

Fluid Mechanics, Water Hammer, Dynamic Stresses, and Piping Design

Robert A. Leishear

Fluid Mechanics, Water Hammer, Dynamic Stresses, and Piping Design

Robert A. Leishear, Ph.D., P. E.

Savannah River National Laboratory

On the cover: Steam plume due to a pipe explosion caused by water hammer in a New York City Steam System, 2009.

This manuscript has been authored by Savannah River Nuclear Solutions, LLC under Contract No. DE-AC09-08SR22470 with the U.S. Department of Energy. The United States Government retains and publisher, by accepting this article for publication, acknowledges that the United States Government retains a non-exclusive, paid-up, irrevocable, worldwide license to publish or reproduce the published form of this work, or allow others to do so, for United States Government purposes.





© 2012, ASME, 3 Park Avenue, New York, NY 10016, USA (www.asme.org)

All rights reserved. Printed in the United States of America. Except as permitted under the United States Copyright Act of 1976, no part of this publication may be reproduced or distributed in any form or by any means, or stored in a database or retrieval system, without the prior written permission of the publisher.

INFORMATION CONTAINED IN THIS WORK HAS BEEN OBTAINED BY THE AMERICAN SOCIETY OF MECHANICAL ENGINEERS FROM SOURCES BELIEVED TO BE RELIABLE. HOWEVER, NEITHER ASME NOR ITS AUTHORS OR EDITORS GUARANTEE THE ACCURACY OR COMPLETENESS OF ANY INFORMATION PUBLISHED IN THIS WORK. NEITHER ASME NOR ITS AUTHORS AND EDITORS SHALL BE RESPONSIBLE FOR ANY ERRORS, OMISSIONS, OR DAMAGES ARISING OUT OF THE USE OF THIS INFORMATION. THE WORK IS PUBLISHED WITH THE UNDERSTANDING THAT ASME AND ITS AUTHORS AND EDITORS ARE SUPPLYING INFORMATION BUT ARE NOT ATTEMPTING TO RENDER ENGINEERING OR OTHER PROFESSIONAL SERVICES. IF SUCH ENGINEERING OR PROFESSIONAL SERVICES ARE REQUIRED, THE ASSISTANCE OF AN APPROPRIATE PROFESSIONAL SHOULD BE SOUGHT.

ASME shall not be responsible for statements or opinions advanced in papers or . . . printed in its publications (B7.1.3). Statement from the Bylaws.

For authorization to photocopy material for internal or personal use under those circumstances not falling within the fair use provisions of the Copyright Act, contact the Copyright Clearance Center (CCC), 222 Rosewood Drive, Danvers, MA 01923, tel: 978-750-8400, www.copyright.com.

Requests for special permission or bulk reproduction should be addressed to the ASME Publishing Department, or submitted online at: http://www.asme.org/Publications/Books/Administration/Permissions.cfm

Library of Congress Cataloging-in-Publication Data

Leishear, Robert Allan.
Fluid mechanics, water hammer, dynamic stresses, and piping design /
Robert A. Leishear.
p. cm.
Includes bibliographical references and index.
ISBN 978-0-7918-5996-4
1. Fluid mechanics. 2. Piping—Design and construction. 3. Water hammer.
I. Title.
QC145.2.L45 2012
660'.283–dc23

2012016745

ACKNOWLEDGMENTS

This book was only possible through the continuous support and sacrifices of Janet Leishear, my wife and best friend. Also, over the past twenty years many technicians, staff, managers, and engineers have contributed to this ongoing research.

In particular, the staff at the University of South Carolina taught graduate school classes, which were required as a basis to invent a new theory that is presented as the crux of this book. In particular, Curtis Rhodes and Jeff Morehouse served as Master's Thesis and PhD Dissertation advisors, respectively, to initially publish the new theory ten years ago. Libby Alford provided substantial instruction on writing techniques to effectively communicate that theory.

Additionally, Department of Energy contractor management from Savannah River Remediation, LLC and Savannah River National Laboratory provided significant financial support over the past twenty years. Corporate funding provided all graduate school education and attendance at many ASME Conferences and Committee meetings that underlie the work presented in this book. ASME staff under Mary Grace Stefanchik and Tara Collins Smith brought this book into publication. Although only one author is listed on the cover of this book, this work was the result of interaction and support from many. Thanks to all of them.

About the Author

Robert A. Leishear, BSME, MSME, Ph.D., P. E.
Savannah River National Laboratory

Dr. Leishear earned a Bachelor's degree in Mechanical Engineering from Johns-Hopkins University in 1982, and a Master of Science and PhD degrees in Mechanical Engineering from the University of South Carolina in 2001 and 2005. Undergraduate and graduate degrees were obtained while employed full time. His Bachelor's degree was obtained while completing a sheet metal apprenticeship and working for 10 years in the construction trades as a Journeyman sheet metal mechanic, structural steel and ship fabricator, steeple jack, welder, and carpenter. Graduate research complemented 25 years of engineering employment and further extensive training as a practicing engineer.

He has held positions as a design engineer, plant engineer, process engineer, test engineer, pump engineer, and research engineer. In these positions he had various responsibilities, which included: water hammer analysis; piping design; troubleshooting and design modifications for fluid systems, cooling towers, heat exchangers, pumps, fans, and motors; plant modifications; vibration analysis of rotating equipment; pressure vessel calculations and inspections; engineering technical oversight of plant operations and maintenance; selection, testing, and installation of pumps up to 300 horsepower; compressor control system design; electronic packaging, machining, and casting design; structural modeling; and large scale experimental fluid mechanics and mass transfer research.

Dr. Leishear has also received additional training in these positions, which included: diesel generators; nuclear waste process equipment and instrumentation; piping, equipment, and instrumentation for compressed air, water, steam, and chemical systems; chemistry; radiochemistry; materials for nuclear service; nuclear waste transfer piping systems and evaporator operations; safety analysis; electrical power systems and electrical distribution; electrical systems training; digital systems training; programmable logic controllers; variable frequency drive controllers; vibration analysis; National Electrical Code; and air conditioning equipment troubleshooting.

Dr. Leishear has also been a member of the ASME Pressure Vessel Division, Design and Analysis Committee, the Task Group for Impulsively Loaded Vessels, ASME B31 Mechanical Design Committee, and the ASME B31.3 Design Subgroup for Process Piping. As an ASME member, he attended the following classes and short courses: ASME Boiler and Pressure Vessel Code, Section VIII; National Board Inspection Code; ASME B31.1 and B31.3 Piping Codes, High temperature piping design; high pressure piping design; Seismic piping design: Failure analysis of piping; and Nondestructive (NDE) inspection techniques for welded assemblies.

Research into water hammer was completed as part of employment as well as University studies. His Master's Thesis and PhD Dissertation focused on the structural response of pipes due to water hammer and the response of simple structures due to impacts by shock waves or colliding objects. Neither of these topics was adequately resolved in the literature prior to this research. To augment research on water hammer, Dr. Leishear completed graduate courses in: advanced fluid flow; fluid transients; gas dynamics; structural vibrations; machinery vibrations; metallurgy; fatigue of materials; fracture mechanics; combustion and explosion dynamics; solid mechanics; theory of structures; computer programming; numerical analysis; advanced engineering mathematics; advanced thermodynamics; nuclear engineering; noise control; heating, ventilation, and air conditioning design; finite element analysis; and stress waves in elastic solids.

Since completing his Master's degree he has authored or coauthored 40 conference and journal publications, which documented the research leading to more than fifty million dollars in cost savings at the Department of Energy's Savannah River Site. Half of these papers were related to dynamic stresses and water hammer. The rest of the papers were related to pumps, vibration analysis, dynamics of rotating machinery, and mixing of nuclear waste in one million gallon storage tanks.

He served as an expert on fluid dynamics, structural dynamics, pumps, and water hammer at various facilities within the Savannah River Site, which included several nuclear waste processing facilities that employ thousands. He has taught engineering classes on water hammer, pumps, and vibration analysis, and is currently working on research for experimental fluid processes as a Fellow Engineer in the Savannah River National Laboratory, Engineering Development Lab, Thermal and Fluids Laboratory.

In short, Dr. Leishear has extensive practical experience coupled with a broad technical and academic education, which resulted in a comprehensive understanding of water hammer and its detrimental effects on personnel and piping systems. Simply stated, the goal of this text is to teach what he has learned on this topic as well as possible.

CONTENTS

Preface **xviii**

CHAPTER 1 Introduction **1**

1.1 Model of a Valve Closure and Fluid Transient 1
1.2 Pipe Stresses 2
1.2.1 Static Stresses 2
1.2.2 Dynamic Stresses 2
1.3 Failure Theories 3
1.4 Valve Closure Model Summary 3

CHAPTER 2 Steady-State Fluid Mechanics and Pipe System Components **5**

2.1 Conservation of Mass and Bernoulli's Equation 5
2.1.1 Conservation of Mass 5
2.1.2 Bernoulli's Equation 6
2.1.3 Limitations of Bernoulli's Equation Due to Localized Flow Characteristics 7
2.2 Hydraulic and Energy Grade Lines 11
2.3 Friction Losses for Pipes 11
2.3.1 Types of Fluids 13
2.3.1.1 Viscosity Definition 13
2.3.1.2 Properties of Newtonian and Non-Newtonian Fluids 14
2.3.1.3 Laminar Flow in Newtonian and Non-Newtonian Fluids 15
2.3.2 Pipe Friction Losses for Newtonian Fluids 16
2.3.3 Friction Factors from the Moody Diagram 16
2.3.3.1 Surface Roughness 19
2.3.3.2 Pipe and Tubing Dimensions 19
2.3.3.3 Density and Viscosity Data and Their Effects on Pressure Drops Due to Flow 23
2.3.4 Tabulated Pressure Drops for Water Flow in Steel Pipe 26
2.3.5 Effects of Aging on Water-Filled Steel Pipes 26
2.3.6 Friction Factors from Churchill's Equation 28
2.3.7 Pipe Friction Losses for Bingham Plastic Fluids and Power Law Fluids 34
2.3.8 Friction Losses in Series Pipes 38
2.3.9 Flow and Friction Losses in Parallel Pipes 40
2.3.10 Inlets, Outlets, and Orifices 41
2.3.11 Fitting Construction 41
2.3.12 Valve Designs 43
2.3.12.1 Gate Valves 55
2.3.12.2 Globe Valves 55
2.3.12.3 Ball Valves 55
2.3.12.4 Butterfly Valves 56
2.3.12.5 Plug Valves 56
2.3.12.6 Diaphragm Valves 56
2.3.12.7 Check Valves 57
2.3.12.8 Relief Valves 62
2.3.12.9 Safety Valves 62
2.3.12.10 Needle Valves 67
2.3.12.11 Pinch Valves 67
2.3.12.12 Traps 67
2.3.12.13 Pressure Regulators 68
2.4 Friction Losses for Fittings and Open Valves 68
2.4.1 Graphic Method for Friction Losses in Fittings and Valves 69
2.4.2 Crane's Method for Friction Losses in Steel Fittings and Valves 69
2.4.3 Modified Crane's Method for Friction Losses in Fittings and Valves of Other Materials and Pipe Diameters 69
2.4.4 Darby's Method for Friction Losses in Fittings and Valves for Newtonian and Non-Newtonian Fluids 69
2.4.5 Tabulated Resistance Coefficients for Fittings and Valves Using Crane's, Darby's, and Hooper's Methods 74
2.5 Valve Performance and Friction Losses for Throttled Valves 74

2.5.1 Valve Flow Characteristics 75
2.5.2 Throttled Valve Characteristics 75
2.5.3 Resistance Coefficients for Throttled Valves 75
2.5.4 Valve Actuators 77
2.5.5 Flow Control 83
2.5.6 P'I'D' Control 84
2.6 Design Flow Rates 88
2.7 Operation of Centrifugal Pumps in Pipe Systems 88
2.7.1 Types of Centrifugal Pumps 88
2.7.2 Pump Curves 89
2.7.2.1 Affinity Laws 89
2.7.2.2 Impeller Diameter 90
2.7.2.3 Impeller Speed 91
2.7.2.4 Acoustic Vibrations in Pumps and Pipe Systems 91
2.7.2.5 Power and Efficiency 92
2.7.2.6 Effects of Other Fluids on Pump Performance 92
2.7.2.7 Net Positive Suction Head and Cavitation 92
2.7.3 Motor Speed Control 99
2.7.3.1 Induction Motors 99
2.7.3.2 Motor Starters 99
2.7.3.3 VFDs 99
2.7.3.4 Pump Shutdown and Inertia of Pumps and Motors 100
2.7.4 Pump Performance as a Function of Specific Speed 100
2.7.5 Pump Heating Due to Flow Through the Pump 102
2.7.6 System Curves 102
2.7.7 Parallel and Series Pumps 107
2.7.8 Parallel and Series Pipes 107
2.8 Jet Pumps 107
2.9 Two Phase Flow Characteristics 108
2.9.1 Liquid/Gas Flows 108
2.9.1.1 Air Entrainment and Dissolved Gas 110
2.9.1.2 Air Binding in Pipes 113
2.9.2 Open Channel Flow 113
2.9.3 Liquid/Vapor Flows 114
2.9.4 Liquid/Solid Flows 114
2.9.5 Siphons 114
2.10 Design Summary for Flow in Steady-State Systems 116

CHAPTER 3 Pipe System Design 119
3.1 Piping and Pressure Vessel Codes and Standards 119
3.1.1 ASME Piping and Pressure Vessel Codes 119
3.1.2 Other Codes and Standards 120
3.1.3 ASME B31.3, Process Piping 120
3.2 Pipe Material Properties 121
3.2.1 Tensile Tests 121
3.2.1.1 Ductile Materials 121
3.2.1.2 True Stress and True Strain 122
3.2.1.3 Strain Hardening 122
3.2.1.4 Loss of Ductility 123
3.2.1.5 Strain Rate Effects on Material Properties 124
3.2.1.6 Brittle Materials 124
3.2.1.7 Elastic Modulus Data 124
3.2.1.8 Yield Strength and Ultimate Strength Data 124
3.2.2 Charpy Impact Test 127
3.2.3 Fatigue Testing and Fatigue Limit 128
3.2.3.1 Fatigue Limit Accuracy 128
3.2.3.2 Fatigue-Testing Methods and Fatigue Data 129
3.2.3.3 Relationship of Fatigue to Vibrations 130
3.2.3.4 Environmental and Surface Effects on Fatigue 131
3.2.3.5 Summary of Fatigue Testing 132
3.2.3.6 Fatigue Testing for Pipe Components 132
3.2.3.7 Fatigue Curves for B31.3 Piping 132
3.2.3.8 Pressure Cycling Fatigue Data 132
3.2.3.9 Fatigue Data for Pressure Vessel Design 132
3.2.4 Poisson's Ratio 136
3.2.5 Material Densities 136
3.2.6 Thermal Expansion and Thermal Stresses 136
3.2.6.1 Thermal Stresses 136
3.2.6.2 Longitudinal Thermal Expansion of a Pipe 148
3.2.6.3 Bending Due to Thermal Expansion 152
3.3 Pipe System Design Stresses 152
3.3.1 Stress Calculations 153
3.3.2 Load-Controlled and Displacement-Controlled Stresses 154
3.3.3 Maximum Stresses 154
3.3.4 Internal Pressure Stresses, Hoop Stresses 154
3.3.4.1 Corrosion and Erosion Allowances 155
3.3.4.2 Hoop Stress and Maximum Pressure 156
3.3.5 Limits for Sustained Longitudinal Stresses, Occasional Stresses, and Displacement Stresses 157
3.3.6 Allowable Stresses 161
3.3.7 Pipe Stresses and Reactions at Pipe Supports 164
3.3.7.1 Axial Stresses and Reactions Due to Pressure and Flow 164

3.3.7.2	Restraint and Control of Forces	168
3.3.7.3	Reactions and Pipe Stresses	168
3.3.7.4	Torsional Stresses and Moments	171
3.3.7.5	Pipe Stresses Due to Pipe and Fluid Weights	171
3.3.7.6	Stress Intensification Factors	171
3.3.7.7	Flexibility Calculation Example	171
3.3.7.8	Comparison of Code Stress Calculations	176
3.3.7.9	Pipe Stresses Due to Wind and Earthquake	179
3.3.7.10	Pipe Supports and Anchor Designs	179
3.3.8	Structural Requirements for Fittings, Flanges, and Valves	180
3.3.9	Pipe Schedule and Pressure Ratings for Fittings, Flanges, and Valves	181
3.3.10	Flange Stresses	182
3.3.11	Limiting Stresses for Rotary Pump Nozzles	182
3.4	Hydrostatic Pressure Tests	182
3.5	Summary of Piping Design	185
CHAPTER 4	**Pipe Failure Analysis and Damage Mechanisms**	**193**
4.1	Failure Theories	193
4.1.1	State of Stress at a Point, Multiaxial Stresses	193
4.1.2	Maximum Stresses	194
4.1.2.1	Principal Stresses	194
4.1.2.2	Maximum Shear Stresses	196
4.1.2.3	Stresses Due to Pipe Restraint	197
4.1.3	Failure Stresses	197
4.1.4	Comparison of Failure Stress Theories	197
4.1.5	Maximum Normal Stress Theory (Rankine)	199
4.1.6	Maximum Shear Stress Theory (Tresca, Guest)	200
4.1.7	Distortion Energy/Octahedral Shear Stress Theory (Von Mises, Huber, Henckey)	201
4.2	Structural Damage Mechanisms/ Failure Criteria	201
4.3	Overload Failure or Rupture	201
4.3.1	Burst Pressure for a Pipe	201
4.3.2	External Pressure Stresses	202
4.4	Plastic Deformation	202
4.4.1	Plasticity Models for Tension	202
4.4.2	Cyclic Plasticity	203
4.4.3	Elastic Follow-Up	203
4.4.4	Cyclic, Plastic Deformation	203
4.4.5	Plastic Cycling for Piping Design	206
4.4.6	Limit Load Analysis for Bending	207
4.4.7	Limit Load Analysis for Equations for Bending of a Pipe	207
4.4.8	Comparison of Limit Load Analysis to Cyclic Plasticity	208
4.4.9	Plastic Deformation Due to Pressure, Hoop Stress	208
4.4.10	Autofrettage	209
4.4.11	Combined Stresses for Plasticity	209
4.4.12	Comparison of Limit Load Analysis to the Bree Diagram	209
4.4.13	Summary of Plastic Failure Analysis	210
4.5	Fatigue Failure	210
4.5.1	High-Cycle Fatigue Mechanism	210
4.5.2	High-Cycle Fatigue Life of Materials	211
4.5.3	Triaxial Fatigue Theories	212
4.5.3.1	Maximum Normal Stress Theory, Triaxial Stresses	212
4.5.3.2	Maximum Shear Stress Theory, Triaxial Stresses	212
4.5.3.3	Octahedral Shear Stress Theory, Triaxial Stresses	213
4.5.4	Cumulative Damage	214
4.5.5	Rain Flow Counting Technique	214
4.5.6	Use of Fatigue Theory and Equations	215
4.5.7	Pressure Vessel Code, Fatigue Calculations	217
4.5.7.1	Method 1: Elastic Stress Method for Fatigue	217
4.5.7.2	Method 2: Elastic-Plastic Stress Method for Fatigue	217
4.5.7.3	Method 3: Structural Stress Method for Fatigue	218
4.5.8	Fatigue Summary	218
4.6	Fracture Mechanics	218
4.6.1	Fracture Mechanics History	219
4.6.2	Applications of Fracture Mechanics and Fitness for Service	219
4.6.3	LEFM	219
4.6.4	Elastic-Plastic Analysis	221
4.6.5	Elastic-Plastic Fracture Mechanisms	221
4.6.6	Crack Propagation	221
4.6.7	Stress Raisers	224
4.6.8	Fracture Mechanics Summary	224
4.7	Corrosion, Erosion, and Stress Corrosion Cracking	225
4.8	Flow-Assisted Corrosion (FAC)	226
4.9	Leak Before Break	226
4.10	Thermal Fatigue	227
4.11	Creep	227
4.11.1	Examples of Creep-Induced Failures	227
4.11.2	Creep in Plastic and Rubber Materials	228

4.12 Other Causes of Piping Failures 228
4.13 Summary of Piping Design and Failure Analysis 229

CHAPTER 5 Fluid Transients in Liquid-Filled Systems 233
5.1 Slug Flow During System Startup 233
5.1.1 Slug Flow Due to Pump Operation 234
5.1.2 Slug Flow During Series Pump Operation 234
5.1.3 Pump Runout Effects on Slug Flow 234
5.2 Draw Down of Systems 235
5.3 Fluid Transients Due to Flow Rate Changes 235
5.3.1 Examples of Pipe System Damages in Liquid-Filled Systems 235
5.3.1.1 Hydroelectric Power Plants 235
5.3.1.2 Valve Closure 235
5.3.1.3 Vapor Collapse in a Liquid-Filled System 236
5.3.1.4 Damages Due to Combined Valve and Pump Flow Rate Changes 237
5.4 Types of Fluid Transient Models for Valve Closure 239
5.5 Rigid Water Column Theory 239
5.5.1 Basic Water Hammer Equation, Elastic Water Column Theory 242
5.5.2 Arithmetic Water Hammer Equation 245
5.6 Shock Waves in Piping 247
5.6.1 Wave Speeds in Thin Wall Metallic Pipes 248
5.6.2 Wave Speeds in Thick Wall Metallic Pipes 249
5.6.3 Wave Speeds in Nonmetallic Pipes 250
5.6.4 Effects of Entrained Solids on Wave Speed 250
5.6.5 Effects of Air Entrainment on Wave Speed 250
5.7 Uncertainty of the Water Hammer Equation 252
5.8 Computer Simulations/Method of Characteristics 253
5.8.1 Differential Equations Describing Fluid Motion 253
5.8.2 Shock Wave Speed Equation 254
5.8.3 MOC Equations 254
5.9 Valve Actuation 257
5.10 Reflected Shock Waves 261
5.11 Reflected Waves in a Dead-End Pipe 261
5.12 Series Pipes and Transitions in Pipe Material 262
5.13 Parallel Pipes/Intersections 262
5.14 Centrifugal Pump Operation During Transients 266
5.14.1 Graphic Water Hammer Solution for Pumps 266
5.14.2 Reverse Pump Operation Due to Flow Reversal 266
5.14.3 Transient Radial Pump Operation 268
5.14.4 MOC Water Hammer Solution for Pumps 268
5.14.5 Use of Valve Closure Speeds to Control Pump Transients 269
5.15 Column Separation and Vapor Collapse 269
5.15.1 Column Separation and Vapor Collapse at a High Point in a System With Both Pipe Ends Submerged 270
5.15.2 Column Separation and Vapor Collapse at a High Point in a Pipe With One End Submerged 273
5.15.3 Column Separation and Vapor Collapse at a Valve 275
5.15.4 Solution Methods to Describe Column Separation and Vapor Collapse 275
5.16 Positive Displacement Pumps 276
5.17 Effect of Trapped Air Pockets on Fluid Transients 277
5.18 Additional Corrective Actions for Fluid Transients 278
5.18.1 Valve Stroking 278
5.18.2 Relief Valves 278
5.18.3 Surge Tanks and Air Chambers 278
5.18.3.1 Fluid Resonance Example 280
5.18.4 Water Hammer Arrestors 280
5.18.5 Surge Suppressors 280
5.18.6 Check Valves 280
5.18.7 Flow Rate Control for Fluid Transients 280
5.19 Summary of Fluid Transients in Liquid-Filled Systems 283

CHAPTER 6 Fluid Transients in Steam Systems 287
6.1 Examples of Water Hammer Accidents in Steam/Condensate Systems 287
6.1.1 Brookhaven Fatalities 287
6.1.2 Hanford Fatality 287
6.1.3 Savannah River Site Pipe Damages 289
6.1.3.1 Pipe Failure During Initial System Startup 289
6.1.3.2 Pipe Damages During System Restart 290
6.1.4 Pipe Failures Due to Condensate-Induced Water Hammer 291

6.2 Water Hammer Mechanisms in Steam/Condensate Systems 291
6.2.1 Water Cannon 292
6.2.2 Steam and Water Counterflow 292
6.2.3 Condensate-Induced Water Hammer in a Horizontal Pipe 292
6.2.4 Steam Pocket Collapse and Filling of Voided Lines 293
6.2.5 Low-Pressure Discharge and Column Separation 295
6.2.6 Steam-Propelled Water Slug 295
6.2.7 Sudden Valve Closure and Pump Operations 295
6.3 Blowdown 295
6.3.1 Sonic Velocity at Discharge Nozzles 296
6.3.2 Piping Loads During Blowdown 297
6.3.3 Steam/Water Flow 298
6.3.4 Pressures in Closed Vessels and Thrust During Blowdown 298
6.4 Appropriate Operation of Steam Systems for Personnel Safety 300
6.4.1 System Startup 300
6.4.2 Steam Traps 301
6.5 Summary of Fluid Transients 301

CHAPTER 7 Shock Waves, Vibrations, and Dynamic Stresses in Elastic Solids 303
7.1 Strain Waves and Vibrations 303
7.1.1 One-Dimensional Strain Waves in a Rod 303
7.1.2 Three-Dimensional Strain Waves in a Solid 304
7.1.3 Vibration Terms 304
7.1.4 Vibrations in a Rod Due to Strain Waves 305
7.1.5 Dilatational Strain Waves in a Rod 305
7.1.6 Wave Reflections in a Rod 305
7.1.7 Strain Wave Examples for Rods 306
7.1.8 Inelastic Damage Due to Wave Reflections 308
7.2 Single Degree of Freedom Models 308
7.2.1 SDOF Oscillators 308
7.2.1.1 SDOF Equation of Motion 309
7.2.1.2 SDOF, Free Vibrations 309
7.2.1.3 Damping Effects 309
7.2.1.4 Damping Ratio 309
7.2.1.5 Log Decrement 309
7.2.1.6 Phase Angle Effects 310
7.2.1.7 SDOF Responses to Applied Forces 311
7.2.2 Step Response for a SDOF Oscillator 311
7.2.2.1 Homogeneous Solution to the Equation of Motion for a Step Response 311
7.2.2.2 Particular Solution to the Equation of Motion for a Step Response 311
7.2.2.3 General Solution to the Equation of Motion for a Step Response 312
7.2.3 Impulse Response for a SDOF Oscillator 312
7.2.4 Ramp Response for a SDOF Oscillator 313
7.2.5 SDOF Harmonic Response 313
7.2.5.1 SDOF Load Control 314
7.2.5.2 Steady-State, SDOF Load-Controlled Vibration 316
7.2.5.3 Frequency Effects on the DMF During SDOF Load-Controlled Vibration 316
7.2.5.4 DMF for SDOF Load Control 317
7.2.6 Multi-DOF Harmonic Response 317
7.2.6.1 Multi-DOF Load Control 317
7.2.6.2 Modal Contributions for Multi-DOF Vibrations 319
7.2.6.3 Participation Factors for SDOF Vibrations 319
7.2.6.4 Resonance for Multi-DOF Vibrations 319
7.2.6.5 Load-Controlled Vibrations for Rods 321
7.2.6.6 Load-Controlled Vibrations for Beams 323
7.3 Dynamic Stress Equations 324
7.3.1 Triaxial Vibrations 324
7.3.2 Damping 325
7.3.2.1 Proportional Damping 325
7.3.2.2 Structural Damping for Pipe Systems 326
7.3.2.3 Fluid Damping and Damping for Hoop 327
7.4 Summary of Dynamic Stresses in Elastic Solids 330

CHAPTER 8 Water Hammer Effects on Breathing Stresses for Pipes and Other Components 331
8.1 Examples of Piping Fatigue Failures 331
8.2 FEA Model of Breathing Stresses for a Short Pipe 331
8.2.1 FEA Assumptions 332
8.2.2 Model Geometry and Dynamic Pressure Loading 334
8.2.3 FEA Model for a Pipe With Fixed Ends 335
8.2.4 Stress Waves and Through-Wall Radial Stresses 336
8.2.5 Hoop Stresses for a Pipe With Fixed Ends 336

8.2.6 Axial Stresses for a Pipe with Fixed Ends 337
8.2.7 Impulse Loads 337
8.2.8 Stresses for a Pipe with One Free End 338
8.2.9 FEA Summary 339
8.3 Theory and Experimental Results for Breathing Stresses 340
8.4 Flexural Resonance 340
8.4.1 Flexural Resonance Theory 340
8.4.1.1 Moment in a Differential Element 340
8.4.1.2 Membrane Forces in a Cylindrical Shell 341
8.4.1.3 Axial Displacement in a Cylindrical Shell 342
8.4.1.4 Equation of Motion for a Cylindrical Shell 342
8.4.1.5 Evaluation of Flexural Resonance 343
8.4.1.6 DMF and the Critical Velocity 344
8.4.1.7 Critical Velocity 344
8.4.1.8 Breathing-Mode Frequency 345
8.4.1.9 Flexural Resonance Assuming Fixed Pipe Ends 345
8.4.2 Flexural Resonance Examples 345
8.4.2.1 Strains in Gun Tubes 345
8.4.2.2 Strains Due to Internal Shocks in a Tube 346
8.4.3 Summary of Flexural Resonance Theory 348
8.5 Dynamic Hoop Stresses 348
8.5.1 Bounded Hoop Stresses from Beam Equations 348
8.5.1.1 Precursor and Aftershock Vibrations 350
8.5.1.2 Pipe Wall Displacement Derivation 350
8.5.1.3 Pipe Wall Displacement Equation 350
8.5.1.4 Critical Velocity 351
8.5.1.5 DMF and Maximum Stresses from Beam Theory 351
8.5.2 Dynamic Stress Theory 351
8.5.2.1 Derivation of Dynamic Stress Equations 351
8.5.2.2 Static Stress 352
8.5.2.3 Equation of Motion for a SDOF Oscillator 352
8.5.2.4 Equation of Motion for a Cylinder Subjected to a Sudden Internal Pressure 352
8.5.2.5 Pipe Stresses Due to a Shock Wave 353
8.5.2.6 Precursor Stresses 353
8.5.2.7 Effects of the Arbitrary Selection of $t = 0$ 354
8.5.2.8 Effects of the Wave Speed 354
8.5.2.9 Maximum Damped Precursor Stress 354
8.5.2.10 Aftershock-Free-Vibration Stresses 354
8.5.2.11 Damping 355
8.5.2.12 Maximum Stress When the Critical Velocity is Not Considered 355
8.5.3 Comparison of Theory to Experimental Results for a Gas-Filled Tube 355
8.5.4 Comparison of Theory to Experimental Results for a Liquid-Filled Pipe 356
8.5.4.1 Test Setup and Raw Data 358
8.5.4.2 Test Results and Discussion 359
8.5.4.3 Breathing Stress Frequency 363
8.5.4.4 Wave Velocities 363
8.5.4.5 Pressure Surge Magnitude 363
8.5.4.6 Equivalent Axial and Hoop Strains 365
8.5.4.7 Example of Corrective Actions and Fitness for Service 365
8.5.4.8 Corrective Actions 365
8.5.4.9 Fitness for Service 365
8.5.5 Comparison of Flexural Resonance Theory to Dynamic Stress Theory 367
8.6 Valves and Fittings 369
8.7 Pressure Vessels 369
8.8 Plastic Hoop Stresses 370
8.8.1 FEA Results for a Shock Wave in a Short Pipe 370
8.8.2 Experimental Results for Explosions in a Thin-Wall Tube 371
8.8.3 Explosions in Pipes 372
8.9 Summary of Elastic and Plastic Hoop Stress Responses to Step Pressure Transients 373

CHAPTER 9 Dynamic Stresses Due to Bending 379
9.1 Deformations, Stresses, and Frequencies for Elastic Frames 379
9.1.1 Static Deflections and Reactions for Simply Supported Beams and Elastic Frames 379
9.1.2 Frequencies for Simple Beams 379
9.1.3 Frequencies for Elastic Frames 381
9.2 Elastic Stresses Due to Bending 383
9.2.1 Step Response Calculation for Bending 384
9.2.1.1 Calculation Assumptions 384
9.2.1.2 Axial Stresses 385
9.2.1.3 Bending Stresses 386

9.2.1.4 Hoop Stresses 387
9.2.1.5 Comparison of Calculated Bending Stress to an FEA Pipe Stress Model 388
9.2.2 Ramp Response for Bending 388
9.2.3 Impulse Response for Bending 390
9.2.4 Multiple Bend FEA Models 392
9.3 FEA Model of Bending Stresses 393
9.4 Plastic Deformation and Stresses Due to Bending 393
9.4.1 Consideration of Earthquake Damages to Pipe Systems 393
9.5 Summary of Stresses During Water Hammer 393

CHAPTER 10 Summary of Water Hammer-Induced Pipe Failures 395
10.1 Troubleshooting a Pipe Failure 396
10.2 Suggested References 396
10.3 Recommended Future Research 397

Appendix A: Notation and Units 399
A.1 Systems of Units 399
A.2 Conversion Factors 400
A.3 Notation: Variables, Constants, and Dimensions 402
References 409
Index 419

PREFACE

The title, "Fluid Mechanics, Water Hammer, Dynamic Stresses, and Piping Design" was selected, even though a more concise title may have been "Fluid Transients and Their Structural Effects on Basic Pipe System Components." "Fluid Mechanics" is discussed to provide a thorough foundation for the text. The term "Fluid Transients" describes the fact that pressure surges occur any time a flow rate changes within a pipe due to a pump startup, a pump shutdown, a valve opening, or a valve closure. A fluid transient always occurs during any of these events. Sometimes the transient pressure is acceptable; sometimes it is not. Water hammer may be defined as an extreme fluid transient recognized by the loud bang, or hammering sound sometimes associated with a fluid transient. In practice, the terms are frequently used interchangeably. However, the term water hammer is commonly associated with accidents and fatalities. For some, the use of this term evokes images of broken and bent piping, multi-million dollar damages, the loss of water supplies to cities, and the deaths of individuals due to water hammer accidents. The primary purpose of this text is to provide practicing engineers with the analytical tools required to identify water hammer concerns and prevent equipment and environmental damage, personnel injury, and fatalities. Consequently, "Water Hammer" seems to be an appropriate term to describe this work.

With respect to the term "Piping Design", the effects of water hammer are considered here for basic pipe system components, such as valves, pipes, and pipe fittings. Complex piping systems are more accurately evaluated using computer models. Although some examples of computer aided design techniques are provided here for fluid transients and structural design calculations, the required computer models are outside the scope of this text. Even so, the constitutive principles provided here should be incorporated into the appropriate computer models.

When I first became involved in water hammer investigations in the early 1990's, a literature review revealed that the pressure surges due to water hammer could be approximately defined, but techniques to find the resulting pipe stresses leading to pipe failure were unavailable. Master's and PhD research (Leishear [1, 2]) focused on the determination of pipe stresses due to water hammer, which are referred to as "Dynamic Stresses". This research resulted in multi-million dollar cost savings by eliminating water hammer damages in a nuclear facility (Leishear [3 - 17]). The research results were paralleled by a short course on water hammer, which I developed and taught to hundreds of engineers, managers, and plant operators. The research publications and the class are the foundation of the text with additional research added as required.

As noted, the text consists of three topics: water hammer and piping design which are related through a third topic of dynamic stresses. Although new developments continue in the field of fluid transients, the basic theory with respect to water hammer is well established. This text provides a review of requisite fluid mechanics in Chapter 2 and static piping design in Chapter 3. Significant piping damages may occur both during initial system startup and shutdown due to a one time material overload, but failures may also occur due to material fatigue after long hours of operation. In other words, a lack of failure at system startup does not guarantee failure free operation in the future. To consider the differences between overload and fatigue failure mechanisms, Chapter 4 reviews available failure theories. Chapters 5 and 6 provide a description of water hammer mechanisms, case studies of water hammer accidents, and recommended techniques to address water hammer concerns for liquid filled systems and steam-condensate systems. For piping design, pipe stresses are greater than those calculated by assuming that a static stress exists due to a slowly applied pressure in a steady-state system. The pipe stresses are greater since the pipe vibrates in response to water hammer. This heightened response is described by vibration equations and dynamic magnification factors, which are described in Chapter 7. The pipe response is comparable to a spring which is suddenly loaded with a force. The spring overshoots its equilibrium, or static position, but gradually returns to equilibrium. The dynamic magnification factor expresses

the value of maximum overshoot above the equilibrium position. Chapters 8 and 9 apply these vibration equations to pipes and equipment, since many cracked pipes and leaking valves in industrial and municipal facilities are the direct result of fluid transients. In short, Chapters 1 through 9 describe water hammer and pipe failures in systems that initially exist at steady state conditions. Specifically, the initial flow rate prior to a fluid transient is typically a constant value or zero. Another type of water hammer analysis concerns some types of positive displacement pumps, where the initial condition prior to the transient is provided by an oscillating, nearly harmonic flow, which is, in itself, a transient condition. Each chapter builds on the material presented in previous chapters, and although research continues, these chapters provide the first comprehensive overview and status of a multidisciplinary technique developed to answer the question, Is the fluid transient in a particular system acceptable, and, if not, how may the transient be corrected?

The text has two primary applications. One is the evaluation of accidents and piping failures. The other is the prevention of these events. For example, recently developed theory contained in this text identified numerous water hammer problems and prevented further multi-million dollar damages at Savannah River Site (SRS). A series of more than two hundred pipe failures which occurred over forty years abruptly came to a halt, but an outstanding milestone to recognize success was nonexistent. The lack of pipe failures over several years was the measure of success. To understand water hammer induced failures, explanations of many other pipe failure mechanisms are discussed to ensure that failure causes can be differentiated by the investigator. Application of this text is hoped to prevent injuries, fatalities, and pipe system damages.

CHAPTER

1

INTRODUCTION

Piping systems are typically designed to the maximum expected design pressure of the system, but water hammer may amplify the system pressure by as much as six to ten, or more, times the original, intended design pressure. This text discusses techniques to estimate those pressures, the stresses caused by the suddenly applied pressures, potential failures due to those pressures, and corrective actions available to reduce those pressures if required. The piping Codes, as written, address static design conditions for elastic materials with little discussion of dynamics. This work reviews some of those static design requirements and provides additional discussion of the dynamic design requirements for pipe systems.

Numerous complexities exist with respect to both the fluid mechanics of water hammer and the dynamic responses of pipe systems subjected to water hammer. Topics such as damping, the effects of trapped air, and trapped vapor in the piping, pump operation, valve operation, steam systems, and piping configurations are presented throughout the text. To introduce the topic, a simplified model is first presented, followed by discussions throughout this work of pertinent topics required to evaluate more complex systems.

A few words about systems of units are required, where US units are predominantly used to be consistent with present practices and referenced works. Including all SI equations would increase the book length appreciably. Deleting the partial list of SI equations shortens this work, but the use of SI equations in the first chapters of the book adequately documents the use of SI units to practically apply this work. This "hybrid" use of SI units seemed satisfactory for communications purposes. Required notation and systems of units used in this text are presented in Appendix A.

1.1 MODEL OF A VALVE CLOSURE AND FLUID TRANSIENT

The classic water hammer problem concerns flow through a pipe and a closing valve as shown in Fig. 1.1 (Joukowski [18]). Initially, the valve is open, and flow is constant. A typical flow velocity in piping systems is 8 to 10 ft/second. When the valve is suddenly closed, a pressure surge is created at the valve with a magnitude equal to P. This pressure surge, or step pressure increase, travels upstream at a sonic velocity, a, along the length of the pipe, where the velocity can approach the acoustic velocity of the fluid, which for water is approximately 4860 ft/second. The magnitude of the pressure change equals

$$\Delta P = P\left(\text{psi}\right) = \frac{\rho\left(\text{lbm/ft}^3\right)\cdot a\left(\text{ft/second}\right)\cdot \Delta V\left(\text{ft/second}\right)}{g_c\left(\text{ft}\cdot\text{lbm/lbf}\cdot\text{second}^2\right)\cdot\left(144\ \text{in}^2/\text{ft}^2\right)} = 2.1584\cdot 10^{-4}\cdot\rho\cdot a\cdot\Delta V \tag{1-1}$$

$$\Delta P = P\left(\text{psi}\right) = \frac{\gamma\left(\text{lbf/in}^3\right)\cdot a\left(\text{ft/second}\right)\cdot V\left(\text{ft/second}\right)}{g\left(\text{ft/second}^2\right)\cdot\left(144\ \text{in}^2/\text{ft}^2\right)} = \frac{\gamma\cdot a\cdot\Delta V}{g\cdot 144} \tag{1-2}$$

where

$$\gamma = \rho\cdot g/g_c \tag{1-3}$$

The change in head across the shock wave (Δh, feet of water) may also be determined using

$$P\left(\text{lbf/ft}^2\right) = \frac{\Delta h\cdot\rho\cdot g}{g_c} \tag{1-4}$$

$$P\left(\text{psi}\right) = \frac{\Delta h\cdot\rho\cdot g}{144\cdot g_c} \tag{1-5}$$

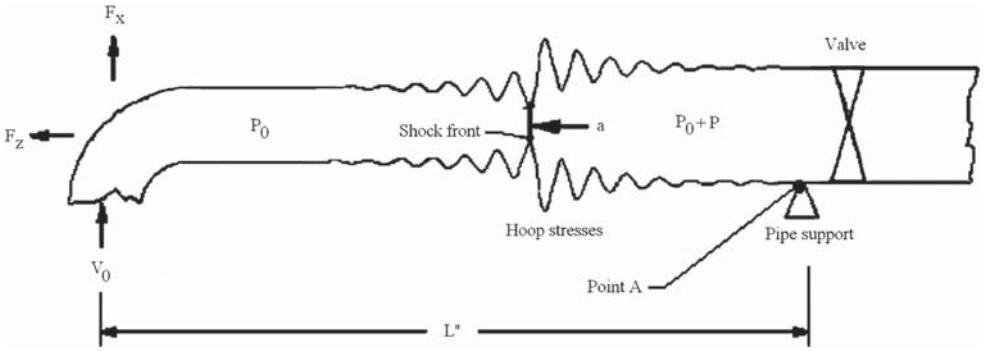


FIG. 1.1 VALVE CLOSURE MODEL

to obtain

$$\Delta h\left(\text{ft}\right)=\frac{a\left(\text{ft/second}\right)\cdot\Delta V\left(\text{ft/second}\right)}{g\left(\text{ft/second}^2\right)}=a\cdot\Delta V/g \qquad (1\text{-}6)$$

In SI units,

$$P=\rho\cdot a\cdot\Delta V \qquad (1\text{-}7)$$

$$P=\Delta h\cdot\rho\cdot g \qquad (1\text{-}8)$$

$$\Delta h=a\cdot\Delta V/g \qquad (1\text{-}9)$$

P_o = initial steady state pressure prior to valve closure
P = increase in pressure across the shock wave
V = V_0 = initial velocity of the liquid
a = velocity of the shock wave
g = local gravitational acceleration
g_c = gravitational constant
ρ = fluid mass density
γ = fluid weight density
ΔV = change in velocity

1.2 PIPE STRESSES

For the simplified model, only the hoop stresses and the stresses due to the shock wave striking the elbow are considered, as shown in Figs. 1.1 and 1.2 (Example 9-1, paragraph 9.2.1). Exaggerated hoop stresses are shown since the actual hoop stresses are visually indiscernible. For a gradually applied load, the static stresses are first determined, and they are then used to establish the dynamic stresses.

1.2.1 Static Stresses

The static hoop stress, σ'_θ, for a thin-walled tube equals

$$\sigma'_\theta\approx\frac{P_0\cdot r_m}{\overline{T}} \qquad (1\text{-}10)$$

For a static axial stress due to an applied force, F_z, in a thin-walled tube, the static axial stress, σ'_z, equals

$$\sigma'_z\approx\frac{P_0\cdot r_m}{2\cdot\overline{T}} \qquad (1\text{-}11)$$

where r_m is the median pipe radius, and $\overline{T}$ is the wall thickness. The maximum static stress due to bending, Sb, due to a force, F, equals

$$Sb\approx\frac{M\cdot c'}{I}=\frac{F\cdot L\cdot r_o}{I}=\frac{4\cdot P_0\cdot L''\cdot r_o^3}{\left(r_o^4-r_i^4\right)} \qquad (1\text{-}12)$$

where
c' = maximum distance from the centroidal axis of an object, and c' = r_o for a pipe
r_o = outer pipe radius
r_i = inner pipe radius
I = moment of inertia
L'' = distance between the pipe support and the applied force, F_x
M = moment

Equations for these static stresses are available in the literature, but dynamic stresses exceeding the static stresses require further examination.

1.2.2 Dynamic Stresses

The approximate dynamic stress, $\sigma(t)$, for simple structures has a general expression of (Leishear [5])

$$\sigma\left(t\right)=\sigma'\cdot V''\left(t\right) \qquad (1\text{-}13)$$

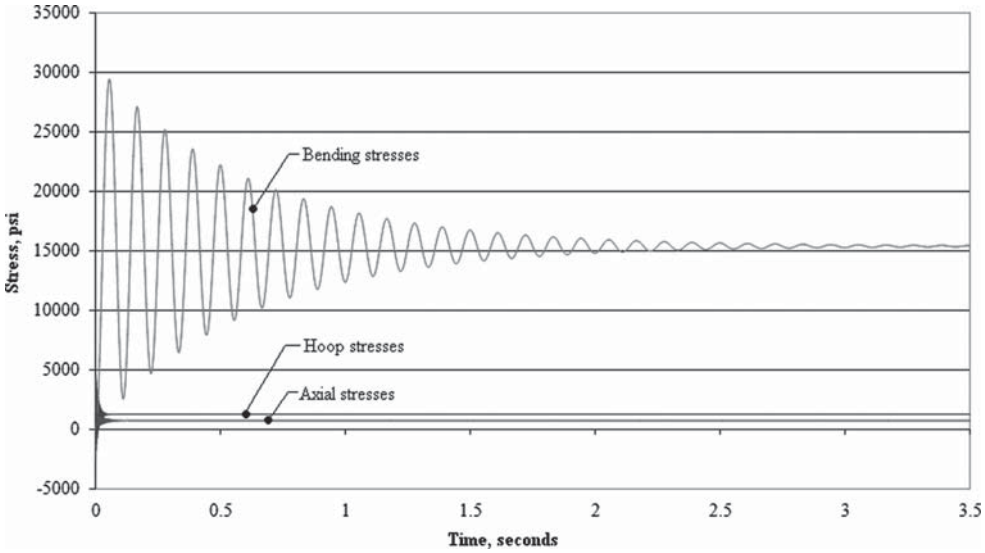


FIG. 1.2 EXAMPLE OF DYNAMIC STRESSES IN A PIPE

where

σ' = static stress
t = time
$V''(t)$ = a vibration response equation, which varies with respect to time, t

Restated, the time-variant, dynamic stress, $\sigma(t)$, equals a constant static stress, σ', times the dynamic response, $V''(t)$. Typically, $V''(t)$ expresses the dynamic stresses in a pipe as a complicated, harmonically decreasing function, which converges to the static stress. While the complexities of $V''(t)$ are further investigated in Chapter 7, the maximum value of the dynamic stress may be stated in a simpler form, such that

$$\sigma_{max} = \sigma' \cdot \text{DMF} \tag{1-14}$$

where the dynamic magnification factor, DMF, is a constant affected by damping. Neglecting damping, Eqs. (1-10) through (1-12) can be substituted into Eq. (1-14) with appropriate DMFs to obtain maximum dynamic stresses for simple cases. The maximum dynamic hoop stress in the vicinity of the shock equals

$$\sigma_{\theta max} = 4 \cdot \sigma'_{\theta} \approx \frac{4 \cdot P \cdot r_m}{\overline{T}} \tag{1-15}$$

The maximum dynamic axial stress after the shock strikes an elbow is

$$\sigma_{z,max} = 2 \cdot \sigma'_z \approx \frac{2 \cdot P \cdot r_m}{\overline{T}} \tag{1-16}$$

The maximum dynamic stress due to bending, after the shock strikes an elbow, is

$$Sb_{max} = 2 \cdot Sb \approx \frac{8 \cdot P_0 \cdot L \cdot r_o^3}{\left(r_o^4 - r_i^4\right)} \tag{1-17}$$

1.3 FAILURE THEORIES

Once the stresses are determined, the appropriate failure theory may be applied. Failure may be determined by comparing the dynamic stress to the yield stress, S_y, the ultimate stress, S_u, allowable design stress, Sa, or the fatigue limit of the material, S_e, or failure may be described in terms of fracture growth through the pipe wall. Detailed descriptions of failure theories and failure modes are listed in Chapter 4.

1.4 VALVE CLOSURE MODEL SUMMARY

For some cases, the equations provided, thus far, are adequate to estimate the pressure surges and pipe stresses due to fluid transients in a system. However, all of the

quantities used in these equations are variable, depending on the system design. Even the yield stresses and ultimate stresses can be described in terms of dynamic yield stresses and dynamic ultimate stresses.

The maximum stresses due to sudden valve closures were also expressed in terms of DMFs multiplied by the calculated static stresses. Although the DMFs were listed as four for hoop stresses and two for bending and axial stresses, the DMFs may be a fraction of these values or multiples of these values depending on the system design. One goal of this text is to provide a sufficient number of mathematical derivations and numerous, practical examples to describe the various influences on the dynamic stresses induced by pressure surges traveling through a pipe system at sonic velocities following the initiation of water hammer.

In short, the text can be considered as three parts: fluid mechanics and water hammer; structural dynamics and the dynamic stress theory; and piping failure analysis. Current piping standards require the user of the standards to consider water hammer, but lack techniques to effectively consider water hammer. This text provides techniques and guidance needed to evaluate water hammer with respect to a given design. Much of the text simply condenses available work in the literature into one source for practicing engineers to resolve pipe failures.

CHAPTER

2

STEADY-STATE FLUID MECHANICS AND PIPE SYSTEM COMPONENTS

Although comprehensive references are available to teach fluid mechanics (White [19] or Shames [20]), some of the fundamentals in these areas are presented here to lay the foundation for a discussion of fluid transients. The basic concepts of theoretical fluid mechanics and some practical aspects of fluid systems (Crane [21]) are applied in this chapter to pipe systems and their system components, such as pumps, piping, valves, and fittings to provide a basic understanding of steady-state fluid system design, which is the first step toward understanding fluid transients. Numerous equations are provided with examples to illustrate their use, but in practice, computer codes are commonly used to establish steady-state conditions in fluid systems.

2.1 CONSERVATION OF MASS AND BERNOULLI'S EQUATION

The extended Bernoulli's equation and the conservation of mass equations are the primary equations used to describe fluid flows in pipe systems. Unless otherwise noted, flows are assumed to be one dimensional and isothermal, and fluids are assumed to be incompressible with constant viscosity. These equations may be derived through vector analysis techniques (Slattery [22]) or through a solution of the equations of motion and continuity of mass (Bird et al [23]). Although equations are not fully developed here, a few of the fundamental assumptions are noted with respect to conservation of mass and Bernoulli's equation.

2.1.1 Conservation of Mass

For differential elements in the Cartesian coordinate system shown in Fig. 2.1, conservation of mass states that the total mass of any system, $\int \rho \cdot dV'$, is invariant with respect to time, such that the mass density, ρ, and the volume, V', are related by

$$\frac{d}{dt}\int \rho \cdot dV' = 0 \qquad \text{US, EE, SI (2.1)}$$

$$\frac{d}{dt}\int \rho \cdot dr \cdot d\theta \cdot dz = 0 \qquad \text{US, EE, SI (2.2)}$$

For a constant density, incompressible fluid,

$$\rho \cdot \frac{d}{dt}\int dr \cdot d\theta \cdot dz = 0 \qquad \text{US, EE, SI (2.3)}$$

Then, for steady-state, one-dimensional flow,

$$\rho \cdot \frac{dz}{dt} \cdot A = \rho \cdot V_z \cdot A = \text{constant} \qquad \text{US, EE, SI (2.4)}$$

where V_z is the axial flow rate, and A is the cross-sectional area of the pipe. This equation then provides expressions for conservation of mass for flow in a pipe, such that

$$\dot{m} = \frac{dm}{dt} = \rho \cdot A \cdot V \Rightarrow \rho_1 \cdot A_1 \cdot V_1 = \rho_2 \cdot A_2 \cdot V_2 \qquad \text{US, SI (2.5)}$$

$$\dot{m} = \frac{\rho(\text{lbm/ft}^3) \cdot A(\text{in}^2) \cdot V(\text{ft/second})}{144(\text{in}^2/\text{ft}^2)} \qquad \text{US (2.6)}$$

where $\dot{m}$ is the mass flow rate, and the subscripts 1 and 2, respectively, represent upstream and downstream locations along the length of a pipe, the cross-sectional areas of the pipe are A_1 and A_2, and the fluid velocities in the pipe equal V_1 and V_2. When the density ρ_1 equals ρ_2 for an incompressible fluid,

$$A_1 \cdot V_1 = A_2 \cdot V_2 \qquad \text{US, EE, SI (2.7)}$$

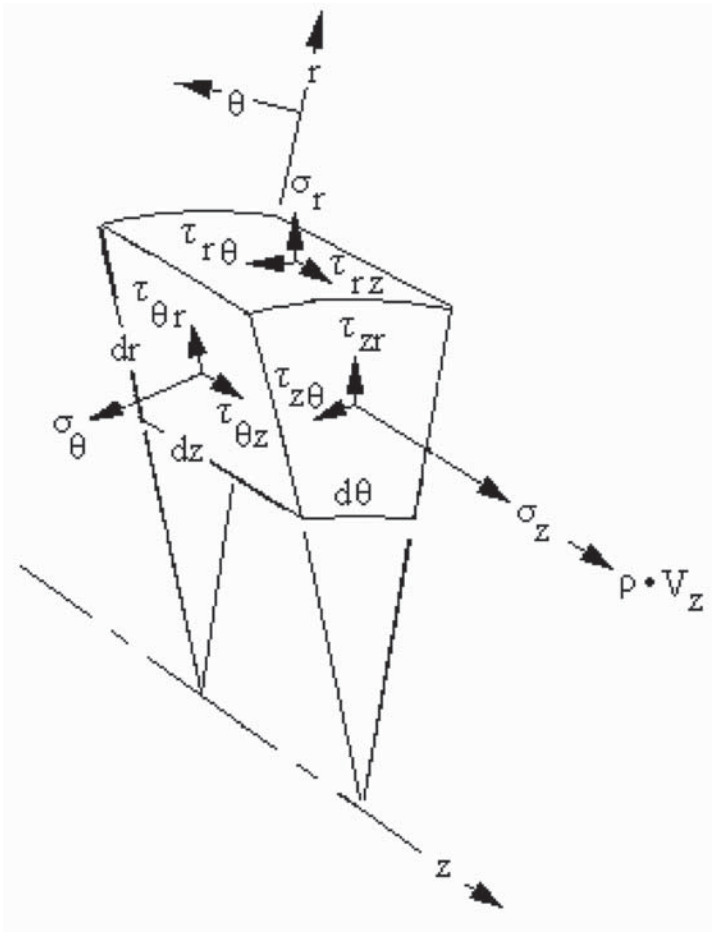


FIG. 2.1 DIFFERENTIAL VOLUME ELEMENT IN CYLINDRICAL COORDINATES

and with appropriate conversions,

$$Q(\text{gpm}) = 2.451 \cdot V(\text{ft/second}) \cdot D^2(\text{in}^2) \quad \text{US (2.8)}$$

where the volumetric flow rate equals Q, and the internal pipe diameter equals D. This one-dimensional approximation for the conservation of mass assumes that the density is constant along streamlines in a pipe and that the calculation error due to compressibility of the fluid is negligible. For most cases, compressibility effects have little effect on calculations for flow problems of liquids and also contribute to minor errors for calculations concerning gases at low velocities below 3% to 10% of the sonic velocity for the gas of concern (John [24]).

2.1.2 Bernoulli's Equation

The cornerstone of fluid calculations in pipe systems is referred to as the extended Bernoulli's equation. A brief mention of its derivation from the equation of motion seems warranted, even though the complexities of the differential equation derivations are outside the scope of this text.

Bird described the equation of motion such that "the accumulation of the rate of momentum in a system equals the rate of momentum in, minus the rate of momentum out, plus the sum of the forces acting on the system . . . where the momentum fluxes equal the stresses on an elemental volume." This statement is based on the change in momentum for the volume element shown in Fig. 2.1, where the momentum equals the unit mass, or density, ρ, times the velocity, V. Differentiating the momentum with respect to time, in the axial, z direction of a pipe, yields

$$\frac{\partial(\rho \cdot V_z)}{\partial t} = -\rho \cdot \left(V_r \cdot \frac{\partial}{\partial r} V_z + \frac{V_\theta}{r} \cdot \frac{\partial}{\partial \theta} V_z + V_z \cdot \frac{\partial}{\partial z} V_z \right) - \left(\frac{1}{r} \cdot \frac{\partial(r \cdot \tau_{rz})}{\partial r} + \frac{1}{r} \cdot \frac{\partial}{\partial \theta} \tau_{\theta z} + \frac{\partial}{\partial_z} \sigma_z \right) - \frac{\partial P_{abs}}{\partial z} + \rho \cdot g \quad \text{SI (2.9)}$$

where P_{abs} is the absolute pressure; V_r, V_θ, and V_z are the velocities in cylindrical coordinates (r, θ, and z); and stresses are shown on three surfaces of the volume element in Fig. 2.1, where the normal stresses (σ_r, σ_θ, σ_z) are perpendicular to the element faces, and the shear stresses ($\tau_{r\theta}$, τ_{rz}, τ_{zr}, $\tau_{z\theta}$, $\tau_{\theta z}$, $\tau_{\theta r}$) are parallel to the element faces. For constant density, one-dimensional flow, most of the terms go to zero, and Eq. (2.9) reduces to

$$0 = \frac{\partial(\rho \cdot V_z)}{\partial t} = -\rho \cdot V_z \cdot \frac{\partial}{\partial z} V_z - \frac{\partial P_{abs}}{\partial z} + \rho \cdot g \quad \text{EE, SI (2.10)}$$

Integrating this expression, Bernoulli's equation is derived for steady-state, isothermal, reversible, irrotational, incompressible, single-phase, one-dimensional fluid flow. In terms of conservation of energy, the total specific energy equals

$$E'_T = E'_p + E'_k + E'_z \quad \text{US, EE, SI (2.11)}$$

where E_p', E_k', and E_z', E_T' are, respectively, the pressure, kinetic, potential, and total specific energies. The total specific energy may then be expressed as

$$E'_T = \frac{P_1}{\rho} + \frac{(V_1)^2}{2} + Z'_1 \cdot g = \frac{P_2}{\rho} + \frac{(V_2)^2}{2} + Z'_2 \cdot g \quad \text{SI (2.12)}$$

$$E'_T = \frac{P_1}{\rho} + \frac{(V_1)^2}{2 \cdot g_c} + Z'_1 \cdot \frac{g}{g_c} = \frac{P_2}{\rho} + \frac{(V_2)^2}{2 \cdot g_c} + Z'_2 \cdot \frac{g}{g_c} \quad \text{EE(2.13)}$$

where Z'_1, Z'_2 = elevation heads, and $Z'_1 - Z'_2$ = change in elevation between the upstream point 1 and the downstream point 2; V_1, V_2 = velocities; P_1, P_2 = absolute pressures; and K = resistance coefficient for head losses due to friction.

Used in this text, the extended Bernoulli's equation is expressed in terms of total feet of head, h_T, where

$$h_T = \frac{P_1}{\gamma} + \frac{(V_1)^2}{2 \cdot g} + Z'_1 + h_{pump} = \frac{P_2}{\gamma} + \frac{(V_2)^2}{2 \cdot g} + Z'_2 + h_L + h_{turbine} \quad \text{EE (2.14)}$$

$$h_T = \frac{144(\text{in}^2/\text{ft}^2) \cdot P_1(\text{psi})}{\gamma(\text{lbf}/\text{ft}^3)} + \frac{(V_1(\text{ft}/\text{second}))^2}{2 \cdot g(\text{ft}/\text{second}^2)} + Z'_1\ (\text{ft}) + h_{pump}(\text{ft}) = \frac{144(\text{in}^2/\text{ft}^2) \cdot P_2}{\gamma(\text{lbf}/\text{ft}^3)} + \frac{(V_2(\text{ft}/\text{second}))^2}{2 \cdot g(\text{ft}/\text{second}^2)} + Z'_2\ (\text{ft}) + h_L\,(\text{ft}) + h_{turbine}\,(\text{ft}) \quad \text{US (2.15)}$$

where h_{pump} = head supplied by a pump, $h_{turbine}$ = head extracted by a turbine, and the head loss, h_L is defined as

$$h_L = K \cdot \frac{(V_2(\text{ft}/\text{second}))^2}{2 \cdot g(\text{ft}/\text{second}^2)} \quad \text{US, EE, SI (2.16)}$$

Similarly, expressing the head in meters

$$h_T = \frac{P_1}{\rho \cdot g} + \frac{(V_1)^2}{2 \cdot g} + Z'_1 + h_{pump} = \frac{P_2}{\rho \cdot g} + \frac{(V_2)^2}{2 \cdot g} + Z'_2 + h_L + h_{turbine} \quad \text{SI (2.17)}$$

Fluid flow equations may be solved in terms of either energy or head, depending on user preference. Head was selected here to be consistent with pump curves supplied by manufacturers, which are typically provided in terms of head in units of feet or meters.

Note that the shear stresses in Eq. (2.9) were replaced by a constant resistance coefficient, K, in the extended Bernoulli's equation, Eq. (2.15), referred to loosely as Bernoulli's equation herein. Although the effects of shear stresses may be calculated for some simple cases, the technique of applying empirical data to determine K is common for both laminar and turbulent pipe system flows. In fact, the determination of K values provides the basis for a description of fluid systems through the use of energy grade lines. Before considering grade lines, additional theoretical limitations on Bernoulli's equation are first considered.

2.1.3 Limitations of Bernoulli's Equation Due to Localized Flow Characteristics

Bernoulli's equation is widely used in design, but the equation is limited to descriptions of the bulk flows of fluids in systems, and calculated flows are frequently 15% to 20%, or more, in error due to fouling of pipes, minor irreversibilities such as heat losses, and the uncertainties in calculated friction coefficients, K. Several examples are used to clarify some additional limitations of Bernoulli's equation.

In one example, velocities through a pipe cross section are shown. In a second example, pressure measurements in an elbow are presented. In a third example, the complexities of flow through a valve are shown. Bernoulli's equation is inadequate to explain the details for any of these examples due to the many simplifying assumptions inherent in the equation.

Example 2.1 Consider the velocity profile in a pipe

The velocity profile through a pipe cross section develops to a nearly constant velocity profile after flow enters

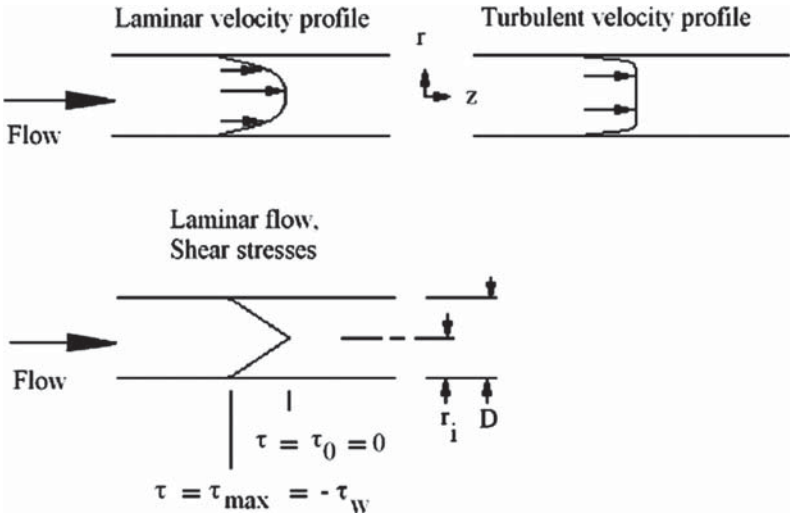


FIG. 2.2 COMPARISON OF LAMINAR AND TURBULENT FLOWS FOR NEWTONIAN FLUIDS

a pipe, and the velocity profile becomes fully developed. Flow regimes are typically classified as laminar, critical, transitional, and turbulent. A simplified comparison between laminar and turbulent flow is shown in Fig. 2.2. For fully developed laminar flow, the profile is parabolic, the velocity varies from zero at the wall to a maximum at the pipe center line, the streamlines in the flow are parallel, and the shear stresses, τ, decrease from $\tau_0 = 0$ at the center line to a maximum negative value of τ_w at the wall, where the shear stress at the wall is defined as the axial force exerted by the fluid along the pipe wall per unit area of pipe surface. For both laminar and turbulent flow, a hydrodynamic entrance length describes the length of pipe required for a boundary layer to develop along the pipe wall. Within this boundary layer, the velocity profile develops until the profile is fully developed as the boundary layers from opposing surfaces converge at the pipe center line. Development of a laminar velocity profile is shown in Figs. 2.3 and 2.4, and turbulent flow is similar except that the formation of a thin laminar boundary layer is formed close to the pipe wall, and a turbulent boundary layer then forms to the pipe center line. For turbulent flow, the turbulent boundary layer is very complex, and research continues in this area. The complexity of turbulent flow is highlighted using an open channel flow, which is shown in Fig. 2.5, which uses flow visualization techniques described in detail by Merzkirch [25]. An additional complexity of turbulent flow is that at any point in the flow, the velocity continuously fluctuates. Velocity measurements at specific points in turbulent flow typically vary by ±30%, or more.

Bernoulli's one-dimensional assumption considers the flow profile to be planar and perpendicular to the pipe wall through any arbitrary pipe cross section, and neglects the complexities of hydrodynamic entrance lengths, streamlines, boundary layers, and velocity profiles. Consequently, techniques used in this text to find pressure losses in pipes are inapplicable to short pipes.

Example 2.2 Consider the measured pressures in an elbow

For this example, pressure measurements were taken at three locations on an 8-in. NPS elbow with an 8-in.

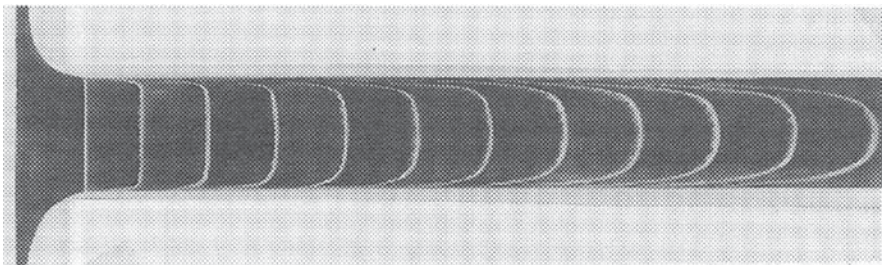


FIG. 2.3 LAMINAR FLOW DEVELOPMENT IN A PIPE, VISUALIZED USING A HYDROGEN BUBBLE METHOD
(Reprinted from "Introduction to Fluid Mechanics", Nakayama and Boucher, Copyright 1999, with permission from Elsevier [26])

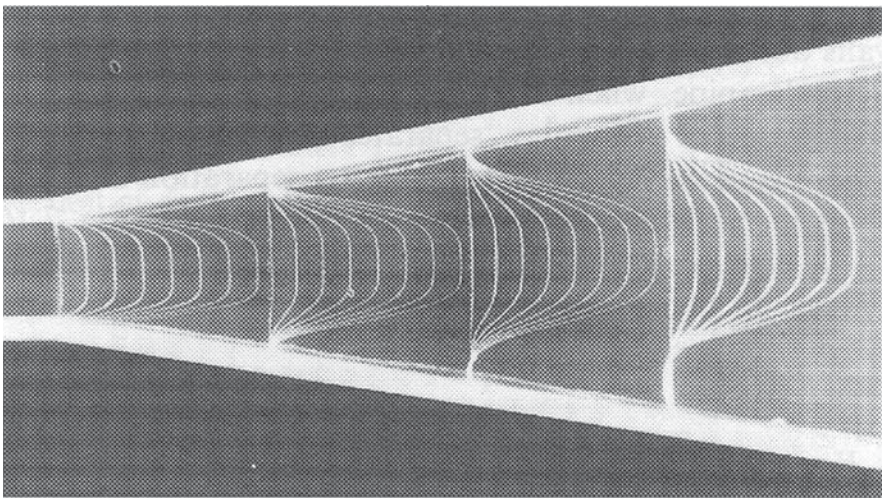


FIG. 2.4 LAMINAR FLOW DEVELOPMENT IN A PIPE EXPANSION (Reprinted from "Introduction to Fluid Mechanics", Nakayama and Boucher, Copyright 1999, with permission from Elsevier [26])

throat radius at a flow rate of approximately 1000 gpm. One might assume that streamlines are parallel to the wall of the elbow, and applying Bernoulli's equation, the velocity would be expected to increase as the elbow radius increases, and the pressure would be expected to decrease from gauge P1 to gauge P2, which is consistent with Fig. 2.6. However, vorticity affects pressure along the inside of the elbow as discussed by Idelchik [28], who also documents flow pattern characteristics for numerous fittings. Eddy currents, helical swirling vortex flows, and vortices all affect the flow patterns within the elbow in question. Fig. 2.6 also shows cross-sectional secondary flow patterns within elbows at different Reynold's numbers. Typically, flow and pressure instruments are placed at least ten, but sometimes as few as two, pipe diameters away from fittings to ensure that the instruments provide accurate readings by preventing measurement inaccuracies due to eddy currents and vortices.

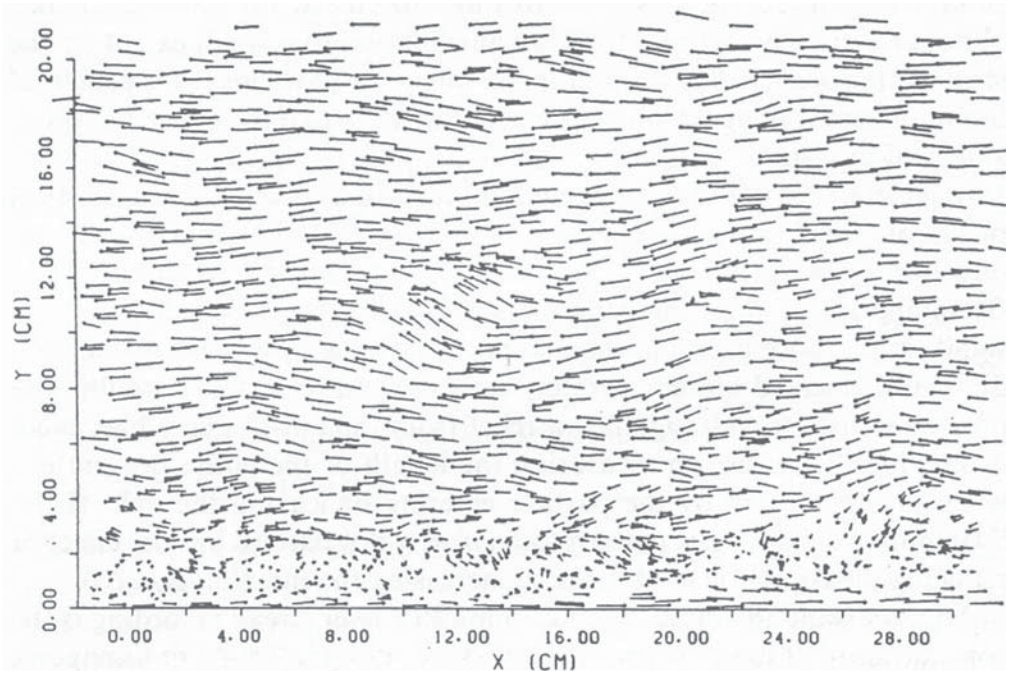


FIG. 2.5 TURBULENT FLOW FIELD IN AN OPEN CHANNEL, VISUALIZED USING PULSED LIGHT IMAGING VELOCIMETRY (PIV) (Adrian [27], Reprinted, with permission, from the Annual Review of Fluid Mechanics, Volume 23, copyright 1987, by Annual Reviews, www.annualreviews.org)

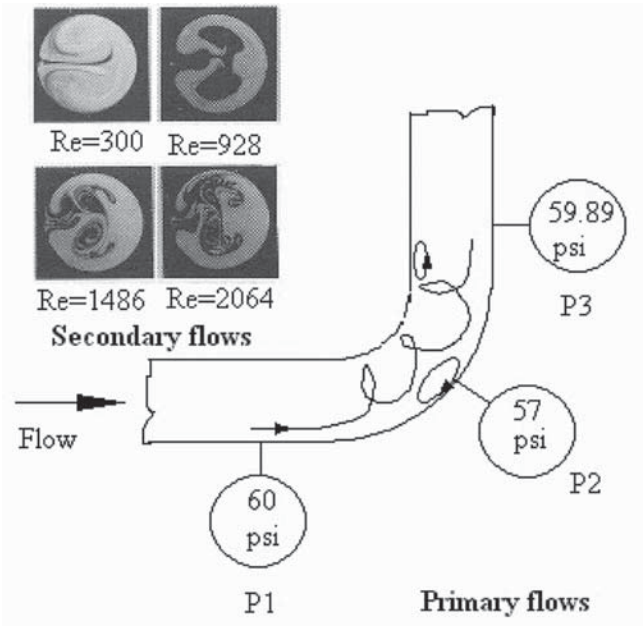


FIG. 2.6 FLOW IN AN ELBOW (Tanida and Miyashiro [29], adapted by permission of Springer-Verlag)

Example 2.3 Consider the flow patterns in a valve

Irregular flow patterns occur in various fittings and valves, and the flow complexity is highlighted by the valve model shown in Figs. 2.7 and 2.8. The model shows the flow streamlines in a 4-in. plug valve. Again, Bernoulli's equation is inadequate to describe detailed fluid mechanics. In short, the use of the extended Bernoulli's equation with resistance coefficients, K, greatly simplifies bulk fluid transport system designs, but flow details must be analyzed using other techniques.

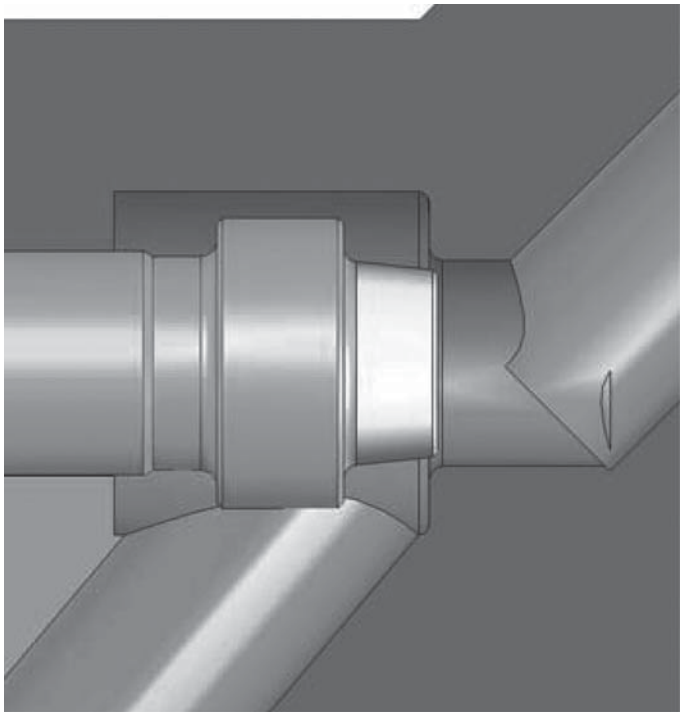


FIG. 2.7 MODEL OF A 4-IN. PLUG VALVE PARTIALLY OPEN (Ahuja et al. [30])

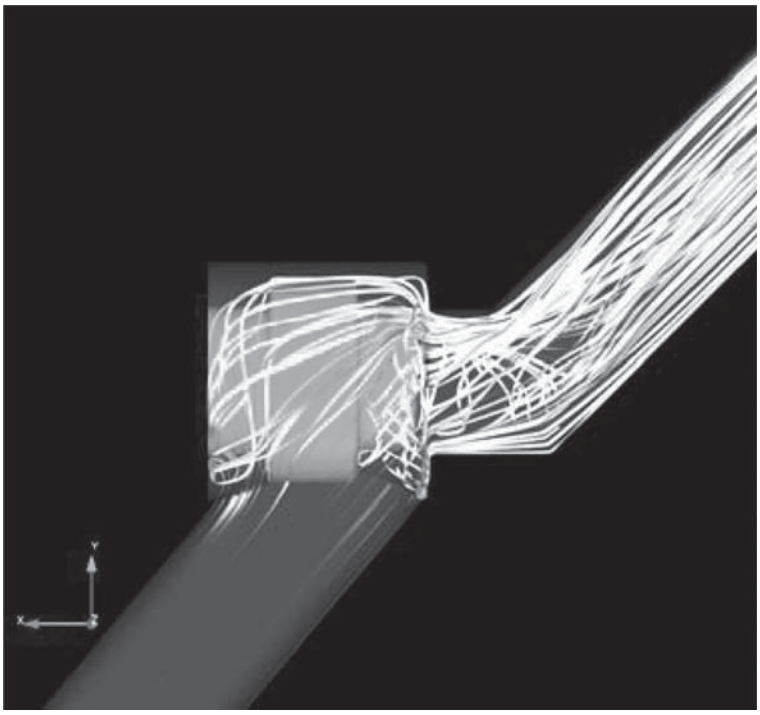


FIG. 2.8 FEA FLOW PATTERNS FOR A 4-IN. PLUG VALVE (Ahuja et al. [30])

2.2 HYDRAULIC AND ENERGY GRADE LINES

To consider hydraulic and energy grade lines, a simplified system is shown in Fig. 2.9. The hydraulic grade line depicts the piezometric head, which is proportional to the pressure in the pipe. That is, any point on the hydraulic grade line equals the height of fluid in a static piezometer tube located at that point (Fig. 2.10), when compensated for density and instrumentation capillarity effects (Liptak and Wenczel [31]). The energy grade line differs from the hydraulic grade line by the velocity head, $V^2/(2 \cdot g)$, and any point on the energy grade line equals the stagnation head, or total head, as measured by a pitot tube, in turbulent flow. To calculate the flow rate in a tube from the velocity head, the velocity head may be measured by subtracting measured piezometric head from the total head measured by a pitot tube. A pitot tube may provide erroneous results in laminar flow, since the velocity distribution varies significantly through the pipe cross section. Together, these grade lines describe the pressure, or head, drops during pipe flow, and each section of the grade lines requires consideration to describe the system.

Starting at the left side of the figure, the tank level may be above the pipe inlet (point 1) for a positive suction head, or the level may be below the pipe inlet when the pump supplies a suction lift, or negative head. Once the flow enters the pipe, there is a minor friction loss due to the entrance, and a more significant change in energy as static head converts to velocity head, which accounts for the magnitude difference between the two grade lines. Past the pipe entrance, the head in the pump suction piping decreases due to pipe friction. The energy then sharply increases at the pump and again linearly decreases due to pipe friction downstream in the pump discharge piping. As the flow passes through fittings and valves, discrete friction losses occur, which are referred to as minor losses. At the end of the pipe (point 2), a minor friction loss occurs due to the pipe exit into the tank, and the hydraulic head is then positive or zero, depending on the level of submergence of the pipe exit. The factors affecting the grade lines, such as friction factors, fluids, pumps, and components, need further consideration.

2.3 FRICTION LOSSES FOR PIPES

The flow for different types of fluids may be characterized by Bernoulli's equation, through the use of friction factors to describe friction losses in pipes. For example, the Moody diagram is an accepted, empirical reference for finding friction losses in pipe systems for Newtonian

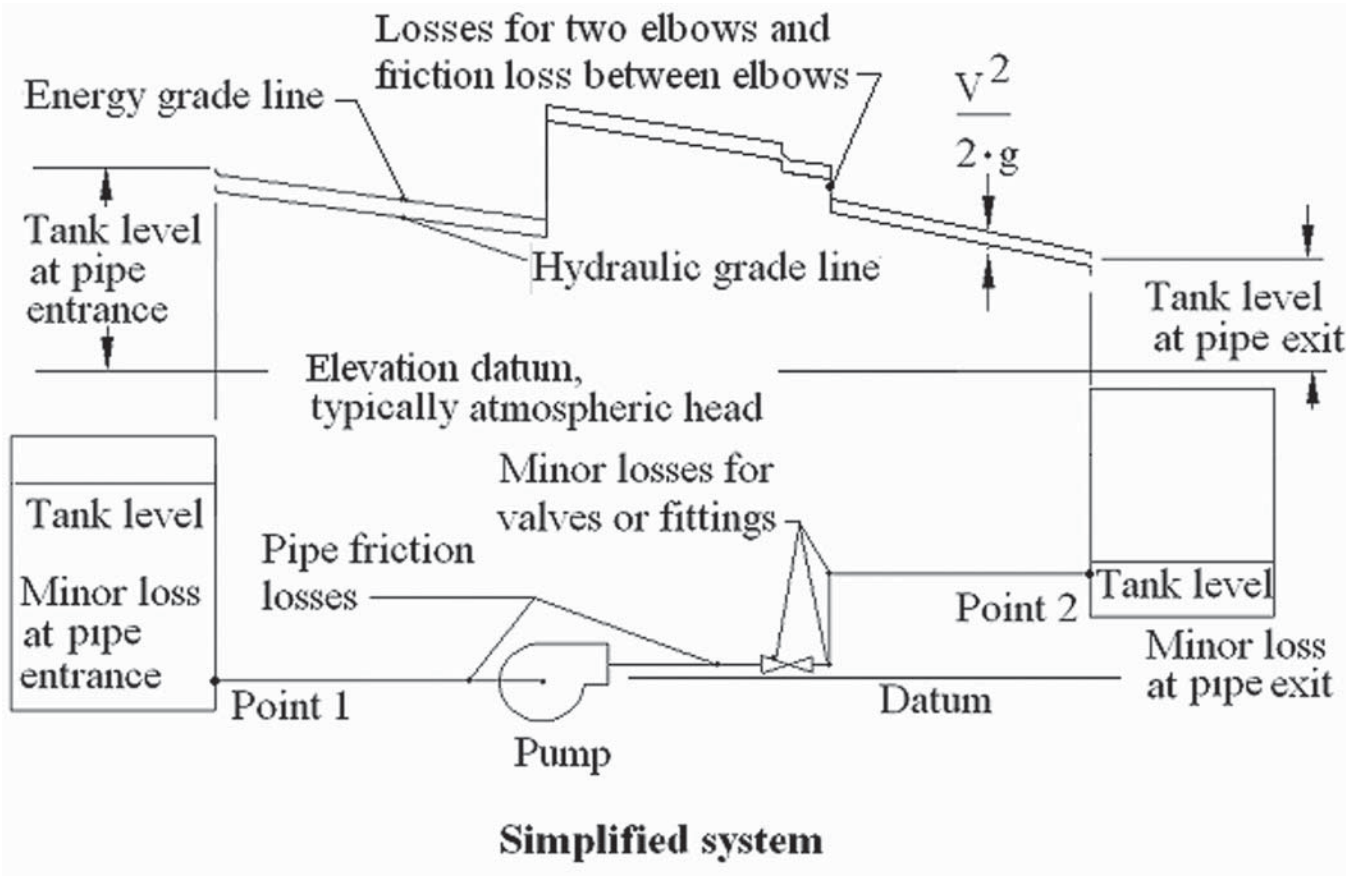


FIG. 2.9 HYDRAULIC AND ENERGY GRADE LINES

fluids. Once the friction factor, f, is determined, it may be substituted into an equation for the resistance coefficient, K, which is then substituted into the head loss term, h_L, in Bernoulli's equation. To find friction factors, the Moody diagram has been reduced to a single equation, which is referred to as Churchill's equation, and equations are available for other types of fluids to estimate friction factors also for use in Bernoulli's equation. Brief descriptions of different fluid types follow, along with the determination of some friction factors and resistance coefficients, required for Bernoulli's equation.

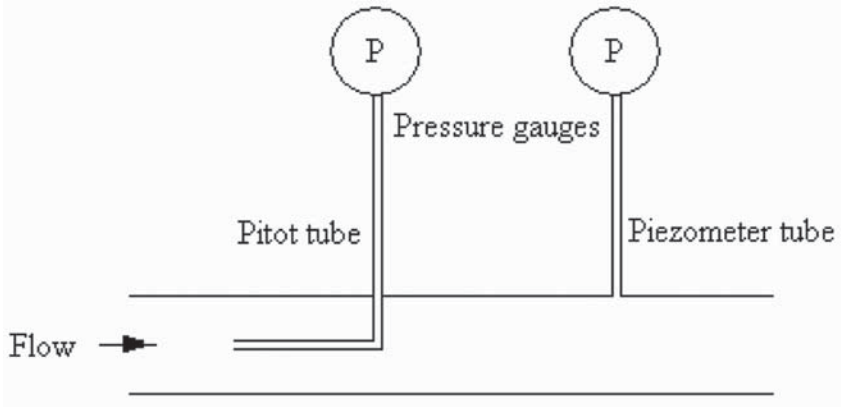


FIG. 2.10 PRESSURE, OR HEAD, MEASUREMENTS IN A PIPE

2.3.1 Types of Fluids

The primary types of Newtonian and non-Newtonian fluids are summarized in Fig. 2.11 (Harnby et al., [32]), where shear stress, viscosity, and strain rate are related. Considering these fluid properties, a description of the experimental techniques used to find viscosity provides a basis for the definition of the different fluid types shown in the figure.

2.3.1.1 Viscosity Definition Absolute dynamic viscosity, μ, is defined using a flat plate viscometer as shown in Fig. 2.12, although numerous viscometers are available for different fluids, as discussed in detail by Liptak and Venczel [31]. A flat plate viscometer is constructed of two parallel plates of surface area, A, with a thin film of fluid between them of film thickness, $\bar{T}$. A constant force, F, is applied to move one of the plates at a constant velocity, V, where the velocity profile between the two plates is experimentally known to be linear.

The experimental shear stress, τ, is related to the absolute dynamic viscosity, μ, by the equation

$$\tau = \frac{F}{A} = \frac{\mu \cdot V}{\bar{T}} \qquad \text{EE, SI (2.18)}$$

$$\tau = \frac{F}{A} = \frac{\mu \cdot V}{\bar{T}} \Rightarrow \tau(\text{lbf/in}^2) = \frac{F(\text{lbf})}{A(\text{in}^2)} = \frac{\mu(\text{lbf} - \text{second/ft}^2) \cdot V(\text{ft/second})}{\bar{T}(\text{in}) \cdot (12 \cdot \text{in/ft})} \qquad \text{US (2.19)}$$

The kinematic viscosity, ν′, is defined as

$$\nu' = \frac{\mu \cdot g_c}{\rho} \Rightarrow \nu'(\text{ft}^2/\text{second}) = \frac{\mu(\text{lbf} - \text{second/ft}^2) \cdot g_c(\text{lbm} \cdot \text{ft/lbf} \cdot \text{second}^2)}{\rho(\text{lbm/ft}^3)} \qquad \text{US, EE (2.20)}$$

$$\nu' = \frac{\mu}{\rho} \qquad \text{SI (2.21)}$$

When the dynamic viscosity, μ, is expressed in metric units of centipoises, cP; the kinematic viscosity, ν, is expressed in metric units of centistokes; and the weight density is defined as ρ = 62.24 lbm at 39.2ºF; the viscosities are related by

$$\nu'\left(\frac{10^{-6}\text{m}^2}{\text{second}}\right) = \frac{\mu\left(10^{-3}\text{kg}/(\text{m} \cdot \text{second})\right)}{\rho(10^3\text{kg/m}^3)} \Rightarrow \upsilon(\text{centistokes}) = \frac{\mu(\text{centipoise})}{\text{Sp}G} \qquad \text{metric (2.22)}$$

A common instrument used to measure viscosity in the US is the Saybolt universal viscometer, which is essentially a calibrated orifice and tube. The time required for a gravity flow of 60 cc through the orifice is measured in Saybolt

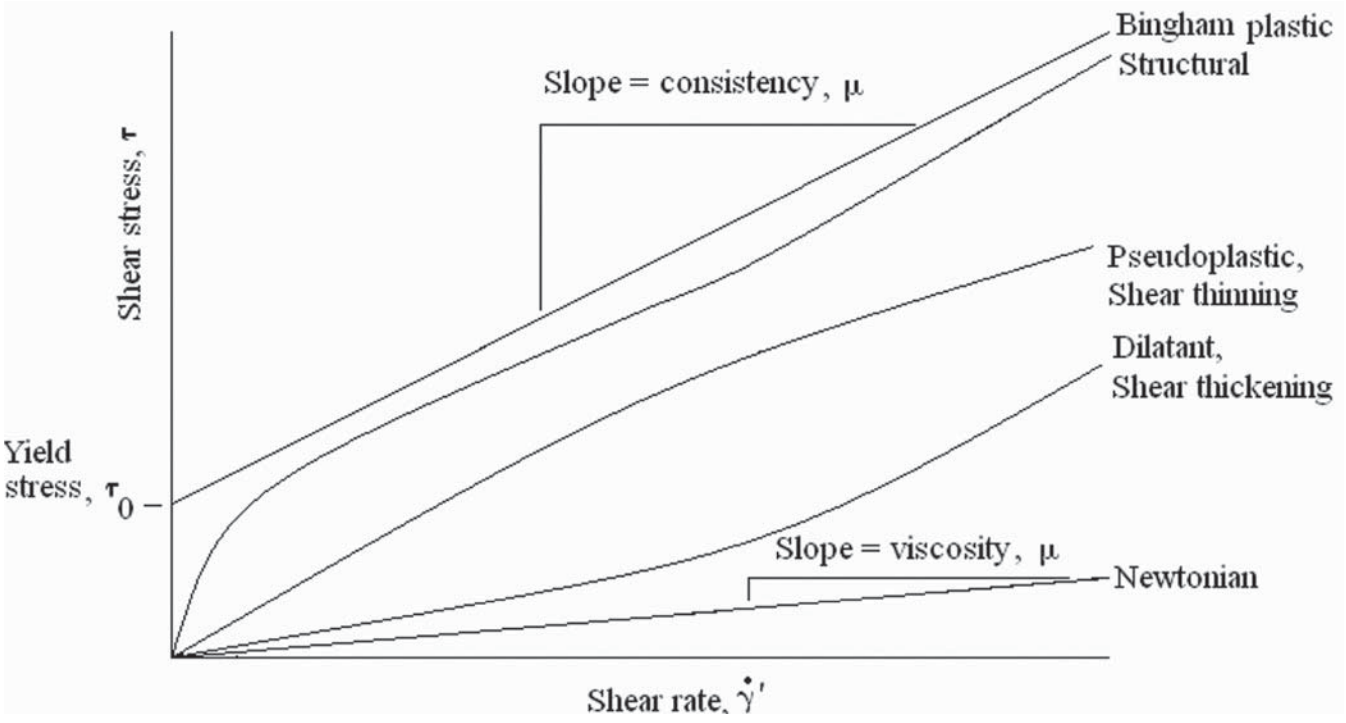


FIG. 2.11 TYPES OF FLUIDS

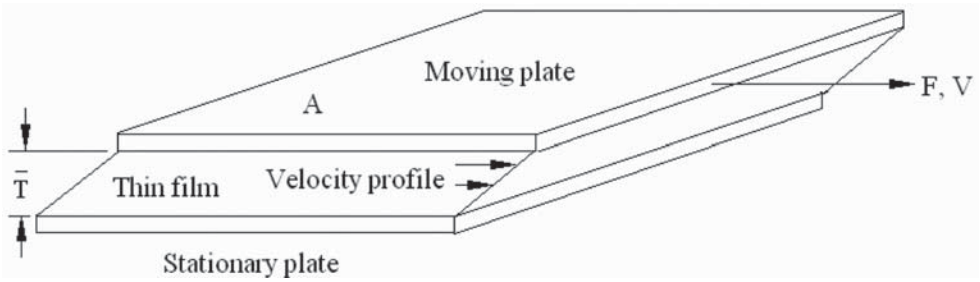


FIG. 2.12 SCHEMATIC OF A FLAT PLATE VISCOMETER

universal seconds, SSU. An approximate conversion for SSU to Stokes (Avallone and Baumeister [33]), is

For $32 < SSU < 100$ seconds,

$$\text{Stokes} = 0.00226 \cdot \text{SSU} - 1.95/\text{SSU} \qquad (2.23)$$

For $SSU > 100$ seconds

$$\text{Stokes} = 0.00220 \cdot \text{SSU} - 1.35/\text{SSU} \qquad (2.24)$$

Having defined viscosity, different types of fluids may be considered.

2.3.1.2 Properties of Newtonian and Non-Newtonian Fluids Fluid properties for the various fluids shown in Fig. 2.11 define the fluid type and are determined using a viscometer. Newtonian fluids are characterized by a constant viscosity with respect to shear rate, and a zero shear stress. Shown in Fig. 2.13, a common type of viscometer, or rheometer, used for highly viscous fluids applies known torques to a vaned impeller, which is submerged in the fluid and rotated, and shear rate versus shear stress is plotted from the measured data to obtain a description of the fluid in question.

There are several types of non-Newtonian fluids. Pseudoplastic, shear thinning fluids, like tooth pastes and extruded plastics, flow easier as the shear rate increases. Examples of dilatant, shear thickening, fluids are china clay and slurry mixtures from mining operations. Fluids that require a defined yield stress before initiating flow are referred to as Bingham fluids, like catsup, sewage, or asphalt. An initial force is required to overcome the yield stress in catsup, but once the yield stress is exceeded, the catsup flows freely.

There are other types of fluids that are not considered here, including thixotropic fluids (Govier and Aziz [34]), which have time-dependent material properties and structural fluids, such as polymeric fluids, flocculated suspensions, colloids, foams, and gels (Darby [35]). Structural fluids have combinations of Newtonian and non-Newtonian properties, but are sometimes approximated as power law or Bingham plastic fluids.

Example 2.4 Approximation of a structural fluid as a Bingham plastic fluid

For example, nuclear waste is considered to have properties similar to a Bingham plastic fluid. Using a rotating rheometer, the material properties shown in Fig. 2.14 were obtained. One set of data was obtained as the strain rate, $\ddot{\gamma}'$, was increased, the other set of data was obtained while the strain rate was decreased. Several data sets were averaged, some of the initial data points were neglected, and a Bingham plastic was modeled (Leishear et al [36]). In other words, once the fluid properties are determined, the appropriate pipe flow model may be selected.

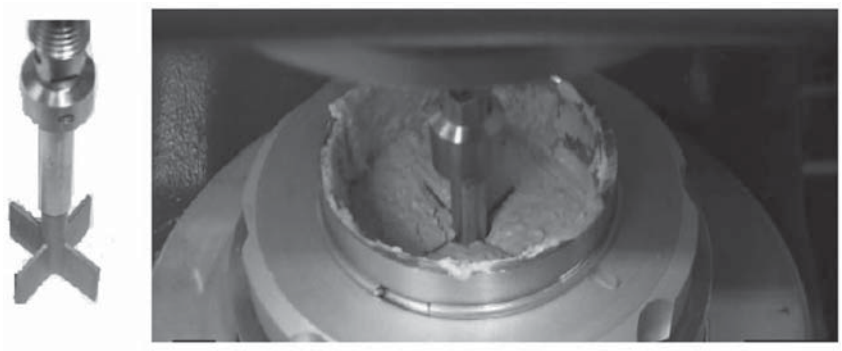


FIG. 2.13 ROTATING VISCOMETER (Rheometer, E. Hansen, SRNL)

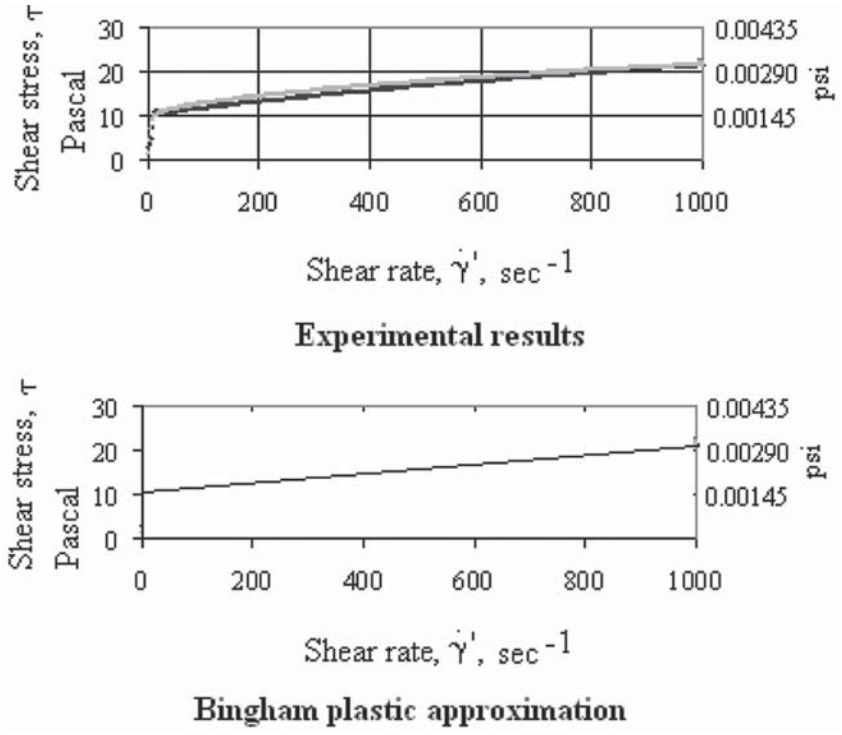


FIG. 2.14 BINGHAM FLUID MODEL APPROXIMATION

2.3.1.3 Laminar Flow in Newtonian and Non-Newtonian Fluids Darby [35] provides derivations for numerous closed form laminar and turbulent flow equations for different fluids with detailed examples. Of these fluids, Newtonian fluids are the most common and will be the focus of most of this text, but water hammer equations are just as valid for these other fluids, and non-Newtonian fluids are also briefly considered in this text.

For various fluids in laminar flow, flow rates are related to shear stresses, τ, and strain rates, $\dot{\gamma}'$, which are described using Figs. 2.2 and 2.11.

For Newtonian fluids,

$$\tau = \mu \cdot \frac{dV_z}{dr} = \mu \cdot \dot{\gamma}' \qquad \text{EE, SI (2.25)}$$

$$Q = \frac{\tau_w \cdot (r_i)^3}{4 \cdot \mu} \qquad \text{EE, SI (2.26)}$$

$$Q(\text{gpm}) = \frac{9.351 \cdot \tau_w(\text{psi}) \cdot (r_i(\text{in}))^3}{\mu(\text{lbf} \cdot \text{second}/\text{ft}^2)} \qquad \text{US (2.27)}$$

For pseudoplastic or dilatant fluids, the shear stresses and shear rates are negative, where

$$\tau = -m' \cdot \left(-\frac{dV_z}{dr}\right)^n = -m' \cdot (-\dot{\gamma}')^n \qquad \text{EE, SI (2.28)}$$

$$Q = \pi \cdot \left(\frac{\tau_w}{m'}\right)^{1/n} \cdot \left(\frac{n}{3 \cdot n + 1}\right) \cdot r_i^3 = \pi \cdot \left(\frac{\tau_w(\text{Pascal})}{m'(\text{Pascal} \cdot \text{second}^n)}\right)^{1/n} \cdot \left(\frac{n}{3 \cdot n + 1}\right) \cdot r_i^3 (m'^3) \qquad \text{EE, SI (2.29)}$$

where the fluid is assumed to act in accordance with a power law. In this case, m' and n are experimentally determined constants for a particular fluid model, where m' is the viscosity at a shear rate of 1/second, and n is nondimensional. In consistent SI units (force · time^n/length^2), the units of m' are Pascal · second^n. When $n = 1$, Eqs. (2.29) and (2.30) describe a Newtonian fluid. In US units,

$$Q(\text{gpm}) = 0.2598 \cdot \pi \cdot \left(\frac{\tau_w(\text{psi})}{m'(\text{psi} \cdot \text{second}^n)}\right)^{1/n} \cdot \left(\frac{n}{3 \cdot n + 1}\right) \cdot r_i^3(\text{in}^3) \qquad \text{US (2.30)}$$

For Bingham plastic fluids where $\tau > \tau_0$,

$$\tau = \tau_0 + \mu \cdot \frac{dV_z}{dr} = \tau_0 + \mu \cdot \dot{\gamma}' \qquad \text{EE, SI (2.31)}$$

$$Q = \frac{\pi \cdot r_i^3 \cdot \tau_w}{4 \cdot \mu} \cdot \left(1 - \frac{4 \cdot \tau_0}{3 \cdot \tau_w} + \frac{\tau_0}{3 \cdot \tau_w}\right) \quad \text{EE, SI (2.32)}$$

$$Q(\text{gpm}) = \frac{9.351 \cdot \pi \cdot r_i^3(\text{in}^3) \cdot \tau_w(\text{psi})}{\mu(\text{lbf} - \text{second}/\text{ft}^2)} \cdot \left(1 - \frac{4 \cdot \tau_0(\text{psi})}{3 \cdot \tau_w(\text{psi})} + \frac{\tau_0(\text{psi})}{3 \cdot \tau_w(\text{psi})}\right) \quad \text{US (2.33)}$$

These laminar flow equations for Newtonian and non-Newtonian fluids highlight basic differences between these types of fluids, and these differences are graphically displayed by the laminar velocity profiles for different types of fluids shown in Fig. 2.15.

Having considered laminar flow for different fluids, Newtonian fluids can be used to begin a discussion of the relationship between laminar and turbulent flow at different velocities with respect to friction losses in pipes, even though non-Newtonian fluid behaviors differ. Moody's diagram provides this relationship.

2.3.2 Pipe Friction Losses for Newtonian Fluids

As mentioned, the Moody diagram is commonly used to describe Newtonian fluid flows, and versions of the diagram are shown in Figs. 2.16 and 2.17. These diagrams provide considerable insight into the effects of flow rates on friction losses. The flow rate is described in terms of the Reynold's number, *Re*, and friction losses are described in terms of the Darcy friction factor, *f*. At low velocities below $Re \approx 2100$, the flow is laminar, and friction factors vary linearly with respect to flow rate in the laminar zone of the diagram. As the flow rate increases for a given pipe size and fluid, the critical zone is entered ($Re \approx 2100$ to 4000) where fluid flow is unstable, and experimental results are therefore inconsistent. At still higher velocities ($Re > 4000$), the flow is turbulent and enters the transition and fully turbulent zones. In the transition zone, flow is still unstable, and the friction factors decrease nonlinearly to nearly constant friction factors. When the friction factors approach almost constant values for a given diameter, fully developed, well-mixed, turbulent flow is established.

2.3.3 Friction Factors From the Moody Diagram

The use of friction factors may be introduced through laminar flow equations. Equation 2.34 is derived to apply friction factors to laminar flow using conservation of mass and momentum equations. Referring to Fig. 2.2, the velocity profile as a function of radial position equals

$$V_z(r) = \frac{\tau_w \cdot r_i}{2 \cdot \mu} \cdot \left(1 - \frac{r^2}{(r_i)^2}\right) \quad \text{EE, SI (2.34)}$$

$$\tau_w = \frac{f \cdot \rho \cdot V^2}{8 \cdot g_c} \quad \text{EE, SI (2.35)}$$

$$\tau_w = \frac{1.5 \cdot f \cdot \rho(\text{psi}) \cdot V^2 \left(\text{ft}^2/\text{second}^2\right)}{g_c \left(\text{ft}/\text{second}^2\right)} \quad \text{US (2.36)}$$

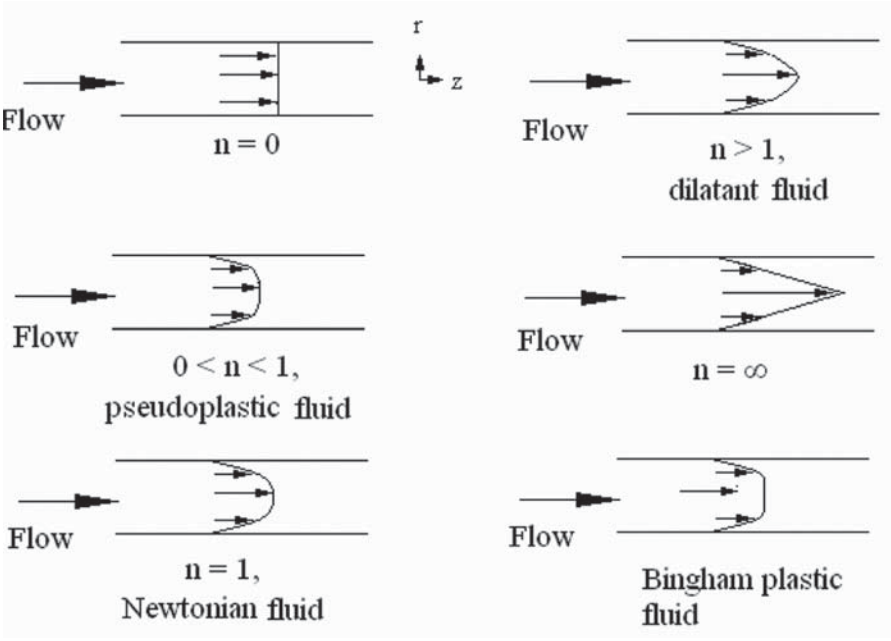


FIG. 2.15 LAMINAR VELOCITY PROFILES FOR DIFFERENT TYPES OF FLUIDS

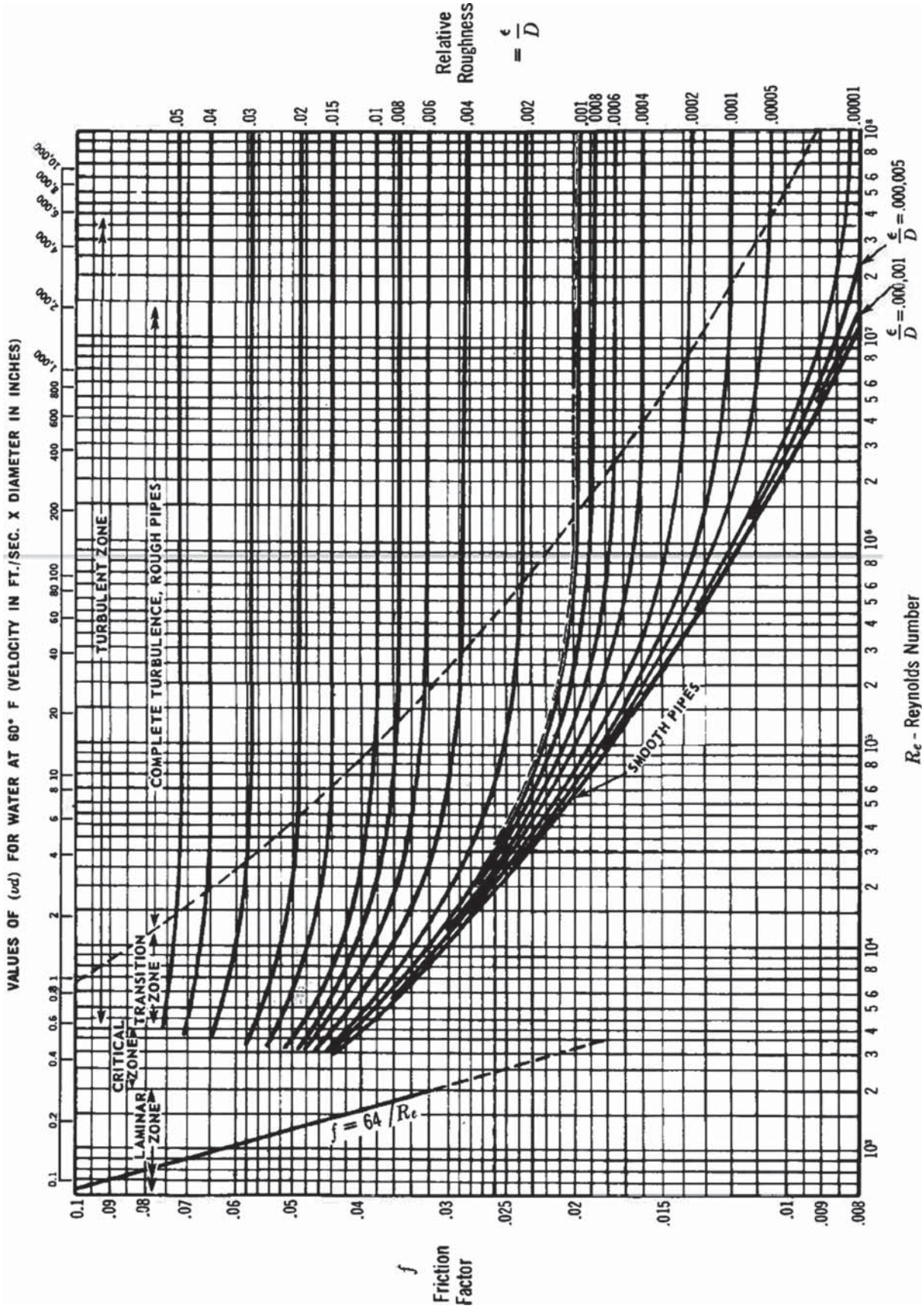


FIG. 2.16 FRICTION FACTORS FOR DIFFERENT FLUIDS AND PIPE MATERIALS (Moody [37])

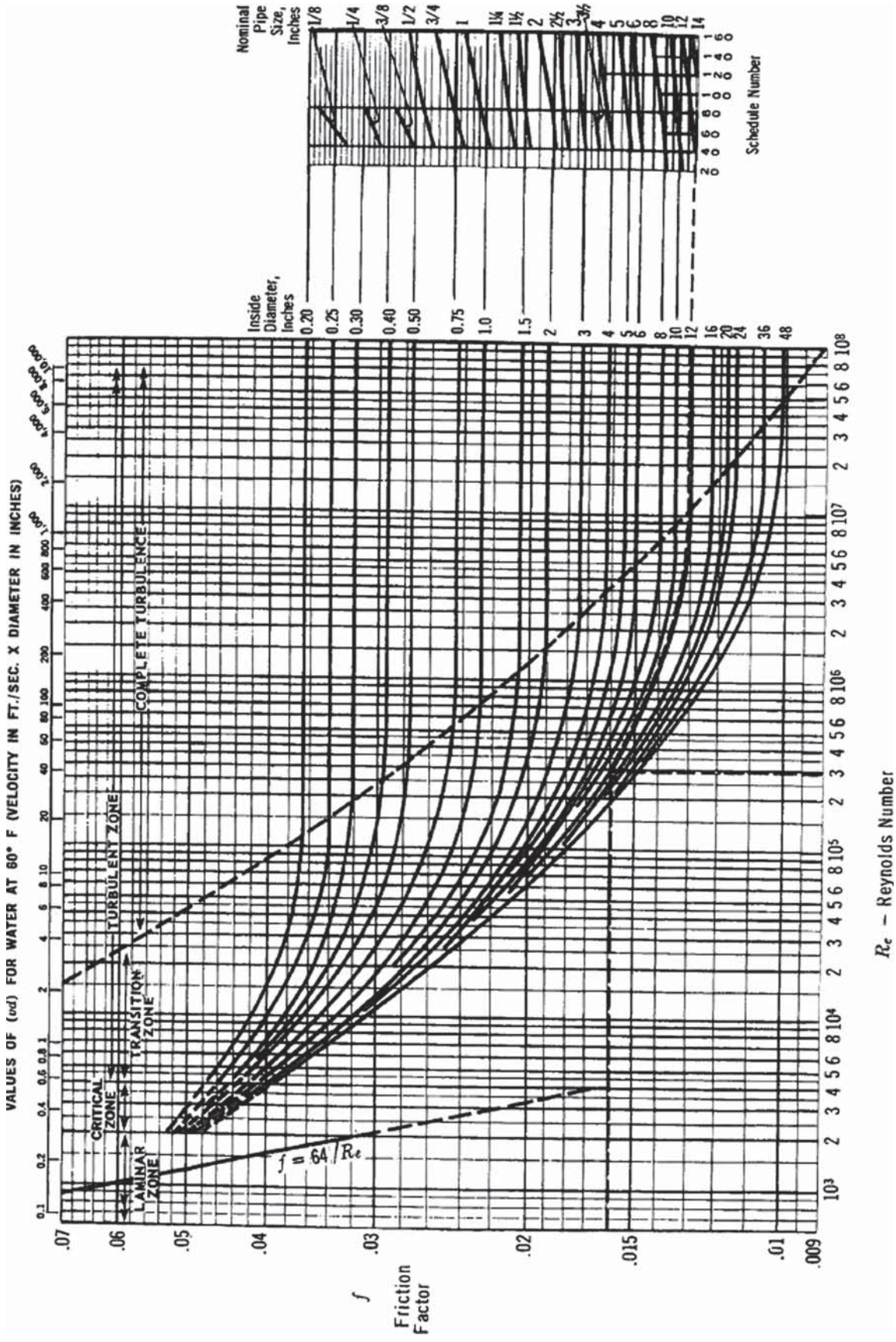


FIG. 2.17 FRICTION FACTORS FOR STEEL PIPE AND WATER (Moody [37])

TABLE 2.1 ROUGHNESS FOR VARIOUS MATERIALS
(Reprinted by permission from Crane, Inc.)

Material	Surface roughness for pipes, ε, in., Moody [37], Crane [21]	Equivalent roughness for fittings, ε_f, in., recommended value in bold, Darby [35]
Steel, stainless steel pipe	0.00015	0.0008–0.0018–0.004 rusted, 0.006–0.1
Wrought iron pipe	---	**0.002**
Cast iron pipe	0.00085	0.01–**0.025**–0.04
Cast iron pipe, asphalted	0.0004	0.004–**0.006**–0.04
Cast iron pipe, galvanized	0.0005	0.001–**0.006**–0.006
Drawn tubing, plastic, steel, copper, brass, glass	0.000005	0.00006–**0.00008**–0.0004
Concrete	0.001–0.01	0.001–0.03
Rubber, smooth	---	0.00025–**0.0004**–0.003
Rubber, wire reinforced	---	0.01–**0.04**–0.15

These equations define the fully developed, parabolic shape of the velocity profile and were derived from the assumption of a linear shear stress profile for laminar flow, where τ_{max} is the shear stress at the pipe wall and the fluid velocity equals zero, as shown in Fig. 2.2. From these equations, laminar flow is defined on the Moody diagram, where $f = 64/Re$. Note that the Fanning friction factor is used in some references, and the Darcy friction factor is used in others. Consequently, on some versions of the Moody diagram, laminar flow is defined as $f_n = 16/Re$. To be consistent, the Darcy friction factors, f, are used throughout this work, where f_n is the Fanning friction factor, and the Darcy friction factor, f, equals

$$f = 4 \cdot f_n \qquad \text{US, EE, SI (2.37)}$$

Turbulent flow is also considered on the Moody diagram. An assumption was made that one equation could be applied to determine the head loss for any friction factor, regardless of whether the flow was laminar or turbulent. This assumption provides the need for the Moody diagram and that equation is expressed as

$$h_L = 0.00259 \cdot \frac{K \cdot Q^2}{D^4} \qquad \text{US (2.38)}$$

where

$$K = \frac{f \cdot L''}{D} \qquad \text{US, EE, SI (2.39)}$$

The Reynolds number is expressed with appropriate conversions by each of the following terms

$$Re = \frac{D \cdot V \cdot \rho}{\mu} = \frac{Q \cdot \rho}{D \cdot \mu} = \frac{D \cdot V}{\nu'} = \frac{Q}{\nu' \cdot D} \qquad \text{SI (2.40)}$$

$$Re = \frac{D(\text{in}) \cdot V(\text{ft/second}) \cdot \rho(\text{lbm/ft}^3)}{386.1 \cdot \mu(\text{lbf} - \text{second/ft})}$$
$$= \frac{Q(\text{gpm}) \cdot \rho(\text{lbm/ft}^3)}{1203.4 \cdot D(\text{in}) \cdot \mu(\text{lbf} - \text{second/ft})}$$
$$= \frac{D(\text{in.}) \cdot V(\text{ft/second})}{12 \cdot \nu'(\text{ft}^2/\text{second})} = \frac{Q(\text{gpm})}{37.405 \cdot \nu' \cdot D(\text{in.})} \qquad \text{US (2.41)}$$

To solve Bernoulli's equation using the Moody diagram and the Reynold's number, the fluid properties, the relative roughness of the pipe, and the pipe dimensions are also required.

2.3.3.1 Surface Roughness On the Moody diagrams, note that the friction losses increase with relative roughness, ε/D, and pipe diameter, where smooth pipes, of course, have the lowest friction loss. Also note that the friction factor significantly increases as the pipe diameter is reduced, which effectively increases the relative roughness. The surface roughness, ε, for various materials are listed in Table 2.1.

2.3.3.2 Pipe and Tubing Dimensions Pipe and tubing dimensions for several common materials are provided in Tables 2.2 to 2.10. Pipe material properties are discussed in Chapter 3. Most of the standards defining these dimensions also provide SI tables. Crane [21] also provides a list of pipe dimensions, along with moments of inertia and pipe weights.

TABLE 2.2 DIMENSIONS FOR WROUGHT STEEL AND STAINLESS STEEL PIPES (ASME B36.10M [38] and ASME B36.19M [39])

Schedule		5S	10S	10	20	30	Std., 40S[2]	40	60	XS, 80S[2]	80	100	120	140	160	XXS
NPS	OD, in.	Inside diameter, *D*, in.														
1/8	0.405	---	0.307	---	---	---	0.269	0.269	---	0.215	0.215	---	---	---	---	---
1/4	0.540	---	0.410	---	---	---	0.364	0.364	---	0.302	0.302	---	---	---	---	---
3/8	0.675	---	0.545	---	---	---	0.493	0.493	---	0.423	0.423	---	---	---	---	---
1/2	0.840	0.710	0.674	---	---	---	0.622	0.622	---	0.546	0.546	---	---	---	0.466	0.252
3/4	1.050	0.920	0.884	---	---	---	0.824	0.824	---	0.742	0.742	---	---	---	0.612	0.434
1	1.315	1.185	1.097	---	---	---	1.049	1.049	---	0.957	0.957	---	---	---	0.815	0.599
1.25	1.660	1.530	1.442	---	---	---	1.380	1.380	---	1.278	1.278	---	---	---	1.160	0.896
1.5	1.900	1.770	1.682	---	---	---	1.610	1.610	---	1.500	1.500	---	---	---	1.338	1.100
2	2.375	2.245	2.157	---	---	---	2.067	2.067	---	1.939	1.939	---	---	---	1.687	1.503
2.5	2.875	2.709	2.635	---	---	---	2.469	2.469	---	2.323	2.323	---	---	---	2.125	1.771
3	3.500	3.334	3.260	---	---	---	3.068	3.068	---	2.900	2.900	---	---	---	2.624	2.300
3.5	4.000	3.834	3.760	---	---	---	3.548	3.548	---	3.364	3.364	---	---	---		
4	4.500	4.334	4.260	---	---	---	4.026	4.026	---	3.826	3.826	---	3.624	---	3.438	3.152
5	5.563	5.345	5.295	---	---	---	5.047	5.047	---	4.813	4.813	---	4.563	---	4.313	4.063
6	6.625	6.407	6.357	---	---	---	6.065	6.065	---	5.761	5.761	---	5.501	---	5.187	4.897
8	8.625	8.407	8.329	---	8.125	8.071	7.981	7.981	7.813	7.625	7.625	7.437	7.187	7.001	6.875	6.813
10	10.75	10.482	10.420	---	10.250	10.136	10.020	10.020	9.750	9.750	9.562	9.312	9.062	8.750	8.500	8.750
12	12.75	12.438	12.390	---	12.250	12.090	12.00	11.938	11.626	11.750	11.374	11.062	10.750	10.500	10.126	10.750
14	14.00	13.688	13.624	13.500	13.376	13.250	13.250	13.124	12.812	13.00	12.500	12.124	11.812	11.500	11.188	---
16	16.00	15.670	15.624	15.500	15.376	15.250	15.250	15.000	14.688	15.000	14.312	13.938	13.562	13.124	12.812	---
18	18.00	17.670	17.624	17.500	17.376	17.124	17.250	16.876	16.500	17.000	16.124	15.688	15.250	14.876	14.438	---
20	20.00	19.624	19.564	19.500	19.250	19.000	19.250	18.812	18.376	19.000	17.938	17.438	17.000	16.500	16.062	---
22	22.00	21.624	21.564	21.500	21.250	21.000	21.250	---	20.250	21.250	19.750	19.250	18.750	18.250	17.750	---
24	24.00	23.564	23.500	23.500	23.250	22.876	23.250	22.624	22.062	23.000	21.562	20.938	20.376	19.876	19.312	---
26	26.00	---	---	25.376	25.000	---	25.250	---	---	25.000	---	---	---	---	---	---
28	28.00	---	---	27.376	---	26.750	27.250	---	---	27.000	---	---	---	---	---	---
30	30.00	29.500	29.376	29.376	29.000	28.750	29.250	---	---	29.000	---	---	---	---	---	---
32	32.00	---	---	31.376	31.000	30.750	31.250	30.624	---	31.000	---	---	---	---	---	---
34	34.00	---	---	33.312	33.000	32.750	33.250	32.624	---	33.000	---	---	---	---	---	---
36	36.00	---	---	35.376	35.00	34.750	35.250	34.500	---	35.000	---	---	---	---	---	---
38	38.00	---	---	---	---	37.25	---	---	37.00	---	---	---	---	---	---	---
40	40.00	---	---	---	---	49.25	---	---	49.00	---	---	---	---	---	---	---
42	42.00	---	---	---	---	41.25	---	---	41.00	---	---	---	---	---	---	---
46	46.00	---	---	---	---	45.25	---	---	45.00	---	---	---	---	---	---	---
48	48.00	---	---	---	---	47.25	---	---	47.00	---	---	---	---	---	---	---

TABLE 2.3 PVC PIPE (ASTM D1785-06 [40], reprinted with permission of ASTM International, 100 Bar Harbor Drive, West Conshohocken, Pa, 19428)

Wall Thicknesses and Tolerances for PVC Plastic Pipe, Schedules 40, 80, and 120,[A,B] in. (mm)

Nominal Pipe Size	Outside Diameter	Wall Thickness[A]					
		Schedule 40		Schedule 80		Schedule 120	
		Minimum	Tolerance	Minimum	Tolerance	Minimum	Tolerance
⅛	0.405 (10.29)	0.068 (1.73)	+0.020 (+0.51)	0.095 (2.41)	+0.020 (+0.51)	...	...
¼	0.540 (13.72)	0.088 (2.24)	+0.020 (+0.51)	0.119 (3.02)	+0.020 (+0.51)	...	...
⅜	0.675 (17.14)	0.091 (2.31)	+0.020 (+0.51)	0.126 (3.20)	+0.020 (+0.51)	...	...
½	0.840 (21.34)	0.109 (2.77)	+0.020 (+0.51)	0.147 (3.73)	+0.020 (+0.51)	0.170 (4.32)	+0.020 (+0.51)
¾	1.050 (26.67)	0.113 (2.87)	+0.020 (+0.51)	0.154 (3.91)	+0.020 (+0.51)	0.170 (4.32)	+0.020 (+0.51)
1	1.315 (33.40)	0.133 (3.38)	+0.020 (+0.51)	0.179 (4.55)	+0.021 (+0.53)	0.200 (5.08)	+0.024 (+0.61)
1¼	1.660 (42.16)	0.140 (3.56)	+0.020 (+0.51)	0.191 (4.85)	+0.023 (+0.58)	0.215 (5.46)	+0.026 (+0.66)
1½	1.900 (48.26)	0.145 (3.68)	+0.020 (+0.51)	0.200 (5.08)	+0.024 (+0.61)	0.225 (5.72)	+0.027 (+0.68)
2	2.375 (60.32)	0.154 (3.91)	+0.020 (+0.51)	0.218 (5.54)	+0.026 (+0.66)	0.250 (6.35)	+0.030 (+0.76)
2½	2.875 (73.02)	0.203 (5.16)	+0.024 (+0.61)	0.276 (7.01)	+0.033 (+0.84)	0.300 (7.62)	+0.036 (+0.91)
3	3.500 (88.90)	0.216 (5.49)	+0.026 (+0.66)	0.300 (7.62)	+0.036 (+0.91)	0.350 (8.89)	+0.042 (+1.07)
3½	4.000 (101.60)	0.226 (5.74)	+0.027 (+0.68)	0.318 (8.08)	+0.038 (+0.96)	0.350 (8.89)	+0.042 (+1.07)
4	4.500 (114.30)	0.237 (6.02)	+0.028 (+0.71)	0.337 (8.56)	+0.040 (+1.02)	0.437 (11.10)	+0.052 (+1.32)
5	5.563 (141.30)	0.258 (6.55)	+0.031 (+0.79)	0.375 (9.52)	+0.045 (+1.14)	0.500 (12.70)	+0.060 (+1.52)
6	6.625 (168.28)	0.280 (7.11)	+0.034 (+0.86)	0.432 (10.97)	+0.052 (+1.32)	0.562 (14.27)	+0.067 (+1.70)
8	8.625 (219.08)	0.322 (8.18)	+0.039 (+0.99)	0.500 (12.70)	+0.060 (+1.52)	0.718 (18.24)	+0.086 (+2.18)
10	10.750 (273.05)	0.365 (9.27)	+0.044 (+1.12)	0.593 (15.06)	+0.071 (+1.80)	0.843 (21.41)	+0.101 (+2.56)
12	12.750 (323.85)	0.406 (10.31)	+0.049 (+1.24)	0.687 (17.45)	+0.082 (+2.08)	1.000 (25.40)	+0.120 (+3.05)
14	14.000 (355.60	0.437 (11.10)	+0.053 (+1.35)	0.750 (19.05)	+0.090 (+2.29)	...	...
16	16.000 (406.40)	0.500 (12.70)	+0.060 (+1.52)	0.843 (21.41)	+0.101 (+2.57)	...	...
18	18.000 (457.20)	0.562 (14.27)	+0.067 (+1.70)	0.937 (23.80)	+0.112 (+2.84)	...	...
20	20.000 (508.00)	0.593 (15.06)	+0.071 (+1.80)	1.031 (26.19)	+0.124 (+3.15)	...	...
24	24.000 (609.60)	0.687 (17.45)	+0.082 (+2.08)	1.218 (30.94)	+0.146 (+3.71)	...	...

[A] The minimum is the lowest wall thickness of the pipe at any cross section. The maximum permitted wall thickness, at any cross section, is the minimum wall thickness plus the stated tolerance. All tolerances are on the plus side of the minimum requirement.

[B] These dimensions conform to nominal IPS dimensions, with the exception that Schedule 120 wall thickness for pipe sizes ½ to 3½ in. (12.5 to 87.5 mm), inclusive, are special PVC plastic pipe sizes.

TABLE 2.4 PRESSURE-RATED PVC PIPE (ASTM D2241-05 [41], reprinted by permission of ASTM International, 100 Bar Harbor Drive, West Conshohocken, Pa, 19428)

Nominal Pipe Size, in.	Average Outside Diameter, in. (mm)		Wall Thickness,[A] in.[B]													
			SDR64		SDR41		SDR32.5		SDR26		SDR21		SDR17		SDR13.5	
			Minimum	Tolerance	Minimum	Tolerance	Minimum	Tolerance	Minimum	Tolerance	Minimum	Tolerance	Minimum	Tolerance	Minimum	Tolerance
⅛	0.405 (10.29)	±0.004 (0.10)	...	...	...	...	...	...	...	...	...	...	...	...	0.060	+0.020
¼	0.540 (13.72)	±0.004 (0.10)	...	...	...	...	...	...	...	...	...	...	...	...	0.060	+0.020
⅜	0.675 (17.14)	±0.004 (0.10)	...	...	...	...	...	...	...	...	...	...	...	...	0.060	+0.020
½	0.840 (21.34)	±0.004 (0.10)	...	...	...	...	...	...	...	...	...	...	...	...	0.062	+0.020
¾	1.050 (26.67)	±0.004 (0.10)	...	...	...	...	...	...	...	...	0.060	+0.020	0.062	+0.020	0.078	+0.020
1	1.315 (33.40)	±0.005 (0.13)	...	...	...	...	...	...	0.060	+0.020	0.063	+0.020	0.077	+0.020	0.097	+0.020
1¼	1.660 (42.16)	±0.005 (0.13)	...	...	...	...	0.060	+0.020	0.064	+0.020	0.079	+0.020	0.098	+0.020	0.123	+0.020
1½	1.900 (48.26)	±0.006 (0.15)	...	...	...	...	0.060	+0.020	0.073	+0.020	0.090	+0.020	0.112	+0.020	0.141	+0.020
2	2.375 (60.32)	±0.006 (0.15)	...	...	...	...	0.073	+0.020	0.091	+0.020	0.113	+0.020	0.140	+0.020	0.176	+0.020
2½	2.875 (73.02)	±0.007 (0.18)	...	...	...	...	0.088	+0.020	0.110	+0.020	0.137	+0.020	0.169	+0.020	0.213	+0.026
3	3.500 (88.90)	±0.008 (0.20)	...	...	0.085	+0.020	0.108	+0.020	0.135	+0.020	0.167	+0.020	0.206	+0.025	0.259	+0.031
3½	4.000 (101.60)	±0.008 (0.20)	...	...	0.098	+0.020	0.123	+0.020	0.154	+0.020	0.190	+0.023	0.235	+0.028	0.296	+0.036
4	4.500 (114.30)	±0.009 (0.23)	0.070	+0.020	0.110	+0.020	0.138	+0.020	0.173	+0.020	0.214	+0.026	0.265	+0.032	0.333	+0.040
5	5.563 (141.30)	±0.010 (0.25)	0.087	+0.020	0.136	+0.020	0.171	+0.021	0.214	+0.027	0.265	+0.032	0.327	+0.039	0.412	+0.049
6	6.625 (168.28)	±0.011 (0.28)	0.104	+0.020	0.162	+0.020	0.204	+0.024	0.255	+0.031	0.316	+0.038	0.390	+0.047	0.491	+0.059
8	8.625 (219.08)	±0.015 (0.38)	0.135	+0.020	0.210	+0.025	0.265	+0.032	0.332	+0.040	0.410	+0.049	0.508	+0.061	...	...
10	10.750 (273.05)	±0.015 (0.38)	0.168	+0.020	0.262	+0.031	0.331	+0.040	0.413	+0.050	0.511	+0.061	0.632	+0.076	...	...
12	12.750 (323.85)	±0.015 (0.38)	0.199	+0.024	0.311	+0.037	0.392	+0.047	0.490	+0.059	0.606	+0.073	0.750	+0.090	...	...
14	14.000 (355.60)	±0.015 (0.38)	...	...	0.341	+0.048	0.430	+0.052	0.538	+0.064	0.666	+0.080	0.823	+0.099	...	...
16	16.000 (406.40)	±0.019 (0.48)	...	...	0.390	+0.055	0.492	+0.059	0.615	+0.074	0.762	+0.091	0.941	+0.113	...	...
18	18.000 (457.20)	±0.019 (0.48)	...	...	0.439	+0.061	0.554	+0.066	0.692	+0.083	0.857	+0.103	1.059	+0.127	...	...
20	20.000 (508.00)	±0.023 (0.58)	...	...	0.488	+0.068	0.615	+0.074	0.769	+0.092	0.952	+0.114	1.176	+0.141	...	...
24	24.000 (609.60)	±0.031 (0.79)	...	...	0.585	+0.082	0.738	+0.088	0.923	+0.111	1.143	+0.137	1.412	+0.169	...	...
30	30.000 (762.00)	±0.041 (1.04)	...	...	0.732	+0.102	0.923	+0.111	1.154	+0.138	1.428	+0.171	1.765	+0.212	...	...
36	36.000 (914.40)	±0.050 (1.27)	...	...	0.878	+0.123	1.108	+0.133	1.385	+0.166	1.714	+0.205	2.118	+0.254	...	...

[A] The minimum is the lowest wall thickness of the pipe at any cross section. The maximum permitted wall thickness, at any cross section, is the minimum wall thickness plus the stated tolerance. All tolerances are on the plus side of the minimum requirement.

[B] 1 in. = 25.4 mm (exact).

TABLE 2.5 ALUMINUM PIPE (ASTM B429/B429M-06 [42], reprinted with permission of ASTM International, 100 Bar Harbor Drive, West Conshohocken, Pa, 19428. See 2010 revision for a more comprehensive list of pipe and tubing sizes)

Nominal Pipe Size Designation	ANSI Schedule No.[B]	OD, in. (mm)			ID, in. (mm)	Wall Thickness, in. (mm)			Weight,[C] lb/ft (M ass per Meter, g)	
		Nominal	Min	Max	Nominal	Nominal	Min	Max[D]	Nominal	Max
½	40	0.840	0.809	0.855	0.622	0.109	0.095	...	0.294	0.317
		(21.30)	(20.50)	(21.70)	(15.76)	(2.77)	(2.42)	...	(0.44)	(0.48)
¾	10	1.050	1.019	1.065	0.884	0.083	0.071	0.095	0.297	...
		(26.70)	(25.90)	(27.10)	(22.4)	(2.11)	(1.80)	(2.41)	(7.54)	...
	40	1.050	1.019	1.065	0.824	0.113	0.099	...	0.391	0.422
		(26.70)	(25.90)	(27.10)	(20.96)	(2.87)	(2.51)	...	(0.58)	(0.63)
1	10	1.315	1.284	1.330	1.097	0.109	0.095	0.123	0.486	...
		(33.40)	(32.60)	(33.80)	(27.86)	(2.77)	(2.41)	(3.12)	(.723)	...
	40	1.315	1.284	1.330	1.049	0.133	0.116	...	0.581	0.627
		(33.40)	(32.60)	(33.80)	(26.64)	(3.38)	(2.95)	...	(.86)	(.93)
1¼	10	1.660	1.629	1.675	1.442	0.109	0.095	0.123	0.625	...
		(42.16)	(41.38)	(42.55)	(36.6)	(2.77)	(2.41)	(3.12)	(.929)	...
	40	1.660	1.629	1.675	1.380	0.140	0.122	...	0.786	0.849
		(42.16)	(41.38)	(42.55)	(35.05)	(3.56)	(3.10)	...	(1.17)	(1.26)
1½	10	1.900	1.869	1.915	1.682	0.109	0.095	0.123	0.721	...
		(48.26)	(47.47)	(48.64)	(42.7)	(2.77)	(2.41)	(3.12)	(1.07)	
	40	1.900	1.869	1.915	1.610	0.145	0.127	...	0.940	1.015
		(48.26)	(47.47)	(48.64)	(40.89)	(3.68)	(3.22)	...	(1.40)	(1.51)
2	10	2.375	2.344	2.406	2.157	0.109	0.095	0.123	0.913	...
		(60.33)	(59.54)	(61.11)	(54.79)	(2.77)	(2.41)	(3.12)	(1.36)	...
	40	2.375	2.351	2.399	2.067	0.154	0.135	...	1.264	1.365
		(60.33)	(59.72)	(60.93)	(52.50)	(3.91)	(3.43)	...	(1.88)	(2.03)
2½	10	2.875	2.844	2.906	2.635	0.120	0.105	0.135	1.221	...
		(73.0)	(72.2)	(73.81)	(66.93)	(3.05)	(2.67)	(3.43)	(1.80)	
	40	2.875	2.846	2.904	2.469	0.203	0.178	...	2.004	2.164
		(73.0)	(72.29)	(73.76)	(62.71)	(5.16)	(4.52)		(2.96)	(3.22)
3	10	3.500	3.469	3.531	3.260	0.120	0.105	0.135	1.498	...
		(88.90)	(88.11)	(89.69)	(82.80)	(3.05)	(2.67)	(3.43)	(2.23)	...
	40	3.500	3.465	3.535	3.068	0.216	0.189	...	2.621	2.830
		(88.90)	(88.00)	(89.79)	(77.92)	(5.49)	(4.80)		(3.90)	(4.21)
3½	40	4.000	3.960	4.040	3.548	0.226	0.198	...	3.151	3.403
		(101.60)	(100.60)	(102.60)	(90.12)	(5.74)	(5.02)	...	(4.67)	(5.04)
4	40	4.500	4.455	4.545	4.026	0.237	0.207	...	3.733	4.031
		(114.30)	(113.20)	(115.40)	(102.26}	(6.02)	(5.27)	...	(5.53)	(5.67)

[A] Soft Metric size conversions shown for reader convenience only. Metric sizes do not exist for standard schedule Pipe.
[B] Schedule 40 is also designated as "standard pipe."
[C] Based on the 6061 alloy density of 0.098 lb/in.^{3} (U.S. Customary) and 2.70 kg/m^3, (Metric). For alloy 6063 multiply by 0.99.
[D] For schedule 40, maximum wall thickness is controlled by weight tolerance.

Notes for Table 2.2

1) STD, XS, and XXS = standard, extra strong, and extra extra strong.
2) Schedule 5S, 10S, 40S, and 80S are available up to 20 NPS. Schedule 22 and 30 are available in 5S and 10S only.
3) Additional pipe wall thicknesses are available per ASME B36.10M and B36.19M, which meet the specifications of API 5L.

2.3.3.3 Density and Viscosity Data and Their Effects on Pressure Drops Due to Flow Viscosity and density are required for various operating temperatures and for fluids other than water. In particular, changes in density and viscosity affect the Reynold's number and predicted pressure drops in pipes.

Densities and other properties for various fluids are presented in Tables 2.11 and 2.12. Fig. 2.18 and Table 2.13 provide more detailed data on water, where the specific gravity of water varies slightly depending on the reference temperature. Additional density data on petroleum products is available in the work of Crane [21], and both Reid [47] and Perry [48] provide techniques for estimating unknown densities for many fluids.

Viscosity data is available for a wide range of fluids, and only some of that data is presented here (Table 2.14). Viscosity effects for some common fluids are presented

TABLE 2.6 ALUMINUM TUBE (ASTM B429/B 429M-06 [42], reprinted with permission of ASTM International, 100 Bar Harbor Drive, West Conshohocken, Pa, 19428)

Standard Structural Tube Sizes

Outside Diameter, OD, in. [mm]	Nominal Wall Thickness, in. [mm]	Nominal Weight,[A] lb/ft [kg/m]	Outside Diameter, OD, in. [mm]	Wall Thickness, in. [mm]	Nominal Weight,[A] lb/ft [kg/m]
1.500 [40]	0.125 [3.20]	0.631 [1.00]	4.000 [100]	0.125 [3.20]	1.790 [2.63]
	0.188 [5.00]	0.911 [1.48]		0.188 [5.00]	2.650 [4.03]
	0.250 [6.30]	1.150 [1.80]		0.250 [6.30]	3.460 [5.01]
2.000 [50]	0.125 [3.20]	0.866 [1.27]	4.500 [120]	0.125 [3.20]	2.020 [3.17]
	0.188 [5.00]	1.260 [1.91]		0.188 [5.00]	2.990 [4.88]
	0.250 [6.30]	1.620 [2.34]		0.250 [6.30]	3.390 [6.08]
2.500 [60]	0.125 [3.20]	1.100 [1.54]	5.000 [130]	0.125 [3.20]	2.250 [3.44]
	0.188 [5.00]	1.610 [2.33]		0.188 [5.00]	3.340 [5.30]
	0.250 [6.30]	2.080 [2.87]		0.250 [6.30]	4.390 [6.62]
3.000 [80]	0.125 [3.20]	1.330 [2.08]	5.500 [140]	0.188 [5.00]	3.690 [5.73]
	0.188 [5.00]	1.950 [3.18]		0.250 [6.30]	4.850 [7.36]
	0.250 [6.30]	2.540 [3.94]			
3.500 [90]	0.125 [3.20]	1.560 [2.36]	6.000 [150]	0.188 [5.00]	4.040 [6.15]
	0.188 [5.00]	2.300 [3.60]			
	0.250 [6.30]	3.000 [4.48]			

[A] Based on the 6005A, 6061 and 6082 alloy densities of 0.098 lb/in.^{3} (U.S. Customary) and 2.70 kg/m^3, (Metric). For alloys 6005, 6105, and 6063 multiply by 0.99.

in Fig. 2.19, and details of viscosity for water and steam are shown in Fig. 2.20, which is expressed in terms of the kinematic viscosity, where both absolute viscosity and density are a function of temperature. Viscosities for some other fluids may be estimated (Perry [48]), using provided data (Table 2.14) and a nomograph (Fig. 2.21).

For additional data, Reid also provides an extensive list of most available experimental data for the viscosity of various fluids, along with techniques to approximate viscosity for different conditions or materials if only one value of density or viscosity is available. For example, an equation that provides estimates similar to that of Fig. 2.21 may be expressed as

$$\mu_L^{-0.2661} = \mu_K^{-0.2661} + \frac{T_L - T_K}{387.4} \qquad \text{US (2.42)}$$

where μ_L (centipoise) is the required liquid viscosity at T_L (°F), and μ_K is a known viscosity at T_K. Reid also noted that calculated viscosities are typically in error by 5% to 15%. In addition to Reid's work, Crane [21] provides viscosity data for numerous petroleum products and refrigerants. Although only some of the available data is provided here, Figs. 2.18 to 2.21 and Table 2.14 provide considerable insight into the behavior of liquids with respect to viscosity and density.

Example 2.5 Temperature effects on density and viscosity

For example, consider water material properties. At 68°F, water has an absolute viscosity of 1 centipoise, a specific gravity, Sp*G*, of 1.0, and a density, ρ, of 62.28 lb/ft^3 (Table 2.13). The viscosity varies by 10% for a 10° temperature change, but the viscosity change is negligible for a pressure change of 500 psig (Fig. 2.20). On the other hand, for compressed water, the density changes less than 1% for a 10° change at different temperatures or a 500 psig change (per ASME tables [51]). The effect of fluid properties on pressure drops is examined further in the next example.

Example 2.6 Temperature effects on flow-induced pressure drop

As another example, consider temperature and material effects on the pressure drop in a pipe for different fluids. The determination of the Reynold's number is shown in Fig. 2.19 for 150°F kerosene flowing through a 6-in., schedule 40 steel pipe at 8.24 ft/second, where $V \cdot D = 8.24 \cdot 6.065 = 50$ ($Re \approx 3.5 \cdot 10^5$). For water at the same conditions, the Reynold's number would be slightly above 10^6.

Substituting these values into the Moody diagram (Fig. 2.16), the friction factors for kerosene and water are approximately 0.0166 and 0.0156, respectively. Consequently, there is approximately a 6% increase in pressure drop when water flows through a straight pipe rather than kerosene for any length of pipe considered. Similarly, considering water flowing at 50°F or 140°F, the difference in pressure drop is also about 6%. This difference in friction accounts for the difference in the sound frequency from a pipe when a valve is opened from a

TABLE 2.7 COPPER WATER TUBE (ASTM B88-03 [43], reprinted with permission of ASTM International, 100 Bar Harbor Drive, West Conshohocken, Pa, 19428)

Nominal or Standard Size, in.	Outside Diameter, in.	Average Outside Diameter[A] Tolerance, in.		Wall Thickness and Tolerances, in.						Theoretical Weight, lb/ft		
				Type K		Type L		Type M				
		Annealed	Drawn	Wall Thickness	Tolerance[B]	Wall Thickness	Tolerance[B]	Wall Thickness	Tolerance[B]	Type K	Type L	Type M
¼	0.375	0.002	0.001	0.035	0.0035	0.030	0.003	[C]	[C]	0.145	0.126	[C]
⅜	0.500	0.0025	0.001	0.049	0.005	0.035	0.004	0.025	0.002	0.269	0.198	0.145
½	0.625	0.0025	0.001	0.049	0.005	0.040	0.004	0.028	0.003	0.344	0.285	0.204
⅝	0.750	0.0025	0.001	0.049	0.005	0.042	0.004	[C]	[C]	0.418	0.362	[C]
¾	0.875	0.003	0.001	0.065	0.006	0.045	0.004	0.032	0.003	0.641	0.455	0.328
1	1.125	0.0035	0.0015	0.065	0.006	0.050	0.005	0.035	0.004	0.839	0.655	0.465
1¼	1.375	0.004	0.0015	0.065	0.006	0.055	0.006	0.042	0.004	1.04	0.884	0.682
1½	1.625	0.0045	0.002	0.072	0.007	0.060	0.006	0.049	0.005	1.36	1.14	0.940
2	2.125	0.005	0.002	0.083	0.008	0.070	0.007	0.058	0.006	2.06	1.75	1.46
2½	2.625	0.005	0.002	0.095	0.010	0.080	0.008	0.065	0.006	2.93	2.48	2.03
3	3.125	0.005	0.002	0.109	0.011	0.090	0.009	0.072	0.007	4.00	3.33	2.68
3½	3.625	0.005	0.002	0.120	0.012	0.100	0.010	0.083	0.008	5.12	4.29	3.58
4	4.125	0.005	0.002	0.134	0.013	0.110	0.011	0.095	0.010	6.51	5.38	4.66
5	5.125	0.005	0.002	0.160	0.016	0.125	0.012	0.109	0.011	9.67	7.61	6.66
6	6.125	0.005	0.002	0.192	0.019	0.140	0.014	0.122	0.012	13.9	10.2	8.92
8	8.125	0.006	+0.002 −0.004	0.271	0.027	0.200	0.020	0.170	0.017	25.9	19.3	16.5
10	10.125	0.008	+0.002 −0.006	0.338	0.034	0.250	0.025	0.212	0.021	40.3	30.1	25.6
12	12.125	0.008	+0.002 −0.006	0.405	0.040	0.280	0.028	0.254	0.025	57.8	40.4	36.7

[A] The average outside diameter of a tube is the average of the maximum and minimum outside diameter, as determined at any one cross section of the tube.
[B] Maximum deviation at any one point.
[C] Indicates that the material is not generally available or that no tolerance has been established.

TABLE 2.8 SEAMLESS COPPER NICKEL TUBING (ASTM B-466 [44], reprinted with permission of ASTM International, 100 Bar Harbor Drive, West Conshohocken, Pa, 19428)

Preferred Wall Thicknesses for Drawn Seamless Pipe Based on SPS Diameter

SPS	Outside Diameter, in. [mm]	Wall Thickness						
		Specials					Regular, in. [mm]	Extra Strong, in. [mm]
		in. [mm]	in. [mm]	in. [mm]	in. [mm]	in. [mm]		
⅛	0.405 [10.3]	0.058 [1.47]	...	...	...	...	0.062 [1.57]	0.100 [2.54]
¼	0.540 [13.7]	0.065 [1.65]	0.072 [1.83]	...	...	...	0.082 [2.08]	0.123 [3.12]
⅜	0.675 [17.1]	0.065 [1.65]	0.072 [1.83]	0.095 [2.41]	0.148 [3.76]	...	0.090 [2.29]	0.127 [3.23]
½	0.840 [21.3]	0.065 [1.65]	0.072 [1.83]	0.120 [3.03]	0.203 [5.16]	...	0.107 [2.72]	0.149 [3.78]
¾	1.050 [26.7]	0.065 [1.65]	0.083 [2.11]	0.148 [3.76]	0.238 [6.05]	...	0.114 [2.90]	0.157 [3.99]
1	1.315 [33.4]	0.065 [1.65]	0.095 [2.41]	0.203 [5.16]	0.340 [8.64]	...	0.126 [3.20]	0.182 [4.62]
1¼	1.650 [42.4]	0.072 [1.83]	0.095 [2.41]	0.120 [3.03]	0.220 [5.59]	0.380 [9.65]	0.146 [3.71]	0.194 [4.93]
1½	1.900 [48.3]	0.072 [1.83]	0.109 [2.77]	0.134 [3.40]	0.250 [6.35]	0.425 [10.8]	0.150 [3.81]	0.203 [5.16]
2	2.375 [60.3]	0.083 [2.11]	0.120 [3.03]	0.165 [4.19]	0.340 [8.64]	0.520 [13.2]	0.156 [3.96]	0.221 [5.61]
2½	2.875 [73.0]	0.083 [2.11]	0.134 [3.40]	0.203 [5.16]	0.380 [9.65]	...	0.187 [4.75]	0.280 [7.11]
3	3.500 [88.9]	0.095 [2.41]	0.165 [4.19]	0.250 [6.35]	0.458 [11.6]	...	0.219 [5.56]	0.304 [7.72]
3½	4.000 [102]	0.095 [2.41]	0.180 [4.57]	0.284 [7.21]	...	...	0.250 [6.35]	0.321 [8.15]
4	4.500 [114]	0.109 [2.77]	0.203 [5.16]	0.340 [8.64]	...	...	0.250 [6.35]	0.341 [8.66]
5	5.552 [141]	0.125 [3.18]	0.220 [5.59]	0.425 [10.8]	...	...	0.250 [6.35]	0.375 [9.52]
6	6.625 [168]	0.134 [3.40]	0.259 [6.58]	0.457 [11.6]	...	...	0.250 [6.35]	0.437 [11.1]

household water heater, where the maximum temperature for water heaters is controlled at 140°F by OSHA regulations. As the viscosity decreases with increasing water temperature, flow increases, and the increased friction in the pipe increases the induced noise as the fluid travels the pipe length. The sound volume of the water increases slightly as the water gets hotter. Only a few fluids are presented in the figures, but the effects of temperature, viscosity, and density clearly demonstrate the need for experimental property data for the fluid of concern.

2.3.4 Tabulated Pressure Drops for Water Flow in Steel Pipe

Crane and Cameron both provide tables of pressure drops versus flow rate for numerous pipe diameters and flow conditions. Cameron [52] provides the more complete data set and notes that a safety factor of 15% to 20% should be used for friction factors, which is also applicable to pressure drop values since friction factors are proportional to pressure drops. These tables provide quick reference for typical conditions for water in steel pipes, as listed in Table 2.15.

Example 2.7 Pressure drop versus pipe diameter

For example, consider the simple case of a lawn sprinkler system with supply conditions of 75 psig and 20 gpm, which are typical values. In Table 2.15, at 20 gpm, the pressure drop per 100 ft of pipe decreases from 37.8 psi for 3/4 NPS pipe to 1.28 psi for 1-1/2 NPS pipe as the velocity drops from 12.03 to 3.06 ft/second. At a distance of 100 ft from the water source, the supply pressure to a sprinkler is half of the pressure at the source for the ¾-in. pipe, and the wetted zone radius due to the sprinkler decreases. On large lawns, sprinklers are occasionally observed to have a small sprinkler radius at the last sprinkler on a pipe when inadequate pipe sizes are installed. An increased pipe diameter would have prevented this inadequate flow, and all sprinkler radii would have been similar.

Similarly, industrial applications require careful consideration of pressure drops, which significantly affect system design. For instance, cross-country oil pipelines require pump stations in series along the pipe lines to overcome friction losses, and NFPA codes provide specific guidance on pipe sizing for fire control systems.

2.3.5 Effects of Aging on Water-Filled Steel Pipes

The Hazen-Williams equation describes the changes in velocity for turbulent flow due to pipe aging, where

$$V\left(\text{ft/second}\right) = 1.318 \cdot f_{\text{H}} \cdot r_{\text{h}}^{0.63} \cdot \left(\frac{h_{\text{L}}}{\text{L}}\right)^{0.54} \quad \text{EE (2.43)}$$

TABLE 2.9 SEAMLESS COPPER PIPE (ASTM B42-02 [45], reprinted with permission of ASTM International, 100 Bar Harbor Drive, West Conshohocken, Pa, 19428)

Standard Dimensions, Weights, and Tolerances

NOTE 1—All tolerances plus and minus except as otherwise indicated.

Nominal or Standard Pipe Size, in.	Outside Diameter, in. (mm)	Average Outside Diameter Tolerance,[A] in. (mm) All Minus	Wall Thickness, in. (mm)	Tolerance,[B] in. (mm)	Theoretical Weight, lb/ft (kg/m)
			Regular		
⅛	0.405 (10.3)	0.004 (0.10)	0.062 (1.57)	0.004 (0.10)	0.259 (0.385)
¼	0.540 (13.7)	0.004 (0.10)	0.082 (2.08)	0.005 (0.13)	0.457 (0.680)
⅜	0.675 (17.1)	0.005 (0.13)	0.090 (2.29)	0.005 (0.13)	0.641 (0.954)
½	0.840 (21.3)	0.005 (0.13)	0.107 (2.72)	0.006 (0.15)	0.955 (1.42)
¾	1.050 (26.7)	0.006 (0.15)	0.114 (2.90)	0.006 (0.15)	1.30 (1.93)
1	1.315 (33.4)	0.006 (0.15)	0.126 (3.20)	0.007 (0.18)	1.82 (2.71)
1¼	1.660 (42.2)	0.006 (0.15)	0.146 (3.71)	0.008 (0.20)	2.69 (4.00)
1½	1.900 (48.3)	0.006 (0.15)	0.150 (3.81)	0.008 (0.20)	3.20 (4.76)
2	2.375 (60.3)	0.008 (0.20)	0.156 (3.96)	0.009 (0.23)	4.22 (6.28)
2½	2.875 (73.0)	0.008 (0.20)	0.187 (4.75)	0.010 (0.25)	6.12 (9.11)
3	3.500 (88.9)	0.010 (0.25)	0.219 (5.56)	0.012 (0.30)	8.76 (13.0)
3½	4.000 (102)	0.010 (0.25)	0.250 (6.35)	0.013 (0.33)	11.4 (17.0)
4	4.500 (114)	0.012 (0.30)	0.250 (6.35)	0.014 (0.36)	12.9 (19.2)
5	5.562 (141)	0.014 (0.36)	0.250 (6.35)	0.014 (0.36)	16.2 (24.1)
6	6.625 (168)	0.016 (0.41)	0.250 (6.35)	0.014 (0.36)	19.4 (28.9)
8	8.625 (219)	0.020 (0.51)	0.312 (7.92)	0.022 (0.56)	31.6 (47.0)
10	10.750 (273)	0.022 (0.56)	0.365 (9.27)	0.030 (0.76)	46.2 (68.7)
12	12.750 (324)	0.024 (0.61)	0.375 (9.52)	0.030 (0.76)	56.5 (84.1)
			Extra Strong		
⅛	0.405 (10.3)	0.004 (0.10)	0.100 (2.54)	0.006 (0.15)	0.371 (0.552)
¼	0.540 (13.7)	0.004 (0.10)	0.123 (3.12)	0.007 (0.18)	0.625 (0.930)
⅜	0.675 (17.1)	0.005 (0.13)	0.127 (3.23)	0.007 (0.18)	0.847 (1.26)
½	0.840 (21.3)	0.005 (0.13)	0.149 (3.78)	0.008 (0.20)	1.25 (1.86)
¾	1.050 (26.7)	0.006 (0.15)	0.157 (3.99)	0.009 (0.23)	1.71 (2.54)
1	1.315 (33.4)	0.006 (0.15)	0.182 (4.62)	0.010 (0.25)	2.51 (3.73)
1¼	1.660 (42.2)	0.006 (0.15)	0.194 (4.93)	0.010 (0.25)	3.46 (5.15)
1½	1.900 (48.3)	0.006 (0.15)	0.203 (5.16)	0.011 (0.28)	4.19 (6.23)
2	2.375 (60.3)	0.008 (0.20)	0.221 (5.61)	0.012 (0.30)	5.80 (8.63)
2½	2.875 (73.0)	0.008 (0.20)	0.280 (7.11)	0.015 (0.38)	8.85 (13.2)
3	3.500 (88.9)	0.010 (0.25)	0.304 (7.72)	0.016 (0.41)	11.8 (17.6)
3½	4.000 (102)	0.010 (0.25)	0.321 (8.15)	0.017 (0.43)	14.4 (21.4)
4	4.500 (114)	0.012 (0.30)	0.341 (8.66)	0.018 (0.46)	17.3 (25.7)
5	5.562 (141)	0.014 (0.36)	0.375 (9.52)	0.019 (0.48)	23.7 (35.3)
6	6.625 (168)	0.016 (0.41)	0.437 (11.1)	0.027 (0.69)	32.9 (49.0)
8	8.625 (219)	0.020 (0.51)	0.500 (12.7)	0.035 (0.89)	49.5 (73.7)
10	10.750 (273)	0.022 (0.56)	0.500 (12.7)	0.040 (1.0)	62.4 (92.9)

[A] The average outside diameter of a tube is the average of the maximum and minimum outside diameters as determined at any one cross section of the pipe.
[B] Maximum deviation at any one point.

TABLE 2.10 DUCTILE IRON PIPE FOR USE WITH THREADED FITTINGS (ANSI/AWWA C115/A21.15-05 [46], reprinted with permission of AWWA)

Nominal Pipe Size *in.*	Maximum Working Pressure *psi*	Pipe Nominal Thickness* *in.*	Pipe OD *in.*	Weight—*lb*		
				Pipe Barrel per ft	One Solid Flange† Only	One Hollow-Back Flange† Only
3	250‡	0.31	3.96	10.9	7	5
4	250‡	0.32	4.80	13.8	11	9
6	250‡	0.34	6.90	21.4	14	11
8	250‡	0.36	9.05	30.1	27	18
10	250‡	0.38	11.10	39.2	32	27
12	250‡	0.40	13.20	49.2	47	38
14	250‡	0.42	15.30	60.1	72	50
16	250‡	0.43	17.40	70.1	90	66
18	250‡	0.44	19.50	80.6	90	73
20	250‡	0.45	21.60	91.5	115	92
24	250‡	0.47	25.80	114.4	160	127
30	250	0.51	32.00	154.4	240	176
36	250	0.58	38.30	210.3	350	275
42	250	0.65	44.50	274.0	500	—
48	250	0.72	50.80	346.6	625	—
54	250	0.81	57.56	441.9	670	—
60	250	0.83	61.61	485.0	1,035	—
64	250	0.87	65.67	542.0	1,510	—

$$V\left(\text{ft/second}\right)=1.318\cdot f_{\text{H}}\cdot\left(\frac{r_{\text{h}}}{12}\right)^{0.63}\cdot\left(\frac{h_{\text{L}}\left(\text{feet}\right)}{L\left(\text{in.}\right)/12}\right)^{0.54}\qquad\text{US (2.44)}$$

$$V(\text{m/second})=0.8492\cdot f_{\text{H}}\cdot r_{\text{h}}^{0.63}\cdot\left(\frac{h_{\text{L}}}{L}\right)^{0.54}\qquad\text{SI (2.45)}$$

where f_{H} is the Hazen-Williams friction factor, h_{L}/L is the head loss per foot of pipe, and r_{h}, (in.) is the hydraulic radius, which equals the inside pipe area divided by the wetted perimeter. For pipe,

$$r_{\text{h}}=D/4\qquad\text{US, EE, SI (2.46)}$$

Karrasik [53] provides some data (Table 2.16), but the friction factor can be drastically affected by water pH (Zipparo [54]). Even so, the data indicates that flow can be cut by 30% to 50% during 35 years of operation.

2.3.6 Friction Factors From Churchill's Equation

Churchill [55] expressed Moody's diagram in a single equation. This equation is considered to be within the accuracy of the data used for Moody's diagram and is expressed as

$$f_{\text{n}}=2\cdot\left(\left(\frac{8}{Re}\right)^{12}+\left(\frac{1}{\left(A'+B'\right)^{1.5}}\right)\right)^{1/12}\qquad\text{US, EE, SI (2.47)}$$

TABLE 2.11 PHYSICAL PROPERTIES OF COMMON LIQUIDS (Pump Characteristics and Applications by Volk, Michael, Copyright 2012. Reproduced with permission of Taylor and Francis Group, LLC. [49])

Liquid	*Sp Gr at 60 F	VISCOSITY		At F
		SSU	Centistokes	
Freon	1.37 to 1.49 @ 70 F		.27–.32	70
Glycerine (100%)	1.26 @ 68 F	2,950 813	648 176	68.6 100
Glycol:				
Propylene	1.038 @ 68 F	240.6	52	70
Triethylene	1.125 @ 68 F	185.7	40	70
Diethylene	1.12	149.7	32	70
Ethylene	1.125	88.4	17.8	70
Hydrochloric Acid (31.5%)	1.05 @ 68 F		1.9	68
Mercury	13.6		.118 .11	70 100
Phenol (Carbolic Acid)	.95 to 1.08	65	11.7	65
Silicate of Soda	40 Baume 42 Baume	365 637.6	79 138	100 100
Sulfuric Acid (100%)	1.83	75.7	14.6	68
FISH AND ANIMAL OILS:				
Bone Oil	.918	220 65	47.5 11.6	130 212
Cod Oil	.928	150 95	32.1 19.4	100 130
Lard	.96	287 160	62.1 34.3	100 130
Lard Oil	.912 to .925	190 to 220 112 to 128	41 to 47.5 23.4 to 27.1	100 130
Menhaden Oil	.933	140 90	29.8 18.2	100 130
Neatsfoot Oil	.917	230 130	49.7 27.5	100 130
Sperm Oil	.883	110 78	23.0 15.2	100 130
Whale Oil	.925	163 to 184 97 to 112	35 to 39.6 19.9 to 23.4	100 130
MINERAL OILS:				
Automobile Crankcase Oils (Average Midcontinent Paraffin Base):				
SAE 10	**.880 to .935	165 to 240 90 to 120	35.4 to 51.9 18.2 to 25.3	100 130
SAE 20	**.880 to .935	240 to 400 120 to 185	51.9 to 86.6 25.3 to 39.9	100 130
SAE 30	**.880 to .935	400 to 580 185 to 255	86.6 to 125.5 39.9 to 55.1	100 130
SAE 40	**.880 to .935	580 to 950 255 to 80	125.5 to 205.6 55.1 to 15.6	100 130 210
SAE 50	**.880 to .935	950 to 1,600 80 to 105	205.6 to 352 15.6 to 21.6	100 210
SAE 60	**.880 to .935	1,600 to 2,300 105 to 125	352 to 507 21.6 to 26.2	100 210
SAE 70	**.880 to .935	2,300 to 3,100 125 to 150	507 to 682 26.2 to 31.8	100 210
SAE 10W	**.880 to .935	5,000 to 10,000	1,100 to 2,200	0
SAE 20W	**.880 to .935	10,000 to 40,000	2,200 to 8,800	0
Automobile Transmission Lubricants:				
SAE 80	**.880 to .935	100,000 max	22,000 max	0
SAE 90	**.880 to .935	800 to 1,500 300 to 500	173.2 to 324.7 64.5 to 108.2	100 130
SAE 140	**.880 to .935	950 to 2,300 120 to 200	205.6 to 507 25.1 to 42.9	130 210
SAE 250	**.880 to .935	Over 2,300 Over 200	Over 507 Over 42.9	130 210
Crude Oils:				
Texas, Oklahoma	.81 to .916	40 to 783 34.2 to 210	4.28 to 169.5 2.45 to 45.3	60 100
Wyoming, Montana	.86 to .88	74 to 1,215 46 to 320	14.1 to 263 6.16 to 69.3	60 100
California	.78 to .92	40 to 4,840 34 to 700	4.28 to 1,063 2.4 to 151.5	60 100
Pennsylvania	.8 to .85	46 to 216 38 to 86	6.16 to 46.7 3.64 to 17.2	60 100
Diesel Engine Lubricating Oils (Based on Average Midcontinent Paraffin Base):				
Federal Specification No. 9110	**.880 to .935	165 to 240 90 to 120	35.4 to 51.9 18.2 to 25.3	100 130

*Unless otherwise noted.

**Depends on origin or percent and type of solvent.

TABLE 2.11 PHYSICAL PROPERTIES OF COMMON LIQUIDS (Continued)

Liquid	*Sp Gr at 60 F	VISCOSITY		At F
		SSU	Centistokes	
Freon	1.37 to 1.49 @ 70 F		.27–.32	70
Glycerine (100%)	1.26 @ 68 F	2,950 813	648 176	68.6 100
Glycol:				
Propylene	1.038 @ 68 F	240.6	52	70
Triethylene	1.125 @ 68 F	185.7	40	70
Diethylene	1.12	149.7	32	70
Ethylene	1.125	88.4	17.8	70
Hydrochloric Acid (31.5%)	1.05 @ 68 F		1.9	68
Mercury	13.6		.118 .11	70 100
Phenol (Carbolic Acid)	.95 to 1.08	65	11.7	65
Silicate of Soda	40 Baume 42 Baume	365 637.6	79 138	100 100
Sulfuric Acid (100%)	1.83	75.7	14.6	68
FISH AND ANIMAL OILS:				
Bone Oil	.918	220 65	47.5 11.6	130 212
Cod Oil	.928	150 95	32.1 19.4	100 130
Lard	.96	287 160	62.1 34.3	100 130
Lard Oil	.912 to .925	190 to 220 112 to 128	41 to 47.5 23.4 to 27.1	100 130
Menhaden Oil	.933	140 90	29.8 18.2	100 130
Neatsfoot Oil	.917	230 130	49.7 27.5	100 130
Sperm Oil	.883	110 78	23.0 15.2	100 130
Whale Oil	.925	163 to 184 97 to 112	35 to 39.6 19.9 to 23.4	100 130
MINERAL OILS:				
Automobile Crankcase Oils (Average Midcontinent Paraffin Base):				
SAE 10	**.880 to .935	165 to 240 90 to 120	35.4 to 51.9 18.2 to 25.3	100 130
SAE 20	**.880 to .935	240 to 400 120 to 185	51.9 to 86.6 25.3 to 39.9	100 130
SAE 30	**.880 to .935	400 to 580 185 to 255	86.6 to 125.5 39.9 to 55.1	100 130
SAE 40	**.880 to .935	580 to 950 255 to 80	125.5 to 205.6 55.1 to 15.6	100 130 210
SAE 50	**.880 to .935	950 to 1,600 80 to 105	205.6 to 352 15.6 to 21.6	100 210
SAE 60	**.880 to .935	1,600 to 2,300 105 to 125	352 to 507 21.6 to 26.2	100 210
SAE 70	**.880 to .935	2,300 to 3,100 125 to 150	507 to 682 26.2 to 31.8	100 210
SAE 10W	**.880 to .935	5,000 to 10,000	1,100 to 2,200	0
SAE 20W	**.880 to .935	10,000 to 40,000	2,200 to 8,800	0
Automobile Transmission Lubricants:				
SAE 80	**.880 to .935	100,000 max	22,000 max	0
SAE 90	**.880 to .935	800 to 1,500 300 to 500	173.2 to 324.7 64.5 to 108.2	100 130
SAE 140	**.880 to .935	950 to 2,300 120 to 200	205.6 to 507 25.1 to 42.9	130 210
SAE 250	**.880 to .935	Over 2,300 Over 200	Over 507 Over 42.9	130 210
Crude Oils:				
Texas, Oklahoma	.81 to .916	40 to 783 34.2 to 210	4.28 to 169.5 2.45 to 45.3	60 100
Wyoming, Montana	.86 to .88	74 to 1,215 46 to 320	14.1 to 263 6.16 to 69.3	60 100
California	.78 to .92	40 to 4,840 34 to 700	4.28 to 1,063 2.4 to 151.5	60 100
Pennsylvania	.8 to .85	46 to 216 38 to 86	6.16 to 46.7 3.64 to 17.2	60 100
Diesel Engine Lubricating Oils (Based on Average Midcontinent Paraffin Base): Federal Specification No. 9110	**.880 to .935	165 to 240 90 to 120	35.4 to 51.9 18.2 to 25.3	100 130

*Unless otherwise noted.

**Depends on origin or percent and type of solvent.

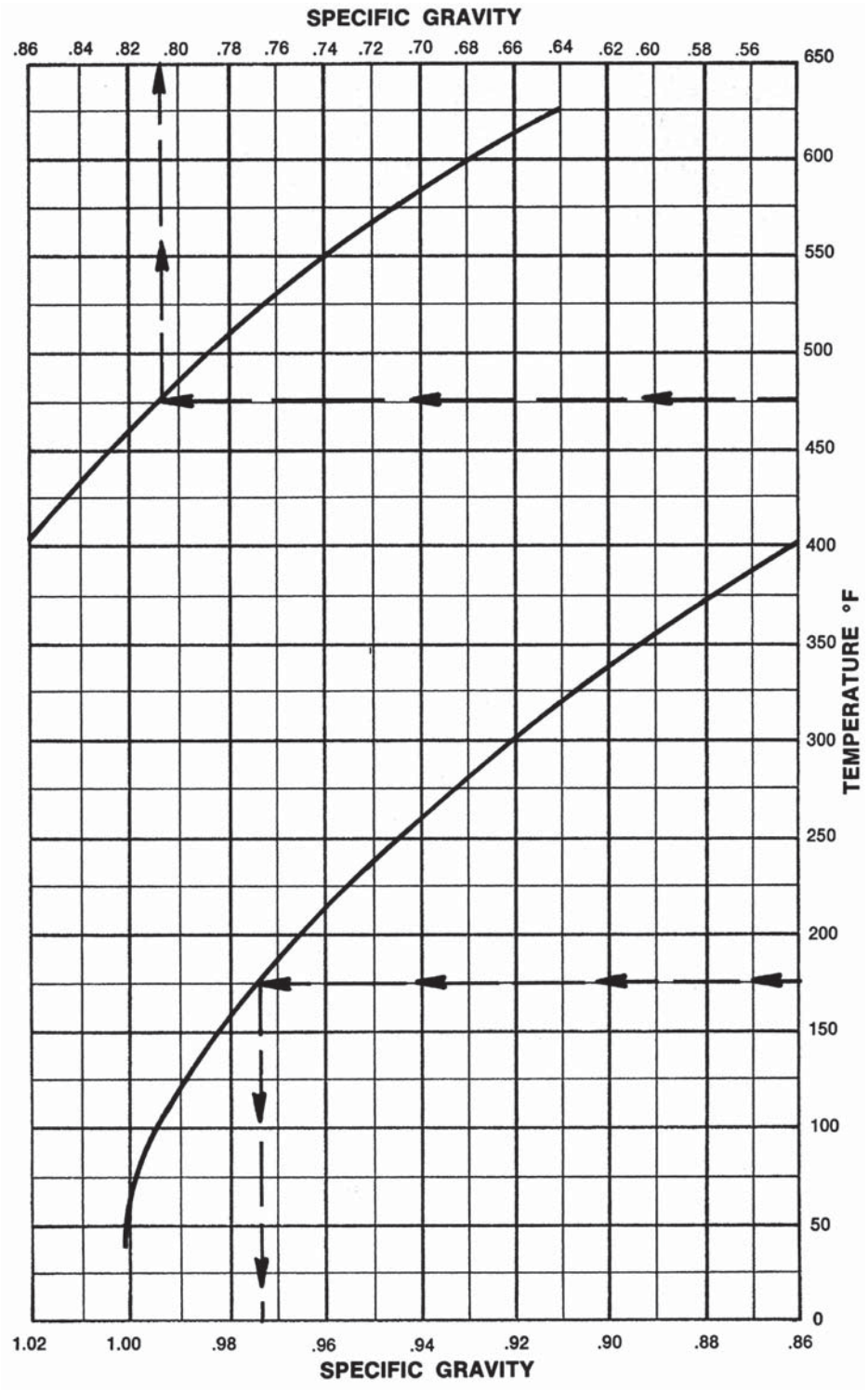


FIG. 2.18 TEMPERATURE EFFECTS ON THE SPECIFIC GRAVITY OF WATER
(Calculated from ASME Steam Tables [51])

TABLE 2.12 BULK MODULUS OF ELASTICITY, RATIO OF SPECIFIC HEATS, AND VELOCITY OF SOUND IN LIQUIDS AT 68°F (Avallone and Baumeister [33])

Liquid	Isothermal (lbf/in.^{2})	Isentropic (lbf/in.^{2})	Speed of sound, c_0 (ft/second)	Cp/Cv
Ethyl alcohol	130,000	155,000	3810	1.19
Benzene	154,000	223,000	4340	1.45
Carbon tetrachloride	139,000	204,000	3080	1.47
Glycerin	654,000	719,000	6510	1.10
Kerosene, SpG = 0.81	188,000	209,000	4390	1.11
Mercury	3,590,000	4,150,000	4770	1.16
Machine oil SpG = 0.907	189,000	219,000	4240	1.13
Water, fresh	316,000	319,000	4860	1.01
Salt water	339,000	344,000	4990	1.01

TABLE 2.13 WATER PROPERTIES (Calculated from ASME Steam Tables [51])

Temp. F	Temp. C	Specific Volume Cu Ft/Lb	SPECIFIC GRAVITY			Wt in Lb/Cu Ft	Vapor Pressure Psi Abs
			39.2 F Reference	60 F Reference	68 F Reference		
32	0	.01602	1.000	1.001	1.002	62.42	0.088
35	1.7	.01602	1.000	1.001	1.002	62.42	0.100
40	4.4	.01602	1.000	1.001	1.002	62.42	0.1217
50	10.0	.01603	.999	1.001	1.002	62.38	0.1781
60	15.6	.01604	.999	1.000	1.001	62.34	0.2563
70	21.1	.01606	.998	.999	1.000	62.27	0.3631
80	26.7	.01608	.996	.998	.999	62.19	0.5069
90	32.2	.01610	.995	.996	.997	62.11	0.6982
100	37.8	.01613	.993	.994	.995	62.00	0.9492
120	48.9	.01620	.989	.990	.991	61.73	1.692
140	60.0	.01629	.983	.985	.986	61.39	2.889
160	71.1	.01639	.977	.979	.979	61.01	4.741
180	82.2	.01651	.970	.972	.973	60.57	7.510
200	93.3	.01663	.963	.964	.966	60.13	11.526
212	100.0	.01672	.958	.959	.960	59.81	14.696
220	104.4	.01677	.955	.956	.957	59.63	17.186
240	115.6	.01692	.947	.948	.949	59.10	24.97
260	126.7	.01709	.938	.939	.940	58.51	35.43
280	137.8	.01726	.928	.929	.930	58.00	49.20
300	148.9	.01745	.918	.919	.920	57.31	67.01
320	160.0	.01765	.908	.909	.910	56.66	89.66
340	171.1	.01787	.896	.898	.899	55.96	118.01
360	182.2	.01811	.885	.886	.887	55.22	153.04
380	193.3	.01836	.873	.874	.875	54.47	195.77
400	204.4	.01864	.859	.860	.862	53.65	247.31
420	215.6	.01894	.846	.847	.848	52.80	308.83
440	226.7	.01926	.832	.833	.834	51.92	381.59
460	237.8	.0196	.817	.818	.819	51.02	466.9
480	248.9	.0200	.801	.802	.803	50.00	566.1
500	260.0	.0204	.785	.786	.787	49.02	680.8
520	271.1	.0209	.765	.766	.767	47.85	812.4
540	282.2	.0215	.746	.747	.748	46.51	962.5
560	293.3	.0221	.726	.727	.728	45.3	1133.1
580	304.4	.0228	.703	.704	.704	43.9	1325.8
600	315.6	.0236	.678	.679	.680	42.3	1542.9
620	326.7	.0247	.649	.650	.650	40.5	1786.6
640	337.8	.0260	.617	.618	.618	38.5	2059.7
660	348.9	.0278	.577	.577	.578	36.0	2365.4
680	360.0	.0305	.525	.526	.527	32.8	2708.1
700	371.1	.0369	.434	.435	.435	27.1	3093.7
705.4	374.1	.0503	.319	.319	.320	19.9	3206.2

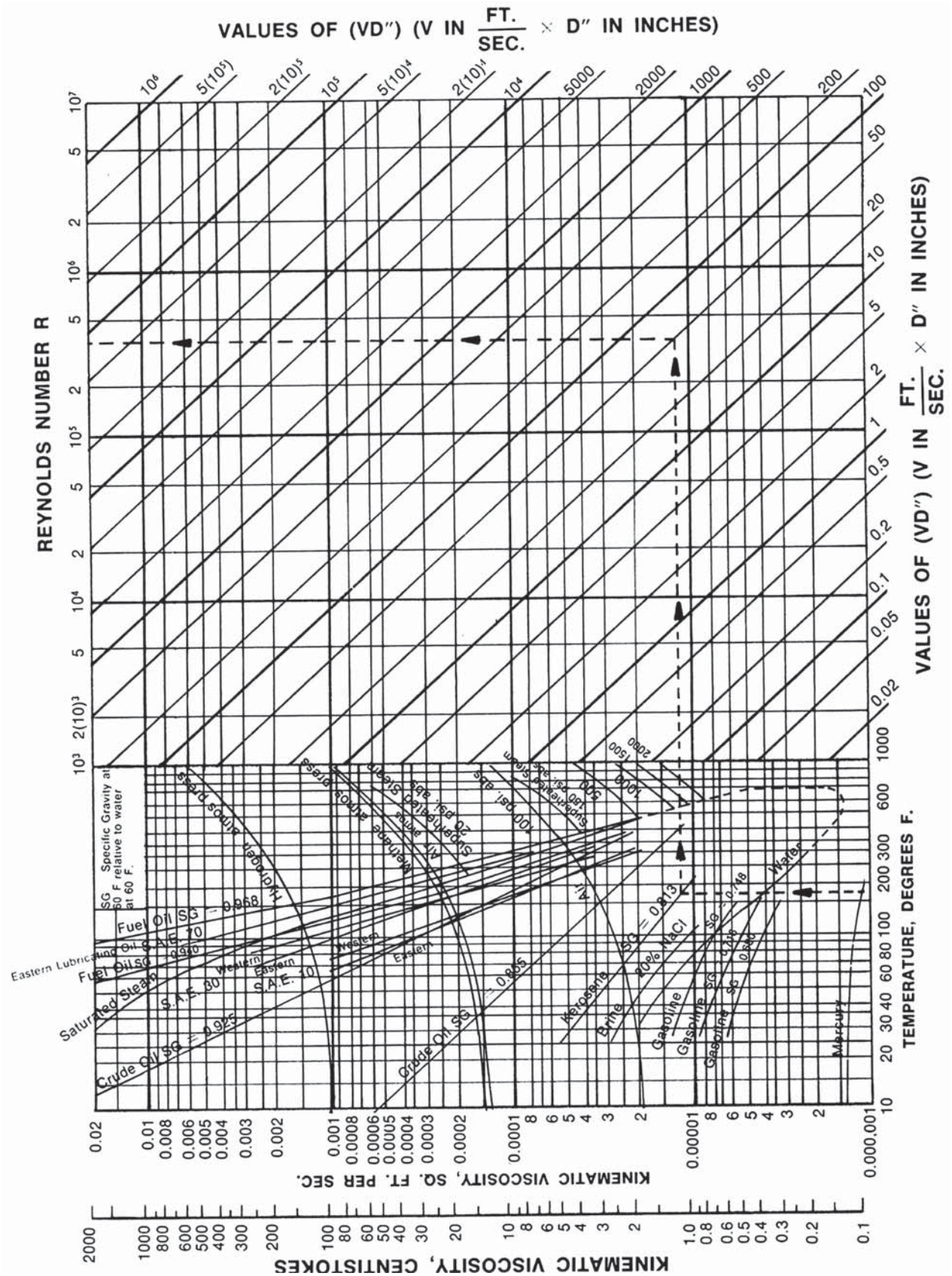


FIG. 2.19 EFFECTS OF VISCOSITY ON REYNOLD'S NUMBER (Moody [37])

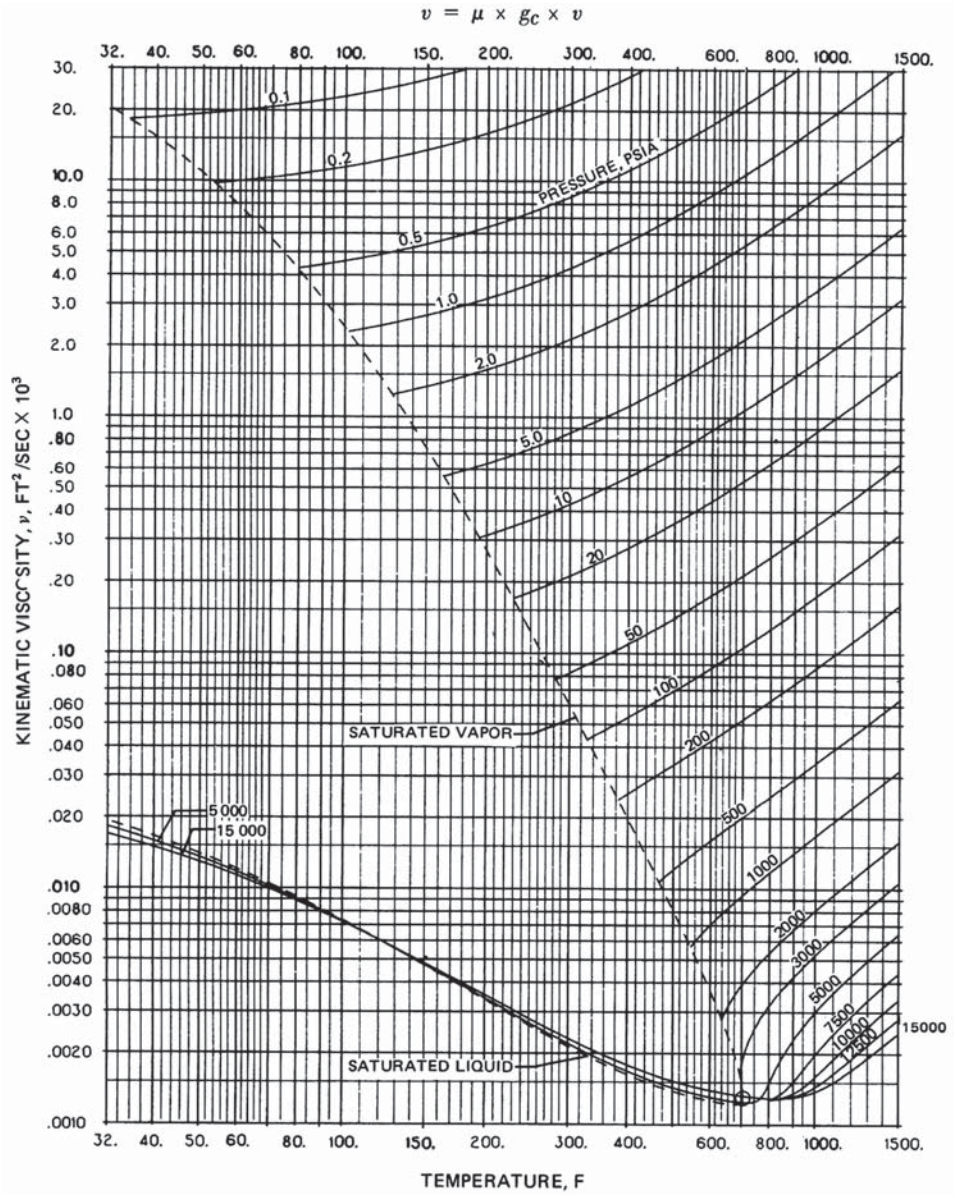


FIG. 2.20 EFFECTS OF PRESSURE AND TEMPERATURE ON THE VISCOSITY OF WATER AND STEAM
(ASME [51])

$$f = 4 \cdot f_n = 8 \cdot \left(\left(\frac{8}{Re} \right)^{12} + \left(\frac{1}{(A' + B')^{1.5}} \right) \right)^{1/12}$$

US, EE, SI (2.48)

where

$$A' = \left(2.457 \cdot \ln \left(\frac{1}{\left(\frac{7}{Re} \right)^{0.9} + \left(\frac{0.27 \cdot \varepsilon}{D} \right)} \right) \right)^{16}$$

US, EE, SI (2.49)

$$B' = \left(\frac{37500}{Re} \right)^{16}$$

US, EE, SI (2.50)

2.3.7 Pipe Friction Losses for Bingham Plastic Fluids and Power Law Fluids

Darby [35] presented friction loss models for both Bingham plastic fluids and power law fluids, which represent pseudoplastic or dilatant fluids. He cautioned that non-Newtonian models may be inadequate if used beyond the range of shear stress and strain rate data used to establish the equations, and he also noted that his

TABLE 2.14 VISCOSITY DATA FOR NOMOGRAPH USE (Perry [48], reprinted by permission of McGraw Hill)

Liquid	X	Y	Liquid	X	Y
Acetaldehyde	15.2	4.8	Freon-113	12.5	11.4
Acetic acid, 100%	12.1	14.2	Glycerol, 100%	2.0	30.0
Acetic acid, 70%	9.5	17.0	Glycerol, 50%	6.9	19.6
Acetic anhydride	12.7	12.8	Heptane	14.1	8.4
Acetone, 100%	14.5	7.2	Hexane	14.7	7.0
Acetone, 35%	7.9	15.0	Hydrochloric acid, 31.5%	13.0	16.6
Acetonitrile	14.4	7.4	Iodobenzene	12.8	15.9
Acrylic acid	12.3	13.9	Isobutyl alcohol	7.1	18.0
Allyl alcohol	10.2	14.3	Isobutyric acid	12.2	14.4
Allyl bromide	14.4	9.6	Isopropyl alcohol	8.2	16.0
Allyl iodide	14.0	11.7	Isopropyl bromide	14.1	9.2
Ammonia, 100%	12.6	2.0	Isopropyl chloride	13.9	7.1
Ammonia, 26%	10.1	13.9	Isopropyl iodide	13.7	11.2
Amyl acetate	11.8	12.5	Kerosene	10.2	16.9
Amyl alcohol	7.5	18.4	Linseed oil, raw	7.5	27.2
Aniline	8.1	18.7	Mercury	18.4	16.4
Anisole	12.3	13.5	Methanol, 100%	12.4	10.5
Arsenic trichloride	13.9	14.5	Methanol, 90%	12.3	11.8
Benzene	12.5	10.9	Methanol, 40%	7.8	15.5
Brine, $CaCl_2$, 25%	6.6	15.9	Methyl acetate	14.2	8.2
Brine, NaCl, 25%	10.2	16.6	Methyl acrylate	13.0	9.5
Bromine	14.2	13.2	Methyl *i*-butyrate	12.3	9.7
Bromotoluene	20.0	15.9	Methyl *n*-butyrate	13.2	10.3
Butyl acetate	12.3	11.0	Methyl chloride	15.0	3.8
Butyl acrylate	11.5	12.6	Methyl ethyl ketone	13.9	8.6
Butyl alcohol	8.6	17.2	Methyl formate	14.2	7.5
Butyric acid	12.1	15.3	Methyl iodide	14.3	9.3
Carbon dioxide	11.6	0.3	Methyl propionate	13.5	9.0
Carbon disulfide	16.1	7.5	Methyl propyl ketone	14.3	9.5
Carbon tetrachloride	12.7	13.1	Methyl sulfide	15.3	6.4
Chlorobenzene	12.3	12.4	Napthalene	7.9	18.1
Chloroform	14.4	10.2	Nitric acid, 95%	12.8	13.8
Chlorosulfonic acid	11.2	18.1	Nitric acid, 60%	10.8	17.0
Chlorotoluene, ortho	13.0	13.3	Nitrobenzene	10.6	16.2
Chlorotoluene, meta	13.3	12.5	Nitrogen dioxide	12.9	8.6
Chlorotoluene, para	13.3	12.5	Nitrotoluene	11.0	17.0
Cresol, meta	2.5	20.8	Octane	13.7	10.0
Cyclohexanol	2.9	24.3	Octyl alcohol	6.6	21.1
Cyclohexane	9.8	12.9	Pentachloroethane	10.9	17.3
Dibromomethane	12.7	15.8	Pentane	14.9	5.2
Dichloroethane	13.2	12.2	Phenol	6.9	20.8
Dichloromethane	14.6	8.9	Phosphorus tribromide	13.8	16.7
Diethyl ketone	13.5	9.2	Phosphorus trichloride	16.2	10.9
Diethyl oxalate	11.0	16.4	Propionic acid	12.8	13.8
Diethylene glycol	5.0	24.7	Propyl acetate	13.1	10.3
Diphenyl	12.0	18.3	Propyl alcohol	9.1	16.5
Dipropyl ether	13.2	8.6	Propyl bromide	14.5	9.6
Dipropyl oxalate	10.3	17.7	Propyl chloride	14.4	7.5
Ethyl acetate	13.7	9.1	Propyl formate	13.1	9.7
Ethyl acrylate	12.7	10.4	Propyl iodide	14.1	11.6
Ethyl alcohol, 100%	10.5	13.8	Sodium	16.4	13.9
Ethyl alcohol, 95%	9.8	14.3	Sodium hydroxide, 50%	3.2	25.8
Ethyl alcohol, 40%	6.5	16.6	Stannic chloride	13.5	12.8
Ethyl benzene	13.2	11.5	Succinonitrile	10.1	20.8
Ethyl bromide	14.5	8.1	Sulfur dioxide	15.2	7.1
2-Ethyl butyl acrylate	11.2	14.0	Sulfuric acid, 110%	7.2	27.4
Ethyl chloride	14.8	6.0	Sulfuric acid, 100%	8.0	25.1
Ethyl ether	14.5	5.3	Sulfuric acid, 98%	7.0	24.8
Ethyl formate	14.2	8.4	Sulfuric acid, 60%	10.2	21.3
2-Ethyl hexyl acrylate	9.0	15.0	Sulfuryl chloride	15.2	12.4
Ethyl iodide	14.7	10.3	Tetrachloroethane	11.9	15.7
Ethyl propionate	13.2	9.9	Thiophene	13.2	11.0
Ethyl propyl ether	14.0	7.0	Titanium tetrachloride	14.4	12.3
Ethyl sulfide	13.8	8.9	Toluene	13.7	10.4
Ethylene bromide	11.9	15.7	Trichloroethylene	14.8	10.5
Ethylene chloride	12.7	12.2	Triethylene glycol	4.7	24.8
Ethylene glycol	6.0	23.6	Turpentine	11.5	14.9
Ethylidene chloride	14.1	8.7	Vinyl acetate	14.0	8.8
Fluorobenzene	13.7	10.4	Vinyl toluene	13.4	12.0
Formic acid	10.7	15.8	Water	10.2	13.0
Freon-11	14.4	9.0	Xylene, ortho	13.5	12.1
Freon-12	16.8	5.6	Xylene, meta	13.9	10.6
Freon-21	15.7	7.5	Xylene, para	13.9	10.9
Freon-22	17.2	4.7			

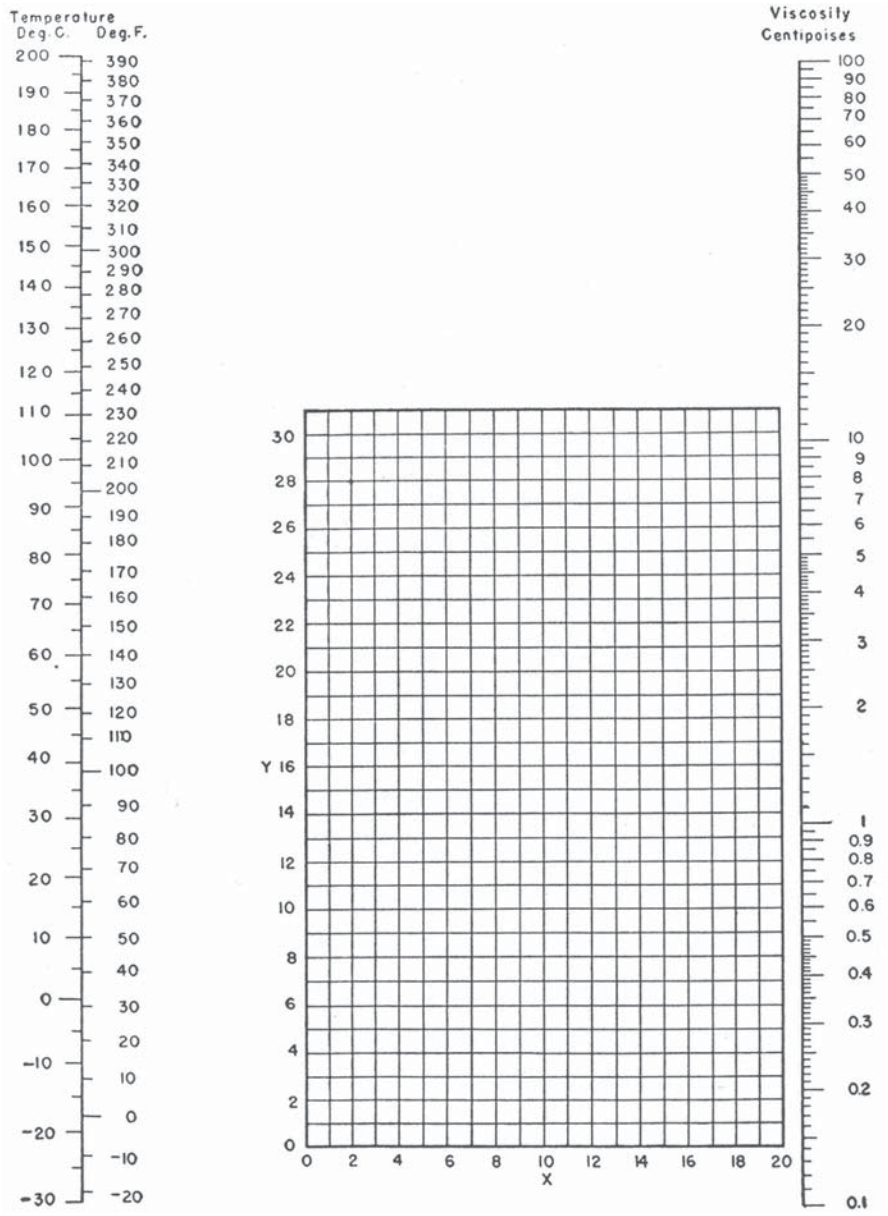


FIG. 2.21 NOMOGRAPH FOR LIQUID VISCOSITIES (Perry [48], reprinted by permission of McGraw Hill)

equations for non-Newtonian fluids assume that the pipes have smooth walls. The reader is referred to his text for further discussion and examples to calculate friction factors for non-Newtonian fluids. However, the equations he presented for laminar and turbulent friction factors for flow in smooth tubes follow.

For power law fluids, the Darcy friction factor is defined by

$$f = 4 \cdot f_n = 4 \cdot \left[\left(1 - \left(\frac{1}{1 + 4^{Re_{pl} - 2100 - 875 \cdot (1-n)}} \right) \right) \cdot f'_L + \frac{1}{\left(1 + 4^{Re_{pl} - 2100 - 875 \cdot (1-n)} \right) \cdot \left(f'^{-8}_T + f'^{-8}_{Tr} \right)^{1/8}} \right]$$

US, EE, SI (2.51)

where f'_L is the Fanning friction factor for laminar flow, and f'_T and f'_{Tr} are turbulent Fanning friction factors in different flow ranges. The Reynold's number for a power law fluid is defined as

TABLE 2.15 PRESSURE DROPS FOR WATER FLOW IN STEEL PIPE (Reprinted by permission from Crane, Inc. [21])

Flow of Water Through Schedule 40 Steel Pipe

Discharge		Pressure Drop per 100 feet and Velocity in Schedule 40 Pipe for Water at 60 F.															
		Veloc- ity	Press. Drop	Veloc- ity	Press. Drop	Veloc- ity	Press. Drop	Veloc- ity	Press. Drop	Veloc- ity	Press. Drop	Veloc- ity	Press. Drop	Veloc- ity	Press. Drop	Veloc- ity	Press. Drop
Gallons per Minute	Cubic Ft. per Second	Feet per Second	Lbs. per Sq. In.	Feet per Second	Lbs. per Sq. In.	Feet per Second	Lbs. per Sq. In.	Feet per Second	Lbs. per Sq. In.	Feet per Second	Lbs. per Sq. In.	Feet per Second	Lbs. per Sq. In.	Feet per Second	Lbs. per Sq. In.	Feet per Second	Lbs. per Sq. In.
		1/8"		1/4"		3/8"		1/2"									
.2	0.000446	1.13	1.86	0.616	0.359												
.3	0.000668	1.69	4.22	0.924	0.903	0.504	0.159	0.317	0.061	3/4"							
.4	0.000891	2.26	6.98	1.23	1.61	0.672	0.345	0.422	0.086								
.5	0.00111	2.82	10.5	1.54	2.39	0.840	0.539	0.528	0.167	0.301	0.033						
.6	0.00134	3.39	14.7	1.85	3.29	1.01	0.751	0.633	0.240	0.361	0.041	1"		1¼"			
.8	0.00178	4.52	25.0	2.46	5.44	1.34	1.25	0.844	0.408	0.481	0.102					1½"	
1	0.00223	5.65	37.2	3.08	8.28	1.68	1.85	1.06	0.600	0.602	0.155	0.371	0.048				
2	0.00446	11.29	134.4	6.16	30.1	3.36	6.58	2.11	2.10	1.20	0.526	0.743	0.164	0.429	0.044		
3	0.00668			9.25	64.1	5.04	13.9	3.17	4.33	1.81	1.09	1.114	0.336	0.644	0.090	0.473	0.043
4	0.00891	2"		12.33	111.2	6.72	23.9	4.22	7.42	2.41	1.83	1.49	0.565	0.858	0.150	0.630	0.071
5	0.01114					8.40	36.7	5.28	11.2	3.01	2.75	1.86	0.835	1.073	0.223	0.788	0.104
6	0.01337	0.574	0.044	2½"		10.08	51.9	6.33	15.8	3.61	3.84	2.23	1.17	1.29	0.309	0.946	0.145
8	0.01782	0.765	0.073			13.44	91.1	8.45	27.7	4.81	6.60	2.97	1.99	1.72	0.518	1.26	0.241
10	0.02228	0.956	0.108	0.670	0.046			10.56	42.4	6.02	9.99	3.71	2.99	2.15	0.774	1.58	0.361
15	0.03342	1.43	0.224	1.01	0.094	3"				9.03	21.6	5.57	6.36	3.22	1.63	2.37	0.755
20	0.04456	1.91	0.375	1.34	0.158	0.868	0.056	3½"		12.03	37.8	7.43	10.9	4.29	2.78	3.16	1.28
25	0.05570	2.39	0.561	1.68	0.234	1.09	0.083	0.812	0.041	4"		9.28	16.7	5.37	4.22	3.94	1.93
30	0.06684	2.87	0.786	2.01	0.327	1.30	0.114	0.974	0.056			11.14	23.8	6.44	5.92	4.73	2.72
35	0.07798	3.35	1.05	2.35	0.436	1.52	0.151	1.14	0.071	0.882	0.041	12.99	32.2	7.51	7.90	5.52	3.64
40	0.08912	3.83	1.35	2.68	0.556	1.74	0.192	1.30	0.095	1.01	0.052	14.85	41.5	8.59	10.24	6.30	4.65
45	0.1003	4.30	1.67	3.02	0.668	1.95	0.239	1.46	0.117	1.13	0.064			9.67	12.80	7.09	5.85
50	0.1114	4.78	2.03	3.35	0.839	2.17	0.288	1.62	0.142	1.26	0.076	5"		10.74	15.66	7.88	7.15
60	0.1337	5.74	2.87	4.02	1.18	2.60	0.406	1.95	0.204	1.51	0.107			12.89	22.2	9.47	10.21
70	0.1560	6.70	3.84	4.69	1.59	3.04	0.540	2.27	0.261	1.76	0.143	1.12	0.047			11.05	13.71
80	0.1782	7.65	4.97	5.36	2.03	3.47	0.687	2.60	0.334	2.02	0.180	1.28	0.060			12.62	17.59
90	0.2005	8.60	6.20	6.03	2.53	3.91	0.861	2.92	0.416	2.27	0.224	1.44	0.074	6"		14.20	22.0
100	0.2228	9.56	7.59	6.70	3.09	4.34	1.05	3.25	0.509	2.52	0.272	1.60	0.090	1.11	0.036	15.78	26.9
125	0.2785	11.97	11.76	8.38	4.71	5.43	1.61	4.06	0.769	3.15	0.415	2.01	0.135	1.39	0.055	19.72	41.4
150	0.3342	14.36	16.70	10.05	6.69	6.51	2.24	4.87	1.08	3.78	0.580	2.41	0.190	1.67	0.077		
175	0.3899	16.75	22.3	11.73	8.97	7.60	3.00	5.68	1.44	4.41	0.774	2.81	0.253	1.94	0.102		
200	0.4456	19.14	28.8	13.42	11.68	8.68	3.87	6.49	1.85	5.04	0.985	3.21	0.323	2.22	0.130	8"	
225	0.5013	...	...	15.09	14.63	9.77	4.83	7.30	2.32	5.67	1.23	3.61	0.401	2.50	0.162	1.44	0.043
250	0.557	...	...	...	...	10.85	5.93	8.12	2.84	6.30	1.46	4.01	0.495	2.78	0.195	1.60	0.051
275	0.6127	...	...	...	...	11.94	7.14	8.93	3.40	6.93	1.79	4.41	0.583	3.05	0.234	1.76	0.061
300	0.6684	...	...	...	...	13.00	8.36	9.74	4.02	7.56	2.11	4.81	0.683	3.33	0.275	1.92	0.072
325	0.7241	...	...	...	...	14.12	9.89	10.53	4.09	8.19	2.47	5.21	0.797	3.61	0.320	2.08	0.083
350	0.7798			...	...	...	...	11.36	5.41	8.82	2.84	5.62	0.919	3.89	0.367	2.24	0.095
375	0.8355			...	...	...	...	12.17	6.18	9.45	3.25	6.02	1.05	4.16	0.416	2.40	0.108
400	0.8912			...	...	...	...	12.98	7.03	10.08	3.68	6.42	1.19	4.44	0.471	2.56	0.121
425	0.9469			...	...	...	...	13.80	7.89	10.71	4.12	6.82	1.33	4.72	0.529	2.73	0.136
450	1.003	10"		...	...	...	...	14.61	8.80	11.34	4.60	7.22	1.48	5.00	0.590	2.89	0.151
475	1.059	1.93	0.054			...	...	...	...	11.97	5.12	7.62	1.64	5.27	0.653	3.04	0.166
500	1.114	2.03	0.059			...	...	...	...	12.60	5.65	8.02	1.81	5.55	0.720	3.21	0.182
550	1.225	2.24	0.071			...	...	...	...	13.85	6.79	8.82	2.17	6.11	0.861	3.53	0.219
600	1.337	2.44	0.083			...	...	...	...	15.12	8.04	9.63	2.55	6.66	1.02	3.85	0.258
650	1.448	2.64	0.097	12"		...	...	...	...	...	...	10.43	2.98	7.22	1.18	4.17	0.301
700	1.560	2.85	0.112	2.01	0.047			...	...	...	...	11.23	3.43	7.78	1.35	4.49	0.343
750	1.671	3.05	0.127	2.15	0.054	14"		...	...	...	...	12.03	3.92	8.33	1.55	4.81	0.392
800	1.782	3.25	0.143	2.29	0.061			...	...	...	...	12.83	4.43	8.88	1.75	5.13	0.443
850	1.894	3.46	0.160	2.44	0.068	2.02	0.042	...	...	...	...	13.64	5.00	9.44	1.96	5.45	0.497
900	2.005	3.66	0.179	2.58	0.075	2.13	0.047	...	...	...	...	14.44	5.58	9.99	2.18	5.77	0.554
950	2.117	3.86	0.198	2.72	0.083	2.25	0.052			...	...	15.24	6.21	10.55	2.42	6.09	0.613
1 000	2.228	4.07	0.218	2.87	0.091	2.37	0.057	16"		...	...	16.04	6.84	11.10	2.68	6.41	0.675
1 100	2.451	4.48	0.260	3.15	0.110	2.61	0.068			...	...	17.65	8.23	12.22	3.22	7.05	0.807
1 200	2.674	4.88	0.306	3.44	0.128	2.85	0.080	2.18	0.042	...	...	...	...	13.33	3.81	7.70	0.948
1 300	2.896	5.29	0.355	3.73	0.150	3.08	0.093	2.36	0.048	...	...	...	...	14.43	4.45	8.33	1.11
1 400	3.119	5.70	0.409	4.01	0.171	3.32	0.107	2.54	0.055					15.55	5.13	8.98	1.28
1 500	3.342	6.10	0.466	4.30	0.195	3.56	0.122	2.72	0.063	18"				16.66	5.85	9.62	1.46
1 600	3.565	6.51	0.527	4.59	0.219	3.79	0.138	2.90	0.071					17.77	6.61	10.26	1.65
1 800	4.010	7.32	0.663	5.16	0.276	4.27	0.172	3.27	0.088	2.58	0.050			19.99	8.37	11.54	2.08
2 000	4.456	8.14	0.808	5.73	0.339	4.74	0.209	3.63	0.107	2.87	0.060	20"		22.21	10.3	12.82	2.55
2 500	5.570	10.17	1.24	7.17	0.515	5.93	0.321	4.54	0.163	3.59	0.091					16.03	3.94
3 000	6.684	12.20	1.76	8.60	0.731	7.11	0.451	5.45	0.232	4.30	0.129	3.46	0.075	24"		19.24	5.59
3 500	7.798	14.24	2.38	10.03	0.982	8.30	0.607	6.35	0.312	5.02	0.173	4.04	0.101			22.44	7.56
4 000	8.912	16.27	3.08	11.47	1.27	9.48	0.787	7.26	0.401	5.74	0.222	4.62	0.129	3.19	0.052	25.65	9.80
4 500	10.03	18.31	3.87	12.90	1.60	10.67	0.990	8.17	0.503	6.46	0.280	5.20	0.162	3.59	0.065	28.87	12.2
5 000	11.14	20.35	4.71	14.33	1.95	11.85	1.21	9.08	0.617	7.17	0.340	5.77	0.199	3.99	0.079	...	...
6 000	13.37	24.41	6.74	17.20	2.77	14.23	1.71	10.89	0.877	8.61	0.483	6.93	0.280	4.79	0.111	...	...
7 000	15.60	28.49	9.11	20.07	3.74	16.60	2.31	12.71	1.18	10.04	0.652	8.08	0.376	5.59	0.150	...	...
8 000	17.82	...	...	22.93	4.84	18.96	2.99	14.52	1.51	11.47	0.839	9.23	0.488	6.38	0.192	...	...
9 000	20.05	...	...	25.79	6.09	21.34	3.76	16.34	1.90	12.91	1.05	10.39	0.608	7.18	0.242	...	...
10 000	22.28	...	...	28.66	7.46	23.71	4.61	18.15	2.34	14.34	1.28	11.54	0.739	7.98	0.294	...	...
12 000	26.74	...	...	34.40	10.7	28.45	6.59	21.79	3.33	17.21	1.83	13.85	1.06	9.58	0.416	...	...
14 000	31.19	...	...	...	...	33.19	8.89	25.42	4.49	20.08	2.45	16.16	1.43	11.17	0.562	...	...
16 000	35.65	...	...	...	...	...	...	29.05	5.83	22.95	3.18	18.47	1.85	12.77	0.723	...	...
18 000	40.10	...	...	...	...	...	...	32.68	7.31	25.82	4.03	20.77	2.32	14.36	0.907	...	...
20 000	44.56	...	...	...	...	...	...	36.31	9.03	28.69	4.93	23.08	2.86	15.96	1.12	...	...

For pipe lengths other than 100 feet, the pressure drop is proportional to the length. Thus, for 50 feet of pipe, the pressure drop is approximately one-half the value given in the table . . . for 300 feet, three times the given value, etc.

Velocity is a function of the cross sectional flow area; thus, it is constant for a given flow rate and is independent of pipe length.

TABLE 2.16 FRICTION FACTORS FOR AGING STEEL PIPE (Karassik [53])

Age, years	D	f_H
0	>12	120
0	8	119
0	4	118
5	>24	113
5	12	111
5	4	107
15	>24	100
15	12	96
15	4	89
25	16	87
25	4	75
35	>30	83
35	16	80
35	4	64

$$Re_{pl} = \frac{8 \cdot D^n \cdot V^{2-n} \cdot \rho}{m' \cdot \left(\frac{2 \cdot (3 \cdot n + 1)}{n} \right)^n} \qquad \text{SI (2.52)}$$

$$Re_{pl} = \frac{8 \cdot D^n \cdot V^{2-n} \cdot \rho}{g_c \cdot m' \cdot \left(\frac{2 \cdot (3 \cdot n + 1)}{n} \right)^n} \qquad \text{EE (2.53)}$$

$$Re_{pl} = \frac{D^n(\text{in}^n) \cdot V^{2-n}((\text{ft/second})^{2-n}) \cdot \rho(\text{lbm/ft}^3)}{6949.6 \cdot m'(\text{psi} \cdot \text{second}^n) \cdot \left(\frac{2 \cdot (3 \cdot n + 1)}{n} \right)^n} \qquad \text{US (2.54)}$$

Additional required terms are

$$f'_L = \frac{16}{Re_{pl}} \qquad \text{US, EE, SI (2.55)}$$

$$f'_T = \frac{0.0682 \cdot n^{-1/2}}{RE_{pl}^{1/(1.87+2.39 \cdot n)}} \qquad \text{US, EE, SI (2.56)}$$

$$f'_{Tr} = 1.79 \cdot 10^{-4} \cdot \exp(-5.24 \cdot n) \cdot Re_{pl}^{0.414+0.757 \cdot n} \qquad \text{US, EE, SI (2.57)}$$

For Bingham plastic fluids, the friction factor is expressed in terms of the laminar Fanning friction factor, f'_L, and the turbulent Fanning friction factor, f'_T, as

$$f = 4 \cdot f'_n = \left(f'^{\left(1.7+\frac{40000}{Re}\right)}_L + f'^{\left(1.7+\frac{40000}{Re}\right)}_T \right)^{1/\left(1.7+\frac{40000}{Re}\right)} \qquad \text{US, EE, SI (2.58)}$$

where the Reynold's number is calculated in the same as that used for Newtonian flow (Eqs. (2.40) and (2.41)). Additional terms required to define the friction factors are expressed as

$$f'_T = \frac{10^{\left(-1.47 \cdot \left(1+0.146 \cdot \exp\left(-2.9 \cdot 10^{-5} \cdot He\right)\right)\right)}}{Re^{0.193}} \qquad \text{US, EE, SI (2.59)}$$

$$f'_L = \frac{16}{Re} \cdot \left(1 + \frac{He}{6 \cdot Re} - \frac{He^4}{3 \cdot \left(f'^3_L\right) \cdot Re^7} \right) \qquad \text{US, EE, SI (2.60)}$$

$$He = \frac{D^2 \cdot \tau_0' \cdot \rho}{g_c \cdot \mu^2} \qquad \text{US, EE (2.61)}$$

$$He = \frac{D^2 \cdot \tau_0' \cdot \rho}{\mu^2} \qquad \text{SI (2.62)}$$

Bingham plastic fluids require not only a required velocity to maintain flow, but the pump must provide sufficient energy to overcome the yield stress on pump restart. Specifically, an empty pipe may be initially filled since the shear stress at the pipe wall increases as the pipe volume is gradually filled from an empty condition, but on restart, the pumps needs to overcome the yield stress along the entire pipe line, and flow may, or may not, be reinitiated, and if not, the pipe may be permanently plugged.

These equations for friction factors, f and f_n, Hedstrom numbers, He, and Reynold's numbers, Re, can be used to iterate flow rates in pipe systems, but these equations demonstrate the increased complexity of non-Newtonian fluids. Again, example calculations for steady state flow are available in Darby's text [35].

2.3.8 Friction Losses in Series Pipes

There are two equations required for series pipes. One relates the volumetric flow rates in the two pipe sections, and the other relates the friction factors to the head loss. The volumetric flow rate for a constant density fluid in a pipe is obtained from conservation of mass by simply rewriting Eq. (2.7).

$$V_1 = \frac{A_2}{A_1} \cdot V_2 \qquad \text{US, EE, SI (2.63)}$$

From conservation of mass and momentum, the resistance coefficients for series pipes are related by

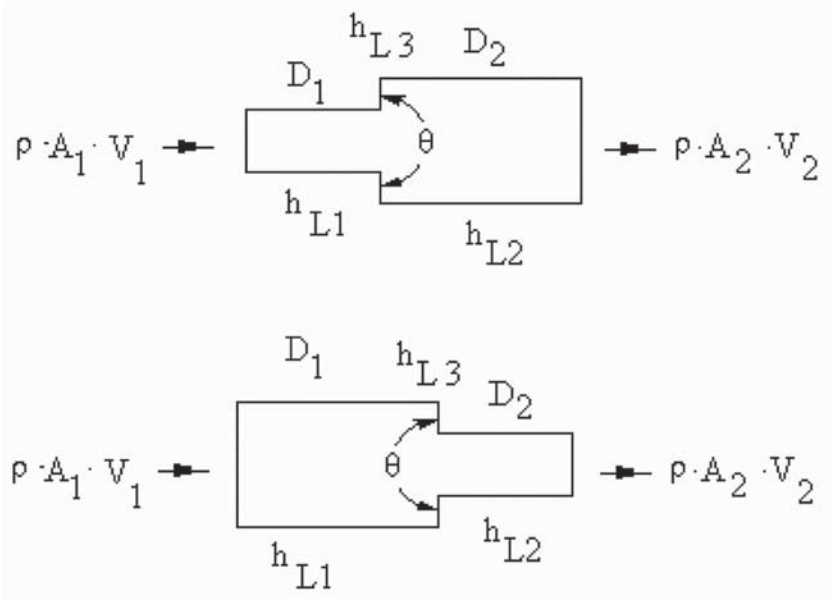


FIG. 2.22 FLOW IN SERIES PIPES

$$K_1 = K_2 \cdot \left(\frac{D_2}{D_1}\right)^4 \quad \text{US, EE, SI (2.64)}$$

This equation describes the relationship between pipe friction for the two series pipes shown in Fig. 2.22 and friction losses at the change in diameter. The total friction loss, h_L, equals the sum of the friction losses for the two pipe sections, h_{L1}, h_{L2} plus the friction loss at the change in pipe diameter, h_{L3}.

$$h_L = h_{L1} + h_{L2} + h_{L3} \quad \text{US, EE, SI (2.65)}$$

Example 2.8 Series pipes

Using Fig. 2.23, find the flow rate, neglecting the friction losses of the reducer, the pipe entrance, and the pipe exit. Using Eq. (2.64)

$$K_3 = K_2 \cdot \left(\frac{D_3}{D_2}\right)^4 = K_2 \cdot \left(\frac{2.067}{3.068}\right)^4 = K_2 \cdot 0.206$$

where K_2 and K_3 are the resistance coefficients for the 2- and 3-in. diameter pipes. Having related K for the two pipes, Churchill's equation or Moody's friction factor charts may be used, or the friction loss tables for water may be used to find the flow rate, since K values are proportional, where

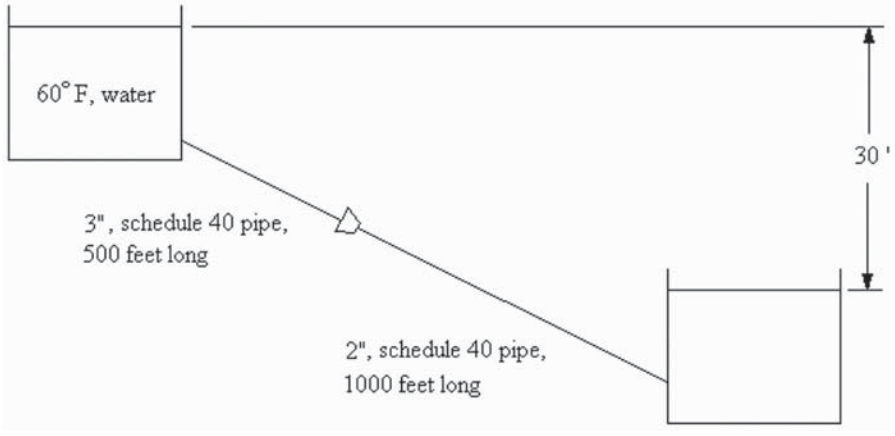


FIG. 2.23 SERIES PIPES

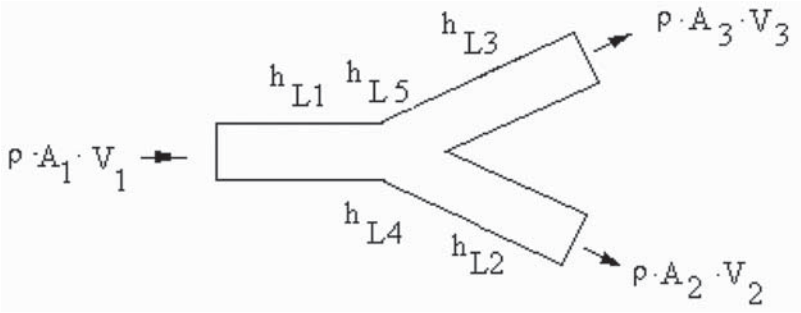


FIG. 2.24 FLOW IN PARALLEL PIPES

$$K_{\text{total}} = K_2 + K_2 \cdot 0.206 \cdot \frac{500\text{ ft}}{1000\text{ ft}} = 1.103 \cdot K_2$$

such that the system pipe length is equivalent to 1.103 · 1000 ft = 1103 ft of 2-in. pipe. The pressure drop equals 30 ft/2.31 ft/psi = 12.98 psi, or 12.98 psi · 100 /(1103 ft) = 1.177 psi pressure drop per 100 ft of 2-in. pipe. Extrapolating from Table 2.15, the flow rate is 37.1 gpm. The error due to neglecting the fittings is minor for this case of a few fitting losses on a long pipeline (<1%). The reader is strongly referred to Crane [21] for several detailed examples of flow rate calculations.

2.3.9 Flow and Friction Losses in Parallel Pipes

Both flow rates and friction losses are required to describe flow in parallel pipes. For a constant density fluid, the volumetric flow rate obtained from Fig. 2.24 can be expressed as

$$A_1 \cdot V_1 = A_2 \cdot V_2 + A_3 \cdot V_3 \quad \text{US, EE, SI (2.66)}$$

The friction losses in parallel flow may be expressed in an equation that is analogous to electrical flow through resistors, in the form

$$h_L = h_{L1} + \frac{1}{\frac{1}{h_{L4} + h_{L2}} + \frac{1}{h_{L5} + h_{L3}}} \quad \text{US, EE, SI (2.67)}$$

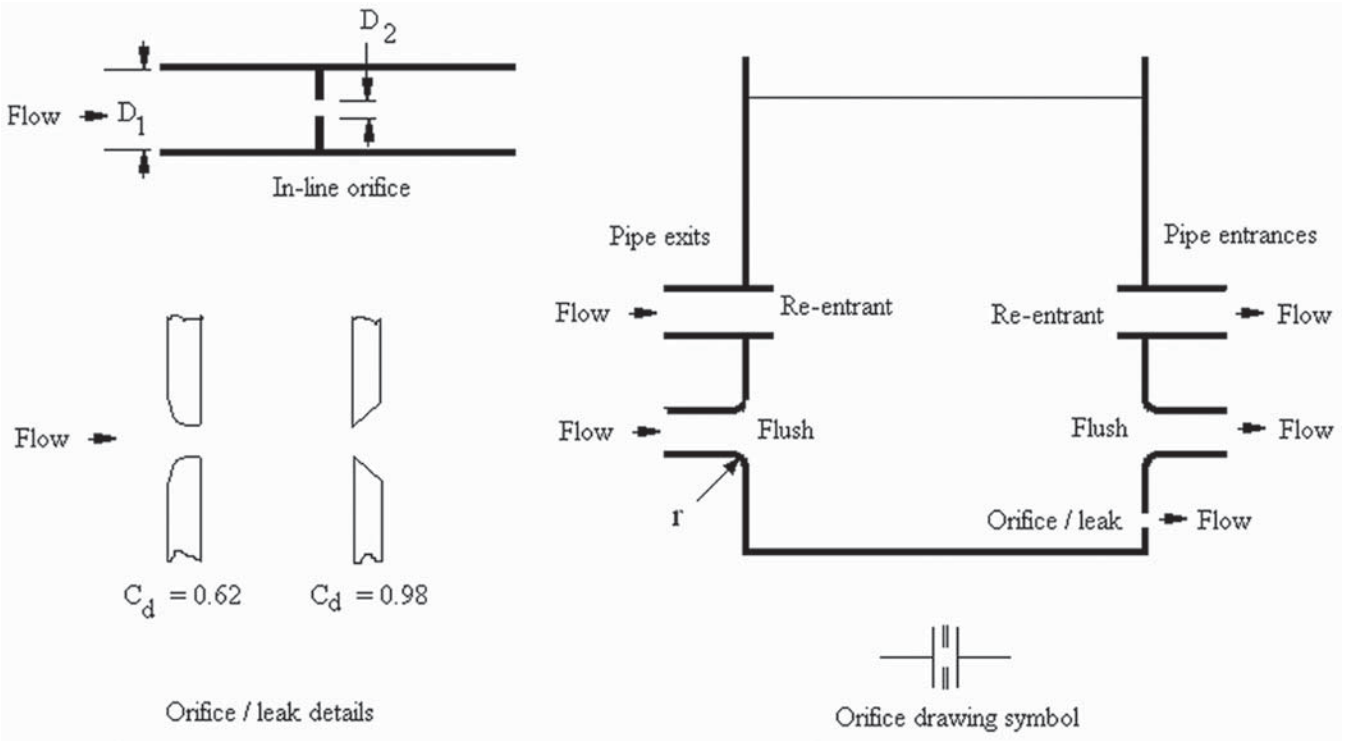


FIG. 2.25 ORIFICES, PIPE INLETS, AND PIPE EXITS

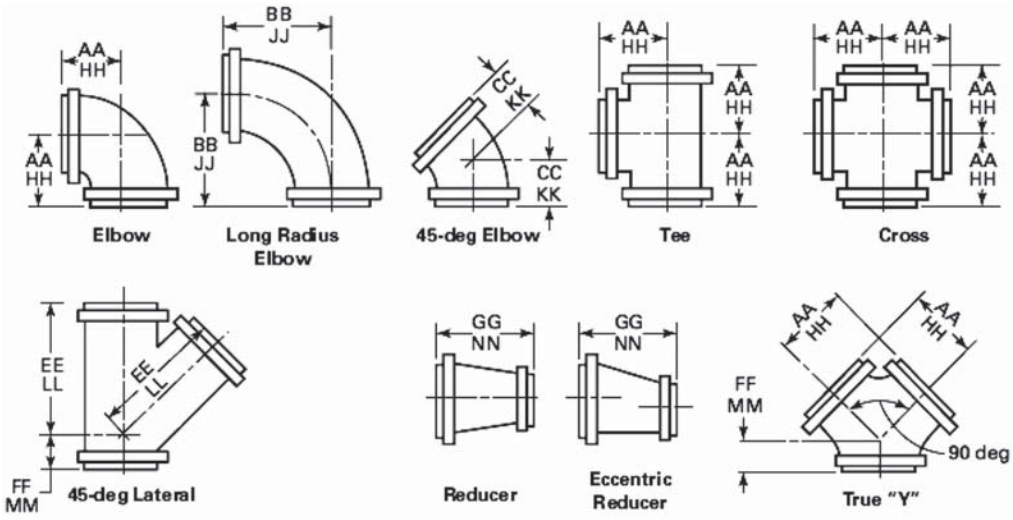


FIG. 2.26 DIMENSIONS FOR FLANGED FITTINGS (DIMENSION JJ = *r* FOR USE WITH FRICTION FACTORS) (ASME B16.5-2003 [60])

where h_L is again the total friction loss; h_{L1}, h_{L2}, and h_{L3} are the pipe friction losses shown in Fig. 2.24; and h_{L4} and h_{L5} are the friction losses of the fittings at the pipe intersection. Miller [56] also provides graphic solutions for parallel pipes.

2.3.10 Inlets, Outlets, and Orifices

Fig. 2.25 provides descriptions for orifices, pipe entrances, and pipe exits. Friction factors for inlets, outlets, and in-line orifices are provided below in Table 2.29. Calculations for a simple leak from a pipe or a tank are expressed in terms of Bernoulli's equation as (Lindeburg [57])

$$Q = C_d \cdot \sqrt{2 \cdot g \cdot P} \qquad \text{EE, SI (2.68)}$$

where P is the internal pressure at the leak site.

2.3.11 Fitting Construction

Before friction losses in valves and fittings may be considered, descriptions of these components are required. Considering fittings first, dimensions are defined for reducers, elbows, returns, crosses, and tees for welded, threaded, and flanged fittings for carbon steel, alloy steel, stainless

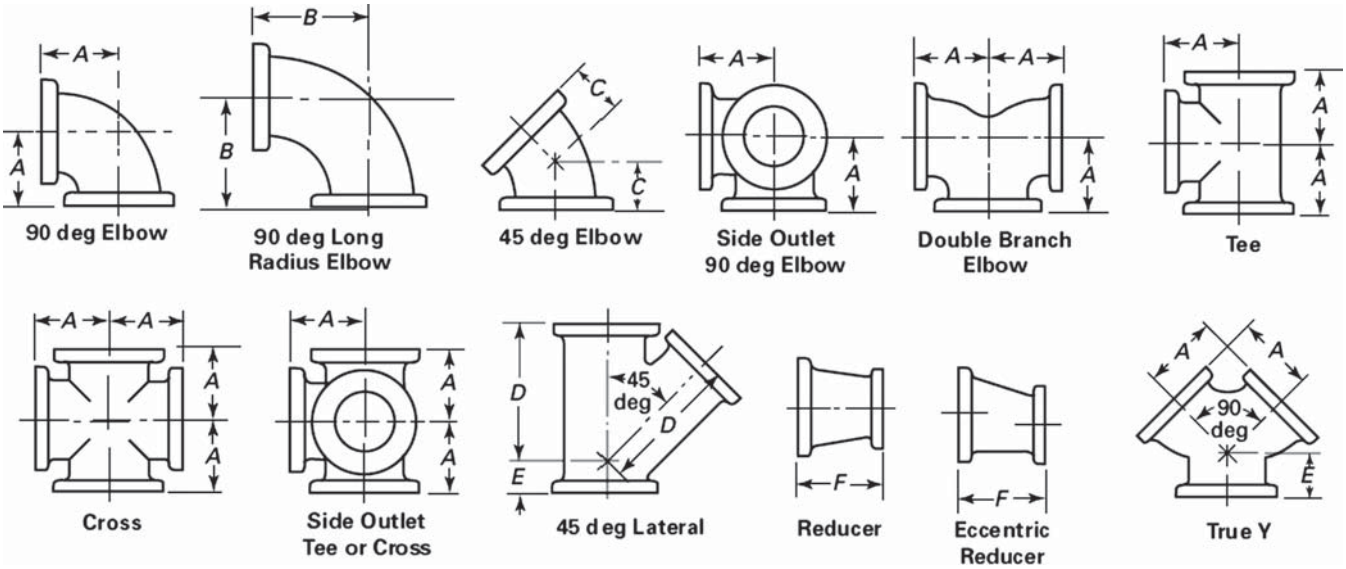
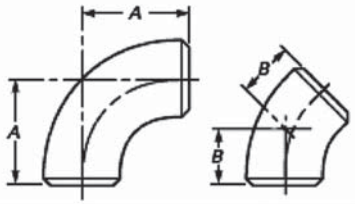


FIG. 2.27 DUCTILE IRON FLANGED FITTING DIMENSIONS (DIMENSION *B* = *r* FOR USE WITH FRICTION FACTORS) (ASME B16.42-1998 [61])

TABLE 2.17 WROUGHT BUTT WELDED ELBOWS (DIMENSION A = *r* FOR USE WITH FRICTION FACTORS)

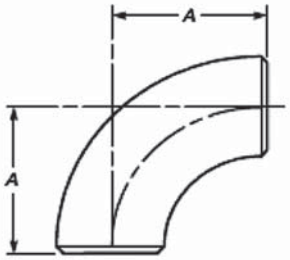
(ASME B16.9-2007 [58])

Dimensions of Long Radius Elbows



Nominal Pipe Size (NPS)	Outside Diameter at Bevel	Center-to-End	
		90-deg Elbows, *A*	45-deg Elbows, *B*
½	0.84	1.50	0.62
¾	1.05	1.50	0.75
1	1.32	1.50	0.88
1¼	1.66	1.88	1.00
1½	1.90	2.25	1.12
2	2.38	3.00	1.38
2½	2.88	3.75	1.75
3	3.50	4.50	2.00
3½	4.00	5.25	2.25
4	4.50	6.00	2.50
5	5.56	7.50	3.12
6	6.62	9.00	3.75
8	8.62	12.00	5.00
10	10.75	15.00	6.25
12	12.75	18.00	7.50
14	14.00	21.00	8.75
16	16.00	24.00	10.00
18	18.00	27.00	11.25
20	20.00	30.00	12.50
22	22.00	33.00	13.50
24	24.00	36.00	15.00
26	26.00	39.00	16.00
28	28.00	42.00	17.25
30	30.00	45.00	18.50
32	32.00	48.00	19.75
34	34.00	51.00	21.00
36	36.00	54.00	22.25
38	38.00	57.00	23.62
40	40.00	60.00	24.88
42	42.00	63.00	26.00
44	44.00	66.00	27.38
46	46.00	69.00	28.62
48	48.00	72.00	29.88

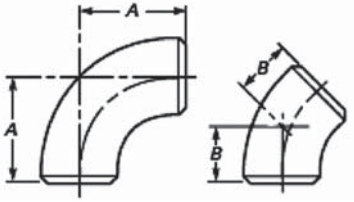
Dimensions of Short Radius Elbows



Nominal Pipe Size (NPS)	Outside Diameter at Bevel	Center-to-End, *A*
1	1.32	1.00
1¼	1.66	1.25
1½	1.90	1.50
2	2.38	2.00
2½	2.88	2.50
3	3.50	3.00
3½	4.00	3.50
4	4.50	4.00
5	5.56	5.00
6	6.62	6.00
8	8.62	8.00
10	10.75	10.00
12	12.75	12.00
14	14.00	14.00
16	16.00	16.00
18	18.00	18.00
20	20.00	20.00
22	22.00	22.00
24	24.00	24.00

All dimensions are in inches

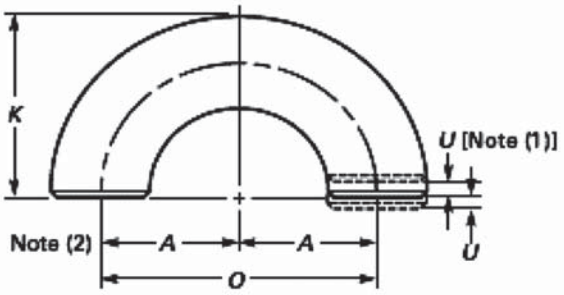
Dimensions of 3D Elbows



Nominal Pipe Size (NPS)	Outside Diameter at Bevel	Center-to-End	
		90-deg Elbows, *A*	45-deg Elbows, *B*
¾	1.05	2.25	0.94
1	1.32	3.00	1.25
1¼	1.66	3.75	1.56
1½	1.90	4.50	1.88
2	2.38	6.00	2.50
2½	2.88	7.50	3.12
3	3.50	9.00	3.75
3½	4.00	10.50	4.38
4	4.50	12.00	5.00
5	5.56	15.00	6.19
6	6.62	18.00	7.44
8	8.62	24.00	9.94
10	10.75	30.00	12.44
12	12.75	36.00	14.88
14	14.00	42.00	17.38
16	16.00	48.00	19.88
18	18.00	54.00	22.38
20	20.00	60.00	24.88
22	22.00	66.00	27.31
24	24.00	72.00	29.81
26	26.00	78.00	32.31
28	28.00	84.00	34.75
30	30.00	90.00	37.25
32	32.00	96.00	39.75
34	34.00	102.00	42.25
36	36.00	108.00	44.69
38	38.00	114.00	47.25
40	40.00	120.00	49.75
42	42.00	126.00	52.19
44	44.00	132.00	54.69
46	46.00	138.00	57.19
48	48.00	144.00	59.69

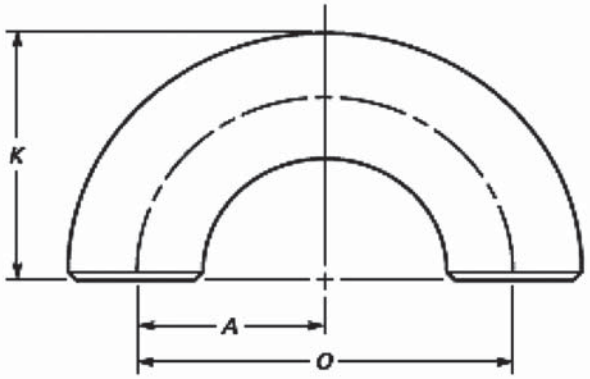
TABLE 2.18 WROUGHT BUTT WELDED RETURNS (ASME B16.9-2007 [58])

Dimensions of Long Radius Returns



Nominal Pipe Size (NPS)	Outside Diameter at Bevel	Center-to-Center, *O*	Back-to-Face, *K*
½	0.84	3.00	1.88
¾	1.05	3.00	2.00
1	1.32	3.00	2.19
1¼	1.66	3.75	2.75
1½	1.90	4.50	3.25
2	2.38	6.00	4.19
2½	2.88	7.50	5.19
3	3.50	9.00	6.25
3½	4.00	10.50	7.25
4	4.50	12.00	8.25
5	5.56	15.00	10.31
6	6.62	18.00	12.31
8	8.62	24.00	16.31
10	10.75	30.00	20.38
12	12.75	36.00	24.38
14	14.00	42.00	28.00
16	16.00	48.00	32.00
18	18.00	54.00	36.00
20	20.00	60.00	40.00
22	22.00	66.00	44.00
24	24.00	72.00	48.00

Dimensions of Short Radius 180-deg Returns



Nominal Pipe Size (NPS)	Outside Diameter at Bevel	Center-to-Center, *O*	Back-to-Face, *K*
1	1.32	2.00	1.62
1¼	1.66	2.50	2.06
1½	1.90	3.00	2.44
2	2.38	4.00	3.19
2½	2.88	5.00	3.94
3	3.50	6.00	4.75
3½	4.00	7.00	5.50
4	4.50	8.00	6.25
5	5.56	10.00	7.75
6	6.62	12.00	9.31
8	8.62	16.00	12.31
10	10.75	20.00	15.38
12	12.75	24.00	18.38
14	14.00	28.00	21.00
16	16.00	32.00	24.00
18	18.00	36.00	27.00
20	20.00	40.00	30.00
22	22.00	44.00	33.00
24	24.00	48.00	36.00

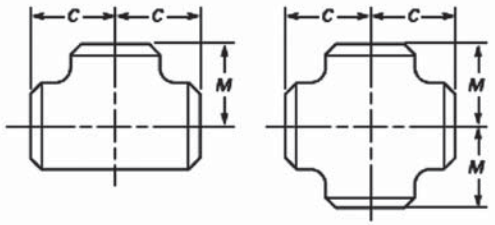
GENERAL NOTES:
(a) All dimensions are in inches.
(b) Dimension *A* is equal to one-half of dimension *O*.

steel, and ductile iron pipe. The standards defining these dimensions provide SI tables. References to applicable standards may have been sufficient for this text, but a ready reference for fitting dimensions in the following figures and tables (Figs. 2.26 and 2.27 and Tables 2.17 to 2.28) should be convenient for use with tables of friction factors.

2.3.12 Valve Designs

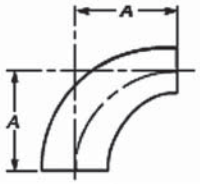
Valve selection depends on the required system control characteristics and costs for the valve application. Liptak and Venczel [31], Driskell [62], Varma [63], and Hutchinson [64] provide detailed discussions of valve design characteristics and selection criteria, but some common valve types and characteristics are considered here since valve characteristics are required to understand fluid transients. Hand wheels (manual actuators) are shown in the figures, but automatic actuators are also available for valves (pneumatic, electromechanical, hydraulic, or electrohydraulic). Face to face and end to end dimensions for valves are available in ASME B16.10-2000 [65]. The

TABLE 2.19 WROUGHT BUTT WELDED REDUCING ELBOWS AND CROSSES (ASME B16.9-2007 [58])



Nominal Pipe Size (NPS)	Outside Diameter at Bevel	Center-to-End	
		Run, C	Outlet, M [Notes (1) and (2)]
½	0.84	1.00	1.00
¾	1.05	1.12	1.12
1	1.32	1.50	1.50
1¼	1.66	1.88	1.88
1½	1.90	2.25	2.25
2	2.38	2.50	2.50
2½	2.88	3.00	3.00
3	3.50	3.38	3.38
3½	4.00	3.75	3.75
4	4.50	4.12	4.12
5	5.56	4.88	4.88
6	6.62	5.62	5.62
8	8.62	7.00	7.00
10	10.75	8.50	8.50
12	12.75	10.00	10.00
14	14.00	11.00	11.00
16	16.00	12.00	12.00
18	18.00	13.50	13.50
20	20.00	15.00	15.00
22	22.00	16.50	16.50
24	24.00	17.00	17.00
26	26.00	19.50	19.50
28	28.00	20.50	20.50
30	30.00	22.00	22.00
32	32.00	23.50	23.50
34	34.00	25.00	25.00
36	36.00	26.50	26.50
38	38.00	28.00	28.00
40	40.00	29.50	29.50
42	42.00	30.00	28.00
44	44.00	32.00	30.00
46	46.00	33.50	31.50
48	48.00	35.00	33.00

NOTES:
(1) Outlet dimension *M* for NPS 26 and larger is recommended but not required.
(2) Dimensions applicable to crosses NPS 24 and smaller.

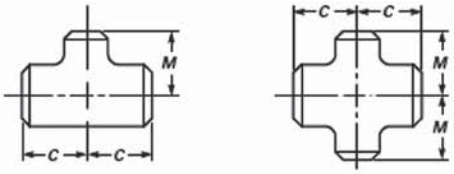


Nominal Pipe Size (NPS)	Outside Diameter at Bevel		Center-to-End, A
	Large End	Small End	
2 × 1½	2.38	1.90	3.00
2 × 1¼	2.38	1.66	3.00
2 × 1	2.38	1.32	3.00
2½ × 2	2.88	2.38	3.75
2½ × 1½	2.88	1.90	3.75
2½ × 1¼	2.88	1.66	3.75
3 × 2½	3.50	2.88	4.50
3 × 2	3.50	2.38	4.50
3 × 1½	3.50	1.90	4.50
3½ × 3	4.00	3.50	5.25
3½ × 2½	4.00	2.88	5.25
3½ × 2	4.00	2.38	5.25
4 × 3½	4.50	4.00	6.00
4 × 3	4.50	3.50	6.00
4 × 2½	4.50	2.88	6.00
4 × 2	4.50	2.38	6.00
5 × 4	5.56	4.50	7.50
5 × 3½	5.56	4.00	7.50
5 × 3	5.56	3.50	7.50
5 × 2½	5.56	2.88	7.50
6 × 5	6.62	5.56	9.00
6 × 4	6.62	4.50	9.00
6 × 3½	6.62	4.00	9.00
6 × 3	6.62	3.50	9.00
8 × 6	8.62	6.62	12.00
8 × 5	8.62	5.56	12.00
8 × 4	8.62	4.50	12.00

Nominal Pipe Size (NPS)	Outside Diameter at Bevel		Center-to-End, A
	Large End	Small End	
10 × 8	10.75	8.62	15.00
10 × 6	10.75	6.62	15.00
10 × 5	10.75	5.56	15.00
12 × 10	12.75	10.75	18.00
12 × 8	12.75	8.62	18.00
12 × 6	12.75	6.62	18.00
14 × 12	14.00	12.75	21.00
14 × 10	14.00	10.75	21.00
14 × 8	14.00	8.62	21.00
16 × 14	16.00	14.00	24.00
16 × 12	16.00	12.75	24.00
16 × 10	16.00	10.75	24.00
18 × 16	18.00	16.00	27.00
18 × 14	18.00	14.00	27.00
18 × 12	18.00	12.75	27.00
18 × 10	18.00	10.75	27.00
20 × 18	20.00	18.00	30.00
20 × 16	20.00	16.00	30.00
20 × 14	20.00	14.00	30.00
20 × 12	20.00	12.75	30.00
20 × 10	20.00	10.75	30.00
24 × 22	24.00	22.00	36.00
24 × 20	24.00	20.00	36.00
24 × 18	24.00	18.00	36.00
24 × 16	24.00	16.00	36.00
24 × 14	24.00	14.00	36.00
24 × 12	24.00	12.75	36.00
...	...	...	...

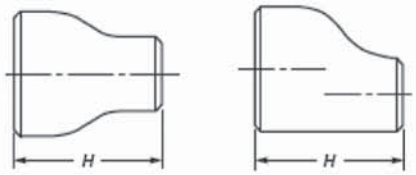
GENERAL NOTE: All dimensions are in inches.

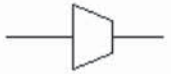
TABLE 2.20 WROUGHT BUTT WELDED REDUCING CROSSES AND TEES (ASME B16.9-2007 [58])



Nominal Pipe Size (NPS)	Outside Diameter at Bevel		Center-to-End	
	Run	Outlet	Run, C	Outlet, M [Note (1)]
½ × ½ × ⅜	0.84	0.68	1.00	1.00
½ × ½ × ¼	0.84	0.54	1.00	1.00
¾ × ¾ × ½	1.05	0.84	1.12	1.12
¾ × ¾ × ⅜	1.05	0.68	1.12	1.12
1 × 1 × ¾	1.32	1.05	1.50	1.50
1 × 1 × ½	1.32	0.84	1.50	1.50
1¼ × 1¼ × 1	1.66	1.32	1.88	1.88
1¼ × 1¼ × ¾	1.66	1.05	1.88	1.88
1¼ × 1¼ × ½	1.66	0.84	1.88	1.88
1½ × 1½ × 1¼	1.90	1.66	2.25	2.25
1½ × 1½ × 1	1.90	1.32	2.25	2.25
1½ × 1½ × ¾	1.90	1.05	2.25	2.25
1½ × 1½ × ½	1.90	0.84	2.25	2.25
2 × 2 × 1½	2.38	1.90	2.50	2.38
2 × 2 × 1¼	2.38	1.66	2.50	2.25
2 × 2 × 1	2.38	1.32	2.50	2.00
2 × 2 × ¾	2.38	1.05	2.50	1.75
2½ × 2½ × 2	2.88	2.38	3.00	2.75
2½ × 2½ × 1½	2.88	1.90	3.00	2.62
2½ × 2½ × 1¼	2.88	1.66	3.00	2.50
2½ × 2½ × 1	2.88	1.32	3.00	2.25
3 × 3 × 2½	3.50	2.88	3.38	3.25
3 × 3 × 2	3.50	2.38	3.38	3.00
3 × 3 × 1½	3.50	1.90	3.38	2.88
3 × 3 × 1¼	3.50	1.66	3.38	2.75
3½ × 3½ × 3	4.00	3.50	3.75	3.62
3½ × 3½ × 2½	4.00	2.88	3.75	3.50
3½ × 3½ × 2	4.00	2.38	3.75	3.25
3½ × 3½ × 1½	4.00	1.90	3.75	3.12
4 × 4 × 3½	4.50	4.00	4.12	4.00
4 × 4 × 3	4.50	3.50	4.12	3.88
4 × 4 × 2½	4.50	2.88	4.12	3.75
4 × 4 × 2	4.50	2.38	4.12	3.50
4 × 4 × 1½	4.50	1.90	4.12	3.38
5 × 5 × 4	5.56	4.50	4.88	4.62
5 × 5 × 3½	5.56	4.00	4.88	4.50
5 × 5 × 3	5.56	3.50	4.88	4.38
5 × 5 × 2½	5.56	2.88	4.88	4.25
5 × 5 × 2	5.56	2.38	4.88	4.12
6 × 6 × 5	6.62	5.56	5.62	5.38
6 × 6 × 4	6.62	4.50	5.62	5.12
6 × 6 × 3½	6.62	4.00	5.62	5.00
6 × 6 × 3	6.62	3.50	5.62	4.88
6 × 6 × 2½	6.62	2.88	5.62	4.75
8 × 8 × 6	8.62	6.62	7.00	6.62
8 × 8 × 5	8.62	5.56	7.00	6.38
8 × 8 × 4	8.62	4.50	7.00	6.12
8 × 8 × 3½	8.62	4.00	7.00	6.00
10 × 10 × 8	10.75	8.62	8.50	8.00
10 × 10 × 6	10.75	6.62	8.50	7.62
10 × 10 × 5	10.75	5.56	8.50	7.50
10 × 10 × 4	10.75	4.50	8.50	7.25
12 × 12 × 10	12.75	10.75	10.00	9.50
12 × 12 × 8	12.75	8.62	10.00	9.00
12 × 12 × 6	12.75	6.62	10.00	8.62
12 × 12 × 5	12.75	5.56	10.00	8.50
14 × 14 × 12	14.00	12.75	11.00	10.62
14 × 14 × 10	14.00	10.75	11.00	10.12
14 × 14 × 8	14.00	8.62	11.00	9.75
14 × 14 × 6	14.00	6.62	11.00	9.38
16 × 16 × 14	16.00	14.00	12.00	12.00
16 × 16 × 12	16.00	12.75	12.00	11.62
16 × 16 × 10	16.00	10.75	12.00	11.12
16 × 16 × 8	16.00	8.62	12.00	10.75
16 × 16 × 6	16.00	6.62	12.00	10.38
18 × 18 × 16	18.00	16.00	13.50	13.00
18 × 18 × 14	18.00	14.00	13.50	13.00
18 × 18 × 12	18.00	12.75	13.50	12.62
18 × 18 × 10	18.00	10.75	13.50	12.12
18 × 18 × 8	18.00	8.62	13.50	11.75
20 × 20 × 18	20.00	18.00	15.00	14.50
20 × 20 × 16	20.00	16.00	15.00	14.00
20 × 20 × 14	20.00	14.00	15.00	14.00
20 × 20 × 12	20.00	12.75	15.00	13.62
20 × 20 × 10	20.00	10.75	15.00	13.12
20 × 20 × 8	20.00	8.62	15.00	12.75
22 × 22 × 20	22.00	20.00	16.50	16.00
22 × 22 × 18	22.00	18.00	16.50	15.50
22 × 22 × 16	22.00	16.00	16.50	15.00
22 × 22 × 14	22.00	14.00	16.50	15.00
22 × 22 × 12	22.00	12.75	16.50	14.62
22 × 22 × 10	22.00	10.75	16.50	14.12
24 × 24 × 22	24.00	22.00	17.00	17.00
24 × 24 × 20	24.00	20.00	17.00	17.00
24 × 24 × 18	24.00	18.00	17.00	16.50
24 × 24 × 16	24.00	16.00	17.00	16.00
24 × 24 × 14	24.00	14.00	17.00	16.00
24 × 24 × 12	24.00	12.75	17.00	15.62
24 × 24 × 10	24.00	10.75	17.00	15.12
26 × 26 × 24	26.00	24.00	19.50	19.00
26 × 26 × 22	26.00	22.00	19.50	18.50
26 × 26 × 20	26.00	20.00	19.50	18.00
26 × 26 × 18	26.00	18.00	19.50	17.50
26 × 26 × 16	26.00	16.00	19.50	17.00
26 × 26 × 14	26.00	14.00	19.50	17.00
26 × 26 × 12	26.00	12.75	19.50	16.62
28 × 28 × 26	28.00	26.00	20.50	20.50
28 × 28 × 24	28.00	24.00	20.50	20.00
28 × 28 × 22	28.00	22.00	20.50	19.50
28 × 28 × 20	28.00	20.00	20.50	19.00
28 × 28 × 18	28.00	18.00	20.50	18.50
28 × 28 × 16	28.00	16.00	20.50	18.00
28 × 28 × 14	28.00	14.00	20.50	18.00
28 × 28 × 12	28.00	12.75	20.50	17.62
30 × 30 × 28	30.00	28.00	22.00	21.50
30 × 30 × 26	30.00	26.00	22.00	21.50
30 × 30 × 24	30.00	24.00	22.00	21.00
30 × 30 × 22	30.00	22.00	22.00	20.50
30 × 30 × 20	30.00	20.00	22.00	20.00
30 × 30 × 18	30.00	18.00	22.00	19.50
30 × 30 × 16	30.00	16.00	22.00	19.00
30 × 30 × 14	30.00	14.00	22.00	19.00
30 × 30 × 12	30.00	12.75	22.00	18.62
30 × 30 × 10	30.00	10.75	22.00	18.12
32 × 32 × 30	32.00	30.00	23.50	23.00
32 × 32 × 28	32.00	28.00	23.50	22.50
32 × 32 × 26	32.00	26.00	23.50	22.50
32 × 32 × 24	32.00	24.00	23.50	22.00
32 × 32 × 22	32.00	22.00	23.50	21.50
32 × 32 × 20	32.00	20.00	23.50	21.00
32 × 32 × 18	32.00	18.00	23.50	20.50
32 × 32 × 16	32.00	16.00	23.50	20.00
32 × 32 × 14	32.00	14.00	23.50	20.00
34 × 34 × 32	34.00	32.00	25.00	24.50
34 × 34 × 30	34.00	30.00	25.00	24.00
34 × 34 × 28	34.00	28.00	25.00	23.50
34 × 34 × 26	34.00	26.00	25.00	23.50
34 × 34 × 24	34.00	24.00	25.00	23.00
34 × 34 × 22	34.00	22.00	25.00	22.50
34 × 34 × 20	34.00	20.00	25.00	22.00
34 × 34 × 18	34.00	18.00	25.00	21.50
34 × 34 × 16	34.00	16.00	25.00	21.00
36 × 36 × 34	36.00	34.00	26.50	26.00
36 × 36 × 32	36.00	32.00	26.50	25.50
36 × 36 × 30	36.00	30.00	26.50	25.00
36 × 36 × 28	36.00	28.00	26.50	24.50
36 × 36 × 26	36.00	26.00	26.50	24.50
36 × 36 × 24	36.00	24.00	26.50	24.00
36 × 36 × 22	36.00	22.00	26.50	23.50
36 × 36 × 20	36.00	20.00	26.50	23.00
36 × 36 × 18	36.00	18.00	26.50	22.50
36 × 36 × 16	36.00	16.00	26.50	22.00
38 × 38 × 36	38.00	36.00	28.00	28.00
38 × 38 × 34	38.00	34.00	28.00	27.50
38 × 38 × 32	38.00	32.00	28.00	27.00
38 × 38 × 30	38.00	30.00	28.00	26.50
38 × 38 × 28	38.00	28.00	28.00	25.50

TABLE 2.21 WROUGHT BUTT WELDED REDUCERS (ASME B16.9-2007 [58])





Drawing symbol

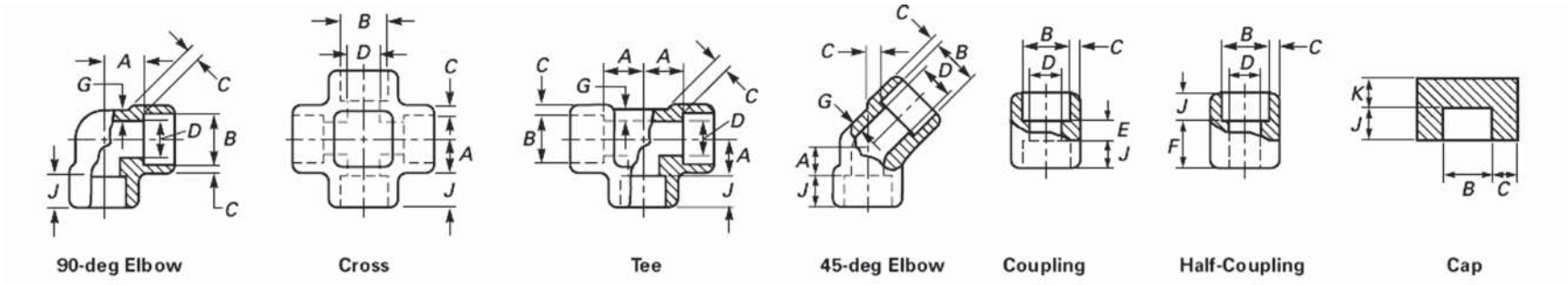
Nominal Pipe Size (NPS)	Outside Diameter at Bevel, Large End	Outside Diameter at Bevel, Small End	End-to-End, *H*
¾ × ½	1.05	0.84	1.50
¾ × ⅜	1.05	0.68	1.50
1 × ¾	1.32	1.05	2.00
1 × ½	1.32	0.84	2.00
1¼ × 1	1.66	1.32	2.00
1¼ × ¾	1.66	1.05	2.00
1¼ × ½	1.66	0.84	2.00
1½ × 1¼	1.90	1.66	2.50
1½ × 1	1.90	1.32	2.50
1½ × ¾	1.90	1.05	2.50
1½ × ½	1.90	0.84	2.50
2 × 1½	2.38	1.90	3.00
2 × 1¼	2.38	1.66	3.00
2 × 1	2.38	1.32	3.00
2 × ¾	2.38	1.05	3.00
2½ × 2	2.88	2.38	3.50
2½ × 1½	2.88	1.90	3.50
2½ × 1¼	2.88	1.66	3.50
2½ × 1	2.88	1.32	3.50
3 × 2½	3.50	2.88	3.50
3 × 2	3.50	2.38	3.50
3 × 1½	3.50	1.90	3.50
3 × 1¼	3.50	1.66	3.50
3½ × 3	4.00	3.50	4.00
3½ × 2½	4.00	2.88	4.00
3½ × 2	4.00	2.38	4.00
3½ × 1½	4.00	1.90	4.00
3½ × 1¼	4.00	1.66	4.00
4 × 3½	4.50	4.00	4.00
4 × 3	4.50	3.50	4.00
4 × 2½	4.50	2.88	4.00
4 × 2	4.50	2.38	4.00
4 × 1½	4.50	1.90	4.00
5 × 4	5.56	4.50	5.00
5 × 3½	5.56	4.00	5.00
5 × 3	5.56	3.50	5.00
5 × 2½	5.56	2.88	5.00
5 × 2	5.56	2.38	5.00
6 × 5	6.62	5.56	5.50
6 × 4	6.62	4.50	5.50
6 × 3½	6.62	4.00	5.50
6 × 3	6.62	3.50	5.50
6 × 2½	6.62	2.88	5.50
8 × 6	8.62	6.62	6.00
8 × 5	8.62	5.56	6.00
8 × 4	8.62	4.50	6.00
8 × 3½	8.62	4.00	6.00
10 × 8	10.75	8.62	7.00
10 × 6	10.75	6.62	7.00
10 × 5	10.75	5.56	7.00
10 × 4	10.75	4.50	7.00
12 × 10	12.75	10.75	8.00
12 × 8	12.75	8.62	8.00
12 × 6	12.75	6.62	8.00
12 × 5	12.75	5.56	8.00
14 × 12	14.00	12.75	13.00
14 × 10	14.00	10.75	13.00
14 × 8	14.00	8.62	13.00
14 × 6	14.00	6.62	13.00
16 × 14	16.00	14.00	14.00
16 × 12	16.00	12.75	14.00
16 × 10	16.00	10.75	14.00
16 × 8	16.00	8.62	14.00
18 × 16	18.00	16.00	15.00
18 × 14	18.00	14.00	15.00
18 × 12	18.00	12.75	15.00
18 × 10	18.00	10.75	15.00
20 × 18	20.00	18.00	20.00
20 × 16	20.00	16.00	20.00
20 × 14	20.00	14.00	20.00
20 × 12	20.00	12.75	20.00
22 × 20	22.00	20.00	20.00
22 × 18	22.00	18.00	20.00
22 × 16	22.00	16.00	20.00
22 × 14	22.00	14.00	20.00
24 × 22	24.00	22.00	20.00
24 × 20	24.00	20.00	20.00
24 × 18	24.00	18.00	20.00
24 × 16	24.00	16.00	20.00
26 × 24	26.00	24.00	24.00
26 × 22	26.00	22.00	24.00
26 × 20	26.00	20.00	24.00
26 × 18	26.00	18.00	24.00
28 × 26	28.00	26.00	24.00
28 × 24	28.00	24.00	24.00
28 × 20	28.00	20.00	24.00
28 × 18	28.00	18.00	24.00
30 × 28	30.00	28.00	24.00
30 × 26	30.00	26.00	24.00
30 × 24	30.00	24.00	24.00
30 × 20	30.00	20.00	24.00
32 × 30	32.00	30.00	24.00
32 × 28	32.00	28.00	24.00
32 × 26	32.00	26.00	24.00
32 × 24	32.00	24.00	24.00
34 × 32	34.00	32.00	24.00
34 × 30	34.00	30.00	24.00
34 × 26	34.00	26.00	24.00
34 × 24	34.00	24.00	24.00
36 × 34	36.00	34.00	24.00
36 × 32	36.00	32.00	24.00
36 × 30	36.00	30.00	24.00
36 × 26	36.00	26.00	24.00
36 × 24	36.00	24.00	24.00
38 × 36	38.00	36.00	24.00
38 × 34	38.00	34.00	24.00
38 × 32	38.00	32.00	24.00
38 × 30	38.00	30.00	24.00
38 × 28	38.00	28.00	24.00
38 × 26	38.00	26.00	24.00
40 × 38	40.00	38.00	24.00
40 × 36	40.00	36.00	24.00
40 × 34	40.00	34.00	24.00
40 × 32	40.00	32.00	24.00
40 × 30	40.00	30.00	24.00
42 × 40	42.00	40.00	24.00
42 × 38	42.00	38.00	24.00
42 × 36	42.00	36.00	24.00
42 × 34	42.00	34.00	24.00
42 × 32	42.00	32.00	24.00
42 × 30	42.00	30.00	24.00
44 × 42	44.00	42.00	24.00
44 × 40	44.00	40.00	24.00
44 × 38	44.00	38.00	24.00
44 × 36	44.00	36.00	24.00
46 × 44	46.00	44.00	28.00
46 × 42	46.00	42.00	28.00
46 × 40	46.00	40.00	28.00
46 × 38	46.00	38.00	28.00
48 × 46	48.00	46.00	28.00
48 × 44	48.00	44.00	28.00
48 × 42	48.00	42.00	28.00
48 × 40	48.00	40.00	28.00

GENERAL NOTES:

(a) All dimensions are in inches.

(b) While the figure illustrates a bell-shaped reducer, the use of a conical reducer is not prohibited.

TABLE 2.22 FORGED SOCKET WELDED FITTINGS (ASME B16.11-2005 [59])



Nominal Pipe Size	Socket Bore Diameter, B [Note (1)]	Bore Diameter of Fittings, D [Note (1)] Class Designation 3000	6000	9000	Socket Wall Thickness, C [Note (2)] Class Designation 3000 Avg.	3000 Min.	6000 Avg.	6000 Min.	9000 Avg.	9000 Min.	Body Wall, G Class Designation 3000 Min.	6000 Min.	9000 Min.	Min. Depth of Socket, J	Center-to-Bottom of Socket, A 90-deg Elbows, Tees, and Crosses Class Designation 3000	6000	9000	45-deg Elbows 3000	6000	9000	Laying Lengths Couplings, E	Half Couplings, F	Tolerances, ± A	E	F	End Wall Thickness, K_{min} Class Designation 3000	6000	9000
⅛	11.2	7.6	4.8	...	3.18	3.18	3.96	3.43	...	...	2.41	3.15	...	9.5	11.0	11.0	...	8.0	8.0	...	6.5	16.0	1.0	1.5	1.0	4.8	6.4	...
	10.8	6.1	3.2	...																								
¼	14.6	10.0	7.1	...	3.78	3.30	4.60	4.01	...	...	3.02	3.68	...	9.5	11.0	13.5	...	8.0	8.0	...	6.5	16.0	1.0	1.5	1.0	4.8	6.4	...
	14.2	8.5	5.6	...																								
⅜	18.0	13.3	9.9	...	4.01	3.50	5.03	4.37	...	...	3.20	4.01	...	9.5	13.5	15.5	...	8.0	11.0	...	6.5	17.5	1.5	3.0	1.5	4.8	6.4	...
	17.6	11.8	8.4	...																								
½	22.2	16.6	12.5	7.2	4.67	4.09	5.97	5.18	9.35	8.18	3.73	4.78	7.47	9.5	15.5	19.0	25.5	11.0	12.5	15.5	9.5	22.5	1.5	3.0	1.5	6.4	7.9	11.2
	21.8	15.0	11.0	5.6																								
¾	27.6	21.7	16.3	11.8	4.90	4.27	6.96	6.04	9.78	8.56	3.91	5.56	7.82	12.5	19.0	22.5	28.5	13.0	14.0	19.0	9.5	24.0	1.5	3.0	1.5	6.4	7.9	12.7
	27.2	20.2	14.8	10.3																								
1	34.3	27.4	21.5	16.0	5.69	4.98	7.92	6.93	11.38	9.96	4.55	6.35	9.09	12.5	22.5	27.0	32.0	14.0	17.5	20.5	12.5	28.5	2.0	4.0	2.0	9.6	11.2	14.2
	33.9	25.9	19.9	14.4																								
1¼	43.1	35.8	30.2	23.5	6.07	5.28	7.92	6.93	12.14	10.62	4.85	6.35	9.70	12.5	27.0	32.0	35.0	17.5	20.5	22.5	12.5	30.0	2.0	4.0	2.0	9.6	11.2	14.2
	42.7	34.3	28.7	22.0																								
1½	49.2	41.6	34.7	28.7	6.35	5.54	8.92	7.80	12.70	11.12	5.08	7.14	10.15	12.5	32.0	38.0	38.0	20.5	25.5	25.5	12.5	32.0	2.0	4.0	2.0	11.2	12.7	15.7
	48.8	40.1	33.2	27.2																								
2	61.7	53.3	43.6	38.9	6.93	6.04	10.92	9.50	13.84	12.12	5.54	8.74	11.07	16.0	38.0	41.0	54.0	25.5	28.5	28.5	19.0	41.0	2.0	4.0	2.0	12.7	15.7	19.0
	61.2	51.7	42.1	37.4																								
2½	74.4	64.2	...	...	8.76	7.67	...	...	...	...	7.01	...	...	16.0	41.0	...	...	28.5	...	...	19.0	43.0	2.5	5.0	2.5	15.7	19.0	...
	73.9	61.2	...	...																								
3	90.3	79.4	...	...	9.52	8.30	...	...	...	...	7.62	...	...	16.0	57.0	...	...	32.0	...	...	19.0	44.5	2.5	5.0	2.5	19.0	22.4	...
	89.8	76.4	...	...																								
4	115.7	103.8	...	...	10.69	9.35	...	...	...	...	8.56	...	...	19.0	66.5	...	...	41.0	...	...	19.0	48.0	2.5	5.0	2.5	22.4	28.4	...
	115.2	100.7	...	...																								

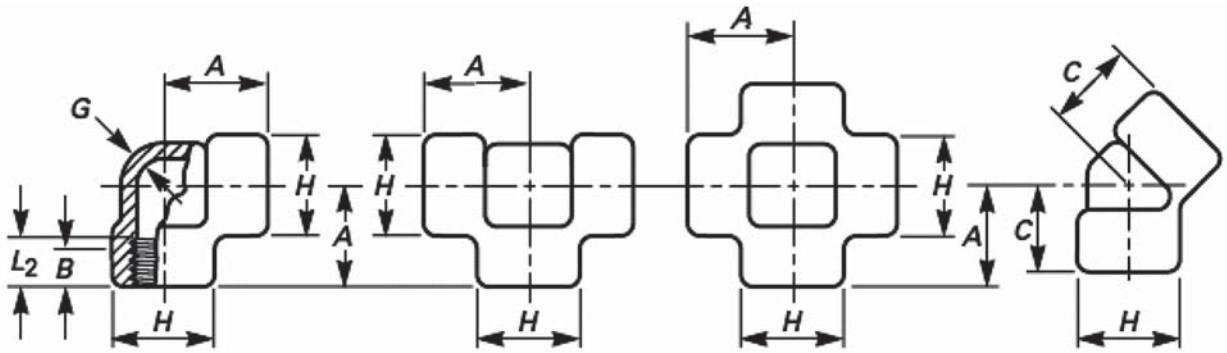
GENERAL NOTE: Dimensions are in millimeters.

NOTES:

(1) Upper and lower values for each size are the respective maximum and minimum dimensions.

(2) Average of socket wall thickness around periphery shall not be less than listed values. The minimum values are permitted in localized areas.

TABLE 2.23 FORGED SCREWED FITTINGS (ASME B16.11-2005 [59])

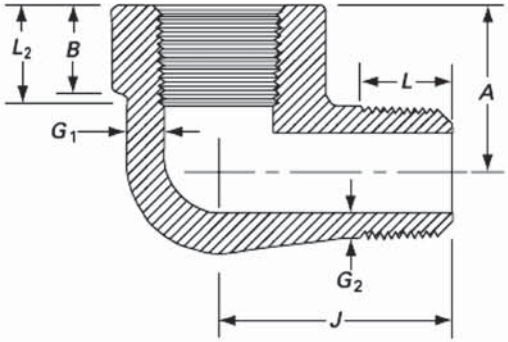


90-deg Elbow Tee Cross 45-deg Elbow

Nominal Pipe Size	Center-to-End Elbows, Tees, Crosses, A			Center-to-End 45-deg Elbow, C			Outside Diameter of Band, H			Min. Wall Thickness, G			Min. Length of Thread [Note (1)]	
	2000	3000	6000	2000	3000	6000	2000	3000	6000	2000	3000	6000	B	L_2
1/8	0.81	0.81	0.97	0.69	0.69	0.75	0.88	0.88	1.00	0.125	0.125	0.250	0.25	0.2639
1/4	0.81	0.97	1.12	0.69	0.75	0.88	0.88	1.00	1.31	0.125	0.130	0.260	0.32	0.4018
3/8	0.97	1.12	1.31	0.75	0.88	1.00	1.00	1.31	1.50	0.125	0.138	0.275	0.36	0.4078
1/2	1.12	1.31	1.50	0.88	1.00	1.12	1.31	1.50	1.81	0.125	0.161	0.321	0.43	0.5337
3/4	1.31	1.50	1.75	1.00	1.12	1.31	1.50	1.81	2.19	0.125	0.170	0.336	0.50	0.5457
1	1.50	1.75	2.00	1.12	1.31	1.38	1.81	2.19	2.44	0.145	0.196	0.391	0.58	0.6828
1 1/4	1.75	2.00	2.38	1.31	1.38	1.69	2.19	2.44	2.97	0.153	0.208	0.417	0.67	0.7068
1 1/2	2.00	2.38	2.50	1.38	1.69	1.72	2.44	2.97	3.31	0.158	0.219	0.436	0.70	0.7235
2	2.38	2.50	3.25	1.69	1.72	2.06	2.97	3.31	4.00	0.168	0.281	0.476	0.75	0.7565
2 1/2	3.00	3.25	3.75	2.06	2.06	2.50	3.62	4.00	4.75	0.221	0.301	0.602	0.93	1.1380
3	3.38	3.75	4.19	2.50	2.50	3.12	4.31	4.75	5.75	0.236	0.348	0.655	1.02	1.2000
4	4.19	4.50	4.50	3.12	3.12	3.12	5.75	6.00	6.00	0.258	0.440	0.735	1.09	1.3000

GENERAL NOTE: Dimensions are in inches.

TABLE 2.24 FORGED THREADED STREET ELBOWS (ASME B16.11-2005 [59])



Nominal Pipe Size, NPS	Center-to-Female End Street Ells, A [Note (1)]		Center-to-Male End Street Ells, J		Outside Diameter of Band, H [Note (2)]		Minimum Wall Thickness, G_1		Minimum Wall Thickness, G_2 [Note (3)]		Minimum Length Internal Thread [Note (4)]		Minimum Length Male Thread, L
	Class Designation		Class Designation		Class Designation		Class Designation		Class Designation				
	3000	6000	3000	6000	3000	6000	3000	6000	3000	6000	B	L_2	
1/8	19	22	25	32	19	25	3.18	5.08	2.74	4.22	6.4	6.7	10
1/4	22	25	32	38	25	32	3.30	5.66	3.22	5.28	8.1	10.2	11
3/8	25	28	38	41	32	38	3.51	6.98	3.50	5.59	9.1	10.4	13
1/2	28	35	41	48	38	44	4.09	8.15	4.16	6.53	10.9	13.6	14
3/4	35	44	48	57	44	51	4.32	8.53	4.88	6.86	12.7	13.9	16
1	44	51	57	66	51	62	4.98	9.93	5.56	7.95	14.7	17.3	19
1 1/4	51	54	66	71	62	70	5.28	10.59	5.56	8.48	17.0	18.0	21
1 1/2	54	64	71	84	70	84	5.56	11.07	6.25	8.89	17.8	18.4	21
2	64	83	84	105	84	102	7.14	12.09	7.64	9.70	19.0	19.2	22

GENERAL NOTE: Dimensions are in millimeters.

NOTES:

(1) Dimension *A* of Table 2 for the appropriate fitting size may also be used at the option of the manufacturer.

(2) Dimension *H* of Table 2 for the appropriate fitting size may also be used at the option of the manufacturer.

(3) Wall thickness before threading.

(4) Dimension *B* is minimum length of perfect thread. The length of useful thread (*B* plus threads with fully formed roots and flat crests) shall not be less than L_2 (effective length of external thread) required by American National Standard for Pipe Threads (ASME B1.20.1; see para. 6.3).

TABLE 2.25 CLASS 150 FLANGED FITTING DIMENSIONS (ASME B16.5-2003 [60])

1	2	3	4	5	6	7	8	9	10	11	12
					0.06-in. Raised Face (Flange Edge) [Note (4)]						
Nominal Pipe Size, NPS	Outside Diameter of Flange, *O*	Minimum Thickness of Flange, t_f [Notes (1)–(3)]	Minimum Wall Thickness of Fitting, t_m	Inside Diameter of Fitting, *d*	Center-to-Contact Surface of Raised Face Elbow, Tee, Cross, and True "Y," AA	Center-to-Contact Surface of Raised Face Long Radius Elbow, BB	Center-to-Contact Surface of Raised Face 45-deg Elbow, CC	Long Center-to-Contact Surface of Raised Face Lateral, EE	Short Center-to-Contact Surface of Raised Face Lateral and True "Y," FF	Contact Surface-to-Contact Surface of Raised Face Reducer, GG [Note (5)]	Ring Joint [Note (4)] Center-to-End Elbow Tee, Cross, and True "Y," HH [Note (6)]
½	3.5	0.31	0.11	0.50	...	...	...	...	...	...	...
¾	3.88	0.34	0.12	0.75	...	...	...	...	...	...	...
1	4.25	0.38	0.16	1.00	3.50	5.00	1.75	5.75	1.75	4.50	3.75
1¼	4.62	0.44	0.19	1.25	3.75	5.50	2.00	6.25	1.75	4.50	4.00
1½	5.00	0.5	0.19	1.50	4.00	6.00	2.25	7.00	2.00	4.50	4.25
2	6.00	0.56	0.22	2.00	4.50	6.50	2.50	8.00	2.50	5.00	4.75
2½	7.00	0.62	0.22	2.50	5.00	7.00	3.00	9.50	2.50	5.50	5.25
3	7.50	0.69	0.22	3.00	5.50	7.75	3.00	10.00	3.00	6.00	5.75
3½	8.50	0.75	0.25	3.50	6.00	8.50	3.50	11.50	3.00	6.50	6.25
4	9.00	0.88	0.25	4.00	6.50	9.00	4.00	12.00	3.00	7.00	6.75
5	10.00	0.88	0.28	5.00	7.50	10.25	4.50	13.50	3.50	8.00	7.75
6	11.00	0.94	0.28	6.00	8.00	11.50	5.00	14.50	3.50	9.00	8.25
8	13.50	1.06	0.31	8.00	9.00	14.00	5.50	17.50	4.50	11.00	9.25
10	16.00	1.12	0.34	10.00	11.00	16.50	6.50	20.50	5.00	12.00	11.25
12	19.00	1.19	0.38	12.00	12.00	19.00	7.50	24.50	6.50	14.00	12.25
14	21.00	1.31	0.41	13.25	14.00	21.50	7.50	27.00	6.00	16.00	14.25
16	23.50	1.38	0.44	15.25	15.00	24.00	8.00	30.00	6.50	18.00	15.25
18	25.00	1.5	0.47	17.25	16.50	26.50	8.50	32.00	7.00	19.00	16.75
20	27.50	1.62	0.50	19.25	18.00	29.00	9.50	35.00	8.00	20.00	18.25
24	32.00	1.81	0.57	23.25	22.00	34.00	11.00	40.50	9.00	24.00	22.25

TABLE 2.26 CLASS 300 FLANGED FITTINGS (ASME B16.5-2003 [60])

1	2	3	4	5	6	7	8	9	10	11	12
					0.06-in. Raised Face (Flange Edge) [Note (4)]						Ring Joint [Note (2)]
Nominal Pipe Size, NPS	Outside Diameter of Flange, O	Minimum Thickness of Flange, t_f [Notes (1)–(3)]	Minimum Wall Thickness of Fitting, t_m	Inside Diameter of Fitting, d	Center-to-Contact Surface of Raised Face Elbow, Tee, Cross, and True "Y," AA	Center-to-Contact Surface of Raised Face Long Radius Elbow, BB	Center-to-Contact Surface of Raised Face 45-deg Elbow, CC	Long Center-to-Contact Surface of Raised Face Lateral, EE	Short Center-to-Contact Surface of Raised Face Lateral and True "Y," FF	Contact Surface-to-Contact Surface of Raised Face Reducer, GG [Note (5)]	Center-to-End Elbow Tee, Cross, and True "Y," HH [Note (4)]
1	4.88	0.62	0.19	1.00	4.00	5.00	2.25	6.50	2.00	4.50	4.25
1¼	5.25	0.69	0.19	1.25	4.25	5.50	2.50	7.25	2.25	4.50	4.50
1½	6.12	0.75	0.19	1.50	4.50	6.00	2.75	8.50	2.50	4.50	4.75
2	6.50	0.81	0.25	2.00	5.00	6.50	3.00	9.00	2.50	5.00	5.31
2½	7.50	0.94	0.25	2.50	5.50	7.00	3.50	10.50	2.50	5.50	5.81
3	8.25	1.06	0.28	3.00	6.00	7.75	3.50	11.00	3.00	6.00	6.31
3½	9.00	1.12	0.29	3.50	6.50	8.50	4.00	12.50	3.00	6.50	6.81
4	10.00	1.19	0.31	4.00	7.00	9.00	4.50	13.50	3.00	7.00	7.31
5	11.00	1.31	0.38	5.00	8.00	10.25	5.00	15.00	3.50	8.00	8.31
6	12.50	1.38	0.38	6.00	8.50	11.50	5.50	17.50	4.00	9.00	8.81
8	15.00	1.56	0.44	8.00	10.00	14.00	6.00	20.50	5.00	11.00	10.31
10	17.50	1.81	0.50	10.00	11.50	16.50	7.00	24.00	5.50	12.00	11.81
12	20.50	1.94	0.56	12.00	13.00	19.00	8.00	27.50	6.00	14.00	13.31
14	23.00	2.06	0.62	13.25	15.00	21.50	8.50	31.00	6.50	16.00	15.31
16	25.50	2.19	0.69	15.25	16.50	24.00	9.50	34.50	7.50	18.00	10.81
18	28.00	2.31	0.75	17.00	18.00	26.50	10.00	37.50	8.00	19.00	18.31
20	30.50	2.44	0.81	19.00	19.50	29.00	10.50	40.50	8.50	20.00	19.89
24	36.00	2.69	0.94	23.00	22.50	34.00	12.00	47.50	10.00	24.00	22.94

TABLE 2.27 CLASS 150 DUCTILE IRON FITTINGS (ASME B16.42-1998 [61])

NPS	Inside Diameter of Fittings	Center-to-Face 90 deg Elbow Tees, Crosses, True Y, and Double Branch Elbow, *A*	Center-to-Face 90 deg Long Radius Elbow, *B*	Center-to-Face 45 deg Elbow, *C*	Center-to-Face Lateral, *D*	Short Center-to-Face True Y and Lateral, *E*	Face-to-Face Reducer, *F*	Diameter of Flange	Minimum Thickness of Flange, *Q*	Minimum Body Wall Thickness
1	1.00	3.50	5.00	1.75	5.75	1.75	4.50	4.25	0.44	0.16
1¼	1.25	3.75	5.50	2.00	6.25	1.75	4.50	4.62	0.50	0.19
1½	1.50	4.00	6.00	2.25	7.00	2.00	4.50	5.00	0.56	0.19
2	2.00	4.50	6.50	2.50	8.00	2.50	5.00	6.00	0.62	0.22
2½	2.50	5.00	7.00	3.00	9.50	2.50	5.50	7.00	0.69	0.22
3	3.00	5.50	7.75	3.00	10.00	3.00	6.00	7.50	0.75	0.22
3½	3.50	6.00	8.50	3.50	11.50	3.00	6.50	8.50	0.81	0.25
4	4.00	6.50	9.00	4.00	12.00	3.00	7.00	9.00	0.94	0.25
5	5.00	7.50	10.25	4.50	13.50	3.50	8.00	10.00	0.94	0.28
6	6.00	8.00	11.50	5.00	14.50	3.50	9.00	11.00	1.00	0.28
8	8.00	9.00	14.00	5.50	17.50	4.50	11.00	13.50	1.12	0.31
10	10.00	11.00	16.50	6.50	20.50	5.00	12.00	16.00	1.19	0.34
12	12.00	12.00	19.00	7.50	24.50	5.50	14.00	19.00	1.25	0.38
14	13.25	14.00	21.50	7.50	27.00	6.00	16.00	21.00	1.38	0.41
16	15.25	15.00	24.00	8.00	30.00	6.50	18.00	23.50	1.44	0.44
18	17.25	16.50	26.50	8.50	32.00	7.00	19.00	25.00	1.56	0.47
20	19.25	18.00	29.00	9.50	35.00	8.00	20.00	27.50	1.69	0.50
24	23.25	22.00	34.00	11.00	40.50	9.00	24.00	32.00	1.88	0.57

TABLE 2.28 CLASS 300 DUCTILE IRON FITTINGS (ASME B16.42-1998 [61])

NPS	Minimum Inside Diameter of Fittings	Center-to-Face 90 deg Elbow Tees, Crosses, and True Y, *A*	Center-to-Face 90 deg Long Radius Elbow, *C*	Center-to-Face 45 deg Elbow, *C*	Center-to-Face Lateral, *D*	Short Center-to-Face True Y and Lateral, *E*	Face-to-Face Reducer, *F*	Diameter of Flange	Minimum Thickness of Flange, *Q*	Minimum Body Wall Thickness
1	1.00	4.00	5.00	2.25	6.50	2.00	4.50	4.88	0.69	0.19
1¼	1.25	4.25	5.50	2.50	7.25	2.25	4.50	5.25	0.75	0.19
1½	1.50	4.50	6.00	2.75	8.50	2.50	4.50	6.12	0.81	0.19
2	2.00	5.00	6.50	3.00	9.00	2.50	5.00	6.50	0.88	0.25
2½	2.50	5.50	7.00	3.50	10.50	2.50	5.50	7.50	1.00	0.25
3	3.00	6.00	7.75	3.50	11.00	3.00	6.00	8.25	1.12	0.28
3½	3.50	6.50	8.50	4.00	12.50	3.00	6.50	9.00	1.19	0.29
4	4.00	7.00	9.00	4.50	13.50	3.00	7.00	10.00	1.25	0.31
5	5.00	8.00	10.25	5.00	15.00	3.50	8.00	11.00	1.38	0.38
6	6.00	8.50	11.50	5.50	17.50	4.00	9.00	12.50	1.44	0.38
8	8.00	10.00	14.00	6.00	20.50	5.00	11.00	15.00	1.62	0.44
10	10.00	11.50	16.50	7.00	24.00	5.50	12.00	17.50	1.88	0.50
12	12.00	13.00	19.00	8.00	27.50	6.00	14.00	20.50	2.00	0.56
14	13.25	15.00	21.50	8.50	31.00	6.50	16.00	23.00	2.12	0.62
16	15.25	16.50	24.00	9.50	34.50	7.50	18.00	25.50	2.25	0.69
18	17.00	18.00	26.50	10.00	37.50	8.00	19.00	28.00	2.38	0.75
20	19.00	19.50	29.00	10.50	40.50	8.50	20.00	30.50	2.50	0.81
24	23.00	22.50	34.00	12.00	47.50	10.00	24.00	36.00	2.75	0.94

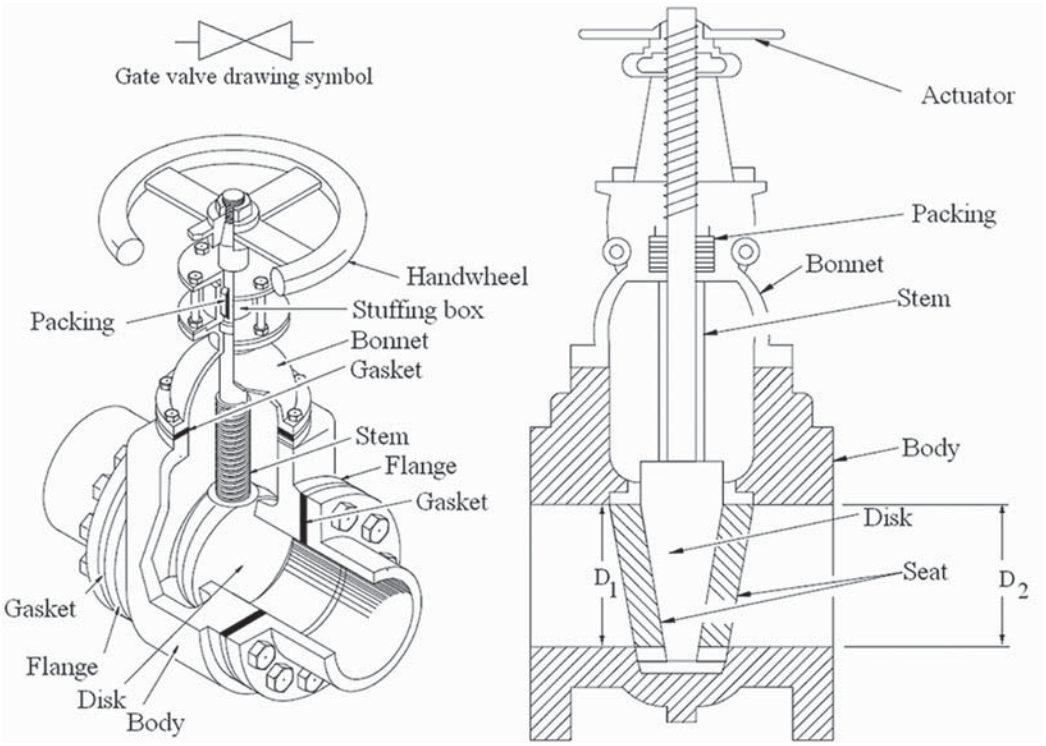


FIG. 2.28 GATE VALVE (US, Department of Energy [66])

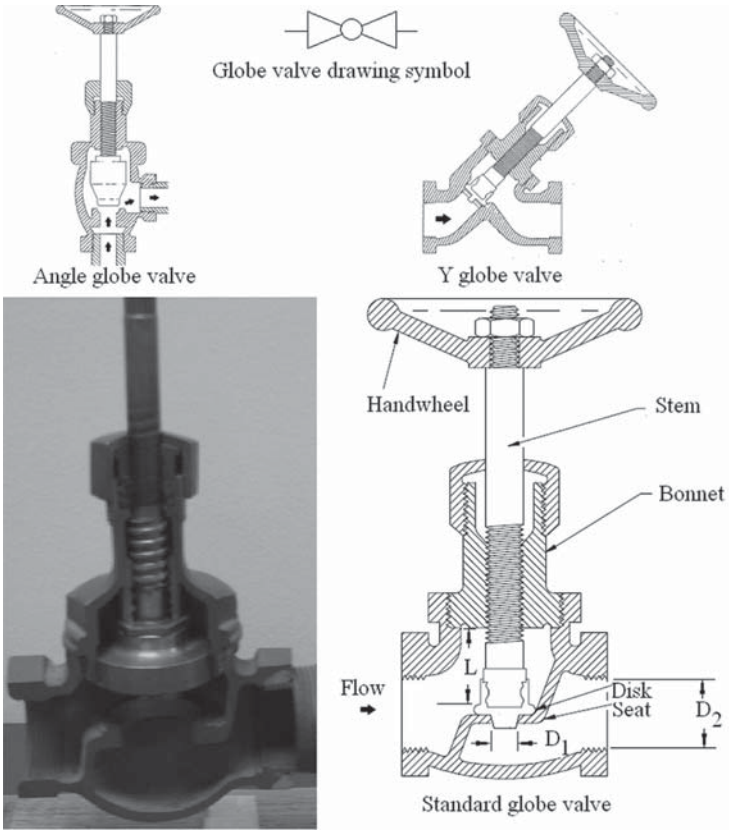


FIG. 2.29 GLOBE VALVES (US, Department of Energy [66])

American Petroleum Institute (API) is in the process of standardizing valve dimensions for numerous valves, and the Manufacturer's Standardization Society of Valves and Fittings (MSS), also provides data for valve dimensions. Descriptions of common valves follow, where line drawings of valves are reprinted from a DOE Valve Handbook [66]. Valves are also classified as standard class valves or special class valves (See ASME B16.34, Valves, Flanged, Threaded, and Welded End), where special class valves receive additional inspection.

2.3.12.1 Gate Valves Gate valves poorly regulate flow in large systems, but can be effectively used for flow control when the valve pressure drop is the primary loss for the system. For example, a gate valve may be used for good volumetric flow control at the end of a discharge pipe or hose. Gate valves have low-pressure drops and provide excellent shutoff capabilities (Fig. 2.28). Gate valves are available in parallel disc and double disc designs (as shown) and nonrising stem designs where the valve handle lifts from the valve or rising stem designs where the valve handle remains at a fixed distance from the valve body when the valve is operated or the stem is threaded through the disc. A valve with a slab-type disc is shown, but gate valves have been fabricated in numerous designs. The positioned disc valve rotates a disc to align holes with a plate in the valve. V-port valves provide a V-shaped opening through the valve, and plate and disc valves provide various openings through a fixed plate in the valve and a rising disc, which aligns the disc and plate openings. A wide range of valve flow characteristics can thus be obtained for gate valves.

2.3.12.2 Globe Valves Globe valves have high-pressure drops, provide good flow control throughout their range of operation by throttling the valve to a partially open position, and have good shutoff capabilities (Fig. 2.29). They are available in numerous designs, which include the standard, angle, and Y globe valves, and the valve discs and valve trims (valve internal designs) are also available in different designs.

2.3.12.3 Ball Valves Ball valves provide quick shutoff, and low-pressure drops, good flow control, and seat materials, such as Teflon or Tefzel, provide good shutoff capability. To improve control characteristics, modifications are available where the ball is modified to U-port, V-port, or parabolic ball valve designs, as shown in Fig. 2.30.

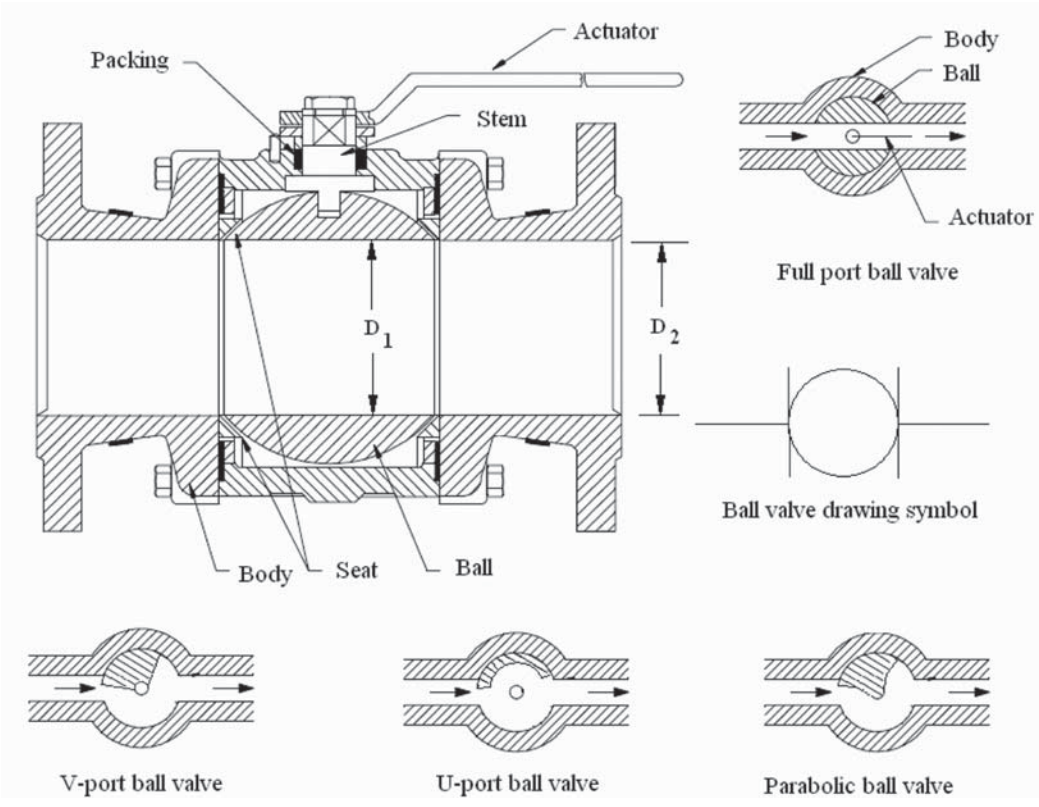


FIG. 2.30 BALL VALVES (US, Department of Energy [66])

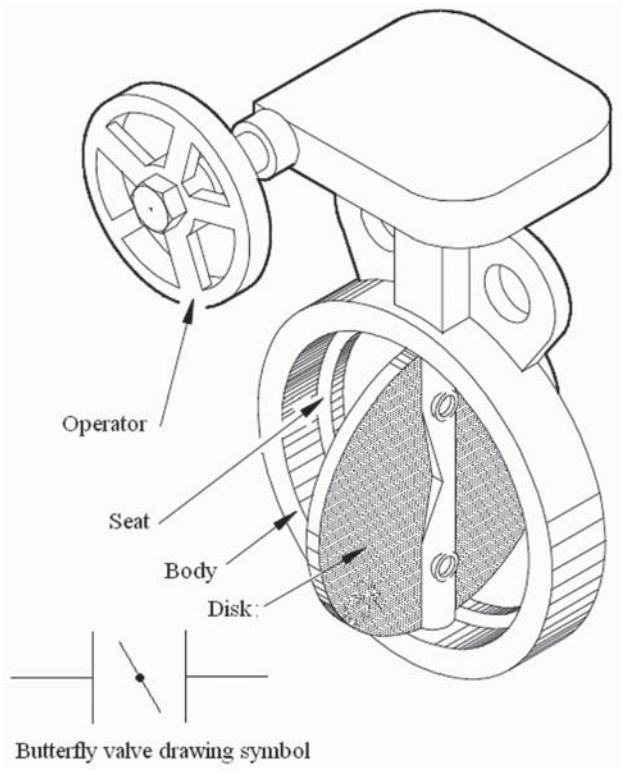


FIG. 2.31 BUTTERFLY VALVE (US, Department of Energy [66])

2.3.12.4 Butterfly Valves Butterfly valves provide quick shutoff and good flow control, but provide poor shutoff control (Fig. 2.31). Some sources in the literature state that this valve provides good control, while others state that this type of valve provides poor control. The fact is that the level of control depends on system characteristics, as described in Chapter 2.5.1. In particular, butterfly valves provide excellent control for large pipe systems, and vendor design modifications improve flow control.

2.3.12.5 Plug Valves Plug valves provide quick shutoff and low-pressure drops (Fig. 2.32). The internal plug and port of the valve comes in different machined configurations to improve flow characteristics of the valve. For example, the plug may be machined to obtain linear, parabolic, or equal percentage flow characteristics as shown, or the port may be modified to the shape of a V, or the port may be modified by an adjustable cylinder, which acts as a moveable curtain to close off flow to the plug.

2.3.12.6 Diaphragm Valves Diaphragm valves provide good flow control, minimize friction-induced damage to fluids, and completely isolate the valve mechanism from the fluid (Fig. 2.33). Different types of diaphragm valve construction are available, which vary the seating surface

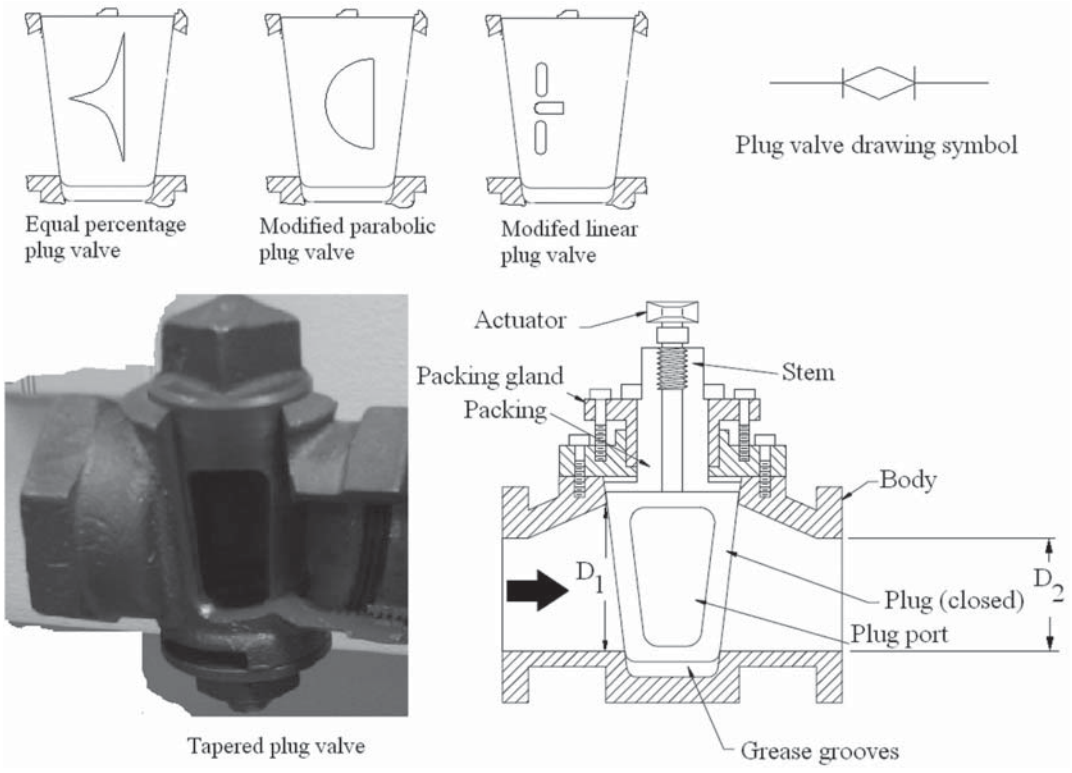


FIG. 2.32 PLUG VALVE (US, Department of Energy [66])

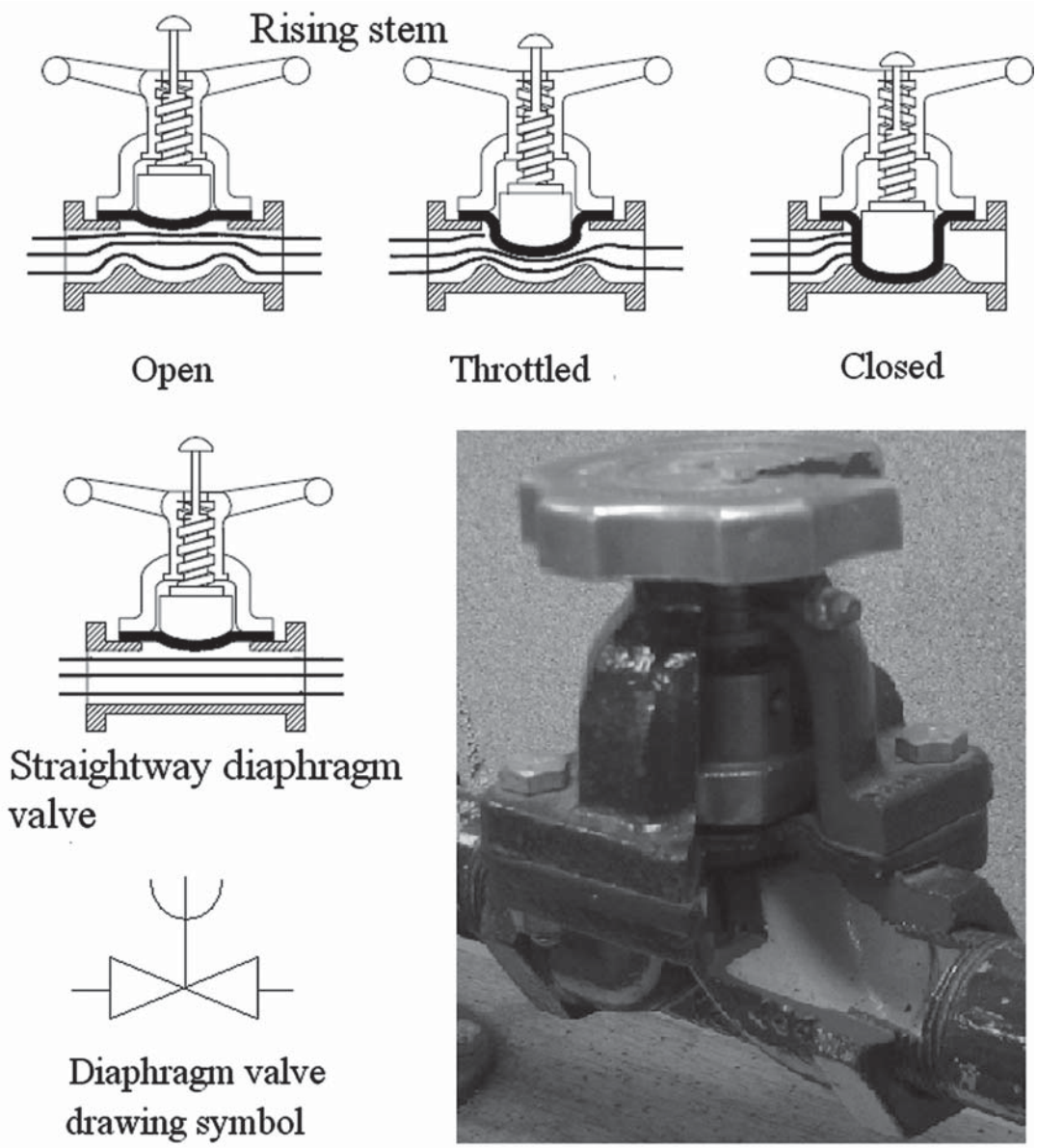


FIG. 2.33 DIAPHRAGM VALVE (US, Department of Energy [66])

for the diaphragm and improve flow through the valve. Flow characteristics vary widely depending on design and material selection.

2.3.12.7 Check Valves Check valves prevent backflow. Typically, check valves require about 5 psi to open them, and a minimum flow is required for them to completely open. They close automatically when flow stops. Several common check valve designs are considered here.

- Swing check valves are used for heavy duty applications (Fig. 2.34). A damped check valve is created by the addition of a lever arm to the check valve to cushion valve closing and to slow the closing time of the valve (Fig. 2.35). Counterweights or air actuators may be applied to the lever to control the disc closing speed.
- Split disc valves are similar to swing check valves, except that two semicircular wafers are attached to a diametrical hinge.
- Tilt check valves provide a lower resistance to flow than swing check valves (Fig. 2.38).
- Piston check (Fig. 2.36) and lift check (Fig. 2.37) valves are similar in design, except that the piston check valve contains a spring to cushion the piston when it rises during operation. These valves are typically used in high-pressure, high-flow services.

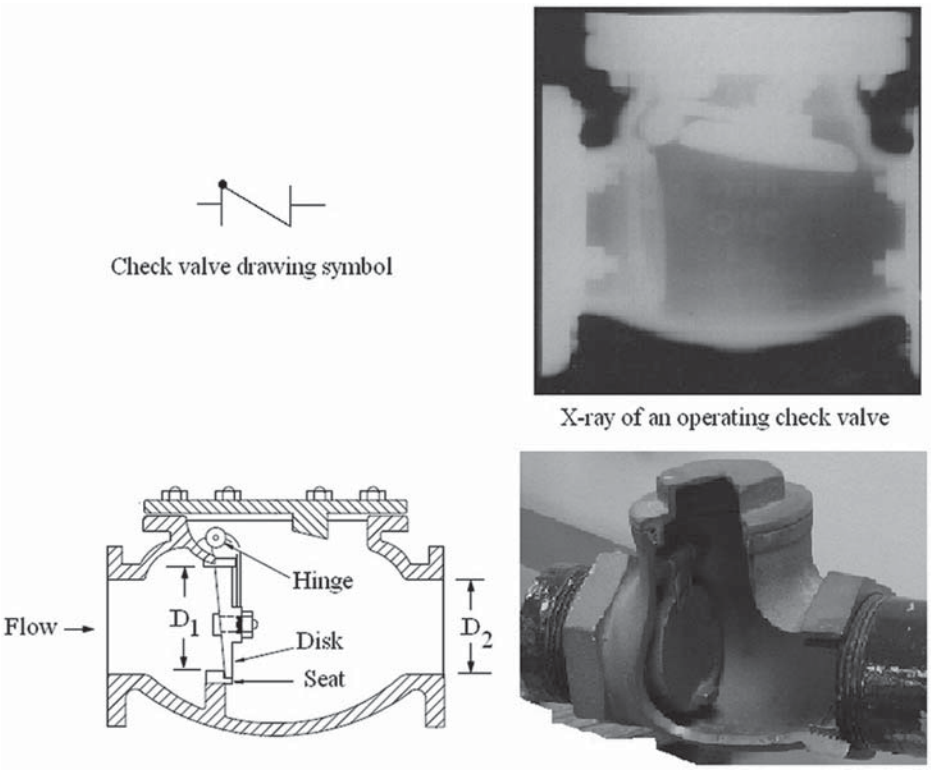


FIG. 2.34 SWING CHECK VALVE

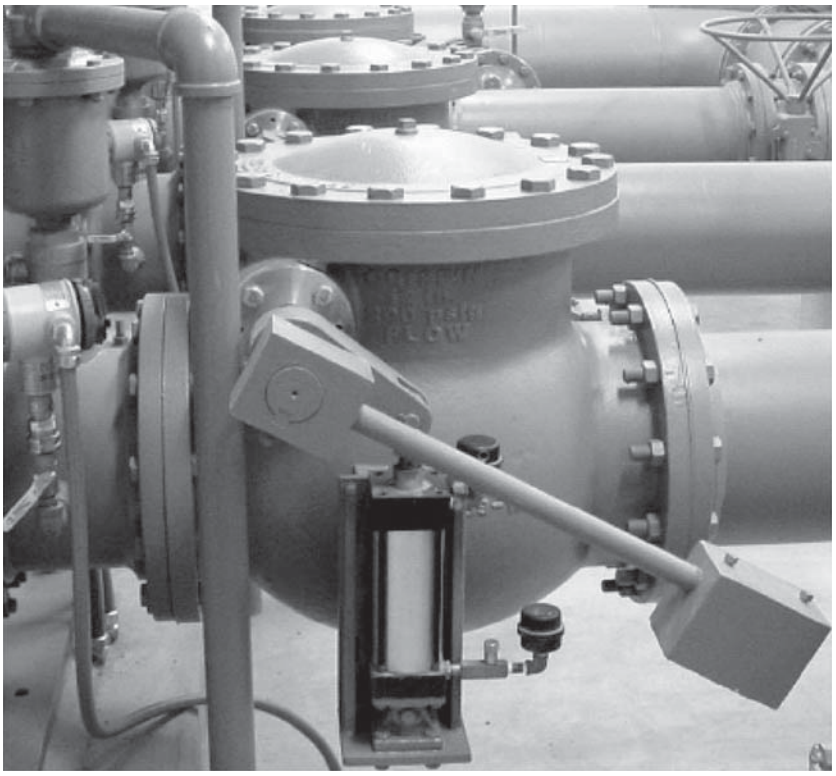


FIG. 2.35 AIR-CUSHIONED SWING CHECK VALVE (Reprinted by permission of Crispin Valve)

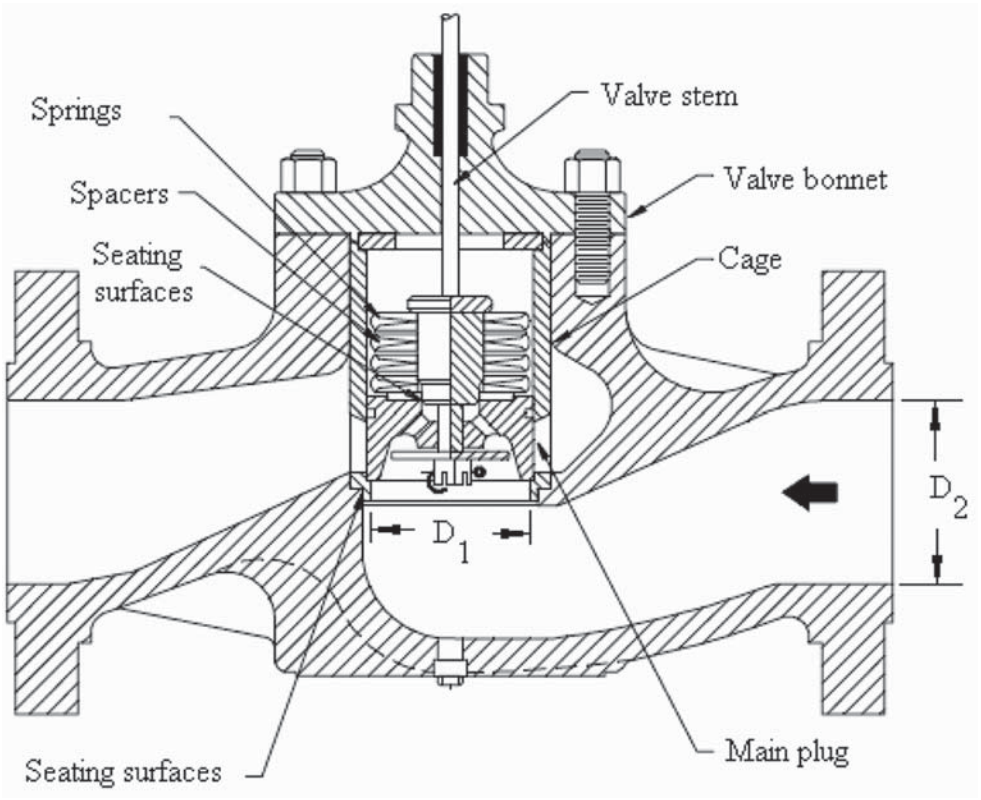


FIG. 2.36 PISTON CHECK VALVE (US, Department of Energy [66])

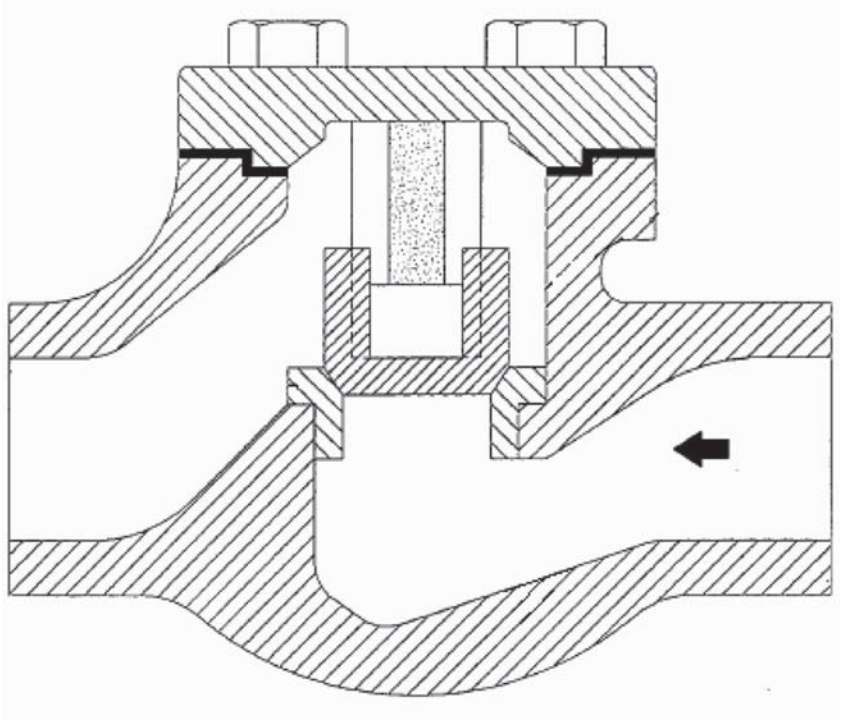


FIG. 2.37 LIFT CHECK VALVE (US, Department of Energy [66])

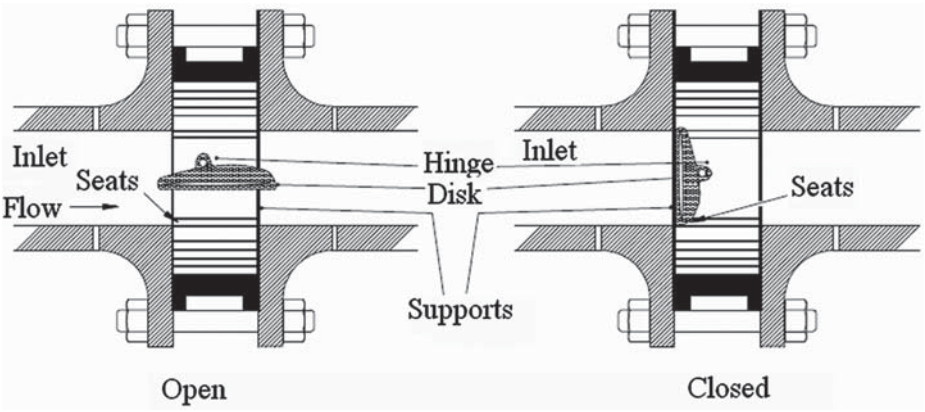


FIG. 2.38 TILT CHECK VALVE (US, Department of Energy [66])

- Ball check valves are similar to lift check valves, except that a ball is used in the valve instead of a piston. A common use for this type of design is the installation as a vacuum breaker in steam systems (Fig. 2.39), where air is admitted through the valve if the system experiences vacuum conditions typical during system cool down.
- Nozzle check valves close as the flow through them slows to reduce valve slam (Fig. 2.40).

There are different approaches to describe check valve closure, and one of those approaches applies the concept of a dynamic check valve, where the type of check valve affects the deceleration of flow in the pipe as it reverses direction. To use this figure, the system deceleration is required in the absence of a check valve, and then the valve type dictates the maximum reverse flow at the moment the valve closes completely. In other words, some backflow occurs through a check valve while it is closing. Fig. 2.41 shows that the magnitude of the flow rate in the reverse direction is much higher for a swing check valve than a no-slam, nozzle check valve. No-slam check valves have a reduced reverse flow at the moment of

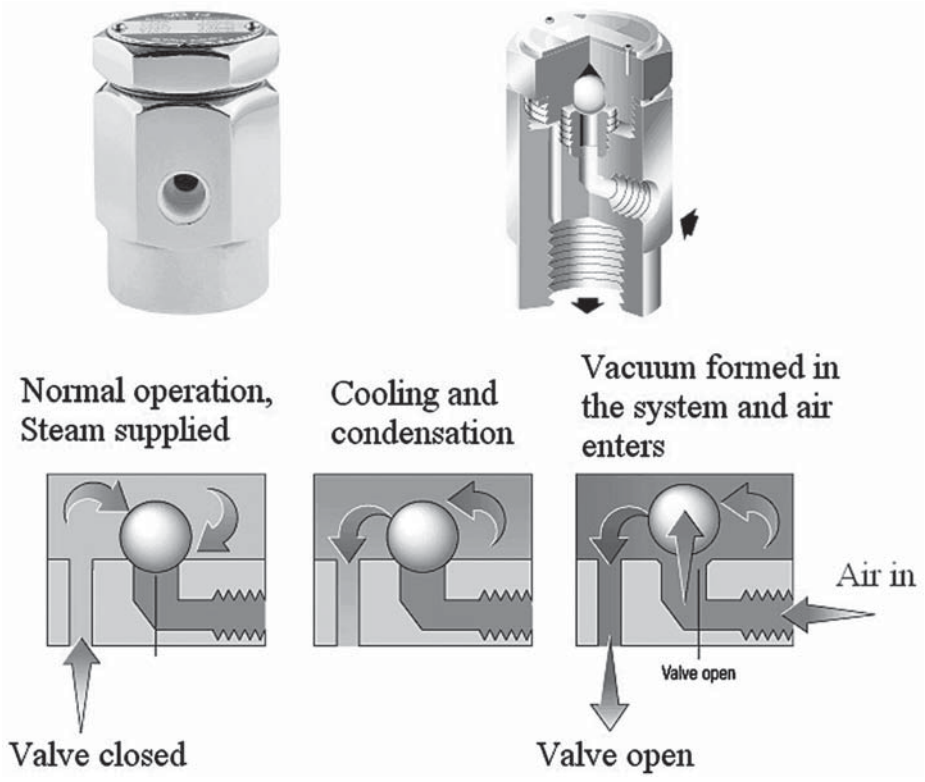


FIG. 2.39 VACUUM BREAKER (Reprinted by permission of Spirax-Sarco)

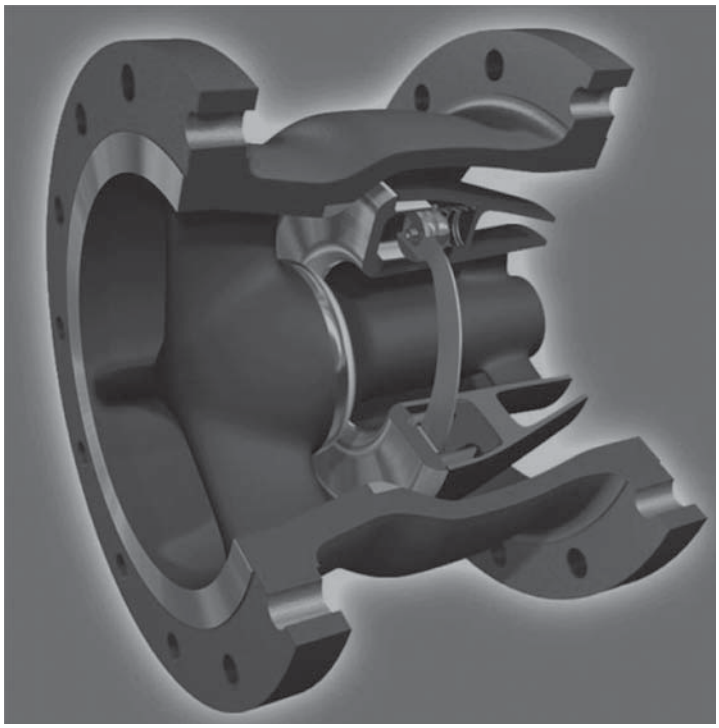


FIG. 2.40 NOZZLE CHECK VALVE (Reprinted by permission of Noreva GmbH)

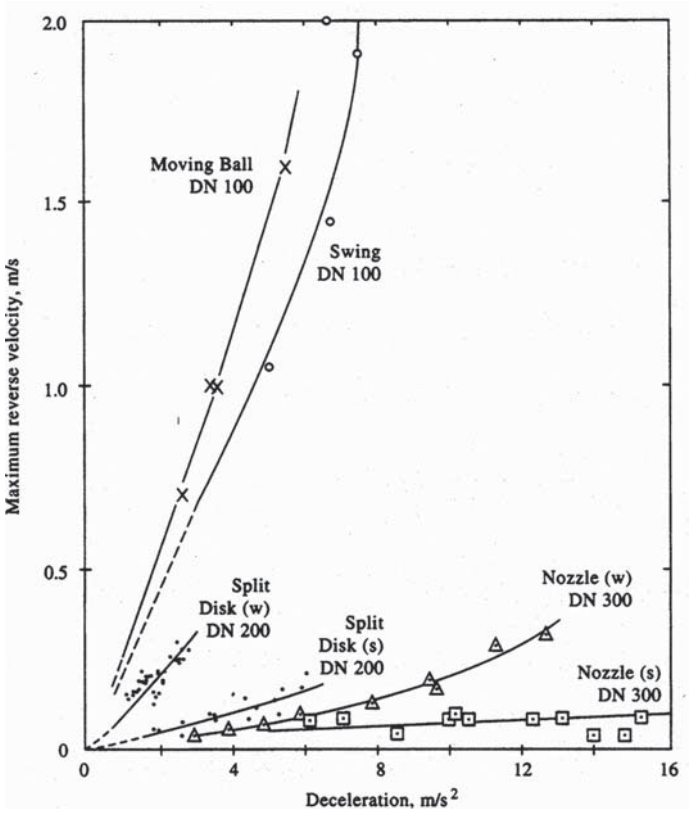


FIG. 2.41 DYNAMIC CHECK VALVE CHARACTERISTICS (s = spring damped, w = without spring (Thorley [68])

closing. Ideally, reverse flow should be zero at the moment the check valve closes completely. Thorley [68] also provided a nondimensional version of this figure.

2.3.12.8 Relief Valves Relief valves are typically used to relieve overpressure conditions for incompressible, liquid services (Fig. 2.42). Relief valves gradually open when the set point is reached and stay open until the system pressure drops below the set point. Relief valves prevent overpressurization during normal operations, and the energy associated with liquid expansion is small when compared to the energy associated with a compressed gas or steam system.

Even so, incompressible fluids store energy, and serious accidents have occurred during hydrostatic testing of incompressible fluid systems. In one case, a technician was decapitated when a test plug dislodged from a pressure vessel under test. In that accident, a rubber plug was compressed into the end of the pipe nozzle to maintain pressure. As the vessel was pressurized, the plug shot from the end of a pipe as a technician walked by the test area, and he was fatally injured. Air may, or may not, have been trapped in the tested pressure vessel.

2.3.12.9 Safety Valves Safety valves are typically used to relieve overpressure conditions for compressible fluids, such as steam or air (Fig. 2.43). These valves fully open (pop off) when the set point is reached and close when the reset pressure is obtained. They are called safety valves instead of relief valves due to the inherent hazards associated with compressible fluids. In fact, the first national safety code was the ASME, Boiler and Pressure Vessel Code, and it was implemented due to the large number of explosions of boilers and compressed gas pressure vessels. In one case, which occurred in the early 1900s, an entire city block was devastated. The national codes resulted in a dramatic decrease in pressure vessel accidents. Compliance with these codes is essential for safety. In another case, as recent as the early 1970s, a maintenance technician gagged (wired shut) safety valves in a small Georgia schoolhouse because the valves were intermittently popping off and were considered to be a nuisance. The resulting boiler explosion leveled the school and killed more than 20 children (Helmut Thielsch, "Piping Design Class").

ASME Codes (Sections I [68], IV [70], and VIII [71]) provide requirements for relief valves, safety valves, and

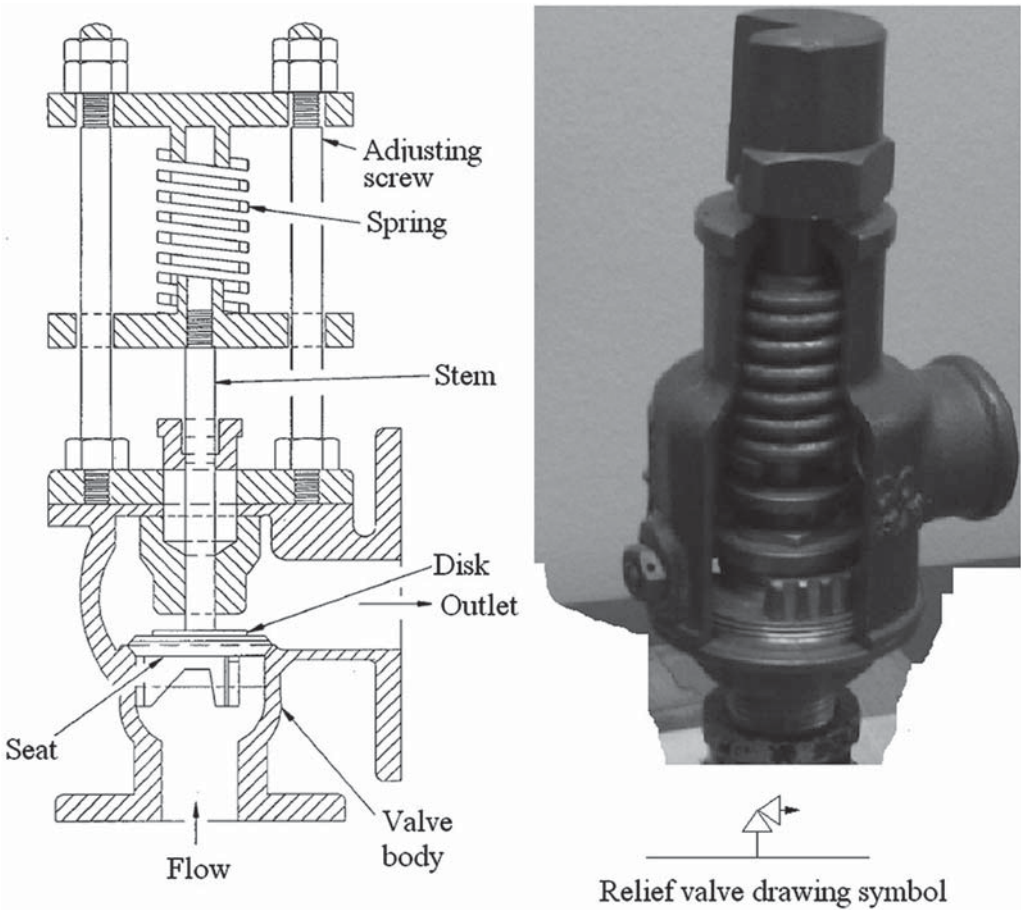


FIG. 2.42 RELIEF VALVE (US, Department of Energy [66])

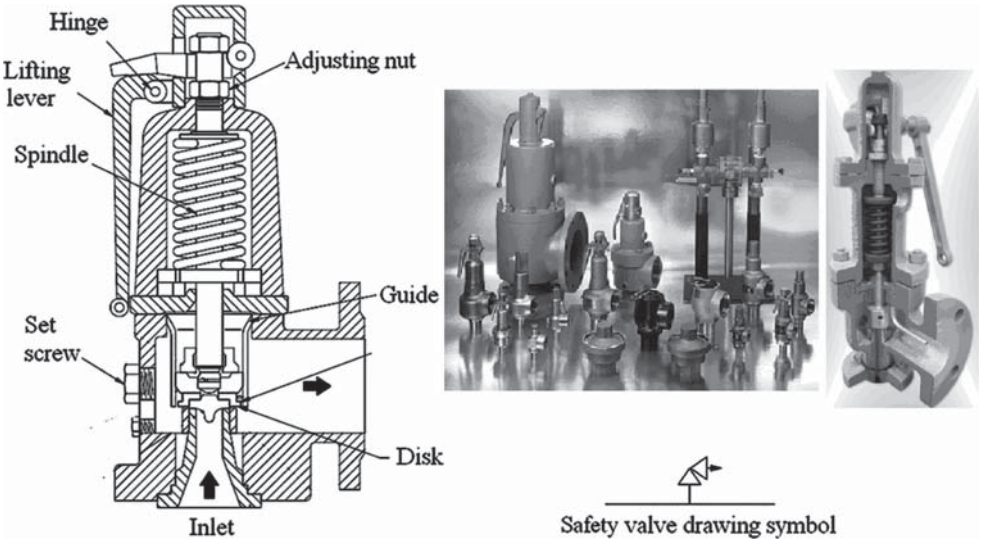


FIG. 2.43 SAFETY VALVES (Photo reprinted by permission of Spence Engineering)

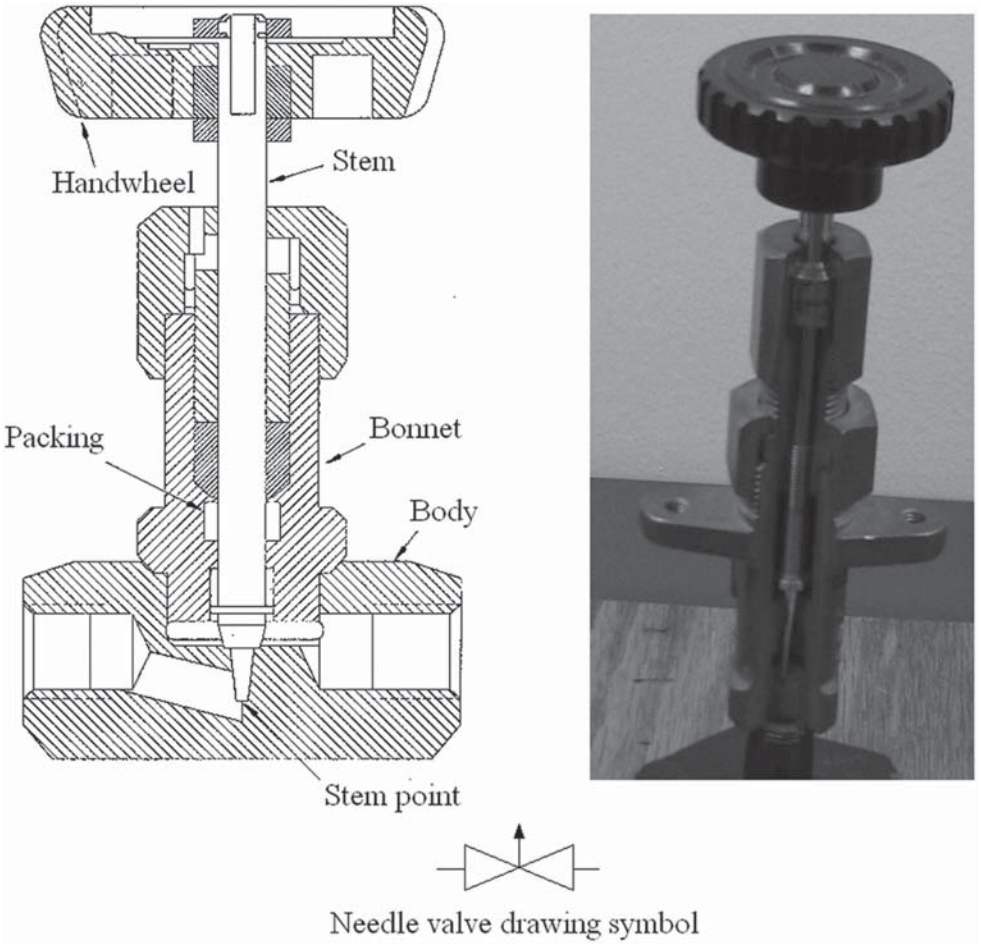


FIG. 2.44 NEEDLE VALVE (US, Department of Energy [66])

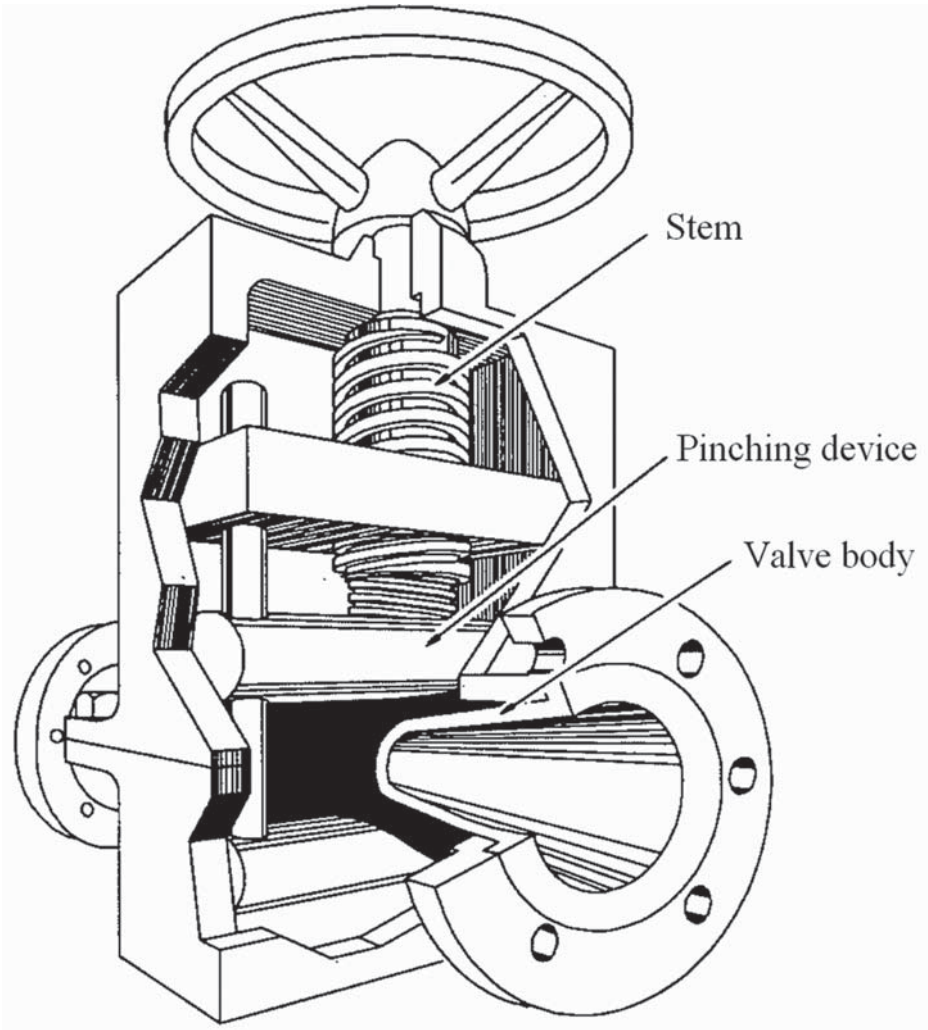


FIG. 2.45 PINCH VALVE (US, Department of Energy [66])

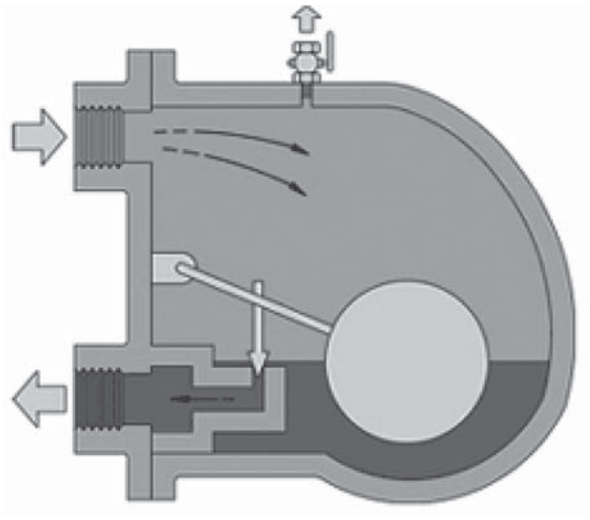


FIG. 2.46 FLOAT TRAP (Reprinted by permission of Spirax-Sarco)

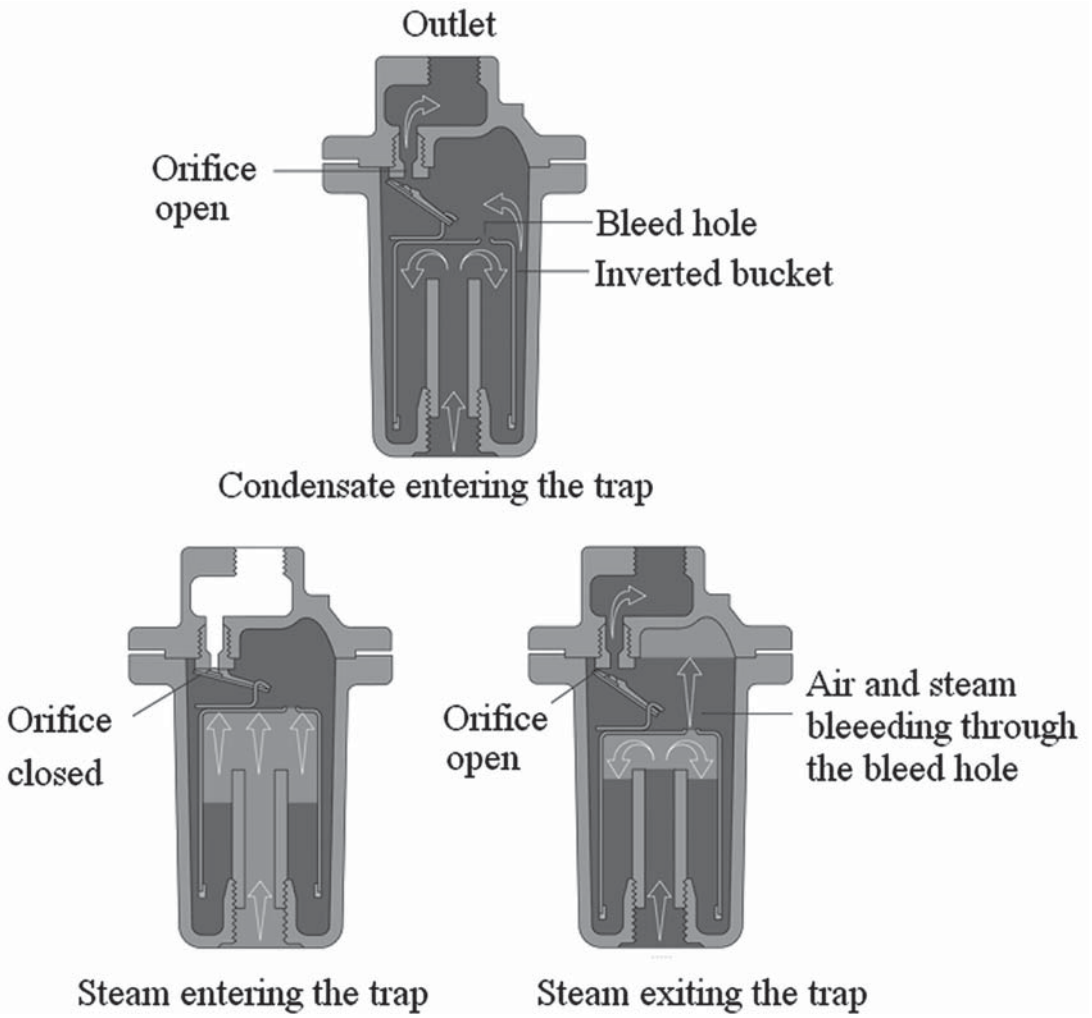


FIG. 2.47 INVERTED BUCKET TRAP (Reprinted by permission of Spirax-Sarco)

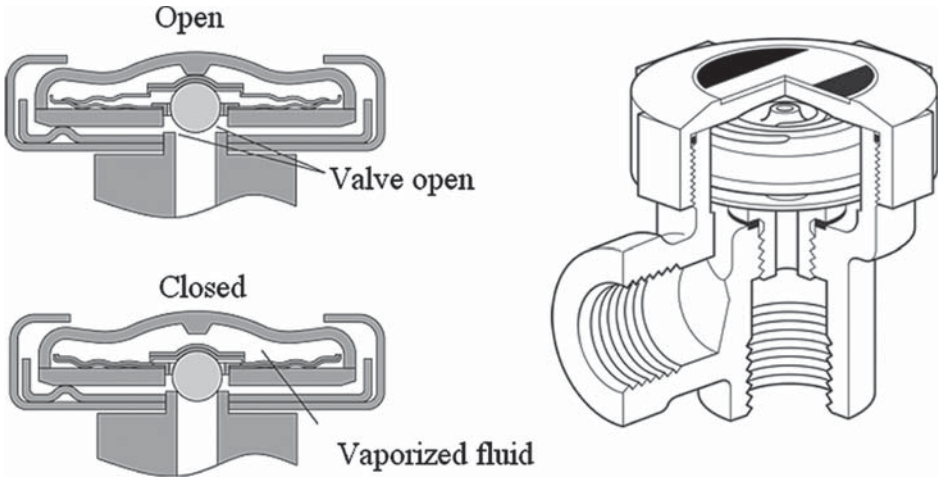


FIG. 2.48 THERMOSTATIC BALANCED PRESSURE TRAP (US, Department of Energy [66])

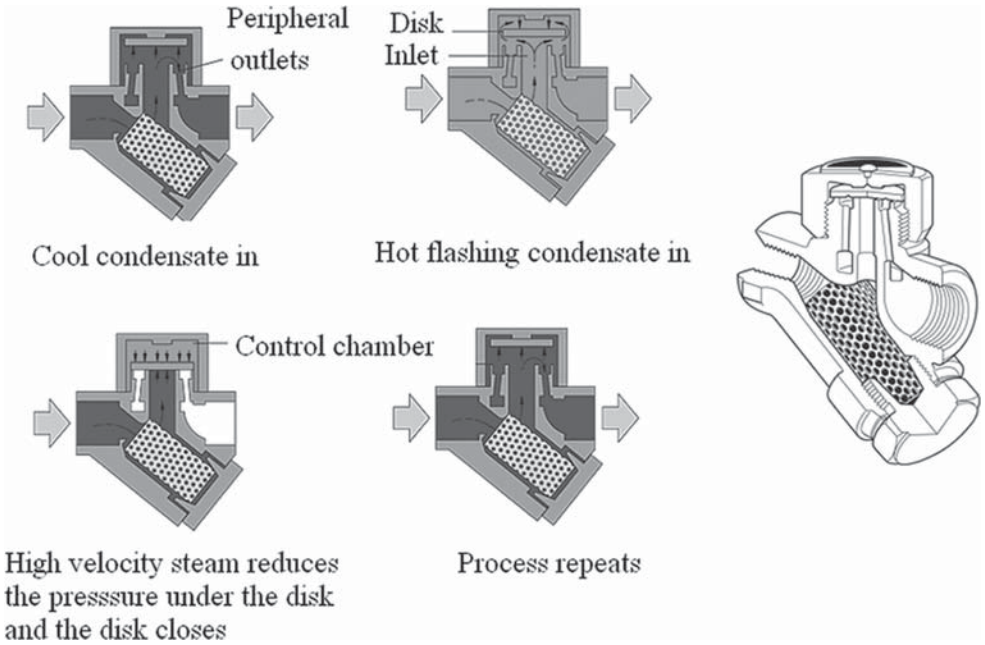


FIG. 2.49 THERMODYNAMIC TRAP (Reprinted by permission of Spirax-Sarco)

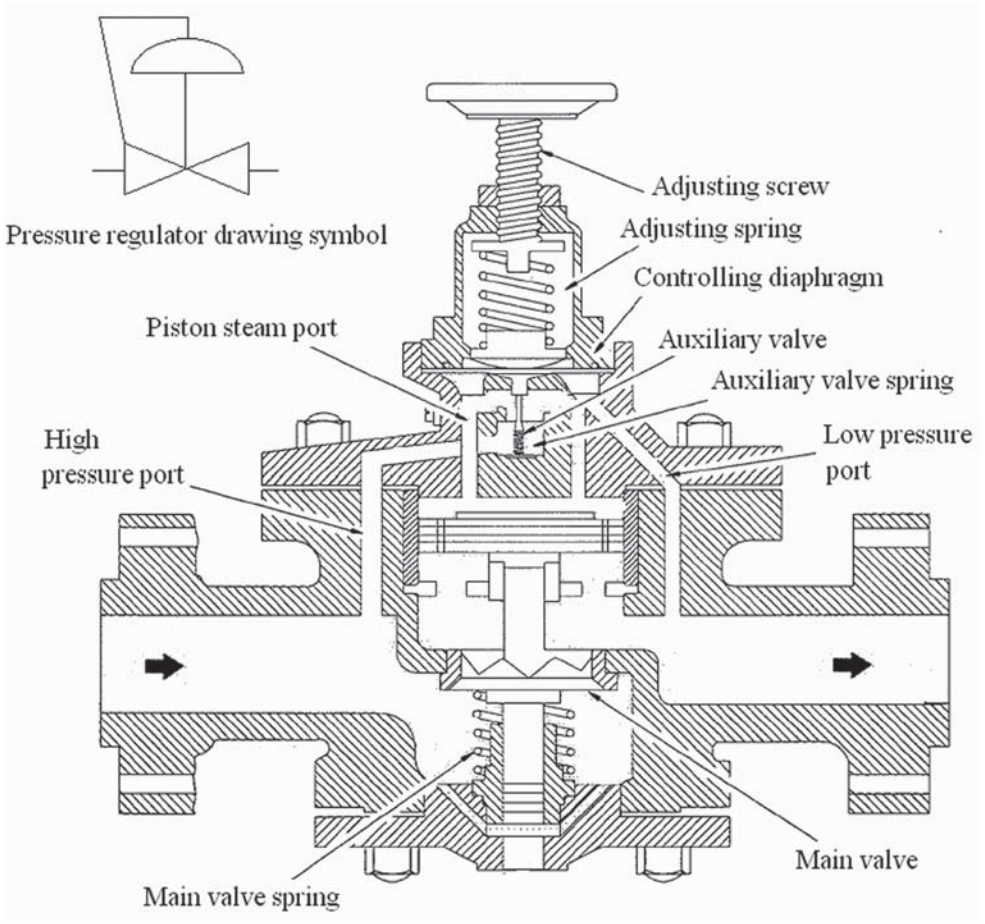


FIG. 2.50 PRESSURE-REDUCING VALVE (US, Department of Energy [66])

safety relief valves, which are suitable for either compressible or incompressible fluid service. Various API (American Petroleum Institute) and ASME B31 piping codes refer to the Pressure Vessel Codes for valve design and testing requirements.

2.3.12.10 Needle Valves Needle valves provide excellent flow control and are typically used for instrumentation and metering of fluids. A partially disassembled valve is shown along with a figure for a complete valve assembly in Fig. 2.44.

2.3.12.11 Pinch Valves Pinch valves provide good flow control and cause the least damage to fluids sensitive to friction (Fig. 2.45). They are available in different materials and designs.

2.3.12.12 Traps Traps are valves used to permit the draining of condensate water from steam systems or to drain liquid from compressed gas systems. When used for steam and condensate, the temperature differential across the trap is typically about 5°F, and temperature measurements can be used to determine if the trap is operating or not. Noncontact radiation thermometers are frequently used for this purpose, since they measure the radiated heat from trap surfaces without touching the trap. Traps are available in numerous designs, and a few of those designs are shown, which are characterized as mechanical, thermodynamic, and thermostatic.

- Two types of mechanical traps are bucket traps and float traps. The inverted bucket trap consists simply of an inverted bucket with a bleed hole floating above the inlet tube into the trap (Fig. 2.46). When the condensate drains, the bucket reseats, and steam or air flow through the trap is prevented. The float trap uses a float to reseat a valve when the condensate is discharged from the trap, which then prevents steam or gas flow through the trap (Fig. 2.47).
- One type of thermostatic trap is a balanced pressure trap (Fig. 2.48), where the disc in the trap contains a

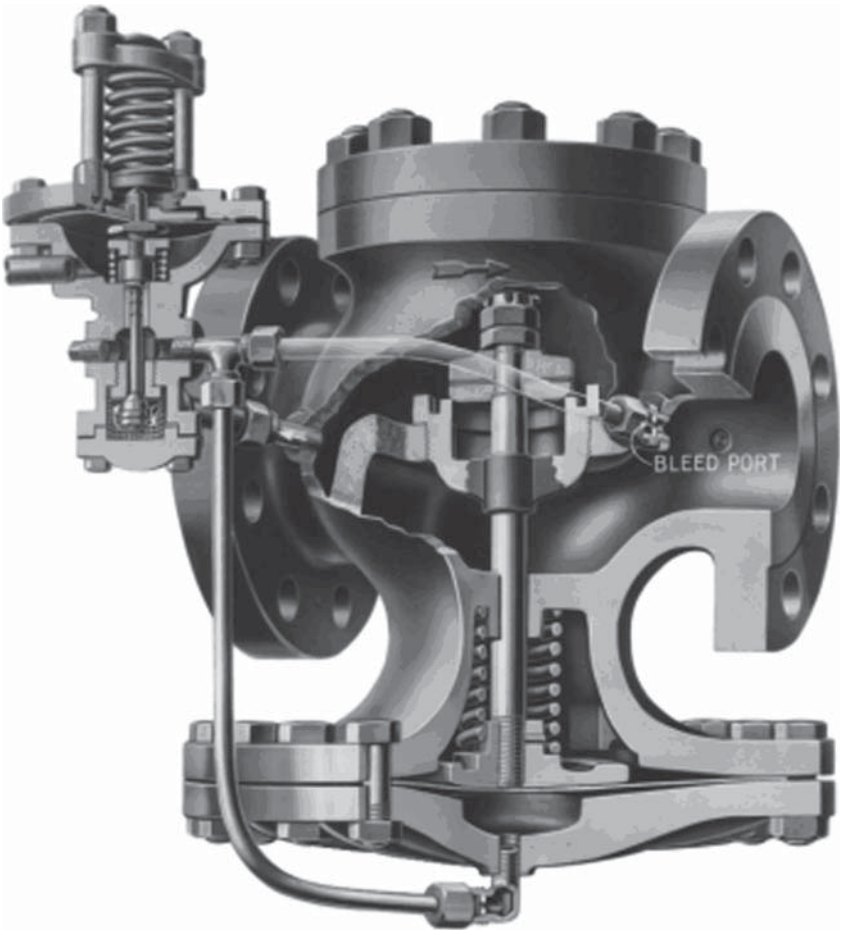


FIG. 2.51 REDUCING VALVE WITH EXTERNAL PILOT (Reprinted with permission of Spence Engineering)

vaporizing fluid, which contracts to permit condensate flow when the system is cold and expands when high-velocity vapors heat the fluid, cause the fluid to expand, and then the disc expands and contstricts the flow passage to prevent steam or gas flow through the valve.

- Thermodynamic traps include the traditional thermodynamic trap (Fig. 2.49), which permits cool condensate to pass through. However, hot condensate entering the control chamber of the trap flashes to steam. Then the steam increases in velocity under the seat, which decreases the pressure under the seat; and the difference in pressure across the disc seats the disc to prevent steam flow through the trap.

2.3.12.13 Pressure Regulators (pressure-reducing valves) are used to control the downstream pressure in a pipe system. The valve spring and diaphragm provide a constant pressure during steady-state operating conditions.

However, upstream pressure changes cause an overshoot of the downstream system pressure, and valve control is required to prevent low flow rates from inducing unstable spring oscillations (hunting) and consequent pressure surges, which may result in visually discernible piping pulsations. For low flow rates, a small diameter bypass in the regulator eliminates unstable operation when adequate flow cannot be assured (Fig. 2.50). Pressure feedback through the bypass prevents low flows across the valve seat and, consequently, an unstable spring operation, which can lead to oscillating pressure excursions well above the design pressure of the system. Larger-capacity valves have a pilot valve, which is a smaller regulating valve on an external bypass line (Fig. 2.51). For upstream pressure changes, the amount of overshoot depends on the pressure change and the design of the regulator where an example of percent overshoot (P.O.) is shown in Fig. 2.52. See also paragraph 7.2.2 for a discussion of the step response, which is applicable to the actuation of pressure regulators.

2.4 FRICTION LOSSES FOR FITTINGS AND OPEN VALVES

Historically, the prediction of friction losses for valves and fittings has improved with the complexity of the solution technique. Three progressively more accurate techniques for predicting friction losses are summarized below.

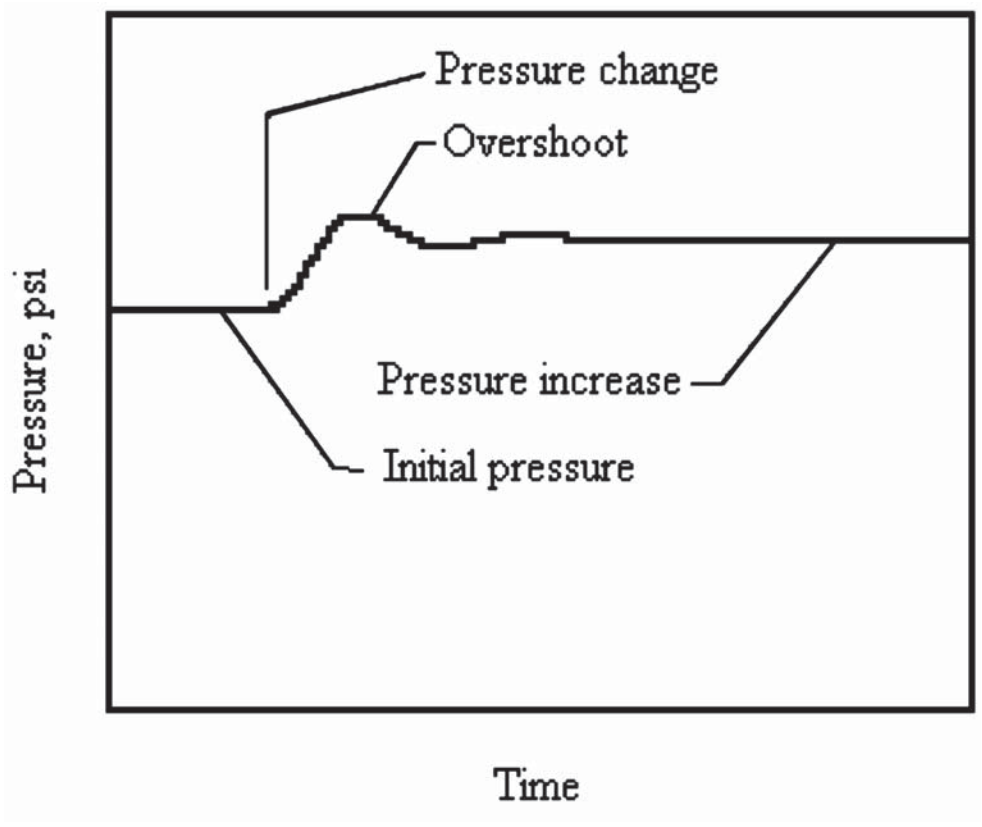


FIG. 2.52 SYSTEM RESPONSE TO A SUDDEN CHANGE IN UPSTREAM PRESSURE

Each of these methods was developed for Newtonian fluids, and only limited experimental data is available for non-Newtonian fluids. The use of manufacturer data for specific components is advised. Following are descriptions of fittings, valves, valve performance, and several methods to find friction losses for these components. With respect to friction losses of components, the more accurate techniques can yield 20% to 30% higher friction losses for small systems where most of the pressure drop is due to fittings rather than pipe.

2.4.1 Graphic Method for Friction Losses in Fittings and Valves

A graphic solution provides quick estimates of system friction losses for Schedule 40 steel pipe, but it inadequately accounts for the relationships between friction factors and flow rates. This method calculates the equivalent length of pipe for some common fittings and valves. Once the equivalent length for the valve or fitting is found per Fig. 2.53, the head loss is found by evaluating the total equivalent pipe length for the system.

2.4.2 Crane's Method for Friction Losses in Steel Fittings and Valves

Crane's method has been widely used for decades and is considered to be reasonably accurate for turbulent flow in steel pipe. This method uses a single value for the resistance coefficient, K, as listed in Table 2.29, but the method assumes the flow to be fully turbulent. Similar to piping (Eq. (2.15)), an (L/D) equivalent is defined such that

$$K_{\text{pipe}} = \frac{f \cdot L''}{D} \Rightarrow K_{\text{fitting}} = K = f \cdot \left(\frac{L''}{D}\right)_{\text{eq}} \qquad \text{US, EE, SI (2.69)}$$

Per Crane, data for K is applicable to steel pipe fitting schedules for steel pipe as listed in Table 2.30, and K values are a function of turbulent friction factors (f_T) as listed in Table 2.31.

Frequently, manufacturer data is provided in terms of a flow coefficient, C_v, instead of a K value. C_v is defined as the flow rate of 60°F water across a valve to cause a 1-psi pressure drop. With appropriate conversions,

$$K = \frac{894 \cdot D^4}{C_v^{\,2}} \qquad \text{US (2.70)}$$

where the pressure drop, ΔP, across the valve equals

$$\Delta P \approx \frac{\rho}{62.4} \cdot \left(\frac{Q}{C_v}\right)^2 \qquad \text{US (2.71)}$$

These two equations both have inconsistent units, and the units are not always the same from different manufacturers.

2.4.3 Modified Crane's Method for Friction Losses in Fittings and Valves of Other Materials and Pipe Diameters

Crane's method can be extended to other materials and pipe sizes for turbulent flow, using the Colebrook equation written in terms of the Darcy friction factor. The Colebrook equation is related to pipe flow for $Re > 4000$, such that

$$\frac{1}{\sqrt{f_n}} = -4 \cdot \log\left(\frac{\varepsilon}{3.7 \cdot D} + \frac{1.255}{Re \cdot \sqrt{f_n}}\right) \qquad \text{US, EE, SI (2.72)}$$

In the turbulent zone for pipe,

$$f = 4 \cdot f_n = \frac{2.5}{\log\left(\frac{3.7 \cdot D}{\varepsilon}\right)^2} \qquad \text{US, EE, SI (2.73)}$$

Assuming that an equivalent length and turbulent friction factor, f_T, exists for fittings, this equation is rewritten as

$$f_T = \frac{2.5}{\log\left(\frac{3.7 \cdot D}{\varepsilon_f}\right)^2} \qquad (2.74)$$

where experimental values for equivalent roughness of fittings, ε_f, are listed in Table 2.1 for several materials. After calculating f_T for a specified material, the Crane values in Table 2.29 can then be extended to other materials and pipe sizes for fully turbulent flow.

Even so, the assumption of complete turbulence can result in significant underestimates of both the friction factor and consequent head loss as the flow approaches laminar. Darby's 3-K method addresses this calculation error. In fact, Darby's method could have been presented as the sole technique for calculating friction losses in fittings along with Churchill's method as the sole technique for calculating friction losses in pipes, but the other methods provide additional insight into the phenomena of friction losses in pipe systems.

2.4.4 Darby's Method for Friction Losses in Fittings and Valves for Newtonian and Non-Newtonian Fluids

Darby's method is considered to be more accurate than Crane's method, since Darby's method increases the accuracy by considering the laminar effects of flow rates and scaling factors for fittings. Preceding Darby's work,

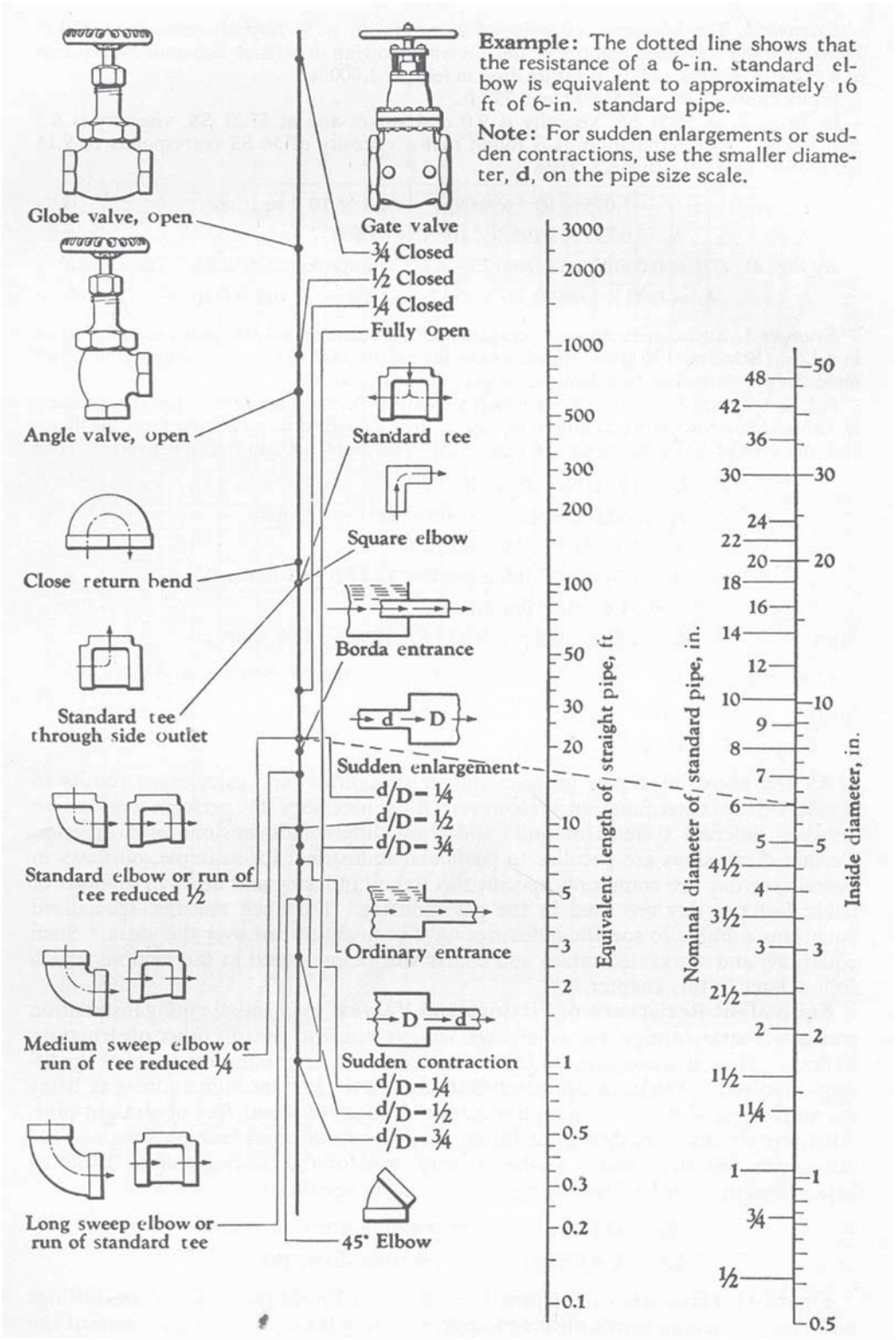


FIG. 2.53 EQUIVALENT PIPE LENGTHS FOR FITTINGS AND VALVES (Reprinted by permission from Crane, Inc. [21])

TABLE 2.29 RESISTANCE, OR LOSS, COEFFICIENTS FOR VALVES AND FITTINGS

Fitting or Valve	K, Crane [21] $K = \left(\frac{L}{\mathrm{ID}}\right)_{eq} \cdot f_T$	K_j, Darby [35], Hooper [73] $K = \frac{K_j}{Re} + K_i \cdot \left(1 + \frac{K_d}{D_{nom,in}^{0.3}}\right)$	K_i, Darby [35], Hooper [73]	K_d, Darby [35]
Threaded Elbows[3,4]				
45 deg, standard	$16 \cdot f_T$	500	0.071	4.2
90 deg, standard	$30 \cdot f_T$	800	0.14	4.0
45 deg, long radius	---	500	0.052	4.0
90 deg, long radius	---	800	0.071	4.2
Welded and Flanged Elbows[3,4]				
90 deg, $r/D = 1$	$20 \cdot f_T$	800	0.091	4.0
90 deg, $r/D = 1.5$	$14 \cdot f_T$	800 (2.K)	$0.20 \cdot \left(1 + \frac{1}{D}\right)$	0
90 deg, $r/D = 2$	$12 \cdot f_T$	800	0.056	3.9
90 deg, $r/D = 3$	$12 \cdot f_T$	----	---	---
90 deg, $r/D = 4$	$14 \cdot f_T$	800	0.066	3.9
90 deg, $r/D = 6$	$17 \cdot f_T$	800	0.075	4.2
90 deg, $r/D = 8$	$24 \cdot f_T$	---	---	---
90 deg, $r/D = 10$	$30 \cdot f_T$	---	---	---
Close Return Bends[3,4]				
Threaded, $r/D = 1$	$50 \cdot f_T$	1000	0.23	4.0
Flanged, $r/D = 1$	---	1000	0.12	4.0
All, $r/D = 1.5$	---	1000	0.10	4.0
Tees, Flow-Through Branch				
Threaded, $r/D = 1$	$60 \cdot f_T$	500	0.274	4.0
Threaded, $r/D = 1.5$	---	800	0.14	4.0
Flanged, $r/D = 1$	---	800	0.28	4.0
Tees, Flow-Through Run				
Threaded, Standard	$20 \cdot f_T$	500 (2.K)	$0.70 \cdot \left(1 + \frac{1}{D}\right)$	0
Threaded, $r/D = 1$	---	200	0.091	4.0
Flanged, $r/D = 1$	---	150	0.017	4.0
Valves[2,5]				
Gate, $\beta = 1$	$8 \cdot f_T$	300 (3-K)	0.037	3.9
Plug, Straight Through, $\beta=1$	$18 \cdot f_T$	300 (3-K)	0.084	3.9
Ball, $\beta = 1$	$3 \cdot f_T$	300 (3-K)	0.017	4.0
Gate, Ball, and Plug, $\beta = 1$	See Crane	300 (2.K)	$0.10 \cdot \left(1 + \frac{1}{D}\right)$	0
Gate, Ball, and Plug, $\beta = 0.9$	See Crane	500 (2.K)	$0.15 \cdot \left(1 + \frac{1}{D}\right)$	0
Gate, Ball, and Plug, $\beta = 0.8$	See Crane	1000 (2.K)	$0.25 \cdot \left(1 + \frac{1}{D}\right)$	0

(continued on next page)

TABLE 2.29 RESISTANCE, OR LOSS, COEFFICIENTS FOR VALVES AND FITTINGS (Continued)

Fitting or Valve	***K*, Crane [21]** $K = \left(\frac{L}{\mathrm{ID}}\right)_{\mathrm{eq}} \cdot f_T$	***K_j*, Darby [35], Hooper [73]** $K = \frac{K_j}{Re} + K_i \cdot \left(1 + \frac{K_d}{D_{\mathrm{nom,in}}^{0.3}}\right)$	***K_i*, Darby [35], Hooper [73]**	**K_d, Darby [35]**
Tees, Flow-Through Run				
Globe, β = 1	$340 \cdot f_T$	1500	1.70	3.6
Globe, Angle (*Y*)	$55 \cdot f_T$	1000 (2.K)	$2.00 \cdot \left(1 + \frac{1}{D}\right)$	0
Globe, Angle	$150 \cdot f_T$	---	---	---
Plug, Three-Way Through flow, β = 1	$30 \cdot f_T$	300	0.14	4.0
Plug, Three-Way Branch Flow, β = 1	$90 \cdot f_T$	500	0.41	4.0
Butterfly, 2–8 in.	$45 \cdot f_T$	800 (2.K)	$0.25 \cdot \left(1 + \frac{1}{D}\right)$	0
Butterfly, 10–14 in.	$35 \cdot f_T$	800 (2.K)	$0.25 \cdot \left(1 + \frac{1}{D}\right)$	0
Butterfly, 16–24 in.	$25 \cdot f_T$	800 (2.K)	$0.25 \cdot \left(1 + \frac{1}{D}\right)$	0
Swing Check, β = 1, Disc Perpendicular to Flow $V_{\min} = 60 \cdot \rho^{-1/2}$ _fps	$50 \cdot f_T$ See Crane for β < 1	---	---	---
Angle Swing Check Valve, β = 1 $V_{\min} = 35 \cdot \rho^{-1/2}$ _fps	$100 \cdot f_T$ See Crane for β < 1	1500	0.46	4.0
Lift Check, β = 1 $V_{\min} = 40 \cdot \rho^{-1/2}$ _fps	$600 \cdot f_T$ See Crane for β<1	< 2000	2.85	3.8
Angle Lift Check, β = 1 $V_{\min} = 140 \cdot \rho^{-1/2}$ _fps	$55 \cdot f_T$ See Crane for β < 1	---	---	---
Tilt Check Valve	See Crane	1000 (2.K)	$0.50 \cdot \left(1 + \frac{1}{D}\right)$	0
Diaphragm	---	1000	0.69	4.9

Pipe Entrances and Exits[4]

	***K*, Crane [21]**	***K*, Hooper [35]**
Exit, Flow Into a Vessel (Any Geometry)	1.0	1.0
Entrance, Flow Into a Pipe That Projects Into a Vessel, Re-entrant	0.78	(160 / *Re*) + 1
Flush Entrance, *r*/*D* = 0, Sharp Corner	0.5	(160/*Re*) + 0.5

(continued on next page)

TABLE 2.29 RESISTANCE, OR LOSS, COEFFICIENTS FOR VALVES AND FITTINGS (Continued)

	***K*, Crane [21]**	***K*, Hooper [35]**
Pipe Entrances and Exits[4]		
Flush Entrance, $r/D = 0.02$	0.28	$(160/Re) + 0.28$
Flush Entrance, $r/D = 0.04$	0.24	$(160/Re) + 0.24$
Flush Entrance, $r/D = 0.06$	0.15	$(160/Re) + 0.15$
Flush Entrance, $r/D = 0.10$	0.09	$(160/Re) + 0.09$
Flush Entrance, $r/D > 0.15$	0.04	$(160/Re) + 0.04$
Expansions and Contractions[2,6] (see Fig. 2.22)		
Contractions $\theta < 45$ deg	$K_1 = \dfrac{0.8 \cdot \left(1 - \left(\frac{D_2}{D_1}\right)^2\right) \cdot \sin\left(\frac{\theta}{2}\right)}{\left(\frac{D_2}{D_1}\right)^4}$	$Re_1 \le 2500$ $\left(1.2 + \dfrac{160}{Re_1}\right) \cdot \left(\left(\dfrac{D_1}{D_2}\right)^4 - 1\right) \cdot 1.6 \cdot \sin\left(\dfrac{\theta}{2}\right)$ $Re_1 > 2500$ $K_1 = (0.6 + 0.48 \cdot f_1) \cdot \dfrac{\left(\left(\frac{D_1}{D_2}\right)^2 - 1\right)}{\left(\frac{D_2}{D_1}\right)^2} \cdot 1.6 \cdot \sin\left(\dfrac{\theta}{2}\right)$
Contractions $45 \text{ deg} > \theta > 180$ deg	$K_1 = \dfrac{0.5 \cdot \left(1 - \left(\frac{D_2}{D_1}\right)^2\right) \cdot \sqrt{\sin\left(\frac{\theta}{2}\right)}}{\left(\frac{D_2}{D_1}\right)^4}$	$Re_1 \le 2500$ $\cdot \left(1.2 + \dfrac{160}{Re_1}\right) \cdot \left(\left(\dfrac{D_1}{D_2}\right)^4 - 1\right) \cdot \sqrt{\sin\left(\dfrac{\theta}{2}\right)}$ $Re_1 > 2500$ $K_1 = (0.6 + 0.48 \cdot f_1) \cdot \dfrac{\left(\left(\frac{D_1}{D_2}\right)^2 - 1\right)}{\left(\frac{D_2}{D_1}\right)^2} \cdot \sqrt{\sin\left(\dfrac{\theta}{2}\right)}$
Expansions $\theta < 45$ deg	$K_2 = \dfrac{2.6 \cdot \left(1 - \left(\frac{D_1}{D_2}\right)^2\right)^2 \cdot \sin\left(\frac{\theta}{2}\right)}{\left(\frac{D_1}{D_2}\right)^4}$	$Re_1 \le 4000$ $K_1 = 5.2 \cdot \left(1 - \left(\dfrac{D_1}{D_2}\right)^4\right) \cdot \sin\left(\dfrac{\theta}{2}\right)$ $Re_1 > 4000$ $K_1 = (2.6 + 2.08 \cdot f_1) \cdot \left(1 - \left(\dfrac{D_1}{D_2}\right)^2\right)^2 \cdot \sin\left(\dfrac{\theta}{2}\right)$
Expansions $45 \text{ deg} > \theta > 180$ deg	$K_2 = \dfrac{\left(1 - \left(\frac{D_1}{D_2}\right)^2\right)^2}{\left(\frac{D_1}{D_2}\right)^4}$	$Re_1 \le 4000$ $K_1 = 2 \cdot \left(1 - \left(\dfrac{D_1}{D_2}\right)^4\right)$ $Re_1 > 4000$ $K_1 = (1.0 + 0.8 \cdot f_1) \cdot \left(1 - \left(\dfrac{D_1}{D_2}\right)^2\right)^2$

(continued on next page)

TABLE 2.29 RESISTANCE, OR LOSS, COEFFICIENTS FOR VALVES AND FITTINGS (Continued)

	K, Crane [21]	*K*, Hooper [35]
In-line Orifice[2]		
Thin Sharp Orifice	See Crane	$Re_1 \le 2500$ $\left(2.72+\left(\frac{D_2}{D_1}\right)^2\cdot\left(\frac{120}{Re_1}-1\right)\right)\cdot\left(1-\left(\frac{D_2}{D_1}\right)^2\right)\cdot\left(\left(\frac{D_1}{D_2}\right)^4-1\right)$ $Re_1 > 2500$ $\left(2.72-\left(\frac{D_2}{D_1}\right)^2\cdot\left(\frac{4000}{Re_1}\right)\right)\cdot\left(1-\left(\frac{D_2}{D_1}\right)^2\right)\cdot\left(\left(\frac{D_1}{D_2}\right)^4-1\right)$

NOTES:

1) In some cases, values to find *K* are unavailable for use in Darby's equation, and values from Hooper's 2-K method are listed in the table. Unless otherwise noted, the 3-K values in the table are Darby's values.
2) Subscripts, 1 and 2, refer to upstream and downstream locations, respectively. For valves, D_1 is the diameter of the valve seat flow area, and D_2 is the valve downstream pipe diameter. For orifices, D_1 is the upstream pipe diameter, and D_2 is the orifice diameter (see Fig. 2.25). Note that the use of subscripts to denote upstream or downstream locations varies for different references, but a consistent use of subscripts is applied to this text.
3) See Crane [21] or Darby [35] for losses in mitered pipe bends.
4) $\beta = D_1/D_2 = 1$ for full port valves. See Crane [21] or the Hydraulic Institute Data Book [50] for additional data on valve resistance coefficients for partial port valves, where $\beta = D_1 / D_2 < 1$.
5) For expansions and contractions, referred to as reducers, see Fig. 2.22 for a description of θ. K_1 and K_2 are calculated using the flow rates at the upstream (D_1) or downstream (D_2) locations, respectively ($K = K_1$ or K_2).

Hooper [73] noted that Crane's method was inaccurate for steel fittings above 6 in. in diameter and when the flow was less than fully turbulent. Hooper described the flow using two parameters that described flow through fittings at high or low velocities, and this technique was referred to as the 2-K method. The 2-K method was further expanded to three variables in Darby's 3-K equation, and values for these variables (K_j, K_i, and K_d) are listed in Table 2.29 for substitution into

$$K = \frac{K_j}{Re} + K_i \cdot \left(1 + \frac{K_d}{D_{nom}^{0.3}}\right) \qquad \text{US, EE, SI(2.75)}$$

This equation expresses *K* for either 2-K or 3-K variables when they are extracted in the format provided in Table 2.29.

Darby also noted that the 3-K method is theoretically applicable to flows of non-Newtonian fluids through fittings, although adequate experimental validation of this technique is presently unavailable. To apply the 3-K method, the Reynold's number, *Re*, is used for Bingham fluids, and the power law Reynold's number, Re_{pl}, is used for power law fluids. Darby noted that this method should give a "good first approximation" to find resistance coefficients for fittings.

TABLE 2.30 APPLICABLE PIPE SCHEDULES FOR CRANE'S METHOD

Class 300 and below	Schedule 40
Class 400 and 600	Schedule 80
Class 1500	Schedule 120
Class 2500 (½ in. to 6 in.)	XXS
Class 2500 (8 in. and up)	Schedule 160

2.4.5 Tabulated Resistance Coefficients for Fittings and Valves Using Crane's, Darby's, and Hooper's Methods

Some resistance coefficients are listed in Table 2.29. The table is set up to either directly find *K* values for use in Crane's method (Eq. (2.69)) or to calculate *K*, using K_j, K_i, and K_d values from Table 2.29. The reader is referred to Crane [21], Darby [35], Hooper [73], and Idelchik [28] for additional data. Manufacturer's data is recommended. Although the recently developed Darby's method will provide more accurate resistance predictions, lower *K* values calculated with a single variable similar to Crane's method are available for a wider range of applications since this method has been in use for many years.

2.5 VALVE PERFORMANCE AND FRICTION LOSSES FOR THROTTLED VALVES

When valves are partially closed, two factors affect their performance. One is the fact that the flow through

TABLE 2.31 FRICTION FACTORS FOR STEEL FITTINGS AND VALVES USING CRANE'S METHOD
(Reprinted by permission from Crane, Inc. [21])

Nominal Pipe Size	½ in.	¾ in.	1 in.	1-¼ in.	1-½ in.	2 in.	2-½–3 in.
Friction Factor, f_T	0.027	0.025	0.023	0.022	0.021	0.019	0.018
Nominal Pipe Size	4 in.	5 in.	6 in.	8–10 in.	12–16 in.	18–24 in.	
Friction Factor, f_T	0.017	0.016	0.015	0.014	0.013	0.012	

the valve decreases as the valve is throttled. The other fact is that the resistance coefficient of friction increases as the valve is throttled. Both flow rate and friction are functions of valve position. Once again, manufacturer or test data is recommended, but data is frequently unavailable. Some of the available data is presented here to provide some insight into the effects of valve selection on system performance. In particular, friction losses and the use of valves as flow control devices are considered.

2.5.1 Valve Flow Characteristics

In this text, the performance of valves with respect to water hammer is the main concern, but valves are typically selected for flow control where water hammer is a secondary concern. Inherent valve characteristics describe valve performance with respect to valve opening and flow through the valve, where defined characteristics are shown in Fig. 2.54. For flow control, linear valves are recommended if most of the system pressure drop is associated with the control valve, and equal percentage valves are recommended if most of the pressure drop is related to other system components (Hutchinson [64]). Linear valves change the flow rate linearly as the valve stem position changes, and equal percentage valves change the flow exponentially with respect to the change in valve stem position.

Although inherent characteristics are theoretically well defined, actual valve characteristics vary within a given type of valve and even vary for similar designs from different manufacturers, as shown in Fig. 2.55. A brief discussion follows to consider valve design details and valve actuation effects on the throttling characteristics of valves.

2.5.2 Throttled Valve Characteristics

As noted, a description of the flow rate through the valve as a function of percent open is required in addition to friction losses to adequately describe valve performance. Valve construction has a significant effect on valve performance, and the fact is that design variations within a specific valve type significantly affect valve performance. Consequently, published valve characteristics sometimes vary considerably for similar valves.

For example, different types of valves (ball, butterfly, plug, and gate) are compared to linear and equal percentage valve characteristics in Fig. 2.56. However, each of these valve types can have different characteristics, as demonstrated by Figs. 2.57 to 2.60. For globe valves, modifications of the valve plug shape permits a full range of valve characteristics, from equal percentage through linear to quick opening (Fig. 2.61).

2.5.3 Resistance Coefficients for Throttled Valves

Resistance coefficient data for throttled valves is far less developed than for fully open valves. The 1-K, 2-K, and 3-K methods developed over time in response to a need for design rules to build pipe systems, but throttled valve characteristics for flow control have not been as thoroughly studied. Consequently, data is typically available for only 1-K models in the turbulent flow regime, and even that data fails to adequately discern friction differences due to valve size, where numerous graphs are available to consider turbulent resistance coefficients as a function of valve opening (Miller [56], Idlechick [28]). Overall, a literature review concludes that many tests have been performed on both open and throttled valves, and the many differences between data cautions one when using generic data to understand flow characteristics for a particular system. Even so, some of the available data for throttled valves is presented to better describe valve performance.

For throttled gate valves of parallel face, slab construction, and $Re > 10{,}000$ (Idlechick [28]),

$$K = \exp\left(2.3 \cdot \sum_{i=0}^{7} a_i \cdot \left(\frac{h}{D_1}\right)^i\right) \quad \text{US, EE, SI (2.76)}$$

where D_1 is the valve seat opening, and h is the stem travel, such that h/D_1 is the percent opening of the valve, and a_i equals the constants $a_0 = 3.22974$, $a_1 = -7.258083$, $a_2 = -44.79518$, $a_3 = 337.6749$, $a_4 = -967.6142$, $a_5 = 1404.989$, $a_6 = -1022.979$, $a_7 = 295.2782$.

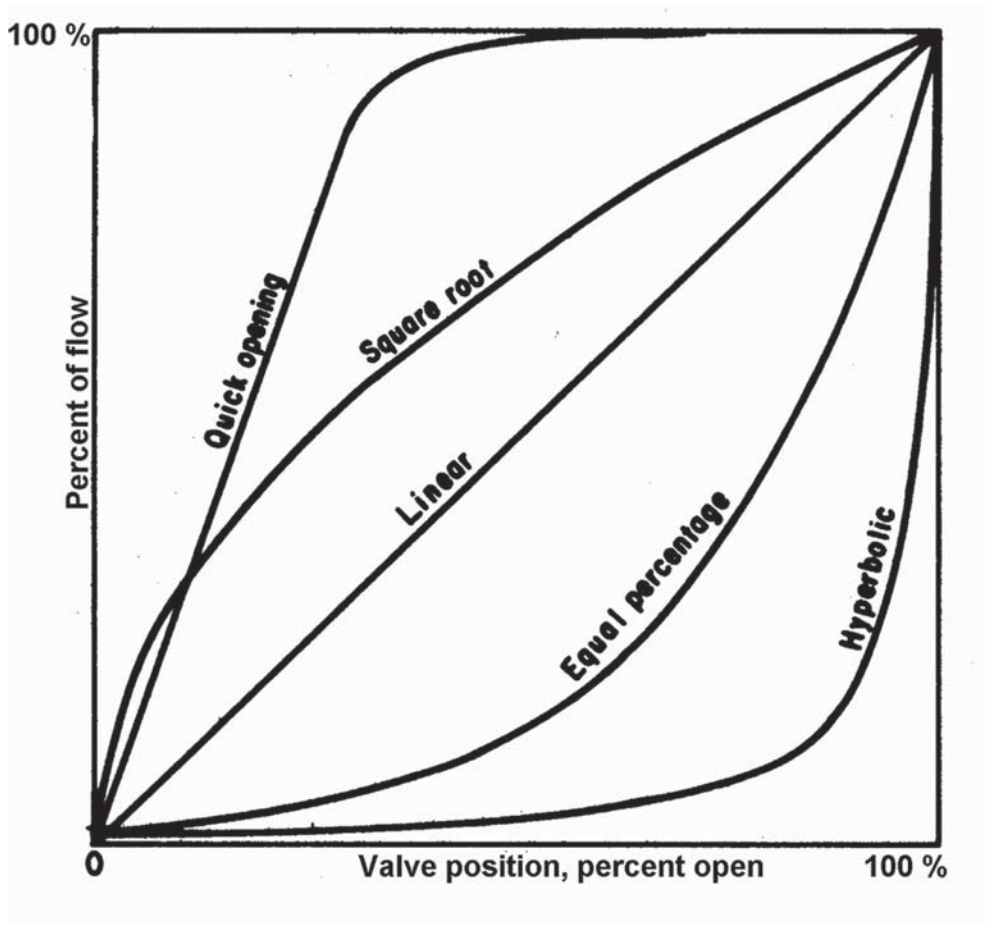


FIG. 2.54 INHERENT VALVE CHARACTERISTICS (Published with permission of ISA. Copyright 1993. All rights reserved. Hutchinson [64])

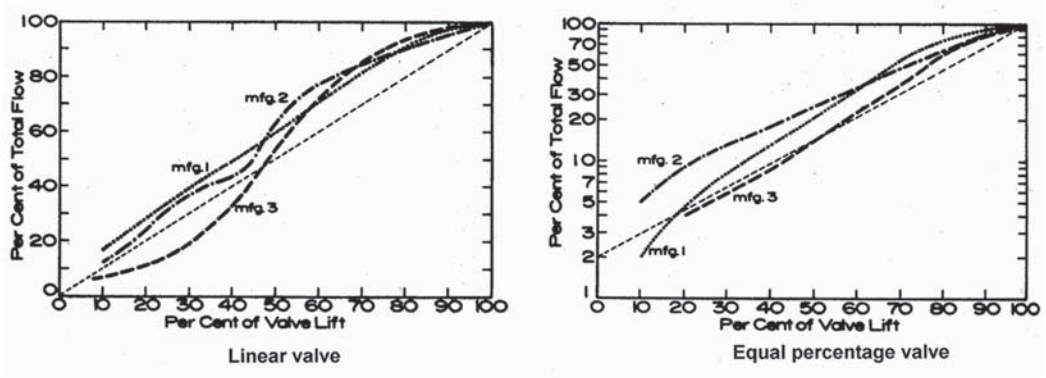


FIG. 2.55 ACTUAL VALVE CHARACTERISTICS FOR SIMILAR VALVES (Published with permission of ISA. Copyright 1993. All rights reserved. Hutchinson [64])

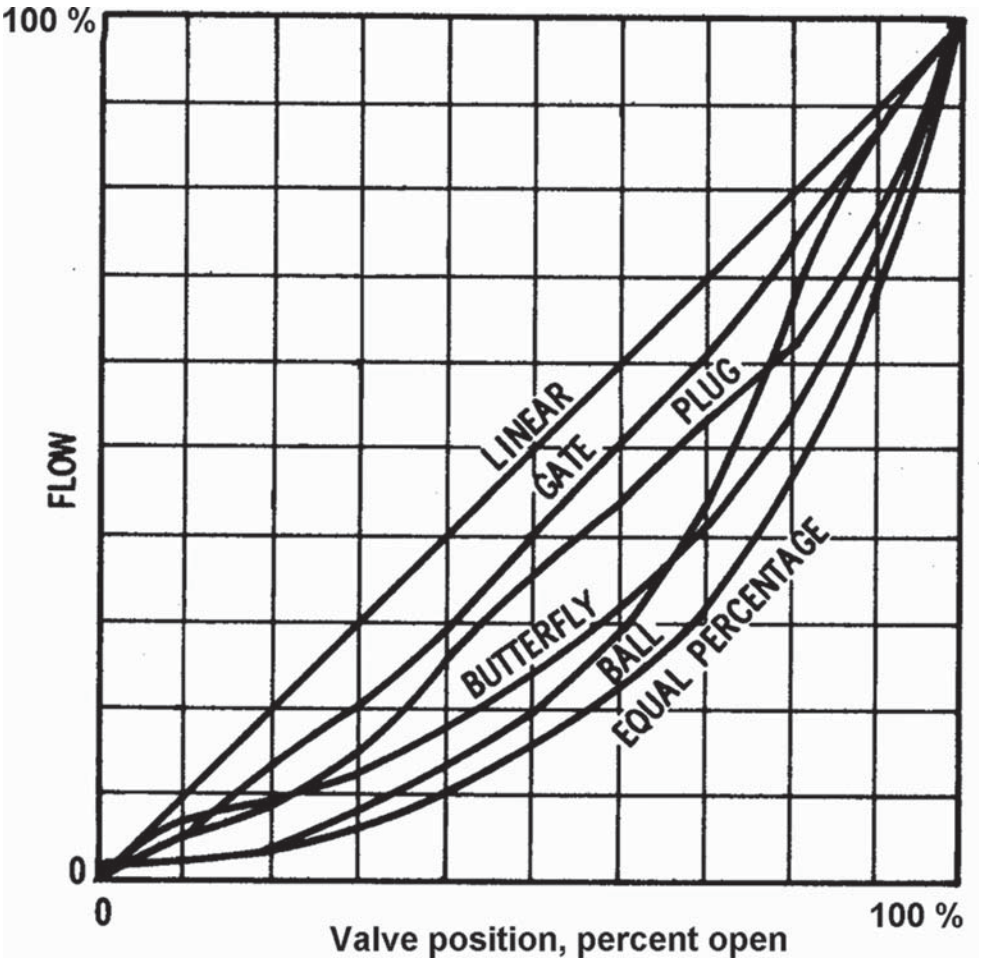


FIG. 2.56 VALVE POSITION VERSUS FLOW (Published with permission of ISA. Copyright 1993. All rights reserved. Hutchinson [64])

For a planar disc butterfly valve, a generic solution is available,

$$K \approx \left(\frac{120}{Re}\right)\cdot\left(\frac{1+0.5\cdot\frac{D_d}{D_1}\cdot\left(1+\sin(\theta)\right)}{\left(1-\left(\frac{D_d}{D_1}\right)^2\cdot\sin(\theta)\right)^2}\right) + \left(1-\frac{50}{\mathrm{Re}}\right)\cdot\left(\frac{1.56}{1-\left(\frac{D_d}{D_1}\right)^2\cdot\sin(\theta)}-1\right)^2 \quad \text{US, EE, SI (2.77)}$$

where D_1 is the pipe diameter, D_d is the disc diameter, and θ is the angle between the disc surface and the pipe centerline. However, turbulent K values for different designs are also available as shown in Fig. 2.62.

For throttled full port ball valves at $Re > 10{,}000$, Fig. 2.63 provides resistance coefficients.

Globe valves have a wide range of characteristics depending on the valve plug design, but some limited data is provided for turbulent pipe flow in Figs. 2.64 and 2.65. Note that valve size has considerable influence on pressure losses.

2.5.4 Valve Actuators

Actuators are controlled by valve positioners, which can be gear operators, solenoid (electromagnet) operators, cam operators, pneumatic operators, etc. Actuators are available in many different designs for different valve types, but they are generally classed as manual actuators; pneumatic diaphragm actuators; piston actuators; electromechanical, geared actuators; and electrohydraulic actuators.

Application and selection of valve actuators for general use is outside the scope of this text (Hutchinson [64]

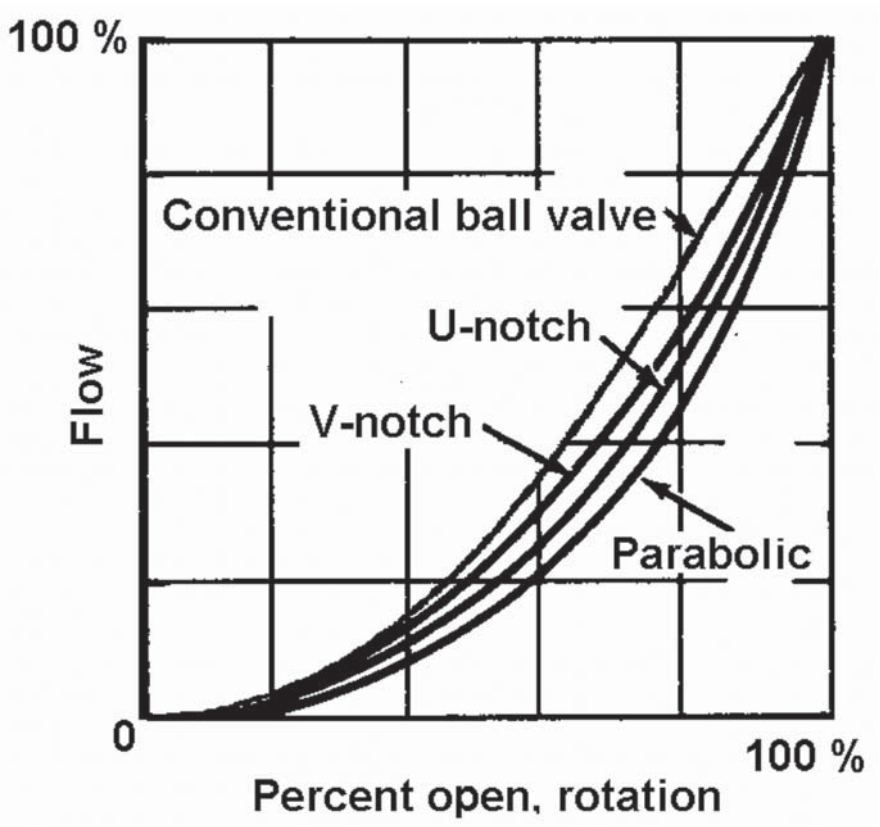


FIG. 2.57 BALL VALVE CHARACTERISTICS (Liptak [31])

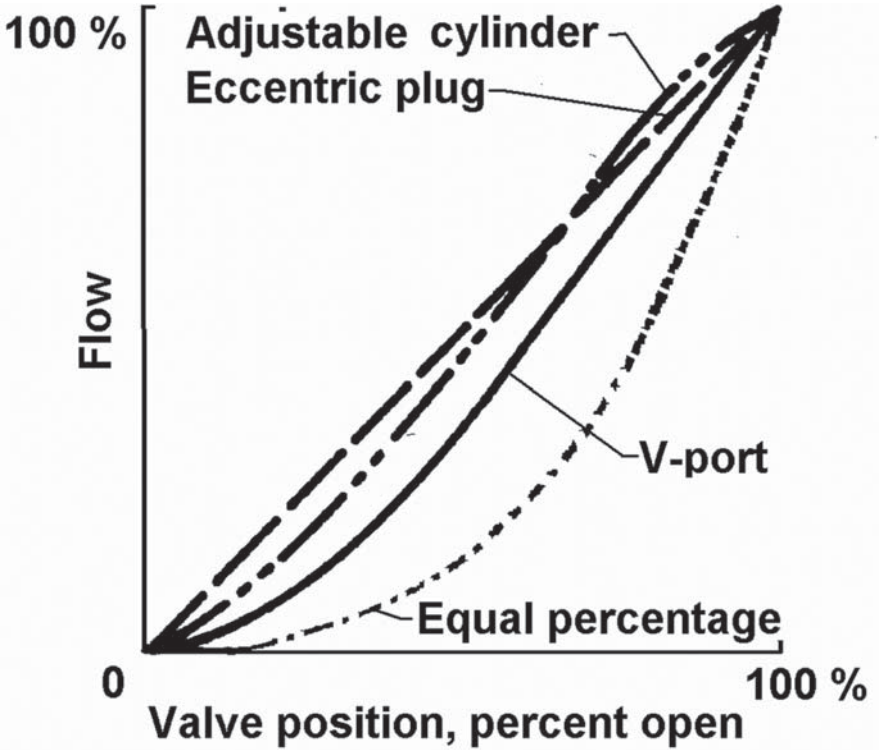


FIG. 2.58 PLUG VALVE CHARACTERISTICS (Liptak [31])

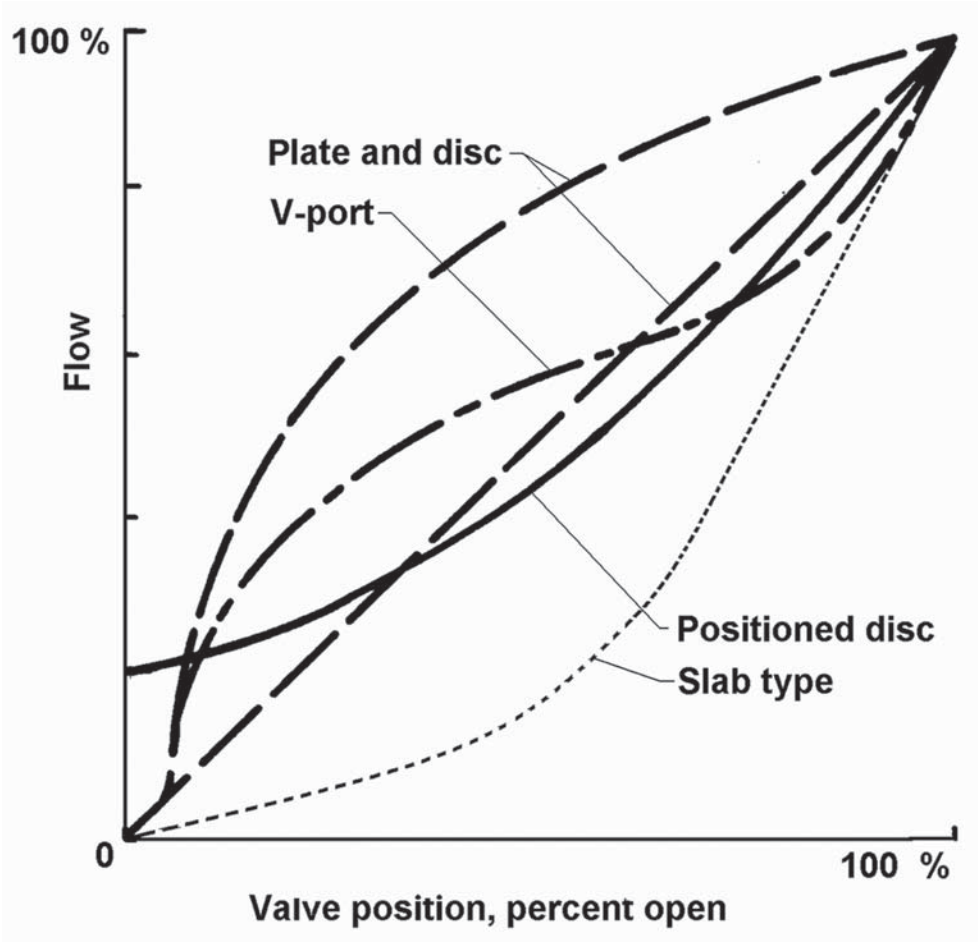


FIG. 2.59 GATE VALVE CHARACTERISTICS (Liptak [31]).

and Liptak [31]), but some mention of actuators and flow control is in order since both valve actuators and control systems affect fluid transients. The pneumatic actuator provides a good example of an actuator, since it is the most frequently used industrial actuator. For a pneumatic actuator (Fig. 2.66), air pressure is controlled against a linear spring to adjust the valve position. Feedback to the controller may, or may not, be supplied from the system flow meter, pressure sensor, or other process variable measurement instrumentation to accurately control the process variable. The positioner, actuator, and valve characteristics combine to provide system control. In fact, the actuator can be used to approximate a linear response from an equal percentage valve or an equal percentage response from a linear valve, by applying suitable multipliers through the control system. The reader is referred to Liptak [31] for a discussion of this technique, which is suited to changing system control without changing valve installations.

With respect to the system response, the distortion coefficient, *Dc*, provides some insight into valve performance with respect to a pipe system. This issue seems relevant since it highlights the fact that a valve's performance is not only a function of design but also of the valve's relationship to the system. Any modeling of a valve must also consider the system application. In Fig. 2.67, the change in flow for linear and equal percentage valves is shown as a function of the distortion coefficient. *Dc*, where

$$Dc = \frac{h_V}{h_L} \tag{2.78}$$

where h_v is the head loss of the valve, and h_L is the system head loss for all of the pump suction and discharge piping components. Note that equal percentage valves are the least affected by increases in pipe length, which is the reason why equal percentage valves are more frequently used than linear valves for control of large systems. Considering Fig. 2.67, another conclusion can be drawn with respect to valve performance in a system. If a pipe is long

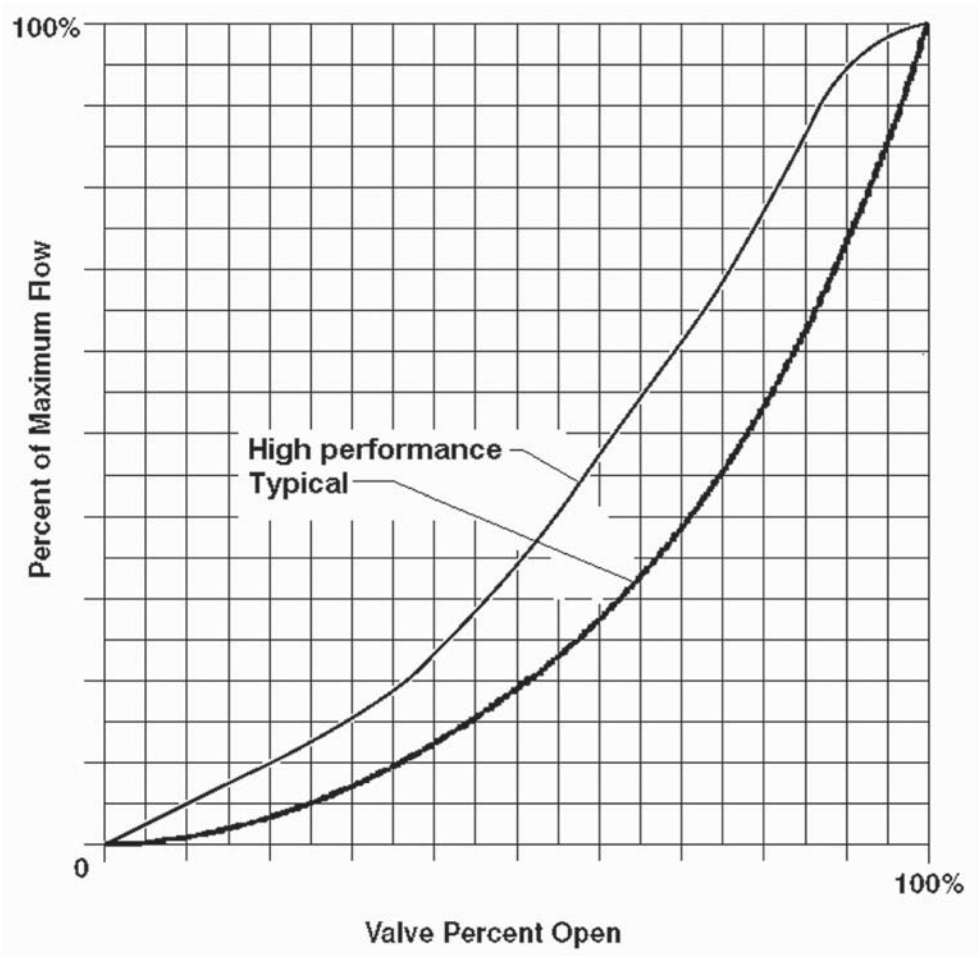


FIG. 2.60 HIGH-PERFORMANCE BUTTERFLY VALVE CHARACTERISTICS (Liptak [31])

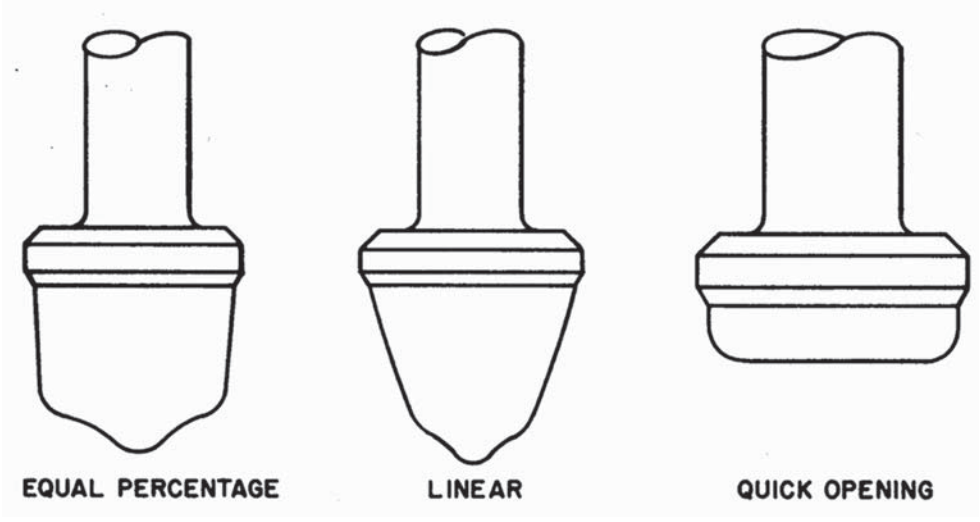


FIG. 2.61 GLOBE VALVE PLUG SHAPES (Liptak [31])

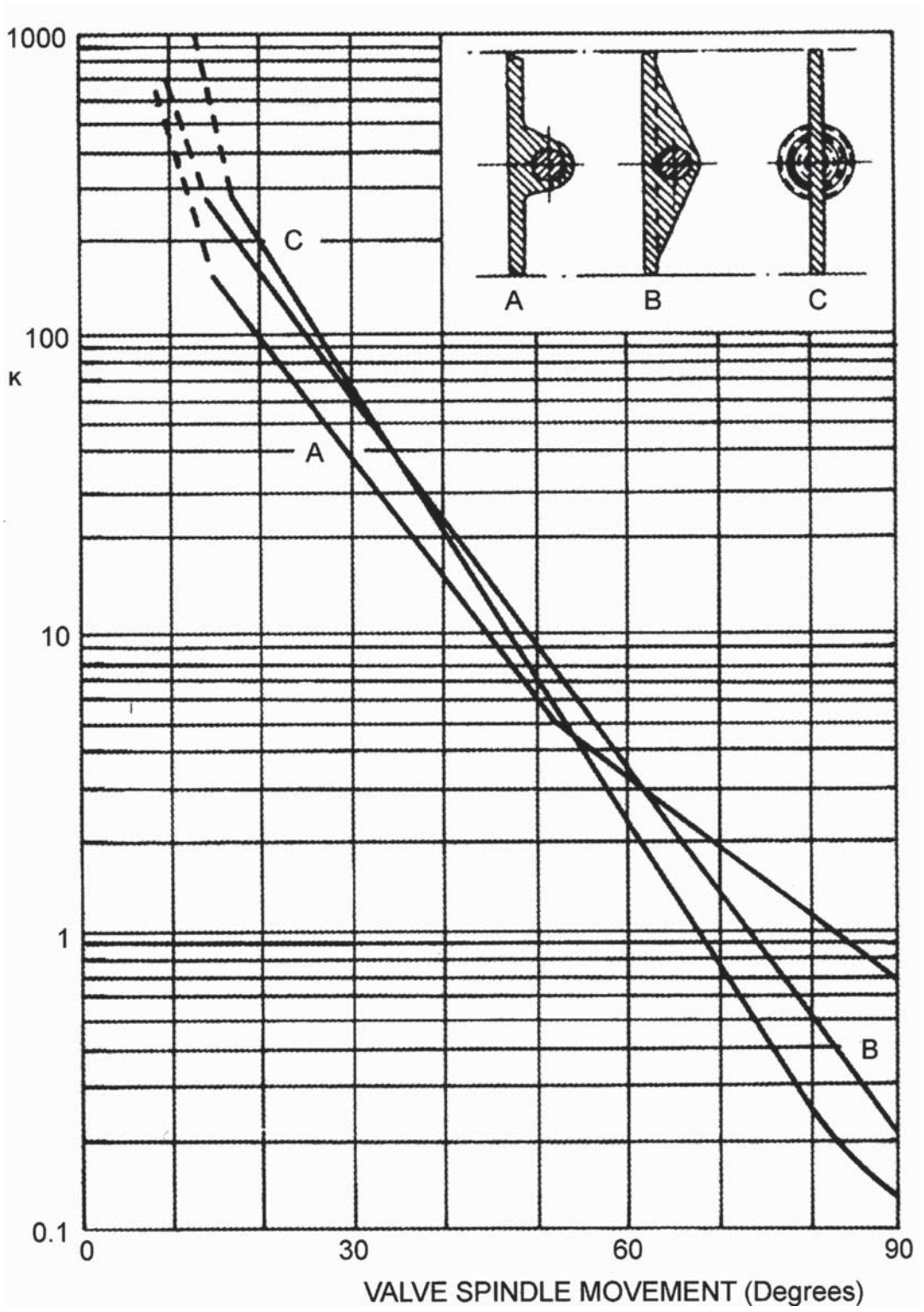


FIG. 2.62 THROTTLED BUTTERFLY VALVE RESISTANCE COEFFICIENTS (Thorley [68])

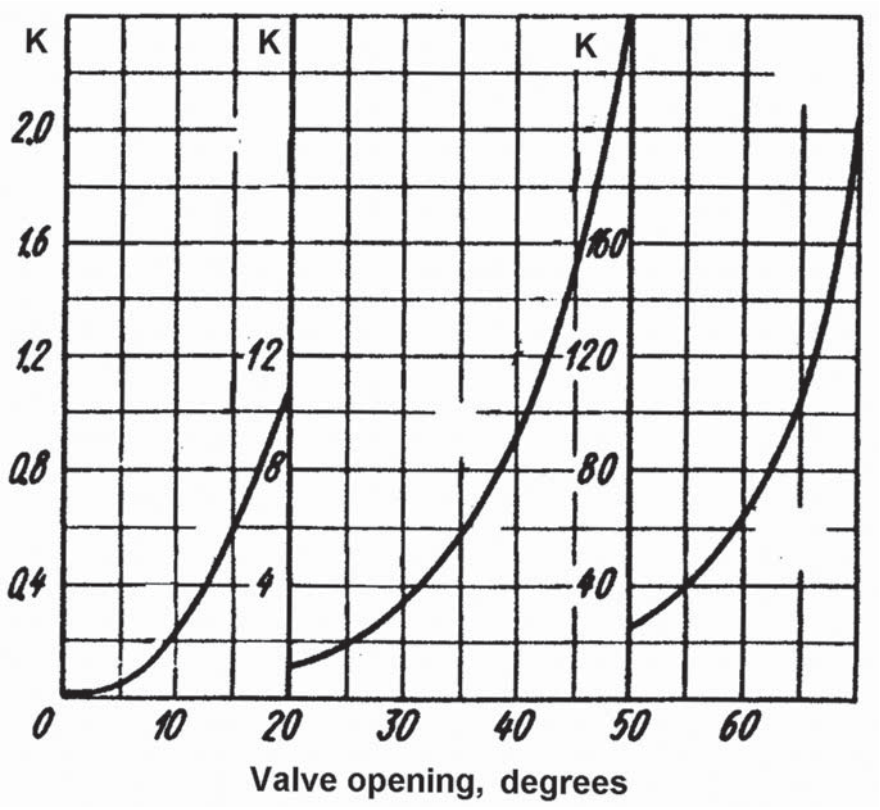


FIG. 2.63 THROTTLED BALL VALVE RESISTANCE COEFFICIENTS (Reprinted by permission of Begell House, Idlechik [28])

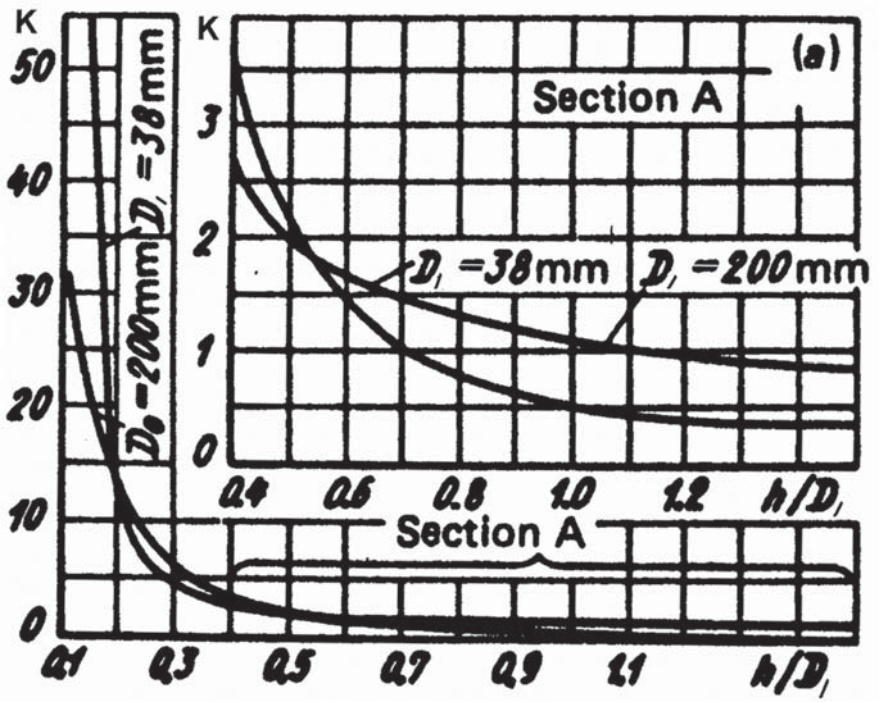


FIG. 2.64 RESISTANCE COEFFICIENTS FOR DIFFERENT-SIZED ANGLE GLOBE VALVES
(Reprinted by permission of Begell House, Idelchik [28]

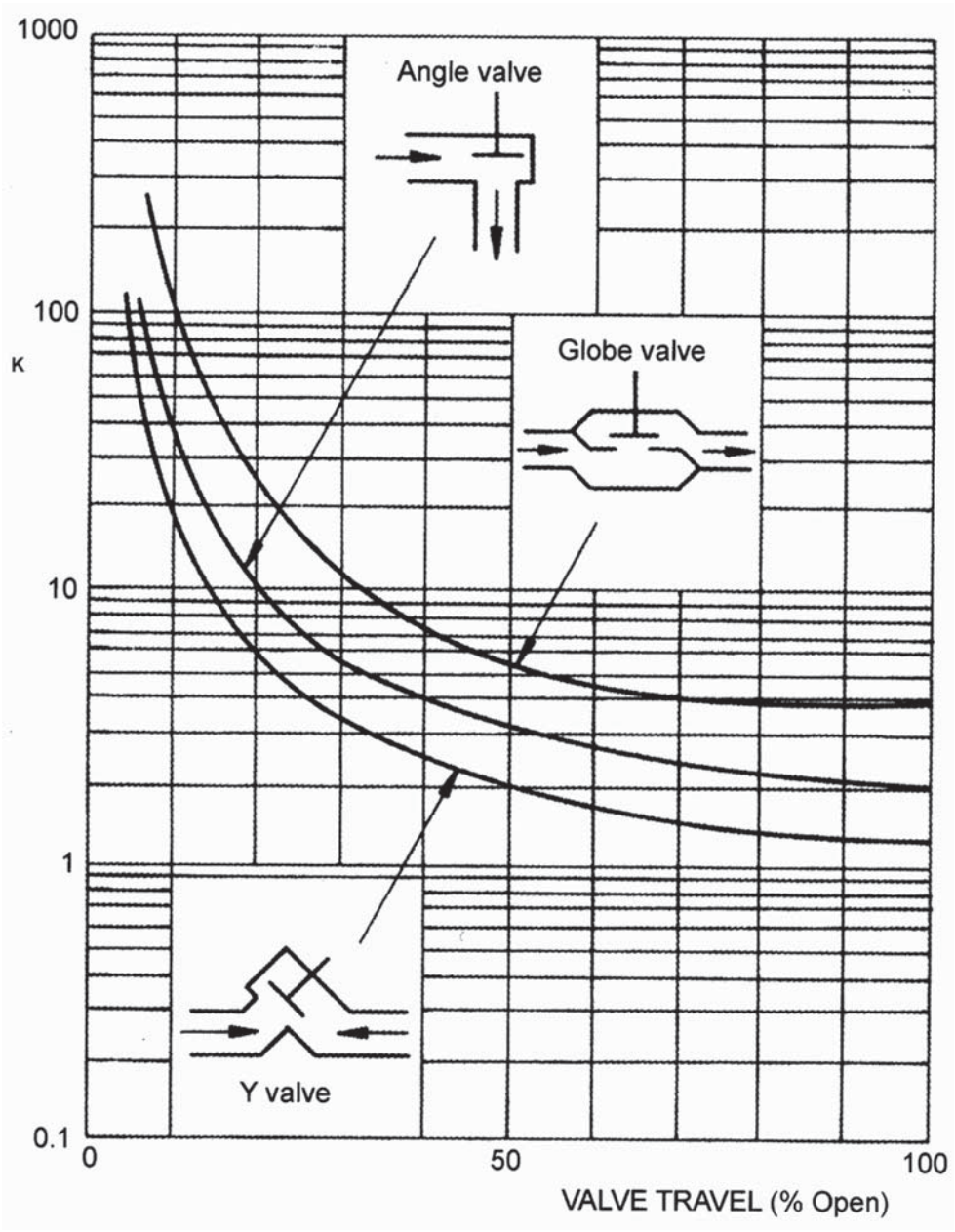


FIG. 2.65 THROTTLED GLOBE VALVE RESISTANCE COEFFICIENTS (Thorley [68])

enough, any valve acts like a quick opening valve, and valve selection has little effect on system performance.

The operation of the actuator affects not only the response of the piping system but also the response of the valve itself. For example, an angle globe valve was tested, and the valve characteristics varied with respect to whether the valve was opening or closing, as shown in Fig. 2.68. With respect to fluid transients, the application of control valves to mitigate water hammer requires careful consideration due to the complex relationship between control valve characteristics and the overall system response. The use of valves to control water hammer is discussed in Chapter 5.

2.5.5 Flow Control

Flow characteristics are controlled through valve positioning or pump speed. This text focuses on the control of water hammer, but controls affect fluid

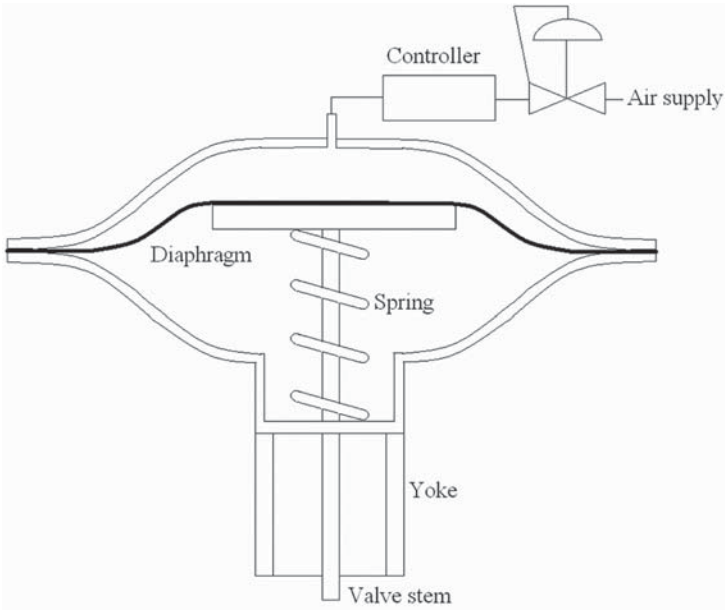


FIG. 2.66 PNEUMATIC ACTUATOR

transients as well as the variables requiring control for the process of concern. In fact, control theory is implicit throughout much of this text, since vibration theory is comparable.

2.5.6 P'I'D' Control

There are three widely used electronic controller modes to stabilize fluid flow. They are proportional, P', integral, I', and derivative, D', modes. The effects of these three P'I'D' modes are shown in Fig. 2.69. The controller changes the flow rates in response to given inputs or flow characteristics by changing the output response of the controller. Proportional control decreases the amplitude of a disturbance in the system. Integral control reduces the disturbance and changes the frequency of the disturbance. Derivative control affects the rate of the disturbance to control flow instabilities. Each of these modes controls fluid transients to yield steady-state conditions.

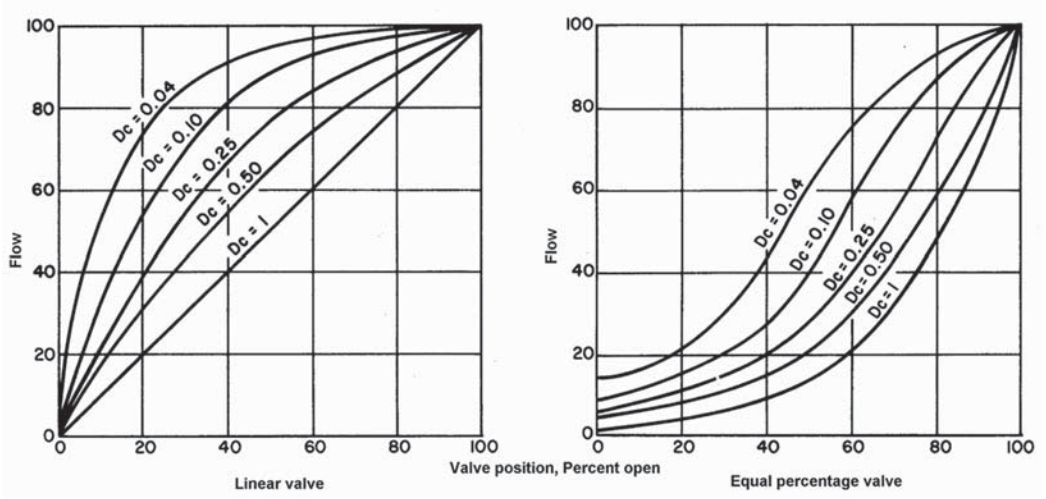


FIG. 2.67 EFFECTS OF SYSTEM PIPING ON THE PERFORMANCE OF LINEAR AND EQUAL PERCENTAGE VALVES (Liptak [31])

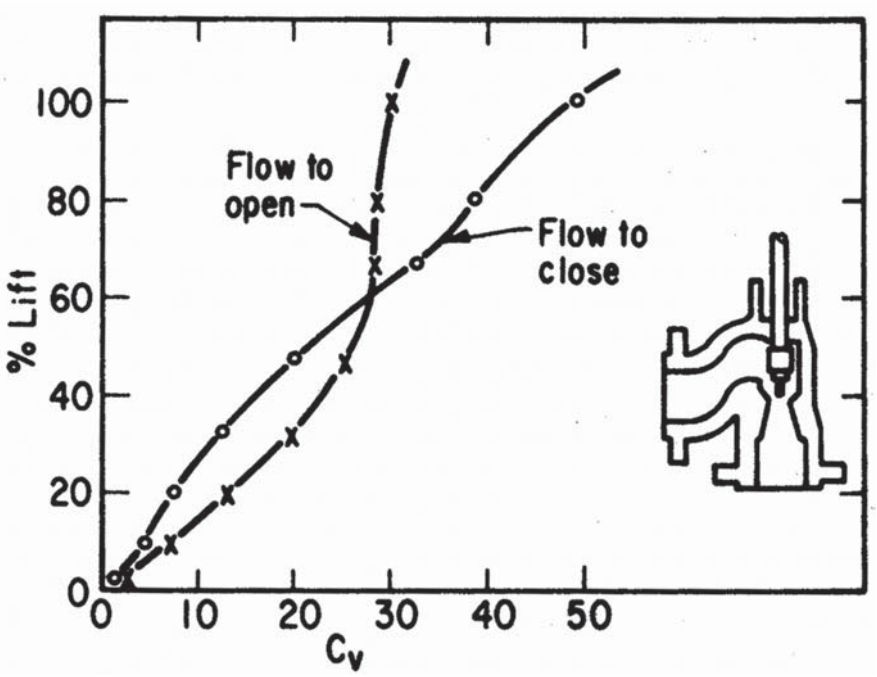


FIG. 2.68 VALVE CHARACTERISTICS FOR OPENING AND CLOSING VALVES
(Published with permission of ISA. Copyright 1993. All rights reserved. Hutchinson [64])

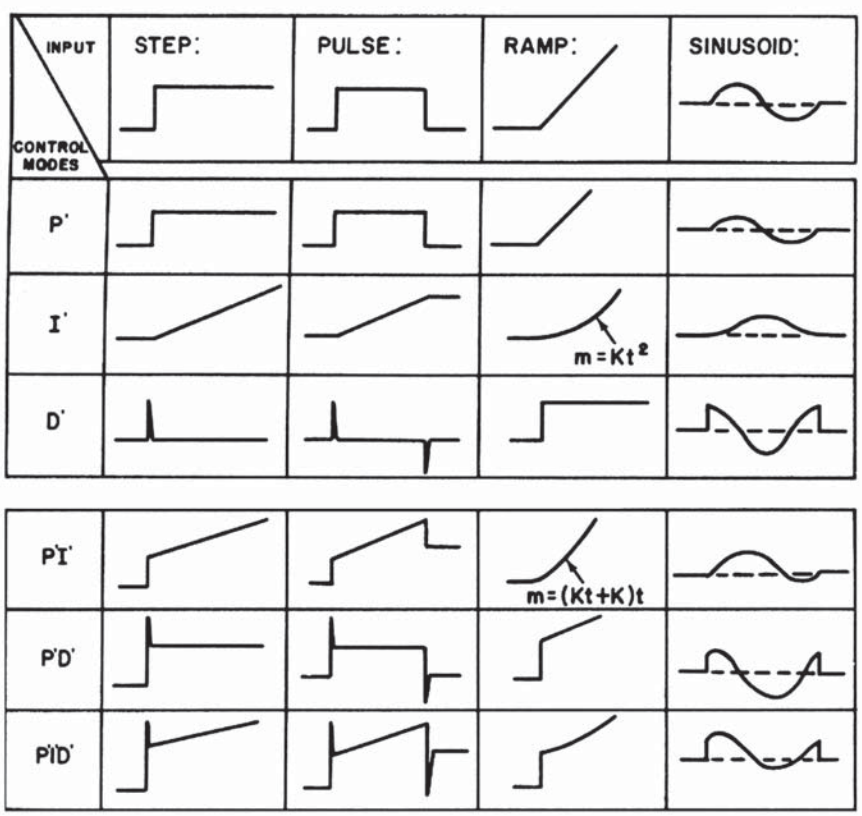


FIG. 2.69 CONTROLLER OUTPUT RESPONSE FOR PROPORTIONAL, INTEGRAL, AND DERIVATIVE MODES
(Hutchinson [64])

The fundamental equations for analogue P'I'D' control are available in the literature, but examples from P'I'D' control provide significant insight into fluid transients and control.

For example, consider Fig. 2.69 with respect to a pipe full of water, which contains a closed valve. If the valve is suddenly opened, the pressure immediately downstream of the valve increases to the upstream pressure. This condition is described by the step input, and the pressure at the downstream end of the valve equals the upstream pressure. Using proportional valve control, the downstream pressure may be decreased. Using integral valve control, the step pressure increase is effectively changed to a ramped pressure. Derivative control is typically used with proportional control, but is frequently difficult to stabilize. The effects of different mode combinations are also shown in the figure.

The actual system response is more complex than indicated in Fig. 2.69. P'I'D' control provides simplified system responses when the fluid flow is described by a step, ramp, sinusoidal, or impulse functions. Actual fluid flow and pressure characteristics are typically more complicated and may contain several different inputs or inputs not described by these three modes. Even so, another example of P'I'D' control provides a broad view of transient control.

Example 2.9 P'I'D' control

To further demonstrate P'I'D' control, an example of control in a closed loop system is summarized here, and a detailed analysis and system description is available from Liptak and Venczel [31]. Figures 2.70, 2.71, and 2.72 describe this typical closed loop response, where the controlled variable could be temperature, pressure, etc.

Pressure control in a pipe system is similar for pressure regulators, water hammer, and pump operations. *P'I'* control describes pressure regulator operation (Fig. 2.52 and 2.70). The set point of the regulator provides proportional control by controlling the regulator spring force and resultant pressure on the regulator diaphragm, while the linear spring in the regulator provides a ramped, integral control for an upstream step pressure increase. Water

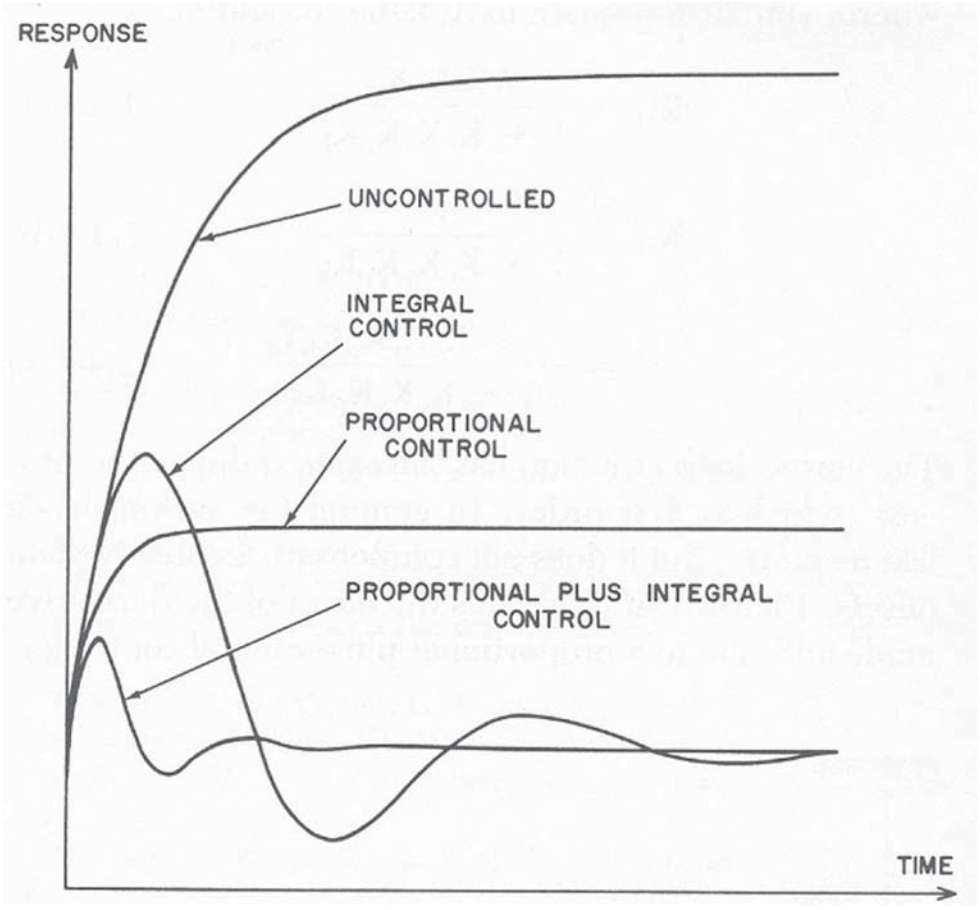


FIG. 2.70 P'I' SYSTEM RESPONSE TO A STEP DISTURBANCE (Hutchinson [64])

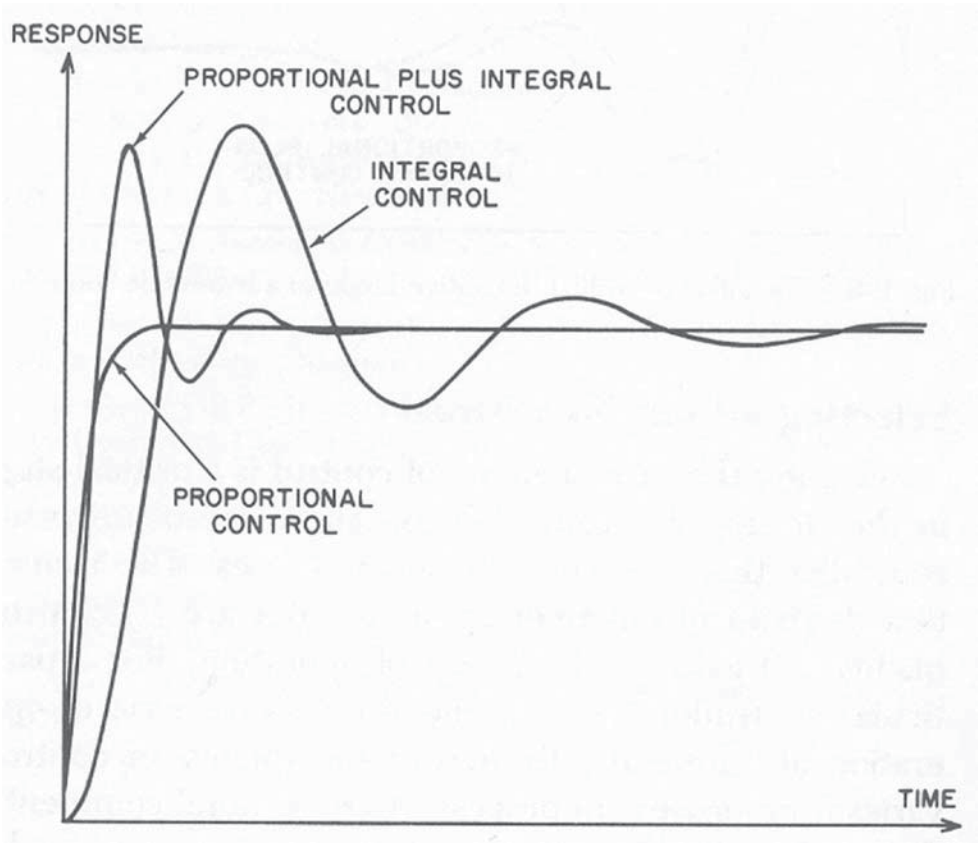


FIG. 2.71 P'I' SYSTEM RESPONSE TO A STEP SET POINT CHANGE (Hutchinson [64])

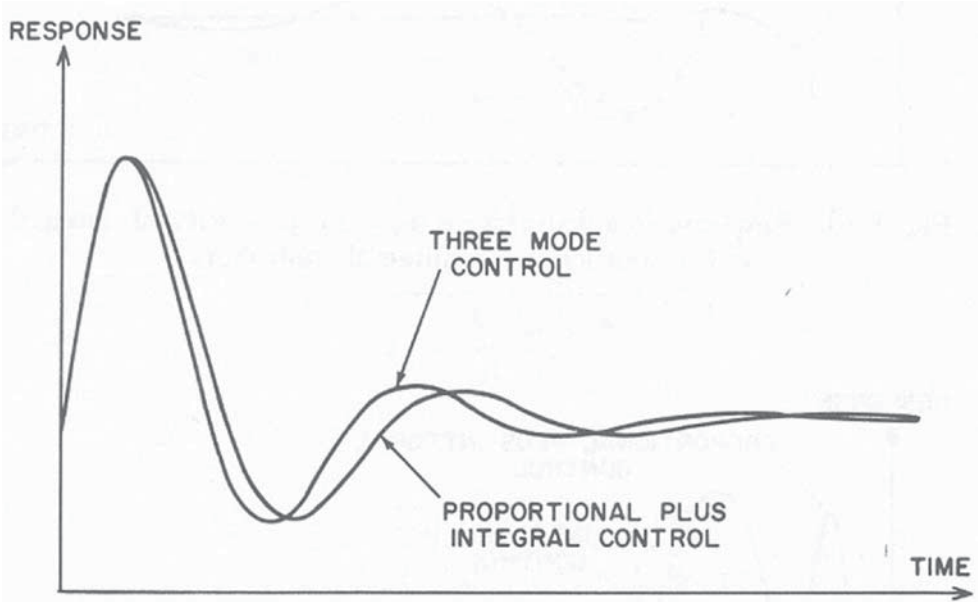


FIG. 2.72 P'I'D' SYSTEM RESPONSE TO STEP DISTURBANCE (Hutchinson [64])

hammer in a closed-end pipe due to a valve opening into the pipe can be described by the uncontrolled response in Fig. 2.70, and the use of a linear actuated valve to control water hammer is described by I' control in Fig. 2.71. Neglecting the inertia of a pump, Figs. 2.71 and 2.72 provide control methods to control transients during pump starting. Either P'I' or P'I'D' can control pump startup transients, where D' converges the system pressure faster. Texts on control theory and control software, such as Matlab®, are available to apply P'I'D' control to fluid transients. Once selected, a P'I'D' controller can be adjusted, or tuned, in the field to account for calculation uncertainties. Other control methods for transients are provided throughout this text.

2.6 DESIGN FLOW RATES

Having reviewed typical pipe system components and techniques to find pressure drops in pipe systems, typical design flow rates may be considered. There are numerous design considerations, or tradeoffs, when selecting optimal flow rates for pipe systems. Karassik [53] recommends a maximum velocity of 8 to 10 ft/second (≈5 to 7 mi/hour) to prevent cavitation through instrumentation and valves, and the American Water Works Association, AWWA, [74] recommends design velocities of 2 to 10 ft/second. Inlet piping to a pump is frequently in the range of 4 to 6 ft/second to prevent pump cavitation. Although particle settling significantly affects required minimum velocities for slurries, minimum velocities of 6 to 8 ft/second are common to prevent settling of particles (Abulnaga [75]), while erosion at pipe elbows is accelerated with increasing slurry velocity. Heat transfer in heat exchangers is improved with higher flow rates. The most recent criteria for determining optimal flow rates are based on economics. Nominal pipe diameters, D_{nom}, are selected with respect to the operating cost of the plant (McKetta [76]). Also, off-design conditions can significantly affect flow, particularly in systems with multiple, varying loads, and some systems, like hydraulic power systems, require flow rates as high as 50 ft/second (Crocker [77]). In other words, both process requirements and economics dictate preferred system flow rates. This range of flow rates is noted here, since the water hammer equation and the dynamic stress equation are both directly proportional to the flow rate. Regardless of flow rate criteria, the design flow rate can only be approximated. In addition to flow rate calculation errors of ±15% to 20%; process temperature changes can cause additional fluctuations in flow rate due to viscosity changes; and fouling, corrosion, or erosion may also affect flow rates. With these minimal comments on system flow rate requirements, coupled with an understanding of system pressure drops, pumps required to supply flow may be considered.

2.7 OPERATION OF CENTRIFUGAL PUMPS IN PIPE SYSTEMS

Once the required flow rate, Q, is approximated, a pump may be selected. There are two general classes of pumps, which are dynamic pumps and positive displacement pumps. This text focuses primarily on the use of dynamic centrifugal pumps, where centrifugal pumps are one type of rotary pump. Rotary pumps also include some positive displacement pumps, such as screw, gear, vane, piston, and lobe pumps. The complete selection criteria for pumps is outside the scope of this text (Karassik [53]), but the operating principles of pumps are essential to understanding fluid transient phenomena.

Since this text limits the discussion to dynamic rather than displacement pumps, a distinction needs to be made between the two classes of pumps. Displacement, or positive displacement, pumps convert energy directly into an increased pressure in a fluid. Dynamic, or kinetic, pumps convert energy to velocity, which is then mechanically converted to an increased pressure. The class of dynamic pumps includes several types, where jets and centrifugal pumps are two types. Centrifugal pumps are further subdivided into radial flow, axial flow, and mixed flow. Pump construction details for other types of pumps are discussed in detail in the *Hydraulic Institute Standards for Centrifugal Pumps* [79]. This chapter includes only jets, centrifugal pumps, and their relationship to system performance. Steady-state flow in centrifugal pump systems is affected by many factors, which include pump types, pump performance, and system performance.

2.7.1 Types of Centrifugal Pumps

The specific speed is typically used to group types of centrifugal pumps. The specific speed, n_S, is defined as

$$n_s = \frac{Q^{0.5} \cdot n}{h_T} \tag{2.79}$$

where n is the pump speed (usually rpm), and h_T is the total head supplied by each pump stage. Specific speeds for various pumps are 1000 to 5000 for radial flow, 5000 to 9000 for mixed flow, and 9000 to 13,000 for axial flow pumps. A diagram of a radial flow pump is shown in Fig. 2.73. Essentially, axial flow pumps are propellers, and mixed flow impellers are designed to provide flow in both axial and radial directions. Although the reader is referred to Karassik [53] for pump construction details, typical pump components are shown in Figs. 2.74 and

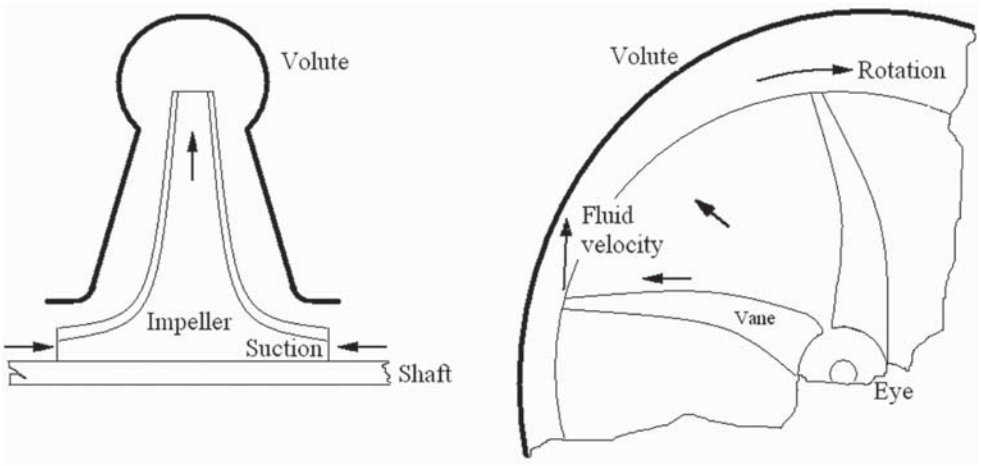


FIG. 2.73 RADIAL FLOW IMPELLER

2.75. For a radial flow pump, liquid is drawn into the impeller through the suction eye, and its velocity increases along the vanes of the rotating pump. The volute expands to decrease the fluid velocity and increase the pressure of the fluid as it is discharged from the pump. Pump curves describe flow and head created by centrifugal pumps. Centrifugal pumps may also run as turbines in reverse, and this mode of operation, and pump curves to describe this mode, are discussed further in Chapter 5.

2.7.2 Pump Curves

The primary operating parameters of pumps are considered with the aid of a typical radial flow pump curve shown in Fig. 2.76. The pump curve provides information on power, efficiency, net positive suction head required for the pump inlet pipe, and flow rate versus head for different impeller diameters, where a commercial practice is to machine various impeller diameters from a standard impeller for a common pump casing design. The operating parameters may be considered in terms of the affinity laws, which are sometimes loosely referred to as the pump laws.

2.7.2.1 Affinity Laws The affinity laws are expressed as

$$\frac{Q_1}{Q_2} = \frac{n_1}{n_2} \qquad \text{US, EE, SI (2.80)}$$

$$\frac{h_1}{h_2} = \left(\frac{n_1}{n_2}\right)^2 \qquad \text{US, EE, SI (2.81)}$$

$$\frac{\text{BHP}_1}{\text{BHP}_2} = \left(\frac{n_1}{n_2}\right)^3 \qquad \text{US, EE, SI (2.82)}$$

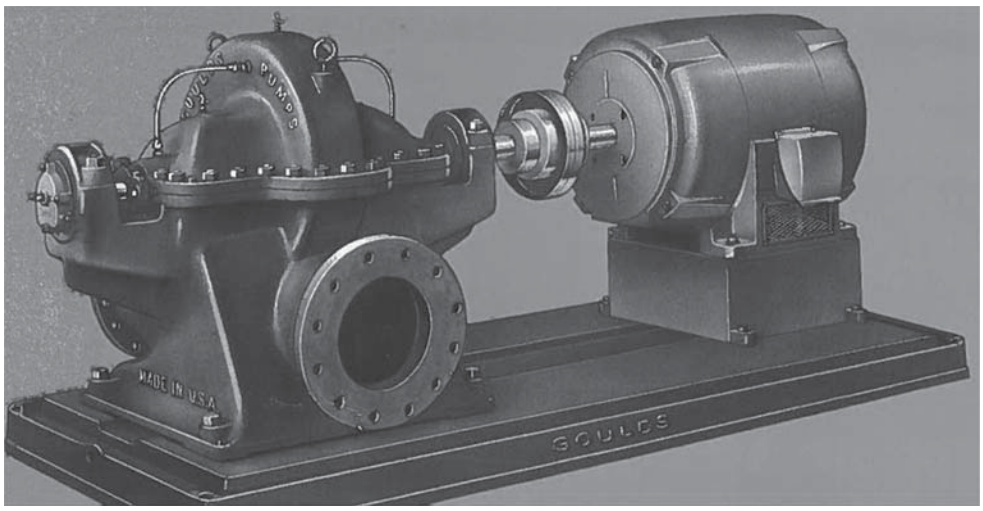


FIG. 2.74 PUMP AND MOTOR INSTALLATION (Reprinted with permission of Gould's Pumps. Inc.)

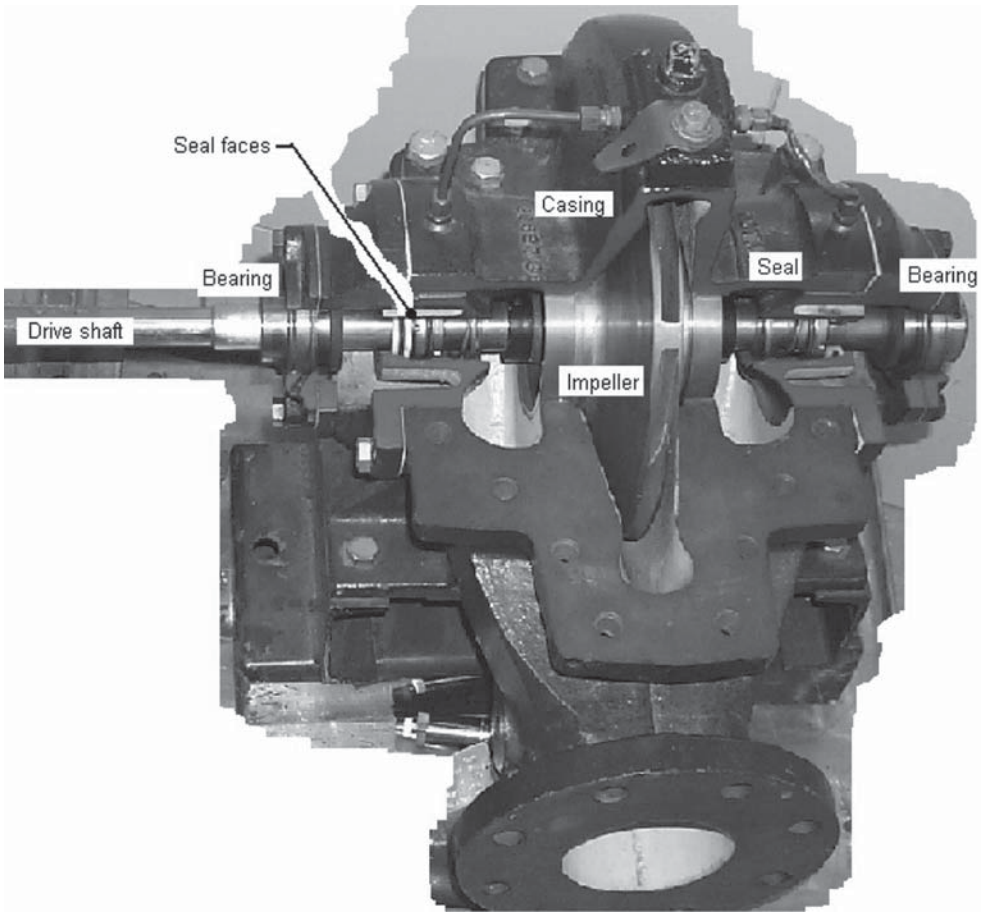


FIG. 2.75 DOUBLE SUCTION, HORIZONTAL SPLIT CASING, RADIAL IMPELLER CENTRIFUGAL PUMP
(Goulds Pumps)

At constant speed,

$$\frac{Q_1}{Q_2} = \frac{D_1}{D_2} \qquad \text{US, EE, SI (2.83)}$$

$$\frac{h_1}{h_2} = \left(\frac{D_1}{D_2}\right)^2 \qquad \text{US, EE, SI (2.84)}$$

$$\frac{\text{BHP}_1}{\text{BHP}_2} = \left(\frac{D_1}{D_2}\right)^3 \qquad \text{US, EE, SI (2.85)}$$

where n is the rotational speed, BHP is the brake horsepower, which is the power required by the pump, h is the head developed by the pump, D is the impeller diameter, Q is the volumetric flow rate, and the subscripts 1 and 2 represent two different design conditions for a given pump. Nonlinearity during speed changes due to motor slip slightly affects speeds calculated from affinity laws.

2.7.2.2 Impeller Diameter Although widely used, the affinity laws are not exact. An implicit assumption of the laws is that the flow in a pump is geometrically similar when speeds are changed. However, streamlines and eddies change when the pump speed or impeller diameter is changed. In fact, Karassik notes that machining an impeller diameter using the affinity laws always results in a flow rate less than the calculated flow rate, due to the change in geometry of the vanes when they are machined. In other words, if the affinity laws are used to calculate a required impeller diameter, the impeller will be machined too small and will need replacement. Manufacturer's data can be used to exemplify these effects of impeller machining.

Example 2.10 Impeller machining

Two impeller data points are compared in Fig. 2.76. Using 700 gpm, at 180 ft of head for a 14.5-in. impeller, a second data point is calculated for an 11-in. diameter impeller:

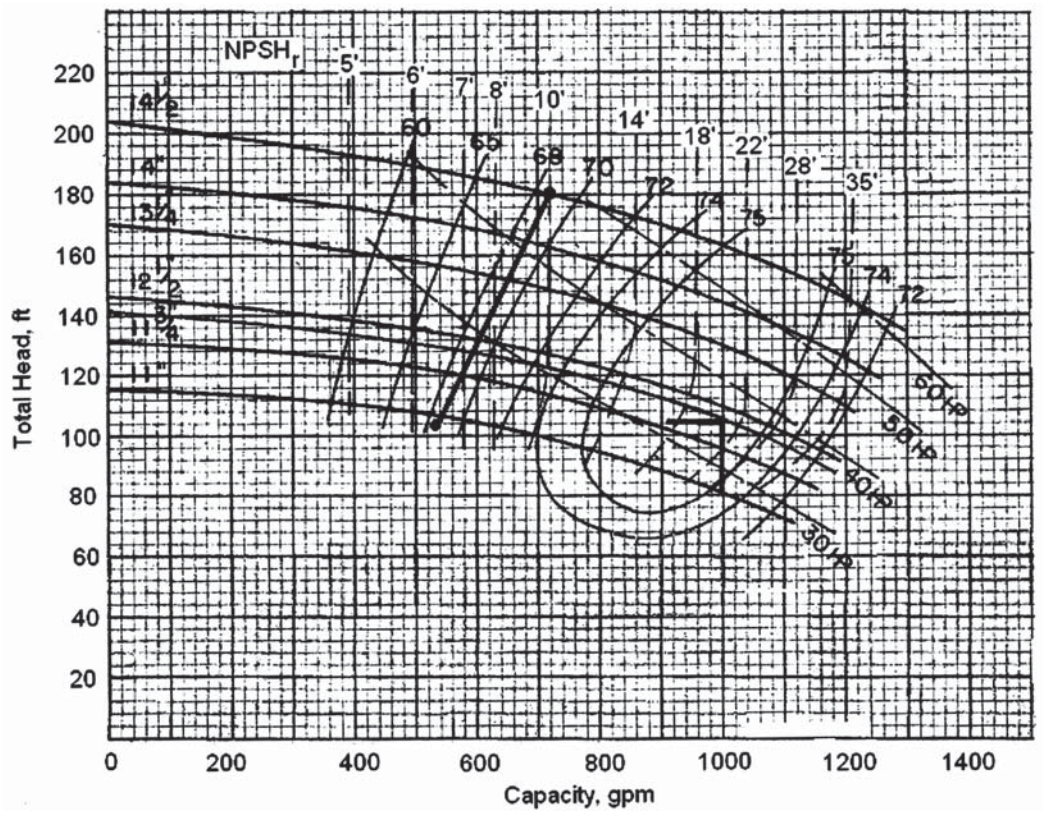


FIG. 2.76 TYPICAL MANUFACTURER'S PUMP CURVE (Reprinted with permission of Gould's Pumps. Inc.)

The predicted head equals 11^2 in.^{2} · 180 ft/14.5^2 in.^{2} = 103.5 ft, and the flow rate equals 11 in. · 700 gpm/14.5 in. = 531 gpm. Other points on the curve are similarly generated. Note that the calculated data point lies slightly below the experimentally determined value for an 11-in. diameter impeller. That is, the affinity laws do not provide an exact prediction for different impeller performances. Note, however, that affinity laws are considered reasonably accurate by the Hydraulic Institute, provided that the impeller diameter is changed by less than 5%.

2.7.2.3 Impeller Speed For different pump speeds, parallel pump curves, similar to Fig. 2.76, may also be generated using the affinity laws, and this calculation technique is occasionally used by pump manufacturers rather than experimental data. Although the errors associated with changing pump speeds are not as large as changing impeller diameters, the affinity laws still have small inherent errors. Again, errors result from the tacit assumption that streamlines can be geometrically scaled. Parallel speed curves are frequently used to describe pump operation when a variable frequency drive (VFD) is used to automatically control the pump speed.

In order of decreasing accuracy, there are three methods to predict pump performance at different speeds.

1. Experimental data from the manufacturer
2. Homologous pump curves (discussed in Chapter 5)
3. Affinity Laws.

2.7.2.4 Acoustic Vibrations in Pumps and Pipe Systems Of passing interest, different events sound different since components vibrate at their natural frequency or the frequency of a forcing function. For example, a 60-Hz electrical transformer and a 3600-rpm pump both vibrate near the 60-Hz forcing frequency, and they sound the same, while an 1800-rpm motor vibrates at an audibly lower, 30-Hz frequency. In comparison, objects that are struck by an object, or force, vibrate at their natural frequency. For example, the pinging of incipient cavitation occurs at a high frequency due to pipe wall erosion caused by single bubble collapse, while fully developed cavitation causes a low frequency gravelly sound as many bubbles collapse near the pipe wall, which vibrates the entire pipe, and in turn vibrates the pipe supports to yield a low-frequency rumbling sound. Similarly, water

hammer induces a loud, low-frequency, 2 to 10 Hz bang as the structural supports vibrate in response to a shock wave. If the pipe is well supported without any looseness of components, water hammer may occur without any banging at all.

2.7.2.5 Power and Efficiency Pumps are typically purchased to run at maximum efficiency for a desired flow rate and head. Referring again to Fig. 2.76, a pair of intersecting lines indicates the requirement supplied to the manufacturer. In this case, a 12.25-in. impeller supplying 1000 gpm at 104 ft of head was required. From the curve, efficiency for this pump is 75% (0.75) at approximately 35 hp. Pump efficiency is affected by fluid friction and mechanical friction, as well as leakage across the wear rings in the pump due to the differential pressure in the pump.

To initially determine pump power and efficiency, the pump manufacturer uses a dynamometer or measures the torque to the pump or input power to the motor, where

$$\mathrm{BHP}(\mathrm{hp}) = \frac{n(\mathrm{rpm}) \cdot T(\mathrm{ft \cdot lbf})}{5250} \qquad \text{US (2.86)}$$

For common three-phase, alternating current, induction motors,

$$\mathrm{BHP}(\mathrm{hp}) = \frac{\eta_\phi \cdot \mathrm{volt} \cdot \mathrm{ampere} \cdot \mathrm{PF} \cdot 1.732}{746} \qquad \text{US (2.87)}$$

For small single phase motors (< 10 hp) and direct current motors,

$$\mathrm{BHP}(\mathrm{hp}) = \frac{\eta_\phi \cdot \mathrm{volt} \cdot \mathrm{ampere} \cdot \mathrm{PF}}{746} \qquad \text{US (2.88)}$$

$$\mathrm{BHP}(\mathrm{hp}) = \frac{\mathrm{WHP}}{\eta} = \frac{Q(\mathrm{gpm}) \cdot h(\mathrm{ft}) \cdot \mathrm{Sp}G}{3960 \cdot \eta} \qquad \text{US (2.89)}$$

$$\mathrm{BHP}(\mathrm{hp}) = \frac{\mathrm{WHP}}{\eta} = \frac{Q(\mathrm{ft}^3/\mathrm{second}) \cdot h(\mathrm{ft}) \cdot \mathrm{Sp}G}{8.82 \cdot \eta} \qquad \text{EE (2.90)}$$

where WHP is the water horsepower provided by the pump, BHP is the actual power supplied by the motor, η is the pump efficiency, which is the combined efficiency of the motor and pump, η_φ and PF are the motor efficiency and power factor supplied by the motor manufacturer's nameplate, T is the torque provided by the motor to the pump, and both volts and amperes are measured at the motor. For the selected design point on the curve in Fig. 2.76, the required horsepower equals (1000 ·104 ·1)/(3960 · 0.75) = 35 hp. Note that manufacturer's pump curves are typically established using water at a SpG = 1, and other fluids and temperatures change the requirements for a pump.

2.7.2.6 Effects of Other Fluids on Pump Performance Even though viscosity is absent from the affinity laws, viscosity does, in fact, affect pump performance. Increased viscosity increases power and decreases both the head and efficiency of a pump. Some data is available (Hydraulics Institute [79]) in graphic format in Fig. 2.77. The figure is applicable to radial flow pumps for Newtonian fluids, where data was obtained from petroleum oils in 2-in. to 8-in. diameter pump discharges. To apply the chart, the following equations are required.

$$Q_\mathrm{w} = \frac{Q}{C_\mathrm{Q}} \qquad \text{US (2.91)}$$

$$h_\mathrm{w} = \frac{h}{C_\mathrm{H}} \qquad \text{US (2.92)}$$

$$\eta_\mathrm{w} = \frac{\eta}{C_\eta} \qquad \text{US (2.93)}$$

where Q_w, h_w, and η_w are the flow, head, and efficiency defined on a pump curve, Q, h, and η are the required actual flow rate, head, and efficiency, and C_Q, C_H, and C_η are constants used in Fig. 2.77.

Example 2.11 Effects of viscosity on pump performance

The Hydraulic Institute [79] provided this example for a viscous fluid of 1000 SSU (220 centistokes) and 0.9 SpG, which from Fig. 2.77 is the viscosity for an 85°F, SAE 30 motor oil. Given the pump curve for water in Fig. 2.76, find the curves for power, head, and efficiency for the specified oil. For example, at 750 gpm and 100 ft of head, the chart is entered at 750 gpm, up to 100 ft of head, over to 1000 SSU, up to the C_Q, C_H, C_η curves, and over to read the values of C_Q, C_H, and C_η. Then,

$Q = C_\mathrm{Q} \cdot Q_\mathrm{w} = 0.95 \cdot 750$ gpm = 712.5 gpm
$h = C_\mathrm{H} \cdot h_\mathrm{w} = 0.92 \cdot 100$ ft = 92 ft
$\eta = C_\eta \cdot \eta_\mathrm{w} = 0.635 \cdot 0.82 = 0.521$
BHP = $Q \cdot h \cdot \mathrm{Sp}G / (3960 \cdot \eta) = 712.5 \cdot 92 \cdot 0.9 / (3960 \cdot 0.521) = 28.6$ hp

Similarly, other points on the curves may be calculated to obtain the curves for the oil shown in Fig. 2.78.

2.7.2.7 Net Positive Suction Head and Cavitation The net positive suction head is usually considered in terms of two quantities, the net positive suction head required, NPSHr, and the net positive suction head available, NPSHa. NPSHr is determined by the pump designs.

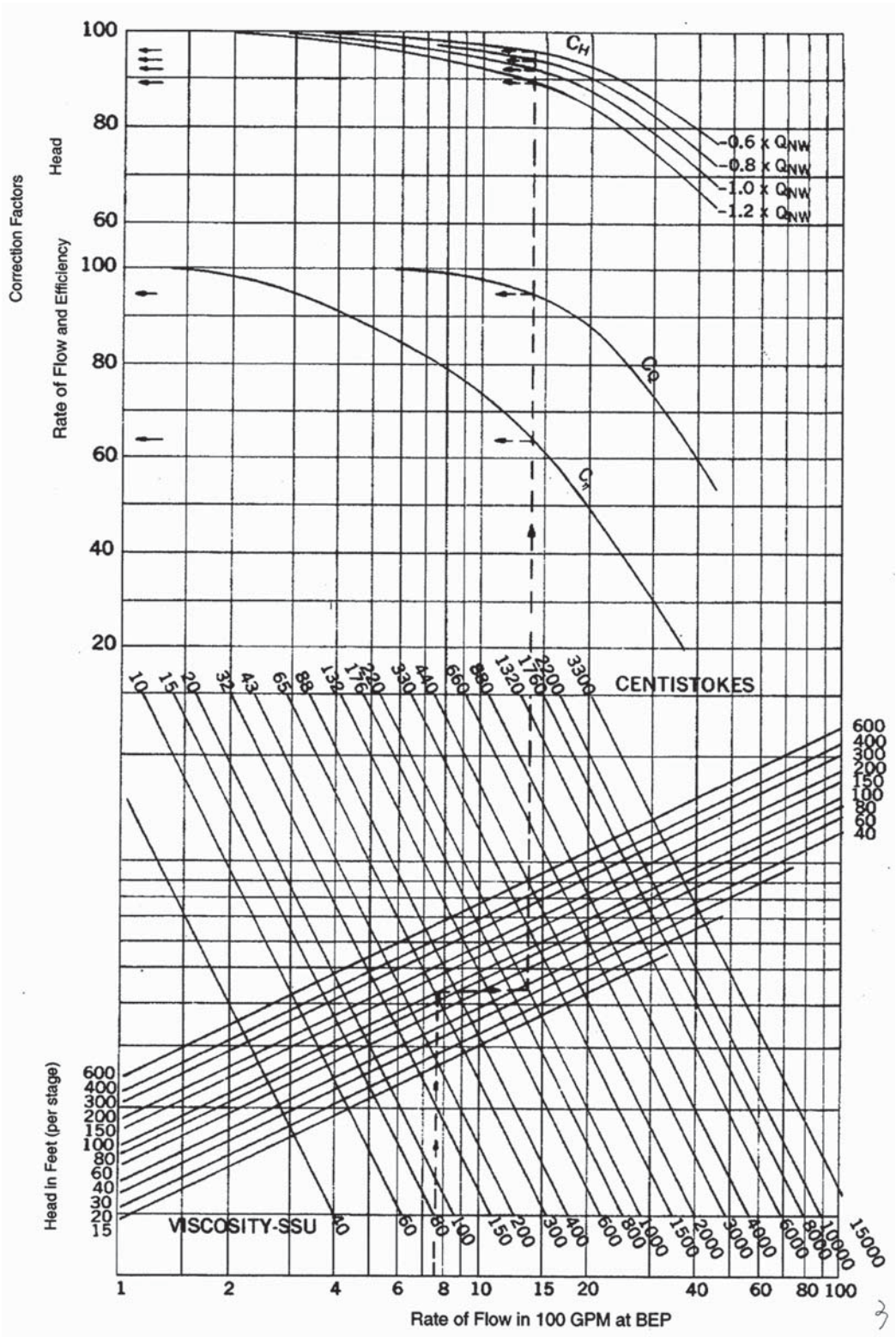


FIG. 2.77 PUMP PERFORMANCE CORRECTION CHART FOR VISCOUS LIQUIDS (Courtesy of Hydraulic Institute, Parsippany, NJ 070504, www.pumps.org [79])

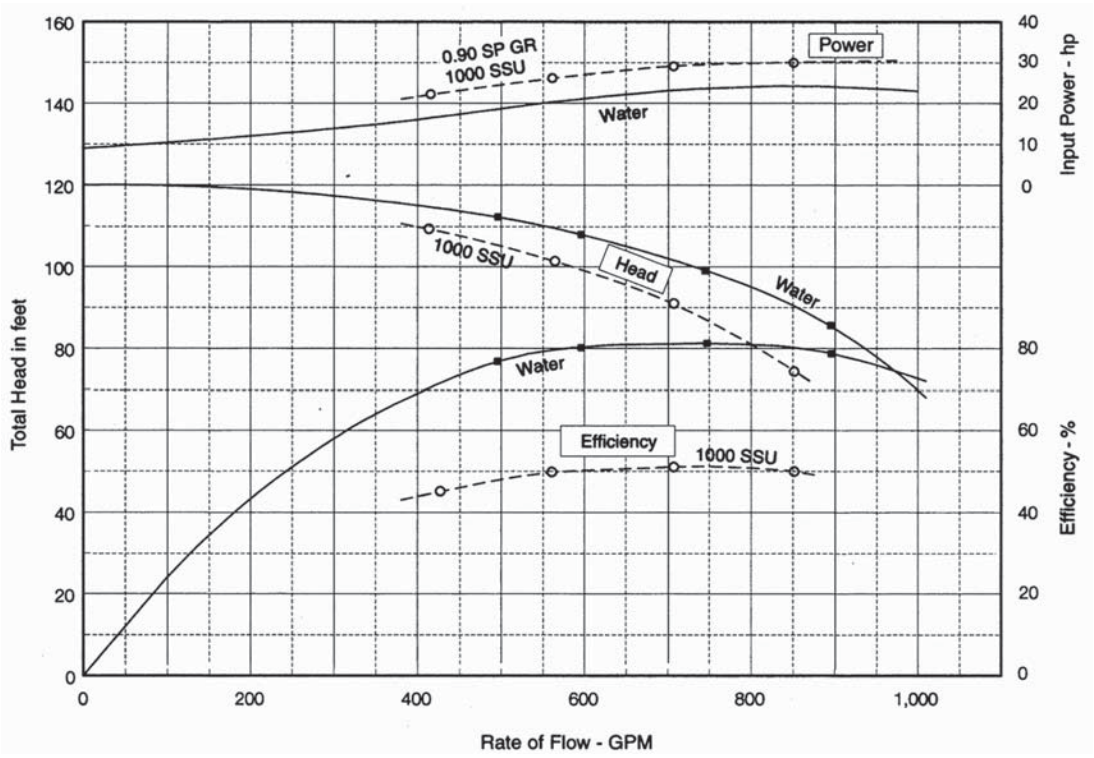


FIG. 2.78 PUMP CURVES FOR A VISCOUS FLUID (Courtesy of Hydraulic Institute, Parsippany, NJ 070504, www.pumps.org [79])

NPSHa is established by the design of the suction piping to the pump.

To consider NPSHr, cavitation requires definition. Although cavitation and cavitation erosion may occur anywhere in a pipe system, it is generally considered with a discussion of pumps. Cavitation is the vaporization of a fluid due to high velocities and low pressures. Considering Bernoulli's equation, if the liquid velocity goes high enough, the pressure drops to the vapor pressure of the liquid, and the liquid vaporizes. Essentially, the liquid boils at a low pressure since the high velocity lowers the liquid pressure to the fluid's vapor pressure. For water, a common vapor pressure is 0.25 psia (0.58 ft = 7 in. of water) from Fig. 2.79. Once cavitation commences, the vapor bubbles travel along fluid streamlines until they reach an area of higher pressure, where the bubbles collapse. If the bubbles collapse near a surface, cavitation erosion occurs. The implosion of the vapor bubbles is still an area of investigation (Blake and Gibson [80]), but a typical vapor bubble collapse is shown in Fig. 2.80, as a jet is formed when the bubble collapses. Near surfaces, the jet may, or may not, form as the bubble collapses. All materials are damaged by cavitation erosion, although some materials are more resistant than others. Cavitation erosion may be inaudible, but frequently, cavitation sounds like stones pinging on the pipe wall at incipient cavitation and sounds like churning gravel in the pipes or pumps as cavitation erosion increases. In addition to pump and piping damage, cavitation results in high vibrations and may also stop flow due to accumulation of vapor in the pump. The stresses in a pipe due to cavitation can be roughly approximated.

Example 2.12 Approximate the average stress in a pipe wall operating at 500°F and 500 psia

Even though the maximum pressure may be higher, the pressure during bubble collapse can be estimated. Once the pressure in the bubble is approximated, the pressure at the wall can be estimated since pressure reflections from a surface double the pressure in a liquid. Then, using a DMF = 2, the average stress can be conservatively estimated. The properties in a vapor bubble change to yield a change in pressure, and these properties can be obtained from the steam tables [ASME 51]. Specifically, the change in pressure, ΔP, can be expressed in terms of the change in energy or enthalpy, $\Delta h'$, and the change in density, $\Delta\rho$, where

$$\int \frac{dP}{dT} = \int \frac{dh' \cdot d\rho}{dT}$$

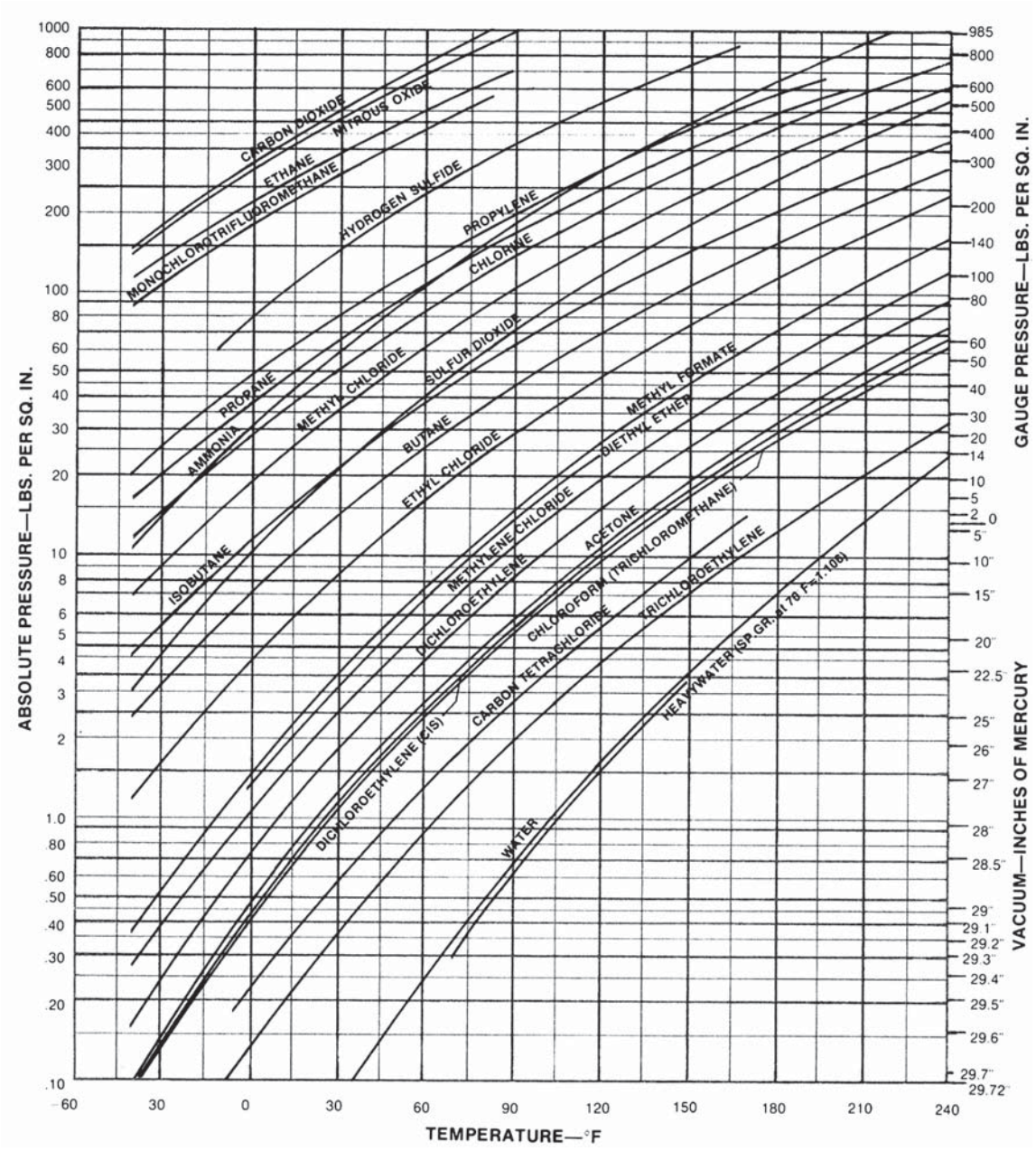


FIG. 2.79 FLUID VAPOR PRESSURES (Courtesy of Hydraulic Institute, Parsippany, NJ 070504, www.pumps.org [79])

Neglecting time dependence, the pressure equals

$$\Delta P = \Delta h' \cdot \Delta \rho$$

For this example,

$$\Delta P = \Delta h' \cdot \Delta \rho$$

$$= (1231.5 - 487.8) \cdot \left(\frac{1}{0.9924 - 0.02048} \right) \cdot \left(\frac{778.26}{144} \right)$$

$$= 4136 \text{ psi}$$

The reflected pressure equals $2 \cdot 4136 = 8272$ psi, and the stress, σ, equals $2 \cdot 8272 = 16544$ psi, which is in the range of the fatigue stress for most materials. Since the pressure may be higher, the stress may also be higher.

Consequently, a failure mechanism to cause cavitation erosion is provided, which depends on the proximity of the bubble to the wall. The complexities of shock wave formation in the bubble may also lead to higher stresses in the material, where the assumptions here are that the bubble collapses isothermally and symmetrically, and the

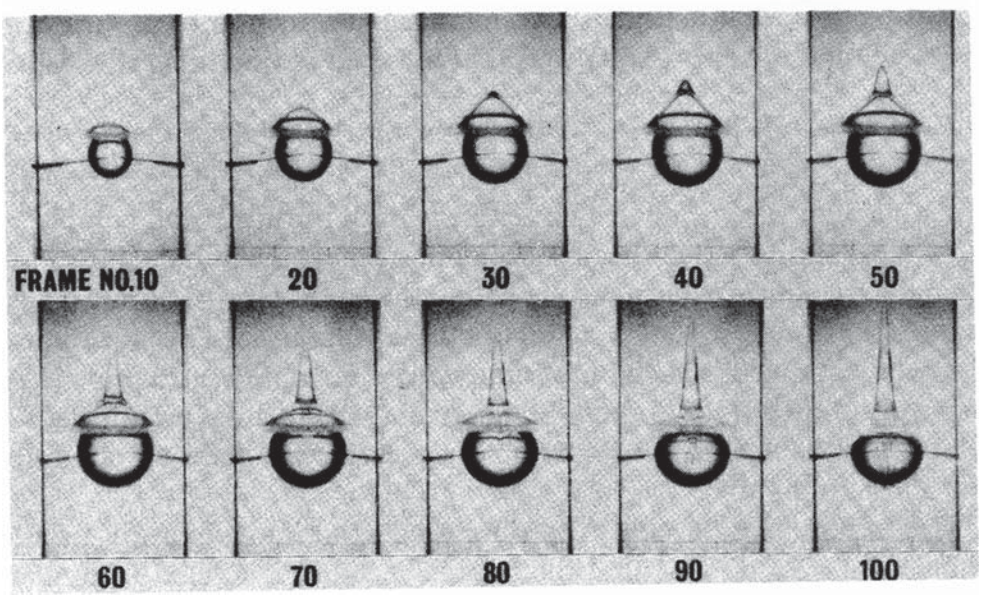


FIG. 2.80 CAVITATION BUBBLE COLLAPSE NEAR A FREE SURFACE (Blake and Gibson [80], Reprinted, with permission, from the Annual Review of Fluid Mechanics, Volume 23, copyright 1987, by Annual Reviews, www.annualreviews.org)

resultant expanding shock wave will have an instantaneous pressure, ΔP, and the pressure will decrease as the shock wave expands in the liquid toward the material surface, where the pressure wave is reflected, the pressure doubles at the surface, and the stress in the material again doubles due to dynamic effects. For further background, Chapter 5 considers reflected pressure waves, and Chapter 7 considers structural dynamic effects.

NPSHr is defined as the throttled, suction flow rate through a pump that causes a 3% decrease in head. The lowered flow rate is obtained by throttling the pump inlet at specified discharge flow rate conditions to produce cavitation within the pump (Hydraulic Institute [79]). Typical test results are shown in Fig. 2.81. Note that as the suction flow is decreased, flow through the pump stops completely soon after the 3% cavitation requirement is

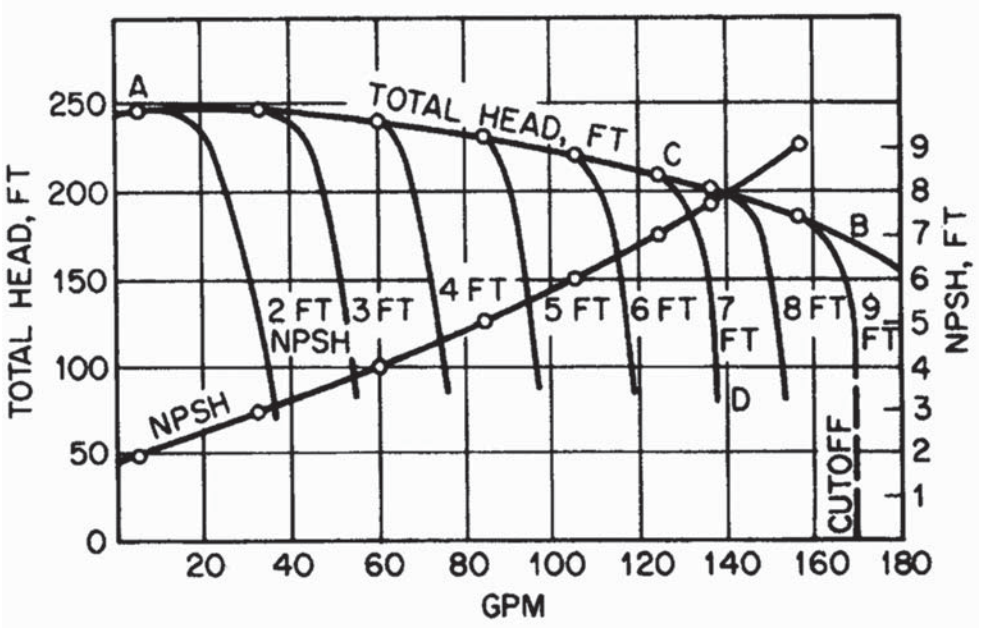


FIG. 2.81 EFFECTS OF CAVITATION ON PUMP OPERATION ("Pump Handbook" by Karrassik, Igor J. Copyright 2012. Reproduced with permission of McGraw Hill Companies, Inc. [53])

reached, where data points for 3% cavitation are denoted by circles on the figure. The pump curve in Fig. 2.81 shows the change in NPSHr with increased flow for a specific pump.

Although this curve demonstrates that NPSHr can be rather complex, even for a single pump design, some generalizations may be applied to fluids used in centrifugal pumps. In particular, the effects of temperature and vapor pressure on NPSHr are shown for some fluids in Fig. 2.82. Using this figure, the NPSHr reduction can be applied to available NPSHr pump curves, which were determined for cold water, providing that the reduction does not exceed 50%. To use the figure, the reduction in NPSHr is found directly from the chart if the NPSHr reduction is less than half of the pump NPSHr. Otherwise, the reduced NPSHr is halved before subtracting it from the pump NPSHr. The NPSHr is also reduced due to entrained air or gases.

If a pump is operated beyond the design conditions for minimum NPSHr, flow rate behavior will vary as flow rates increase. At first, flow will fluctuate as it is increased. Then, flow may actually pulse forward and backward,

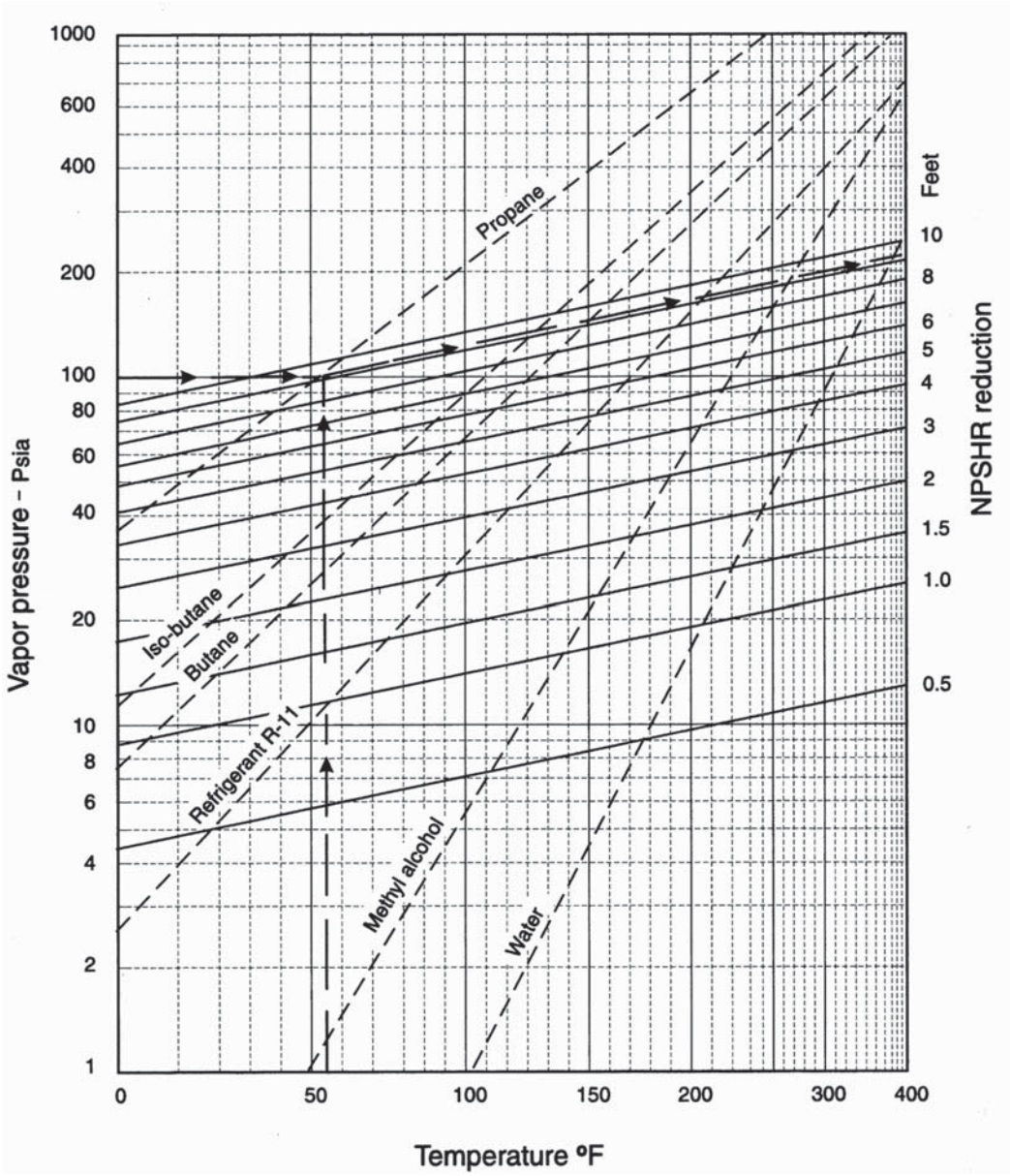


FIG. 2.82 EFFECTS OF VAPOR PRESSURE AND TEMPERATURE ON NPSHR (Courtesy of Hydraulic Institute, Parsippany, NJ 070504, www.pumps.org [79])

before a flow rate is obtained where pump flow is completely stopped, and the pump prime is lost. To ensure that a pump is primed for operation, design should ensure that the NPSHr is met.

To use a given pump, the NPSHa must exceed the NPSHr by an acceptable margin for operating conditions (ANSI/HI 9.6-1998, Centrifugal and Vertical Pumps for NPSH Margin [ANSI 81]). NPSHa is defined using Fig. 2.83 and the following equations.

$$\text{NPSHa} = h_b + h_s \qquad \text{US (2.94)}$$

At the pump suction flange,

$$h_b\,(\text{ft}) = \frac{\left(P_a\,(\text{psi}) - P_v\,(\text{psi})\right)\cdot 144}{\gamma\left(\text{lbf}/\text{ft}^3\right)} \qquad \text{US (2.95)}$$

$$h_s = \frac{P_s\,(\text{psi})}{\gamma\left(\text{lbf}\cdot\text{ft}^2\right)} + Z'_{ps} + \frac{V^2}{2\cdot g} \qquad \text{US (2.96)}$$

$$\text{NPSHa} = h_b + h_s \qquad \text{US (2.97)}$$

For the piping between the tank and the suction flange

$$\text{NPSHa} = \frac{\left(P_t - P_v\right)\cdot 144}{\gamma} + Z' - h_{LS} \qquad \text{US (2.98)}$$

$$\text{NPSHa} = \frac{\left(P_t - P_v\right)}{\rho\cdot g} + Z' - h_{LS} \qquad \text{SI (2.99)}$$

where h_b is the barometric head of fluid as described by Fig. 2.84, h_S is the suction head if positive and h_S is the suction lift if negative, Z' is positive for suction head and negative for suction lift, P_t is the tank pressure or atmospheric pressure as applicable, h_{LS} is the head loss of the suction piping, P_v is the vapor pressure of the fluid, Z_{ps} is the height of a pressure gauge above the pump datum plane, P_s is the gauge pressure at the pump suction inlet, and $P_a = P_g + P_{abs}$ is the atmospheric pressure as defined in Table 2.32. If required, pressures may be determined according to

$$P_a\,(\text{psia}) = 14.696\cdot\left(1 - 7.399\cdot 10^{-5}\cdot Z'\,(\text{ft})\right)^{5.2559} \qquad (2.100)$$

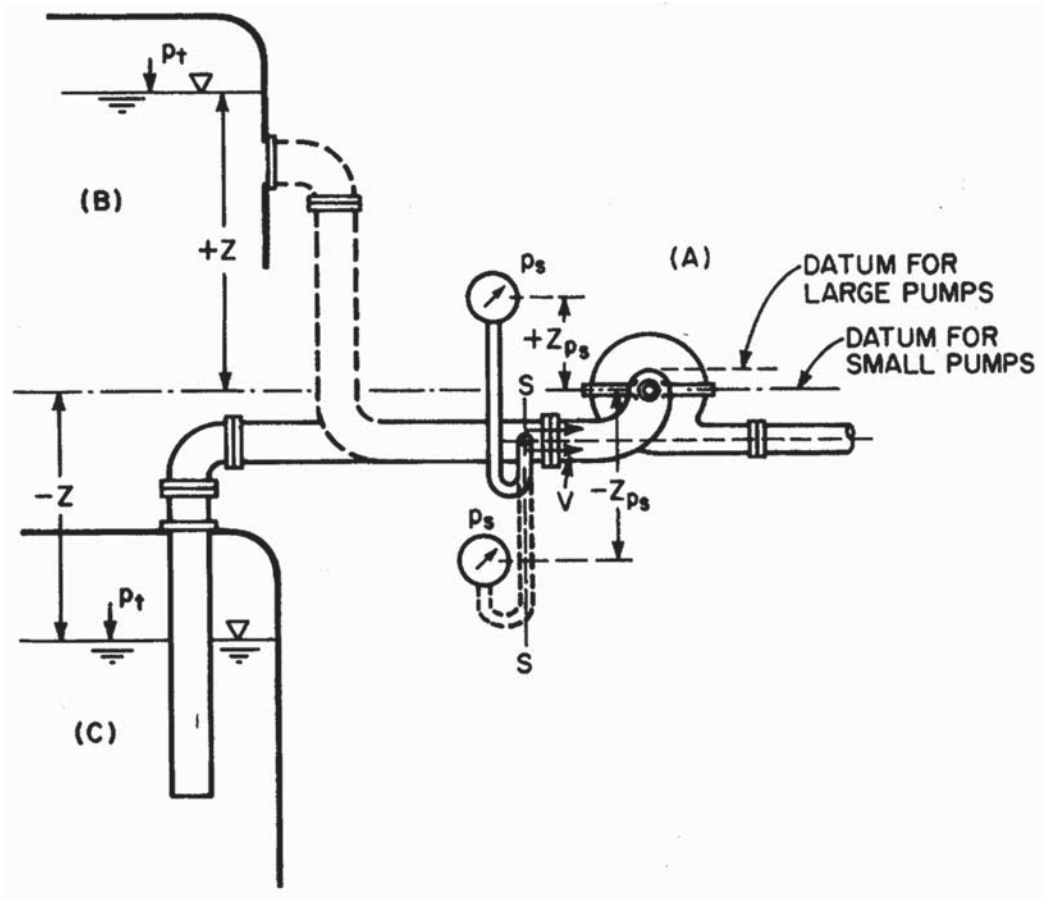


FIG. 2.83 NPSHR TEST CONDITIONS AND DEFINITIONS ("Pump Handbook" by Karrassik, Igor J. Copyright 2012. Reproduced with permission of McGraw Hill Companies, Inc. [53])

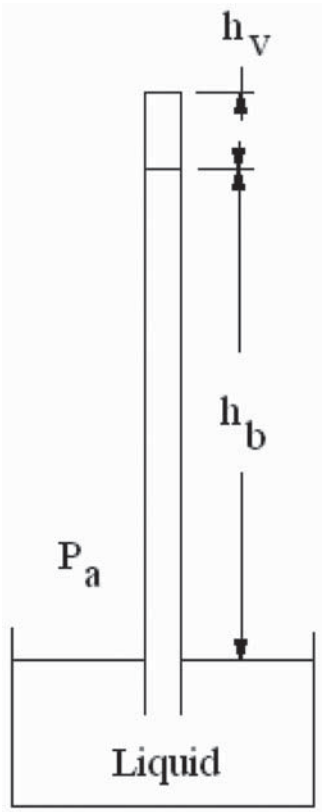


FIG. 2.84 BAROMETRIC HEAD

where *Z*' is the altitude (ASHRAE [82]). Atmospheric pressures are also affected by weather conditions, where pressure extremes in the US typically vary between 14.0 and 14.9 psia, and the lowest recorded tornadic pressure is 13 psia.

2.7.3 Motor Speed Control

Several different types of electric motor controllers and starters are available for industrial applications, such as pumps. Starters are commonly used to turn pumps on, and controllers are used for both starting the pump, controlling flow rates, and shutdown.

2.7.3.1 Induction Motors AC induction motors are commonly used motors for pumps. A motor typically consist of housing, drive shaft, bearings, a rotor with coil windings, and a stationary stator, which electromagnetically induces a current into the rotor to cause rotation. Since 60-Hz power is supplied in the US, motors are typically rated at 1200, 1800, and 3600 rpm, depending on the design of the motor.

Operating speed, service factor, SF, current, and rated horsepower are provided on the motor name plate. The service factor provides a factor to be applied to the rated horsepower to obtain the maximum operating horsepower for the motor. Motor slip accounts for friction and heat losses in motors, since motors run at speeds less than theoretical. Operating speeds for a 1800-rpm motor typically vary between 1725 and 1765 rpm. A 3600-rpm motor may operate at a slip speed of as low as 3450 rpm. As the motor slows, slip is nonlinear.

2.7.3.2 Motor Starters The most common starters are direct line contactors. When a pump is started from a local switch or remote location, an electromagnet pulls in, or engages, the contactor to complete the circuit and energize the motor. A copper bar, or stab, is pulled in to complete the circuit. For this type of starter, the initial current draw is typically 6–8 times the operating current (steady state operations shown in Fig. 2.85). To prevent damage to the motor windings, overloads, or heaters are supplied with the motor. The overloads trip if the current is too high. To prevent damage to wiring attached to the motor, fuses or circuit breakers are installed per NEC (National Electrical Code) specifications. Time delay, or slow blow, fuses are commonly used to compensate the excessive startup currents when direct line contactors are used. VFD's may be installed to minimize inrush currents.

2.7.3.3 VFDs VFDs are a control device used to vary the motor speed by varying the frequency and voltage. Specifically, motor speed can be gradually ramped-up on starting, and speed can then be controlled during operation. To do so, a 60-Hz line frequency is input into the VFD, which is then converted to frequencies as low as 2 Hz, where maximum inrush currents may be limited to 150% of operating currents. Different ramp-up functions are frequently available with VFDs, where the ramp up time may be a linear function or quadratic function. VFDs may also be used to control flow rates during pump operation. If a P'I'D' controller is added to the motor controls, significant flexibility can be obtained during operations, as well as during startup and shutdown. Compatibility of the VFD and motor should be considered for prolonged

TABLE 2.32 STANDARD ATMOSPHERE
(Reprinted by permission of McGraw Hill, Avallone and Baumeister [33])

Altitude (ft)	Temperature (°F)	Pressure (psi)	Speed of sound, c_0 (ft/second)
Sea level	59.00	14.696	1116
5000	41.17	12.227	1097
10,000	23.34	10.106	1077
15,000	5.51	8.293	1057

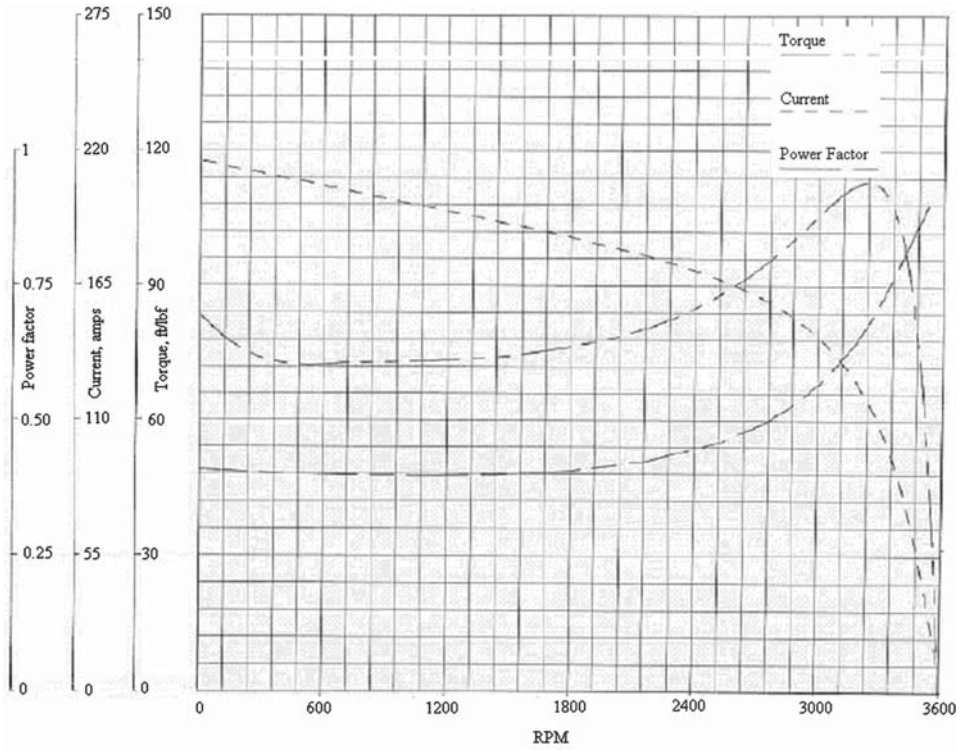


FIG. 2.85 TYPICAL CURRENT REQUIREMENTS DURING MOTOR STARTUP

low-speed operation, where cooling may be a concern. Other controller designs are available, but are outside the scope of this work (Smeaton [83], Jaeschke [84], Siskind [85], and NEMA [86]). DC motors are also outside the scope of this work.

2.7.3.4 Pump Shutdown and Inertia of Pumps and Motors When pumps are turned off, the inertia of the pump controls the time for the pump to stop. Inertial data should be obtained from motor manufacturers, but data for numerous pumps has been established (Thorley [68]), according to

$$I_p = 0.2435 \cdot \left(\frac{P'}{n^3}\right)^{0.9556} \qquad \text{US (2.101)}$$

$$I_m = 0.0043 \cdot \left(\frac{P'}{n^3}\right)^{1.48} \qquad \text{US (2.102)}$$

To find the power required for Eqs. (2.101) and (2.102), rewrite Eq. (2.89), such that

$$P' = \text{BHP}(\text{hp}) = \frac{Q(\text{gpm}) \cdot h(\text{ft}) \cdot \text{Sp}G}{3960 \cdot \eta} \qquad \text{US (2.103)}$$

$$I_{\text{total}} \approx I_p + I_m \qquad \text{US (2.104)}$$

where I_{total} is the total mass moment of inertia compensated for minor mechanical coupling losses, I_p is the pump rotary inertia in lbf/ft^2, I_m is the motor rotary inertia, P' is the horsepower, and n is the rotational speed at rated speed. VFDs may also be used to control pump flow rate during shutdown for cases other than power loss. Also, in large systems, the inertia of the fluid in the system overcomes the motor and pump inertia, and equipment inertia is negligible.

2.7.4 Pump Performance as a Function of Specific Speed

Centrifugal pump performance for various specific speeds is summarized in Figs. 2.86 and 2.87. Normal operating conditions are 100% of flow at 100% of the normal efficiency or best efficiency point. This set of curves provides considerable insight into pump performance, since generic pump curves are used to describe the complete range of centrifugal pump designs from the lower specific speed radial pumps to the higher specific speed axial pumps. The type of centrifugal pump affects the dead head pressure and torque at zero flow. Note that for lower specific speed radial pumps, the dead head pressure and torque exceed the normal operating pressure somewhat, but for the high specific speed axial flow pumps,

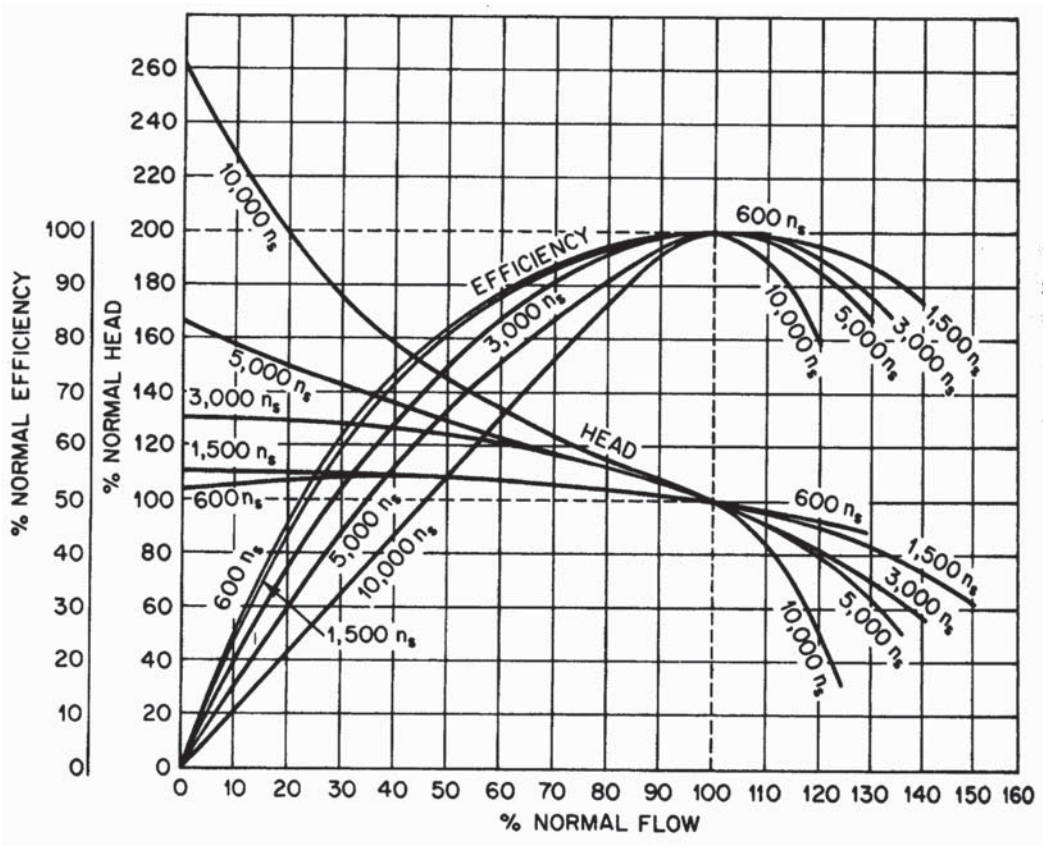


FIG. 2.86 EFFECT OF SPECIFIC SPEED ON HEAD AND EFFICIENCY ("Pump Handbook" by Karrassik, Igor J. Copyright 2012. Reproduced with permission of McGraw Hill Companies, Inc. [53])

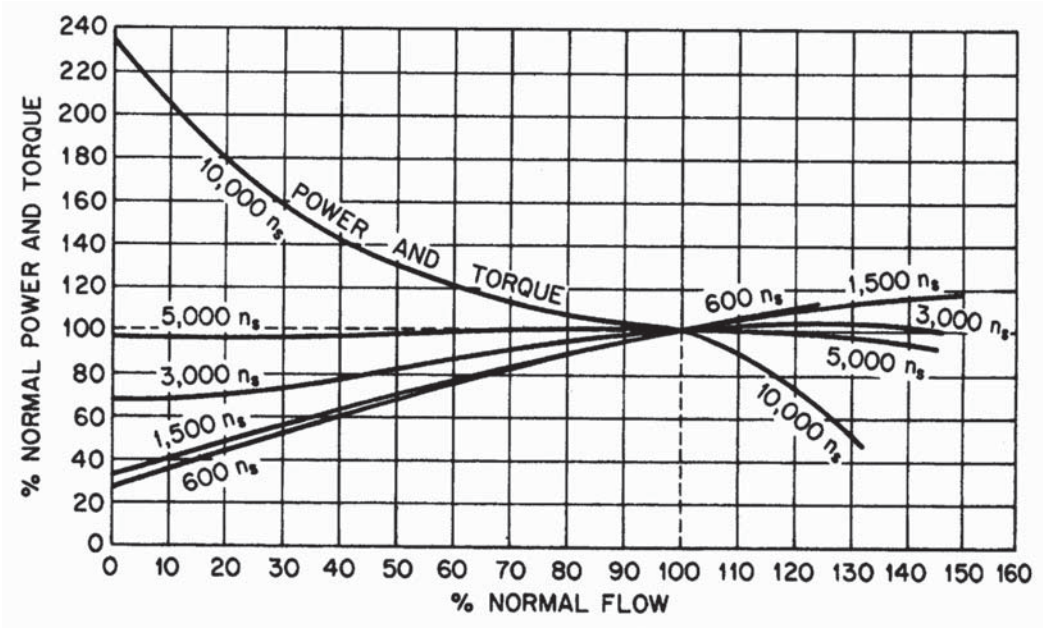


FIG. 2.87 EFFECTS OF SPECIFIC SPEED ON POWER AND TORQUE ("Pump Handbook" by Karrassik, Igor J. Copyright 2012. Reproduced with permission of McGraw Hill Companies, Inc. [53])

TABLE 2.33 MEAN SPECIFIC HEATS OF FLUIDS (32°F TO 212°F)
(Avallone and Baumeister [33])

Acetic acid	0.51	Ethylene glycol	0.60	Mercury	0.03
Acetone	0.51	Fusel oil	0.56	Paraffin oil	0.52
Alcohol	0.58	Gasoline	0.50	Petroleum	0.50
Aniline	0.51	Glycerin	0.58	Sulfuric acid	0.33
Benzol	0.40	Hydrochloric acid	0.60	Sea water	0.94
Chloroform	0.23	Kerosene	0.50	Toluene	0.44
Ether	0.54	Napthalene	0.31	Turpentine	0.42
Ethyl acetate	0.47	Machine oil	0.40	Water	1.002

the dead head pressure more than doubles the normal operating head if the pump is started against a closed valve. High starting torques may be eliminated by installing a bypass on the pump if the pump must be started against a closed valve. Again, Karassik provides a more detailed discussion of this topic.

2.7.5 Pump Heating Due to Flow Through the Pump

Also, the power to the pump heats the fluid as it passes through the pump (Hydraulic Institute [79]). The effects of temperature increases range between acceptable temperature increases, which have a negligible effect on pump components, to explosion of the pump due to vapor generation in the casing. The increase in pump temperature, ΔT, equals

$$\Delta T(^\circ\mathrm{F}) = \frac{h(\mathrm{ft})}{778 \cdot C_\mathrm{p}(\mathrm{Btu/lbm} \cdot ^\circ\mathrm{F})} \cdot \left(\frac{1}{\eta} - 1\right) \text{ US} \qquad (2.105)$$

$$\Delta T(^\circ\mathrm{C}) = \frac{h(\mathrm{m})}{10400 \cdot C_\mathrm{p}(\mathrm{N \cdot m/kg} \cdot ^\circ\mathrm{C})} \cdot \left(\frac{1}{\eta} - 1\right) \text{ SI} \qquad (2.106)$$

where C_p is the specific heat of the fluid, and η is the pump efficiency. To obtain values for the specific heat of some liquids, Table 2.33 is provided. For water, the mean value is accurate to within 0.5% throughout the range of temperatures between 32°F and 212°F.

The specific heat is defined as the ratio of the amount of heat transfer required to raise a unit mass of a material 1° divided by the heat required to raise a unit mass of water 1°; the specific heat is measured in terms of Btu/lbm·°F (US), where the Btu (778.26 ft·lbf) is defined at an arbitrary temperature to equal the heat required to raise 1 lbm of water 1°F.

When the pump is deadheaded (also referred to as the shutoff condition), the approximate rate of temperature increase, $\Delta T / \Delta t$, in the pump is described by

$$\frac{\Delta T}{\Delta t}(^\circ\mathrm{F/minute}) = \frac{5.09 \cdot P'(\mathrm{hp})}{V'(\mathrm{gal}) \cdot C_\mathrm{p}(\mathrm{Btu/lbm} \cdot ^\circ\mathrm{F}) \cdot \mathrm{Sp}G} \qquad \text{US} \quad (2.107)$$

$$\frac{\Delta T}{\Delta t}(^\circ\mathrm{C/minute}) = \frac{60 \cdot P'(\mathrm{watts})}{V'(\mathrm{m}^3) \cdot C_\mathrm{p}(\mathrm{J/kg} \cdot ^\circ\mathrm{C}) \cdot \rho(\mathrm{kg/m}^3)} \qquad (2.108)$$

where V' is the fluid volume of the pump casing, and P' is the power at shutoff.

2.7.6 System Curves

System curves depict the head loss in a system with respect to flow rate, and examples provide some insight into system curves. Several examples are provided to demonstrate the effects on system performance due to viscosity, system head, parallel and series pumps, and parallel and series pipes.

Example 2.13 Effects of viscosity on system curves
Using the system shown in Fig. 2.88 and the pump curve shown in Fig. 2.76 determine;

1. System curve and operating point (design condition) for pumping water at 60°F. That is, find Q, h, and Re
2. System curve and design condition for pumping water at 208°F
3. System curve and design condition for pumping SAE 30 oil at 80°F. Oil was arbitrarily selected to demonstrate principles

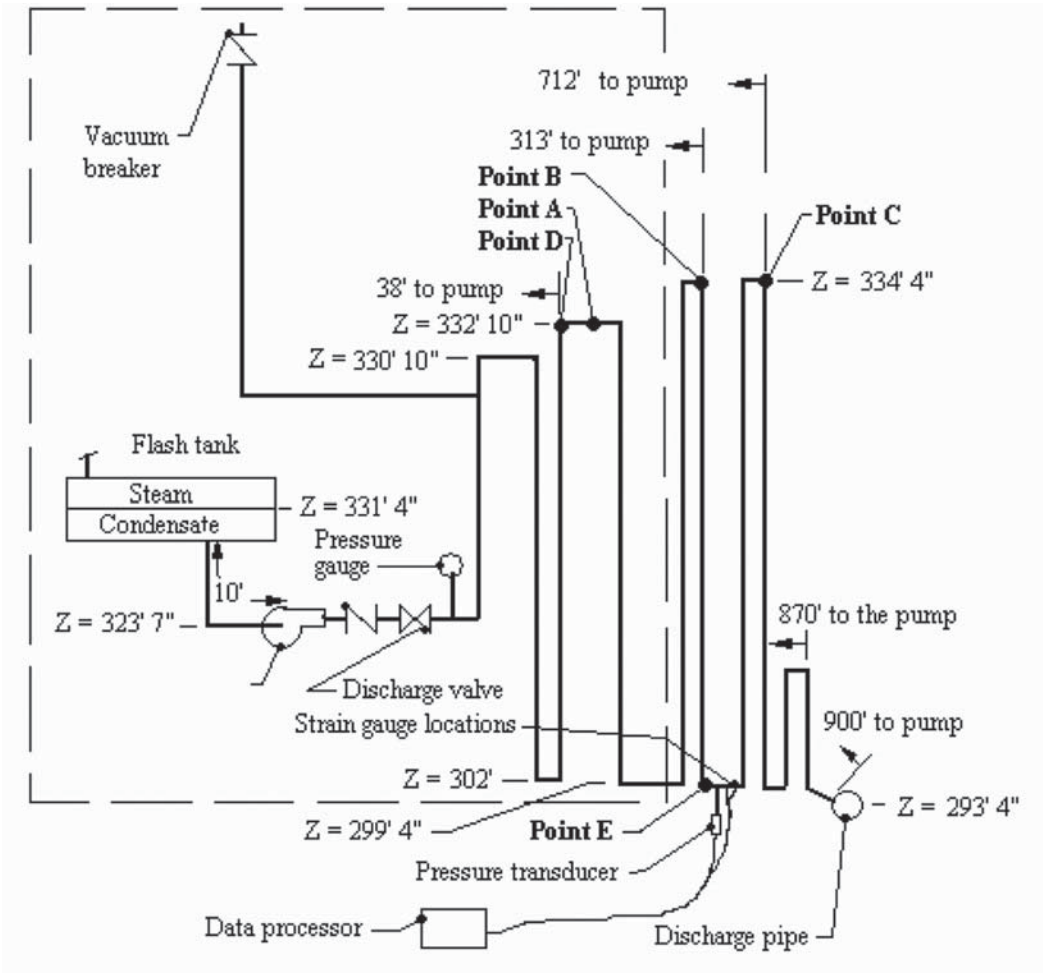


FIG. 2.88 DESCRIPTION OF A CONDENSATE SYSTEM

This system curve also provides an example of droop as the pump curve approaches shutoff. This condition associated with low specific speed pumps may lead to unstable surging of the system in some designs, since Q exists at two different values of head on the pump curve. A dip in the curve for axial flow pumps may also lead to unstable operations at some low flows (Volk [49]).
Given:

L' = total system pipe length = 910 ft of 2-in. NPS pipe,
$Z_2 - Z_1$ = 293 ft 4 in. to 331 ft 4 in. = −38 ft
$\nu' = 1.22 \cdot 10^{-5}$ for 60°F water; $\nu' = 3.26 \cdot 10^{-6}$ for 208°F water; and $\nu' = 0.0022$ for 85°F oil
D = 2.067 in.
ε = 0.00015 in.

K values for components are calculated using Churchill's equation for pipe, and the 2-K and 3-K resistance coefficients for fittings:
20, 2-in. diameter elbows, $r/D = 1.5$,

$$K = 20 \cdot \frac{800}{Re} + 0.2 \cdot \left(1 + \frac{1}{D}\right)$$

1 check valve, $K = 1 \cdot \frac{1500}{Re} + 0.46 \cdot \left(1 + \frac{4}{D^{0.3}}\right)$

1 gate valve, $K = 1 \cdot \frac{300}{Re} + 0.1 \cdot \left(1 + \frac{1}{D}\right)$

1 pipe entrance $K = 1 \cdot \frac{160}{Re} + 0.5$

1 pipe exit $K = 1 \cdot 1$

1 through tee $K = 1 \cdot \frac{500}{Re} + 0.7 \cdot \left(1 + \frac{1}{D}\right)$

Adding the friction terms for the fittings,

$$K_{\text{total}} = \frac{18460}{Re} + 1.0 \cdot \left(1 + \frac{1}{D}\right) + 1.5 + 0.46 \cdot \left(1 + \frac{4}{D^{0.3}}\right)$$

The system curves and pump curve were first established to find the design conditions at the points where the system curves intersected the pump curve. Calculations for the 208°F condensate system design condition on the pump curve at 35.7 gpm follow, along with calculations for the *Re* number at design conditions for the other two fluid models.

$$Re(208\_\text{F}\_\text{water}) = \frac{Q}{37.405 \cdot \nu' \cdot D} = \frac{35.7}{37.405 \cdot \left(3.26 \cdot 10^{-6}\right) \cdot 2.067} = 141638$$

$$f = 8 \cdot \left(\left(\frac{8}{Re}\right)^{12} + \left(\frac{1}{\left(\left(2.457 \cdot \ln\left(\frac{1}{\left(\frac{7}{Re}\right)^{0.9} + \left(\frac{0.27 \cdot \varepsilon}{D}\right)} \right) \right)^{16} + \left(\frac{37500}{Re}\right)^{16} \right)^{1.5}} \right) \right)^{1/12}$$

$$f = 8 \cdot \left(\left(\frac{8}{141638}\right)^{12} + \left(\frac{1}{\left(\left(2.457 \cdot \ln\left(\frac{1}{\left(\frac{7}{141638}\right)^{0.9} + \left(\frac{0.27 \cdot 0.00015}{2.067}\right)} \right) \right)^{16} + \left(\frac{37500}{141638}\right)^{16} \right)^{1.5}} \right) \right)^{1/12}$$

$$f = 0.09101$$

$$K_{\text{pipe}} = \frac{f \cdot L}{D} = \frac{0.09101 \cdot 910 \cdot 12}{2.067} = 480.81$$

$$h_{\text{L}} = \frac{0.00259 \cdot K \cdot Q^2}{D^4} = \frac{0.00259 \cdot (5.05 + 480.81) \cdot 35.7^2}{2.067^4} = 87.87\_\text{ft}$$

As shown in Fig. 2.76, the design point on the curve is defined for 208°F water as:

Re =141,638 Q = 35.7 gpm head, $h_L = -38 + 87.87 = 49.87$ ft.
Similarly, for laminar flow of oil at 85°F,
Re = 61 Q = 10.4 gpm h_L = 51.7 ft.
For water at 60°F,
Re = 32,229 Q = 30.4 gpm h_L = 52 ft.

This example for 208°F water was thoroughly investigated for water hammer concerns and will be referenced throughout this text to illustrate the relationships between fluid mechanics, pipe stresses, and failure analysis. The system curves for each fluid are provided in Fig. 2.89, and the pump curve is unaffected by viscosity for the flow rates and viscosities of this example. Note that the system behavior of oil is different than water. Referring to the Moody diagram and considering the calculated Re number, the oil is laminar throughout the flow range considered, while water is in the turbulent transition zone of the diagram at both temperatures. For laminar flow, $f = 64/Re$, and $h_L = 0.0968 \cdot Q \cdot \nu'/D^3$, where the head loss is linear for oil instead of quadratic as it is for water at both temperatures considered. Also note that the initial head is shown on the system curves as −38 feet at 0 gpm, which will cause siphon flow even if the pump is turned off.

Example 2.14 Effects of system head on system curves:
Consider the system of Example 2.13, but assume that all of the piping beyond point D is disconnected. In this example, all of the parameters for this example are the same as Example 2.13 except that the pipe length is given as

L' = 38 + 10 = 48 ft = total pipe system pipe length,
$Z_2 - Z_1$ = 1.5 ft,

and fitting losses are given as

$$K_{\text{total}} = \frac{8060}{Re} + 1.0 \cdot \left(1 + \frac{1}{D}\right) + 0.5 + 0.46 \cdot \left(1 + \frac{4}{D^{0.3}}\right)$$

This case is shown in Fig. 2.90 for each of the same fluids considered in Example 2.13, where operation near run out is shown for the pump with a shorter length of pipe at the pump discharge. Run out is defined when a pump is permitted to operate without friction losses at the pump discharge.

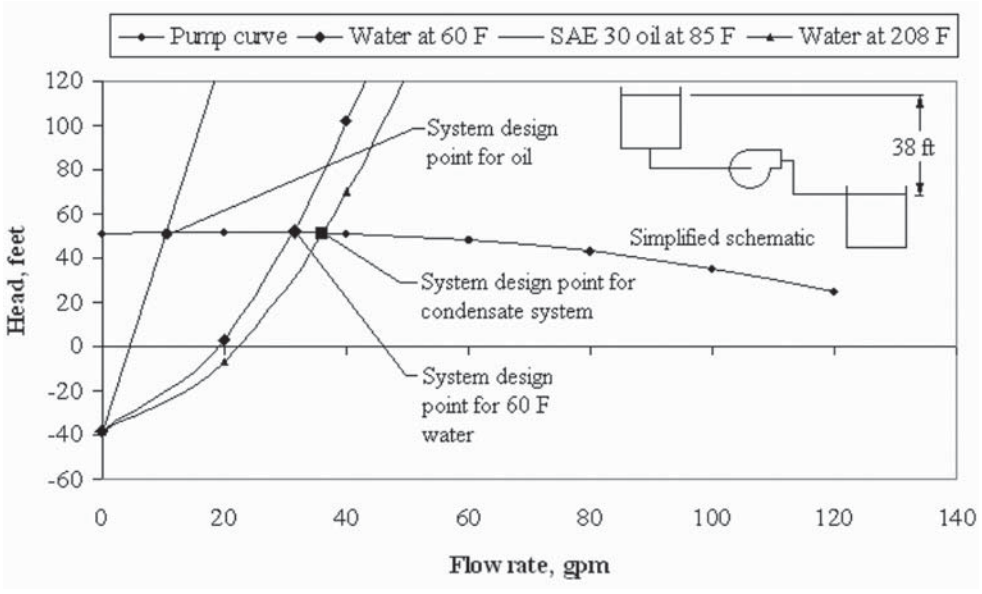


FIG. 2.89 PUMP CURVE AND SYSTEM CURVES FOR DIFFERENT FLUIDS AND CONDITIONS

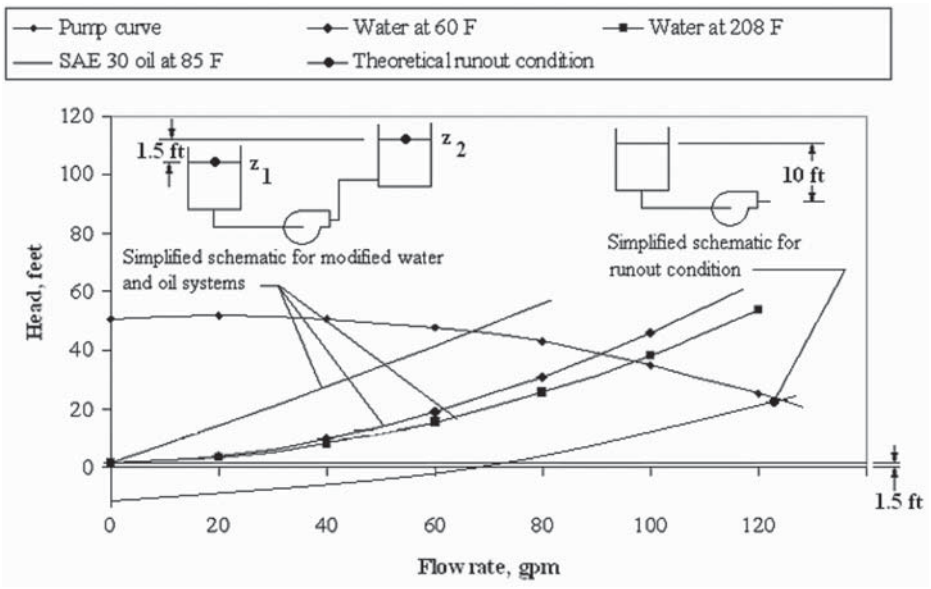


FIG. 2.90 DECREASED FRICTION RESISTANCE AND RUN OUT CONDITIONS

Example 2.15 Closed loop systems

System head also affects curves for closed loop systems. In particular, the static head is 0 ft of head. Assuming that a system has the same head losses as the modified condensate system of Example 2.13, the system curve looks like Fig. 2.91. The system curve simply moves vertically with respect to the pump curve, depending on the elevation differences of the system. Although this curve represents operating conditions for this system, the pump may need to have a larger head requirement if the system is filled at the pump. This additional head is required to overcome the elevation head needed to fill the system. Off-normal conditions would also require calculations.

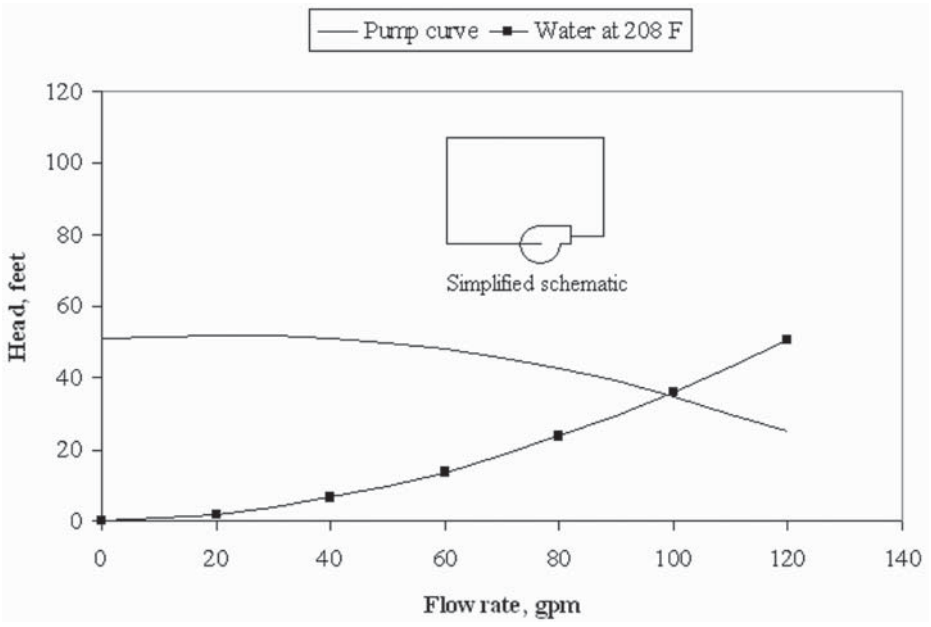


FIG. 2.91 CLOSED LOOP SYSTEM

2.7.7 Parallel and Series Pumps

The performance of parallel and series pumps is depicted in Fig. 2.92 using the modified condensate system of Example 2.13. To obtain a series pump curve, the head from two series pumps is simply added together to obtain points on the combined pump curve. To obtain a parallel pump curve, volumetric flow rates of each pump are added together to obtain the combined curve. In both cases, the piping connecting the pumps is neglected. Note that only a minor flow increase is obtained by using parallel pumps in Example 2.13.

The use of dissimilar pumps in parallel may lead to unexpected off-normal operations. Operating parallel pumps with significantly different operating heads can cause deadheading of the lower head pump since its discharge check valve will be held closed by the other pump at low system flows.

2.7.8 Parallel and Series Pipes

Karassik [53] provided a classic graphic description of parallel pipe systems, shown in Figs. 2.93 and 2.94. Series pipe system curves are obtained by adding the system head for the two curves, and parallel pipe system curves are obtained by adding the system flow rates. At a junction, the combined elevation and friction heads are equal for each pipe branch. With these few rules and the equations provided in this text, each of the system curves may be constructed. At each point on every curve, hydraulic and energy grade lines may also be drawn. Accordingly, comprehensive calculations for static system design readily lend themselves to computer simulations.

2.8 JET PUMPS

The basic construction of jet pumps is shown in Fig. 2.95, where a fluid provides the motive force for the pump by entering a nozzle and increasing velocity to create a suction pressure. The suction pressure draws fluid into the pump prior to a converging-diverging nozzle, which pressurizes the mixed fluid. Jet pumps are available as eductors (liquid as the motive fluid), injectors (gas or air as the motive fluid), or siphon jets (condensable vapor as the motive fluid). This type of pump has the advantage of no moving parts. Only one head is supplied by a specific applied pressure. Karassik [53] provides a comprehensive discussion of this type of pump.

This brief discussion of jet pumps concludes the basic considerations for dynamic pumps, but system performance also needs to be considered, where the influence of multiphase flows significantly affects system operations.

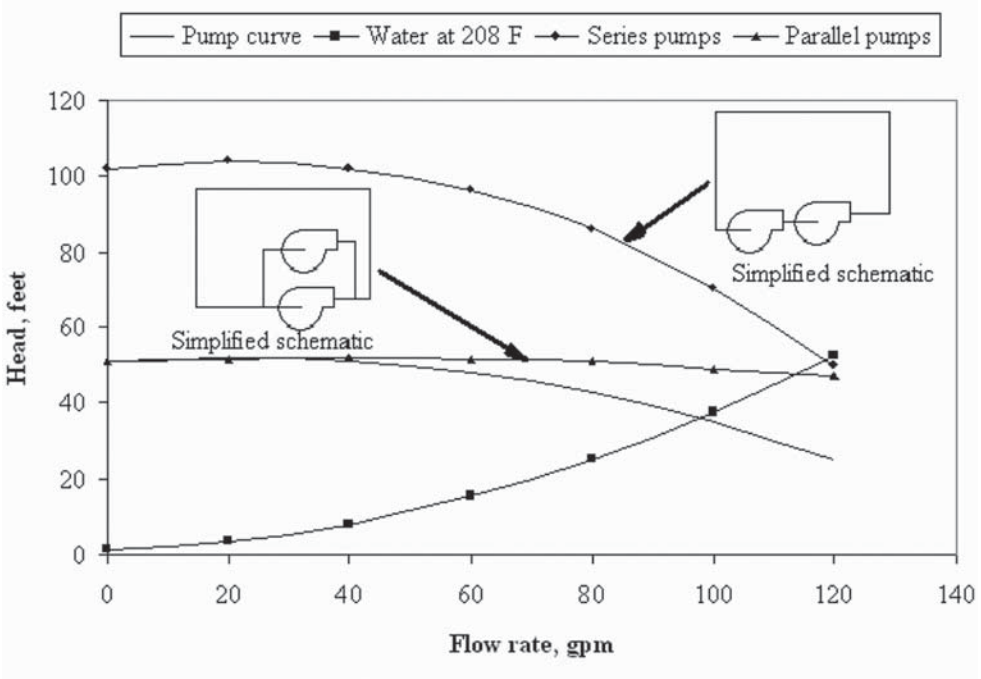


FIG. 2.92 SERIES AND PARALLEL PUMPS

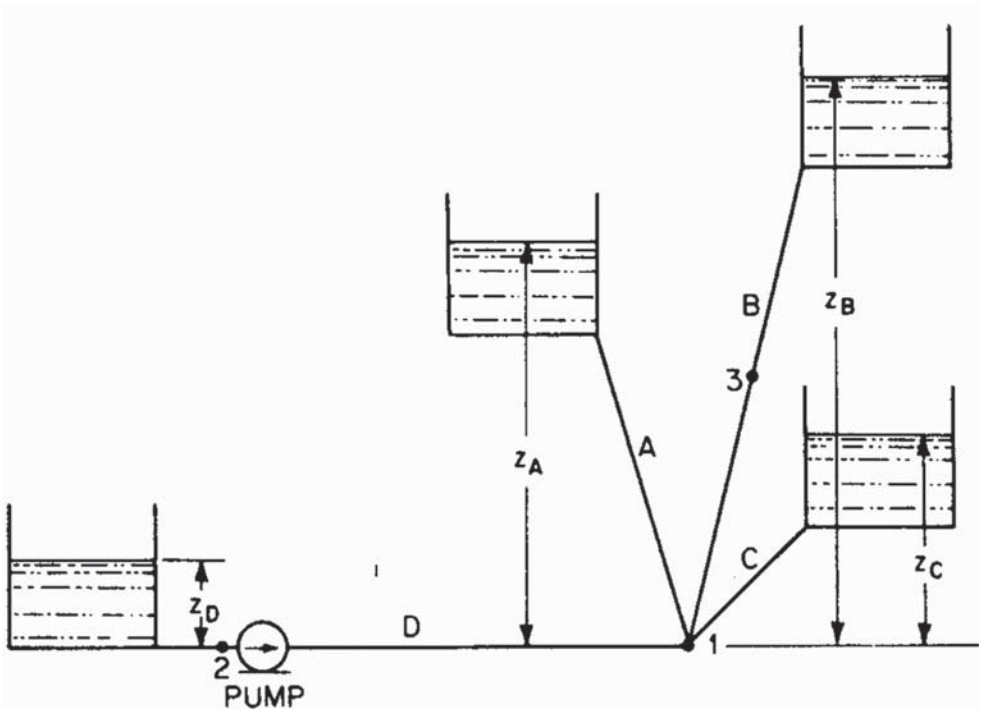


FIG. 2.93 MULTIPLE BRANCH SYSTEM (Pump Handbook by Karrassik, Igor J. Copyright 2012. Reproduced with permission of McGraw Hill Companies, Inc. [53])

2.9 TWO-PHASE FLOW CHARACTERISTICS

Although a reasonable study of two-phase flow is outside the scope of this text, some mention of the topic is provided. The effect of solid particles, gas bubbles, such as air in water, or vapor bubbles, such as steam in water, each complicate the fluid mechanics of flow through a pipe. Also, one should recognize when a pipe flows partially full and theory from open channel hydraulics is applicable. Since fluid transients are affected by two-phase fluids, basic descriptions for these fluids are warranted before transients are considered in Chapters 5 and 6. In fact, considerations of two-phase flow begin the discussion of unsteady flows and fluid transients.

2.9.1 Liquid/Gas Flows

The study of gas flow in fluids is rather complex, and new research is routinely published. The rise of bubbles complicates the flow in vertical pipes, since there is a free stream velocity associated with rising bubbles. A brief presentation of gas/liquid flow in horizontal pipes is presented here, where several flow patterns are shown in Fig. 2.96. Friction factors for various types of flow are available in the literature.

Fluid behavior is related to the gas and liquid flow rates, using the figure and the following equations.

$$\lambda = \left(\frac{\rho_g}{0.075}\right)\cdot\left(\frac{\rho_L}{62.3}\right) \qquad \text{US (2.109)}$$

$$\psi = \left(\left(\frac{\mu}{1}\right)\cdot\left(\frac{4.99}{\sigma''}\right)\cdot\left(\frac{\rho_g}{62.3}\right)^2\right)^{1/3} \qquad \text{US (2.110)}$$

where λ and ψ are fluid property parameters, G_g is the mass flux of the gas (lbm/(ft^2 · hour)), G_L is the mass flux of the liquid (lbm/(ft^2 · hour)), ρ_L is the density of the liquid, μ is the viscosity of the liquid, σ is the surface tension of the liquid, ρ_g is the density of the gas, 0.075 lbf/ft^3 is the density of air, and water properties are included in the equations as 62.3 lbf/ft^3 = density, 1 centipoise (cP) = viscosity, and 4.99 lbf/ft = surface tension (Avallone and Baumeister [33]).

Referring to the figure, the vertical axis is a function of gas flow rate, and the horizontal axis is a function of the ratio of liquid flow rate to gas flow rate. For water and air, the axes reduce to the air flow rate versus the water flow rate divided by the air flow rate. At the middle of the

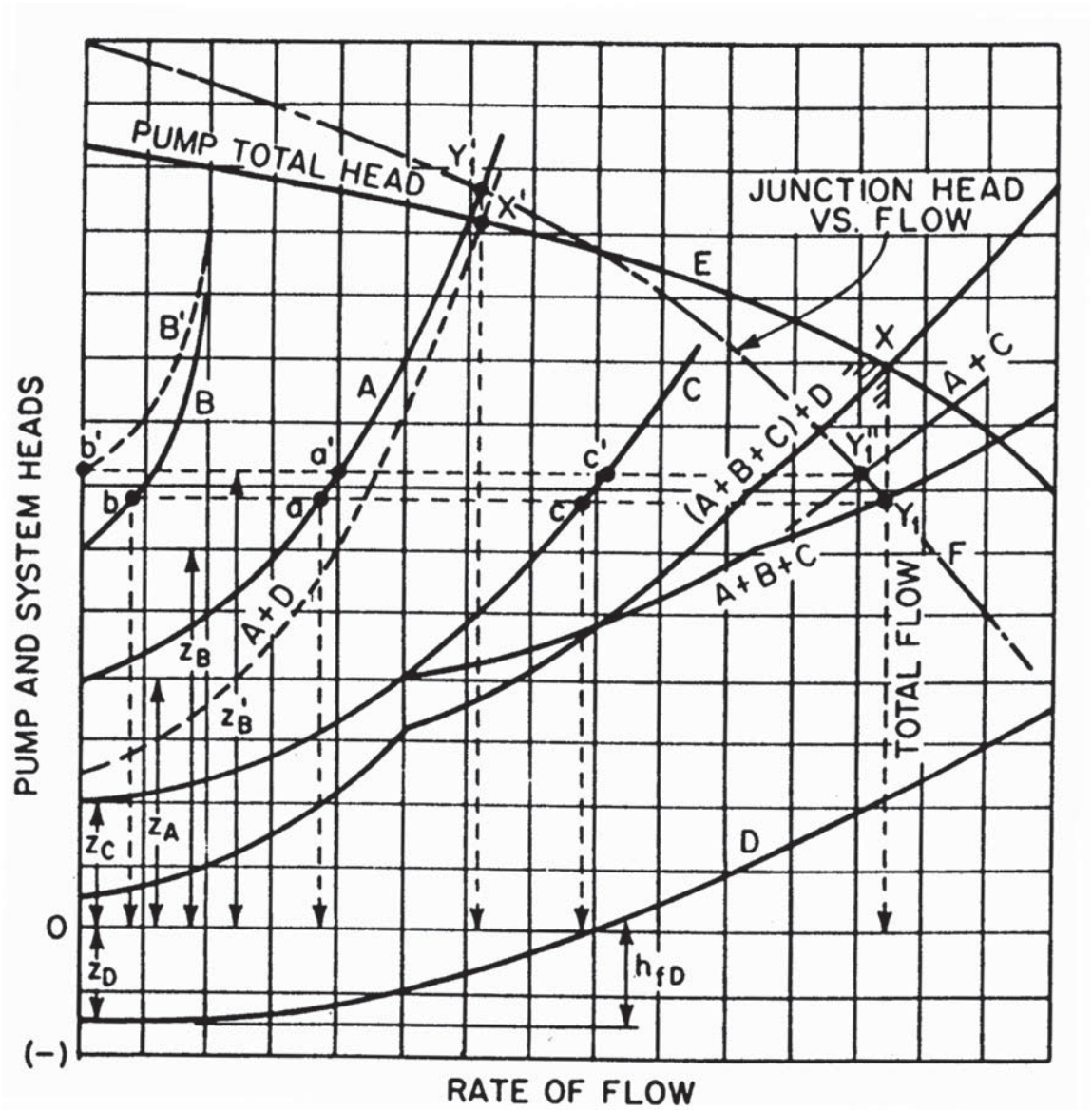


FIG. 2.94 PUMP CURVES FOR A MULTIPLE BRANCH SYSTEM ("Pump Handbook" by Karrassik, Igor J. Copyright 2012. Reproduced with permission of McGraw Hill Companies, Inc. [53])

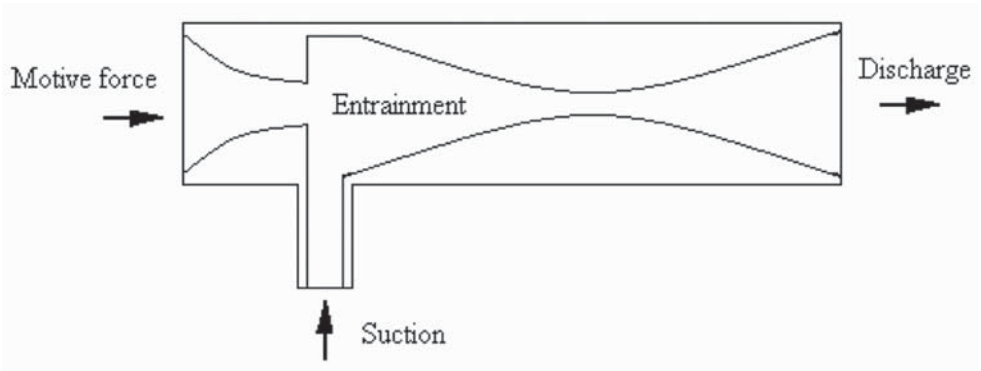


FIG. 2.95 JET PUMPS

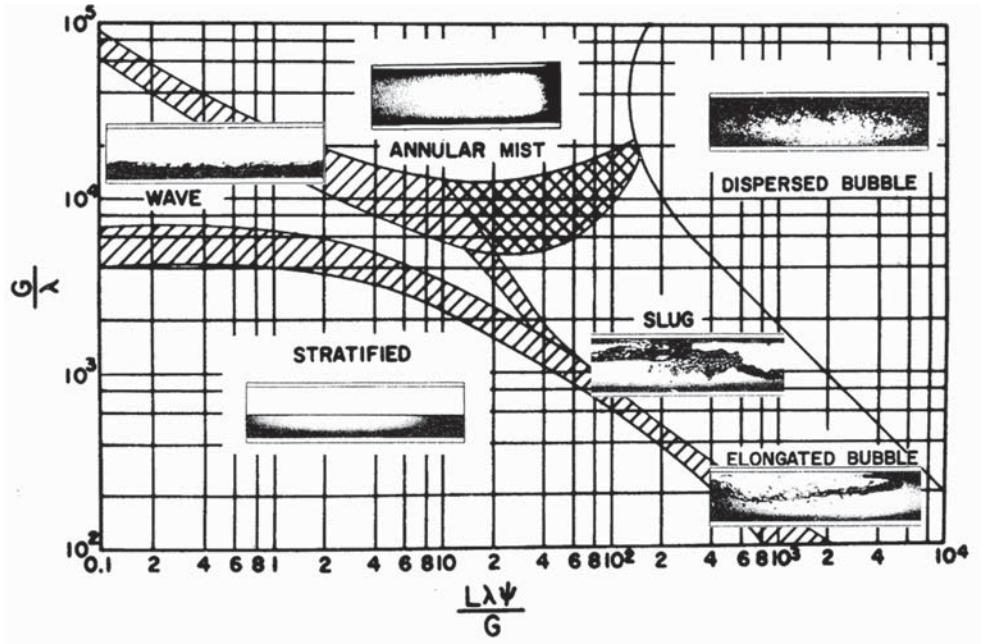


FIG. 2.96 FLOW PATTERNS FOR GAS/LIQUID FLOW (Scott [87] and Hoogendorn [88], Govier and Aziz [34])

chart, the flow is stratified (open channel flow) for low gas flow rates. As the gas flow increases, waves appear on the fluid surface, then annular liquid flow occurs. If the gas flow rate continues to increase, a mist is created throughout the pipe volume. Viewing the figure from left to right, the fluids change from open channel flow to elongated bubble or slug flow and then to dispersed bubbles. Dispersed bubble flows include froths and small bubbles entrained depending on flow rates. Gas may be introduced into the system either intentionally for processing or unintentionally due to design conditions.

2.9.1.1 Air Entrainment and Dissolved Gas Air and gas are frequently introduced into pipe systems, where dissolved gas is related to the maximum solubility of gas in liquid, and entrainment is related to air or gas forced into solution by recirculation or other causes. Either dissolved gas or entrained gas may affect flow rates through a pump, as shown in Figs. 2.97 and 2.98.

Air is occasionally introduced into pump inlets subjected to vortexing at the pump inlet, where up to 10% air by volume may be drawn into the piping (Karassik [53]). In some cases, slug flow is produced due to air entrainment when the pipe slopes upward from the pump (Haupt [78]). In other cases, 2% to 3% air by volume is usually sufficient to prevent flow through a pump at deadhead as the pump becomes air bound. The Hydraulic Institute [79] indicates that pumps may continue to operate at higher speeds for as much as 6% of trapped air in some pumps. On the other hand, positive displacement pumps can handle large volumes of air. Once air passes through the pump, it can also affect performance elsewhere in the system. The general nature of air effects on pump performance are shown in Fig. 2.99, and an example provides insight into this figure.

Example 2.16 Air entrainment in a pump

Pump startup was extremely difficult for the system shown in Fig. 2.100 due to air entrainment into the pump from the cooling tower. In the cooling tower, a baffle was installed to prevent vortexing, but corrosion permitted some air through the plate into the pump inlet piping. The problem was simply corrected by replacing the plate, but analyzing the problem was not so simple. The system was in service for many years, records were inadequate, and the impeller size was increased after initial system operation. The known facts were that priming the pump took as long as 10 to 15 minutes, while the pump discharge valve was very slowly opened, and the pump sometimes stopped after many hours of operation. The pump curve was evaluated, and the NPSHa and NPSHr were nearly equal, and a loss of prime due to faulty design was initially considered to be the problem. In fact, pitting of internal pump surfaces was caused by cavitation erosion,

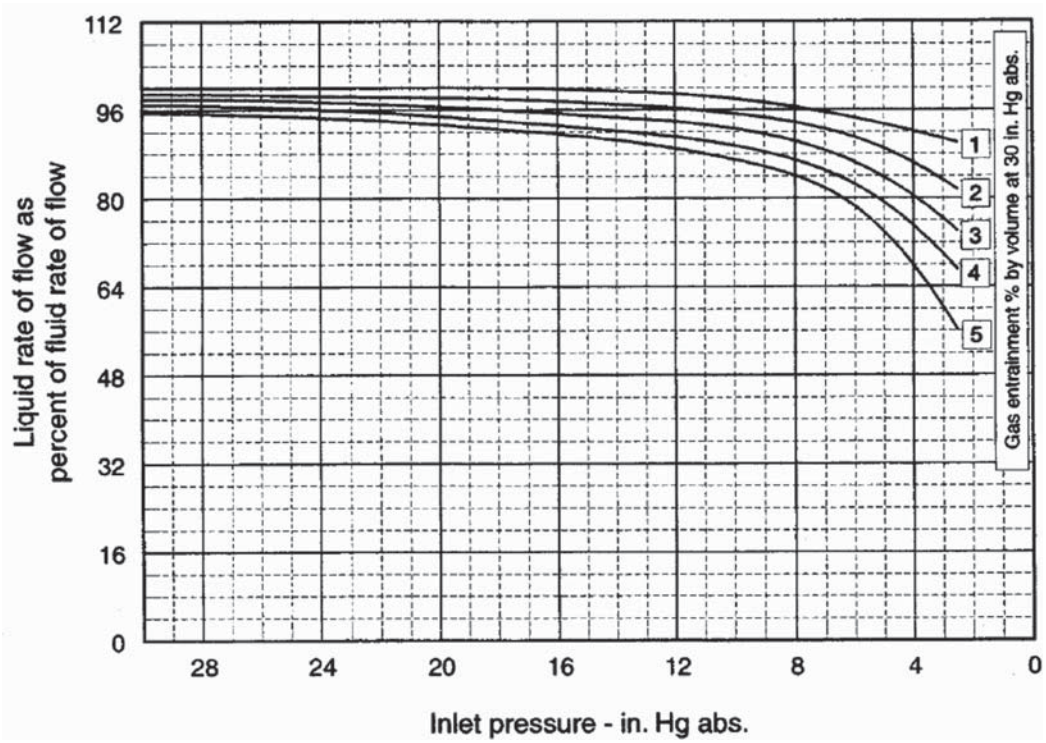


FIG. 2.97 EFFECT OF ENTRAINED GAS ON FLOW RATE OF ROTARY PUMPS (Courtesy of Hydraulic Institute, Parsippany, NJ 070504, www.pumps.org [79])

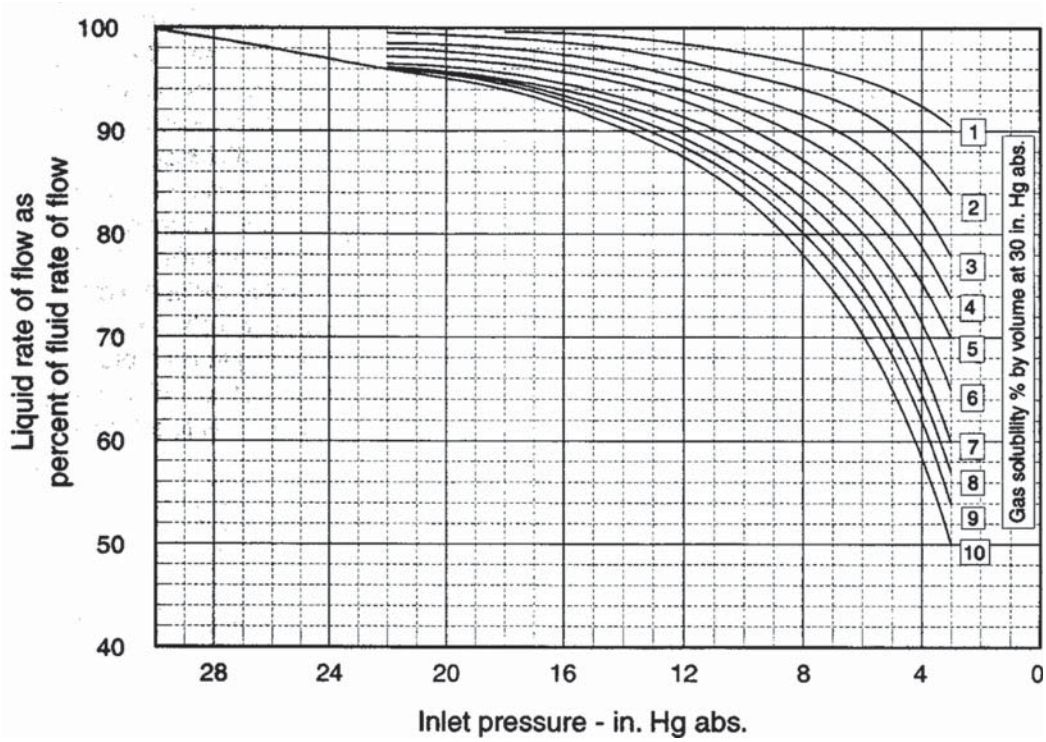


FIG. 2.98 EFFECT OF DISSOLVED GAS ON FLOW RATE OF ROTARY PUMPS (Courtesy of Hydraulic Institute, Parsippany, NJ 070504, www.pumps.org [79])

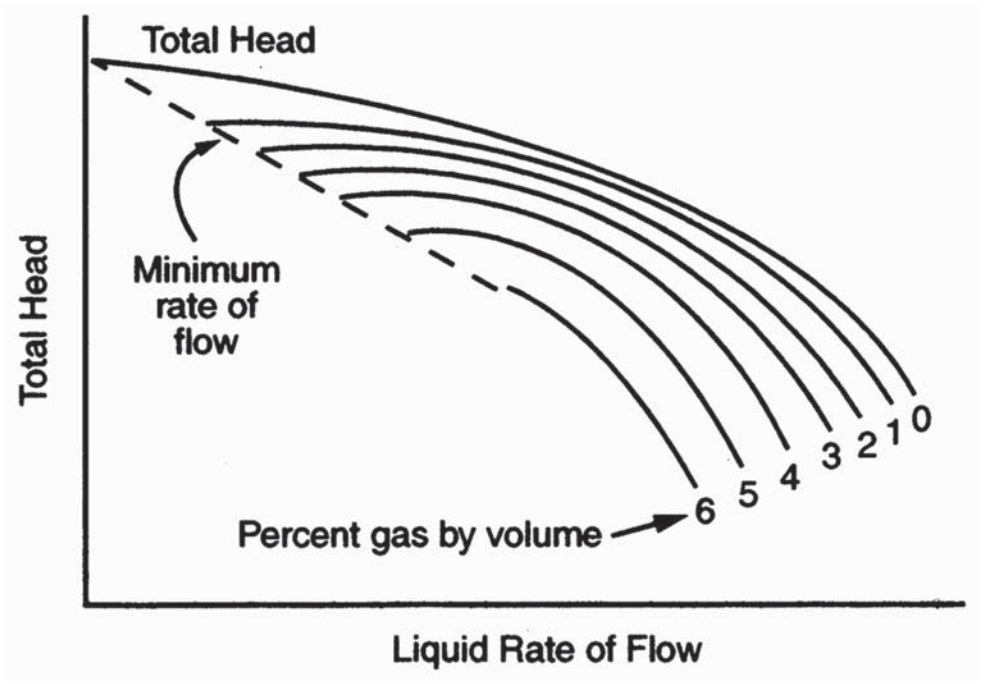


FIG. 2.99 GAS EFFECTS ON PUMP PERFORMANCE (Reprinted by permission of Hydraulic Institute [79])

and vibration analysis equipment demonstrated increased pump vibration due to cavitation bubble collapse. On further investigation, the corroded baffle plate was discovered. Even so, the faulty operation can be explained using Fig. 2.100. At startup, the pump would not operate properly due to air entrainment, but once a flow rate was established, the pump operated continually above the minimum rate of flow on the curve until sufficient additional air was introduced into the pump to stop operation at some later time. For cases where repair is not so simple,

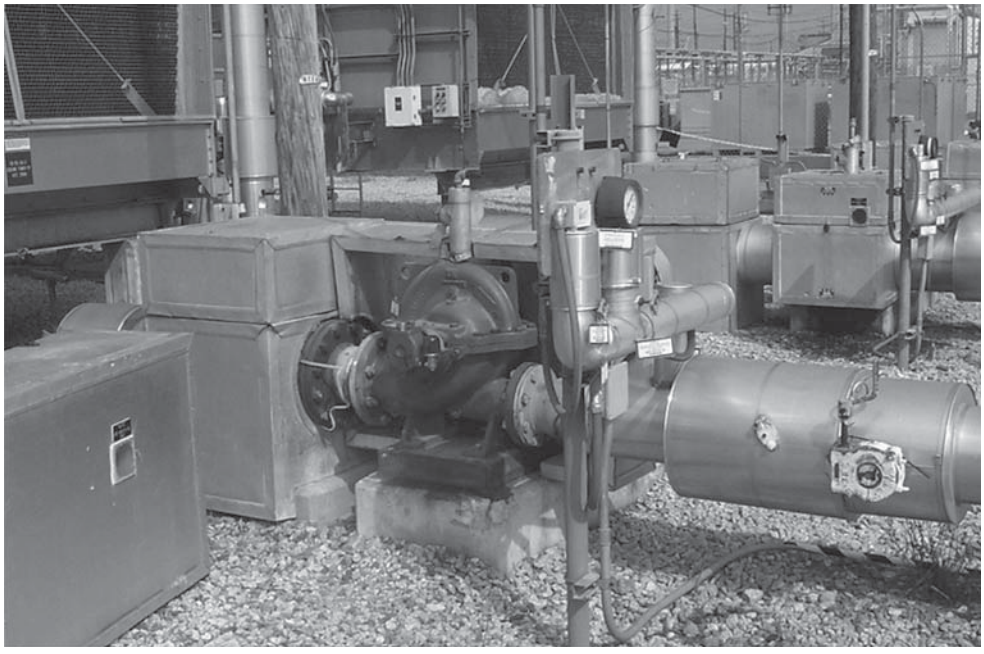


FIG. 2.100 AIR ENTRAINMENT EXAMPLE

vents may be installed on the pump to correct an air entrainment problem at the pump.

2.9.1.2 Air Binding in Pipes SRS operations experience has shown that entrained air typically separates from solution at localized high points in a system, and the net effect is that air pockets occur in the system. If air pockets form in one of two, or more, parallel pipes, flow through that path may be obstructed, or air bound, since flow moves through the less-obstructed flow path. Additionally, when the system is depressurized, a sudden expansion of the air pocket may occur and result in a system volume increase, which can lead to overflow of surge tanks connected to the system. Venting the system at high points controls air accumulation during system startup and subsequent operations.

2.9.2 Open Channel Flow

Although open channel flow is worthy of textbooks to study the field, the basic equations for open channel flow need consideration here. Referring to Fig. 2.101, open channel flow in a long pipe occurs if the hydraulic grade line has a steeper slope than the pipe, where

$$\frac{P_1}{\gamma} + Z_1 < \frac{P_2}{\gamma} + Z_2 \qquad \text{US (2.111)}$$

This condition defines critical flow, where the fluid depth in the pipe is constant. At subcritical flow, the pipe cannot flow full. At supercritical flow, a point exists along the pipe where the pipe will start to flow full. The velocity at any flow rate in the pipe is obtained using the Manning equation, which yields

$$V_2 = \frac{Q}{A} = \sqrt{\frac{8 \cdot r_h \cdot h_L \cdot g}{f_m \cdot L}} = \frac{1.486 \cdot (r_h)^{1/6}}{\varepsilon_m} \cdot \sqrt{\frac{r_h \cdot h_L}{L}} \qquad \text{EE, SI (2.112)}$$

$$V(\text{ft/sec}) = \sqrt{\frac{8 \cdot r_h(\text{in}) \cdot h_L(\text{ft}) \cdot g(\text{ft/sec}^2)}{f_m \cdot L''(\text{in})}} = \frac{0.1238 \cdot \left((r_h)^{1/6}(\text{in})\right)}{\varepsilon_m} \cdot \sqrt{\frac{r_h(\text{in}) \cdot h_L(\text{ft})}{L''(\text{in})}} \qquad (2.113)$$

where r_h is the hydraulic radius, $D/4$, and the Manning friction factor, f_m, and the nondimensional roughness factor, ε_m, differ from roughness and friction factors for full flow in pipes. For turbulent flow in water, $\varepsilon_m = 0.015$ for steel and cast iron, 0.012 to 0.015 for concrete, and 0.010 for brass (Avallone and Baumeister [33]).

If the pipe is flowing full under gravity forces only, and the pipe is open at both ends, frictional forces balance

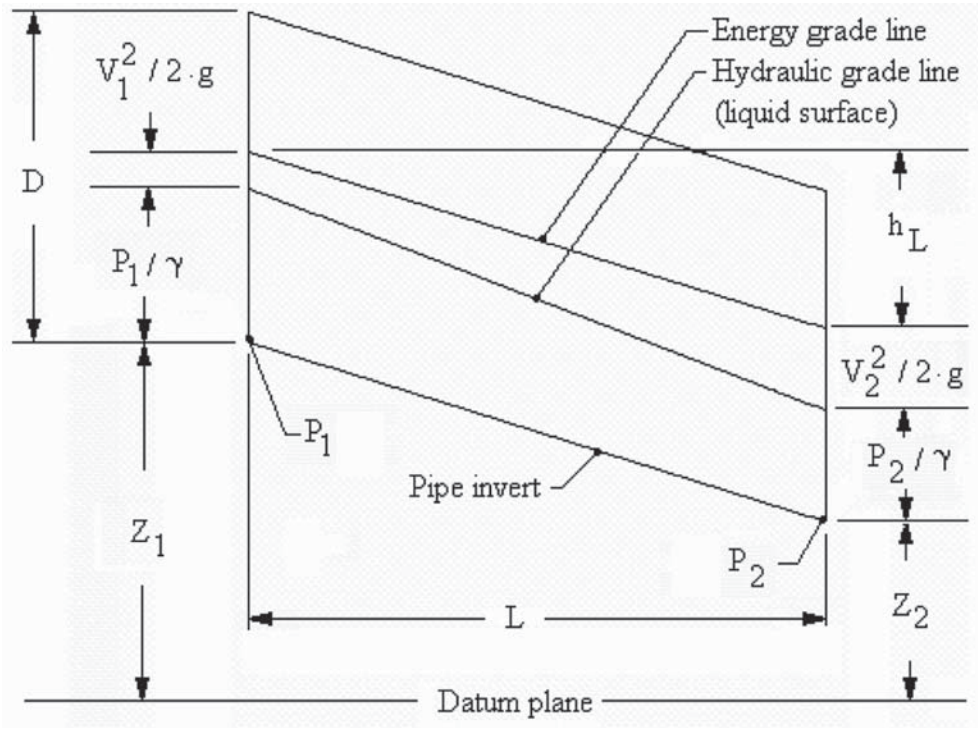


FIG. 2.101 OPEN CHANNEL FLOW IN A PIPE

gravity forces, and the estimated terminal velocity of the fluid in the pipe equals

$$V = \sqrt{\frac{D \cdot g \cdot h}{2 \cdot f \cdot L \cdot 12}} \qquad \text{US (2.114)}$$

$$V = \sqrt{\frac{D \cdot g \cdot h}{2 \cdot f \cdot L}} \qquad \text{SI (2.115)}$$

2.9.3 Liquid/Vapor Flows

Steam/condensate systems are an example of liquid/vapor flows. Flow characteristics are very similar to gas/liquid flows, except that vapor collapse occurs. If gas is entrapped within a liquid, the gas provides resistance as it compresses, and a pressurized bubble may form. If a steam vapor is entrapped within a liquid, the vapor condenses and offers negligible resistance when pressurized (Wylie [173]). When the vapor cavities are small, collapse of cavitation bubbles occurs, and when the cavities are large, shock waves are created in the liquid. This shock wave creation is sometimes referred to as condensate-induced water hammer or steam hammer.

2.9.4 Liquid/Solid Flows

Slurries are a mixture of solid particles and a liquid, and slurry performance in pipe systems is well outside the scope of this text, but an example seems relevant. In this example, 60-μm glass particles were suspended in water in ¾-in. NPS pipe, and the results shown in Fig. 2.102 were obtained. Note that a minimum velocity was required to suspend all of the particles, and particles tumbled along the pipe bottom as a moving bed when the velocity was lowered and that as the velocity was lowered further, a stationary bed of particles formed as saltation of particles occurred.

2.9.5 Siphons

Siphons may seem rather simple, but they are rather complicated in actual systems. Testing performed at SRS demonstrated the characteristics of siphons, as shown in the following example.

Example 2.17 Siphons

Consider siphons where the dimensions are provided in Fig. 2.103, and test results are shown in Fig. 2.104. Valves were initially closed before all tests. When both ends of the tube are submerged, a siphon occurs as expected to empty one reservoir to the other if the elevation $Z' < h_b - h_L$. In other words, a continuous flow from the high to low point, or siphon, occurs if the pressure in the tube does not reduce to the vapor pressure of the fluid. However, if one, or both, ends of the tube are open to atmosphere, fluid behavior changes significantly.

First, consider the case of a tube with neither end submerged. If only the lower end of the tube is opened, liquid slug flow occurs in the tube as air enters the bottom of the tube, and the upper sections of the tube compress due to vacuum formation in the tube. Air then bubbles into the upper tube section, and the tube expands. Equilibrium is reached in less than a minute. The sequence of valve opening affects only the height of liquid left in the tube.

Intuitively, one might expect that the fluid would remain in the vertical tube. After all, a classic example is to hold one's finger over the end of a straw, and a column

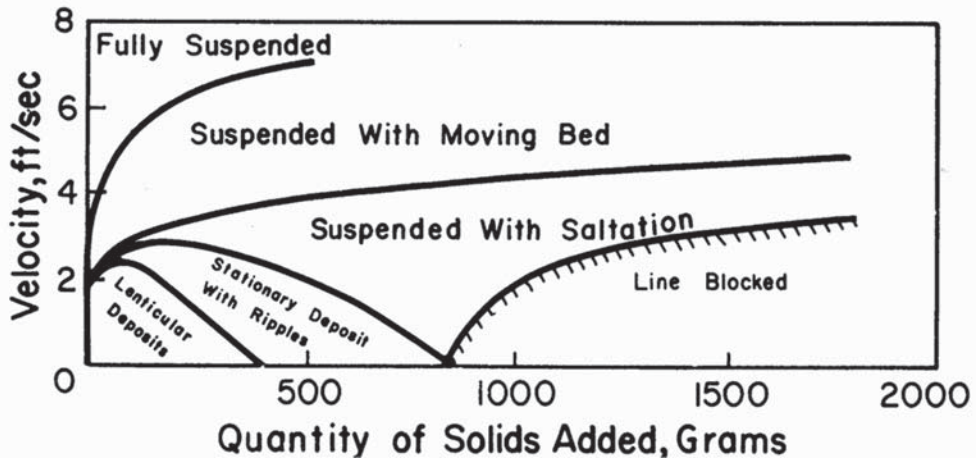


FIG. 2.102 GLASS PARTICLE SLURRY (Reprinted by permission of Institution of Chemical Engineers, Govier [34])

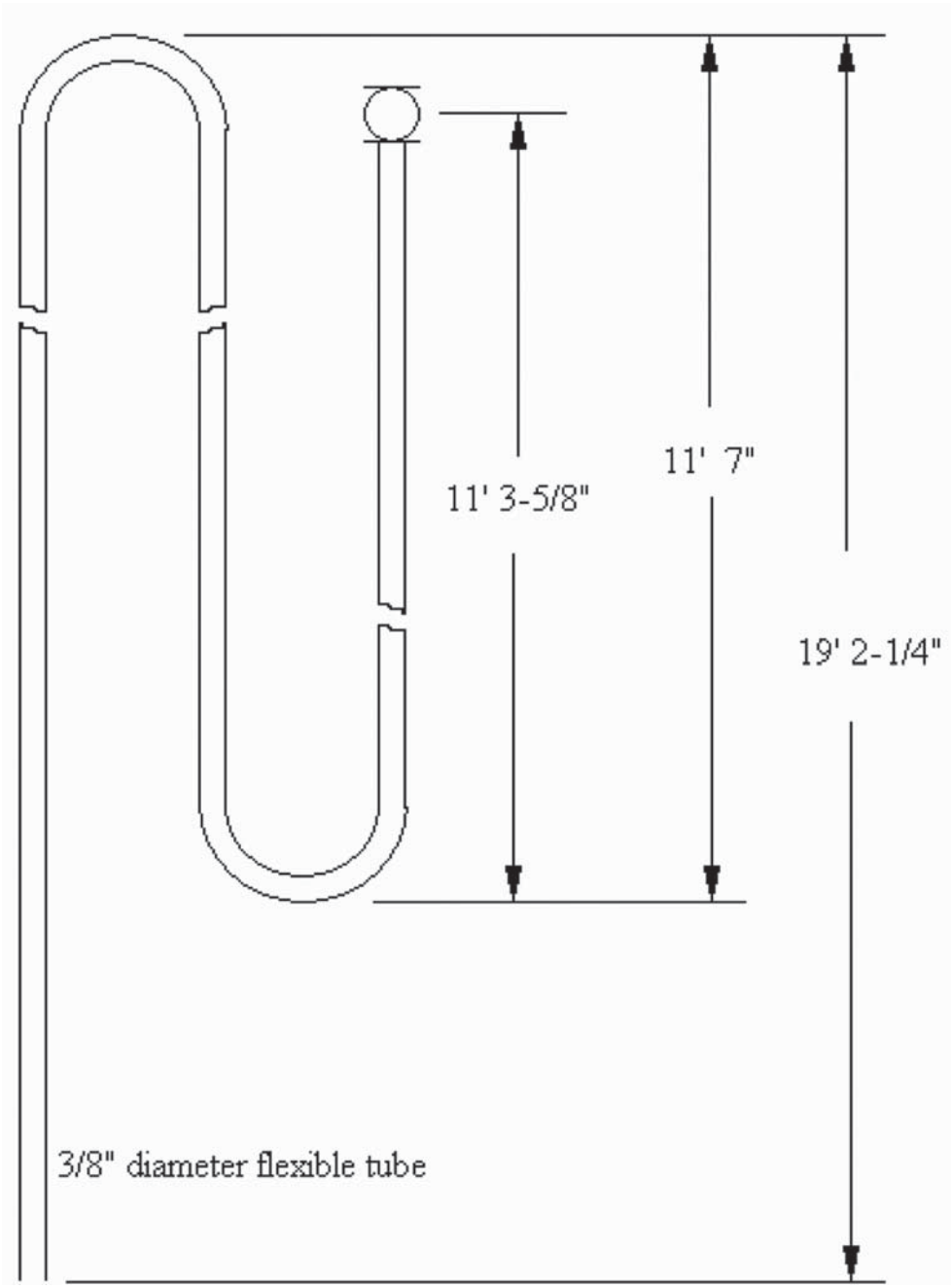


FIG. 2.103 SIPHON TEST SETUP

of fluid remains in the straw when it is lifted. Up to about 1/8 to ¼ of an inch diameter this technique works, but for larger diameters, air bubbles up into the tube for either horizontal or vertical tubes or pipes.

Now, consider the case of a tube with only one end submerged. Intuitively, one may assume that all of the fluid in the tube siphons into the reservoir when both valves are opened. Results prove otherwise. When valves are opened, liquid drops into the reservoir, and the upper loop of the tube collapses due to vacuum. Then, air bubbles into the tube from the upper end mix with the vapor as the tube expands. Again, this process occurs in less than a minute as the liquid rapidly flows back and forth in the tube. Most, but not all, of the liquid siphoned from the tube. Again, the sequence of valving only affected the final liquid levels in the tube.

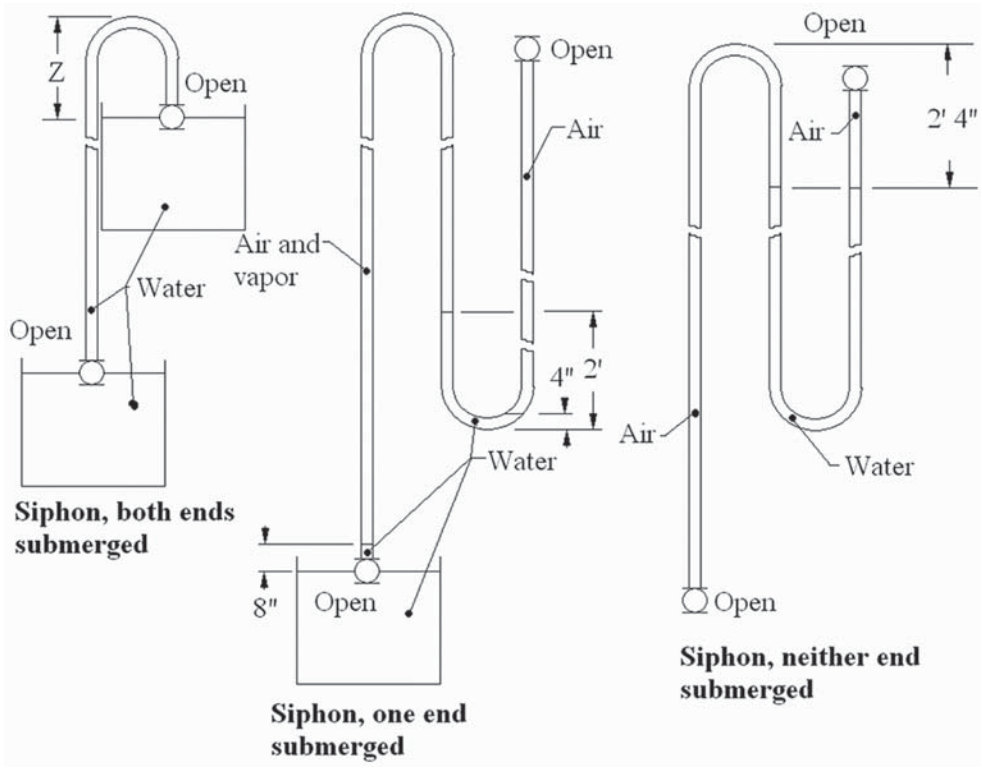


FIG. 2.104 SIPHON TEST RESULTS

This model of one tube end submerged in a liquid closely paralleled the results of a siphon through a 3-in. NPS pipe, which connected two 1.3 million gallon tanks at Savannah River Site. The tubing elevations for test were selected and were comparable to a pipe system where an actual siphon left a small percentage of liquid in the piping. The percentage of liquid left in the pipe was comparable to the percentage of liquid left in the tube, and test results were consequently shown to be comparable to actual facility conditions.

2.10 DESIGN SUMMARY FOR FLOW IN STEADY-STATE SYSTEMS

A simplified example shown in Fig. 2.105 provides an overview of this chapter. In this example, a pump lifts fluid from one tank to another tank, and the pressures and velocities at the surfaces are assumed to equal zero. The required head, h_p, for the pump is then determined from Bernoulli's equation, calculated between points 1 and 2. A pump curve is selected to meet head and power requirements at the design condition and also for off-normal operations. The NPSHr is supplied with the pump curve and is compared to the NPSHa for the suction piping. Details for more complicated pipe systems are presented in this chapter.

In short, this chapter of the text reviews the fluid mechanics for steady-state operating conditions required for the design of pipe systems. System curves, pump curves, and hydraulic and energy grade lines provide a graphic understanding of the head, or pressure, changes throughout a system, and the factors affecting these curves and grade lines are considered here. In particular, appropriate constitutive equations, experimental data, equipment descriptions, and material properties are provided, along with additional references for details not included herein. Overall, approximate flow rates, power requirements, and system pressures may be obtained throughout pipe systems containing Newtonian fluids, such as water or gasoline flowing in pipes or tubes, but flow rates for more complex, non-Newtonian, fluids are less understood.

In other texts on water hammer, the reader is assumed to be already familiar with the topics presented in this chapter, but a reasonable understanding of steady-state fluid design and pipe system components is essential to understanding fluid transients, and the basics are therefore provided in this chapter. The primary objective of this chapter is to provide references as required and some

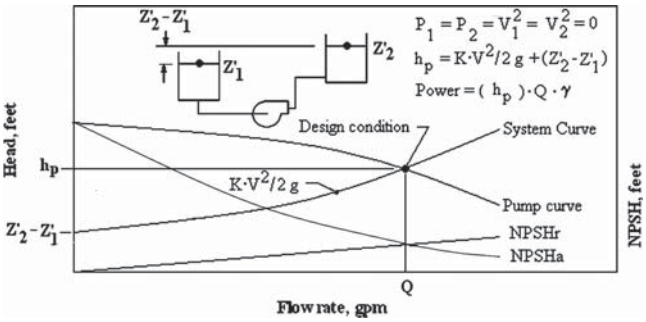


FIG. 2.105 APPLICATION OF BERNOULLI'S EQUATION TO PUMP CURVE SELECTION

insight into the many complexities associated with steady-state flows. As with the topics in each chapter of this text, research continues to improve current technology, which for this chapter leads to a better understanding of steady-state flow in pipes.

Even so, available techniques for estimating flow and head are the foundation of this text. Specifically, the steady-state velocity, *V*, is proportional to pressure transient magnitudes and the additional forces on pipe system components due to pressure transients.

CHAPTER

3

PIPE SYSTEM DESIGN

This chapter on piping design could just as well follow the chapter on fluid transients, but some of the pipe failures used to describe transients are related to piping design. Consequently, the basics of piping design are first introduced. Piping design constitutes entire textbooks and is the subject of piping design Codes and computer programs used to design to those Codes. Accordingly, a complete set of design rules for piping is outside the scope of this text. The intent here is to provide a basic introduction to piping design as a foundation to consider the effects of fluid transients on pipe systems.

Different systems of units were used in Chapters 1 and 2 to clarify the relationships between systems of units for this work, but US units will be consistently used throughout the remainder of the text for stresses. The earlier chapters and Appendix A-2 provide sufficient information to convert between systems of units.

3.1 PIPING AND PRESSURE VESSEL CODES AND STANDARDS

Codes and standards provide design and operating requirements for systems requirements for individual components. Codes and Standards are available for valves, flanges, and other components, pipe systems, and pressure vessels. Neither Codes nor Standards purport to provide a complete set of design procedures. Instead, the Codes and Standards provide uniform acceptance requirements to ensure safe operation. Current revisions to the Codes and Standards should be consulted.

3.1.1 ASME Piping and Pressure Vessel Codes

A partial list of ASME piping and pressure vessel design Codes follows, although numerous other Standards are available to describe valves, fittings, and piping design. Postconstruction Codes are also available through ASME.

The ASME B31 Code for Pressure Piping consists of a number of individually published Sections, each an American National Standard, under the direction of ASME Committee B31, Code for Pressure Piping.
Rules for each Section reflect the kinds of piping installations considered during its development, as follows:

- B31.1 Power Piping: piping typically found in electric power generating stations, in industrial and institutional plants, geothermal heating systems, and central and district heating and cooling systems
- B31.3 Process Piping: piping typically found in petroleum refineries; chemical, pharmaceutical, textile, paper, semiconductor, and cryogenic plants; and related processing plants and terminals
- B31.4 Pipeline Transportation Systems for Liquid Hydrocarbons and Other Liquids: piping transporting products that are predominately liquid between plants and terminals and within terminals, pumping, regulating, and metering stations
- B31.5 Refrigeration Piping: piping for refrigerants and secondary coolants
- B31.8 Gas Transportation and Distribution Piping Systems: piping transporting products that are predominately gas between sources and terminals, including compressor, regulating, and metering stations; gas gathering pipelines
- B31.9 Building Services Piping: piping typically found in industrial, institutional, commercial, and public buildings, and in multi-unit residences, which does not require the range of sizes, pressures, and temperatures covered in B31.1
- B31.11 Slurry Transportation Piping Systems: piping transporting aqueous slurries between plants and terminals and within terminals, pumping, and regulating stations
- B31.12 Hydrogen Piping and Pipelines: piping in gaseous and liquid hydrogen service and pipelines in gaseous hydrogen service

2010 ASME

BOILER AND PRESSURE VESSEL CODE

SECTIONS

I Rules for Construction of Power Boilers
II Materials
- Part A − Ferrous Material Specifications
- Part B − Nonferrous Material Specifications
- Part C − Specifications for Welding Rods, Electrodes, and Filler Metals
- Part D − Properties (Customary)
- Part D − Properties (Metric)

III Rules for Construction of Nuclear Facility Components
- Subsection NCA − General Requirements for Division 1 and Division 2

Division 1
- Subsection NB − Class 1 Components
- Subsection NC − Class 2 Components
- Subsection ND − Class 3 Components
- Subsection NE − Class MC Components
- Subsection NF − Supports
- Subsection NG − Core Support Structures
- Subsection NH − Class 1 Components in Elevated Temperature Service
- Appendices

Division 2 − Code for Concrete Containments
Division 3 − Containments for Transportation and Storage of Spent Nuclear Fuel and High Level Radioactive Material and Waste

IV Rules for Construction of Heating Boilers
V Nondestructive Examination
VI Recommended Rules for the Care and Operation of Heating Boilers
VII Recommended Guidelines for the Care of Power Boilers
VIII Rules for Construction of Pressure Vessels
- Division 1
- Division 2 − Alternative Rules
- Division 3 − Alternative Rules for Construction of High Pressure Vessels

IX Welding and Brazing Qualifications
X Fiber-Reinforced Plastic Pressure Vessels
XI Rules for Inservice Inspection of Nuclear Power Plant Components
XII Rules for Construction and Continued Service of Transport Tanks

3.1.2 Other Codes and Standards

Other Codes and Standards may be pertinent to specific designs, such as American Petroleum Institute (API), Pipe Fabrication Institute, National Association of Corrosion Engineers, American Concrete Institute, Welding Research Council, American Society of Testing and Materials, Manufacturers Standardization Society, American Water Works Association, National Board of Pressure Vessels, Flow Control Institute, Process Industry Practices, and the National Fire Protection Association.

3.1.3 ASME B31.3, Process Piping

Applications of the ASME B31.3 Piping Code [89], as supported by Section VIII [90, 91], is considered here with respect to pipe system design. B31.3 provides design rules to ensure structural integrity at operating temperatures and pressures for pipe systems, compares material properties to pipe stresses, and also provides rules for fabrication and examination to ensure safe design. Examination techniques for welds and fabrication methods are excluded here, but considerations of the interaction between piping, pipe supports, and components, such as pumps and pressure vessels, are added to this B31.3 Code summary. Design rules for pipes containing dangerous fluids and high pressures are also excluded here, although they are considered in B31.3. Further discussion of the use and application of B31.3 is available (Becht [92]). Comprehensive lists of Codes, Standards, and reference

textbooks are listed in Antaki's text [93]. Both Standards and Codes include other pertinent reference standards, although the references used to create those standards are frequently not supplied.

Using the Codes requires some understanding of their structure. The Scope and Foreword for each document are not informal introductions, as would be found in a textbook. The Scope provides the limitations of the Code, and the Foreword provides the guiding philosophy implicit throughout a specific Code. Similarly, notes are not some additional insight as found in a textbook. The notes in a Code provide additional design, inspection, or fabrication rules to clarify table use. Code Committees are responsible for writing new Codes and interpreting or revising existing Codes. Frequently, a polite response to a request for interpretation is to read the entire Code. Another frequent response is that the Code is not a design document. That is, many design techniques are not found in the Codes, even though the Code is responsible for providing acceptance criteria for design. In short, the user of a Code is responsible to read all of the Code and referenced documents before applying that Code and is further expected to provide competent design to meet the Code of record. Additionally, the inspection and testing requirements are expected to be performed as specified, since they enforce the design rules presented in the Codes.

3.2 PIPE MATERIAL PROPERTIES

Several material properties are of interest to Code calculations. Much of the discussion of material properties presented here applies available ASME, ASM, ASTM, and SAE metallurgical background to develop and explain theory. Definitions follow for the yield stress, S_y, the ultimate stress, S_u, the endurance or fatigue limit, S_e, thermal expansion coefficients, α, and Poisson's ratio, ν.

3.2.1 Tensile Tests

Tensile tests establish several material properties, which include the yield strength, the ultimate strength, and the elastic modulus, E (Young's Modulus of Elasticity). The yield strength is also referred to as the yield stress. The ultimate strength is also referred to as the ultimate stress and the tensile strength. One type of tensile test uses a 2-in. long, 0.50-in. diameter test section of a bar, which is elongated at a maximum strain rate of 1/16 to 1/2 in. per in. per minute for determination of yield and tensile strengths. The bar is strained until it snaps. Alternatively, standards permit smaller diameter bars or flat or curved plate specimens to be tested as required (ASTM A370).

Material properties vary significantly for different materials and temperatures. Ductile and brittle classifications can be used to divide metals into two failure types, and much research has been directed toward understanding these different types of failure at the microscopic level. In general, at the macroscopic level, ductile material failures are preceded by plastic deformation, and the fracture surfaces have a fibrous or smooth appearance. Brittle materials have negligible deformation before fracture, and the fracture surface appears to be crystalline.

Boyer [108] provides stress-strain curves for numerous materials, and metals have higher strengths in compression than tension. Also, cold working from rolling or drawing operations increases the material strength. One implication for pipe is that pipes will be stronger along their axis than along their circumference, since more cold work occurs in the axial direction when pipes are formed. Also, a submerged hydrostatically loaded part resists substantially higher compressive stresses indicated by tensile tests (Bridgeman [94]).

3.2.1.1 Ductile Materials Ductile materials are considered to be materials that stretch, or strain, at least 5% before fracture occurs. An example of ductile material tensile test results is shown on a stress/strain diagram for one type of common steel, shown in Fig. 3.1. Two different curves are drawn on the figure, using two different scales to show both the complete stress/strain diagram and the details of the stress/strain diagram near the yield point. Initially, the stress and strain are linear until the proportional limit is reached. The slope in this linear elastic region is described by the elastic modulus, E, which is considered to be nearly the same for tension and compression of ductile materials. The one-dimensional Hooke's Law is expressed as

$$E = \frac{\sigma_e}{\varepsilon_e} \qquad \text{US, EE, SI (3.1)}$$

where ε_e is the engineering strain (in. per in.), and σ_e is the engineering stress (applied force per unit area). The terms engineering stress and strain are determined using the original cross-sectional area, A_0, of the test specimen. Beyond the elastic limit, the material is permanently, or plastically, deformed.

For some ductile materials, a slight overshoot of stress at the yield point occurs as shown, but for many materials, a concise yield point is not observed in testing. Consequently, a 0.2% plastic offset is a criteria used to uniformly define yield strength for pipes (0.5% offset or greater may be applied in other applications). For ductile materials like carbon steel, significant plastic deformation, stretching, or necking occurs before rupture. Up to the ultimate strength, the stretching is uniform throughout the bar, but near the ultimate strength, necking becomes

localized, and negligible additional force is required to fracture the bar.

Stress/strain diagrams for different materials are shown in Fig. 3.2. Ductile failures during tensile testing are shown in Figs. 3.3 and 3.4. In Fig. 3.3, a typical cup and cone fracture expected for ductile materials is observed. For ductile failures, significant plastic deformation occurs on the outside of the test specimen. When the tensile specimen snaps, the crack can be heard throughout a test facility. This fracture phenomenon during tensile testing is attributed to the formation of microvoids at material imperfections, as shown in Fig. 3.5. In Fig. 3.4, the fracture is more like a brittle fracture, where the tensile test was performed at low temperatures.

For extremely ductile materials, like aluminum at high temperature, necking continues until failure, as shown in Fig. 3.6 (Brooks and Choudhury [95]). This case is atypical of pipe materials, but highlights the fact that tensile properties and fractures of ductile materials depend on the type of material, their microstructures, and temperatures.

3.2.1.2 True Stress and True Strain Although engineering stresses and strains are used in design where elastic response is expected, true stresses and strains provide insight into actual performance of materials subjected to failure loads. The true stresses, σ_t, and true strains, ε_t, are one-dimensional stresses and strains that occur if the reducing dimensions of the cross-sectional area of the tensile test specimen are considered. In this case,

$$\varepsilon_t = \ln\left(1+\varepsilon_e\right) = \ln\frac{A}{A_0} \quad \text{US, EE, SI (3.2)}$$

$$\sigma_t = \sigma_e \cdot \left(1+\varepsilon_e\right) \quad \text{US, EE, SI (3.3)}$$

The relationship of engineering to true stresses and strains is shown in Fig. 3.7.

3.2.1.3 Strain Hardening Once a ductile material is plastically strained, additional force is required to strain it further. This phenomenon is referred to as strain hardening or work hardening. For many pipe materials, the relationship of the log of the true stress to the log of true strain is linear, where Collins provides some limited data to describe materials in terms of power law constants, where k''' is a strength coefficient, and n' is a strain hardening exponent. Commonly reported values of n' for steels vary between 0.11 and 0.284, and values of k''' vary between

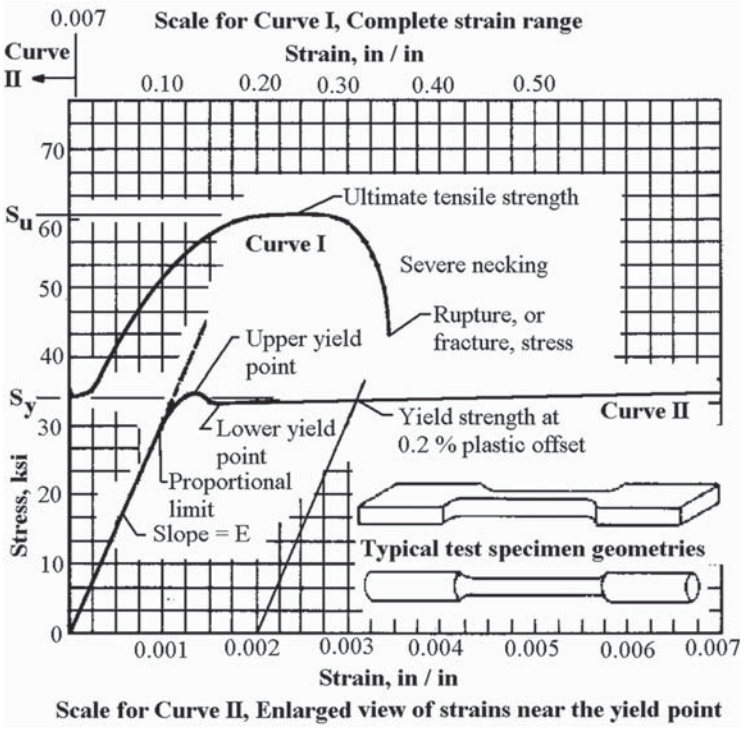


FIG. 3.1 ENGINEERING STRESS/STRAIN DIAGRAM FOR 0.25% CARBON STEEL (By permission of Van Nostrand Reinhold, Adapted from Harvey [97])

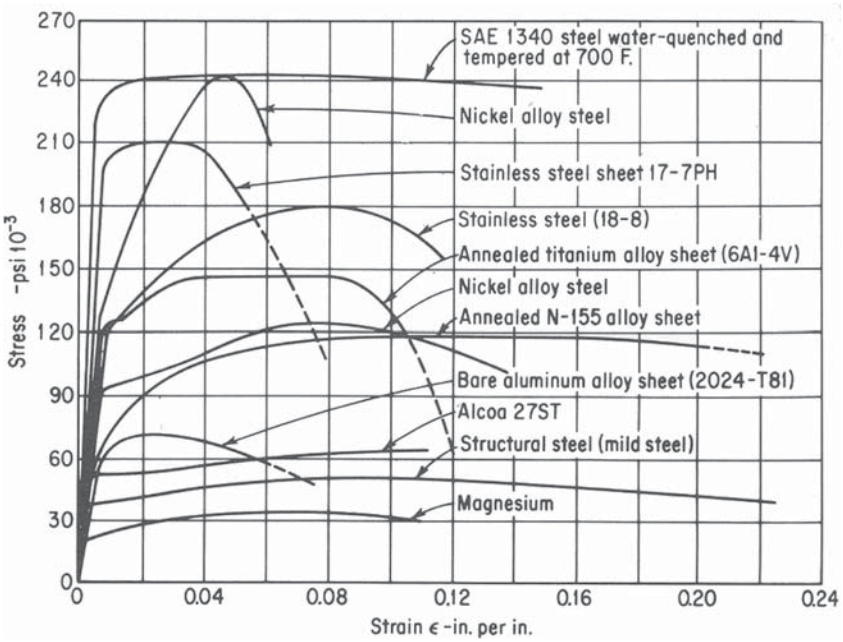


FIG. 3.2 ENGINEERING STRESS/STRAIN CURVES (Marin, Mechanical Behavior of Engineering Materials, 1st Edition, copyright 1926, pp. 24, reprinted by permission of Pearson Education, Inc Upper Saddle River, N.J. [100]) (See also Pilkey [99])

75,500 and 169,400 for 0.05 %, decarburized, carbon steel and SAE 4130 annealed steel, respectively. The power law relation is approximated as

$$\sigma_t = k''' \cdot (\varepsilon_t)^{n'} \qquad \text{US, EE, SI (3.4)}$$

Accordingly, strain hardening is linear on a log-log scale. The strain hardening exponent is affected by both material properties and part geometry. Fig. 3.8 and Table 3.1 demonstrate material effects on n'.

3.2.1.4 Loss of Ductility Loss of ductility occurs when a part is initially plastically deformed, is then elastically unloaded, and then reloaded until plastic deformation reoccurs, as shown in Fig. 3.9. Loss of ductility results in a reduction of a material's ability to resist brittle fracture. Loss of ductility may be caused by cold working, such as drawing, forging, or bending, or by welding. If time lapses between the time when the part is unloaded and reloaded, strain aging occurs where the yield point increases, and the overshoot and the yield point is changed. An implication from ductility losses is that when pipes are cold drawn, the pipes are more ductile in the hoop direction than the axial direction. That is, pipes are anisotropic due to cold forming, where the hoop direction has lower yield strength.

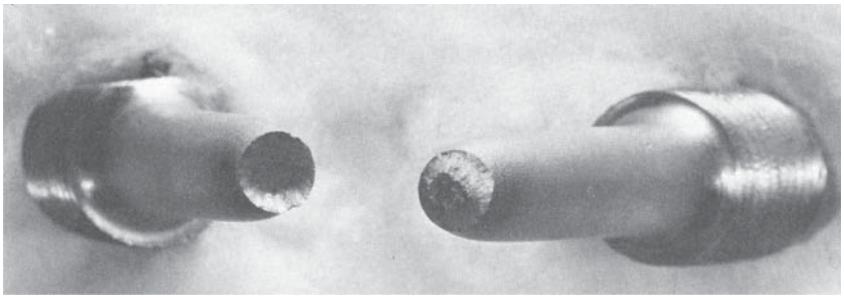


FIG. 3.3 CUP AND CONE FRACTURE OF MILD STEEL DURING TENSILE TEST (Reprinted with permission of ASM [101])

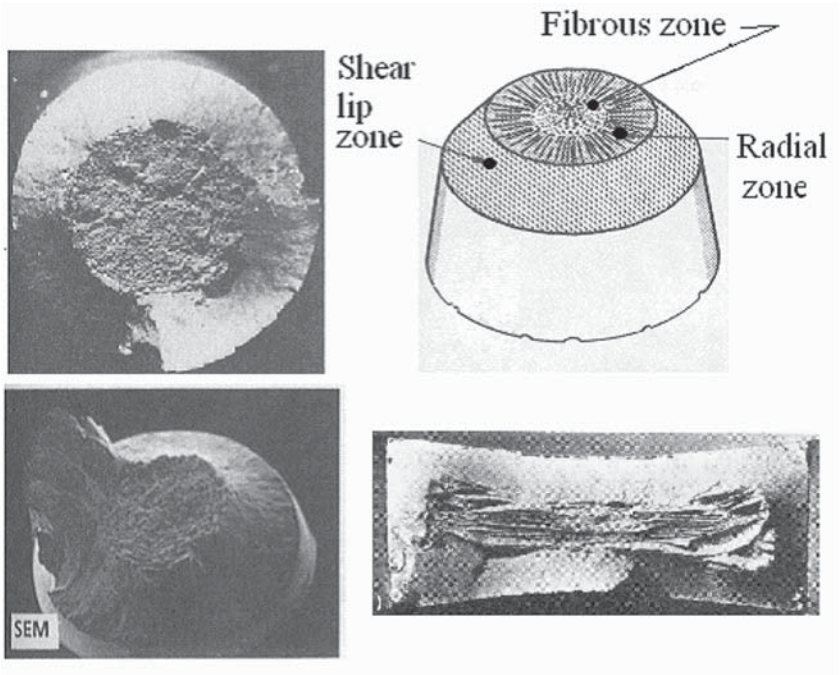


FIG. 3.4 TENSILE TEST RESULTS FOR DIFFERENT DUCTILE MATERIALS USING ROUND AND FLAT BAR SPECIMENS (Hoorstman [104], Reprinted with permission, ASM [102])

3.2.1.5 Strain Rate Effects on Material Properties Strain rates affect the material properties as shown in Fig. 3.10. As mentioned, tensile test strain rates are controlled to provide comparative tensile test data in the Codes (ASTM A370 [107]). However, in-service parts may be subject to different strain rates, and the effects of strain rate are pertinent during dynamic loading. Note that as the strain rate increases, both yield and ultimate strengths increase, and the yield strength approaches the value of the ultimate strength. One implication is that at very high strain rates, the material may respond to sudden loads elastically rather than plastically. This effect is not as pronounced as material temperatures increase, as shown in Fig. 3.11 Boyer [108] provides strain rate data for a few other materials.

3.2.1.6 Brittle Materials Negligible plastic deformation occurs during brittle fractures, as shown in Figs. 3.12 and 3.13. Brittle materials are generally assumed to strain linearly with respect to stress up to the point of fracture. However, Fig. 3.12 shows that the elastic modulus may vary when the material is elastically nonlinear. To define the elastic modulus for nonlinear, elastic materials, the secant or initial tangent modulus is used, where the slope is defined between zero stress and the elastic limit. The elastic limit is the point on the stress/strain curve where the material deviates from linear elastic behavior. The figure also shows that the ultimate stress varies significantly for cast iron, depending on whether the test is performed in tension or compression. Even so, B31.3 provides a comprehensive list of material properties including the elastic modulus and ultimate strength in tension for commonly used pipe materials. Typical examples of brittle, nonlinear materials are cast iron and concrete. Cast iron is presented here as an example of a common pipe material. Concrete data is not presented since properties vary widely, and specific data for the installed pipe should be obtained. Many ductile materials fail in a brittle manner at low temperatures. ASME, B31T [109], and paragraph 3.2.2 provide more detail on ductile to brittle transition with respect to material, temperature, shape, and thickness.

3.2.1.7 Elastic Modulus Data Data for the elastic modulus for different materials is obtained from B31.3, App. C. Data is listed in Table 3.2 for both metallic and nonmetallic materials.

3.2.1.8 Yield Strength and Ultimate Strength Data Most allowable stresses for piping materials are derived from ASME Section II [110], Part D, Appendix 1 and Appendix 2 (Flenner [111]). In some cases, ASME Standards replace existing ASTM Standards to provide additional requirements. For example, ASME, SA106 replaces ASTM, A106 in some Codes. For most steels, a safety factor of 3 to 5 based on tensile strength is applied. For B31.1, a safety fac-

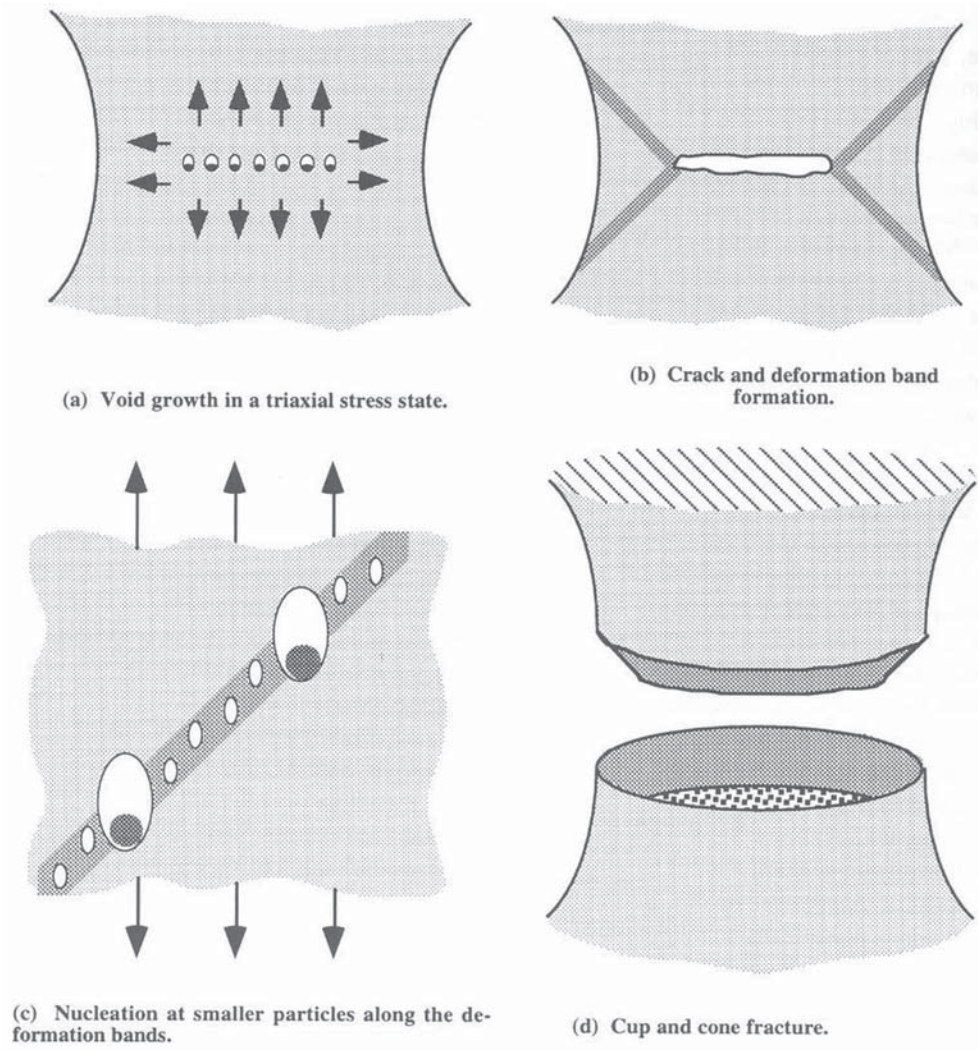


FIG. 3.5 FORMATION OF MICROVOIDS AT IMPERFECTIONS DURING TENSILE TEST FRACTURE (Anderson [103], Reprinted by permission of Marcel Dekker, Inc.)

tor of 5 is used, and for B31.3 a safety factor of 3.0 based on tensile strength is presently applied. This 3.0 value was reduced from 3.5 to align with European Standards. Determination of allowable stresses is rather complicated, and the Appendices in Section II should be consulted for further details, but the basic rules to obtain an allowable stress may be expressed as the lowest of the following values, based on ultimate strength and creep conditions:

1. For brittle materials, $S_u/10$
   For ductile materials
2. $S_u/3.5$ (ASME B31.1) or $S_u/3.0$ ASME B31.3) for ductile materials
3. $2 \cdot S_y/3$
4. 100% of the average stress to create 0.01% strain in 1000 hours
5. 67% of the average stress to create rupture in 100,000 hours (≈12 years)
6. 80% of the minimum stress to create rupture in 100,000 hours

An example of B31.1 allowable stresses for an SA-516, Grade 65 steel is shown in Fig. 3.14 (Frey [112]). Stresses are similarly calculated for B31.3 material properties.

Table 3.3 provides a partial list of material properties directly from B31.3. Properties for carbon steel, low- and intermediate-alloy carbon steels, and stainless steel pipe are included here. The reader is referred to B31.3 for a complete list of pipe properties for titanium, aluminum, copper, nickel, zirconium, and their alloys, along with properties for castings, forgings, fittings,

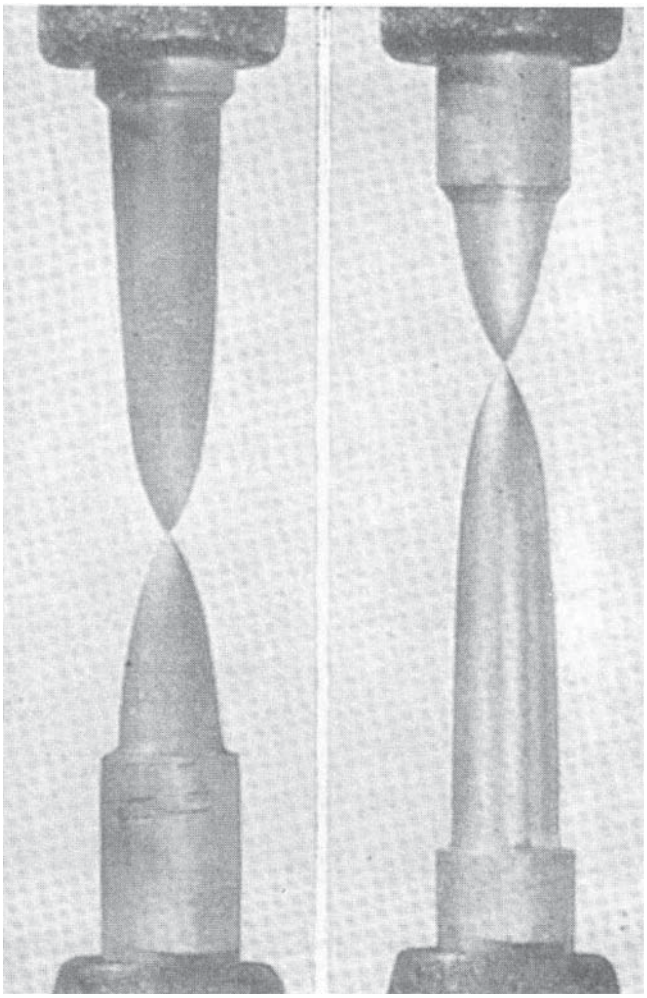


FIG. 3.6 DUCTILE FAILURE OF ALUMINUM AT 1110°F (Henry and Hoorstman [104], Reprinted by permission Verlag Stahleisen)

bolts, sheets, plates, plastic piping, and high-pressure piping. The list provided here provides a reasonable overview of material properties used in pipe system design.

Since steel pipe is the most commonly used industrial pipe, a few words about steels are in order. Steels are grouped as general use low-carbon steels (0.05% to 0.25%), which includes high-strength low-alloy steels (HSLA), machinery steels generally used in the automotive industry (0.30% to 0.55% carbon), and tool steels for cutting, forming, and rolling (less than 1.3% carbon) (Avallone and Baumeister [33]). Of interest to piping, the low-carbon steels are very ductile, and ASTM, A53, and A106 steels are widely used carbon steel pipe. The ductility of these materials permit significant plastic deformation before failure. HSLA steels provide higher yield and ultimate strengths, but in general, the fatigue limits are not significantly increased.

In Table 3.3, note that the basic allowable stresses, *S*, are provided in addition to the yield and tensile strengths. The allowable stress used for design to the Code reflects safety factors associated with different materials. For example, A48, gray iron castings have a tensile strength of 20 ksi and an allowable stress of 2 ksi, which yields a safety factor of 10. ASTM, A53 carbon steel pipe has a tensile strength of 60 ksi, a yield strength of 35 ksi, and an allowable stress of 20 ksi, which yields a safety factor of 3 based on the ultimate strength. These safety factors are reasonable, given the tolerances for material properties, permissible processing defects, permissible overpressure conditions, and the approximate calculation techniques used in the Code. Note also that the allowable stress decreases with increasing temperature as material strengths decrease. Additionally, lower temperature limits are listed in the table, and they are considered further with respect to Charpy impact tests.

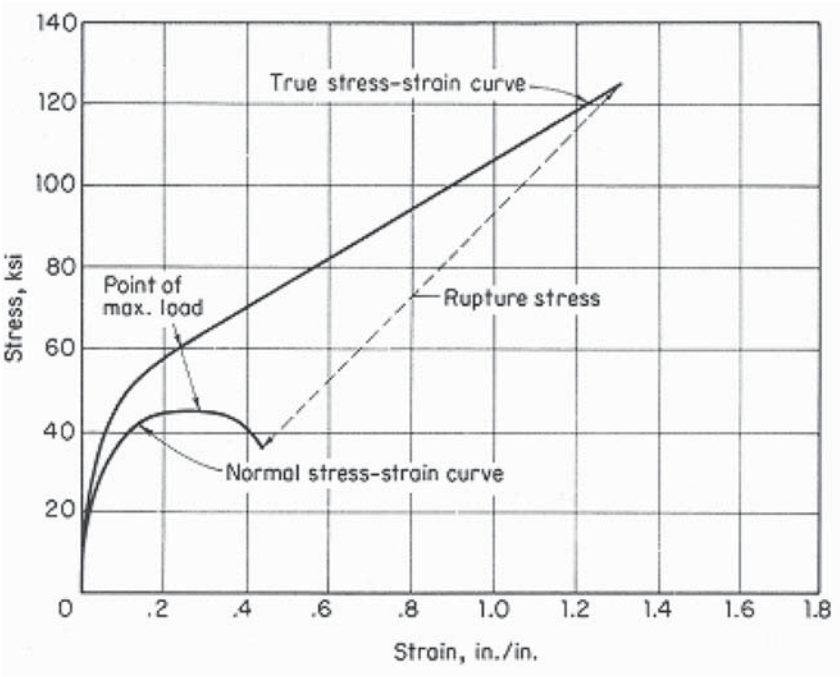


FIG. 3.7 TRUE STRESS AND TRUE STRAIN, TEMPER ROLLED, LOW CARBON, DEEP DRAWN, SHEET STEEL, 44% ELONGATION IN 2 IN., AREA REDUCTION = 75% (Reprinted by permission of ASM, Low [105])

3.2.2 Charpy Impact Test

Although drop tests are more commonly used at present, Charpy impact tests have also been used to determine the temperature at which materials have a ductile to brittle transition. Below this temperature, some metals (carbon steels in particular) fail in a brittle failure mode rather than ductile. Since brittle fractures may lead to catastrophic failures, operation below the ductile to brittle transition

TABLE 3.1 STRAIN HARDENING EXPONENTS (Cooper [106])

Material	*Condition*		*n*
SAE 1020	Yield strength, psi	= 26,000	0.28
		= 45,000	0.19
		= 52,000	0.17
		= 74,000	0.12
		= 82,000	0.098
		= 91,000	0.092
Various 0.25 to 0.45% C forged medium alloy steels	Yield strength, psi	= 180,000	0.054
		= 85,000	0.16
SAE 1045	Yield strength, psi	= 230,000	0.05
		= 100,000	0.13
		= 64,000	0.18
		= 48,000	0.23
0.45 C, Cr, Mo, V alloy steel	Yield strength, psi	= 88,000	0.186
		= 110,000	0.159
		= 150,000	0.095
		= 200,000	0.078
Alpha brass	Yield strength, psi	= 13,000	0.70
		= 20,000	0.55
Copper	Annealed		0.54
0.05% C steel sheet	Annealed and temper rolled		0.235
24S aluminum alloy	Precipitation hardened		0.16
	Annealed		0.21

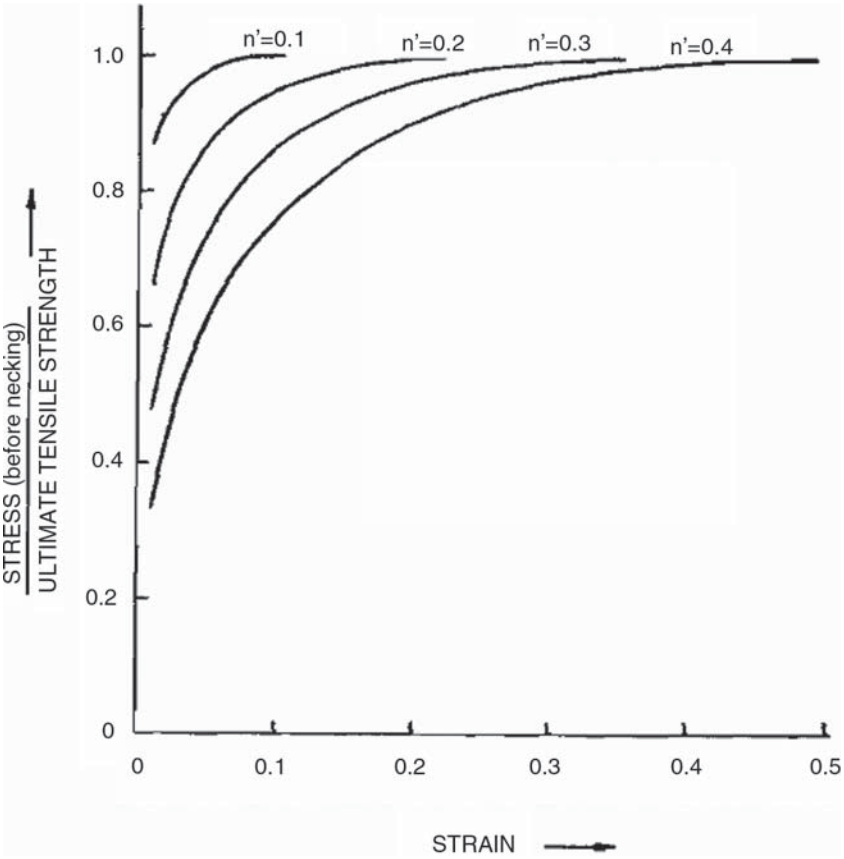


FIG. 3.8 CHARACTERISTIC SHAPE OF STRESS/STRAIN CURVES FOR VARYING STRAIN HARDENING EXPONENTS, *N´* (Cooper [106], Reprinted with permission of the Welding Research Council)

temperature is prohibited. If a material brittle fracture occurs in a material during impact test, it may experience brittle fracture in tension.

Tests are performed using a notched specimen and striker, using one of the two configurations shown in Fig. 3.15. To ensure consistent results, the impact speed of the striker is controlled within 10 to 20 ft per second. Verification of ductile to brittle transition is performed by surface inspections at different temperatures, as shown in Fig. 3.16. Different values of percent of shear are shown in the figure. For metallic pipe materials, the temperature at which 100% ductile shear occurs is the ductile to brittle transition temperature. Below this value, brittle fracture occurs as different percentages of the fracture process.

3.2.3 Fatigue Testing and Fatigue Limit

The endurance limit, S_e, or fatigue limit is the maximum fully reversing stress that a material can theoretically withstand for a specified or infinite number of cycles. Steel is considered to clarify this statement. Referring to Fig. 3.17, the fatigue limit for this steel is about 47 ksi at 10 million cycles. The steel is assumed to last indefinitely if the reversing stress is less than ±47 ksi. However, recent data indicates that the fatigue limit continues to decrease slightly for steels as the number of cycles increase, and a theoretical infinite life is unlikely for any material subject to alternating loads. For practical purposes, an infinite life is assumed.

3.2.3.1 Fatigue Limit Accuracy Note also that the recorded data has a large scatter of ± an order of magnitude. For example, for a 60-ksi stress, the data indicates that failure may occur in a few hundred cycles or as many as 10,000 cycles. This data scatter answers questions often asked when fatigue pipe failures occur. If the pipes failed in fatigue, why have only one or two pipes failed? Should not all of the pipes fail? The answer is that fatigue failures occur throughout a range of applied loads and that continued system operation will result in many more pipe failures after initial failures are observed. The fundamentals of fatigue as a material property follow, but fatigue failures are discussed further throughout the text. In fact, fatigue is a primary concern with respect to water hammer damages.

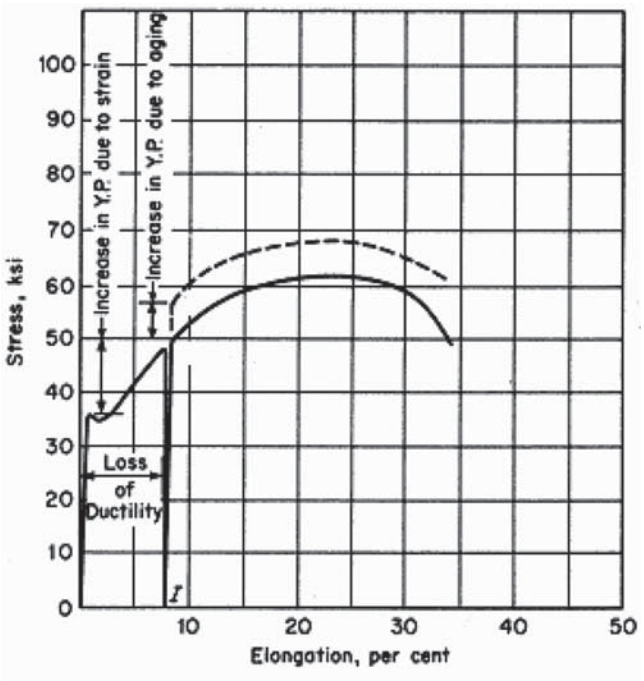


FIG. 3.9 TENSILE LOADING AND UNLOADING
(Reprinted by permission, Harvey [97])

3.2.3.2 Fatigue-Testing Methods and Fatigue Data To obtain fatigue data, various types of fatigue-testing machines are available, which apply cyclic loads differently to test specimens. Boyer [108] provides an extensive, but dated, collection of fatigue data for different materials. Swanson [116] provides a summary of fatigue-testing techniques. The load may be applied axially, in torsion, by bending the specimen in-plane (reversed beam loading), rotationally bending the specimen (rotating beam loading), or in combined stress. Harmonically varying loads are typically applied with a constant, maximum stress level, which varies about a zero mean stress, $\pm S_e$, until fracture is initiated. Loads may also be varied during test, where the load is applied for different values of the stress ratio, R' where

$$R' = \frac{S_{\min}}{S_{\max}} \qquad \text{US, EE, SI (3.5)}$$

and R' is defined in accordance with Fig. 3.18, where S'_a equals the alternating stress, S_m equals the mean stress, S_r equals the range stress, $S_{\min}$ equals the minimum stress, and $S_{\max}$ equals the maximum stress during test. Looking at the figure, R' varies from $R' = -1$ for typical fatigue tests to $R' = 1$ for constant load creep tests. Discussed in Chapters 7 and 8, $R' > 0$ applies to pipe stresses during water hammer, where a load is suddenly applied, and the pipe system is prestressed. Master curves provide data for the full range of R', but are available for only a few materials in graphs similar to Fig. 3.19.

In general, the fatigue limit is considered to be independent of the frequency of loading, but tests indicate that frequency has an effect in some cases. For example, testing of nodular iron and some alloys showed that the fatigue limit varied below 1000 cycles per minute, but was independent of frequency above 1000 cycles per minute (Boyer [108]). Roth [117] concluded that fatigue limits were unaffected up to 20 kHz for face-centered cubic stainless steels. Furuya, et al. [118] also showed that fatigue limits for low-alloy steels were constant when frequencies were increased from 100 to 20 kHz. Grover et al. [119] also noted that fatigue limits were independent of frequency for steels and other metals for tests preformed between 3 and 116 Hz. Although extensive data not available, data indicates that fatigue limits are unaffected by

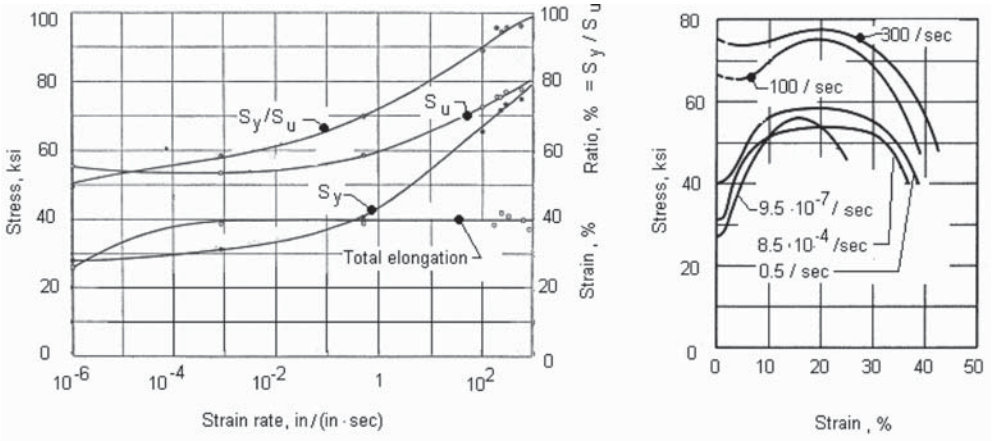


FIG. 3.10 EFFECTS OF STRAIN RATES ON MILD STEEL TENSILE PROPERTIES AT ROOM TEMPERATURE
(Manjoine [113])

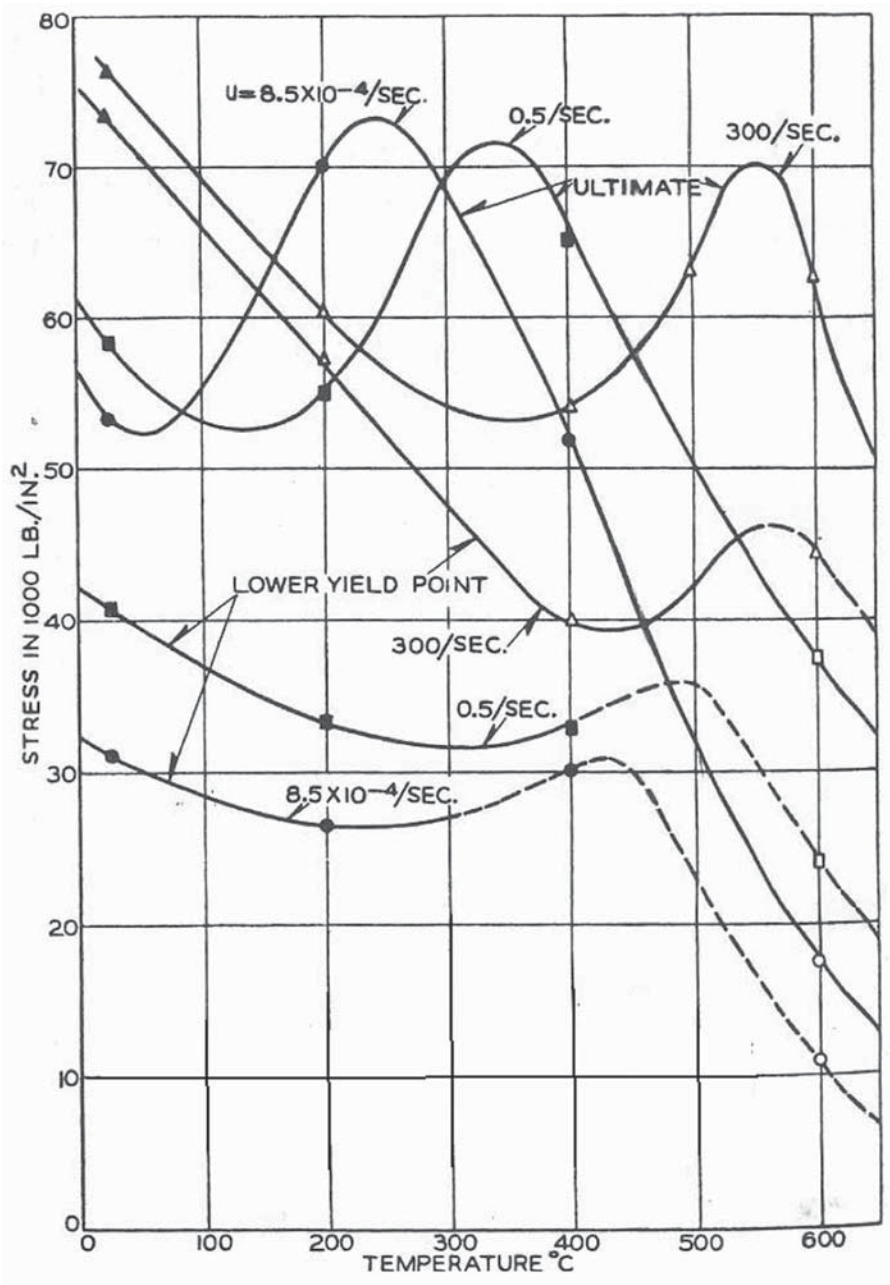


FIG. 3.11 ULTIMATE STRESSES AND YIELD STRESSES OF MILD STEEL AT VARIOUS TEMPERATURES AND RATES OF STRAIN (Manjoine [113])

frequency and that inclusion or defect sizes are the primary factor leading to fatigue.

3.2.3.3 Relationship of Fatigue to Vibrations Vibrations in structures may lead to fatigue damage, where the vibrations appear to be quite random. Accordingly, variable stress fatigue tests (Collins [121]) may also be performed as shown in Fig. 3.19. Stress/time waveforms for actual fatigue loads in service are considerably more complex than those typically tested.

As an example of complex vibrations in a real structure, vibrations were measured on a 12 ft by 12 ft, structural steel, I-beam construction platform excited by motor vibrations, and the vibration results are also shown in Fig. 3.18 (Leishear [122]). The vibrations were caused by discrete vibrations from many interconnected components. Each

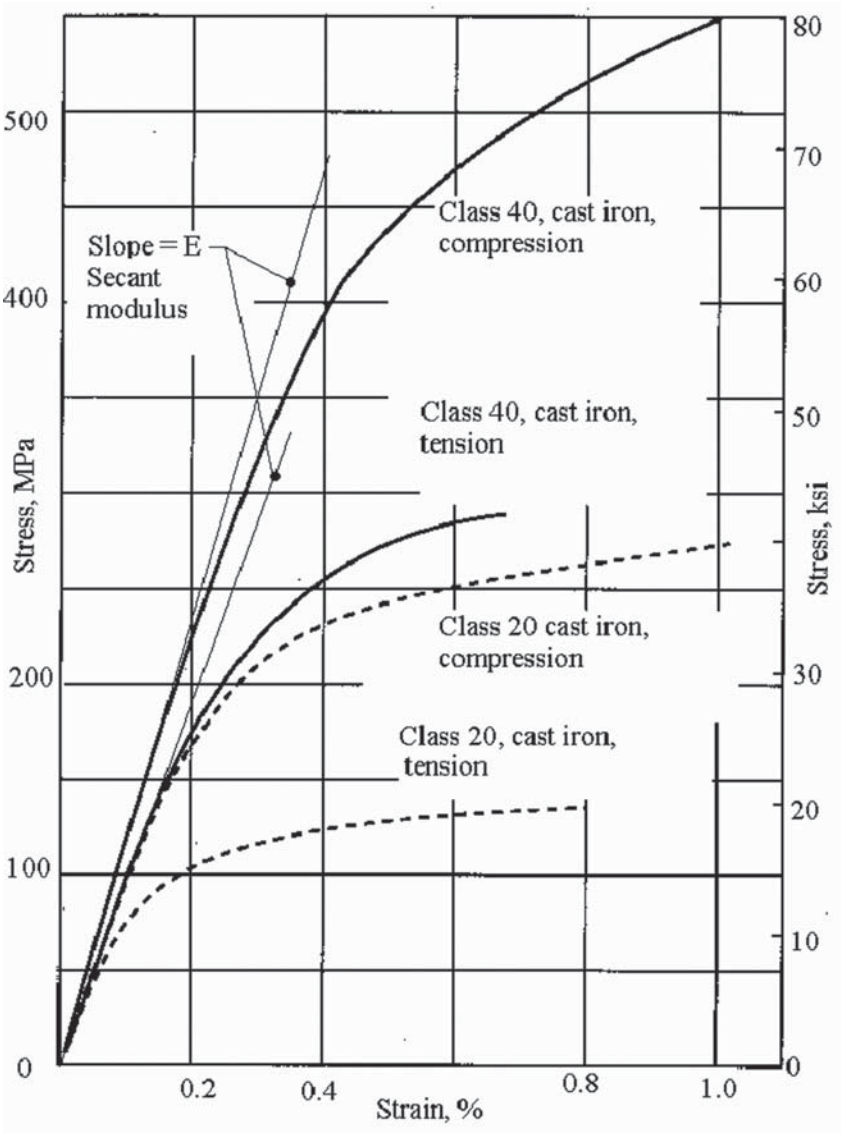


FIG. 3.12 TENSILE TESTS FOR CAST IRONS (Reprinted by permission of ASM [114])

component vibrated at its natural frequency and all of the vibrations added by the elastic principle of superposition to form the complex, seemingly random waveform shown. Vibration analysis of machinery is founded on this basic principal. Vibration analyzers from different manufacturers measure the complex vibrations of a structure and convert the time waveforms into discrete vibrations, which occur predominantly at the natural frequencies of different members. Typically, failures occur at one of the measured frequencies. Natural frequencies are discussed further in Chapter 7.

3.2.3.4 Environmental and Surface Effects on Fatigue Fatigue data is affected by the type of material, operating temperature, notches or scratches, the surface finish of the material, and specific material properties such as microstructure, grain direction, heat treatment, and corrosion, (Collins [121]). For example, Fig. 3.20 shows that aluminum does not have a clearly defined fatigue limit near 1 to 10 million cycles like steel, and Figs. 3.21 and 3.22 show that fatigue lives for various steels are dramatically affected by surface finish, corrosion, and tensile strength. In fact, test specimens are frequently polished, and corrections for the expected number of cycles to failure have been recommended for round bars in service (Juvinall [125]), such that

$$N_{\text{design}} = N \cdot K_1^{'} \cdot K_d^{'} \cdot K_s^{'} \text{ US, EE, SI (3.6)}$$

where N is the number of cycles obtained from a fatigue curve, N_{design} is the predicted number of cycles to failure for

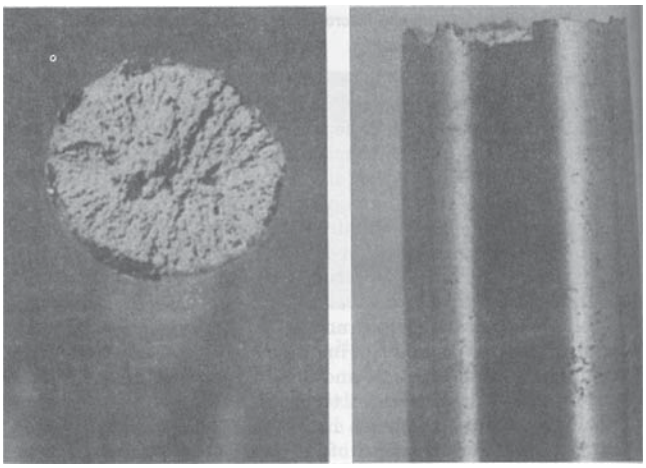


FIG. 3.13 TYPICAL BRITTLE FRACTURES
(Reprinted by permission, ASM [101])

a part, K'_1 is a correction factor for the type of load, K'_d is a correction factor for the part diameter, and K'_S is a correction for surface finish, corrosion, and tensile strength of the material. Microstructure also affects fatigue life, but was not considered in Juvinall's work. The effects of surface finish are also considered in ASME, Section III [124].

3.2.3.5 Summary of Fatigue Testing The dependence of fatigue limit on these numerous parameters implies that fatigue tests can be significantly different than in-service results. As the size of the equipment increases, the potential for errors increases with respect to predicted fatigue life. Preferably full size fatigue tests should be performed at the operating condition, but this option is frequently impractical. For pipes, full size testing has been performed.

3.2.3.6 Fatigue Testing for Pipe Components Significant fatigue test data is available for pipe components, such as elbows, tees, and flanges, where Markl's results [126, 127] are the basis for the present B31.3 design rules for fatigue. Markl's tests included standard fatigue tests for polished bars where he noted that test speed had little effect on fatigue limit, reversed bending fatigue tests for pipe, and reversed bending tests for fittings, both in-plane and out of plane, where tests were performed until pipes leaked. The equipment that Markl used for testing is shown in Figs. 3.23 and 3.24. All of his tests were performed on 4-in. diameter, A106 steel pipe, and some of his results are shown in Figs. 3.25 through 3.30. His work applies to cyclic loads, which fully reverse the pipe stress from tension to compression of identical magnitude ($R' = -1$), and the maximum stresses always occurred at elbows and tees. For other than fully reversed loads, Chapter 4 of this text provides some discussion. Temperature and corrosion affects were not considered in Markl's tests.

3.2.3.7 Fatigue Curves for B31.3 Piping Markl's work was adapted to B31.3, as shown in Fig. 3.31. A stress range factor, f'', is used to multiply allowable stresses when a specified number of cycles is required. Note that below 7000 cycles, the allowable stress for cyclic loads increases by a factor greater than 1. Also of note, the Markl research focused primarily on high-cycle fatigue, and limited data was provided below 7000 cycles, where some low-yield strength materials may be used down to 3125 cycles to failure. Per B31.3, the stress range factor is used to find the number of cycles, n, such that

$$f'' = 6.0 \cdot n^{-0.2} \qquad \text{US, EE, SI (3.7)}$$

B31.3 Committee work is in process to change the definition of f', in an effort to be consistent with Section VIII and to account for high-cycle fatigue data (>10^6 cycles), where Markl's data was approximated within 20% for high-cycle fatigue. A more accurate interpretation of Markl's data plus more recent data yielded

$$f'' = 17.0 \cdot n^{-0.32} \qquad \text{US, EE, SI (3.8)}$$

3.2.3.8 Pressure Cycling Fatigue Data Fatigue data for pressure cycling of pipe intersections is available from several sources and is presently under investigation by the B31 Committees for Code recommendations. From that investigation, test data of pressure vessels with tie-in connections is provided in Fig. 3.32.

3.2.3.9 Fatigue Data for Pressure Vessel Design Although pressure vessels are outside the scope of this text, Section VIII provides additional data on fatigue that is applicable to pipe systems in some cases. Numerous fatigue curves are presently available in Section VIII, Division 2, Annex 3.F. Also, Section VIII, Sub-group Fatigue is also in the process of generating fatigue curves that include corrosion data. Some of that data is shown in Figs. 3.33 and 3.34 and Tables 3.4 and 3.5. The curves are corrected for environmental effect at 700°F. Note that high strain rates are indicated as 1% strain on the curves, which is less than the strains used in standard tensile tests (1/16 to ½ in./in./second → 6% to 50%). In other words, strain rates of 1% percent are considered to be high for applications to pipe systems that are slowly loaded in service. Note also that the fatigue limit is constant for different strain rates, which is consistent with statements in the literature that fatigue limits are frequently independent of cycle rate during testing. Some high-cycle fatigue data is available (PD 5500 [129]). However, finite fatigue strength (<10^6 cycles) is reduced as the strain rate is reduced as shown in Figs. 3.33 and 3.34 as well as Tables 3.4 and 3.5.

TABLE 3.2 MODULUS OF ELASTICITY METALS AND NONMETALS (ASME B31.3)

Material	E = Modulus of Elasticity, Msi (Millions of psi), at Temperature, °F									
	−425	−400	−350	−325	−200	−100	70	200	300	400
Ferrous Metals										
Gray cast iron	...	...	...	...	...	...	13.4	13.2	12.9	12.6
Carbon steels, C ≤ 0.3%	31.9	...	...	31.4	30.8	30.2	29.5	28.8	28.3	27.7
Carbon steels, C > 0.3%	31.7	...	...	31.2	30.6	30.0	29.3	28.6	28.1	27.5
Carbon–moly steels	31.7	...	...	31.1	30.5	29.9	29.2	28.5	28.0	27.4
Nickel steels, Ni 2%–9%	30.1	...	...	29.6	29.1	28.5	27.8	27.1	26.7	26.1
Cr–Mo steels, Cr ½%–2%	32.1	...	...	31.6	31.0	30.4	29.7	29.0	28.5	27.9
Cr–Mo steels, Cr 2¼%–3%	33.1	...	...	32.6	32.0	31.4	30.6	29.8	29.4	28.8
Cr–Mo steels, Cr 5%–9%	33.4	...	...	32.9	32.3	31.7	30.9	30.1	29.7	29.0
Chromium steels, Cr 12%, 17%, 27%	31.8	...	...	31.2	30.7	30.1	29.2	28.5	27.9	27.3
Austenitic steels (TP304, 310, 316, 321, 347)	30.8	...	...	30.3	29.7	29.0	28.3	27.6	27.0	26.5
Copper and Copper Alloys (UNS Nos.)										
Comp. and leaded Sn–bronze (C83600, C92200)	...	...	...	14.8	14.6	14.4	14.0	13.7	13.4	13.2
Naval brass, Si– & Al–bronze (C46400, C65500, C95200, C95400)	...	...	...	15.9	15.6	15.4	15.0	14.6	14.4	14.1
Copper (C11000)	...	...	...	16.9	16.6	16.5	16.0	15.6	15.4	15.0
Copper, red brass, Al–bronze (C10200, C12000, C12200, C12500, C14200, C23000, C61400)	...	...	...	18.0	17.7	17.5	17.0	16.6	16.3	16.0
90Cu–10Ni (C70600)	...	...	...	19.0	18.7	18.5	18.0	17.6	17.3	16.9
Leaded Ni–bronze	...	...	...	20.1	19.8	19.6	19.0	18.5	18.2	17.9
80Cu–20Ni (C71000)	...	...	...	21.2	20.8	20.6	20.0	19.5	19.2	18.8
70Cu–30Ni (C71500)	...	...	...	23.3	22.9	22.7	22.0	21.5	21.1	20.7
Nickel and Nickel Alloys (UNS Nos.)										
Alloy 400 N04400	28.3	...	...	27.8	27.3	26.8	26.0	25.4	25.0	24.7
Alloy N06035	29.2	...	...	29.1	29.0	28.8	28.5	28.1	27.8	27.5
Alloys N06007, N08320	30.3	...	...	29.5	29.2	28.6	27.8	27.1	26.7	26.4
Alloys N08800, N08810, N06002	31.1	...	...	30.5	29.9	29.4	28.5	27.8	27.4	27.1
Alloys N06455, N10276	32.5	...	...	31.6	31.3	30.6	29.8	29.1	28.6	28.3
Alloys N02200, N02201, N06625	32.7	...	...	32.1	31.5	30.9	30.0	29.3	28.8	28.5
Alloy N06600	33.8	...	...	33.2	32.6	31.9	31.0	30.2	29.9	29.5
Alloy N10001	33.9	...	...	33.3	32.7	32.0	31.1	30.3	29.9	29.5
Alloy N10665	34.2	...	...	33.3	33.0	32.3	31.4	30.6	30.1	29.8
Alloy N10675	...	...	...	33.7	32.9	32.3	31.4	30.7	30.2	29.8
Unalloyed Titanium										
Grades 1, 2, 3, and 7	...	...	...	...	...	...	15.5	15.0	14.6	14.0
Zirconium Alloys										
R60702	...	...	...	...	...	...	14.4	14.4	14.4	14.4

TABLE 3.2 MODULUS OF ELASTICITY METALS AND NONMETALS (CONTINUED)

E = Modulus of Elasticity, Msi (Millions of psi), at Temperature, °F											
500	600	700	800	900	1000	1100	1200	1300	1400	1500	Material
											Ferrous Metals
12.2	11.7	11.0	10.2	...	...	...	...	...	...	...	Gray cast iron
27.3	26.7	25.5	24.2	22.4	20.4	18.0	...	...	...	...	Carbon steels, C ≤ 0.3%
27.1	26.5	25.3	24.0	22.2	20.2	17.9	15.4	...	...	...	Carbon steels, C > 0.3%
27.0	26.4	25.3	23.9	22.2	20.1	17.8	15.3	...	...	...	Carbon–moly steels
25.7	25.2	24.6	23.0	...	...	...	...	...	...	...	Nickel steels, Ni 2%–9%
27.5	26.9	26.3	25.5	24.8	23.9	23.0	21.8	20.5	18.9	...	Cr–Mo steels, Cr ½%–2%
28.3	27.7	27.1	26.3	25.6	24.6	23.7	22.5	21.1	19.4	...	Cr–Mo steels, Cr 2¼%–3%
28.6	28.0	27.3	26.1	24.7	22.7	20.4	18.2	15.5	12.7	...	Cr–Mo steels, Cr 5%–9%
26.7	26.1	25.6	24.7	22.2	21.5	19.1	16.6	...	...	...	Chromium steels, Cr 12%, 17%, 27%
25.8	25.3	24.8	24.1	23.5	22.8	22.1	21.2	20.2	19.2	18.1	Austenitic steels (TP304, 310, 316, 321, 347)
											Copper and Copper Alloys (UNS Nos.)
12.9	12.5	12.0	...	...	...	...	...	...	...	...	Comp. and leaded Sn–bronze (C83600, C92200)
13.8	13.4	12.8	...	...	...	...	...	...	...	...	Naval brass, Si– & Al–bronze (C46400, C65500, C95200, C95400)
14.7	14.2	13.7	...	...	...	...	...	...	...	...	Copper (C11000)
15.6	15.1	14.5	...	...	...	...	...	...	...	...	Copper, red brass, Al–bronze (C10200, C12000, C12200, C12500, C14200, C23000, C61400)
16.6	16.0	15.4	...	...	...	...	...	...	...	...	90Cu–10Ni (C70600)
17.5	16.9	16.2	...	...	...	...	...	...	...	...	Leaded Ni-bronze
18.4	17.8	17.1	...	...	...	...	...	...	...	...	80Cu–20Ni (C71000)
20.2	19.6	18.8	...	...	...	...	...	...	...	...	70Cu–30Ni (C71500)
											Nickel and Nickel Alloys (UNS Nos.)
24.3	24.1	23.7	23.1	22.6	22.1	21.7	21.2	...	...	...	Alloy 400 N04400
27.1	26.7	26.3	25.8	25.3	24.8	24.2	23.6	...	...	...	Alloy N06035
26.0	25.7	25.3	24.7	24.2	23.6	23.2	22.7	...	...	...	Alloys N06007, N08320
26.6	26.4	25.9	25.4	24.8	24.2	23.8	23.2	...	...	...	Alloys N08800, N08810, N06002
27.9	27.6	27.1	26.5	25.9	25.3	24.9	24.3	...	...	...	Alloys N06455, N10276
28.1	27.8	27.3	26.7	26.1	25.5	25.1	24.5	...	...	...	Alloys N02200, N02201, N06625
29.0	28.7	28.2	27.6	27.0	26.4	25.9	25.3	...	...	...	Alloy N06600
29.1	28.8	28.3	27.7	27.1	26.4	26.0	25.3	...	...	...	Alloy N10001
29.4	29.0	28.6	27.9	27.3	26.7	26.2	25.6	...	...	...	Alloy N10665
29.3	28.9	28.4	27.9	27.4	26.8	26.2	25.6	24.9	24.2	23.4	Alloy N10675
											Unalloyed Titanium
13.3	12.6	11.9	11.2	...	...	...	...	...	...	...	Grades 1, 2, 3, and 7
											Zirconium Alloys
14.4	14.4	14.4	14.4	...	...	...	...	...	...	...	R60702
14.2	14.2	14.2	14.2	...	...	...	...	...	...	...	R60705

TABLE 3.2 MODULUS OF ELASTICITY METALS AND NONMETALS (CONTINUED)

Material	E = Modulus of Elasticity, Msi (Millions of psi), at Temperature, °F									
	−425	−400	−350	−325	−200	−100	70	200	300	400
Aluminum and Aluminum Alloys (UNS Nos.)										
Grades 443, 1060, 1100, 3003, 3004, 6061, 6063 (A24430, A91060, A91100, A93003, A93004, A96061, A96063)	11.4	...	...	11.1	10.8	10.5	10.0	9.6	9.2	8.7
Grades 5052, 5154, 5454, 5652 (A95052, A95154, A95454, A95652)	11.6	...	...	11.3	11.0	10.7	10.2	9.7	9.4	8.9
Grades 356, 5083, 5086, 5456 (A03560, A95083, A95086, A95456)	11.7	...	...	11.4	11.1	10.8	10.3	9.8	9.5	9.0

Material Description	E, ksi (73.4°F)	E, MPa (23°C)
Thermoplastics [Note (1)]		
Acetal	410	2 830
ABS, Type 1210	250	1 725
ABS, Type 1316	340	2 345
CAB	120	825
PVC, TYPE 1120	420	2 895
PVC, Type 1220	410	2 825
PVC, Type 2110	340	2 345
PVC, Type 2116	380	2 620
Chlorinated PVC	420	2 895
Chlorinated polyether	160	1 105
PE, Type 2306	90	620
PE, Type 3306	130	895
PE, Type 3406	150	1 035
Polypropylene	120	825
Poly(vinylidene chloride)	100	690
Poly(vinylidene fluoride)	194	1 340
Poly(tetrafluorethylene)	57	395
Poly(fluorinated ethylenepropylene)	67	460
Poly(perfluoroalkoxy alkane)	100	690
Thermosetting Resins, Axially Reinforced		
Epoxy-glass, centrifugally cast	1,200–1,900	8 275–13 100
Epoxy-glass, filament-wound	1,100–2,000	7 585–13 790
Polyester-glass, centrifugally cast	1,200–1,900	8 275–13 100
Polyester-glass, hand lay-up	800–1,000	5 515–6 895
Other		
Borosilicate glass	9,800	67 570

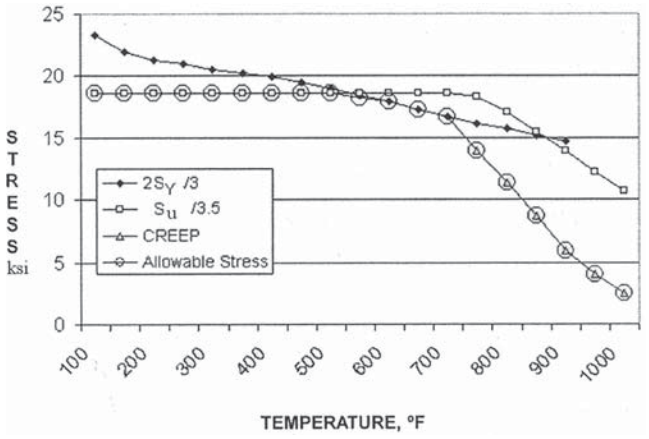


FIG. 3.14 ALLOWABLE STRESSES FOR SA-516 STEEL (Frey [112])

3.2.4 Poisson's Ratio

Poisson's ratio defines a dimensional change in an object at right angles to the applied load. Experiments show that a transverse strain accompanies any static strain on an object, such that

$$\nu \cdot \varepsilon_z = -\varepsilon_y \qquad \text{US, EE, SI (3.9)}$$

where ε_z is the axial tensile strain (+) applied to an object along its z axis, and ε_y is the transverse compressive (−) strain normal to the tensile strain. In compression, the results are similar, except that the sign of the transverse tensile strain (+) is reversed. B31.3 permits the use of 0.3 as the value of Poisson's ratio for elastic materials at all temperatures, unless other data is available, where limited data is provided in Table 3.6. Poisson's ratio is 0.5 for plastic deformation of metals, where the materials are essentially incompressible, and the volume remains the same.

3.2.5 Material Densities

The densities of various metals are provided in Table 3.7. Densities for some plastics are provided in Table 3.8.

3.2.6 Thermal Expansion and Thermal Stresses

Thermal expansion exerts significant loads on pipe systems. A rule of thumb is that steel expands 0.007 in. per ft per 100°F ($e = 6.07 \cdot 10^{-6} \cdot 12 \cdot 100 = 0.007$). B31.3 provides tables for thermal expansion coefficients, α, throughout the range of temperatures permitted for Code-approved materials, and the thermal coefficients vary by 20% to 30% in this range. Values from B31.3 are provided at 70°F for some materials in Table 3.9. The effects of thermal expansion on pipe stresses are critical to piping design.

3.2.6.1 Thermal Stresses Thermal stresses are induced by a differential temperature distribution through a thick-walled cylinder (Harvey [97]). For many cases, thermally induced stresses through the wall are negligible, but there are cases when they affect piping. A few different examples show the effects of operating temperature on pipe stresses.

Example 3.1, Insulated pipe wall stresses due to thermal loading.

For example, consider an ASTM, A53, 0.3%, carbon steel 3 in. NPS, Schedule 40, steel pipe, which is insulated with 1 in. of calcium silicate insulation. McKetta [76] provides a list of recommended insulation thicknesses for low-temperature pipe systems (<60°F). Calcium silicate and fiberglass are the most widely used pipe insulations ($\rho_{\text{fiberglass}}$ = 0.6 to 3.0 lbm/ft^3, $\rho_{\text{calcium silicate}}$ = 11.9 lbm/ft^3, Kutz [130]). The system is operating at a 70°F ambient temperature with a 200°F fluid temperature, where $E = 9.5 \cdot 10^6$ psi, $\alpha = 6.07 \cdot 10^{-6}$, $\nu = 0.3$, OD = 3.5 in., and D = 3.068 in.

The outer wall temperature can be found from the equation for the heat flux through a hollow cylinder (Lindeburg [57]), where

$$q = \frac{1}{\dfrac{1}{h''_{\text{fluid}}} + \dfrac{\ln\dfrac{\text{OD}}{D}}{k''_{\text{steel}}} + \dfrac{\ln\dfrac{\text{OD} + \bar{T}\,(\text{insulation})}{\text{OD}}}{k''_{\text{insulation}}} + \dfrac{1}{h''\text{air}}} \qquad \text{US, EE, SI (3.10)}$$

where q is the heat flux, h_{fluid} is the film coefficient for the fluid in the pipe (neglecting fluid convection inside the pipe, h''_{fluid} = infinity), k''_{steel} is the thermal conductivity of steel (27 Btu/(hour·ft^2·F)), $k''_{\text{insulation}}$ is the thermal conductivity of calcium silicate at 70°F, and h''_{air} is the film coefficient of air at 70°F (6 Btu/(hour·ft^2·F)). Lists of h'' and k'' are available from Lindeburg [57] or heat transfer texts.

Since the quantities in the denominator represent the thermal resistances through the pipe wall, and temperatures are proportional to thermal resistances, the temperature change between the inside of the pipe and the outer pipe wall surface equals

$$\Delta T = \frac{(T_{\text{fluid}} - T_{\text{ambient}}) \cdot \dfrac{\ln\dfrac{\text{OD}}{D}}{k''_{\text{steel}}}}{\dfrac{1}{h''_{\text{air}}} + \dfrac{\ln\dfrac{\text{OD} + \bar{T}}{\text{OD}}}{k''_{\text{insulation}}}} \qquad \text{US, EE, SI (3.11)}$$

where $\bar{T}$ is the insulation thickness. The maximum stresses occur on the pipe surfaces (Harvey [97]), such that

TABLE 3.3 ALLOWABLE STRESSES FOR PIPE MATERIALS (ASME B31.3, APP. A1)

Specifications Are ASTM Unless Otherwise Indicated

Material	Spec. No.	P-No. or S-No. (5)	Grade	Notes	Min. Temp., °F (6)	Specified Min. Strength, ksi		Basic Allowable Stress, *S*, ksi (1), at Metal Temperature, °F						
						Tensile	Yield	Min. Temp. to 100	200	300	400	500	600	650
Iron Castings (2)														
Gray	A 48	...	20	(8e)(48)	−20	20	...	2.0	2.0	2.0	2.0	...	...	...
Gray	A 278	...	20	(8e)(48)	−20	20	...	2.0	2.0	2.0	2.0	...	...	...
Gray	A 126	...	A	(8e)(9)(48)	−20	21	...	2.0	2.0	2.0	2.0	...	...	...
Gray	A 48	...	25	(8e)(48)	−20	25	...	2.5	2.5	2.5	2.5	...	...	...
Gray	A 278	...	25	(8e)(48)	−20	25	...	2.5	2.5	2.5	2.5	...	...	...
Gray	A 48	...	30	(8e)(48)	−20	30	...	3.0	3.0	3.0	3.0	...	...	...
Gray	A 278	...	30	(8e)(48)	−20	30	...	3.0	3.0	3.0	3.0	...	...	...
Gray	A 126	...	B	(8e)(9)(48)	−20	31	...	3.0	3.0	3.0	3.0	...	...	...
Gray	A 48	...	35	(8e)(48)	−20	35	...	3.5	3.5	3.5	3.5	...	...	...
Gray	A 278	...	35	(8e)(48)	−20	35	...	3.5	3.5	3.5	3.5	...	...	...
Gray	A 48	...	40	(8e)(9)(48)	−20	40	...	4.0	4.0	4.0	4.0	...	...	...
Gray	A 126	...	C	(8e)(9)(48)	−20	41	...	4.0	4.0	4.0	4.0	...	...	...
Gray	A 278	...	40	(8e)(9)(53)	−20	40	...	4.0	4.0	4.0	4.0	4.0	4.0	4.0
Gray	A 48	...	45	(8e)(48)	−20	45	...	4.5	4.5	4.5	4.5	...	...	...
Gray	A 48	...	50	(8e)(48)	−20	50	...	5.0	5.0	5.0	5.0	...	...	...
Gray	A 278	...	50	(8e)(53)	−20	50	...	5.0	5.0	5.0	5.0	5.0	5.0	5.0
Gray	A 48	...	55	(8e)(48)	−20	55	...	5.5	5.5	5.5	5.5	...	...	...
Gray	A 48	...	60	(8e)(48)	−20	60	...	6.0	6.0	6.0	6.0	...	...	...
Gray	A 278	...	60	(8e)(53)	−20	60	...	6.0	6.0	6.0	6.0	6.0	6.0	6.0
Cupola malleable	A 197	...	...	(8e)(9)	−20	40	30	8.0	8.0	8.0	8.0	8.0	8.0	8.0
Malleable	A 47	...	32510	(8e)(9)	−20	50	32.5	10.0	10.0	10.0	10.0	10.0	10.0	10.0
Ferritic ductile	A 395	...	...	(8d)(9)	−20	60	40	20.0	19.0	17.9	16.9	15.9	14.9	14.1
Austenitic ductile	A 571	...	Type D-2M, Cl.1	(8d)	−20	65	30	20.0	...	...	...	...	...	...

TABLE 3.3 ALLOWABLE STRESSES FOR PIPE MATERIALS (CONTINUED)

Specifications Are ASTM Unless Otherwise Indicated

Material	Spec. No.	P-No. or S-No. (5)	Grade	UNS No.	Notes	Min. Temp., °F (6)	Specified Min. Strength, ksi		Min. Temp.		
							Tensile	Yield	to 100	200	300
Carbon Steel Pipes and Tubes (2)											
A 285 Gr. A	A 134	1	...	...	(8b)(57)	B	45	24	15.0	14.7	14.2
A 285 Gr. A	A 672	1	A45	K01700	(57)(59)(67)	B	45	24	15.0	14.7	14.2
Butt weld	API 5L	S-1	A25	...	(8a)	−20	45	25	15.0	15.0	14.7
Smls & ERW	API 5L	S-1	A25	...	(57)(59)	B	45	25	15.0	15.0	14.7
...	A 179	1	...	K01200	(57)(59)	−20	47	26	15.7	15.7	15.3
Type F	A 53	1	A	K02504	(8a)(77)	20	48	30	16.0	16.0	16.0
...	A 139	S-1	A	...	(8b)(77)	A	48	30	16.0	16.0	16.0
...	A 587	1	...	K11500	(57)(59)	−20	48	30	16.0	16.0	16.0
...	A 53	1	A	K02504	(57)(59)	B	48	30	16.0	16.0	16.0
...	A 106	1	A	K02501	(57)	B	48	30	16.0	16.0	16.0
...	A 135	1	A	...	(57)(59)	B	48	30	16.0	16.0	16.0
...	A 369	1	FPA	K02501	(57)	B	48	30	16.0	16.0	16.0
...	API 5L	S-1	A	...	(57)(59)(77)	B	48	30	16.0	16.0	16.0
A 285 Gr. B	A 134	1	...	...	(8b)(57)	B	50	27	16.7	16.5	15.9
A 285 Gr. B	A 672	1	A50	K02200	(57)(59)(67)	B	50	27	16.7	16.5	15.9
A 285 Gr. C	A 134	1	...	...	(8b)(57)	A	55	30	18.3	18.3	17.7
...	A 524	1	II	K02104	(57)	−20	55	30	18.3	18.3	17.7
...	A 333	1	1	K03008	(57)(59)	−50	55	30	18.3	18.3	17.7
...	A 334	1	1	K03008	(57)(59)	−50	55	30	18.3	18.3	17.7
A 285 Gr. C	A 671	1	CA55	K02801	(59)(67)	A	55	30	18.3	18.3	17.7
A 285 Gr. C	A 672	1	A55	K02801	(57)(59)(67)	A	55	30	18.3	18.3	17.7
A 516 Gr. 55	A 672	1	C55	K01800	(57)(67)	C	55	30	18.3	18.3	17.7
A 516 Gr. 60	A 671	1	CC60	K02100	(57)(67)	C	60	32	20.0	19.5	18.9
A 515 Gr. 60	A 671	1	CB60	K02401	(57)(67)	B	60	32	20.0	19.5	18.9
A 515 Gr. 60	A 672	1	B60	K02401	(57)(67)	B	60	32	20.0	19.5	18.9
A 516 Gr. 60	A 672	1	C60	K02100	(57)(67)	C	60	32	20.0	19.5	18.9
...	A 139	S-1	B	K03003	(8b)	A	60	35	20.0	20.0	20.0
...	A 135	1	B	K03018	(57)(59)	B	60	35	20.0	20.0	20.0
...	A 524	1	I	K02104	(57)	−20	60	35	20.0	20.0	20.0
...	A 53	1	B	K03005	(57)(59)	B	60	35	20.0	20.0	20.0
...	A 106	1	B	K03006	(57)	B	60	35	20.0	20.0	20.0
...	A 333	1	6	K03006	(57)	−50	60	35	20.0	20.0	20.0
...	A 334	1	6	K03006	(57)	−50	60	35	20.0	20.0	20.0
...	A 369	1	FPB	K03006	(57)	−20	60	35	20.0	20.0	20.0
...	A 381	S-1	Y35	...	...	A	60	35	20.0	20.0	20.0
...	API 5L	S-1	B	...	(57)(59)(77)	B	60	35	20.0	20.0	20.0

TABLE 3.3 ALLOWABLE STRESSES FOR PIPE MATERIALS (CONTINUED)

Specifications Are ASTM Unless Otherwise Indicated

Basic Allowable Stress, *S*, ksi (1), at Metal Temperature, °F														
400	500	600	650	700	750	800	850	900	950	1000	1050	1100	Grade	Spec. No.
														Carbon Steel Pipes and Tubes (2)
13.7	13.0	12.3	11.9	11.5	10.7	9.2	7.9	5.9	...	...	...	...	...	A 134
13.7	13.0	12.3	11.9	11.5	10.7	9.2	7.9	5.9	4.0	2.5	1.6	1.0	A45	A 672
14.2	...	...	...	...	...	...	...	...	...	...	...	...	A25	API 5L
14.2	...	...	...	...	...	...	...	...	...	...	...	...	A25	API 5L
14.8	14.1	13.3	12.8	12.4	10.7	9.2	7.9	5.9	4.0	2.5	1.6	1.0	...	A 179
16.0	...	...	...	...	...	...	...	...	...	...	...	...	A	A 53
...	...	...	...	...	...	...	...	...	...	...	...	...	A	A 139
16.0	16.0	15.3	14.6	12.5	10.7	9.2	7.9	...	...	...	...	...	...	A 587
16.0	16.0	15.3	14.6	12.5	10.7	9.2	7.9	5.9	4.0	2.5	1.6	1.0	A	A 53
16.0	16.0	15.3	14.6	12.5	10.7	9.2	7.9	5.9	4.0	2.5	1.6	1.0	A	A 106
16.0	16.0	15.3	14.6	12.5	10.7	9.2	7.9	5.9	4.0	2.5	1.6	1.0	A	A 135
16.0	16.0	15.3	14.6	12.5	10.7	9.2	7.9	5.9	4.0	2.5	1.6	1.0	FPA	A 369
16.0	16.0	15.3	14.6	12.5	10.7	9.2	7.9	5.9	4.0	2.5	1.6	1.0	A	API 5L
15.4	14.7	13.8	13.3	12.5	10.7	9.2	7.9	5.9	...	...	...	...	...	A 134
15.4	14.7	13.8	13.3	12.5	10.7	9.2	7.9	5.9	4.0	2.5	1.6	1.0	A50	A 672
17.1	16.3	15.3	14.8	14.3	13.0	10.8	8.7	5.9	...	...	...	...	...	A 134
17.1	16.3	15.3	14.8	14.3	13.0	10.8	8.7	5.9	4.0	2.5	...	...	II	A 524
17.1	16.3	15.3	14.8	14.3	13.0	10.8	8.7	5.9	4.0	2.5	1.6	1.0	1	A 333
17.1	16.3	15.3	14.8	14.3	13.0	10.8	8.7	5.9	4.0	2.5	1.6	1.0	1	A 334
17.1	16.3	15.3	14.8	14.3	13.0	10.8	8.7	5.9	4.0	2.5	1.6	1.0	CA55	A 671
17.1	16.3	15.3	14.8	14.3	13.0	10.8	8.7	5.9	4.0	2.5	1.6	1.0	A55	A 672
17.1	16.3	15.3	14.8	14.3	13.0	10.8	8.7	5.9	4.0	2.5	1.6	1.0	C55	A 672
18.2	17.4	16.4	15.8	15.3	13.9	11.4	8.7	5.9	4.0	2.5	...	...	CC60	A 671
18.2	17.4	16.4	15.8	15.3	13.9	11.4	8.7	5.9	4.0	2.5	1.6	1.0	CB60	A 671
18.2	17.4	16.4	15.8	15.3	13.9	11.4	8.7	5.9	4.0	2.5	1.6	1.0	B60	A 672
18.2	17.4	16.4	15.8	15.3	13.9	11.4	8.7	5.9	4.0	2.5	1.6	1.0	C60	A 672
...	...	...	...	...	...	...	...	...	...	...	...	...	B	A 139
19.9	19.0	17.9	17.3	16.7	13.9	11.4	8.7	5.9	4.0	2.5	...	...	B	A 135
19.9	19.0	17.9	17.3	16.7	13.9	11.4	8.7	5.9	4.0	2.5	...	...	I	A 524
19.9	19.0	17.9	17.3	16.7	13.9	11.4	8.7	5.9	4.0	2.5	1.6	1.0	B	A 53
19.9	19.0	17.9	17.3	16.7	13.9	11.4	8.7	5.9	4.0	2.5	1.6	1.0	B	A 106
19.9	19.0	17.9	17.3	16.7	13.9	11.4	8.7	5.9	4.0	2.5	1.6	1.0	6	A 333
19.9	19.0	17.9	17.3	16.7	13.9	11.4	8.7	5.9	4.0	2.5	1.6	1.0	6	A 334
19.9	19.0	17.9	17.3	16.7	13.9	11.4	8.7	5.9	4.0	2.5	1.6	1.0	FPB	A 369
19.9	19.0	17.9	17.3	16.7	13.9	11.4	8.7	5.9	4.0	2.5	1.6	1.0	Y35	A 381
19.9	19.0	17.9	17.3	16.7	13.9	11.4	8.7	5.9	4.0	2.5	1.6	1.0	B	API 5L

TABLE 3.3 ALLOWABLE STRESSES FOR PIPE MATERIALS (CONTINUED)

Specifications Are ASTM Unless Otherwise Indicated

Material	Spec. No.	P-No. or S-No. (5)	Grade	UNS No.	Notes	Min. Temp., °F (6)	Specified Min. Strength, ksi		Allowable Stress, ksi, for Metal Temperature, °F, Not Exceeding		
							Tensile	Yield	Min. Temp. to 100	200	300
Carbon Steel (Cont'd)											
Pipes and Tubes (2) (Cont'd)											
...	A 139	S-1	C	K03004	(8b)	A	60	42	20.0	20.0	20.0
...	A 139	S-1	D	K03010	(8b)	A	60	46	20.0	20.0	20.0
...	API 5L	S-1	X42	...	(55)(77)	A	60	42	20.0	20.0	20.0
...	A 381	S-1	Y42	...	...	A	60	42	20.0	20.0	20.0
...	A 381	S-1	Y48	...	...	A	62	48	20.7	20.7	20.7
...	API 5L	S-1	X46	...	(55)(77)	A	63	46	21.0	21.0	21.0
...	A 381	S-1	Y46	...	...	A	63	46	21.0	21.0	21.0
...	A 381	S-1	Y50	...	...	A	64	50	21.3	21.3	21.3
A 516 Gr. 65	A 671	1	CC65	K02403	(57)(67)	B	65	35	21.7	21.4	20.6
A 515 Gr. 65	A 671	1	CB65	K02800	(57)(67)	A	65	35	21.7	21.4	20.6
A 515 Gr. 65	A 672	1	B65	K02800	(57)(67)	A	65	35	21.7	21.4	20.6
A 516 Gr. 65	A 672	1	C65	K02403	(57)(67)	B	65	35	21.7	21.4	20.6
...	A 139	S-1	E	K03012	(8b)	A	66	52	22.0	22.0	22.0
...	API 5L	S-1	X52	...	(55)(77)	A	66	52	22.0	22.0	22.0
...	A 381	S-1	Y52	...	...	A	66	52	22.0	22.0	22.0
A 516 Gr. 70	A 671	1	CC70	K02700	(57)(67)	B	70	38	23.3	23.2	22.4
A 515 Gr. 70	A 671	1	CB70	K03101	(57)(67)	A	70	38	23.3	23.2	22.4
A 515 Gr. 70	A 672	1	B70	K03101	(57)(67)	A	70	38	23.3	23.2	22.4
A 516 Gr. 70	A 672	1	C70	K02700	(57)(67)	B	70	38	23.3	23.2	22.4
...	A 106	1	C	K03501	(57)	B	70	40	23.3	23.3	23.3
A 537 Cl. 1 (≤ 2½ in. thick)	A 671	1	CD70	K12437	(67)	D	70	50	23.3	23.3	22.8
A 537 Cl. 1 (≤ 2½ in. thick)	A 672	1	D70	K12437	(67)	D	70	50	23.3	23.3	22.8
A 537 Cl. 1 (≤ 2½ in. thick)	A 691	1	CMSH70	K12437	(67)	D	70	50	23.3	23.3	22.8
...	API 5L	S-1	X56	...	(51)(55)(71)(77)	A	71	56	23.7	23.7	23.7
...	A 381	S-1	Y56	...	(51)(55)(71)	A	71	56	23.7	23.7	23.7
A 299 (> 1 in. thick)	A 671	1	CK75	K02803	(57)(67)	A	75	40	25.0	24.4	23.6
A 299 (> 1 in. thick)	A 672	1	N75	K02803	(57)(67)	A	75	40	25.0	24.4	23.6
A 299 (> 1 in. thick)	A 691	1	CMS75	K02803	(57)(67)	A	75	40	25.0	24.4	23.6
A 299 (≤ 1 in. thick)	A 671	1	CK75	K02803	(57)(67)	A	75	42	25.0	25.0	24.8
A 299 (> 1 in. thick)	A 672	1	N75	K02803	(57)(67)	A	75	42	25.0	25.0	24.8
A 299 (> 1 in. thick)	A 672	1	N75	K02803	(57)(67)	A	75	40	25.0	24.4	23.6
A 299 (> 1 in. thick)	A 691	1	CMS75	K02803	(57)(67)	A	75	40	25.0	24.4	23.6
A 299 (≤ 1 in. thick)	A 671	1	CK75	K02803	(57)(67)	A	75	42	25.0	25.0	24.8
A 299 (≤ 1 in. thick)	A 672	1	N75	K02803	(57)(67)	A	75	42	25.0	25.0	24.8
A 299 (≤ 1 in. thick)	A 691	1	CMS75	K02803	(57)(67)	A	75	42	25.0	25.0	24.8
...	API 5L	S-1	X60	...	(51)(55)(71)(77)	A	75	60	25.0	25.0	25.0
...	API 5L	S-1	X65	...	(51)(55)(71)(77)	A	77	65	25.7	25.7	25.7
...	API 5L	S-1	X70	...	(51)(55)(71)(77)	A	82	70	27.3	27.3	27.3
...	API 5L	S-1	X80	...	(51)(55)(71)(77)	A	90	80	30.0	30.0	30.0
...	A 381	S-1	Y60	...	(51)(71)	A	75	60	25.0	25.0	25.0

TABLE 3.3 ALLOWABLE STRESSES FOR PIPE MATERIALS (CONTINUED)

Specifications Are ASTM Unless Otherwise Indicate

Basic Allowable Stress, *S*, ksi (1), at Metal Temperature, °F														
400	500	600	650	700	750	800	850	900	950	1000	1050	1100	Grade	Spec. N
														Carbon Steel (Cont'd) Pipes and Tubes (2) (Cont'd)
...	...	...	...	...	...	...	...	...	...	...	...	...	C	A 139
...	...	...	...	...	...	...	...	...	...	...	...	...	D	A 139
20.0	...	...	...	...	...	...	...	...	...	...	...	...	X42	API 5L
20.0	...	...	...	...	...	...	...	...	...	...	...	...	Y42	A 381
20.7	20.7	20.7	18.7	...	...	...	...	...	...	...	...	...	Y48	A 381
21.0	...	...	...	...	...	...	...	...	...	...	...	...	X46	API 5L
21.0	...	...	...	...	...	...	...	...	...	...	...	...	Y46	A 381
21.3	21.3	21.3	18.7	...	...	...	...	...	...	...	...	...	Y50	A 381
19.9	19.0	17.9	17.3	16.7	13.9	11.4	9.0	6.3	4.0	2.5	...	...	CC65	A 671
19.9	19.0	17.9	17.3	16.7	13.9	11.4	9.0	6.3	4.0	2.5	1.6	1.0	CB65	A 671
19.9	19.0	17.9	17.3	16.7	13.9	11.4	9.0	6.3	4.0	2.5	1.6	1.0	B65	A 672
19.9	19.0	17.9	17.3	16.7	13.9	11.4	9.0	6.3	4.0	2.5	1.6	1.0	C65	A 672
...	...	...	...	...	...	...	...	...	...	...	...	...	E	A 139
22.0	...	...	...	...	...	...	...	...	...	...	...	...	X52	API 5L
22.0	...	...	...	...	...	...	...	...	...	...	...	...	Y52	A 381
21.6	20.6	19.4	18.8	18.1	14.8	12.0	9.3	6.7	4.0	2.5	...	...	CC70	A 671
21.6	20.6	19.4	18.8	18.1	14.8	12.0	9.3	6.7	4.0	2.5	1.6	1.0	CB70	A 671
21.6	20.6	19.4	18.8	18.1	14.8	12.0	9.3	6.7	4.0	2.5	1.6	1.0	B70	A 672
21.6	20.6	19.4	18.8	18.1	14.8	12.0	9.3	6.7	4.0	2.5	1.6	1.0	C70	A 672
22.8	21.7	20.4	19.8	18.3	14.8	12.0	...	...	...	...	...	...	C	A 106
22.7	22.7	22.4	21.9	18.3	...	...	...	...	...	...	...	...	CD70	A 671
22.7	22.7	22.4	21.9	18.3	...	...	...	...	...	...	...	...	D70	A 672
22.7	22.7	22.4	21.9	18.3	...	...	...	...	...	...	...	...	CMSH70	A 691
23.7	...	...	...	...	...	...	...	...	...	...	...	...	X56	API 5L
23.7	...	...	...	...	...	...	...	...	...	...	...	...	Y56	A 381
22.8	21.7	20.4	19.8	19.1	15.7	12.6	9.3	6.7	4.0	2.5	1.6	1.0	CK75	A 671
22.8	21.7	20.4	19.8	19.1	15.7	12.6	9.3	6.7	4.0	2.5	1.6	1.0	N75	A 672
22.8	21.7	20.4	19.8	19.1	15.7	12.6	9.3	6.7	4.0	2.5	1.6	1.0	CMS75	A 691
23.9	22.8	21.5	20.8	19.6	...	...	...	...	...	...	...	...	CK75	A 671
23.9	22.8	21.5	20.8	19.6	...	...	...	...	...	...	...	...	N75	A 672
23.9	22.8	21.5	20.8	19.6	...	...	...	...	...	...	...	...	CMS75	A 691
25.0	...	...	...	...	...	...	...	...	...	...	...	...	X60	API 5L
25.7	...	...	...	...	...	...	...	...	...	...	...	...	X65	API 5L
27.3	...	...	...	...	...	...	...	...	...	...	...	...	X70	API 5L
30.0	...	...	...	...	...	...	...	...	...	...	...	...	X80	API 5L
25.0	...	...	...	...	...	...	...	...	...	...	...	...	Y60	A 381

TABLE 3.3 ALLOWABLE STRESSES FOR PIPE MATERIALS (CONTINUED)

Specifications Are ASTM Unless Otherwise Indicated

Material	Spec. No.	P-No. or S-No. (5)	Grade	Notes	Min. Temp., °F (6)	Specified Min. Strength, ksi		Min. Temp.	
						Tensile	Yield	to 100	200
Low and Intermediate Alloy Steel Pipes (2)									
½Cr–½Mo	A 335	3	P2	. . .	–20	55	30	18.3	18.3
½Cr–½Mo A 387 Gr. 2 Cl. 1	A 691	3	½CR	(11)(67)	–20	55	33	18.3	18.3
C–½Mo	A 335	3	P1	(58)	–20	55	30	18.3	18.3
C–½Mo	A 369	3	FP1	(58)	–20	55	30	18.3	18.3
½Cr–½Mo	A 369	3	FP2	. . .	–20	55	30	18.3	18.3
1Cr–½Mo A 387 Gr. 12 Cl. 1	A 691	4	1CR	(11)(67)	–20	55	33	18.3	18.3
½Cr–½Mo	A 426	3	CP2	(10)	–20	60	30	18.4	17.7
1½Si–½Mo	A 335	3	P15	. . .	–20	60	30	18.8	18.2
1½Si–½Mo	A 426	3	CP15	(10)	–20	60	30	18.8	18.2
1Cr–½Mo	A 426	4	CP12	(10)	–20	60	30	18.8	18.3
5Cr–½Mo–1½Si	A 426	5B	CP5b	(10)	–20	60	30	18.8	17.9
3Cr–Mo	A 426	5A	CP21	(10)	–20	60	30	18.8	18.1
¾Cr–¾Ni–Cu–Al	A 333	4	4	. . .	–150	60	35	20.0	19.1
2Cr–½Mo	A 369	4	FP3b	. . .	–20	60	30	20.0	18.5
1Cr–½Mo	A 335	4	P12	. . .	–20	60	32	20.0	18.7
1Cr–½Mo	A 369	4	FP12	. . .	–20	60	32	20.0	18.7
1¼Cr–½Mo	A 335	4	P11	. . .	–20	60	30	20.0	18.7
1¼Cr–½Mo	A 369	4	FP11	. . .	–20	60	30	20.0	18.7
1¼Cr–½Mo A 387 Gr. 11 Cl. 1	A 691	4	1¼CR	(11)(67)	–20	60	35	20.0	20.0
5Cr–½Mo A 387 Gr. 5 Cl. 1	A 691	5B	5CR	(11)(67)	–20	60	30	20.0	18.1
5Cr–½Mo	A 335	5B	P5	. . .	–20	60	30	20.0	18.1
5Cr–½Mo–Si	A 335	5B	P5b	. . .	–20	60	30	20.0	18.1
5Cr–½Mo–Ti	A 335	5B	P5c	. . .	–20	60	30	20.0	18.1
5Cr–½Mo	A 369	5B	FP5	. . .	–20	60	30	20.0	18.1
9Cr–1Mo	A 335	5B	P9	. . .	–20	60	30	20.0	18.1
9Cr–1Mo	A 369	5B	FP9	. . .	–20	60	30	20.0	18.1
9Cr–1Mo A 387 Gr. 9 Cl. 1	A 691	5B	9CR	. . .	–20	60	30	20.0	18.1
3Cr–1Mo	A 335	5A	P21	. . .	–20	60	30	20.0	18.7
3Cr–1Mo	A 369	5A	FP21	. . .	–20	60	30	20.0	18.7
3Cr–1Mo A 387 Gr. 21 Cl. 1	A 691	5A	3CR	(11)(67)	–20	60	30	20.0	18.5

TABLE 3.3 ALLOWABLE STRESSES FOR PIPE MATERIALS (CONTINUED)

Specifications Are ASTM Unless Otherwise Indicated

Basic Allowable Stress, *S*, ksi (1), at Metal Temperature, °F																	
300	400	500	600	650	700	750	800	850	900	950	1000	1050	1100	1150	1200	Grade	Spec. No.
																Low and Intermediate Alloy Steel Pipes (2)	
17.5	16.9	16.3	15.7	15.4	15.1	13.8	13.5	13.2	12.8	9.2	5.9	...	...	...	...	P2	A 335
18.3	18.3	17.9	17.3	16.9	16.6	13.8	13.8	13.4	12.8	9.2	5.9	...	...	...	...	½CR	A 691
17.5	16.9	16.3	15.7	15.4	15.1	13.8	13.5	13.2	12.7	8.2	4.8	4.0	2.4	...	...	P1	A 335
17.5	16.9	16.3	15.7	15.4	15.1	13.8	13.5	13.2	12.7	8.2	4.8	4.0	2.4	...	...	FP1	A 369
17.5	16.9	16.3	15.7	15.4	15.1	13.8	13.5	13.2	12.8	9.2	5.9	4.0	2.4	...	...	FP2	A 369
18.3	18.3	17.9	17.3	16.9	16.6	16.3	15.9	15.4	14.0	11.3	7.2	4.5	2.8	1.8	1.1	1CR	A 691
17.0	16.3	15.6	14.9	14.6	14.2	13.9	13.5	13.2	12.5	10.0	6.3	4.0	2.4	...	...	CP2	A 426
17.6	17.0	16.5	15.9	15.6	15.3	15.0	14.4	13.8	12.5	10.0	6.3	4.0	2.4	...	...	P15	A 335
17.6	17.0	16.5	15.9	15.6	15.3	15.0	14.4	13.8	12.5	10.0	6.3	4.0	2.4	...	...	CP15	A 426
17.6	17.1	16.5	15.9	15.7	15.4	15.1	14.8	14.2	13.1	11.3	7.2	4.5	2.8	1.8	1.1	CP12	A 426
17.1	16.2	15.4	14.5	14.1	13.7	13.3	12.8	12.4	10.9	9.0	5.5	3.5	2.5	1.8	1.2	CP5b	A 426
17.4	16.8	16.1	15.5	15.2	14.8	14.5	13.9	13.2	12.0	9.0	7.0	5.5	4.0	2.7	1.5	CP21	A 426
18.2	17.3	16.4	15.5	15.0	...	...	...	...	...	...	...	...	...	...	...	4	A 333
17.5	16.4	16.3	15.7	15.4	15.1	13.9	13.5	13.1	12.5	10.0	6.2	4.2	2.6	1.4	1.0	FP3b	A 369
18.0	17.5	17.2	16.7	16.2	15.6	15.2	15.0	14.5	12.8	11.3	7.2	4.5	2.8	1.8	1.1	P12	A 335
18.0	17.5	17.2	16.7	16.2	15.6	15.2	15.0	14.5	12.8	11.3	7.2	4.5	2.8	1.8	1.1	FP12	A 369
18.0	17.5	17.2	16.7	16.2	15.6	15.2	15.0	14.5	12.8	9.3	6.3	4.2	2.8	1.9	1.2	P11	A 335
18.0	17.5	17.2	16.7	16.2	15.6	15.2	15.0	14.5	12.8	9.3	6.3	4.2	2.8	1.9	1.2	FP11	A 369
20.0	19.7	18.9	18.3	18.0	17.6	17.3	16.8	16.3	15.0	9.9	6.3	4.2	2.8	1.9	1.2	1¼CR	A 691
17.4	17.2	17.1	16.8	16.6	16.3	13.2	12.8	12.1	10.9	8.0	5.8	4.2	2.8	2.0	1.3	5CR	A 691
17.4	17.2	17.1	16.8	16.6	16.3	13.2	12.8	12.1	10.9	8.0	5.8	4.2	2.9	1.8	1.0	P5	A 335
17.4	17.2	17.1	16.8	16.6	16.3	13.2	12.8	12.1	10.9	8.0	5.8	4.2	2.9	1.8	1.0	P5b	A 335
17.4	17.2	17.1	16.8	16.6	16.3	13.2	12.8	12.1	10.9	8.0	5.8	4.2	2.9	1.8	1.0	P5c	A 335
17.4	17.2	17.1	16.8	16.6	16.3	13.2	12.8	12.1	10.9	8.0	5.8	4.2	2.9	1.8	1.0	FP5	A 369
17.4	17.2	17.1	16.8	16.6	16.3	13.2	12.8	12.1	11.4	10.6	7.4	5.0	3.3	2.2	1.5	P9	A 335
17.4	17.2	17.1	16.8	16.6	16.3	13.2	12.8	12.1	11.4	10.6	7.4	5.0	3.3	2.2	1.5	FP9	A 369
17.4	17.2	17.1	16.8	16.6	16.3	13.2	12.8	12.1	11.4	10.6	7.4	5.0	3.3	2.2	1.5	9CR	A 691
18.0	17.5	17.2	16.7	16.2	15.6	15.2	15.0	14.0	12.0	9.0	7.0	5.5	4.0	2.7	1.5	P21	A 335
18.0	17.5	17.2	16.7	16.2	15.6	15.2	15.0	14.0	12.0	9.0	7.0	5.5	4.0	2.7	1.5	FP21	A 369
18.1	17.9	17.9	17.9	17.9	17.9	17.9	17.8	14.0	12.0	9.0	7.0	5.5	4.0	2.7	1.5	3CR	A 691

TABLE 3.3 ALLOWABLE STRESSES FOR PIPE MATERIALS (CONTINUED)

Specifications Are ASTM Unless Otherwise Indicated

Material	Spec. No.	P-No. or S-No. (5)	Grade	Notes	Min. Temp., °F (6)	Specified Min. Strength, ksi		Min. Temp.	
						Tensile	Yield	to 100	200
Low and Intermediate Alloy Steel (Cont'd) Pipes (2) (Cont'd)									
2¼Cr–1Mo A 387 Gr. 22 Cl. 1	A 691	5A	2¼CR	(11)(67) (72)(75)	–20	60	30	20.0	18.5
2¼Cr–1Mo	A 369	5A	FP22	(72)(75)	–20	60	30	20.0	18.5
2¼Cr–1Mo	A 335	5A	P22	(72)(75)	–20	60	30	20.0	18.5
2Ni–1Cu	A 333	9A	9	. . .	–100	63	46	21.0	. . .
2Ni–1Cu	A 334	9A	9	. . .	–100	63	46	21.0	. . .
2¼Ni	A 333	9A	7	. . .	–100	65	35	21.7	19.6
2¼Ni	A 334	9A	7	. . .	–100	65	35	21.7	19.6
3½Ni	A 333	9B	3	. . .	–150	65	35	21.7	19.6
3½Ni	A 334	9B	3	. . .	–150	65	35	21.7	19.6
C–½Mo	A 426	3	CP1	(10)(58)	–20	65	35	21.7	21.7
C–Mo A 204 Gr. A	A 672	3	L65	(11)(58)(67)	–20	65	37	21.7	21.7
C–Mo A 204 Gr. A	A 691	3	CM65	(11)(58)(67)	–20	65	37	21.7	21.7
2¼Ni A 203 Gr. B	A 671	9A	CF70	(11)(65)(67)	–20	70	40	23.3	. . .
3½Ni A 203 Gr. E	A 671	9B	CF71	(11)(65)(67)	–20	70	40	23.3	. . .
C–Mo A 204 Gr. B	A 672	3	L70	(11)(58)(67)	–20	70	40	23.3	23.3
C–Mo A 204 Gr. B	A 691	3	CM70	(11)(58)(67)	–20	70	40	23.3	23.3
1¼Cr–½Mo	A 426	4	CP11	(10)	–20	70	40	23.3	23.3
2¼Cr–1Mo	A 426	5A	CP22	(10)(72)	–20	70	40	23.3	23.3
C–Mo A 204 Gr. C	A 672	3	L75	(11)(58)(67)	–20	75	43	25.0	25.0
C–Mo A 204 Gr. C	A 691	3	CM75	(11)(58)(67)	–20	75	43	25.0	25.0
9Cr–1Mo–V ≤ 3 in. thick	A 335	15E	P91	. . .	–20	85	60	28.3	28.3
9Cr–1Mo–V ≤ 3 in. thick	A 691	15E	P91	. . .	–20	85	60	28.3	28.3
5Cr–½Mo	A 426	5B	CP5	(10)	–20	90	60	30.0	28.0
9Cr–1Mo	A 426	5B	CP9	(10)	–20	90	60	30.0	22.5
9Ni	A 333	11A	8	(47)	–320	100	75	31.7	31.7
9Ni	A 334	11A	8	. . .	–320	100	75	31.7	31.7

TABLE 3.3 ALLOWABLE STRESSES FOR PIPE MATERIALS (CONTINUED)

Specifications Are ASTM Unless Otherwise Indicated

Basic Allowable Stress, *S*, ksi (1), at Metal Temperature, °F																	
300	400	500	600	650	700	750	800	850	900	950	1000	1050	1100	1150	1200	Grade	Spec. No
																Low and Intermediate Alloy Steel (Cont'd) Pipes (2) (Cont'd)	
18.0	17.9	17.9	17.9	17.9	17.9	17.9	17.8	14.5	12.8	10.8	7.8	5.1	3.2	2.0	1.6	2¼CR	A 691
18.0	17.9	17.9	17.9	17.9	17.9	17.9	17.8	14.5	12.8	10.8	7.8	5.1	3.2	2.0	1.6	FP22	A 369
18.0	17.9	17.9	17.9	17.9	17.9	17.9	17.8	14.5	12.8	10.8	7.8	5.1	3.2	2.0	1.6	P22	A 335
...	...	...	...	...	...	...	...	...	...	...	...	...	...	...	...	9	A 333
...	...	...	...	...	...	...	...	...	...	...	...	...	...	...	...	9	A 334
19.6	18.7	17.6	16.8	16.3	15.5	13.9	11.4	9.0	6.5	4.5	2.5	1.6	1.0	...	...	7	A 333
19.6	18.7	17.6	16.8	16.3	15.5	13.9	11.4	9.0	6.5	4.5	2.5	1.6	1.0	...	...	7	A 334
19.6	18.7	17.8	16.8	16.3	15.5	13.9	11.4	9.0	6.5	4.5	2.5	1.6	1.0	...	...	3	A 333
19.6	18.7	17.8	16.8	16.3	15.5	13.9	11.4	9.0	6.5	4.5	2.5	1.6	1.0	...	...	3	A 334
21.7	21.7	21.3	20.7	20.4	20.0	16.3	15.7	14.4	12.5	10.0	6.3	4.0	2.4	...	...	CP1	A 426
21.7	20.7	20.0	19.3	19.0	18.6	16.3	15.8	15.3	13.7	8.2	4.8	4.0	2.4	...	...	L65	A 672
21.7	20.7	20.0	19.3	19.0	18.6	16.3	15.8	15.3	13.7	8.2	4.8	4.0	2.4	...	...	CM65	A 691
...	...	...	...	...	...	...	...	...	...	...	...	...	...	...	...	CF70	A 671
...	...	...	...	...	...	...	...	...	...	...	...	...	...	...	...	CF71	A 671
23.3	22.5	21.7	20.9	20.5	20.1	17.5	17.5	17.1	13.7	8.2	4.8	4.0	2.4	...	...	L70	A 672
23.3	22.5	21.7	20.9	20.5	20.1	17.5	17.5	17.1	13.7	8.2	4.8	4.0	2.4	...	...	CM70	A 691
23.3	23.3	22.9	22.3	21.6	20.9	15.5	15.0	14.4	13.7	9.3	6.3	4.2	2.8	1.9	1.2	CP11	A 426
23.3	23.3	22.9	22.3	21.6	20.9	17.5	17.5	16.0	14.0	11.0	7.8	5.1	3.2	2.0	1.2	CP22	A 426
25.0	24.1	23.3	22.5	22.1	21.7	18.8	18.8	18.3	13.7	8.2	4.8	4.0	2.4	...	...	L75	A 672
25.0	24.1	23.3	22.5	22.1	21.7	18.8	18.8	18.3	13.7	8.2	4.8	4.0	2.4	...	...	CM75	A 691
28.3	28.2	28.1	27.7	27.3	26.7	25.9	24.9	23.7	22.3	20.7	18.0	14.0	10.3	7.0	4.3	P91	A 335
28.3	28.2	28.1	27.7	27.3	26.7	25.9	24.9	23.7	22.3	20.7	18.0	14.0	10.3	7.0	4.3	P91	A 691
26.1	24.1	22.1	20.1	19.0	17.5	16.0	14.5	12.8	10.4	7.6	5.6	4.2	3.1	1.8	1.0	CP5	A 426
22.5	22.5	22.5	22.5	22.5	22.0	21.0	19.4	17.3	15.0	10.7	8.5	5.5	3.3	2.2	1.5	CP9	A 426
...	...	...	...	...	...	...	...	...	...	...	...	...	...	...	...	8	A 333
...	...	...	...	...	...	...	...	...	...	...	...	...	...	...	...	8	A 334

TABLE 3.3 ALLOWABLE STRESSES FOR PIPE MATERIALS (CONTINUED)

Specifications Are ASTM Unless Otherwise Indicated

Material	Spec. No.	P-No. or S-No. (5)	Grade	UNS No.	Notes	Min. Temp., °F (6)	Specified Min. Strength, ksi		Min. Temp. to 100	200	300	400	500	600
							Tensile	Yield						
Stainless Steel (3)(4a) Pipes and Tubes (2)														
18Cr–10Ni–Ti pipe smls > 3/8 in. thick	A 312	8	TP321	S32100	(30)(36)	–425	70	25	16.7	16.7	16.7	16.7	16.1	15.2
18Cr–10Ni–Ti pipe > 3/8 in. thick	A 376	8	TP321	S32100	(30)(36)	–425	70	25	16.7	16.7	16.7	16.7	16.1	15.2
18Cr–8Ni tube	A 269	8	TP304L	S30403	(14)(36)	–425	70	25	16.7	16.7	16.7	15.8	14.7	14.0
18Cr–8Ni pipe	A 312	8	TP304L	S30403	...	–425	70	25	16.7	16.7	16.7	15.8	14.7	14.0
Type 304L A 240	A 358	8	304L	S30403	(36)	–425	70	25	16.7	16.7	16.7	15.8	14.7	14.0
16Cr–12Ni–2Mo tube	A 269	8	TP316L	S31603	(14)(36)	–425	70	25	16.7	16.7	16.7	15.7	14.8	14.0
16Cr–12Ni–2Mo pipe	A 312	8	TP316L	S31603	...	–425	70	25	16.7	16.7	16.7	15.7	14.8	14.0
Type 316L A 240	A 358	8	316L	S31603	(36)	–425	70	25	16.7	16.7	16.7	15.7	14.8	14.0
18Cr–10Ni–Ti pipe smls > 3/8 in. thick	A 312	8	TP321	S32100	(28)(30)(36)	–425	70	25	16.7	16.7	16.7	16.7	16.1	15.2
18Cr–10Ni–Ti pipe > 3/8 in. thick	A 376	8	TP321	S32100	(28)(30)(36)	–425	70	25	16.7	16.7	16.7	16.7	16.1	15.2
18Cr–10Ni–Ti pipe smls > 3/8 in. thick	A 312	8	TP321H	S32109	(30)(36)	–325	70	25	16.7	16.7	16.7	16.7	16.1	15.2
18Cr–10Ni–Ti pipe > 3/8 in. thick	A 376	8	TP321H	S32109	...	–325	70	25	16.7	16.7	16.7	16.7	16.1	15.2
23Cr–13Ni	A 451	8	CPH8	J93400	(26)(28)(35)	–325	65	28	18.7	18.7	18.5	18.0	17.7	17.1
25Cr–20Ni	A 451	8	CPK20	J94202	(12)(28)(35)(39)	–325	65	28	18.7	18.7	18.5	18.0	17.7	17.1
11Cr–Ti tube	A 268	7	TP409	S40900	(35)	–20	60	30	20.0	...	...	...	...	...
18Cr–Ti tube	A 268	7	TP430Ti	S43036	(35)(49)	–20	60	40	20.0	...	...	...	...	...
15Cr–13Ni–2Mo–Cb	A 451	S-8	CPF10MC	...	(28)	–325	70	30	20.0	...	...	...	...	...
16Cr–8Ni–2Mo pipe	A 376	8	16-8-2H	S16800	(26)(31)(35)	–325	75	30	20.0	...	...	...	...	...
12Cr–Al tube	A 268	7	TP405	S40500	(35)	–20	60	30	20.0	20.0	19.6	19.3	19.0	18.5
13Cr tube	A 268	6	TP410	S41000	(35)	–20	60	30	20.0	20.0	19.6	19.3	19.0	18.5
16Cr tube	A 268	7	TP430	S43000	(35)(49)	–20	60	35	20.0	20.0	19.6	19.3	19.0	18.5
18Cr–13Ni–3Mo pipe	A 312	8	TP317L	S31703	...	–325	75	30	20.0	20.0	20.0	18.9	17.7	16.9
25Cr–20Ni pipe	A 312	8	TP310	...	(28)(35)(39)	–325	75	30	20.0	20.0	20.0	20.0	19.3	18.5
Type 310S A 240	A 358	8	310S	S31008	(28)(31)(35)(36)	–325	75	30	20.0	20.0	20.0	20.0	19.3	18.5
25Cr–20Ni pipe	A 409	8	TP310	S31000	(28)(31)(35)(36)(39)	–325	75	30	20.0	20.0	20.0	20.0	19.3	18.5
18Cr–10Ni–Ti pipe smls ≤ 3/8 in. thk & wld	A 312	8	TP321	S32100	(30)	–425	75	30	20.0	20.0	20.0	20.0	19.3	18.3
18Cr–10Ni–Ti pipe	A 358	8	321	S32100	(30)(36)	–425	75	30	20.0	20.0	20.0	20.0	19.3	18.3
18Cr–10Ni–Ti pipe ≤ 3/8 in. thick	A 376	8	TP321	S32100	(30)(36)	–425	75	30	20.0	20.0	20.0	20.0	19.3	18.3
18Cr–10Ni–Ti pipe	A 409	8	TP321	S32100	(30)(36)	–425	75	30	20.0	20.0	20.0	20.0	19.3	18.3
23Cr–12Ni pipe	A 312	8	TP309	...	(28)(35)(39)	–325	75	30	20.0	20.0	20.0	20.0	19.4	18.8
Type 309S A 240	A 358	8	309S	S30908	(28)(31)(35)(36)	–325	75	30	20.0	20.0	20.0	20.0	19.4	18.8
23Cr–12Ni pipe	A 409	8	TP309	S30900	(28)(31)(35)(36)(39)	–325	75	30	20.0	20.0	20.0	20.0	19.4	18.8
18Cr–8Ni	A 451	8	CPF8	J92600	(26)(28)	–425	70	30	20.0	20.0	20.0	18.6	17.5	16.6

TABLE 3.3 ALLOWABLE STRESSES FOR PIPE MATERIALS (CONTINUED)

Specifications Are ASTM Unless Otherwise Indicated

Basic Allowable Stress, *S*, ksi (1), at Metal Temperature, °F																			
650	700	750	800	850	900	950	1000	1050	1100	1150	1200	1250	1300	1350	1400	1450	1500	Grade	Spec. No.
																		Stainless Steel (3)(4a) Pipes and Tubes (2)	
14.9	14.6	14.3	14.1	14.0	13.8	13.6	13.5	9.6	6.9	5.0	3.6	2.6	1.7	1.1	0.8	0.5	0.3	TP321	A 312
14.9	14.6	14.3	14.1	14.0	13.8	13.6	13.5	9.6	6.9	5.0	3.6	2.6	1.7	1.1	0.8	0.5	0.3	TP321	A 376
13.7	13.5	13.3	13.0	12.8	12.6	12.3	12.0	6.3	5.1	4.0	3.2	2.6	2.1	1.7	1.1	1.0	0.9	TP304L	A 269
13.7	13.5	13.3	13.0	12.8	12.6	12.3	12.0	6.3	5.1	4.0	3.2	2.6	2.1	1.7	1.1	1.0	0.9	TP304L	A 312
13.7	13.5	13.3	13.0	12.8	12.6	12.3	12.0	6.3	5.1	4.0	3.2	2.6	2.1	1.7	1.1	1.0	0.9	304L	A 358
13.7	13.5	13.2	12.9	12.7	12.4	12.1	11.8	11.6	11.4	8.8	6.4	4.7	3.5	2.5	1.8	1.3	1.0	TP316L	A 269
13.7	13.5	13.2	12.9	12.7	12.4	12.1	11.8	11.6	11.4	8.8	6.4	4.7	3.5	2.5	1.8	1.3	1.0	TP316L	A 312
13.7	13.5	13.2	12.9	12.7	12.4	12.1	11.8	11.6	11.4	8.8	6.4	4.7	3.5	2.5	1.8	1.3	1.0	316L	A 358
14.9	14.6	14.3	14.1	13.9	13.8	13.6	13.5	12.3	9.1	6.9	5.4	4.1	3.2	2.5	1.9	1.5	1.1	TP321	A 312
14.9	14.6	14.3	14.1	13.9	13.8	13.6	13.5	12.3	9.1	6.9	5.4	4.1	3.2	2.5	1.9	1.5	1.1	TP321	A 376
14.9	14.6	14.3	14.1	13.9	13.8	13.6	13.5	12.3	9.1	6.9	5.4	4.1	3.2	2.5	1.9	1.5	1.1	TP321H	A 312
14.9	14.6	14.3	14.1	13.9	13.8	13.6	13.5	12.3	9.1	6.9	5.4	4.1	3.2	2.5	1.9	1.5	1.1	TP321H	A 376
16.7	16.3	15.9	15.4	14.9	14.4	13.9	11.1	8.5	6.5	5.0	3.8	2.9	2.3	1.8	1.3	0.9	0.8	CPH8	A 451
16.7	16.3	15.9	15.4	14.9	14.4	13.9	11.3	9.8	8.5	7.3	6.0	4.8	3.5	2.4	1.6	1.1	0.8	CPK20	A 451
...	...	...	...	...	...	...	...	...	...	...	...	...	...	...	...	...	...	TP409	A 268
...	...	...	...	...	...	...	...	...	...	...	...	...	...	...	...	...	...	TP430Ti	A 268
...	...	...	...	...	...	...	...	...	...	...	...	...	...	...	...	...	...	CPF10MC	A 451
...	...	...	...	...	...	...	...	...	...	...	...	...	...	...	...	...	...	16-8-2H	A 376
18.1	17.7	17.1	16.4	15.6	14.3	8.4	4.0	...	...	...	...	...	...	...	...	...	...	TP405	A 268
18.1	17.7	17.1	16.4	15.6	12.3	8.8	6.4	4.4	2.9	1.8	1.0	...	...	...	...	...	...	TP410	A 268
18.1	17.7	17.1	16.4	15.6	12.0	9.2	6.5	4.5	3.2	2.4	1.8	...	...	...	...	...	...	TP430	A 268
16.5	16.2	15.8	15.5	15.2	...	...	...	...	...	...	...	...	...	...	...	...	...	TP317L	A 312
18.2	17.9	17.7	17.4	17.2	16.9	15.9	9.9	7.1	5.0	3.6	2.5	1.5	0.8	0.5	0.4	0.3	0.2	TP310	A 312
18.2	17.9	17.7	17.4	17.2	16.9	15.9	9.9	7.1	5.0	3.6	2.5	1.5	0.8	0.5	0.4	0.3	0.2	310S	A 358
18.2	17.9	17.7	17.4	17.2	16.9	15.9	9.9	7.1	5.0	3.6	2.5	1.5	0.8	0.5	0.4	0.3	0.2	TP310	A 409
17.9	17.5	17.2	16.9	16.7	16.5	16.4	16.2	9.6	6.9	5.0	3.6	2.6	1.7	1.1	0.8	0.5	0.3	TP321	A 312
17.9	17.5	17.2	16.9	16.7	16.5	16.4	16.2	9.6	6.9	5.0	3.6	2.6	1.7	1.1	0.8	0.5	0.3	321	A 358
17.9	17.5	17.2	16.9	16.7	16.5	16.4	16.2	9.6	6.9	5.0	3.6	2.6	1.7	1.1	0.8	0.5	0.3	TP321	A 376
17.9	17.5	17.2	16.9	16.7	16.5	16.4	16.2	9.6	6.9	5.0	3.6	2.6	1.7	1.1	0.8	0.5	0.3	TP321	A 409
18.5	18.2	18.0	17.7	17.5	17.2	16.9	13.8	10.3	7.6	5.5	4.0	3.0	2.2	1.7	1.3	1.0	0.8	TP309	A 312
18.5	18.2	18.0	17.7	17.5	17.2	16.9	13.8	10.3	7.6	5.5	4.0	3.0	2.2	1.7	1.3	1.0	0.8	309S	A 358
18.5	18.2	18.0	17.7	17.5	17.2	16.9	13.8	10.3	7.6	5.5	4.0	3.0	2.2	1.7	1.3	1.0	0.8	TP309	A 409
16.2	15.8	15.5	15.2	14.9	14.6	14.3	12.2	9.5	7.5	6.0	4.8	3.9	3.3	2.7	2.3	2.0	1.7	CPF8	A 451

$$\sigma_{\vartheta}\left(\text{inner\_wall}\right)=\sigma_{z}\left(\text{inner\_wall}\right)=\frac{\alpha\cdot E\cdot\Delta T}{2\cdot\left(1-\nu\right)\cdot\ln\left(\frac{\text{OD}}{D}\right)}\cdot\left(1-\frac{2\cdot\text{OD}^{2}\cdot\ln\left(\frac{\text{OD}}{D}\right)}{\text{OD}^{2}-D^{2}}\right)$$

US, EE, SI (3.12)

$$\sigma_{\vartheta}\left(\text{outer\_wall}\right)=\sigma_{z}\left(\text{outer\_wall}\right)=\frac{\alpha\cdot E\cdot\Delta T}{2\cdot\left(1-\nu\right)\cdot\ln\left(\frac{\text{OD}}{D}\right)}\cdot\left(1-\frac{2\cdot\text{OD}^{2}\cdot\ln\left(\frac{\text{OD}}{D}\right)}{\text{OD}^{2}-D^{2}}\right)$$

US, EE, SI (3.13)

In this example, the stresses on the inner and outer pipe walls are −6.5 and 6.0 psi, respectively. In other words, for an effectively insulated pipe, thermal stresses through the pipe wall are negligible.

Example 3.2 Uninsulated pipe wall stresses due to thermal loading.

If the insulation is removed from the pipe, the same conditions (70°F ambient temperature with a 200°F fluid temperature) yield pipe stresses of −1778 and 1629 psi. For an Uninsulated, 3 in. XXS steel pipe at the same conditions, where the OD = 3.5 and D = 2.3, the stresses are −6181 and 4679 psi. If the fluid temperature is increased to 440°F for the uninsulated 3 in. XXS pipe, the stresses are − 49,400 and 45250 psi. Both insulation and wall thickness have an appreciable effect on thermal stresses through the pipe wall. Also, a sudden change in wall temperature or fluctuating temperatures may induce significant thermal stresses.

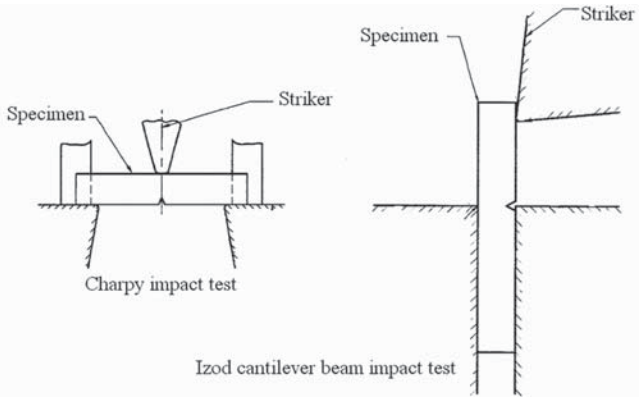


FIG. 3.15 IMPACT TESTING (Reprinted by permission, ASTM E23.07a)

Example 3.3 Transient thermal stresses.

Consider the same 3 in., Schedule 40, steel pipe at 70°F, suddenly flooded with 200°F water or steam. Assuming a linear temperature distribution through the wall, the momentary hoop stress through the wall (Harvey [97]) approximately equals

$$\sigma'_{\theta}=\sigma'_{z}=-\frac{E\cdot\alpha\cdot\Delta T}{1-\nu}\quad\text{US, EE, SI (3.14)}$$

In this case, the calculated stress is 33,250 psi, where the stress is independent of wall thickness. This example highlights the need to slowly add steam or hot fluids to a pipe system on initial startup to prevent excessive pipe stresses and possible thermal fatigue of pipe system components.

Steam systems operate at hundreds of degrees F or more, and one precaution for their use is the gradual heating of the piping during restart. Suddenly applied steam at 350 psia has a temperature of 440°F, yielding a stress of 94,600 psi, which is well above the fatigue limit for ASTM, A53 steel (see Table 3.3). Although these approximations are rather coarse, and FEA models would provide better stress predictions, these examples clearly demonstrate the inherent danger in sudden flooding of a system with a hot fluid. Also, thermal fatigue may occur at pipe junctions when different temperature fluids mix, where analysis techniques are rather complex and are presented in recent publications (Beaufils and Courtin [96]).

3.2.6.2 Longitudinal Thermal Expansion of a Pipe

Thermal fatigue may also be a concern due to repeated loading due to bending caused by temperature changes. Thermal stresses can be bounded for a pipe, which is rigidly fixed or restrained at both ends (Harvey [97]), using

$$\sigma'=E\cdot\varepsilon'=-E\cdot\alpha\cdot\Delta T\quad\text{US, EE, SI (3.15)}$$

Example 3.4 Thermal expansion.

Consider a length of carbon steel pipe with fixed ends subject to a temperature change from 70°F to 200°F. Although a fixed restraint is only theoretical, the compressive stress in the pipe is calculated as,

$$-29.5\cdot10^{6}\cdot6.07\cdot10^{-6}\cdot130=-23{,}278\text{ psi}$$

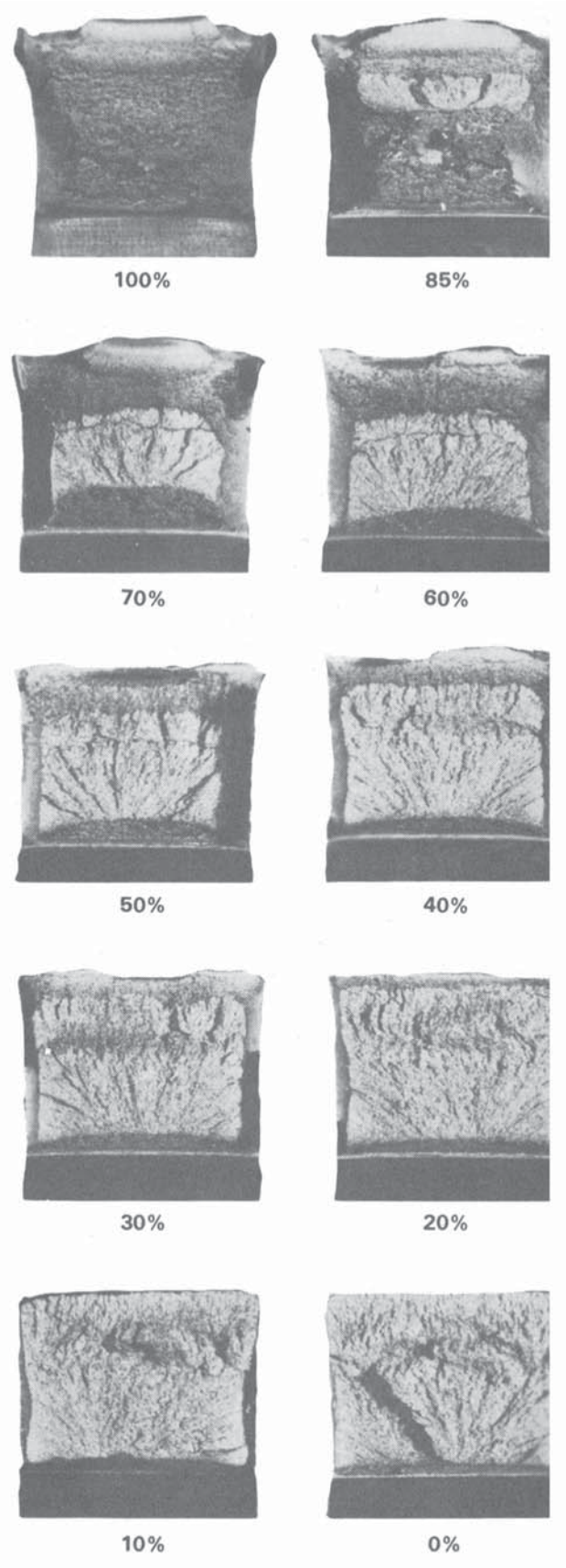


FIG. 3.16 PERCENT OF DUCTILE FRACTURE ON IMPACT TEST FRACTURE SURFACES FOR 4340 STEEL
("Reprinted with permission of ASTM International, 100 Bar Harbor Drive, West Conshohocken, Pa, 19428." by permission, ASTM E23.07a)

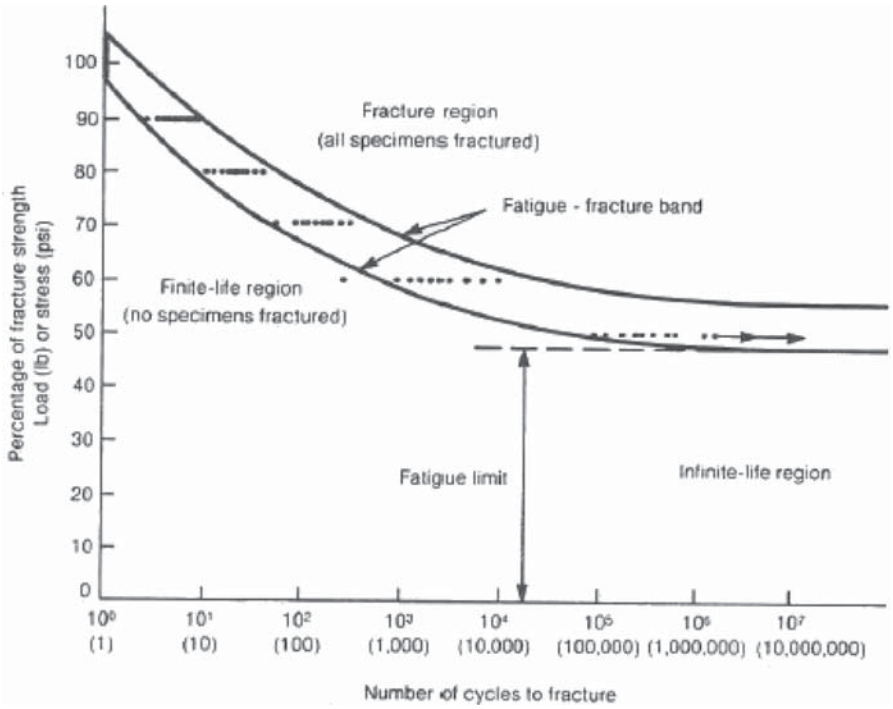


FIG. 3.17 TYPICAL FATIGUE TEST DATA (Permission of American Society of Metals [115])

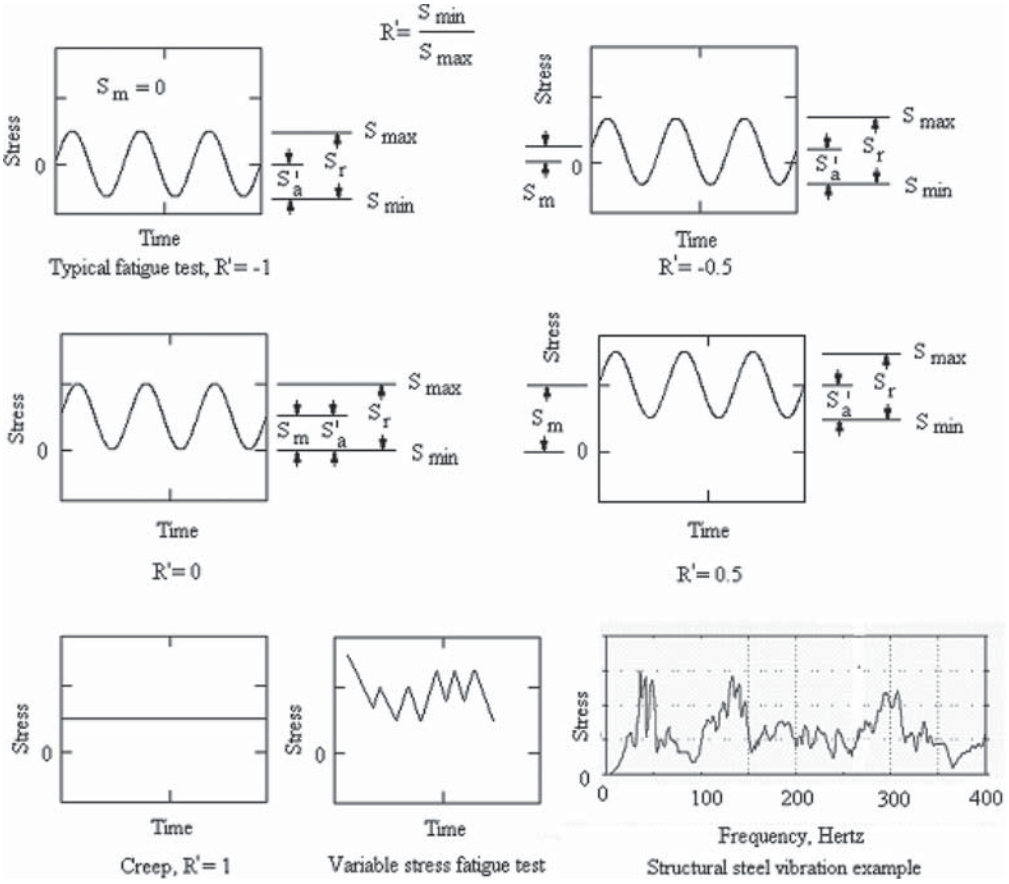


FIG. 3.18 STRESS RANGES FOR FATIGUE TESTING

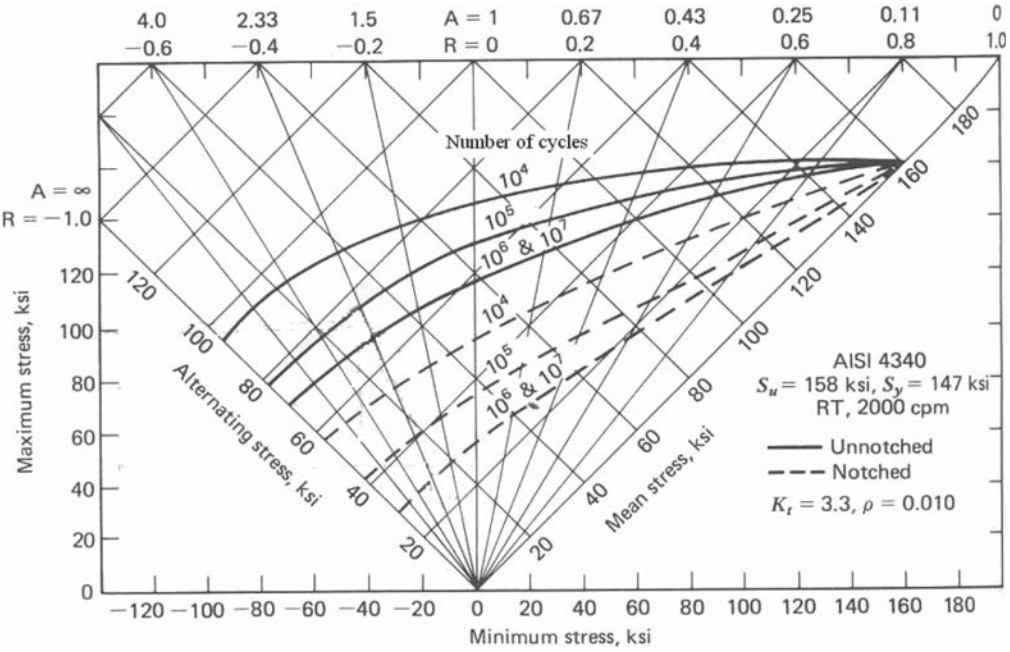


FIG. 3.19 MASTER FATIGUE CURVE FOR A STEEL (Grover [120])

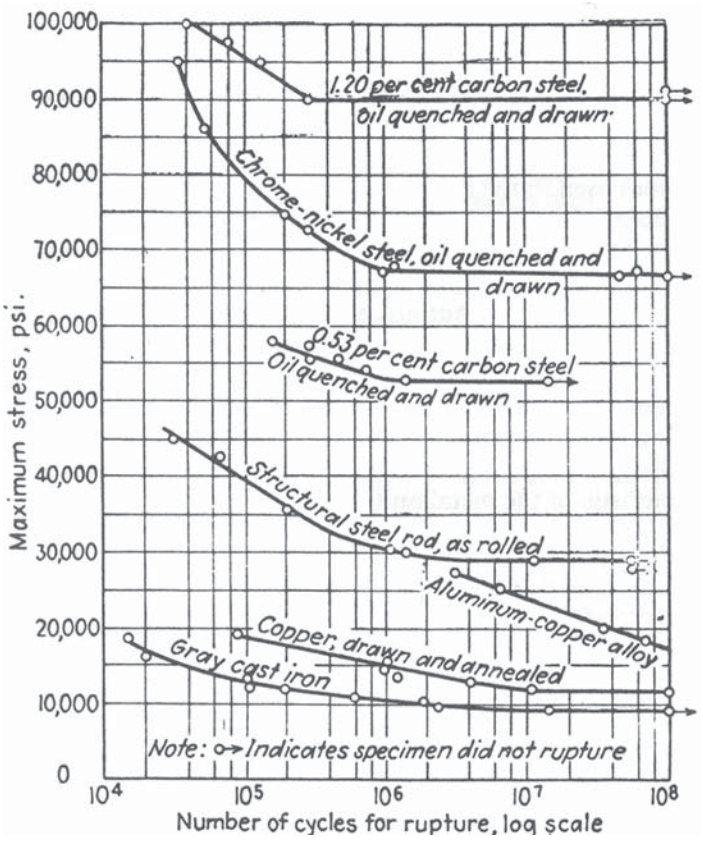
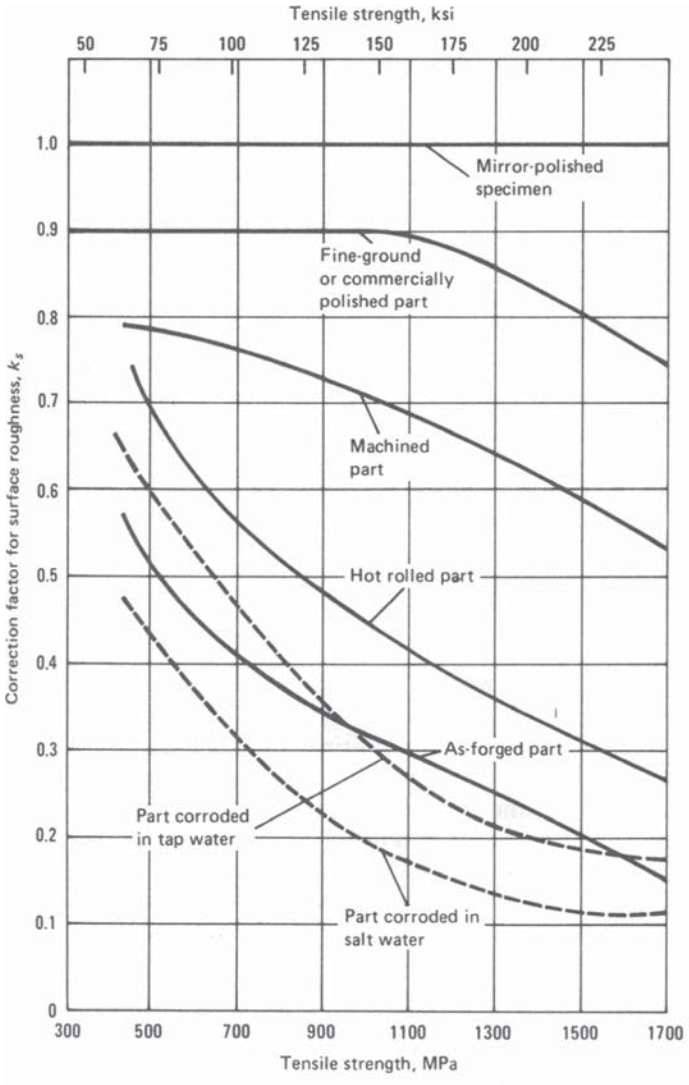


FIG. 3.20 FATIGUE LIMITS FOR DIFFERENT MATERIALS (Boyer [108], Permission of American Society of Metals)



Factor	Value for loading in Bending	Torsion	Tension
K_l	1.0	0.58	0.9(a)
K_d, where: $d \leq 0.4$ in. . .	1.0	1.0	1.0
0.4 in. $< d \leq 2$ in.	0.9	0.9	1.0
K_s	From chart above		

(a) A lower value (0.06 to 0.85) may be used to account for known or suspected undetermined bending because of load eccentricity.

Correction factors for surface roughness (K_s), type of loading (K_l), and part diameter (K_d), for fatigue life of steel parts.

FIG. 3.21 EFFECTS OF SURFACE FINISH ON FATIGUE LIMITS (Boyer [108], Permission of American Society of Metals)

3.2.6.3 Bending Due to Thermal Expansion Thermal stresses are a primary reason for flexibility analyses. The pipe system must be flexible enough to prevent excessive stresses in piping and components due to pipe support or anchor restraints. When a pipe axially extends due to temperature, the pipe is frequently restrained by attached piping, which bends in response to the displacement. Displacement-controlled bending is a primary design concern, and B31.3 is sometimes referred to as a "hot" piping code. The design rules of the Code address cold piping as well, but more detailed analysis is required to ensure that hot piping is not overstressed (paragraph 3.3.7.3).

3.3 PIPE SYSTEM DESIGN STRESSES

Although loads due to water hammer are the focus of this text, other loads need to first be considered, since stresses due to those loads add to the stresses induced by water hammer. Consideration of pipe stresses is the subject of several pipe codes, and as noted, B31.3 is discussed here. Even so, the reader should thoroughly review B31.3 or the applicable Code to supplement this abridged discussion.

An allowable stress range, *S*a, are established by the Code and compared to sustained, occasional, and cyclic

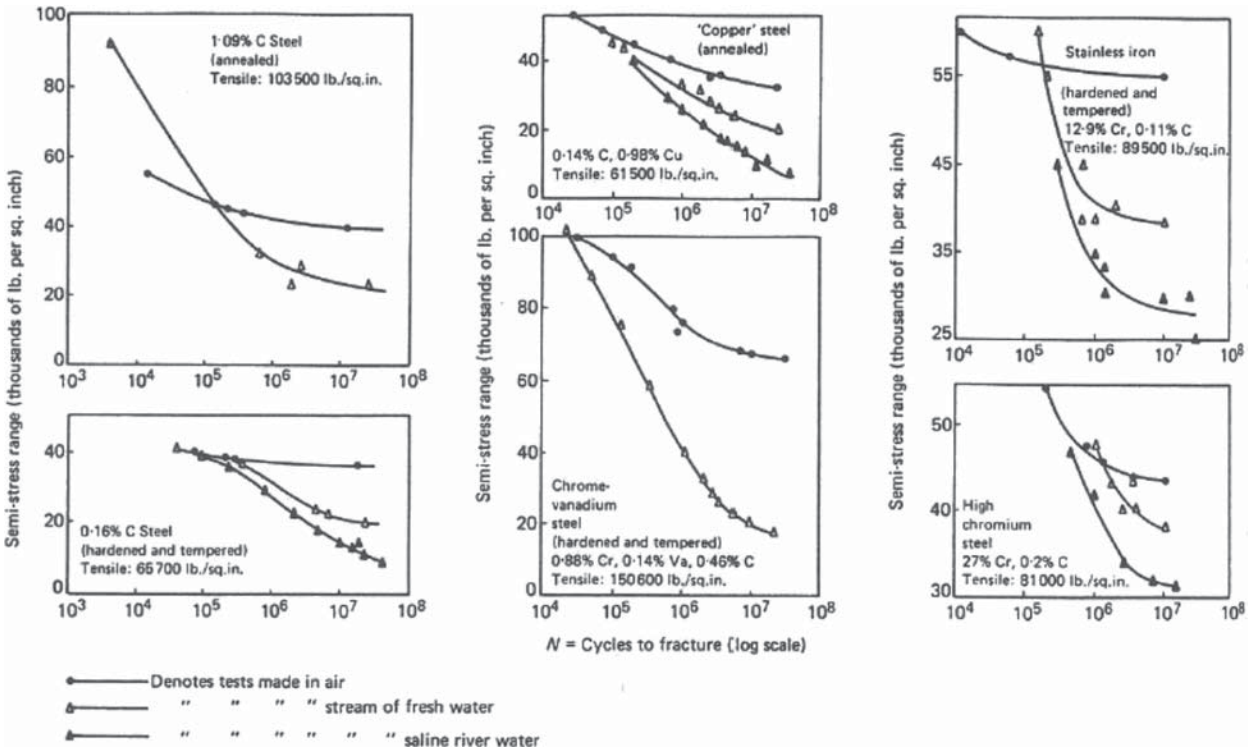


FIG. 3.22 EFFECTS OF CORROSION ON FATIGUE LIMITS (Boyer [108], Permission of American Society of Metals)

loads. Although not specifically defined in the Codes, sustained loads include pressure, ice or snow, and the weight of pipe, insulation, and fluid. Occasional loads include wind and earthquake, safety valve operation, and transient loads with a number of cycles less than 1000. Cyclic, displacement loads are caused by operating temperature changes and dynamic loads, such as earthquakes, vibrations, or water hammer with a number of cycles greater than 1000. These loads are evaluated through a set of Code rules, which were developed from experience plus experimental and analytical data.

3.3.1 Stress Calculations

The application of Code rules is inconsistent with stress calculations obtained from a typical strength of materials stress analysis. For example, internal pressure is used in the Code to determine the wall thickness of a pipe, but hoop stresses are not included when the maximum stress is calculated at a point on a pipe. In the strength of materials stress calculation, hoop stresses are included when resultant stresses at a point are calculated. The difference between the two techniques is clarified in Chapter 4 and is also important with respect to selected software. Code programs like Autopipe® and Caesar® include Code design rules, but non-Code programs like Abaqus® and Ansys® use the strength of materials approach. Consequently, Code programs may provide different results than non-Code programs. Other programs include Caepipe, Triflex, Simflex, and Pipepak. Since computer programs are commonly used to determine pipe stresses, B31.3 provides several examples of pipe designs performed with different software, which obtained similar results. Some of the Code rules and their application are addressed here, where pipe stresses can be grouped as internal, external, sustained longitudinal, or displacement stresses. Recommendations on when to use computer codes, or not, are available (Becht [92]). Errors between different approaches for identical stress calculations may occur. A 30% to 40% error may be observed in hand calculations for stresses, and 5% to 10% differences in calculated stresses have been noted for different computer programs. In fact, slightly different results may be obtained using the same program, depending on the selection of boundary conditions within the program.

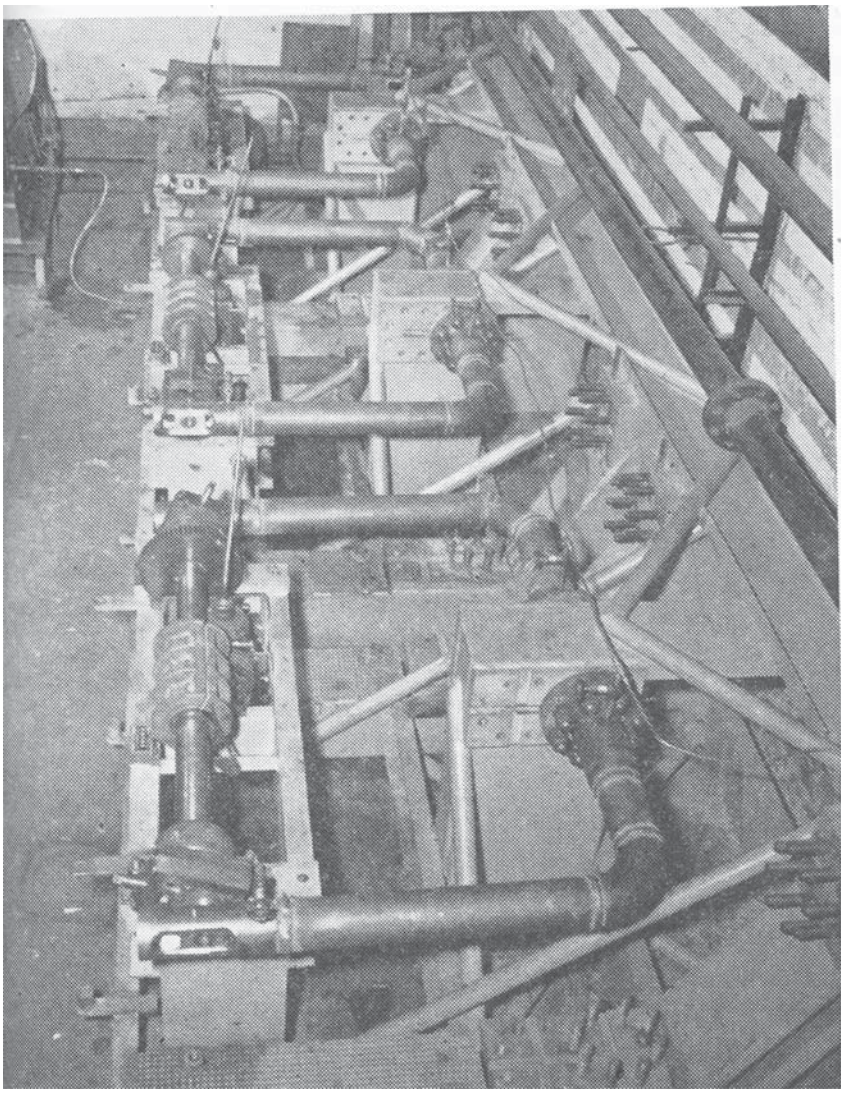


FIG. 3.23 TEST SETUP FOR PIPE COMPONENT FATIGUE TESTS (Markl [126])

3.3.2 Load-Controlled and Displacement-Controlled Stresses

The terms load control and displacement controls are also used to describe stresses. Load-controlled stresses are induced by applied forces, such as weight, wind, and water hammer. Displacement-controlled stresses are induced by inducing a deformation in a structure, where thermal pipe expansion is an example of displacement control.

3.3.3 Maximum Stresses

The maximum stresses for structures occur on the material surface, except in the case of subsurface contact stresses, where two objects are forced against each other. With respect to piping, the maximum bending stress occurs on the outside pipe wall, the maximum torsional stress occurs on the outside pipe wall, the maximum hoop stress occurs on the inside pipe wall, axial stresses are constant throughout the pipe cross section, and contact stresses occur near pipe supports below the pipe surface. In general, bending stresses dominate the pipe system response. Consideration of piping requirements for both hoop stress and longitudinal stress follow.

3.3.4 Internal Pressure Stresses, Hoop Stresses

In ASME B31.3, the hoop stresses due to hydrostatic pressure are considered independently of pipe stresses induced through axial, bending, and torsional deformation of a pipe. At a minimum, a straight pipe must meet the minimum thickness requirements of the Code, where

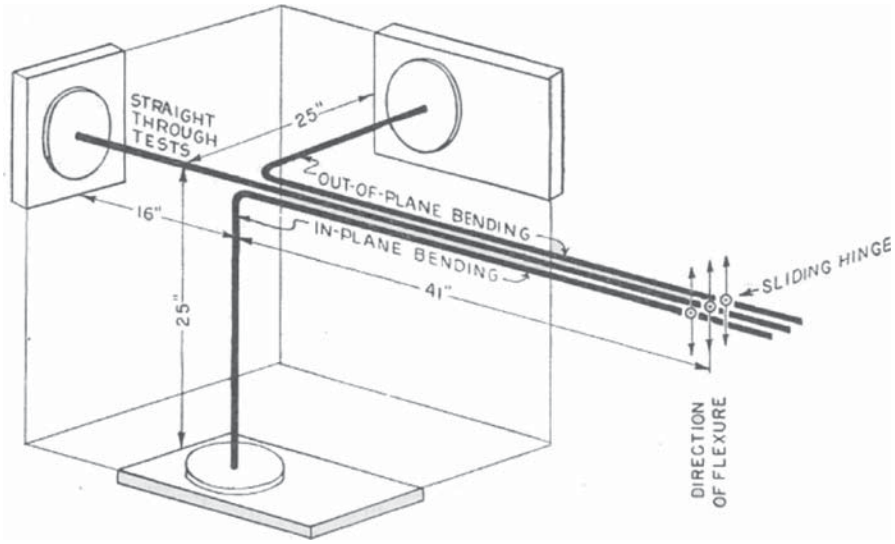


FIG. 3.24 MARKL'S FATIGUE TEST ASSEMBLY AND LOADING (Markl [126])

the minimum wall thickness is specified by one of two equations.

$$\bar{T}_{\min} = \frac{\mathrm{P}\cdot\mathrm{OD}}{2\cdot\left(\mathrm{S}\cdot\mathrm{E}'''\cdot\mathrm{W}'+\mathrm{P}\cdot\mathrm{Y}'\right)} \quad \text{US, EE, SI} \quad (3.16)$$

$$\bar{T}_{\min} = \frac{P\cdot\left(D+2\cdot c''\right)}{2\cdot\left(S\cdot E'''\cdot W'+P\cdot\left(Y'\right)-P\right)} \quad \text{US, EE, SI} \quad (3.17)$$

where D is the inside pipe diameter, OD is the outside pipe diameter, E''' is a quality factor (Table 3.10), W' is a weld joint strength reduction factor (Table 3.11), c' is the sum of the thread or groove depth plus a 0.2-in. machining tolerance plus corrosion and erosion allowances, and Y' varies from 0.4 to 0.7 for temperatures up to 900°F and above 1100°F for $\bar{T} \le \mathrm{OD}/6$. For $\bar{T} \ge \mathrm{OD}/6$, $Y' = \left(\dfrac{D+2\cdot c''}{\mathrm{OD}+D+2\cdot c''}\right)$ the design margin, or safety factor, against ultimate strength for B31.3 piping equals 3 for pressure.

3.3.4.1 Corrosion and Erosion Allowances Corrosion and erosion allowances have been frequently assumed to be 1/16 in. in the past, but the corrosion allowance is much more complicated. The corrosion rates for a particular service must be considered, as well as the expected life of the facility and factors such as flow-

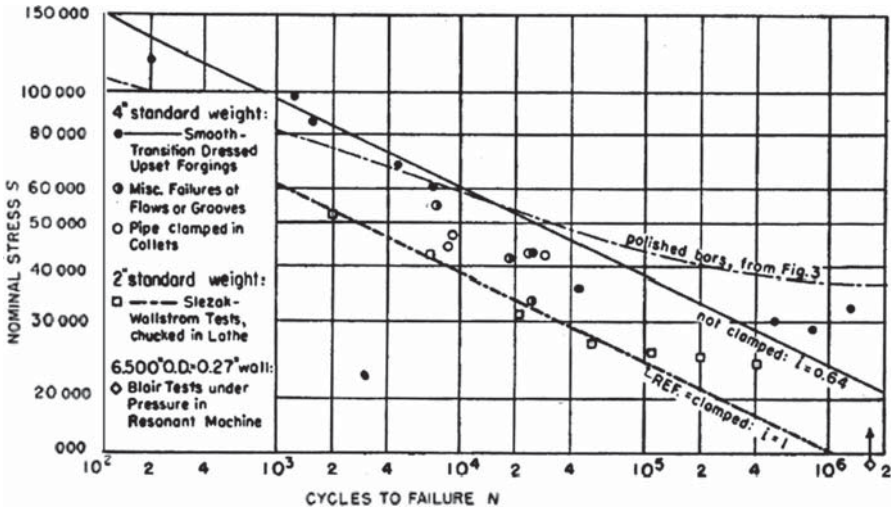


FIG. 3.25 FATIGUE DATA FOR POLISHED ROTATING BEAM FATIGUE TESTS (Markl [126])

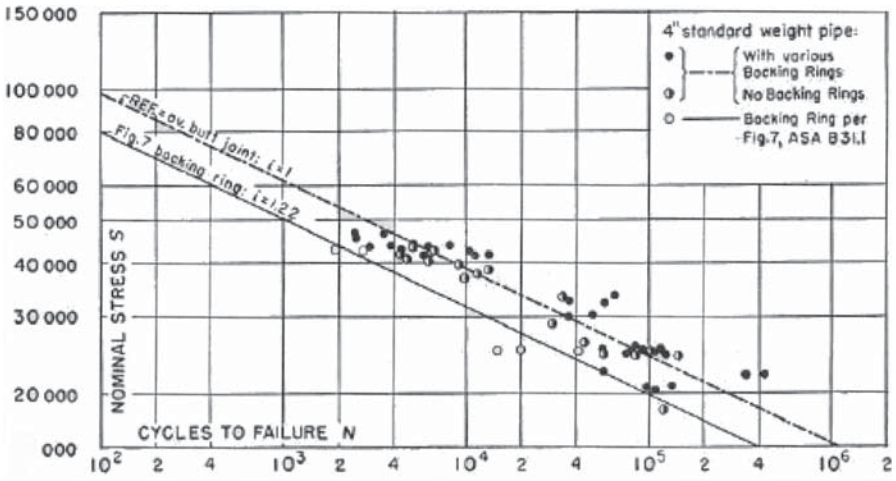


FIG. 3.26 FATIGUE DATA FOR WELDED PIPE (Markl [126])

accelerated corrosion, crevice corrosion, galvanic corrosion, and microbial-induced corrosion. Also, significant galvanic corrosion may occur in underground piping, where the differences in electric potential induce currents between the soil and pipe (similar to a battery). Erosion is affected by both flow rates and entrained solids in the fluid. Leakage due to erosion at an elbow commonly occurs when localized thinning reaches about 10% of the wall thickness. In other words, corrosion and erosion allowances need to be determined specifically for the system in question. Some examples of corrosion and erosion are provided in paragraph 4.7, along with references. Also, Antaki [131] provides a more complete discussion of corrosion and applicable standards. For Eqs. (3.18) and (3.19), the inside diameter, D, equals the nominal inside pipe diameter minus pipe fabrication tolerances, which are typically ±12.5%. Requirements for wall thicknesses of fabricated elbows are also discussed in B31.3.

3.3.4.2 Hoop Stress and Maximum Pressure The hoop stresses may be approximated by the thin wall hoop stress equation (1-10), or the hoop stresses may be more accurately calculated by the thick wall hoop stress equation, where the maximum stress occurs at the inner wall according to

$$\sigma_\theta = \frac{P \cdot D^2 \cdot \left(\mathrm{OD}^2 + r^2\right)}{r^2 \cdot \left(\mathrm{OD}^2 - D^2\right)} = \frac{P \cdot \left(\mathrm{OD}^2 + D^2\right)}{\left(\mathrm{OD}^2 - D^2\right)}$$

US, EE, SI (3.18)

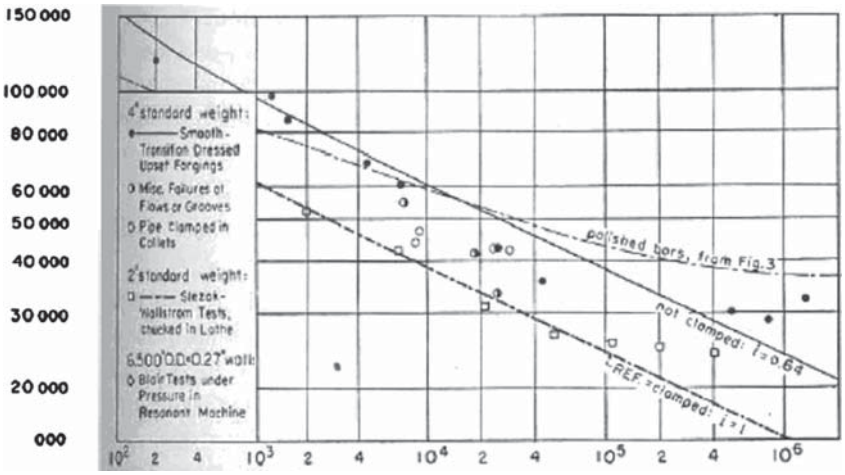


FIG. 3.27 FATIGUE DATA FOR STRAIGHT PIPE (Markl [126])

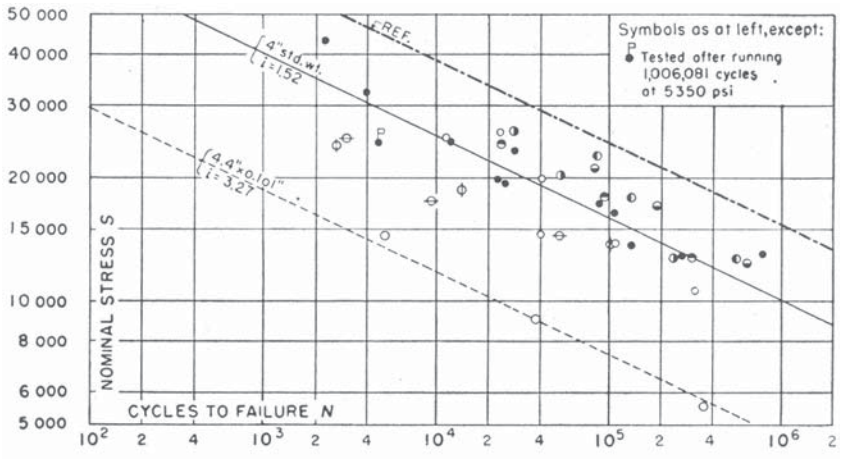


FIG. 3.28 FATIGUE DATA FOR LONG RADIUS ELBOWS, OUT OF PLANE LOADING (Markl [126])

At the outer wall, the hoop stress equals

$$\sigma_\theta = \frac{P \cdot 2 \cdot \mathrm{ID}^2}{\left(\mathrm{OD}^2 - D^2\right)} \quad \text{US, EE, SI (3.19)}$$

Example 3.5 Hoop stresses.

What is the required wall thickness for an A106, Type F, 6-in. NPS pipe operating at 70°F and 200 psig, assuming a corrosion allowance of 0.065 in. = c' and a 12.5% mill tolerance equal to 0.125 · 0.280 = 0.035 in.

$$\bar{T}_{\min} = \frac{200 \cdot (6.625)}{2 \cdot \left(16000 \cdot 0.8 \cdot 1.00 + 200 \cdot (0.4)\right)} = 0.051\_\text{in}$$

For this wall thickness, the maximum *ID* then equals *OD* − 2 · 0.051 = 6.57 in., and Schedule 5 pipe is selected from Table 2-2, where D = 6.407 in.

What is the maximum hoop stress in this selected pipe? Calculating the maximum stress, using a nominal Schedule 5S ID (0.109-in. wall thickness), the nominal stress is well below yield and equals

$$\sigma_\theta = \frac{200 \cdot \left(6.625^2 + 6.407^2\right)}{\left(6.625^2 - 6.407^2\right)} = 5980\_\text{psi}$$

3.3.5 Limits for Sustained Longitudinal Stresses and Occasional Stresses (Displacement stresses)

The acceptance criteria or limits for different pipe stresses are first considered here, followed by a description of the various loads, which contribute to these stresses. Per B31.3, sustained longitudinal stresses, S_L, for a nominal

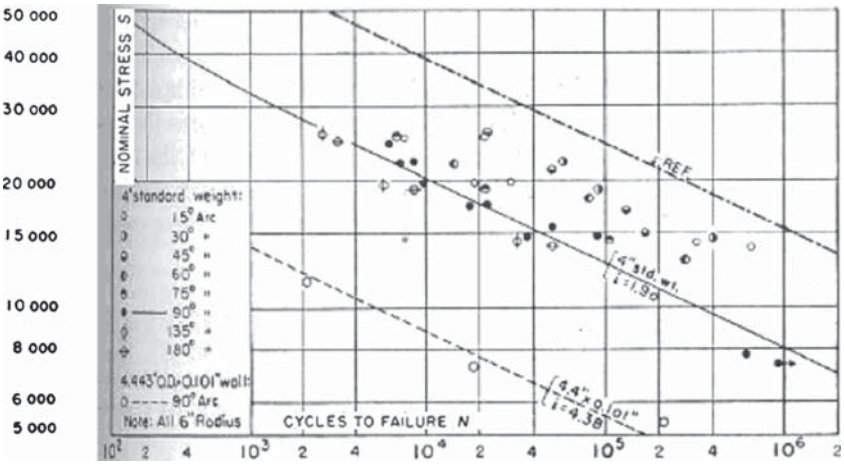


FIG. 3.29 FATIGUE DATA FOR LONG RADIUS ELBOWS, IN-PLANE LOADING (Markl [126])

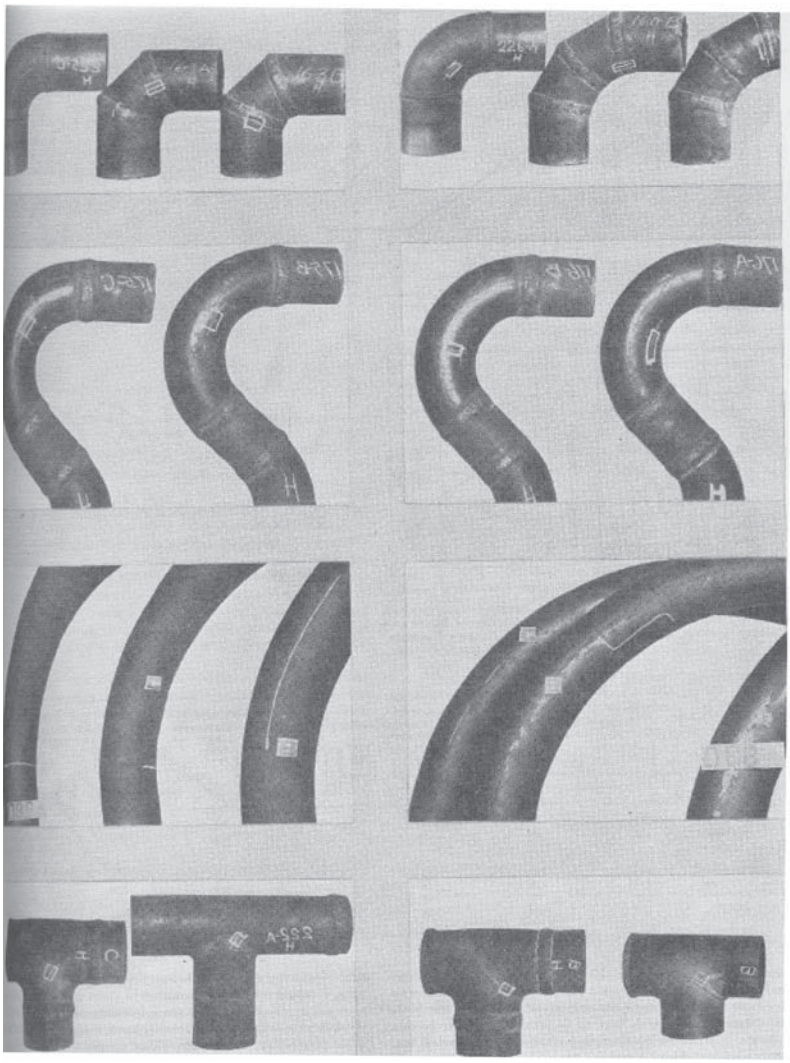


FIG. 3.30 EXAMPLES OF PIPE FAILURES DURING FATIGUE TESTING (Markl [127])

pipe of thickness, $\bar{T}_{\text{nom}}$, due to weight and pressure must meet the requirement that

$$S_{\text{L}} < S_{\text{h}} \qquad \text{US, EE, SI (3.20)}$$

Occasional stresses below 800°F, which occur less than 100 hours per year and less than 10 hours at a time, may exceed the allowable stress, such that

$$S_{\text{L}} < 1.33 \cdot S_{\text{h}} \qquad \text{US, EE, SI (3.21)}$$

Displacement stresses are typically only required for flexibility analyses, and a flexibility analysis is not required if the system essentially duplicates an existing system, or uniform piping is fixed between two points and meets the requirements of

$$\frac{\text{OD}\,(\text{in}) \cdot \Delta\,(\text{in})}{\left(L\,(\text{ft}) - L_s\,(\text{ft})\right)^2} < \frac{30 \cdot S_{\text{A}}\,(\text{psi})}{E_{70°F}\,(\text{psi})}\,(\text{in./ft})$$

US, EE (3.22)

$$\frac{\text{OD}\,(\text{m}) \cdot \Delta\,(\text{m})}{\left(L\,(\text{m}) - L_s\,(\text{m})\right)^2} < \frac{208 \cdot S_{\text{A}}}{E_{70°F}}\,(\text{m/m})$$

SI (3.23)

where L is the developed pipe length, L_s is the linear distance between anchors, and Δ is the resultant of the total strain displacements. Accordingly, systems operated at low or ambient temperatures frequently are exempt from flexibility analyses. When an analysis is required, bend-

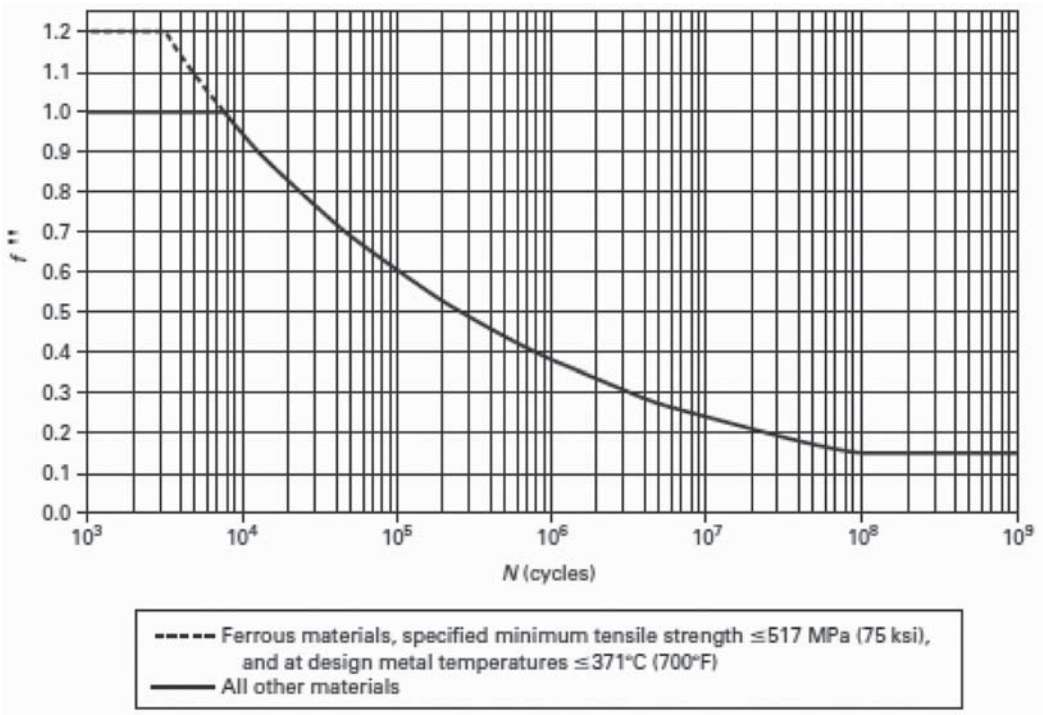


FIG. 3.31 STRESS RANGE FACTOR, f″ (ASME B31.3)

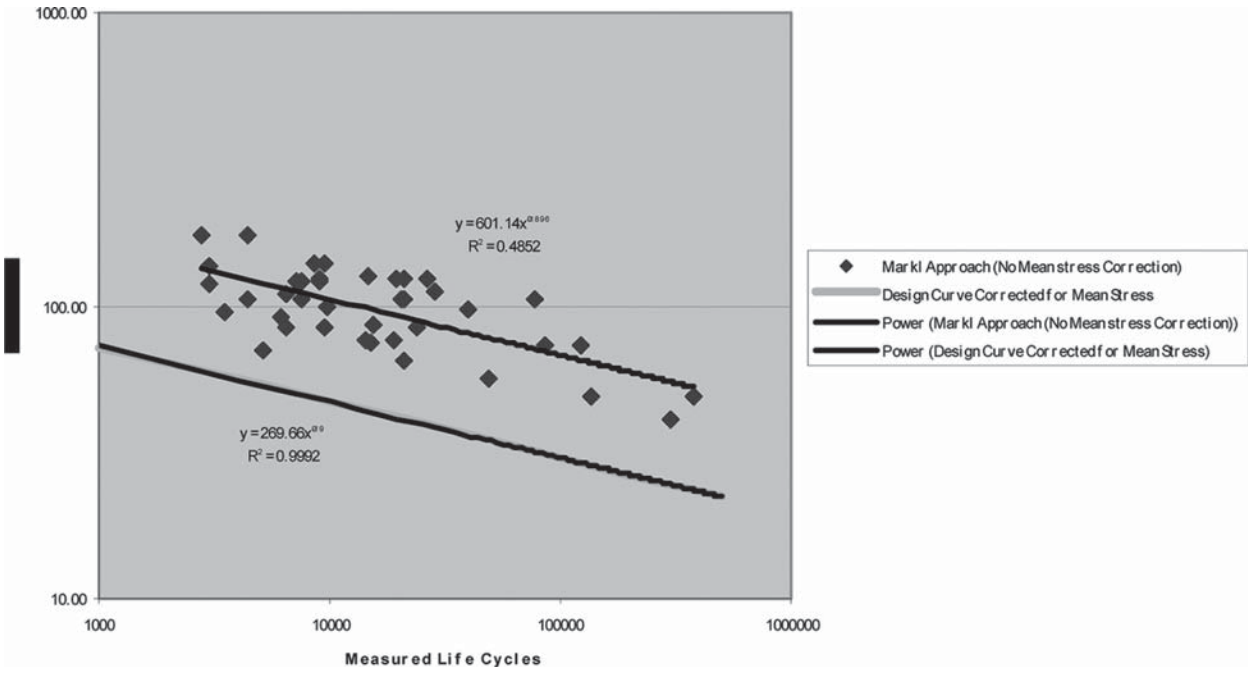


FIG. 3.32 CYCLIC PRESSURE FATIGUE FOR PIPE INTERSECTIONS (Kapp [128])

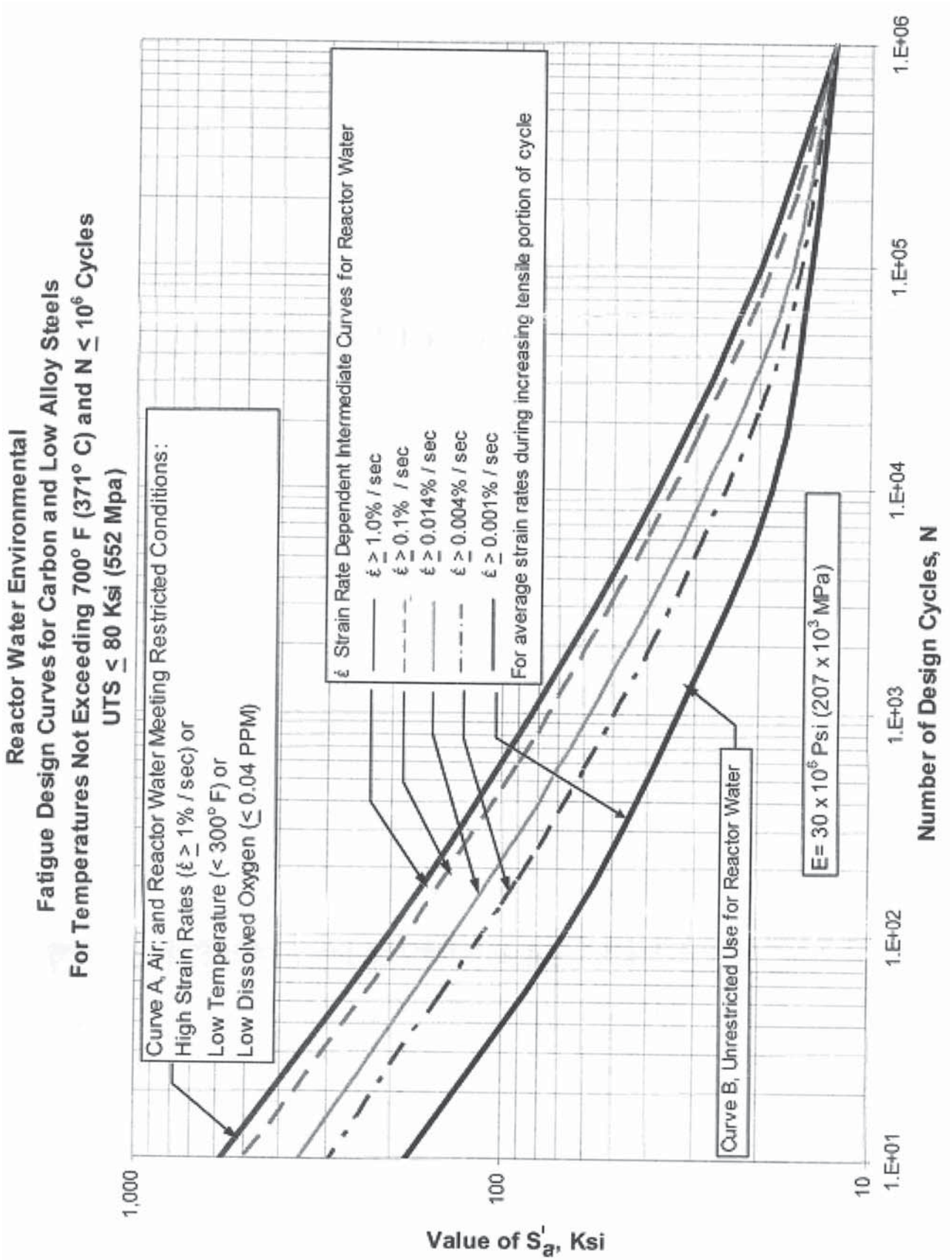


FIG. 3.33 FATIGUE CURVES FOR CARBON AND LOW-ALLOY STEELS

TABLE 3.4 FATIGUE DATA FOR CARBON AND LOW-ALLOY STEELS (See Fig. 3.33)

N (cycles)	Sa (Ksi) Curve A	ε̇ in % / sec			Curve B
	ε̇ =1.0	ε̇ =.1	ε̇ =.014	ε̇ =.004	ε̇ =.001
1.E+01	580	500	351	295	180
2.E+01	410	368	262	223	134
5.E+01	275	245	185	150	91.0
1.E+02	205	183	137	114	70.0
2.E+02	155	138	104	87.0	55.0
5.E+02	105	96.0	74.0	63.0	41.0
1.E+03	83.0	75.0	58.0	50.0	33.0
2.E+03	64.0	59.0	46.0	40.0	27.5
5.E+03	48.0	44.0	35.0	30.0	21.5
1.E+04	38.0	35.0	28.5	24.8	18.5
2.E+04	31.0	28.5	23.3	20.5	16.5
5.E+04	23.0	22.0	18.5	17.3	15.0
1.E+05	20.0	18.5	16.3	15.7	14.1
2.E+05	16.5	16.0	14.8	14.5	13.5
5.E+05	13.5	13.5	13.5	13.3	12.9
1.E+06	12.5	12.5	12.5	12.5	12.5

ing and torsional stresses are used to find displacement stresses.

3.3.6 Allowable Stresses

Per the 2008 edition of B31.3, allowable stresses are calculated as follows

For $S_L < S_h$

$$Sa = f'' \cdot \left(1.25 \cdot S_c + 0.25 \cdot S_h\right) = S_E \quad \text{US, EE, SI (3.24)}$$

For $S_L > S_h$

$$Sa = f'' \cdot \left(1.25 \cdot \left(S_c + S_h\right) - S_L\right) = S_E \quad \text{US, EE, SI (3.25)}$$

Sa is the allowable displacement stress range, S_L is the cumulative longitudinal stress due to sustained loads such as weight and pressure, and S_h and S_c are the allowable stresses, S, from Table 3.3 for hot and cold operating conditions, respectively. (Calculation techniques for flexibility analyses were changed in the 2012 edition of B31.3, and other changes are in process.) Note that the allowable stress S_a does not always equal the alternating stress, S'_a, used in fatigue calculations, but $Sa \geq S'_a$. For B31.3, $Sa = S_E = S'_a$. The stress range factor, f'', accounts for fatigue and is obtained from Fig. 3.31. Once the allowable stress range, Sa is established, it is compared to the calculated stress range for the pipe component, S'_E. For straight pipe, the calculated stress range equals the resultant stress obtained from the resultant of the bending and torsional moments, such that

$$S'_E = \sqrt{\frac{\left(M_b^2 + M_T^2\right) \cdot \mathrm{OD}}{I}} = \sqrt{S_b^2 + 4 \cdot S_T^2} \quad \text{US, EE, SI (3.26)}$$

and the required variables equal

$$S_T = \frac{M_T}{2 \cdot Z} \quad \text{US, EE, SI (3.27)}$$

$$I = \frac{\pi \cdot \left(\mathrm{OD}^4 - D^4\right)}{64} \quad \text{US, EE, SI (3.28)}$$

$$Z = \frac{I}{c'} = \frac{I}{\mathrm{OD}/2} = \frac{\pi \cdot \left(\mathrm{OD}^4 - D^4\right)}{32 \cdot \mathrm{OD}} \quad \text{US, EE, SI (3.29)}$$

where I is the moment of inertia for a pipe, Z is the section modulus of the pipe, M_b is the bending moment, M_T is the torsional moment, S_b is the bending stress, and S_T is the torsional stress.

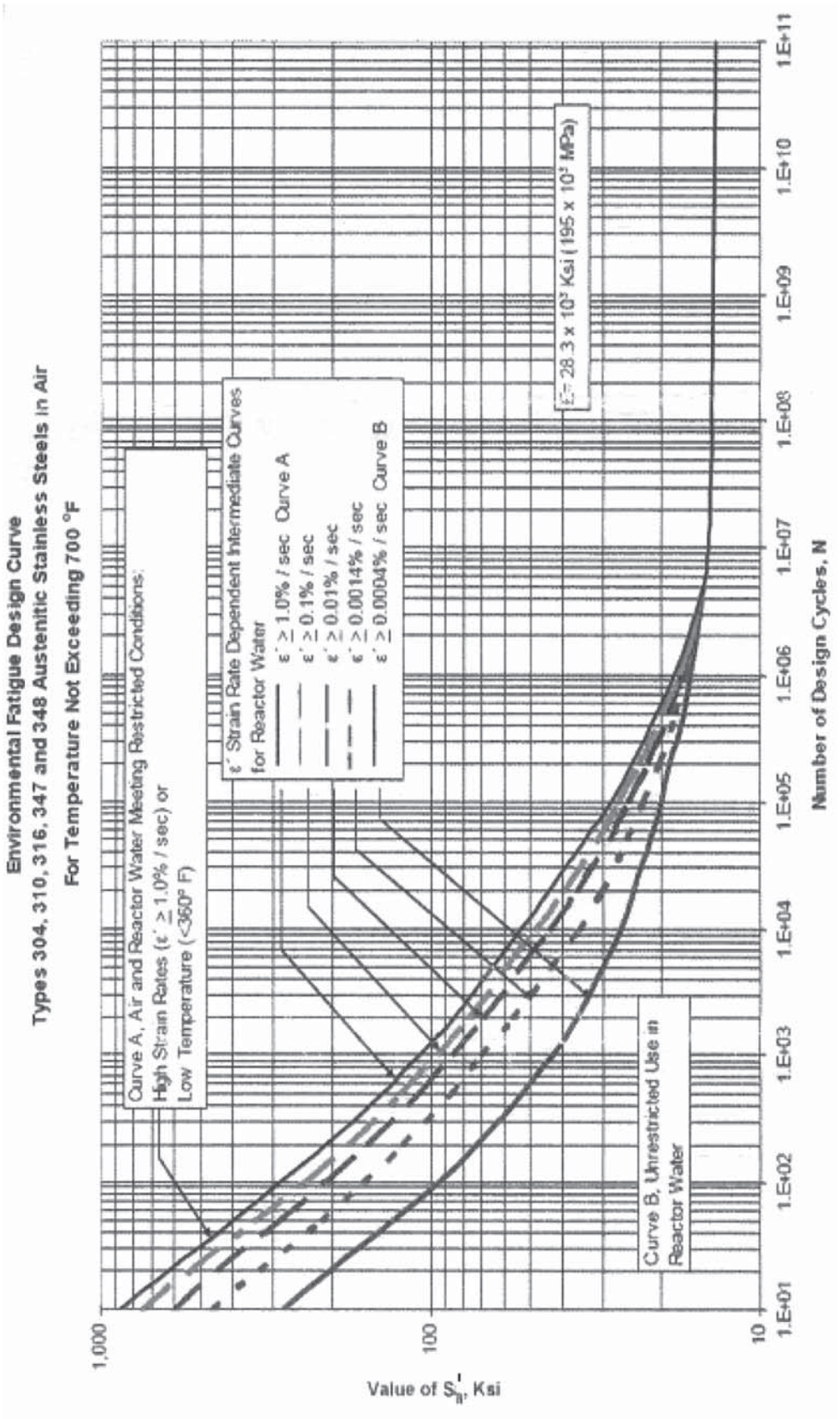


FIG. 3.34 FATIGUE CURVES FOR STAINLESS STEELS

TABLE 3.5 FATIGUE DATA FOR STAINLESS STEELS (See Fig. 3.34)

N (Cycles)	Sa (ksi) Curve A	ε˙ in % / sec			Curve B
	ε˙=1.0	ε˙=0.1	ε˙=0.01	ε˙=0.0014	ε˙=0.0004
1.E+01	870	750	600	460	280
2.E+01	624	537	445	334	202
5.E+01	399	343	292	217	131.0
1.E+02	287	243	208	161.0	94.9
2.E+02	209	178.0	158.0	123.0	73.2
5.E+02	141.0	124.0	109.0	87.0	52.7
1.E+03	108.0	95.5	86.0	70.3	42.6
2.E+03	85.6	76.9	69.6	56.8	36.0
5.E+03	65.3	59.4	53.4	43.2	29.9
1.E+04	53.4	48.2	43.5	35.7	26.6
2.E+04	43.5	39.6	35.9	30.0	24.3
5.E+04	34.1	31.1	28.7	25.4	21.6
1.E+05	28.4	26.7	25.0	22.6	20.0
2.E+05	24.4	23.2	21.9	20.2	18.80
5.E+05	20.6	19.70	18.90	18.10	17.10
1.E+06	18.30	17.50	17.20	16.70	16.20
2.E+06	16.40	16.00	15.90	15.70	15.50
5.E+06	14.80	14.80	14.80	14.80	14.80
1.E+07	14.40				
1.E+08	14.10				
1.E+09	13.90				
1.E+10	13.70				
1.E+11	13.60				

For elbows, the calculated bending stress equals

$$S_b = \sqrt{\frac{\left(i_i \cdot M_i\right)^2 + \left(i_o \cdot M_o\right)^2}{Z}} \quad \text{US, EE, SI (3.30)}$$

And for tees, the calculated bending stresses equal:
For the header

$$S_b = \sqrt{\frac{\left(i_i \cdot M_i\right)^2 + \left(i_o \cdot M_o\right)^2}{Z_e}} \quad \text{US, EE, SI (3.31)}$$

For the branch

$$S_b = \sqrt{\frac{\left(i_i \cdot M_i\right)^2 + \left(i_o \cdot M_o\right)^2}{Z_e}} \quad \text{US, EE, SI (3.32)}$$

$$Z_e = \pi \cdot r_m^{\,2} \cdot \bar{T}_s \quad \text{US, EE, SI (3.33)}$$

where $\bar{T}_s$ is the effective wall thickness equal to the lesser of the header pipe wall thickness or i_i times the branch pipe wall thickness, Z_e is the effective section modulus, M_i is the in-plane moment, M_o is the out-plane moment, and r_m is the mean branch cross-sectional radius. The stress intensification factors, i_i and i_o, are considered in Section 3.3.7.6 below. B31.3 also permits an alternative calculation, which adds axial pressure-induced stresses to the bending stresses. Having defined the piping stress limits, some theory to calculate pertinent stresses and resulting pipe reactions follow.

TABLE 3.6 POISSON'S RATIO AND BULK MODULUS OF METALS (Avallone [33])

Material	Bulk modulus, k, 10^6 psi	Poisson's ratio, ν
Cast steel	20.2	0.265
Cold rolled steel	23.1	0.287
Stainless steel, 18–8	23.6	0.305
All other steels, including high carbon, heat treated	22.6–24.0	0.283–0.292
Cast iron	8.4–15.5	0.211–0.299
Malleable iron	17.2	0.271
Copper	17.9	0.355
Brass, 70–30	15.7	0.331
Cast brass	16.8	0.357
Tobin brass	16.3	0.359
Phosphor bronze	17.8	0.350
Aluminum alloys	9.9–10.2	0.330–0.334
Monel metal	22.5	0.315
Inconel	—	0.27-0.38
Titanium, 99.0 Ti, annealed bar	—	0.34

3.3.7 Pipe Stresses and Reactions at Pipe Supports

Both sustained longitudinal stresses and displacement stresses are related to reactions at pipe supports. Calculation methods for different stresses are grouped together here since axial forces, bending moments, and torsional moments each contribute to reactions and pipe stresses. Stresses in a pipe are typically determined using available software, due to the complexity of the equations. For the general case, at each end of a pipe, there are three translations, three rotations, three moments, and three forces, which may be addressed using linear algebra techniques. Even though stress calculations can be quite complex, various stresses are considered here, along with some simplified examples.

3.3.7.1 Axial Stresses and Reactions Due to Pressure and Flow In most steady-state cases, axial pipe stresses are small, and pipe reactions are cancelled by opposing axial forces, where exceptions are parallel unequal diameter pipes and hot underground pipes. Pipes subject to blowdown, venting, and water hammer are unsteady-state examples of applied axial forces, where the axial forces may lead to fatigue, plastic deformation, or rupture. Again, the following chapters of this text address pipe failures due to fluid transients.

Axial stresses due to internal pressure (Young and Budynas [132]) are found, such that for a thick-walled cylinder with closed ends, the through-wall axial stress equals

$$\sigma'_z = \frac{P \cdot D^2}{\mathrm{OD}^2 - D^2} \quad \text{US, EE, SI} \quad (3.34)$$

and the maximum radial stress occurs at the inner wall, where

$$\sigma'_r = \frac{-P \cdot D^2 \cdot \left(\mathrm{OD}^2 - r^2\right)}{r^2 \cdot \left(\mathrm{OD}^2 - D^2\right)} = -P \quad \text{US, EE, SI} \quad (3.35)$$

For a thin-walled cylinder

$$\sigma'_z = \frac{P \cdot \mathrm{OD}}{4 \cdot \bar{T}} \quad \text{US, EE, SI} \quad (3.36)$$

Example 3.6 Axial stresses and reactions.

To understand the axial stresses in a pipe, consider a 6-in., schedule 40 pipe with an internal pressure of 200 psig. From Eq. (3.36), the nominal axial pipe stress through the pipe wall equals $200 \cdot 6.025^2/(6.625^2 - 6.025^2) = 957$ psi. Per Code, the pipe thickness must be compensated for mill tolerances and corrosion. Assuming 0.065 in. of corrosion, and using a 12.5% mill tolerance per ASTM standards, the corrected axial stress equals $200 \cdot 6.225^2/(6.625^2 - 6.225^2) = 1507.8$ psi $= \sigma_{min} > 0$. As noted, the axial stresses are considered as sustained loads in B31.3, but the Code neglects the axial stresses for flexibility analyses even though the fatigue life will be decreased somewhat, since $R' = \sigma_{min}/\sigma_{max} > 0$, and the Code fatigue curve was generated for $R' = 0$. Consideration of axial stresses is presently being evaluated by B31.3 Committees. Also for this example, the radial stress is zero at the outer wall and has a compressive magnitude equal to the pressure at the inner wall, where $\sigma'_r = -200$ psi. Radial

TABLE 3.7 Densities of metals (Reprinted with permission of ASM)

Metal or alloy	Density g/cm³	Density lb/in.³
Aluminum and aluminum alloys		
Aluminum (99.996%)	2.6989	0.0975
Wrought alloys		
EC, 1060 alloys	2.70	0.098
1100	2.71	0.098
2011	2.82	0.102
2014	2.80	0.101
2024	2.77	0.100
2218	2.81	0.101
3003	2.73	0.099
4032	2.69	0.097
5005	2.70	0.098
5050	2.69	0.097
5052	2.68	0.097
5056	2.64	0.095
5083	2.66	0.096
5086	2.65	0.096
5154	2.66	0.096
5357	2.70	0.098
5456	2.66	0.096
6061, 6063	2.70	0.098
6101, 6151	2.70	0.098
7075	2.80	0.101
7079	2.74	0.099
7178	2.82	0.102
Casting alloys		
A13	2.66	0.096
43	2.69	0.097
108, A108	2.79	0.101
A132	2.72	0.098
D132	2.76	0.100
F132	2.74	0.099
138	2.95	0.107
142	2.81	0.101
195, B195	2.81	0.101
214	2.65	0.096
220	2.57	0.093
319	2.79	0.101
355	2.71	0.098
356	2.68	0.097
360	2.64	0.095
380	2.71	0.098
750	2.88	0.104
40E	2.81	0.101
Copper and copper alloys		
Wrought coppers		
Pure copper	8.96	0.324
Electrolytic tough pitch copper (ETP)	8.89	0.321
Deoxidized copper, high residual phosphorus (DHP)	8.94	0.323
Free-machining copper		
0.5% Te	8.94	0.323
1.0% Pb	8.94	0.323
Wrought alloys		
Gilding, 95%	8.86	0.320
Commercial bronze, 90%	8.80	0.318
Jewelry bronze, 87.5%	8.78	0.317
Red brass, 85%	8.75	0.316
Low brass, 80%	8.67	0.313
Cartridge brass, 70%	8.53	0.308
Yellow brass	8.47	0.306
Muntz metal	8.39	0.303
Leaded commercial bronze	8.83	0.319
Low-leaded brass (tube)	8.50	0.307
Medium-leaded brass	8.47	0.306
High-leaded brass (tube)	8.53	0.308
High-leaded brass	8.50	0.307
Extra-high-leaded brass	8.50	0.307
Free-cutting brass	8.50	0.307
Leaded Muntz metal	8.41	0.304
Forging brass	8.44	0.305
Architectural bronze	8.47	0.306
Inhibited admiralty	8.53	0.308
Naval brass	8.41	0.304
Leaded naval brass	8.44	0.305
Manganese bronze (A)	8.36	0.302
Phosphor bronze, 5% (A)	8.86	0.320
Phosphor bronze, 8% (C)	8.80	0.318
Phosphor bronze, 10% (D)	8.78	0.317
Phosphor bronze, 1.25%	8.89	0.321
Free-cutting phosphor bronze	8.89	0.321
Cupro-nickel, 30%	8.94	0.323
Cupro-nickel, 10%	8.94	0.323
Nickel silver, 65-18	8.73	0.315
Nickel silver, 55-18	8.70	0.314
High-silicon bronze (A)	8.53	0.308
Low-silicon bronze (B)	8.75	0.316
Aluminum bronze, 5% Al	8.17	0.294
Aluminum bronze, (3)	7.78	0.281
Aluminum-silicon bronze	7.69	0.278
Aluminum bronze, (1)	7.58	0.274
Aluminum bronze, (2)	7.58	0.274
Beryllium copper	8.23	0.297
Casting alloys		
Chromium copper (1% Cr)	8.7	0.31
88Cu-10Sn-2Zn	8.7	0.31
88Cu-8Sn-4Zn	8.8	0.32
89Cu-11Sn	8.78	0.317
88Cu-6Sn-1.5Pb-4.5Zn	8.7	0.31
87Cu-8Sn-1Pb-4Zn	8.8	0.32
87Cu-10Sn-1Pb-2Zn	8.8	0.32
80Cu-10Sn-10Pb	8.95	0.323
83Cu-7Sn-7Pb-3Zn	8.93	0.322
85Cu-5Sn-9Pb-1Zn	8.87	0.320
78Cu-7Sn-15Pb	9.25	0.334
70Cu-5Sn-25Pb	9.30	0.336
85Cu-5Sn-5Pb-5Zn	8.80	0.318
83Cu-4Sn-6Pb-7Zn	8.6	0.31
81Cu-3Sn-7Pb-9Zn	8.7	0.31
76Cu-2.5Sn-6.5Pb-15Zn	8.77	0.317
72Cu-1Sn-3Pb-24Zn	8.50	0.307
67Cu-1Sn-3Pb-29Zn	8.45	0.305
61Cu-1Sn-1Pb-37Zn	8.40	0.304
Manganese bronze		
60 ksi	8.2	0.30
65 ksi	8.3	0.30
90 ksi	7.9	0.29
110 ksi	7.7	0.28
Aluminum bronze		
Alloy 9A	7.8	0.28
Alloy 9B	7.55	0.272
Alloy 9C	7.5	0.27
Alloy 9D	7.7	0.28
Nickel silver		
12% Ni	8.95	0.323
16% Ni	8.95	0.323
20% Ni	8.85	0.319
25% Ni	8.8	0.32
Silicon bronze	8.30	0.300
Silicon brass	8.30	0.300
Iron and iron alloys		
Pure iron	7.874	0.2845
Ingot iron	7.866	0.2842
Wrought iron	7.7	0.28
Gray cast iron	7.15(a)	0.258(a)
Malleable iron	7.27(b)	0.262(b)
0.06% C steel	7.871	0.2844
0.23% C steel	7.859	0.2839
0.435% C steel	7.844	0.2834
1.22% C steel	7.830	0.2829
Low-carbon chromium-molybdenum steels		
0.5% Mo steel	7.86	0.283
1Cr-0.5Mo steel	7.86	0.283
1.25Cr-0.5Mo steel	7.86	0.283
2.25Cr-1.0Mo steel	7.86	0.283
5Cr-0.5Mo steel	7.78	0.278
7Cr-0.5Mo steel	7.78	0.278
9Cr-1Mo steel	7.67	0.276
Medium-carbon alloy steels		
1Cr-0.35Mo-0.25V steel	7.86	0.283
H11 die steel (5Cr-1.5Mo-0.4V)	7.79	0.281
Other iron-base alloys		
A-286	7.94	0.286
16-25-6 alloy	8.08	0.292
RA-330	8.03	0.290
Incoloy	8.02	0.290
Incoloy T	7.98	0.288
Incoloy 901	8.23	0.297
T1 tool steel	8.67	0.313
M2 tool steel	8.16	0.295
H41 tool steel	7.88	0.285
20W-4Cr-2V-12Co steel	8.89	0.321
Invar (36% Ni)	8.00	0.289
Hipernik (50% Ni)	8.25	0.298
4% Si	7.6	0.27
10.27% Si	6.97	0.252
Stainless steels and heat-resistant alloys		
Corrosion-resistant steel castings		
CA-15	7.612	0.2750
CA-40	7.612	0.2750
CB-30	7.53	0.272
CC-50	7.53	0.272
CE-30	7.67	0.277
CF-8	7.75	0.280
CF-20	7.75	0.280
CF-8M, CF-12M	7.75	0.280
CF-8C	7.75	0.280
CF-16F	7.75	0.280
CH-20	7.72	0.279
CK-20	7.75	0.280
CN-7M	8.00	0.289

(a) 6.95 to 7.35 g/cm³ (0.251 to 0.265 lb/in.³). (b) 7.20 to 7.34 g/cm³ (0.260 to 0.265 lb/in.³). (c) Annealed. (d) As cast. (e) Face-centered cubic. (f) Hexagonal. (g) Body-centered cubic. (h) Close-packed hexagonal. (j) Rhombohedral

TABLE 3.7 DENSITIES OF METALS (CONTINUED)

Metal or alloy	Density g/cm³	Density lb/in.³
Heat-resistant alloy castings		
HA	7.72	0.279
HC	7.53	0.272
HD	7.58	0.274
HE	7.67	0.277
HF	7.75	0.280
HH	7.72	0.279
HI	7.72	0.279
HK	7.75	0.280
HL	7.72	0.279
HN	7.83	0.283
HT	7.92	0.286
HU	8.04	0.290
HW	8.14	0.294
HX	8.14	0.294
Wrought stainless and heat-resisting steels		
Type 301	7.9	0.29
Type 302	7.9	0.29
Type 302B	8.0	0.29
Type 303	7.9	0.29
Type 304	7.9	0.29
Type 305	8.0	0.29
Type 308	8.0	0.29
Type 309	7.9	0.29
Type 310	7.9	0.29
Type 314	7.72	0.279
Type 316	8.0	0.29
Type 317	8.0	0.29
Type 321	7.9	0.29
Type 347	8.0	0.29
Type 403	7.7	0.28
Type 405	7.7	0.28
Type 410	7.7	0.28
Type 416	7.7	0.28
Type 420	7.7	0.28
Type 430	7.7	0.28
Type 430F	7.7	0.28
Type 431	7.7	0.28
Types 440A, 440B, 440C	7.7	0.28
Type 446	7.6	0.27
Type 501	7.7	0.28
Type 502	7.8	0.28
19-9DL	7.97	0.29
Precipitation-hardening stainless steels		
PH15-7 Mo	7.804	0.2819
17-4 PH	7.8	0.28
17-7 PH	7.81	0.282
Nickel-base alloys		
D-979	8.27	0.299
Nimonic 80A	8.25	0.298
Nimonic 90	8.27	0.299
M-252	8.27	0.298
Inconel	8.51	0.307
Inconel "X" 550	8.30	0.300
Inconel 700	8.17	0.295
Inconel "713C"	7.913	0.2859
Waspaloy	8.23	0.296
René 41	8.27	0.298
Hastelloy alloy B	9.24	0.334
Hastelloy alloy C	8.94	0.323
Hastelloy alloy X	8.23	0.297
Udimet 500	8.07	0.291
GMR-235	8.03	0.290
Cobalt-chromium-nickel-base alloys		
N-155 (HS-95)	8.23	0.296
S-590	8.36	0.301
Cobalt-base alloys		
S-816	8.68	0.314
V-36	8.60	0.311
HS-25	9.13	0.330
HS-36	9.04	0.327
HS-31	8.61	0.311
HS-21	8.30	0.300
Molybdenum-base alloy		
Mo-0.5Ti	10.2	0.368
Lead and lead alloys		
Chemical lead (99.90+% Pb)	11.34	0.4097
Corroding lead (99.73+% Pb)	11.36	0.4104
Arsenical lead	11.34	0.4097
Calcium lead	11.34	0.4097
5-95 solder	11.0	0.397
20-80 solder	10.2	0.368
50-50 solder	8.89	0.321
Antimonial lead alloys		
1% antimonial lead	11.27	0.407
Hard lead (96Pb-4Sb)	11.04	0.399
Hard lead (94Pb-6Sb)	10.88	0.393
8% antimonial lead	10.74	0.388
9% antimonial lead	10.66	0.385
Lead-base babbitt alloys		
Lead-base babbitt		
SAE 13	10.24	0.370
SAE 14	9.73	0.352
Alloy 8	10.04	0.363
Arsenical lead		
Babbitt (SAE 15)	10.1	0.365
"G" Babbitt	10.1	0.365
Magnesium and magnesium alloys		
Magnesium (99.8%)	1.738	0.06279
Casting alloys		
AM100A	1.81	0.065
AZ63A	1.84	0.066
AZ81A	1.80	0.065
AZ91A, B, C	1.81	0.065
AZ92A	1.82	0.066
HK31A	1.79	0.065
HZ32A	1.83	0.066
ZH42, ZH62A	1.86	0.067
ZK51A	1.81	0.065
ZE41A	1.82	0.066
EZ33A	1.83	0.066
EK30A	1.79	0.065
EK41A	1.81	0.065
Wrought alloys		
M1A	1.76	0.064
A3A	1.77	0.064
AZ31B	1.77	0.064
PE	1.76	0.064
AZ61A	1.80	0.065
AZ80A	1.80	0.065
ZK60A, B	1.83	0.066
ZE10A	1.76	0.064
HM21A	1.78	0.064
HM31A	1.81	0.065
Nickel and nickel alloys		
Nickel (99.95% Ni + Co)	8.902	0.322
"A" Nickel	8.885	0.321
"D" Nickel	8.78	0.317
Duranickel	8.26	0.298
Cast nickel	8.34	0.301
Monel	8.84	0.319
"K" Monel	8.47	0.306
Monel (cast)	8.63	0.312
"H" Monel (cast)	8.5	0.31
"S" Monel (cast)	8.36	0.302
Inconel	8.51	0.307
Inconel (cast)	8.3	0.30
Ni-o-nel	7.86	0.294
Nickel-molybdenum-chromium-iron alloys		
Hastelloy B	9.24	0.334
Hastelloy C	8.94	0.323
Hastelloy D	7.8	0.282
Hastelloy F	8.17	0.295
Hastelloy N	8.79	0.317
Hastelloy W	9.03	0.326
Hastelloy X	8.23	0.297
Nickel-chromium-molybdenum-copper alloys		
Illium G	8.58	0.310
Illium R	8.58	0.310
Electrical resistance alloys		
80Ni-20Cr	8.4	0.30
60Ni-24Fe-16Cr	8.247	0.298
35Ni-45Fe-20Cr	7.95	0.287
Constantan	8.9	0.32
Tin and tin alloys		
Pure tin	7.3	0.264
Soft solder (30% Pb)	8.32	0.301
Soft solder (37% Pb)	8.42	0.304
Tin babbitt		
Alloy 1	7.34	0.265
Alloy 2	7.39	0.267
Alloy 3	7.46	0.269
Alloy 4	7.53	0.272
Alloy 5	7.75	0.280
White metal	7.28	0.263
Pewter	7.28	0.263
Titanium and titanium alloys		
99.9% Ti	4.507	0.1628
99.2% Ti	4.507	0.1628
99.0% Ti	4.52	0.163
Ti-6Al-4V	4.43	0.160
Ti-5Al-2.5Sn	4.46	0.161
Ti-2Fe-2Cr-2Mo	4.65	0.168
Ti-8Mn	4.71	0.171
Ti-7Al-4Mo	4.48	0.162
Ti-4Al-4Mn	4.52	0.163
Ti-4Al-3Mo-1V	4.507	0.1628
Ti-2.5Al-16V	4.65	0.168
Zinc and zinc alloys		
Pure zinc	7.133	0.2577
AG40A alloy	6.6	0.24
AC41A alloy	6.7	0.24

(a) 6.95 to 7.35 g/cm³ (0.251 to 0.265 lb/in.³). (b) 7.20 to 7.34 g/cm³ (0.260 to 0.265 lb/in.³). (c) Annealed. (d) As cast. (e) Face-centered cubic. (f) Hexagonal. (g) Body-centered cubic (h) Close-packed hexagonal. (j) Rhombohedral

TABLE 3.7 DENSITIES OF METALS (CONTINUED)

Metal or alloy	Density g/cm³	Density lb/in.³
Commercial rolled zinc		
0.08% Pb	7.14	0.258
0.06 Pb, 0.06 Cd	7.14	0.258
0.3 Pb, 0.3 Cd	7.14	0.258
Copper-hardened, rolled zinc (1% Cu)	7.18	0.259
Rolled zinc alloy (1 Cu, 0.010 Mg)	7.18	0.259
Zn-Cu-Ti alloy (0.8 Cu, 0.15 Ti)	7.18	0.259
Precious metals		
Silver	10.49	0.379
Gold	19.32	0.698
70Au-30Pt	19.92	...
Platinum	21.45	0.775
Pt-3.5Rh	20.9	...
Pt-5Rh	20.65	...
Pt-10Rh	19.97	...
Pt-20Rh	18.74	...
Pt-30Rh	17.62	...
Pt-40Rh	16.63	...
Pt-5Ir	21.49	...
Pt-10Ir	21.53	...
Pt-15Ir	21.57	...
Pt-20Ir	21.61	...
Pt-25Ir	21.66	...
Pt-30Ir	21.70	...
Pt-35Ir	21.79	...
Pt-5Ru	20.67	...
Pt-10Ru	19.94	...
Palladium	12.02	0.4343
60Pd-40Cu	10.6	0.383
95.5Pd-4.5Ru	12.07(a)	...
95.5Pd-4.5Ru	11.62(b)	...

Metal or alloy	Density g/cm³	Density lb/in.³
Permanent magnet materials		
Cunico	8.30	0.300
Cunife	8.61	0.311
Comol	8.16	0.295
Alnico I	6.89	0.249
Alnico II	7.09	0.256
Alnico III	6.89	0.249
Alnico IV	7.00	0.253
Alnico V	7.31	0.264
Alnico VI	7.42	0.268
Barium ferrite	4.7	0.17
Vectolite	3.13	0.113
Pure metals		
Antimony	6.62	0.239
Beryllium	1.848	0.067
Bismuth	9.80	0.354
Cadmium	8.65	0.313
Calcium	1.55	0.056
Cesium	1.903	0.069
Chromium	7.19	0.260
Cobalt	8.85	0.322
Gallium	5.907	0.213
Germanium	5.323	0.192
Hafnium	13.1	0.473
Indium	7.31	0.264
Iridium	22.5	0.813
Lithium	0.534	0.019
Manganese	7.43	0.270
Mercury	13.546	0.489
Molybdenum	10.22	0.369
Niobium	8.57	0.310
Osmium	22.583	0.816
Plutonium	19.84	0.717
Potassium	0.86	0.031
Rhenium	21.04	0.756

Metal or alloy	Density g/cm³	Density lb/in.³
Rhodium	12.44[c]	0.447
Ruthenium	12.2	0.441
Selenium	4.79	0.174
Silicon	2.33	0.084
Silver	10.49	0.379
Sodium	0.97	0.035
Tantalum	16.6	0.600
Thalium	11.85	0.428
Thorium	11.72	0.423
Tungsten	19.3	0.697
Uranium	19.07	0.689
Vanadium	6.1	0.22
Zirconium	6.5	0.23
Rare earth metals		
Cerium	8.23(c)	...
Cerium	6.66(d)	...
Cerium	6.77(e)	...
Dysprosium	8.55(f)	...
Erbium	9.15(f)	...
Europium	5.245(e)	...
Gadolinium	7.86(f)	...
Holmium	6.79(f)	...
Lanthanum	6.19(d)	...
Lanthanum	6.18(c)	...
Lanthanum	5.97(e)	...
Lutetium	9.85(f)	...
Neodymium	7.00(d)	...
Neodymium	6.80(e)	...
Praseodymium	6.77(d)	...
Praseodymium	6.64(e)	...
Samarium	7.49(g)	...
Scandium	2.99(f)	...
Terbium	8.25(f)	...
Thulium	9.31(f)	...
Ytterbium	6.96(c)	...
Yttrium	4.47(f)	...

(a) 6.95 to 7.35 g/cm³ (0.251 to 0.265 lb/in.³). (b) 7.20 to 7.34 g/cm³ (0.260 to 0.265 lb/in.³). (c) Face-centered cubic. (d) Hexagonal. (e) Body-centered cubic. (f) Close-packed hexagonal. (g) Rhombohedral

stresses are neglected in Code calculations, since they are zero at the outer wall, and bending is unaffected.

The reaction force at an elbow or pipe cap equals the pressure times the internal cross-sectional area, but this force is usually countered by an opposing force in steady-state systems. For example, a force is exerted on an elbow in line with a pump discharge, but an equal force is exerted against the pump, and the net resultant force of the axial pipe reactions is zero. For a 6-in. pipe discharging from a pump to an elbow at 200 psi (D = 6.225 in.), axial forces exist at both the elbow and the pump equal to $200 \cdot \pi \cdot D^2/4 = 6087$ lb, but the forces are balanced. However, the use of a bellows expansion joint to compensate thermal growth or equipment vibration may cause significant reaction forces. Since the pipe ends are disconnected from each other by the bellows, the approximate reaction force at each pipe end equals the pressure in the pipe times the mean diameter of the bellows (U. S. Bellows). If a bellows with a 7.0-in. OD and a 6-in. inside diameter is used for the 6-in. pipe of this example, the axial reaction at

TABLE 3.8 TYPICAL PLASTIC DENSITIES (Kutz [130])

Material	Density, lbm/ft³	Material	Density, lbm/ft³
Polyvinyl chloride, PVC	83.5–91	Polypropylene	56.1–56.7
PVC 1120 (Harvel, Inc.)	91	Polyethylene, PE, HDPE	59.8–60.4
CPVC (Harvel, Inc.)	93.5	ABS	65.4–66.7
Poly(tetraflouroethylene) PTFE, Teflon®	134.6	Poly (fluorinated ethylene-propylene) FEP	133.9

TABLE 3.9 THERMAL EXPANSION COEFFICIENTS AT 70°F (ASME B31.3)

Carbon steel, Carbon moly low chrome (through 3Cr-Mo) 10^{-6} in./(in·°F)	5Cr-Mo through 9Cr-Mo 10^{-6} in./(in·°F)	Austenitic stainless steels 10^{-6} in./(in·°F)	12Cr, 17Cr, 27Cr 10^{-6} in./(in·°F)
6.07	5.73	9.11	5.24
UNS N40440 Monel 67Ni-30Cu	3½ Ni	Copper and copper alloys	Aluminum
7.48	6.25	9.32	12.25
Bronze	Brass	70Cu-30Ni	Ductile iron
9.57	9.34	8.16	5.74
CPVC 4120	PVC1120	PVC1220	PVC2110
35	30	35	50

both pipe ends would equal 6637 lb. Applying B31.3, the required bellows diameter equals the outside diameter, and the reaction force equals 7697 lb.

In addition to pressure-induced axial forces, a velocity-induced axial force is also present at elbows and changes in pipe flow direction, but these axial stresses due to a change in flow direction are typically negligible. For example, Bernoulli's equation shows that a 10 ft per second flow rate impinging on a nominal 6-in. elbow yields a minor force of 19.16 lb, where

$$F(\text{lbf}) = \frac{V^2 \cdot A}{2 \cdot g} = \frac{V^2 \cdot A}{2 \cdot 32.2\left(\text{ft/second}^2\right) \cdot 2.31(\text{ft/psi})}$$

$$= \frac{10^2 \cdot \pi \cdot D^2/4}{2 \cdot 32.2\left(\text{ft/second}^2\right) \cdot 2.31(\text{ft/psi})} = 19.16\_\text{lbf}$$

However, larger axial forces are sometimes exerted on pipe systems. The total axial force is described by

$$F = \pi \cdot \frac{D^2}{2} \cdot \left(\rho_L \cdot \frac{V^2}{g} + P\right) \cdot \cos\left(\frac{\theta}{2}\right) \quad \text{US, EE, SI (3.37)}$$

where θ is the angle between pipe centerlines, and F is the resultant force at an angle θ/2 with respect to the pipe centerline. The effect of pressure losses and changes in velocity on the resultant force is neglected.

3.3.7.2 Restraint and Control of Forces These pipe reactions may be reduced by using thrust blocks, pipe supports, or pressure-equalizing bellows, as shown in Fig. 3.36. Vendors should be contacted for bellows application and fatigue data. Similarly, for an open-ended pressurized pipe, unbalanced forces are present since an opposing force is absent at the open end of the pipe. Although unbalanced forces are the crux of this text with respect to fluid transients in pipes, unbalanced forces similar to an open-end pipe are responsible for other industrial accidents. In particular, industrial personnel have been injured when a hose is quickly pressurized, and an unbalanced force caused an unrestrained hose to whip uncontrollably. In fact, hose whip is an example of a fluid transient.

3.3.7.3 Reactions and Pipe Stresses As noted, a flexibility analysis is not required for all systems, and computer programs are often used to perform flexibility analyses, but graphic calculations provide ready insight into flexibility to find pipe stresses for simple systems, like expansion loops and fixed-end pipes. To present some typical pipe configurations, graphs for fixed-end pipes are shown in Figs. 3.37, 3.38, 3.39, and 3.40 for cases of thermal pipe expansion and pipe displacement due to pipe end displacements. The reader is referred to Kellogg [133], McKetta [76], and Crocker and King [77] for hand calculation techniques and additional graphs of moments and forces in thermal expansion loops, which compensate thermal expansion and discussions of rotating joints to increase flexibility. Other piping design references include Peng and Peng [135], Kannapann [136], and Grinnel [137]. Kellogg noted that the assumption of fixed restraints can lead to overdesigned nozzles on attached pressure vessels since the vessel flexibility reduces the stiffness at the attachment flange. Even so, these figures conveniently provide maximum predicted stresses. To use the figures, the pipe is assumed to change by a total length,

$$\Delta = \alpha \cdot 12 \cdot L \cdot \Delta T = e \cdot L \quad \text{US, EE, SI (3.38)}$$

where α is the thermal expansion coefficient from Table 3.9, and e is the total strain (in./ft). Other terms are defined as required in the figures.

TABLE 3.10 QUALITY FACTORS, *E″* (ASME B31.3)

Spec. No.	Class (or Type)	Description	E_j (2)
Carbon Steel			
API 5L	...	Seamless pipe	1.00
		Electric resistance welded pipe	0.85
		Electric fusion welded pipe, double butt, straight or spiral seam	0.95
		Furnace butt welded	0.60
A 53	Type S	Seamless pipe	1.00
	Type E	Electric resistance welded pipe	0.85
	Type F	Furnace butt welded pipe	0.60
A 105	...	Forgings and fittings	1.00
A 106	...	Seamless pipe	1.00
A 134	...	Electric fusion welded pipe, single butt, straight or spiral seam	0.80
A 135	...	Electric resistance welded pipe	0.85
A 139	...	Electric fusion welded pipe, straight or spiral seam	0.80
A 179	...	Seamless tube	1.00
A 181	...	Forgings and fittings	1.00
A 234	...	Seamless and welded fittings	1.00
A 333	...	Seamless pipe	1.00
		Electric resistance welded pipe	0.85
A 334	...	Seamless tube	1.00
A 350	...	Forgings and fittings	1.00
A 369	...	Seamless pipe	1.00
A 381	...	Electric fusion welded pipe, 100% radiographed	1.00
		Electric fusion welded pipe, spot radiographed	0.90
		Electric fusion welded pipe, as manufactured	0.85
A 420	...	Welded fittings, 100% radiographed	1.00
A 524	...	Seamless pipe	1.00
A 587	...	Electric resistance welded pipe	0.85
A 671	12, 22, 32, 42, 52	Electric fusion welded pipe, 100% radiographed	1.00
	13, 23, 33, 43, 53	Electric fusion welded pipe, double butt seam	0.85
A 672	12, 22, 32, 42, 52	Electric fusion welded pipe, 100% radiographed	1.00
	13, 23, 33, 43, 53	Electric fusion welded pipe, double butt seam	0.85
A 691	12, 22, 32, 42, 52	Electric fusion welded pipe, 100% radiographed	1.00
	13, 23, 33, 43, 53	Electric fusion welded pipe, double butt seam	0.85
Low and Intermediate Alloy Steel			
A 182	...	Forgings and fittings	1.00
A 234	...	Seamless and welded fittings	1.00
A 333	...	Seamless pipe	1.00
		Electric resistance welded pipe	0.85
A 334	...	Seamless tube	1.00
A 335	...	Seamless pipe	1.00
A 350	...	Forgings and fittings	1.00
A 369	...	Seamless pipe	1.00
A 420	...	Welded fittings, 100% radiographed	1.00
A 671	12, 22, 32, 42, 52	Electric fusion welded pipe, 100% radiographed	1.00
	13, 23, 33, 43, 53	Electric fusion welded pipe, double butt seam	0.85

TABLE 3.11 WELD JOINT STRENGTH REDUCTION FACTOR, *W*′ (ASME B31.3)

Steel Group	Component Temperature, T_i, °C (°F)														
	427 (800)	454 (850)	482 (900)	510 (950)	538 (1,000)	566 (1,050)	593 (1,100)	621 (1,150)	649 (1,200)	677 (1,250)	704 (1,300)	732 (1,350)	760 (1,400)	788 (1,450)	816 (1,500)
CrMo [Notes (1)–(3)]	1	0.95	0.91	0.86	0.82	0.77	0.73	0.68	0.64	...	...	...	...	...	...
CSEF (N + T) [Notes (3)–(5)]	...	...	...	1	0.95	0.91	0.86	0.82	0.77	...	...	...	...	...	...
CSEF [Notes (3) and (4)] (Subcritical PWHT)	...	...	1	0.5	0.5	0.5	0.5	0.5	0.5	...	...	...	...	...	...
Autogenous welds in austenitic stainless grade 3xx, and N088xx and N066xx nickel alloys [Note (6)]	...	...	...	1	1	1	1	1	1	1	1	1	1	1	1
Austenitic stainless grade 3xx and N088xx nickel alloys [Notes (7) and (8)]	...	...	...	1	0.95	0.91	0.86	0.82	0.77	0.73	0.68	0.64	0.59	0.55	0.5
Other materials [Note (9)]	...	...	...	...	...	...	...	...	...	...	...	...	...	...	...

Following Kellogg, Mcketta [76] provided several examples of hand calculations to determine the maximum moments and stresses in two anchor systems without intermediate supports for any piping geometry between the supports. One of his recommended techniques provides equations for the maximum force and moment, which lie in a plane along the axis between two fixed pipe supports, as shown in Fig. 3.41, where L_s is the distance between the supports, and L is the developed length of the pipe between supports compensated for length reductions at elbows.

$$F = \frac{E(\text{psi})I(\text{in}^4)\cdot\Delta(\text{in})\cdot 2900}{L_s^3(\text{ft}^3)\cdot 1728\left(\frac{\text{in}^3}{\text{ft}^3}\right)\cdot\left(\frac{L(\text{ft})}{L_s(\text{ft})}\right)^8} \qquad \text{US, EE, SI (3.39)}$$

$$M = \frac{\left(\frac{L}{L_s}\right)^{4.83}\cdot F\cdot L_s}{50} \qquad \text{US, EE, SI (3.40)}$$

Beam deflection equations can approximate pipe forces and moments when the pipe is guided, as shown in Fig. 3.41. The actual bending stresses are less since some rotation is expected, which reduces stress at the elbow.

The deflection equations (Young and Budynas [132]) describing a force applied at an elbow are

$$\Delta = \frac{F\cdot L''^3}{12\cdot E\cdot I} \qquad \text{US, EE, SI (3.41)}$$

$$M_i = \frac{F\cdot L''}{2} \qquad \text{US, EE, SI (3.42)}$$

At point A,

$$S_b = \frac{i_i\cdot M_i}{Z} \qquad \text{US, EE, SI (3.43)}$$

where i_i is the stress intensification factor. At point B,

$$S_b = \frac{M_i}{Z} \qquad \text{US, EE, SI (3.44)}$$

Depending on the design of the guide, localized contact stresses may also occur at point B. Equations for guided supports may be combined with Kellogg's charts to approximate bending stresses in simple systems.

To find bending stresses in an open-end pipe (Fig. 3.43), formulas for a cantilevered beam from Young and Budynas [132] may be used.

$$\Delta = \frac{F\cdot L''^3}{3\cdot E\cdot I} \qquad \text{US, EE, SI (3.45)}$$

$$S_b = \frac{F\cdot L''}{Z} \qquad \text{US, EE, SI (3.46)}$$

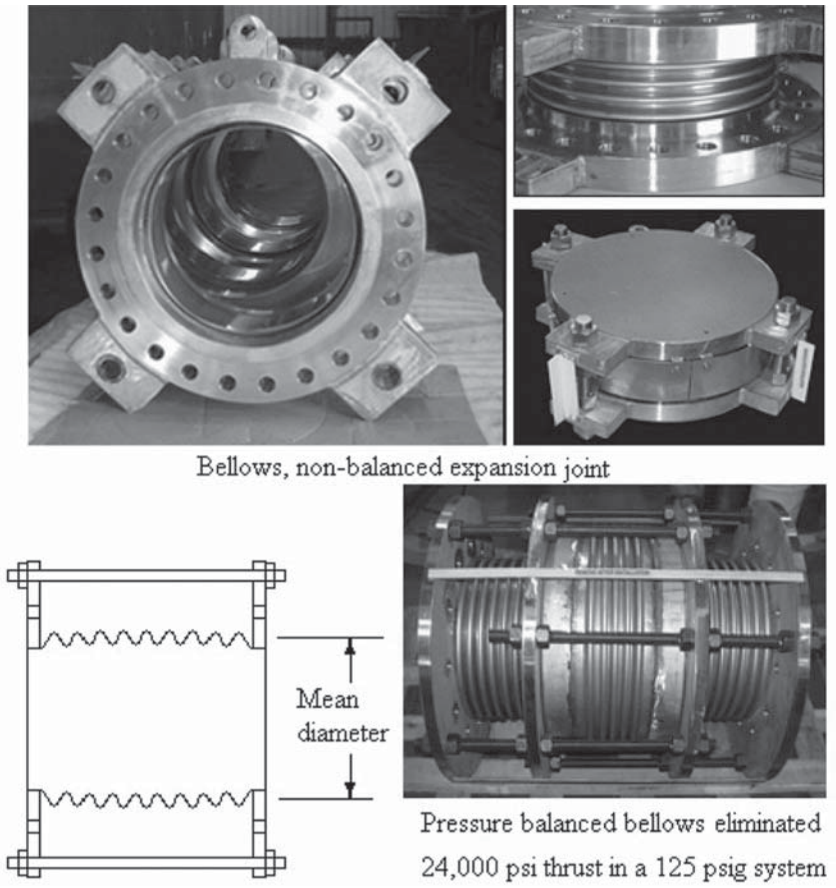


FIG. 3.36 BELLOWS (Reprinted by permission of (U. S. Bellows, Inc.)

3.3.7.4 Torsional Stresses and Moments Similar calculations for simple pipe systems may be performed to analyze torsion or pipes with free ends by applying the provided figures and equations. As mentioned, computer codes are typically used for flexibility analyses on complex pipe systems. When the moment, or torque, is calculated, maximum torsional shear stresses at the outer pipe wall are determined using the pipe wall minimum thickness, according to the equations

$$S_T = \frac{M \cdot (r_o - r_i)}{J} = \frac{2 \cdot M}{\pi \cdot \left(r_o^3 - r_i^3\right)} \quad \text{US, EE, SI (3.47)}$$

$$J = \frac{\pi \cdot \left(r_o^4 - r_i^4\right)}{2} \quad \text{US, EE, SI (3.48)}$$

where S_T is the torsional stress, and J is the polar moment of inertia.

3.3.7.5 Pipe Stresses Due to Pipe and Fluid Weights Stresses due to fluid weight can be calculated, but to simplify design, Table 3.12 for pipe support spacing is available from ASME B31.1 [138]. Figs. 3.44 and 3.45 provide pipe stresses due to pipe weight for a water-filled or empty pipe. Support spacings in MSS SP-127 [134], which is applicable to B31.3 design.

3.3.7.6 Stress Intensification Factors Stresses in elbows and other pipe fittings are larger than expected since the fittings flex under load. Locally, the stresses increase as the outer fibers of the pipe fitting stretch. To account for this additional flexural stress, Markl adapted fatigue test data to determine stress intensification factors, where k equals a flexibility factor, and i equals a stress intensification factor. These factors were incorporated into B31.3 (Figs. 3.46 and 3.47), but B31.3 Committee efforts are in process to update their application and values.

3.3.7.7 Flexibility Calculation Example There are numerous techniques available to calculate pipe stresses, depending on the reference text or FEA program used for

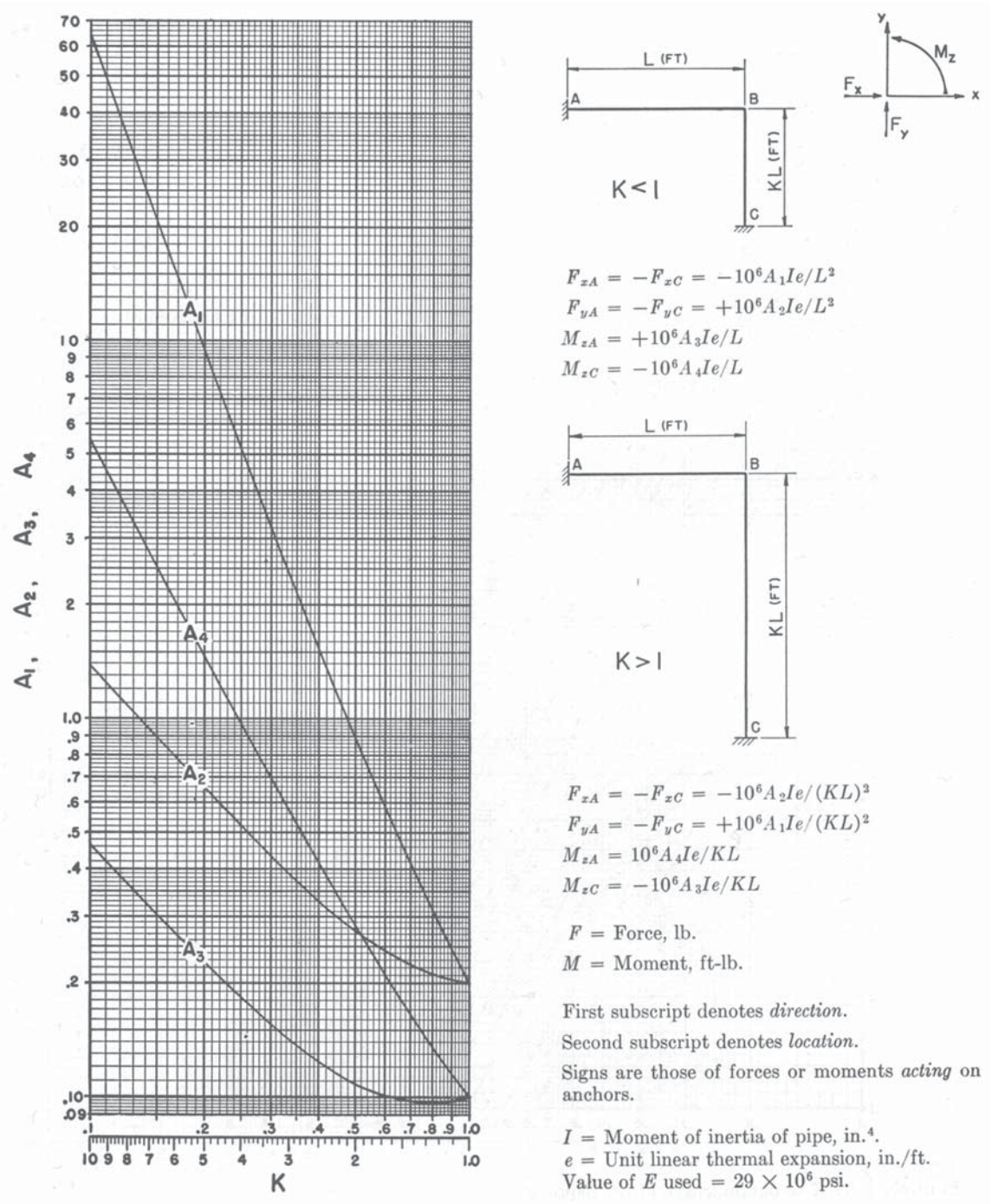


FIG. 3.37 THERMAL STRESSES FOR A PIPE WITH FIXED ENDS (Kellogg [133])

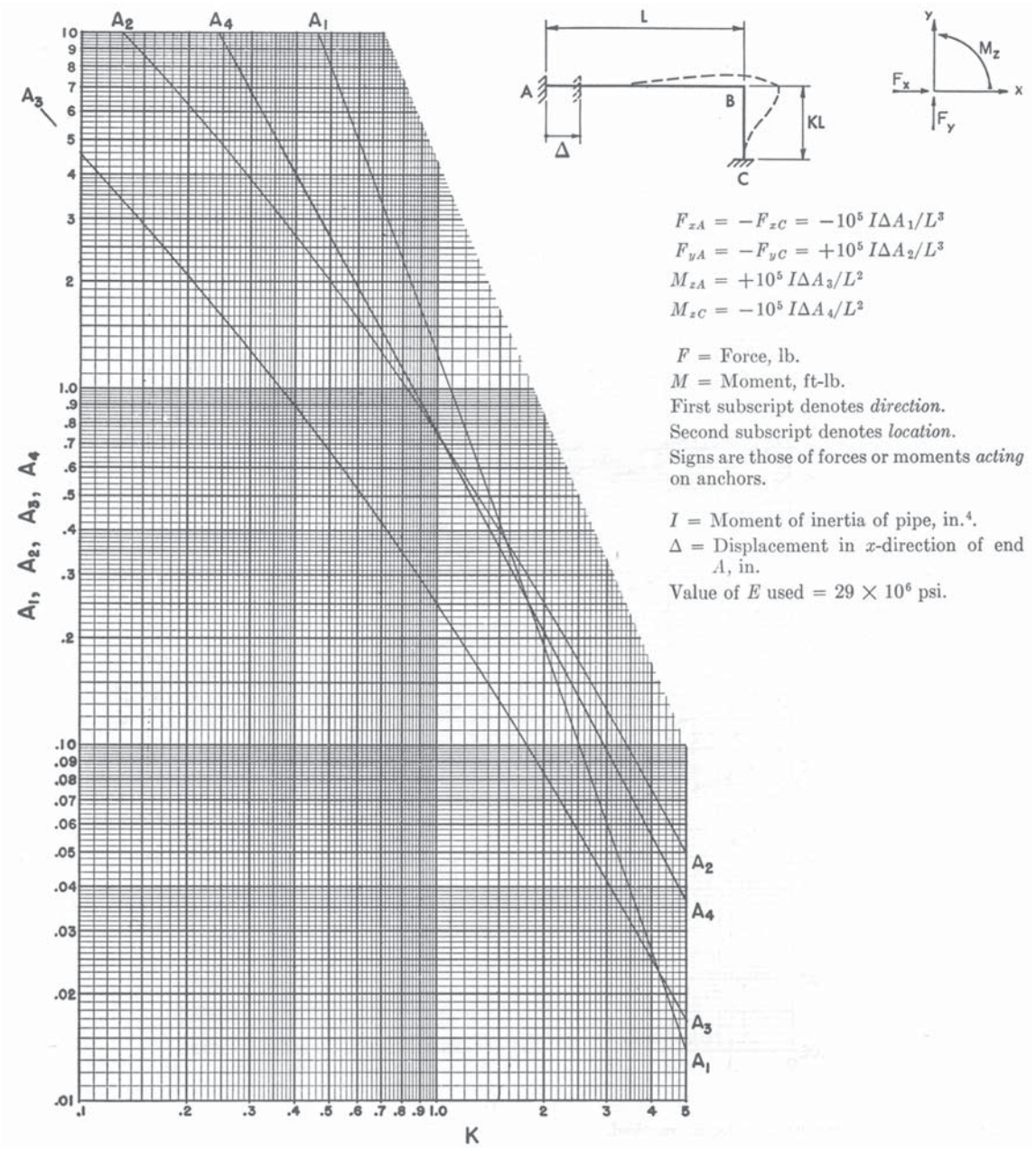


FIG. 3.38 BENDING STRESSES DUE TO DISPLACEMENT OF A PIPE END (Kellogg [133])

the calculation. One type of calculation follows to determine stresses due to thermal expansion.

Example 3.7, Flexibility calculation.

Determine the stresses due to thermal expansion using Fig. 3.37 for ASTM A106, Grade A, 0.25% carbon, 6 NPS, Schedule 40 pipe and long radius elbows, operating at 200°F. Assume a corrosion allowance of 0.065 in., a mill tolerance of 12.5%, and a thermal expansion coefficient of $e = 6.07 \cdot 10^{-6} \cdot 12 \cdot 100 = 0.007$. For A106 steel, $E = 28.8 \cdot 10^6$ at 200°F and $29.5 \cdot 10^6$ at 70°F. Let $L = 10$ ft, $K = 1.2$, and KL = 12 ft. Using Fig. 3.37, the error in stress magnitude due to the difference in elastic modulus at different temperatures is negligible since $E = 28.8 \cdot 10^6$ for this example, the figure uses $E = 29 \cdot 10^6$ psi, and the deflections, forces, and moments are inversely proportional to the modulus of elasticity.

Thermal deflection is first required for both members (A-B and B-C), where

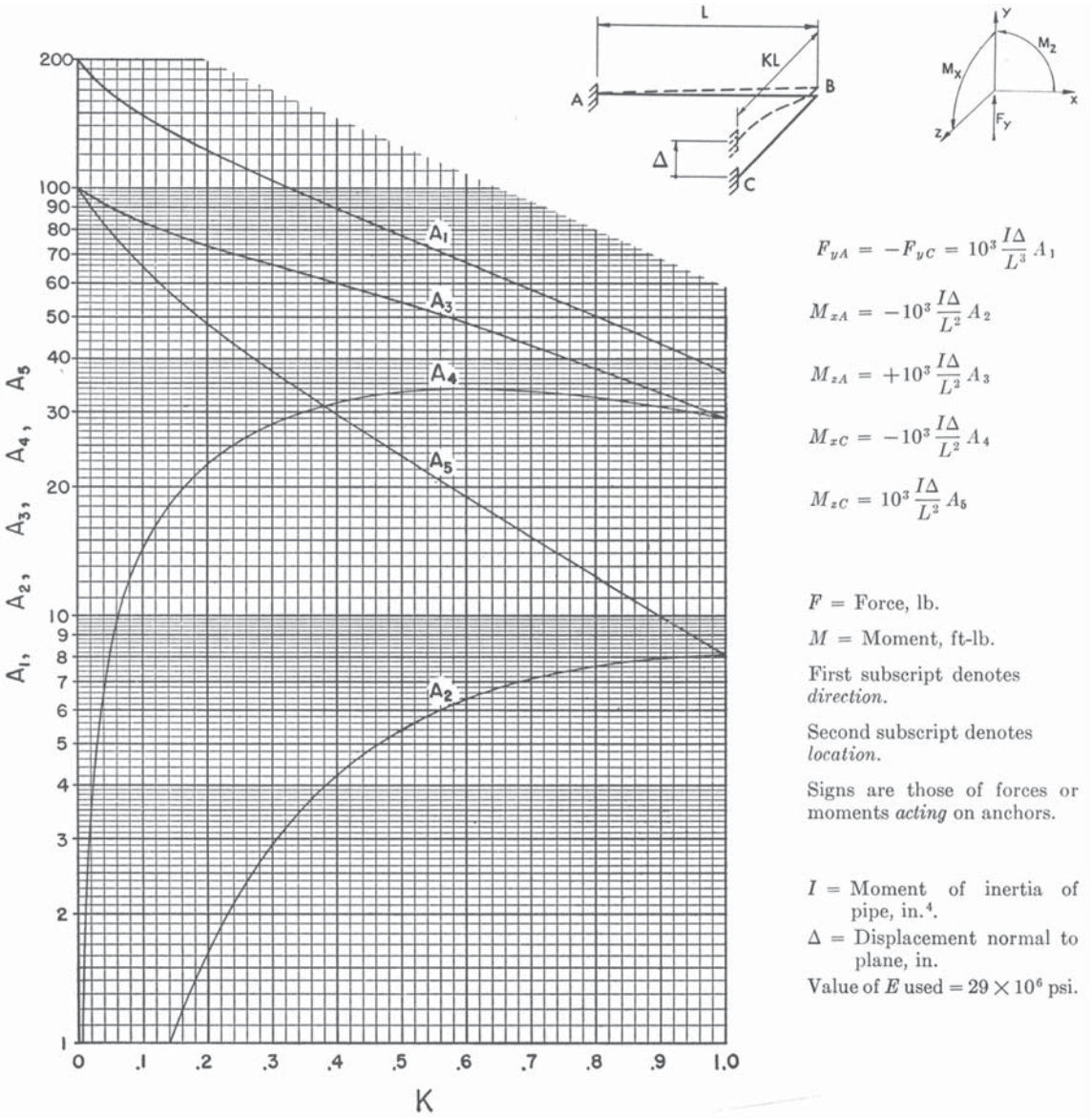


FIG. 3.39 TORSIONAL STRESSES DUE TO DISPLACEMENT OF A PIPE END (Kellogg [133])

$\Delta = \sum \delta L_i = \alpha \cdot 12 \cdot L \cdot \Delta T \cdot L \cdot \Delta T = (6.07 \cdot 10^{-6}) \cdot (200 - 70) \cdot (10 + 12) \cdot 12 = 0.208$ in.

From B31.3, a flexibility analysis is not required for this configuration, since

$$0.034 = \frac{6.625 \cdot 0.208}{\left(\left((10+12) - \left(\sqrt{10^2 + 12^2} \right) \right)^2 \right)}$$

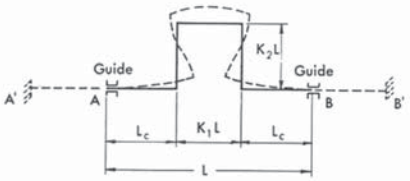
$$= \frac{\mathrm{OD} \cdot \Delta}{(L - L_s)^2} < \frac{30 \cdot S_A}{E_{70°F}} = \frac{30 \cdot 16{,}000}{29{,}500{,}000} = 0.163$$

However, a flexibility analysis is performed for this example to demonstrate calculation techniques.

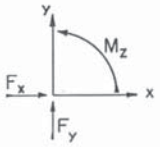
Since the inside and outside diameters are $D = 6.225$ and OD = 6.625 in., the moment of inertia equals

$$I = \frac{\pi \cdot (\mathrm{OD}^4 - D^4)}{64} = \frac{\pi \cdot (6.625^4 - 6.065^4)}{64} = 28.14 \_ \mathrm{in}^4$$

$$Z = \frac{2 \cdot \mathrm{I}}{\mathrm{OD}} = 8.495 \_ \mathrm{in}^3$$



$$F_{xA'} = -F_{xB'} = -10^6 A_1 I\Delta/L^3$$
$$M_{xA} = -M_{xB} = 10^5 A_2 I\Delta/L^2$$



I = Moment of inertia of pipe, in.^{4}.
Δ = Expansion from A' to B', in.
Value of E used = 29×10^6 psi.

F = Force, lb.
M = Moment, ft-lb.
First subscript denotes *direction*.
Second subscript denotes *location*.
Signs are those of forces or moments *acting* on anchors.

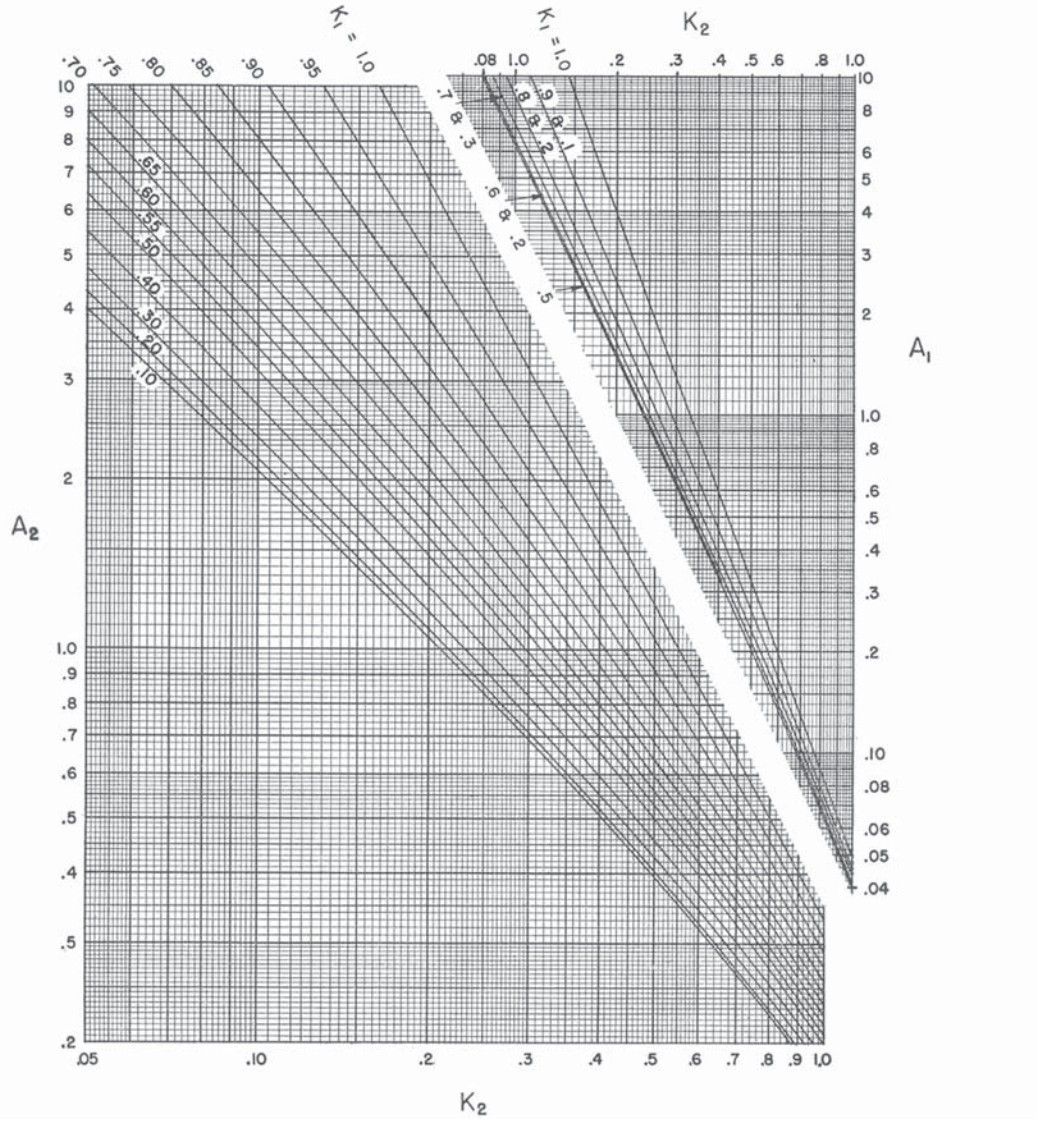


FIG. 3.40 PIPE STRESSES IN A LOOP RESTRAINED AT BOTH ENDS (Kellogg [133])

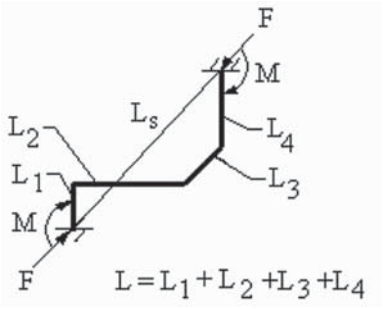


FIG. 3.41 MAXIMUM FORCE AND MOMENT DIAGRAM

From Fig. 3.37, $A_1 = 0.28$, $A_2 = 0.21$, $A_3 = 0.098$, and $A_4 = 0.13$. Then, the forces and moments at points A and B equal

$$F_{xA} = -10^6 \cdot A_2 \cdot I \cdot e/(\mathrm{KL})^2 = -299\_\mathrm{lbf}$$

$$F_{yA} = 10^6 \cdot A_1 \cdot I \cdot e/(\mathrm{KL})^2 = 399\_\mathrm{lbf}$$

$$M_{zA} = 10^6 \cdot A_4 \cdot I \cdot e/(\mathrm{KL}) = 2221\_\mathrm{ft-lbf}$$

$$M_{zC} = -10^6 \cdot A_3 \cdot I \cdot e/(\mathrm{KL}) = -1674\_\mathrm{ft-lbf}$$

To find the stresses at the elbow (point B), the sum of the moments for member A-B can be used, such that

$$\sum M_{zA} = 0 \Rightarrow 2221 - 10 \cdot 399 = -1769\_\mathrm{ft-lbf} = M_{zB}$$

To find the maximum stress at the elbow, the stress intensification factor requires consideration. The stress

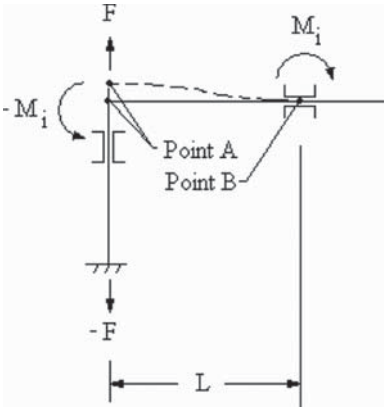


FIG. 3.42 PIPE STRESSES FOR PIPES WITH GUIDED SUPPORTS

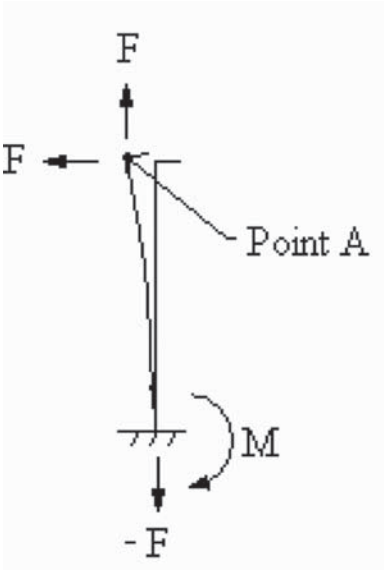


FIG. 3.43 STRESSES IN AN OPEN-END PIPE

intensification factor for in-plane bending of a 6-in. diameter elbow equals

$$i_i = \frac{0.9}{\left(\dfrac{\overline{T}_{\min} \cdot \mathrm{r}}{r_m^2}\right)^{2/3}} = 2.88$$

where r is the sweep radius to the elbow centerline (9 in.), and r_m is the mean radius of the pipe cross section (3.212 in.), and $\overline{T}_{\min}$ is the wall thickness (0.2 in.). Then,

$$S_A = \frac{M_{zA}}{Z} = 2221 \cdot 12/8.495 = 3137\_\mathrm{psi}$$

$$S_C = \frac{M_{zC}}{Z} = -1674 \cdot 12/8.495 = 2365\_\mathrm{psi}$$

$$S_B = \frac{i_1 \cdot M_{zB}}{Z} = 2.88 \cdot 1769 \cdot 12/8.495 = 7197\_\mathrm{psi}$$

Note that the maximum stress is much less than the 20-ksi allowable stress for A106 steel provided in Table 3.3, which was expected since flexibility analysis was not required for this piping design.

3.3.7.8 Comparison of Code Stress Calculations The use of different ASME codes presently yields different design stresses for identical design conditions. Antaki provided the following example to highlight this discrepancy. Even so, different design, fabrication, examination, and testing criteria for different Codes affects the design margins, and the design rules for each Code have been successfully applied during years of use.

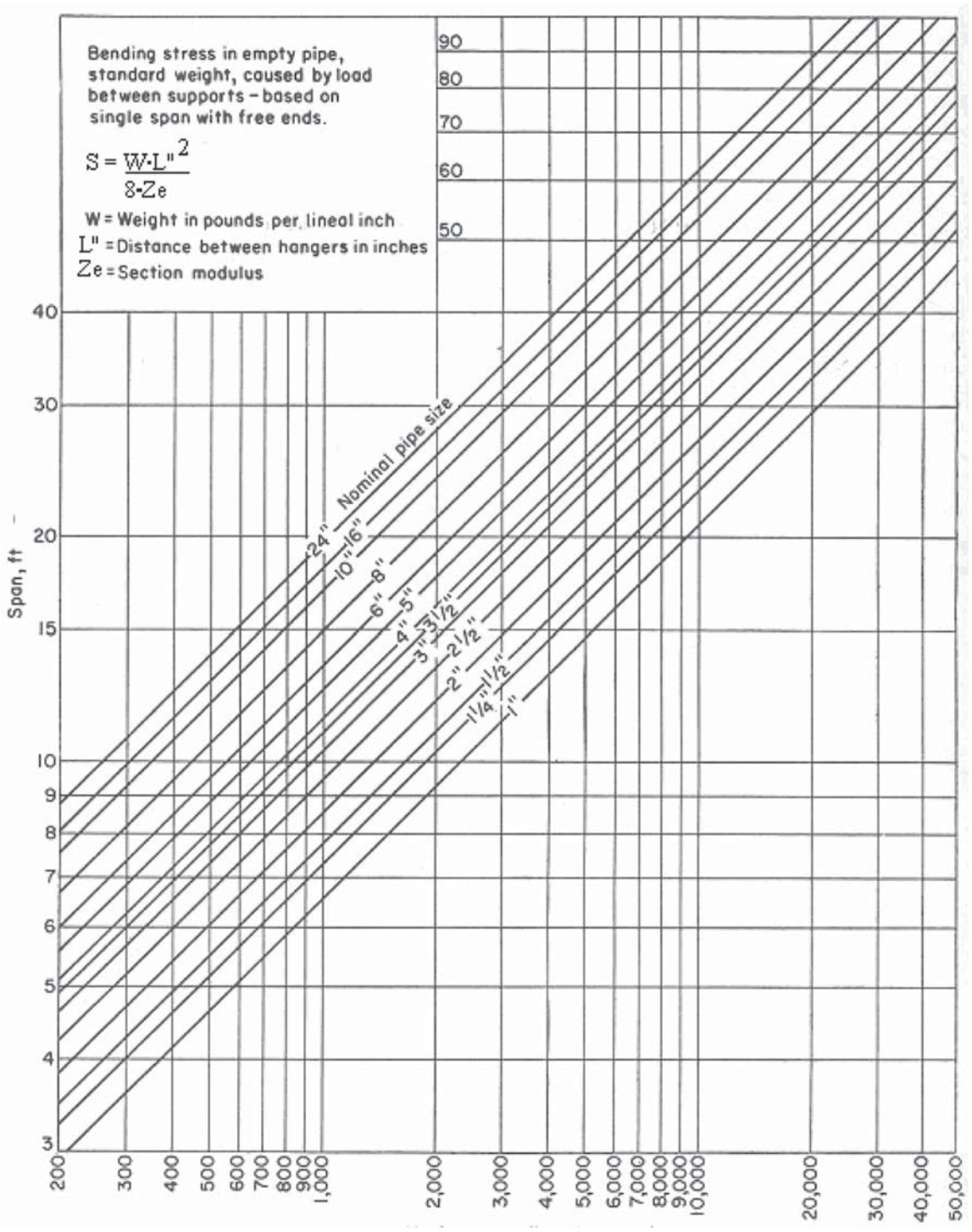


FIG. 3.44 BENDING STRESS IN WATER-FILLED PIPE (Crocker and King, Reprinted by permission of McGraw Hill)

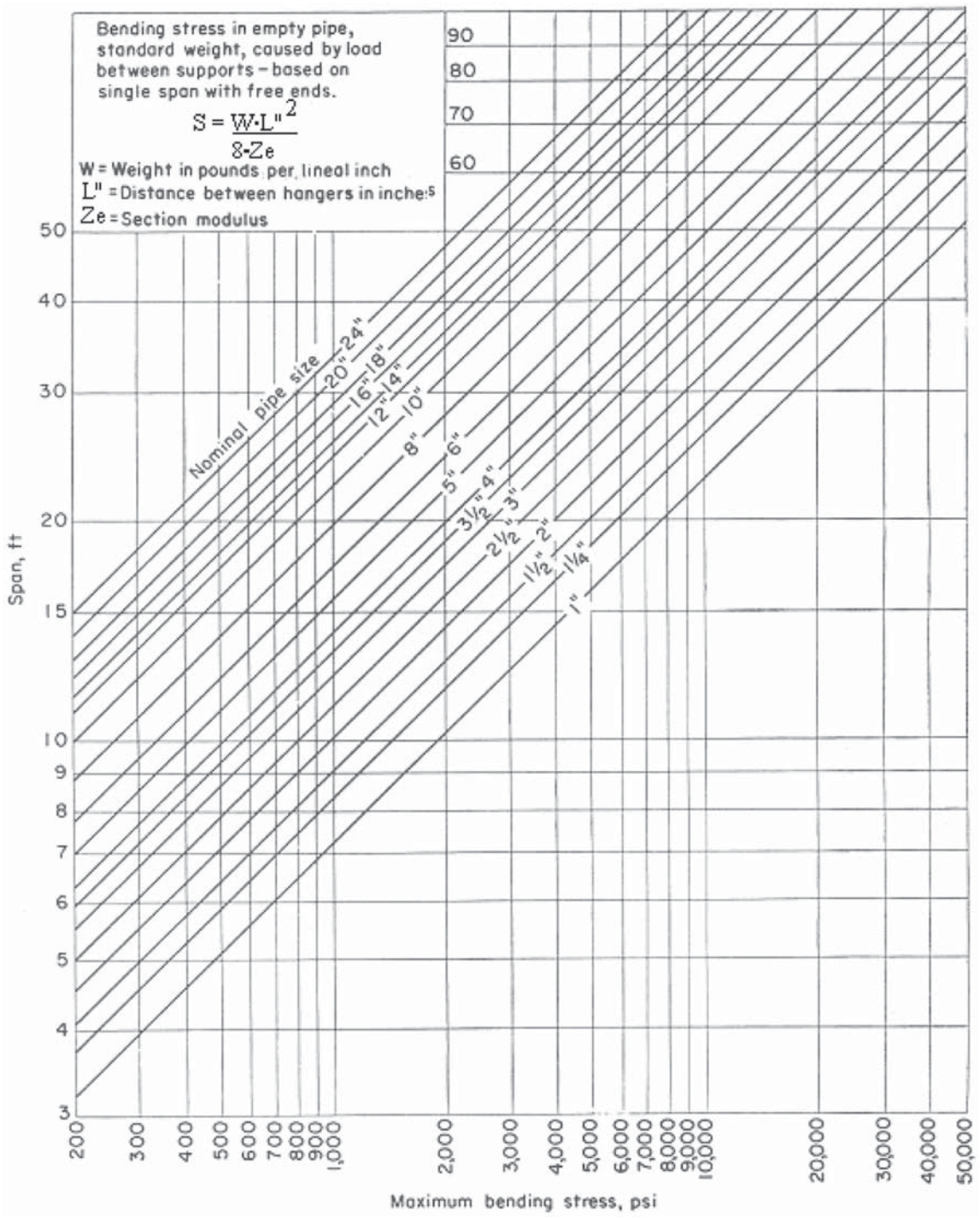


FIG. 3.45 BENDING STRESSES IN AN EMPTY PIPE (Crocker and King, Reprinted by permission of McGraw Hill)

Example 3.8 Design stresses using different ASME Codes (Antaki [139]).

The differences in equations and differences in allowable stresses between codes result in differences in design margins, as illustrated in Fig. 3.48. This example corresponds to a long radius elbow in a horizontal water-filled 3 inch Schedule 40 carbon steel pipe (3.5 inch OD, 0.216 inch wall). The loads from deadweight are M_o (out-of-plane moment in the horizontal elbow) of 2900 in-lb, with the other loads and

TABLE 3.12 SUPPORT SPACING FOR PIPE SYSTEMS (ASME B31.1 [138])

Nominal Pipe Size, NPS	Suggested Maximum Span			
	Water Service		Steam, Gas, or Air Service	
	ft	m	ft	m
1	7	2.1	9	2.7
2	10	3.0	13	4.0
3	12	3.7	15	4.6
4	14	4.3	17	5.2
6	17	5.2	21	6.4
8	19	5.8	24	7.3
12	23	7.0	30	9.1
16	27	8.2	35	10.7
20	30	9.1	39	11.9
24	32	9.8	42	12.8

GENERAL NOTES:

(a) Suggested maximum spacing between pipe supports for horizontal straight runs of standard and heavier pipe at maximum operating temperature of 750°F (400°C).

(b) Does not apply where span calculations are made or where there are concentrated loads between supports, such as flanges, valves, specialties, etc.

(c) The spacing is based on a fixed beam support with a bending stress not exceeding 2,300 psi (15.86 MPa) and insulated pipe filled with water or the equivalent weight of steel pipe for steam, gas, or air service, and the pitch of the line is such that a sag of 0.1 in. (2.5 mm) between supports is permissible.

moments, including the axial force, being zero. The system design pressure is 500 psi and its design temperature is 100 F. The design stress ratios are shown in the figure. For the B31.3 calculation summarized in Fig. 3.48,

$$\frac{\left(\dfrac{P\cdot D}{4\cdot \bar{T}}+\dfrac{\sqrt{(i_{\mathrm{i}}\cdot M_{\mathrm{i}})^2+(i_{\mathrm{o}}\cdot M_{\mathrm{o}})^2+(i_{\mathrm{i}}\cdot M_{\mathrm{t}})^2}}{Z}\right)}{S_h=20{,}000}$$

US, EE, SI (3.49)

NC/ND corresponds to stress equation from ASME, Section III, NC/ND-3600, with an allowable stress of 1.5S.

3.3.7.9 Pipe Stresses Due to Wind and Earthquake Wind and earthquake loads are discussed in the appropriate Codes (ASCE 7 [140], International Building Code (IBC) [141]), but have little impact on water hammer considerations. Water hammer-induced fatigue damage prior to wind or earthquake loads may reduce the ability of pipe systems to withstand wind or earthquake loading.

3.3.7.10 Pipe Supports and Anchor Designs Reactions at the pipe supports are calculated, and pipe supports to resist these loads consist of anchors, saddles, snubbers, and spring supports. Anchors rigidly support the piping, while other supports permit some motion. Snubbers act as shock absorbers, spring supports allow vertical motion, and saddles permit horizontal motion. Several types of pipe supports are shown in Figs. 3.49, and 3.50. Design guidance for pipe supports is available (MSS SP-58 [142]).

Pipe supports are attached to concrete or structural steel to support piping and are designed in accordance with applicable civil engineering Codes (ACI-318 [143], ACI-349 [144], and AISC Manual of Steel Construction [145]). When supports are suspended, the carrying capacity

Description	Flexibility Factor, k	Stress Intensification Factor [Notes (2), (3)] Out-of-Plane, i_o	In-Plane, i_i	Flexibility Characteristic, h	Sketch
Welding elbow or pipe bend [Notes (2), (4)-(7)]	$\frac{1.65}{h}$	$\frac{0.75}{h^{2/3}}$	$\frac{0.9}{h^{2/3}}$	$\frac{\overline{T}R_1}{r_2^2}$	R_1 = bend radius
Closely spaced miter bend $s < r_2(1 + \tan\theta)$ [Notes (2), (4), (5), (7)]	$\frac{1.52}{h^{5/6}}$	$\frac{0.9}{h^{2/3}}$	$\frac{0.9}{h^{2/3}}$	$\frac{\cot\theta}{2}\left(\frac{s\overline{T}}{r_2^2}\right)$	$R_1 = \frac{s\cot\theta}{2}$
Single miter bend or widely spaced miter bend $s \geq r_2(1 + \tan\theta)$ [Notes (2), (4), (7)]	$\frac{1.52}{h^{5/6}}$	$\frac{0.9}{h^{2/3}}$	$\frac{0.9}{h^{2/3}}$	$\frac{1 + \cot\theta}{2}\left(\frac{\overline{T}}{r_2}\right)$	$R_1 = \frac{r_2(1 + \cot\theta)}{2}$
Welding tee in accordance with ASME B16.9 [Notes (2), (4), (6), (8), (9)]	1	$\frac{0.9}{h^{2/3}}$	$\frac{3}{4}i_o + \frac{1}{4}$	$3.1\frac{\overline{T}}{r_2}$	
Reinforced fabricated tee with pad or saddle [Notes (2), (4), (9), (10), (11)]	1	$\frac{0.9}{h^{2/3}}$	$\frac{3}{4}i_o + \frac{1}{4}$	$\frac{(\overline{T} + \frac{1}{2}\overline{T}_r)^{2.5}}{\overline{T}^{1.5}r_2}$	Pad Saddle

FIG. 3.46 STRESS INTENSIFICATION FACTORS (ASME B31.3)

for rods to hold the pipe supports, or hangers, are listed in Tables 3.13 and 3.14.

Hanger and anchor designs are complicated by numerous factors. Cold spring should be considered for support design, where the piping is initially displaced when it is cold to minimize pipe stresses after heating the pipe. Also, localized stresses occur at the pipe support, which may exceed three times the calculated static stress, and is calculated using graphs or computer codes.

Example 3.9 Contact stresses at pipe supports.

An example of localized contact stress is shown in Fig. 3.51, where a discontinuous stress is modeled (Williams and Ranson [146], Leishear [17]). Assuming that a pipe is supported by a saddle, which does not bend, and that the average pressure due to the saddle on the outside of the pipe is 150 psi, the maximum subsurface shear stress is 450 psi.

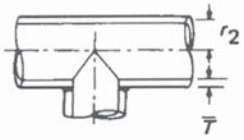
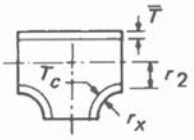
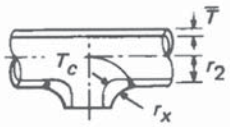
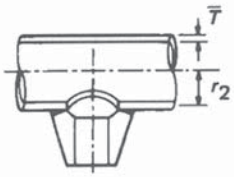
3.3.8 Structural Requirements for Fittings, Flanges, and Valves

As discussed, the use and application of piping components depend on pressure ratings and loading, which both need consideration. Following MSS Standards for fittings, ASME, B16 Standards provide dimensions for most pipe fittings. Crocker and King [77] provide a comprehensive listing of dimensions, descriptions, and pressure ratings for common valves, fittings, and flanges as specified by B16, ASTM, and other applicable standards. ASME Section VIII provides guidance on load considerations for flanged joints. Welded joints are considered per the applicable pipe code. A recommendation for the maximum moments on flanges is available (Koves [147]), such that

$$M_b(\text{ft}-\text{lbf}) = \frac{S_{a1}(\text{psi}) \cdot A_1 \cdot D(\text{in}) \cdot A_b(\text{in}^2)}{96}$$

US, EE, SI (3.50)

where M_b is the moment at the flange, S_{a1} is the allowable stress of the bolt at ambient temperature, S_{a2} is the allowable stress of the bolt at operating temperature, D is the bolt circle diameter, S_y is the flange yield strength, and A_1 is a temperature correction factor equal to the lesser of S_{a2} / S_{a1} or S_y / 36,000.

Description	Flexibility Factor, k	Stress Intensification Factor [Notes (2), (3)] Out-of-Plane, i_o	Stress Intensification Factor [Notes (2), (3)] In-Plane, i_i	Flexibility Characteristic, h	Sketch
Unreinforced fabricated tee [Notes (2), (4), (9), (11)]	1	$\frac{0.9}{h^{2/3}}$	$\frac{3}{4}i_o + \frac{1}{4}$	$\frac{\overline{T}}{r_2}$	
Extruded welding tee with $r_x \geq 0.05\ D_b$ $T_c < 1.5\ \overline{T}$ [Notes (2), (4), (9)]	1	$\frac{0.9}{h^{2/3}}$	$\frac{3}{4}i_o + \frac{1}{4}$	$\left(1 + \frac{r_x}{r_2}\right)\frac{\overline{T}}{r_2}$	
Welded-in contour insert [Notes (2), (4), (8), (9)]	1	$\frac{0.9}{h^{2/3}}$	$\frac{3}{4}i_o + \frac{1}{4}$	$3.1\frac{\overline{T}}{r_2}$	
Branch welded-on fitting (integrally reinforced) [Notes (2), (4), (11), (12)]	1	$\frac{0.9}{h^{2/3}}$	$\frac{0.9}{h^{2/3}}$	$3.3\frac{\overline{T}}{r_2}$	

Description	Flexibility Factor, k	Stress Intensification Factor, i [Note (1)]
Butt welded joint, reducer, or weld neck flange	1	1.0
Double-welded slip-on flange	1	1.2
Fillet or socket weld	1	1.3 [Note (13)]
Lap joint flange (with ASME B16.9 lap joint stub)	1	1.6
Threaded pipe joint or threaded flange	1	2.3
Corrugated straight pipe, or corrugated or creased bend [Note (14)]	5	2.5

FIG. 3.47 STRESS INTENSIFICATION FACTORS, CONT'D (ASME B31.3)

3.3.9 Pipe Schedule and Pressure Ratings for Fittings, Flanges, and Valves

Fittings, elbows, reducers, etc., are available for most materials and pipe sizes between ½ and 24 in. for Schedule 40 and Schedule 80 pipe. Stainless steel fittings are available for both Schedules 5S and 10S, and nickel/nickel alloy fittings are also available in Schedule 5S.

Flanges and valves are specified by pressure ratings: 150, 300, 400, 600, 900, 1500, and 2500 pound. Valves are available for many sizes in the range of ½ to 24 in., depending on valve type and material. Typical flange designs are shown in Fig. 3.52, and flange ratings are shown in Figs. 3.53 and 3.54. Blind flanges are frequently used to cap a pipe, weld neck flanges are used for highest

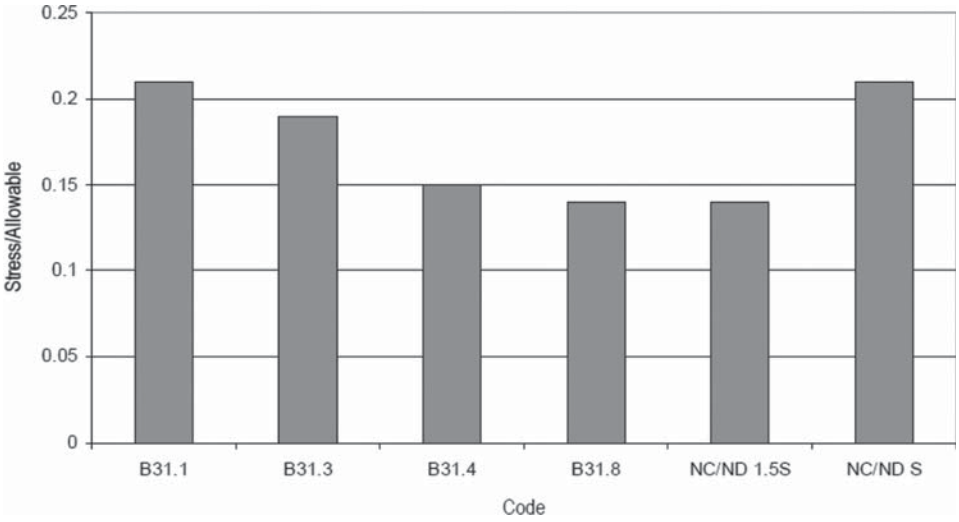


FIG. 3.48 DESIGN MARGINS, COMPARISON OF CALCULATED SUSTAINED STRESS/ALLOWABLE STRESS
(Antaki [139])

strength and reliability, and threaded and slip-on welded flanges are used for reduced cost. Slip on and threaded flanges are more likely to fail in fatigue than weld neck flanges when vibrations are induced at pump or compressor connections, where vibrations are prevalent. Most flanges are available for sizes between ½ and 24 in. up to 1500 lb, and up to 12 in. for 2500 lb. Historically, the ratings referred to an approximate maximum pressure (psi) rating throughout a specified temperature range. As Standards evolved, and material properties became better understood, the temperature/pressure relationship has varied. For example, consider a stainless steel ball valve.

Example 3.10, Pressure/temperature rating for ball valves.

Pressure/temperature ratings for ball valves meeting the 300-lb requirements are shown in Figs. 3.55 and 3.56. For a valve with metal seats, note that the pressure rating is 760 psig at ambient temperature conditions and decreases to 300 psi at 1275°F. Also note that the pressure rating is affected not only by the body material but by the valve trim material. In other words, valve ratings need consideration on a case by case basis.

3.3.10 Flange Stresses

Publications on flange stresses, gaskets, and bolted joints appear frequently in the literature. To determine acceptable design conditions, ASME Section VIII provides a comprehensive set of step by step rules to analyze the forces in bolts and flanges for pipe systems and pressure vessels.

3.3.11 Limiting Stresses for Rotary Pump Nozzles

The Hydraulic Institute Standards (Hydraulic Institute [149]) provide maximum forces and moments to be applied to pump flanges for rotary pump designs, which include centrifugal pumps. Nozzle stresses for centrifugal pumps are limited to 26,250 psi in tension and 90,000 psi in shear for ASTM A216 carbon steel. Applicable forces and moments at the pump flanges are listed in Table 3.15. Force and moment correction factors for the following equations are listed for different materials in Table 3.16.

$$F_{\text{actual}} = F_{\text{table}} \cdot \frac{\text{Actual\_allowable\_stress}}{\text{Allowable\_stress\_at\_ambient}}$$

US, EE, SI (3.51)

$$M_{\text{actual}} = M_{\text{table}} \cdot \frac{\text{Actual\_allowable\_stress}}{\text{Allowable\_stress\_at\_ambient}}$$

US, EE, SI (3.52)

Also, correction factors for grouting techniques and different pump designs vary from 0.8 to 1, as listed by the Hydraulic Institute. API RP-686 [150] provides requirements for pump alignments during installation.

3.4 HYDROSTATIC PRESSURE TESTS

During and after installation, pipe systems are typically tested hydrostatically, but there are also limited alternative tests specified in the Code, such as in-service leak tests and pneumatic leak tests. Per B31.3, piping is pressurized with water to 1-½ times the maximum expected pressure, which is corrected for operating temperature. During hydrotesting of large systems, creaking is often heard as the piping plastically deforms. The hydrotest is the last step

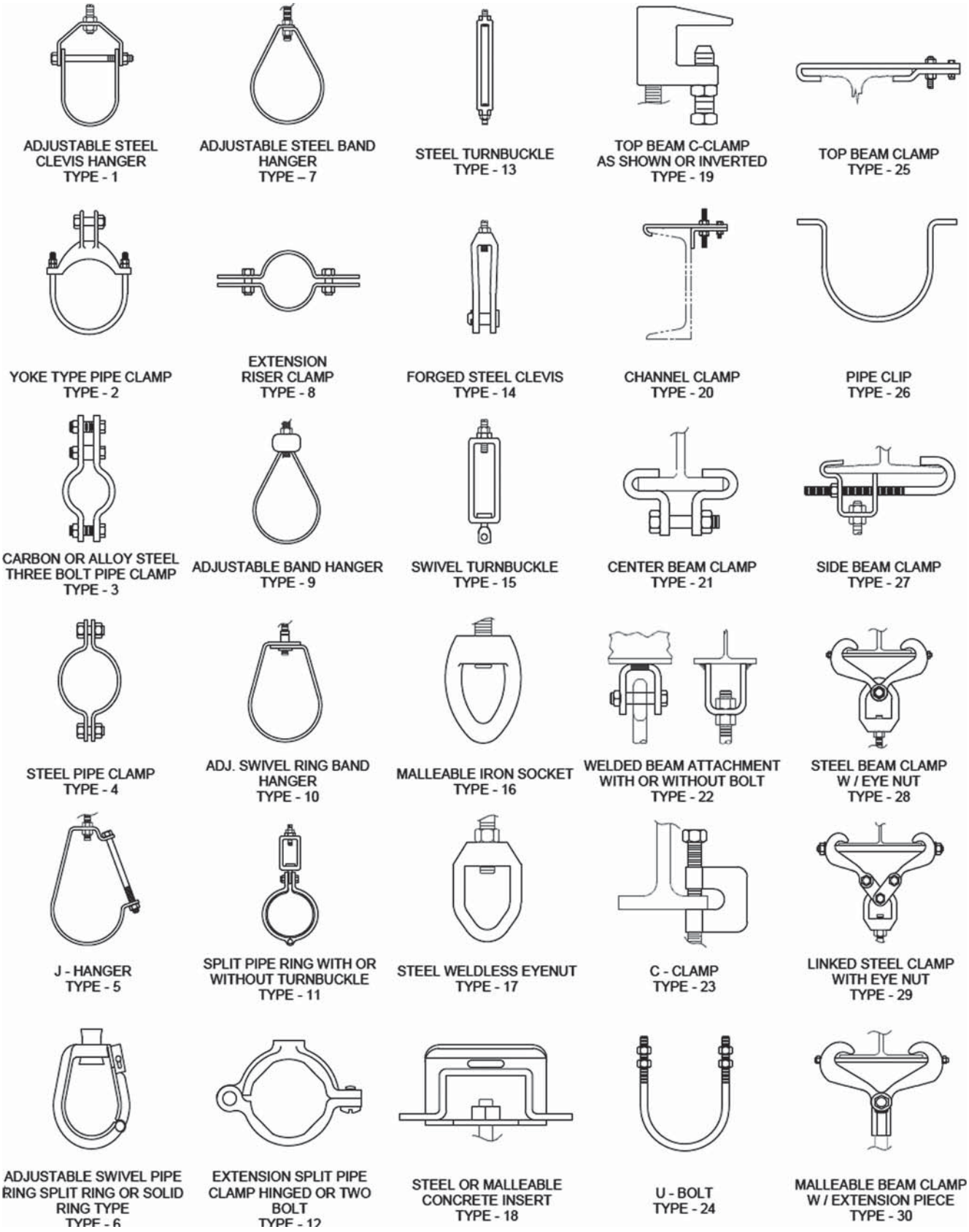


FIG. 3.49 PIPE SUPPORTS ASSEMBLIES (Extracted from ANSI/MSS SP-58-2009 with permission of the publisher, Manufacturers Standardization Society of the Valve and Fitting Industry, Inc.)

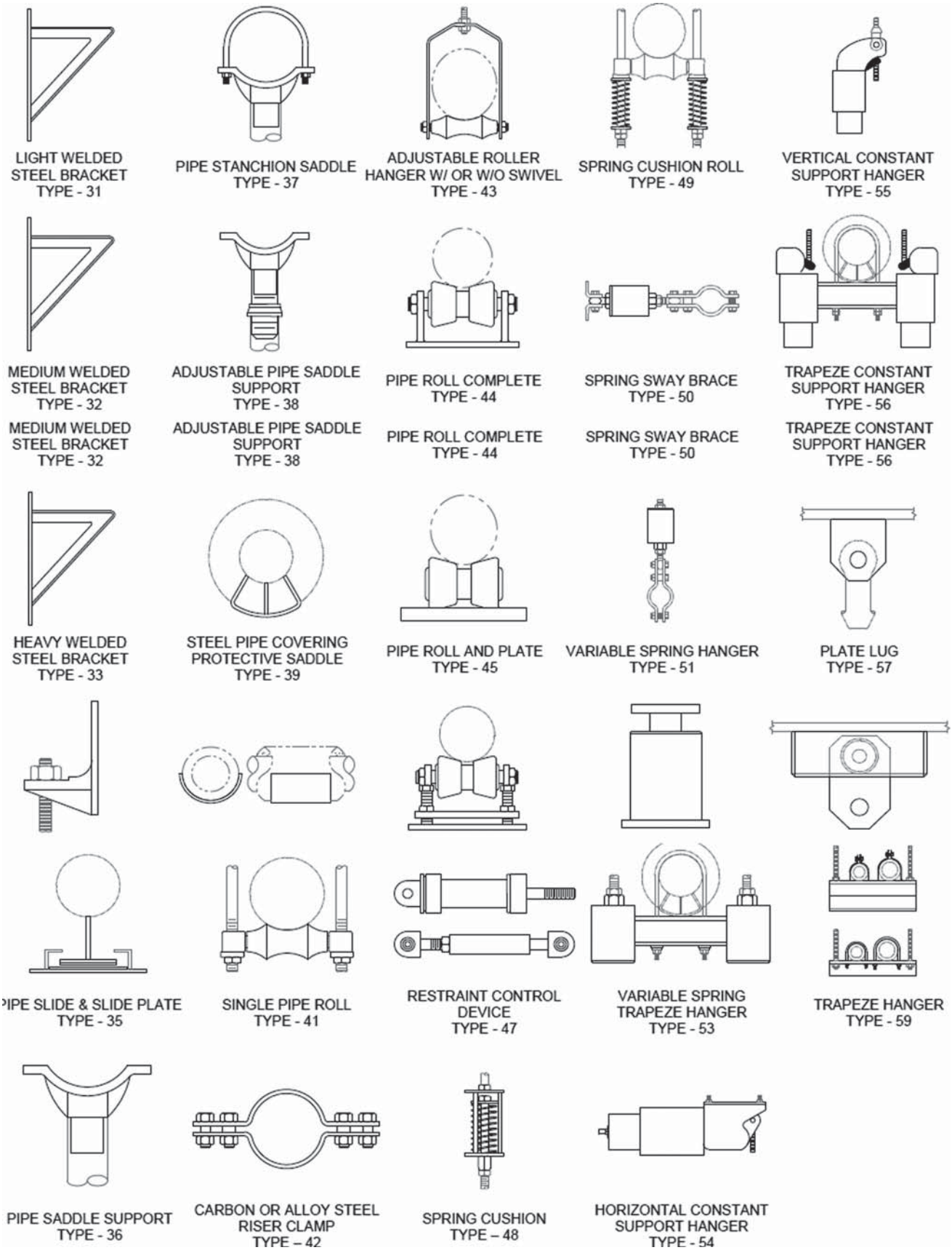


FIG. 3.50 PIPE ANCHORS ASSEMBLIES (Extracted from ANSI/MSS SP-58-2009 with permission of the publisher, Manufacturers Standardization Society of the Valve and Fitting Industry, Inc.)

TABLE 3.13 MINIMUM DESIGN LOADS FOR PIPE HANGER ASSEMBLIES (Extracted from ANSI/MSS SP-58-2009 with permission of the publisher, Manufacturers Standardization Society of the Valve and Fitting Industry, Inc.)

Applicable to all components of complete assembly; including pipe attachment, rod, fixtures, and building attachment.			
Nominal Pipe or Tube Size		Minimum Design Load Ratings at Normal Temperature Range[b]	
NPS - Inch	DN - mm	Pounds	kN
3/8	10	150	0.67
1/2	15	150	0.67
3/4	20	150	0.67
1	25	150	0.67
1 1/4	32	150	0.67
1 1/2	40	150	0.67
2	50	150	0.67
2 1/2	65	150	0.67
3	80	200	0.89
3 1/2	90	210	0.93
4	100	250	1.11
5	125	360	1.60
6	150	480	2.14
8	200	760	3.38
10	250	1120	4.98
12	300	1480	6.58
14	350	1710	7.61
16	400	2130	9.47
18	450	2580	11.48
20	500	3060	13.61
24	600	3060	13.61
30	750	3500	15.57

Notes:

a. See Section 4 for allowable stresses and temperatures.

b. Normal temperature range is -20°F to 650°F (-29°C to 343°C) for carbon steel, -20°F to 450°F (-29°C to 231°C) for malleable iron and -20°F to 400°F (-29°C to 204°C) for gray iron.

c. See Section 7.2.1 for minimum rod diameter restrictions.

d. For loads greater than those tabulated, hanger component load ratings shall be established by the manufacturer. Design shall be in accordance with all criteria as outlined in this document.

e. Pipe attachment ratings for temperature ranges between 650°F to 750°F (343°C to 398°C) shall be reduced by the ratio of allowable stress at service temperature to the allowable stress at 650°F (343°C).

f. For services over 750°F (398°C), attachments in direct contact with the pipe shall be designed to allowable stresses listed in Tables A2 and A2M.

to ensure system safety before placing the system in service. After initial system installation, testing to 110% of the design pressure is performed to ensure system integrity (National Board Inspection Code, NBIC [151]). Per B31.3, pipe systems are permitted to exceed design pressure for short durations, but in no case are pipe system-operating pressures permitted to exceed the hydrostatic test pressure. Water hammer-induced pressures frequently exceed design pressures and hydrostatic test pressures in practice.

3.5 SUMMARY OF PIPING DESIGN

A brief summary of piping design provides some understanding of the complexities of pipe design. Material properties, components, stress calculations, acceptance criteria, and testing were all considered with respect to Code design. Both fatigue and allowable stress criteria were considered in some detail, and hydrotesting was mentioned as a test criterion for pipe systems. Common system components were described, along with material properties. Pressure vessel Codes were mentioned with respect to piping, although pressure vessel design is outside the scope of this text. The intent of this chapter is to provide the fundamentals of pipe system design and components, since a better understanding of these topics leads to prevention of pipe system failures.

TABLE 3.14 LOAD CAPACITY FOR THREADED RODS (Extracted from ANSI/MSS SP-58-2009 with permission of the publisher, Manufacturers Standardization Society of the Valve and Fitting Industry, Inc.)

Nominal Rod Diameter	Root Area of Thread	Maximum Safe Load at Rod Temperature of 650°F (343°C)	
Inch	in^2	Pounds	kN
3/8	.0678	730	3.23
1/2	.126	1350	5.98
5/8	.202	2160	9.61
3/4	.302	3230	14.4
7/8	.419	4480	19.9
1	.551	5900	26.2
1 1/4	.890	9500	42.4
1 1/2	1.29	13800	61.6
1 3/4	1.74	18600	82.8
2	2.30	24600	109
2 1/4	3.02	32300	144
2 1/2	3.72	39800	177
2 3/4	4.62	49400	220
3	5.62	60100	267
3 1/4	6.72	71900	320
3 1/2	7.92	84700	377
3 3/4	9.21	98500	438
4	10.6	114000	505
4 1/4	12.1	129000	576
4 1/2	13.7	146000	652
4 3/4	15.4	165000	733
5	17.2	184000	819

Notes:

a. For materials other than carbon steel, see requirements of Section 4.8 and Table A2.

b. Tabulated loads are based on a minimum actual tensile stress of 50ksi (345MPa) divided by a safety factor of 3.5, reduced by 25% resulting in an allowable stress of 10.7ksi. (The 25% reduction is to allow for normal installation and service conditions.)

c. Root area threads are based upon the following thread series:

diameter 4" and below—coarse thread (UNC)

diameter above 4"—4 thread (4-UN)

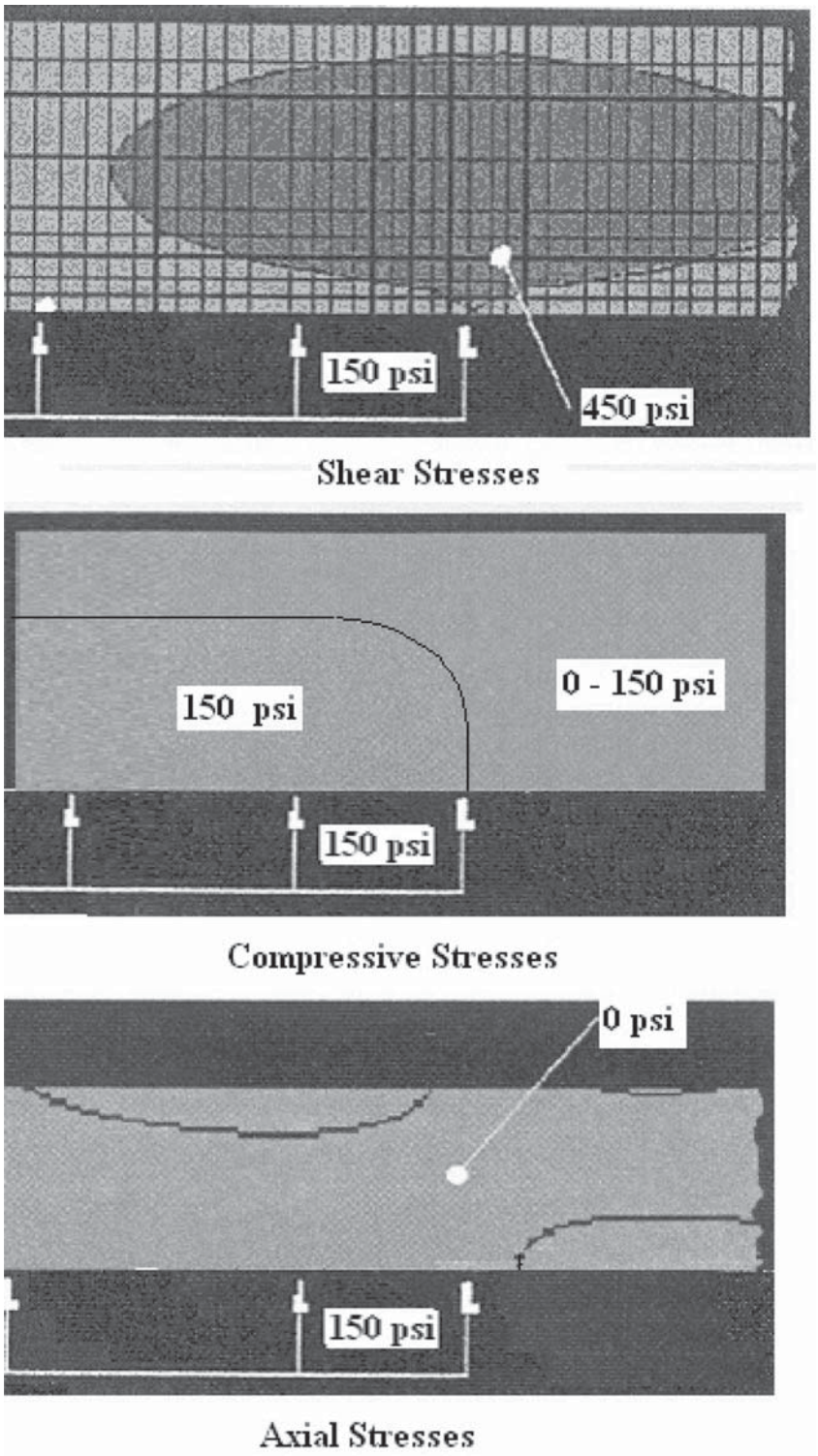


FIG. 3.51 FEA MODEL OF A DISCONTINUOUS STATIC STRESS (Leishear et al. [17])

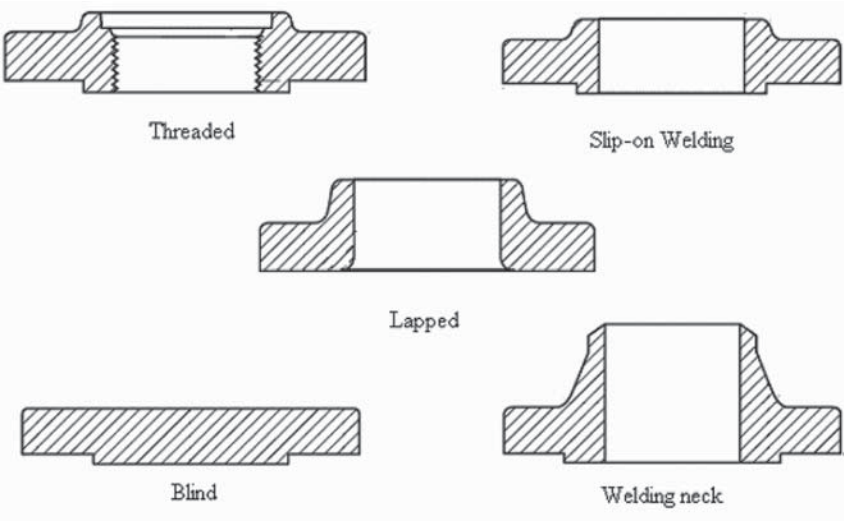


FIG. 3.52 TYPES OF FLANGES (ASME B16.5)

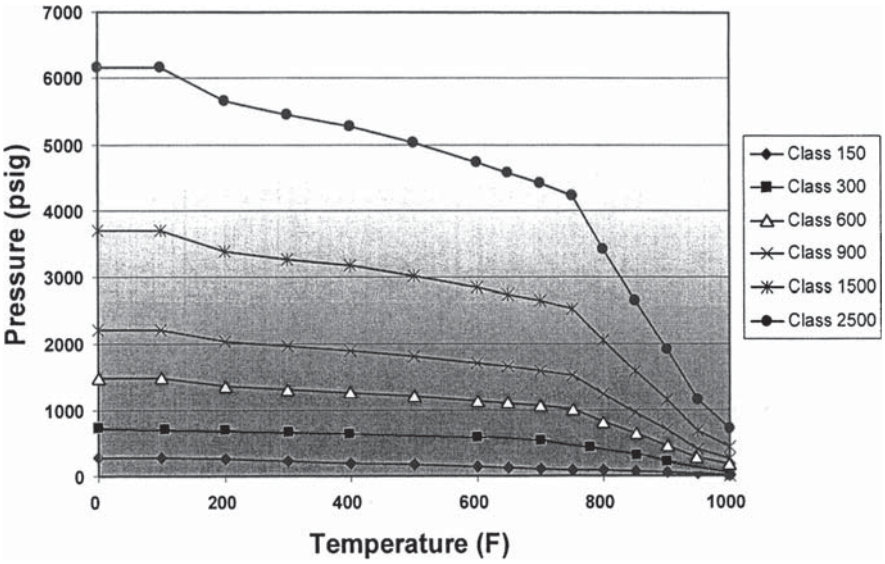


FIG. 3.53 GROUP 1.1, CARBON STEEL FLANGE RATINGS (ASME B16.5, Reprinted from D. Frikken [148])

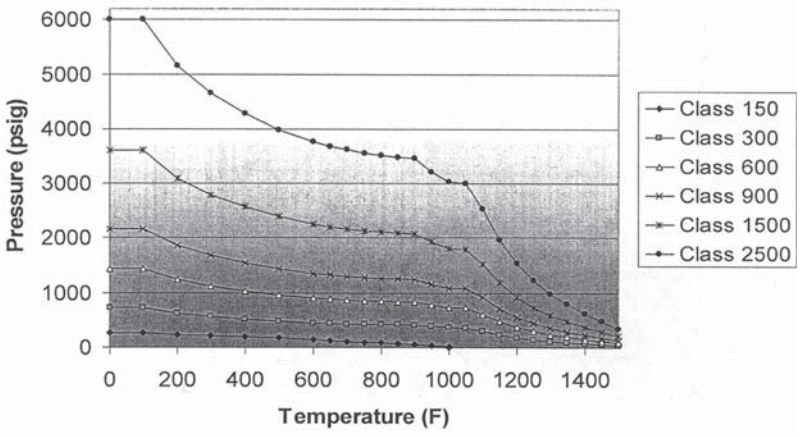


FIG. 3.54 GROUP 2.2, STAINLESS STEEL FLANGE RATINGS (ASME B16.5, Reprinted from D. Frikken [148])

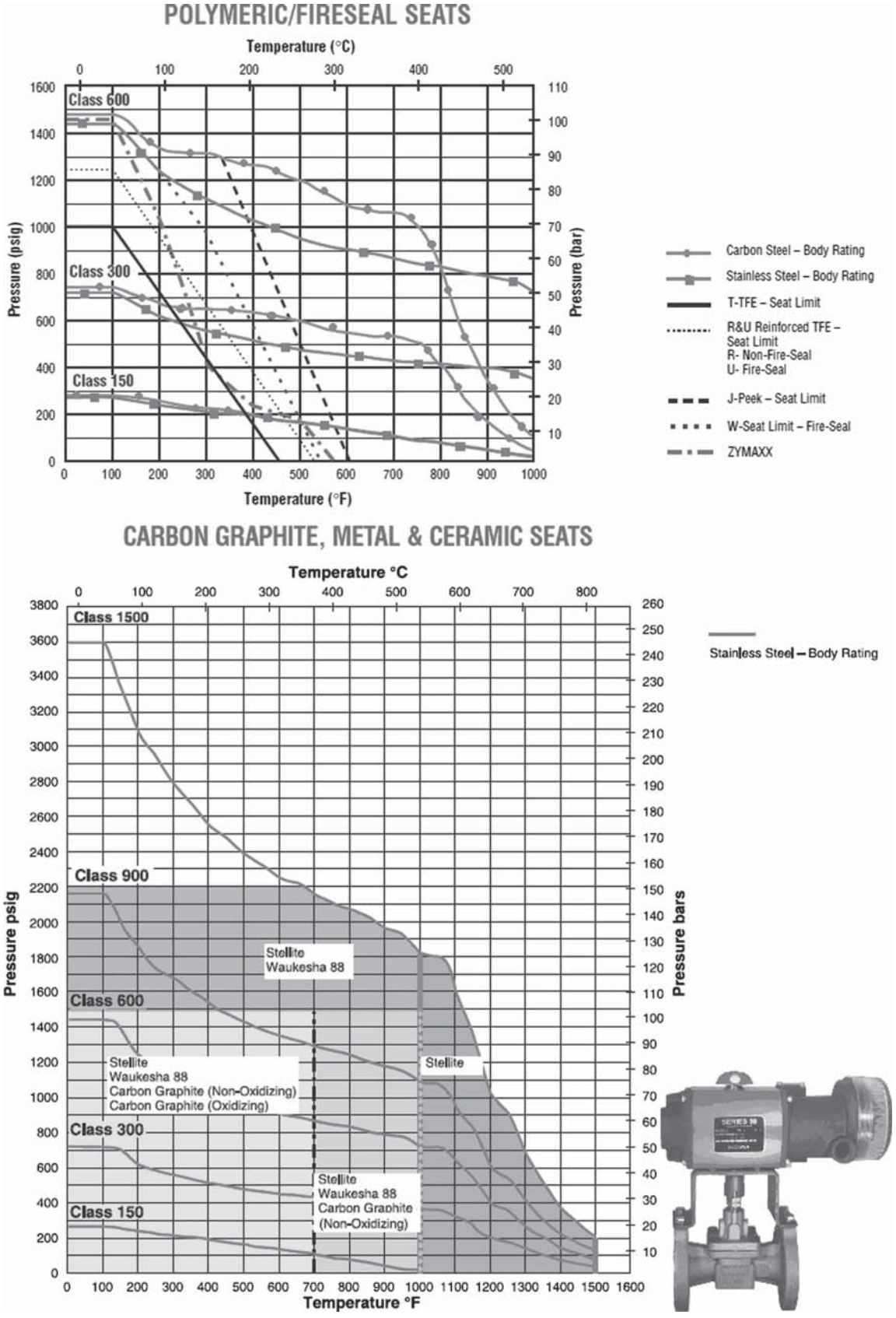


FIG. 3.55 STAINLESS STEEL BALL VALVE, PRESSURE RATINGS (McCanna ball valve, reprinted by permission of Flowserve)

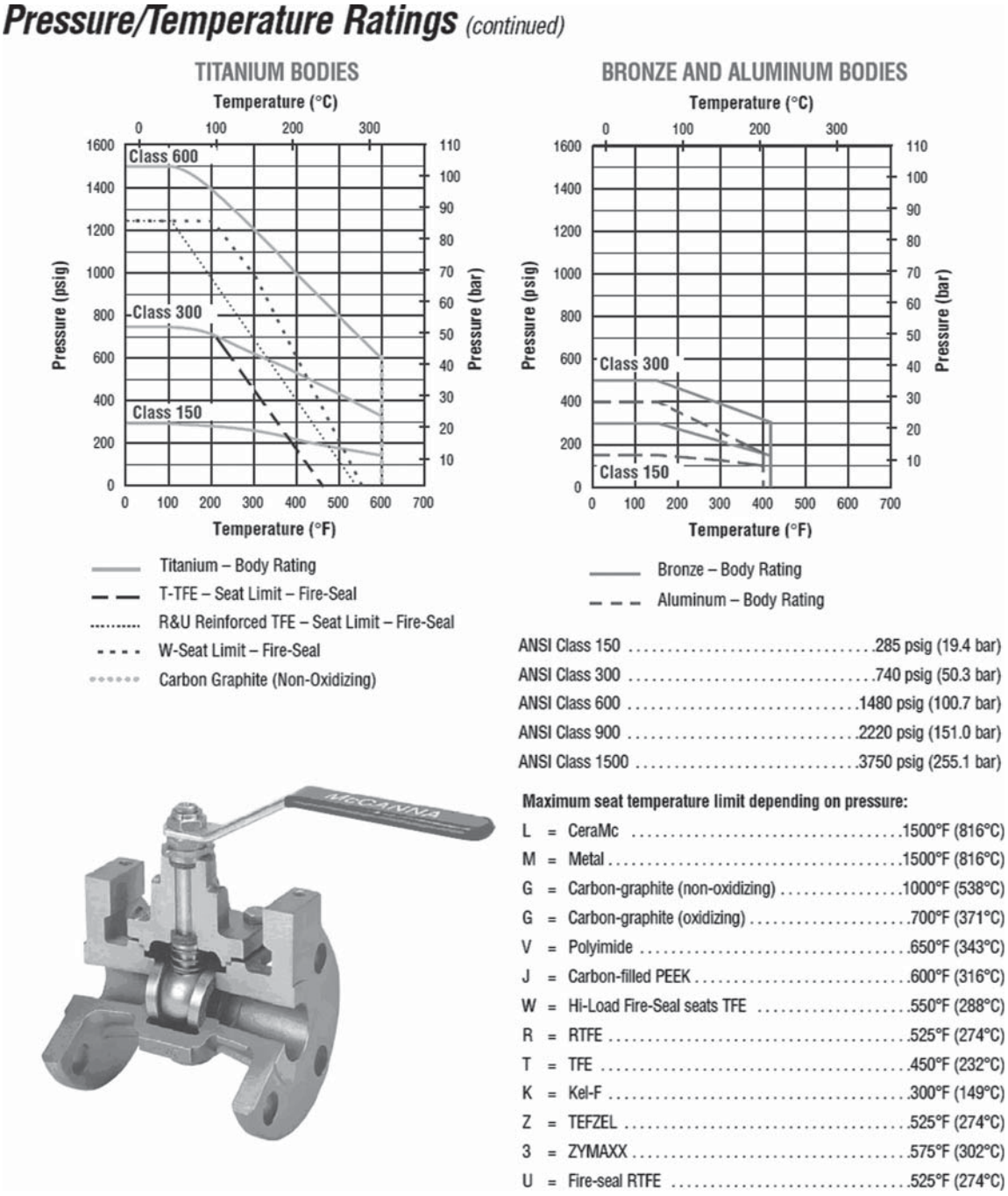


FIG. 3.56 TITANIUM, BRONZE, AND ALUMINUM BALL VALVES, PRESSURE RATINGS (McCanna ball valve, reprinted by permission of Flowserve)

TABLE 3.15 ALLOWABLE FORCES AND MOMENTS FOR PUMP NOZZLES (Reprinted by permission of Hydraulic Institute [149])

Inlet/Outlet Size (mm)	Maximum Forces F_x, F_y, F_z (Newton)	Maximum Moment M_x, M_y, M_z (Newton meter)	Inlet/Outlet Size (in.)	Maximum Forces F_x, F_y, F_z (lbs)	Maximum Moment M_x, M_y, M_z (ft-lbs)
40	500	255	1.5	112	187
50	665	340	2	150	250
65	830	425	2.5	187	312
80	1000	510	3	225	375
100	1335	680	4	300	500
150	2000	1020	6	450	750
200	2670	1360	8	600	1000
250	3340	1700	10	750	1250
300	4000	2035	12	900	1500
350	4670	2375	14	1050	1750
400	5340	2710	16	1200	2000
450	6000	3050	18	1350	2250
500	6670	3400	20	1500	2500

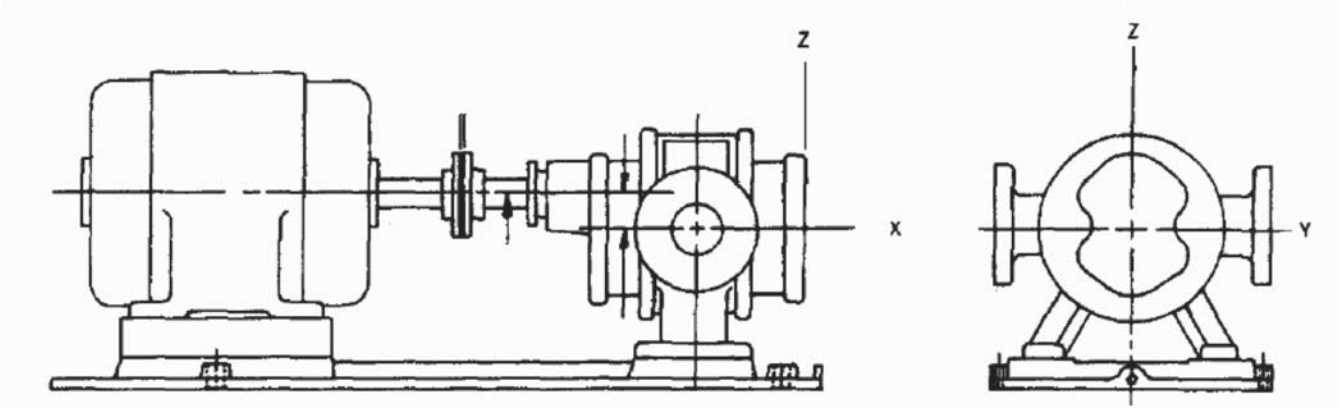


TABLE 3.16 CORRECTION FACTORS FOR PUMP NOZZLES (Reprinted by permission of Hydraulic Institute [151])

$$\left(\frac{\text{Actual allowable stress}}{\text{Ambient allowable stress}}\right)$$

Temp °C	Temp °F	Carbon Steel	Cast Iron	Type 304	Type 316	Type 304L Type 316L	Alloy 20	Hast B, C, CD4MCu
–29 to 38	–20 to 100	1.0	.526	.965	.965	.807	.807	1.0
95	200	.912	.474	.825	.842	.684	.754	.912
150	300	.807	.386	.719	.754	.614	.702	.807
205	400	.702	—	.632	.684	.561	.649	.702
260	500	.596	—	.596	.596	.509	.596	.596
315	600	.491	—	.491	.491	.491	.491	.491

CHAPTER

4

PIPE FAILURE ANALYSIS AND DAMAGE MECHANISMS

Failure theories provide techniques to calculate stresses, and damage mechanisms describe material failures due to those stresses. Code techniques provide safe, conservative rules for initial pipe design, but the analysis of pipe failures requires added understanding of failure theories, plastic deformation, fatigue cracks, and crack growth after initial fracture. What is the appropriate response to a cracked, ruptured, collapsed, or bent pipe, which was designed to meet Code design requirements? Obviously, Code-allowable stresses are exceeded, but an understanding of the damage and its cause are required to prevent further damage. To either repair a damaged system or return it to service, several questions need to be answered. Is the damage localized? What was the cause of damage? Can the cause be eliminated? If so, what are the costs, and can the system return to service without risk? If not, what are the risks, and can the system return to service at risk?

Some of these decisions are not always left to engineers, but engineers are frequently responsible to provide sound, technical recommendations to support those responsible for decisions. In the past, adequate theory to support recommendations related to water hammer was unavailable, and some pertinent data is still unavailable, but the fact remains: these questions must be addressed when a pipe failure occurs, and the better the understanding of the failure, the better the recommendations. An essential part of any recommendation is recognition and understanding of the failure mechanisms for pipes and components. Similar to Chapter 3, this chapter could follow the chapters on water hammer, but a preliminary discussion of pipe failure analysis provides insight into what is happening to the pipe while it is subjected to water hammer.

4.1 FAILURE THEORIES

Material failures start at local points in a structure, and failure theories are used combined with the calculated stresses at a point to predict failure. There are numerous failure theories available in the literature, and Collins [121] provides a comprehensive review of those theories, where a few of those theories are summarized here. In particular, the octahedral shear stress theory (Von Mises theory), maximum shear stress theory (Tresca theory), and maximum normal stress theory (Rankine theory) are presented here, since they are commonly used in practice. To understand these failure theories, the stresses at a point first need consideration.

4.1.1 State of Stress at a Point, Multiaxial Stresses

Stresses are referred to as biaxial (two dimensional), or triaxial (three dimensional) stresses. The stresses at a point are typically described using a stress cube at a point as shown in Fig. 4.1, where, σ_x, σ_y, σ_z are normal stresses, and τ_{xy}, τ_{yx}, τ_{xz}, τ_{zx}, τ_{yz}, and τ_{zy} are shear stresses. Normal stresses are perpendicular to the stress cube and describe the compression or tension at a point, and shear stresses are on the surfaces of the stress cube. This common nomenclature is used to introduce failure stress theory, followed by pipe stresses expressed in terms of r, θ, and z. The stresses at a point are due to the applied forces (F_x, F_y, and F_z) at that point (Fig. 4.2), where $\tau_{xy} = \tau_{yx}$, $\tau_{xz} = \tau_{zx}$, and $\tau_{yz} = \tau_{zy}$, and the principal stresses on opposite faces of the stress cube are equal at equilibrium. In the cylindrical coordinate system describing a pipe, the normal stresses are described by σ_θ, σ_r, and σ_z, and the shear

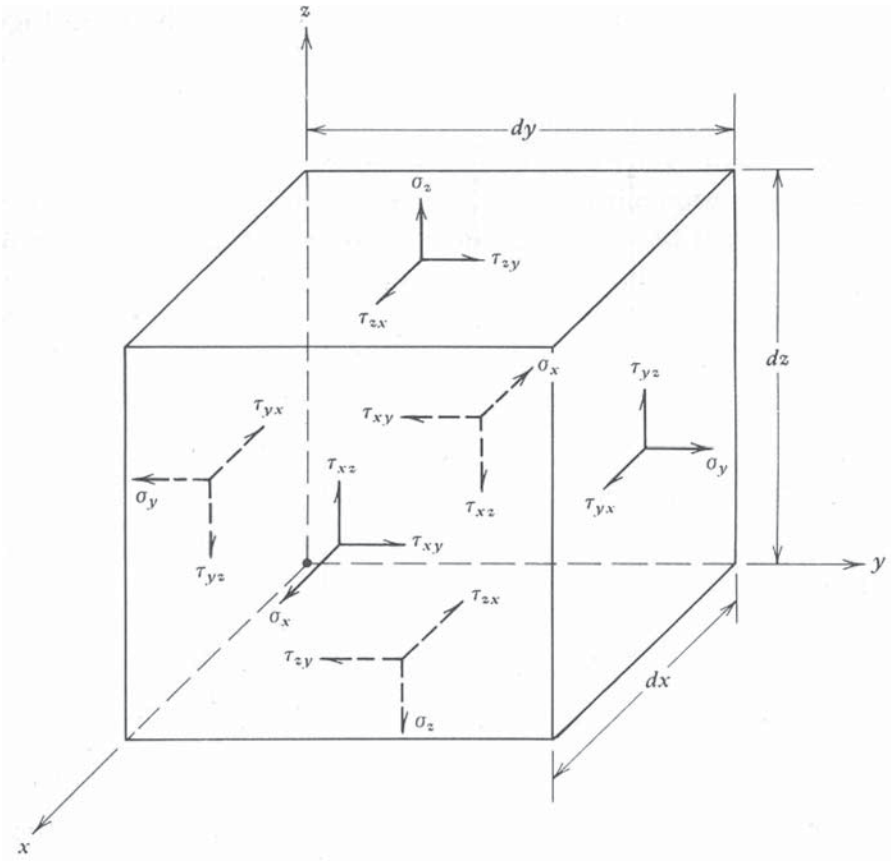


FIG. 4.1 STRESSES AT A POINT (Collins [121], Reprinted by permission of John Wiley, and Sons)

stresses are described by $\tau_{r\theta} = \tau_{\theta r}$, $\tau_{\theta z}$, $= \tau_{z\theta}$, and $\tau_{rz} = \tau_{zr}$ (Fig. 4.3). However, the stresses of interest in design are the maximum stresses at that point.

4.1.2 Maximum Stresses

Maximum normal stresses, or principal stresses, occur on three, orthogonal principal planes where the shear stresses are zero as shown in Fig. 4.4, and the maximum shear stresses occur on planes at 45° to the principal stress planes as shown in Fig. 4.5. Note that the principal plane axes, 1, 2, and 3, may not be coincident to the axes of the applied forces, *x*, *y*, and *z*.

4.1.2.1 Principal Stresses Collins [121] provides detailed derivations, solution techniques, and examples for triaxial stresses. The stresses at a point shown in Fig. 4.1 can be expressed as a stress matrix, such that

$$\begin{vmatrix} \sigma - \sigma_x & -\tau_{xy} & -\tau_{xz} \\ -\tau_{xy} & \sigma - \sigma_y & -\tau_{yz} \\ -\tau_{xz} & -\tau_{yz} & \sigma - \sigma_z \end{vmatrix} = 0 \qquad \text{US (4.1)}$$

This equation has three solutions for the principal stresses, where $\sigma = \sigma_1, \sigma_2, \sigma_3$. The sign conventions for these equations and all following equations are "+" for the shear rotations shown in Fig. 4.1 and are "+" for tension and "–" for compression. To solve Eq. (4.1), the principal stresses equal the eigenvalues of this matrix (Krieyszig [153]), which can be calculated on some hand calculators. The resultant principal stress has a magnitude of

$$\sigma_{\text{resultant}} = \sqrt{\sigma_1^2 + \sigma_2^2 + \sigma_3^2} \qquad \text{US (4.2)}$$

The angles of the resultant principal stress with respect to the *x*-*y*-*z* axes equal the eigenvectors of the stress matrix (Eq. (4.1)), where the angles (α, β, γ) are defined in Fig. 4.2, and the eigenvectors provide those angles in units of radians. Consequently, the principal stresses can be found for any given combined stress state at a point.

However, most stresses of concern to this work occur on the pipe surfaces, and two-dimensional stress equations are adequate. In this case, the principal stresses equal

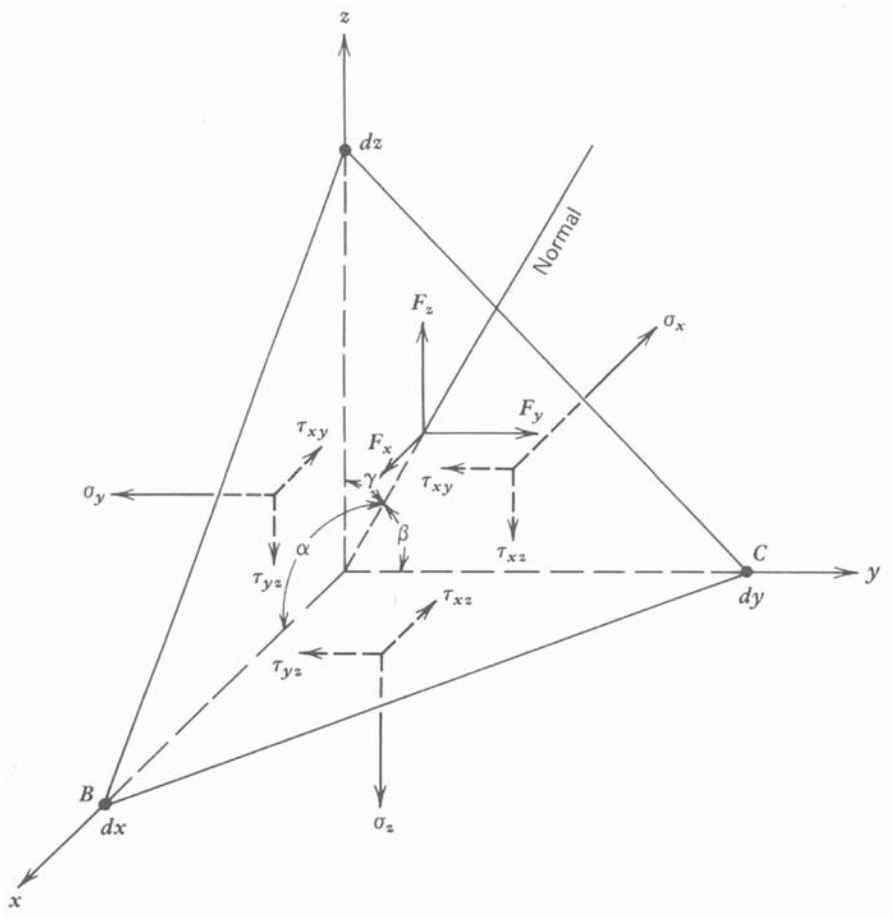


FIG. 4.2 FORCES AT A POINT (Collins [121], Reprinted by permission of John Wiley, and Sons)

$$\sigma_1 = \frac{\sigma_x + \sigma_y}{2} + \sqrt{\left(\frac{\sigma_x - \sigma_y}{2}\right)^2 + \tau_{xy}^2} \qquad \text{US (4.3)}$$

$$\sigma_2 = \frac{\sigma_x + \sigma_y}{2} - \sqrt{\left(\frac{\sigma_x - \sigma_y}{2}\right)^2 + \tau_{xy}^2} \qquad \text{US (4.4)}$$

When the shear equals zero, these equations reduce to

$$\sigma_1 = \sigma_x \qquad \text{US (4.5)}$$

$$\sigma_2 = \sigma_y \qquad \text{US (4.6)}$$

In a three-dimensional, cylindrical coordinate system,

$$\begin{vmatrix} \sigma - \sigma_r & -\tau_{r\theta} & -\tau_{rz} \\ -\tau_{r\theta} & \sigma - \sigma_\theta & -\tau_{\theta z} \\ -\tau_{rz} & -\tau_{\theta z} & \sigma - \sigma_z \end{vmatrix} = 0 \qquad \text{US (4.7)}$$

Simplifying Eq. (4.7) to two dimensions yields,

$$\sigma_1 = \frac{\sigma_\theta + \sigma_z}{2} + \sqrt{\left(\frac{\sigma_\theta - \sigma_z}{2}\right)^2 + \tau_{z\theta}^2} \qquad \text{US (4.8)}$$

$$\sigma_2 = \frac{\sigma_\theta + \sigma_z}{2} - \sqrt{\left(\frac{\sigma_\theta - \sigma_z}{2}\right)^2 + \tau_{z\theta}^2} \qquad \text{US (4.9)}$$

When the shear equals zero in the absence of torque, the principal stresses equal

$$\sigma_1 = \sigma'_z = S_b + S_L \qquad \text{US (4.10)}$$

$$\sigma_2 = \sigma'_\theta \qquad \text{US (4.11)}$$

$$\sigma_3 = \sigma'_r \qquad \text{US (4.12)}$$

where σ'_θ is the hoop stress, σ'_r is the radial stress, which equals zero at the outer pipe wall and equals the pressure at

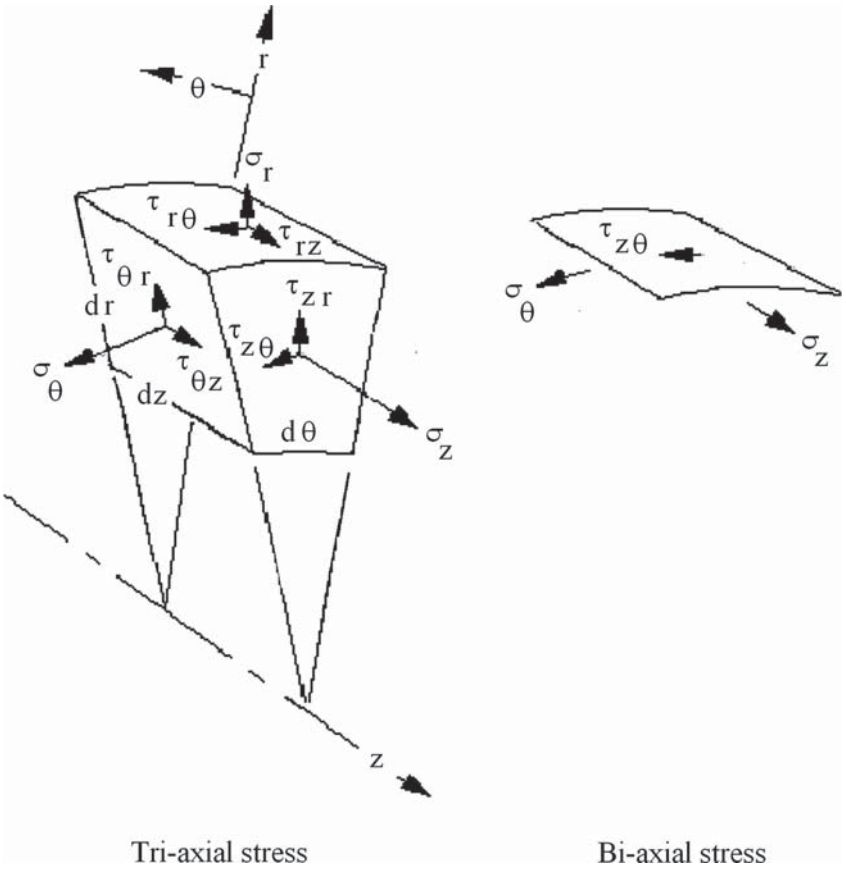


FIG. 4.3 PIPE STRESSES

the inner pipe wall, and σ'_z is the stress due to bending and axial extension or compression as applicable. At the outer pipe wall, the radial stress equals zero, $\sigma_3 = \sigma'_r = 0$, and the bending stress is at a maximum. At the inner pipe wall, the static radial stress equals the internal pressure, $\sigma_3 = \sigma'_r = P$.

4.1.2.2 Maximum Shear Stresses Shear stresses are related to normal stresses by the relationship

$$\tau = \gamma' \cdot G \qquad \text{US (4.13)}$$

The angular strain, γ', deforms the square surface of a stress cube (Fig. 4.5) into a parallelogram by an angle of γ' from its equilibrium position. G is the shear modulus, where

$$G = \frac{E}{2 \cdot \left(1 + \nu^2\right)} \qquad \text{US (4.14)}$$

For maximum shear stresses,

$$\tau_{\max} = \sqrt{\left(\frac{\sigma_x - \sigma_y}{2}\right)^2 + \tau_{xy}^2} \qquad \text{US (4.15)}$$

$$\tau_{\max} = \frac{\sigma_1 - \sigma_2}{2} \qquad \text{US (4.16)}$$

At a point of maximum shear, the normal stresses (σ'_1 and σ'_2) are equal, such that

$$\sigma'_1 = \sigma'_2 = \frac{\sigma_x + \sigma_y}{2} \qquad \text{US (4.17)}$$

In a cylindrical coordinate system,

$$\tau_{\max} = \sqrt{\left(\frac{\sigma_\theta - \sigma_z}{2}\right)^2 + \tau_{z\theta}^2} \qquad \text{US (4.18)}$$

$$\tau_{\max} = \frac{\sigma_1 - \sigma_2}{2} \qquad \text{US (4.19)}$$

These equations summarize the maximum stresses required for design, and discussions are also available for Mohr's circle (Collins [121]), which provides graphic descriptions of the maximum stresses and the stresses on any plane through a point.

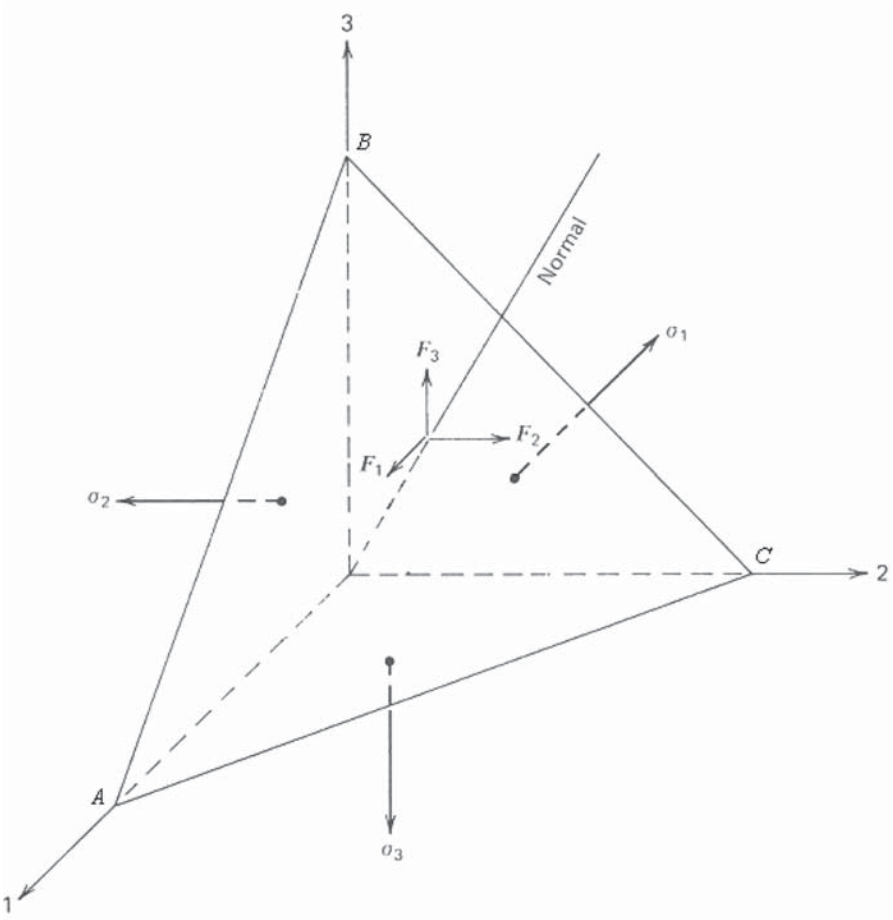


FIG. 4.4 PRINCIPAL STRESSES AND PRINCIPAL PLANES (Collins [121], Reprinted by permission of John Wiley, and Sons)

4.1.2.3 Stresses Due to Pipe Restraint Additional three-dimensional stresses can contribute to the principal stresses if the pipe ends are restrained. In terms of strain, Hooke's law can be rewritten as

$$\varepsilon_1 \cdot E = \left(\sigma_1 - \nu \cdot \left(\sigma_2 + \sigma_3\right)\right) \qquad \text{US (4.20)}$$

$$\varepsilon_2 \cdot E = \left(\sigma_2 - \nu \cdot \left(\sigma_1 + \sigma_3\right)\right) \qquad \text{US (4.21)}$$

$$\varepsilon_3 \cdot E = \left(\sigma_3 - \nu \cdot \left(\sigma_2 + \sigma_1\right)\right) \qquad \text{US (4.22)}$$

where ε_1, ε_2, and ε_3 are the principal strains, and σ_1, σ_2, and σ_3 are the principal stresses.

4.1.3 Failure Stresses

Once they are calculated, maximum stresses are compared to uniaxial tensile and fatigue test data to evaluate material failure using failure theories. As required, the failure stress, σ_f, can be the yield strength, the ultimate strength, or the fatigue limit. For piping and pressure vessel codes, the yield stress, S_y, is related to the allowable stress, S_a.

4.1.4 Comparison of Failure Stress Theories

Numerous failure theories and triaxial stresses are discussed in detail by Collins [121]. Comparisons between different failure theories are shown in Fig. 4.6 for biaxial stresses. Three theories are summarized here, since they best agree with experimental biaxial results for brittle and ductile materials. In general, brittle materials fail at less than 5% strain in 2 in., and ductile materials fail above 5% strain. Figure 4.7 was obtained for material failures exceeding the ultimate strength, such that:

1. The maximum normal stress theory agrees reasonably well with experimental results for brittle materials, but is inadequate for ductile materials.
2. The maximum shear stress theory, which is commonly referred to as the Tresca theory, provides

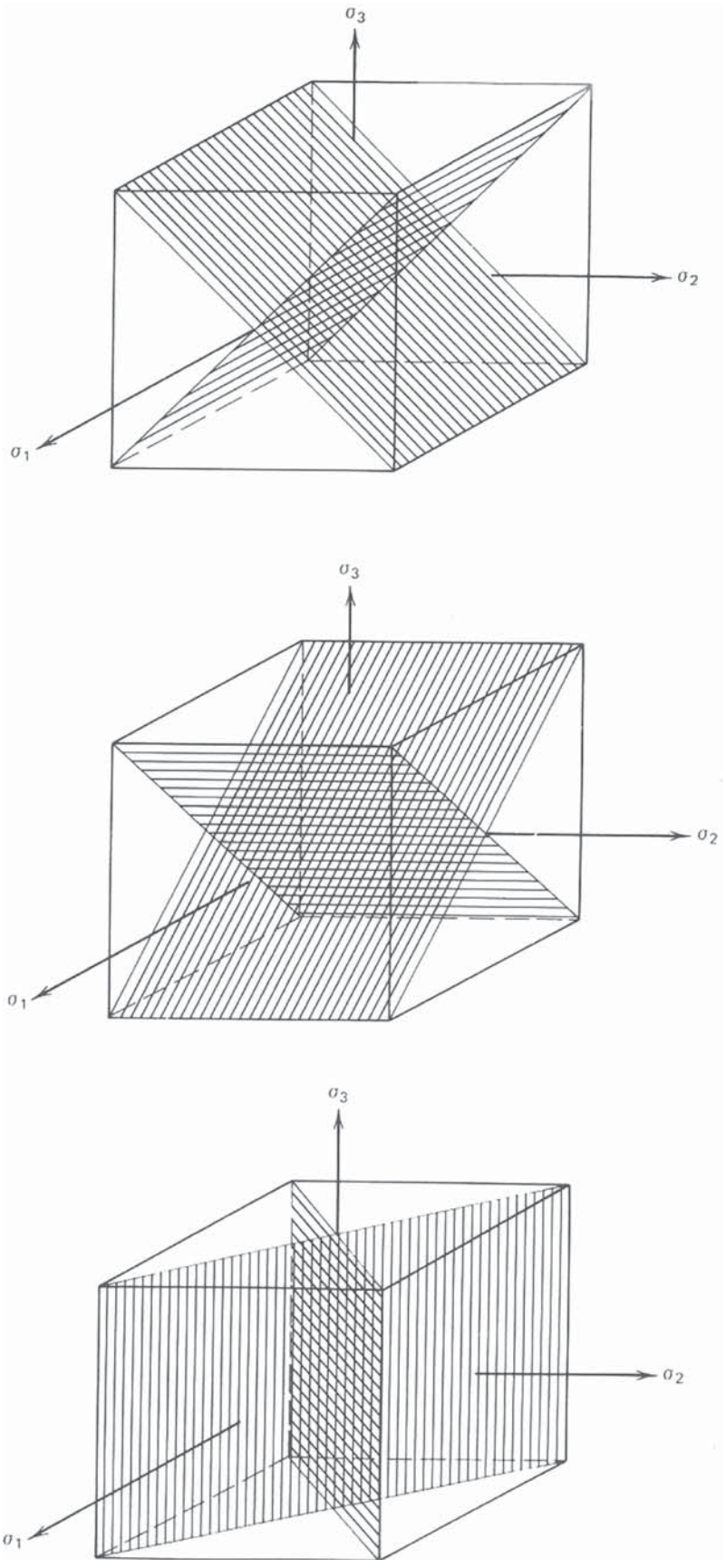


FIG. 4.5 MAXIMUM SHEAR STRESSES (Collins [121], Reprinted by permission of John Wiley, and Sons)

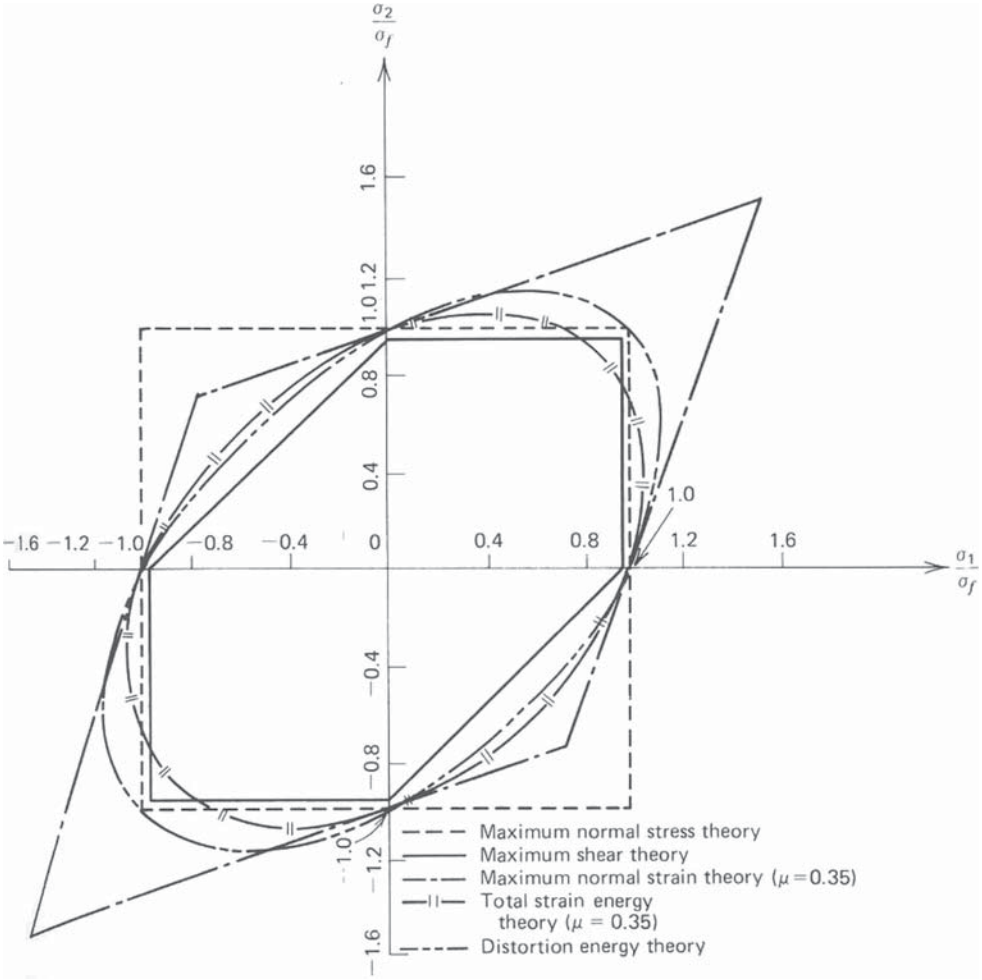


FIG. 4.6 COMPARISON OF DIFFERENT STRESS THEORIES OF FAILURE (Marin, Mechanical Behavior of Engineering Materials, 1st Edition, copyright 1962, p. 123, reprinted by permission of Pearson Education, Inc. Upper Saddle River, N. J. [100])

lower limits for experimental data in most cases. This failure theory provides a tentative basis for most piping codes.

3. The distortion energy, or octahedral shear stress theory, is commonly referred to as the Von Mises' theory. This theory provides a better estimate of the actual stresses in an object than other theories, and is frequently more appropriate for analyzing pipes that have failed in service. This theory is the basis of some pressure vessel calculations. Review of the applicable code is required to ascertain which theory is applicable.
4. The principal stresses are compared to the failure stress, σ_f, in each of the theories. For uniaxial specimens, σ_f may equal the yield strength, the ultimate strength, or the fatigue limit. For pipes and other structures, geometry affects σ_f, as well. Calculations of the stresses causing material damage are followed here by a discussion of part geometry effects on failure.

4.1.5 Maximum Normal Stress Theory (Rankine)

The Rankine theory is commonly used for brittle materials, where failure is predicted to occur when a stress from a uniaxial material test is exceeded by any one of the principal stresses. Failure is predicted when a principal stress in any direction exceeds the specified failure criteria, such that

$$|\sigma_1| \geq |\sigma_f| \qquad \text{US (4.23)}$$

$$|\sigma_2| \geq |\sigma_f| \qquad \text{US (4.24)}$$

$$|\sigma_3| \geq |\sigma_f| \qquad \text{US (4.25)}$$

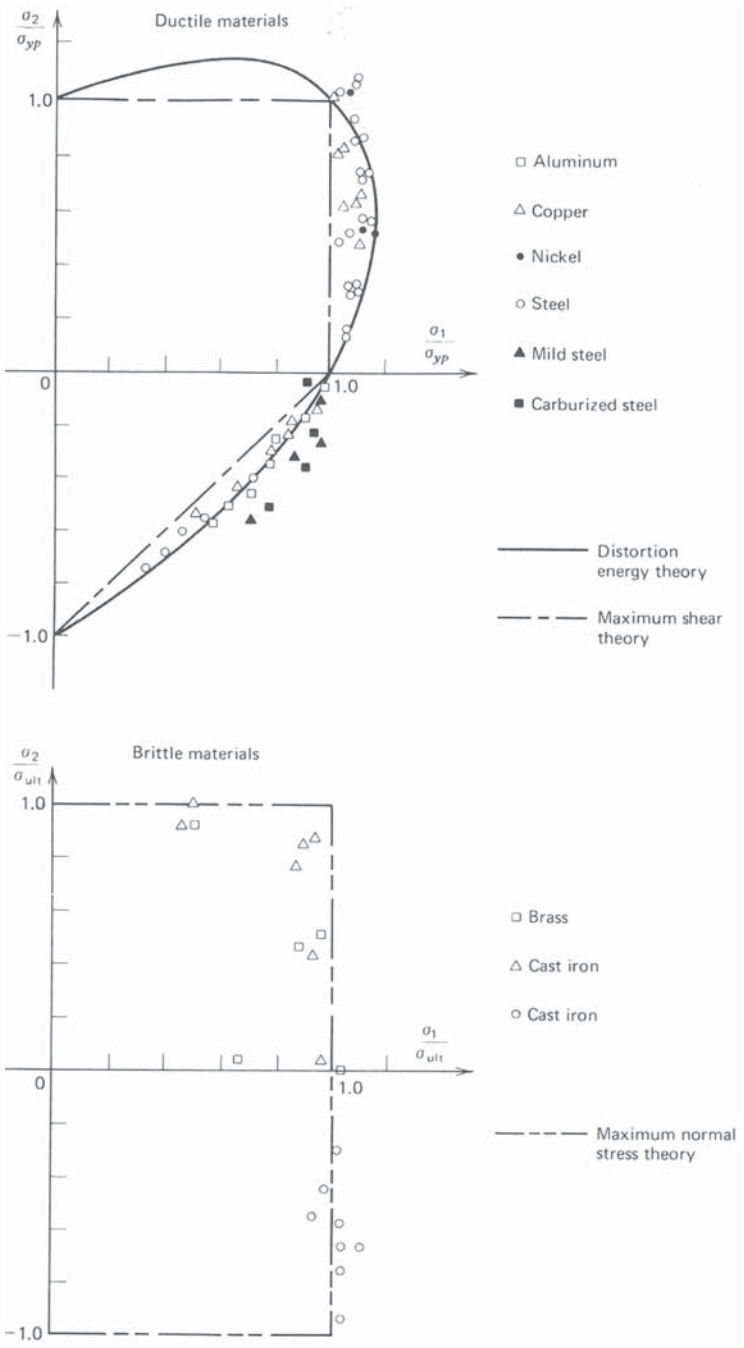


FIG. 4.7 COMPARISON OF FAILURE THEORIES TO EXPERIMENTAL RESULTS (Collins [121], Reprinted by permission of John Wiley, and Sons)

4.1.6 Maximum Shear Stress Theory (Tresca, Guest)

Failure is predicted when the shear stress of a structure equals the shear stress in a uniaxial, material test. The shear stresses are related to the principal stresses (Eq. (4.19) and Fig. 4.5), and the maximum shear stresses for predicted failures equal

$$\left|\frac{\sigma_1 - \sigma_2}{2}\right| \geq \left|\frac{\sigma_f}{2}\right| \qquad \text{US (4.26)}$$

$$\left|\frac{\sigma_2 - \sigma_3}{2}\right| \geq \left|\frac{\sigma_f}{2}\right| \qquad \text{US (4.27)}$$

$$\left|\frac{\sigma_3 - \sigma_1}{2}\right| \geq \left|\frac{\sigma_f}{2}\right| \qquad \text{US (4.28)}$$

Then, failure is predicted when

$$|\sigma_1 - \sigma_2| \geq |\sigma_f| \qquad \text{US (4.29)}$$

$$|\sigma_2 - \sigma_3| \geq |\sigma_f| \qquad \text{US (4.30)}$$

$$|\sigma_3 - \sigma_1| \geq |\sigma_f| \qquad \text{US (4.31)}$$

Eqs. (4.29), (4.30), and (4.31) are referred to as the Tresca failure criteria. At the outer pipe wall, the Tresca failure criteria become,

$$|S_b + S_L \pm \sigma_\theta| \geq |\sigma_f| \qquad \text{US (4.32)}$$

$$|\sigma_\theta| \geq |\sigma_f| \qquad \text{US (4.33)}$$

$$|S_b + S_L| \geq |\sigma_f| \qquad \text{US (4.34)}$$

Note that the Tresca Eqs. (4.32) through (4.34) are expressed differently than Eqs. (3.23) and (3.24), as excerpted from B31.3. The theoretical stress range from the Tresca equations is replaced by a stress state in B31.3 to describe failure criteria based on the Tresca criteria and material yield strengths. The Tresca theory is also used in Sections III and VIII of the Boiler and Pressure Vessel Code to predict yield.

4.1.7 Distortion Energy/Octahedral Shear Stress Theory (Von Mises, Huber, Henckey)

The distortion energy theory and the octahedral shear stress theory provide identical results through different assumptions. For the octahedral shear stress theory, failure occurs on an octahedral shear plane at a point in a structure. One of the eight octahedral planes of a stress cube is depicted by Plane *A-B-C* in Fig. 4.4. The maximum, resultant shear stress on any of the octahedral shear planes equals

$$\tau_{max} = \frac{\sqrt{(\sigma_1 - \sigma_2)^2 + (\sigma_2 - \sigma_3)^2 + (\sigma_3 - \sigma_1)^2}}{3} \qquad \text{US (4.35)}$$

For a uniaxial test

$$\tau_{max} = \frac{\sqrt{2 \cdot \sigma_f^2}}{3} \qquad \text{US (4.36)}$$

Then, failure is predicted when

$$\sqrt{\frac{(\sigma_1 - \sigma_2)^2 + (\sigma_2 - \sigma_3)^2 + (\sigma_3 - \sigma_1)^2}{2}} \geq \sigma_f \qquad \text{US (4.37)}$$

Eq. (4.37) is referred to as the Von Mises failure criterion. When the yield strength is used for σ_f, the equations are referred to as the Von Mises yield criterion.

4.2 STRUCTURAL DAMAGE MECHANISMS/FAILURE CRITERIA

Damage mechanisms may be described as excessive plastic deformation above yield, corrosion, rupture, buckling, fatigue, or fracture. Both loading and damage are quite complex in practice. Plastic deformation is complicated by the fact that both elastic and plastic deformations simultaneously occur at different parts of a structure. Fatigue occurs at low cycles and high cycles, and the strain history over time is frequently important. Once a crack forms, the principles of fracture mechanics may be employed to investigate fitness for service of the pipe system. Corrosion is a damage mechanism in itself, but also influences other damage mechanisms. Descriptions of different types of damage follow.

4.3 OVERLOAD FAILURE OR RUPTURE

One time, overload failures occur when a pipe suddenly ruptures and is well outside design requirements. Even so, this type of failure does occur, and consideration is warranted. Both bursting and external pressure effects on stresses are briefly considered here.

4.3.1 Burst Pressure for a Pipe

Burst pressures provide some insight into the applicability of tensile strengths to material failures. The ultimate strength of the material and shape of the part must also be considered, where failures may occur above the ultimate strength when statically loaded. Experimentally determined burst pressures for a pipe were found to be

$$P = \left(\frac{4 \cdot \overline{T} \cdot S_u}{D}\right) \cdot 3^{-\left(n' + 1/2\right)} \qquad \text{US (4.38)}$$

where P is the burst pressure, and n' is the strain-hardening exponent (Cooper [106]). From Fig. 4.8, the calculated circumferential stress typically exceeds the tensile pipe stress for most steels ($n' < 0.28$, Table 3.1).

Another important aspect of overload failure is the dynamic change in material properties due to load rate

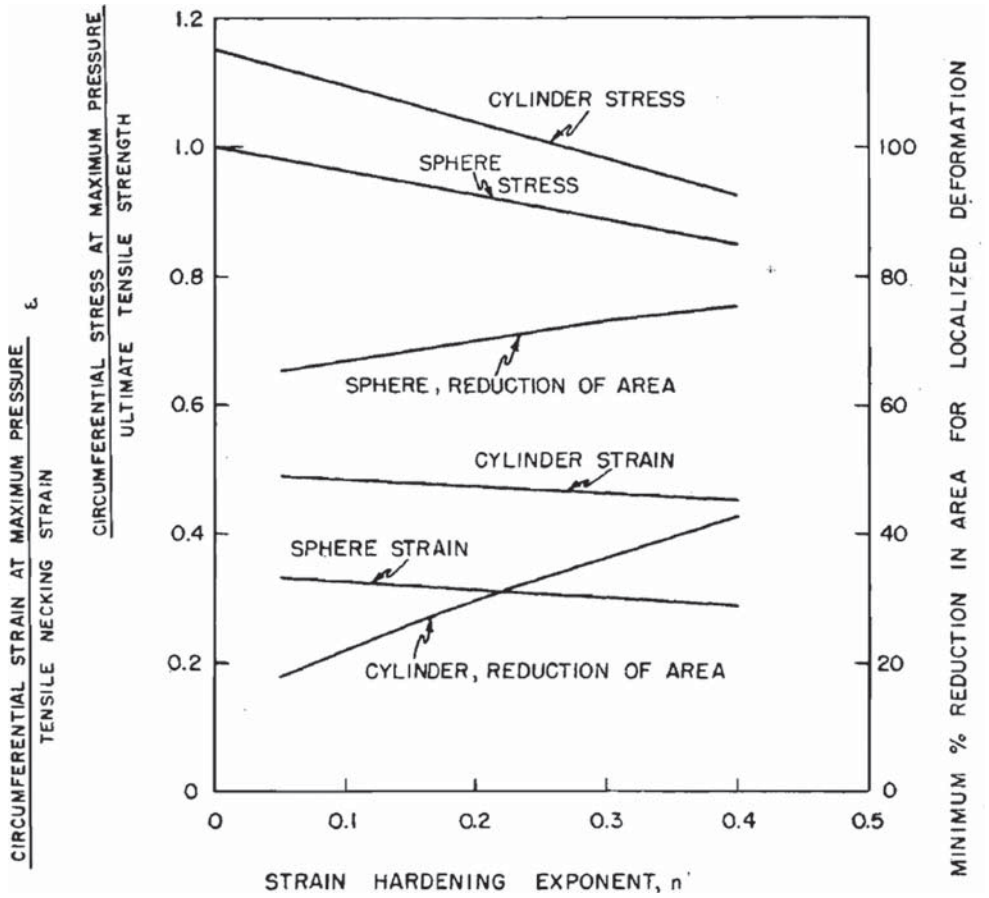


FIG. 4.8 STRAIN-HARDENING EXPONENT, *N′* (Cooper [106], Reprinted with Permission of the American Welding Society)

(paragraph 3.2.1.5). As the load rate increases, the stress effects due to a specific applied pressure decrease. Dynamic material data is unavailable for many materials, but the limited data available for steels indicates that both yield and ultimate strengths increase with increasing strain rates. Even so, the use of standard stress-strain data is sometimes used to approximate dynamic loading in the absence of available data (Blodgett [154]), since failure is predicted at stresses less than the actual dynamic stresses.

4.3.2 External Pressure Stresses

Buckling due to external pressure on a pipe may be analyzed in accordance with ASME, Section II, Part D. With respect to water hammer, external pressures simply counter the applied internal pressures. A simple expression for the minimum pipe wall required to resist buckling is (Cooper [106])

$$\overline{T} = D_{\text{nom}} \cdot 3\sqrt{\frac{6 \cdot P}{E}} \qquad \text{US (4.39)}$$

To determine the load on a pipe due to soil pressure, Merritt [155] provides equations for pipe loads related to soil properties. He further explains that the load on the pipe may be different than the load expected due to the weight of the soil above the pipe, since shear stresses in the soil may increase or decrease the load on the pipe.

4.4 PLASTIC DEFORMATION

Plasticity models are used to analyze both overload and cyclic plastic stresses. Plastic deformation can be modeled using different modeling approximations for both tensile loading and fully reversed loading. Also of note, materials act incompressibly during plastic deformation, and Poisson's ratio equals 0.5 (Mendelson [156]).

4.4.1 Plasticity Models for Tension

Plasticity models are used to develop failure theories. For tensile stresses, Fig. 4.9 shows a true stress-strain curve compared to (1) a linear strain-hardening model, and (2) a perfectly plastic material with a constant stress at

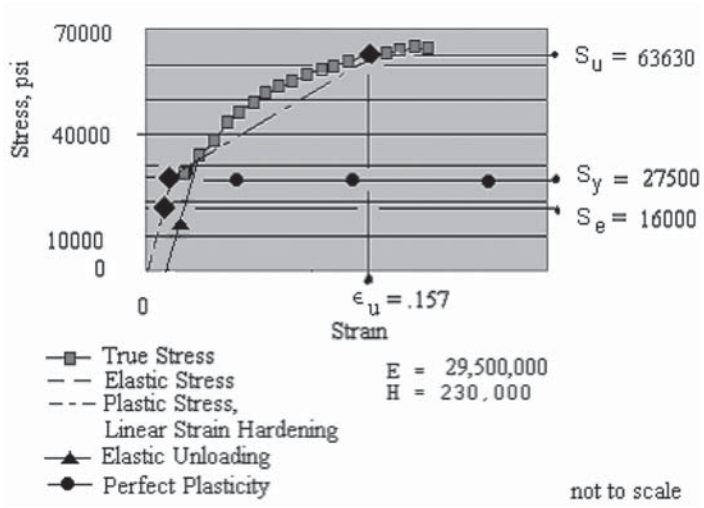


FIG. 4.9 PLASTICITY MODELS FOR A CARBON STEEL IN TENSION

yield. For the linear strain-hardening model, *H* equals the slope of the strain hardening or plastic modulus. In linear models, elastic unloading is approximated linearly.

4.4.2 Cyclic Plasticity

To consider plastic cycling, compressive strengths need comparison to tensile strengths. They are frequently considered to be the same, but the compressive strength is usually greater in magnitude. For example, Boyer [108] provides stress-strain curves for tension and compression for several materials. Of those figures provided, both the yield and ultimate strengths increase in compression for various carbon steels. However, for 304L stainless steel, only the ultimate strength increases in compression, where yield strength varies little between tension and compression. Even the slope of strain hardening changes between tension and compression for some materials. Stress-strain diagrams are further complicated by the Bauschinger effect, which notes that when a material is cycled between tension and compression, the compressive yield is lowered after tensile yielding, and vice versa. The stress-strain curves may even be different for uniaxial (monotonic) tensile tests when compared to cyclic tests, as shown in Fig. 4.10. Suresh [157] provides a thorough discussion of plasticity models and their complexity. In short, plasticity models only approximate material behavior.

Of particular interest here, the perfectly plastic model provides one assumption for cyclic plasticity in piping and limit load analysis. Limit load analysis assumes that failure occurs when a plastic hinge forms in a structure, and this technique predicts higher allowable permissible stresses then elasticity theories. A discussion of cyclic plasticity introduces concepts required to explain limit loads.

4.4.3 Elastic Follow-Up

Elastic follow-up can be described using Fig. 4.10. If a section of a pipe system is hotter, thinner, or of lower strength, that section may act differently than the overall system. For example, assume that 2-in. reducers are used to reduce the pipe to a smaller diameter flow device placed in a 6-in. pipeline. Then, the system will act elastically as if the entire pipe system is 6-in. in diameter during heat up. The stresses on the 2-in. reducer may then be plastically deformed as the 6-in. pipe elastically expands. On cool down, cyclic loading to point A occurs as shown in Fig. 4.10, since the elastic strain of the system returns to zero. These weak points in the system may require added analysis to evaluate follow-up.

4.4.4 Cyclic, Plastic Deformation

Cyclic plasticity may result in shakedown, captive plastic cycling, or ratcheting, and each of these terms requires definition with respect to material properties. These definitions can be explained in terms of the Bree diagram, shown in Fig. 4.11 (Bree [159]). The assumptions for the diagram are that the pressure is constant, bending stresses, S_b, are due to thermal cycling (displacement control), the material is perfectly plastic with no strain hardening, the pipe wall is treated as a membrane with pressure-induced stresses, σ'_0, stresses are calculated using elastic stress calculation techniques, the Tresca yield criteria is assumed, and temperature distributions through the wall are linear. The definitions are followed by an example to clarify the use of Bree's diagram. Hodge [160] provides

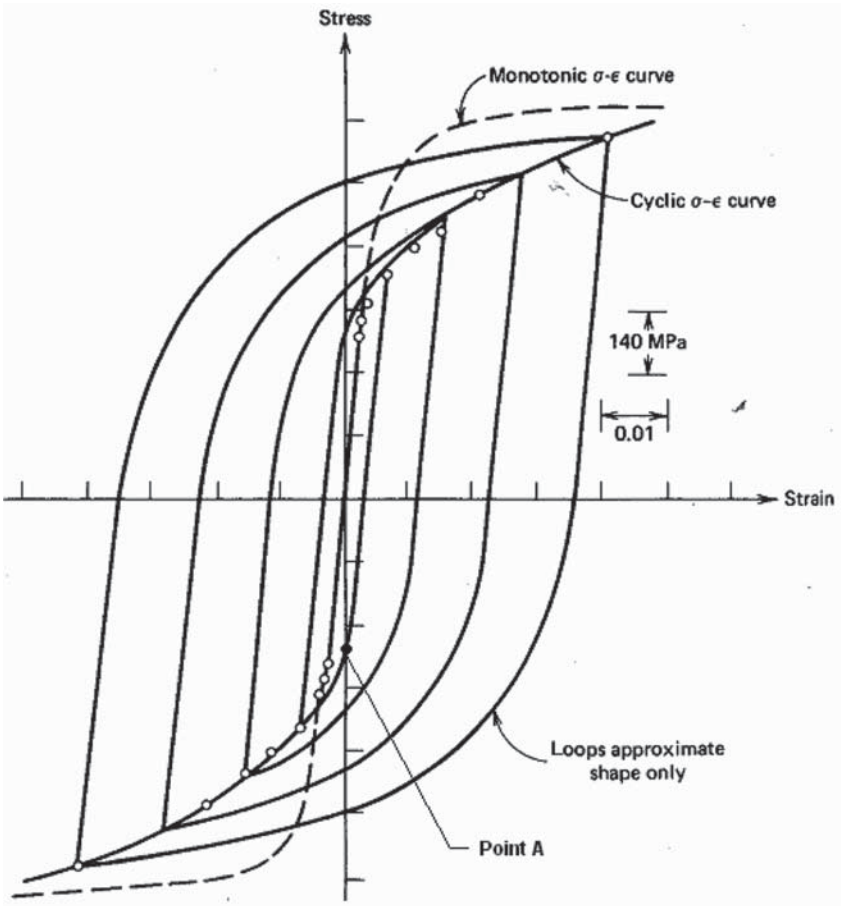


FIG. 4.10 COMPARISON OF CYCLIC STRESS STRAIN TESTING TO UNIAXIAL STRESS-STRAIN TESTING FOR 4340 STEEL (Landgraf [158], Reprinted with permission of ASTM International, 100 Bar Harbor Drive, Conshohocken, Pa 19428)

additional discussion on shakedown and ratcheting in three-dimensional frames, which is applicable to pipe networks.

Definition of terms:

1. Elastic deformation occurs in regime *E*, which is defined between the elastic limits, $S_b = S_y$ and $\sigma'_\theta = S_y$.
2. Plastic deformation due solely to bending occurs on the left, vertical, S_b axis, where plastic yielding occurs above $S_b = S_y$. Note that the predicted failure stress is above the ultimate strengths for piping materials. Failure is assumed to occur after the entire pipe cross section becomes fully plastic.
3. Plastic deformation due solely to pressure occurs on the lower, horizontal, σ'_θ axis where plastic yielding occurs above $\sigma'_\theta = S_y$.
4. Shakedown occurs when cycling achieves steady-state plastic deformations with associated residual stresses on the material surfaces, where the remainder of the pipe wall (elastic core) remains elastic. After this steady-state condition is reached, continuous cycling at this shakedown-limit stress will not increase plastic deformation. During shakedown, an elastic core exists where plastic deformation commences at one or both surfaces and increases incrementally through the pipe wall as the elastic core diminishes. Note that the shakedown limit is $S_b = 2 \cdot S_y$ for $\sigma'_\theta = 0.5 \cdot S_y$ through $\sigma'_\theta = 0.5 \cdot S_y$, and then decreases to $\sigma'_\theta = S_y$. Shakedown occurs only at the inner pipe wall in regime S_1 of the Bree diagram, and shakedown occurs on both inner and outer surfaces in regime S_2. Elastic unloading, or shakedown, is also shown in Fig. 4.11. Shakedown may continue without detrimental pipe system damages, unless fatigue is induced.
5. Captive plastic cycling occurs in regime *P*, where the pipe wall is plastic through the thickness, and the pipe is plastically bent back and forth. Captive, or contained, plastic cycling describes plastic deformations that occur when planar sections remain planar in a

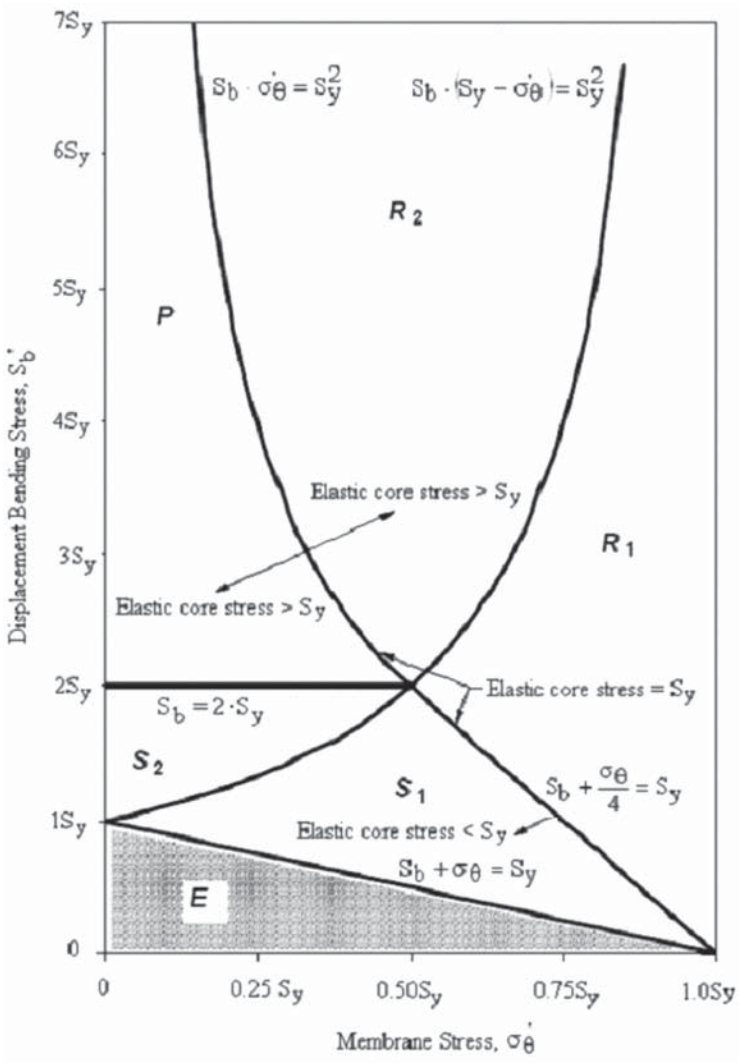


FIG. 4.11 BREE'S STRESS DIAGRAM FOR PLASTIC DEFORMATION DUE TO CYCLING (Bree, [159], Adapted with permission of Sage Publishing)

structure. Buckling and shearing are examples where planar sections change. The plastic strain required to cause buckling in this regime is not very well understood, and operating in this regime is discouraged.

6. Ratcheting occurs when the shakedown limit is exceeded, and plastic deformation increases during each cycle. Note that ratcheting occurs when the elastic core is eliminated as the stress throughout the pipe wall exceeds yield during ratcheting. That is, plastic deformations ratchet, or increase, within the pipe wall as cycling continues. Ratcheting is also referred to as cyclic creep or incremental collapse (Suresh [157]). In regime R_1 of the Bree diagram, ratcheting proceeds from the inside of the pipe. In regime R_2, ratcheting proceeds from both sides of the pipe.
7. Shakedown, ratcheting, and captive plastic cycling also occur at points to the right of the Bree curve. Although shakedown is expected at $S_b = 0$ and $\sigma'_\theta = S_y$, shakedown, ratcheting, captive plastic cycling, and bursting have not been related to each other to the right of the Bree diagram for $\sigma'_\theta > S_y$.
8. Plastic collapse and plastic flow are terms used in the literature to describe static loading, where the elastic core is eliminated.

Example 4.1 Demonstrate the use of the Bree diagram.

Porowski and O'Donnell [161] provided an example of FEA calculations for a 4-in. thick wall with end covers subjected to internal thermal transients, which are shown in Fig. 4.12. Shakedown was demonstrated in regime S_1

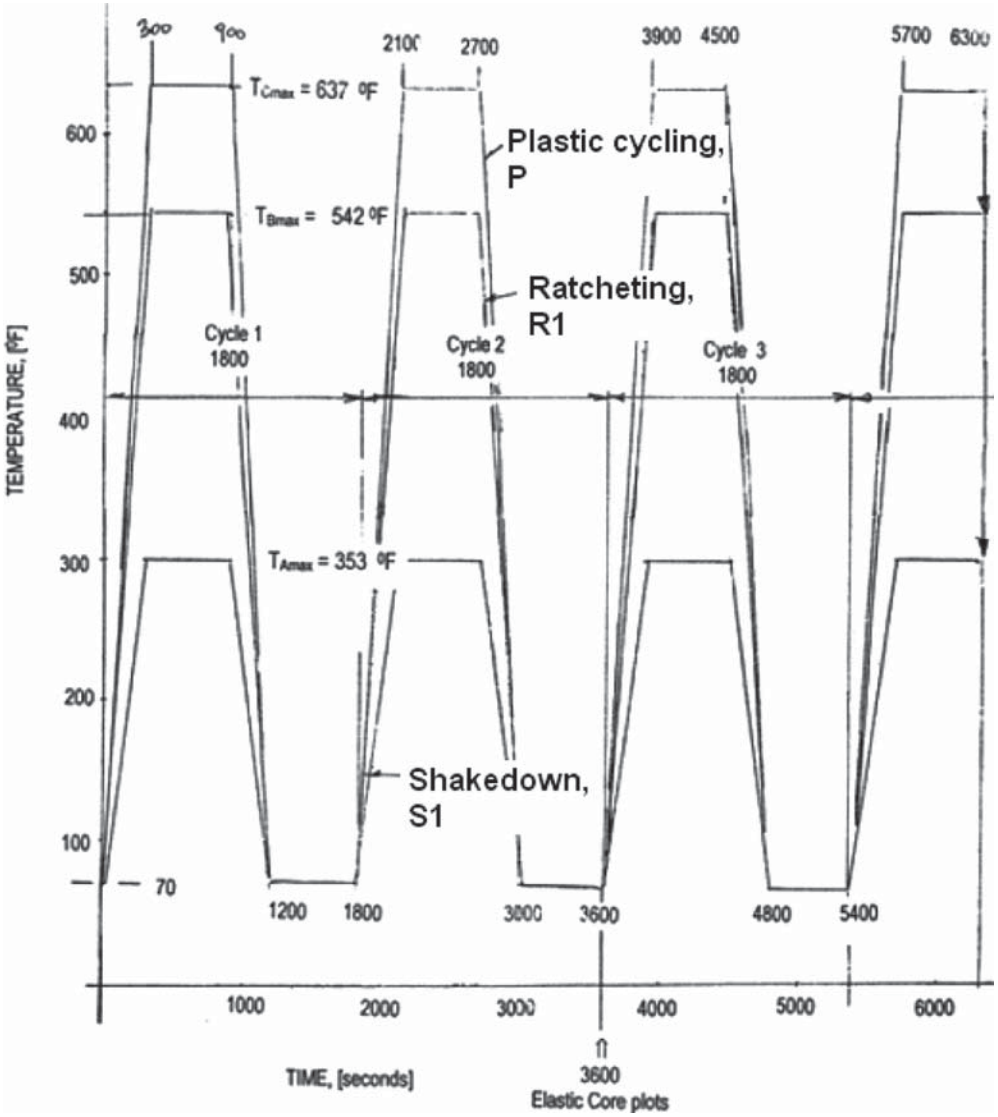


FIG. 4.12 TYPICAL CYCLIC TEMPERATURES FOR SHAKEDOWN AND RATCHETING ANALYSIS (Porowski and O'Donnell [161])

for several examples, where thermal cycles of increasing magnitude were applied to the inside of the wall, and stresses reached equilibrium. Results for those FEA models are shown in Fig. 4.13. One of those models is shown in Fig. 4.14. Ratcheting was also investigated for several models as shown in Fig. 4.15, and one example is shown in Fig. 4.16. Porowski and O'Donnell also provide a more in-depth discussion of shakedown and ratcheting.

4.4.5 Plastic Cycling for Piping Design

B31.3 does not incorporate the results of the Bree diagram. However, B31.3 does permit the use of allowable stresses above yield per Eqs. (3.24) and (3.25) of B31.3, as shown in the following example, which compares a specific case for B31.3 to the Bree diagram.

Example 4.2 Comparison of allowable stresses to the Bree diagram.

Consider stresses per B31.3 for comparison to the Bree diagram, assuming that an ASTM, A53 pipe system is operated at 800°F. Also, assume that the system operates at the maximum allowable bending stress, the longitudinal stress is less than the allowable stress, and that the system will be started up 7000 times. From Eq. (3.7), $f' = 1.0$, and from Table 3.3, $S_c = 20$ ksi, $S_h = 10.8$ ksi, and $S_y = 35$ ksi. Then, Eq. (3.24) yields

$$Sa = 1.0 \cdot \left(1.25 \cdot 20 + 0.25 \cdot 10.8\right) = 27.7\_\text{ksi} = 0.79 \cdot S_y$$

The allowable bending stress is less than yield. Further assume that the system operates at 1000 psi and the pipe

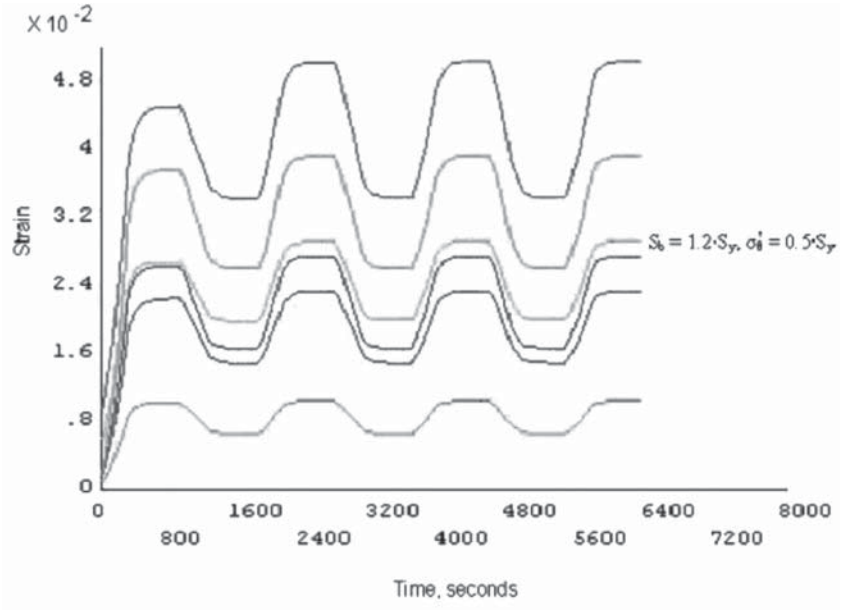


FIG. 4.13 SHAKEDOWN IN REGIME S_1 (Porowski and O'Donnell [161])

size is 6 in., schedule 40. Then, from Eq. (1.10) and Table 2.2, the hoop stress equals 1000 psi·3.03 in./0.28 in. = 10.82 ksi = $0.31 \cdot S_y$. In this example, shakedown can be expected, since $S_b = 0.79 \cdot S_y + \sigma_0' = 1.1 \cdot S_y > S_y$. In general, pressures and temperatures need to be rather high to induce ratcheting caused by internal temperature increases. But what happens when other types of loads or displacements are applied to pipes?

4.4.6 Limit Load Analysis for Bending

Limit load analysis is another technique used to determine the failure load in structures when plastic deformation is permitted. Failure is assumed to occur when a cross section of a member becomes fully plastic, and a plastic hinge or hinges occur that will no longer support the member when the centroidal plane of that member reaches the yield strength in bending. Complete plastic flow is assumed at an elastic hinge. However, the results of the Bree diagram show that when the elastic core stress equals the yield strength, ratcheting instability or contained plastic cycling will occur. The beam does not completely collapse when an elastic hinge forms. In other words, the beam does not necessarily buckle at the limit load, but this condition of full plasticity is a failure condition, based on the assumption of perfect plasticity. Furthermore, membrane effects from the large deformation associated with collapse restrain deformation.

Example 4.3 Elastic-plastic bending of a beam.

Mendelson provides additional discussion on the complexities of this analysis technique, but a simple beam subjected to bending provides insight into limit load analysis. When a load is applied to a beam, or pipe, the pipe bends, and the minimum stress occurs at the centroid of the pipe, and maximum stresses occur at a distance c' from the centroid as shown in Fig. 4.17. Neglecting deformation at the pipe supports, the outer fibers first reach yield, and plastic deformation occurs on both surfaces. As the stresses increase, the plastic zone increases, and an elastic core forms. Plastic flow cannot occur until the entire pipe cross section becomes plastic. For static structural design, the limit or collapse, load occurs when complete plasticity occurs through a cross section of a loaded member. The extent of plastic deformation or buckling is not considered. The fact that plastic flow may occur throughout the cross section is a sufficient failure criterion.

4.4.7 Limit Load Analysis for Equations for Bending of a Pipe

For a pipe subjected to bending, Mendelson derived an equation for M_e, which equals the moment required to exceed yield in the outer fibers of a member, and he also derived an equation for M_0' which equals the moment required to form a plastic hinge and is referred to as the yield moment, limiting moment, or fully plastic moment. Perfect plasticity was assumed in his analysis, similar to Bree's assumptions. The moments for a pipe equal

$$M_e = \frac{\pi \cdot S_y \cdot \left(\mathrm{OD}^3 - D^3\right)}{32} \qquad \text{US (4.40)}$$

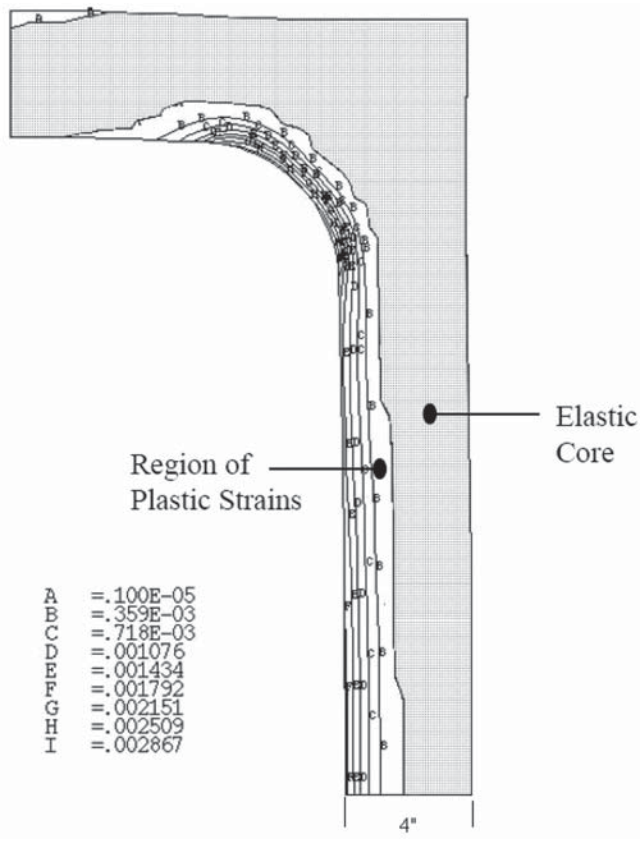


FIG. 4.14 SHAKEDOWN IN REGIME S_1, $S_b = 1.2 \cdot S_y$, $\sigma'_\theta = 0.5 \cdot S_y$ (Porowski and O'Donnell [161])

$$M'_0 = \frac{S_y \cdot \left(\mathrm{OD}^3 - D^3\right)}{6} \tag{4.41}$$

Using these equations, consider an example of limit load analysis for piping.

Example 4.4 Compare the limit load of a pipe to the Bree diagram.

That is, determine the limit load stress for a 6-in., schedule 40 pipe in bending.

Substituting ID = 6.065 in., OD = 6.625 in., and M'_0 for M in the equation for the bending stress in a beam,

$$\sigma = \frac{M \cdot c'}{I} = \frac{M \cdot \mathrm{OD}}{2 \cdot I} = \frac{M_0 \cdot \mathrm{OD} \cdot 64}{2 \cdot \pi \cdot (\mathrm{OD}^4 - D^4)}$$
$$= \frac{32 \cdot S_y \cdot \left((\mathrm{OD})^3 - (D)^3\right) \cdot \mathrm{OD}}{6 \cdot \pi \cdot \left(\mathrm{OD}^4 - D^4\right)} = 1.215 \cdot S_y = S_b$$

This value of $1.215 \cdot S_y$ for the limit load will, of course, vary depending on wall thickness and pipe diameter, but this limiting stress value is less than the $2 \cdot S_y$ stress obtained from the Bree diagram for bending. Also, more complicated pipe systems, which include bends, may form elastic hinges at support points for applied moments, which are significantly less than the yield moment (see Mendelson for examples [156]). Consequently, pipe system geometry influences the onset of ratcheting and shakedown, and the Bree diagram has limited application to piping design.

4.4.8 Comparison of Limit Load Analysis to Cyclic Plasticity

For cyclic plasticity, plastic deformation is similar. The force, F, is applied cyclically. When an elastic core is present, shakedown occurs. For this condition, permanent plastic deformation occurs at the surfaces, but for repeated constant loads, stresses do not increase from cycle to cycle. When the cross section becomes fully plastic, ratcheting or contained plastic cycling occurs. On repeated loading during ratcheting, the stresses increase during each cycle as plastic flow occurs. In contained plasticity, stresses do not increase from cycle to cycle. Again, the onset of bucking is not defined, but the presence of ratcheting at the onset of plastic flow is a sufficient condition for pipe failure.

4.4.9 Plastic Deformation Due to Pressure, Hoop Stress

For hoop stresses, limit loads and ratcheting are similar to bending except that plastic deformation proceeds from the inner pipe wall, and the elastic core occurs at the outside of the pipe. For combined bending and hoop stresses, plastic deformation occurs at one or both surfaces depending on loading.

There are several available models for hoop stresses affected by plasticity (Mendelson [156]). Each of those models assumes that a plastic core exists and that plastic deformation commences at the inner pipe wall. As temperature or pressure increases, the elastic core decreases until yield is reached at the outer pipe wall. At this limit load point, ratcheting occurs for cyclic loading. Bland [162] also provided a set of equations that considered temperature and pressure applied to a pipe. For a linear strain-hardening material, iterative techniques are provided by Mendelson. Note that the Bree diagram indicates that ratcheting occurs for all when yield is initially reached at the surface, but plastic zones will form due to internal pressure, and ratcheting will not occur as soon as yield is reached on the inner pipe surface. Closed form solutions are unavailable for plastic deformation due to combined bending and hoop stresses for pipe, and computer models are generally required for plastic analysis.

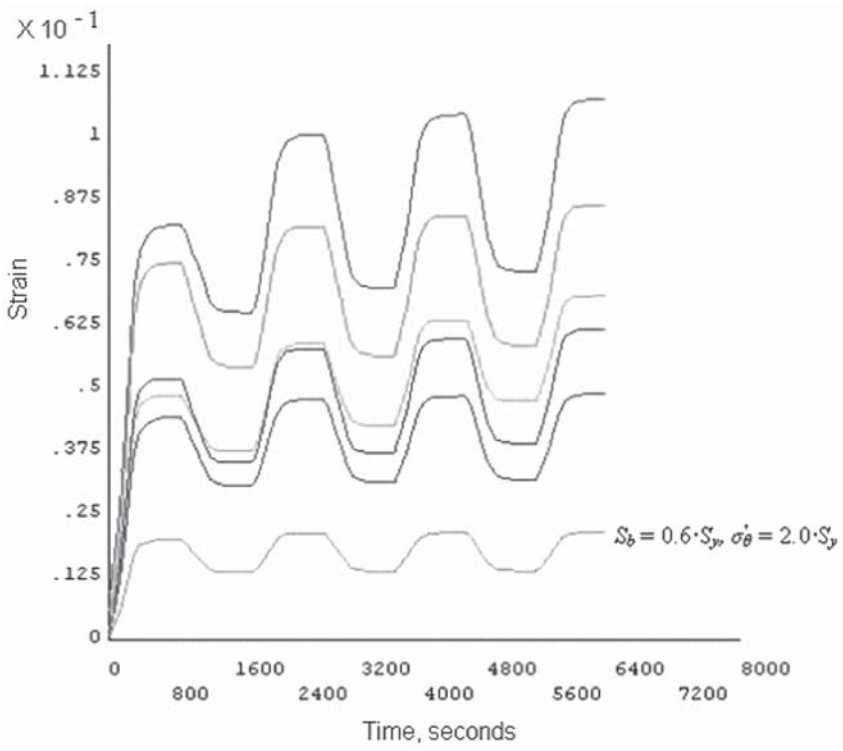


FIG. 4.15 RATCHETING IN REGIME R_1 (Porowski and O'Donnell [161])

4.4.10 Autofrettage

Autofrettage is the practice of intentionally inducing plastic strain at the inner pipe wall to increase the yield strength, fatigue resistance, and resistance to fracture. The practice and application is discussed in ASME, Section VIII, Division 3 [123].

4.4.11 Combined Stresses for Plasticity

Combined stresses during plastic deformation are not necessarily additive by the principle of superposition, but up to yield, stresses are additive. This observation permits evaluation of combined stresses at limit loads for the onset of ratcheting and contained plasticity. Also, any one of the stresses for bending, hoop, or torsion will exert a transverse Poisson's stress, which will add to stresses on other axes if the pipe is restrained.

4.4.12 Comparison of Limit Load Analysis to the Bree Diagram

The Bree diagram indicates that systems may operate in regimes S_1 and S_2. However, limit load analysis indicates that the operating stress range may be further restricted for bending. For hoop stresses, failure is expected at higher stresses than predicted by the Bree diagram.

Example 4.5 Compare limit load bending stresses to the Bree diagram.

What bending stress will induce the limit load for an ASTM, A53, 6-in., schedule 40 pipe operating at 1000 psi? From the above Examples 4.3 and 4.4, S_y = 35,000, $S_b = 1.215 \cdot S_y$, and $\sigma'_\theta = 0.31 \cdot S_y$. If the pipe ends are unrestrained, a transverse force will not be present. If the pipe ends are restrained, the hoop stress will exert a transverse force. Assume for this example that the pipe ends are unrestrained. Then, using the Tresca theory, the bending stress required to reach the limit load equals $S_b = 1.215 \cdot S_y = 42.5$ ksi. The Bree diagram indicates that full plasticity through a cross section occurs at $\sigma'_\theta = 2 \cdot S_y$. An implication of this result is that ratcheting may occur at the lower stress of $1.215 \cdot S_y$.

Example 4.6 Compare the bursting stress for a pipe to the Bree diagram.

Using data from Cooper's paper and SAE 1045 material properties, S_y = 64,000 psi, S_u = 74,000 psi, and n' = 0.18, Fig. 4.8 can be used to find $\sigma'_\theta / S_u = 1.2$. The bursting stress then equals σ'_θ = 88,800, and the bursting stress ratio to yield strength equals $\sigma'_\theta / S_y = 1.39$. The axis on the Bree diagram indicates that S_y is the maximum permissible stress. In short, bending stresses are less than predicted, and hoop stresses are greater than predicted by the Bree diagram. These examples conclude considerations for plastic failure, which may cause buckling, where ratcheting causes incremental increases in deformation

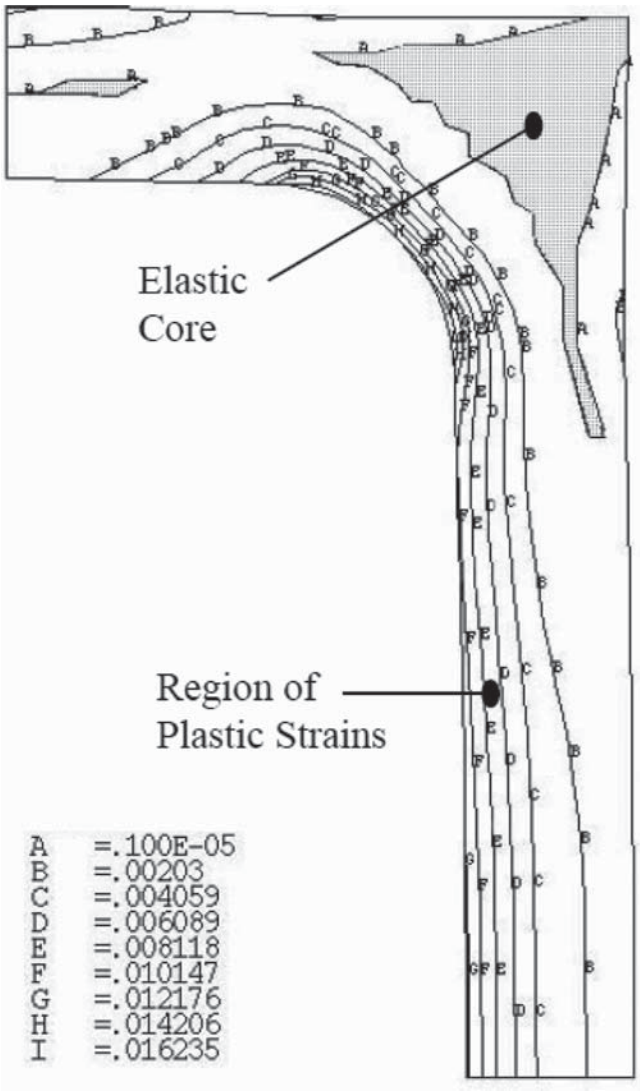


FIG. 4.16 RATCHETING IN REGIME R_1, $S_b = 0.6 \cdot S_y$, $\sigma'_\theta = 2.0 \cdot S_y$ (Porowski and O'Donnell [161])

during successive load applications, and contained cyclic plasticity does not.

4.4.13 Summary of Plastic Failure Analysis

An overview of plasticity theory was presented here. References for further details were presented, but plastic analysis generally requires computer simulations to adequately determine failure stresses. Plastic failure occurs above the yield stress of a material due to the formation of an elastic core, where loads may be either statically or cyclically applied. Plasticity calculations provide insight into why pipe systems do not fail when operated above the initial occurrence of yield strength in a pipe wall. In fact, limit load analysis is an accepted static design method for structural steel design of buildings. Shakedown occurs during cyclic loading, and collapse may not occur until stresses exceed yield through a cross section of a pipe.

With respect to failure analysis, many plastic failures may be addressed, but the presented theory is inadequate to fully assess some failures. When buckling occurs, stresses can be calculated to find the limit loads or shakedown limits, but calculations for the actual stresses to induce failure are unavailable. Even so, the prevention of ratcheting provides a reasonable upper bound for plastic deformation. The next failure mechanism to be considered here is fatigue, where pipe cracks initiate.

4.5 FATIGUE FAILURE

Fatigue failures are theoretically considered to be high cycle or low cycle (below ≈50,000 cycles). Nominal stresses are in the elastic range for high-cycle fatigue where local plastic deformation at stress risers or inclusions may initiate fracture, and for low-cycle fatigue, the stresses are plastic, and large deformations may occur. Low-cycle fatigue theory relates failure to plastic strain and is outside the scope of this work (see Collins [121] or Suresh [157]). Even so, fatigue curves are generally applied to both low- and high-cycle fatigue and are used in the pressure vessel and piping codes. High-cycle fatigue life is introduced in paragraph 3.2.3, but application of fatigue test data to pipe systems requires some additional discussion. Fatigue may result from load- or displacement-controlled stresses or thermal cycling. The end results are similar. An example of thermal fatigue is shown in Fig. 4.18.

4.5.1 High-Cycle Fatigue Mechanism

The fatigue mechanism is not fully understood. Consequently, approximate techniques are used to evaluate fatigue, where the Strength of Materials approach is presented here. This approach assumes that material failures can be described by continuum theories. Research continues to relate continuum theory to failures in material crystals, at grain boundaries, and even at the molecular scale, but the complexities of the fracture process historically led to continuum simplifications for material failures.

Fatigue theory is limited to the initiation of cracks, and fracture mechanics describes the generation of the crack after formation. Fatigue, fracture mechanics, and plasticity theories have developed independently. However, local plastic deformation at fatigue cracks has been reported in the literature, and strain hardening has been observed in the vicinity of cracks during fatigue. In fact, the use of a nondestructive Vickers' hardness tester demonstrated this fact during a fatigue failure analysis.

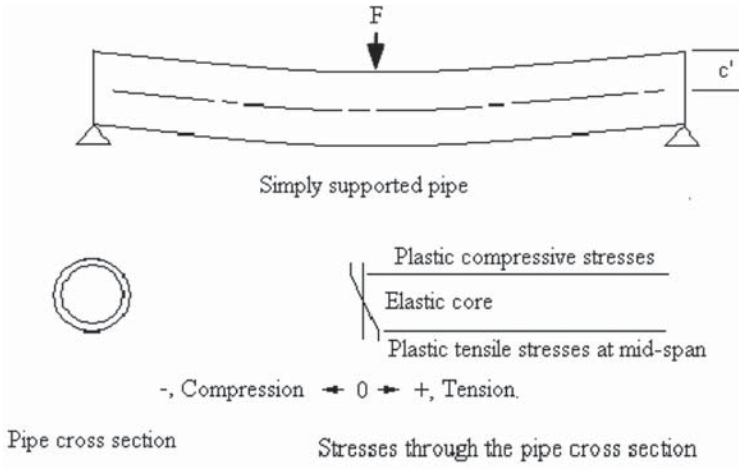


FIG. 4.17 PLASTIC DEFORMATION FOR BENDING

Example 4.7 Evaluation of a pressure vessel crack in a compressed air system at SRS. Repetitive pressure pulsations in a compressed air system led to the formation of a 3-in. long crack in a 30-in. diameter pressure vessel. A Vickers' hardness tester was used as part of the failure evaluation process, where the tester impinged a small spherical striker against a surface to determine the surface hardness. Near the crack, the hardness was 20% higher than at other locations on the vessel. A relationship between surface hardness and fatigue has not been established. Even though fatigue mechanics are unclear, fatigue life has been extensively studied.

4.5.2 High-Cycle Fatigue Life of Materials

Fatigue life depends not only on the number of cycles but on the mean stress, S_m, and maximum stresses, S_{max}, that may vary in service. Fig. 3.17 provides definitions for these terms. Fatigue data is available for completely reversed, zero mean stress for many materials, and only a few materials have been sufficiently tested to provide master diagrams that account for nonzero mean stresses. Several theories are available to approximate the effects of mean stress in the absence of a master diagram for specific materials. Of those theories, Collins [121] recommends the modified Goodman relationship, which relates the mean stress to the yield strength and fatigue limit using four different mean stress ranges. Failure is predicted to occur if

$$S_{max} - 2 \cdot S_m \geq S_y \text{ when } -S_y \leq S_m \leq \left(S_e - S_y\right) \quad \text{US (4.42)}$$

$$S_{max} - S_m \geq S_e \text{ when } \left(S_e - S_y\right) \leq S_m \leq 0 \quad \text{US (4.43)}$$

$$S_{max} - \left(1 - \frac{S_e}{S_u}\right) \cdot S_m \geq S_e \quad \text{when} \quad 0 \leq S_m \leq \left(\frac{S_y - S_e}{1 - \frac{S_e}{S_u}}\right) \quad \text{US (4.44)}$$

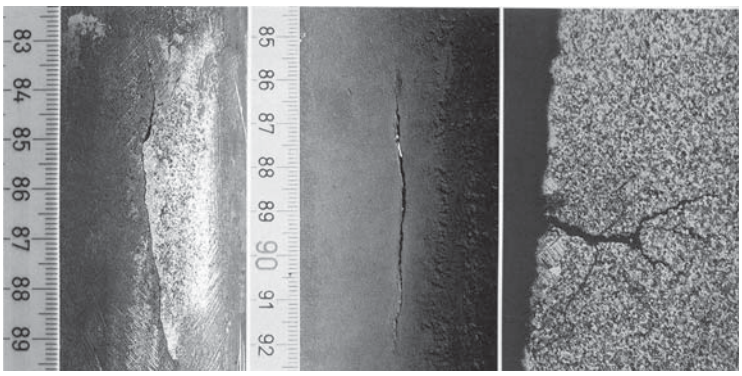


FIG. 4.18 THERMAL FATIGUE OF CARBON STEEL (During [164], Reprinted by permission of Elsevier Publishing)

$$S_{max} \geq S_y \quad \text{when} \quad \left(\frac{S_y - S_e}{1 - \frac{S_e}{S_u}} \right) \leq S_m \leq S_y \qquad \text{US (4.45)}$$

4.5.3 Triaxial Fatigue Theories

The modified Goodman relationship may be combined with failure theories to obtain triaxial fatigue failure theories. Collins [121] derived equations for different failure criteria, using the modified Goodman relationship. Those equations are listed here with the range of application for each equation.

4.5.3.1 Maximum Normal Stress Theory, Triaxial Stresses Principal stresses are determined by combining Rankine's and Goodman's theories. Failure occurs for σ_1 if

$$\sigma_{1max} - 2 \cdot \sigma_{1m} - S_y \geq 0 \quad \text{when} \quad -S_y \leq \sigma_{1m} \leq \left(S_e - S_y \right) \qquad \text{US (4.46)}$$

$$\sigma_{1max} - \sigma_{1m} - S_e \geq 0 \text{ when } \left(S_e - S_y \right) \leq \sigma_{1m} \leq 0 \qquad \text{US (4.47)}$$

$$\sigma_{1max} - \sigma_{1m} \cdot \left(1 - \frac{S_e}{S_u} \right) - S_e \geq 0 \text{ when } 0 \leq \sigma_{1m} \leq \left(\frac{S_y - S_e}{1 - \frac{S_e}{S_u}} \right) \qquad \text{US (4.48)}$$

$$\sigma_{1max} - S_y \geq 0 \text{ when } \left(\frac{S_y - S_e}{1 - \frac{S_e}{S_u}} \right) \leq \sigma_{1m} \leq S_y \qquad \text{US (4.49)}$$

Failure occurs for σ_2 if

$$\sigma_{2max} - 2 \cdot \sigma_{2m} - S_y \geq 0 \quad \text{when} \quad -S_y \leq \sigma_{2m} \leq \left(S_e - S_y \right) \qquad \text{US (4.50)}$$

$$\sigma_{2max} - \sigma_{2m} - S_e \geq 0 \text{ when } \left(S_e - S_y \right) \leq \sigma_{2m} \leq 0 \qquad \text{US (4.51)}$$

$$\sigma_{2max} - \sigma_{2m} \cdot \left(1 - \frac{S_e}{S_u} \right) - S_e \geq 0 \text{ when } 0 \leq \sigma_{2m} \leq \left(\frac{S_y - S_e}{1 - \frac{S_e}{S_u}} \right) \qquad \text{US (4.52)}$$

$$\sigma_{2max} - S_y \geq 0 \text{ when } \left(\frac{S_y - S_e}{1 - \frac{S_e}{S_u}} \right) \leq \sigma_{2m} \leq S_y \qquad \text{US (4.53)}$$

Failure occurs for σ_3 if

$$\sigma_{3max} - 2 \cdot \sigma_{3m} - S_y \geq 0 \text{ when } -S_y \leq \sigma_{3m} \leq \left(S_e - S_y \right) \qquad \text{US (4.54)}$$

$$\sigma_{3max} - \sigma_{1m} - S_e \geq 0 \text{ when } \left(S_e - S_y \right) \leq \sigma_{3m} \leq 0 \qquad \text{US (4.55)}$$

$$\sigma_{3max} - \sigma_{3m} \cdot \left(1 - \frac{S_e}{S_u} \right) - S_e \geq 0 \text{ when } 0 \leq \sigma_{3m} \leq \left(\frac{S_y - S_e}{1 - \frac{S_e}{S_u}} \right) \qquad \text{US (4.56)}$$

$$\sigma_{3max} - S_y \geq 0 \text{ when } \left(\frac{S_y - S_e}{1 - \frac{S_e}{S_u}} \right) \leq \sigma_{3m} \leq S_y \qquad \text{US (4.57)}$$

4.5.3.2 Maximum Shear Stress Theory, Triaxial Stresses Maximum shear stresses on shear planes are determined in terms of principal stresses by combining Tresca's and Goodman's theories. Failure occurs for τ_1 if

$$\left(\sigma_{2max} - \sigma_{3max} \right) - 2 \cdot \left(\sigma_{2m} - \sigma_{3m} \right) - S_y \geq 0 \text{ when } -S_y \leq \left(\sigma_{2m} - \sigma_{3m} \right) \leq \left(S_e - S_y \right) \qquad \text{US (4.58)}$$

$$\left(\sigma_{2max} - \sigma_{3max} \right) - 2 \cdot \left(\sigma_{2m} - \sigma_{3m} \right) - S_y \geq 0 \text{ when } \left(S_e - S_y \right) \leq \sigma_{2m} \leq 0 \qquad \text{US (4.59)}$$

$$\left(\sigma_{2max} - \sigma_{3max} \right) - 2 \cdot \left(\sigma_{2m} - \sigma_{3m} \right) - S_y \geq 0 \text{ when } 0 \leq \sigma_{3m} \leq \left(\frac{S_y - S_e}{1 - \frac{S_e}{S_u}} \right) \qquad \text{US (4.60)}$$

$$\left(\sigma_{2max} - \sigma_{3max} \right) - 2 \cdot \left(\sigma_{2m} - \sigma_{3m} \right) - S_y \geq 0 \text{ when}$$

$$\left(\frac{S_y - S_e}{1 - \frac{S_e}{S_u}}\right) \le \sigma_{3m} \le S_y \qquad \text{US (4.61)}$$

Failure occurs for τ_2 if

$$\left(\sigma_{3max} - \sigma_{1max}\right) - 2 \cdot \left(\sigma_{3m} - \sigma_{1m}\right) - S_y \ge 0 \text{ when}$$
$$-S_y \le \left(\sigma_{3m} - \sigma_{1m}\right) \le \left(S_e - S_y\right) \qquad \text{US (4.62)}$$

$$\left(\sigma_{3max} - \sigma_{1max}\right) - 2 \cdot \left(\sigma_{3m} - \sigma_{1m}\right) - S_y \ge 0 \text{ when}$$
$$\left(S_e - S_y\right) \le \left(\sigma_{3m} - \sigma_{1m}\right) \le 0 \qquad \text{US (4.63)}$$

$$\left(\sigma_{3max} - \sigma_{1max}\right) - 2 \cdot \left(\sigma_{3m} - \sigma_{1m}\right) - S_y \ge 0 \text{ when}$$
$$0 \le \left(\sigma_{3m} - \sigma_{1m}\right) \le \left(\frac{S_y - S_e}{1 - \frac{S_e}{S_u}}\right) \qquad \text{US (4.64)}$$

$$\left(\sigma_{3max} - \sigma_{1max}\right) - 2 \cdot \left(\sigma_{3m} - \sigma_{1m}\right) - S_y \ge 0 \text{ when}$$
$$\left(\frac{S_y - S_e}{1 - \frac{S_e}{S_u}}\right) \le \left(\sigma_{3m} - \sigma_{1m}\right) \le S_y \qquad \text{US (4.65)}$$

Failure occurs for τ_3 if

$$\left(\sigma_{1max} - \sigma_{2max}\right) - 2 \cdot \left(\sigma_{1m} - \sigma_{2m}\right) - S_y \ge 0 \text{ when}$$
$$-S_y \le \left(\sigma_{1m} - \sigma_{2m}\right) \le \left(S_e - S_y\right) \qquad \text{US (4.66)}$$

$$\left(\sigma_{1max} - \sigma_{2max}\right) - 2 \cdot \left(\sigma_{1m} - \sigma_{2m}\right) - S_y \ge 0 \text{ when}$$
$$\left(S_e - S_y\right) \le \left(\sigma_{1m} - \sigma_{2m}\right) \le 0 \qquad \text{US (4.67)}$$

$$\left(\sigma_{1max} - \sigma_{2max}\right) - 2 \cdot \left(\sigma_{1m} - \sigma_{2m}\right) - S_y \ge 0 \text{ when}$$
$$0 \le \left(\sigma_{1m} - \sigma_{2m}\right) \le \left(\frac{S_y - S_e}{1 - \frac{S_e}{S_u}}\right) \qquad \text{US (4.68)}$$

$$\left(\sigma_{1max} - \sigma_{2max}\right) - 2 \cdot \left(\sigma_{1m} - \sigma_{2m}\right) - S_y \ge 0 \text{ when}$$
$$\left(\frac{S_y - S_e}{1 - \frac{S_e}{S_u}}\right) \le \left(\sigma_{1m} - \sigma_{2m}\right) \le S_y \qquad \text{US (4.69)}$$

4.5.3.3 Octahedral Shear Stress Theory, Triaxial Stresses Octahedral shear stresses are determined by combining Von Mises' and Goodman's theories. Failures occur on the octahedral shear planes if

$$\left(\sqrt{(\sigma_{1max} - \sigma_{2max})^2 + (\sigma_{2max} - \sigma_{3max})^2 + (\sigma_{3max} - \sigma_{1max})^2}\right)$$
$$- 2 \cdot \left(\sqrt{(\sigma_{1m} - \sigma_{2m})^2 + (\sigma_{2m} - \sigma_{3m})^2 + (\sigma_{3m} - \sigma_{1m})^2}\right)$$
$$- S_y \ge 0$$

when

$$-S_y \le \left(\sqrt{\frac{(\sigma_{1m} - \sigma_{2m})^2 + (\sigma_{2m} - \sigma_{3m})^2 + (\sigma_{3m} - \sigma_{1m})^2}{2}}\right)$$
$$\le (S_e - S_y) \qquad \text{US (4.70)}$$

$$\left(\sqrt{(\sigma_{1max} - \sigma_{2max})^2 + (\sigma_{2max} - \sigma_{3max})^2 + (\sigma_{3max} - \sigma_{1max})^2}\right)$$
$$- 2 \cdot \left(\sqrt{(\sigma_{1m} - \sigma_{2m})^2 + (\sigma_{2m} - \sigma_{3m})^2 + (\sigma_{3m} - \sigma_{1m})^2}\right)$$
$$- S_y \ge 0$$

when

$$(S_e - S_y) \le$$
$$\left(\sqrt{\frac{(\sigma_{1m} - \sigma_{2m})^2 + (\sigma_{2m} - \sigma_{3m})^2 + (\sigma_{3m} - \sigma_{1m})^2}{2}}\right) \le 0$$

US (4.71)

$$\left(\sqrt{(\sigma_{1max} - \sigma_{2max})^2 + (\sigma_{2max} - \sigma_{3max})^2 + (\sigma_{3max} - \sigma_{1max})^2}\right)$$
$$- 2 \cdot \left(\sqrt{(\sigma_{1m} - \sigma_{2m})^2 + (\sigma_{2m} - \sigma_{3m})^2 + (\sigma_{3m} - \sigma_{1m})^2}\right)$$
$$- S_y \ge 0$$

when

$$0 \le \left(\sqrt{\frac{(\sigma_{1m}-\sigma_{2m})^2+(\sigma_{2m}-\sigma_{3m})^2+(\sigma_{3m}-\sigma_{1m})^2}{2}} \right) \le \left(\frac{S_y - S_e}{1-\frac{S_e}{S_u}} \right) \qquad \text{US (4.72)}$$

$$\left(\sqrt{(\sigma_{1max}-\sigma_{2max})^2+(\sigma_{2max}-\sigma_{3max})^2+(\sigma_{3max}-\sigma_{1max})^2} \right) - 2 \cdot \left(\sqrt{(\sigma_{1m}-\sigma_{2m})^2+(\sigma_{2m}-\sigma_{3m})^2+(\sigma_{3m}-\sigma_{1m})^2} \right) - S_y \ge 0$$

when

$$\left(\frac{S_y - S_e}{1-\frac{S_e}{S_u}} \right) \le \left(\sqrt{\frac{(\sigma_{1m}-\sigma_{2m})^2+(\sigma_{2m}-\sigma_{3m})^2+(\sigma_{3m}-\sigma_{1m})^2}{2}} \right) \le S_y^{\wedge} \qquad \text{US (4.73)}$$

4.5.4 Cumulative Damage

Cumulative damage theories account for the fact that stresses and resultant damage may vary from cycle to cycle. Collins summarizes numerous damage theories and states that the Palmgren-Miner linear damage theory provides accuracy comparable to the more complex nonlinear damage theories. The Palmgren-Miner theory used in B31.3 states that

$$\sum_{j=1}^{i} \frac{n_j}{N_j} = \frac{n_1}{N_1} + \frac{n_2}{N_2} + \ldots + \frac{n_{i-1}}{N_{i-1}} + \frac{n_i}{N_i} \ge 1 \qquad \text{US (4.74)}$$

where N is the number of cycles to failure at a specific stress, S, and n is the number of cycles operated at that stress. Definitions for n, N, and S are shown in Fig. 4.19.

4.5.5 Rain Flow Counting Technique

For complex stress cycles, the rain flow counting technique is commonly used. The reader is referred to Suresh [157] and ASTM E1049 [165] for elaboration of the technique. This technique can be applied to any stress cycle, such as the structural steel vibration example shown in Fig. 3.17.

Example 4.8 Demonstrate the use of the rain flow counting technique.

ASTM E1049 provides details for an example of the rain flow counting technique, but the results are shown in

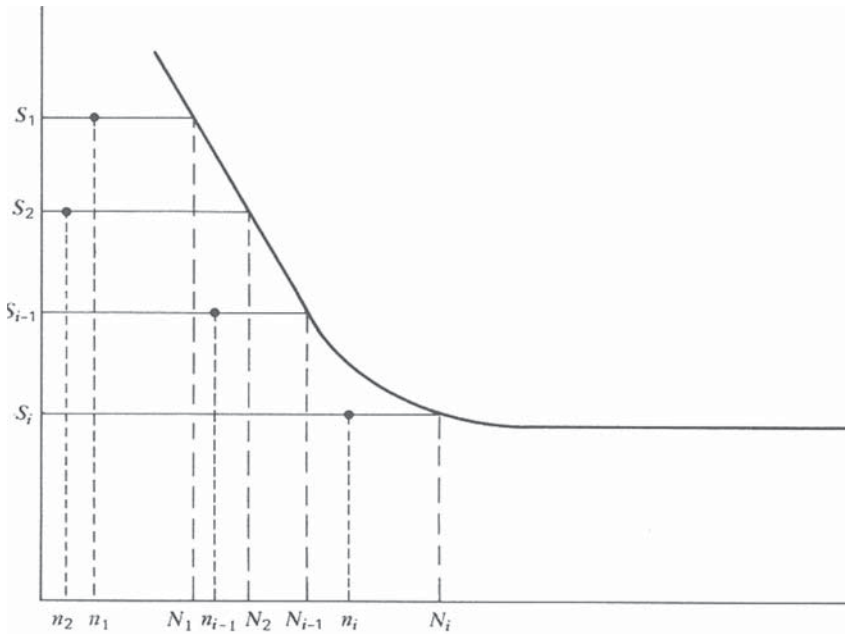


FIG. 4.19 LINEAR DAMAGE RULE (Collins [121], Reprinted by permission of John Wiley, and Sons)

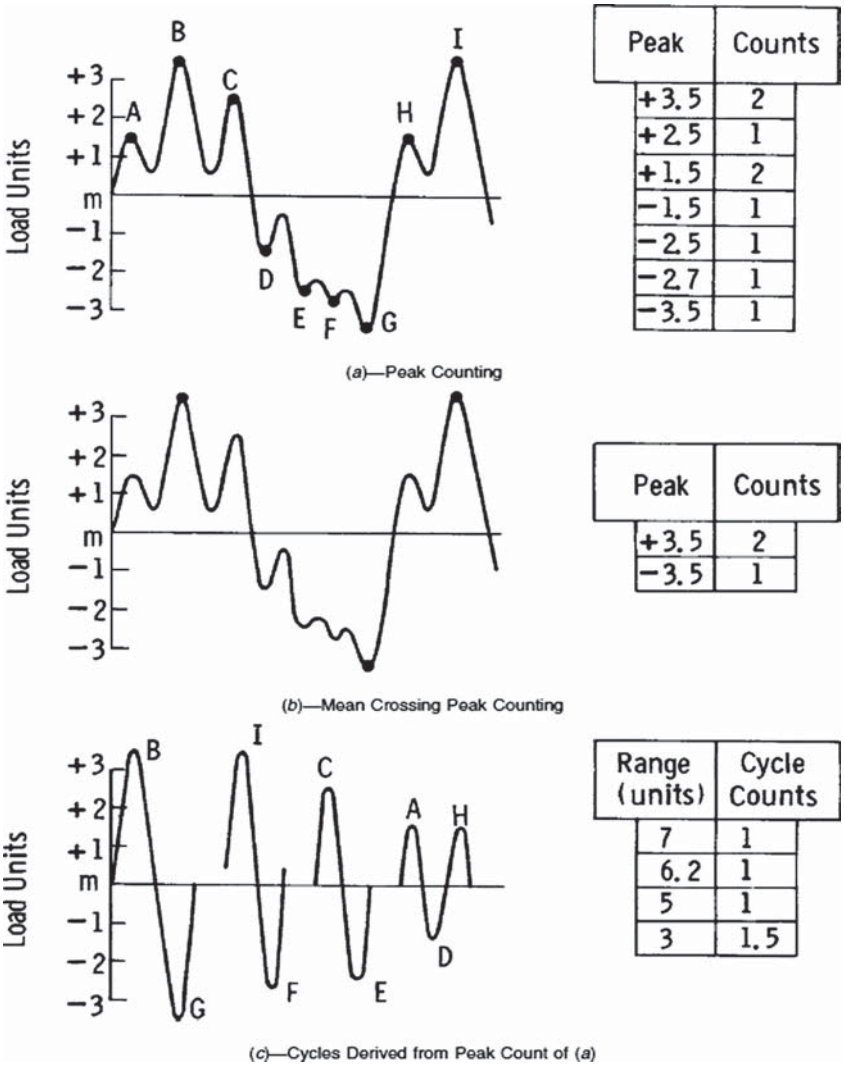


FIG. 4.20 RAIN FLOW COUNTING TECHNIQUE (ASTM E1049 [165], reprinted with permission of ASTM International, 100 Bar Harbor Drive, Conshohocken, Pa 19428)

Fig. 4.20. A typical complex load cycle is shown along with its representative loads. The reader is referred to ASTM E1049 or Collins [121] for further details.

4.5.6 Use of Fatigue Theory and Equations

This chapter provides equations and techniques that are commonly adapted to apply both full- and small-scale fatigue test data. The following example applies some of these techniques.

Example 4.9 Fatigue calculation example.

Determine the cycles to failure for a 2-in., schedule 40, ASTM, A53 seamless pipe at 200°F, which had measured strains shown in Fig. 4.21 for both axial and hoop strains along the pipe and along a long radius elbow. Assume that the pipe is well supported and neglect dead loads due to weight. This example determines the failure stress, $S_n < S_e$, required for fatigue to occur, when the number of cycles is less than the number of cycles at the fatigue limit ($N_j < N$).

Then, E = 29,500,000 psi, S_y = 35,000 psi, S_u = 60,000 psi. Using the B31.3 fatigue curve (Fig. 3.32), the fatigue limit at $\approx 10^8$ cycles equals

$$S_n = S_a \cdot f'' = S_a \cdot 6.0 \cdot N^{-0.2} = 20{,}000 \cdot 6.0 \cdot (10^8)^{-0.2} = 3014 \text{ psi}$$

Using the pressure vessel fatigue curve (Fig. 3.32), the fatigue limit equals, S_n = 12,500 psi at 10^6 cycles. Since measured strains are used along the length of a pipe and at an elbow, the pressure vessel curve may be used to assess failure, even though the B31.3 curve is recommended for use with calculated design stresses at elbows. Since the

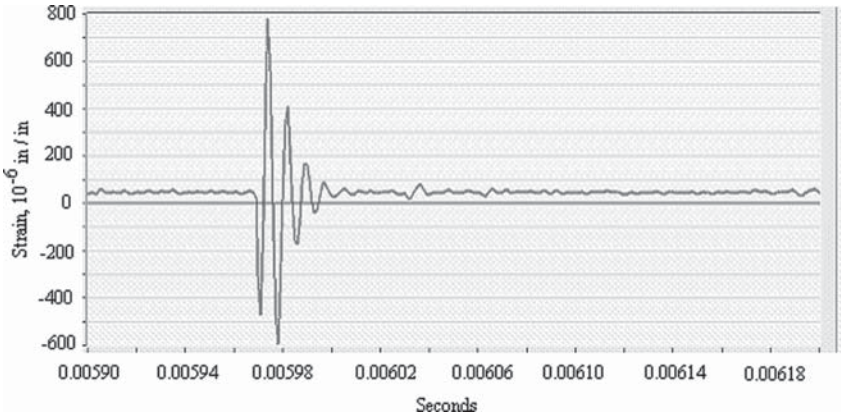


FIG. 4.21 MEASURED AXIAL AND HOOP STRAINS

fatigue limits vary by a factor of four for the two techniques, this example shows the importance of full-scale test data. However, this example demonstrates that other factors, such as strain rate, significantly affect the predicted fatigue life.

For the three largest cyclic stresses in Fig. 4.21, the maximum axial and hoop strains are 780, 400, and 180 microstrain, and the minimum strains are −470, −800, and −160 μ strain. Since

$$S_b = \sigma'_\theta,\ \sigma = \varepsilon \cdot E, \text{ and } S'_a = \frac{\sigma_{max} - \sigma_{min}}{2}$$

the stress amplitude and mean stress for the first cycle equal

$$S'_a = \frac{780 \cdot 10^{-6} \cdot 29{,}500{,}000 - (-470 \cdot 10^{-6} \cdot 29{,}500{,}000)}{2}$$
$$= 18438 \text{ psi}$$

$$\sigma_{1m} = S_b = \sigma_{2m} = \sigma_\theta = S_{max} - S'_a$$
$$= 780 \cdot 10^{-6} \cdot 29{,}500{,}000 - 18438 = 4572 \text{ psi}$$

Conservatively assume the Tresca failure criteria, and review Eqs. (4.46) through (4.49). From the problem statement, $\sigma_3 = 0$, and $S_b = \sigma'_\theta = \sigma_1$. The mean stress is within the stress range of Eq. (4.5), and

$$0 \le \sigma_{1m} \le \left(\frac{S_y - S_e}{1 - \frac{S_e}{S_u}} \right) \Rightarrow 0 \le 4572 \le \left(\frac{35000 - 3014}{1 - \frac{3014}{60000}} \right)$$
$$\Rightarrow 0 \le 4572 \le (33678) \text{ psi}$$

$$\sigma_{1max} - \sigma_{1m} \cdot \left(1 - \frac{S_e}{S_u} \right) - S_e \ge 0 \Rightarrow 23010$$
$$- 4572 \cdot \left(1 - \frac{3014}{60000} \right) - 3014 = 15654 \ge 0$$

Consequently, an infinite life cannot be obtained for this example, since repetition of the first cycle alone will cause fatigue failure in $<10^8$ sets of cycles. What is the maximum permitted stress for this example?

$$\sigma_{1max} - \sigma_{1m} \cdot \left(1 - \frac{S_e}{S_u} \right) - S_e = 0 \Rightarrow \frac{23010 - 4572}{1 - \frac{4572}{60000}}$$
$$= S_n = 19959 \text{ psi}$$

Careful application of fatigue curves is required for this example. What number of cycles is required to cause fatigue failure for this example?

Another question first needs to be addressed. What strain rate should be used for high-frequency stresses? An average strain rate during increasing tension is required to use Curve A. For this example, the frequency approximately equals 150,000 cycles per second, and the average strain rate in increasing tension equals

(150,000 cycles · (780 − (−470) in/ (in. cycle) · 10^{-6}) · 1/2 cycle) = 93.75 in./in./second = 9375% strain/second

which is well above the range of available fatigue test data. That is, the strain rate for this example exceeds the 1% average strain rate by a factor of 10,000, and fatigue may occur at a higher number of cycles. Even so, the 1% strain limit data may be used as a lower limit

approximation in lieu of other data. In that case, Curve A is used, and at 19,959 psi, the maximum number of cycles at 1% strain may be linearly interpolated from Table 3.4, where

$$N_j = N_1 = \left(\frac{20000-165000}{20000-19959}\right)\cdot\left(\log(200000) - \log(100000)\right) + \left(\log(100000)\right) = 100814$$

$$N_1 = 100{,}814 \text{ cycles}$$

Similarly, for the second cycle,

$$S'_a = \frac{400\cdot10^{-6}\cdot 29{,}500{,}000 - \left(-800\cdot10^{-6}\cdot 29{,}500{,}000\right)}{2} = 17700 \text{ psi}$$

$$S_m = S_{max} - S'_a = 400\cdot10^{-6}\cdot 29{,}500{,}000 - 17700 = -590 \text{ psi}$$

$$\sigma_{1max} - \sigma_{1m}\cdot\left(1-\frac{S_e}{S_u}\right) - S_e = 0 \Rightarrow \frac{11800-(-5900)}{1-\frac{(-5900)}{60000}} = S_n = 16115 \text{ psi}$$

$N_j = N_2 = 224{,}888$ cycles

For the third cycle,

$$S'_a = \frac{180\cdot10^{-6}\cdot 29{,}500{,}000 - \left(-160\cdot10^{-6}\cdot 29{,}500{,}000\right)}{2} = 5015 \text{ psi}$$

$$S_m = S_{max} - S'_a = 780\cdot10^{-6}\cdot 29{,}500{,}000 - 18438 = 4572 \text{ psi}$$

$$\sigma_{1max} - \sigma_{1m}\cdot\left(1-\frac{S_e}{S_u}\right) - S_e = 0 \Rightarrow \frac{5310-(5015)}{1-\frac{(5015)}{60000}} \text{ psi} = S_n = 322$$

This latter stress and all other cyclic stresses may be neglected since they are below the fatigue limit. Consider the first two cycles using the linear damage rule (Eq. (4.74)). Since the number of cycles is the same for both maximum stresses, failure occurs when

$$\frac{n_1}{N_1} + \frac{n_2}{N_2} = \frac{n_1}{100814} + \frac{n_2}{224888} = \frac{n_1}{100814} + \frac{n_1}{224888} = 1$$

Solving for the number of cycles, $n_1 = 69{,}609$ cycles, which is the minimum number of stress cycles shown in Fig. 4.21 required to cause fatigue failure. The fact that this example is significantly different than fatigue during bending is clear. Bending fatigue data implied that the system should not be operated above 7000 cycles, while a detailed analysis showed that failure will occur above 69,609 cycles due to the high-frequency nature of the stress cycles of concern. An actual system operated under these conditions for 150,000 to 300,000 stress cycles without fracture indications, which implies that the fatigue limit is higher than the value obtained from the pressure vessel fatigue curve.

4.5.7 Pressure Vessel Code, Fatigue Calculations

ASME Section III and Section VIII, Divisions I, II, III provide other techniques to determine triaxial stresses, the number of fatigue cycles, cumulative damage, permissible elastic-plastic stresses, and applications of fracture mechanics principles. With respect to fatigue, Section III, Article KD-3 provides a step by step analysis technique for calculating stresses for use of fatigue curves for welded and nonwelded structures. That technique is an option to the technique presented in Example 4.9. Section III also provides equations to compensate plasticity effects during low-cycle fatigue. Again, Codes should be thoroughly reviewed when piping calculations are performed. Pinsha Dong Martin Prager, and David Osage provided a background document used for revisions to ASME Section VIII, Division III fatigue rules, which summarized the use of different fatigue approaches and resultant design margins used in the different ASME Codes. They separated the techniques into three methods for use with FEA pipe system design: elastic stress analysis, elastic-plastic stress analysis, and the structural stress method.

4.5.7.1 Method 1: Elastic Stress Method for Fatigue The elastic stress method presented, so far, in this text can be summarized by use of graphs similar to Fig. 4.22. A maximum stress is calculated and compared to the figure to estimate piping life.

4.5.7.2 Method 2: Elastic-Plastic Stress Method for Fatigue For the elastic-plastic method, stresses are calculated from

$$S_{alt,k} = \frac{E_{yf}\cdot\Delta\varepsilon_{eff,k}}{2} \qquad \Delta\varepsilon_{eff,k} = \frac{\Delta S_{P,k}}{E_{ya,k}} + \Delta\varepsilon_{peq,k}$$

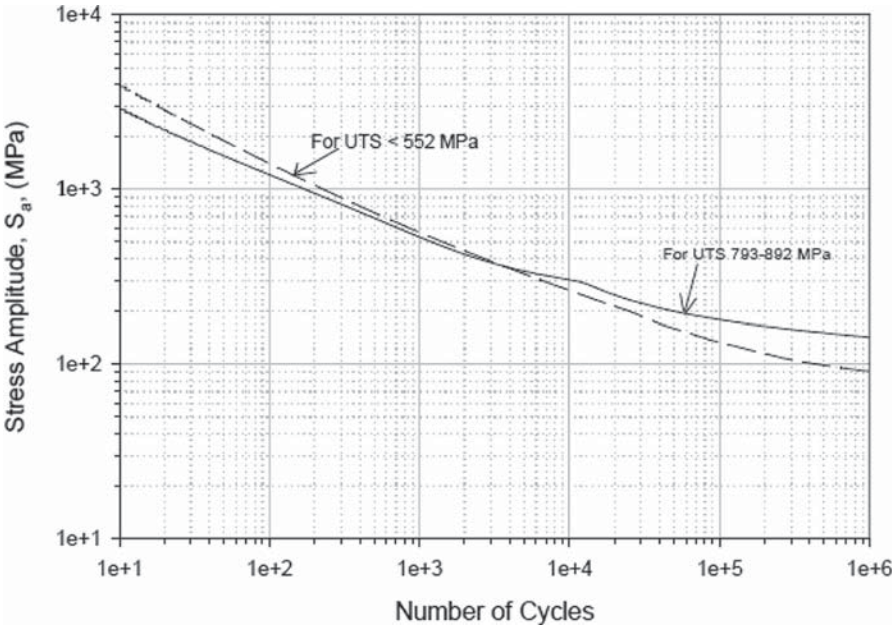


FIG. 4.22 FATIGUE CURVE FOR CARBON, LOW ALLOY, SERIES 4XX, HIGH-ALLOY STEELS, AND HIGH-TENSILE STRENGTH STEELS (ASME, Section VIII [71])

$$\Delta\varepsilon_{\text{peq},k} = \frac{\sqrt{2}}{3}\left[\begin{array}{l}(\Delta p_{11,k} - \Delta p_{22,k})^2 + (\Delta p_{22,k} - \Delta p_{33,k})^2 + \\ (\Delta p_{33,k} - \Delta p_{11,k})^2 + \\ 6\left(\Delta p_{12,k}^2 + \Delta p_{23,k}^2 + \Delta p_{31,k}^2\right)\end{array}\right]^{0.5}$$

$$\Delta\varepsilon_{\text{peq},k} = \frac{1}{\sqrt{2}}\left[\begin{array}{l}(\Delta\sigma_{11,k} - \Delta\sigma_{22,k})^2 + (\Delta\sigma_{11,k} - \Delta\sigma_{33,k})^2 + \\ (\Delta\sigma_{22,k} - \Delta\sigma_{33,k})^2 + \\ 6\left(\Delta\sigma_{12,k}^2 + \Delta\sigma_{13,k}^2 + \Delta\sigma_{23,k}^2\right)\end{array}\right]^{0.5}$$

Once stresses are determined, they are compared to Fig. 4.22 or similar graphs to determine the estimated life.

4.5.7.3 Method 3: Structural Stress Method for Fatigue The Structural Stress Method or the use of fracture mechanics is permitted in Section VIII, Division 3 for the design of high-pressure vessels (>10,000 psi), where lower design margins are permitted due to the use of more stringent design, testing, fabrication, and examination requirements. To support this method, Pinsha Dong (ASME B31.3 Committee minutes), recently developed a technique, which combined available steel weldment fatigue data. From his analysis, a single master curve for steel weldments was obtained, which is independent of ultimate strength and also provided corrections for thickness and environment. He recommended the 99% confidence level (Lower 99) for design, as shown in Fig. 4.23. A summary of the data considered by Dong is presented in Fig. 4.24. An important aspect of this data is that a fatigue limit is not apparent for welded steel structures. That is, the assumption of infinite life beyond the fatigue limit is invalid.

4.5.8 Fatigue Summary

Fatigue has been considered in several chapters of this text. As a rule, full-scale fatigue data is recommended, but full-scale data is frequently unavailable. B31.3 provides fatigue data based on limited full-scale testing, and the pressure vessel codes use data from both small- and large-scale fatigue tests. Fatigue curves from each of these sources have applicability to piping design and failure analysis. Overall, sufficient data and theory is provided here to prevent and evaluate many piping fatigue failures.

4.6 FRACTURE MECHANICS

Once a crack forms due to fatigue, further growth of that crack can be evaluated using the principles of fracture mechanics. This field of study is extensive, and only a cursory overview is presented here. Although fracture mechanics publications are prolific, a few references elucidate techniques to evaluate fractures in pipe systems. A thorough history of fracture mechanics development to 1965 is provided by Barsom [166]. To understand the principles of fracture mechanics, Anderson [103] provides a comprehensive text.

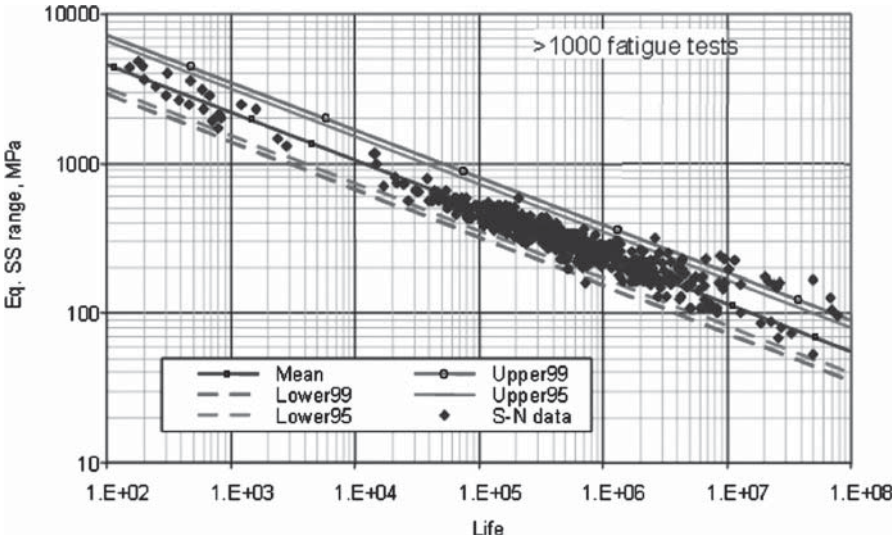


FIG. 4.23 MASTER FATIGUE CURVE FOR STEEL WELDMENTS

4.6.1 Fracture Mechanics History

Griffith performed classic experiments that started the field of fracture mechanics in 1920. He loaded glass fibers in tension and found that a fiber failed at the tensile strength of 24,900 psi when the diameter equaled 0.04 in. As the diameter was decreased to 0.00013 in., the breaking stress increased to 491,000 psi. Imperfections in glass fibers resulted in drastic differences in tensile strength. These test results led to the conclusion that imperfections reduce the ability of all materials to resist fracture.

The field of fracture mechanics developed little until ship fractures occurred during World War II. Following that research, various researchers further developed the fundamentals of fracture mechanics to address failures of jet aircraft, turbine motor casings, and missile components in the 1950s. Since that time, extensive study and experimentation has been performed. Both linear elastic fracture mechanics (LEFM) and elastic-plastic fracture methods were developed.

4.6.2 Applications of Fracture Mechanics and Fitness for Service

LEFM has been adapted to apply fracture mechanics principles to pipe systems and pressure vessels. ASME, Section XI [167] applies LEFM principles with elastic-plastic correction factors to assess subsurface and surface flaws that exist following initial fabrication. For in-service cracks, API 579-1/ASME FFS-1 and API 579-2 [168 and 169] provide accepted methods and worked example problems of how to assess in-service fractures of various types, including circumferential cracks, elliptical surface cracks, circumferential cracks, longitudinal cracks, and cracks at socket welds. The API techniques permit continued operation of pipe systems and pressure vessels once they are determined to be fit for continued service, even though a crack may be present. To meet the requirements of fitness for service, combinations of inspections and fracture mechanics calculations are performed. Codes and standards supply extensive information with respect to fracture mechanics, but a short discussion of LEFM and elastic-plastic fracture mechanics provides added insight into pipe failure analysis.

4.6.3 LEFM

LEFM techniques assume that nonlinear material behavior near the crack tip has a negligible effect on crack formation. Essentially, the crack is assumed to be atomically sharp, and the breaking of molecular bonds at the crack tip causes fracture. To present LEFM, consider a through crack of length, $2 \cdot a$, in an infinite plate, subjected to a stress, σ (Fig. 4.25). Failure occurs when the stress intensity factor, K_I, exceeds the fracture toughness, K_{Ic}. That is, a crack will grow in length if $K_I \geq K_{Ic}$ where,

$$K_I = \sigma \cdot \sqrt{\pi \cdot a} \qquad \text{US (4.75)}$$

Fracture toughness constants (K_{Ic}, K_{IIc}, and K_{IIIc}) are experimentally determined constants for Modes I, II, and III fractures. These modes are associated with the direction of the applied displacement or load during tests, as shown in Fig. 4.26. Fracture toughness is measured with either load or displacement tests using various test specimen geometries, as shown in Figs. 4.27 and 4.28.

For an edge crack in a flat plate,

$$K_I = 1.12 \cdot \sigma \cdot \sqrt{\pi \cdot a} \qquad \text{US (4.76)}$$

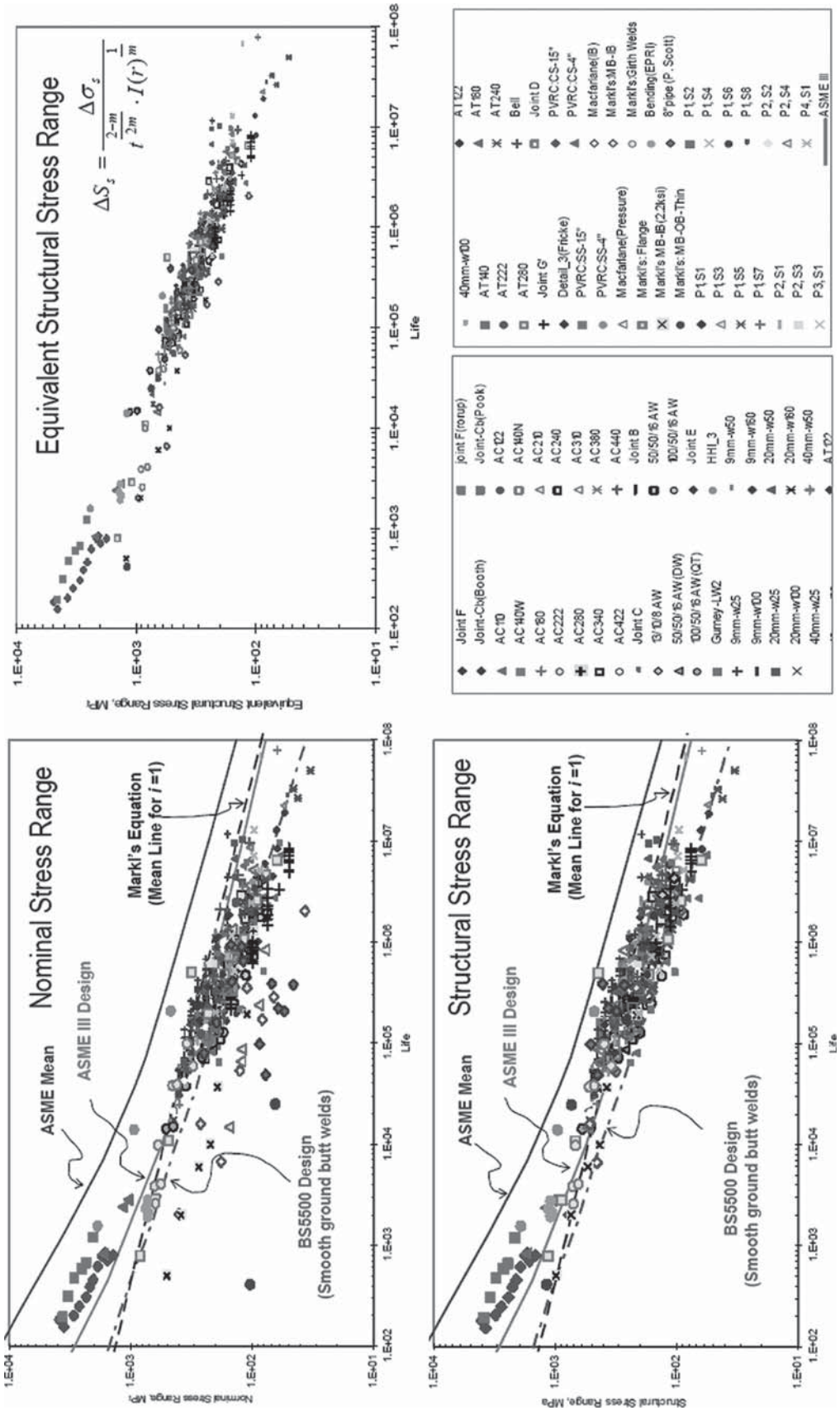


FIG. 4.24 COMPARISON OF FATIGUE METHODS AND SUPPORTING DATA (Pinsha Dong)

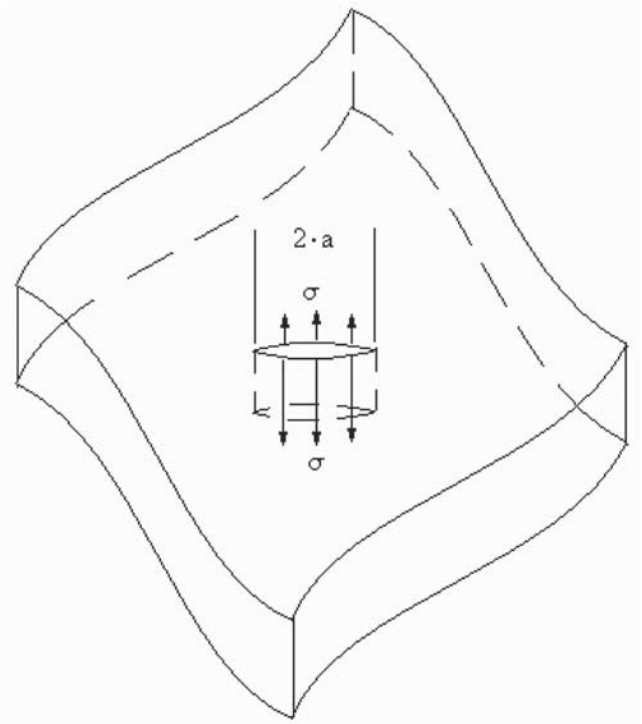


FIG. 4.25 CRACK IN AN INFINITE PLATE

where a is the depth of the crack. Anderson [103] provides numerous LEFM solutions for various crack geometries in terms of principal stresses and geometry. These simplifications of fracture mechanics serve to demonstrate the principles of LEFM.

However, when surface and subsurface cracks are analyzed in accordance with ASME, Section XI, Article A-3000, K_1 is a function of yield strength, hoop stress, bending stress, and crack dimensions. Section XIII, Article H-7000, addresses pipe flaws. Even the rate of crack growth may be calculated using Section XI techniques. More complex crack geometries are considered in API 579/ASME FFS-1. In these codes, LEFM techniques are corrected for elastic-plastic effects at the crack tip, using yield strength and geometry correction factors. These correction factors and elastic-plastic analysis developed to address the issue that LEFM inadequately described ductile material cracking.

4.6.4 Elastic-Plastic Analysis

Elastic-plastic fracture mechanics methods assume that a plastic zone forms near the tip of a crack. The crack tip blunts due to plastic deformation as the crack grows. Since this behavior is typical of steels, elastic-plastic effects are important to piping design. Two of the models used to describe plastic deformation at the crack tip, and the effects of those models on K_{eff} are shown in Fig. 4.29, where K_{eff} compensates K_1 for an effective crack length due to the plastic zones. Irwin [170] provides a short, comprehensive comparison between LEFM and elastic-plastic fracture mechanics.

4.6.5 Elastic-Plastic Fracture Mechanisms

Ductile metallic fractures are further complicated by the micromechanisms associated with fracture. Some micromechanisms of fracture are shown in Fig. 4.30. Fig. 4.31 shows a pattern of void growth on a fracture surface, which initiates at material imperfections.

As an example of ductile material failure, a fracture surface is shown in Fig. 4.32. Microvoids are formed, which coalesce to initiate fracture. Then, cleavage or intergranular cracking occurs as the crack surfaces separate, followed by the formation of striations, which occur during successive cycles. Also of note, abrasion and corrosion during crack growth frequently prevent photomicrographs of this quality, since surfaces are damaged.

4.6.6 Crack Propagation

LEFM also provides a method to estimate the rate of crack growth, and the LEFM method is corrected for

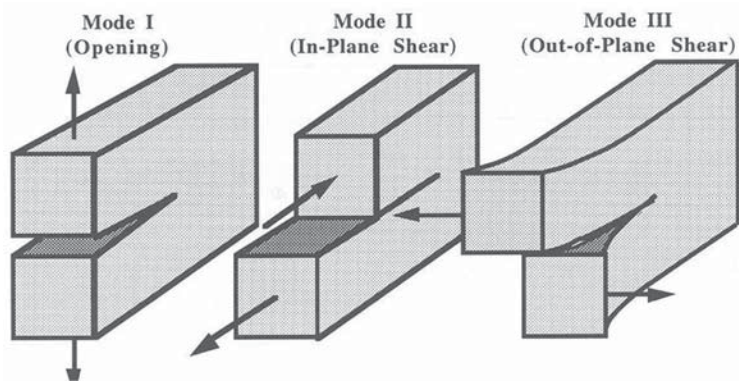


FIG. 4.26 FRACTURE MODES ("Fracture Mechanics": Fundamentals and Applications" by Anderson, Ted L. Copyright 2012. Reproduced with permission of Taylor and Francis Group, LLC. [103])

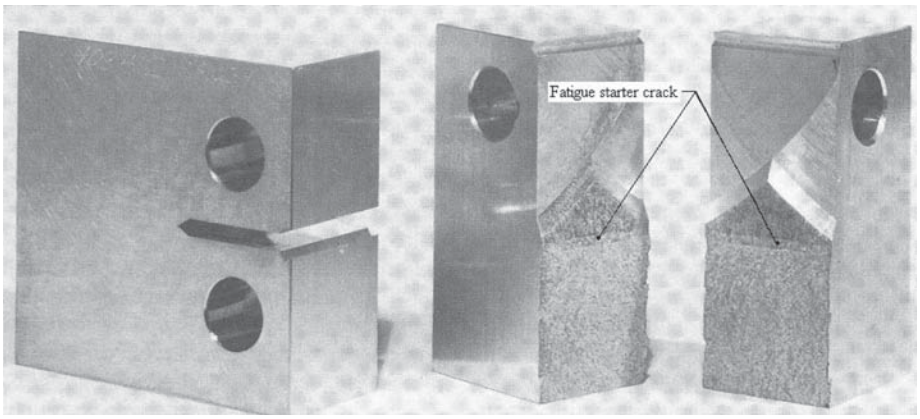


FIG. 4.27 FRACTURE TEST SPECIMEN (ASM [170], Reprinted by permission)

plasticity effects at the crack tip. Cracks propagate, or grow, above a threshold fracture toughness, K_{thr}, but below the critical fracture toughness, K_{1c}, which equals the fracture toughness of a material. When K_{1c} is approached, the rate of fracture increases sharply, as shown in Fig. 4.33. Below K_{thr}, a crack will not propagate. To consider the figure, da/dn is the rate of crack length, a, increase per cycle, n, and $\Delta K = K_{I,max} - K_{I,min}$, which is the difference between maximum and minimum stress intensity factors, which are calculated from service conditions. Crack growth is diminished when the operating temperature is 30 degrees F above the ductile to brittle transition temperature.

Using Section VIII (Division 3, Article KD-4 and Appendix D), one technique is provided to evaluate the rate of crack growth. A comprehensive example for this technique requires several pages and is excluded from this text. However, presentation of the equations provides insight into crack growth.

Example 4.10 Present the general equations for the growth of an elliptical shaped, longitudinal, surface crack in a pipe.

Assume that a crack has occurred or that the fatigue limit has been exceeded and complete inspection of the pipe system cannot be performed. If a crack has been observed, then API 579/ASME FFS-1 techniques can be directly applied. If not, then an assumption is required for crack dimensions. Per Section VIII, Division 3, surface cracks grow with a length, L''), to a depth ratio of L''/a = 3/1. Per API 579/ASME FFS-1, a critical crack depth can be determined

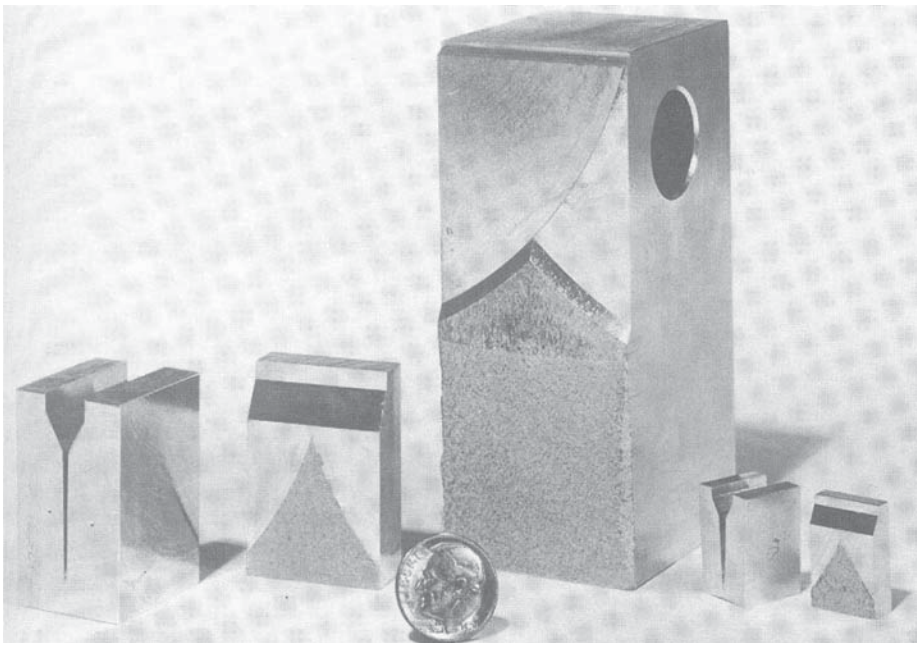


FIG. 4.28 FRACTURE TEST SPECIMENS (ASM [170], Reprinted by permission)

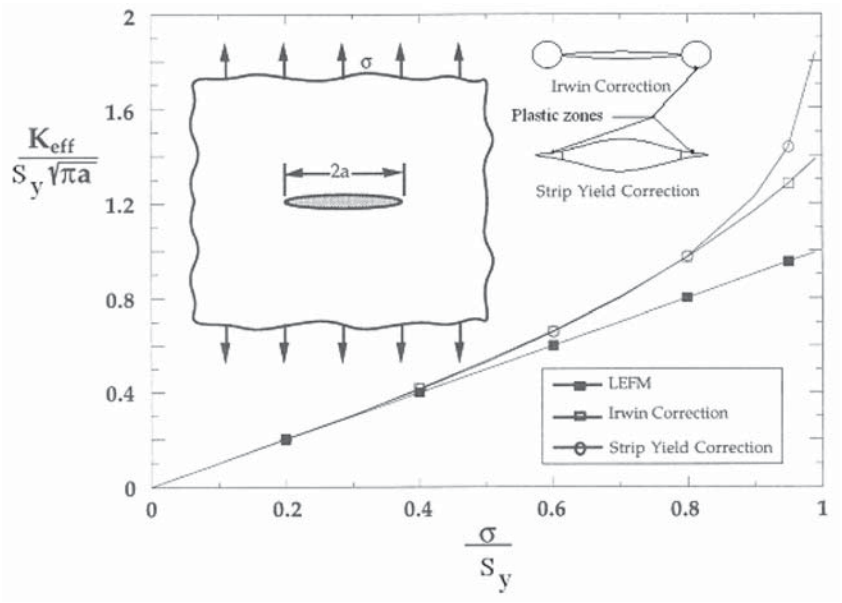


FIG. 4.29 COMPARISON OF LEFM TO ELASTIC-PLASTIC FRACTURE ("Fracture Mechanics": Fundamentals and Applications" by Anderson, Ted L. Copyright 2012. Reproduced with permission of Taylor and Francis Group, LLC. [103])

beyond which the crack will rapidly grow. To this critical crack depth, the rate of crack growth per cycle at any crack depth can be determined. Then da/dn, equals

$$\frac{da}{dn} = C \cdot f(R_K) \cdot (\Delta K)^m = C \cdot f\left(\frac{K_{I,min} + K_{I,res}}{K_{I,max} + K_{I,res}}\right) \cdot (K_{I,max} - K_{I,min})^m \quad \text{US (4.77)}$$

where C and m are material constants, and $K_{I,res}$ is a stress intensity factor due to residual stresses from autofrettage. Note that when $(K_{I,max} + K_{I,res}) \leq 0$, d$a$/d$n$ = 0, and a crack will not propagate. To calculate the required stress intensity factors,

$$K_I = \left((A_0 + P) \cdot G_0 + A_1 \cdot G_1 + A_2 \cdot G_2 + A_3 \cdot G_3\right) \cdot \sqrt{\frac{\pi \cdot a}{Q}} \quad \text{US (4.78)}$$

where P is the applied pressure on the crack, Q, $A_0 - A_4$, and $G_0 - G_3$ are constants related to crack geometry and plasticity effects, and $f(R_K)$ is a material property.

Note also that when $\Delta K < K_{thr}$, da/dn = 0, and a crack will not propagate. This observation may be critical to continued use of a system subjected to water hammer or other cyclic loads. Fracture mechanics may demonstrate that unseen cracks on the inside of a pipe cannot grow once water hammer-induced stresses are eliminated. That is, the system may be fit for service even if cracks are

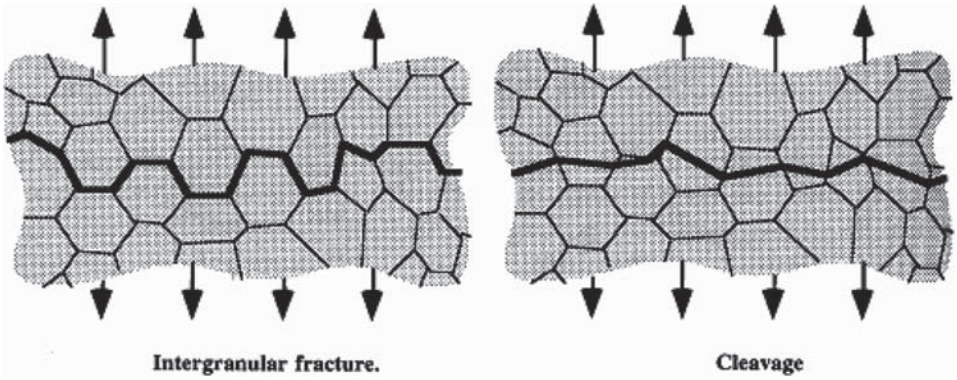


FIG. 4.30 MICROMECHANISMS OF FRACTURE IN METALS ("Fracture Mechanics": Fundamentals and Applications" by Anderson, Ted L. Copyright 2012. Reproduced with permission of Taylor and Francis Group, LLC. [103])

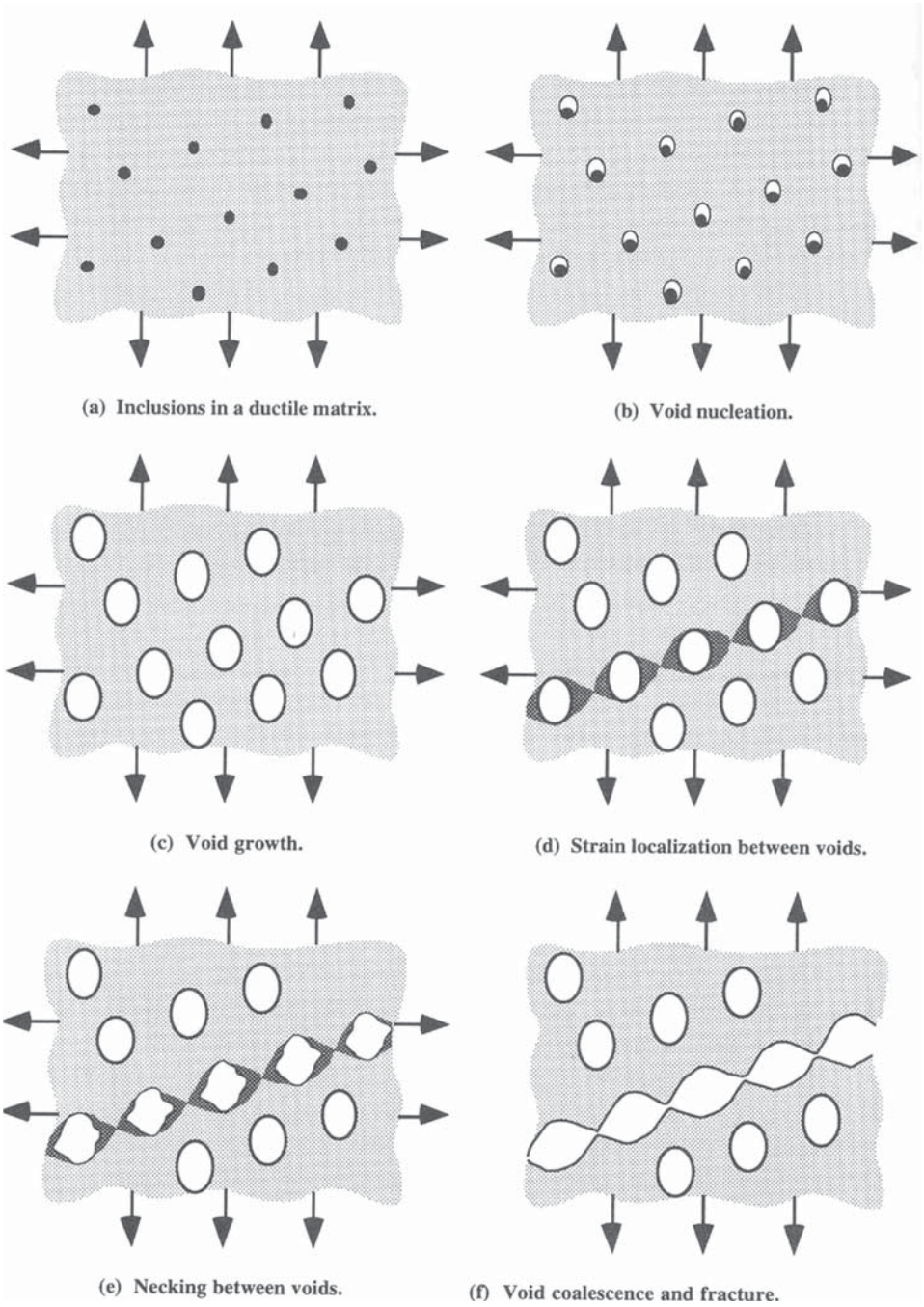


FIG. 4.31 CRACK FORMATION ON CRACK SURFACES ("Fracture Mechanics": Fundamentals and Applications" by Anderson, Ted L. Copyright 2012. Reproduced with permission of Taylor and Francis Group, LLC. [103])

present, and further growth of those cracks can be eliminated by eliminating the fluid transient.

4.6.7 Stress Raisers

Stress raisers caused by structural discontinuities are not typically addressed in the pipe codes, since localized plastic deformation generally corrects stress discontinuity problems at installation by local yielding. However, discontinuities occurring at socket welds frequently lead to failures in service when exposed to thermal or mechanical cycling. Cracks at socket welds may also be evaluated using API 579/ASME FFS-1.

4.6.8 Fracture Mechanics Summary

Fracture mechanics is useful for determining the remaining life of a pipe system when cracks are detected in

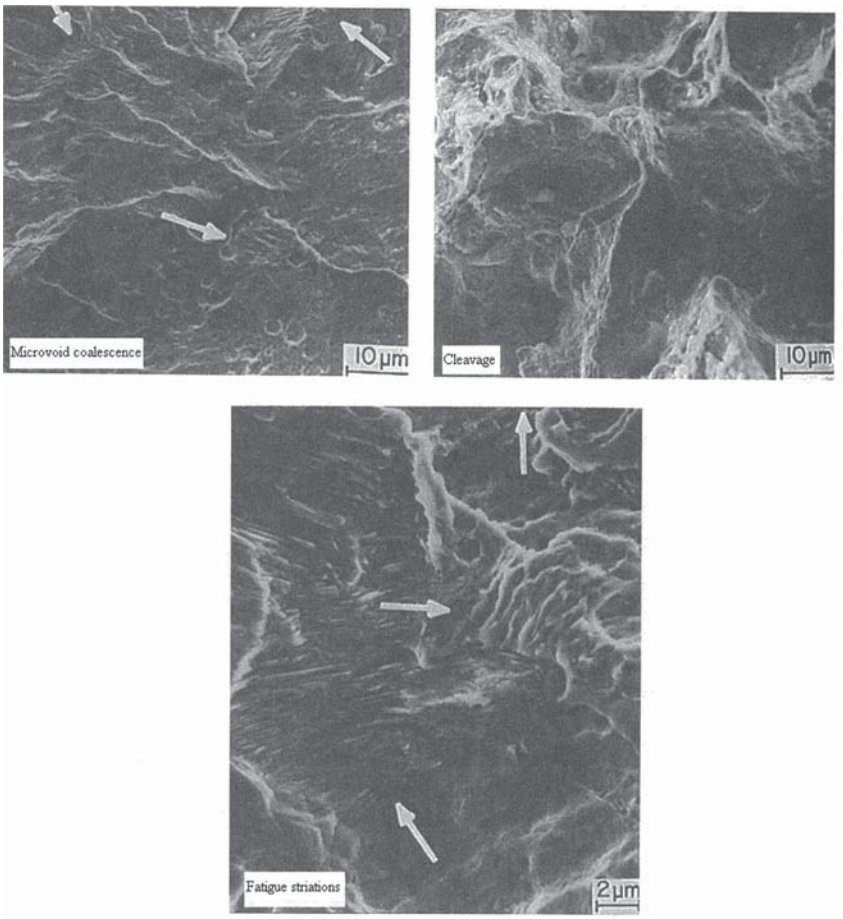


FIG. 4.32 PHOTOMICROGRAPHS OF FRACTURE SURFACES (Brooks and Choudhury [95], Reprinted by permission of McGraw Hill)

operation. Calculation techniques are available, but outside the scope of this work. Books and standards are available for both Fracture Mechanics and Fitness for Service to perform calculations and assessments of fracture damage (Anderson [103] and Antaki [131]). One aspect of fracture mechanics is that further pipe cracks may be prevented by simply reducing the loads on the system after initial cracks are detected. To do so, pipe stresses, fracture toughness, and remaining life require calculation. For fatigue cracks due to fluid transients, an implication is that the system may be returned to service by preventing further fluid transients. A risk of this type of decision is that other incipient cracks may have already formed in the pipes, and another unexpected transient may induce further leaks.

4.7 CORROSION, EROSION, AND STRESS CORROSION CRACKING

In general, corrosion and erosion are identified by irregular thinning, pitting, crevices, or holes through a pipe wall. Stress corrosion cracking is an acceleration of crack growth due to corrosion. In fact, stress corrosion cracking may initiate at a grain boundary, where a crack might not otherwise be created (intergranular stress corrosion cracking). Stress corrosion also accelerates during chemical attack within cracks. Significant detail is available in the literature from many sources. For example, McEvily [171] provides graphs for fatigue and fracture of many materials. Craig and Anderson [163] provide comprehensive tables of corrosion rate data for different material combinations to describe galvanic corrosion, which is induced by the current through an electrolyte between two different materials of different electrical charges. A specific example is the galvanic corrosion between pipes and soil for buried piping. API 579/FFS-1 can also be used to assess corrosion damage for fitness for service. During [164] provides hundreds of case studies for different types of corrosion in pipe systems. One of the goals of this text is to note that water hammer damage is frequently attributed to corrosion when the root cause may,

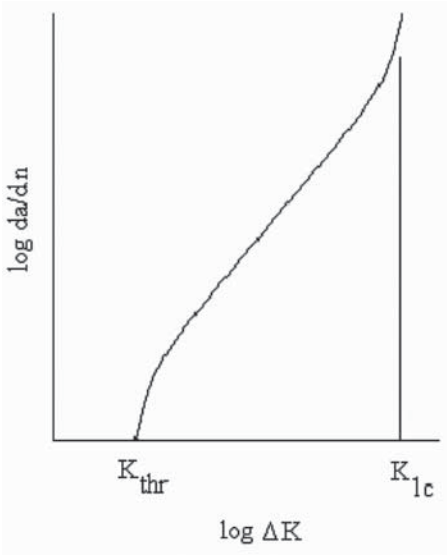


FIG. 4.33 CRACK PROPAGATION

in fact, be water hammer, although stress corrosion may accelerate crack growth caused by fluid transients.

A few corrosion examples from During are presented here. Figs. 4.34, 4.35, and 4.36 are obviously due to corrosion only. However, Fig. 4.37 shows a classic fatigue fracture, where the fracture initiated at the bottom of a shallow pit in the pipe surface. A possible, uninvestigated cause was fatigue due to water hammer.

4.8 FLOW-ASSISTED CORROSION (FAC)

Flow-assisted corrosion typically occurs at flow rates above 15 ft/second, where the oxide layer of a steel is removed by the fluid flow. Examples of FAC-induced pipe failures are shown in Fig. 4.38 (five fatalities) and Fig. 4.39 (four fatalities). As a result of these accidents, A106 steel was investigated, and wear rates were shown to be related



FIG. 4.34 EROSION OF CARBON STEEL (During [164], Reprinted by permission of Elsevier Publishing)

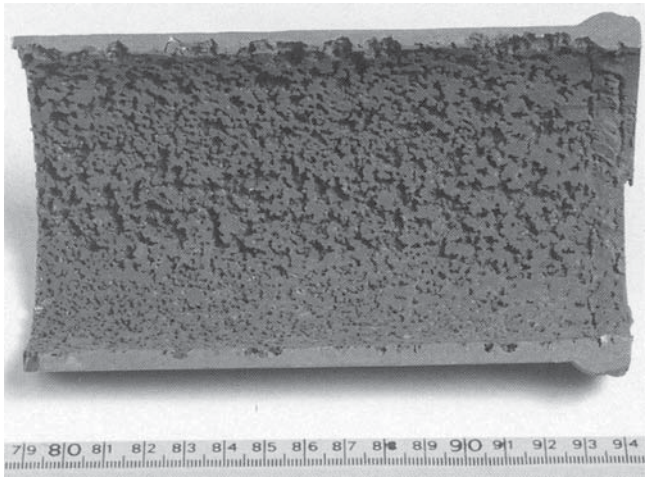


FIG. 4.35 CAVITATION EROSION OF CARBON STEEL (During [164], Reprinted by permission of Elsevier Publishing)

to alloy content, as shown in Fig. 4.40 (Nayyar [152]). Accordingly, factors affecting FAC include water chemistry, temperatures between 200°F and 500°F, alloy content < 0.1% for single-phase flow, alloy content < 0.5% for two-phase flow, and geometry such as elbows and reducers. Wall thicknesses have been observed to be as low as 1 / 10 of the initial wall thicknesses at the time of pipe rupture (Frey [112]). Several "Lessons Learned" have been concluded from accidents as recent as 2007 (Frey [112]), which include (1) analysis for FAC can be performed using software, such as CHECWORKS, (2) alloy content control, and (3) routine inspections. The potential influences of fluid transients were not evaluated in these studies.

4.9 LEAK BEFORE BREAK

There are many publications on the leak before break theory, and the theory is implemented in Section VIII, Divison 3 of the Pressure Vessel Codes. Essentially, cracks incrementally increase in size during the fatigue process. Accordingly, sudden rupture is not expected due to high-cycle fatigue, and the pipe system leaks before catastrophic failure, while sudden fracture may occur for low-cycle fatigue or overload. In practice, fatigue cracks from water hammer frequently start as smaller leaks, which progressively increase as cycles continue. In fact, valves have frequently been observed to leak before pipe leaks occur. Although the leak before break phenomenon may provide protection against major failures, many cracks can be induced throughout a pipe system by the time the first leak is noticed. Also, if the pressure surge magnitude is high enough, low-cycle fatigue and rupture may occur during a single water hammer event.

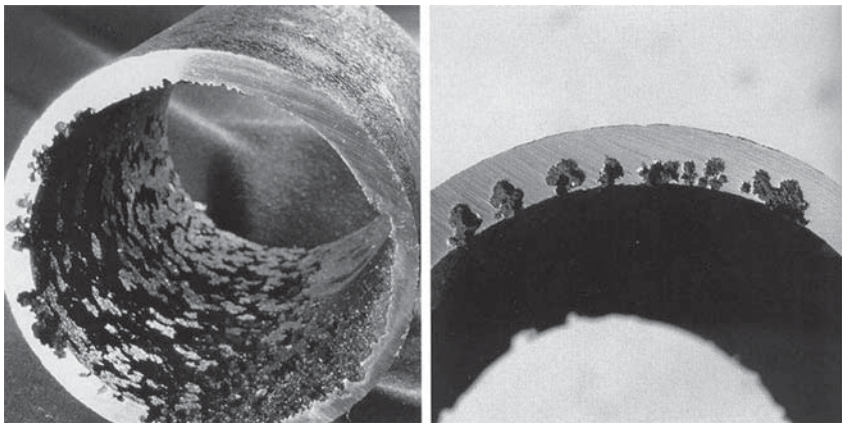


FIG. 4.36 ACID EROSION OF CARBON STEEL (During [164], Reprinted by permission of Elsevier Publishing)

4.10 THERMAL FATIGUE

Many examples of thermal fatigue failures are available in the literature, and a recent investigation highlights the effects of this failure mechanism (Frey [112]). In this case, cooler condensate intermittently flowed down into a steam line and suddenly cooled the piping at the transition (stress raiser) to an elbow. Some of pipe damages are shown in Figs. 4.41 through 4.43, where some of the piping spun loose from the side of the building and smashed a car 1200 ft away from the accident.

4.11 CREEP

Although outside the scope of this text, creep should at least be noted. Creep is an increasing strain in a material over time. For metals, creep is negligible up to 700°F. One of the few examples of creep at ambient conditions for steels is the use of ball bearings in rotating equipment. If a pump or motor is not rotated every few months, the balls will form flat spots due to low-temperature creep.

4.11.1 Examples of Creep-Induced Failures

However, for metallic pipe systems, creep is only a concern at high temperatures, which equal about ½ of a metal's melting temperature. For example, creep occurs above 1000°F for iron, 800°F for carbon steel, 850°F for molybdenum, 950°F for P11, and 1000°F for P22. Examples where high-temperature creep is of concern are boilers, furnaces, supersonic aircraft, and turbines. In general, leak before break does not occur during catastrophic failure of piping due to creep (Frey [112]). P11 and P22 materials were superseded by P91 and P92 materials for boiler construction, following the pipe failure shown in Fig. 4.44, which killed seven operators as the steam blew through several walls into the control room. Another of

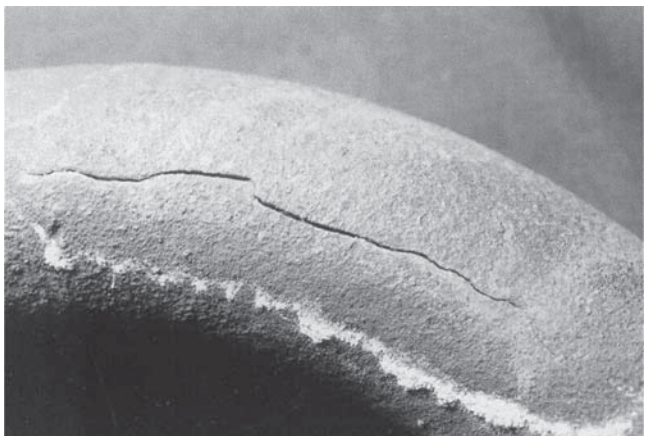


FIG. 4.37 INTERGRANULAR STRESS CORROSION CRACKING OF CARBON STEEL (During [164], Reprinted by permission of Elsevier Publishing)

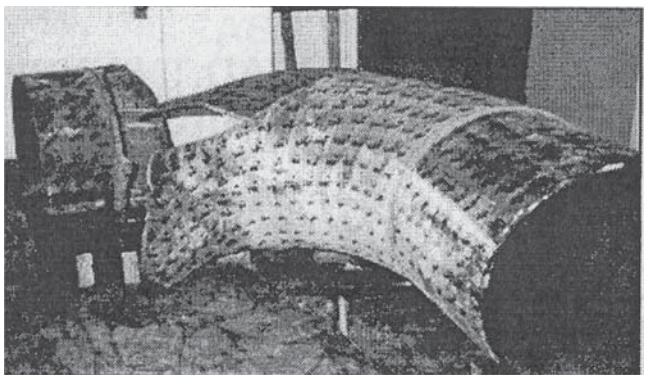


FIG. 4.38 SURRY POWER PLANT, 1986, FAC FAILURE, NPS 18 CONDENSATE PIPING (Nayyar [152])

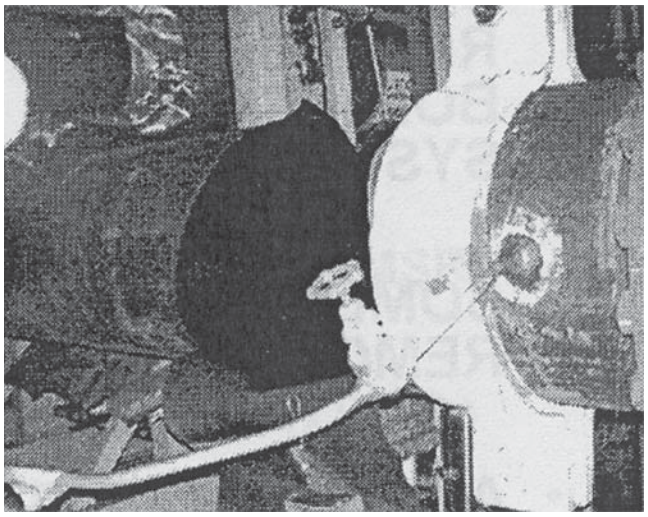


FIG. 4.39 MIHAMA POWER PLANT, 2004, FAC FAILURE, NPS 22 CONDENSATE PIPING (Nayyar [152])

eight catastrophic creep failures, which occurred in power plants between 1979 and 1998, is shown in Fig. 4.45.

4.11.2 Creep in Plastic and Rubber Materials

Creep is also important for plastics and rubbers, where significant creep may occur at room temperature, and strains induced during installation of plastic pipe may reduce ductility. If either assembly stresses for above-grade PVC and CPVC piping or settlement stresses for underground PVC or CPVC piping are induced during installation of plastic piping, loss of ductility can render the pipe in a near-failure condition. On the other hand, HDPE piping is quite ductile. Other properties of plastics and rubbers, like the elastic modulus, may also change over time. Work is presently underway by ASME to create a new Standard for plastic piping. At present, design rules for creep, fatigue, pipe hanger spacings, and molded parts are unavailable. In fact, ASME, B31.9 restricts the size of plastic pipe. Also, plastic liners and unreinforced tubing may be subject to collapse during water hammer for those cases where vacuum pressures are created.

4.12 OTHER CAUSES OF PIPING FAILURES

ASME, Section III, Section 2, Part B, App A. provides a comprehensive list of piping failure mechanisms. In addition to those mentioned here, other failure mechanisms include:

1. Graphitization which is a time-dependent, localized breakdown of steel into carbon and iron. Graphitization occurs above 800°F for carbon steels and above 875°F for chrome-molybdenum steels and usually occurs in the heat-affected zone of welds.
2. Pipe supports: frozen or not operational; improperly routed or spaced, elastic follow-up.
3. Hydrogen embrittlement caused by the absorption of hydrogen by steels to increase hardness and reduce resistance to impacts.
4. Hydrogen attack and cracking at temperatures between 600°F and 1000°F occurs when steels are subjected to wet hydrogen sulfide, H_2S.
5. Corrosion under insulation.
6. Microbiologically induced corrosion (MIC) caused in stagnant or low-flow water, where sulfur, ammonia, or H_2S are present.
7. Counterfeit material and improper identification of piping.
8. Improper welding techniques or heat treatment. Preheating before welding prevents subsurface cracks on some low-alloy carbon steels, and postheating of welds prevents residual stresses due to hardening and strengthening near the weld for some carbon

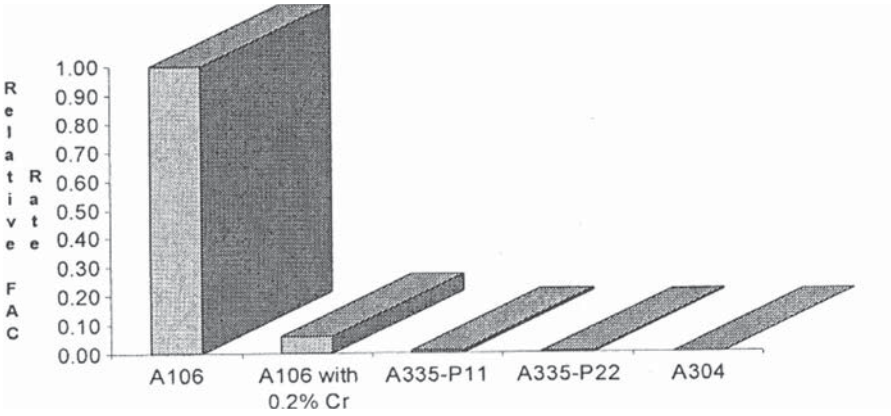


FIG. 4.40 MATERIAL VS. WEAR RATE (Nayyar [152])

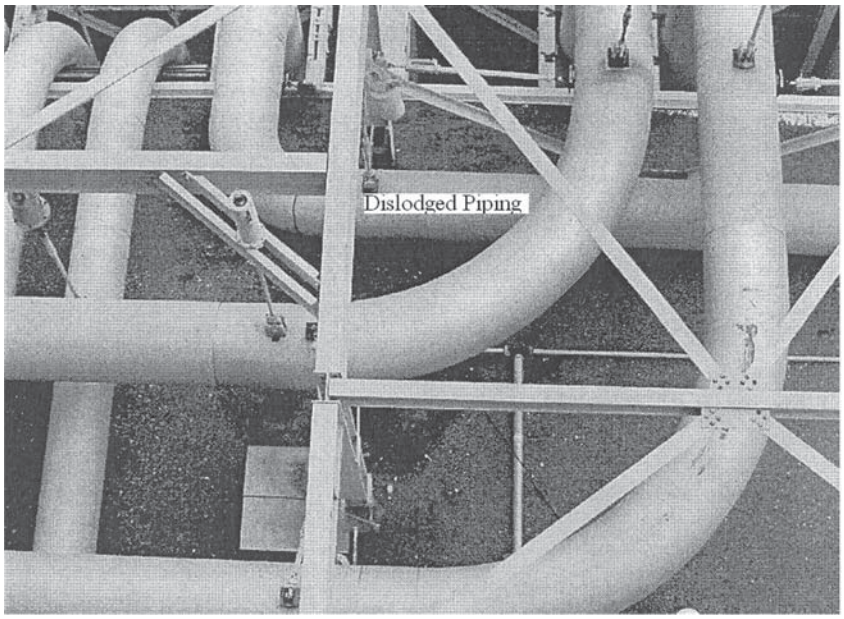


FIG. 4.41 W. A. PARISH POWER PLANT, 2003, NPS 30, ASTM A155 (Frey [112])

and alloy steels. Postheating anneals the weld and reduces residual stresses.

4.13 SUMMARY OF PIPING DESIGN AND FAILURE ANALYSIS

This chapter concludes a presentation of the fundamentals required for pipe system design and failure analysis. Appropriate references for added explanations and derivations of equations are provided as required. Pipe systems are designed to operate below the yield strength of selected pipe materials, but fatigue may occur at even lower stresses. As a rule of thumb, cracks due to internal pressure and temperature excursions start at the inside of the pipe and decrease in length toward the outer wall, and failures due to pipe support stresses start at the outer wall and decrease in length toward the inside of the pipe. Once

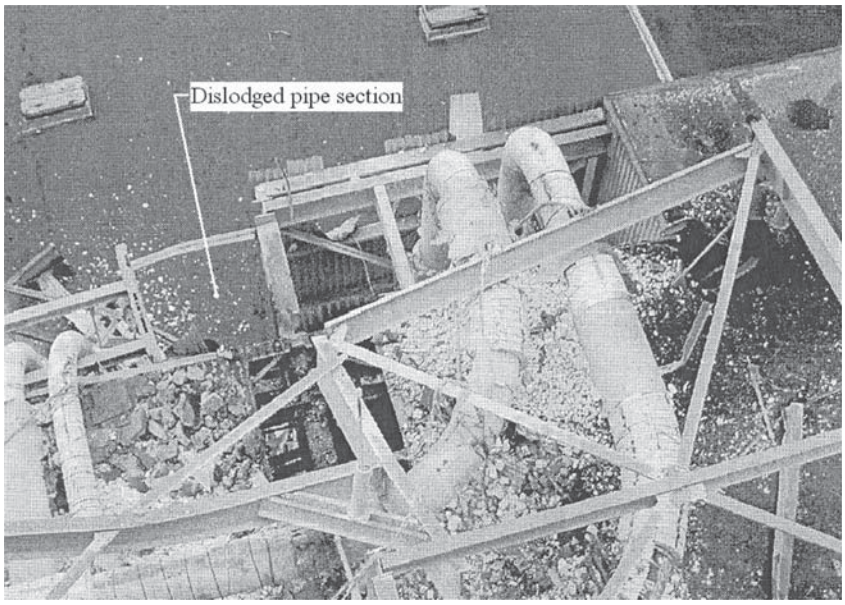


FIG. 4.42 W. A. PARISH POWER PLANT, 2003, NPS 30, ROOFTOP PIPING AFTER ACCIDENT (Frey [112])

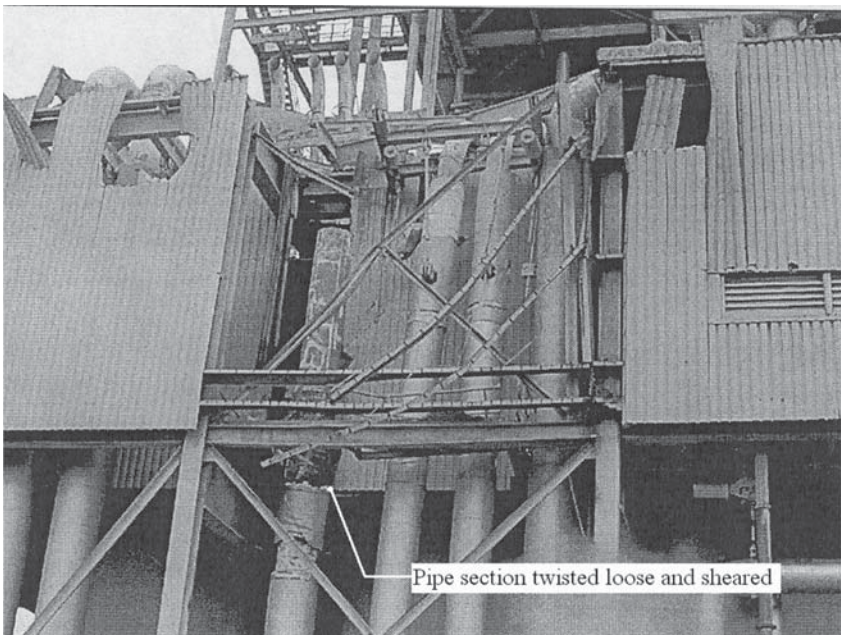


FIG. 4.43 W. A. PARISH POWER PLANT, 2003, NPS 30, VERTICAL PIPING AFTER ACCIDENT (Frey [112])

a fatigue crack occurs, fracture mechanics may be used in some cases to extend the service life of the pipe system.

The goals of Chapters 2–4 are to provide sufficient information on fluid flow and structures to design and analyze simple pipe systems. More complex pipe systems also incorporate the fundamentals and data presented here, but computer simulations are generally performed.

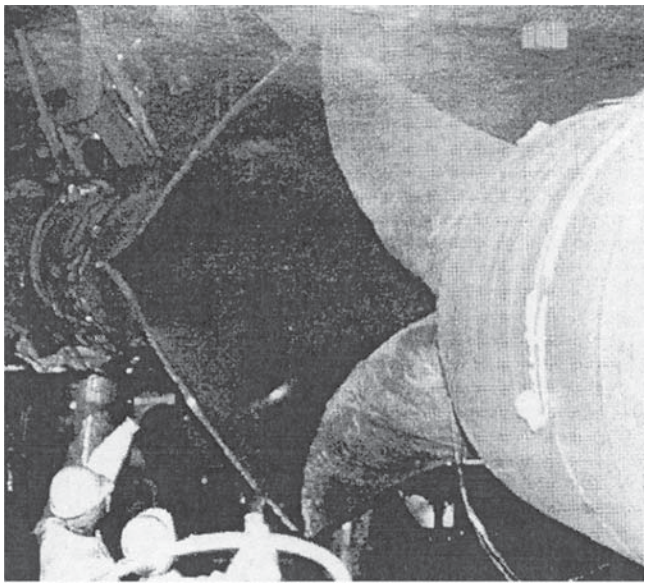


FIG. 4.44 MOHAVE POWER PLANT, CREEP FAILURE, P11, SEAM WELD FAILURE (Frey [112])

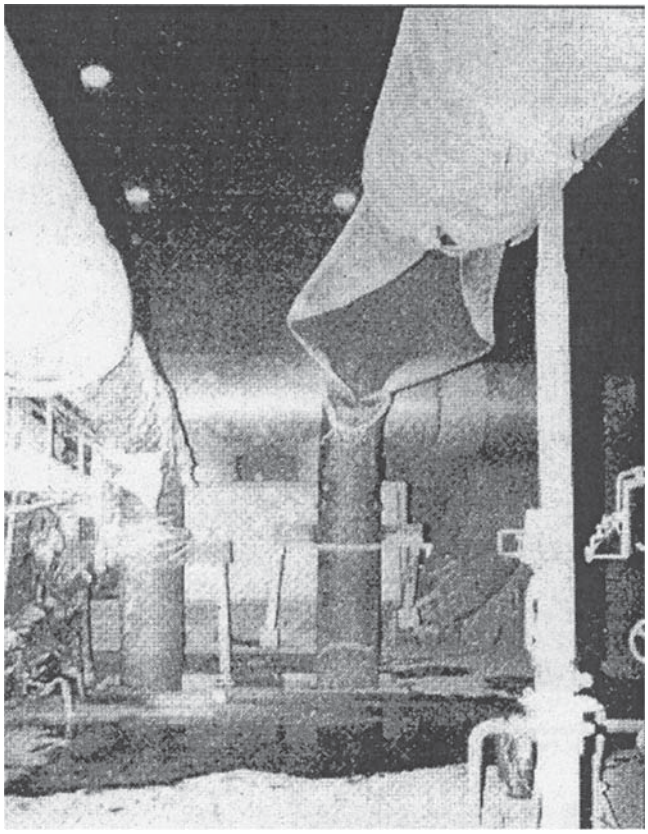


FIG. 4.45 MONROE POWER PLANT, CREEP FAILURE, P22, SEAM WELD FAILURE (Frey [112])

Chapter 2 provides a comprehensive discussion of fluid mechanics, materials, and equipment required to size and design pipe systems for liquid flow. Different types of fluids and two-phase flow were also considered in that chapter.

Chapter 3 provides sufficient design equations and data to analyze structural designs for simple pipe systems and determine allowable stresses. Different pipe codes were noted to yield different allowable stresses for comparable designs. In each code, the allowable stress is related to yield stresses at operating temperatures, where pipe failures occur at stresses above the allowable stresses.

To determine the stresses required to cause failure, Chapter 4 provides methods to analyze most pipe failures. Damages are caused by either cyclic or statically applied loads. Both static and cyclic loads may lead to plastic failure, which occurs above yield and is beyond pipe code design limits. Cyclic loads also induce fatigue and fracture, which occur at stresses below yield. Fracture mechanics and corrosion failure mechanisms were superficially considered. However, appropriate references were provided to analyze corrosion and fracture failures to determine if they are acceptable for continued system operation. The background provided in these chapters is tacitly assumed for the following discussions of fluid dynamics and dynamic piping response.

CHAPTER

5

FLUID TRANSIENTS IN LIQUID-FILLED SYSTEMS

Fluid transients in liquid-filled systems and steam condensate systems are a focus of this text, and a brief overview of fluid transient mechanisms is first warranted. Parmakian [172] provided a discussion of dated graphic techniques. Although thousands of papers on water hammer are available, Wylie and Streeter [173] provide comprehensive references describing theory, experiments, computer programs, and calculation techniques for fluid transients for pumps, valves, turbines, liquids, vapors, and gases. Moody [174] provided thermal and fluid transient theory. Chaudry [175] provided a thorough discussion of calculation techniques and numerous examples of water hammer in liquid-filled systems. Larock et al [176] provided computer programs and derivations of equations for water hammer, as well as steady-state fluid flow for pipe systems. Popescu et al [177] provided discussions of transients and calculation techniques for hydroelectric power plants. Popescu cited many accidents and provides a comprehensive discussion of fluid transients as they affected power-generation facilities. A recent review of theory provides an extensive list of references for water hammer (Ghidaoui [178]). Wiggert and Tijsseling [179] also provided a summary of theory with numerous references. For a comprehensive understanding of fluid transient theory, the reader is referred to these works, since a comprehensive understanding of the mathematical development of theory is required to prevent misapplication of that theory. This text only provides a broad overview of several fluid transient mechanisms, or causes, which affect pipe system response and damages. These mechanisms can be grouped into categories, such as:

1. Slug flow (paragraph 5.1)
2. Draw down, or emptying, of systems (paragraph 5.2)
3. Flow rate changes in liquid-filled systems during valve closures and pump startup and shutdown, which cause shock waves and pressure surges (paragraph 5.3)
4. Column separation and subsequent vapor cavity collapse in liquid-filled systems (paragraph 5.15.1)
5. Trapped air in liquid-filled systems (paragraph 5.17)
6. Vapor cavity collapse in steam condensate systems (paragraph 6.2)
7. Blow down in vapor-filled (steam) systems (paragraph 6.3)
8. Flow rate changes in condensable fluid systems. See Streeter for analysis techniques [172] since this topic is not fully addressed here. Even so, piping and pressure vessel damages are caused by valve operations in gas-filled pipes and by pressure surges due to compressor operations (Rollins [180])

Examples for each of the first five mechanisms (1 to 5) are presented in this chapter, along with technical discussions for each mechanism. Mechanisms 6 and 7 are considered separately in Chapter 6, even though there are similarities between different mechanisms.

5.1 SLUG FLOW DURING SYSTEM STARTUP

Slug flow can be initiated during initial system startup, when the pipe is empty or partially full and typically filled with air or vapor. As the system is filled, slug flow rushes through the pipe, and the liquid wave front impinges on elbows, valves, and tees throughout the system. All components are suddenly, rather than gradually, loaded, and pipe stresses may be dynamically magnified. In cases where the piping is initially empty near the pump, the pump operates near runout, and velocities are considerably higher than normal operating conditions. Accordingly, the change in fluid momentum at components can be considerably higher, which also increases stresses.

The basic water hammer equation describes valve closure, and a modification of that equation can be used for

simple cases of vapor collapse. Collapse occurs when vapor pockets are formed at high points in systems, and the water column is suddenly rejoined. Vapor pockets may be formed during a transient or may be present before the transient starts. A simplified calculation to find the maximum velocity and pressure due to slug flow where a moving column of water impacts a stationary column of water is derived from Eq. (5.1) and is expressed as

$$V_s\left(\text{ft/sec}\right)=\sqrt{\frac{2\cdot L_V\left(\text{ft}\right)\cdot P\left(\text{psi}\right)\cdot 144}{\rho\left(\text{lbf/ft}^3\right)\cdot L_S\left(\text{ft}\right)}} \quad \text{US (5.1)}$$

$$P\left(\text{psi}\right)=\rho\left(\text{lbf/ft}^3\right)\cdot a\left(\text{ft/sec}\right)\cdot\frac{V_s\left(\text{ft/sec}\right)}{2\cdot g\left(\text{ft/sec}^2\right)\cdot 144} \quad \text{US (5.2)}$$

where V_s is the velocity of the slug at impact, L_v is the length of a voided section of pipe, and L_s is the length of the slug. If the slug impacts the dead end of a pipe, the pressure is doubled. Note that frictional effects are not included in Eqs. (5.1) and (5.2), and consequently, pressure surges may be significantly overpredicted when these equations are used.

5.1.1 Slug Flow Due to Pump Operation

For, example, H. Thielsch [181] provided an example of a startup failure in a class that he taught from his text. He reported that a 12-in. diameter header was designed with the run of a tee installed perpendicular to a pump discharge. The pipe was initially filled with air, and when the pump was started using a direct on line motor starter, a slug of water hit the tee and moved the piping from its supports. The corrective action for that case was the installation of stronger supports. A VFD could have also corrected the problem. That choice was the designer's decision, which was to eliminate the cause or to counter the effect. In short, when a pump was suddenly started to provide water to an empty pipe system, damage occurred since the system was not designed to withstand transient flows.

5.1.2 Slug Flow During Series Pump Operation

Another example is the formation of individual slugs during the use of series pumps. If two pumps are in series, and the upstream pump has a lower flow rate than the downstream pump, insufficient flow will be provided to the downstream pump, slugs will be periodically propelled from the downstream pump, and vapor cavities will form between the pumps. Further discussion of this slug flow is available (Edwards and Haupt [78]).

5.1.3 Pump Runout Effects on Slug Flow

Also, examples 2.13 and 2.14 can be reconsidered with respect to runout. In those examples, the system length was 910 ft plus numerous fittings. Between the pump and an elbow at the system high point, there was only 48 ft of pipe, and the pipe was filled with water to this point when the pump started. At that time, the startup flow rate at this



FIG. 5.1 TANK DAMAGE DURING DRAW DOWN

elbow was nearly double the typical flow rate during normal operations. This particular example did not result in pipe damages, but quantifies the effects of runout conditions during startup. That is, pipe stresses can be significantly higher than expected when increased momentum is coupled with the dynamic magnification.

5.2 DRAW DOWN OF SYSTEMS

Emptying systems can cause subatmospheric pressures that may damage some components. Damages to pressure vessels have been reported at various facilities and also during the emptying of tanker trucks, where the truck container folds, and the center of the container drops to the ground between the wheels.

Example 5.1 Draw down for a storage tank

Shown in Fig. 5.1, tank damages were caused when a tank was emptied, and a vent valve on top of the tank had been covered with a plastic bag to protect the vent while the tank was painted. Failure to remove the plastic blocked the vent, caused the internal tank pressure to drop to the vapor pressure of the contents, a pressure near atmospheric was applied over the entire tank surface, and the tank collapsed.

5.3 FLUID TRANSIENTS DUE TO FLOW RATE CHANGES

The basic water hammer equation was derived by Joukowski [18] and is rewritten from Eq. (1.1) as

$$\Delta P(\text{psi}) = 2.1584 \cdot 10^{-4} \cdot \rho(\text{lbf}/\text{ft}^3) \cdot a(\text{ft}/\text{sec}) \cdot \Delta V(\text{ft}/\text{sec}) \quad \text{US} \quad (5.3)$$

The study of fluid transients has developed from this equation, which describes the pressure surge following a shock wave traveling at a sonic velocity along the bore of a pipe, due to sudden changes in flow. A few examples of pipe system damages follow to exemplify the importance of fluid transient theory. Following these examples, the water hammer equation will be considered with respect to assumptions, applications, factors that modify the basic equation, calculation techniques, and corrective actions. A few examples of water hammer accidents lead into a discussion of water hammer theory and applications.

5.3.1 Examples of Pipe System Damages in Liquid-Filled Systems

Hundreds of examples of water hammer damages are available in the literature, many other damages are unreported, and damages continue to routinely occur throughout the industry. Water hammer has resulted in the temporary loss of water supplies to various cities, in addition to process upsets considered here. The selected examples highlight water hammer.

5.3.1.1 Hydroelectric Power Plants Popescu et al [177] dedicated their text to transients in power-generation plants and large-scale pumping systems. Along with calculation techniques, they list a number of accidents and fatalities that occurred during power plant operations due to gate closures and fluid resonance. Since that publication, one of the most catastrophic power plant accidents in history has occurred.

Example 5.2 Hydroelectric Power Plant Accident

At the largest power plant in Russia, catastrophic damages were due to fatigue failures of mounting bolts caused by pressure fluctuation-induced vibrations. Piping supplied water from behind the dam down to the turbines, and fluid oscillations along with rotor imbalance due to recent repairs were considered to be the cause of higher than normal vibrations, which were considered to be within design specifications (Wikipedia). The control room at the bottom of the dam was flooded and destroyed, and 75 operators were drowned in the accident. Damages are expected to cost in excess of $630,000,000 and are shown in Figs. 5.2 through 5.6. Analysis following the accident concluded that vibration-induced fatigue failures of mounting bolts permitted the 1000 ton rotor to lift out of its seat through the turbine cover as the rotor spun at full speed. This particular example of fluid equipment damage is really outside the scope of this text, which focuses on industrial piping damages, but this disaster seems to be of interest here. Immediately following the accident, the photos below were widely circulated on the Internet with a brief, informal report, which incorrectly stated that water hammer was the cause.

5.3.1.2 Valve Closure Valve closure may result in shock waves initiated by valve closure, or shock waves may be initiated by vapor collapse. The following examples demonstrate the damages and pressure surges caused by seemingly simple actions of starting and stopping pumps or turbines and closing valves.

Example 5.3 Hydroelectric power plant pressure surges due to unexpected pressure surges

Fig. 5.8 shows the pressure surges for a power plant when flow is stopped at the turbine. Note that a surge tank is installed to protect piping between sections 4 and 5 on the figure, but significant pressure surges occur near the turbine in sections 1 to 3. For this reason, multiple surge tanks are frequently installed on large systems.

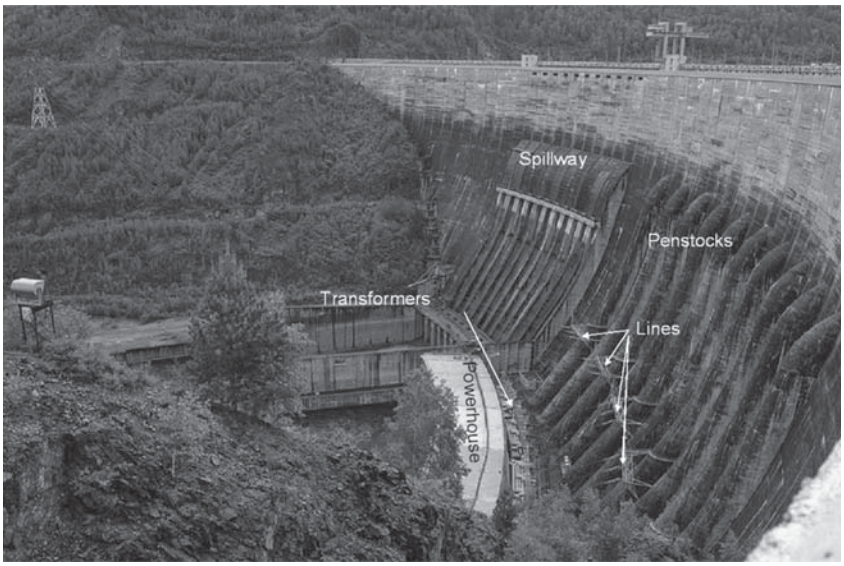


FIG. 5.2 SAYANO-SHUSHENSKAYA POWER PLANT (Environmental Protection Agency)

Example 5.4 Pressure surges in a pumping station

Fig. 5.9 shows pressure surges in a pumping station, where a check valve was installed to prevent reverse flow through the pump. As expected, pressure surge magnitudes decrease as the elevation increases from section 1 to section 12 of the pipe system. The surge tanks protect the piping between sections 4 and 5, but have a much smaller effect on the piping near the turbine. Calculations were performed using the method of characteristics (MOC), discussed in paragraph 5.8.3.

5.3.1.3 Vapor Collapse in a Liquid-Filled System

When a vapor pocket forms in a system, and later collapses, there is essentially no resistance to the forces of the recombining slugs of water. Essentially, the slugs slam together as the water condenses, and shock waves are formed, which in turn propagate through the fluid. An example of this potentially destructive force follows.

Example 5.5 Vapor collapse

Arastu et al [182] investigated a vapor collapse and corrective actions for a fire protection system accident. For this accident, a valve was opened, and vapor at the top of the stand pipe attached to the valve collapsed, sending shock waves through the system and cracking a valve (Fig. 5.8). The valve was actuated by smoke detection devices when smoke was detected, and the system previously actuated properly on multiple occasions without failure. In this case, the pressure surge cracked the valve and leaked more than 163,000 gal to fill a stairwell to more than 10 ft before the leak was stopped.



FIG. 5.3 SAYANO-SHUSHENSKAYA POWER PLANT (Environmental Protection Agency)



FIG. 5.4 TURBINE INSTALLATION (Environmental Protection Agency)

Typically, the system operated at 125 to 150 psig, but calculations showed that a pressure increase of 311 psi occurred due to opening the valve (Fig. 5.9), and a 1102-psi pressure increase occurred due to vapor collapse (Fig. 5.10). Calculations were performed using the MOC.

Both interim and long-term corrective actions were performed to address the problem. Interim corrective actions included replacement of cast iron valves with steel valves, continuous pump operation to prevent void formation, and installation of an accumulator tank at high points. This tank contained a 2-ft diameter bubble of nitrogen to cushion vapor collapse. Long-term corrective actions included adding relief valves to the pump recirculation lines, adding vent valves at the system high points, and installing a VFD to slowly start and stop pumps.

5.3.1.4 Damages Due to Combined Valve and Pump Flow Rate Changes System fatigue failures may be caused by pressure surges due to a combination of both pump and valve operational transients. The following example considers such a case.

Example 5.6 Cooling system damages

A cooling system for 1 million gal, radioactive liquid waste storage tanks suffered hundreds of cooling coil and underground piping fatigue cracks during more than 40 years of operation due to valve- and pump-induced fluid transients. Since the cracks were in a potentially corrosive radioactive environment, inspection was typically impossible, and corrosion was long assumed to be the cause of pipe leaks in the 2-in. NPS, carbon steel, cooling coils in the tanks. Several underground leaks also occurred and were attributed to other causes. Water hammer was identi-



FIG. 5.5 POWER HOUSE BEFORE THE ACCIDENT (Environmental Protection Agency)



FIG. 5.6 POWER HOUSE AFTER THE ACCIDENT (Environmental Protection Agency)

fied and corrected in the early 1990s, and only one leak has occurred since for systems that were modified to control water hammer. That leak was quickly shown to be a malfunction of the water hammer-control equipment. Fluid transients due to both pump operation and valve closures contributed to water hammer damages. Since this example was thoroughly investigated, it will be used to demonstrate numerous aspects of fluid transients in this chapter.

As a matter of fact, the dynamic stress theory presented in this text was developed to resolve these pipe failures. Without a failure theory to relate water hammer to pipe failures, justifying costs to modify pipe systems was impractical. The dynamic stress theory provided that relationship, and the application of that theory provided proof of the theory. In particular, the more damaged systems were corrected first, but systems that were undamaged failed before modifications corrected water hammer. The estimated cost of repairs was $5,000,000. The theory was new and unproven prior to that time. Modifications were expedited upon realization of the



FIG. 5.7 POWER HOUSE AFTER THE ACCIDENT (Environmental Protection Agency)

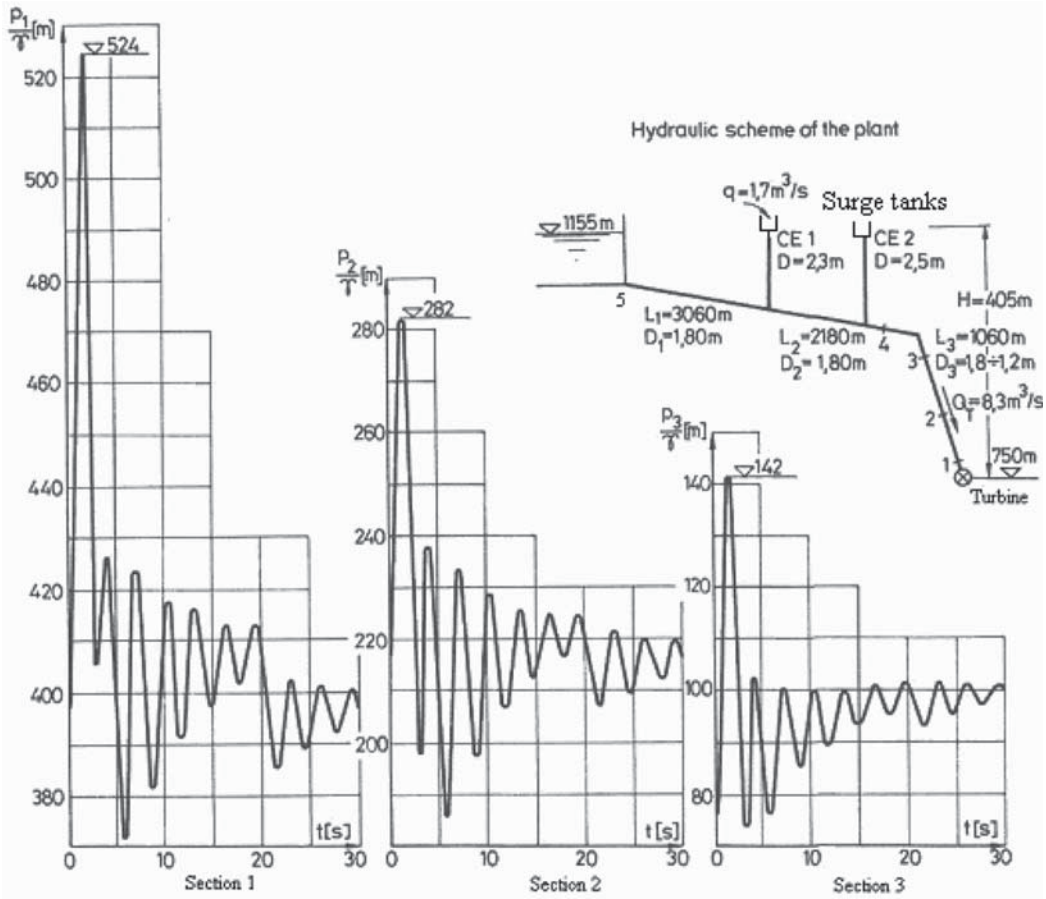


FIG. 5.8 THEORETICAL POWER PLANT HALT AT A TURBINE, SADU V PLANT (From: M. Popescu et al [177], "Applied Hydraulic Transients for Hydroelectric Power Plants", A. A. Balkeema Publishing, copyright 2003. Reproduced by Permission of Taylor and Francis Books UK.)

risks, and tens of millions of dollars in damages were prevented.

Since this pipe system is the focus of numerous examples here, the cooling system layout is shown for one of two facilities, along with photos of 2-in., NPS, pipe failures. In Figs. 5.10 and 5.11, a liquid radioactive waste storage facility is shown. In addition to numerous underground leaks identified in the figure, cooling coils failed in 43 of the storage tanks at SRS. Typical fatigue cracks are shown in Fig. 5.12. Having provided examples of both catastrophic and fatigue pipe failures, the theory to understand the mechanics of fluid transients follows.

5.4 TYPES OF FLUID TRANSIENT MODELS FOR VALVE CLOSURE

There are many theories to describe the intricacies of water hammer, but water hammer theory is first divided into two broad categories:

1. rigid water column theory
2. elastic water column theory

The first assumes that the pipe remains rigid for an incompressible fluid, while the second assumes that the pipe wall elastically deforms in response to a pressure surge. The rigid water column theory has applications and is briefly considered, followed by elastic theory, which is a primary focus of this work.

5.5 RIGID WATER COLUMN THEORY

When the transients in a system do not occur rapidly, the rigid water column theory is applicable. However, rapid is not clearly defined in the literature. The fluid transient theory initially developed from a civil engineering need to understand fluid flow between reservoirs. Many of the examples in the literature concern pumping stations and power plants. Rigid water hammer column was one of the earlier methods to describe simple systems, but Larock

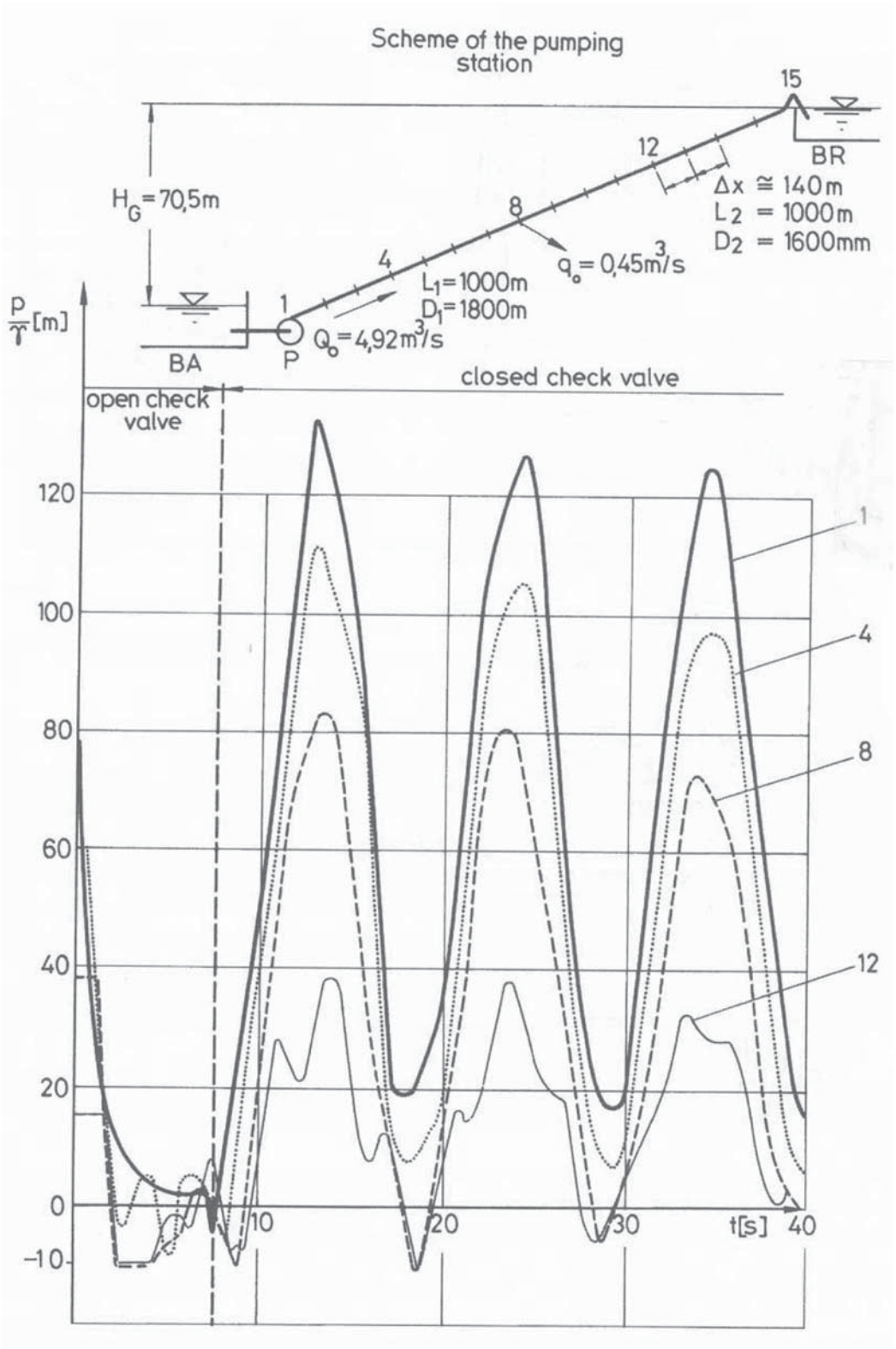


FIG. 5.9 CHECK VALVE CLOSURE IN A PUMPING STATION, SRPA 1-5 SINOE (From: M. Popescu et al [177], "Applied Hydraulic Transients for Hydroelectric Power Plants", A. A. Balkeema Publishing, copyright 2003. Reproduced by permission of Taylor and Francis Books UK.)

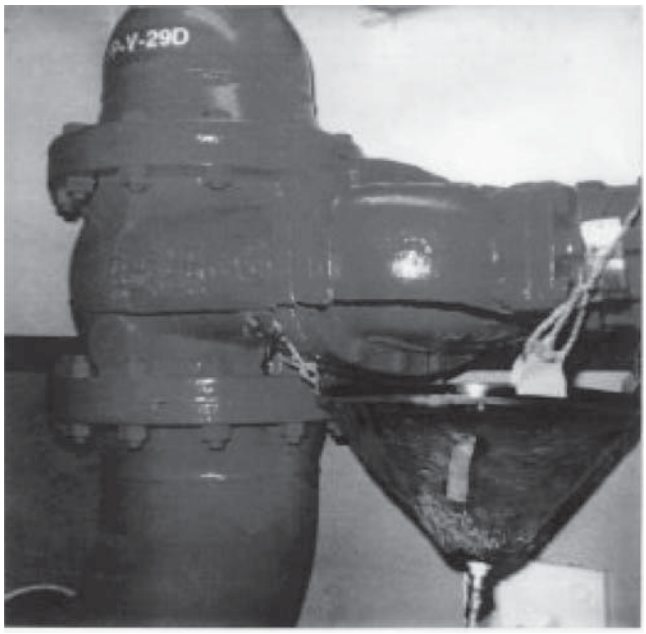


FIG. 5.8 VALVE FRACTURE DUE TO WATER HAMMER (Arastu et al [182])

et al [176] have extended its application to more complex systems, and they provide programs to do so. Even so, Parmakian [172] derived equations and a graphic solution for rigid water columns. The equations determine the head rise in a pipe for a linearly operating gate with negligible friction losses in the pipe and are expressed as:

For gate closure,

$$\frac{h_{a,max}}{h_0} = \frac{B'}{2} + \sqrt{B' + \frac{(B')^2}{4}} \qquad \text{US (5.4)}$$

$$B' = \left(\frac{L \cdot (V_f - V_0)}{g \cdot h_0 \cdot T} \right) \qquad \text{US (5.5)}$$

For gate opening,

$$\frac{h'_{a,max}}{h_0} = \frac{B'}{2} - \sqrt{B' + \frac{(B')^2}{4}} \qquad \text{US (5.6)}$$

where terms are defined in Fig. 5.15, and a graphic solution is provided in Fig. 5.16. h_a is the pressure rise due to a full or partial valve closure, h'_a is the pressure drop

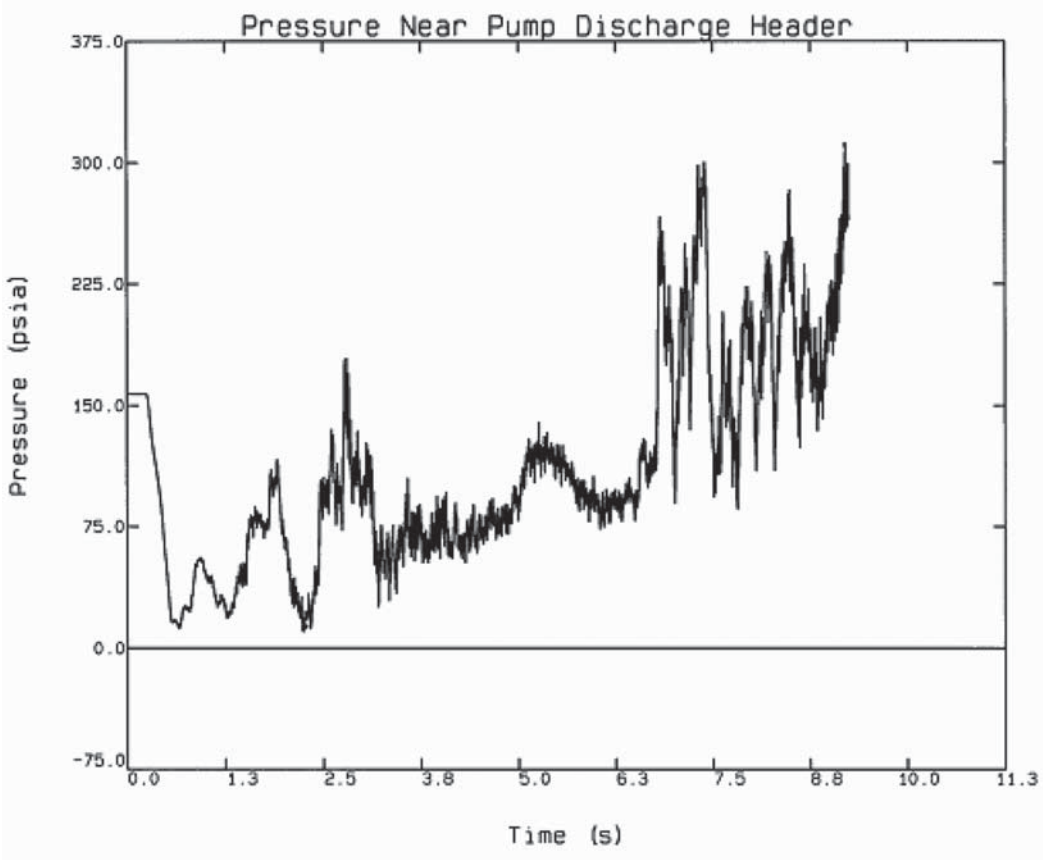


FIG. 5.9 CALCULATED PRESSURE SURGES DUE TO VALVE OPENING (Arastu et al [182])

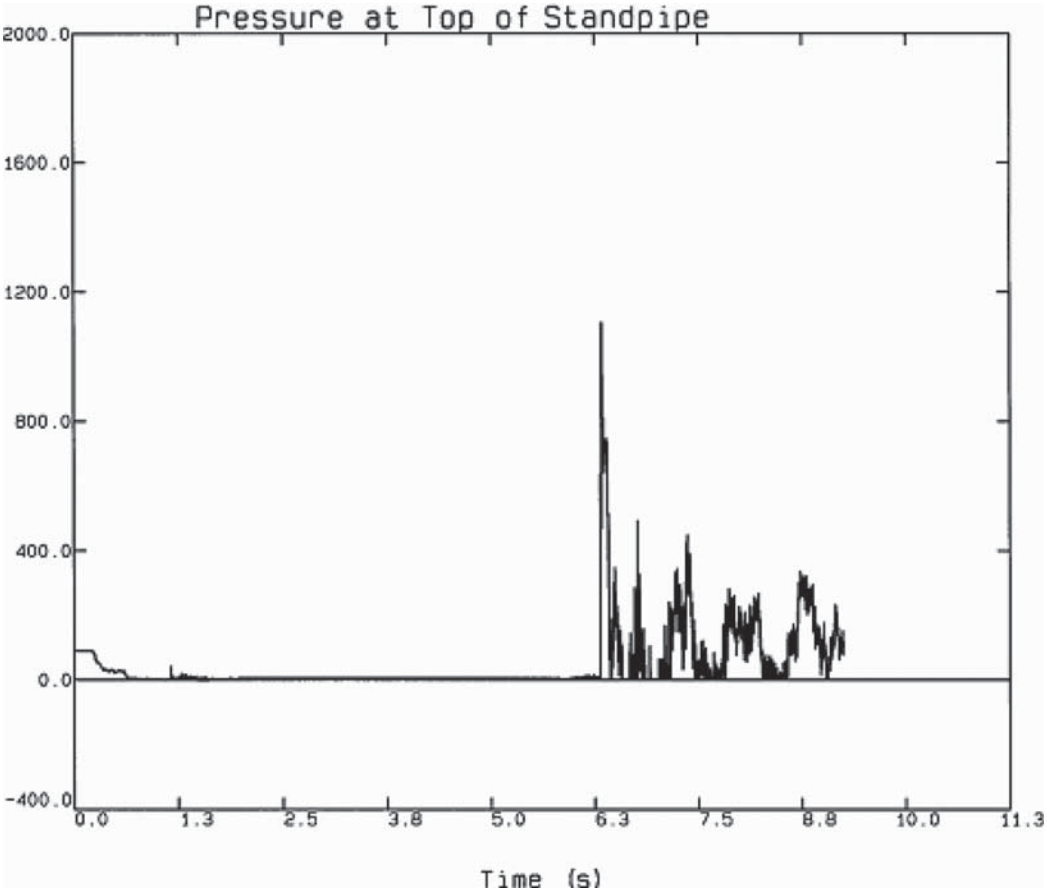


FIG. 5.10 CALCULATED PRESSURE SURGES DUE TO VAPOR COLLAPSE (Arastu et al [182])

due to an opening valve, h_0 is the total head at the valve, V_f is the final velocity in the pipe, V_0 is the initial velocity in the pipe, B' is an arbitrary constant, and T is the closure time of the gate. These equations can be solved graphically using Fig. 5.16 if the initial and final velocities are known.

Example 5.7 Determine the pressure rise in a pipe when a downstream valve is closed

Parmakian [172] provided the following example: Assume that $D = 10$ ft, $L = 3000$ ft, $T = 12$ seconds, the initial flow rate is 1500 ft^3/second, and the final flow rate is 500 ft^3/second. Then, from Fig. 5.16,

$$\frac{L \cdot (V_f - V_0)}{g \cdot h_0 \cdot T} = 0.20$$

$$\frac{h_a(\max)}{h_0} = 0.22$$

and the head increase at the gate equals $h_a(\max) = 110$ ft.

Although this example provides a convenient calculation technique, transients are frequently far more complex. A deficiency of this technique is that pressure changes are assumed to be transmitted instantaneously throughout the piping, and elastic water column theory addresses this concern.

5.5.1 Basic Water Hammer Equation, Elastic Water Column Theory

Larock [176] provides a detailed derivation of the water hammer equation using differential equations, but the arithmetic derivation as presented by Wiley and Streeter [173] is presented here. This technique considers the elastic expansion of the pipe wall in the wake of a shock wave in the pipe and is referred to as the arithmetic method, which was the technique of choice until the 1930s. At about that time, graphical techniques were developed to better describe water hammer, and a few examples are provided to develop insight into transients. Presently, the method of characteristics is widely accepted, but several other computer-aided techniques are also available. Complete derivations and explanations of equations will not be provided here. Entire texts are dedicated to that purpose. For the purposes of this work, only a summary of pertinent equations is presented.

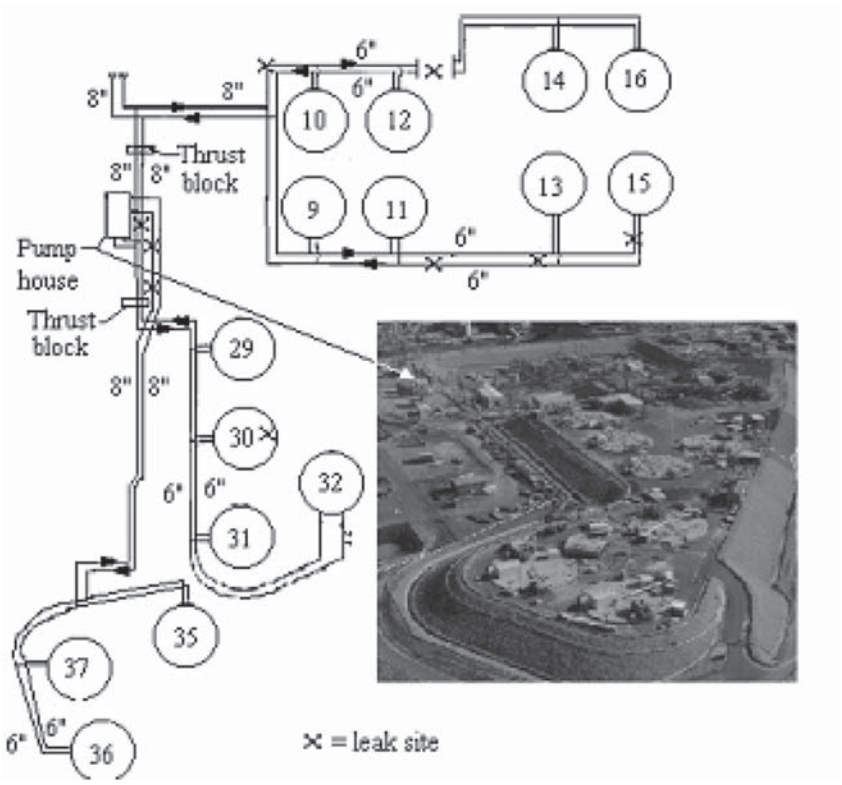


FIG. 5.11 COOLING SYSTEM LAYOUT

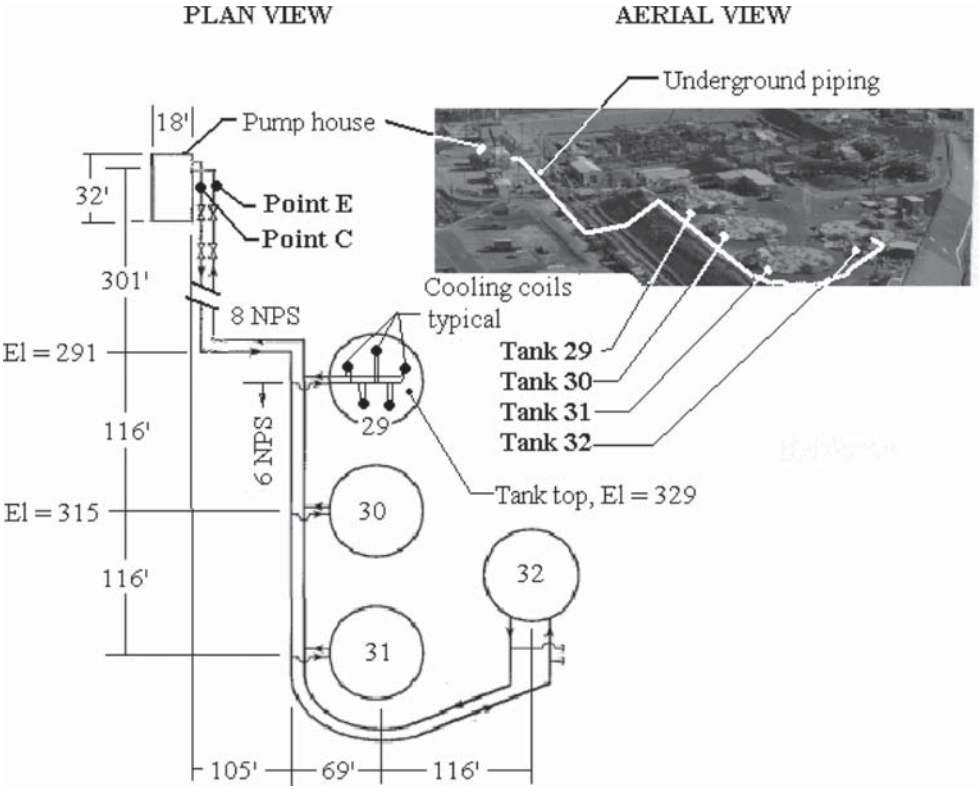


FIG. 5.12 PARTIAL COOLING SYSTEM LAYOUT

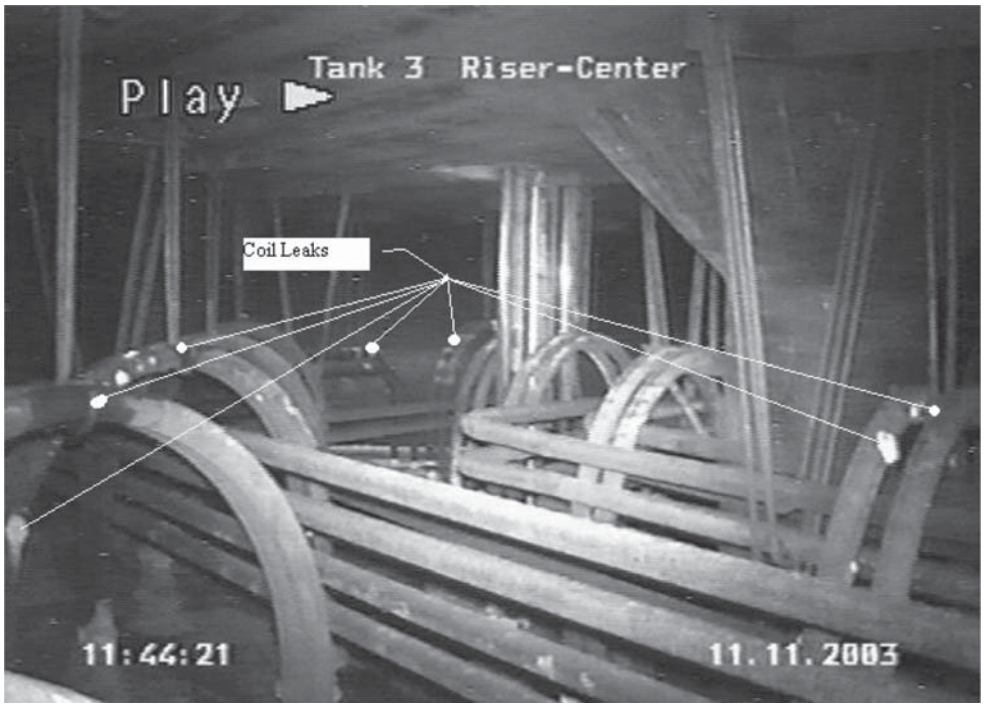


FIG. 5.13 COOLING COIL DAMAGES

The elastic water column theory is demonstrated in Fig. 5.17. Initially, steady-state flow exists in the pipe at $V = V_0$, and the valve is suddenly closed at $t = 0$. At the valve, the fluid velocity goes to zero, and a shock wave of magnitude, Δh, travels upstream as the fluid comes to rest throughout the pipe behind the shock. The shock wave returns from the reservoir at $t = L/a$, and the fluid velocity again equals V_0 as the head decreases to initial

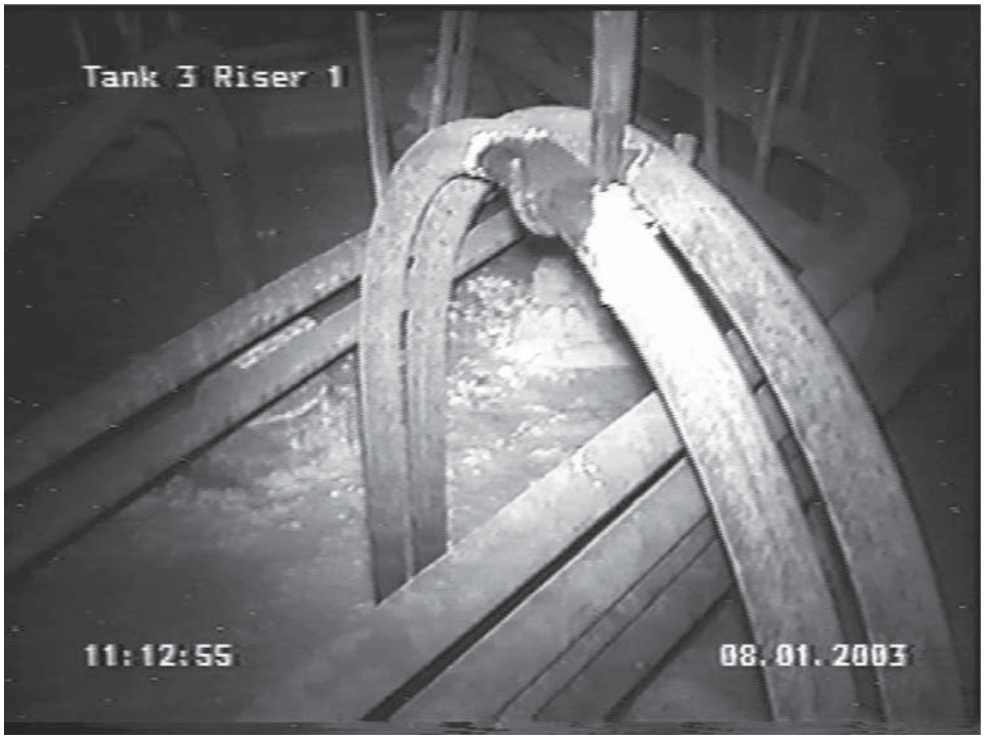


FIG. 5.14 COOLING COIL DAMAGES

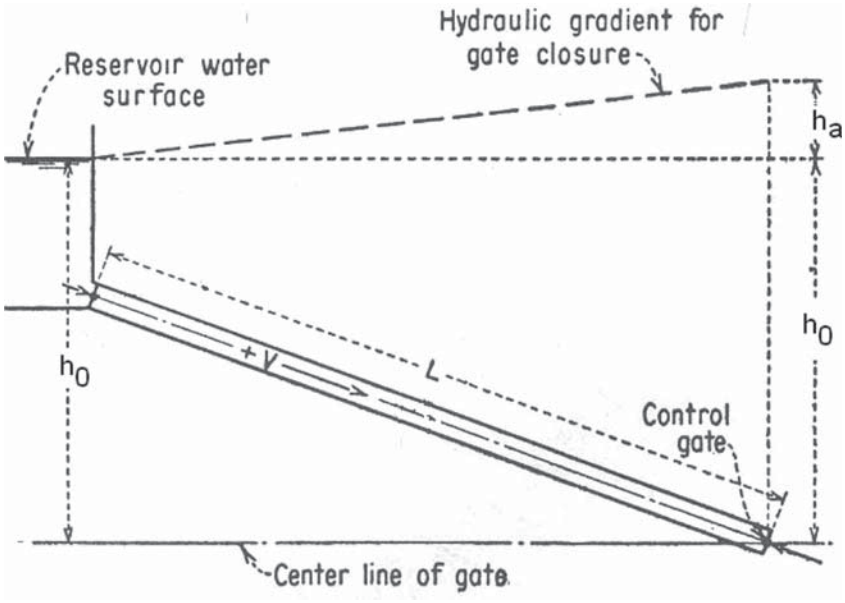


FIG. 5.15 GATE OPERATION (Parmakian [172], reprinted with permission of Dover Publications)

conditions ($h = h_0$). When the shock reflects from the valve, the magnitude of the head is negative, $-\Delta h$, and the velocity behind the shock again equals zero. Not shown, the head decreases to $h = h_0$ when the shock reflects from the reservoir. Then, the cycle repeats: four cycles for each time period of $4 \cdot L/a$ seconds. Note that if $\Delta h > h_0$, the head is below atmospheric pressure and is therefore limited by the vapor pressure of the fluid. The arithmetic water hammer equation describes this process.

5.5.2 Arithmetic Water Hammer Equation

For this technique, the pipe wall elastically expands, the fluid is compressible, and a shock wave travels from the valve when it is operated. Fig. 5.18 defines terms, where V_0 is the initial steady-state velocity in the pipe, ΔV is the incremental change in velocity, $\Delta\rho$ is the change in mass density, A is the cross-sectional area, the specific weight equals $\gamma = \rho \cdot g$, and a is the wave velocity.

For analysis, a wave is assumed to be traveling away from the valve at a speed equal to $a - V_0$ due to an incremental change in valve position. The control volume of Fig. 5.18 is considered to find the basic water hammer equation.

The time rate increase in linear momentum is expressed as

$$\frac{A \cdot (a - V_0) \cdot \Delta t}{\Delta t} \cdot \left((\rho + \Delta\rho) \cdot (V_0 + \Delta V) - \rho \cdot V_0 \right) \quad \text{SI (5.7)}$$

The momentum equation is expressed as

$$-\Delta P \cdot A = A \cdot (a - V_0) \cdot \left((\rho + \Delta\rho) \cdot (V_0 + \Delta V) - \rho \cdot V_0 \right) + (\rho + \Delta\rho) \cdot (V_0 + \Delta V)^2 - \rho \cdot A \cdot V_0^2 \quad \text{SI (5.8)}$$

and conservation of mass is expressed as

$$\frac{\rho \cdot A \cdot V_0 - (\rho + \Delta\rho) \cdot A \cdot (V_0 + \Delta V)}{\Delta t} = \frac{A \mp \cdot (a - V_0) \cdot \left((\rho + \Delta\rho) - \rho \right)}{\Delta t} \quad \text{SI (5.9)}$$

Combining these three equations, the basic water hammer equation is derived, where Eqs. (1.1), (1.2), and (1.6) are restated. For a downstream valve closure, a has a negative value as it travels upstream, and

$$\Delta h(\text{ft}) = \frac{a(\text{ft/sec}) \cdot \Delta V(\text{ft/sec})}{g(\text{ft/}l\,\text{sec}^2)} = -a \cdot \Delta V/g \quad \text{US (5.10)}$$

$$P(\text{psi}) = \frac{\rho(\text{lbm/ft}^3) \cdot a(\text{ft/sec}) \cdot \Delta V(\text{ft/sec})}{g_c(\text{ft} \cdot \text{lbm/lbf} \cdot \text{sec}^2) \cdot (144\text{in}^2/\text{ft}^2)} = -2.1584 \cdot 10^{-4} \cdot \rho \cdot a \cdot \Delta V \quad \text{US (5.11)}$$

$$P\left(\text{psi}\right) = \frac{\gamma\left(\text{lbf/in}^3\right) \cdot a\left(\text{ft/sec}\right) \cdot V\left(\text{ft/sec}\right)}{g\left(\text{ft/sec}^2\right) \cdot \left(144\text{in}^2/\text{ft}^2\right)} = -\frac{\gamma \cdot a \cdot \Delta V}{g \cdot 144} \quad \text{US (5.12)}$$

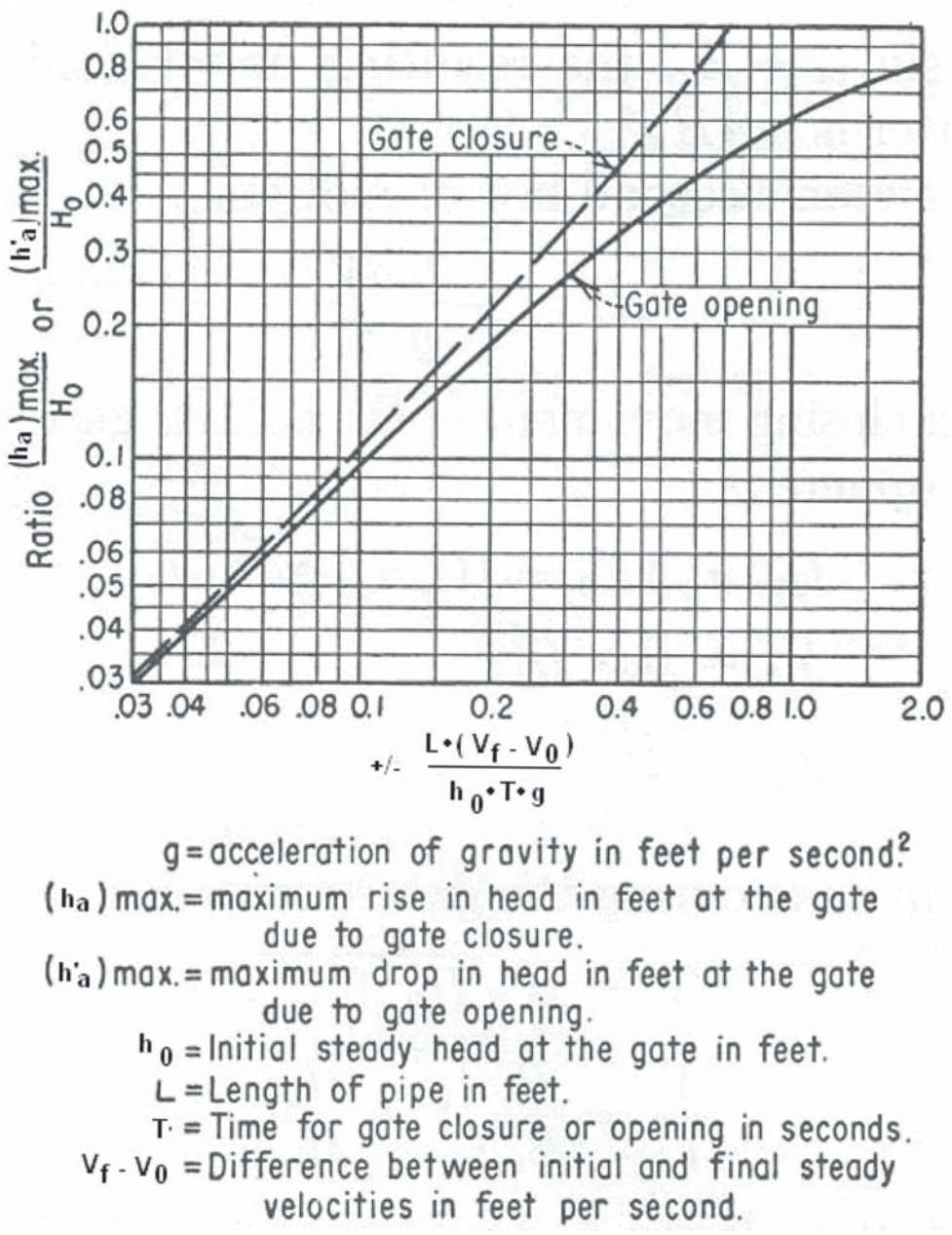


FIG. 5.16 GRAPHIC SOLUTION FOR HEAD INCREASE DUE TO VALVE OPERATION (Parmakian [172], reprinted with permission of Dover Publications)

For an instantaneously closed downstream valve,

$$P(\text{psi}) = -\frac{\gamma \cdot a \cdot V_0}{g \cdot 144} \qquad \text{US (5.13)}$$

$$P = -\rho \cdot a \cdot V_0 \qquad \text{SI (5.14)}$$

For an instantaneously closed upstream valve, a has a positive value as it travels downstream, and

$$P(\text{psi}) = +\frac{\gamma \cdot a \cdot V_0}{g \cdot 144} \qquad \text{US (5.15)}$$

$$P = +\rho \cdot a \cdot V_0 \qquad \text{SI (5.16)}$$

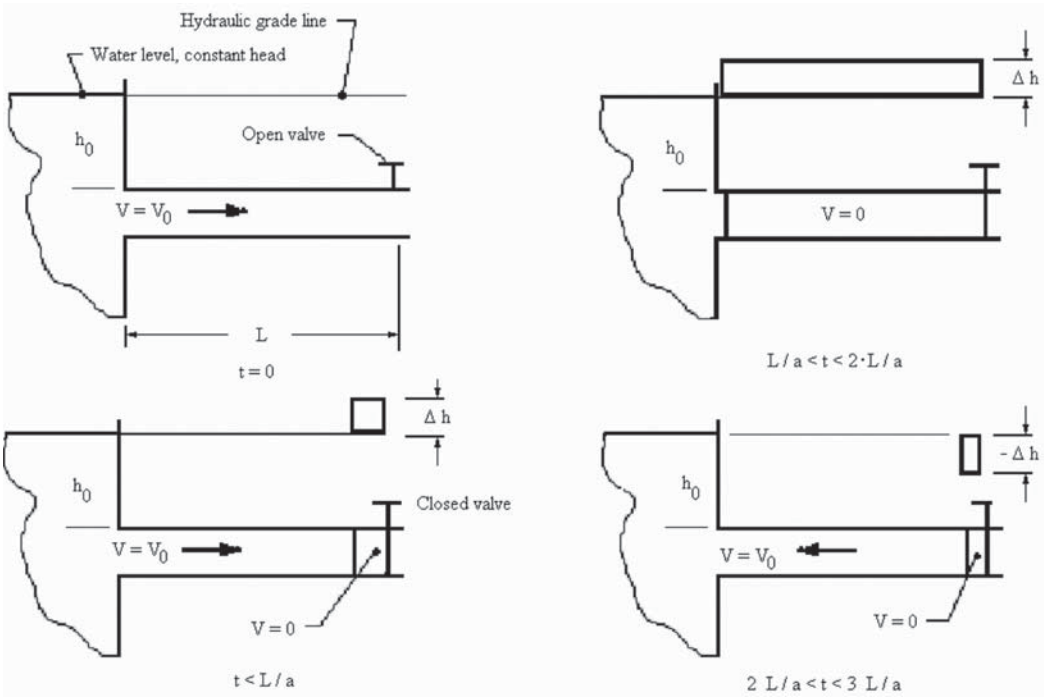


FIG. 5.17 ELASTIC WATER COLUMN THEORY

In a closed loop system, or for the case of a valve located between the upstream and downstream ends of a pipe, pressure waves travel in both directions away from a closing valve.

Eqs. (5.10) through (5.14) define the basic water hammer equation in different formats, but the equations require a definition for the wave velocity, *a*. Before determining a magnitude for the wave velocity, shock waves require a brief description.

5.6 SHOCK WAVES IN PIPING

For water hammer analysis, shock waves are assumed to be planar waves traveling the bore of the pipe. Although this assumption is reasonable, actual shock waves in piping need consideration. Based on available data, shocks in gas-filled piping are considered here in lieu of adequate data for shocks in liquid-filled pipes.

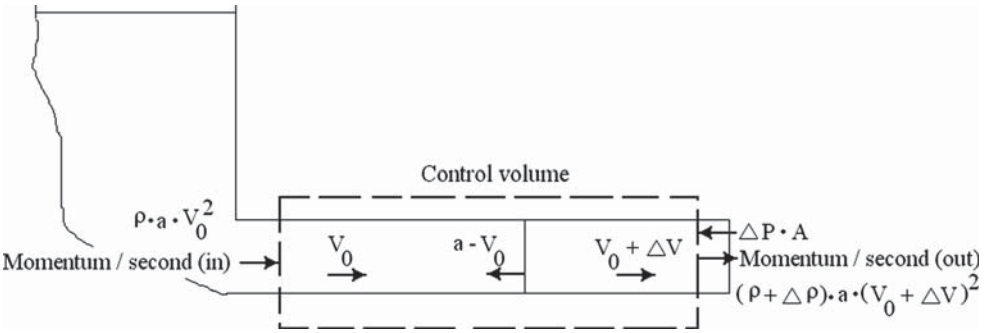


FIG. 5.18 VALVE CLOSURE AND CONTROL VOLUME (Wylie, E. B. , Streeter, V. L., "Fluid Transients in Systems, 1st" Edition, copyright 1993. adapted by permission of Pearson Education, Inc., Upper Saddle River, NJ)

Example 5.8 Consider a shock wave traveling through an elbow

In Fig. 5.19, a shock wave is shown as it passes through air in either a rectangular elbow or a pipe. The photo shows the entire time history as the shock travels from left to right. The deformations of the planar wave and reflections of the wave within the pipe elbow may be observed in Fig. 5.19. The dynamics of the shock wave are very complex as it reflects from the walls of the tubes during passage. Compressibility effects are not as pronounced in water-filled pipes, but the complexities of shock passage through an elbow are assumed to be similar.

5.6.1 Wave Speeds in Thin Wall Metallic Pipes

Attributed to Joukowski, Wiley and Streeter [173] also provided an arithmetic derivation for the wave velocity in a thin wall tube. For a thin wall tube fixed at both ends, the bulk modulus equals the normal stress applied to a cube divided by the volume change due to that stress, and the wave velocity equals

$$a = \sqrt{\frac{\frac{k}{\rho}}{1+\left(\frac{k}{E}\right)\cdot\left(\frac{D}{\overline{T}}\right)}} \qquad \text{SI (5.17)}$$

$$a = \sqrt{\frac{k(\text{psi})\cdot g\left(\text{ft/sec}^2\right)\cdot 144\left(\text{in}^2/ft^2\right)}{\gamma\left(\text{lbf/ft}^3\right)}} \qquad \text{US (5.18)}$$

Note that the wave velocity is reduced due to the pipe flexibility, where the wave velocity for a rigid pipe equals the acoustic velocity of sound in the liquid:

$$a = \sqrt{\frac{k\cdot g\cdot 144}{\rho}} \qquad \text{US (5.19)}$$

Wave velocities for different pipe restraints are also listed by Wiley and Streeter [173]. Wave velocities can be summarized in the format

$$a = \sqrt{\frac{\frac{k}{\rho}}{1+\left(\frac{k}{E}\right)\cdot\left(\frac{D}{\overline{T}}\right)\cdot c_1}} \qquad \text{SI (5.20)}$$

$$a = \sqrt{\frac{\frac{k\cdot g\cdot 144}{\gamma}}{1+\left(\frac{k}{E}\right)\cdot\left(\frac{D}{\overline{T}}\right)\cdot c_1}} \qquad \text{US (5.21)}$$

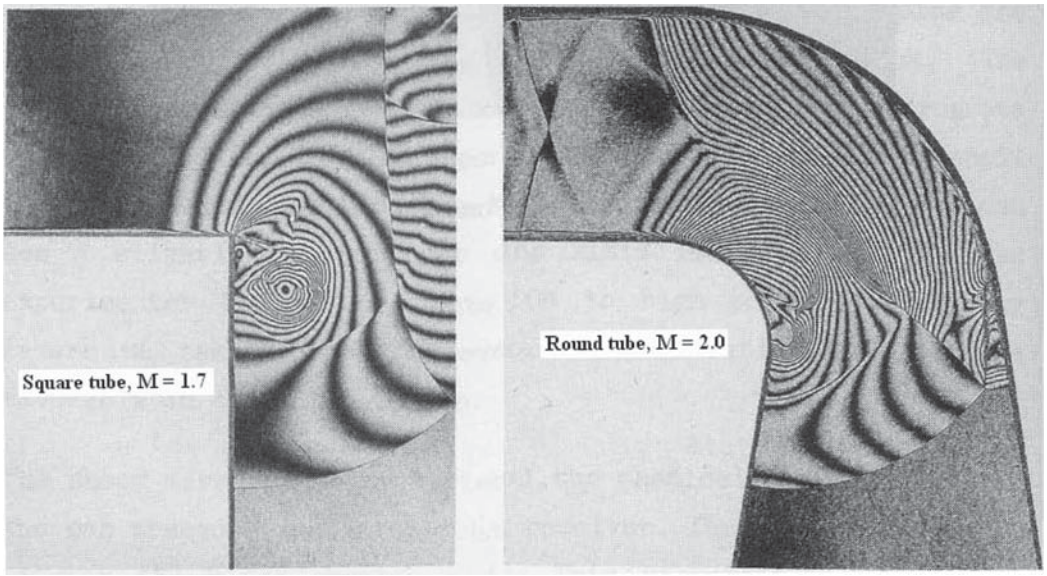


FIG. 5.19 SHOCK WAVES IN AIR-FILLED TUBES (Tanida and Miyashiro [29], reprinted by permission of Springer-Verlag)

where c_1 corrects the equation for restraint conditions, and the Bulk Modulus, k, equals the ratio of the applied pressure stress to the volumetric change due to that stress (Table 2.12).

For thin wall pipes, and for a pipe with a free downstream end,

$$c_1 = 1 - \frac{\nu}{2} \qquad \text{US (5.22)}$$

For a pipe restrained along its entire length,

$$c_1 = 1 - \nu^2 \qquad \text{US (5.23)}$$

Example 5.9 Consider wave velocities for thin wall pipes

To summarize Eqs. (5.21) to (5.23), Parmakian [172] provided a graphic solution for wave speeds in thin wall pipes. As expected, the wave speed approaches the acoustic wave speed as the pipe thickness increases.

5.6.2 Wave Speeds in Thick Wall Metallic Pipes

More accurate wave speeds may also be found, using the thick wall approximation for pipes. For a thick wall pipe with a free downstream end,

$$c_1 = \frac{2 \cdot \overline{T}}{D} \cdot (1 + \nu) + \frac{D}{D + \overline{T}} \cdot \left(1 - \frac{\nu}{2}\right) \qquad \text{US (5.24)}$$

For a thick wall pipe restrained along its entire length,

$$c_1 = \frac{2 \cdot \overline{T}}{D} \cdot (1 + \nu) + \frac{D}{D + \overline{T}} \cdot \left(1 - \nu^2\right) \qquad \text{US (5.25)}$$

Example 5.10 Compare the effects of different pipe models for 2- and 24-in. Schedule 40, carbon steel pipes, containing water at 68°F

For these conditions, $\overline{T}$ = 0.154 in., D = 2.067 in., k = 319,000 psi, ν = 0.29, E = 29,500,000 psi). Eqs. (5.19) through (5.25) yield the following table of results.

2-in. Schedule 40, 24-in., Schedule 40

$D/\overline{T}$ = 13.42 $D/\overline{T}$ = 32.88

For a rigid pipe, a = 4872 ft/second,

For a thin wall pipe with a free end, a = 4595 ft/second, a = 4267 ft/second.

For a restrained thin wall pipe, a = 4577 ft/second, a = 4232 ft/second.

For a thick wall pipe with a free end, a = 4556 ft/second, a = 4236 ft/second.

For a restrained thick wall pipe, a = 4540 ft/second, a = 4203 ft/second.

Note that throughout this range, the errors between thin wall and thick wall pipe approximations are 1% to 1.5%,

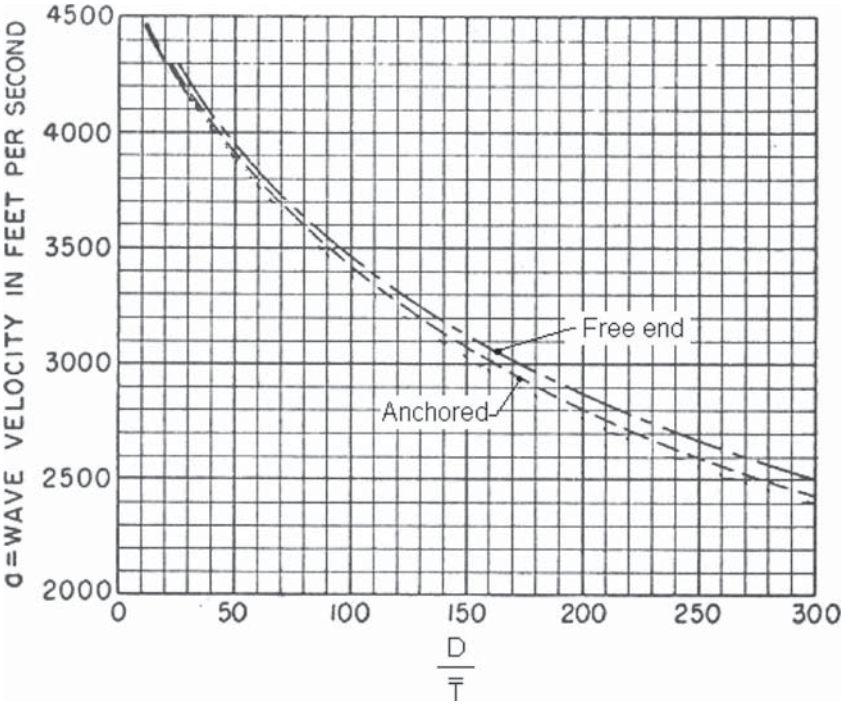


FIG. 5.20 WAVE VELOCITIES IN STEEL PIPES (Parmakian [172], reprinted with permission of Dover Publications)

but the differences between a rigid pipe approximation and other wave speed calculations vary by nearly 12%. Therefore, from the water hammer equation, the magnitude of a pressure surge in any Schedule 40 pipe between 2- and 24-in. diameters also varies by 12% for an equivalent initial velocity, V_0, in the pipeline. Note also that each of the thick wall equations approach the thin wall approximations as $D/\overline{T} \rightarrow 0$. The above wave speed equations are applicable to metals and materials that have a linear elastic modulus, but not all materials meet that requirement.

5.6.3 Wave Speeds in Nonmetallic Pipes

For nonmetallic materials, calculation techniques are more complicated. For cast iron pipe, the water hammer equation may be used, but the wave speed is variable, since the elastic modulus varies with load. For plastic pipe, the basic water hammer equations are applicable (Suo and Wylie [183]), but the elastic modulus also varies with respect to load and, in some cases, varies with aging. For reinforced concrete pipe, one method is to use an equivalent steel pipe diameter, but the concrete modulus also varies with load. Larock et al [176] recommends using the equation:

$$A_{\text{steel}} = \frac{E_{\text{concrete}}}{E_{\text{steel}}} \cdot A_{\text{concrete}} = \frac{57{,}000\sqrt{f_c}}{E_{\text{steel}}} \cdot A_{\text{concrete}}$$

where f_c is the 28-day concrete strength, and $\nu = 0.24$.

If the tangent modulus is used for calculations, the estimated water hammer pressures will exceed expected actual pressures. For plastic and cast iron pipes, these values are listed in B31.3 tables included in Chapter 2.

Outside the scope of this work, Wiley and Streeter [173] also provide discussions of wave speeds in tunnels, lined tunnels, and tubes of rectangular cross section. Even so, the equations for the wave speed for a tunnel through rock or concrete in a dam or other structure is expressed as

$$a = \sqrt{\frac{\frac{k \cdot g \cdot 144}{\gamma}}{1 + \left(\frac{k}{E_R}\right) \cdot (1 + \nu)}} \qquad \text{US (5.26)}$$

where E_R equals the modulus of rigidity for the rock or concrete. When a steel liner is installed in a tunnel or a pipe is encased in concrete the wave speed equals,

$$a = \sqrt{\frac{\frac{k \cdot g \cdot 144}{\gamma}}{1 + \left(\frac{k}{E_R}\right) \cdot \left(\frac{2 \cdot E \cdot \overline{T}}{E_R \cdot D + 2 \cdot E \cdot \overline{T}}\right)}} \qquad \text{US (5.27)}$$

5.6.4 Effects of Entrained Solids on Wave Speed

For solutions containing suspended fine particles, equivalent values for the bulk modulus and density may be substituted into the water hammer equations to find waves speeds and pressure transients. To do so, the basic water hammer equation may be used for any restraint condition, where the equivalent bulk modulus and density are expressed as

$$k = \frac{k_L}{1 + \left(\frac{V_s'}{V'}\right) \cdot \left(\frac{k_L}{k_s} - 1\right)} \qquad \text{SI (5.28)}$$

$$\gamma = \frac{\gamma_g \cdot V_g'}{V'} + \frac{\gamma_L \cdot V_L'}{V'} \qquad \text{US (5.29)}$$

$$\rho = \frac{\rho_s \cdot V_s'}{V'} + \frac{\rho_L \cdot V_L'}{V'} p \qquad \text{SI, EE, US (5.30)}$$

where V_s', V_L', V' are the solid, liquid, and the total volumes, ρ_s, ρ_L, ρ are the solid, liquid, and total mass densities, γ_s, γ_L, γ are the solid, liquid, and total weight densities.

5.6.5 Effects of Air Entrainment on Wave Speed

Air or vapor entrainment significantly reduces the wave speed. A 1% gas content can reduce the speed by an order of magnitude (Wylie and Streeter [173]). Wave speed effects due to air bubbles in solution are shown in Fig. 5.21. The effects of air bubbles in solution are clearly evident. The technique of forcing gas into solution can reduce shock wave magnitudes. Even during normal operations, entrained air may affect the wave speed. The theoretical wave speed equation shown in Fig. 5.21 assumes isothermal expansion of the air in solution in a thin wall tube. To determine the wave speed, the bulk modulus of the gas, k_g, and density are required. The wave speed may be determined using the water hammer equations with different restraint conditions when expressed in terms of

$$\rho = \frac{\rho_g \cdot V_g'}{V'} + \frac{\rho_L \cdot V_L'}{V'} \qquad \text{SI, EE, US (5.31)}$$

$$\gamma = \frac{\gamma_g \cdot V_g'}{V'} + \frac{\gamma_L \cdot V_L'}{V'} \qquad \text{SI, EE, US (5.32)}$$

$$k = \frac{k_L}{1 + \frac{V'g}{V} \cdot \left(\frac{k}{k_g} - 1\right)} \qquad \text{SI, EE, US (5.33)}$$

k_g is the bulk modulus, ρ_g is mass density of the gas, V_g' is the volume of the gas at temperature, γ_L is the liquid weight density, γ_g is the gas weight density, and T is the absolute temperature. For isentropic processes, $k_g = 1.4 \cdot P_{\text{abs}}$, for

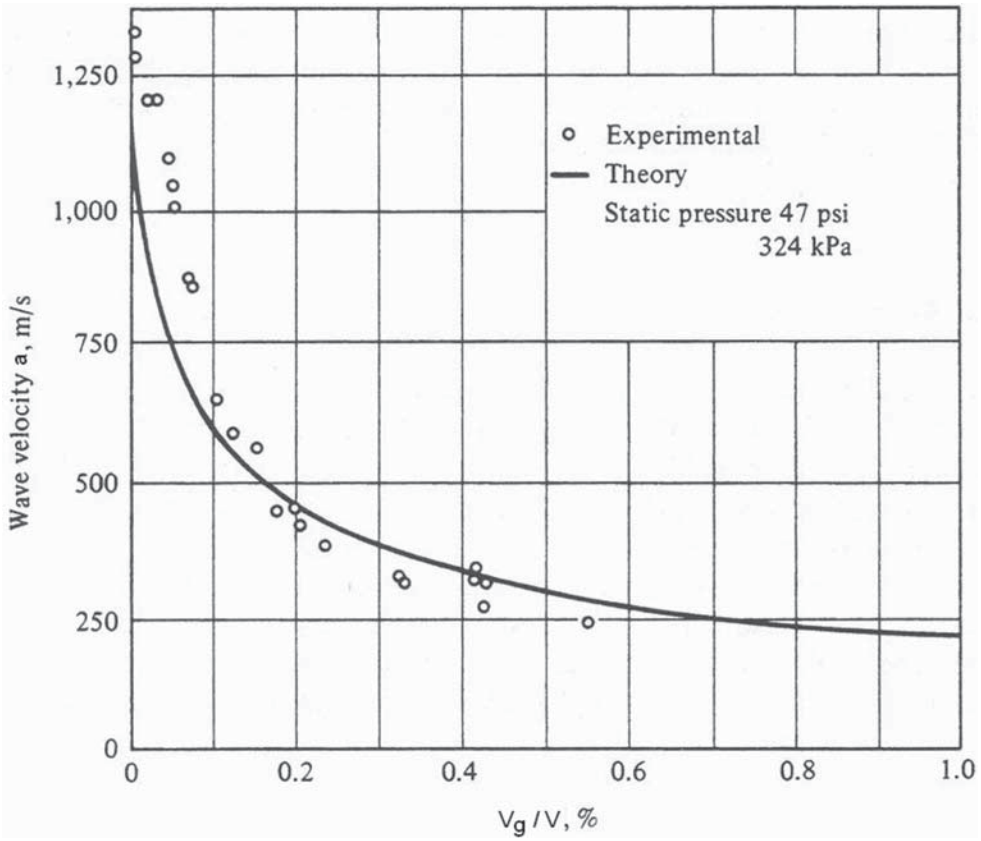


FIG. 5.21 EFFECTS OF AIR CONTENT ON WAVE SPEED (Kobori et al [185] Wylie, E. B., Streeter, V. L., "Fluid Transients in Systems, 1st" Edition, copyright 1993. Reprinted by permission of Pearson Education, Inc., Upper Saddle River, NJ)

polytropic processes, $k_g = 1.2 \cdot P_{abs}$, and for isothermal processes in air, $k_g = P_{abs}$ (Larock et al [176]) The difference in wave speeds for different assumptions of the bulk modulus is therefore proportional to the square root of 1.4, which implies that a 14% wave speed error is possible depending on whether, or not, the process is isentropic or isothermal. An adiabatic assumption seems reasonable, given the fact that temperatures change across shock waves, which are generally assumed to behave isentropically.

Example 5.11 Consider the effects of air content on wave speed

Even though subatmospheric pressures occur during many pump shutdowns, assume that the pressure is reduced to atmospheric pressure during a pump shutdown. To demonstrate the effects of air release in water, consider the concentration of air in water. Henry's law for oxygen concentration in water is shown in Fig. 5.22, where Henry's law states that gas concentration in solution is proportional to the applied pressure. Extrapolating experimental results provided in the figure, air contains 0.016 weight percent air at 47 psig and 72°F. At atmospheric pressure, water contains 0.0038 weight percent air. Most of the air bubbles are released from solution as the pump stops, and the final weight percent of air then equals 0.012. From Fig. 5.21, an approximate 46% wave speed reduction is noted at 0.012 weight percent, where the wave speed is approximately 1000 m/second, and the acoustic wave speed equals 1463 m/second. The change in theoretical wave speed may also be calculated using Eqs. (5.21), (5.30), and (5.31).

Additional research is yet required to fully quantify this estimate, since the dynamics of air bubble formation and release are quite complicated. In fact, the wave speed is not affected as a wave initially passes a point in a pipe, since air is not yet released. That is, air release affects reflected pressure waves only. Depending on the time of wave return, air bubble rise to the fluid surface may also affect the wave speed. For this example, entrained air in solution may introduce an approximate 46% error into wave speed calculations for pressure waves following the initial shock wave, but calculations are unaffected for the magnitude of the initial shock wave, using the water hammer equation.

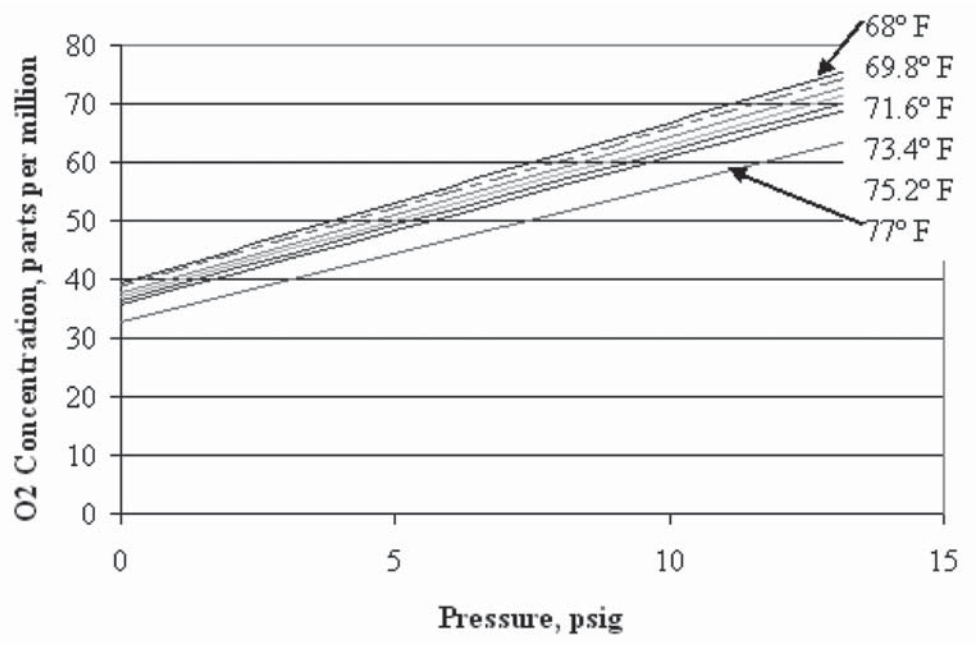


FIG. 5.22 EXTRAPOLATED OXYGEN CONCENTRATIONS FROM TEST DATA AT 0 TO 1.5 PSIG

5.7 UNCERTAINTY OF THE WATER HAMMER EQUATION

The accuracy of the water hammer equation merits attention, and that accuracy depends on the variables in the water hammer equation, $\rho \cdot a \cdot V$. Uncertainty calculations can be used to estimate calculation errors (Coleman and Steele [184]).

Example 5.12 Determine errors for the water hammer equation

The error for ρ, a, and V are required to find the total error. Previous paragraphs noted that a 10% change in density occurs for a 10°F change in water temperature, the wave speed varies by 2% to 3% depending on restraint conditions, and calculated velocities may vary by 20% to 30%. The approximate total error for a calculation using these variables can then be expressed as the root mean sum of the squares (RMS) of the errors.

$$\%\_\text{Error} = \text{RMS} = 100 \cdot \sqrt{0.10^2 + 0.30^2 + 0.03^2} = 30.1\%$$

However, if measured values are used, the calculation error is significantly reduced. Flow meters typically have instrument errors less than 5%. Substituting this velocity error,

$$\%\_\text{Error} = 100 \cdot \sqrt{0.10^2 + 0.05^2 + 0.03^2} = 13.4\%$$

Note that the error is directly related to process measurements. If the velocity is not well known, then the total error nearly equals the error in velocity. If the velocity is well defined, the density error varies with temperature, and density dominates the total error. If the temperature and velocity are both well defined, then the error would be further reduced. For example, thermocouples are common instruments used to measure process temperatures, and instrument errors are typically less than 3°F. For a 3°F temperature change in water, the density varies by about 3%. If a process temperature is constant, the instrument error can then be assumed to be proportional to the density change. Substituting this density error,

$$\%\_\text{Error} = 100 \cdot \sqrt{0.03^2 + 0.05^2 + 0.03^2} = 6.6\%$$

In short, the RMS error of the water hammer equation varies by as much as 6% to 30%, depending on the knowledge of the specific process under consideration. Since all computer simulations are based on these variables, computer simulations implicitly contain these inherent errors. For plastic, cast iron, and concrete pipe, the wave speed approximations may have even higher errors. The RMS error has a confidence level of 68% and is also referred to as the one sigma error. To obtain a commonly used two sigma error, the RMS is doubled. For the cases considered here, the error is 12% to 60% with 95% confidence.

5.8 COMPUTER SIMULATIONS/ METHOD OF CHARACTERISTICS

The method of characteristics is a widely accepted numerical simulation of water hammer. This technique, as well as other techniques discussed in the literature, compensates friction effects that the arithmetic water hammer technique neglects. How much discussion should be devoted to the theoretical basis of the MOC? There are several fundamental equations that are the basis of this finite difference technique. The derivations for each require several pages of differential equations, and the application of those equations is the focus of chapters in Wiley's text. The reader is referred to that work for further detail. However, a few of the equations and a qualitative discussion of the technique are certainly warranted. There are two fundamental equation sets required to describe water hammer. One set describes fluid flow, while the other set describes shock wave speeds. Together, these equations of motion are the basis for the method of characteristics and other fluid flow algorithms.

5.8.1 Differential Equations Describing Fluid Motion

Referring to Fig. 2.1 for nomenclature, the fundamental equation for fluid flow is the Reynold's transport theorem. In fact, a mathematical treatment of this work would open with this theorem. Neglecting diffusion and heat transfer, this theorem is expressed as

$$\frac{\mathrm{d}(m\cdot V)}{\mathrm{d}t}=\frac{\partial\left(\int_{\mathrm{cv}}\rho\cdot\mathrm{d}V'+\int_{\mathrm{cs}}V\cdot\mathrm{d}A\right)}{\partial t}\quad\text{EE, SI, US (5.34)}$$

where cv is the control volume, cs is the surface of the control volume, and A is the cross-sectional area. Essentially, the change in momentum equals the change in both mass and flow rate through the control volume with respect to time. This momentum equation is subtracted from the continuity equation (Eq. (2-10)) multiplied by the velocity to derive

$$\frac{\partial(V)}{\partial t}+V\cdot\frac{\partial(V)}{\partial z}+\frac{1}{\rho}\cdot\frac{\partial(P_{\mathrm{abs}})}{\partial z}+g\cdot\sin(\alpha)+\frac{f\cdot V\cdot|V|}{2\cdot D}=0$$

EE, SI (5.35)

$$\frac{\partial(V)}{\partial t}+V\cdot\frac{\partial(V)}{\partial z}+g\cdot\frac{\partial(h)}{\partial z}+g\cdot\sin(\alpha)+\frac{f\cdot V\cdot|V|}{2\cdot D}=0$$

US (5.36)

where $\acute{\alpha}$ is the angle of the pipe to a horizontal plane. This differential equation for water hammer is the basis for the MOC, but is also the basis for all fluid mechanics discussed in this text. For example, Streeter lists several derivations from this equation.

Power law fluids can be described by

$$\frac{\partial(V)}{\partial t}+V\cdot\frac{\partial(V)}{\partial x}+\frac{1}{\rho}\cdot\frac{\partial(P_{\mathrm{abs}})}{\partial x}+g\cdot\sin(\alpha)+\frac{\lambda\cdot V\cdot|V^{n-1}|}{2\cdot D^{m}}=0$$

EE, SI (5.37)

where n is the power law exponent, and λ and m are experimentally determined constants. A significant implication of this equation is that commercial water hammer programs need to be reviewed when considering non-Newtonian fluids, such as dilatant, pseudoplastic, or structural fluids.

Also, non-Newtonian, Bingham plastic fluids are similar to Newtonian fluids for shock waves, but when the fluid comes to rest, it will stay at rest, unless a motive force is reapplied to overcome the yield stress. That is, shock waves in the fluid can be described using the water hammer equation, but changes in flow rate are not well understood. In fact, many pipelines have been plugged when Bingham fluid flows were interrupted, and the installed pumps did not have sufficient head to overcome the yield stresses at the wall in a long pipe. Sufficient head was available to fill the pipes, but once the pipes were full, additional head was required to reinitiate fluid motion.

Bernoulli's equation and other results presented in Chapter 2 follow directly from Eq. (5.36), and a mass oscillation equation may also be derived from Eq. (5.36). In the literature, the terms rigid column flow and mass oscillation are used interchangeably. Mass oscillation is described as slowly varying fluid flow in systems for incompressible fluids. Rigid column flow does not account for elasticity effects in the pipe wall or compressibility. Either assumption results in the same equation. Shock waves are neglected, pressure changes are assumed to occur instantaneously throughout the pipe, and the transient term is then dropped from Eq. (5.36). The resulting equation is used to approximate mass oscillations, which are calculated according to

$$\frac{P_{\mathrm{abs}}}{\rho}+\frac{\partial(V)}{\partial t}+g\cdot\sin(\alpha)+\frac{f\cdot V\cdot|V|}{2\cdot D}=0\quad\text{EE, SI (5.38)}$$

This equation is appropriate for many cases where fluid mass oscillations in a system occur slowly, but the limits of applicability are a concern. Even so, the water hammer equation is used throughout the remainder of this work, with the exception of the following example.

Example 5.13 Compare the mass oscillation equations to the water hammer equations

Popescu et al provided several examples for comparison of results, based on the water hammer equation (Eq. (5.37)) or the mass oscillation equation (Eq. (5.38)). In general, the mass oscillation technique predicted higher pressure surges at slightly higher frequencies, as shown in Figs. 5.23 and 5.24. They also provided criteria to relate the two theories, which are not presented here.

5.8.2 Shock Wave Speed Equation

The wave speed equation is applicable to waves in gases, fluids, or solids. In fact, the wave speed equation can be used to derive vibration equations, which is appropriate since shock waves on structures induce vibrations. The general form of the wave speed equation in elastic materials is frequently referred to as the D'Alembert equation and is expressed as

$$\frac{\partial^2(U)}{\partial t^2} = a^2 \cdot \frac{\partial^2(U)}{\partial z^2} \qquad \text{EE, SI, US} \quad (5.39)$$

where a is a constant wave velocity, and U is a variable such as strain, pressure, or stress. For fluid flow equations, this equation is rewritten in terms of head as

$$g \cdot \frac{\partial^2(h)}{\partial t^2} = a^2 \cdot \frac{\partial^2(h)}{\partial z^2} \qquad \text{US} \quad (5.40)$$

This equation can also be derived from Eq. (5.36). The solution to Eq. (5.40) equals

$$h - h_0 = F\left(t + \frac{z}{a}\right) - f\left(t - \frac{z}{a}\right) \qquad \text{US} \quad (5.41)$$

where h is the variation in head, h_0 is the initial head, the function, F, describes a wave traveling in the $-z$ direction, and f describes a wave traveling in the $+z$ direction.

In short, any time-dependent pressure perturbation is transmitted at sonic velocities in a fluid, and the wave shapes are described by f waves and F waves. For fluid transients, the resulting wave shape is dependent on both the initiating event and the pipe length. For example, a linear closing valve causes a ramped shaped pressure wave transmission in a short pipeline. The same valve closure in a long pipeline causes a step pressure increase throughout the pipe. The cause of the surge is the same, but the characteristic impedance, or resistance, of the attached pipe influences the wave shape. As another example, pump shutdowns are very complex in short pipelines, but in long pipelines, pump shutdowns are also simplified to step pressure changes at the wave front. For transients due to pump operations, the change in wave front is also caused by the characteristic impedance of the system. As system resistance to momentum change increases, the time dependence of the wave shape diminishes, and the wave shape approaches a steep-fronted shock wave for any flow perturbation. Unfortunately, a concise definition of a short pipe versus a long pipe is unavailable for this phenomenon. For practical purposes, one implication is that a steep-fronted wave can be assumed using the basic water hammer equation. This assumption can lead to serious error, and computer simulations are frequently required.

Another aspect of the f and F wave equations is the sign of these equations. For fluid transients, the direction of the wave depends on the valve location. Shock waves travel from the valve in the direction of an open pipe, either upstream (–), downstream (+), or both. These wave speed equations and the equations of fluid motion are adapted to describe the Method of Characteristics.

5.8.3 MOC Equations

Both Wiley and Streeter [173] and Larock et al [176] provide detailed discussions and derivations of the MOC technique. For this work, only the basic equations are presented to provide some insight into the method. The MOC equations are derived from Eqs. (5.36) and (5.40), where two characteristics (C^+ and C^-) are developed. For a constant wave speed,

$$C^+: \frac{\mathrm{d}(V)}{\mathrm{d}t} + \frac{g}{a} \cdot \frac{\mathrm{d}(h)}{\mathrm{d}t} + \frac{g}{a} \cdot \frac{\mathrm{d}(Z')}{\mathrm{d}z} + \frac{f \cdot V \cdot |V|}{2 \cdot D} = 0 \qquad \text{US} \quad (5.42)$$

when

$$\frac{\mathrm{d}z}{\mathrm{d}t} = V + a \qquad \text{US} \quad (5.43)$$

$$C^-: \frac{\mathrm{d}(V)}{\mathrm{d}t} - \frac{g}{a} \cdot \frac{\mathrm{d}(h)}{\mathrm{d}z} + \frac{g}{a} \cdot \frac{\mathrm{d}(Z')}{\mathrm{d}z} + \frac{f \cdot V \cdot |V|}{2 \cdot D} = 0 \qquad \text{US} \quad (5.44)$$

when

$$\frac{\mathrm{d}z}{\mathrm{d}t} = V - a \qquad \text{US} \quad (5.45)$$

These equations are then solved to yield a finite difference approximation. To do so, the pipe is divided into N reaches, or pipe sections, as shown in the z-t plane of Fig. 5.25. The accuracy of the numerical solution is somewhat affected by the number of reaches, but the selection of the time increment significantly affects both accuracy and stability of the numerical solution. Wiley and Streeter consider the Courant condition for selection of a stable time increment, Δt, and numerical techniques can readily check accuracy for selection of N.

Applying Fig. 5.25, the MOC technique solves the characteristic equations at each node on the z-t plane. To use MOC, the governing equations (Eqs. (5.42) and (5.43)) yield

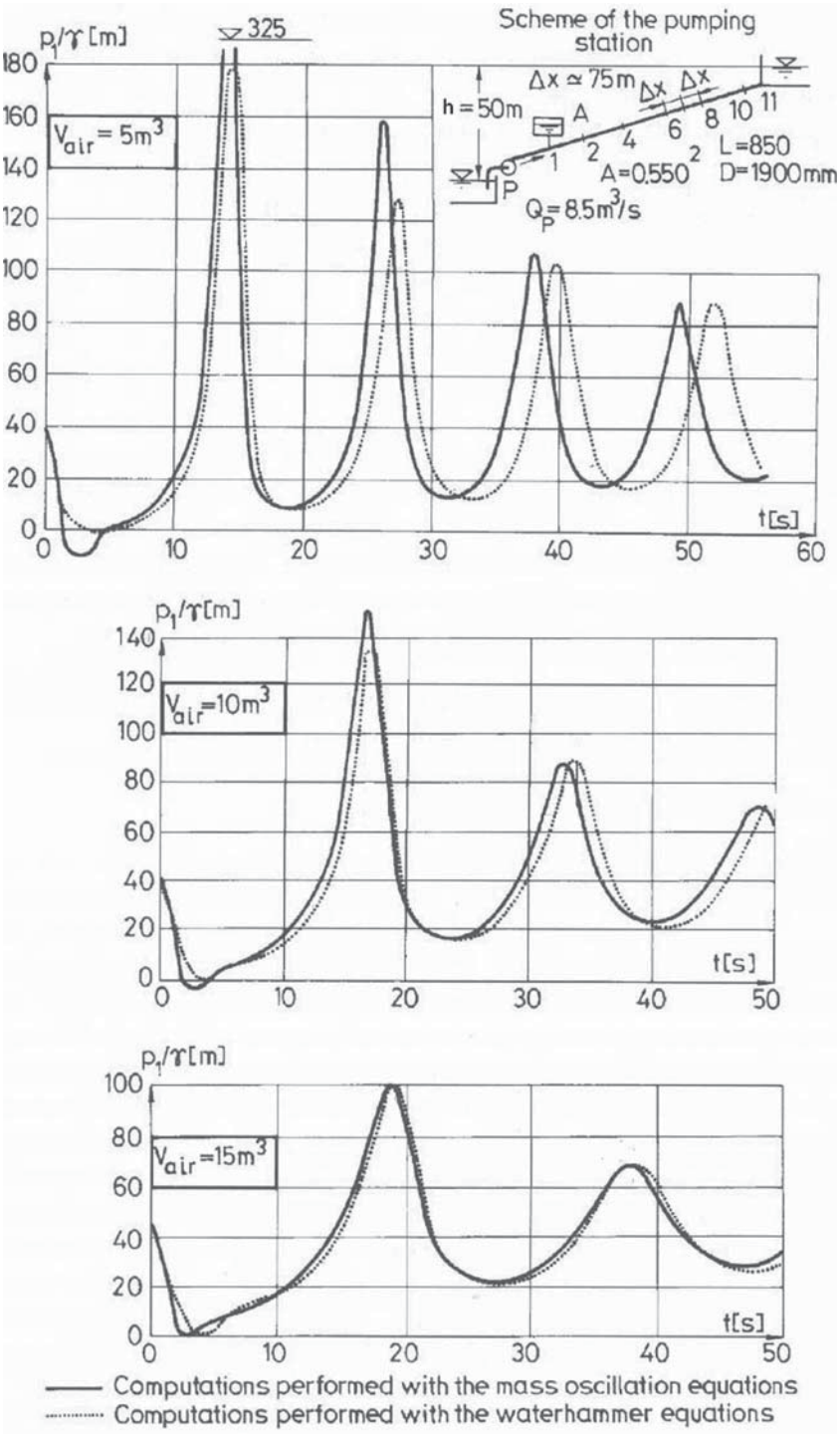


FIG. 5.23 COMPARISON OF NUMERICAL SIMULATIONS FOR AN AIR CHAMBER (From: M. Popescu et al [177], "Applied Hydraulic Transients for Hydroelectric Power Plants", A. A. Balkeema Publishing, copyright 2003. Reproduced by permission of Taylor and Francis Books UK)

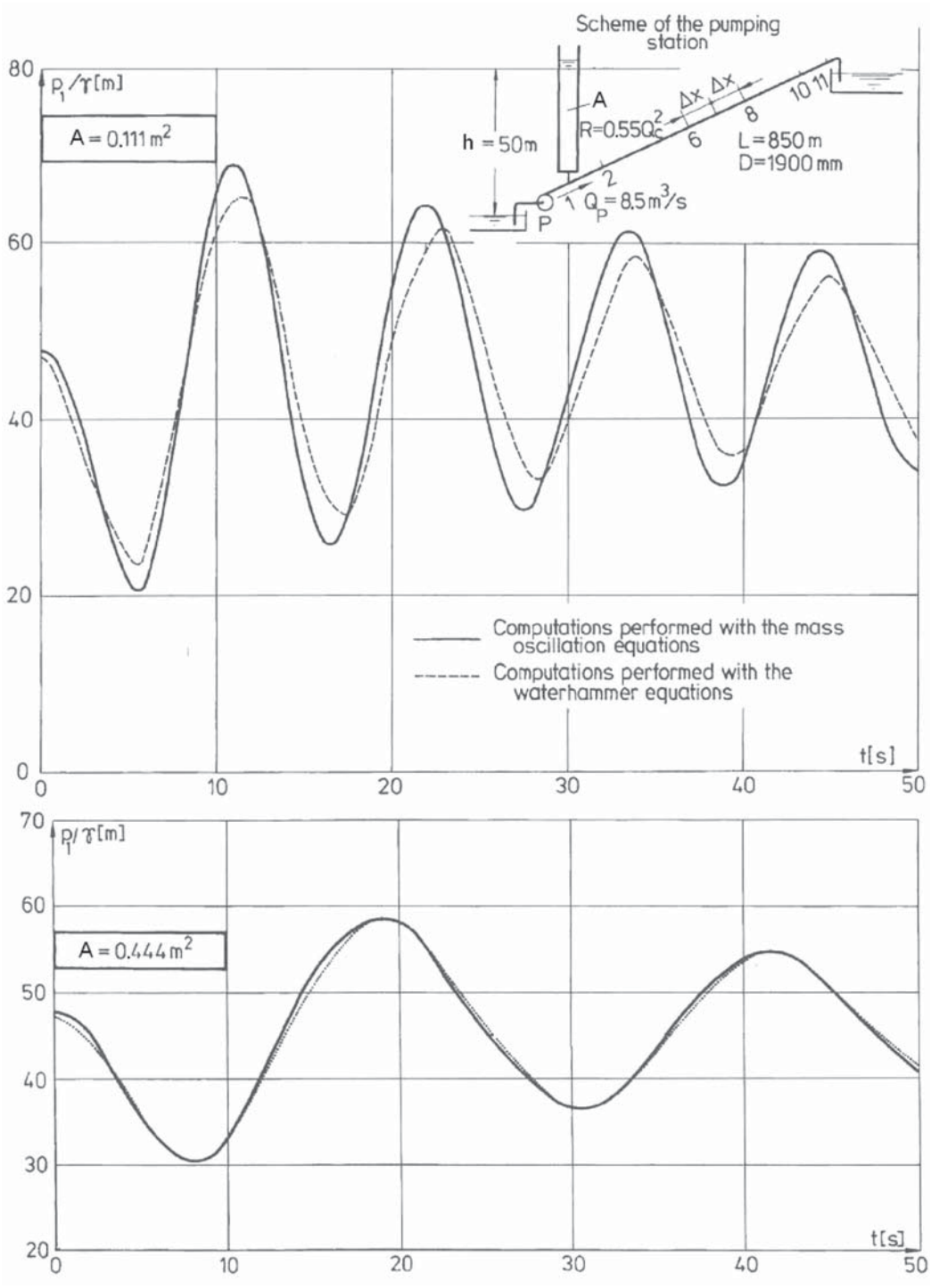


FIG. 5.24 COMPARISON OF NUMERICAL SIMULATIONS FOR A SURGE TANK (From: M. Popescu et al [177], "Applied Hydraulic Transients for Hydroelectric Power Plants", A. A. Balkeema Publishing, copyright 2003. Reproduced by permission of Taylor and Francis Books UK)

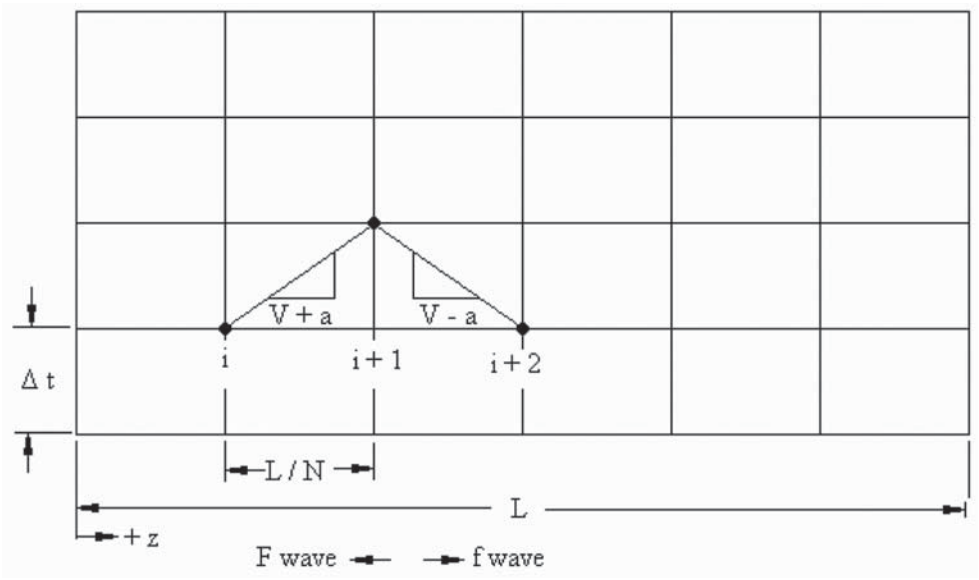


FIG. 5.25 FINITE DIFFERENCE SOLUTION FOR THE MOC

$$C^+ : V_{i+1} = 0 = \frac{1}{2} \cdot \left(\begin{array}{l} (V_i + V_{i+2}) + \dfrac{g \cdot (h_i + h_{i+2})}{a} \\ + \dfrac{g \cdot \Delta t \cdot (V_i - V_{i+2}) \cdot \sin(\alpha)}{a} \\ + \dfrac{f \cdot \Delta t \cdot \left(V_i \cdot |V_i| + V_{i+2} \cdot |V_{i+2}| \right)}{2 \cdot D} \end{array} \right) \quad \text{US (5.46)}$$

$$C^+ : H_{i+1} = 0 = \frac{1}{2} \cdot \left(\begin{array}{l} \dfrac{a}{g}(V_i + V_{i+2}) + (h_i + h_{i+2}) \\ + \Delta t \cdot (V_i - V_{i+2}) \cdot \sin(\alpha) \\ + \dfrac{a \cdot f \cdot \Delta t \cdot \left(V_i \cdot |V_i| + V_{i+2} \cdot |V_{i+2}| \right)}{g \cdot 2 \cdot D} \end{array} \right) \quad \text{US (5.47)}$$

$$C^- : V_{i+1} = 0 = \frac{1}{2} \cdot \left(\begin{array}{l} (V_i + V_{i+2}) + \dfrac{g \cdot (h_i + h_{i+2})}{a} \\ - \dfrac{g \cdot \Delta t \cdot (V_i - V_{i+2}) \cdot \sin(\alpha)}{a} \\ + \dfrac{f \cdot \Delta t \cdot \left(V_i \cdot |V_i| + V_{i+2} \cdot |V_{i+2}| \right)}{2 \cdot D} \end{array} \right) \quad \text{US (5.48)}$$

$$C^- : H_{i+1} = 0 = \frac{1}{2} \cdot \left(\begin{array}{l} \dfrac{a}{g}(V_i + V_{i+2}) + (h_i + h_{i+2}) \\ - \Delta t \cdot (V_i - V_{i+2}) \cdot \sin(\alpha) \\ + \dfrac{a \cdot f \cdot \Delta t \cdot \left(V_i \cdot |V_i| + V_{i+2} \cdot |V_{i+2}| \right)}{g \cdot 2 \cdot D} \end{array} \right) \quad \text{US (5.49)}$$

These equations provide a technique to calculate the head and flow rate at any arbitrary point at node $i + 1$ if the conditions at node i and node $i + 2$ are known. The steady-state conditions provide conditions at all nodes along the $\Delta t = 0$ axis (Eq. (2.36)). Then, to complete any finite difference calculation for fluid transients in a straight pipe, all that is required are the boundary conditions at $z = 0$ and $z = L$. Boundary conditions at pipe ends may consist of constant head, constant flow, variable flow due to pump or valve operations, or variable head and flow due to surge tank operations.

5.9 VALVE ACTUATION

Valve actuations provide classic examples of water hammer. Joukowski's equation quantifies the pressure surge, but the transient pressures in a pipe are more complex as shown by the following valve actuation examples. The first and second examples visually present the

changes in flow and head that occur in a pipe when a valve is closed. The third example compares the MOC theory to experimental results for liquid-filled pipes. The fourth example demonstrates one application of the use of the MOC to correct pipe system failures. Other examples follow throughout this chapter.

Example 5.14 Use MOC to consider a suddenly closed valve in a pipe

Fig. 5.26 provides the results of a MOC calculation for a suddenly closed valve in a pipeline connected to a reservoir. Both changes in head and velocity are plotted for different times following valve closure. The phenomenon referred to as line pack is evidenced, where friction affects the head in the wake of the shock wave. Note also that frictional effects reduce the magnitude of the shock with respect to time, as expected. For examples like this, the MOC has gained wide acceptance due to its agreement with experimental data for fluid transients in systems for liquid-filled systems.

Example 5.15 Consider a slowly opened valve in a pipe

Calculations were performed by C. Liou for a slowly opened valve in a pipe between two reservoirs. After the valve opens fully, the level in the upstream reservoir drops until the level is the same in each reservoir, and flow stops. The results are shown in Fig. 5.27 as the valve opens, where the head, velocity, and valve position as a function of time are shown. For this example, the f wave is described by a ramp function. Note that the pressure surge, Δh, is completely eliminated by using valve closure speed control, and only the head of the reservoir is exerted on the pipeline.

Example 5.16 Compare the MOC to experimental results for a suddenly closed valve in a pipe

Numerous experimental examples are available in the literature, and two of those examples cited by Wiley and Streeter are provided here. In Fig. 5.28, a comparison between an MOC solution and experiment are shown for sudden valve closure in a 40-ft long, ½-in. diameter copper tube with orifice's installed in the tube. Pressure was measured 10 ft from the solenoid closed valve. In Fig. 5.29, an MOC solution is compared to experiment for a reservoir, pipeline, and valve system. Note that unsteady friction terms are required to ensure accuracy for the MOC after the first shock wave. One implication of this result is that the DMF may be only applicable to the first water hammer cycle, and fatigue effects may be limited to that cycle when evaluating pipe failure.

Example 5.17 Consider valve leaks caused by water hammer and corrective actions

During facility operations, different below-grade valves were operated, and several water hammers occurred that caused leaks in several valves, as shown in Fig. 5.30 (Leishear [7]). Although the leaks were contained by designed safety features, repairs were costly since radioactive liquid waste was leaked from the valves. To consider the leaks, a rather complex piping system is simplified in Fig. 5.31, where the pipe layout is shown in Fig. 5.32. The system consisted of a flush water tank at the high point of the system connected to a pump and piping, where water flowed down into the 1000-ft long pipe system to flush it after transferring radioactive liquid waste. Valves were damaged during flushing operations.

Water hammer magnitudes were calculated using the MOC for calculations at different times that transients occurred, and the magnitudes of several different transients were directly related to leaks that occurred in that facility. In Fig. 5.33, several calculation results are shown along with control room records that indicated the exact time that leaks occurred in the facility. Points 2, 8, 10, and 12 in the figure indicate the occurrence of different water hammers, as indicated by fluid level increases in a sump below the leaking valves.

These leaks were not corrected until they had occurred on three different occasions, since water hammer was not identified as a cause. In each case, a valve was actuated, and leaks occurred hundreds of feet away at different valves. The facts were not related between valve or pump operations in one place and leaks occurring in another place.

To troubleshoot these leaks, the valves were evaluated, and the maximum calculated pressure of 547 psi was less than the rated 760-psi valve rating. A DMF of 1.8 was estimated to determine an equivalent valve load of 985 psi, which resulted in packing leaks. Further investigation revealed a long history of valve leaks and that special procedures were developed to rebuild and improve the life of these valves. These rebuilt valves were shown to withstand 1000-psi pressures without leaking, as shown in Fig. 5.34. Essentially, water hammer had occurred repeatedly for years without operator awareness, and the valves were essentially strengthened to withstand beyond design conditions that had become routine.

To control fluid transients, operator training and procedure corrections were implemented to ensure that valves are slowly operated to prevent transients. Also, a slow-acting valve was installed at the pump as considered in Example 5.18.

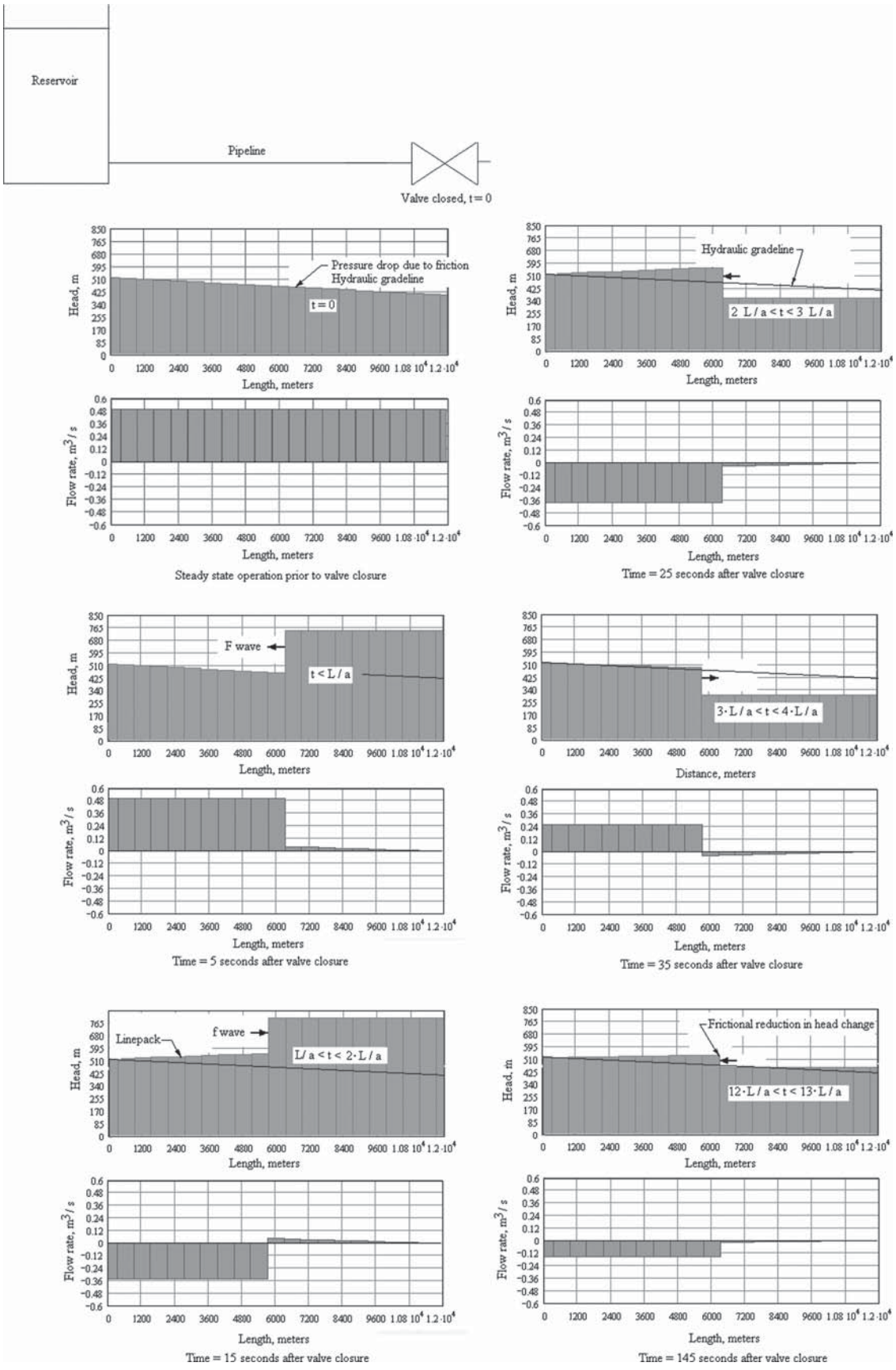


FIG. 5.26 SUDDENLY CLOSED VALVE ("Fluid Transients" class example," C. Liou, U. of Idaho)

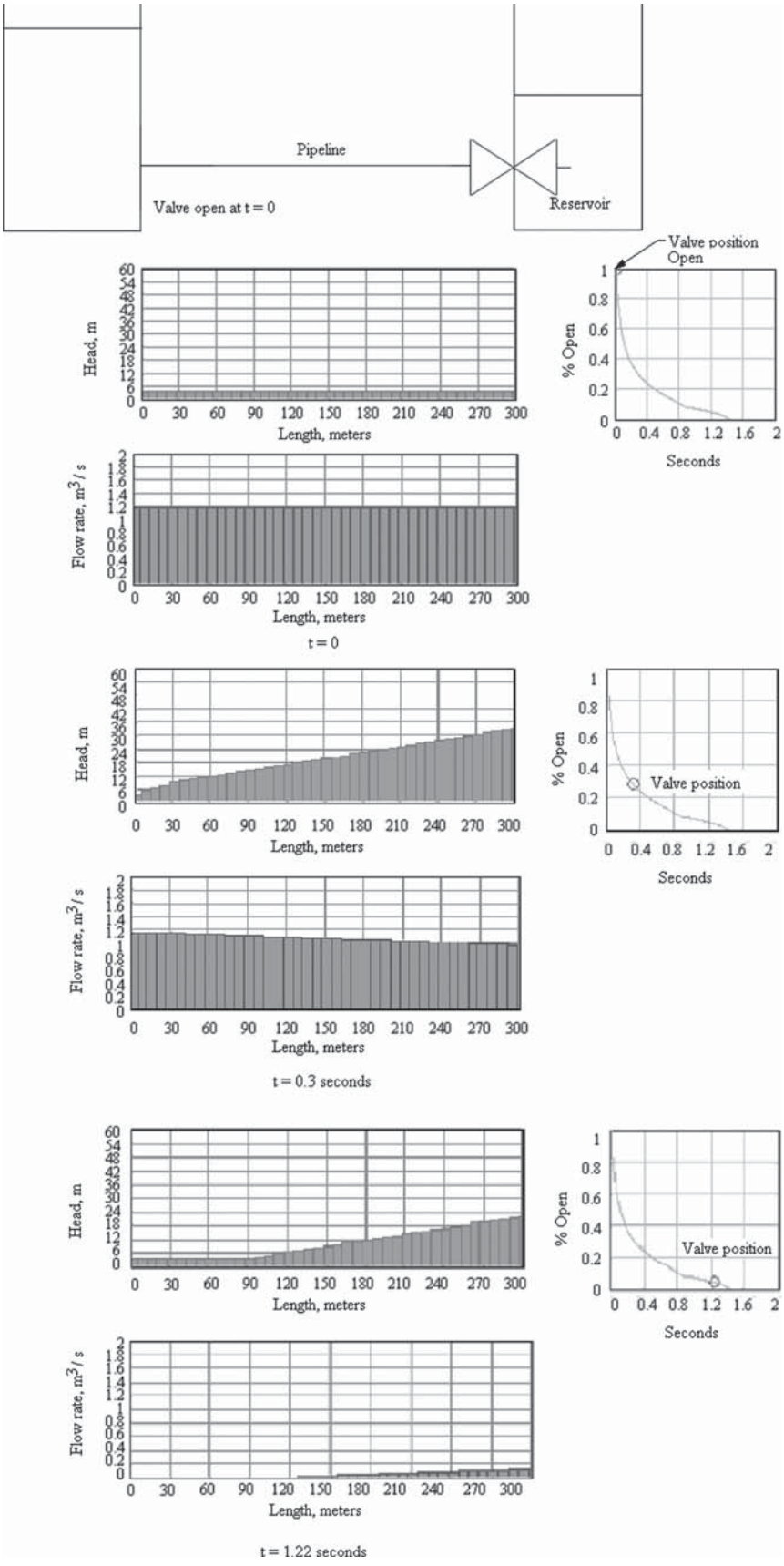


FIG. 5.27 SLOWLY OPENING VALVE ("Fluid Transients" class example," C. Liou, U. of Idaho)

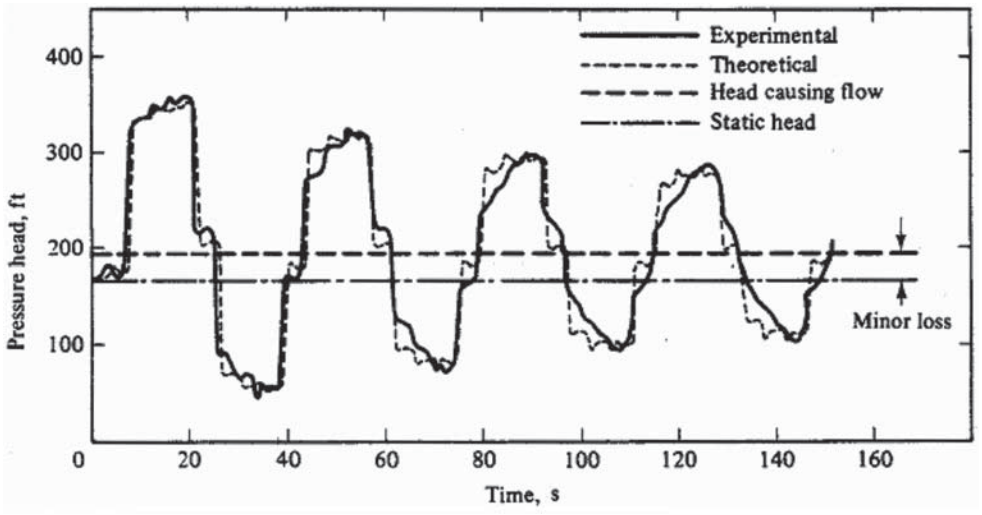


FIG. 5.28 VALVE CLOSURE IN A SHORT TUBE (Contractor [186])

5.10 REFLECTED SHOCK WAVES

Shock wave reflections occur at all boundary changes in a system, which include dimensional and property changes. For example, reconsider Example 5.14 and note that the wave is fully reflected from the reservoir, but reversed in sign, which is similar for a wave reflection from a free surface. For both cases, $f = -F$. Other boundaries are more complicated.

5.11 REFLECTED WAVES IN A DEAD-END PIPE

For a dead-end pipe, the wave is reflected intact, and the pressure magnitude of the shock is doubled in the pipe. One reflected wave concern occurs for dead-end branches in pipe systems where any shock wave occurs. The basic water hammer equation can be used to approximate the shock wave in the main header, but all dead-end branches will experience a doubling of that pressure. A similar reflected wave concern occurs in pipe systems that have closed valves on pump startup, where the closed valve acts as a dead end, and again, the expected maximum pressure can be doubled.

The effects of reflected pressure waves are also frequently observed during pump startups in long pipelines that do not have dead ends. If a pump is suddenly started, the momentum of the fluid inhibits flow, and pressure spikes doubling the steady-state pressure are frequently noted in calculations. The fluid momentum prevents free fluid movement throughout the pipe. Refer to Fig. 5.9 for an example of wave reflections during pump startup. In that figure, the pressure doubles immediately after startup Reflected shocks can cause pipe rupture near dead ends and pump explosions for some conditions..

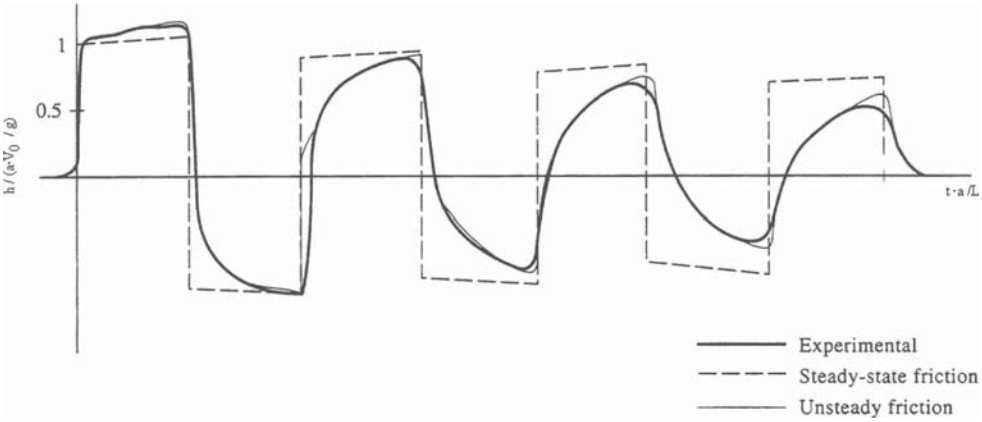


FIG. 5.29 VALVE CLOSURE IN A LONG PIPE (Wiley and Streeter [173], Holmboe [187], and Zielke [188], Wylie, E. B., Streeter, V. L., "Fluid Transients in Systems, 1st" Edition, copyright 1993. Reprinted by permission of Pearson Education, Inc., Upper Saddle River, NJ)

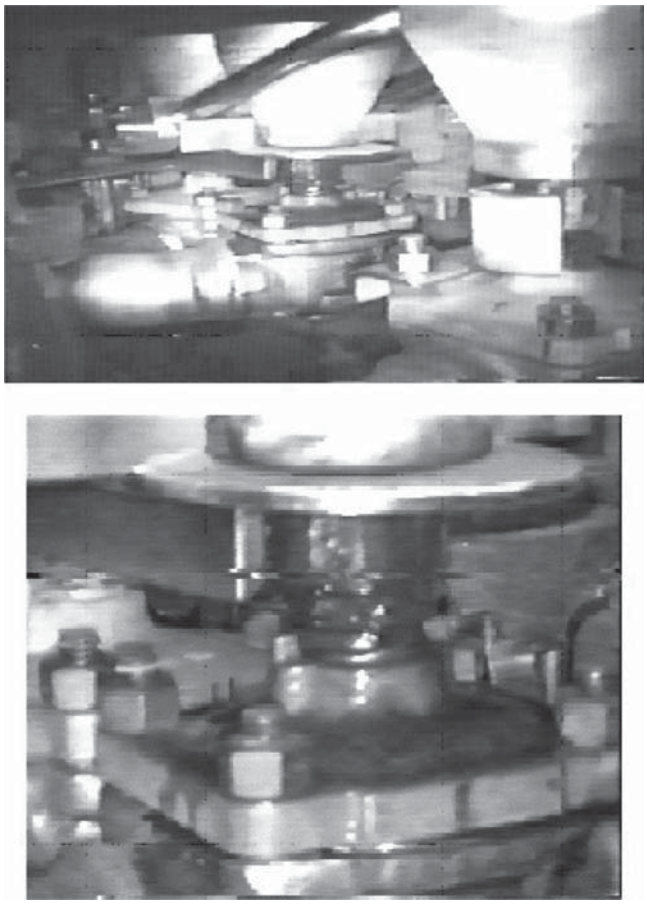


FIG. 5.30 REMOTE PHOTO OF PACKING

Example 5.18 Consider a valve opening into a closed-end system

Fig. 5.33 describes several fluid transients, but the 300-psi transients noted to occur during the first two leaks resulted from wave reflections at the end of a pipe. The schematic of Fig. 5.31 is further simplified in Fig. 5.35, along with pressure calculations. Referring to Fig. 5.31, repeated hammering of the system occurred after the pump was started. Valve 1073 was opened on numerous occasions when the pipe was plugged with salt precipitated from solution. This plugging was the equivalent of opening Valve 1073 against closed Valves 39 and 61. Analyzing the system accordingly using the MOC, the indicated 300-psi pressures were calculated.

The pressure surge was eliminated by using a slow-closing ball valve as demonstrated by Fig. 5.36. Note that the pressure is nearly cut in half as the reflected pressure wave is eliminated. Since the flow is downward, there was also the potential for slug flow on startup, which was not evaluated.

5.12 SERIES PIPES AND TRANSITIONS IN PIPE MATERIAL

When pipe diameters, thicknesses, or materials change, wave reflections occur. When an incident wave arrives at a transition, a wave of different magnitude is transmitted through the transition, while another wave is reflected back in the direction of the approaching incident wave. For waves traveling in the $+z$ direction, waves at the transition may be described in terms of incident, f_i, transmitted, f_t, and reflected waves, F_r. For waves in the $-z$ direction, the roles of f and F are simply reversed. Neglecting friction in the $+z$ direction and referring to Fig. 5.37,

$$f_t = f_i \cdot \frac{\dfrac{2 \cdot A_1}{a_1}}{\dfrac{A_1}{a_1} + \dfrac{A_2}{a_2}} \qquad \text{US (5.50)}$$

$$f_r = f_i \cdot \frac{\dfrac{A_1}{a_1} - \dfrac{A_2}{a_2}}{\dfrac{A_1}{a_1} + \dfrac{A_2}{a_2}} \qquad \text{US (5.51)}$$

where A_1 and A_2 are the pipe areas, and a_1 and a_2 are the wave speeds.

Equations (5.50) and (5.51) describe the initial shock waves at a transition, but the wave mechanics for even a single pipe are far more complex than these simple equations indicate.

Example 5.19 Consider wave reflections due to a material change in a pipe

In another of C. Liou's "Fluid Transient" class examples, he provided an excellent demonstration of the complexities of wave transmission during fluid transients. Fig. 5.38 shows the approaching wave, its division into a reflected and transmitted wave, and then combined reflections from the pipe ends and additional reflections at the transition. In large pipe systems, reflected waves occur at every transition, as well as at all intersections. All in all, the complexities of large systems demand computerized solutions.

5.13 PARALLEL PIPES/ INTERSECTIONS

The MOC technique is used to describe parallel pipe systems and also used throughout the remainder of this work unless otherwise noted. Even so, other methods of solution should be noted.

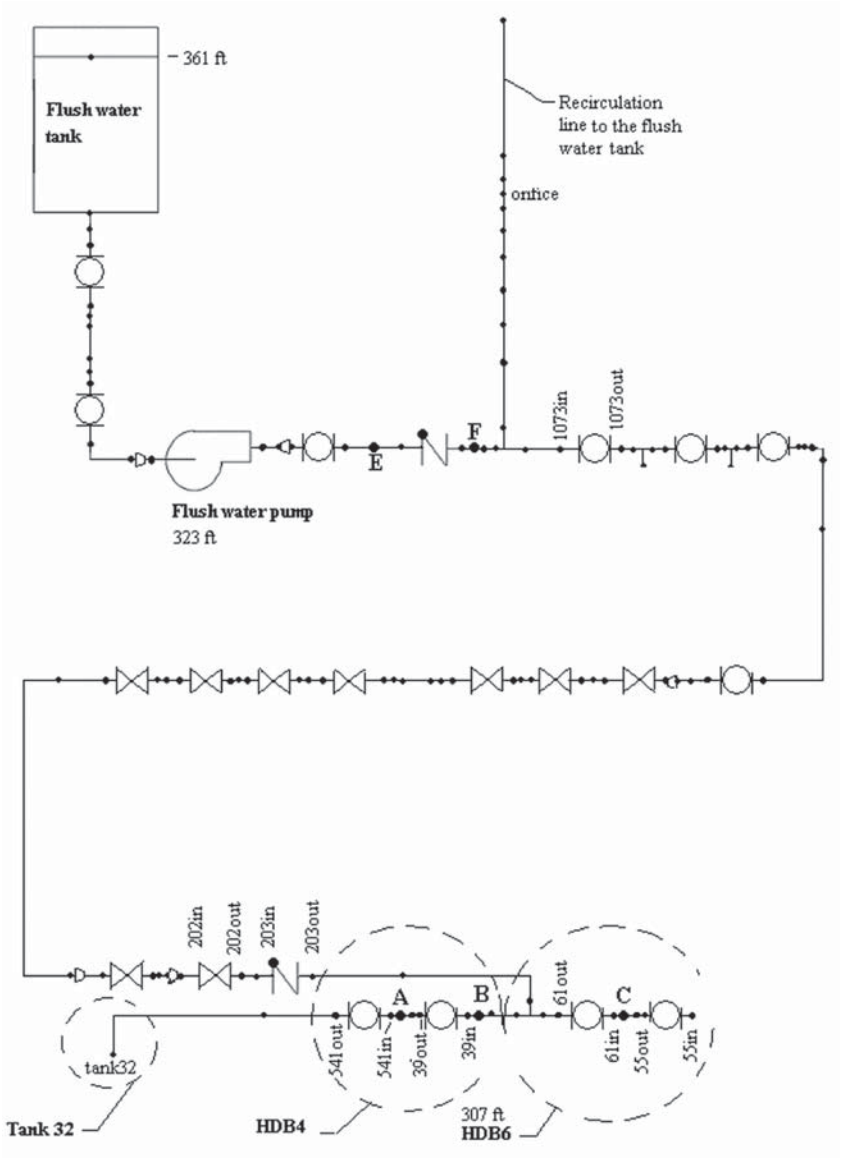


FIG. 5.31 PIPING SCHEMATIC

In particular, Larock et al [176] provides computer programs to establish flow in networks of parallel pipes, using rigid water column techniques for solving a set of algebraic simultaneous equations to describe flow through parallel paths. Larock also adapts this technique to relief valves in pipe networks.

For the elastic water column theory, Parmakian [172] expressed the wave equations at the intersection as

$$f_t = f_i \cdot \frac{\dfrac{2 \cdot A_1}{a_1}}{\dfrac{A_1}{a_1} + \dfrac{A_2}{a_2} + \dfrac{A_3}{a_3}} \qquad \text{US (5.52)}$$

$$f_r = f_i \cdot \frac{\dfrac{A_1}{a_1} - \dfrac{A_2}{a_2} - \dfrac{A_3}{a_3}}{\dfrac{A_1}{a_1} + \dfrac{A_2}{a_2} + \dfrac{A_3}{a_3}} \qquad \text{US (5.53)}$$

where a_3 and A_3 are wave speeds and areas, and terms are defined in Fig. 5.39. Once again, actual systems are far more complex, but the simplified equations provide some insight into the physics of the processes. The following example demonstrates the usefulness of the MOC technique for evaluation of normal and off-normal operations.

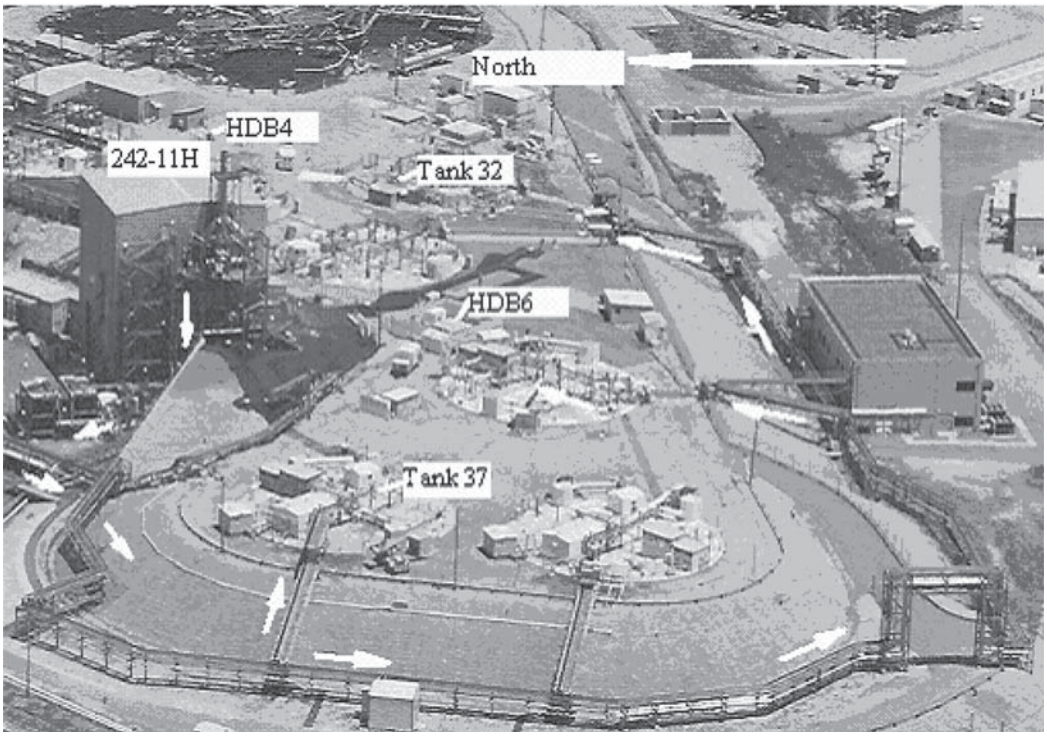


FIG. 5.32 FACILITY LAYOUT AND PIPELINE PATHS

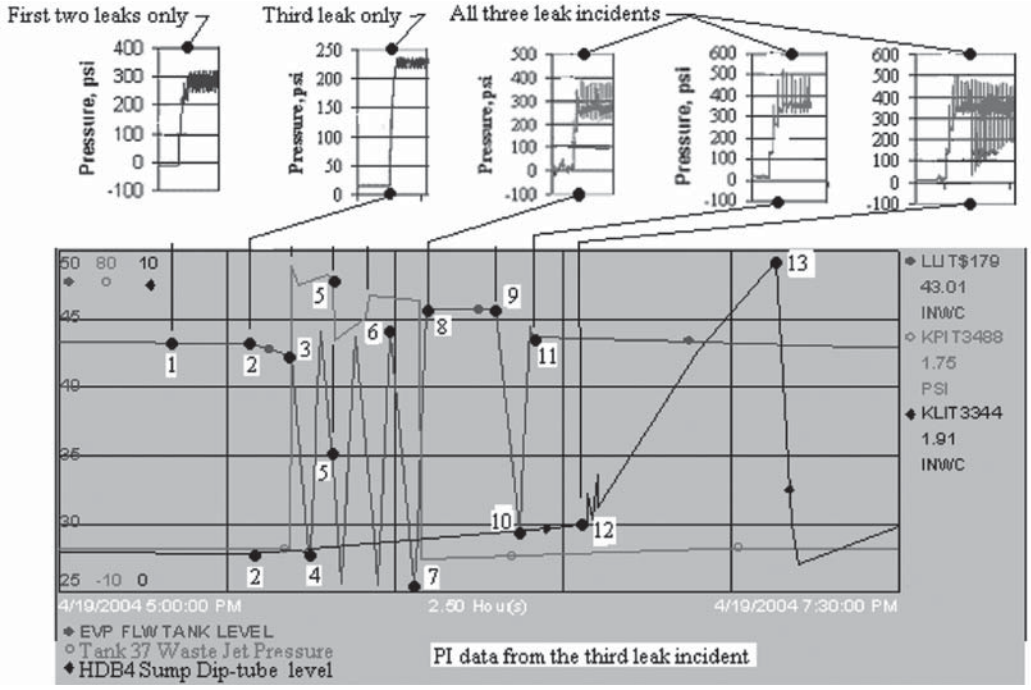


FIG. 5.33 VALVE LEAKS AND PRESSURE CALCULATIONS

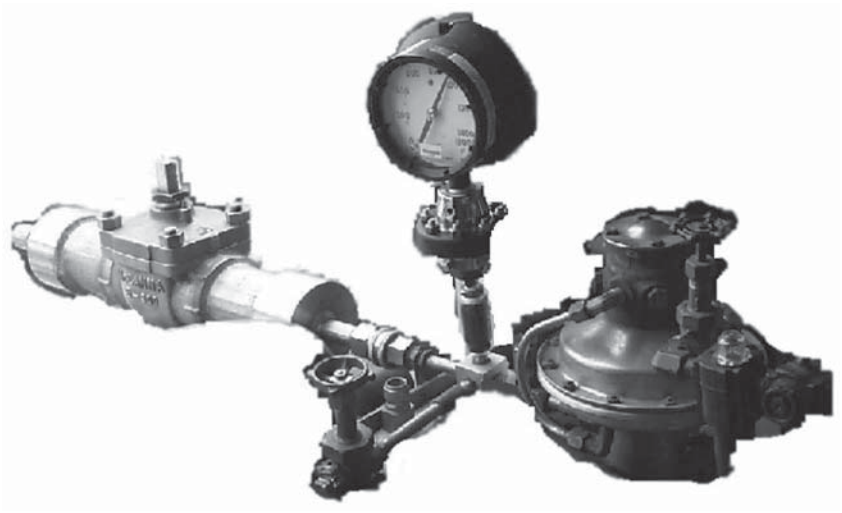


FIG. 5.34 HYDROSTATIC LEAK TEST OF REBUILT VALVE

Example 5.20 consider normal and off-normal valve operations

For the system shown in Example 5.6, water hammer was induced by several causes, and this example focuses on valve-induced transients. An MOC program written by Gerry Schohl of the Tennessee Valley Authority was used for examples in this text. Additional details of the pipe system and calculations are available (Leishear [1]). TFSIM uses variable friction and approximates wave speeds in parallel branches by adjusting the wave speed in one branch to ensure that the waves recombine at the end of the parallel paths. This simplification affects the timing of wave speeds throughout the system and needs consideration. In Fig. 5.40, the maximum pressure surge is nearly 500 psi due to a valve closure at point D when flow is present through all the valves shown. When the last valve is closed, the pressure surge is over 700 psi, as shown in Fig. 5.41. That is, increasing pressure shocks were introduced into the system as each valve was successively closed during shutdown. Note also that a higher pressure occurs during the second pressure peak. These additional pressures are due to wave reflections in the pipe system, and these reflected wave additions are occasionally referred to as rebound. Since TFSIM approximates the wave speeds in parallel paths, the exact location and magnitude of the rebound is indiscernible, but reflected waves are expected to double, and pressures may be as high as 2·700 psi = 1400 psi.

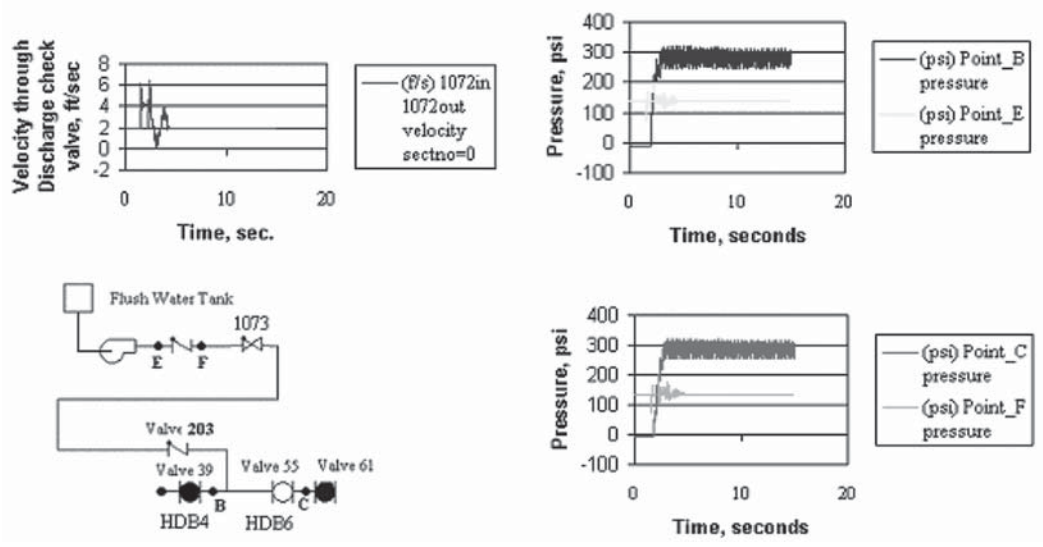


FIG. 5.35 PUMP STARTUP AGAINST CLOSED VALVES IN A LONG PIPE SYSTEM

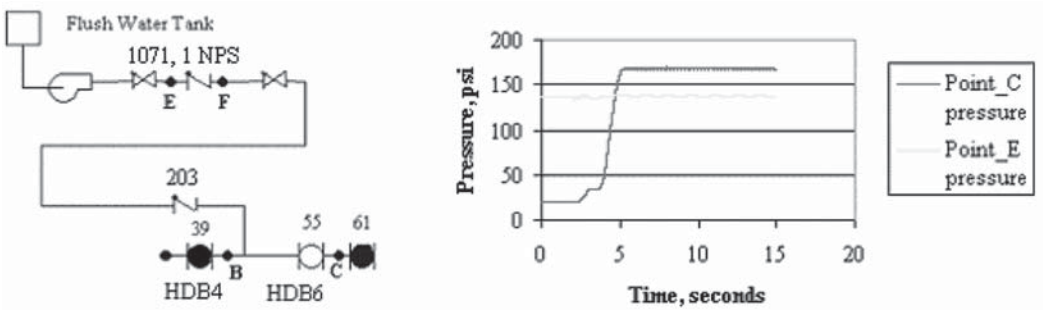


FIG. 5.36 SLOW-ACTING VALVE TO ELIMINATE REFLECTED PRESSURE WAVES

Historically, more leaks occurred during shutdown of this system, once a leak was identified. When a leak occurred, the system was repetitively hammered during shutdown as valves were successively closed, and the flow rates at valves were increased from 6 to 8 ft/second to above 20 ft/second. Water hammer was long unidentified, since the cracked cooling coils could not be accessed, a dynamic stress theory was not yet available, and pipes frequently broke a half mile away from the source of water hammer. A thorough investigation of facility records showed that either valve actuations or pump operations were in process every time a leak in the systems occurred. Ball valves have a non-linear closing action, but a linear-actuator can be installed with the response shown in Fig. 5.42 to adequately reduce transients.

5.14 CENTRIFUGAL PUMP OPERATION DURING TRANSIENTS

Centrifugal pump performance changes depending on the system. If flow is uphill, liquid can flow in reverse through the pump, and the pump acts as a turbine. If the flow is downhill, vapor pockets can form, and slug flow is initiated on re-start. If flow is in a closed loop system, the flow simply coasts to a stop on pump shutdown. If one of two, or more, parallel pumps are shut down while the others are still operating, flow will suddenly reverse through the stopped pump. The MOC is the method of choice to investigate these different conditions, but the graphic technique provides insight perhaps not gleaned from the MOC method.

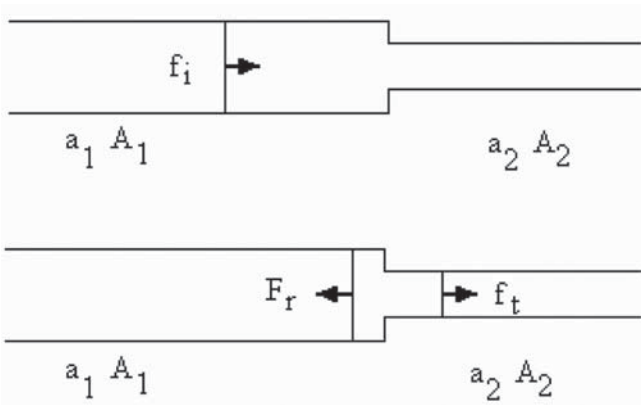


FIG. 5.37 WAVES AT PIPE TRANSITIONS

5.14.1 Graphic Water Hammer Solution for Pumps

Example 5.21 Consider a power loss to pump

Parmakian [172] provided numerous graphic examples of water hammer. One of those examples shows the pressure transients shown in Fig. 5.43 for the case of power loss at pumps equipped with instantaneously closing discharge check valves. The water hammer equations were used to calculate velocity and head to establish different points in the figure, and that technique is not presented here. In the figure, the pressure and flow decrease from steady state at $t = 0$ through $t = 3 \cdot L/a$, where the flow reverses, and increases to $1.9 \cdot h_0$. This example is another classic water hammer problem, where flow reversal needs to be stopped, but valve slamming causes pressure surges in the piping. As noted in chapter 3, check valves behave dynamically, and the pressure surges are affected by the valve characteristics. The MOC technique addresses this issue and, again, is a presently accepted methodology.

5.14.2 Reverse Pump Operation Due to Flow Reversal

Check valves are typically installed on pump discharge piping to prevent flow reversal, but there are some cases where the pump is intentionally operated in reverse. In those cases, pumps act as turbines and run at the line frequency provided to the pump. That is, pumps will provide power at 60 Hz as water runs backward through the pumps.

When pumps operate in reverse, a pump curve for reverse operation is required, and some are available in the

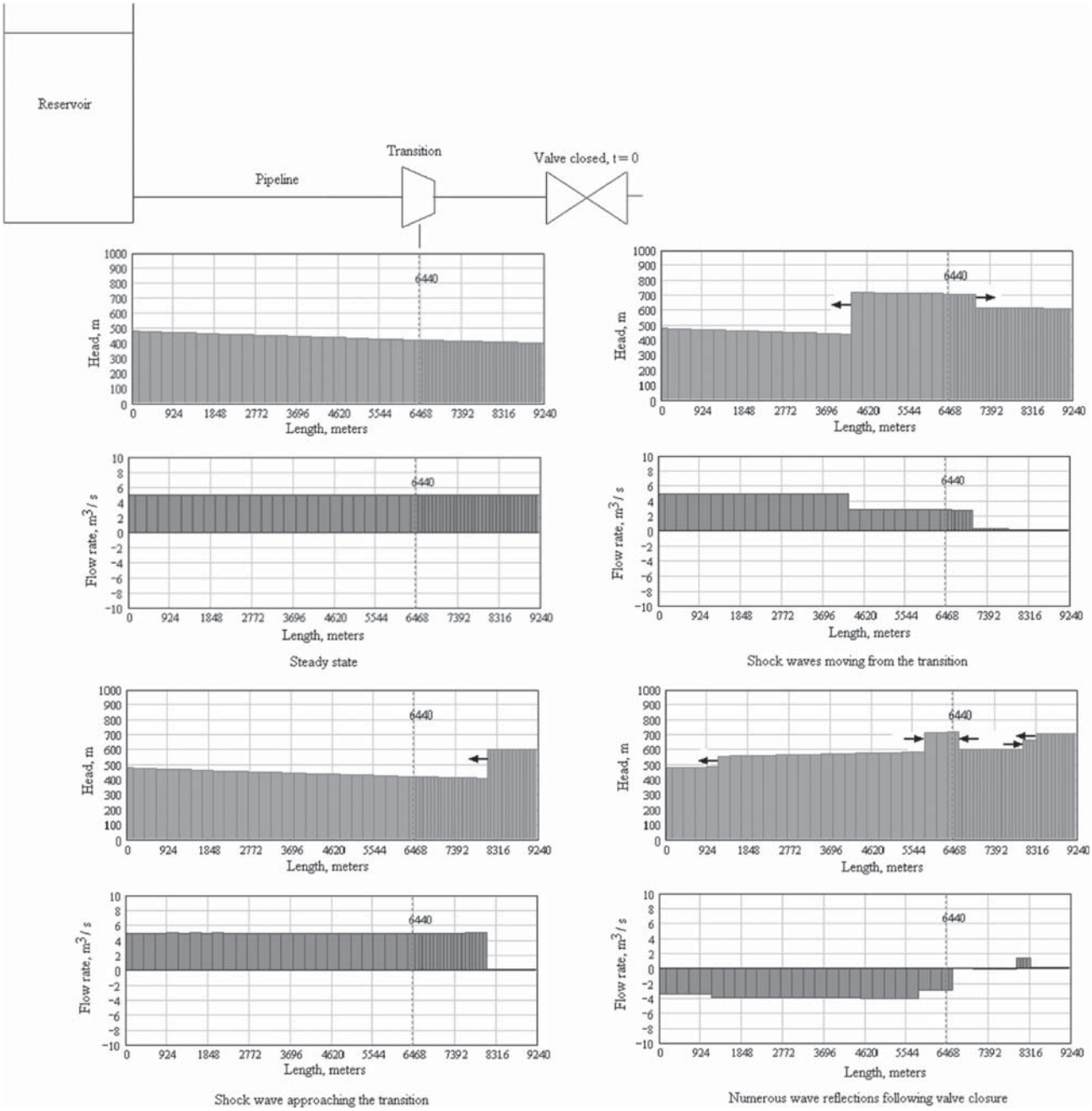


FIG. 5.38 SHOCK WAVES DUE TO A PIPE TRANSITION
("Fluid Transients" Class Example from C. Liou, University of Idaho)

literature. Although errors may be induced in calculations, a common practice to approximate pump performance is to use a pump curve with a similar specific speed, where the term homologous pump applies to pumps with similar specific speeds.

Donsky provided some of the earliest pump curves that included reverse operations. Those curves provide some generic insight into pump operations during flow reversal, using the ratios of input torque at any time divided by the rated torque ($T/T_R = \beta$) and the operating speed divided by the rated speed ($N/N_R = \alpha$). Also, at least 23 different pump curves are available in the literature (Donsky [189], Wylie et al [173], Brown and Rogers [190], and Thorley [191]), which are similar to Figs. 5.44 and 5.45. Thorley's

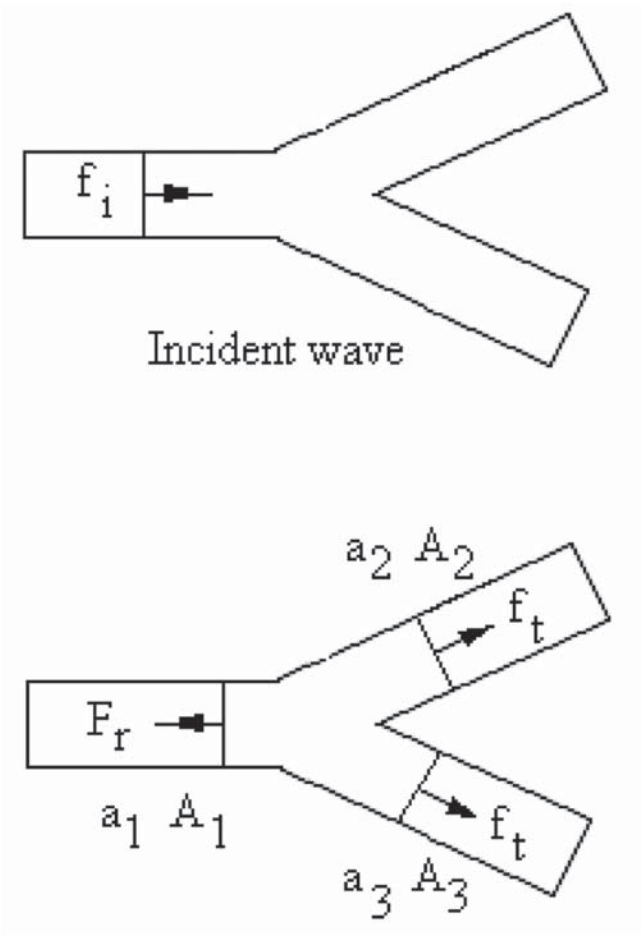


FIG. 5.39 SHOCK WAVES AT A PIPE INTERSECTION

text [68] suggests the use of nondimensional shape factors instead of specific speeds. His text provides curves from 14 different pump tests.

5.14.3 Transient Radial Pump Operation

For a typical radial pump operation, Fig. 5.44 describes normal, or forward, pumping operations for a specific radial pump, where the design point is provided at $V/V_0 = 1$, and $h/h_0 = 1$. From Fig. 5.44, the shutoff head equals 129% of the rated head. Fig. 5.45 describes reverse rotation for a radial pump, where the maximum, reverse flow at runout is 55% of rated flow, and the maximum head during reverse flow is 63% of rated head at full speed in reverse. Note that the affinity laws only approximate the curves shown for an actual pump shutdown.

However, the affinity laws and pump curves for forward and reverse operation can be combined to obtain a series of curves to describe pump shutdowns, which are referred to as four-quadrant or four-zone homologous pump curves. Wylie presents techniques to adapt homologous pump curves and pump inertia to the MOC technique, which is outside the scope of this text. This technique overcomes calculation problems where the velocity and head equal zero and also better explains the concept of energy dissipation. Energy dissipation occurs when the flow rate is in the opposite direction of pump rotation, and energy is lost. That is, during pump shutdown, there are four zones of operation. One is normal pump operation in forward pump rotation. Another is turbine operation, where the pump rotates in reverse and generates energy. The other two zones of operation occur as the pump transitions between these two zones, and the flow moves in the opposite direction of the impeller rotation. Since flow and mechanical motion are opposite in direction, energy is dissipated, and the pump flow performs no useful work during dissipation. The reader is referred to Wylie and Streeter for a full discussion of four-quadrant pump operation. All in all, the fluid transients are very complex during pump shutdown and flow reversal through the pump, as the pump head, speeds, power, and flow rates change. Even so, computer programs are presently accepted solution techniques to address these complexities.

5.14.4 MOC Water Hammer Solution for Pumps

Using pump curves, the pump operation in forward or reverse can be evaluated. Reverse flow typically occurs when the head due to downstream frictional losses is less than the elevation head between the pump and an elevated reservoir. A special case of reverse flow occurs when pumps are in parallel.

Example 5.22 Consider dynamic check valve closure during parallel pump operation

Check valves are typically installed on pump discharge piping, but not without problems. Again, considering Example 5.6, transients due to pump shutdown also contributed to fatigue fractures. The system schematic is shown in Fig. 5.46. When one pump (Pump 1) is turned off, flow reverses through the pump, and the check valve, Valve 1, slams shut. In fact, when this operation was observed, the crack was loud enough that one engineer thought that the 15-ft long, 2-ft diameter heat exchangers attached to the piping were going to fall off the wall. The crack sounded like an 8-lb mall was swung overhead and down into a steel plate. The shock wave traveled from the check valve into the exchangers, which acted like amplifiers. For this example, and many others, pump inertia has a negligible effect on the transient, since the inertia for many industrial applications is relatively small.

As shown in Fig. 5.47, the calculated pressure due to the pump shutdown is nearly three times the operating

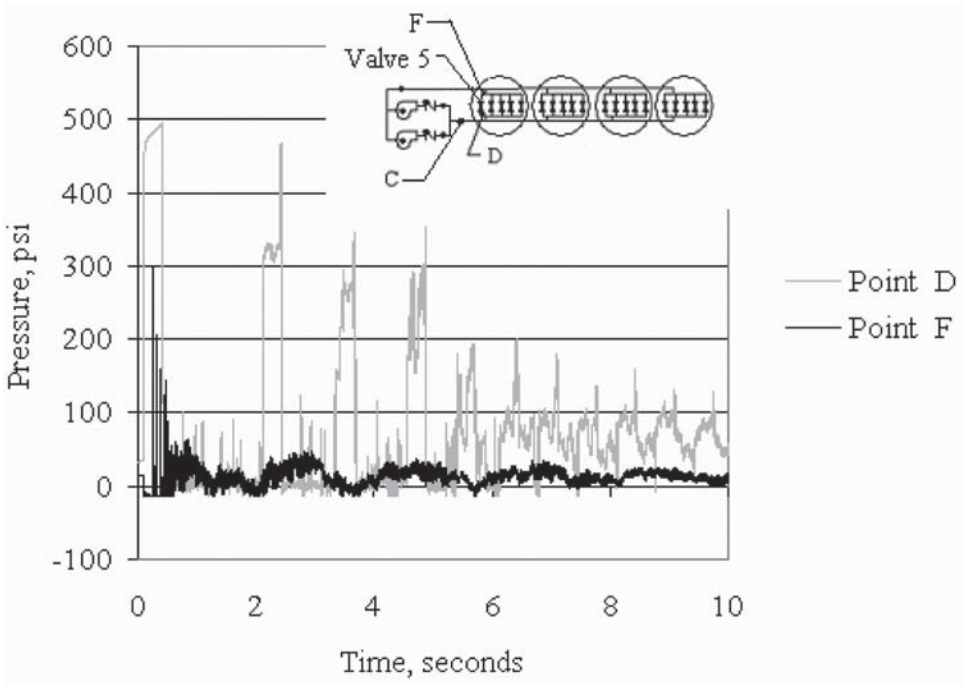


FIG. 5.40 SUDDEN VALVE CLOSURE FOR PARALLEL PATH PIPING

pressure. One corrective action was the use of a linear actuated ball valve that operated automatically when one pump was turned off or power was lost to one pump.

5.14.5 Use of Valve Closure Speeds to Control Pump Transients

Valve selection and closure speed are important factors for transient control. Different valve types, and their use, are discussed in Chapter 2.5. With respect to water hammer, ball and plug valves provide comparable performance for linear valve actuation, since most of the flow is reduced during initial valve closure. Other valves can be controlled to provide similar performance, but linear control is, in general, simpler to implement. An example of a linearly controlled ball valve follows.

Example 5.23 Reduce the pressure surge of Example 5.22, using a slow-closing ball valve

The resulting pressure transient for slow-valve closure during single pump shutdown is shown in Fig. 5.48. Closure time was selected to ensure that relief valves were not actuated. Air-actuated valves and solenoids ensured that the valves would function properly during loss of power.

The dead head condition that momentarily occurs when a pump is operated in this manner should be considered with respect to pump operation. Pump temperatures can increase, and flow imbalances may occur in the pump which induce vibrations and possible bearing damages.

5.15 COLUMN SEPARATION AND VAPOR COLLAPSE

During a fluid transient, column separation occurs in a pipe system when the pressure in the pipe drops below the vapor pressure and a vapor pocket, cavitation bubbles, or a combination of both are created. Vapor collapse occurs when the vapor is suddenly condensed, and since the vapor offers no resistance to collapse, a shock wave is created when the fluid columns rejoin. The process is extremely complicated due to bubble formation, rejoining of bubbles, and subsequent disintegration of those bubbles. Techniques have been developed to approximate the pressure surges due to vapor collapse, but the application of these techniques is further complicated by the fact that the pressure surges vary in magnitude for different conditions. For example, the magnitude of the pressure surge depends on whether the void occurs at a high point in the pipe system or at a valve in the system. Also, the pressure surge depends on whether, or not, the pipe ends are both submerged. Careful consideration of the system is required when analyzing vapor collapse.

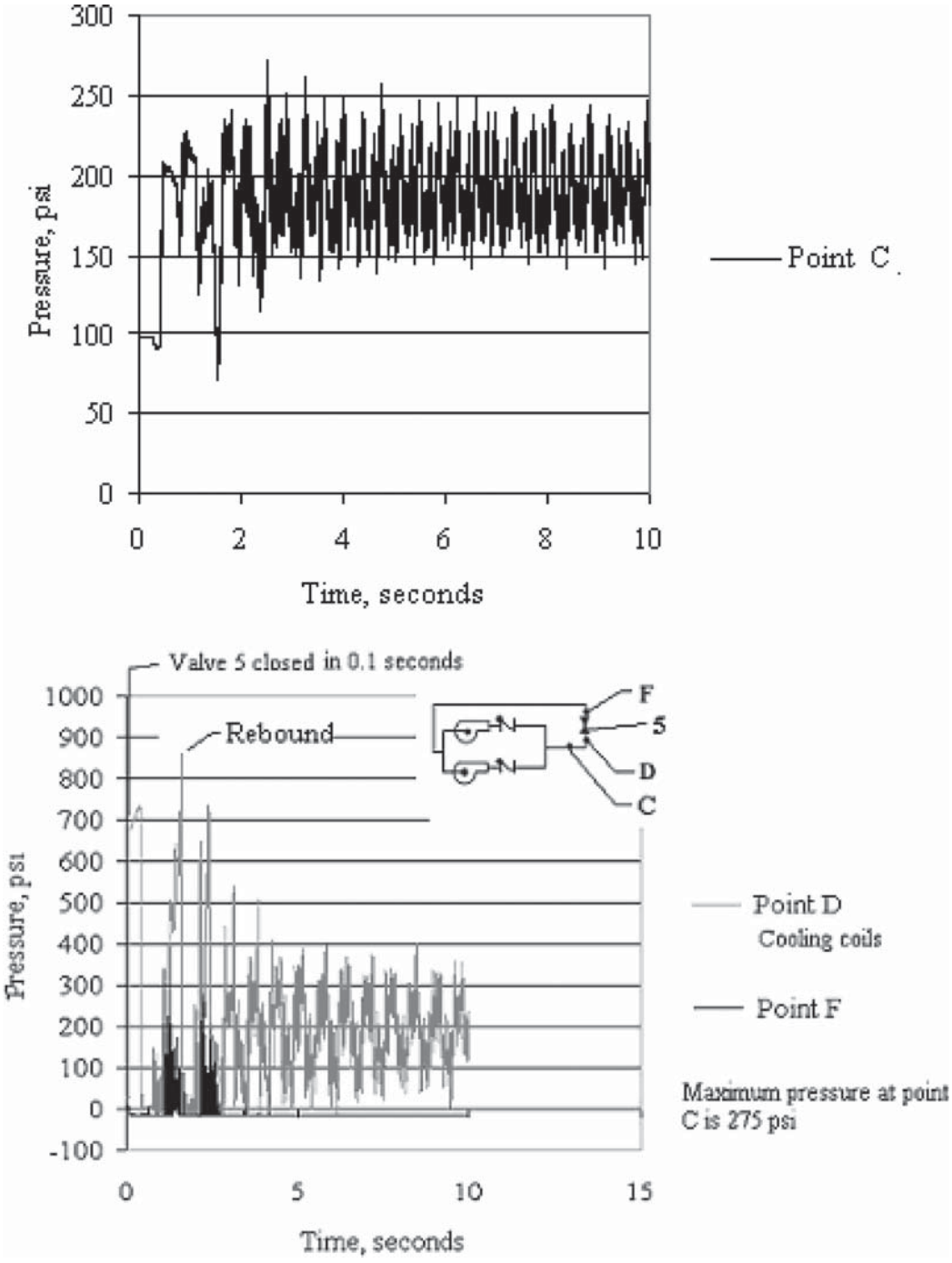


FIG. 5.41 REFLECTED PRESSURE WAVE DUE TO SINGLE VALVE CLOSURE

5.15.1 Column Separation and Vapor Collapse at a High Point in a System With Both Pipe Ends Submerged

Vapor pockets are formed when the pipe elevation exceeds the hydraulic grade line sufficiently so that the liquid in the pipe vaporizes. If both pipe ends are submerged, a vapor pocket may form and collapse during transients when a pump is stopped, which causes shocks at the void. Typically, the voids occur at the high point, but in some cases, voids may form at both the high point and the closing valve.

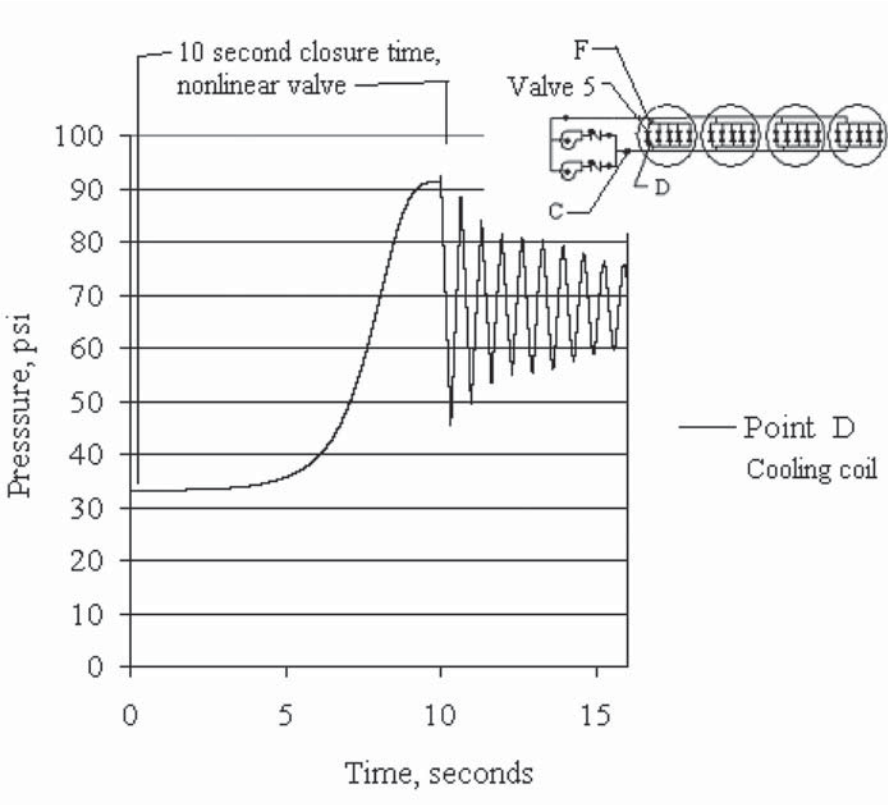


FIG. 5.42 EFFECTS OF LINEAR ACTUATED, BALL VALVE CLOSURE TIME ON PRESSURES

Example 5.24 Consider vapor void formation and collapse for a pipe with both ends submerged

When flow rates change in systems, voids may form as a fluid vaporizes, and the collapse of these voids during the transients causes pressure surges. To consider this phenomenon, the hydraulic grade line for a simplified system is shown in Fig. 5.49 (similar to Fig. 2.9).

For specific conditions, vapor forms between points 3 and 4. To describe these conditions, the relationship between the vapor head, the barometric head, and the head of the fluid at a point in the pipe are graphically shown in Fig. 5.50, where tank levels are assumed constant. For the system to operate at steady-state conditions, the hydraulic grade line must exceed the pipe elevation at all points along the pipe. Otherwise, sufficient head is unavailable to pump over the high points in the system. When a transient occurs due to a valve closure, the hydraulic grade line (piezometric head) and energy grade line (total head) both decrease as the flow rate in the pipe decreases. For a vapor pocket to form during a transient, the difference between the barometric head and the absolute value of the vapor head must be less than the hydraulic grade line of fluid in the pipe, which may be expressed as $(h_b - h_v) < h$. When this temporal condition is met, the fluid vaporizes. As the flow at point 4 slows down and the flow at point 3 speeds up, the head in the pipe decreases to vaporize the fluid. Fig. 5.50 shows this phenomenon in a different format. As the flow, Q_1, slows down and the flow, Q_2, speeds up, the head in the pipe decreases to vaporize the fluid. The grade line varies as a function of flow rate with a different slope on each side of the system high point. After the vapor pocket forms, the flow reverses direction, the fluid condenses, and the fluid columns impact to create a fluid transient. Whether the pocket collapses immediately following pump shutdown or during re-start of the pump depends on system geometry and flow rates. Fluid separation may also occur at the closing valve in some cases. Moreover, computer calculations are required to describe flow separation and vapor collapse for discrete systems.

When column separation occurs for a pipe submerged at both ends, the head at point 3 varies as the flow rates in the pipe change. In Fig. 5.50, for example, Q_1 reduces to a flow rate below Q_2 following an upstream pump valve closure, and a void forms at point 3. Then, Q_2 reverses direction, and the void collapses as the vapor condenses without resistance to flow, and the cycle repeats itself. During this process, the hydraulic head is continually changing both before and after the void, as the flow rates vary. A shock wave in the pipe is created of a maximum theoretical magnitude equal to

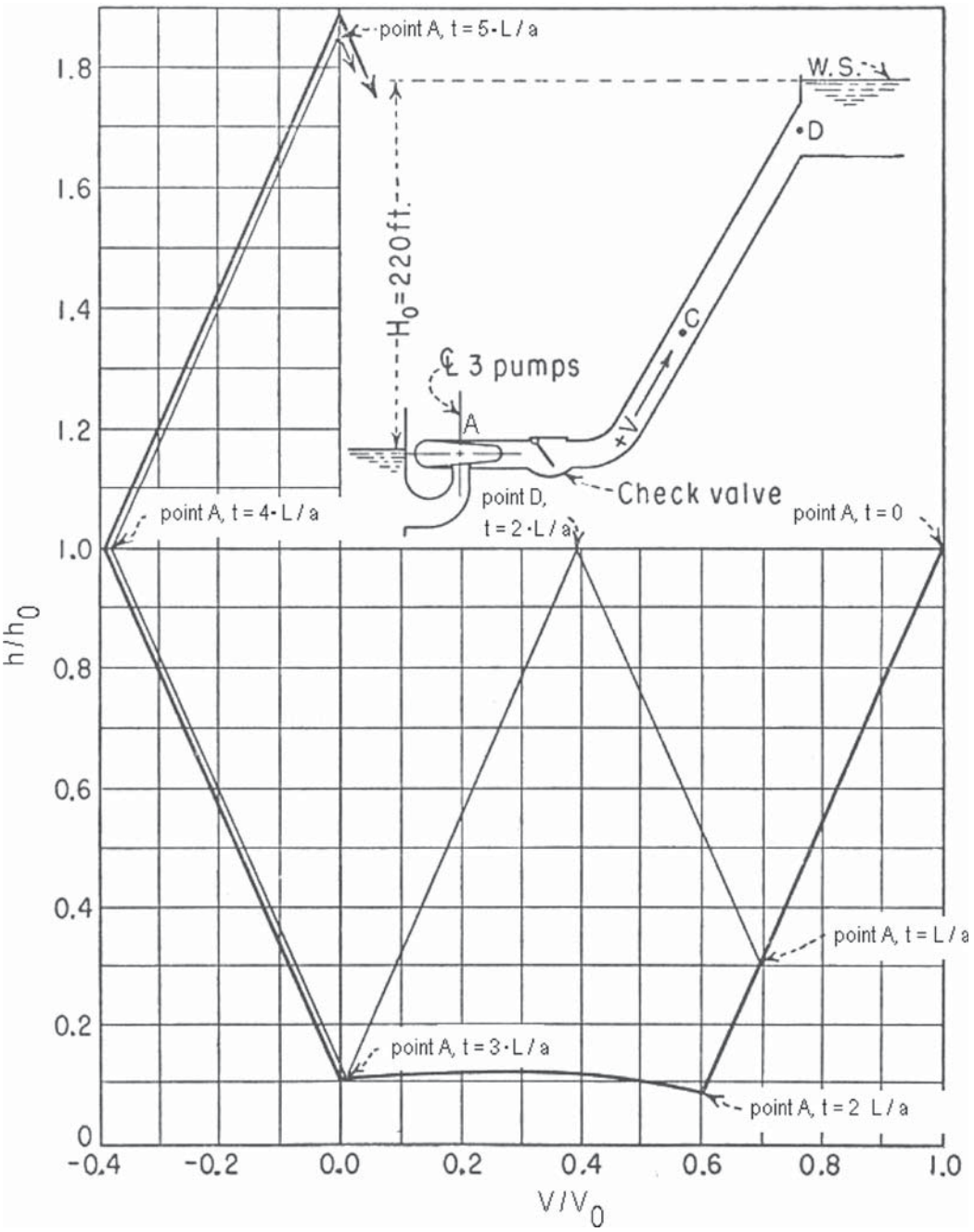


FIG. 5.43 SUDDEN CHECK VALVE CLOSURE FOLLOWING PUMP SHUTDOWN (Parmakian [172], reprinted with permission of Dover Publications)

$$\Delta P(\text{psi}) = (2.1584 \cdot 10^{-4} \cdot \rho(\text{lbf/ft}^3) \cdot a(\text{ft/sec}) \cdot \Delta V(\text{ft/sec}))/2 = 1.0792 \cdot 10^{-4} \cdot \rho(\text{lbf/ft})^3 \cdot a(\text{ft/sec}) \cdot \Delta V(\text{ft/sec}) \quad \text{US (5.54)}$$

This equation is derived similar to the basic water hammer equation with a change in boundary conditions. The fluid column is assumed to be free to move in both directions at the void, rather than being restrained from movement at a valve. When solving the arithmetic water hammer equation, this change in the boundary conditions results in a pressure surge magnitude equal to half the pressure obtained for the case of a suddenly closed pump discharge valve. In some cases, a void is also formed at the valve as the fluid moves away from the valve. A comparable pressure surge

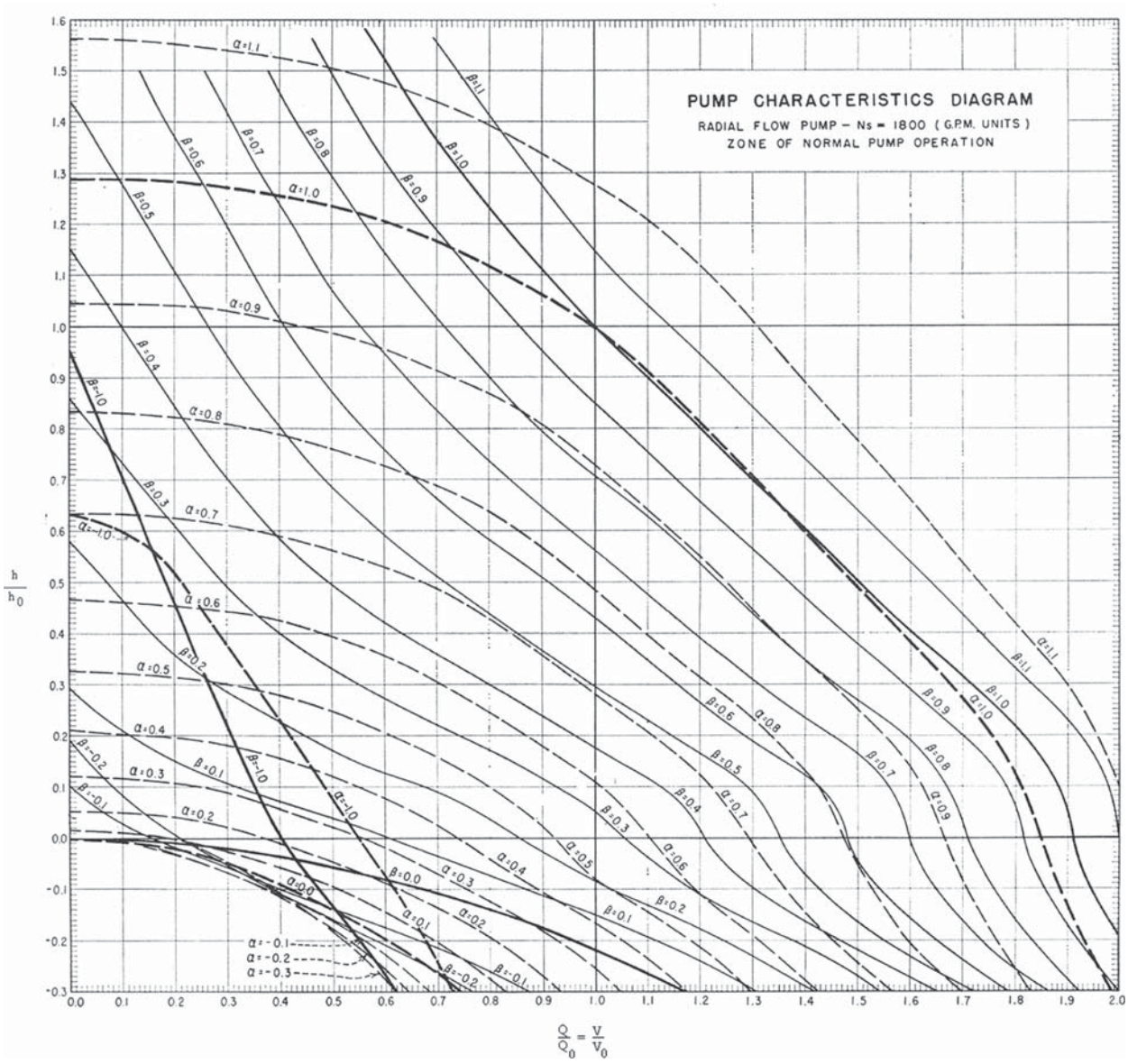


FIG. 5.44 TYPICAL RADIAL PUMP CURVES IN NORMAL OPERATION (Donsky [189])

occurs when a pump is restarted for a pipe with one end submerged.

5.15.2 Column Separation and Vapor Collapse at a High Point in a Pipe With One End Submerged

If only one pipe end is submerged, a void may form that collapses when the pump restarts. This case is different from Example 5.24, where collapse occurred during pump shutdown. When only one end of a pipe is submerged, the transients may be even more complex, since fluid exits the end of the pipe. If there is only one high point in the pipe, a transient will only occur if the pump is restarted before the pipe fully drains. However, if the pipe has multiple high points, vapor collapse may occur at each point when the pump is restarted.

Example 5.25 Consider a fluid transient for a pipe with one end submerged

Reconsider Example 2.13, but consider fluid transient operations. That example can be simplified as shown in Fig. 5.51. When the pump was shut down, fluid exited the end of the pipe, and voids were formed at points A and B, while the pipe emptied between point C and the end of

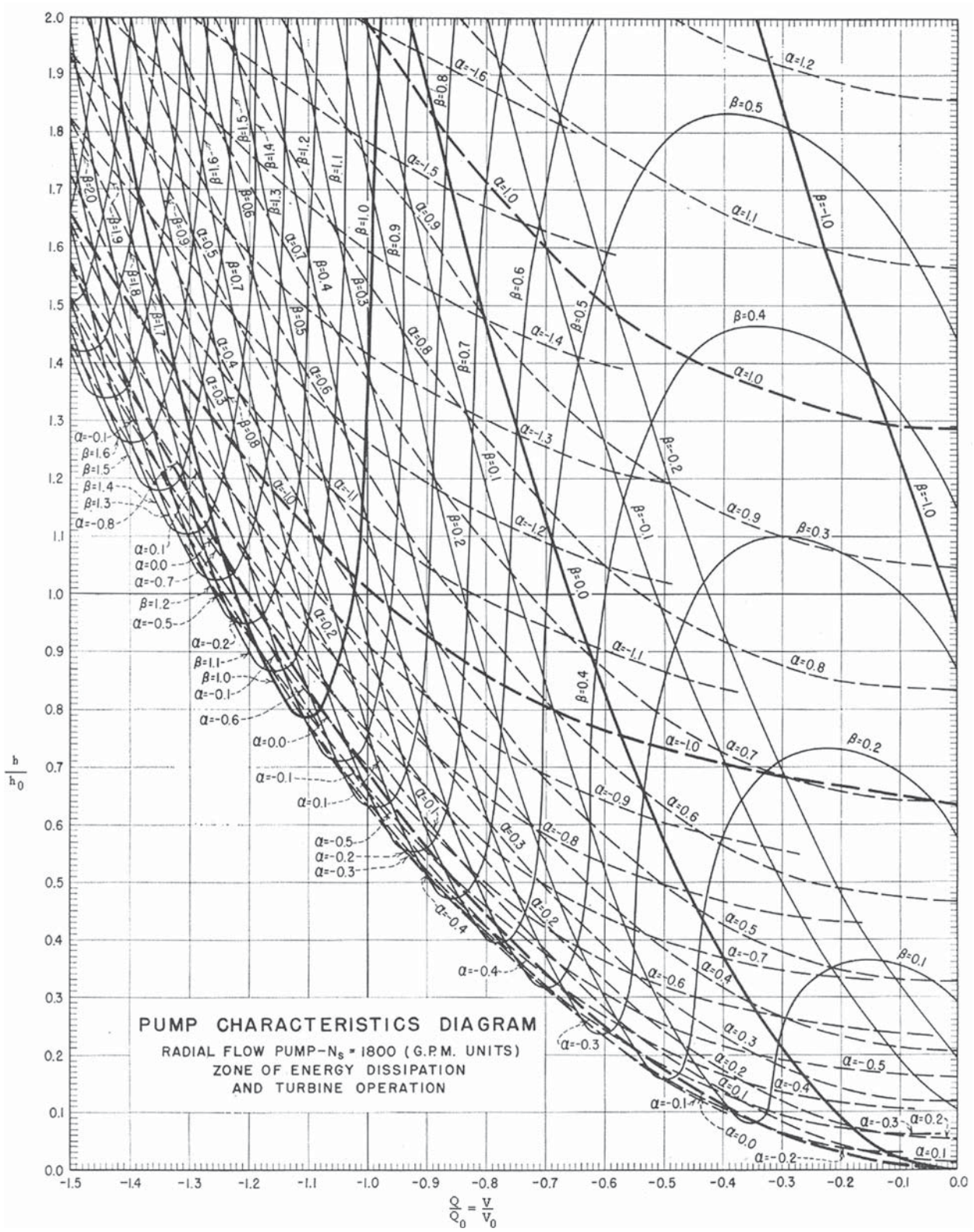


FIG. 5.45 TYPICAL CURVES FOR A RADIAL PUMP IN REVERSE OPERATION (Donsky [189])

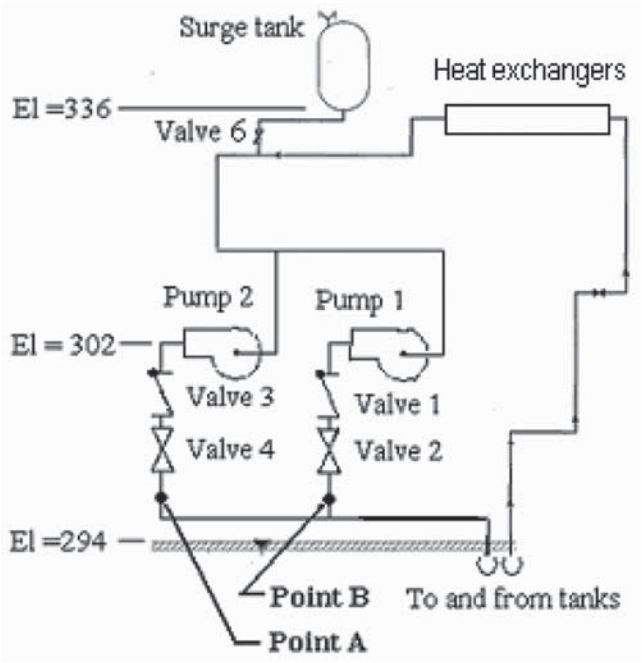


FIG. 5.46 SYSTEM SCHEMATIC FOR THE PUMP HOUSE

the pipe. When the pump restarted, the voids at A and B collapsed, and shock waves were formed (Leishear [8]). Pressure surges were measured downstream of point B as shown in Fig. 5.52. A VFD was installed on the pump motor used to reduce the pressures as shown in Fig. 5.53. The linear valve closure time was set at 3 minutes.

5.15.3 Column Separation and Vapor Collapse at a Valve

Column separation may also occur when the vapor pressure decreases below the vapor pressure at a valve, and numerous experimental results for vapor collapse are available for vapor collapse at valves. For this case, the pressure increases the pressure predicted by Joukowski for a suddenly closed valve, such that

$$\Delta P(\text{psi}) = 2 \cdot P_0 + (2.1584 \cdot 10^{-4} \cdot \rho(\text{lbf/ft}^3) \cdot a(\text{ft/sec}) \cdot \Delta V(\text{ft/sec})) \quad \text{US} \quad (5.55)$$

where P_0 is the initial pressure before the transient.

5.15.4 Solution Methods to Describe Column Separation and Vapor Collapse

Although MOC is commonly used to completely describe a transient, numerous techniques are available in the literature to describe pressure surges due to vapor collapse. Bergant et al [192], provide an excellent discussion of the numerous techniques with supporting experimental results. In particular, they considered classic discrete vapor cavity models (CDVM) and single vaporous zone (SVZ) models where the former technique assumes that cavitation bubbles may be collected into several vaporous zones, and the latter technique assumes that all cavitation bubbles may be considered as a single vaporous zone.

Example 5.26 Compare different calculation methods for the analysis of vapor collapse at a valve

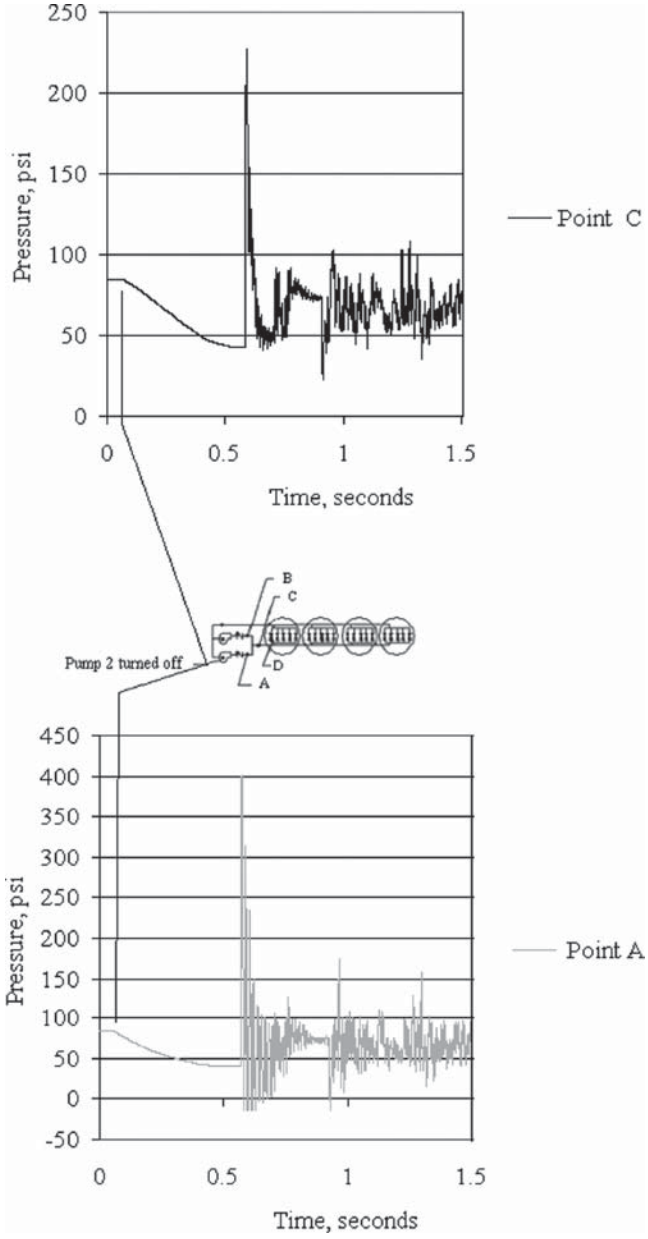


FIG. 5.47 PRESSURES DUE TO STOPPING ONE OF TWO PUMPS

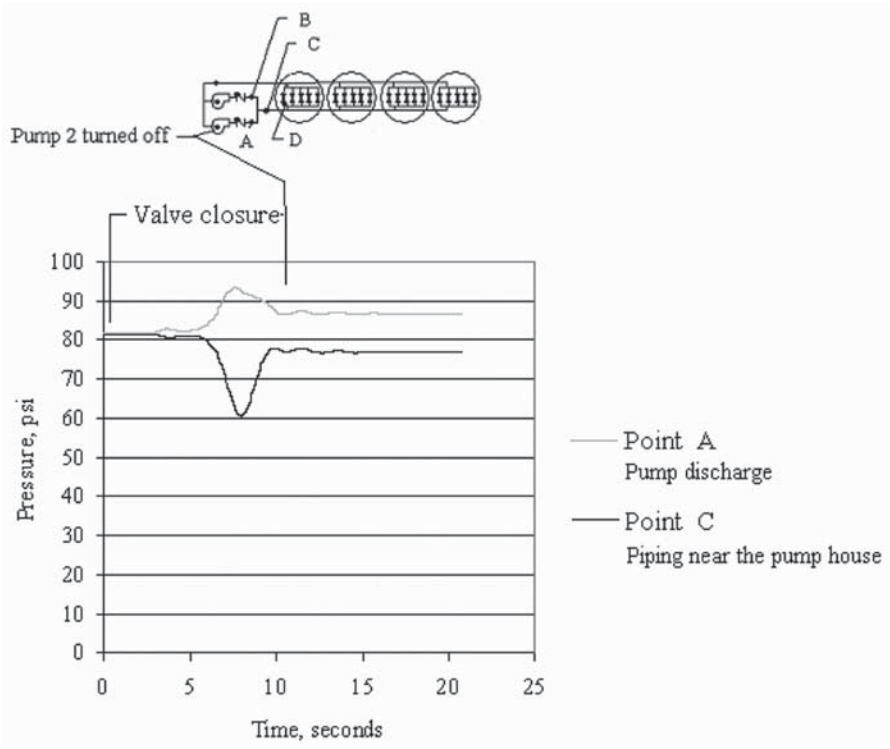


FIG. 5.48 EFFECTS ON A SINGLE PUMP SHUTDOWN USING A LINEAR CLOSING BALL VALVE

One of the more recent studies of vapor collapse was performed by Adamkowski and Lewandowski [193]. Their method uses an unsteady friction model and assumes vapor zones throughout the pipe where the vapor pressure is realized. Specific details are available in their paper.

To describe their theory, they first presented a theoretical example of the use of their technique in Fig. 5.54. From this figure, note that most of the change in vapor volume occurs at the valve, while some vapor condenses elsewhere along the pipe.

They performed a series of experiments using the test setup shown in Fig. 5.55, and they compared their test results to DVCM and SVZ methods. To demonstrate their theory, they further provided experimental results for comparison to theory, as shown in Fig. 5.56. Note that their technique provides a marked improvement between experiment and theory, when compared to earlier theory.

However, also note that a pressure spike of more than 30% is neglected when the pressure surge is initiated. That is, this method predicts a maximum pressure head of approximately 270 m, while the actual surge is approximately 350 m of head. This 30% error is in addition to the 6% to 30% uncertainty discussed in paragraph 5.7. In other words, caution should be used when applying computer simulations to analyze vapor collapse.

5.16 POSITIVE DISPLACEMENT PUMPS

Although outside the scope of this work, positive displacement pumps require a few comments. A primary difference between positive displacement and centrifugal pumps is that a positive displacement pump will provide whatever load the system requires until the pump reaches its maximum pressure capacity. With respect to water hammer, these pumps do not reverse direction, and the pressure increases if a downstream valve is closed. In other words, the head pressure increases, while the shock wave travels back and forth in the pipeline. Pressure transients may be considerably larger than observed in centrifugal pump systems.

Another attribute of positive displacement pumps, diaphragm pumps in particular, regards pulsations caused by the pumps. Frequently, these pulsations are in the frequency range of the pipe system, and resonance may occur (Lesmez et al [194]). Depending on the pump and piping frequency, changing the pump speed may still lead to excessive pipe vibrations. Much research is available in the literature on resonant fluid-structure interaction. Even so, Chapters 7 to 9 will show that predicting structural piping frequencies is an approximate technique, and tuning techniques to correct vibrations con-

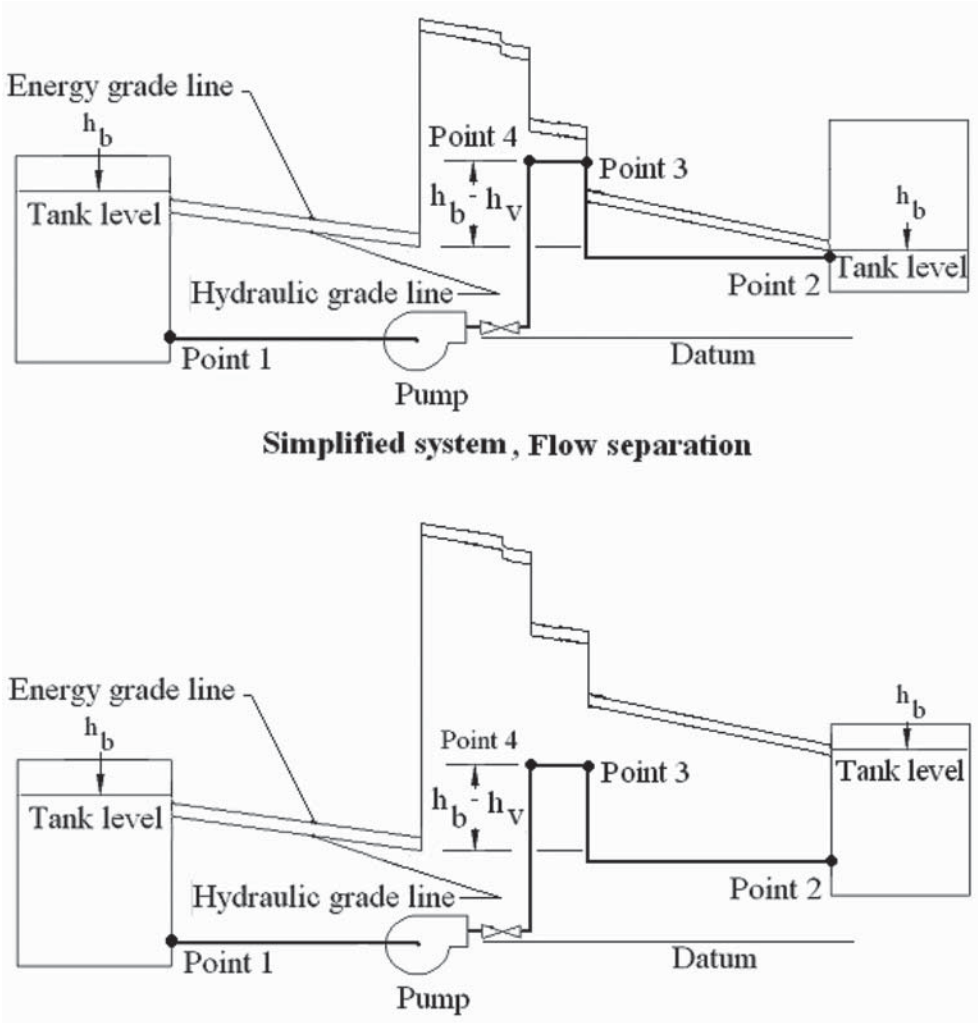


FIG. 5.49 COLUMN SEPARATION IN A PIPE WITH SUBMERGED ENDS

sequently may need to be variable. A common technique to reduce pressure pulsations from displacement pumps is to install a flexible connection between the pump and the piping. These water hammer arrestors are typically manufactured from flexible, rubber, or rubber-like, materials. These materials are not always adequate to overcome the pulsations.

5.17 EFFECT OF TRAPPED AIR POCKETS ON FLUID TRANSIENTS

Entrained air in systems has a tendency to migrate to system high points, and air pockets result. A long-standing transient concern in pipe systems is whether air is good or bad for the system. The answer is that the amount of air is important. If there is much air in the system, runout conditions exist, and slug flow occurs. In other applications, air is used in an air chamber to decrease the pressure surge (paragraph 5.18.3). In still other situations, trapped air may act as a cushion to water hammer in the system.

Example 5.27 Consider the effects of trapped air at a closing valve

However, for small quantities of air, the air may act as a cushion, as shown in Fig. 5.57. The system described in Examples 5.6 and 5.20 is the basis for this example. In those examples, the maximum pressures following a 0.1-second valve closure exceeded 700 psi for the first shock wave and exceeded 800 psi during rebound, as shown in Fig. 5.41. In both examples, the pump is operating continuously, and the valve is closed in 0.1 second, which is generally considered to be the fastest rate that a valve can be closed by hand. Note that the pressure surge of

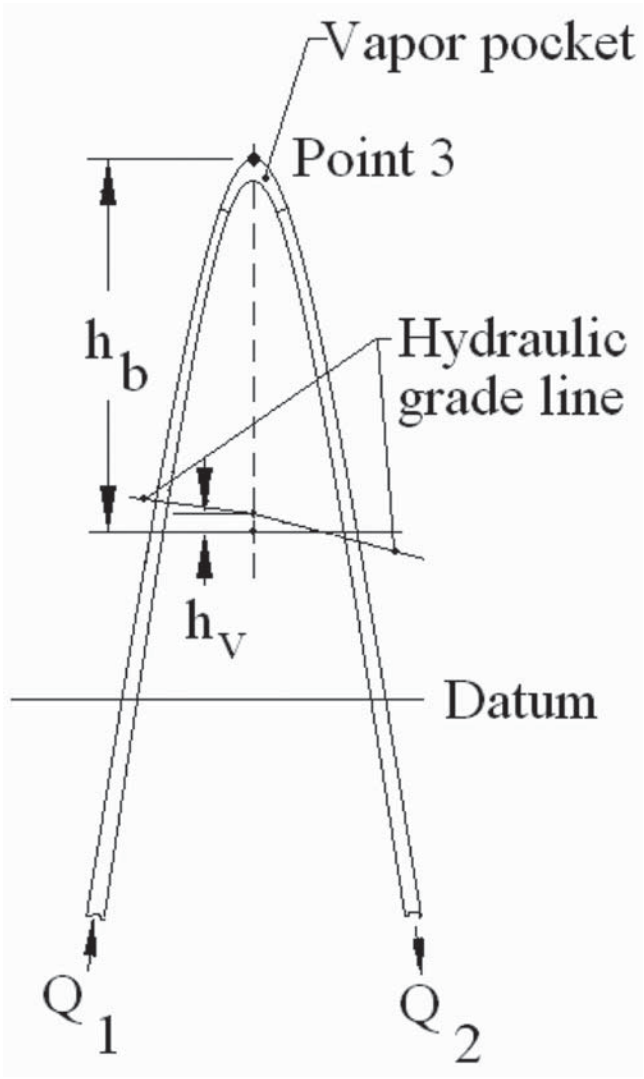


FIG. 5.50 COLUMN SEPARATION DURING A TRANSIENT

Fig. 5.54 is less than 275 psig, which is a pressure decrease by a factor of 2.5 to 3. That is, the air pocket acts as an air chamber at a valve to minimize transient pressures. However, an air pocket at a distance from the closing valve may have a lesser effect when a shock wave is generated at the valve and compresses the air pocket as the shock reaches the air pocket. That is, the size and location of the air pocket affects the system response and needs to be considered on a case by case basis.

Another aspect to trapped air is related to pump shutdown. When the pump pressure is removed, the air pocket rapidly expands and causes a transient in the system. For example, a pressurized air pocket in a system containing a surge tank can lead to overflow of the surge tank when the pump is shut down.

5.18 ADDITIONAL CORRECTIVE ACTIONS FOR FLUID TRANSIENTS

Some causes and corrective actions for fluid transients were considered above, and additional transient control devices are listed here to expand the techniques for fluid transient control. As with many engineering problems, multiple solutions are available.

Popescu et al [177] summarized fluid transient controls as belonging to one of two types. Examples of each type of control will be considered in this chapter.

I. Protection devices, which limit the amplitude of pressure oscillations, while still changing the fluid flow rapidly. This type is assessed by water hammer calculations, and it includes relief valves, valve bypass lines, valve speed closure, inertial fly wheels on a pump motor, and VFD control of a pump motor.

II. Protection devices, which change the amplitude of pressure oscillations into a slowly varying flow rate. This type may be assessed by a water hammer calculation or by a mass oscillation calculation and includes one way reservoirs, surge tanks, and air chambers.

5.18.1 Valve Stroking

Another technique for transient control is referred to as valve stroking. The valve is operated at different speeds during different times of the closing valve stroke. An example of valve stroking is shown in Fig. 5.58 for different valve strokes for a gate in a pumping station. Percentage of valve opening versus closure time are shown, where S_0 is the cross-sectional area of the gate. Wylie and Streeter [173] provided a chapter on valve stroking with constitutive equations and numerous examples.

5.18.2 Relief Valves

Relief valves provide excellent protection against overpressure when the overpressure condition is slowly applied, but water hammer occurs too quickly for adequate control by relief valves or rupture discs. Although the spring in a relief valve acts fast with respect to an observer, the response time of relief valves is too slow to inhibit a passing sonic velocity shock wave. Popescu et al [177] provided some excellent laboratory research on the response of turbine (gravitational) and pumping systems. One of their tests showed that pressure surges were negligibly affected as the wave initially passed the relief valve, and pressure surges were significantly reduced for subsequent pressure waves.

5.18.3 Surge Tanks and Air Chambers

Surge tanks and air chambers minimize fluid transients by alleviating the pressure behind the pressure

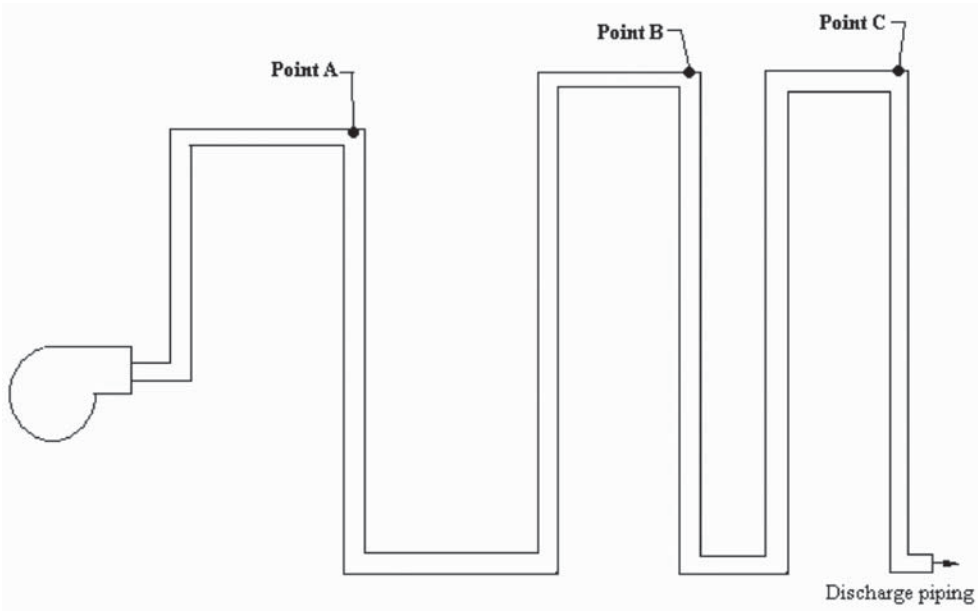


FIG. 5.51 PIPE WITH ONE SUBMERGED END

wave as it passes. Surge tanks are open to atmosphere, and the tank level changes to limit fluid transients. Air tanks are closed pressure vessels, and the internal pressure increases to limit fluid transients. Accumulators are another term for air chambers, but the term is generally used for smaller tanks, where the tank may be fitted with a diaphragm to prevent loss through absorption of the air or nitrogen contained in the accumulator. Surge tanks and air chambers significantly affect pressure surges. However, pressure surges are not eliminated, and shock waves between the source of the shock and the protective device are not affected. Consequently, stronger piping and supports may be required for some pipe sections.

The basic mechanism for these devices is that water flows into the cavity behind the shock wave to reduce the pressure surge. Thorley [68] provides a chapter of graphs to perform hand calculations for air chamber design, and of course, computer simulations are available.

Example 5.28 Demonstrate the effects of surge tanks and air chambers

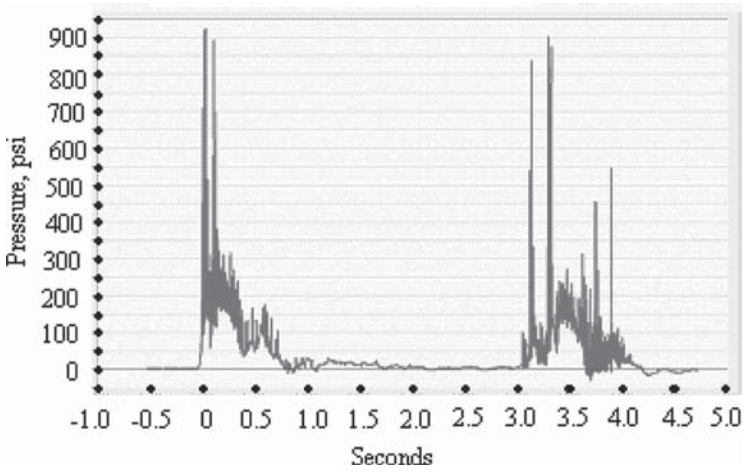


FIG. 5.52 PRESSURE SURGES DUE TO VAPOR COLLAPSE

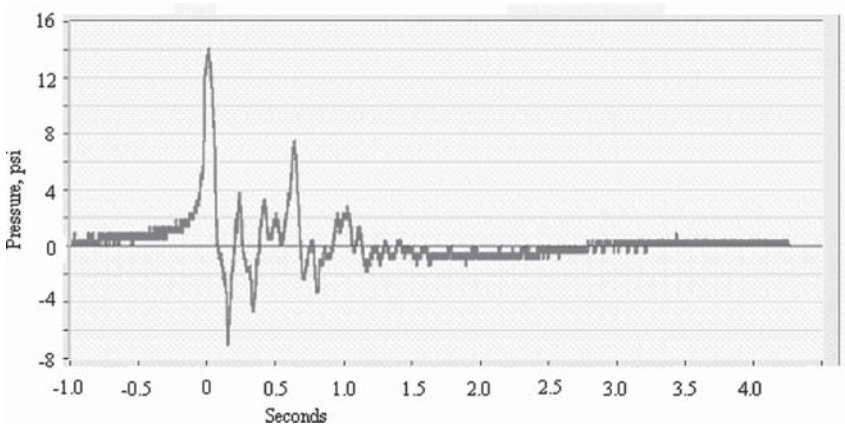


FIG. 5.53 PRESSURE SURGES REDUCED DUE TO VFD CONTROL OF THE PUMP SPEED ON STARTUP

Popescu provided a good example of the use of surge tanks or air chambers, where he obtained the same results for either device through judicious selection of design parameters. Note that a significant pressure reduction may be obtained by using these devices, as shown in Fig. 5.59.

5.18.3.1 Fluid Resonance Example Although surge tanks correct fluid transients, they introduce an additional problem in the system referred to as fluid resonance. The reader is referred to Popescu's book for a discussion of the calculation techniques, but an example is warranted.

Fluid resonance has multiple causes. Essentially, a fluid instability is generated when an excitation force has a frequency coincident to a frequency of the water column in a pipe. In industrial systems, valves provide oscillatory flow at low flow rates. In particular, pressure regulators "hunt" as the spring oscillates during low flow conditions. Pressure vessels attached to pipe systems with hunting regulators can be observed to pulsate. In power plant and pumping systems, numerous accidents have been attributed to resonance induced by surge tank operations.

Example 5.29 Resonance in systems with an installed surge tank

Fig. 5.60 provides an example of resonance-induced pressure surges for a pumping system with an installed surge tank, for a system similar to Example 5.4. Popescu et al [177] provided a detailed discussion of calculation techniques and recommendations to correct resonance due to pressure oscillations in systems of this type. Specifically, the surge tank diameter can be increased to an appropriate diameter to minimize oscillations. Popescu provided another example of a power plant with a surge tank, which showed that an installed diaphragm in the surge tank reduced the pressure oscillations in a surge tank during routine operations. He also provided sound advice that safety devices such as surge tanks should be installed even though techniques such as valve stroking are used. If the valve stroke fails, significant damage can occur without a surge tank.

5.18.4 Water Hammer Arrestors

Water hammer arrestors are small accumulators used in residential and small commercial systems to reduce transients at the end of a pipeline, e.g., lavatory facilities. There is much literature on this topic, but arrestors are outside the scope of this work.

5.18.5 Surge Suppressors

Essentially, surge suppressors are flexible hoses that are well designed to reduce pressure surges. They may be of multiple layer construction, which may include rubber, steel fabric, or plastics. The basic principle is that the suppressor will expand to absorb energy from the shock. Design guidance from manufacturers is typically required for specific applications.

5.18.6 Check Valves

Check valves frequently are the cause of water hammer as discussed in Example 5.22, but specially designed check valves may significantly reduce water hammer. Specifically, air cushion check valves and nozzle check valves (paragraph 2.3.12.7) close at rates designed to ensure that the valve closes near the time that the flow rate approaches zero.

5.18.7 Flow Rate Control for Fluid Transients

Controlling flow rates by controlling the motor speed during startup and shutdown is an effective means of transient control. Example 5.25 provides experimental

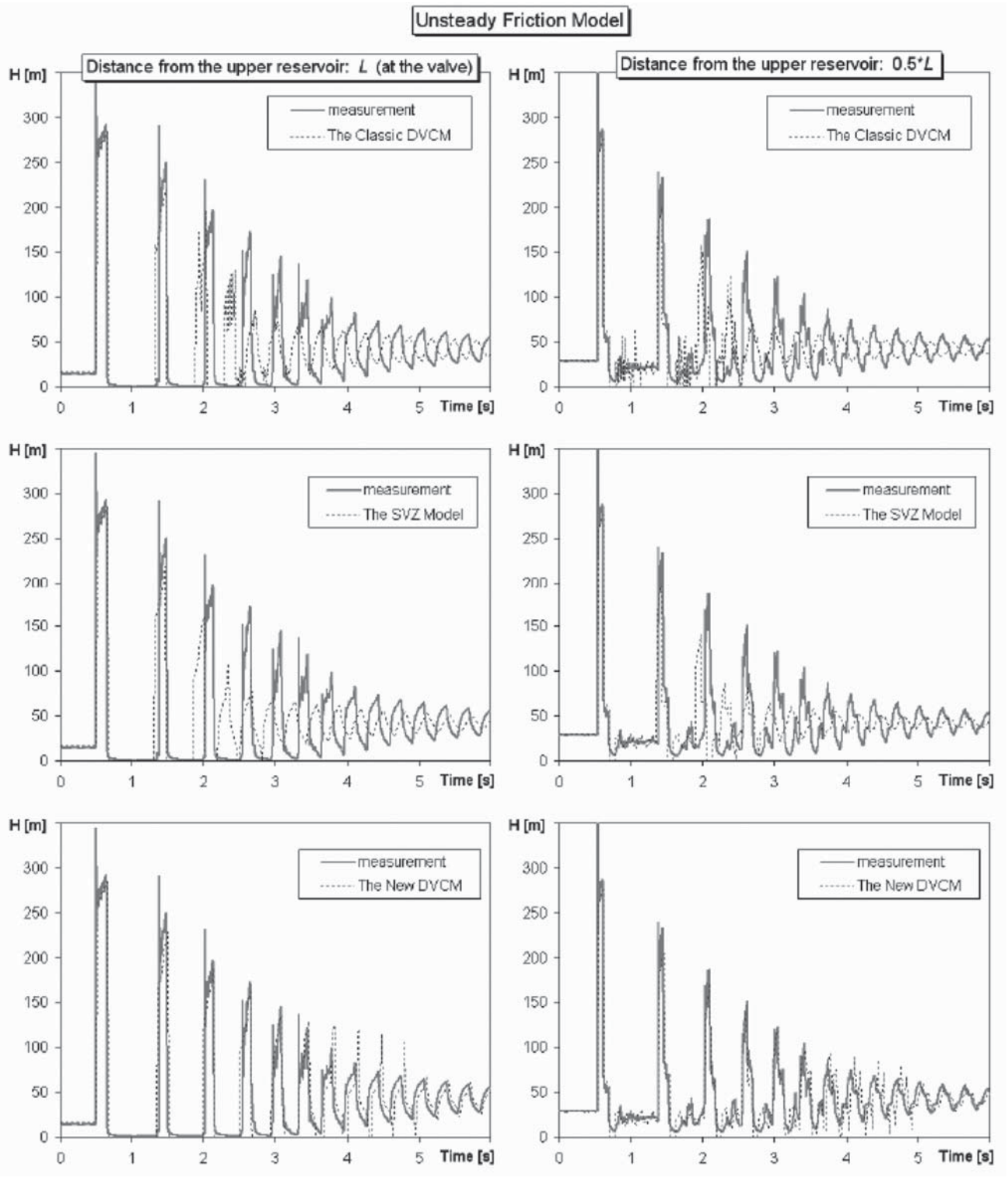
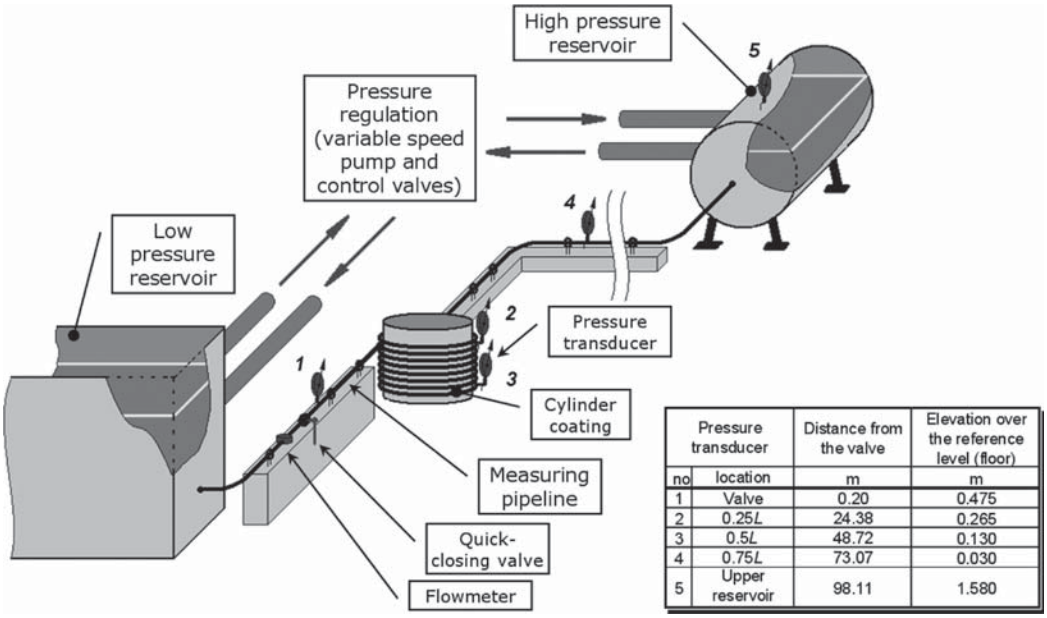


FIG. 5.54 EXPERIMENTAL VALIDATION OF NEW DVCM TECHNIQUE (Adamkowski and Lewandowski [193])



Pressure transducer		Distance from the valve	Elevation over the reference level (floor)
no	location	m	m
1	Valve	0.20	0.475
2	0.25*L*	24.38	0.265
3	0.5*L*	48.72	0.130
4	0.75*L*	73.07	0.030
5	Upper reservoir	98.11	1.580

FIG. 5.55 EXPERIMENTAL SETUP FOR COLUMN SEPARATION TESTS (Adamkowski and Lewandowski [193])

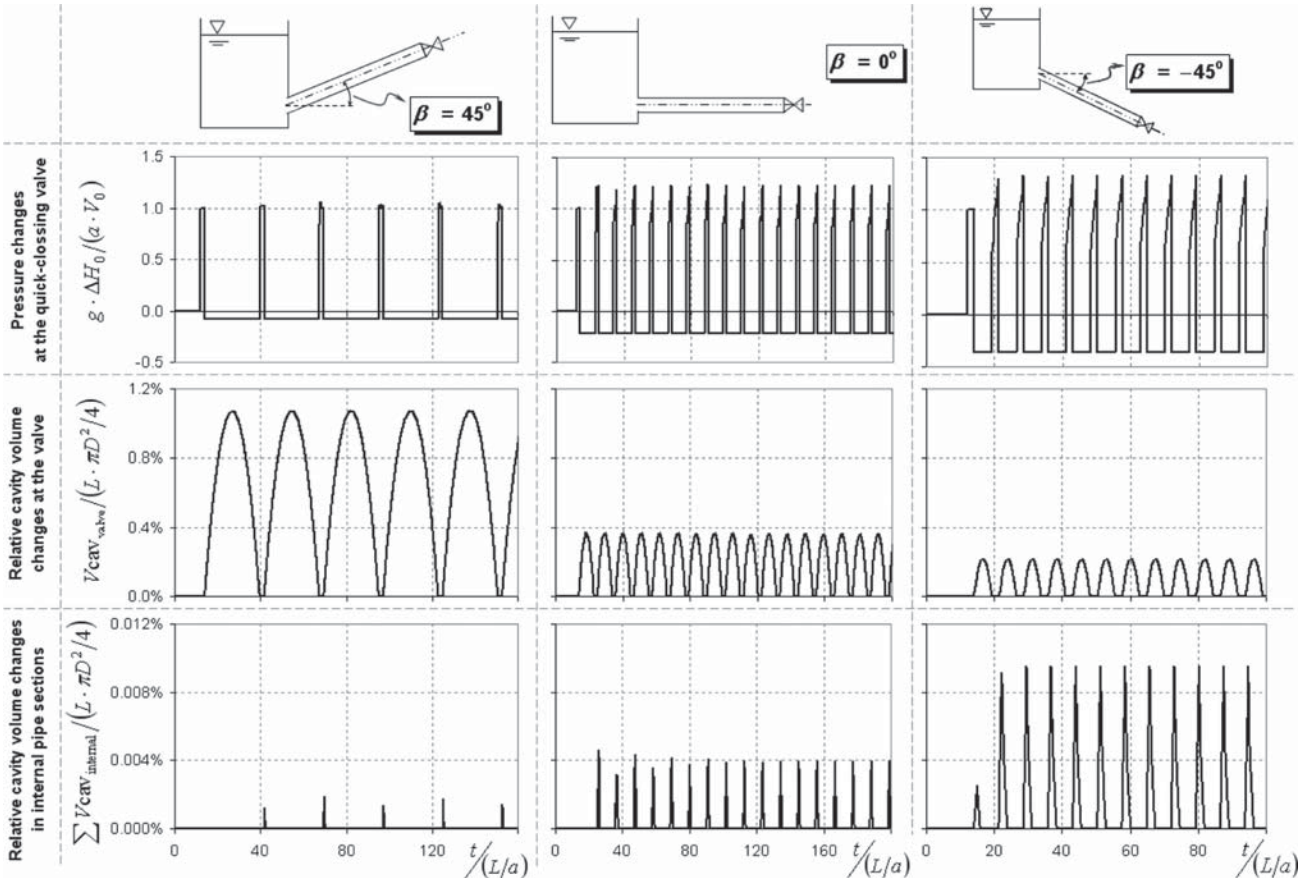


FIG. 5.56 NEW DVCM TECHNIQUE (Adamkowski and Lewandowski [193])

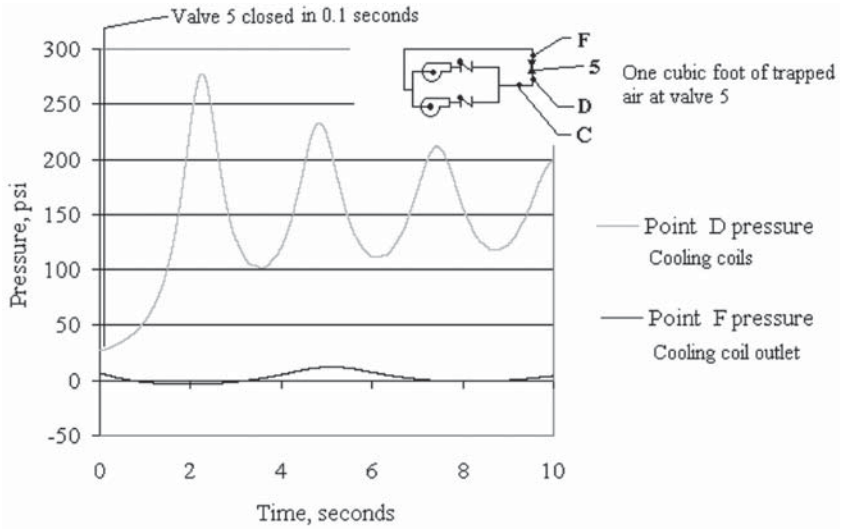


FIG. 5.57 TRAPPED AIR AT A RAPIDLY CLOSING VALVE

results for using flow rate control. Similar results may be obtained for pump shutdown, where the MOC technique can be applied.

5.19 SUMMARY OF FLUID TRANSIENTS IN LIQUID-FILLED SYSTEMS

Transients in systems completely filled with a liquid are reasonably well understood, but trapped air and vapors significantly complicate the system response to sudden changes in flow. A discussion was provided here to inform the reader of some of the issues that need to be considered in pipe system operations. That is, a brief survey of transient mechanisms was presented, along with corrective actions. The goal was to provide sufficient information to enable the reader to identify transient problems and solutions for liquid-filled systems. Although all of the skills needed to solve transient problems were not presented, references were provided to lead the reader to required solution approaches to specific transient problems. In fact, there are some transient problems that are not yet fully understood.

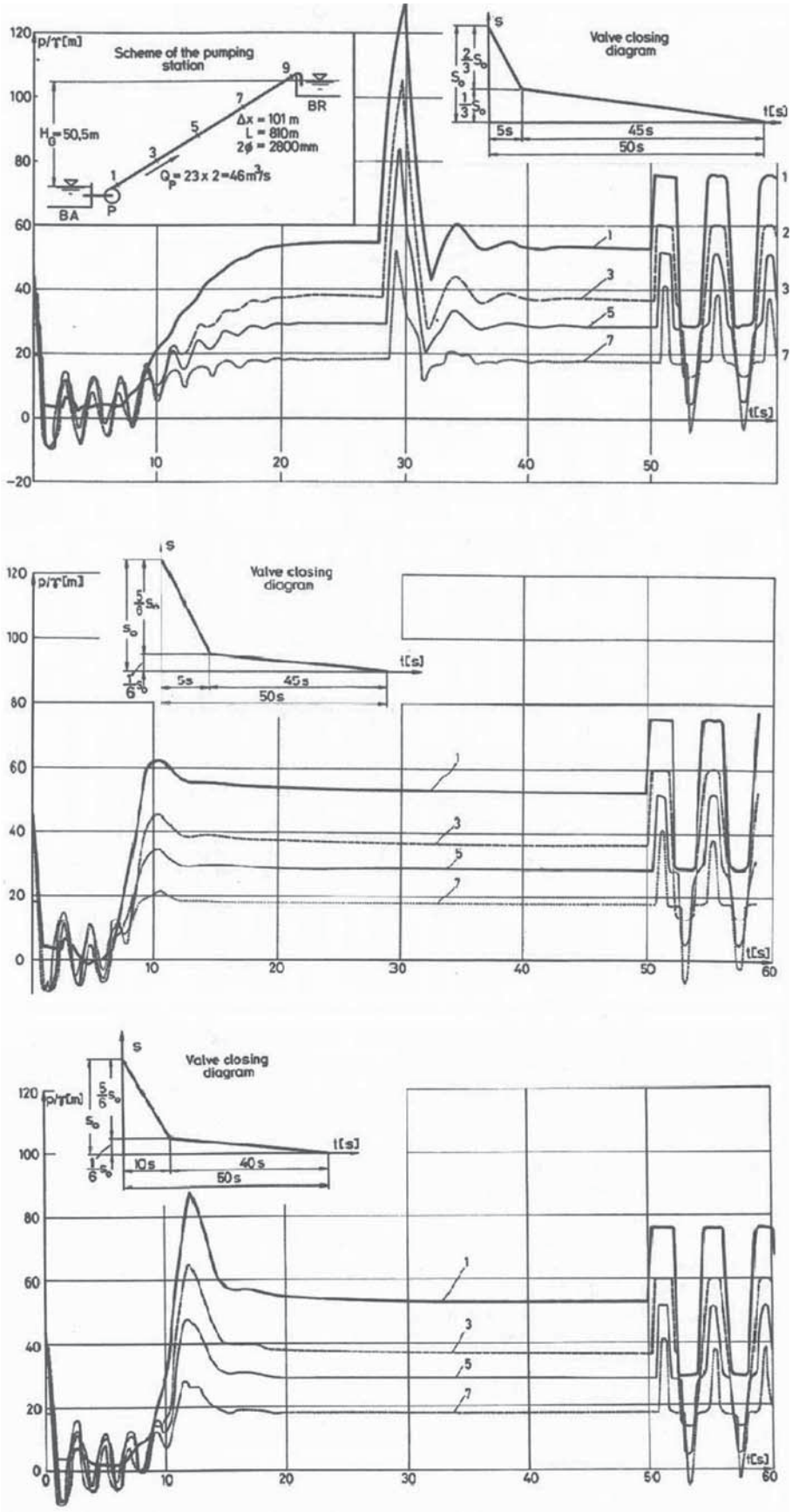


FIG. 5.58 VALVE STROKING (From: M. Popescu et al [177], "Applied Hydraulic Transients for Hydroelectric Power Plants", A. A. Balkeema Publishing, copyright 2003. Reproduced by permission of Taylor and Francis Books UK)

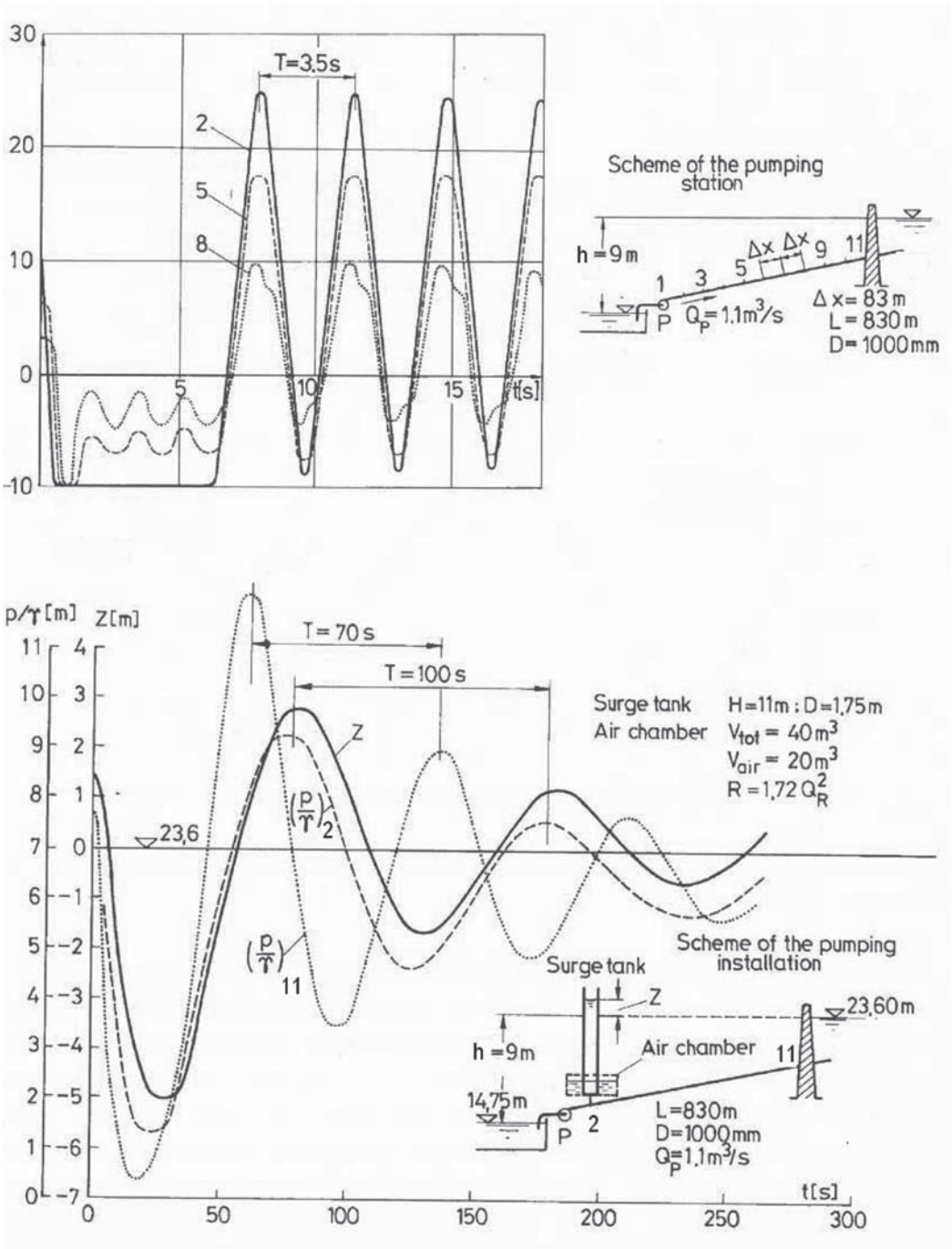


FIG. 5.59 SURGE TANK AND AIR CHAMBER EFFECTS ON PRESSURE SURGES (From: M. Popescu et al [177], "Applied Hydraulic Transients for Hydroelectric Power Plants", A. A. Balkeema Publishing, copyright 2003. Reproduced by permission of Taylor and Francis Books UK.)

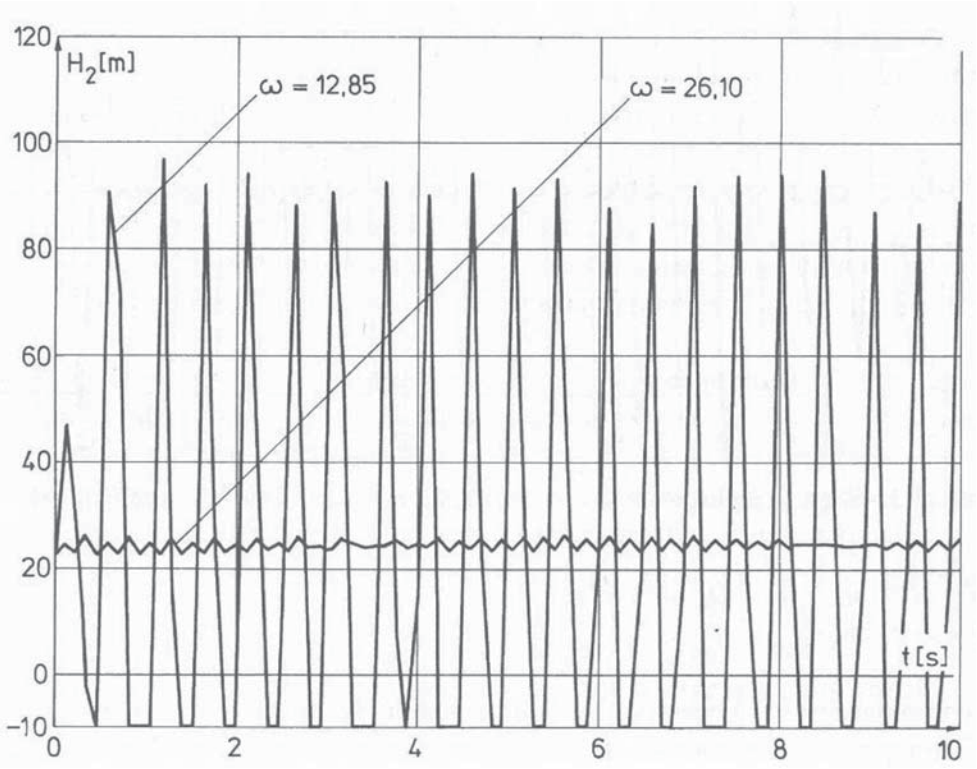


FIG. 5.60 FLUID RESONANCE, RAZELM-TULCEA PUMPING STATION (From: M. Popescu et al [177], "Applied Hydraulic Transients for Hydroelectric Power Plants", A. A. Balkeema Publishing, copyright 2003. Reproduced by permission of Taylor and Francis Books UK)

CHAPTER

6

FLUID TRANSIENTS IN STEAM SYSTEMS

Steam systems and steam condensate systems provide tragic examples of vapor collapse during fluid transients. Chapter 5 provided examples of vapor collapse during liquid/vapor fluid transients, where small quantities of vapor were present. When larger quantities of vapor are present in steam systems, the fluid mechanics of two-phase flow are far more complex. This chapter provides historical examples of water hammer, a discussion of two-phase transients (vapor collapse), a brief discussion of single-phase transients (blowdown), and some actions to prevent damages during steam system operation.

Significant damages occur during operation as well as during system startup. An example of a steam system failure occurred in New York City in 2009. Reportedly, a pipe trap failed following coating of the pipe wall interiors, where some of the plastic coating seeped into the trap. Condensate accumulated in the underground pipe line and condensate-induced water hammer (steam hammer) occurred, which is a form of vapor collapse. An 8-ft diameter hole was created in the sidewalk above the exploding cast iron pipe, and a bystander died of a heart attack at the scene. Photos of the resulting steam plume are shown in Figs. 6.1 and 6.2.

6.1 EXAMPLES OF WATER HAMMER ACCIDENTS IN STEAM/ CONDENSATE SYSTEMS

Water hammer accidents in steam systems and steam condensate systems are common throughout industry, and many go unreported. Condensate systems are used to collect condensed steam, and condensate also accumulates in steam systems under different operating conditions. For example, condensate accumulates in pipe lines after system shut down and trapped steam in the piping cools.

To ensure personnel safety, U.S. Department of Energy (DOE) facilities have made significant investments in research and training as a result of previous accidents. A few examples of water hammer at DOE facilities follow, since those accidents were extensively investigated and much data is available with respect to the accidents and resultant pipe failures.

6.1.1 Brookhaven Fatalities

In an accident at the Brookhaven National Laboratory [195], two operators were killed, and one survived. The operators' individual responses to the accident highlighted the dangers of steam in enclosed spaces, like rooms. When steam exits a pipe crack, air is entrained to cool the steam. For this accident, the supplied steam was 70 psi (303°F), leaking from a gasket blown out of a flange during water hammer. Independent testing showed that the steam will cool to 106°F in 15 in. of travel, as shown in Fig. 6.3. However, in an enclosed space, air does not mix completely with the steam to cool it. The operator who survived the accident ran through the steam and was burned, but the two operators who remained behind were exposed to the 303°F steam as the temperature in the room increased, and they died of steam inhalation. In a similar accident, an operator was killed when the bolts on a flange stripped during a condensate-induced water hammer (Kirsner [196]).

6.1.2 Hanford Fatality

Steam inhalation was also the cause of a fatality at a Hanford, Washington, nuclear waste facility (Fig. 6.4). An operator entered the underground steam valve pit to open the 6 in. valve at the left side of the figure (MSS-25). The underground pipe was filled with 55°F condensate on one side of the valve. On the other side of the valve, the pipe contained 110 psig steam. When the operator opened the valve, a second operator at ground level heard him say, "Oh, no." Three days later, he died from burns to his lungs.

An extensive investigation was performed to understand the cause of the accident and actions required to prevent future accidents. Chemical analysis of the valve material



FIG. 6.1 STEAM PLUME FOLLOWING WATER HAMMER ACCIDENT (Wikipedia)

was performed, scanning electron microscopy was performed on the fracture surfaces, material properties were measured, fluid transient calculations were performed, simulated fluid transient tests were performed, and valve failure was induced on a similar valve (Green [198]). The valve fracture was thoroughly evaluated.

When the valve opened, slug flow was propelled upward toward a 6 in. valve near MSS-26, which was cracked from the fluid impact. "The failed valve had been blown suddenly from its place," and the pit was filled with steam. Investigation showed that the cast iron valve cracked due to impact from the water slug, where no plastic deformation



FIG. 6.2 STEAM PLUME FOLLOWING WATER HAMMER ACCIDENT (Wikipedia)

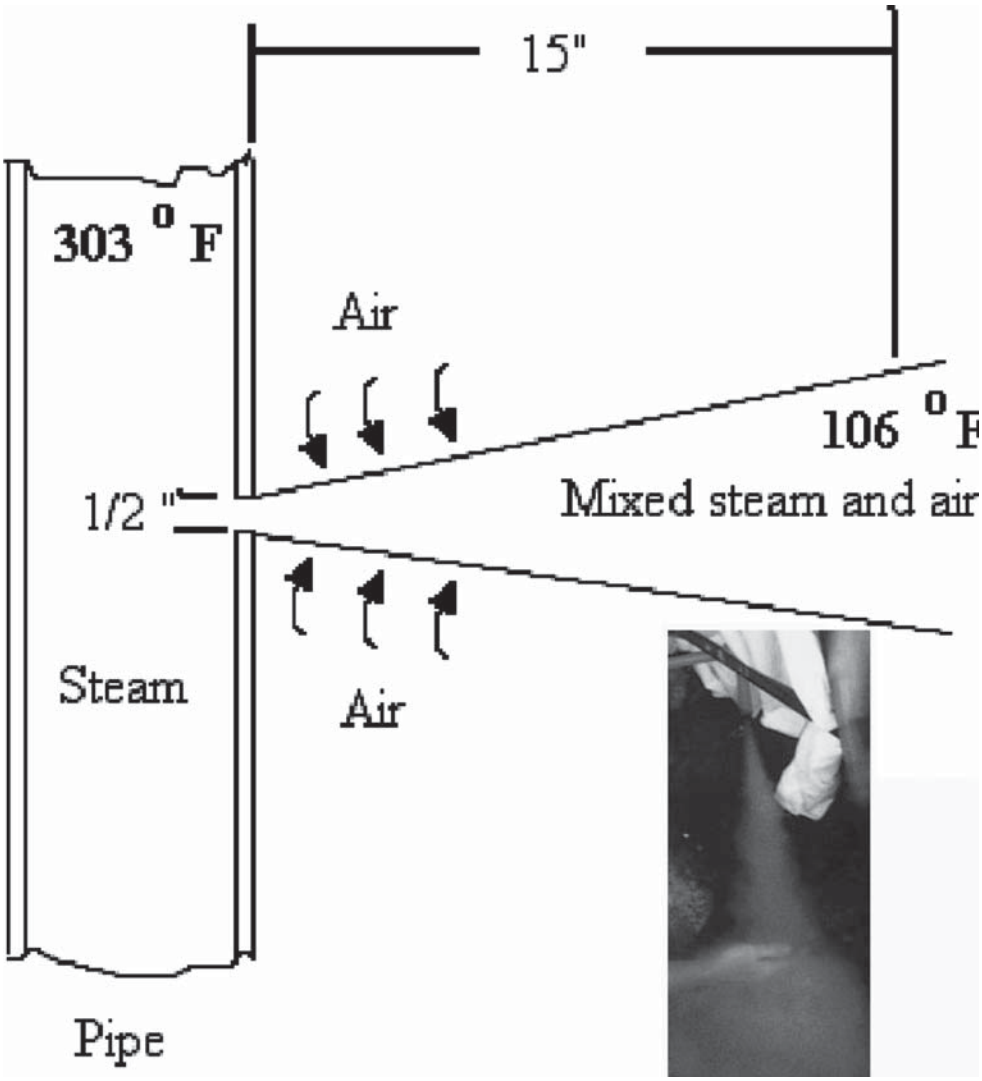


FIG. 6.3 AIR ENTRAINMENT INTO A STEAM JET (Kirsner [196])

was observed for any components. Estimated pressures were 1500 to 3000 psig, which were an order of magnitude higher than the 110-psig operating pressure.

Further testing showed that when a similar valve was hydrostatically tested at the maximum calculated pressure for the accident, the valve did not crack. The hydrostatic pressure was increased until valve failure occurred. One of the report conclusions was that a steel valve would not have failed. Another conclusion was that a dynamic amplification factor, or DMF, of at least 1.7 existed for this brittle fracture to occur in the valve body. The tensile strength of the valve material was measured at S_U = 15,900 psi. The work presented here shows that the maximum, equivalent DMF may have been as high as 4, since the effects of reflected pressure waves at the end of a pipe double the incident pressure at the pipe end. That is, the DMF includes the doubled pressure effects as well as the dynamic response effects (DMF < 2).

6.1.3 Savannah River Site Pipe Damages

Two different water hammer incidents at Savannah River Site are cited here. Damages in both cases could have been prevented through proper use of steam traps.

6.1.3.1 Pipe Failure During Initial System Startup Significant pipe damages occurred during startup of a newly constructed 4800-ft long, 385-psig steam system in 1984, due to design and operational errors. The pipe system was designed with an inadequate number of steam traps, installed traps were partially blocked, and the pipe line was filled with water from hydrostatic testing when steam was introduced into the pipe system during startup.

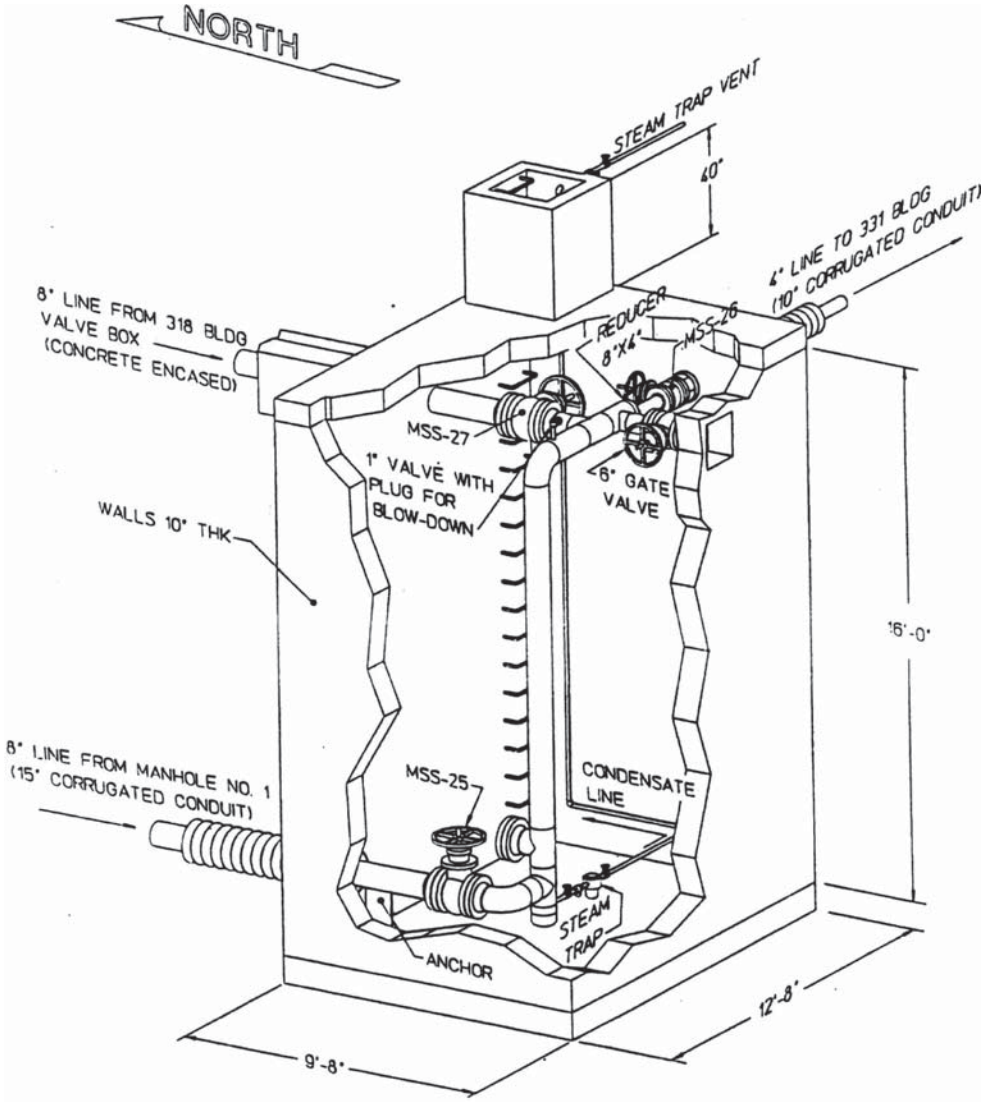


FIG. 6.4 HANFORD ACCIDENT PIPING CONFIGURATION (Green [195])

Steam was partially introduced at first, and only a minor hammer was observed by the operators. They then opened the steam regulator completely to permit steam into the pipe, water hammer commenced, and shock waves traveled back and forth in the pipe. As the operators drove back and forth to each end of the 4500-ft long pipeline, they observed the water hammer at each location. They failed to recognize that a water hammer shock wave was traveling back and forth between the pipe ends at a sonic velocity. More than 2000 ft of 24-in. pipe was knocked off the pipe supports, and another 3000 ft of piping and pipe supports were damaged. Damages may have been reduced if the steam was shut down immediately. Some of those damages are shown in Fig. 6.5. Interestingly, the pipe was not ruptured, and only plastic deformation occurred.

6.1.3.2 Pipe Damages During System Restart Significant water hammer occurred in a system that had been previously restarted on numerous occasions. At the time of this incident, steam traps were operating improperly, condensate was accumulated in a pipeline, and the pipe was not drained prior to opening the steam regulator. Pressures were estimated at 1400 psig, and water hammer continued for 15 min in the building, where banging was heard outside of the concrete building. Once again, pipe damages resulted from failed steam traps, and further damage could have been minimized by closing the steam



FIG. 6.5 PIPE FAILURE DURING INITIAL SYSTEM STARTUP (Savannah River Site, Steam Supply Piping Incident, 1984)

regulator. The resulting damages are shown in Fig. 6.6. Some plastic deformation occurred in the pipe, and an expansion joint was significantly deflected, but pipe fracture did not occur. Training and preventive maintenance programs were reinforced to prevent future reoccurrence but additional damages have since occured at SRS.

6.1.4 Pipe Failures Due to Condensate-Induced Water Hammer

The incidents considered here bring up an important point about condensate-induced water hammer and pipe system response. Although Code design requirements were certainly exceeded, and pipes were damaged, the pipe failure mechanism for steel piping was typically plastic deformation. Only the cast iron fractured. That is, the ductile response of carbon steel frequently prevents catastrophic failures due to overload in pipe systems.

6.2 WATER HAMMER MECHANISMS IN STEAM/ CONDENSATE SYSTEMS

Several studies have been performed to estimate pressure surges due to water hammer in steam condensate systems. The only equation for use is Eq. (5.1), and computer codes

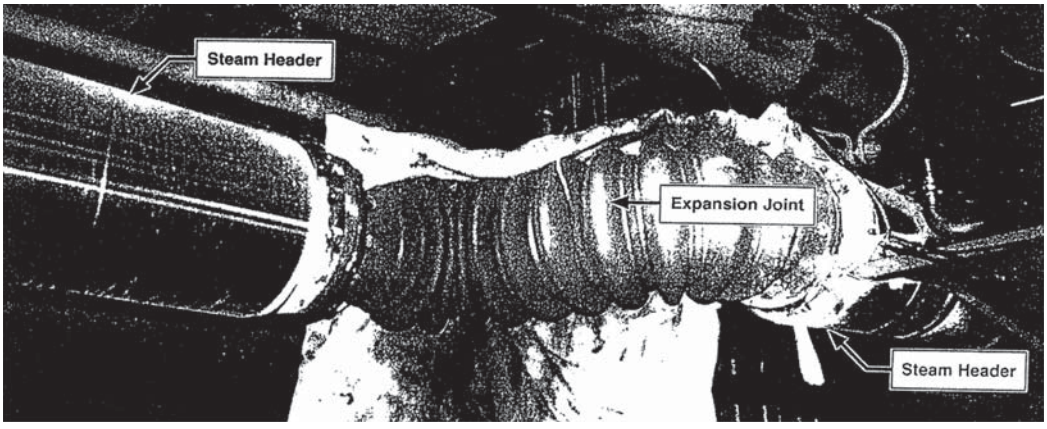


FIG. 6.6 EXPANSION JOINT DAMAGE DURING STEAM SYSTEM RESTART (Savannah River Site, Steam Supply Piping Incident, 1993 (WSRC-MS-94-0474)

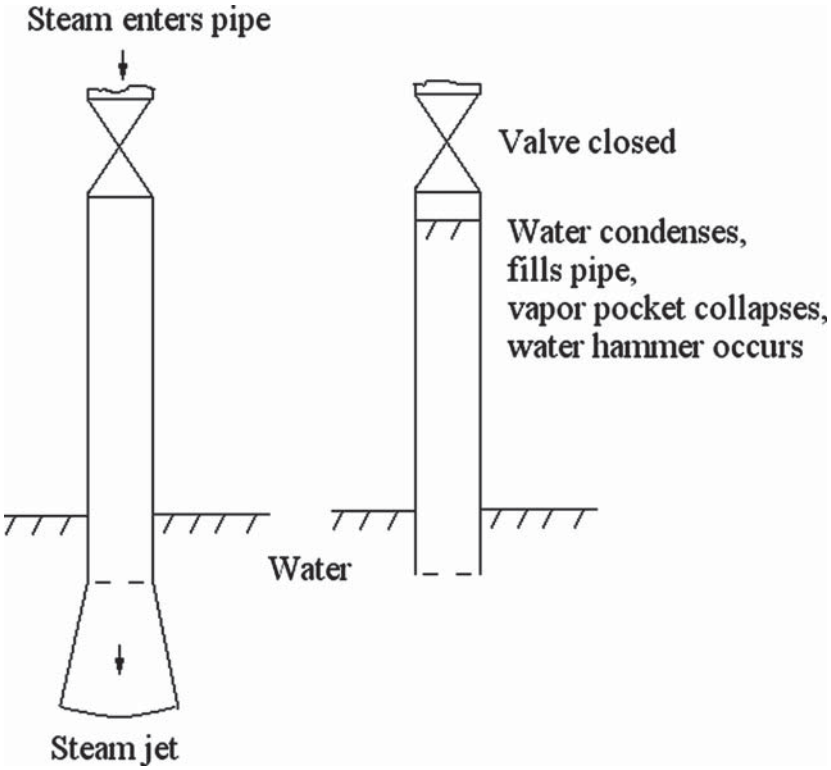


FIG. 6.7 SUBCOOLED WATER WITH CONDENSING STEAM IN A VERTICAL PIPE, WATER CANNON (EPRI [199])

are sometimes developed on a case by case basis. As a general rule, water hammer in steam systems should be avoided since Code design conditions are typically exceeded. However, water hammer in steam systems is commonplace in industrial pipe systems, and operators frequently learn to accept water hammer when it is observed without damage to the pipe system. Even so, a description of various water hammer mechanisms in steam systems is required.

The Electric Power Research Institute (EPRI) investigated nearly 400 water hammer incidents in nuclear reactor facilities between 1969 and 1988, and provided a summary of different water hammer mechanisms and recommended mitigations [199 and 200]. Several of these mechanisms were considered in Chapter 5, but a comprehensive summary of water hammer mechanisms is warranted since those mechanisms are also applicable to steam/condensate systems. Water hammer continues to occur in nuclear facilities as documented in various NRC Bulletins (Nuclear Regulatory Commission). Different mechanisms are discussed in the following sections as summarized by EPRI.

6.2.1 Water Cannon

The water cannon mechanism is described using Fig. 6.7.

- Steam enters a cooler fluid
- A valve is closed to throttle or stop the flow
- Steam condenses, and liquid is drawn up into the pipe
- Vapor and liquid mix to form vapor pockets, which then collapse and cause shock waves

A common method to prevent water cannon is to introduce air into the pipe to displace the steam prior to sudden valve closure, using control valves.

6.2.2 Steam and Water Counterflow

The steam and water counterflow mechanism is described in Fig. 6.8. The liquid and vapor flow in opposite directions. Considering Fig. 6.8:

- Condensate slowly fills a pipe supplied with steam
- Unstable wave growth
- Steam void formed
- Void collapse

This mechanism is the assumed cause of the Hanford accident (paragraph 6.1.2).

To prevent water hammer due to counter flow, condensate should not be added to steam-filled systems.

6.2.3 Condensate-Induced Water Hammer in a Horizontal Pipe

Similar to cross flow, condensate-induced water hammer in a horizontal pipe is independent of flow directions.

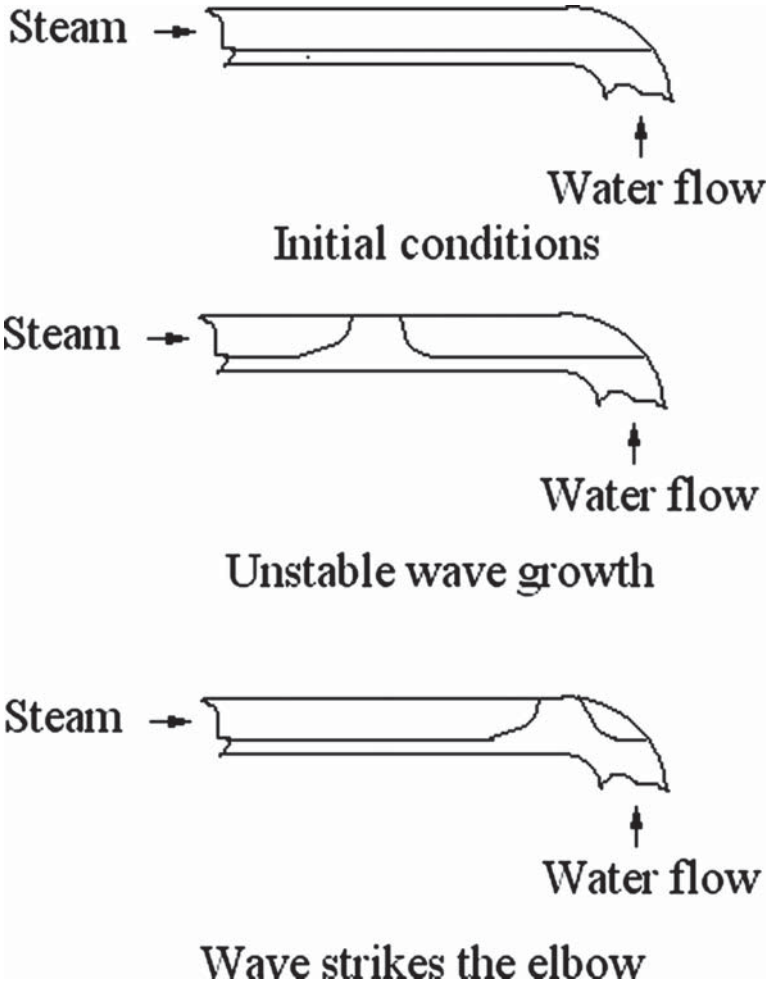


FIG. 6.8 STEAM AND WATER COUNTERFLOW IN A HORIZONTAL PIPE (EPRI [199])

Testing following the Hanford accident (paragraph 6.1.2) showed that water hammer may be induced with as little as ½ in. of water in the bottom of a 4-in. diameter pipe. Fig. 6.9 describes formation of and collapse of voids, which generate pressure pulses in steam/condensate systems.

- Steam enters a pipe partially filled with water
- Waves are initiated
- Unstable waves form
- Slug forms
- Slug grows and accelerates
- Steam void collapses due to slug impact

Videos were performed of tests for slug formation in transparent pipes (Figs. 6.10 and 6.11), using a 15-psig pressure regulator, which permitted steam into one end of a horizontal, 4-in. diameter pipe. A tee was placed at the other end of the pipe. Upward flow at the tee slowly added 55°F water to the steam-filled horizontal pipe section. The combined steam and condensate exited through a second horizontal pipe. When the steam filled the pipe with about ½ in. of water, unstable wave growth and slug impacts were observed as slugs filled the entire pipe cross section, similar to Fig. 6.9. Slug impacts repeated numerous times over several minutes before the water hammer event subsided. To prevent this water hammer mechanism, the condensate should be completely drained before adding steam to horizontal pipes.

6.2.4 Steam Pocket Collapse and Filling of Voided Lines

Filling a vertical or sloped pipeline may result in water hammer due to the inertial effects of the fluid, caused by a pump. Various mechanisms are shown in Figs. 6.12 and 6.13. A comprehensive example of this mechanism is provided in Example 5-25, where vapor pockets were experimentally shown to collapse as quickly as the pressure was applied.

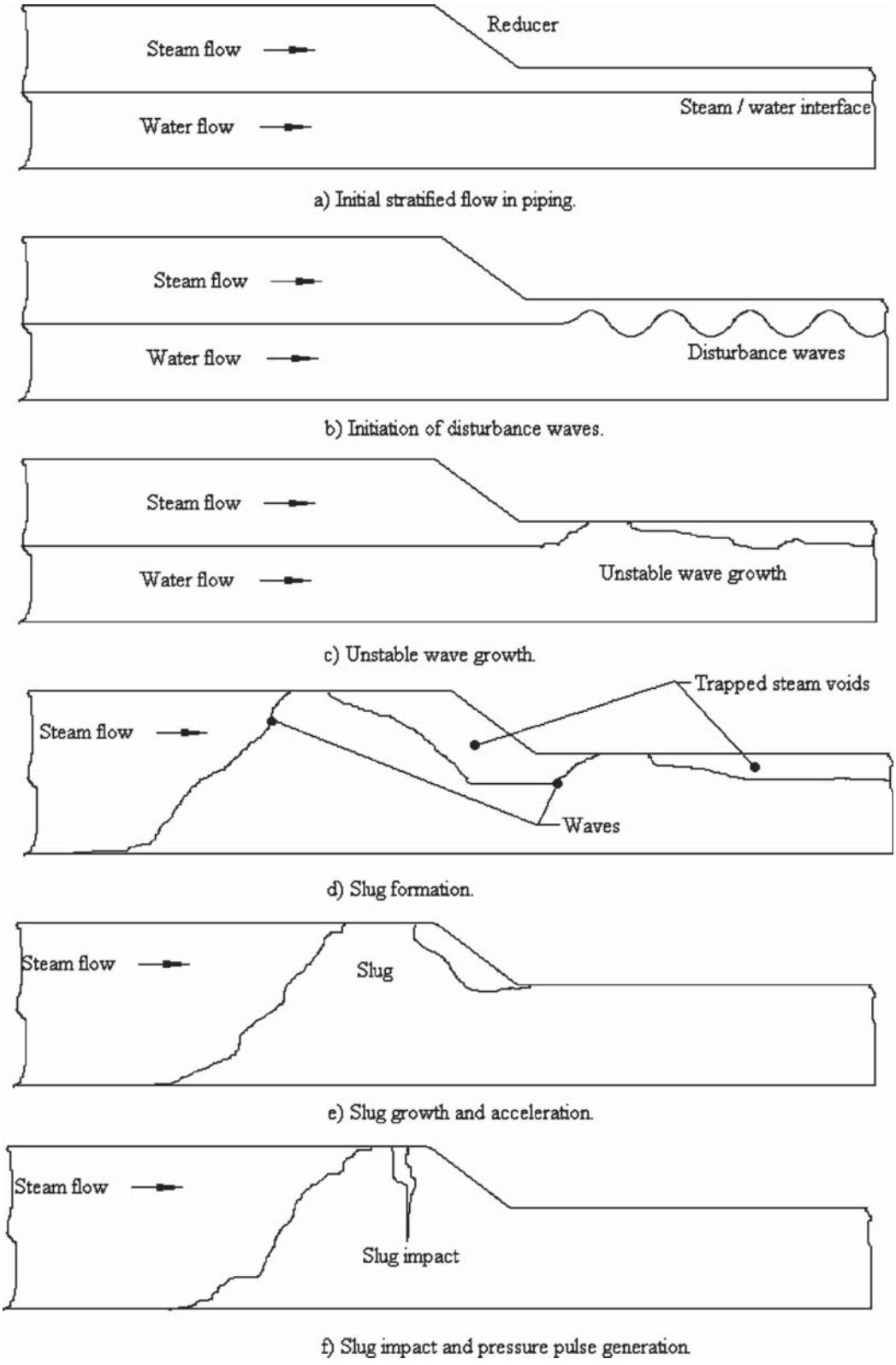


FIG. 6.9 SCHEMATIC OF SLUG FORMATION IN A HORIZONTAL PIPE (Green [198])

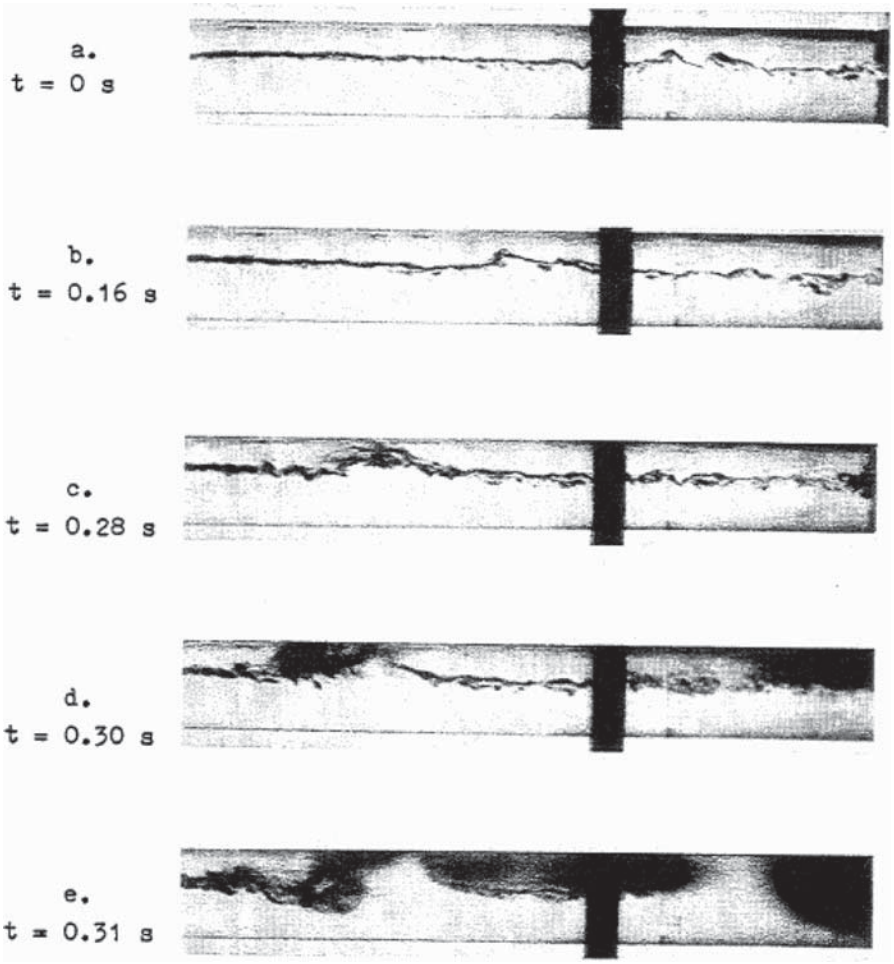


FIG. 6.10 SLUG FORMATION EXPERIMENTS (Bjorge and Griffith [201])

6.2.5 Low-Pressure Discharge and Column Separation

Column separation for condensate systems is the same as separation for any other liquid-filled system except that the system is operating much closer to the vapor pressure of the fluid, and separation is easier to induce. In addition to the examples provided in paragraph 5.15, another mechanism is shown in Fig. 6.14, where hot water enters a lower-pressure pipe system.

6.2.6 Steam-Propelled Water Slug

Water slugs may also cause large forces at pipe supports during startup or restart of systems (Fig. 6.15). Normally, empty pipes may have accumulated water that forms into steam-propelled slugs. The mechanism noted in paragraph 6.2.3 may also occur, depending on the quantity of water in the pipe.

6.2.7 Sudden Valve Closure and Pump Operations

Sudden valve closure and pump operations are the same in condensate systems as in other fluid systems (see paragraphs 5.9 and 5.14) except that column separation is more likely to occur. A schematic of a stuck check valve slamming closed is shown in Fig. 6.16. Check valve slamming causes higher pressures than shutting down one of two operating parallel pumps, which was considered in Example 5.22.

6.3 BLOWDOWN

Blowdown of steam and gas systems is outside the scope of this work, but minimal discussion of the topic still seems warranted. Blowdown includes the sonic discharge of gases or vapors from pipe systems (typi-

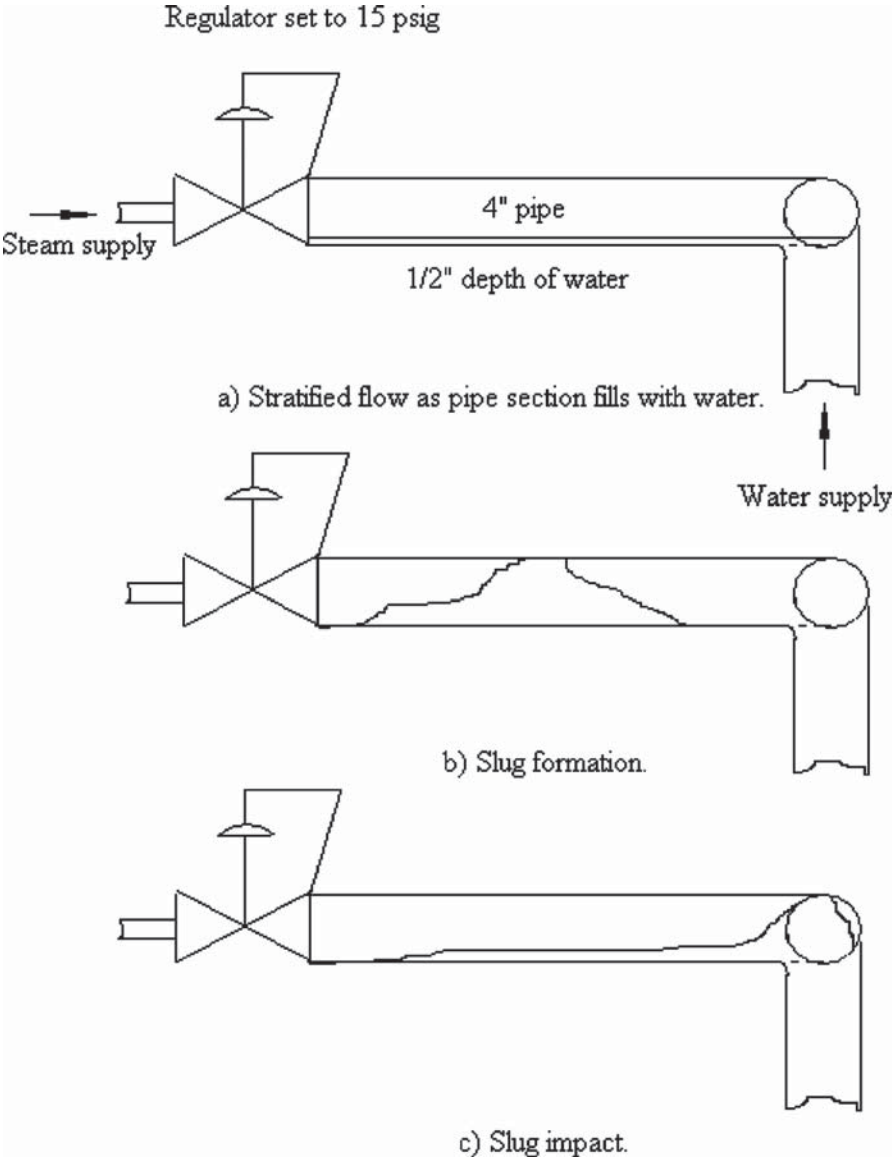


FIG. 6.11 SCHEMATIC OF SLUG FORMATION IN A HORIZONTAL PIPE

cally to atmosphere). For steam systems, blowdown may include steam or a combination of steam and water. Forces on pipe supports are similar to those caused by liquids.

6.3.1 Sonic Velocity at Discharge Nozzles

A major distinction between liquid and gas flows is that compressibility changes the flow characteristics of the fluid (John [24]). Specifically, compressible gases may flow at subsonic, sonic, or supersonic, velocities. Gas dynamics and the reaction forces on pipe systems are rather complex, but the underlying equations are presented here.

If a nozzle converges as shown in Fig. 6.17, which is a reasonable assumption for a discharge pipe from a steam system, the velocity at the smallest pipe cross section is sonic. The pressure at this point is referred to as the critical pressure, P_c, where,

$$P_c = P_0 \cdot \left(\frac{2}{k+1} \right)^{\frac{k}{k-1}} \qquad \text{US, SI (6.1)}$$

This critical pressure is referred to as the choked pressure, since this pressure is the largest pressure that can

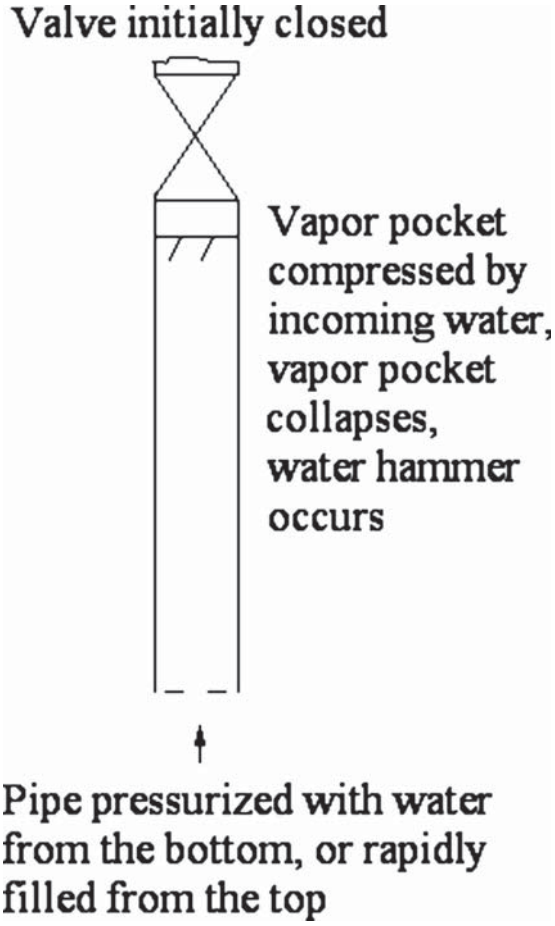


FIG. 6.12 PRESSURIZED WATER ENTERING A VERTICAL STEAM-FILLED PIPE, VAPOR COLLAPSE, STEAM POCKET COLLAPSE (EPRI [199])

be obtained at sonic velocity due to an operating system stagnation pressure, P_0.

If the nozzle diverges, then supersonic velocity may be obtained, but the choked flow pressure cannot exceed P_c. For example, the maximum pressure at a restriction during choked flow equals approximately 55% of the steam pressure in a vessel or pipe. For an air-filled pipe, P_c equals 52.8% of the vessel pressure.

Also, the gas temperature decreases from the stagnation temperature, T_0, to the critical temperature, T_c, when choked. From the ideal gas laws,

$$P_c = P_0 \cdot \left(\frac{T_c}{T_0} \right)^{\frac{k}{k-1}} \qquad \text{US, SI (6.2)}$$

The maximum flow rate through the choked nozzle for a perfect gas equals

$$\dot{m} = \sqrt{k \cdot g_c \cdot P_0 \cdot \rho_0} \left(\frac{2}{k+1} \right)^{(k+1)/2(k-1)} \cdot A \qquad \text{US, SI (6.3)}$$

where the bulk modulus (specific heat ratio) at 70°F, equals $k = 1.4$ for air, and $k = 1.33$ for steam. At 1282°F, $k = 1.25$ for steam. The bulk modulus increases with pressure. The reader is referred to John's text [24] for a full discussion of shock waves in pipes and nozzles. Note also that as the pipe pressure decreases, the mass flow rate decreases, which is the case for small-diameter pipes of long dimensions. That is, the pressure drop due to gas flow in a pipe may lead to a reduced pressure at the nozzle.

6.3.2 Piping Loads During Blowdown

Loads on piping due to relief valve opening during blowdown can be estimated from Fig. 6.18. The period of the piping vibration, τ', is required along with the linear relief valve opening time, t_o. The DMFs shown in Fig. 6.18 are applicable to relief valves without discharge piping installed. That is, the DMF is applied to the support piping of the relief valve, and discharge piping requires a more complex analysis.

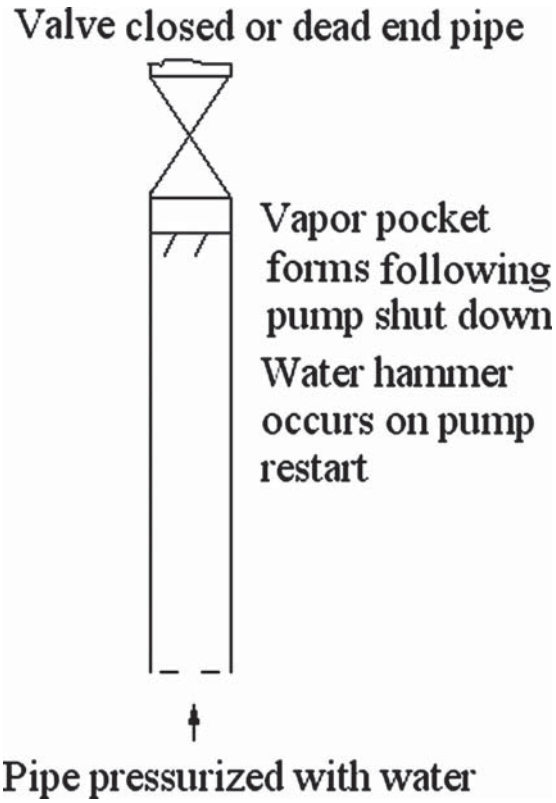


FIG. 6.13 FILLING OF A VOIDED LINE, COLUMN REJOINING, VAPOR COLLAPSE (EPRI [199])

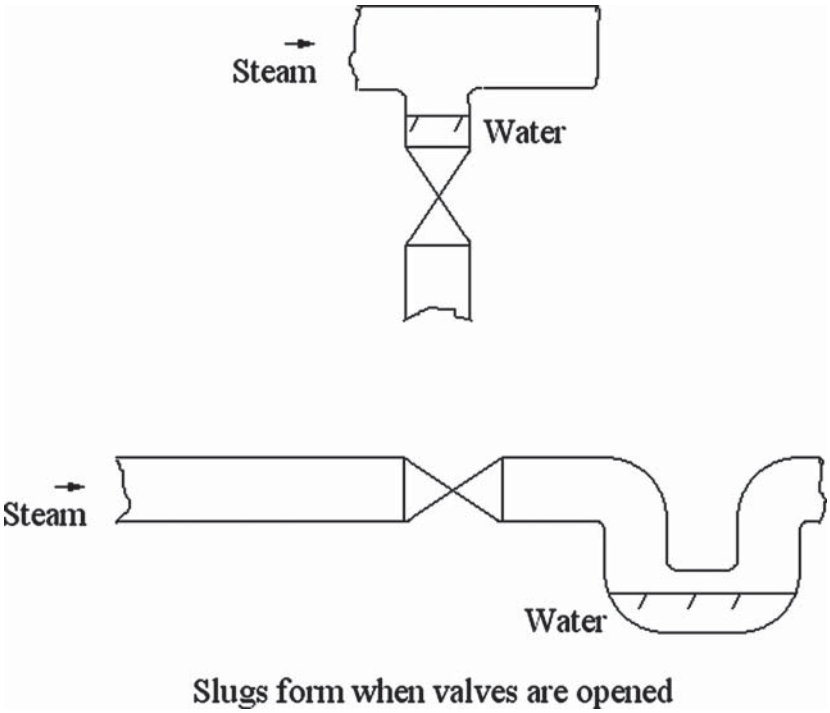


FIG. 6.14 HOT WATER ENTERING A LOW-PRESSURE LINE, LOW-PRESSURE DISCHARGE (EPRI [199])

6.3.3 Steam/Water Flow

The maximum flow rate for steam occurs for pure steam, but the maximum flow rate decreases as the water quality changes. That is, the maximum flow rate through a restricted orifice decreases as the percentage of water content in the vapor increases.

6.3.4 Pressures in Closed Vessels and Thrust During Blowdown

Pressures decrease in closed vessels as gas is exhausted through a discharge nozzle. This asymptotically decreasing pressure, P, can be determined by differentiating Bernoulli's equation with respect to time and assuming adiabatic conditions to obtain

$$P = P_0 \cdot \left(1 + \left(\frac{k-1}{2} \right) \cdot \left(\frac{2}{k+1} \right)^{\frac{k+1}{2\cdot(k-1)}} \cdot \sqrt{\frac{k \cdot g \cdot P_0}{12 \cdot \rho_0}} \cdot \frac{A \cdot t \cdot 12}{V'} \right)$$

US (6.4)

As the pressure decreases in a pipe system, the pressure regulator will counter this decrease in pressure. De-

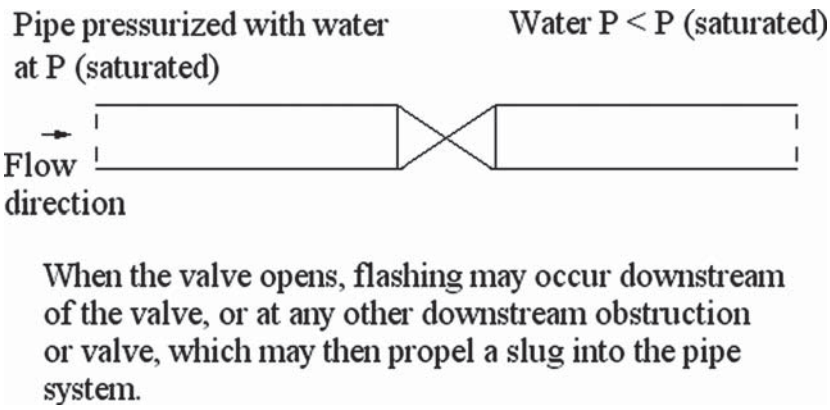


FIG. 6.15 STEAM-PROPELLED WATER SLUG, SLUG FLOW (EPRI [199])

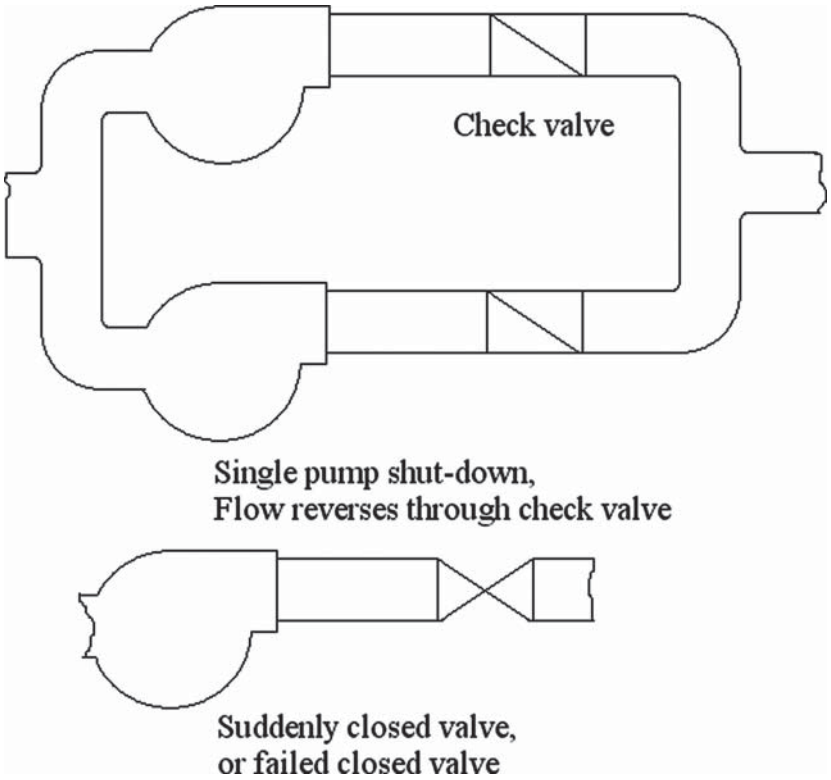


FIG. 6.16 SUDDEN VALVE CLOSURE, VALVE SLAM (EPRI [199])

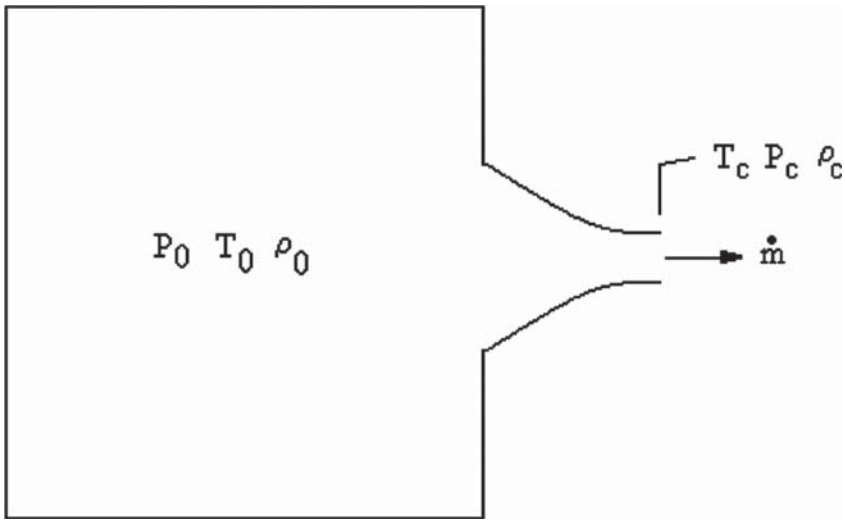


FIG. 6.17 NOZZLE FLOW RATE

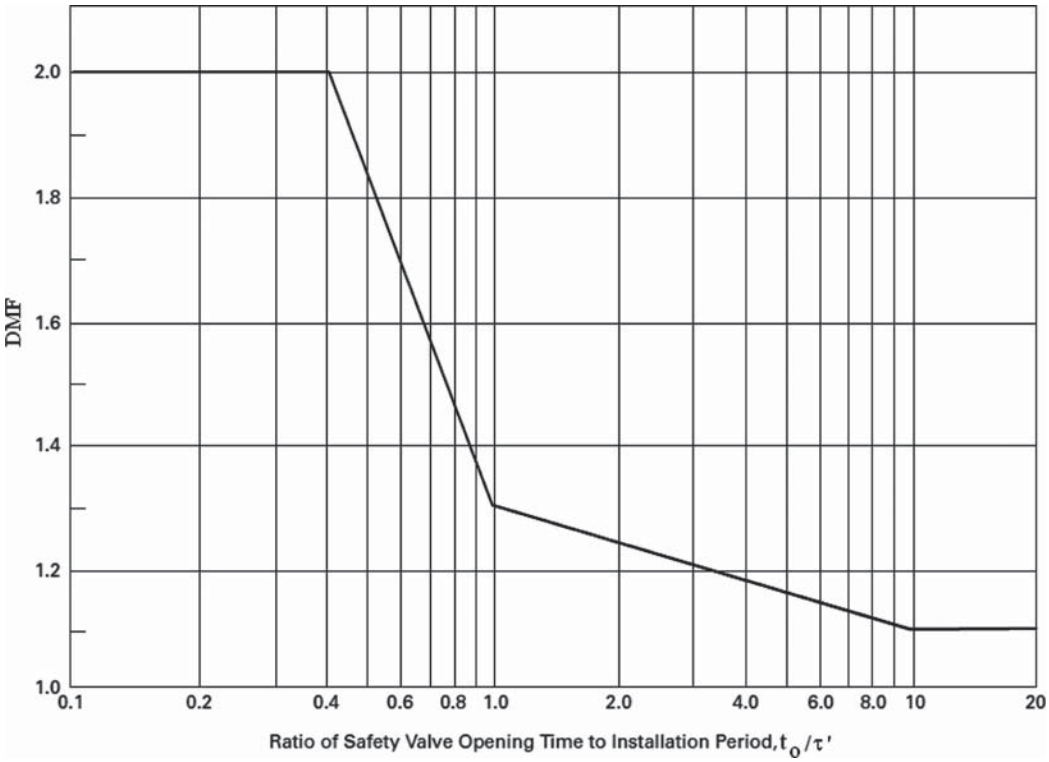


FIG. 6.18 DMF's FOR RELIEF VALVE OPENING IN A PIPE SYSTEM (ASME, B31.1, Appendix II)

pending on the length of the pipe, pressure decreases will be minor, and thrust forces depend on the pressure at the nozzle (Fig. 6.19). The maximum thrust or force, F, on a vessel or pipe equals

$$F = A \cdot (k+1) \cdot P_c \qquad \text{US (6.5)}$$

The forces on relief valves and attached piping can be large and require careful consideration, but are outside the scope of this text.

6.4 APPROPRIATE OPERATION OF STEAM SYSTEMS FOR PERSONNEL SAFETY

Although there are numerous pressure and safety considerations for steam systems, only a brief discussion of issues related to water hammer are presented here. Numerous design recommendations are provided as required throughout this text.

6.4.1 System Startup

During startup, condensate should be removed from the system prior to opening the regulator fully to prevent water hammer. A common method is to open the regulator bypass line to apply a force to drain the system. Vent/drain valves are typically opened along the pipe length to discharge condensate. When steam blowdown is observed, each valve is closed. Another method is to open the regulator bypass for a prescribed time to ensure that

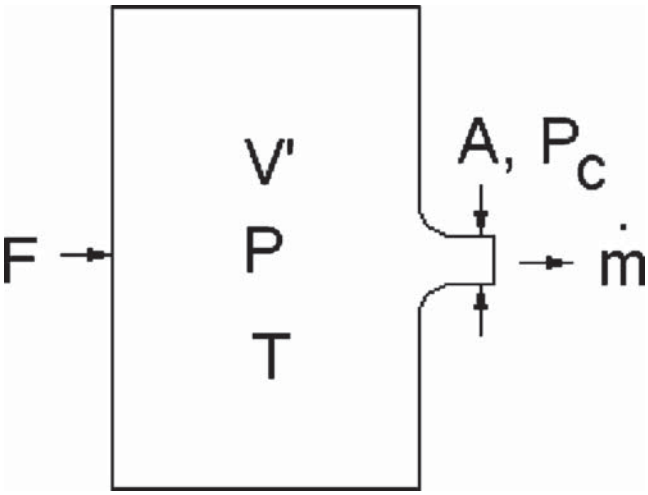


FIG. 6.19 PRESSURE VESSEL AND NOZZLE NOMENCLATURE

condensate is removed, e.g., typically 30 minutes, or longer. Once the condensate is removed, the main valve of the regulator is used to incrementally increase the system pressure and temperature.

6.4.2 Steam Traps

Steam traps should be installed and operated appropriately to both reduce operating costs and prevent water hammer. Resources are available for further discussion [202, 203, 204]. Typically, a 5° to 10° temperature difference exists across a steam trap, which can be periodically monitored or preferably continuously monitored.

6.5 SUMMARY OF FLUID TRANSIENTS

Steam condensate systems provide examples of most fluid transient types, where excessive pressures occur when operating conditions change. Although many transients occur during startup and shutdown, transients also occur during equipment failures and changes in flow conditions while in operation. Pressure magnitudes may be calculated for some, but not all, transients. Several catastrophic examples of transients were provided here, as well as examples of equipment damage due to fatigue. The relationship between pipe failures and fluid transients is the focus of the following chapters.

CHAPTER

7

SHOCK WAVES, VIBRATIONS, AND DYNAMIC STRESSES IN ELASTIC SOLIDS

To understand pipe failures due to water hammer, the dynamics of generalized stresses first require consideration. Elastic stresses are the focus of this dynamic analysis, even though dynamic plastic stresses are briefly treated in this text. The fact is that plastic deformation dynamics is far from being fully understood. Even elastic structural dynamics needs much work. In short, suddenly applied loads induce shock waves, which in turn cause vibrations and dynamic strains, where these strains are related to dynamic failure stresses through material properties.

Several steps are provided here to explain elastic stresses in objects. First, shock waves are created in objects when they are suddenly loaded, and examples are provided to describe vibrations in rods following impact. Second, the equation of motion is adapted to a simple model to describe vibrations in basic structures, like rods or beams. Once the model is presented, different types of loads on structures are considered. These loads include a suddenly applied constant load and a slowly applied load, which are of concern for water hammer and corrective actions. Also, periodic loads are considered to better understand structural response, in general, and to understand pipe response to cyclic loads provided by some types of positive displacement pumps (paragraph 5.16). Following a discussion of vibration, the equation of vibration is used to calculate the dynamic strains, which create dynamic stresses in objects due to various load types. All dynamic stresses decrease over time due to damping, so damping closes the discussion on stresses due to dynamic loading.

7.1 STRAIN WAVES AND VIBRATIONS

When an object or shock wave strikes an object, a strain wave develops in the object due to the induced stress at the rod tip. This process may also be described as a stress wave, but strain, or deflection, is technically the correct term for use, since strain is the measurable quantity in a structure. However, the terms stress waves and strain waves are used interchangeably in the literature, since they are readily converted by using the elastic modulus for an elastic material. To describe this process, the wave equation was developed from the equation of motion in 1776 by D'Alembert (Graff [206]). The case of a strain wave in a rod simplifies the discussion of strain waves.

7.1.1 One-Dimensional Strain Waves in a Rod

For a rod struck on one end, D'Alembert's wave equation is expressed as follows.

$$u(x,t) = f(x - c \cdot t) + g(x + c \cdot t) \tag{7.1}$$

The deflection $u(x,t)$ was derived from the equation of motion, such that the sum of the applied forces, $\sum F$, equal

$$\sum F = m \cdot a = \rho \cdot A \cdot dx \cdot \frac{\partial^2 u}{\partial t^2} \tag{7.2}$$

In these equations, the quantity $u(x,t)$ is any function that describes the displacement of the end of the rod where a force or displacement is applied, $f(x - c \cdot t)$ describes forward traveling waves into the rod away from the struck end, and $g(x + c \cdot t)$ describes reverse waves traveling back to the struck end. If a general equation is available to describe $u(x,t)$ in terms of applied pressure or strain, that equation is then used to describe the stress or motion at any point, x, in the rod in terms of the one-dimensional wave velocity of the rod material, $c = c_0$ where

TABLE 7.1 APPROXIMATE VELOCITY OF SOUND FOR METALS (Avallone and Bumeister [33])

Material	Sound velocity (ft/second)	Density (lbm/ft^3)
Aluminum	16,740	168
Brass	11,480	530
Copper	11,670	555
Iron and soft steel	16,410	486
Lead	1610	1125

$$c_0 = \sqrt{\frac{E \cdot g_c \cdot 144}{\rho}} \qquad \text{US (7.3)}$$

$$c_0 = \sqrt{\frac{E}{\rho}} \qquad \text{SI (7.4)}$$

Differing slightly from these approximations, measured velocities of sound for some materials are provided in Table 7.1. Note that the velocities of sound in liquids (Table 2.12) is about four to six times the velocity of sound in air, and the velocities of sound in metals are about three to four times the velocity of sound in water (air, 1116 ft/second; water, 4860 ft/second; steel, 16,410 ft/second).

7.1.2 Three-Dimensional Strain Waves in a Solid

For some applications, one-dimensional wave speed approximations are reasonable. However, three distinct waves are present in three-dimensional solids, where each type of wave travels at a different velocity. Strain waves are described in terms of Lame's constants (λ' and G), where G equals the shear modulus (Eq. (4.14)). In texts on wave motion, μ is a commonly used symbol for the shear modulus, instead of G, which is used here and in texts on structural mechanics. Lame's constants are described in terms of other material properties, in the forms:

$$\lambda' = k - \frac{2 \cdot G}{3} \qquad \text{US, SI (7.5)}$$

$$E = \frac{G \cdot (3 \cdot \lambda' + 2 \cdot G)}{(\lambda' + G)} \qquad \text{US, SI (7.6)}$$

$$\nu = \frac{\lambda'}{2 \cdot (\lambda' + G)} \qquad \text{US, SI (7.7)}$$

Also referred to as axial waves, pressure waves, or strain waves, dilatational waves travel in the direction of the applied load at a velocity, c_1, which equals

$$c_1 = \sqrt{\frac{(\lambda' + 2 \cdot G) \cdot g}{\rho}} = \sqrt{\frac{E \cdot (1-\nu) \cdot g}{\rho \cdot (1+\nu) \cdot (1-2 \cdot \nu)}} = \sqrt{\frac{3 \cdot k \cdot (3 \cdot k + E) \cdot g}{\rho \cdot (9 \cdot k - E)}} = \sqrt{\frac{G \cdot (4 \cdot G - E) \cdot g}{\rho \cdot (3 \cdot G - E)}} \qquad \text{US, SI (7.8)}$$

$$c_1 = \sqrt{\frac{(\lambda' + 2 \cdot G)}{\rho}} \qquad \text{SI (7.9)}$$

Also referred to as shear waves and torsion waves since they result in shear or torsion, respectively, traction waves are orthogonal to dilatational waves and travel at wave velocities, c_2, equal to

$$c_2 = \sqrt{\frac{G \cdot g}{\rho}} = \sqrt{\frac{E \cdot g}{2 \cdot \rho \cdot (1 + \nu^2)}} \qquad \text{US (7.10)}$$

$$c_2 = \sqrt{\frac{G}{\rho}} \qquad \text{SI (7.11)}$$

Frequently referred to as Rayleigh waves, surface waves are also present on the surface of a solid. These waves penetrate minor distances into the solid material surface and were initially investigated to explain surface waves during earthquakes. Rayleigh waves have wave velocities, c_R, slightly less than traction wave velocities, and are a function of Poisson's ratio, as shown in Fig. 7.1 and expressed by

$$c_R \approx \frac{c_2 \cdot (0.87 + 1.12 \cdot \nu)}{(1 + \nu)} \qquad \text{US, SI (7.12)}$$

In short, a shock to an object results in three distinct waves within the object. 1) A dilatational wave travels in the direction of the shock. 2) Traction waves are perpendicular to the dilatational wave. Traction waves may be in the form of rotational waves, torsion waves, or two-dimensional shear waves. 3) In addition to these waves occurring throughout the volume of the solid, surface waves are also present.

7.1.3 Vibration Terms

To describe vibrations, relevant terms require definition, such that:

A'' = amplitude
c = wave speed
f = frequency, time required to complete a vibration cycle
f_n = natural frequency
$f_1, f_2, \ldots, f_n$ = modal frequencies, higher-mode natural frequencies

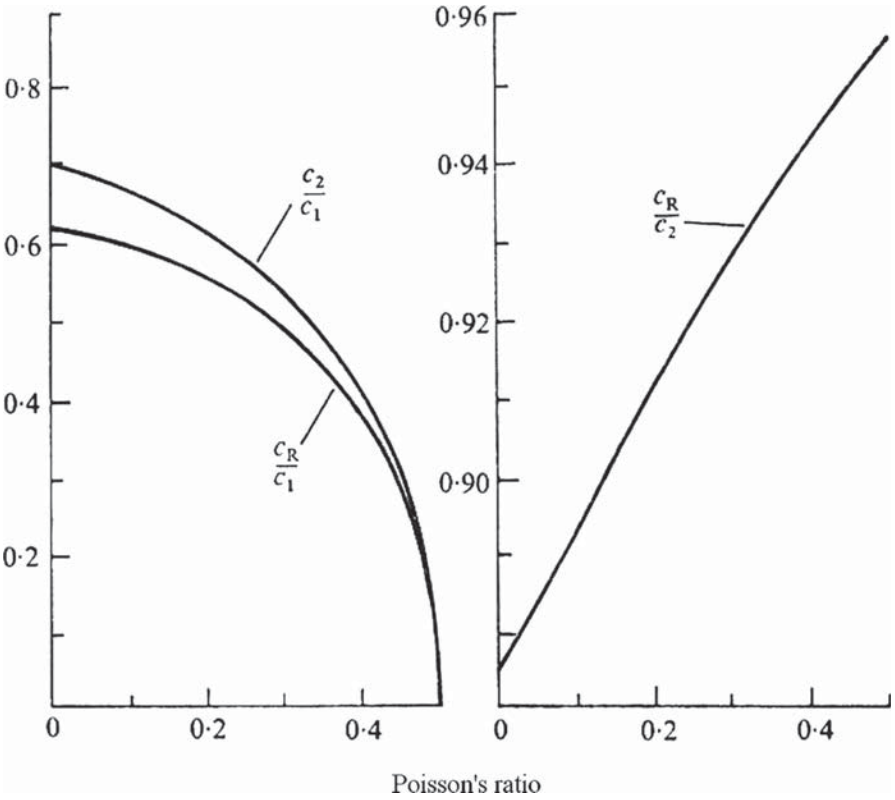


FIG. 7.1 RATIO OF SURFACE WAVE VELOCITIES TO DILATATIONAL AND TRACTION WAVE VELOCITIES
(Knopoff [207], Reprinted by permission of the Seismological Society of America)

γ' = wavenumber
$\lambda = 2 \cdot \pi/\gamma'$ = wavelength, total length of a single wave
$\tau' = 1/f$ = period
$\omega = 2 \cdot \pi \cdot f = \gamma' \cdot c$ = radial frequency
$\omega_1, \omega_2, \ldots, \omega_n$ = modal radial frequencies

7.1.4 Vibrations in a Rod Due to Strain Waves

To discuss vibrations in a cantilevered rod due to strain waves, a general observation with respect to vibrations can start the discussion. That is, when an object is struck with a hammer, it vibrates at its natural frequency, f_n, and this condition is referred to as free vibration where the induced shock wave results in a vibration. As the shock wave travels back and forth in the rod at a velocity = c_1, a standing vibration is set up in the rod as the reflected and incident waves combine to form a standing wave. The reader is referred to Graff [206] for derivations of standing wave equations from discrete wave equations, where Fourier transforms, elasticity equations, and Navier equations are combined to perform these complex derivations, which typically require many pages of vector differential equations.

If the applied excitation force or load varies, the frequency response of the rod depends on both the frequency of the rod and the mass and frequency causing the excitation. For the case of an applied pressure, which is important to this work, the frequency response of a rod (or plate) depends only on the rod (or plate) frequency. In other words, when an excitation force (pressure) is applied, the rod vibrates at its natural frequency, similar to free vibrations caused by striking an object with a hammer. Strain waves in a rod are discussed in the following paragraphs to describe the relationship between shock waves and vibrations.

7.1.5 Dilatational Strain Waves in a Rod

Ideally, whatever action happens at the end of a uniform rod in terms of force or deflection causes a shock wave to transmit down the length of the rod at a sonic velocity, where the vibration frequencies of the rod are controlled by the end constraints of the rod. Again, the terms stress wave and strain wave are used interchangeably, using the elastic modulus relationship between stress and strain.

7.1.6 Wave Reflections in a Rod

Eq. (7.1) can be extended to evaluate wave reflections from the end of a rod (Graff [206]), where similar results are obtained for a flat plate. A pressure applied to the end

of a rod will transmit a strain down the length of the rod at the sonic velocity of the rod material. Strains will be reflected as dictated by the boundary conditions at the ends of the rod, where reflected strains are doubled for fixed-end restraint conditions and cancel each other for free-end conditions. In real structures, the end restraint is seldom rigidly fixed, and reflected waves do not necessarily double completely, since the incident and reflected waves are out of phase, and dispersion of the load may also occur at the point of incidence. Examples of impacts on free and fixed rods clarify the relationships between shock waves and vibrations.

7.1.7 Strain Wave Examples for Rods

The cases of both cantilevered and free ends are considered, as shown in Fig. 7.2. Each example considers the effects of both incident and reflected waves in the rods.

Example 7.1, Consider a suddenly (instantly) applied constant pressure to the end of a rod with both ends free.

Consider the rod with free ends first. The frequency is incidentally the same for the rod with both ends fixed or both ends free. For a constantly applied pressure, the first-mode frequency, f_1, will be the primary natural frequency to be excited (Den Hartog [209]). Higher-mode frequency vibrations are typically less than 10% of the total vibration and are frequently neglected in calculations (see paragraph 7.2.6). The free bar vibrates at a frequency and period equal to

$$\omega_n = \frac{n \cdot \pi}{L''} \cdot \sqrt{\frac{E \cdot g''}{\rho''}} = \frac{n \cdot \pi}{L''} \cdot \sqrt{\frac{A \cdot E \cdot g''}{\left(\frac{W}{L''}\right)}} \qquad \text{US (7.13)}$$

$$\tau_1' = 2 \cdot L'' \cdot \sqrt{\frac{\rho''}{E \cdot g''}} \qquad \text{US (7.14)}$$

where τ_1' equals the period of the first-mode frequency.

If a step pressure is applied at the tip of the rod, an equivalent average stress occurs at the tip of the rod. However, an elastic strain is expected to vary from zero up to the maximum strain as the rod compresses at the frequency of a free rod as shown in Fig. 7.3. Intuitively, one might conclude that the stress at the tip of the rod should instantly increase to the magnitude of the applied pressure. However, an instantaneous increase in stress at the tip of the rod will occur only in a theoretically rigid material. That is, an elastic material does not instantly deform to a condition of maximum compression.

Also for a rod with free ends, a wave of equal but opposite sign is reflected when the incident wave reaches the far end of the rod. That is, a compression strain will reflect from a free end as a tension strain of equal magnitude but opposite direction, and the strain waves will effectively cancel each other as shown in Fig. 7.3. In short, the forward-traveling shock waves due to impact are cancelled within the rod by the reflected waves (reverse traveling) at the free end, and the energy imparted to the rod then translates, or moves, the bar. That is, if the rod was suspended from strings, the rod would swing like a pendulum, following initial vibrations as the shock wave travels down the length of the bar and back a single time.

Example 7.2, Consider a suddenly (instantly) applied constant pressure to the free end of a fixed cantilevered rod.

For a cantilevered rod, waves are reflected at the same sign, and the strains add to double the strain magnitude, where an incident compression strain wave is reflected as a compression strain from the fixed end of the rod. Figure 7.4 shows the strain at the tip of a rod struck by a suddenly applied constant pressure.

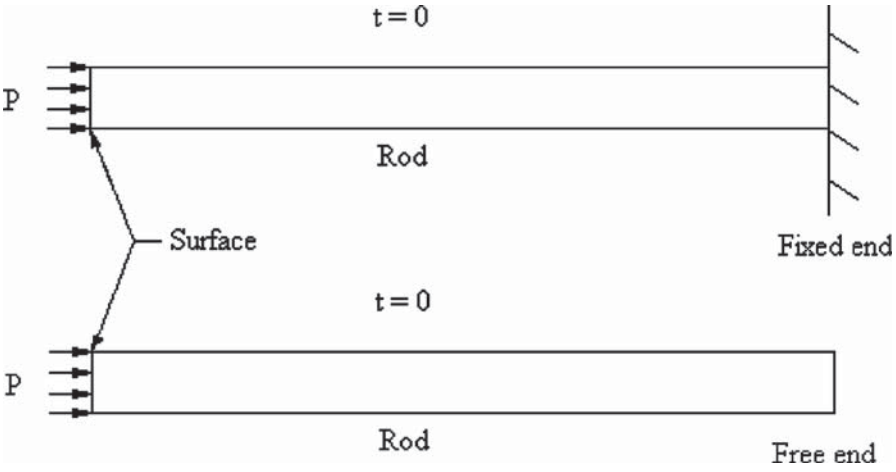


FIG. 7.2 SUDDENLY APPLIED PRESSURE TO A ROD WITH FIXED OR FREE-END CONSTRAINTS

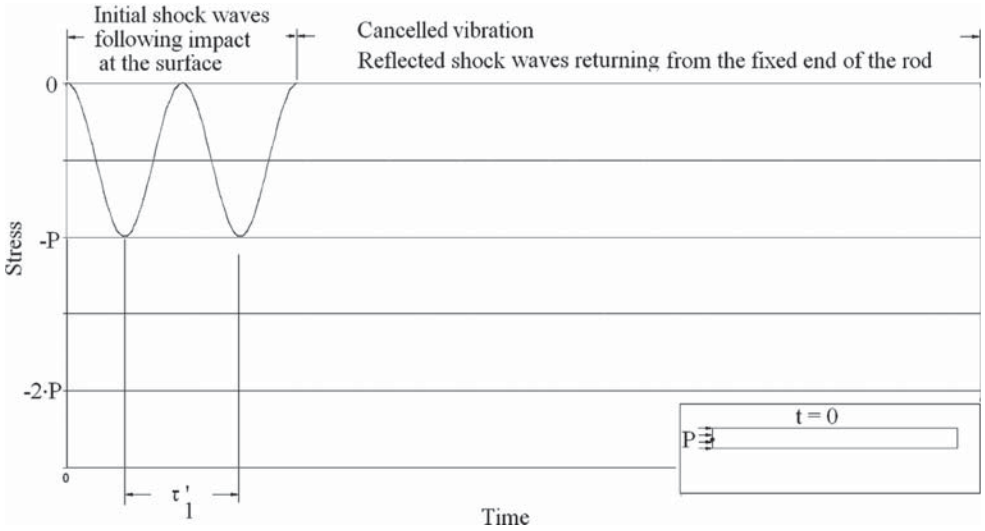


FIG. 7.3 SHOCK WAVES AND VIBRATIONS AT THE IMPACTED SURFACE OF A FREE ROD

In Fig. 7.4, the longitudinal frequency and period for a cantilevered rod with one fixed end equal

$$\omega_n = \frac{(2 \cdot n - 1) \cdot \pi}{2 \cdot L''} \cdot \sqrt{\frac{E \cdot g''}{\rho''}} \qquad \text{US (7.15)}$$

$$\tau_1' = 4 \cdot L'' \cdot \sqrt{\frac{\rho''}{E \cdot g''}} \qquad \text{US (7.16)}$$

where W/L'' is the weight per unit length (Den Hartog [209]). Note that the suddenly applied pressure induces a harmonic strain with a vibration period equal to the period of a cantilevered rod, which equals

Note also that a rod with both ends fixed has a higher frequency than a rod with only one end fixed, due to an increased stiffness.

Once the shock travels the length of the rod from the struck end, the wave reflects from the fixed end and doubles in magnitude to form a standing wave or vibration in the rod. In the absence of damping, the standing wave would continue indefinitely.

This basic mechanism for shock-induced vibrations is similar for other structures. Other structural shapes react similarly to compressive forces, but shock waves may dissipate, or scatter, as they expand through nonuniform cross sections of an object, such as a beam. Graff [206]

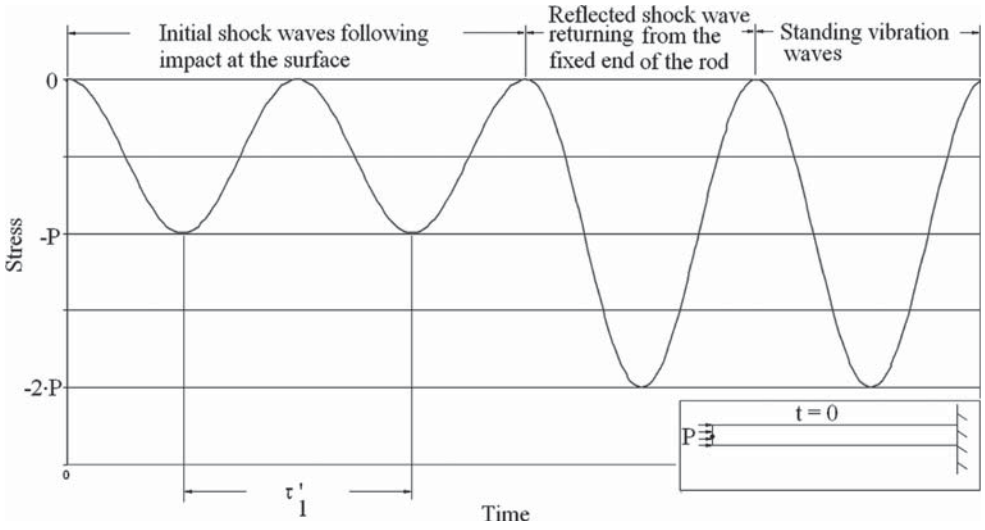


FIG. 7.4 SHOCK WAVES AND VIBRATIONS AT THE IMPACTED SURFACE OF A CANTILEVERED ROD

and Morse and Ingard [208] also provide more details on wave motion in simple structures, such as plates and shells. Computer simulations are required for more complicated structures.

7.1.8 Inelastic Damage Due to Wave Reflections

The maximum stress frequently occurs on the surface of the object, but the maximum stress may occur internal to an object following impact loading. If the shock wave to the solid is of large magnitude, the doubling of reflected, plastic, shock waves inside a solid may lead to damage. Although outside the scope of this work, but providing some insight into wave mechanics, spalling of plates occurs away from the point of contact of an artillery shell. That is, there are three primary outcomes discussed in the literature for an artillery shell impact to a steel plate (Kolsky [210]):

1. A through hole in the plate
2. Spalling of the plate on the opposite side of impact, where a reflected wave doubles the stress magnitude below the surface of the plate, and a disc of metal detaches from the plate
3. Bending and plastic deformation of the plate at the impact location

There may also be bending stresses that contribute to this type of failure.

7.2 SINGLE DEGREE OF FREEDOM MODELS

Rather than derive the vibration equations from wave theory for numerous different structures, a single degree of freedom (SDOF) oscillator can be used as a model for simple structures, and the frequency equations for those structures can be obtained from the literature to complete the SDOF equations for use. Specifically, SDOF models will be used in this work to describe dynamic radial wall stresses, hoop stresses, and bending stresses. Treatment of torsion stresses is similar, but not discussed here. SDOF vibration equations are first developed, followed by the application of these equations to describe stresses. Thomson [212] provided an excellent presentation of vibration theory, which provides an introduction to the following discussion of vibrations, where SDOF oscillators are described as follows.

7.2.1 SDOF Oscillators

The SDOF model shown in Fig. 7.5 is applicable to materials with linear stress-strain relationships, where the principle of superposition applies to orthogonal strains. The oscillator vibrates in response to an excitation force, which can model a changing force (load control), a changing displacement of the supports (displacement control), or a free vibration, which represents stretching the spring to a known position and releasing the mass. Specifically,

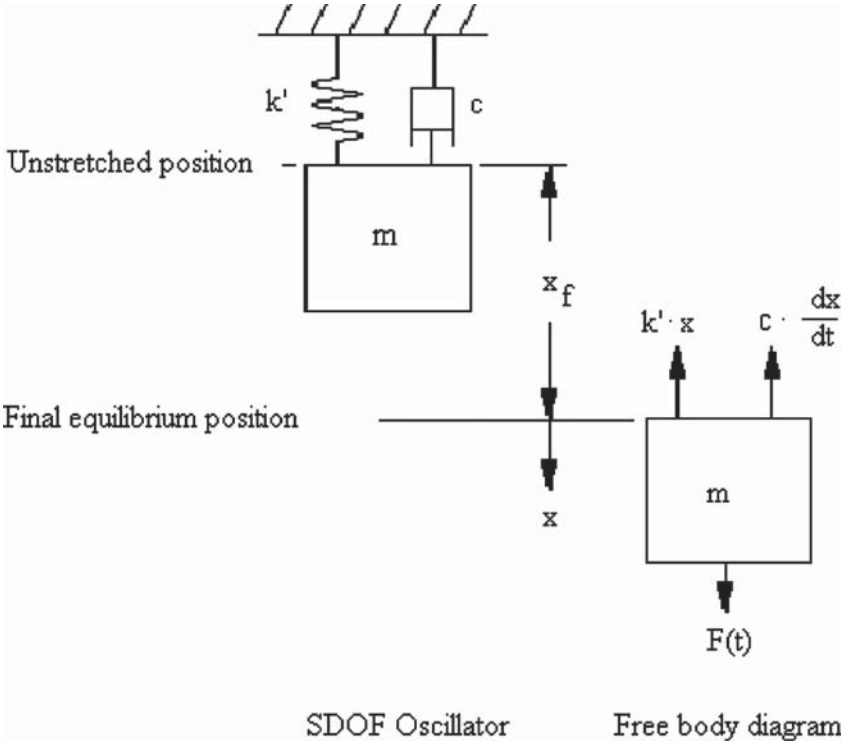


FIG. 7.5 MODEL FOR A SDOF OSCILLATOR

free vibration and load control are applicable to this work. Subscripts are frequently used to describe orthogonal vibrations in some texts, but were dropped in this initial discussion, since a single dimension is being considered (SDOF). That is, ω_j, ζ, and x_j are shortened to ω, ζ, and x. Subscripts, j, will be used as applicable in later paragraphs to describe coordinate directions.

7.2.1.1 SDOF Equation of Motion The dynamic response of an oscillator is described in terms of Newton's equation of motion, such that

$$m \cdot \frac{d^2x}{dt^2} + c \cdot \frac{dx}{dt} + k' \cdot x = F(t) \cdot g \qquad \text{US (7.17)}$$

$$m \cdot \frac{d^2x}{dt^2} + c \cdot \frac{dx}{dt} + k' \cdot x = F(t) \qquad \text{SI (7.18)}$$

where m is the mass of the object; k' is the spring constant, c is a constant linear damping coefficient, $F(t)$ describes the excitation force as a function of time, t, and

$$\frac{d^2x}{dt^2} \qquad \text{SI, US (7.19)}$$

equals the instantaneous acceleration of the mass, and

$$\frac{dx}{dt} \qquad \text{SI, US (7.20)}$$

equals the instantaneous velocity of the mass. For constant, linear damping coefficients, Eq. (7.17) yields

$$m \cdot \frac{d^2x}{dt^2} + 2 \cdot \zeta \cdot \omega_n \cdot \frac{dx}{dt} + \omega_n^2 \cdot x = F(t) \cdot g \qquad \text{SI, US (7.21)}$$

$$\zeta = \frac{c}{2 \cdot m \cdot \omega_n} = \frac{c}{c_{critical}} \qquad \text{SI, US (7.22)}$$

$$\omega_n = \sqrt{\frac{k' \cdot g}{m}} = 2 \cdot \pi \cdot f_n \qquad \text{US (7.23)}$$

$$\tau'_n = \frac{1}{f_n} = \frac{2\pi}{\omega_n} \qquad \text{SI, US (7.24)}$$

where ω_n is the natural frequency in radians/second, f_n is the natural frequency in cycles per second, τ'_n equals the period of the natural frequency, which is the time between successive peaks of vibration, $c_{critical}$ is the critical damping coefficient, and ζ is the damping factor. Damping and frequency effects can be described using a free vibration equation.

7.2.1.2 SDOF, Free Vibrations Free vibrations provide an example to clarify and relate vibration terms. To evaluate free vibrations, assume that a spring has an initial displacement, x_f, such that $x = x_f$ = constant at $t = 0$. Eq. (7.21) yields

$$m \cdot \frac{d^2x}{dt^2} + 2 \cdot \zeta \cdot \omega_n \cdot \frac{dx}{dt} + \omega_n^2 \cdot x = 0 \qquad \text{SI, US (7.25)}$$

$$x = x_f \cdot e^{-\zeta \cdot \omega \cdot t} \cdot \sin\left(\sqrt{1-\zeta^2} \cdot \omega_n \cdot t + \varphi\right) \qquad \text{SI, US (7.26)}$$

$$\omega_d = \omega_n \cdot \sqrt{1-\zeta^2} \qquad \text{SI, US (7.27)}$$

$$\tau'_d = \frac{1}{f_d} = \frac{2\pi}{\omega_d} \qquad \text{SI, US (7.28)}$$

where ω_d, f_d, τ'_d are the circular frequency, frequency, and period for damped vibrations, respectively, and φ is the phase angle.

7.2.1.3 Damping Effects

Example 7.3 Damping effects on SDOF responses.

Free vibrations are graphed in Fig. 7.6 to demonstrate the effects of damping and clarify nomenclature. In the figure, τ'_d is shown for 40% damping, since τ'_d for 1% damping is near the undamped period, τ'_n, of the natural frequency. Note that $e^{-\zeta \cdot \omega_n \cdot t}$ bounds each sinusoidal response and varies with the damping ratio, ζ. The exponential function of Eq. (7.26) is only shown for the 40% damping case.

7.2.1.4 Damping Ratio Vibrations in structures occur for positive damping ratios, $1 > \zeta > 0$. Vibrations are critically damped when $c = c_{critical}$, $\zeta = 1$, and vibrations do not occur after a load is applied. Below $\zeta = 1$, nonoscillatory, overdamped, motion occurs, and the system returns to equilibrium. Between $\zeta = 0$ and $\zeta = 1$, vibrations decay, or vibrate, to equilibrium in the absence of a forcing function. For $\zeta = 0$, the system is undamped, and the amplitude remains constant as the natural frequency vibrations theoretically continue unabated even in the absence of a forcing function. For $\zeta < 0$, the system is unstable, and once initiated, vibrations increase without limit in the absence of a forcing function, following an initial excitation. Although numerous damping models are available, constant damping used here provides many simplifications to approximate structural behavior.

7.2.1.5 Log Decrement The log decrement, δ, provides a technique to determine the rate of vibration decay, where the natural log of the ratio of any two successive amplitudes equals δ. The log decrement is defined as

$$\delta = \frac{2 \cdot \pi \cdot \zeta}{\sqrt{1-\zeta^2}} \qquad \text{SI, US (7.29)}$$

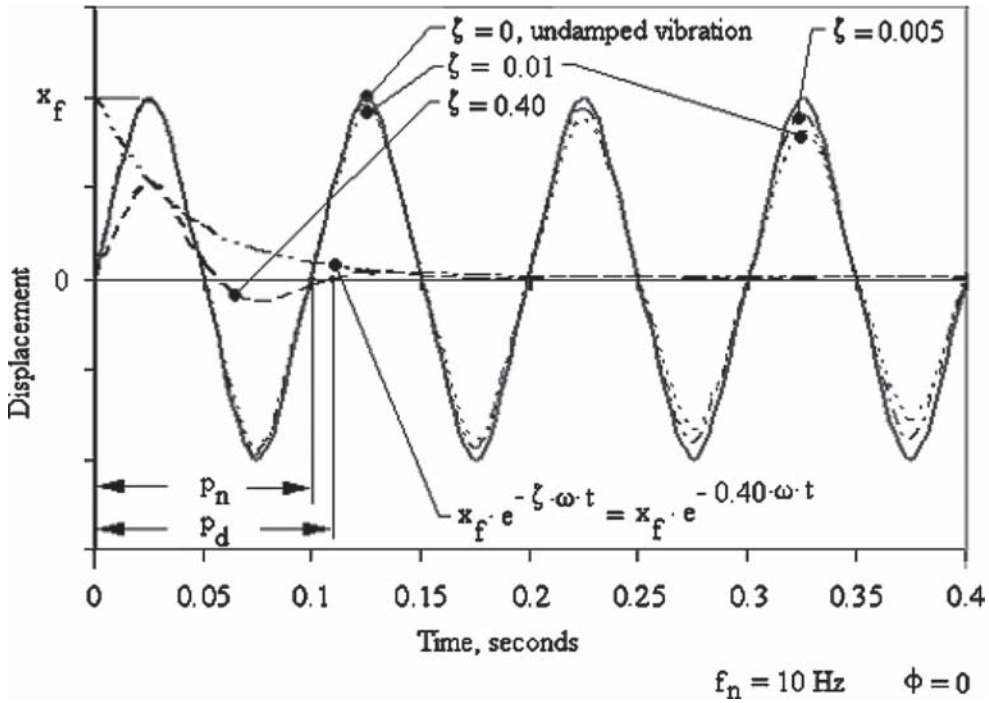


FIG. 7.6 EXAMPLE OF DAMPED AND UNDAMPED FREE VIBRATIONS, EQ. (7.26)

To find the ratio of any two successive amplitudes, x_1 and x_2,

$$\frac{x_1}{x_2} = e^{\delta} \qquad \text{SI, US (7.30)}$$

7.2.1.6 Phase Angle Effects

Example 7.4 Phase angle effects on SDOF responses.

The relationship of phase angle to vibration is shown in Fig. 7.7. As a special case, a spring is stretched to a length, x_f, and then released. Then, $\varphi = \pi/2$, and the response is

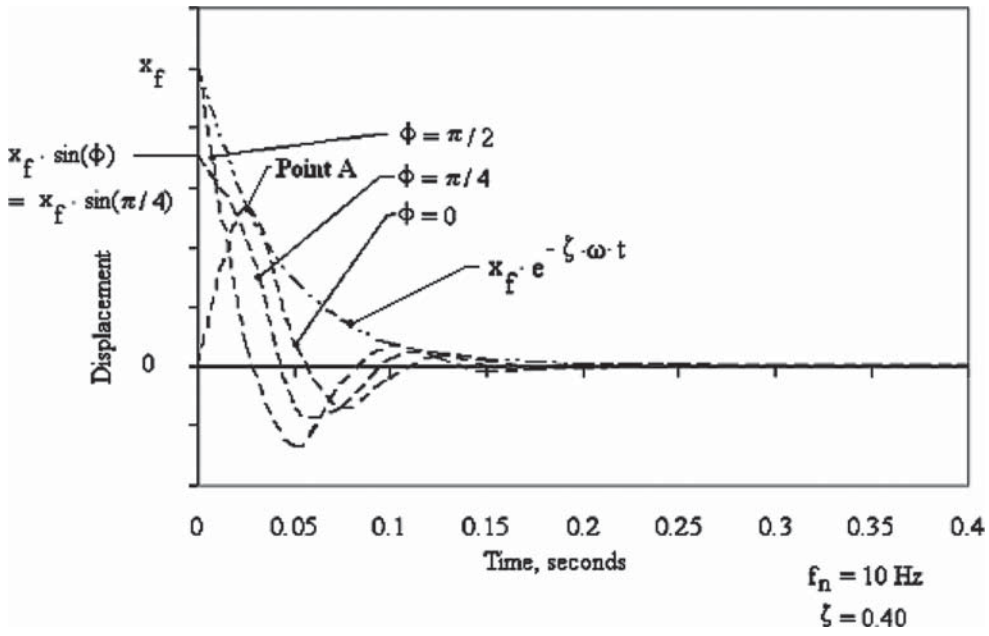


FIG. 7.7 PHASE ANGLE EFFECTS ON FREE VIBRATION AMPLITUDE, EQ. (7.26)

shown in the figure. An arbitrarily selected phase angle of $\varphi = \pi/4$ is also shown in the figure.

The maximum value at point A is frequently referred to as the maxi-max amplitude in vibration texts. In this work, that amplitude is the basis for the DMF. Note also that point A is slightly below the bounding curve described by $x_f \cdot e^{-\zeta \cdot \omega \cdot t}$, since the vibration ($\varphi = 0$) is tangent to that curve. Vibration texts provide additional discussion for SDOF vibrations, but this basic presentation seems adequate to introduce SDOF responses.

7.2.1.7 SDOF Responses to Applied Forces There has been much study on the response of SDOF oscillators, and Harris [213] provided a summary of responses to numerous excitation forces. A few of those are the basis for dynamic stress equations commonly used in this text, i.e., responses to step, ramp, impulse, and harmonic excitation forces, which are also referred to as forcing functions (Fig. 7.8). The reader is referred to Harris' text for responses to some other more complex excitation forces and impulses. Also, having defined vibration nomenclature using Eqs. (7.17) through (7.30), those mathematical relationships for periods, frequencies, and damping ratios are, of course, applicable to all vibrations considered in this work.

7.2.2 Step Response for a SDOF Oscillator

Fig. 7.8 shows a damped spring-mass system with a constant, suddenly applied exciting force $F(t) = F$ commencing at $t = 0$, which is the definition of a step input. Since the step response is crucial to the development of dynamic stress theory as applied to water hammer, a complete derivation of the response is warranted.

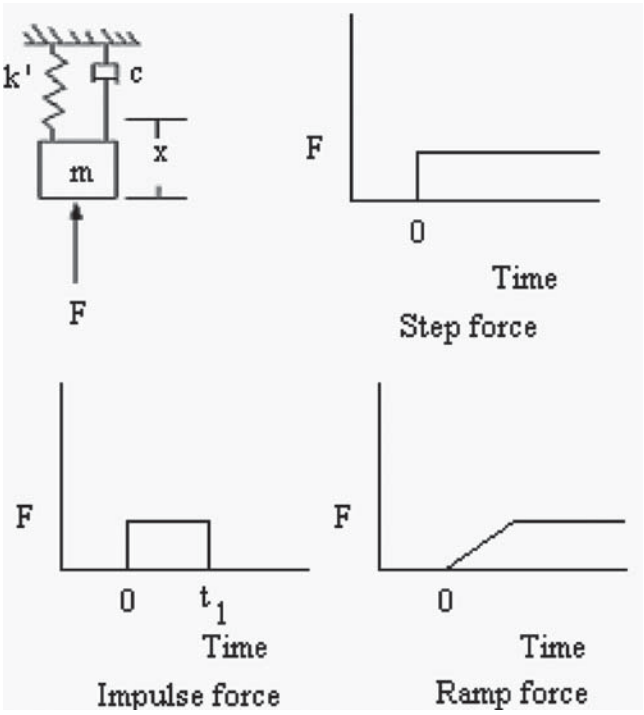


FIG. 7.8 SDOF EXCITATIONS/APPLIED FORCES

Substituting the excitation force into Eq. (7.21), the equation of motion for a step response is given by

$$m \cdot \frac{d^2x}{dt^2} + 2 \cdot \zeta \cdot \omega_n \cdot \frac{dx}{dt} + \omega_n^2 \cdot x = F \cdot g \qquad \text{US (7.31)}$$

where x is the system response or the displacement of the mass with respect to time. To find a general solution to Eq. (7.31), the homogeneous and particular solutions are required for this differential equation (Spiegel [214]).

7.2.2.1 Homogeneous Solution to the Equation of Motion for a Step Response The homogeneous solution to Eq. (7.31) is

$$\frac{d^2(m \cdot x)}{dt^2} + \frac{d(c \cdot x)}{dt} + k' \cdot x = 0 \qquad \text{US (7.32)}$$

Assuming

$$x = e^{s \cdot t} \qquad \text{US (7.33)}$$

where s is a constant, and substituting Eq. (7.33) into Eq. (7.32) yields

$$\left(m \cdot s^2 + c \cdot s + K\right) \cdot e^{s \cdot t} = 0 \qquad \text{US (7.34)}$$

which has two roots equal to

$$s_{1,2} = \left(-\zeta \pm \sqrt{\zeta^2 - 1}\right) \cdot \omega \qquad \text{US (7.35)}$$

When the motion is oscillatory, $\xi \le 1$, the general solution to Eq. (7.34) is expressed as

$$\begin{aligned} x_h &= A_1 \cdot e^{s_1 \cdot t} + A_2 \cdot e^{-s_2 \cdot t} = e^{-\zeta \cdot \omega \cdot t} \cdot \\ &\left(A_1 \cdot e^{i \cdot \omega \cdot t \cdot \sqrt{1-\zeta^2}} + A_2 \cdot e^{-i \cdot \omega \cdot t \cdot \sqrt{1-\zeta^2}}\right) \\ &= A_3 \cdot e^{-\zeta \cdot \omega \cdot t} \cdot \sin\left(\sqrt{1-\zeta^2} \cdot \omega \cdot t + A_4\right) \end{aligned} \qquad \text{US (7.36)}$$

7.2.2.2 Particular Solution to the Equation of Motion for a Step Response The particular solution to Eq. (7.31) is found by using the method of undetermined coefficients (Spiegel [214]). Assuming a particular solution of the form

$$x_p = A_5 \cdot \sin(\omega \cdot t) + A_6 \cdot \cos(\omega \cdot t) \qquad \text{US (7.37)}$$

and substituting x_p (Eq. 7.37) into Eq. (7.31) and differentiating yields

$$x_p = -A_5 \cdot \omega^2 \cdot \sin(\omega \cdot t) - A_6 \cdot \omega^2 \cdot \cos(\omega \cdot t) + 2 \cdot \zeta \cdot \omega \cdot (\omega \cdot A_5 \cdot \cos(\omega \cdot t) - \omega \cdot A_6 \cdot \sin(\omega \cdot t)) + \omega^2 \cdot (A_5 \cdot \sin(\omega \cdot t + A_6 \cdot \cos(\omega \cdot t) + A_7)) = \frac{F \cdot g}{m} \quad \text{US (7.38)}$$

Using the boundary conditions,

$$t = 0,\ x = 0 \text{ and } dx/dt = 0 \quad \text{US (7.39)}$$

like coefficients of Eq. (7.38) can be determined such that

$$A_7 = \frac{F \cdot g}{m \cdot \omega^2} = \frac{F}{k'} \quad \text{US (7.40)}$$

$$A_5 = A_6 = 0 \quad \text{US (7.41)}$$

Then,

$$x_p = \frac{F}{k'} \quad \text{US (7.42)}$$

7.2.2.3 General Solution to the Equation of Motion for a Step Response The general solution for the step response is found by adding the homogeneous and particular solutions (Eqs. (7.36) and (7.42)) and substituting the boundary conditions (Eq. (7.39)) to find the constants A_3 and A_4. The general solution for the response to a suddenly applied force is then expressed as

$$x(t) = \frac{F}{k'} \cdot \left(1 - \frac{e^{-\zeta \cdot \omega \cdot t}}{\sqrt{1-\zeta^2}} \cdot \cos\left(\left(t \cdot \omega \cdot \sqrt{1-\zeta^2}\right) - \left(\frac{\zeta}{\sqrt{1-\zeta^2}}\right)\right)\right) \quad \text{US (7.43)}$$

In nondimensional form, Eq. (7.43) is rewritten as

$$\frac{x(t) \cdot k'}{F} = \left(1 - \frac{e^{-\zeta \cdot \omega \cdot t}}{\sqrt{1-\zeta^2}} \cdot \cos\left(\left(t \cdot \omega \cdot \sqrt{1-\zeta^2}\right) - \left(\frac{\zeta}{\sqrt{1-\zeta^2}}\right)\right)\right) = S(t, \omega, \zeta) \quad \text{US (7.44)}$$

where $S(t, \omega, \xi)$ is the nondimensional step response, expressed as a function of time, radial frequency, and damping. For the undamped case, Eq. (7.44) reduces to

$$\frac{x(t) \cdot k'}{F} = (1 - \cos(\omega \cdot t)) = S(t, \omega, \zeta = 0) \quad \text{US (7.45)}$$

Note that Eq. (7.45) has a maximum value equal to

$$\text{DMF} = \frac{x_{\max} \cdot k'}{F} = 2 \quad \text{US (7.46)}$$

The dynamic magnification factor, DMF, has several equivalent terms in the literature and is referred to as the dynamic load factor, maxi-max response, impact factor, percent overshoot plus 1 (P.O. + 1), transmissibility, and dynamic amplification factor. The term DMF is being used in this work for consistency, since DMF has gained some acceptance in the piping industry.

According to Eq. (7.46), the maximum displacement of an undamped spring due to a step force increase, F, is therefore twice as much as the displacement obtained during free vibration for a force, F, induced by an identical mass (DMF = 2). This observation is also depicted by the step response provided in Example 7.5, which considers both step and impulse responses.

7.2.3 Impulse Response for a SDOF Oscillator

The impulse response shown in Fig. 7.8 is the sum of two step responses, where t_1 is the pulse duration time. For $t \le t_1$, Eq. (7.43) describes the response. For $t > t_1$, the response is described by

$$\begin{aligned} x = {} & \frac{F}{k'} \cdot \left(1 - \left(\frac{\zeta}{\sqrt{1-\zeta^2}}\right) - \frac{e^{-\zeta \cdot \omega \cdot t}}{\sqrt{1-\zeta^2}} \cdot \right. \\ & \left. \cos\left(\left((t - t_1) \cdot \omega \cdot \sqrt{1-\zeta^2}\right) - \left(\frac{\zeta}{\sqrt{1-\zeta^2}}\right)\right)\right) \\ & \left(1 - \left(\frac{\zeta}{\sqrt{1-\zeta^2}}\right) - \frac{e^{-\zeta \cdot \omega \cdot t}}{\sqrt{1-\zeta^2}} \cdot \right. \\ & \left. \cos\left(\left(t \cdot \omega \cdot \sqrt{1-\zeta^2}\right) - \left(\frac{\zeta}{\sqrt{1-\zeta^2}}\right)\right)\right) \\ = {} & \frac{F}{k'} \cdot \left(\left(\frac{\zeta}{\sqrt{1-\zeta^2}}\right) - \frac{e^{-\zeta \cdot \omega \cdot t}}{\sqrt{1-\zeta^2}} \cdot \right. \\ & \left. \cos\left(\left((t - t_1) \cdot \omega \cdot \sqrt{1-\zeta^2}\right) - \left(\frac{\zeta}{\sqrt{1-\zeta^2}}\right)\right)\right) - \\ & \left(\frac{\zeta}{\sqrt{1-\zeta^2}}\right) - \frac{e^{-\zeta \cdot \omega \cdot t}}{\sqrt{1-\zeta^2}} \cdot \\ & \cos\left(\left(t \cdot \omega \cdot \sqrt{1-\zeta^2}\right) - \left(\frac{\zeta}{\sqrt{1-\zeta^2}}\right)\right) \end{aligned} \quad \text{US (7.47)}$$

For the undamped case,

$$\frac{x(t)\cdot k'}{F} = \left(\cos\left(\omega\cdot\left(t-t_1\right)\right)-\cos\left(\omega\cdot t\right)\right) = I(t,\omega,\zeta=0) \qquad \text{US (7.48)}$$

where $I(t, \omega, \zeta = 0)$ is the nondimensional impulse response.

Example 7.5 Consider the effects of an impulse response on a SDOF oscillator.

An example of the effects of short-duration pulses is portrayed in Fig. 7.9. The lower curve is subtracted from the upper curve to obtain the curve in the middle, which describes the resultant vibrations presented by Eq. (7.48). Note that as the pulse length decreases, the amplitude of the deflection decreases. With respect to water hammer, the pulse duration of the transient may affect the piping response, which implies that very short impulses may produce negligible piping responses in some cases.

7.2.4 Ramp Response for a SDOF Oscillator

The undamped response to a constant slope, ramp excitation force similar to that shown in Fig. 7.8 may be derived, such that

$$R(T,\omega,\zeta=0) = \frac{x(t)\cdot k'}{F} = \left[1-\frac{\sin(\omega\cdot t)}{\omega\cdot t_1}+\frac{\sin(\omega\cdot(t-t_1))}{\omega\cdot t_1}\right]\cdot H(t-t_1) + \left[\frac{t}{t_1}-\frac{\sin(\omega\cdot(t))}{\omega\cdot t_1}\right]\cdot H(t_1-t) \qquad \text{US (7.49)}$$

where $R(t, \omega, \zeta = 0)$ is the nondimensional ramp response. $H(\ldots)$ is the Heaviside step function, which equals 1 when the argument is positive or 0 or equals 0 when the argument is negative. The Heaviside function is used to capture the response before and after the rise time, t_1. The overall influence of rise time for the ramp function is shown by the maximum amplitudes as a function of rise time with respect to the vibration period (Fig. 7.10). Fig. 7.10 also shows rise times that are nonlinear (Harris [213]). Note that the DMF = 2 at point A when the rise time equals zero for a step function, that the DMF is approximately 1.2 when the ratio of the rise time to the SDOF system period (t_1/τ') equals 1.5 at point B, and that the DMF = 1.1 when the rise time is 3.5 times the SDOF period at point C. In general, a ramp input reduces the vibration response as the rise time increases, where the step input is a special case of zero rise time.

7.2.5 SDOF Harmonic Response

The harmonic response describes physical processes pertinent to this work, such as machinery vibrations of rotating equipment that induce fatigue failures in attached piping, pump pressure pulsations that cause structural resonance and consequent fatigue failures of piping and associated equipment, and pipe system pressure pulsations that cause fluid resonance. The harmonic excitation force is simply a continuing cyclic loading on a solid structure or fluid. Both load-controlled and displacement-controlled vibrations (support motion) may be considered, but only load control is pertinent to the topic of water hammer.

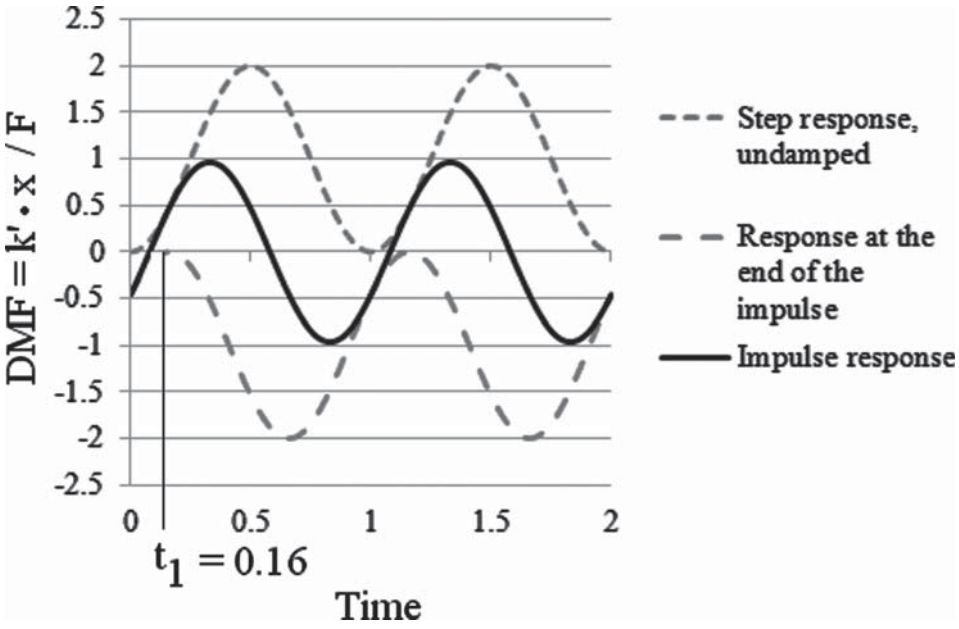


FIG. 7.9 UNDAMPED RESPONSE FOR $t_1 / \tau'_n = 0.16$ (Thomson, William T., "Theory of Vibration with Applications", 4th Edition, copyright 1993. Reprinted by permission of Pearson Education, Inc., Upper Saddle River, NJ)

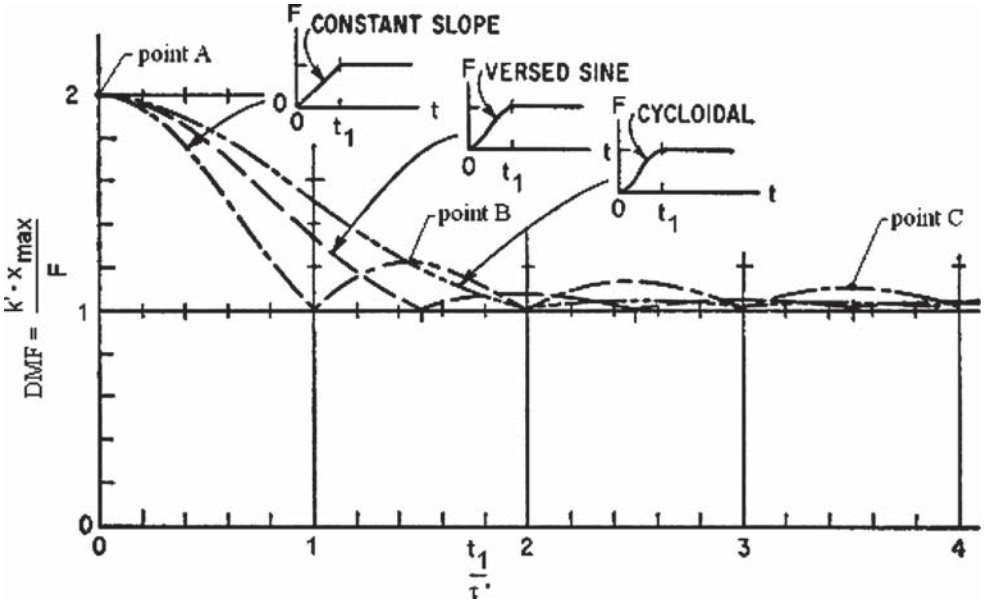


FIG. 7.10 EFFECTS OF RISE TIMES ON THE MAXIMUM AMPLITUDES (DMFs) OF RAMP RESPONSES (Harris [213], reprinted by permission of McGraw Hill)

Displacement control is more appropriate to earthquake response, where ground motion occurs. To introduce the reader to various harmonic vibration inputs to SDOF systems, a discussion of SDOF systems is accented by discussions of rods and beams. In particular, the system response is complicated by resonance, which is considered here for SDOF and multiple degree of freedom (multi-DOF) systems.

To simplify this discussion of resonance, the maximum values of harmonic vibrations will be considered for linear, elastic structures. The structural material is assumed to be elastic and linear, where elastic materials will not permanently deform, and linear materials have constant stiffness. When a structure vibrates due to a varying applied load, the structure vibrates at multiple frequencies principally associated with first-mode vibrations of various components. These natural frequencies are known for many simple structures, such as axially loaded rods and helical springs and transversely loaded beams with different support conditions, such as fixed or free ends. The vibration at any point in a structure is simply the sum of the vibrations acting at that point due to each of the vibrations, or responses, of each modal frequency caused by the excitation force, which may be either a changing force applied to the structure, or a changing position, or displacement, of the structural supports. For the examples considered here, the applied forces and displacements are assumed to act as steady-state sinusoidal functions.

When the frequency of the forcing function equals a natural frequency of a structure, resonance exists, and in the absence of damping, the structure vibrates with an infinite magnitude. However, all real structures have some damping, and the maximum vibration is limited. Even so, the response of the structure is magnified.

For example, common helical springs frequently have DMFs exceeding 100 (Thomson [212]). For the case of a spring with DMF = 100, a weight slowly added to the end of a spring will stretch the spring to a specific length at rest or static equilibrium. If that same weight is applied using a sinusoidal forcing function at resonance, the maximum length of the spring equals 100 times the length of the spring at rest.

In other words, acceptable vibrations may be greatly magnified and cause equipment damage if a resonant condition exists. Resonance will first be considered here for simple systems with a single natural frequency, followed by consideration of systems with multiple natural, or modal, frequencies, i.e., first mode, second mode, etc.

7.2.5.1 SDOF Load Control Load control is described by Fig. 7.11, and to describe the oscillator motion assume that

$$m \cdot \frac{\mathrm{d}^2 x}{\mathrm{d}t^2} + 2 \cdot \zeta \cdot \omega_\mathrm{n} \cdot \frac{\mathrm{d}x}{\mathrm{d}t} + \omega_\mathrm{n}^2 \cdot x = F \cdot \sin\left(\omega \cdot t\right) \cdot g \quad \text{US (7.50)}$$

To solve this differential equation, a particular solution for the displacement is assumed to be

$$x\left(t\right) = x_\mathrm{f} \cdot \sin\left(\omega \cdot t - \theta\right) \quad \text{US (7.51)}$$

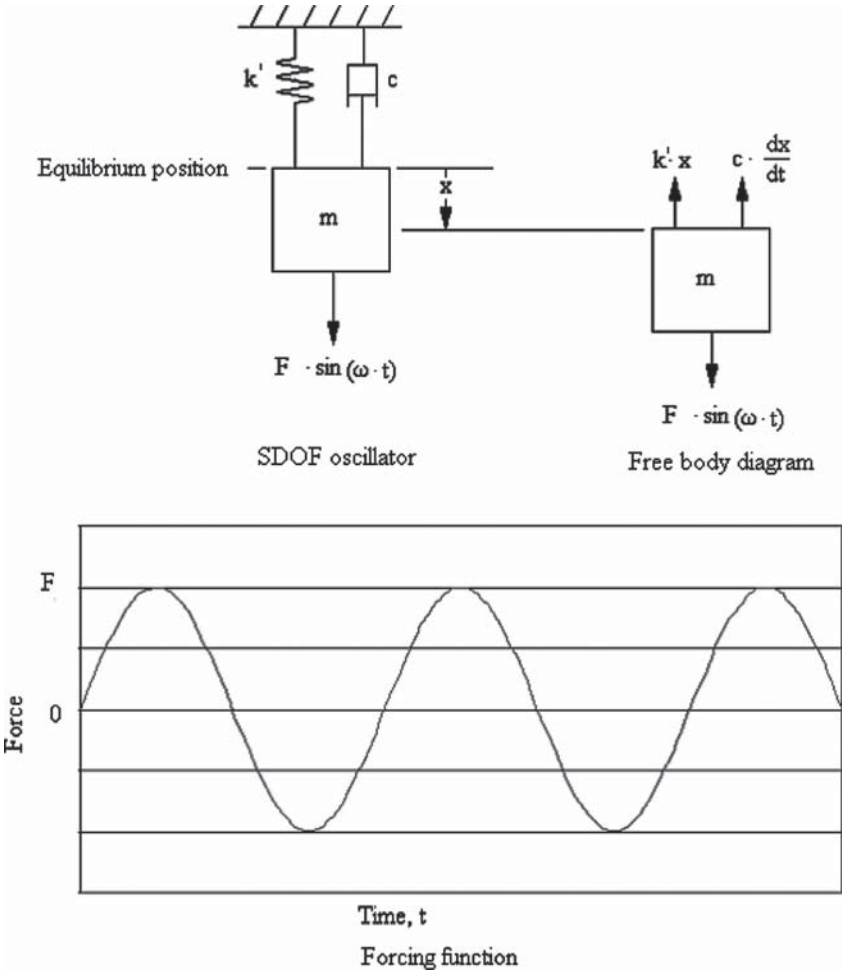


FIG. 7.11 LOAD-CONTROLLED SDOF OSCILLATOR

where ω is the circular frequency of the applied force, x_f is the amplitude of the impressed vibration, φ is the phase angle, and θ is the phase of the displacement vibration with respect to the phase of the excitation force. Note that θ and φ may be the same, but need not be equal, depending on the boundary conditions. Eqs (7.50) and (7.51) can be solved to yield the displacement and phase angle at any time, *t*, to yield

$$x(t,\omega,\zeta) = \frac{F \cdot \sin(\omega \cdot t - \theta)}{k' \cdot \sqrt{\left(1-\left(\frac{\omega}{\omega_n}\right)^2\right)^2 + \left(\frac{2\cdot\zeta\cdot\omega}{\omega_n}\right)^2}} + x_f \cdot e^{-\zeta\cdot\omega_n\cdot t} \cdot \sin\left(\sqrt{1-\zeta^2}\cdot\omega_n\cdot t + \varphi\right) \quad \text{US (7.52)}$$

$$\varphi = \tan^{-1}\left(\frac{2\cdot\zeta\cdot\omega_n}{1-\left(\frac{\omega}{\omega_n}\right)^2}\right) \quad \text{US (7.53)}$$

Example 7.6 Demonstrate the effects of free and forced vibration for a SDOF response.

An example of load control (Eq. (7.52)) is shown in Fig. 7.12. This example displays the vibration when a spring is stretched, and the applied load is in phase with the free vibration, where the total initial force is applied at time, $t = 0$. Terms were arbitrarily selected, where the initial position ratio is expressed as a unit displacement ($x_f = F/k' = 1$), and the frequency was arbitrarily selected.

Compare the steady-state vibration to the cumulative vibration shown in Fig. 7.12 to justify neglecting the free vibration transient. Note that the free vibration (for $\varphi = \pi/2$) has a decreasing effect on vibrations, and the transient vibration reduces x_{max}, which is the length that the spring is initially stretched. That is, the transient and steady-state vibrations are additive from Eq. (7.52), and the negative transient vibration subtracts from the amplitude. In successive periods, the transient approaches zero. The damped transient affects vibration for only the initial vibration cycles, and as shown in this example, the

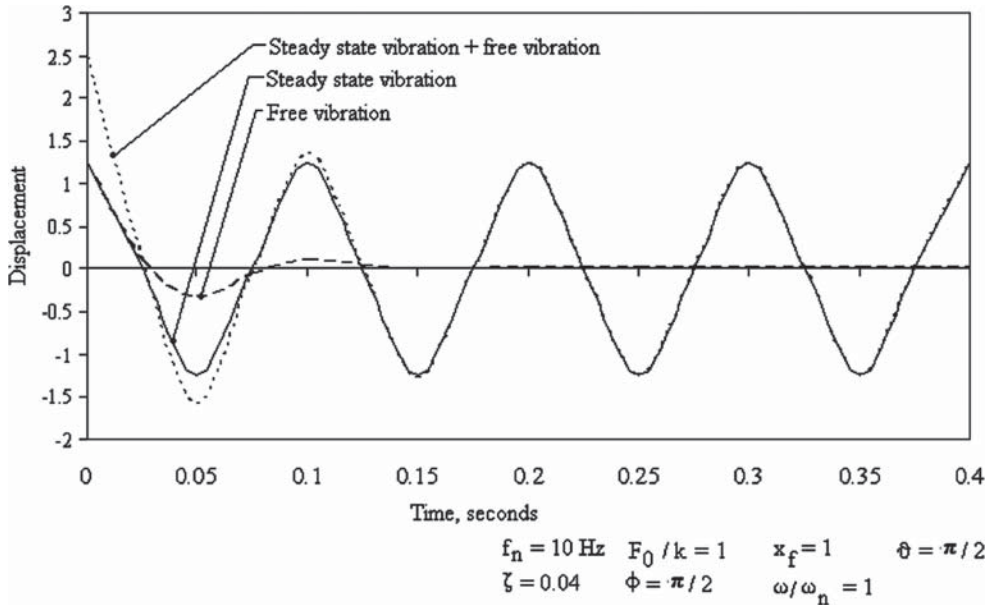


FIG. 7.12 SDOF LOAD-CONTROLLED VIBRATIONS, FREE VIBRATION AND STEADY-STATE VIBRATION, EQ. (7.52)

damped vibration serves to increase the maximum amplitude. If θ and φ are equal, and the vibrations are in phase, the free and steady-state vibrations add, and the total vibration is higher during the initial cycles. In other words, the free vibration may have an effect on vibration during the initial vibration cycles. For $\varphi = 0$, x_f equals zero and so does the free vibration.

7.2.5.2 Steady-State, SDOF Load-Controlled Vibration Considering only the steady-state forced vibration, the free vibration term may be neglected to simplify calculations for demonstration purposes. To do so, assume that the system is initially at rest, and the spring is stretched to the equilibrium position, where $t = 0$, $x = x_f = 0$, $\varphi = 0$. These boundary conditions were selected for this work to be consistent with the boundary conditions required for the use of the dynamic stress theory, considered in paragraph 7.3. Load-controlled vibrations are then described, using

$$x(t,\omega,\zeta) = \frac{F \cdot \sin(\omega \cdot t - \theta)}{k' \cdot \sqrt{\left(1 - \left(\frac{\omega}{\omega_n}\right)^2\right)^2 + \left(\frac{2 \cdot \zeta \cdot \omega}{\omega_n}\right)^2}} \qquad \text{US (7.54)}$$

$$\frac{x(t,\omega,\zeta) \cdot k'}{F} = \frac{F \cdot \sin(\omega \cdot t - \theta)}{k' \cdot \sqrt{\left(1 - \left(\frac{\omega}{\omega_n}\right)^2\right)^2 + \left(\frac{2 \cdot \zeta \cdot \omega}{\omega_n}\right)^2}} \qquad \text{US (7.55)}$$

$$= C(t,\omega,\zeta)$$

where $C(t, \omega, \zeta)$ is the cyclic, harmonic response when $x_f = 0$ and $\varphi = 0$.

From Eq. (7.56) the DMF theoretically goes to infinity as damping goes to zero and $\omega = \omega_n$, since the maximum amplitude at resonance equals

$$\text{DMF} = \frac{x_{max} \cdot k'}{F} = \frac{1}{2 \cdot \zeta'} \qquad \text{US (7.56)}$$

7.2.5.3 Frequency Effects on the DMF During SDOF Load-Controlled Vibration

Example 7.7 Demonstrate the effects of the excitation frequency for a SDOF response.

Fig. 7.13 provides examples for the effects of forcing frequency, where different ratios of forcing frequency to the SDOF frequency are shown. Vibrations with common damping values of 1% are displayed for values of $\omega/\omega_n = 0.5$ and $\omega/\omega_n \approx 1.0$. A unit displacement, $1 = k'/F_0$, is used to simplify Fig. 7.13, although unit displacement is atypical for most systems. Effects on both amplitude and phase are readily observed, since only the frequency of the impressed force is altered for the figure. For 1% damping, the amplitude, x_{max} increases, such that DMF = 1.3 at point B and DMF = 50 at point A when ω/ω_n is doubled from 0.5 to 1.0. That is, the amplitude due to static deflection loading increases by a factor of 50 for 1% damping when the excitation frequency equals the SDOF frequency. This large increase in amplitude clearly demonstrates the impact of resonance on system response. In short, when the ratio of frequencies decreases, so does the amplitude of the vibrations.

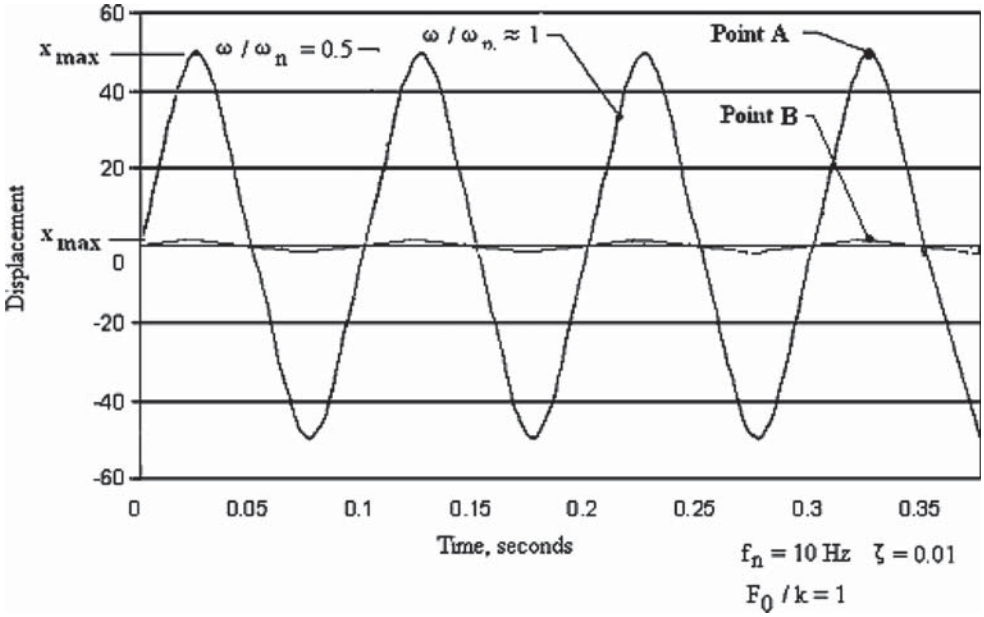


FIG. 7.13 EXAMPLE OF STEADY-STATE, LOAD-CONTROLLED VIBRATIONS, EQ. (7.54)

7.2.5.4 DMF for SDOF Load Control To visualize the DMF over a range of frequencies and damping ratios, nondimensional DMFs are typically presented in graphic formats (Leishear [211]). An expression for the DMF is derived from Eq. (7.55) ($t = 0$, $x = x_f = 0$, $\varphi = 0$), such that

$$\text{DMF} = \frac{x_{max} \cdot k'}{F} = \frac{1}{\sqrt{\left(1 - \left(\frac{\omega}{\omega_n}\right)^2\right)^2 + \left(\frac{2 \cdot \zeta \cdot \omega}{\omega_n}\right)^2}} \quad \text{U (7.57)}$$

Fig. 7.14 logarithmically shows DMFs as functions of forcing frequency and damping, and Fig. 7.15 shows the same data to scale.

7.2.6 Multi-DOF Harmonic Response

For harmonic responses, operating near or above a critical frequency ($\omega = \omega_n$) results in magnified displacements, and in many cases results in equipment damage. Operating midway between resonant vibrations decreases the vibrations, but vibrations may, or may not, be adequately reduced. Classic SDOF approximations of Fig. 7.15 inadequately describe higher mode frequency effects, and graphs provided here attempt to clarify this shortcoming in previous vibration theory. In short, new theory advances the understanding of DMFs with respect to multi-DOF systems by providing simplified graphs, which can be used to understand the overall system dynamics associated with higher mode frequencies in structures.

7.2.6.1 Multi-DOF Load Control Structures are multi-DOF systems, where the degrees of freedom are represented by a series of natural frequencies at which a structure vibrates, $\omega_i = \omega_1, \omega_2 \ldots \omega_\infty$. For the case of linear damping, the equations of motion are uncoupled. That is, each higher-mode frequency of a system may be considered independently using the principle of superposition (see paragraph 7.3.1). Equations to describe higher mode DMFs are presented here for load-controlled vibrations of springs, rods, and simply supported beams to investigate modal effects on structural response.

For load-controlled vibrations, each modal vibration is described by a sin response, where

$$m \cdot \frac{d^2 x_i}{dt^2} + 2 \cdot \zeta \cdot \omega \cdot \frac{dx_i}{dt} + \omega \cdot x_i = F \cdot \sin(\omega \cdot t) \cdot g \quad \text{US (7.58)}$$

$$\frac{x(t) \cdot k'}{F} = \frac{\sin(\omega \cdot t - \theta)}{\sqrt{\left(1 - \left(\frac{\omega_k}{\omega_i}\right)^2\right)^2 + \left(\frac{2 \cdot \zeta \cdot \omega_k}{\omega_i}\right)^2}} \quad \text{US (7.59)}$$

where ω_i are frequencies associated with each mode numbers, i, and ω_k are the forcing frequencies with mode numbers, k. These equations are used here to describe the maximum response of springs, axially loaded rods, and simply supported beams. Although damping may vary as frequency increases, a constant damping ratio is assumed here for illustrative purposes (see paragraph 7.2.1.3).

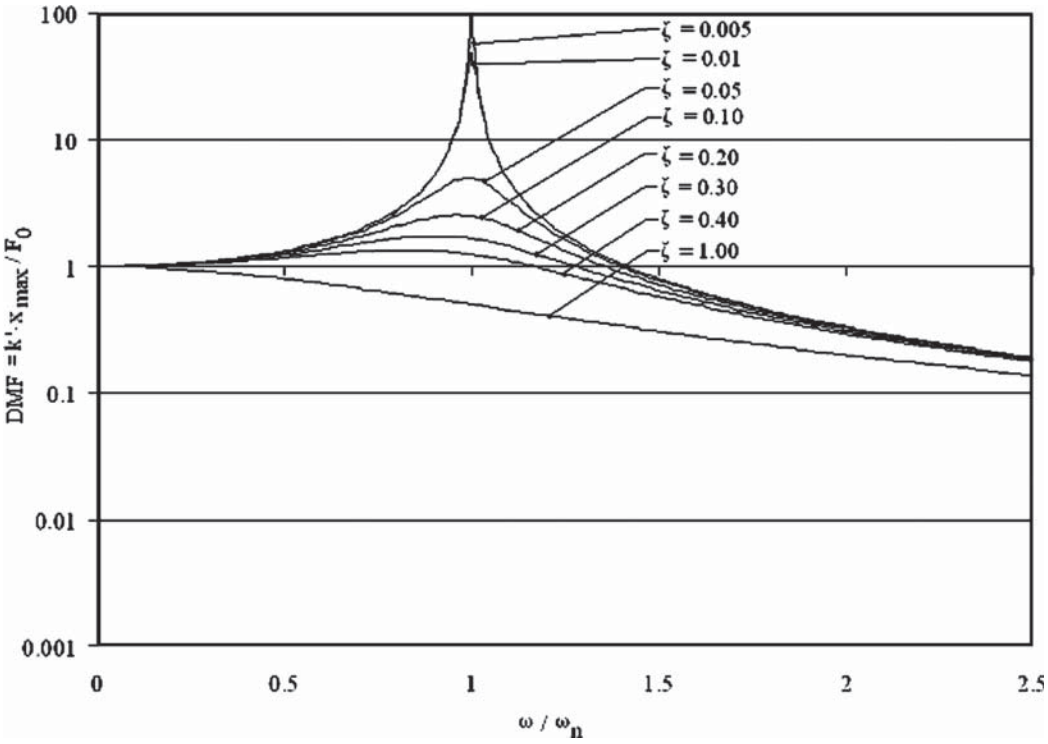


FIG. 7.14 DMF FOR STEADY-STATE LOAD CONTROL (LOG SCALE), EQ. (7.57)

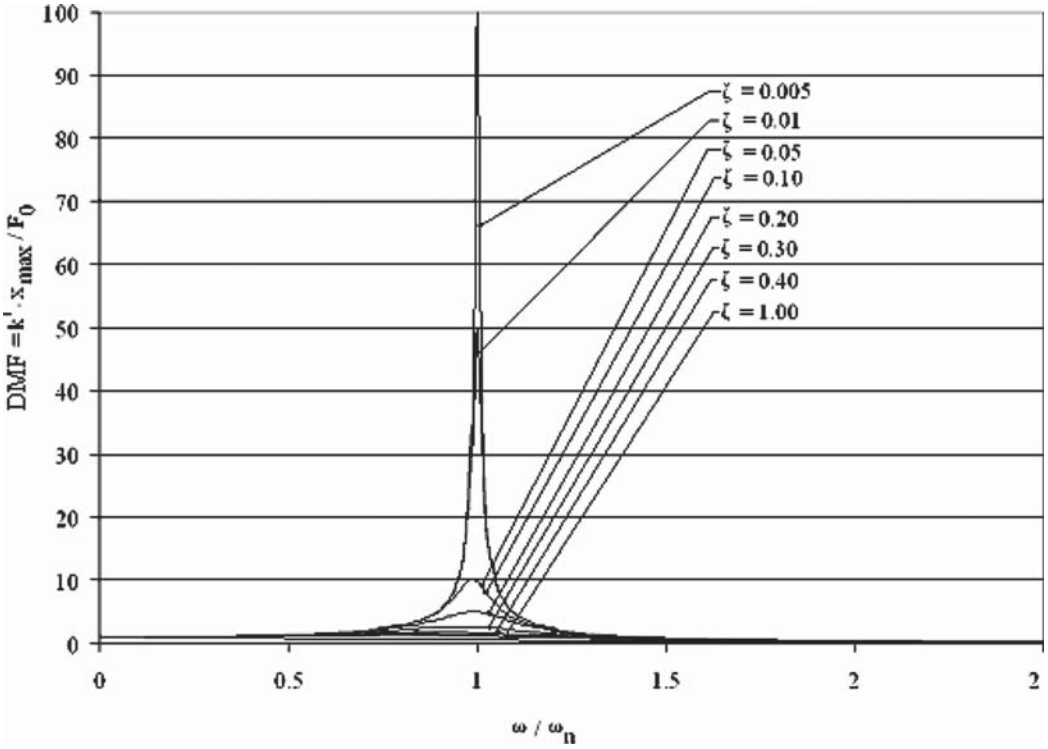


FIG. 7.15 DMF FOR STEADY-STATE LOAD CONTROL (LINEAR SCALE), EQ. (7.58) (Thomson [212])

7.2.6.2 Modal Contributions for Multi-DOF Vibrations As shown in Fig. 7.16, the discrete modal vibration magnitudes add to yield the total vibration. Long recognized in the literature, modal participation factors approximate the contribution of each of these modes to the total vibration. Also in Fig. 7.16, the raw complex vibration signal represents the effects of other vibrations, which is the definition of the participation factor.

7.2.6.3 Participation Factors for SDOF Vibrations

Example 7.8 Determine the effects of higher-mode frequencies on a spring.

Fig. 7.17 shows the contribution of other vibration frequencies on the first-mode frequency. This contribution to the overall vibration is sometimes referred to as a participation factor. Also of significance to this work: 1) Note that the primary response to impacts and step forcing functions occurs in the first mode, and 2) Note that the assumption that the effects of higher-mode frequencies may be neglected is in error by 8% for this example.

To obtain Fig. 7.17 by considering the effects due to other modes on a primary mode of vibration for springs, first substitute and rewrite Eq. (7.59) to describe each modal response, such that

$$\sum_{i=1}^{\infty}\frac{x_i\cdot k'}{F}\approx\sum_{i=1}^{25}\frac{x_i\cdot k'}{F}=\sum_{i=1}^{25}\frac{\sin\left(\omega\cdot t-\theta\right)}{\sqrt{\left(1-\left(\frac{\omega_k}{\omega_i}\right)^2\right)^2+\left(\frac{2\cdot\zeta\cdot\omega_k}{\omega_i}\right)^2}} \qquad \text{US (7.60)}$$

where the mode number of participating vibrations, i = 1,…25, was selected for accuracy. That is, the total vibrations for the first 25 modes of vibration are shown in Fig. 7.17, along with the first four vibration modes. Setting $F/k'_1 = x = 1$, the first mode of a spring, i is a function of ω, such that

$$\frac{\omega^2}{\omega_i^2}=\frac{1}{i^2} \qquad \text{US (7.61)}$$

For example, to find the effect of the second mode on the first mode, the relationship between i and ω is

$$\frac{\omega^2}{\omega_i^2}=\frac{\omega_1^2}{\omega_2^2}=\frac{1}{2^2} \qquad \text{US (7.62)}$$

Substitution of Eq. (7.61) into Eq. (7.60) yields the resonant response for the first mode coupled with participating vibrations from the first 25 modes of a spring (Fig. 7.17), where

$$\sum_{i=1}^{25}\frac{x_{i,\max}\cdot k'}{F}\approx \text{DMF}=1+\sum_{i=1}^{25}\left(\frac{1}{\sqrt{\left(1-\left(\frac{1}{i}\right)^2\right)^2+\left(\frac{2\cdot\zeta\cdot 1}{i}\right)^2}}\right)-1 \qquad \text{US (7.63)}$$

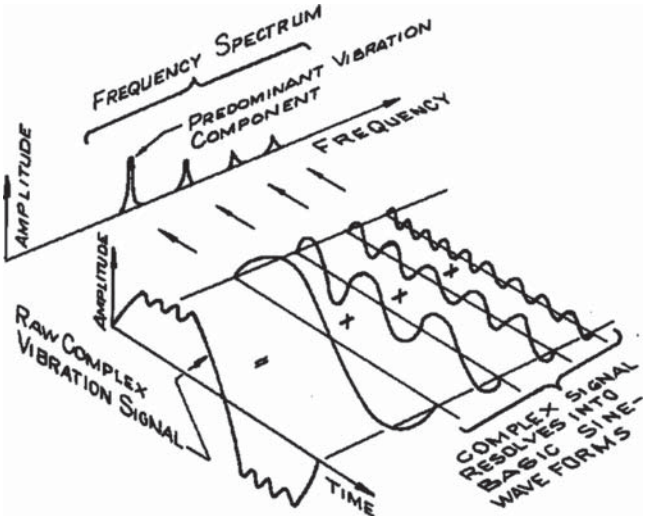


FIG. 7.16 MODAL VIBRATION FREQUENCIES
(Reprinted by permission of Taylor and Francis Group, LLC., Karassik [53])

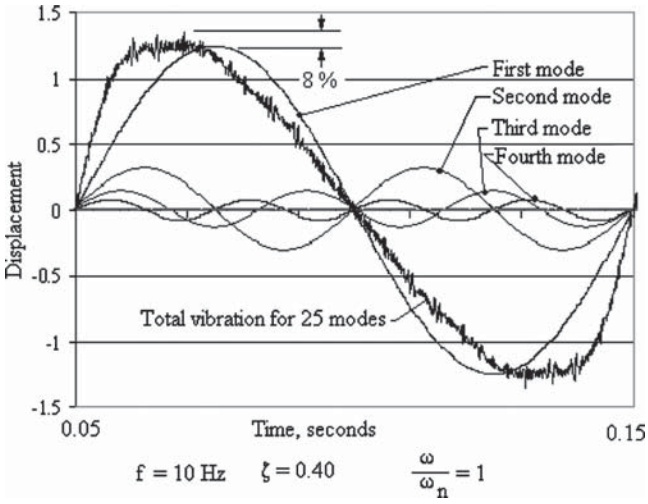


FIG. 7.17 EFFECTS OF HIGHER-MODE FREQUENCIES ON THE FIRST-MODE FREQUENCY OF A SPRING, EQ. (7.63)

7.2.6.4 Resonance for Multi-DOF Vibrations Resonance occurs for each mode, and as the excitation frequency increases, different modes are excited. To relate DMFs for multiple modes, the vibrations need to be reconsidered. Each of the resonant vibrations is

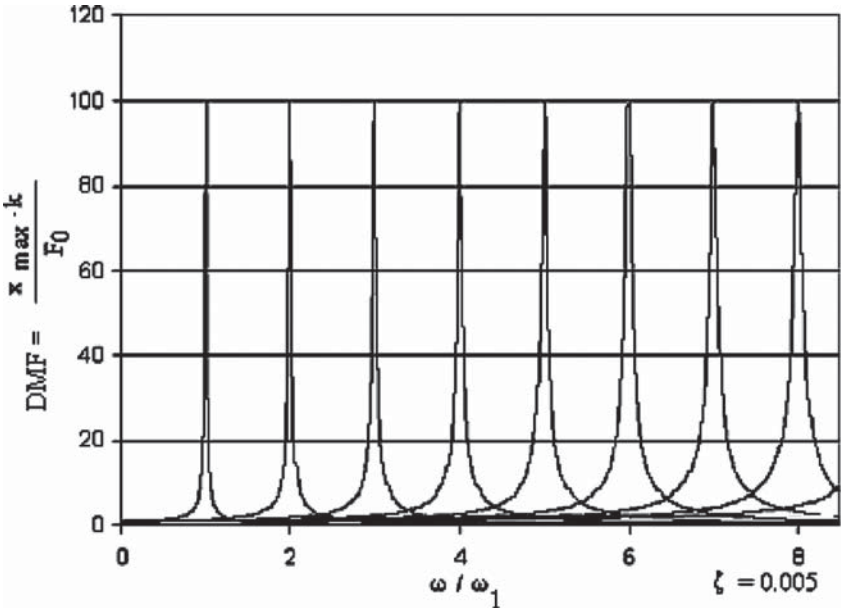


FIG. 7.18 EXAMPLE OF MODAL FREQUENCIES FOR MULTI-DOF LOAD CONTROL, EQ. (7.64)

first considered separately, as shown in Fig. 7.18. To accumulate the resonant frequency effects for a spring, Fig. 7.19 adds the DMFs as higher-mode frequencies are excited for an example where $\xi = 0.005$. Fig. 7.20 combines the results of Fig. 7.19 with the responses for other values of ξ, where Fig. 7.20 provides predictions for the DMF of a spring, which includes the spring response throughout a range of different modal excitation frequencies. The derivations for the equations to prepare Figs. 7.18 through 7.20 follow with an example of their use.

As noted, each of the resonant frequencies is first plotted in Fig. 7.18, where Eq. (7.60) is rewritten for any modal response as

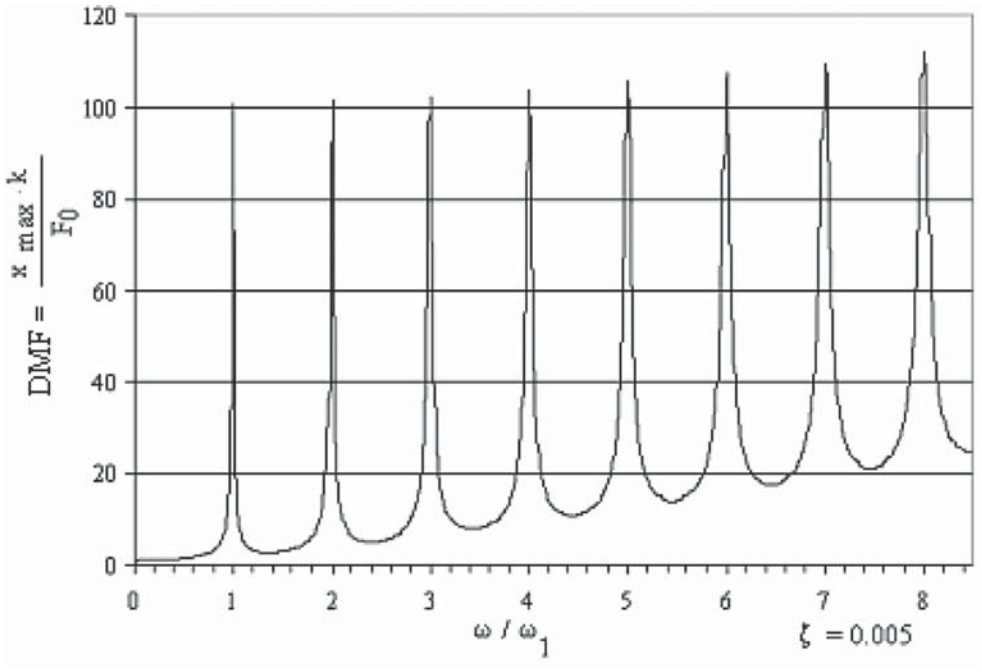


FIG. 7.19 DMF EXAMPLE FOR MULTI-DOF LOAD CONTROL, EQ. (7.65)

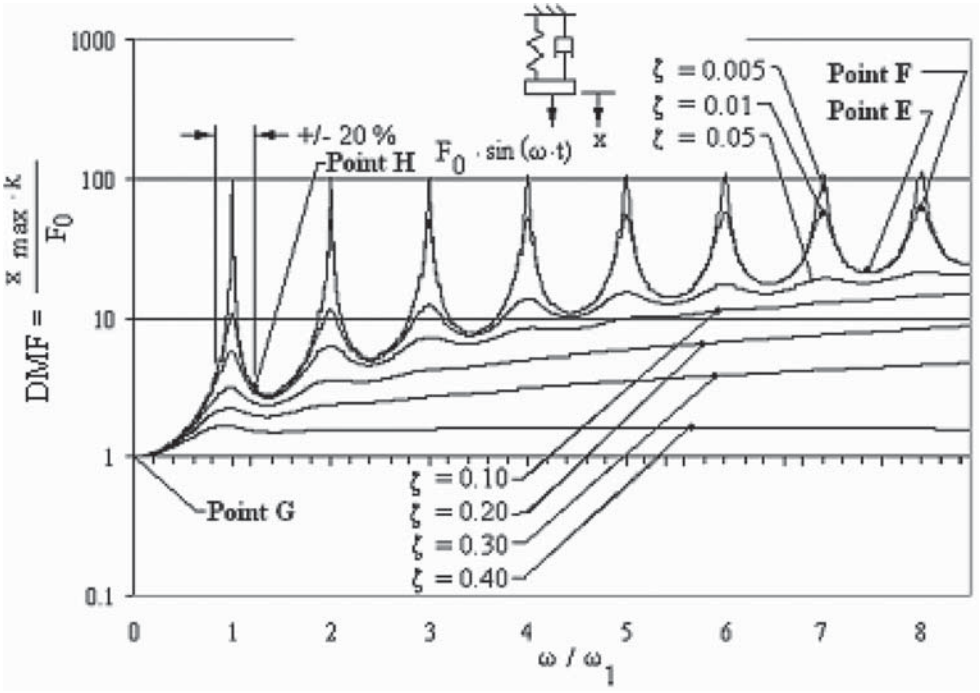


FIG. 7.20 MULTI-DOF DMF LOAD CONTROL OF A SPRING, EQ. (7.65)

$$\frac{x_{i,\max}\cdot k'}{F}\approx 1+\sum_{i=1}^{25}\left(\left(\frac{1}{\sqrt{\left(1-\left(\frac{\omega_k}{\omega_i}\right)^2\right)^2+\left(\frac{2\cdot\zeta\cdot\omega_k}{\omega_i}\right)^2}}\right)-1\right) \quad \text{US (7.64)}$$

where k is the mode number of the excitation frequency and $\omega = \omega_k$. Then, for the first eight nodes of the forcing functions, $k = 1,\ldots 8$, and

$$\sum_{k=1}^{8}\sum_{i=1}^{25}\frac{x_{i,\max}\cdot k'}{F}\approx \text{DMF}$$

$$=1+\sum_{k=1}^{8}\sum_{i=1}^{25}\left(\left(\frac{1}{\sqrt{\left(1-\left(\frac{\omega_k}{\omega_i}\right)^2\right)^2+\left(\frac{2\cdot\zeta\cdot\omega_k}{\omega_i}\right)^2}}\right)-1\right) \quad \text{US (7.65)}$$

Example 7.9 Consider the effects of exciting a spring at different frequencies.

Assume that a cyclic force is applied to a spring, and vary the excitation frequency. Consider initial operation at point F in Fig. 7.20, where the DMF equals 62 at $\xi = 1\%$ due to an eighth mode excitation frequency. If the excitation frequency is changed to $\omega/\omega_k = 7.5$ at point E, the DMF is reduced from 62 for resonance at point F to 21 at point E. In other words, vibrations can be reduced by operating at point E, but vibration magnitudes are still significant. If the forcing frequency can be reduced to Point H, the DMF = 3.4, and vibration is significantly reduced. Point G represents static design. Overall, Fig. 7.20 provides a means to assess the DMF across a range of forcing frequencies for multi-DOF springs.

7.2.6.5 Load-Controlled Vibrations for Rods SDOF vibrations are similar to vibrations of axially loaded rods or transversely loaded beams. A rod that is fixed at one end and free to move at the other end is considered here. The participation factor for the first mode frequency is shown in Fig. 7.21, and the multi-DOF response to a range of forcing functions is expected to be similar to Fig. 7.19, as shown in Fig. 7.22. Note that the response at the even-numbered antinodes ($\omega = \omega_k$, $k = 0, 2, 4,\ldots$) is significantly less than the response at the odd-numbered nodes ($\omega = \omega_k$, $k = 1, 3, 5,\ldots$).

To calculate the DMF for a rod, use Eq. (7.60) and substitute

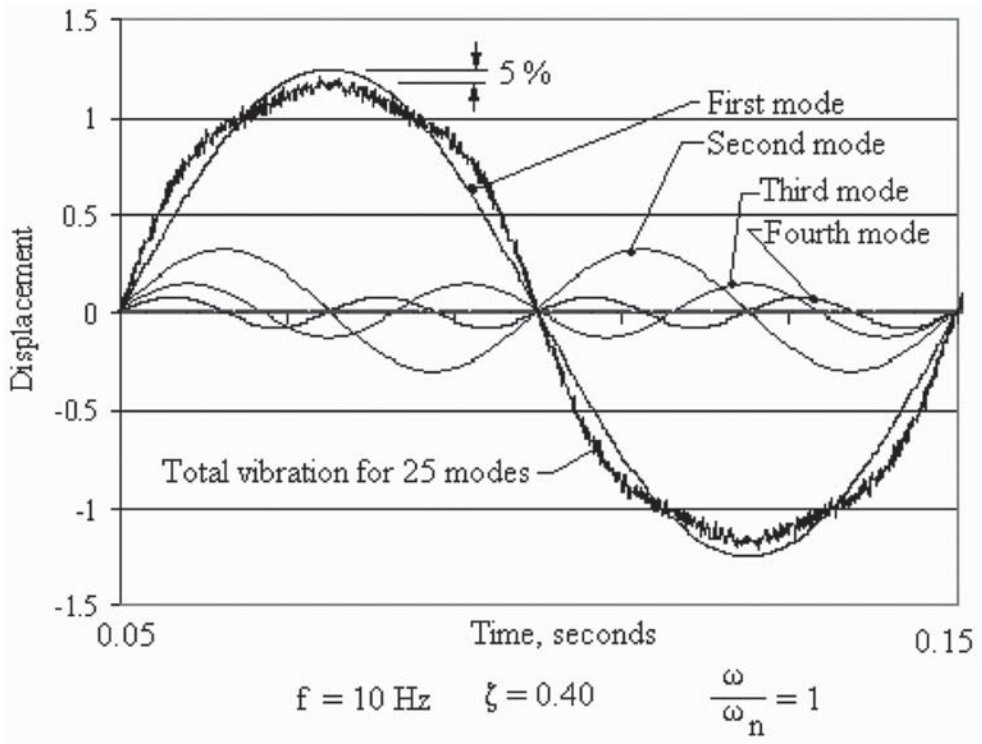


FIG. 7.21 EFFECTS OF HIGHER MODES ON THE FIRST MODE RESPONSE OF A LOADED ROD, EQ. (7.68)

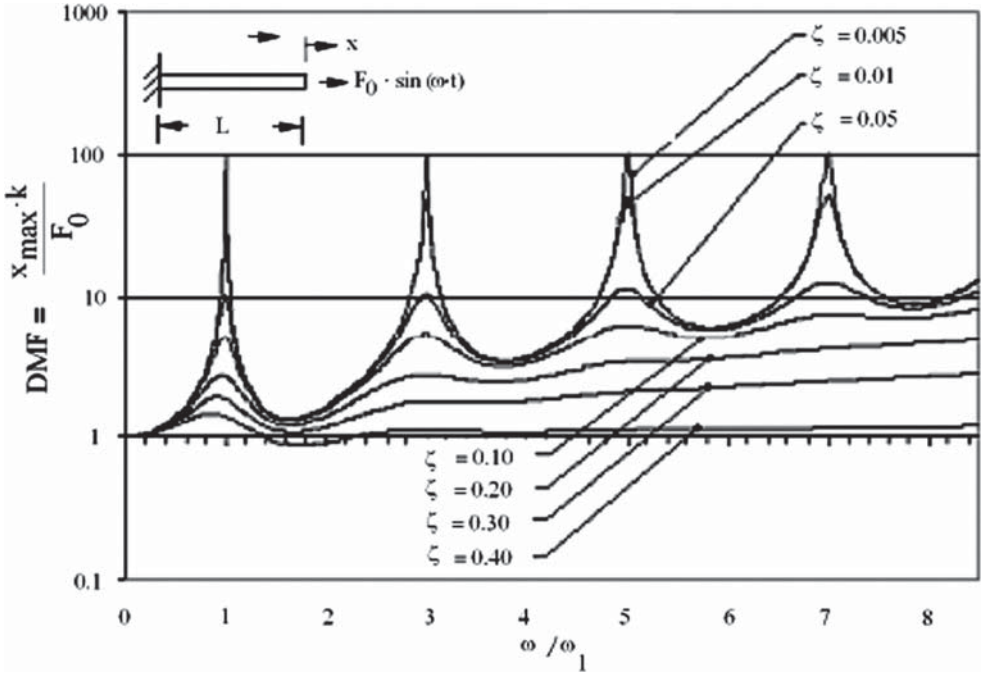


FIG. 7.22 DMFS FOR AN AXIALLY LOADED ROD

$$\omega_i = \frac{(2\cdot i - 1)\cdot \pi}{2\cdot L}\cdot\sqrt{\frac{E}{\rho}} \qquad \text{US (7.67)}$$

Then, the effects of higher modes with respect to the first mode of a rod may be expressed as (Leishear [211])

$$\frac{x_{i,\max}\cdot k'}{F} \approx 1+\sum_{i=1}^{25}\left(\left(\frac{1}{\sqrt{\left(1-\left(\frac{1}{(2\cdot i)-1}\right)^2\right)^2+\left(\frac{2\cdot\zeta\cdot 1}{(2\cdot i)-1}\right)^2}}\right)-1\right) \qquad \text{US (7.68)}$$

7.2.6.6 Load-Controlled Vibrations for Beams The response for beams with different types of end supports can be evaluated using the techniques presented here, but this discussion is limited to the case of a beam with pinned, or hinged, supports. The response of a beam simply supported at both ends, subjected to higher-mode excitations, is shown in Fig. 7.23. For this case, the mode shape and frequencies are listed by Pilkey [99], such that

$$\text{beam deflection mode shape} = \sin\left(\frac{i\cdot\pi\cdot z}{L}\right) \qquad \text{US (7.69)}$$

$$\omega_i = \frac{(i\cdot\pi)^2}{L^2}\cdot\sqrt{\frac{E\cdot I}{\rho}} \qquad \text{US (7.70)}$$

Then, the effect of higher modes with respect to the first mode of a simply supported beam may be expressed as the sum of several resonant responses. (Leishear [211]). A significant implication of these results is that changing the forcing frequency can reduce the response, but a static response can only be obtained at static conditions.

$$\sum_{i=1}^{75}\frac{x_{i,\max}\cdot k_i}{F_0} \approx DMF = \left|1+\sum_{i=1}^{\infty}\left(\left(\frac{1}{\sqrt{\left(1-\left(\frac{1}{i^2}\right)^2\right)^2+\left(\frac{2\cdot\zeta\cdot 1}{i^2}\right)^2}}\right)-1\right)\right| \qquad \text{US (7.71)}$$

Example 7.10 Consider resonant effects of a pipe excited by pump vibrations.

For example, consider a pipe attached to a motor, and assume that the pipe response approximates a free-end beam and that damping is 1%. Further assume that a forcing frequency is induced by vibration from a motor and pump attached to a pump system near higher-mode beam frequency. Changing the motor speed will change the

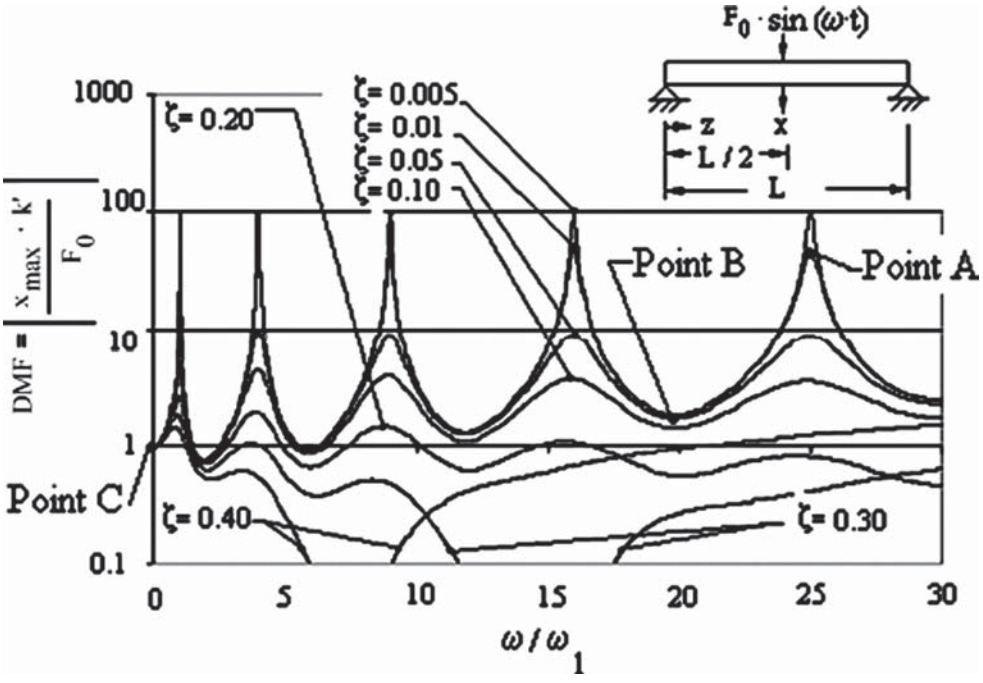


FIG. 7.23 DMFS FOR A SIMPLY SUPPORTED BEAM

pipe response from point A to point B in Fig. 7.23, and the beam vibrations are reduced substantially: from DMF = 21 to DMF = 3.4, but the vibrations and consequent stresses are still several times the static stress. Comparable results may be obtained by assuming that the pipe is fixed at both ends. In practice, excited pipe frequencies are typically expected for first- and second-mode responses, but higher modes may be excited in some cases.

7.3 DYNAMIC STRESS EQUATIONS

The dynamic stress equation provides a simplified expression for the response of simple systems, such as pipes, beams, or pipe supports. A general expression for the DMF of a SDOF structure is

$$V''(t) = \frac{x''(t) \cdot k''}{F} \qquad \text{US (7.72)}$$

where $V''(t) = S(t)$, $I(t)$, $R(t)$, or $C(t)$. Responses other than the step, impulse, ramp, or harmonic responses may be derived as required from Harris [213].

The derivation of the dynamic stress equation follows. The spring force is defined as

$$F = k'' \cdot \Delta x'' \qquad \text{US (7.73)}$$

where k'' is the spring constant in units of lbf/in., and $\Delta x''$ is the displacement in inches. The strain in an object equals

$$\Delta x'' / x'' = \varepsilon \qquad \text{US (7.74)}$$

Combining Eq. (7.73) with Eq. (7.74)

$$F = k'' \cdot \Delta x = k'' \cdot x \cdot \varepsilon = k'' \cdot x'' \cdot \mathrm{St}/E \qquad \text{US (7.75)}$$

Hooke's Law states that

$$\mathrm{E} = \sigma'/\varepsilon \qquad \text{US (7.76)}$$

The static stress in an object, σ', equals

$$\sigma' = \frac{F}{A} \qquad \text{US (7.77)}$$

Assuming a unit cross-sectional area, and substituting Eqs. (7.75) and (7.77) into Eq. (7.72) yields

$$\sigma(t) = \sigma' \cdot V''(t) \qquad \text{US (7.78)}$$

which is the general equation for a dynamic stress for a SDOF system. Note that the inherent errors are approximately ±10%, since higher-mode frequencies are neglected in Eq. (7.78). The errors due to higher-mode frequencies are considered in paragraphs 7.2.6.3 and 7.2.6.5.

The dynamic stress equation (Eq. 7.78) is the crux of this text, where the equation is used to relate static piping design principles to dynamic pipe stresses for the evaluation of pipe design and pipe failures. The remainder of this text focuses on considering this equation to describe different dynamic pipe stresses. The step response provides an important example of the dynamic stress equation for this work, where the step response approximates suddenly applied constant loads to pipes, which are characteristic of some water hammer loads. Equations (7.44) and (7.78) combine to yield

$$\sigma(t) = \sigma' \cdot \left(1 - \frac{e^{-\zeta \cdot \omega \cdot t}}{\sqrt{1-\zeta^2}} \cdot \cos\left(t \cdot \omega \cdot \sqrt{1-\zeta^2} \right) - a\tan\left(\frac{\zeta}{\sqrt{1-\zeta^2}} \right) \right) \qquad \text{US (7.79)}$$

where $\sigma(t)$ is the dynamic stress, and σ' is a static stress.

7.3.1 Triaxial Vibrations

Triaxial vibrations need consideration, even though coordinate axes were neglected above to simplify discussions and notations. As an example, the step vibration response of Eq. (7.79) is rewritten as

$$\sigma_j(t) = \sigma'_j \cdot \left(1 - \frac{e^{-\zeta_j \cdot \omega_j \cdot t}}{\sqrt{1-\zeta_j^2}} \cdot \cos\left(t \cdot \omega_j \cdot \sqrt{1-\zeta_j^2} \right) - a\tan\left(\frac{\zeta_j}{\sqrt{1-\zeta_j^2}} \right) \right) \qquad \text{US (7.80)}$$

where j describes orthogonal directions, and $j = x, y, z$ or $j = r, \theta, z$.

The fact is that vibrations in a structure affect each other and are said to be coupled vibrations. To use the dynamic stress equation as written, the vibrations need to be uncoupled. Otherwise, matrix techniques must be employed to analyze vibrations, where Meirovitch [215] provided a comprehensive discussion of these techniques, and matrix techniques are also the basis of FEA structural models, which are outside the scope of this work. To use SDOF models and apply the principle of superposition, the equation of motion requires further consideration to uncouple orthogonal vibrations. Rewriting Eq. (7.21) in terms of a displacement, δ_j,

$$m \cdot \frac{\mathrm{d}^2\delta_j}{\mathrm{d}t^2} + 2 \cdot \zeta_j \cdot \omega_j \cdot \frac{\mathrm{d}\delta_j}{\mathrm{d}t} + \omega_j^2 \cdot \delta_j = F(t) \cdot g \qquad \text{US (7.81)}$$

There are two methods to uncouple Eq. (7.81):

1) If the frequencies are significantly different, then, the vibrations have a negligible effect on each other. For example, through-wall radial vibrations have much higher frequencies than hoop vibrations (paragraph 8.2). Consequently, when the hoop vibrations obtain maximum amplitudes, the radial vibrations are already damped to a static value, and the radial and hoop stresses are therefore uncoupled. Similarly, hoop vibrations have much higher frequencies than bending vibrations, and the hoop vibrations are damped when the maximum bending vibration amplitudes occur. In short, through-wall vibrations, hoop vibrations, and bending vibrations may be uncoupled and considered separately. Uncoupling Eq. (7.81), the step responses for stresses (Eq. (7.80)) may be expressed as

$$\sigma_\theta(t) = \sigma'_\theta \cdot \left(1 - \frac{e^{-\zeta_\theta \cdot \omega_\theta \cdot t}}{\sqrt{1-\zeta_\theta^2}} \cdot \cos\left(t \cdot \omega_\theta \cdot \sqrt{1-\zeta_\theta^2} \right) - a\tan\left(\frac{\zeta_\theta}{\sqrt{1-\zeta_\theta^2}} \right) \right) \quad \text{US (7.82)}$$

$$\sigma_r(t) = \sigma'_r \cdot \left(1 - \frac{e^{-\zeta_r \cdot \omega_r \cdot t}}{\sqrt{1-\zeta_r^2}} \cdot \cos\left(t \cdot \omega_r \cdot \sqrt{1-\zeta_r^2} \right) - a\tan\left(\frac{\zeta_r}{\sqrt{1-\zeta_r^2}} \right) \right) \quad \text{US (7.83)}$$

$$\sigma_b(t) = \sigma'_b \cdot \left(1 - \frac{e^{-\zeta_b \cdot \omega_b \cdot t}}{\sqrt{1-\zeta_b^2}} \cdot \cos\left(t \cdot \omega_b \cdot \sqrt{1-\zeta_b^2} \right) - a\tan\left(\frac{\zeta_b}{\sqrt{1-\zeta_b^2}} \right) \right) \quad \text{US (7.84)}$$

where the subscripts r and θ are the radial and circumferential hoop directions, respectively, and the subscript b represents bending. Note that Eqs. (7.82) through (7.86) are applicable to step, impulse, and ramp responses but may have exceptions when harmonic responses are considered due to resonant responses at different forcing frequencies.

2) If the damping ratios are the same in each direction, the equation of motion is uncoupled. For example, when $\zeta = 0$, all vibration equations are uncoupled since the damping ratios are identical. A tacit assumption for SDOF and many FEA models is that damping is constant, which is typically not true. However, for bending in pipe systems, approximations hold this assumption to be reasonable, where an approximation for damping of 2% for pipes under 12 in. in diameter, or 3% for pipes over 12 in., is was assumed in earlier versions of Section VIII for bending and torsional vibrations. Using this constant damping assumption, bending, torsion, and axial vibrations may be uncoupled. Uncoupled vibrations for torsion and axial stresses are expressed as

$$\sigma_T(t) = \sigma'_T \cdot \left(1 - \frac{e^{-\zeta_T \cdot \omega_T \cdot t}}{\sqrt{1-\zeta_T^2}} \cdot \cos\left(t \cdot \omega_T \cdot \sqrt{1-\zeta_T^2} \right) - a\tan\left(\frac{\zeta_T}{\sqrt{1-\zeta_T^2}} \right) \right) \quad \text{US (7.85)}$$

$$\sigma_z(t) = \sigma'_z \cdot \left(1 - \frac{e^{-\zeta_z \cdot \omega_z \cdot t}}{\sqrt{1-\zeta_z^2}} \cdot \cos\left(t \cdot \omega_z \cdot \sqrt{1-\zeta_z^2} \right) - a\tan\left(\frac{\zeta_z}{\sqrt{1-\zeta_z^2}} \right) \right) \quad \text{US (7.86)}$$

where the subscript z is the axial direction, and the subscript T represents torsion. The basis for 2% to 3% damping in pipe systems is discussed in the following paragraphs, along with other considerations of damping.

7.3.2 Damping

A discussion of damping could have been provided throughout the text as needed, but is presented here in one place to focus the topic. Damping is required to more accurately predict pipe stresses for fatigue analysis and to evaluate experimental results, but to only determine a maximum overload pipe stress, an upper bound for the maximum stress can be obtained by neglecting damping. Different types of damping mechanisms are discussed here, which are pertinent to the response of pipe systems during a water hammer event.

7.3.2.1 Proportional Damping Rayleigh proportional damping provides some insight into the nature of damping and is described by rewriting the equation of motion (Eq. (7.17)) as

$$m \cdot \frac{d^2x}{dt^2} + \left(\alpha \cdot m + \beta \cdot k' \right)' \cdot \frac{dx}{dt} + k' \cdot x = F(t) \cdot g \quad \text{US (7.87)}$$

$$c = \alpha \cdot m + \beta \cdot k' \quad \text{US (7.88)}$$

where ά is a mass proportional damping coefficient, and β is a stiffness proportional damping coefficient. Damping for all modal frequencies is then found to be

$$\zeta_i = \frac{\alpha}{2 \cdot \omega_i} + \beta \cdot \omega_i \qquad \text{US (7.88)}$$

Note that for proportional damping, the stiffness of the structure dominates the damping response as the frequency increases and also note that higher-mode frequencies are damped more than lower-mode frequencies.

7.3.2.2 Structural Damping for Pipe Systems For structural materials, frequency has been shown to have little effect on damping. Meirovitch [215] provided detailed discussion of structural damping, which is simplified here using Eq. (7.87). Neglecting mass proportional damping, ά = 0 and neglecting frequency effects

$$m \cdot \frac{d^2x}{dt^2} + \frac{\beta}{\omega} \cdot \frac{dx}{dt} + k' \cdot x = F(t) \cdot g \qquad \text{US (7.90)}$$

$$\zeta_i = \frac{0}{2 \cdot \omega_i^2} + \beta \cdot \frac{\omega_i}{\omega_i} = \beta_i = \zeta_s \qquad \text{US (7.91)}$$

There are different methods to determine structural damping ratios, ξ_s. One is an analytical method developed by Lazan [216], and the other is a statistical method developed by Hadjian [216]. Thomson [218] recommended a 0.01 damping ratio for high-frequency acoustic vibrations in aircraft.

In the early 1980s, ASME, Section VIII, Division 1 provided a 2% damping ratio for bending of pipes under 12 NPS and 3% damping for pipes over 12 NPS. However, those values have since been removed from the Code, and damping values for piping from ASCE-43 are specified as 5%.

More concise damping estimates are based on experimental data from Hadjian as shown in Fig. 7.24. This data was obtained from steam piping in power plants, where structural damping was the primary damping mechanism. These values are applicable to lower-frequency pipe responses due to earthquakes and, as such, are considered to be reasonable damping estimates for torsion and axial stresses as well as bending stresses. Statistical research investigated damping by considering the effects of welding, insulation, and miscellaneous loads, such as valves. Note that liquid in the pipe changes the frequency, but the damping ratio has only minor changes when the pipe is filled. To obtain a more concise estimate of damping than provided by ASCE-43, Hadjian's equations may be used.

$$\zeta_s = 0.0053 + 0.0024 \cdot D_{\text{nom}} + 0.0166 \cdot R + 0.009 \cdot F - 0.0019 \cdot L \qquad \text{US (7.92)}$$

where D_{nom} is the nominal pipe diameter, $R = 0$ if yielding occurs, $R = 1$ if there is no yielding, $F = 1$ for the first mode, $F = 0$ for all other modes, $L = 1$ if there are equipment or loads on the pipe, and $L = 0$ for no loads on the pipe. Eq. (7.92) is recommended for damping of through-wall radial stresses, where fluid damping is expected to be negligible since the contained fluid has a much lower frequency than the pipe wall. For heavily insulated piping,

$$\zeta_s = 0.0924 - 0.0074 \cdot D_{\text{nom}} - 0.022 \cdot H - 0.043 \cdot S \qquad \text{US (7.93)}$$

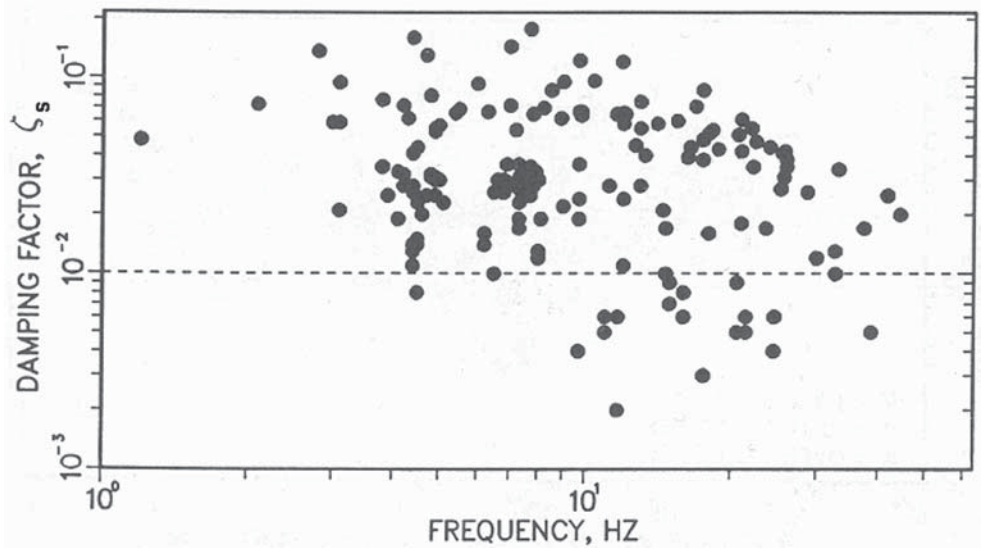


FIG. 7.24 DAMPING RATIOS IN POWER PLANT PIPING (Hadjian [216])

where $H = 0$ for the first mode, and $H = 1$ for all other modes, and $S = 1$ if snubbers are installed, and $S = 0$ if snubbers are not installed.

Also, for stiffness proportional damping, Lazan provided an empirical equation for structural damping for common structural materials, where

$$\varsigma_s = \frac{D \cdot E}{2 \cdot \pi \cdot S_r^2} \qquad \text{US (7.94)}$$

$$D = \left(\frac{S_r}{S_e}\right)^{2.3} + 6 \cdot \left(\frac{S_r}{S_e}\right)^{8} \qquad \text{US (7.95)}$$

$$S_r = 2 \cdot \alpha' \qquad \text{US (7.96)}$$

where D is the specific damping for a structural material, and E is the elastic modulus. The stress range, S_r, is the magnitude of the completely reversed stress in fatigue testing, and the fatigue limit is S_e. Experimental raw data for different structural materials is provided in Fig. 7.25, and Eq. (7.95) is shown for numerous structural materials and is recommended for damping of hoop stresses.

Also of note, Blevins [219] provided an excellent compilation of damping data for different structures, such as bridges, buildings, towers, piping, and heat exchanger tube banks. Some other structural damping values are available, where 0.5% to 6.0% damping is the range of damping values for steel structures, 7% to 145% is the range for concrete structures, 15% to 40% is the range for masonry structures (Pilkey [99]), and damping for helical springs drops below 0.005% (Harris and Piersol [213]). Note that the 145% damping ratio for concrete implies that a structure would be overdamped, and the DMF = 1 for a suddenly applied load (step response).

Also, Fig. 7.26 implies that damping for plastic stresses converges to DMF = 1, but experimental data for plastic response is limited. That is, the damping increases by a factor of 1000 between stress amplitudes equal to the fatigue strength up to nearly the ultimate strength.

7.3.2.3 Fluid Damping and Damping for Hoop Stresses The hoop stress is expected to be affected by damping from both the pipe wall and the fluid in the pipe, since the contained fluid has stiffness as it compresses. Damping is approximated in the form of a structural damping coefficient ζ_s, and a fluid damping coefficient, ζ_f, by assuming that

$$\zeta = 1/(1\zeta_f + 1/\zeta_s) \qquad \text{US (7.97)}$$

Eq. (7.97) is recommended and conservatively assumes that the water and pipe wall act as series springs. Another option is to assume that the pipe wall and contained liquid act as parallel springs, where

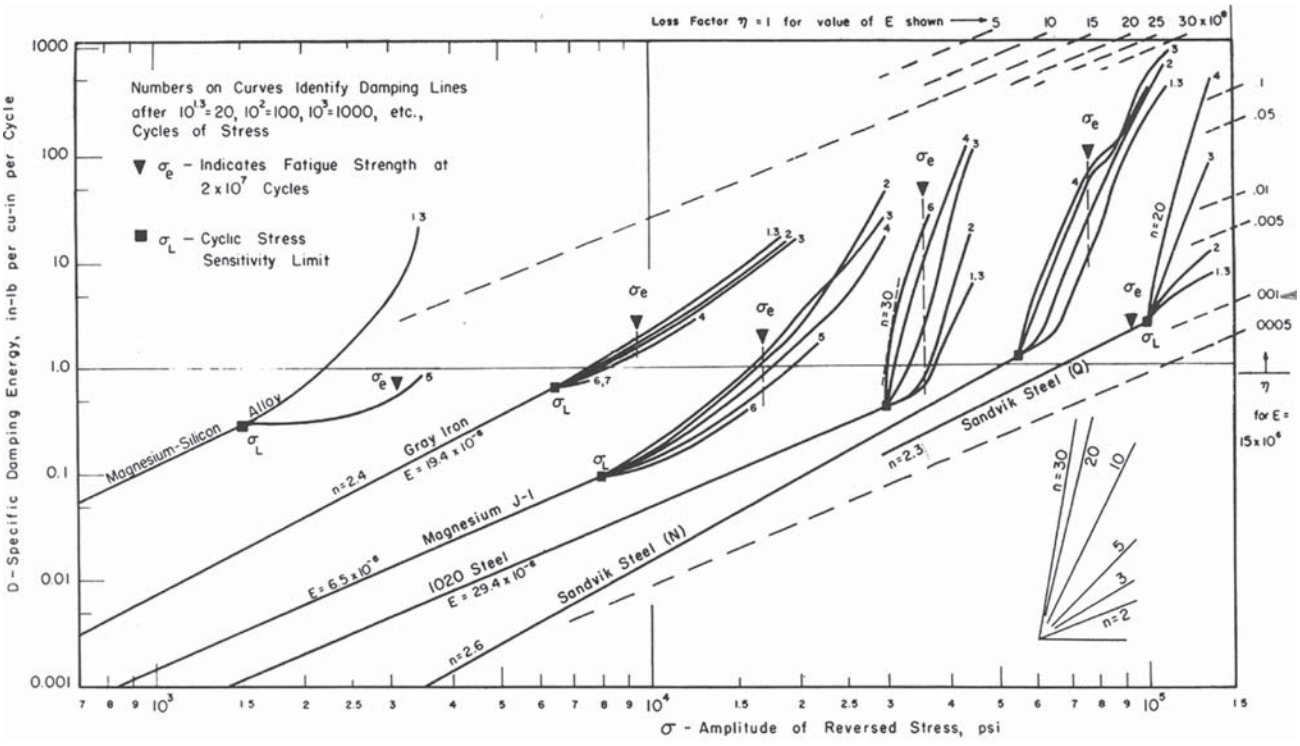


FIG. 7.25 EXPERIMENTAL DATA FOR STRUCTURAL DAMPING (Lazan [216])

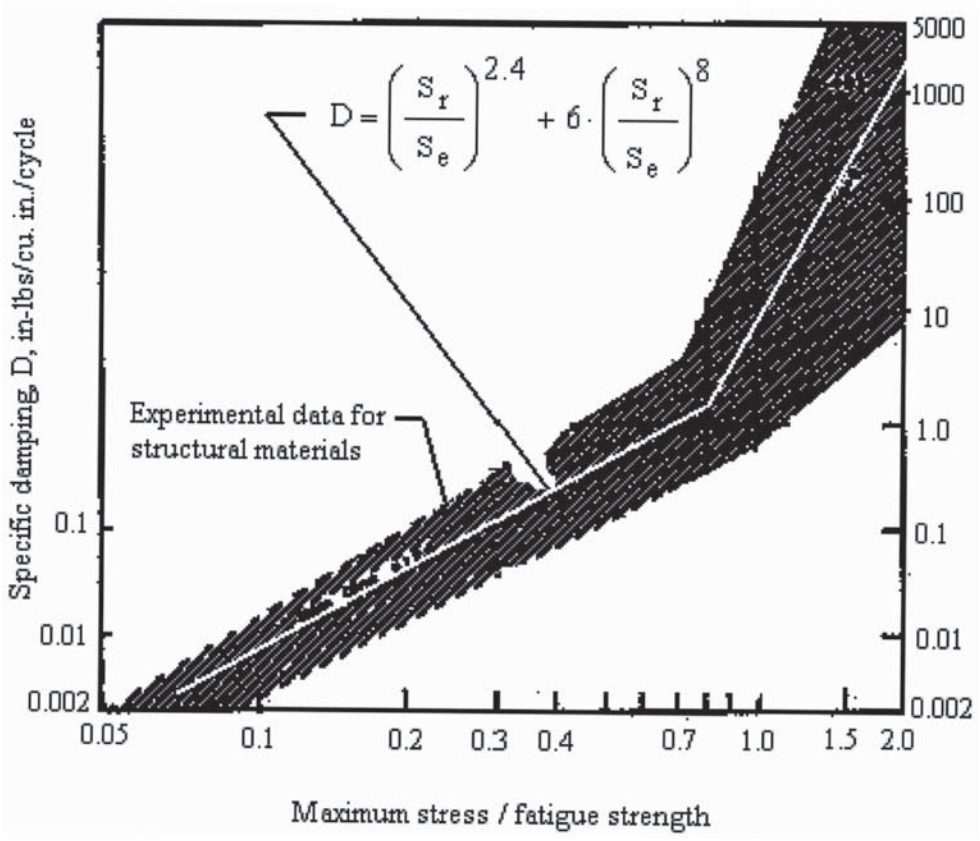


FIG. 7.26 DAMPING FOR STRUCTURAL MATERIALS (Lazan [216])

$$\zeta = \zeta_f + \zeta_s \qquad \text{US (7.98)}$$

The structural damping coefficient can be estimated from Eq. (7.94), and fluid damping coefficients were determined by relating the thermodynamic changes in the fluid properties to a dynamic magnification factor. To do so for a step response, a dynamic magnification factor is first expressed in terms of the percent overshoot (P.O.) as

$$\text{DMF} = 1 + \text{P.O.} = \left(1 + e^{\left[\frac{-\zeta \cdot \pi}{\sqrt{1-\zeta^2}}\right]}\right) \qquad \text{US (7.99)}$$

For critical damping, P.O. = 0, and DMF = 1, and adding the P.O. to one gives the DMF for the SDOF model, as shown in Fig. 7.27.

To apply thermodynamics to fluid damping, the Second Law of thermodynamic efficiency was considered where the efficiency is defined as the maximum work that can be obtained from a system (Wark [220]). Terms to relate thermodynamics to dynamics are shown in Fig. 7.28. For a compression cycle, the efficiency, ε', is defined as

$$\varepsilon' = \frac{\Delta h - T_0 \cdot \Delta s}{\Delta h} \qquad \text{US (7.100)}$$

where Δh is the change in enthalpy, Δs is the change in entropy, and T_0 is the ambient temperature. The thermodynamic properties are obtained at the initial or dead state, and the final or equilibrium state. Assuming the fluid properties to vary linearly, and only fluid damping is present, the maximum achievable stress must, of necessity, be governed by this Second Law relationship. In that case, the undamped maximum stress is related to the DMF as

$$2 \cdot \varepsilon' = \text{DMF} \qquad \text{US (7.101)}$$

Using Eqs. (7.97) or (7.98) and (7.100), the fluid damping can be determined. There may be other losses associated with cavitation at the pipe wall/fluid interface, but at a minimum, this fluid damping coefficient should be considered. Once the fluid damping coefficient is established, the structural damping coefficient can be considered. Expressing the percent overshoot, P.O., in terms of thermodynamic properties

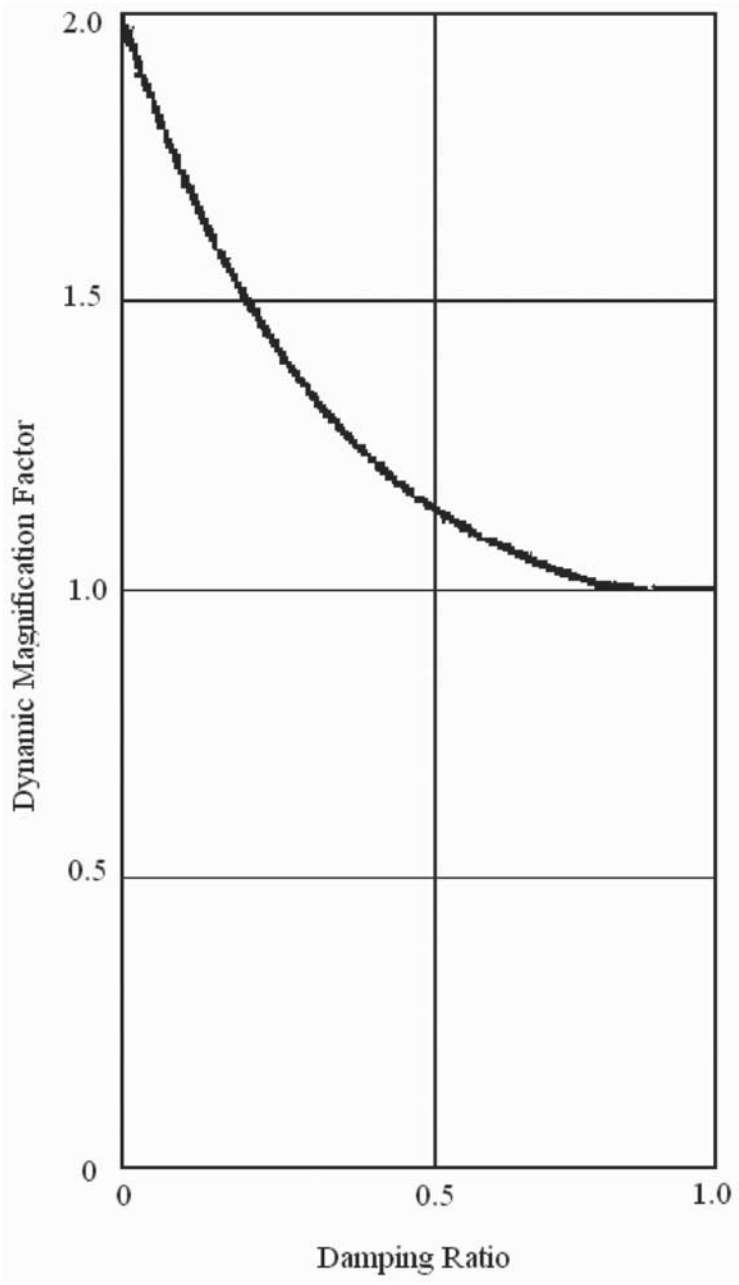


FIG. 7.27 DAMPING EFFECTS ON THE DYNAMIC MAGNIFICATION FACTOR

$$\varepsilon' = \frac{\Delta h - T_0 \cdot \Delta s}{\Delta h} \qquad \text{US (7.102)}$$

$$2 \cdot \varepsilon' = 1 + \text{P.O.} = \text{DMF} \qquad \text{US (7.103)}$$

Combining Eqs. (7.98) through (7.103),

$$\zeta_f = \frac{-\ln(\varepsilon')}{\left(\left(\ln(\varepsilon')^2 + \pi^2\right)^{\frac{1}{2}}\right)} \qquad \text{US (7.104)}$$

Substituting Eqs. (7.94) and (7.103) into Eq. (7.97), the total damping for hoop stresses in a fluid-filled pipe equals

$$\zeta = \frac{-\ln(\varepsilon')}{\left(\left(\ln(\varepsilon')^2 + \pi^2\right)^{\frac{1}{2}}\right)} + \frac{D \cdot E}{2 \cdot \pi \cdot S_r^2} \qquad \text{US (7.105)}$$

In short, different damping coefficients are recommended for different stresses. Damping for hoop stresses is described

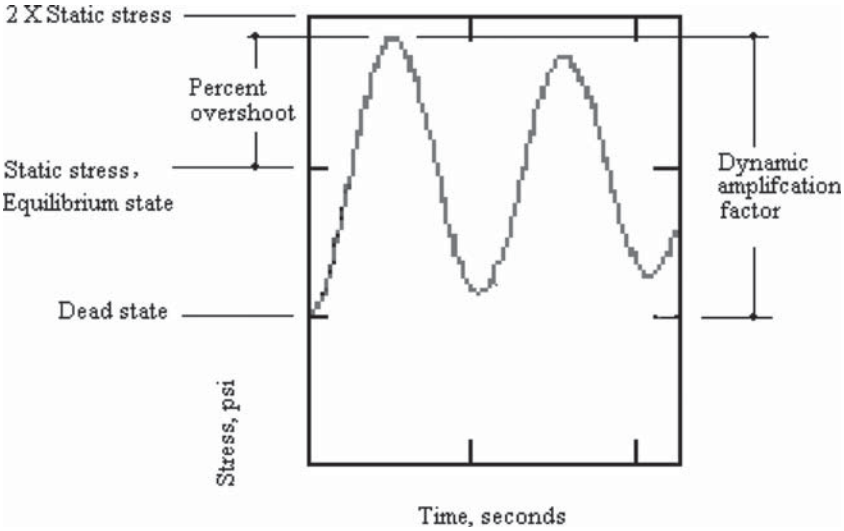


FIG. 7.28 RELATIONSHIPS BETWEEN THE DYNAMIC MAGNIFICATION FACTOR AND THERMODYNAMIC EFFICIENCY

by structural and fluid damping coefficients, which are related directly to material properties. Material properties are also used to describe damping of through-wall stresses. For bending, torsion, and axial stresses, statistical data from in-service systems was used to estimate damping effects. These damping coefficients are coupled with the dynamic stress equations to describe piping responses to water hammer.

7.4 SUMMARY OF DYNAMIC STRESSES IN ELASTIC SOLIDS

Dynamic stress equations were derived from shock wave theory and vibration theory, based on Newton's Law. Shock waves induced by impact travel at sonic velocity in solids, and induce vibrations in those solids. Those vibrations occur at multiple natural frequencies in all structures, and dissipate over time due to damping. Structural vibrations induce strains and proportional stresses in elastic materials, and those stresses are related to the applied loads; which may be applied forces or displacements on the structure. Equations describing dynamic stresses as a function of the applied load were presented in this chapter to provide a sound technical basis for the following chapters on the dynamic responses of pipe systems.

CHAPTER

8

WATER HAMMER EFFECTS ON BREATHING STRESSES FOR PIPES AND OTHER COMPONENTS

Hoop stresses are seldom the maximum pipe stresses in a pipe system, but their study is fundamental to the concept of dynamic stresses, since most of the available experimental data to support dynamic stress theory was found for cases of simple, cylindrical, pipe sections. Dynamic hoop stresses are frequently referred to as breathing stresses, due to the pulsating, albeit rapid, motion of pipes subjected to sudden internal pressures. Breathing stresses consist of a primary stress that occurs in the wake of a shock wave traveling the bore of a pipe. In front of the shock wave, precursor waves similar to Rayleigh surface waves also occur, and examples are provided here to describe dynamic hoop stresses along with appropriate derivations.

For all examples, a sudden increase in pressure at the shock front was evaluated as a step response of the piping, where the width of the shock wave was neglected. That is, a step pressure was transmitted along the inside of the pipe at a sonic velocity. The first example is an FEA model of a short pipe, which is unaffected by precursor waves, and DMF = 2 in the absence of damping. Other examples provide experimental results and supporting analysis that demonstrate the presence of precursor waves, where DMF = 4 in the absence of damping. As another example, the presence of flexural vibrations (Fig. 8.1) was considered, since both flexural stresses and hoop stresses are coincident. Additionally, experimental results are considered to demonstrate the effectiveness of using a ramp pressure increase, instead of a step increase to reduce dynamic stresses.

Although first-mode frequencies are expected to be excited by typical step responses, the response of pipes to harmonic excitation lend some understanding to pipe vibrations. Applying different forcing frequencies to pipes, Dweib [221] presented several higher mode frequency pipe responses, as shown in Figs. 8.2 to 8.5.

8.1 EXAMPLES OF PIPING FATIGUE FAILURES

As an example of failure due to breathing stresses, fatigue cracks in a 2-in. NPS, Schedule 10 pipe are shown in Fig. 8.6. Cracks in the pipe started on the inside of the pipe. Hoop stresses were the cause of these axial cracks, but circumferential cracks have also been observed at SRS in ductile iron pipes halfway between pipe flanges, which were located on the ends of 20-ft pipe sections. These ductile pipe fractures indicated that first-mode flexural stresses caused fatigue.

8.2 FEA MODEL OF BREATHING STRESSES FOR A SHORT PIPE

Finite element analysis provided a means for determining the shock-induced pipe stresses in a pipe due to shock wave in an empty pipe. The cross section of a typical pipe and the water hammer as modeled in the FEA are shown in Fig. 8.7. This figure shows that the pressure, P, increases from 0 to P_0 across the wave front as the wave moves along the pipe from left to right. This step pressure is assumed to be a one-dimensional planar wave, which is a standard approximation in the literature. This planar wave travels in a pipe at a sonic velocity, where Eq. (5.18) was revised to compensate the effects of fixed-end conditions. The velocity equals

$$a'' = \sqrt{\frac{\dfrac{k \cdot g''}{\rho_{water}}}{1 + \left(\dfrac{2 \cdot k \cdot r_m}{E \cdot \bar{T}}\right) \cdot \left[\dfrac{\bar{T}}{r_m} \cdot (1 + \nu) + \dfrac{2 \cdot r_m \cdot (1 - \nu^2)}{2 \cdot r_m + \bar{T}}\right]}} \tag{8.1}$$

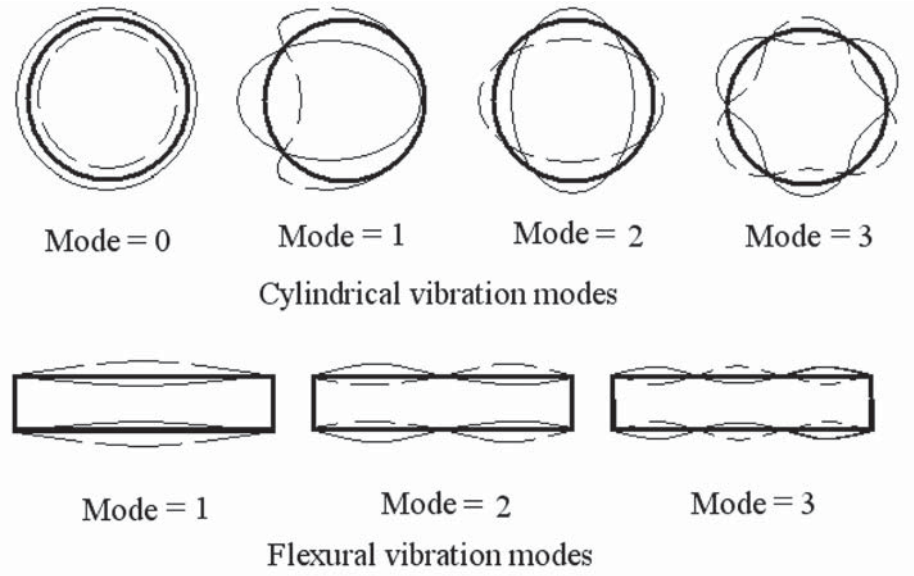


FIG. 8.1 VIBRATION MODES FOR CYLINDRICAL AND FLEXURAL VIBRATIONS (Adapted from Blevins [222], Adapted by permission of Engineering Dynamics, Inc. Wachel et al [223])

where k equals the bulk modulus of the fluid, E, equals the modulus of elasticity of the pipe material, and v equals Poisson's ratio. The fluid velocity, in the pipe was assumed to be negligible, since typical piping design flow velocities are 6 to 10 ft per second, while the wave speed equaled 4386 ft per second for an 8-in. diameter steel pipe, containing water. The pipe stresses in the wake of the pressure wave traveling at this velocity were explored in the FEA model.

8.2.1 FEA Assumptions

Several assumptions were required for the FEA models. A moving step pressure increase of P_0 = 150 psig was as-

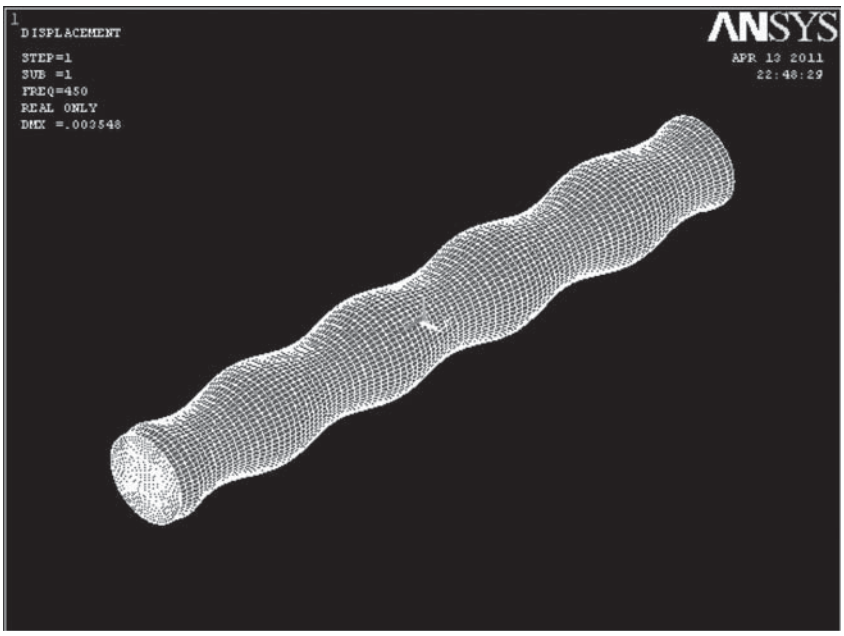


FIG. 8.2 DEFORMED PIPE AT A 450-HZ FORCING FREQUENCY (Dweib [221])

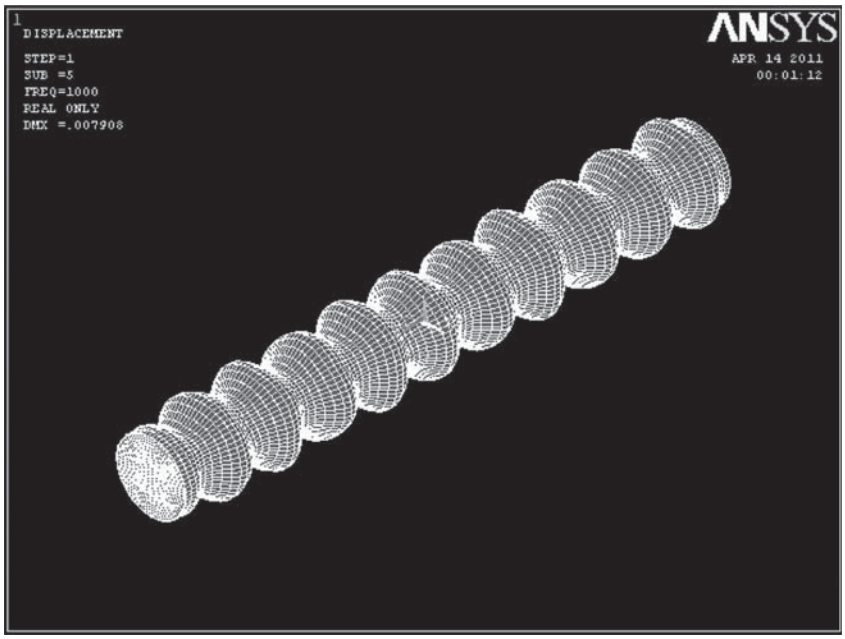


FIG. 8.3 DEFORMED PIPE AT A 1000-HZ FORCING FREQUENCY (Dweib [221])

sumed in an 8 in. NPS Schedule 40 pipe, for both steel and aluminum materials. The length of pipe, $L' = 14$ in., shown in Fig. 8.7 was used in the FEA model. The properties of the pipe at a 70°C temperature were used. Linear elastic, isotropic, homogeneous material behavior was also assumed. The anisotropic properties of cold worked pipe support the isotropic material assumption required in this work for elastic stress calculations since the elastic modulus of the pipe is unaffected. Shear stresses, τ_{rz}, $\tau_{r\theta}$, and $\tau_{z\theta}$ at the inner pipe wall were assumed to be negligible. The effects of material, fluid, and structural damping were neglected. Strain rate effects were neglected. A continuously

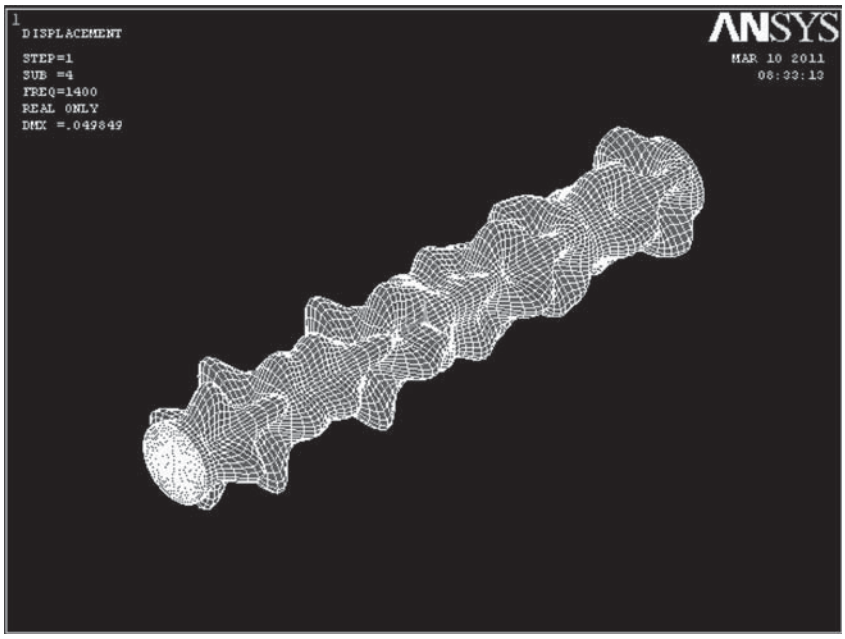


FIG. 8.4 DEFORMED SHAPE AT A 1400-HZ FORCING FREQUENCY (Dweib [221])

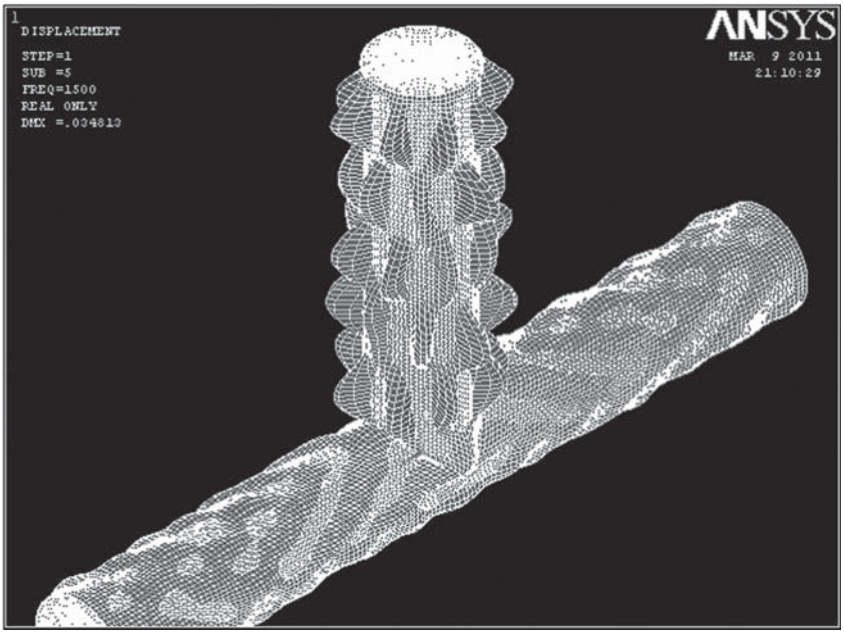


FIG. 8.5 DEFORMED SHAPE AT A 1500-HZ FORCING FREQUENCY (DWEIB [221])

applied pressure was assumed to exist on the inner pipe wall after the shock passed. Thus, the fluid was coupled to the pipe wall, and therefore, the radial fluid velocity at the wall was assumed to equal the radial wall velocity. Additionally, stress wave transmissions into the surrounding air and water were assumed to be negligible. Pipe models with both ends fixed and one end fixed were considered.

8.2.2 Model Geometry and Dynamic Pressure Loading

A three-dimensional view of the FEA model is shown in Fig. 8.8. The solid finite elements are subjected to the moving pressure wave sequentially as the wave moves along the model's inner wall. A Fortran® program used in the Abaqus® code simulated the dynamic pressure load

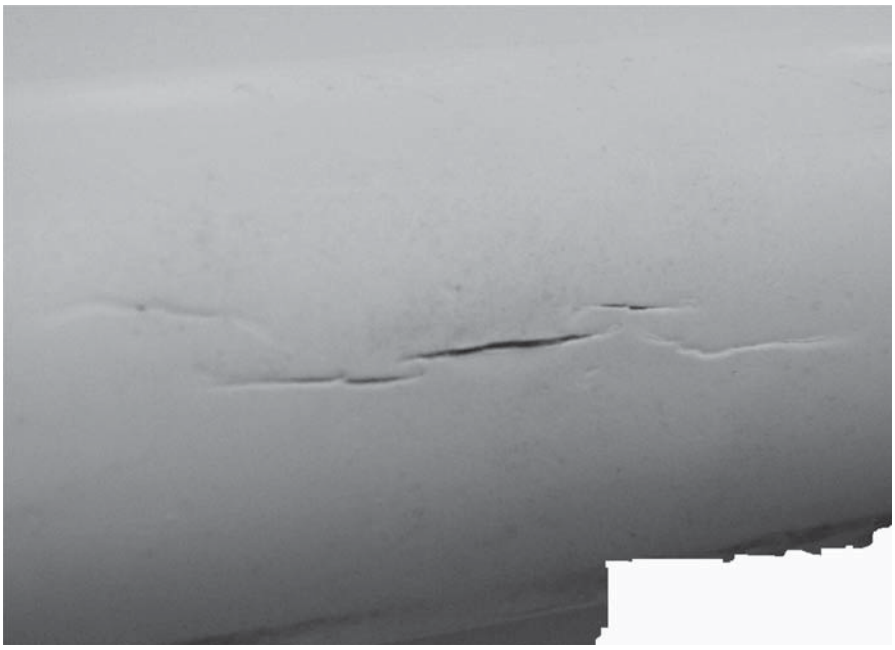


FIG. 8.6 FATIGUE CRACKS IN PVC PIPE

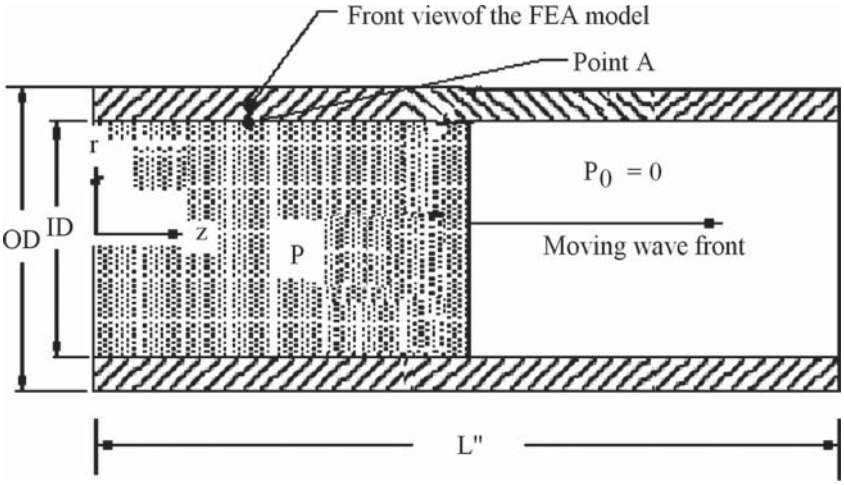


FIG. 8.7 FEA MODEL CROSS SECTION

due to the motion of a pressure wave moving along the inner pipe wall (Leishear [1, 224]). The pressure step commenced at $z = 0$ when the time equaled zero. The pressure step traveled along the pipe at a wave speed equal to a, for an arbitrarily selected 14-in. pipe length.

8.2.3 FEA Model for a Pipe With Fixed Ends

Example 8.1 Consider an FEA model of an internal shock in a pipe with fixed ends.

For a pipe with both ends fixed, the maximum stresses were found in the wake of the shock after the wave passed. The maximum stresses in the pipe wall occurred at point A at the inner surface the pipe wall, and the stresses calculated at that point are shown in Fig. 8.9. There are three distinguishable stresses. One stress is due to the initial radial stress waves reflecting back and forth within the wall. The second stress is due to a bulk motion of the wall as it expands and contracts back to its original position, creating the hoop stresses. The third motion is due to the Poisson's stresses induced by the hoop stresses. Also, Fig. 8.9 indicates that subsurface contact stresses do not have time to form at the leading edge of the wave front as it moves along the pipe length. Radial stresses are considered first, since they lead to hoop stresses. In addition, note that radial vibrations shown in Fig. 8.9 are inaccurate due to computer memory limitations for this specific model, but the harmonic nature of the radial vibrations can be shown using Abaqus® as required. The FEA results provide insight into short pipe response,

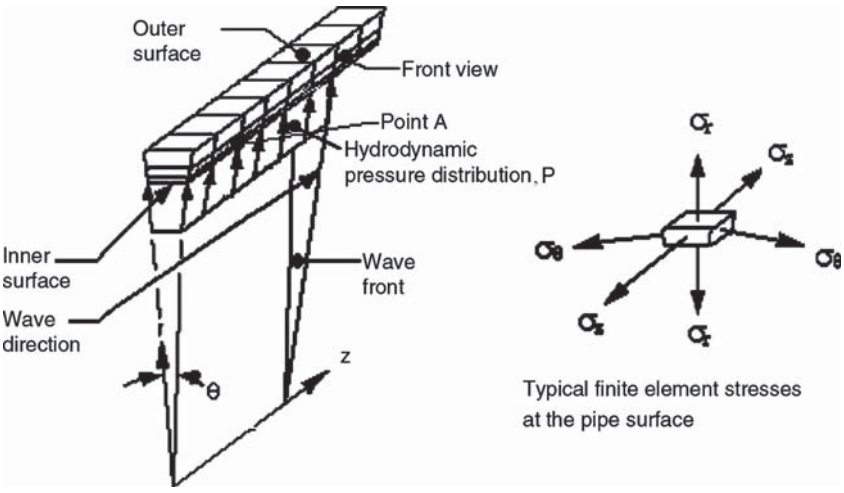


FIG. 8.8 THREE-DIMENSIONAL FEA MODEL

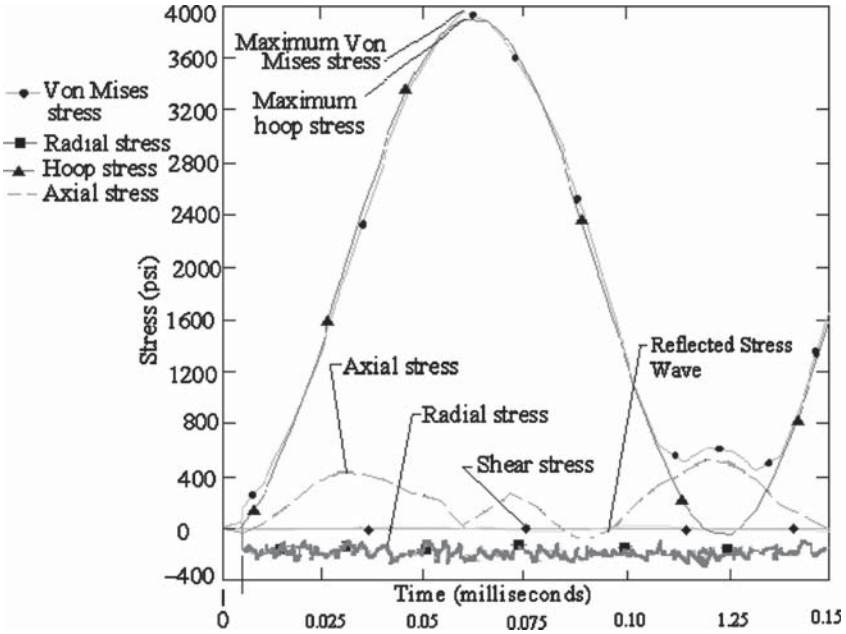


FIG. 8.9 FEA CALCULATED STRESSES

but a precaution should be noted. A DMF = 2 was observed, and for longer pipes, DMF = 4 for an undamped pipe. This issue is discussed in paragraph 8.5.

8.2.4 Stress Waves and Through-Wall Radial Stresses

Once the traveling shock wave in the fluid first reached point A on the pipe wall, the pressure increased to P_0, compressed the pipe wall, and induced a continuous compressive pressure of 150 psig. Resultant stress waves induce vibrations similar to Fig. 7.4, where the compressive pressure caused σ_r to vary between 0 and $2 \cdot P = -300$ psi. Shown in Fig. 8.10, compressive stress waves travel back and forth perpendicular to the pipe wall at a wave velocity, c_1, in excess of five times the water hammer wave velocity. Fig. 8.11 shows the variance of the radial stress, σ_r, as it changes through the pipe wall. The radial vibration frequency, ω_r, can be found from the relationship $\omega_r = 2 \cdot \pi \cdot \tau'$, where a / τ' equals the period shown in Fig. 8.11. This frequency is slightly higher than the first-mode frequency of a flat plate (Eq. (7.13)). In short, the maximum undamped radial stress is twice the magnitude of the applied pressure, and the stresses occur at a frequency near the frequency of a flat plate.

8.2.5 Hoop Stresses for a Pipe with Fixed Ends

The initial deflection of the pipe wall is shown in Fig. 8.12, and the final deflection and hoop stresses of a pipe wall are shown in Fig. 8.13. When point A was initially loaded with the step pressure, the hoop stress had not yet formed and was noted to be equal to zero. As the pipe wall expanded, the hoop stress increased to 3900 psi, and oscillated about a stress of 1950 psi, which is, in fact, the static hoop stress resulting from an applied pressure of 150 psi on a thick walled cylinder. The static hoop stress is expressed as (Young, et al [132]).

$$\sigma_\theta = \frac{\left(P \cdot ID^2 \cdot (OD^2 + ID^2)\right)}{r^2 \cdot (OD^2 - ID^2)} \qquad \text{US (8.2)}$$

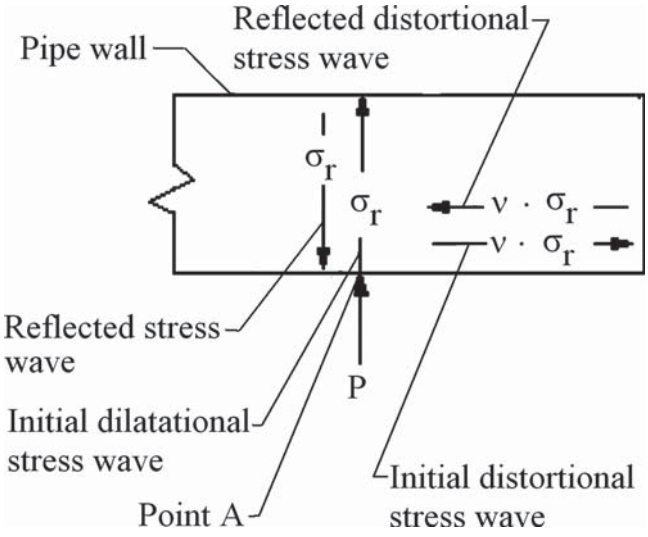


FIG. 8.10 RADIAL STRESS WAVES IN A PIPE WALL

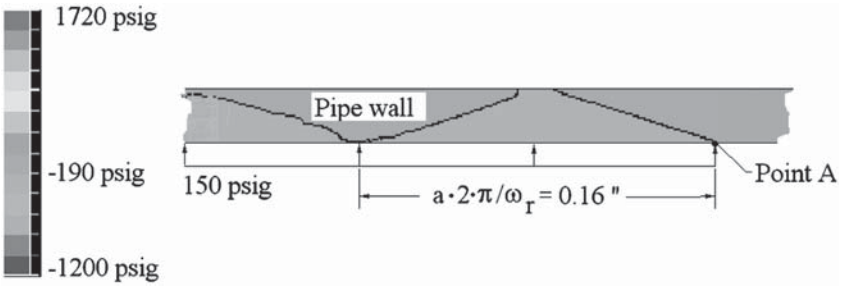


FIG. 8.11 RADIAL STRESSES IN THE PIPE WALL

where *r* is the position at which the stress is calculated. Moreover, at maximum deflection, the maximum stress at the inner wall calculated by FEA was twice the static value found by Eq. (8.2). Also, see Eq. (1.10) for stresses in a thin-wall cylinder, where the difference between thin and thick wall stress predictions is frequently about 10%. Similar maximum stresses were obtained for an aluminum pipe (not shown here (Leishear [1]) and a pipe with one end fixed and one end free. Note that the DMF = 2 for this idealized case of a short pipe. In paragraph 7.3, the DMF for longer pipes is shown to be DMF < 4. For this example, the hoop stress has not had time to develop at the shock wave. The FEA model also lacks the effects of reflected waves in a fluid that may occur at the end of the pipe, and the effects of shortening the pulse time of the pressure excursion (paragraphs 7.2.3 and 7.3), where maximum stresses in a dead end pipe may be significantly diminished or doubled, depending on the pipe length.

8.2.6 Axial Stresses for a Pipe with Fixed Ends

Axial stresses at point A (Fig. 8.9) were caused primarily by hoop stresses and wave reflections in the solid material. The maximum axial stress at point A was 525 psi, which was less than expected for a Poisson's stress due to the hoop stresses, and the minimum axial stress was equal to zero when the hoop stress reached a maximum.

To explain the disparity of the axial stresses, the boundary conditions, and stresses due to reflected waves were considered. When the pipe initially expands, the pipe cannot compress in the axial direction, and an axial tensile stress is formed. The maximum axial stress due to the hoop stress is found from

$$\sigma'_z = \nu \cdot \sigma'_\theta \qquad \text{US (8.3)}$$

A negligible stress due to the radial stress is also present, where

$$\sigma'_z = \nu \cdot \sigma'_r \qquad \text{US (8.4)}$$

Axial strain waves are reflected back and forth along the pipe, where stresses due to wave reflections combine with the initial axial stresses to reduce the amplitude of the axial stresses. In the absence of wave reflections, the maximum stress would have been higher in accordance with the static stress predictions of Eq. (8.3). In short, the complex nature of axial stresses and the effects of wave reflections appear in the FEA model. The final axial stress curve is seen in Fig. 8.9.

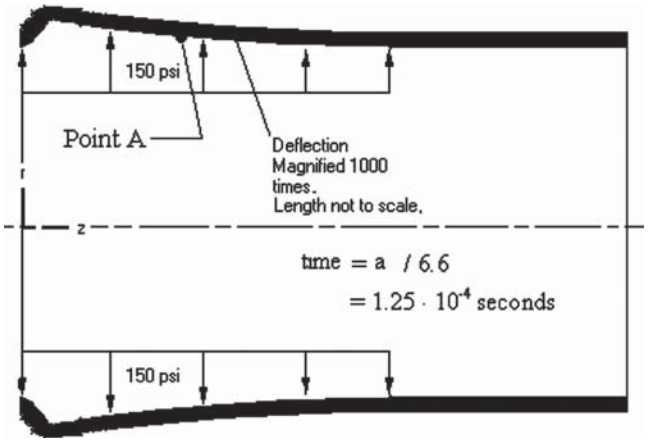


FIG. 8.12 INITIAL PIPE WALL DEFLECTIONS

8.2.7 Impulse Loads

Example 8.2 Using the FEA fixed-end model in Example 8.1, determine the effects of a short impulse pressure surge.

Damping effects on breathing stresses for this pipe were first evaluated using step response equations, where a 2% damping ratio was assumed, as shown in Fig. 8.14. Note that the reflected axial stresses observed in the FEA model are not captured by the SDOF model. Also, reflected waves in the fluid were not considered.

After considering a damped response, a step impulse, pressure transient was considered. Using the damped SDOF

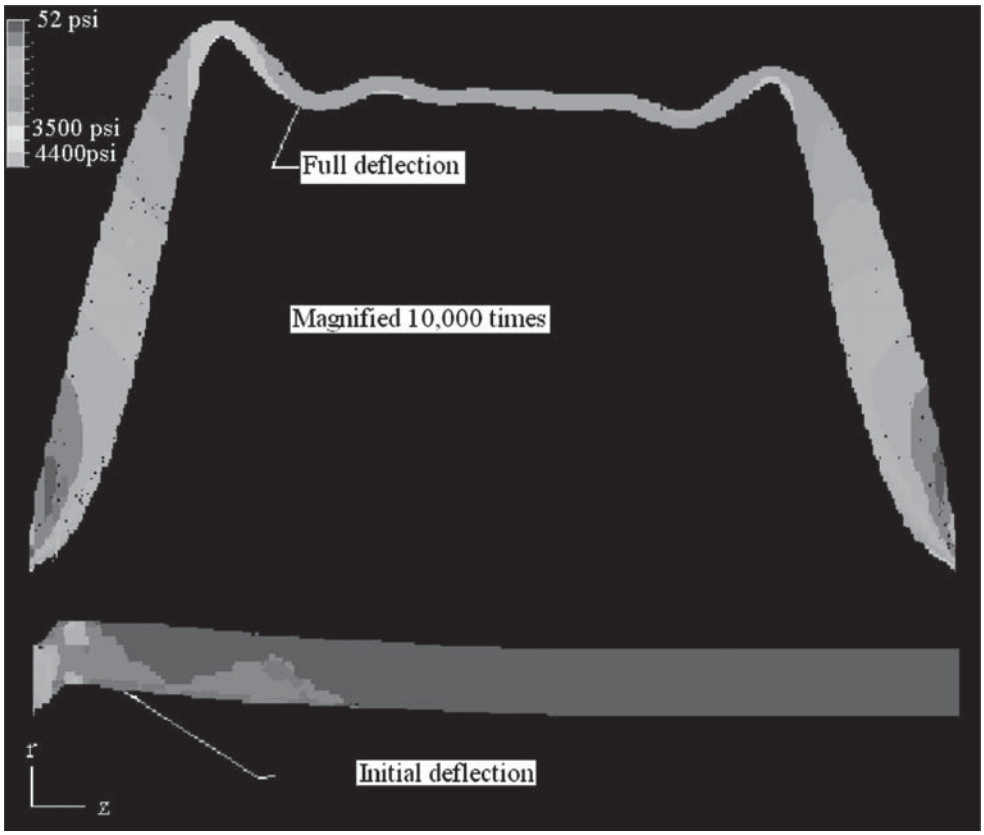


FIG. 8.13 MAXIMUM PIPE WALL DEFLECTIONS AND PIPE STRESSES

model, the effects of an extremely short impulse ($t_1 = 0.003$ seconds) were considered, as shown in Fig. 8.15.

8.2.8 Stresses for a Pipe with One Free End

Example 8.3 Consider an FEA model of an internal shock in a pipe with one fixed end and one free end.

The deflections and maximum stresses in a free-end pipe are shown in Figs. 8.16 and 8.17. The maximum hoop stresses again equaled twice the calculated static stress, but there were no axial stresses, since the pipe end was unrestrained. FEA assumptions were the same as those used for a fixed-end pipe, except that the end condi-

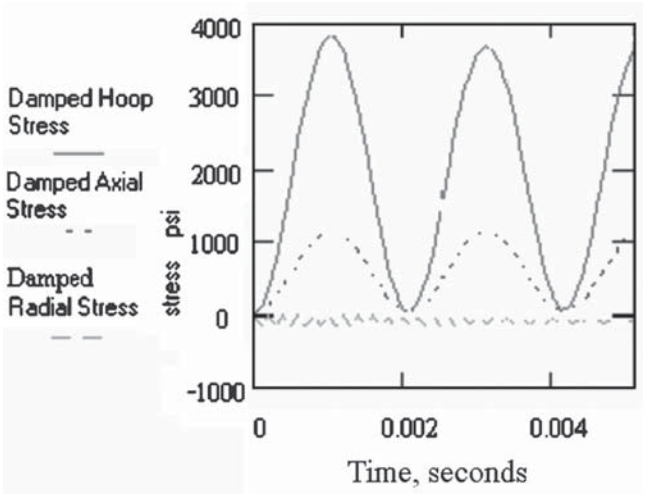


FIG. 8.14 DAMPED RESPONSE OF BREATHING STRESSES IN A SHORT PIPE

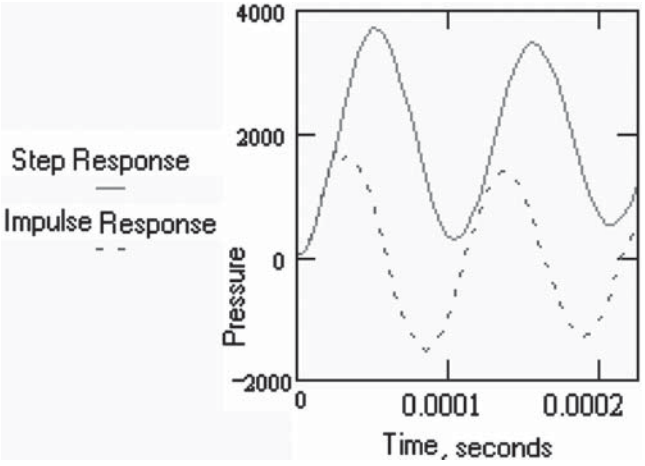


FIG. 8.15 IMPULSE RESPONSE OF HOOP STRESS IN A SHORT PIPE

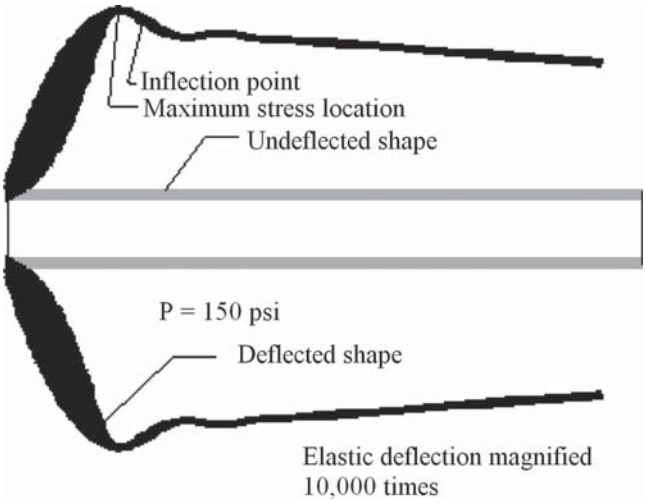


FIG. 8.16 DEFLECTION IN A FREE-END PIPE

tions differed and that the wave speed was determined for free-end conditions, such that

$$a'' = \sqrt{\frac{\frac{k \cdot g''}{\rho_{water}}}{1 + \left(\frac{2 \cdot k \cdot r_m}{E \cdot \bar{T}}\right) \cdot \left[\frac{t}{r_m} \cdot (1+\nu) + \frac{2 \cdot r_m \cdot \left(1 - \frac{\nu}{2}\right)}{2 \cdot r_m + \bar{T}}\right]}} \qquad \text{US (8.5)}$$

8.2.9 FEA Summary

In short, FEA models for a short pipe used to quantify stresses due to shock waves accompanied by a step increase in pressure for short steel and aluminum pipes. For cases of undamped vibrations in elastic materials, the FEA solution provided several conclusions. The maximum breathing stresses in a pipe resulted directly from vibrations due to shocks, and the stresses were created at a significant time after the wave front had passed. That is, the maximum stress did not occur at either the wave front or near the ends of the pipe. The maximum dynamic hoop stresses were twice the magnitude of the static stresses that would be expected from an equivalent static load regardless of boundary conditions at the pipe end or material. The median dynamic hoop stress in the FEA model equaled the static equilibrium hoop stress. The maximum stress was equivalent when the load was applied sequentially to the finite elements or when all of the elements were loaded simultaneously.

The effects of pipe length on the maximum stresses due to shock waves were not considered in the FEA models, which led to a major shortcoming in the analysis of water hammer-induced stresses. In particular, precursor waves did not have time to form in the pipe wall, since the shock would have long since passed when the pipe vibration created the maximum stress. For the FEA examples considered here, the wave would have traveled more than 5 ft ($L = a/\omega_0$) before the maximum hoop stress occurred. Also, the effects of water in the pipe and damping were not considered in the FEA models.

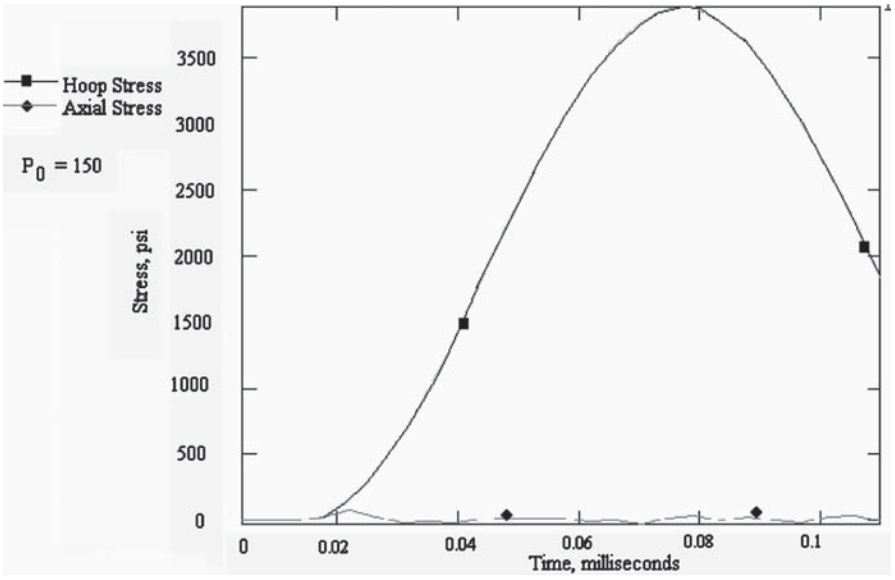


FIG. 8.17 MAXIMUM STRESSES IN A FREE-END PIPE

8.3 THEORY AND EXPERIMENTAL RESULTS FOR BREATHING STRESSES

Experimental data shows that dynamic hoop stresses occur in pipe systems, where the maximum stresses are nearly four times the magnitude predicted by static stress equations in many cases. Two different theories are considered to describe maximum hoop stresses here, i.e., flexural resonance theory and dynamic stress theory. The complete derivations for both dynamic hoop stresses and flexural stresses have been recorded (Leishear [225, 226]), and those derivations are presented here, along with examples and added discussion not previously presented.

The two theories seem to be mutually exclusive, but they may, in fact, describe the same stresses. Flexural resonance has been shown to describe stresses in short tubes such as gun barrels, and the dynamic stress theory is consistent with longer tubes, such as steel pipes. Each approach has limitations, but a reasonable approximation of pipe stresses can be established for design or failure analysis, using the dynamic stress theory. Flexural resonance leads logically into a discussion of dynamic stress theory.

8.4 FLEXURAL RESONANCE

The stresses in a tube, or pipe, are caused by the vibrations of the pipe wall as the shock travels through the pipe, as shown in Fig. 8.18. The shock wave travels at a velocity, a, and a pressure increase occurs from P_0 to $P + P_0$ across the shock. The initial pressure in the pipe, P_0, is neglected in the remainder of this discussion. A precursor vibration occurs in front of the wave, and an aftershock vibration occurs in the wake of the shock. The strain jump is related to the median change in diameter of the pipe. The concept of flexural resonance is one approach to describe hoop stresses.

Experiments have been performed in gas-filled tubes and in artillery barrels. Simkins [227 and 228] applied the flexural resonance theory to analyze measured strains in gun barrels, and Beltman et al [229], experimentally investigated strains due to internal shock waves in gas-filled tubes. In this theory, an infinite stress was assumed to exist at the shock wave, but there is no experimental or theoretical justification for this assumption. Even though flexural resonance and dynamic hoop stress theory describe different pipe responses, the maximum measured flexural stresses are consistent with the stresses calculated from dynamic stress theory (DMF < 4), and these maximum stresses are shown to a occur at a critical velocity, V_{cr}. In fact, Simkins used a step response in his derivations, in addition to results reported in terms of an infinite strain. The derivation of theory is followed here by examples of that theory.

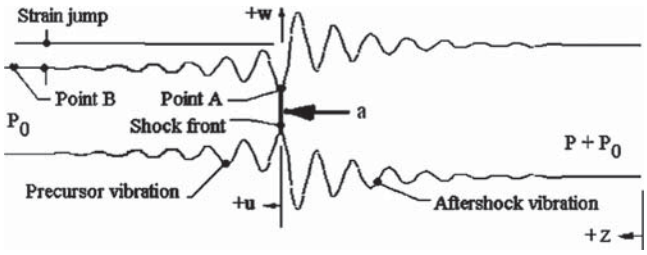


FIG. 8.18 PIPE WALL VIBRATIONS

8.4.1 Flexural Resonance Theory

The derivation for a tube with free ends was presented by Simkins, but is rewritten and elaborated here to show all of the steps used in his analysis to provide a solid understanding of the pipe response. Further details are available in the references, but the following derivation presents applicable equations used in the original referenced analyses.

8.4.1.1 Moment in a Differential Element The response of a thin-walled tube may be developed by first considering the bending of a differential element of the tube wall as shown in Fig. 8.19, where σ_z is the axial stress, y is measured from the center of a tube wall of thickness, T, dy is the width of a differential element, and M_z is the resultant moment due to bending of the tube wall.

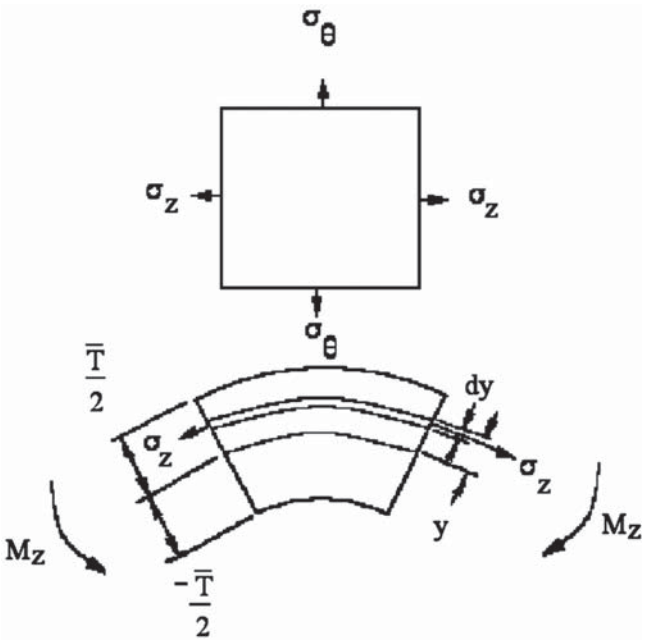


FIG. 8.19 DIFFERENTIAL AXIAL ELEMENT IN THE TUBE WALL

The moment was determined as follows (Timoshenko and Woinowski-Krieger [231]). Using Hooke's law for free-end conditions

$$\varepsilon_z = \frac{\sigma'_z}{E} - \frac{\nu \cdot \sigma'_\theta}{E} \qquad \text{US (8.6)}$$

$$\varepsilon_\theta = \frac{\sigma'_\theta}{E} - \frac{\nu \cdot \sigma'_z}{E} = 0 \qquad \text{US (8.7)}$$

where the local coordinate system in terms of u and w is shown in Fig. 8.19; ε_z, ε_θ, σ_z, and σ_θ are the axial and hoop strains and stresses; E is the modulus of elasticity; and ν is Poisson's ratio. The curvature of the tube deflection equals

$$-d^2w / dz^2 \qquad \text{US (8.8)}$$

The unit elongation then equals

$$\varepsilon_u = -y \cdot \ d^2w / dz^2 \qquad \text{US (8.9)}$$

where u and w are the axial and radial displacements, respectively. On substitution,

$$\varepsilon_z = \frac{\left(1-\nu^2\right)\cdot\sigma_z}{E} \qquad \text{US (8.10)}$$

$$\sigma_z = \frac{E \cdot y}{(1-\nu^2)} \cdot \frac{d^2w}{dz^2} \qquad \text{US (8.11)}$$

The bending moment is then calculated using the differential element.

$$M_z = \int_{-\bar{T}/2}^{\bar{T}/2} (\sigma_z \cdot y) dy = \int_{-\bar{T}/2}^{\bar{T}/2} \left(\frac{E \cdot y^2}{(1-\nu^2)} \cdot \frac{d^2w}{dz^2} \right) dy = \frac{E \cdot \bar{T}^3}{12 \cdot (1-\nu^2)} \cdot \frac{d^2w}{dz^2} \qquad \text{US (8.12)}$$

and M_z is expressed as

$$M_z = \frac{M_\theta}{\nu} = -D \cdot \frac{d^2w}{dz^2} \qquad \text{US (8.13)}$$

where D is the flexural rigidity, such that

$$D = \frac{E \cdot \bar{T}^3}{12 \cdot \left(1-\nu^2\right)} \qquad \text{US (8.14)}$$

8.4.1.2 Membrane Forces in a Cylindrical Shell Once the moment is determined for a differential element of the shell, the forces due to a statically applied pressure, P, can be determined using Fig. 8.20, where F_r is a shear force per unit length, and F_z is a normal force per unit length, M_z is the moment per unit length in the z direction, M_θ is the moment per unit length in the tangential direction, F_θ is the circumferential force per unit length, $d\theta$ is the differential length of the element along the circumference, r is the radius, and dz is the differential length of the element in the z direction.

The equilibrium equations in the radial direction for a shell are expressed as (Timoshenko and Woinowski-Krieger [231]),

$$\frac{dF_r}{dz} \cdot r \cdot dz \cdot d\theta + F_\theta \cdot dz \cdot d\theta + P \cdot r \cdot dz \cdot d\theta = 0 \qquad \text{US (8.15)}$$

The moment equilibrium about the radial direction equals

$$\frac{dM_z}{dz} \cdot r \cdot dz \cdot d\theta - r \cdot F_r \cdot dz \cdot d\theta = 0 \qquad \text{US (8.16)}$$

These two equations are further reduced to

$$\frac{dF_r}{dz} + \frac{F_\theta}{r} + P = 0 \qquad \text{US (8.17)}$$

$$\frac{dM_z}{dz} - F_r = 0 \qquad \text{US (8.18)}$$

Assume that the strains equal

$$\varepsilon_z = \frac{du}{dz} \qquad \text{US (8.19)}$$

$$\varepsilon_\theta = \frac{-w}{r} \qquad \text{US (8.20)}$$

The normal force is then equal to

$$F_z = \frac{E \cdot \bar{T}}{1-\nu^2} \cdot \left(\varepsilon_z + \nu \cdot \varepsilon_z\right) = \frac{E \cdot \bar{T}}{1-\nu^2} \cdot \left(\frac{du}{dz} - \frac{\nu \cdot w}{r} \right) = 0 \qquad \text{US (8.21)}$$

which yields

$$\frac{du}{dz} = \frac{\nu \cdot w}{r} \qquad \text{US (8.22)}$$

On substitution, the hoop stress resultant equals

$$F_\theta = \frac{E \cdot \bar{T}}{1-\nu^2} \cdot \left(\varepsilon_\theta + \nu \cdot \varepsilon_z\right) = \frac{E \cdot \bar{T}}{1-\nu^2} \cdot \left(\frac{-w}{r} + \frac{\nu \cdot du}{dz} \right) \qquad \text{US (8.23)}$$

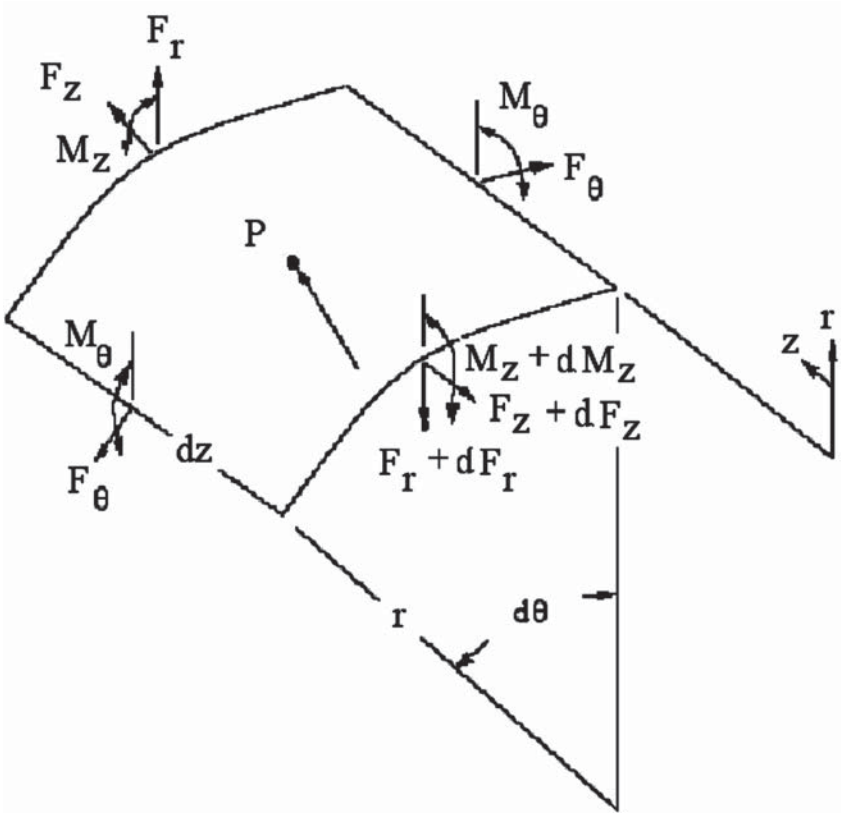


FIG. 8.20 DIFFERENTIAL SHELL ELEMENT

The circumferential force is found to be

$$F_\theta = \frac{-E \cdot \bar{T} \cdot w}{r} \tag{8.24}$$

8.4.1.3 Axial Displacement in a Cylindrical Shell The hoop stress resultant is used to determine the axial displacement of a shell. Eliminating F_r from Eqs. (8.17) and (8.18) yields

$$\frac{d^2 M_z}{dz^2} + \frac{F_\theta}{r} + P = 0 \qquad \text{US (8.25)}$$

Substitution of Eqs. (8.13) and (8.24) into Eq. (8.25) describes the axial displacement of a shell subjected to a pressure, P, such that

$$D \cdot \frac{d^4 w}{dz^4} + \frac{E \cdot \bar{T} \cdot w}{r^2} = P \qquad \text{US (8.26)}$$

8.4.1.4 Equation of Motion for a Cylindrical Shell The equation of motion for a cylinder can be determined with the aid of Eq. (8.17), which describes the radial forces on the shell. The radial forces per unit length on the shell element must equal the mass per unit length, $\rho \cdot t$ times the radial acceleration of the shell wall, d^2w/dx^2, such that

$$\frac{\partial (F_r)}{\partial z} + \frac{F_\theta}{r} + P = \rho'' \Big/ g'' \cdot t \cdot \frac{\partial^2 w}{\partial t^2} \qquad \text{US (8.27)}$$

On substitution of Eqs. (8.13), (8.18), and (8.24), Eq. (8.27) yields

$$\frac{D \cdot \partial^4 w}{\partial z^4} + \frac{\rho'' \Big/ g \cdot \bar{T} \cdot \partial^2 w}{\partial t^2} + \frac{E \cdot \bar{T} \cdot w}{r^2} = P(1 - H(z - a'' \cdot t)) \qquad \text{US (8.28)}$$

where t is the time, V_0, is the velocity of the coordinate system or shock wave in this case, and $H(\ldots)$ is the Heaviside step function expressing the pressure as a function of time. By a change of variables, Eq. (8.28) is referenced to a moving coordinate system using the chain rule for differential equations, such that

$$\frac{D \cdot \partial^4 w}{\partial (z - V \cdot t)^4} \cdot \frac{\partial^4 (z - a'' \cdot t)}{\partial z^4} + \frac{E \cdot \bar{T} \cdot w}{r^2} + \frac{\rho \Big/ g \cdot \bar{T} \cdot \partial^2 w}{\partial (z - V \cdot t)^2} \cdot \frac{\partial^2 (z - a'' \cdot t)}{\partial t^2} = P \cdot (1 - H(z - a'' \cdot t)) \qquad \text{US (8.29)}$$

Simplifying,

$$\frac{d^4w}{d\xi^4} + w + \frac{2\cdot\lambda\cdot d^2w}{d\xi^2} = P\cdot(1 - H(z - a''\cdot t) \qquad \text{US (8.30)}$$

where

$$\gamma = \sqrt[4]{\frac{E\cdot\bar{T}}{r^2\cdot D}} \qquad \text{US (8.31)}$$

$$\xi = \gamma\cdot\left(z - a''\cdot t\right) \qquad \text{US (8.32)}$$

$$2\cdot\lambda = \rho''/g''\cdot a''^2\sqrt{\frac{r^2}{E\cdot\bar{T}\cdot D}} \qquad \text{US (8.33)}$$

where γ, λ, and ξ are variables to simplify notation. Note that $\xi = 0$ at the shock for an observer moving with the shock wave.

8.4.1.5 Evaluation of Flexural Resonance Eq. (8.28) is the basis of the following evaluation of flexural resonance provided by Simkins [227]. This equation was the beginning of his analysis. The equation is rewritten in terms of displacements before and after the shock wave.

$$\frac{d^4w1}{d\xi^4} + w_1 + \frac{2\cdot\lambda\cdot d^2w_1}{d\xi^2} = \frac{P\cdot r^2}{E\cdot\bar{T}} \qquad \text{US (8.34)}$$

$$\frac{d^4w_2}{d\xi^4} + w_2 + \frac{2\cdot\lambda\cdot d^2w_2}{d\xi^2} = 0 \qquad \text{US (8.35)}$$

where the subscripts (2) and (1) indicate the displacements before and after a shock, respectively. To further consider the displacement, assume that Eq. (8.34) has a solution of the form

$$\lim_{\alpha\to 0}\frac{R^2\cdot P\cdot e^{i\cdot\alpha\cdot\xi}}{E\cdot\bar{T}} = \lim_{\alpha\to 0}\left(\alpha^4 - 2\cdot\lambda\cdot\alpha^2 + 1\right)\cdot A\cdot e^{i\cdot\alpha\cdot\xi} \qquad \text{US (8.36)}$$

where $w_1 = A\cdot e^{-i\cdot\alpha\cdot\xi}$. For the homogeneous solution, let

$$\alpha^4 - 2\cdot\lambda\cdot\alpha^2 + 1 = 0 \qquad \text{US (8.37)}$$

$$\alpha^2 = \lambda \pm \sqrt{\lambda^2 - 1} \qquad \text{US (8.38)}$$

Then, the four roots for α from Eq. (8.37) equal

$$\alpha = \pm\frac{\left(i\sqrt{1-\lambda} \pm \sqrt{1+\lambda}\right)}{\sqrt{2}} = \pm c \pm d\cdot i \qquad \text{US (8.39)}$$

where

$$d = \sqrt{\frac{1-\lambda}{2}} \qquad \text{US (8.40)}$$

$$c = \sqrt{\frac{1+\lambda}{2}} \qquad \text{US (8.41)}$$

By inspection, the particular solution, w_p, for Eq. (8.34) is expressed as Lame's equation for a cylinder, such that

$$w_p = \frac{P\cdot r^2}{E\cdot\bar{T}} \qquad \text{US (8.42)}$$

Similarly, the roots of the homogeneous solution to Eq. (8.35) are the same as those listed in Eq. (8.39) and the particular solution is

$$w_p = 0 \qquad \text{US (8.43)}$$

The general solutions to Eqs. (8.34) and (8.35) are then written as

$$w_1 = A_1e^{(i\cdot c+d)\cdot\xi} + A_2e^{-(i\cdot c+d)\cdot\xi} + A_3\cdot e^{(i\cdot c-d)\cdot\xi} + A_4e^{(-i\cdot c-d)\cdot\xi} + w_p \qquad \text{US (8.44)}$$

$$w_2 = A_5\cdot e^{(i\cdot c+d)\cdot\xi} + A_6\cdot e^{-(i\cdot c+d)\cdot\xi} + A_7\cdot e^{(i\cdot c-d)\cdot\xi} + A_8\cdot e^{(-i\cdot c-d)\cdot\xi} \qquad \text{US (8.45)}$$

where w_1 is the wall deflection upstream and behind the shock, and w_2 is the wall deflection downstream of the shock before the shock arrives at a point on the pipe wall. The boundary conditions to solve these equations assume continuity at the shock where $\xi = 0$ and are stated as:

Displacement continuity, $w_1 - w_2 = 0$ US (8.46)

Rotational continuity, $\frac{dw_2}{d\xi} - \frac{dw_1}{d\xi} = 0$ US (8.47)

Moment continuity, $\frac{d^2w_2}{d\xi^2} - \frac{d^2w_1}{d\xi^2} = 0$ US (8.48)

Shear continuity, $\frac{d^3w_2}{d\xi^3} - \frac{d^3w_1}{d\xi^3} = 0$ US (8.49)

Velocities dictate three different solutions to these equations. Below the critical velocity, $\lambda < 1$; at the critical velocity, $\lambda = 1$, and above the critical velocity, $\lambda > 1$. To reduce the number of equations, the boundary condition at the ends of the pipe were considered. Below the critical velocity, assume that as $z \to \pm\infty$, $\xi \to \pm\infty$. When $\lambda < 1$, $A_3 = A_4 = A_5 = A_6 = 0$ and

$$w_1 = A_1e^{(ic+d)\cdot\xi} + A_2e^{-(ic+d)\cdot\xi} + w_p \qquad \text{US (8.50)}$$

$$w_2 = A_7 \cdot e^{(i\cdot c - d)\cdot \xi} + A_8 \cdot e^{(-i\cdot c - d)\cdot \xi} \qquad \text{US (8.51)}$$

Substituting the boundary conditions of Eqs. (8.46) to (8.49) into Eqs. (8.44) and (8.45) yields

$$\begin{vmatrix} A_1 + A_2 - A_7 - A_8 = -\dfrac{P\cdot R^2}{E\cdot t} \\ \alpha_1 \cdot A_1 + \alpha_2 \cdot A_2 - \alpha_3 \cdot A_7 - \alpha_4 \cdot A_8 = 0 \\ \alpha_1{}^2 \cdot A_1 + \alpha_2{}^2 \cdot A_2 - \alpha_2{}^2 \cdot A_7 - \alpha_4{}^2 \cdot A_8 = 0 \\ \alpha_1{}^3 \cdot A_1 + \alpha_2{}^3 \cdot A_2 - \alpha_2{}^3 \cdot A_7 - \alpha_4{}^3 \cdot A_8 = 0 \end{vmatrix} \qquad (8.52)$$

Solving Eqs. (8.50) to (8.52),

$$w_1 = \frac{P\cdot r^2}{2\cdot E\cdot \bar{T}} \cdot \left(e^{d\cdot\xi} \cdot \left(-\cos(c\cdot\xi) + \frac{d^2 - c^2}{2\cdot c\cdot d} \cdot \sin(c\cdot\xi) \right) + 1 \right) \qquad \text{US (8.53)}$$

for $\xi \le 0$ behind the shock, and

$$w_2 = \frac{P\cdot r^2 \cdot}{2\cdot E\cdot \bar{T}} \cdot \left(e^{-d\cdot\xi} \cdot \left(\cos(c\cdot\xi) + \frac{d^2 - c^2}{2\cdot c\cdot d} - \sin(c\cdot\xi) \right) \right) \qquad \text{US (8.54)}$$

for $\xi \ge 0$ in front of the shock.

At the critical velocity, $\lambda = 1$, $d = 0$, and a solution similar to Eq. (8.52) is nonexistent since

$$|\text{coef}| = 0 \qquad \text{US (8.55)}$$

Above the critical velocity, $\lambda > 1$, and Simkins solved the pertinent equations to show that

$$w_1 = \frac{P\cdot r^2}{2\cdot E\cdot \bar{T}} \cdot \left(\frac{b^2 \cdot \cos(a\cdot\xi)}{b^2 - a^2} + 1 \right) \qquad \text{US (8.56)}$$

$$w_2 = \frac{P\cdot r^2}{2\cdot E\cdot \bar{T}} \cdot \left(\frac{-a^2 \cdot \cos(b\cdot\xi)}{b^2 - a^2} \right) \qquad \text{US (8.57)}$$

where

$$a = \sqrt{\frac{1+\lambda}{2}} - \sqrt{\frac{\lambda - 1}{2}} \qquad \text{US (8.58)}$$

$$b = \sqrt{\frac{1+\lambda}{2}} + \sqrt{\frac{\lambda - 1}{2}} \qquad \text{US (8.59)}$$

Eqs. (8.53) to (8.57) describe the tube wall motion. Note that for velocities above critical, the frequencies change across the shock, a precursor wave is present in the form of w_2 and the vibrations are undamped.

Below the critical velocity, Simkins described the wall deflection equations in matrix format and combined his results to obtain a graph to relate DMF to the critical velocity. Frequencies do not change across the shock for subcritical velocities.

8.4.1.6 DMF and the Critical Velocity Simkins derived Fig. 8.21 by expressing the DMF as

$$\text{DMF} = \frac{w}{\left(\dfrac{P\cdot r^2}{2\cdot E\cdot \bar{T}} \right)} \qquad \text{US (8.60)}$$

8.4.1.7 Critical Velocity Once all of the equations were developed, the critical velocity and frequency were determined. The critical velocity occurs at $\lambda = 1$, where the strain at the step pressure increase is assumed to be infinite. The physical explanation for resonance at the step is that energy must flow away from a shock, and at the critical velocity, energy cannot flow away from the shock and accumulates to create a resonant condition. Eq. (8.33) can be shown to yield

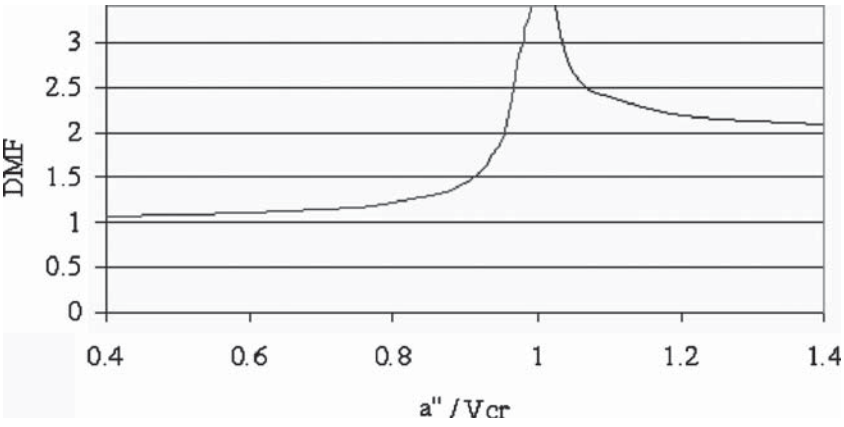


FIG. 8.21 DMF AND CRITICAL VELOCITY (Simkins [227])

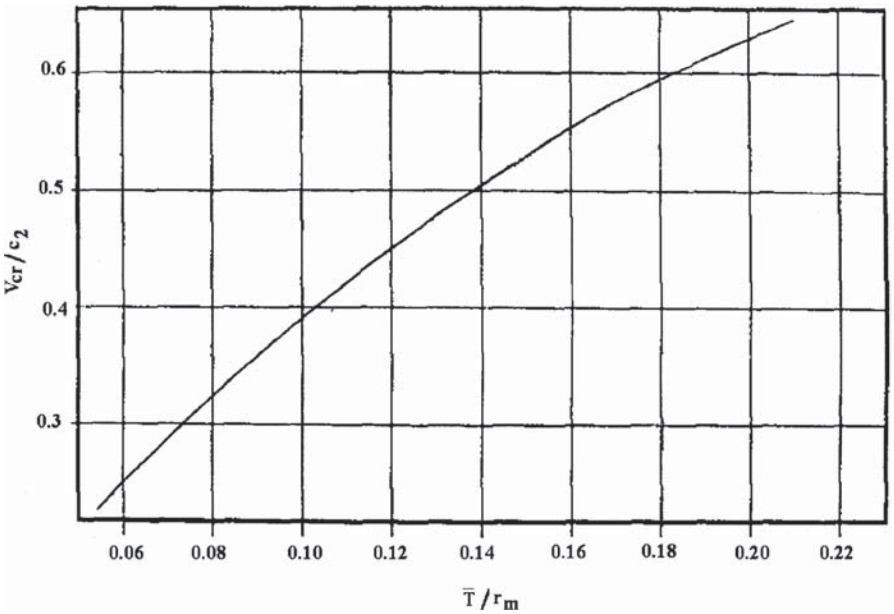


FIG. 8.22 WALL THICKNESS EFFECTS ON CRITICAL VELOCITY (Simkins [227])

$$V_{cr}\left(\frac{ft}{\sec}\right)=\frac{1}{12}\left(\frac{ft}{in}\right)\cdot\sqrt{\frac{E\cdot\bar{T}\cdot g''}{\rho''\cdot r\cdot\sqrt{3\cdot\left(1-\nu^2\right)}}} \qquad \text{US (8.61)}$$

8.4.1.8 Breathing-Mode Frequency Inspection of Eq. (8.32) shows that the frequency seen by a stationary observer equals

$$\omega = a''\cdot\gamma \qquad \text{US (8.62)}$$

At the critical velocity, Eqs. (8.61) and (8.62) yield the critical frequency, ω_{cr}

$$\omega_{cr}=\sqrt{\frac{2\cdot E\cdot g''}{\rho''\cdot r^2}} \qquad \text{US (8.63)}$$

Simkins noted that the critical velocity and frequencies were significantly different for thick-walled tubes, and the reader is referred to his work for further details. Even so, relationships between critical velocity and wall thickness are shown in Fig. 8.22. A closed form solution for thick-wall frequencies was not derived, but Herman and Mirsky [230] recommended four equation solutions to find thick-wall frequencies.

8.4.1.9 Flexural Resonance Assuming Fixed Pipe Ends The analysis for a pipe with fixed ends is identical to that for free ends, except that the initial boundary conditions are different. By substitution of the boundary conditions into Eq. (8.61), the critical velocity for a fixed-end pipe equals

$$V_{cr}=\sqrt{\frac{E\cdot\bar{T}\cdot g}{\rho\cdot r\cdot\sqrt{3\cdot(1)}}} \qquad (8.64)$$

Essentially, the ν^2 term is dropped from the critical velocity equation. For typical structural materials, where $\nu = 0.3$, the difference in the critical velocity due to end restraints of the tube is approximately only 5%. Frequencies are the same for either end constraint, as shown by substitution of the appropriate terms into Eq. (8.62).

8.4.2 Flexural Resonance Examples

Several investigators have performed tests to investigate flexural resonance. All vibration magnitudes occur for DMF < 4.

8.4.2.1 Strains in Gun Tubes

Example 8.4 Present some of Simkins' results for gun tubes.

Simkins pioneered experimental research for high-frequency vibrations in tubes, and he solved the flexural resonance equations for two specific gun barrels, as shown in Figs. 8.23 and 8.24. In both cases, the projectile velocity was less than the critical speed, and reasonable agreement was obtained between theory and experiment. Results from a series of tests are presented in Fig. 8.25 to demonstrate the use of the flexural resonance theory for short tubes.

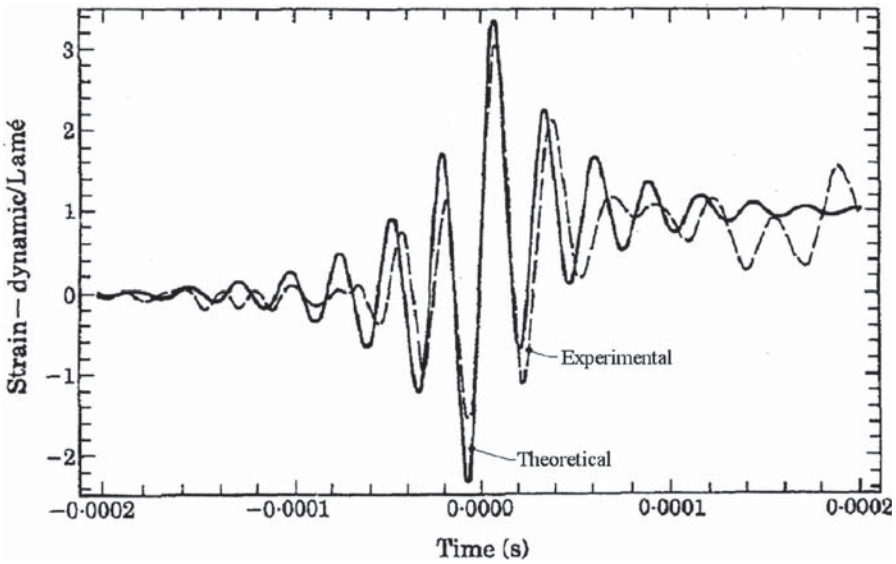


FIG. 8.23 FLEXURAL RESONANCE FOR A 60-MM GUN TUBE, $a = 0.993 \cdot V_{cr}$ (Simkins [227 and 228])

8.4.2.2 Strains Due to Internal Shocks in a Tube Example 8.5 Present some of Beltman's and Shepherd's results for internal shocks in a tube.

Beltman's shock tube was instrumented to measure the pressure in a tube and the hoop strains on the outer wall of the tube as a step pressure increase traveled axially along the inner wall of the tube. A step pressure measured at a point on the inner wall of the tube is shown in Fig. 8.26. The strains resulting from this applied pressure on the outside diameter of the tube are shown in Figs. 8.27 and 8.28 for two different velocities. Although Beltman instrumented several points along the tube, only partial data for the pipe wall is represented here. Note that a precursor vibration occurs before the shock wave arrives, and an aftershock vibration occurs in the wake of the shock.

The velocity of the pressure front was varied in the shock tube, so that the maximum strains were found over a range of different shock wave velocities. The relationships between strain and the different velocities of the pressure front are shown in Fig. 8.29. The relationship is

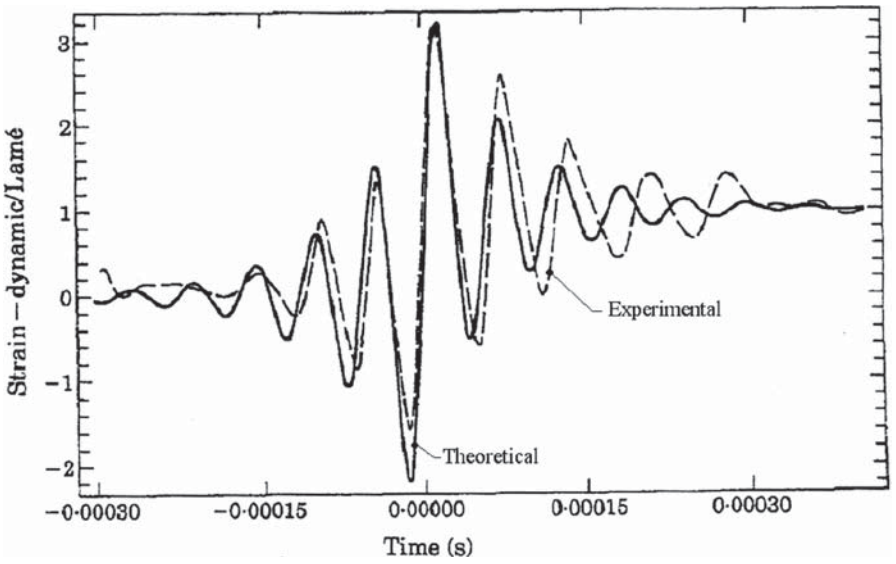


FIG. 8.24 NEAR FLEXURAL RESONANCE FOR A 120-MM GUN TUBE (Simkins [227 and 228])

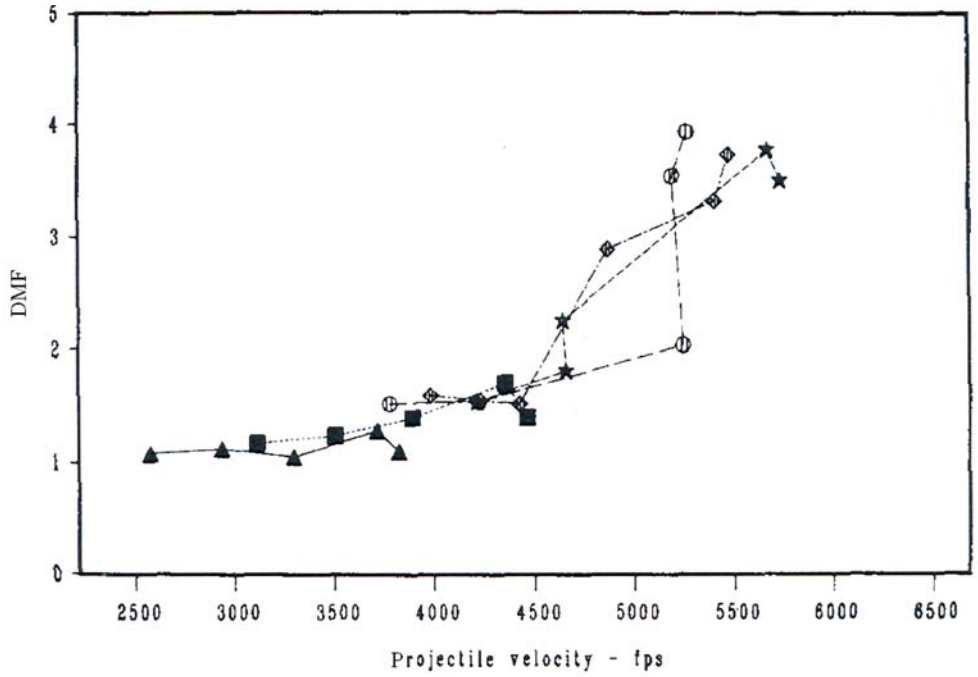


FIG. 8.25 TEST RESULTS FOR A 120-MM GUN TUBE (Simkins [227 and 228])

described by using the DMF. Beltman et al stated that the dynamic load factor equaled approximately one for low-wave velocities, approached maximum values of three to three and one half at the critical velocity, and then tapered off to values below two for higher velocities. The vibrations changed as they moved along the pipe wall. Beltman also provided Tang's flexural resonance solution for the hoop strain equation and the results of FEA models, which used thin-wall shell elements. The FEA models predicted maximum strains at the critical velocity.

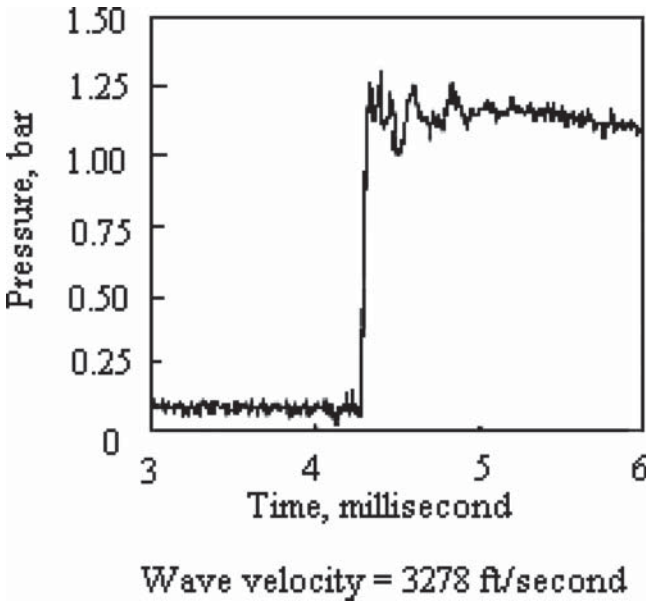


FIG. 8.26 PRESSURE BEHIND THE SHOCK WAVE IN THE TUBE
(Beltman et al [229])

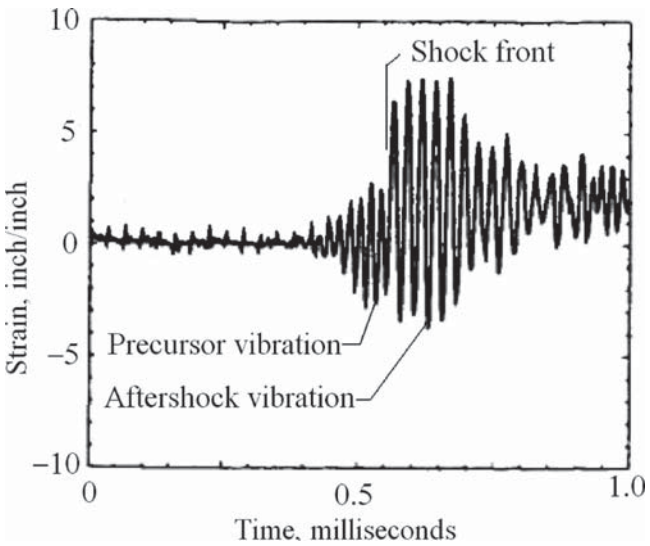


FIG. 8.27 STRAINS AT A POINT ON THE OUTER PIPE WALL, SHOCK VELOCITY = 3278 FT/SECOND
(Beltman et al [229])

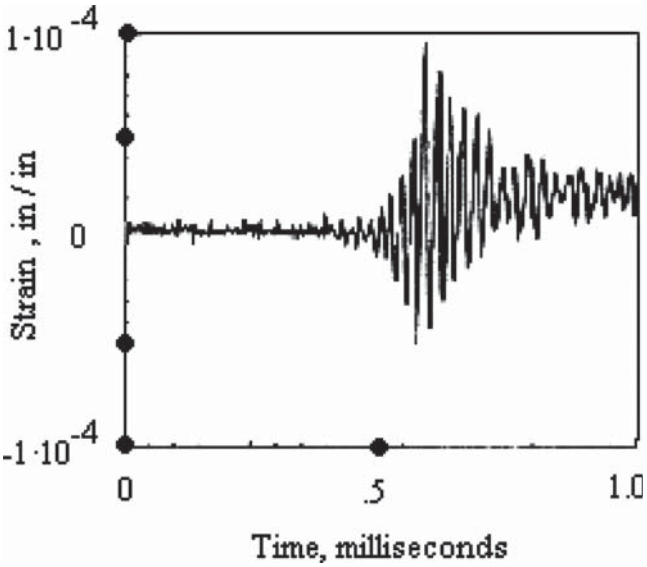


FIG. 8.28 STRAINS AT A POINT ON THE OUTER PIPE WALL, SHOCK VELOCITY = 3175 FT/SECOND (Beltman et al [229])

Example 8.6 Determine the DMF at the critical velocity for common pipe sizes.

For some common diameters of steel pipe with free ends, find the wave speeds due to water hammer (Eq. (5.20)), and find the critical velocities using Figs. 8.21 and 8.22 to find the DMF. Results are shown in Table 8.1 and Fig. 8.30, where wall thickness has a pronounced effect on the critical velocity.

8.4.3 Summary of Flexural Resonance Theory

Both Simkins and Beltman demonstrated that the DMF increases near the critical velocity in short tubes. However, the very high predicted strains at the critical speed never occurred in testing. In fact, the highest values of the DMF were typically between 3 and 4. This inconsistency between experiment and theory suggested a different solution technique.

8.5 DYNAMIC HOOP STRESSES

There are two additional solution techniques considered here to explain dynamic hoop stresses. One technique is similar to flexural resonance theory, except that the stresses are bounded. The other technique is referred to as the dynamic stress theory and is derived from the equations for SDOF oscillators, using step pressure responses to describe the hoop stresses. While flexural resonance and beam theory may be preferred for short tubes, the dynamic stress theory is endorsed for longer pipes, and the following discussion supports this opinion.

8.5.1 Bounded Hoop Stresses from Beam Equations

This technique starts with the same beam equations used to define flexural resonance, but the assumption of resonance at the step pressure is not used. Consequently, the displacements and stresses at the shock are bounded. For clarity, a few of the equations from flexural resonance theory (paragraph 8.4) are rewritten to describe dynamic hoop stresses. Rewriting Eqs. (8.28), (8.44), and (8.45),

$$\frac{D\cdot\partial^4 w}{\partial z^4}+\frac{\rho/g\cdot\bar{T}\cdot\partial^2 w}{\partial t^2}+\frac{E\cdot\bar{T}\cdot w}{r^2}=P(1-H(z-a''\cdot t)) \qquad \text{US (8.65)}$$

$$w_1=A_1\cdot e^{(i\cdot c+d)\cdot\xi}+A_2\cdot e^{(-i\cdot c+d)\cdot\xi}+A_3\cdot e^{(i\cdot c-d)\cdot\xi}+A_4 e^{(-i\cdot c-d)\cdot\xi}+w_p \qquad \text{US (8.66)}$$

$$w_2=A_5\cdot e^{(i\cdot c+d)\cdot\xi}+A_6\cdot e^{(-i\cdot c+d)\cdot\xi}+A_7\cdot e^{(i\cdot c-d)\cdot\xi}+A_8\cdot e^{(-i\cdot c-d)\cdot\xi} \qquad \text{US (8.67)}$$

where w_1 describes the vibration after the shock due to the step response, and w_2 describes the free vibration near the shock. Let us change the flexural resonance assumptions to solve these equations. Flexural resonance theory

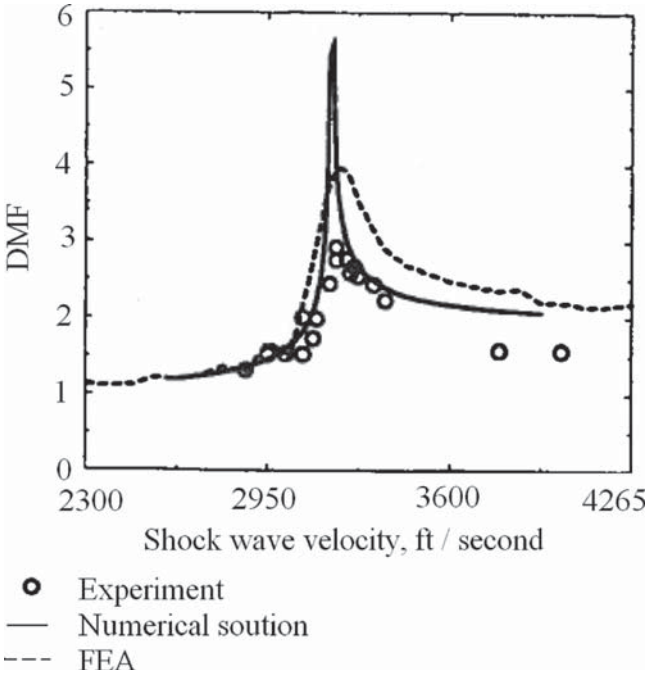


FIG. 8.29 EXAMPLE OF DYNAMIC AMPLIFICATION DATA (Beltman et al [229])

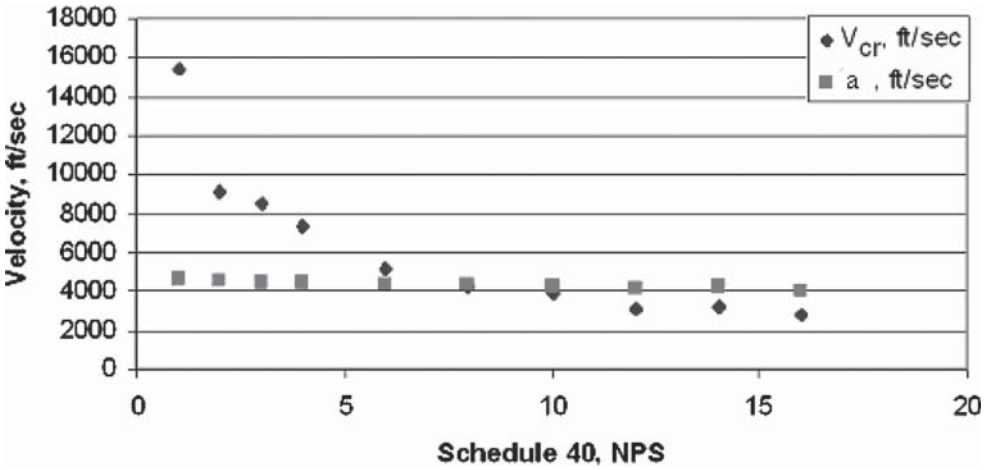


FIG. 8.30 WATER HAMMER WAVE SPEEDS AND CRITICAL VELOCITIES FOR PIPING

assumed that an infinite strain occurred at the step pressure increase, which has not been demonstrated. In fact, an assumption for ordinary structural vibrations (paragraph 7.2) was that the vibrations are stable, to the extent that $0 \le \zeta \le 1$ for real materials. Also, measured vibrations are always below a factor of four times the expected static stress. In other words, assume that the response is bounded at the shock. Also assume that the response is the sum of the step and free vibrations at the shock. Further assume that at $z = 0$, $t = 0^-$ occurs at the initiation of the step pressure input, and $t = 0^+$ occurs at the conclusion of step pressure input. The deflections before the shock, at the shock, and after the shock need descriptions. Before the shock, assume that

$$w_{2p} = w_{pr} \qquad \text{US (8.68)}$$

After the shock, assume that

$$w_{1a} + w_{2a} = w_a \qquad \text{US (8.69)}$$

At the shock, the vibration, or displacement, transitions nearly instantly between Eqs. (8.68) and (8.69), where the precursor displacement, w_{2p}, equals the precursor-free vibration, w_{pr}, ahead of the shock, and the total aftershock

TABLE 8.1 DMF FOR FLEXURAL RESONANCE IN FIXED-END PIPES

Sch 40, NPS	V_{cr}, ft/second, Eq. (8.61)	Water hammer wave speed, a, ft/second, Eq. (5.20)	Ratio of speeds, a/V_{cr}, Fig. 8.22	DMF, Fig. 8.21
1	15,383	4625	0.30	1.1
2	9067	4515	0.50	1.1
3	8469	4499	0.51	1.1
4	7353	4483	0.61	1.2
6	5140	4355	0.85	1.3
8	4245	4299	1.01	4.5
10	3909	4252	1.09	3.3
12	3118	4176	1.34	2.2
14	3216	4210	1.31	2.2
16	2806	4052	1.44	2.1
Sch. 5S, NPS				
1	6401	4419	0.69	1.2
2	3008	4136	1.37	2.2

vibration equals the sum of the step and free vibrations ($w_{1a} + w_{2a}$). That is, the total vibration, w_a, after the shock is the sum of free and aftershock vibrations imposed on the differential element shown in Fig. 8.20. This assumption to sum the vibrations after the shock, instead of assuming an infinite response, is a major transition from flexural response theory.

8.5.1.1 Precursor and Aftershock Vibrations For the aftershock wave, Eqs. (8.66) and (8.67) must be bounded as $z \to \pm\infty$, and $\xi \to \pm\infty$, $A_3 = A_4 = A_7 = A_8 = 0$. Therefore,

$$w_{1a} = A_1 \cdot e^{(i\cdot c+d)\cdot\xi} + A_2 \cdot e^{-(i\cdot c+d)\cdot\xi} + w_p \quad \text{US (8.70)}$$

$$w_{2a} = A_5 \cdot e^{(i\cdot c+d)\cdot\xi} + A_6 \cdot e^{-(i\cdot c+d)\cdot\xi} \quad \text{US (8.71)}$$

For the precursor wave, Eq. (8.66) must be bounded as $z \to +\infty$, and $\xi \to +\infty$, $A_5 = A_6 = 0$, and

$$w_{2p} = A_7 \cdot e^{(i\cdot c-d)\cdot\xi} + A_8 \cdot e^{(-i\cdot c-d)\cdot\xi} \quad \text{US (8.72)}$$

At $t = 0^-$, $w_{2p} = w_{2a} = 0$, $z = 0^-$, and Eq. (8.72) yields

$$A_5 = A_6 = A_7 = A_8 \quad \text{US (8.73)}$$

At the initiation of the pressure step at $t = 0^-$, $z = 0^-$, $W_p = 0$, and Eq. (8.70) reduces to

$$w_{1a} = A_1 \cdot e^{(i\cdot c+d)\cdot\xi} + A_2 \cdot e^{(-i\cdot c+d)\cdot\xi} \quad \text{US (8.74)}$$

Then, $w_1 = 0$, and Eqs. (8.73) and (8.74) yield

$$A_1 = A_2 \quad \text{US (8.75)}$$

By substitution of Eqs. (8.73) and (8.75) into Eqs. (8.70), (8.71), and (8.72)

$$w_{1a} = A_1 \cdot e^{(i\cdot c+d)\cdot\xi} + A_1 \cdot e^{(-i\cdot c+d)\cdot\xi} + w_p \quad \text{US (8.76)}$$

$$w_{2a} = A_5 \cdot e^{(i\cdot c+d)\cdot\xi} + A_5 \cdot e^{-(i\cdot c+d)\cdot\xi} \quad \text{US (8.77)}$$

$$w_{2p} = A_7 \cdot e^{(i\cdot c-d)\cdot\xi} + A_7 \cdot e^{(-i\cdot c-d)\cdot\xi} \quad \text{US (8.78)}$$

Rewriting these equations,

$$w_{1a} = e^{d\cdot\xi} \cdot \left(A_1 \cdot e^{(i\cdot c)\cdot\xi} + A_1 \cdot e^{(-i\cdot c)\cdot\xi}\right) + w_p \quad \text{US (8.79)}$$

$$w_{2a} = e^{d\cdot\xi} \cdot \left(A_5 \cdot e^{(i\cdot c)\cdot\xi} + A_5 \cdot e^{(-i\cdot c)\cdot\xi}\right) \quad \text{US (8.80)}$$

$$w_{2p} = e^{-d\cdot\xi} \cdot \left(A_5 \cdot e^{(i\cdot c-d)\cdot\xi} + A_5 \cdot e^{(-i\cdot c-d)\cdot\xi}\right) \quad \text{US (8.81)}$$

8.5.1.2 Pipe Wall Displacement Derivation Similar to the derivations of Eqs. (7.36) and (7.44), Eqs. (8.79) and (8.81) yield the pipe wall displacements.

$$w_{1a} = A_1 \cdot e^{d\cdot\xi} \cdot e^{\xi} \cdot \left(-\cos\left(c\cdot\xi\right)\right) + w_p \quad \text{US (8.82)}$$

$$w_{2a} = A_5 \cdot e^{d\cdot\xi} \cdot e^{\xi} \cdot \left(-\cos\left(c\cdot\xi\right)\right) \quad \text{US (8.83)}$$

$$w_{2p} = A_5 \cdot e^{-d\cdot\xi} \cdot e^{-\xi} \cdot \left(-\cos\left(c\cdot\xi\right)\right) \quad \text{US (8.84)}$$

At $t = 0^+$, $z = 0^+$, the initial deflection due to the step pressure equals 0, and Eq. (8.82) yields

$$w_{1a} = 0 \Rightarrow A_1 = w_p \quad \text{US (8.85)}$$

Another boundary condition is required to solve for A_5, and the derivatives of the displacements are inadequate. At $t = 0^+$, $z = 0^+$, w_{2p} and w_{1a} exist, but w_{2a} has yet to form. Rewriting Eqs. (8.82) and (8.84) at the moment the pressure step fully forms, the magnitude of the vibrations are equal, such that

$$\begin{aligned} w_{1a} &= e^{d\cdot\xi} \cdot \left(w_p \cdot e^{(i\cdot c)\xi} + w_p \cdot e^{-(i\cdot c)\xi}\right) + w_p \\ &= w_{2p} = e^{-d\cdot\xi} \cdot \left(A_5 \cdot e^{(i\cdot c)\xi} + A_5 \cdot e^{(-i\cdot c)\xi}\right) \end{aligned} \quad \text{US (8.86)}$$

Setting $\xi = 0$ at the shock,

$$w_{2p} = w_{2a} \Rightarrow A_5 = 2 \cdot w_p \quad (8.87)$$

Then,

$$w_{1a} = w_p \cdot \left(1 - e^{-d\cdot\xi} \cdot e^{-\xi} \cdot \left(\cos\left(c\cdot\xi\right)\right)\right) + w_p \quad (8.88)$$

$$w_{2a} = 2 \cdot w_p \cdot e^{-d\cdot\xi} \cdot e^{-\xi} \cdot \left(-\cos\left(c\cdot\xi\right)\right) \quad (8.89)$$

$$w_{2p} = w_{pr} = 2 \cdot w_p \cdot e^{d\cdot\xi} \cdot e^{\xi} \cdot \left(-\cos\left(c\cdot\xi\right)\right) \quad (8.90)$$

8.5.1.3 Pipe Wall Displacement Equation Substituting the Lame' equation from Eq. (8.42),

$$w_a = \frac{P\cdot r^2}{E\cdot\bar{T}} \cdot c \cdot \left(1 - 3\cdot e^{-d\cdot\xi} \cdot e^{-\xi} \cdot \left(\cos\left(c\cdot\xi\right)\right)\right) \quad \text{US (8.91)}$$

$$w_{pr} = -2 \cdot \frac{P \cdot r^2}{E \cdot \bar{T}} \cdot e^{d \cdot \xi} \cdot e^{\xi} \cdot \left(\cos\left(c \cdot \xi\right)\right) \quad \text{US (8.92)}$$

where applicable constants are obtained by rewriting Eqs. (8.31), (8.33), (8.40), and (8.41), and (8.61) to (8.63), such that

$$\lambda = \frac{\rho''}{2 \cdot g''} \cdot V_0''^2 \sqrt{\frac{r^2}{E \cdot \bar{T} \cdot D}} \quad \text{US (8.93)}$$

$$d = \sqrt{\frac{1-\lambda}{2}} \quad \text{US (8.94)}$$

$$c = \sqrt{\frac{1+\lambda}{2}} \quad \text{US (8.95)}$$

$$\omega = V \cdot \gamma \quad \text{US (8.96)}$$

$$\gamma = \sqrt[4]{\frac{E \cdot \bar{T}}{r^2 \cdot D}} \quad \text{US (8.97)}$$

8.5.1.4 Critical Velocity At the critical velocity,

$$V_{cr}\left(\frac{ft}{\sec}\right) = \frac{1}{12}\left(\frac{\text{ft}}{\text{in}}\right) \cdot \sqrt{\frac{E \cdot \bar{T} \cdot g''}{\rho'' \cdot r \cdot \sqrt{3 \cdot \left(1-\nu^2\right)}}} \quad \text{US (8.98)}$$

$$\omega_{cr} = \sqrt{\frac{2 \cdot E \cdot g''}{\rho'' \cdot r^2}} \quad \text{US (8.99)}$$

8.5.1.5 DMF and Maximum Stresses From Beam Theory By inspection of Eqs. (8.91) and (8.92) at the critical velocity, the maximum DMF = 4 for the aftershock wave, and the maximum DMF = 2 for the precursor wave, where $d = 0$, $c = 1$, and $\xi = \gamma \cdot (z - V_{cr} \cdot t) = 0$. In all cases, the waves decrease in magnitude in both directions away from the step pressure. Eqs. (8.91) to (8.99) may be used to estimate the displacements and resultant hoop stresses in tubes. Hoop stresses for a thin-wall pipe are obtained by multiplying the DMF times the stress, where

$$\sigma_\theta = \text{DMF} \cdot \frac{P \cdot r}{\bar{T}} \quad \text{US (8.100)}$$

8.5.2 Dynamic Stress Theory

The dynamic stress theory is a preferred, optional method to find dynamic hoop stresses for piping, and the theory incorporates damping and relies on the step response of a pipe at the shock. When compared to flexural resonance theory, the dynamic stress method predicts higher displacements and stresses (DMF < 4) for most wave speeds. Even so, this optional method agrees well with experimental results. The theory is developed here along with two different examples. The first example considers a gas-filled tube, which was a 3.06-ft long, 0.063-in. thick wall, 2-in. ID aluminum tube. The second example considers a water-filled pipe, which was a several hundred ft long, 2-in. NPS steel pipe. Both examples reasonably predict the maximum stresses determined during tests, but the frequencies are inaccurately predicted for thick-wall pipe. Even so, the maximum stresses are unaffected by frequency, and the dynamic stress theory can be used to adequately predict dynamic hoop stresses in piping.

8.5.2.1 Derivation of Dynamic Stress Equations Similar to the flexural resonance derivation, the equations describing the step response derivation are scattered throughout numerous references. The intent here is to provide the requisite equations to provide a thorough review of the analysis technique. All of the referenced equations have been published, and further details are available in the applicable references. Fig. 8.18 shows the problem to be addressed. Essentially, the step response technique assumes that the response of a shell can be calculated for a suddenly applied load and that this dynamic load is continually applied to the tube wall at the velocity of the shock wave, V. To start the discussion, a suddenly applied load at $V = V_0$ is considered, using Fig. 8.31.

The stresses due to expansion of the tube, or breathing stresses, are the focus of this discussion. Through-wall radial stresses are negligible. An isotropic tube is assumed

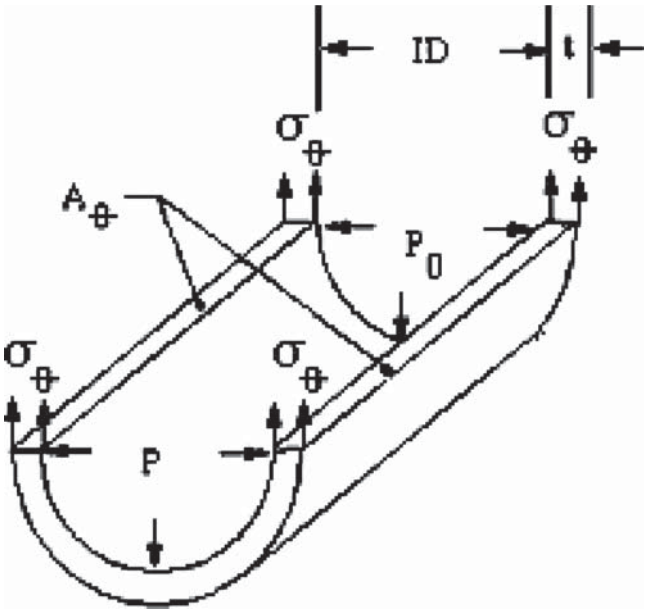


FIG. 8.31 SDOF PIPE MODEL

to act as a single degree of freedom (SDOF) oscillator subjected to a suddenly applied step increase in pressure. To evaluate the dynamic stresses, the static stress is first required, followed by the equation of motion. Once these equations are presented, the dynamics of the step pressure moving at a sonic velocity are discussed below.

8.5.2.2 Static Stress The static Lame' stress is determined by assuming a unit length subjected to a pressure, P, with opposing hoop stresses equal to $2 \cdot \sigma'_\theta$. This thin-wall approximation stress is expressed as

$$\sigma'_\theta = P \cdot \frac{r}{\bar{T}} \qquad \text{US (8.101)}$$

A more informative, and slightly more accurate, form of the hoop stress is the thick-wall approximation, which can be found as follows (Lubliner [9]).

$$\varepsilon_r = \frac{\mathrm{d}\left(r \cdot \varepsilon_\theta\right)}{\mathrm{dr}} = \frac{\sigma'_r - \nu \cdot \sigma'_\theta}{E} \qquad \text{US (8.102)}$$

$$\varepsilon'_\theta = \frac{\sigma'_\theta - \nu \cdot \sigma_r}{E} \qquad \text{US (8.103)}$$

On substitution,

$$\frac{\mathrm{d}\left(\left(1-\nu\right) \cdot \sigma'_\theta - \nu \cdot \sigma'_r\right)}{\mathrm{dr}} = \frac{\sigma'_r - \sigma'_\theta}{E} \qquad \text{US (8.104)}$$

By symmetry,

$$\frac{\mathrm{d}\sigma'_r}{\mathrm{dr}} + \frac{\sigma'_r - \sigma'_\theta}{r} = 0 \qquad \text{US (8.105)}$$

Substituting Eq. (8.104) into (8.105) yields

$$\frac{\mathrm{d}\left(\sigma'_\theta - \sigma'_r\right)}{\mathrm{dr}} + \frac{2 \cdot \left(\sigma'_\theta - \sigma'_r\right)}{r} = 0 \qquad \text{US (8.106)}$$

which can be solved by assuming two constants A_1 and A_2 such that

$$\sigma'_\theta - \sigma'_r = \frac{2 \cdot A_2}{r^2} \qquad \text{US (8.107)}$$

$$\sigma'_\theta + \sigma'_r = 2 \cdot A_1 \qquad \text{US (8.108)}$$

Then

$$\sigma'_\theta = -\frac{\left(\sigma'_r\big|_{r=ID}\right)}{2} + \frac{\sigma'_r\big|_{r=ID}}{2 \cdot \left(1 - \left(\frac{\mathrm{ID}}{\mathrm{OD}}\right)^2\right) \cdot \left(1 + \left(\frac{\mathrm{ID}}{\mathrm{OD}}\right)^2 + 2 \cdot \left(\frac{\mathrm{ID}}{r}\right)^2\right)} \qquad \text{US (8.109)}$$

which simplifies to

$$\sigma'_\theta = P \cdot \frac{\mathrm{ID}^2 \cdot \left(\mathrm{OD}^2 + \mathrm{ID}^2\right)}{r^2 \cdot \left(\mathrm{OD}^2 - \mathrm{ID}^2\right)} \qquad \text{US (8.110)}$$

Therefore, the maximum stress occurs at the inside diameter, such that

$$\sigma'_\theta = P \cdot \frac{\left(\mathrm{OD}^2 + \mathrm{ID}^2\right)}{\left(\mathrm{OD}^2 - \mathrm{ID}^2\right)} \qquad \text{US (8.111)}$$

where σ'_θ is the static hoop stress, and $\sigma_\theta(t)$ is considered to be the dynamic hoop stress for the remainder of this paper. Having established the static hoop stress for the cylinder, this stress needed to be related to the equation of motion.

8.5.2.3 Equation of Motion for a SDOF Oscillator The SDOF equation of motion is discussed in detail in Chapter 7.2.2. To clarify discussion, Eqs. (7.44) to (7.46) are rewritten, where the step response is expressed non-dimensionally as

$$\frac{x(t) \cdot k'}{F} = \left(1 - \frac{e^{-\zeta \cdot \omega \cdot t}}{\sqrt{1-\zeta^2}} \cdot \cos\left(\left(t \cdot \omega \cdot \sqrt{1-\zeta^2}\right) - \left(\frac{\zeta}{\sqrt{1-\zeta^2}}\right)\right)\right) = S(t, \omega, \zeta) \qquad \text{US (8.112)}$$

In the absence of damping, the step response is expressed as

$$\frac{x(t) \cdot k'}{F} = \left(1 - \cos\left(\omega \cdot t\right)\right) = S\left(t, \omega, \zeta = 0\right) \qquad \text{US (8.113)}$$

where

$$\mathrm{DMF} = \frac{x_{\max} \cdot k'}{F} = 2 \qquad \text{US (8.114)}$$

8.5.2.4 Equation of Motion for a Cylinder Subjected to a Sudden Internal Pressure Having defined the step response for a SDOF oscillator, a cylinder needed to be described in terms of this response. Returning to Fig. 8.31, the variable, σ'_θ, can be expressed in terms of x by a change of variables.

To change the variables, the circumference of the pipe is compared to the SDOF system using Hooke's law such that,

$$F_x = k' \cdot \Delta x'' = k' \cdot L' \cdot \varepsilon_x \qquad \text{US (8.115)}$$

where L" is the length of the spring, and $\varepsilon_x = \Delta x"/L"$. Similarly, the circumference, c, increases by a length equal to Δc when it expands. The static circumferential force expands the pipe wall with a force equal to

$$F_\theta = k' \cdot \Delta c = k' \cdot c \cdot \varepsilon_\theta = k'' \cdot c \cdot \sigma''_\theta / E \qquad \text{US (8.116)}$$

where $\varepsilon_\theta = \Delta c / c$. From the basic definition of a static stress

$$F_\theta = \sigma'_\theta \cdot A_\theta \qquad \text{US (8.117)}$$

Assuming a unit area, substituting Eqs. (8.112) and (8.117) into (8.115), using Hooke's law, and equating $F = P / A$

$$\sigma(t) = \sigma'_\theta \cdot \left(1 - \frac{e^{-\zeta \cdot \omega \cdot t}}{\sqrt{1-\zeta^2}} \cdot \cos\left(\left(t \cdot \omega \cdot \sqrt{1-\zeta^2} \right) - a\tan\left(\frac{\zeta}{\sqrt{1-\zeta^2}} \right) \right) \right) \qquad \text{US (8.118)}$$

$$\sigma_s(T) = P \cdot \frac{\left(OD^2 + ID^2 \right)}{\left(OD^2 - ID^2 \right)} \cdot H\left(t - \frac{z}{a"} \right) \cdot \left(1 - \frac{e^{-\zeta \cdot \omega \cdot t}}{\sqrt{1-\zeta^2}} \cdot \cos\left(\left(\left(t - \frac{z}{a"} \right) \cdot \omega \cdot \sqrt{1-\zeta^2} \right) - a\tan\left(\frac{\zeta}{\sqrt{1-\zeta^2}} \right) \right) \right) \qquad \text{US (8.119)}$$

where $H(\ldots)$ is the Heaviside step function, used to describe the response as the shock arrives at a point at time $t = z/V_0$. This equation describes the stresses in the pipe when the entire inner pipe wall is subjected to a suddenly applied pressure and is appropriate to predict the maximum response for short pipes (paragraph 8.2). However, the response of a long pipe is much more complex due to the moving pressure discontinuity at the shock wave, which induces the pipe stresses.

8.5.2.5 Pipe Stresses Due to a Shock Wave Referring to Fig. 8.18, the response of the pipe wall is assumed to consist of a precursor vibration and an aftershock vibration. Furthermore, the aftershock vibration is assumed to consist of two separate vibrations. Consequently, three vibrations needed consideration.

First of all, one vibration is due to the step response after a shock. Stresses, $\sigma_S(t)$, are assumed to act in accordance with Eq. (8.119) as the shock moves at a sonic velocity in the tube. The pipe is assumed to vibrate at its damped natural frequency in response to an excitation force.

Second, a precursor-free vibration stress, $\sigma_P(t)$, due to the step response is assumed. If the wall vibrates behind the shock, the wall in front of the shock must also vibrate in response to the applied step pressure to maintain continuity. However, the vibration must be a free vibration since an applied load on the pipe wall in front of the shock is nonexistent.

Third, a free-vibration stress, $\sigma_a(t)$, is also assumed to exist as part of the aftershock vibration. This vibration is assumed to exist due to the motion of the shock. If a discontinuous step pressure is applied to the pipe wall, and the shock is not moving (a" = 0), both the step response and precursor vibration exist. However, if the shock is moving, an observer at the shock experiences an additional effect. As he moves into the precursor vibration, the wall is already vibrating, and this additional vibration needs to be added to the other two vibration-induced stresses, such that the total vibration is described as

$$\sigma_\theta(t) = \sigma_p(t) + \sigma_s(t) + \sigma_a(t) \qquad \text{US (8.120)}$$

The stress due to the step response is presented in Eq. (8.119), but the other two stresses require further discussion.

8.5.2.6 Precursor Stresses The precursor stresses are visualized easier if damping is excluded from the equations of motion. Consider Fig. 8.32 to evaluate precursor-free vibrations due to a step response. One vibration occurs at an arbitrary time, $t = 0$, behind the shock. In front of the shock, a free vibration exists. What is the nature of the free vibration? Assume that the vibration behind the shock is due to the step pressure increase and that the vibration in front of the shock equals the sum of the pressure increase to P and a pressure decrease back to $P = 0$. Then, the total vibration equals the sum of two step responses, such that

$$\sigma_p(t) = \sigma'_\theta \cdot \left(1 - \cos(\omega \cdot t) \right) - \left(1 - \cos\left(\omega \cdot \left(t - \frac{z}{a''} \right) \right) \right)$$

$$= \sigma'_\theta \cdot \left(\cos\left(\omega \cdot \left(t - \frac{z}{a''} \right) \right) - \cos(\omega \cdot t) \right) \qquad \text{US (8.121)}$$

However, this assumption does not compensate shock wave speeds, and the arbitrary selection of $t = 0$ at $z = 0$ also affects the pipe response.

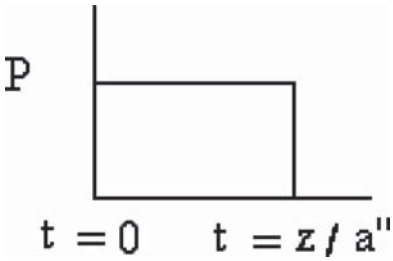


FIG. 8.32 FREE-VIBRATION MODEL

8.5.2.7 Effects of the Arbitrary Selection of $t = 0$ The location of $t = 0$ with respect to the shock wave affects the pipe response. As z/a' approaches t, the maximum value of Eq. (8.121) reduces from $2 \cdot \sigma'_\theta$ to 0. Since the boundary condition is arbitrary, the most that can be claimed is that the maximum precursor stress lies within a range of stresses equal to 0 through $2 \cdot \sigma'_\theta$, which is consistent with the variation in maximum strains observed in tests (Leishear [10]). Tests showed that the precursor stresses varied between approximately σ'_θ and $2 \cdot \sigma'_\theta$. The maximum stress is therefore adequately described by Eq. (8.121).

8.5.2.8 Effects of the Wave Speed If the precursor vibration travels at the speed of the shock, the vibration frequency will appear different to a stationary observer. The higher the wave velocity, the higher the frequency appears. A significant assumption is made at this point in this analysis. The critical velocity defined by Eq. (8.98) is assumed to be the velocity at which the maximum stress occurs. Accordingly, at this velocity, the frequencies before and after the shock are nearly equal, and this assumption provides a requisite boundary condition to apply step response equations to the stresses induced by shock waves in the pipe. The frequency after the shock is assumed to equal the frequency for a tube. For an undamped frequency

$$\omega = a'' \cdot \gamma \qquad \text{US (8.122)}$$

$$\omega_1 = \sqrt{\frac{E \cdot g''}{\rho'' \cdot r^2}}, \text{ (Barez [232])} \qquad \text{US (8.123)}$$

Note that Eq. (8.123) differs from Eq. (8.99) by a factor of $\sqrt{2}$; hence, the significance of assuming maximum stresses occur at the critical velocity. The assumption introduces an approximation based on experimental data. Tests performed by Beltman et al [229] measured aftershock frequencies equal to the frequencies predicted by assuming that the pipe vibrates at its damped natural frequency, which is

$$\omega = \sqrt{1-\zeta^2} \cdot \sqrt{\frac{E \cdot g''}{\rho'' \cdot r^2}} \qquad \text{US (8.124)}$$

Assuming the pipe response frequency equals this equation at the critical velocity, the apparent frequency to a stationary observer can be obtained, such that

$$\sigma_p(t) = \sigma'_\theta \cdot \left(\cos\left(\tau \cdot \omega \cdot \left(t - \frac{z}{a''} \right) \right) - \cos(\omega \cdot t) \right) \qquad \text{US (8.125)}$$

where the velocity ratio equals

$$\tau = \frac{a}{V_{cr}} \qquad \text{US (8.126)}$$

8.5.2.9 Maximum Damped Precursor Stress To determine the damped maximum precursor stress, Eq. (8.125) can be rewritten similar to Eq. (8.119), by recognizing that the exponential function increases with respect to time. Then,

$$\sigma_p(t) = -2 \cdot P \cdot \frac{\left(OD^2 + ID^2\right)}{\left(OD^2 - ID^2\right)} \cdot H\left(\frac{z}{a''} - t \right) \cdot \left(\frac{e^{\tau \cdot \zeta \cdot \omega \cdot \left(t - \frac{z}{a''} \right)}}{\sqrt{1-\zeta^2}} \cdot \cos\left(\left(\left(t - \frac{z}{a''} \right) \cdot \tau \cdot \omega \cdot \sqrt{1-\zeta^2} \right) - a\tan\left(\frac{\zeta}{\sqrt{1-\zeta^2}} \right) \right) \right) \qquad \text{US (8.127)}$$

8.5.2.10 Aftershock-Free-Vibration Stresses The stresses behind the shock due to free vibrations are assumed to be identical to the precursor vibrations, except that the exponential function decreases with respect to time. That is,

$$\sigma_a(t) = -2 \cdot P \cdot \frac{\left(OD^2 + ID^2\right)}{\left(OD^2 - ID^2\right)} \cdot H\left(t - \frac{z}{a''} \right) \cdot \left(\frac{e^{\tau \cdot \zeta \cdot \omega \cdot \left(t - \frac{z}{V_0} \right)}}{\sqrt{1-\zeta^2}} \cdot \cos\left(\left(\left(t - \frac{z}{a''} \right) \cdot \tau \cdot \omega \cdot \sqrt{1-\zeta^2} \right) - a\tan\left(\frac{\zeta}{\sqrt{1-\zeta^2}} \right) \right) \right) \qquad \text{US (8.128)}$$

Similar to the precursor stress, this stress varies between a maximum predicted by Eq. (8.128) and zero. Again, a range of stresses are expected along the pipe wall, and Eq. (8.128) predicts the maximum possible stresses along the pipe.

8.5.2.11 Damping Damping for hoop stresses in pipes was discussed in paragraph 7.3.2.3 (Eq. (7.100)) and was expressed as

$$\zeta = \frac{-\ln(\varepsilon')}{\left(\ln(\varepsilon')^2 + \pi^2\right)^{\frac{1}{2}}} + \frac{D \cdot E}{2 \cdot \pi \cdot S_r^2} \quad \text{US (8.129)}$$

8.5.2.12 Maximum Stress When the Critical Velocity is Not Considered If the maximum stress is assumed to be independent of the critical velocity, the maximum stress can be determined by Eq. (8.120) by substituting

$$\tau = 1 \quad \text{US (8.130)}$$

into the constitutive equations. The net result of this substitution is that the DMFs will be conservatively higher than when the critical velocity was compensated. In thick-wall solutions, the critical velocity and frequencies are yet to be clearly understood, but this approximation can be used to find a conservative, albeit somewhat high, maximum stress, since the maximum stress will be independent of frequency. Then, the hoop stress equals

$$\sigma_s(t) = P \cdot \frac{\left(OD^2 + ID^2\right)}{\left(OD^2 - ID^2\right)} \cdot H\left(t - \frac{z}{a''}\right)$$

$$\cdot\left(1 - \frac{e^{-\zeta \cdot \omega \cdot t}}{\sqrt{1-\zeta^2}} \cdot \cos\left(\left(t \cdot \omega \cdot \sqrt{1-\zeta^2}\right) - a\tan\left(\frac{\zeta}{\sqrt{1-\zeta^2}}\right)\right)\right) \quad \text{US (8.131)}$$

$$\sigma_a(t) = -2 \cdot P \cdot \frac{\left(OD^2 + ID^2\right)}{\left(OD^2 - ID^2\right)} \cdot H\left(t - \frac{z}{a''}\right)$$

$$\cdot\left(\frac{e^{-\zeta \cdot \omega \cdot}}{\sqrt{1-\zeta^2}} \cdot \cos\left(\left(\cdot\omega \cdot \sqrt{1-\zeta^2}\right) - a\tan\left(\frac{\zeta}{\sqrt{1-\zeta^2}}\right)\right)\right) \quad \text{US (8.132)}$$

The dynamic stress after the shock then equals

$$\sigma_\theta(t) = P \cdot \frac{\left(OD^2 + ID^2\right)}{\left(OD^2 - ID^2\right)} \cdot H\left(t - \frac{z}{a''}\right)$$

$$\cdot\left(1 - 3 \cdot \frac{e^{-\zeta \cdot \omega \cdot t}}{\sqrt{1-\zeta^2}} \cdot \cos\left(\left(t \cdot \omega \cdot \sqrt{1-\zeta^2}\right) - a\tan\left(\frac{\zeta}{\sqrt{1-\zeta^2}}\right)\right)\right) \quad \text{US (8.133)}$$

and the dynamic stress before the shock equals

$$\sigma_p(t) = -2 \cdot P \cdot \frac{\left(OD^2 + ID^2\right)}{\left(OD^2 - ID^2\right)} \cdot H\left(\frac{z}{a''} - t\right)$$

$$\cdot\left(\frac{e^{\zeta \cdot \omega \cdot \left(t - \frac{z}{a''}\right)}}{\sqrt{1-\zeta^2}} \cdot \cos\left(\left(\omega \cdot \sqrt{1-\zeta^2}\right) - a\tan\left(\frac{\zeta}{\sqrt{1-\zeta^2}}\right)\right)\right) \quad \text{US (8.134)}$$

From these equations, the maximum stress is the product of the static stress times the DMF. The maximum stress is independent of frequency and equals the maximum stress during the first vibration cycle. Similar to the derivation of Eq. (7.95), the maximum hoop stress equals

$$\sigma_{\theta,\max} = 2 \cdot \sigma'_\theta \cdot \left(1 + e^{\left[\frac{-\zeta \cdot \pi}{\sqrt{1-\zeta^2}}\right]}\right) \quad \text{US (8.135)}$$

For fatigue calculations, subsequent stresses may be calculated from the ratio of any two successive amplitudes, $\sigma_{\theta 1}$ and $\sigma_{\theta 2}$, which are also independent of frequency. Successive stress cycle maximums are predicted by the log decrement (Eq. (7.29)), such that

$$\frac{\sigma_{\theta 1}}{\sigma_{\theta 2}} = e^{\left(\frac{2 \cdot \pi \cdot \zeta}{\sqrt{1-\zeta^2}}\right)} \quad \text{US (8.136)}$$

where σ_1 and σ_2 are successive peak stress amplitudes in a vibration response.

8.5.3 Comparison of Theory to Experimental Results for a Gas-Filled Tube

Example 8.7 Compare the dynamic stress theory to Beltman's results, shown in Fig. 8.28 of Example 8.5.

To calculate the stresses in a tube wall, critical velocity was considered by using Eqs. (8.119), (8.127), (8.128), and (8.129), and dimensions and material properties were substituted into the equations. The results are summarized here, but calculation details are available (Leishear [3]). In short, the dynamic stress theory described stresses accurately near the critical velocity for a short tube, but did not accurately predict stresses away from the critical velocity for a short tube. Equations were also modified to indicate strain,

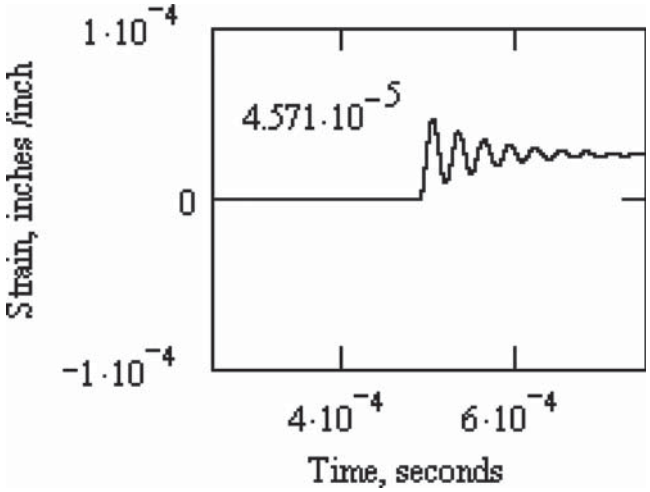


FIG. 8.33 STEP RESPONSE OF THE HOOP STRAIN AT THE OUTER WALL AFTER A SHOCK, A/V_{CR} = 0.98

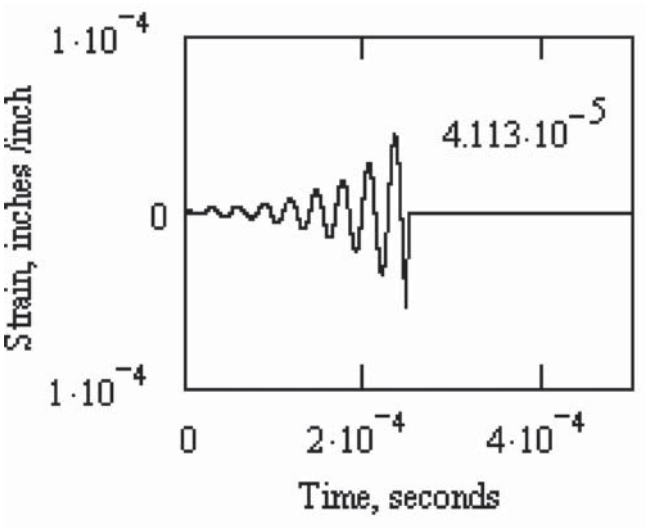


FIG. 8.35 MAXIMUM PRECURSOR STRAIN AT THE OUTER WALL PRIOR TO A SHOCK

using Hooke's law. Figs. 8.33 to 8.36 capture the discrete vibrations on the inner pipe wall, which contribute to the total vibration, shown in Fig. 8.37. The total vibrations at the outer pipe wall are shown in Fig. 8.38, and these vibrations are consistent with measurements shown in Fig. 8.28 (DMF = 3.41). Considering Fig. 8.27, theory does not describe all strains at the pipe wall. Simkins noted that bending may be a cause of variable strains along a tube, but the motion of the tube ahead of the shock also changes the boundary conditions and the resultant strains. For all tests to date, these effects reduce the strains, and theory is adequate to predict maximum strains. However, the number of strain cycles may increase during shock wave response. Also, strains were calculated at higher wave speeds as shown in Figs. 8.39 and 8.40, and the calculated results were significantly higher than reported in Beltman's experimental work (Fig. 8.29).

8.5.4 Comparison of Theory to Experimental Results for a Liquid-Filled Pipe

Example 8.8 Compare the dynamic stress theory to experimental results in a long pipe, which was described in Examples 4.9 and 5.25.

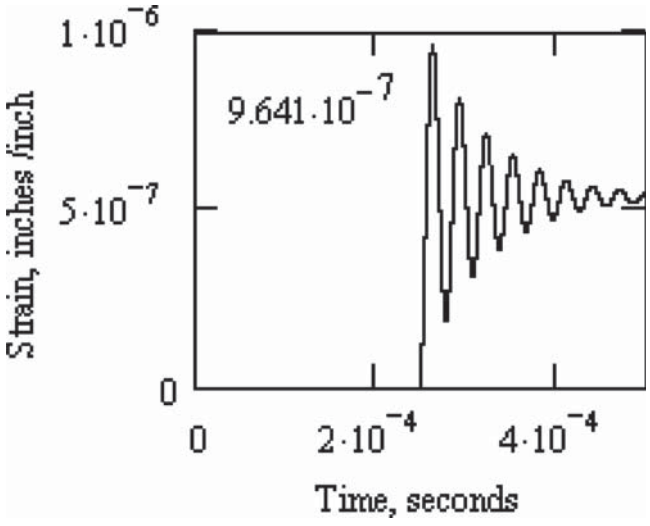


FIG. 8.34 HOOP STRAIN DUE AT THE INNER WALL DUE TO THROUGH-WALL RADIAL COMPRESSION

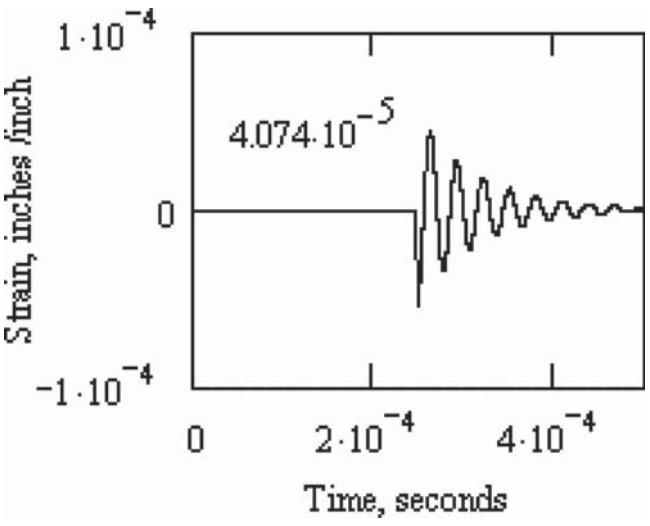


FIG. 8.36 MAXIMUM FREE VIBRATION AT THE OUTER WALL AFTER THE SHOCK

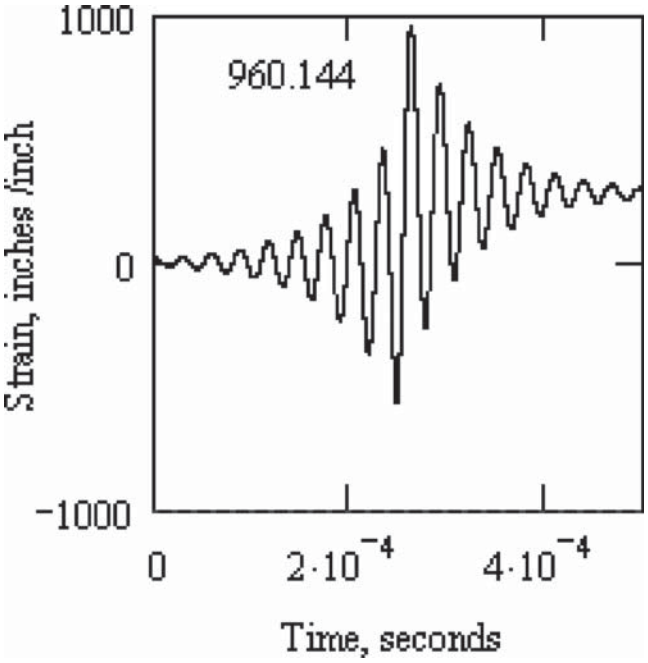


FIG. 8.37 MAXIMUM HOOP STRESS AT THE INNER WALL DUE TO A SHOCK

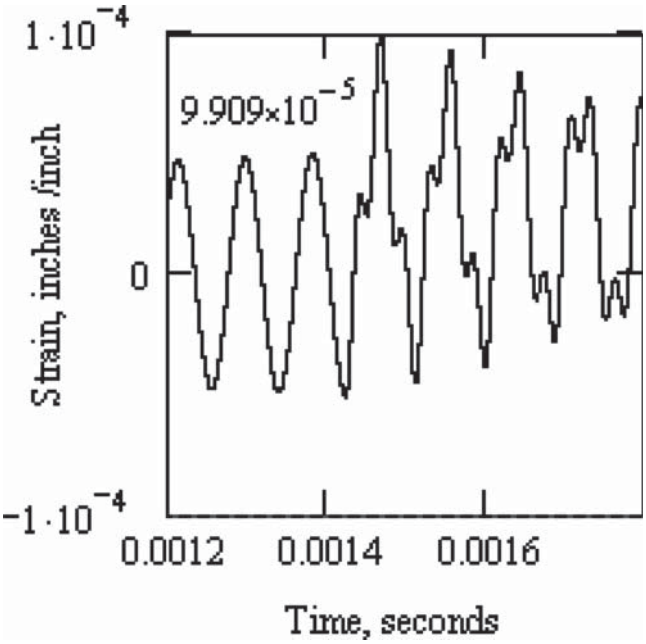


FIG. 8.39 MAXIMUM STRAIN AT $A/V_{CR} = 1.1$

Experimental tests were performed on a 2-in. NPS, schedule 40, steel pipe to measure pressures caused by vapor collapse, and the resultant pipe strains were compared to dynamic stress theory. An earlier version of the dynamic stress theory was applied (Leishear [6]), and data from that research was reevaluated here using updated Eqs. (8.129) to (8.135). The frequency for a water-filled tube was also used as derived by Barez [233], where

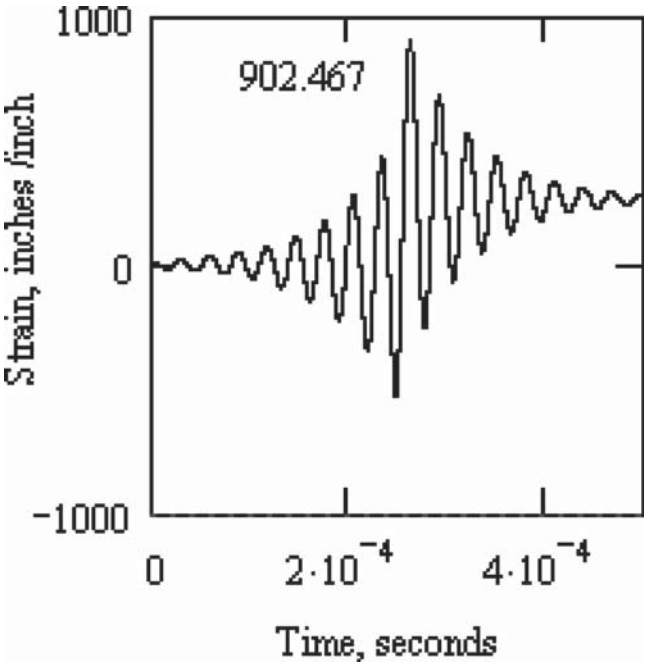


FIG. 8.38 MAXIMUM HOOP STRESS AT THE OUTER WALL DUE TO A SHOCK

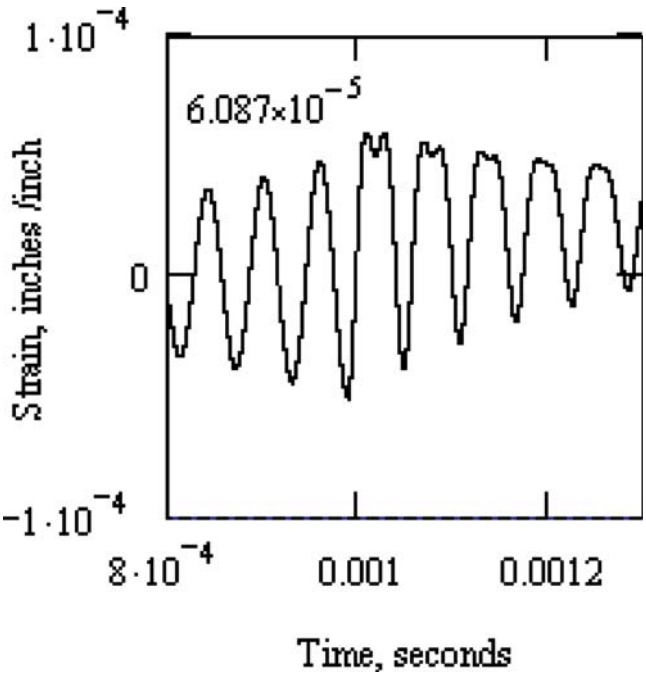


FIG. 8.40 MAXIMUM STRAIN AT $A/V_{CR} = 1.44$

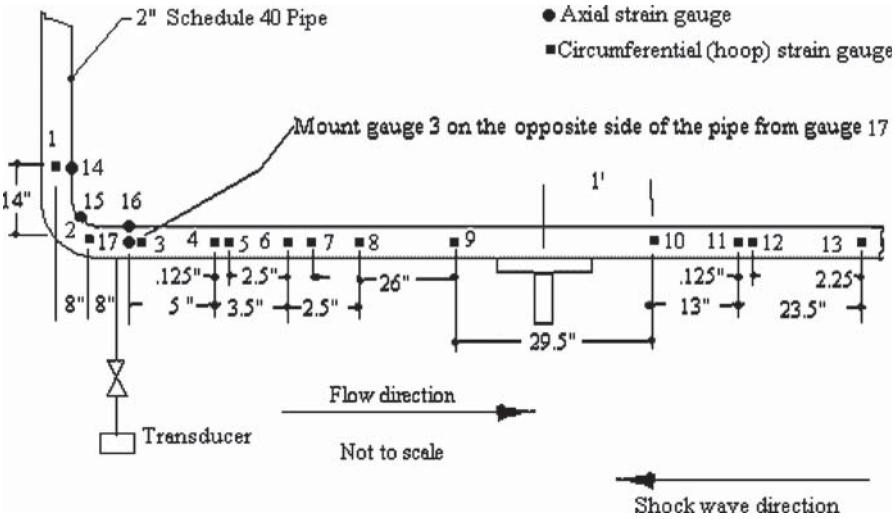


FIG. 8.41 TEST SETUP FOR WATER HAMMER STRAIN EVALUATION

$$\omega_\theta = \sqrt{g''.\frac{\left(\frac{2\cdot k}{(r_m)\cdot \bar{T}}\right)+\left(\frac{E}{(r)^2\cdot(1-\nu^2)}\right)}{\rho_{pipe}+\frac{(r_m)\cdot\rho_{water}}{4\cdot\bar{T}}}} \qquad (8.137)$$

8.5.4.1 Test Setup and Raw Data The test setup is shown in Fig. 8.41, where strain gauges were located along 10 ft of a 1000-ft long pipe. Pressure data is displayed in Figs. 8.42 and 8.43, and the largest measured pressure peak, labeled Pr1, was selected for investigation. Strain data was recorded as shown in Fig. 8.44 for the complete recorded strain history of one strain gauge. Fig. 8.45 zooms in on typical strains associated with the Pr1 pressure wave. Fig. 8.46 demonstrates the potential data inaccuracy due to limited sampling of strains. Also, accuracy of the new instrumentation as supplied from the manufacturer was not verified. Test data is provided in Table 8.2.

Measured strains provide much insight into pipe response. Strains from a sequential set of strain gauges is shown in Figs. 8.47 to 8.54 to demonstrate wave travel at advancing times as the shock travels at a sonic velocity along the bore of the pipe. Also, strains traveling around the elbow are shown in Fig. 8.55. Note that strains are comparable to the strains elsewhere on the pipe, indicat-

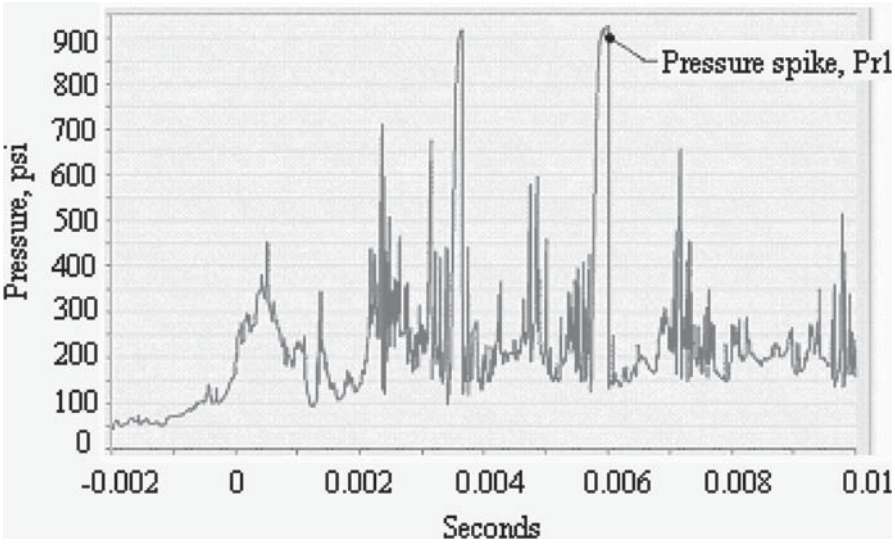


FIG. 8.42 TYPICAL PRESSURE DATA (zoomed in from Fig. 5.52)

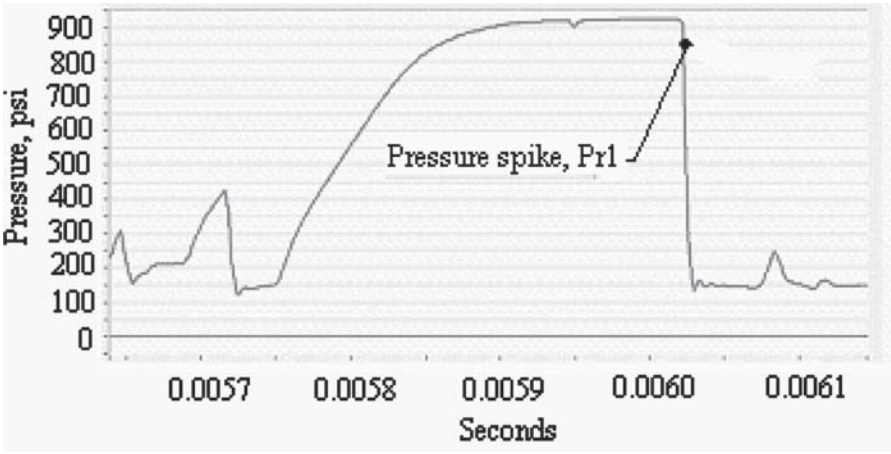


FIG. 8.43 PRESSURE DATA (zoomed in on Pr1)

ing that hoop stresses in the elbow are equivalent to hoop stresses in the straight pipe.

8.5.4.2 Test Results and Discussion The DMF and Table 8.2 can be used to compare theory to experiment. From Eq. (8.135),

$$\text{DMF} = 2 \cdot \left(1 + e^{\left[\frac{-\zeta \cdot \pi}{\sqrt{1-\zeta^2}} \right]} \right) \qquad \text{US (8.138)}$$

The DMF depends on the assumptions for damping. If the pipe wall and water are assumed to act as series springs, the DMF = 3.96. If the water and pipe act in parallel, the DMF = 3.51. From the experimental data (Leishear [6]) partially shown in Figs. 8.47 to 8.55, the average experimental DMF = 3.78, and with 95% confidence, this DMF is within ±26%. Both the 3.51% and 3.96% damping estimates are within experimental error. The series assumption provides the higher, conservative estimate, and the parallel assumption provides an estimate where vibrations decay faster, which is more consistent with the actual stresses and strains.

In short, the dynamic stress theory predicts that the maximum vibration magnitudes are consistent between theory and experiment for a liquid-filled pipe. Although further research is recommended, this observation provides a favorable comparison between theory and experiment to assess damages due to induced shock waves in a pipe. In fact, the dynamic stress theory provides better results for piping than flexural resonance theory. In Example 8.6 (paragraph 8.4.2.2), the DMF = 1.1 for shocks in 2-in., schedule 40 pipe, which is much lower than the experimental DMF = 3.78. To provide closure to this example, details with respect to pipe wall frequency, wave velocity, and pressure magnitude follow.

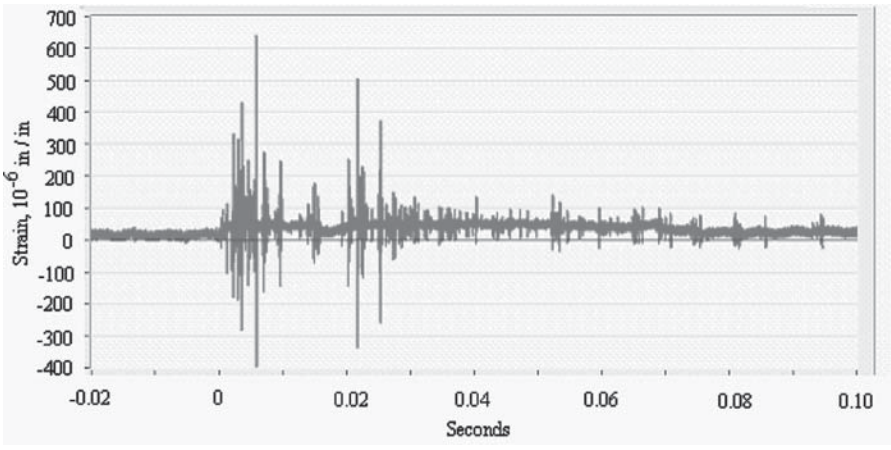


FIG. 8.44 TYPICAL HOOP STRAIN MEASUREMENTS AT POINT 13

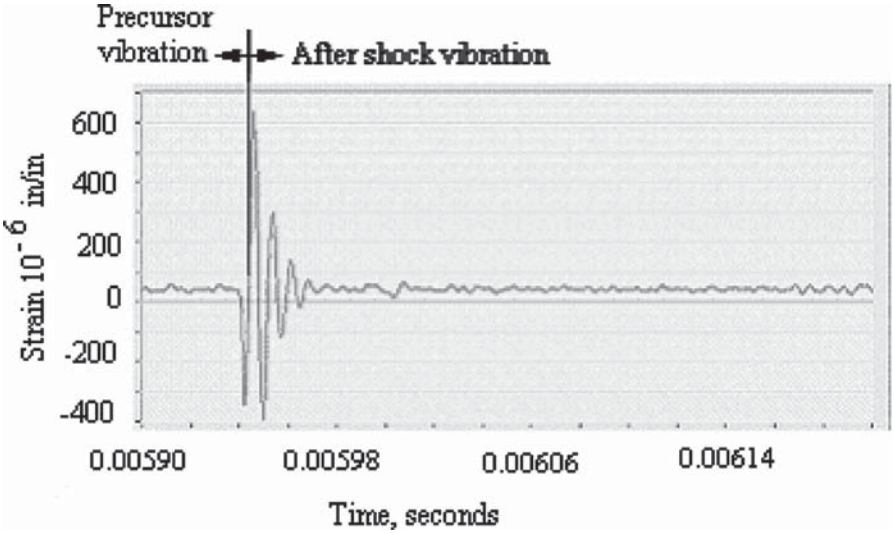


FIG. 8.45 TYPICAL HOOP STRAIN MEASUREMENTS AT POINT 13 (zoomed in from Fig. 8.44)

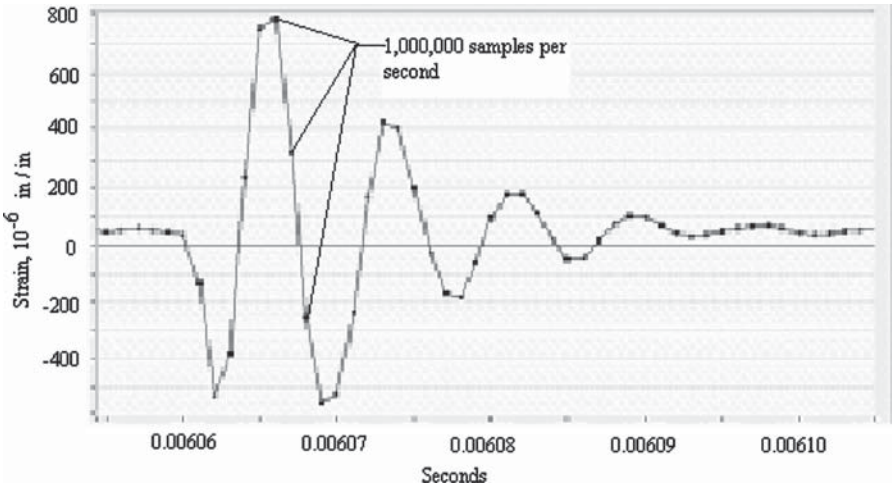


FIG. 8.46 EFFECTS OF THE SAMPLE RATE ON THE ACCURACY OF MEASURED STRAINS

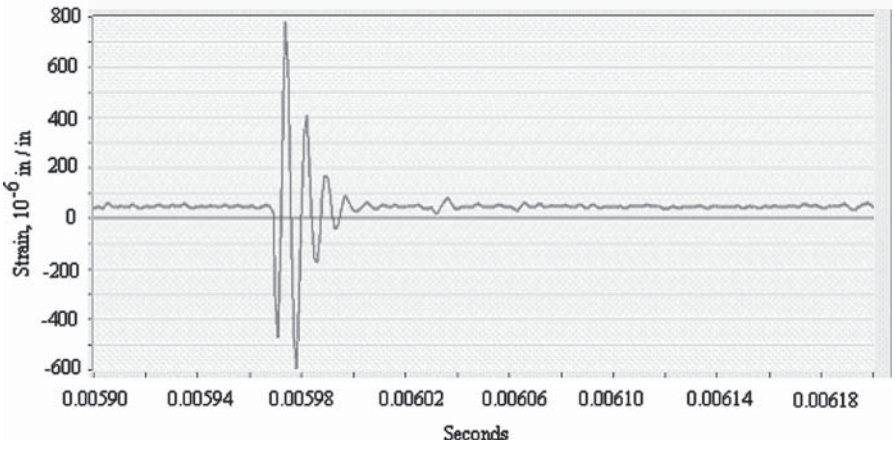


FIG. 8.47 TYPICAL HOOP STRAIN MEASUREMENTS AT POINT 12

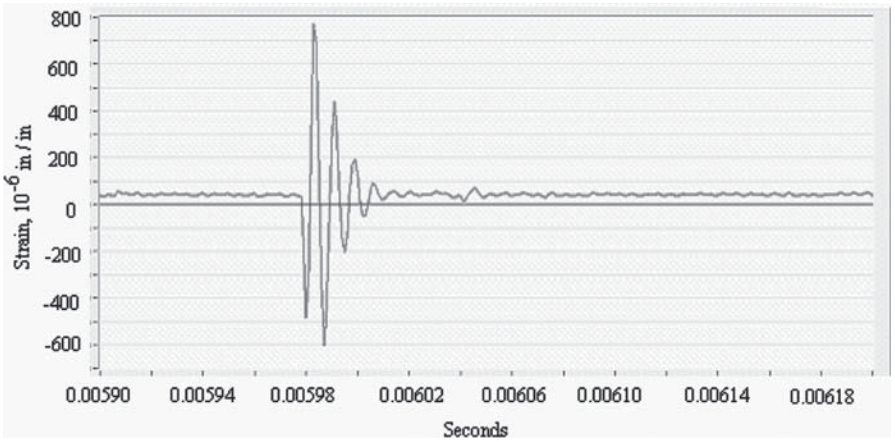


FIG. 8.48 TYPICAL HOOP STRAIN MEASUREMENTS AT POINT 11

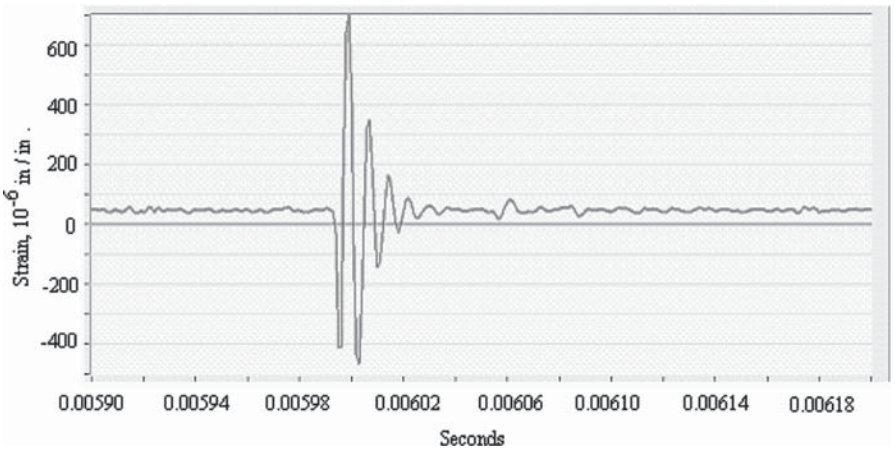


FIG. 8.49 TYPICAL HOOP STRAIN MEASUREMENTS AT POINT 10

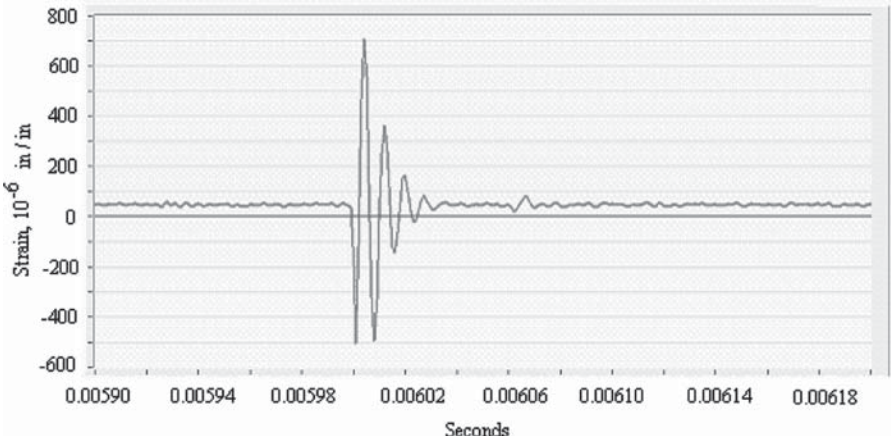


FIG. 8.50 TYPICAL HOOP STRAIN MEASUREMENTS AT POINT 9

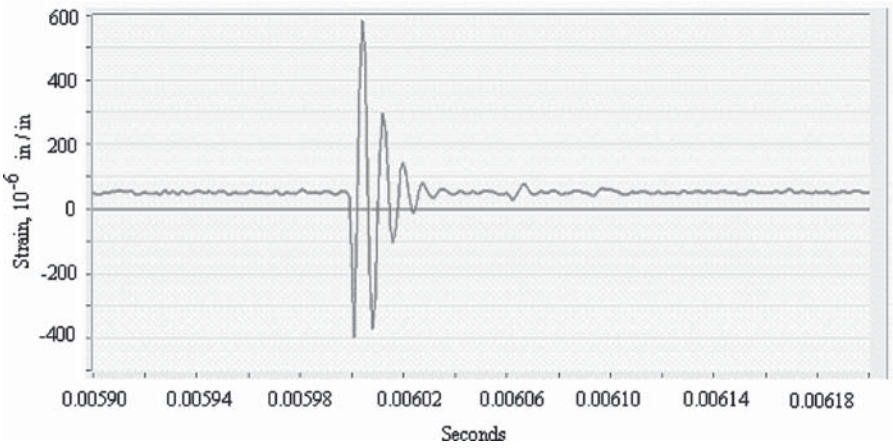


FIG. 8.51 TYPICAL HOOP STRAIN MEASUREMENTS AT POINT 8

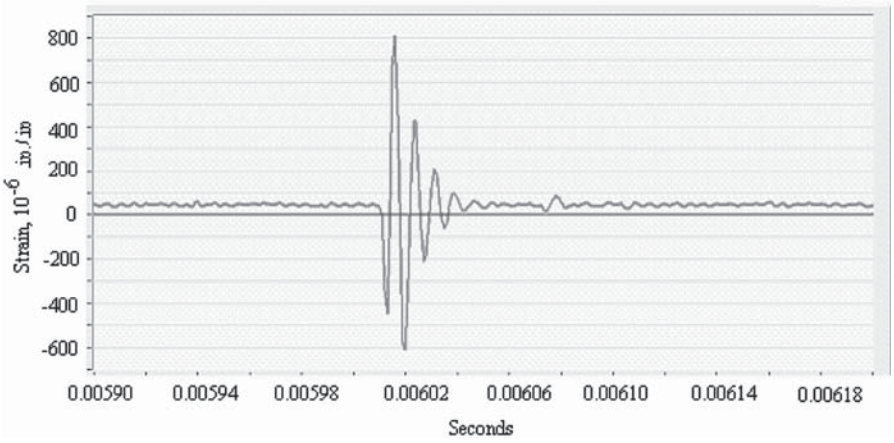


FIG. 8.52 TYPICAL HOOP STRAIN MEASUREMENTS AT POINT 7

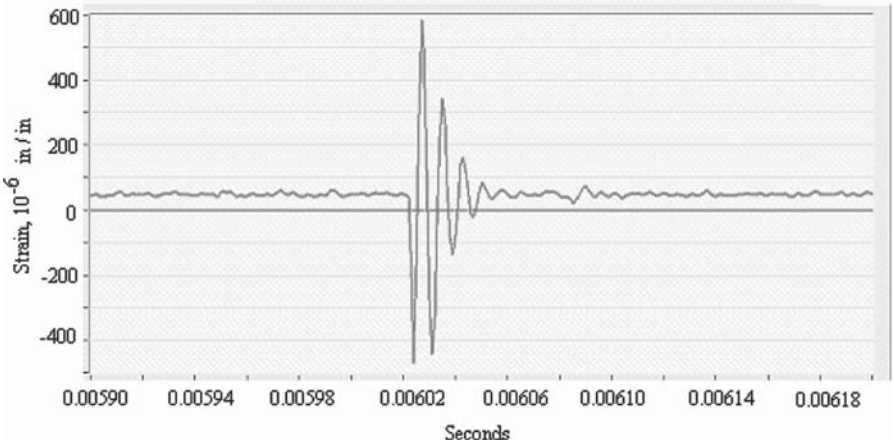


FIG. 8.53 TYPICAL HOOP STRAIN MEASUREMENTS AT POINT 6

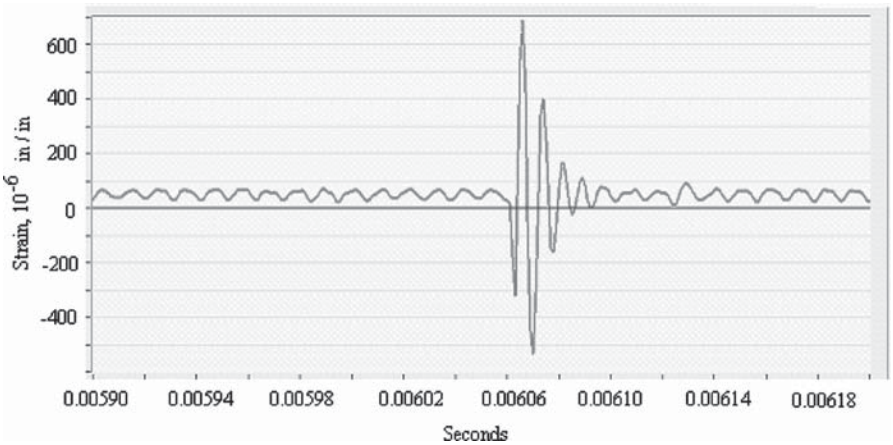


FIG. 8.54 TYPICAL HOOP STRAIN MEASUREMENTS AT POINT 5

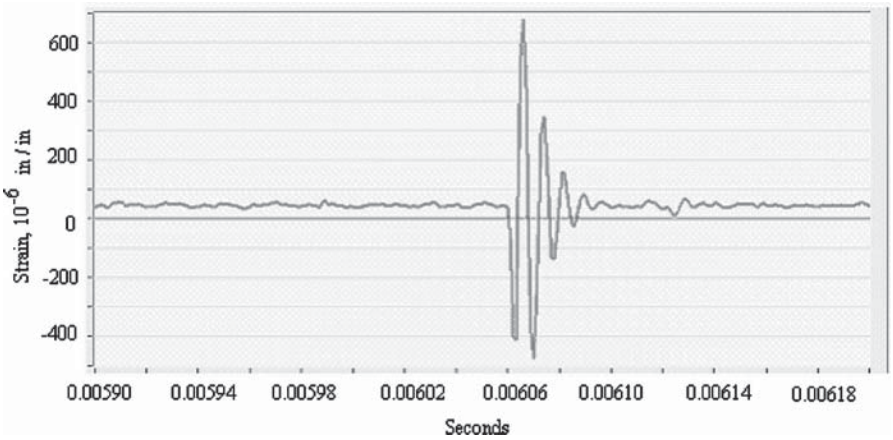


FIG. 8.55 TYPICAL HOOP STRAIN MEASUREMENTS AT POINT 2 ON THE ELBOW

8.5.4.3 Breathing Stress Frequency Although frequencies are reasonably predicted for thin-wall tubes, the measured frequency of a thick-wall pipe was different than predicted by dynamic stress theory (50% error). This inconsistency may require further research, but frequency differences have negligible effect on the maximum stress amplitude or the number and magnitude of subsequent vibration cycles. Consequently, an interest in frequency response has academic merit, but adds little to predictions of pipe failures from either overload or fatigue.

8.5.4.4 Wave Velocities Several different wave velocities may be calculated by using different end-constraint assumptions. Calculated wave velocities, a = 4515 ft/second, significantly exceeded the measured wave velocities during testing at the Pr1 shock of interest, a = 2679 ft/second. This wave speed anomaly was attributed to the formation of cavitation bubbles in the wake of other preceding pressure waves. On closer inspection of vibration plots, each successive wave travels slightly slower than the wave in front of it. The change in the average pipe volume leads to a vapor fraction of 0.05%, which provides a cause of cavitation. That is, a change in wave velocity occurs when vapor in solution reduces the wave velocity, and vapor formed in the wake of a shock cannot be replaced by slower inrushing liquid, due to the sonic wave velocity at the shock front. These factors combined to support a conclusion that cavitation affected shock velocity. Even so, the wave velocity has negligible impact on predicted maximum stresses and strains when the dynamic stress theory is applied.

8.5.4.5 Pressure Surge Magnitude Near the point of measured pressures, a void was present in the overhead piping. When the pump started, slug flow and vapor collapse was initiated at that point. To find the maximum pressure in the pipe, the velocity of the slug equals

$$Vs = \sqrt{\frac{2 \cdot Lv \cdot P_{pump}}{\rho_{water} \cdot Ls}} \qquad \text{US (8.139)}$$

TABLE 8.2. MATERIAL AND PIPE DATA

Operating temperature	178°F	Poisson's ratio, ν	0.29
Pipe wall material	P53 steel	Critical velocity, V_{cr}, ft/second	4604
Elastic modulus, E, psi	28,600,000	Shock velocity, a, ft/second	30,400
Bulk modulus of water, k, psi	319,000	Initial head , P_0, psi	9.35
Water density, ρ''_{water}, lbm, in^3	0.035	Pressure change, P, psi	925
Pipe density, ρ''_{pipe}, lbm, in^3	0.283	Theoretical shock velocity, a, ft/second	4515
Theoretical vibration period, seconds	$4.02 \cdot 10^{-5}$	Measured shock velocity, a, ft/second	2679
Measured vibration period, seconds	$6.5 \cdot 10^{-5}$	Damping, $\zeta = \zeta_{f+}\zeta_s$	0.089
Static strain at the OD, $\varepsilon'_\theta = P \cdot \frac{ID^2 \cdot \left(OD^2 + ID^2\right)}{E \cdot r^2 \cdot \left(OD^2 - ID^2\right)}$	0.00178	Damping, $\zeta = 1 / (1 / \zeta_f + 1 / \zeta_s)$	0.006
Average measured strain	670.7	Experimental strain uncertainty	±174.1
Pipe outside diameter, OD, in.	2.375	Efficiency, ε	0.766
Pipe inside diameter, ID, in.	2.067	Enthalpy, Δh	0.273
Structural damping, $\overset{s}{\zeta}$	0.006	Entropy, Δs	0.0001
Fluid damping, $\overset{f}{\zeta}$	0.083	Specific damping, D	0.035
Ultimate strength, S_u, psi	60,000	Endurance limit, S_e, psi	21,900

A 50-gpm rate was determined from measurements, and the pressure was obtained from the pump curve in Fig. 8.58. The pressure, p_{pump}, supplied by the pump during normal operation at 50 gpm is

$$p_{pump} = 21.2 \text{ psi} \qquad \text{US (8.140)}$$

The slug length and void length were determined from field observations. Slug velocity and resulting maximum overpressure were calculated. Accordingly,

$$L_S = 712 \text{ ft} \qquad \text{US (8.141)}$$

$$L_V = 36.5 + 3 = 39.5 \text{ ft} \qquad \text{US (8.142)}$$

$$Vs = \sqrt{\frac{2 \cdot (36.5 + 3) \cdot 21.2 \cdot 144 \cdot 32.174}{60.13 \cdot 712}} \qquad (8.143)$$

$$V_s = 13.463 \text{ ft/second} \qquad (8.144)$$

$$P = 969 \text{ psi} \qquad (8.145)$$

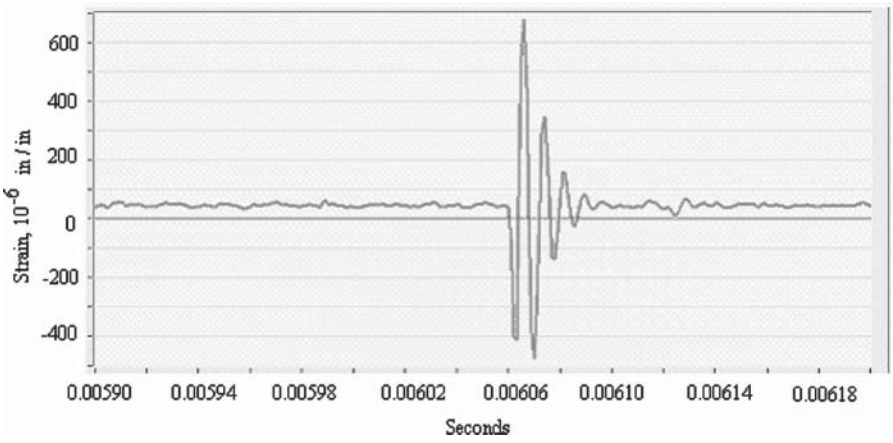


FIG. 8.56 TYPICAL HOOP STRAIN MEASUREMENTS AT POINT 3 ON THE SIDE OF THE PIPE

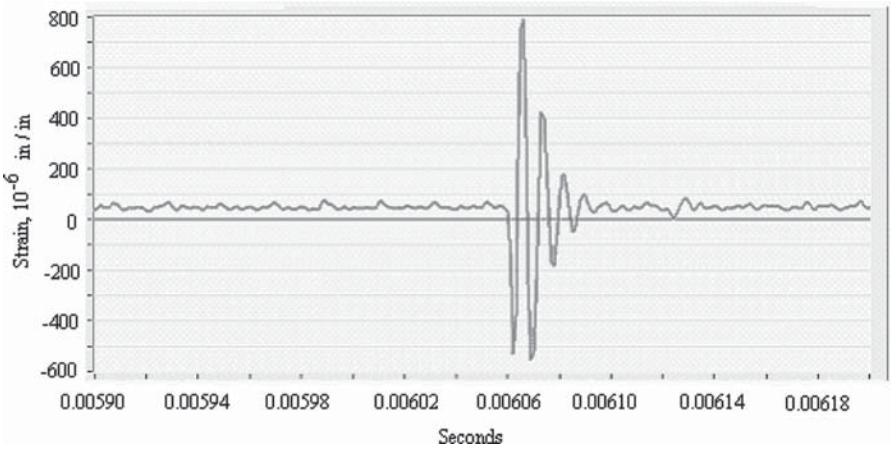


FIG. 8.57 AXIAL STRAINS AT POINT 17 ON THE SIDE OF THE PIPE

This 969 psi calculated pressure is consistent with the measured 925 psi pressure spike. This observation demonstrates that slug flow calculations provide reasonable estimates for pressure surges.

8.5.4.6 Equivalent Axial and Hoop Strains Unexpectedly, the axial and hoop strains were experimentally shown to be nearly the same (points 3 and 17 in Fig. 8.41), as shown in Figs. 8.56 and 8.57. Since,

$$\varepsilon_z = \varepsilon_\theta \qquad \text{US (8.146)}$$

the axial and hoop stresses must also be equal by Hooke's Law (Eq. 3.1), such that

$$\sigma_z = \sigma_\theta \qquad \text{US (8.147)}$$

Instead of these two stresses being equal, note that (Eq. 3.9) concludes that these two stresses should be related by a factor of Poisson's ratio. This anomaly was an unexpected finding during testing. A theoretical explanation of this experimental result has not been determined. Strain gauge installation and calibration were checked to ensure that results were accurate. However, other tests to investigate plastic strains showed that Poisson's ratio was approximately followed in short tubes (Example 8.12, paragraph 8.8.2).

8.5.4.7 Example of Fitness for Service

Previous examples in this text considered this same system with respect to fitness for this service. Example 8.8 (paragraph 8.5.4) for a water-filled pipe subjected to vapor collapse provided substantial data with respect to water hammer-induced stresses and strains. However, the continued use of the system required evaluation, and Example 4.9 demonstrated that the fatigue limit had been exceeded for piping in this system. Experimental data was coupled with a fracture mechanics analysis to establish fitness for (example 8.10, paragraph 8.5.4.9).

8.5.4.8 Corrective Actions

Example 8.9 Consider Example 8.8 (paragraph 8.5.4) corrective actions, which included installing the VFD modifications discussed in Example 5.25.

The pump and system head curves are shown in Fig. 8.58. Preliminary tests were performed by linearly operating a gate valve to obtain the pressures shown in Figs. 8.59 to 8.61, where the pressure surge was reduced to as low as 120 psig. Using a VFD-controlled pump, the pressure surge was typically reduced to 14 psig (Figs. 5.52 and 5.53), but an occasional surge was observed near 80 psig (Fig. 8.62). Strains were negligible, following the VFD modifications, as shown in Fig. 8.63.

8.5.4.9 Fitness for Service

Example 8.10 Consider the system of Example 8.8 (paragraph 8.5.4) for fitness for service after installing the VFD modifications discussed in Example 5.25.

Even though the strains seemed to be negligible, fitness for service was demonstrated using the principles presented in API 579/ASME FFS-1. The crack growth is defined by

$$\frac{da}{dn} = C \cdot \left(\Delta K\right)^m \qquad \text{US (8.148)}$$

where da/dn is the rate of crack growth, C and m are constants, and ΔK characterizes the initiation of fracture and equals the maximum stress intensity factor minus the minimum stress intensity factor, such that

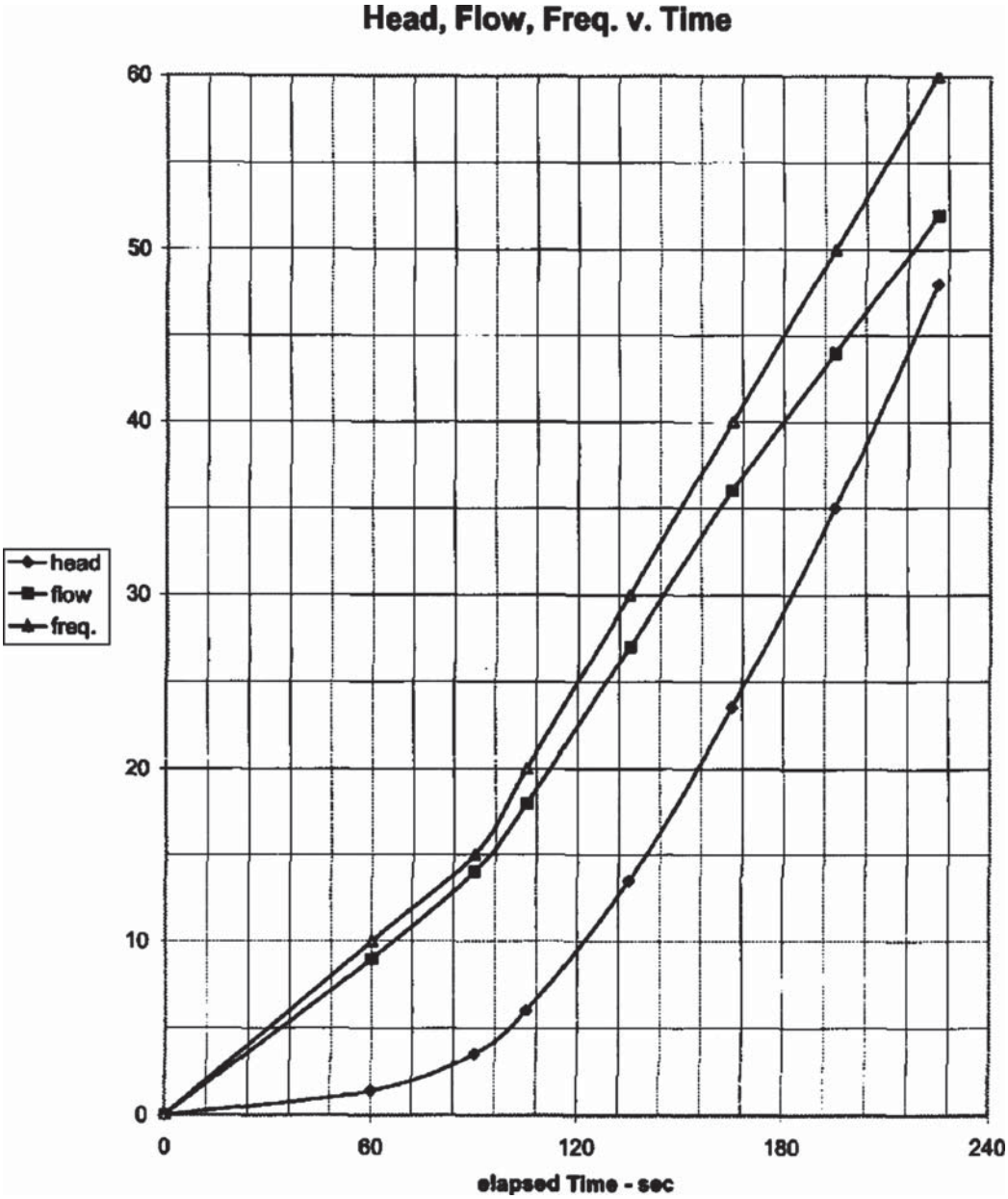


FIG. 8.58 SYSTEM HEAD CURVES, A. SOSSAIPILLAI, SRS

$$K = K_{\max} - K_{\min} \qquad \text{US (8.149)}$$

The crack will not grow if ΔK is less than the threshold stress intensity factor, K_{th}. Therefore, using API 579/ASME FFS-1, a crack will not grow if

$$\Delta K < Kthr = 1.82\_ksi\sqrt{in} \qquad \text{US (8.150)}$$

To find ΔK, crack dimensions in the pipe needed to be defined. API 579/ASME FFS-1 provided direction for evaluating measured cracks, but postulated cracks were not discussed. The maximum stress occurs on the inner surface of the pipe where crack initiation is expected. An assumption to find the minimum crack width, c, for a semicircular crack was assumed. Cracks typically grow with a width to depth ratio of 3 to 1, but a 1 to 1 ratio was conservatively assumed (Fig. 8.64). The code was then used to predict the crack growth due to a through-wall crack of width $2 \cdot a = 2 \cdot \bar{T}$, which was subjected to the maximum hoop stress caused by the 80-psi pressure surge shown in Fig. 8.62.

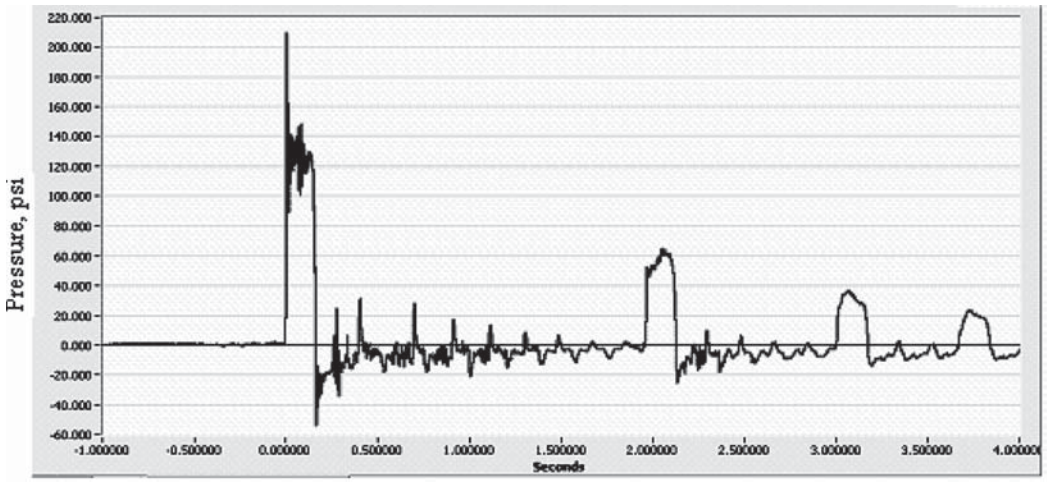


FIG. 8.59 VALVE CLOSURE IN 50 SECONDS

Using API 579/ASME FFS-1,

$$\mathrm{K1} = \Delta K = 0.677 < K_{\mathrm{thr}} = 1.82 \quad \text{US (8.151)}$$

Eq. (8.151) defines the criteria for any crack to grow in the 2-in. piping. The maximum allowable pressure in the system would then be

$$K_{\mathrm{thr}} \cdot P/\mathrm{K1} = 215 \text{ psi} \quad \text{US (8.152)}$$

which is well above the measured 80-psi transient. Similar results were obtained for other components and pipes in the system. Bending stresses had an even smaller effect. The system has been returned to service for 6 years without incident, cycling every 10 minutes. This example and referenced examples provided a complete description of the uses of the dynamic stress theory, i.e., (1) determination of the maximum stresses and stress cycles, (2) fatigue failure assessment, (3) corrective actions to minimize the transient, and (4) fracture mechanics analysis to return the pipe system to service.

8.5.5 Comparison of Flexural Resonance Theory to Dynamic Stress Theory

Constitutive equations for each theory are fundamentally different. Dynamic stress theory responses are derived from

$$m \cdot \frac{d^2 z}{dt^2} + 2 \cdot \zeta \cdot \omega_n \cdot \frac{dz}{dt} + \omega_n^2 \cdot z = F(t) \cdot g \quad \text{US (8.153)}$$

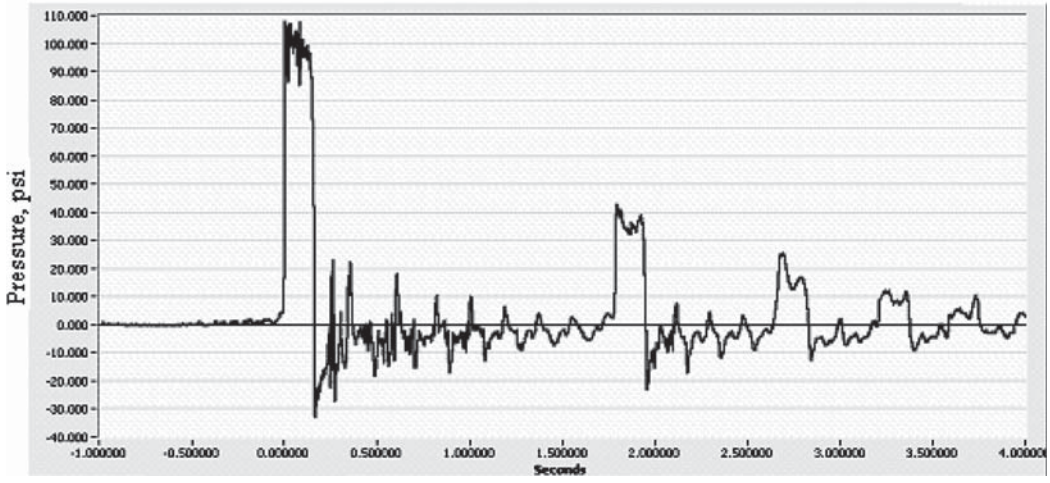


FIG. 8.60 VALVE CLOSURE IN 120 SECONDS

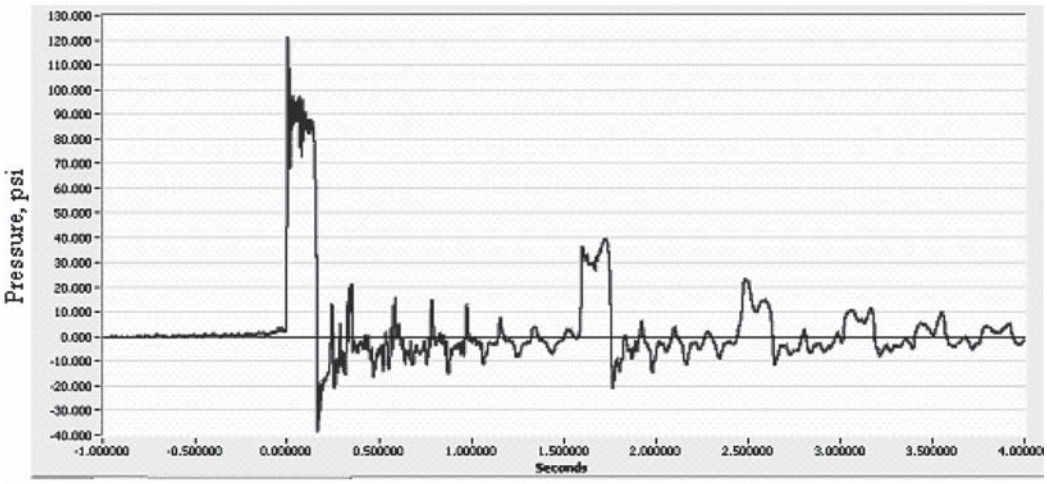


FIG. 8.61 VALVE CLOSURE IN 150 SECONDS

Flexural resonance theory responses are derived from

$$\frac{d^4 w_1}{d\xi^4} + w_1 + \frac{2 \cdot \lambda \cdot d^2 w_1}{d\xi^2} = \frac{P \cdot r^2}{E \cdot \bar{T}} \qquad (8.154)$$

An intractable problem, the actual solution may be a combination of these two equations. Even so, several observations were noted in this work.

For flexural resonance theory in short tubes:

1. Near the critical velocity, the stress was shown to increase as observed in experiments with short tubes; (DMF < 4)
2. Below the critical velocity, strains were calculated with reasonable accuracy
3. Above the critical velocity, the DMF = 2, but experiment showed that DMF varied between 1 and 2
4. At low velocities, DMF = 1 by experiment and theory
5. Using beam theory, flexural resonance theory was modified by assuming that the strains were bounded at the critical velocity. This modification yielded more accurate strain predictions near the critical velocity

For dynamic stress theory:

1. Near the critical velocity, strains were accurately predicted for both short tubes and long pipes (DMF < 4)

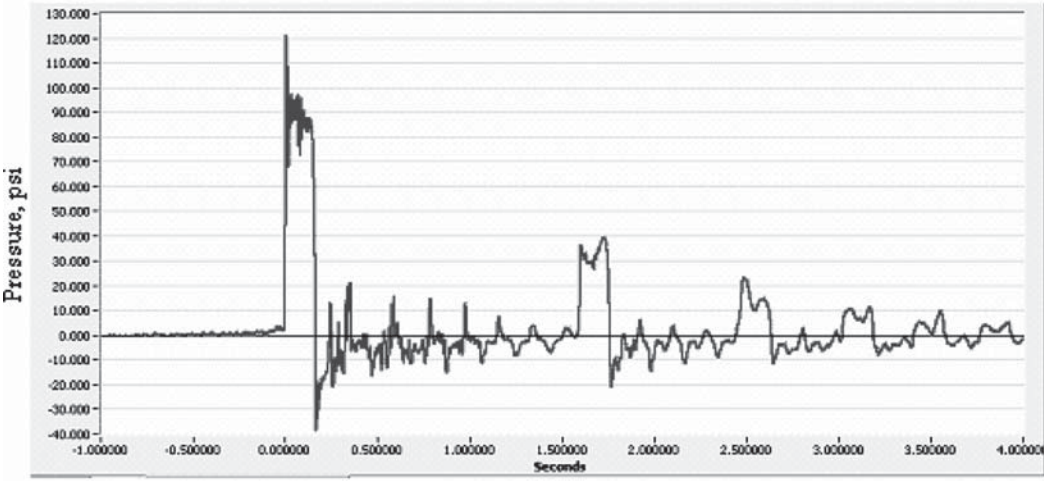


FIG. 8.62 INFREQUENT PRESSURE SPIKE

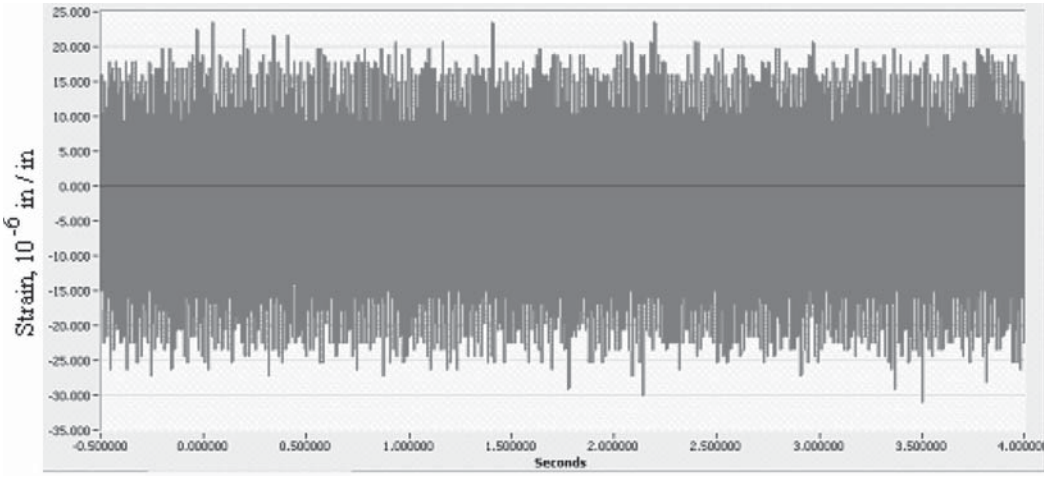


FIG. 8.63 TYPICAL STRAIN RATE DATA FOLLOWING MODIFICATIONS

2. Above and below the critical velocity, strains were overpredicted for short tubes
3. Below the critical velocity, experimental strains were much higher than predicted by flexural resonance, and the dynamic stress theory provided reasonable predictions

In short, flexural resonance provides good insight into the response of short tubes. However, the dynamic stress theory consistently bounds experimental results and is endorsed here for pressure design of piping subject to pressure transients during water hammer.

For both theories, the maximum stress depends on a constant step pressure increase in a pipe. Note that:

1. As described in paragraph 7.2.3, the length of an impulse reduces the overall response. That is, short duration pulses of a time span less than ¼ of the vibration period ($t_1 < \tau / 4$) of the yield stress reduce the maximum stress
2. Ramp responses described in paragraph 7.2.4 also reduce the maximum stress
3. Stresses may be doubled at closed end pipes if the pipe is long enough to preclude the effects of impulse loading, and reflected waves occur within the fluid inside the pipe

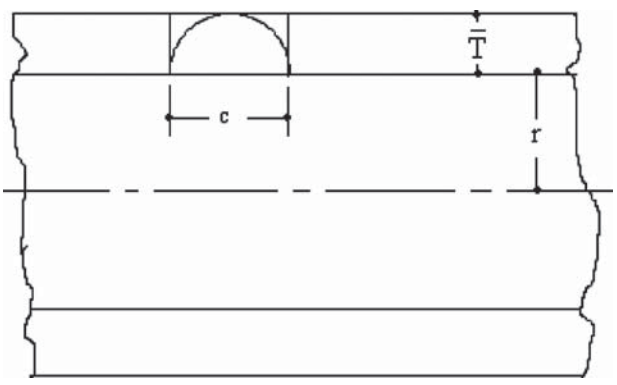


FIG. 8.64 POSTULATED MINIMUM CRACK SIZE

8.6 VALVES AND FITTINGS

The sudden changes in diameter and geometry cause valves and fittings to act similar to the short FEA model (paragraph 8.2), where the maximum DMF ≤ 2. Also, Example 5.17 (paragraph 5.9) successfully applied a DMF = 1.8 to assess valve leaks. An argument can easily be made that the complex geometry and different materials used in valve construction may negate the use of damping, and therefore, DMF = 2 is a reasonable recommendation for valves subjected to sudden pressures. At the welded connection of a valve to a pipe, DMF ≤ 4. For hoop stresses in elbows the DMF ≤ 4, and for other fittings, the DMF will vary between 2 and 4.

8.7 PRESSURE VESSELS

For pressure vessels, the DMF is expected to be near 2, but reflected waves in the vessel may cause DMF ≤ 4 near the corners of the vessel, and stress raisers may be present depending on vessel design. Also, the wave

expansion from a small-diameter pipe entering a larger vessel container significantly reduces the pressure magnitude, similar to the reduction in pressure for series pipes. Pressure vessel data during water hammer is unavailable, but explosive detonations in pressure vessels have seen much attention.

For example, experimental stress/strain results were obtained in a 2-ft diameter, 20-ft long pressure vessel (Malherbee et al [234]). An explosive charge was detonated at one end of the cylinder, and strains were measured at distances of 13 and 17 ft from the charge. Strains were measured at 2-1/2 times the calculated static hoop stress (DMF = 2.5). FEA models are recommended for analysis of pressure vessels if there is a concern.

8.8 PLASTIC HOOP STRESSES

Plastic deformation during transients is poorly understood, and limited insight is consequently provided here. During cycling and fatigue, piping hoop response is complicated by plasticity effects and strain rate-dependent material properties. An FEA model and an experimental result supported by FEA calculations are provided here as examples of plastic hoop strains.

Together, these two examples infer that ratcheting is the expected hoop strain mechanism during many cases of water hammer. The first example demonstrated the initiation of shakedown during elastoplastic pipe response. The second example demonstrated fully plastic deformation, where ratcheting occurred in a thin-tube wall for impulse load tests performed to 5000 psi. Well below this pressure, water hammer pressures have been noted to occur up to about 3000 psi in thicker-pipe wall examples in this work. In other words, fractures of ductile piping and components are not expected during water hammer, which is consistent with observations. There may be exceptions to this observation for high-pressure piping where burst pressure calculations are advised using a DMF = 2, but in general, bursting of ductile pipes is not observed due to water hammer. There may also be exceptions for ductile pipe failures where reflected waves occur near pipe ends. Ruptured pipes have been observed in power plants near the ends of long pipelines, which were dead ended. Further investigation is recommended.

8.8.1 FEA Results for a Shock Wave in a Short Pipe

Example 8.11 Consider plastic deformation of a short tube, using FEA.

An FEA model was evaluated for plastic response due to a 1000-psig step pressure wave traveling at a water hammer wave speed (Leishear [14]), using the same model geometry for a pipe with fixed ends provided in paragraph 8.2.3. Elastic and plastic deformations are compared in Fig. 8.65. Linear elasticity and linear strain rate hardening were assumed. When strain rates were neglected, the strain continued to rise while the pressure was exerted on the pipe wall, as shown in Fig. 8.66. When strain rates were included in the FEA model, results were markedly different, as shown in Fig. 8.67. The pipe wall vibrated elastically, and the elastic deformation was cut off when the dynamic yield stress was reached, and plastic deformation and shakedown occurred.

To better understand the complicated response of the pipe wall, SDOF oscillators were considered where the pipe wall was assumed to act as a bilinear oscillator. That is, the frequency of the oscillator changed when the dynamic yield stress was achieved. Figs. 8.68 and 8.69 provide a trial and error solution for a SDOF response. The effects of filling the pipe with fluid were addressed, and strain rate effects were also addressed. The concept of plastic frequency was introduced, where

$$\omega = \sqrt{g'' \cdot \frac{\left(\frac{2 \cdot k}{(r) \cdot t}\right) + \left(\frac{H}{(r)^2 \cdot (1 - \nu^2)}\right)}{\rho_{pipe} + \frac{(r) \cdot \rho_{water}}{4 \cdot \bar{T}}}} \qquad (8.155)$$

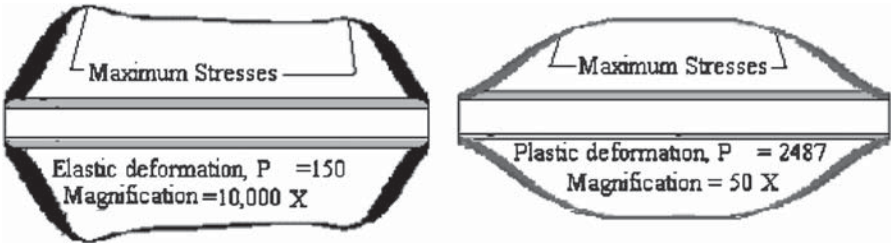


FIG. 8.65 COMPARISON OF ELASTIC TO PLASTIC DEFECTIONS OF SHORT PIPE, NO STRAIN RATE EFFECTS

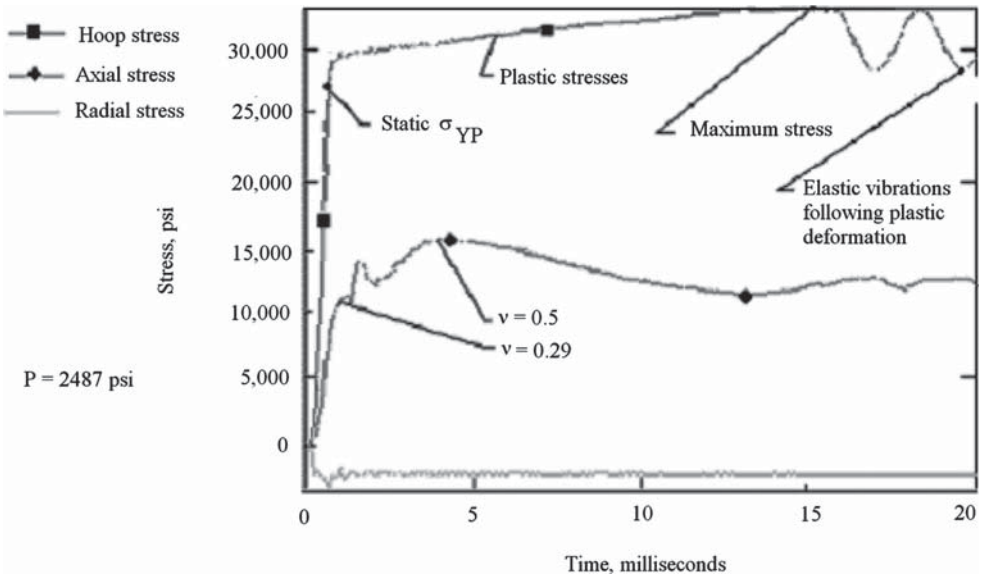


FIG. 8.66 PLASTIC STRESSES WITHOUT STRAIN RATE EFFECTS

The plastic modulus equals *H*, which is the slope of the linear strain hardening on the assumed stress/strain diagram (Fig. 8.70). Since the plastic frequency is approximately 11 times higher than the elastic frequency, the pipe wall response markedly changed at the dynamic yield stress, and shakedown occurred. To further consider plastic deformations, the example in the following paragraph investigated explosions in tubes and consequent strains due to high-pressure shocks.

8.8.2 Experimental Results for Explosions in a Thin-Wall Tube

Example 8.12 Consider experimental results and analysis for deformations in short, thin-wall tubes.

In some excellent research, Shepherd et al [235] investigated plastic deformation in gas-filled, thin-wall tubes subjected to internal pressures up to 5000 psi (35 MPa = 5076 psi). Tests were performed in A513, mild steel, 5-in. ID, 0.059-in. thick wall, 47.24-in. long tubes. One end of

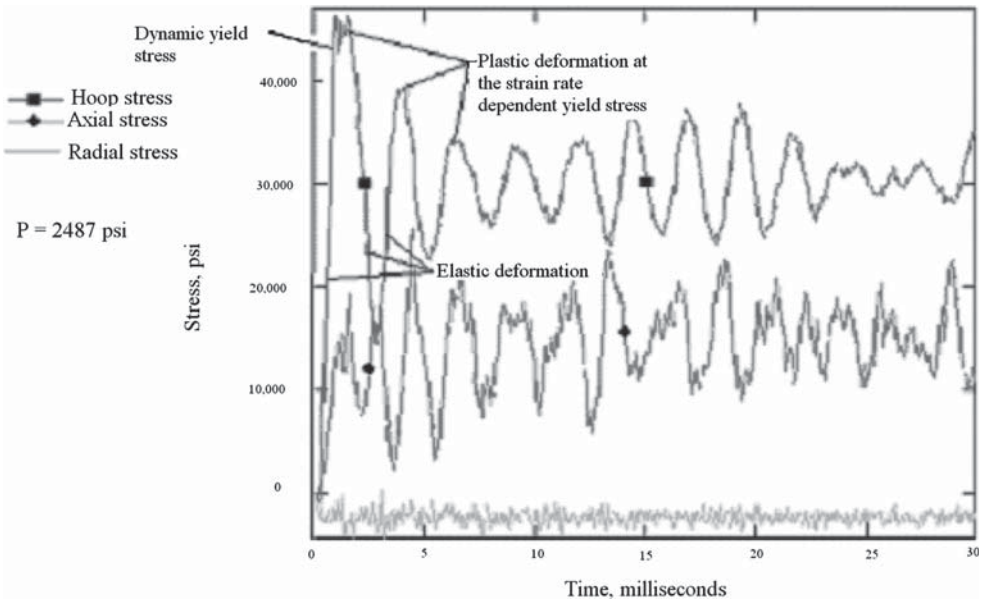


FIG. 8.67 PLASTIC STRESSES WITH STRAIN RATE EFFECTS

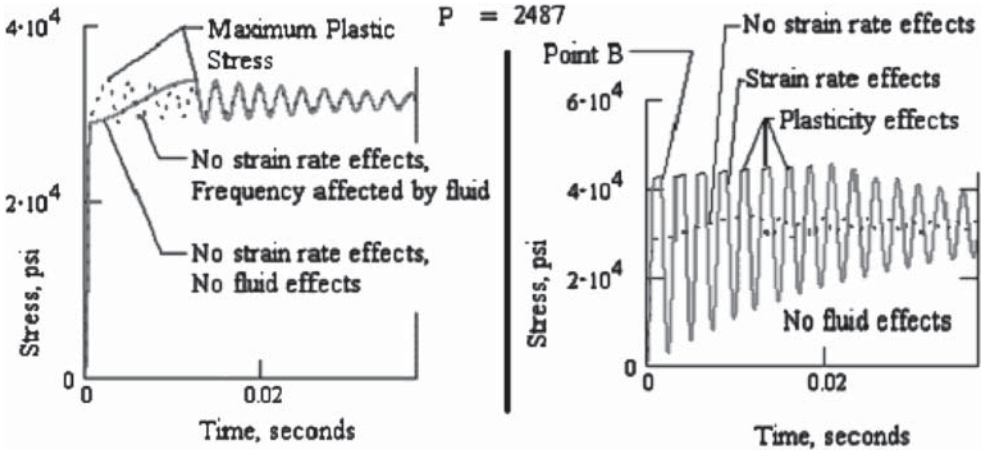


FIG. 8.68 COMPARISON OF FACTORS AFFECTING ELASTOPLASTIC HOOP STRESSES

the tube was blanked off, and a repeatable shock wave was initiated into the other end of the tube. Multiple tubes were tested, and multiple shocks were successively initiated in each tube. Wavelike deformations formed near the ends of the tubes, as shown in Fig. 8.71. Pressures near the end of the tube where the largest deformations occurred are shown in Fig. 8.72. Data analysis was performed to evaluate the use of a SDOF and FEA models.

A SDOF model with linear strain hardening was used, but did not agree well with data as shown in Fig. 8.73, where experiment and theory are both presented. Note in the figure that the pipe wall ratcheted as successive shots were performed and that the frequency of the pipe wall changed with distance from the sealed end of the pipe. Also of interest, the DMF equals 4 up the yield point. Since plastic precursor stresses are not expected, values of the DMF are expected to be less than 2 when the hoop response is fully plastic. The few examples presented here clearly demonstrate that more research is required to accurately predict DMFs during dynamic elastoplastic response.

An FEA model was performed using LS-Dyna®, where linear strain hardening and strain rate properties were included in the model. The FEA model provided a reasonable prediction of the maximum strains for successive shots, but the FEA model strain predictions lost accuracy at distances from the pipe end (Fig. 8.74). Another aspect of the test results showed that the Poisson's ratio, σ_z/σ_θ, varied from 0.5 during the initial shots to 0.3 in later shots (Fig. 8.75). In short, neither overload nor low-cycle fatigue occurred for 5000 psi pressure shocks in a 6-in. diameter tube with a wall thickness less than 1/16 in.

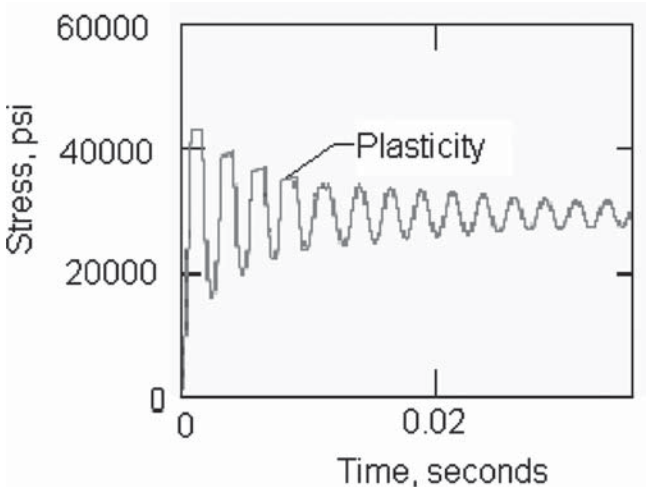


FIG. 8.69 ELASTOPLASTIC DEFORMATIONS OF A FLUID-FILLED PIPE WITH STRAIN RATE EFFECTS CONSIDERED

8.8.3 Explosions in Pipes

Outside the scope of this work, explosions in pipes are noted to conclude this discussion of pressure-induced pipe failures. Pipeline explosions in nuclear reactor facilities have been attributed to hydrogen detonation within the pipes (Naitoh [236], Leishear [237]). Specifically, Naitoh concluded that the pressure required to cause the damage at Hamaoka (Fig. 8.76) was due to hydrogen detonation. The explosion occurred on system startup of a steam system, and water was found in the piping near the rupture. The detonation mechanism was not identified. One postulated cause was a spark from Gadolinium exposed to steam flow in the piping. Another was compression of the stoichiometric hydrogen/oxygen mixture and auto-ignition due to fluid transient compression of

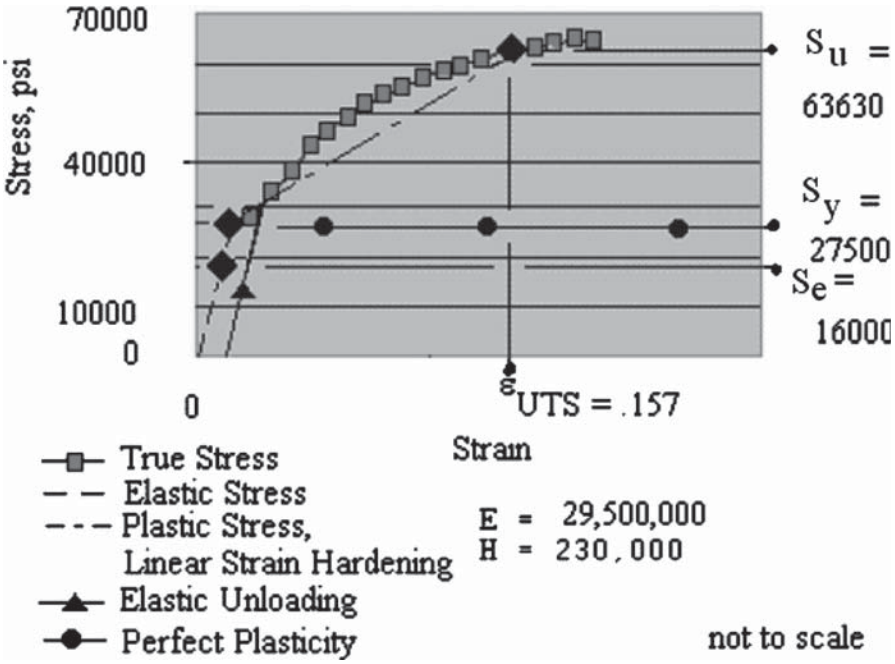


FIG. 8.70 STRESS/STRAIN DIAGRAM FOR MILD STEEL

the vapors. Theoretically, water hammer may have compressed the trapped hydrogen gas to cause auto-ignition of the hydrogen/oxygen mixture in the pipe. Given sufficient gas accumulation in the pipe due to radiolytic decomposition of water, a flame front to explosion transition may have occurred to burst the pipe. Research is required to adequately demonstrate either theory.

8.9 SUMMARY OF ELASTIC AND PLASTIC HOOP STRESS RESPONSES TO STEP PRESSURE TRANSIENTS

For elastic hoop stresses caused by step pressure increases, where the stress is below yield strength, the DMF

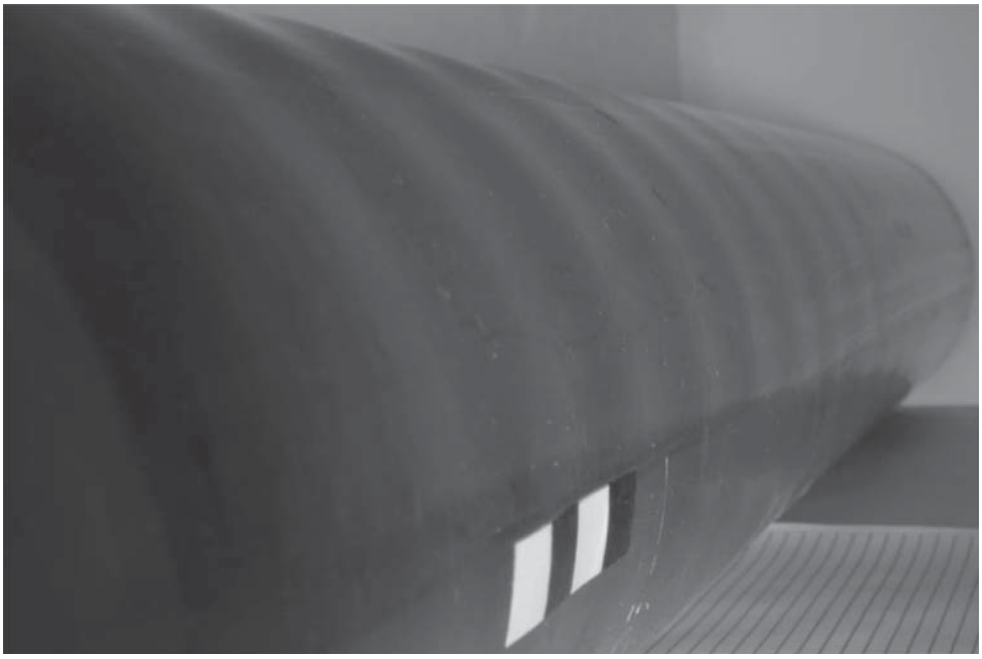


FIG. 8.71 PIPE WALL DEFLECTIONS DUE TO SUCCESSIVE BLAST LOADS (Shepherd et al [235])

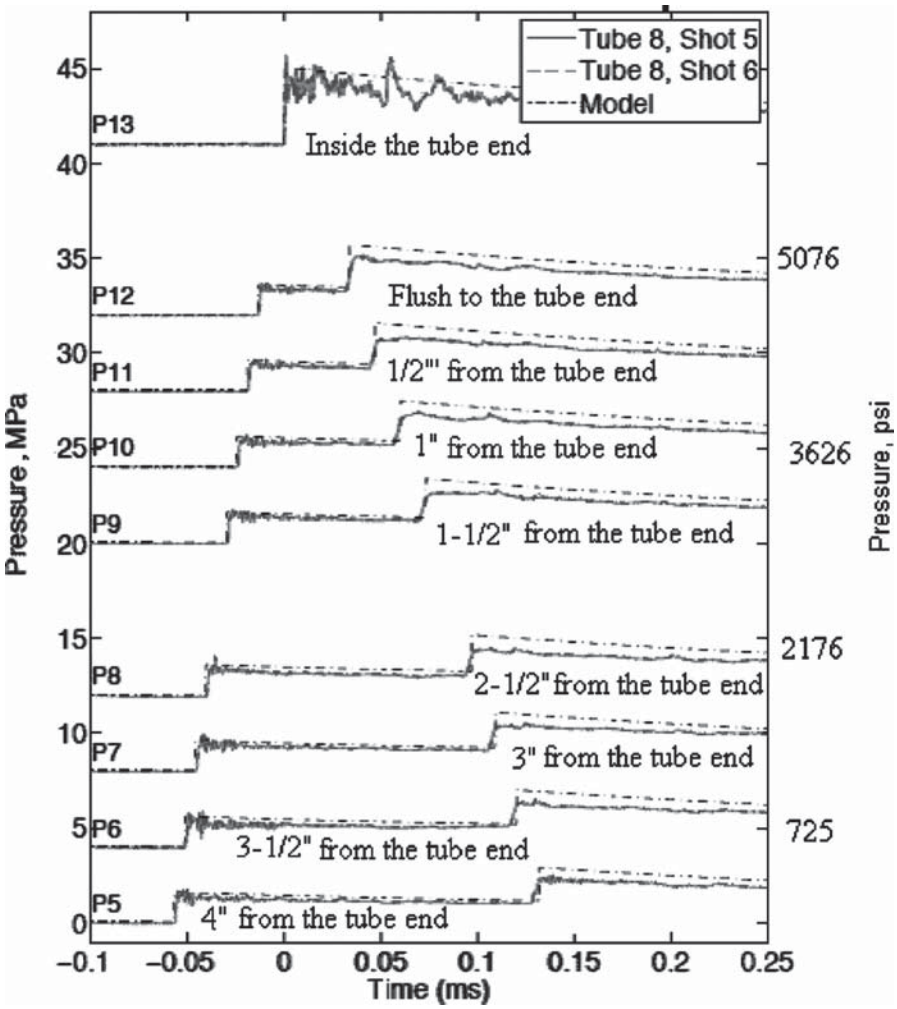


FIG. 8.72 MEASURED PRESSURES ALONG THE TUBE LENGTH (Shepherd et al [235])

3 < 4. For plastic hoop stresses above the yield strength, 1 < DMF < 4. An example follows, which highlights the ambiguity of the DMF above the yield.

Example 8.13 Determine maximum stresses due to a suddenly closed valve.

Neglecting damping at 70°F, Figs. 8.77 and 8.78 provide some insight into the pressures caused by suddenly closed valves and the resultant maximum Lame' stresses in typical industrial piping. Note that at common design flow rates of 10 ft/second, pipe stresses are below yield for mild steel, Schedule 40 pipes under 16-in. NPS, where S_y = 30,000 to 35,000 psi, and fatigue is not expected for any number of cycles for pipe sizes under 4-in. NPS, assuming S_e = 12.5 ksi. Also note that presented stresses are invalid if the yield strength of the pipe is exceeded, since further elastoplastic research is required. That is, the DMF does not suddenly drop to a value of 1 or 2 when the yield point is reached. See paragraph 7.3.2.2 for overdamping effects, which will affect any determination of a DMF. Furthermore, a clear understanding of plastic hoop stresses and DMFs is further complicated by strain rate-dependent yield strengths and the formation of a plastic core in the pipe. In short, the present theory provides reasonable maximum stress estimates for dynamic elastic hoop stresses, but dynamic plastic hoop stress estimates require further research.

Additionally, the pressures displayed in Fig. 8.77 highlight another issue. Pressures during water hammer may subject the system to the requirements of high-pressure design, which may not have been an initial design condition. The fact is that most industrial gate or globe are hand operated, and sudden closure cannot occur unless butterfly, ball, or plug valves are installed. This issue also implies that installation of automatic fast-acting valves should be evaluated for transient flow system effects.

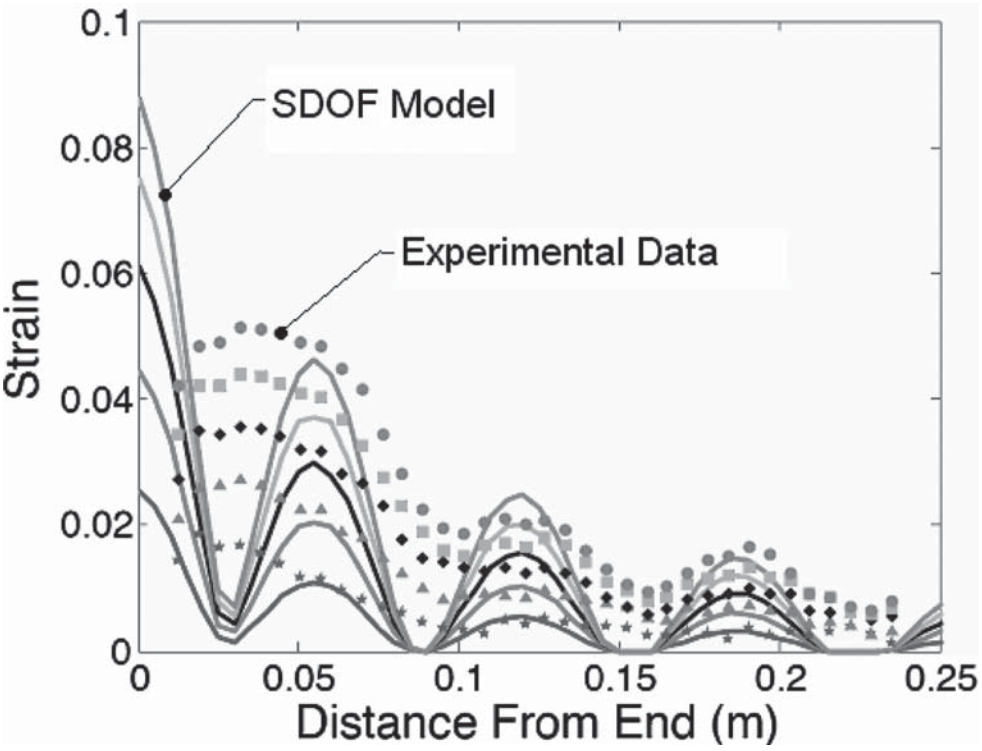


FIG. 8.73 RESIDUAL PLASTIC STRAIN: SDOF MODEL CALCULATIONS COMPARED TO EXPERIMENT FOR A LINEAR STRAIN HARDENING MATERIAL (Shepherd et al [235])

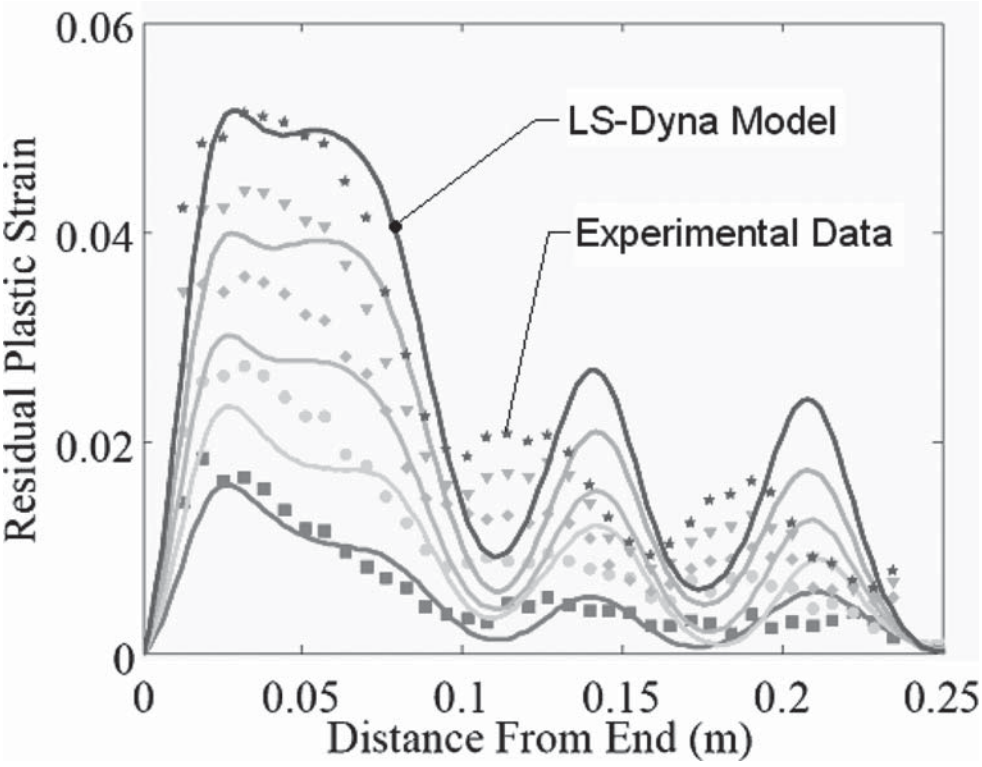


FIG. 8.74 RESIDUAL PLASTIC STRAIN: LS-DYNA® FEA CALCULATIONS COMPARED TO EXPERIMENT FOR A LINEAR STRAIN HARDENING MATERIAL, INCLUDING STRAIN RATE EFFECTS ON YIELD STRENGTH (Shepherd et al [235])

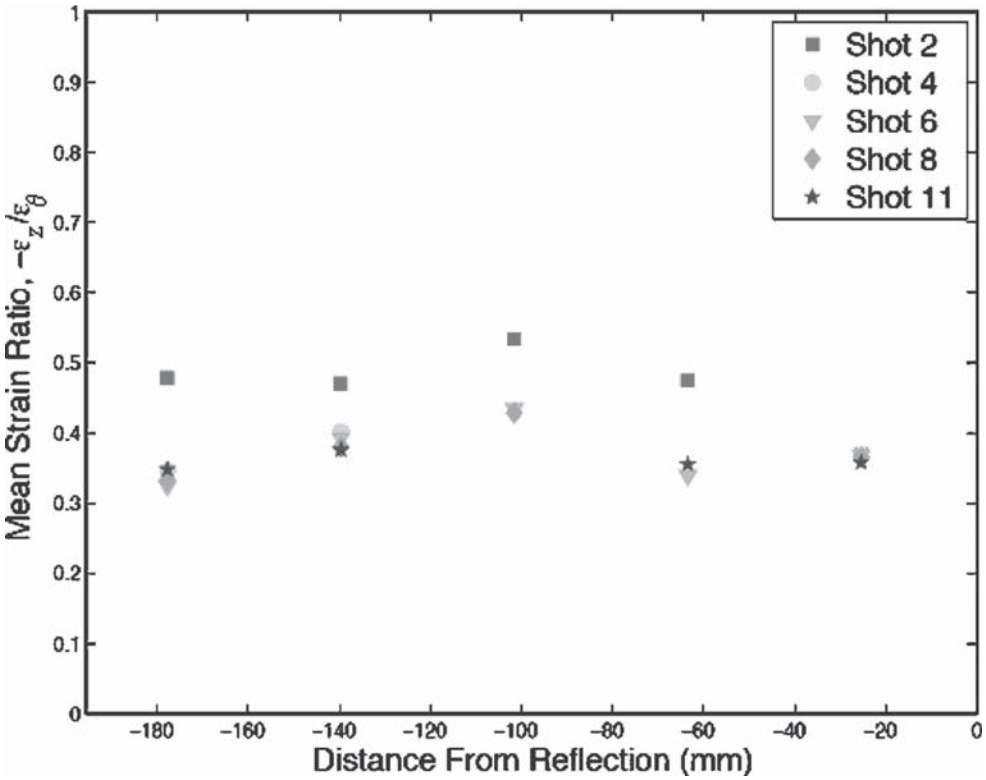


FIG. 8.75 POISSON'S RATIO DURING SUCCESSIVE SHOCK WAVES (Shots) (Shepherd et al [235])

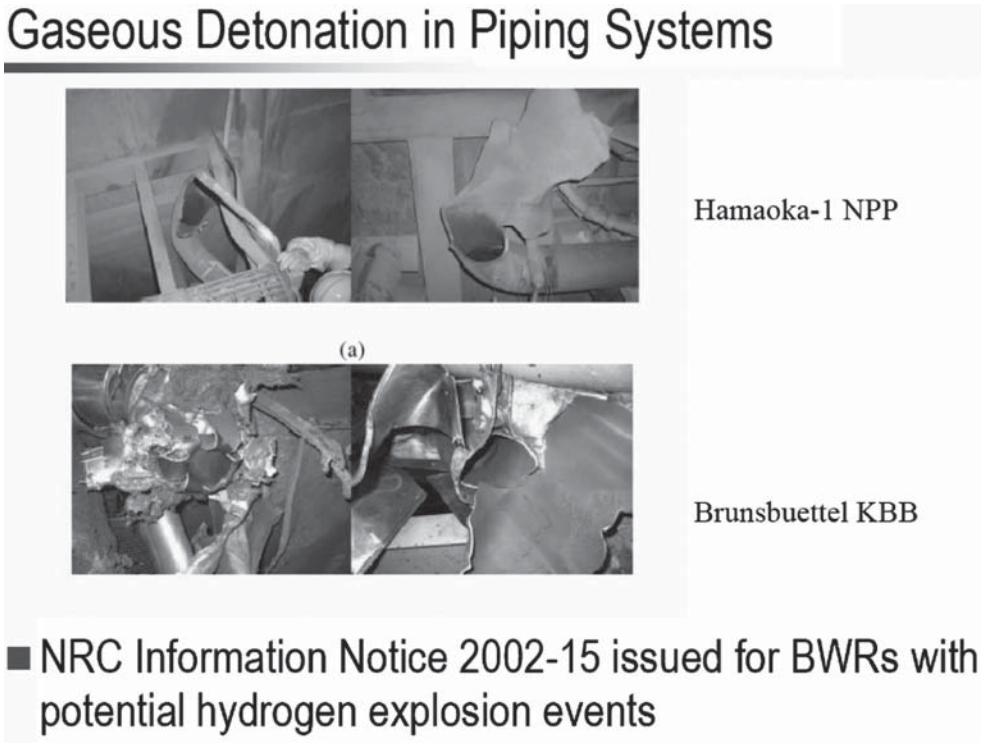


FIG. 8.76 HYDROGEN EXPLOSION DAMAGE IN NUCLEAR FACILITIES (ASME, Task Group on IMPULSIVELY LOADED VESSELS, BOB NICKELL)

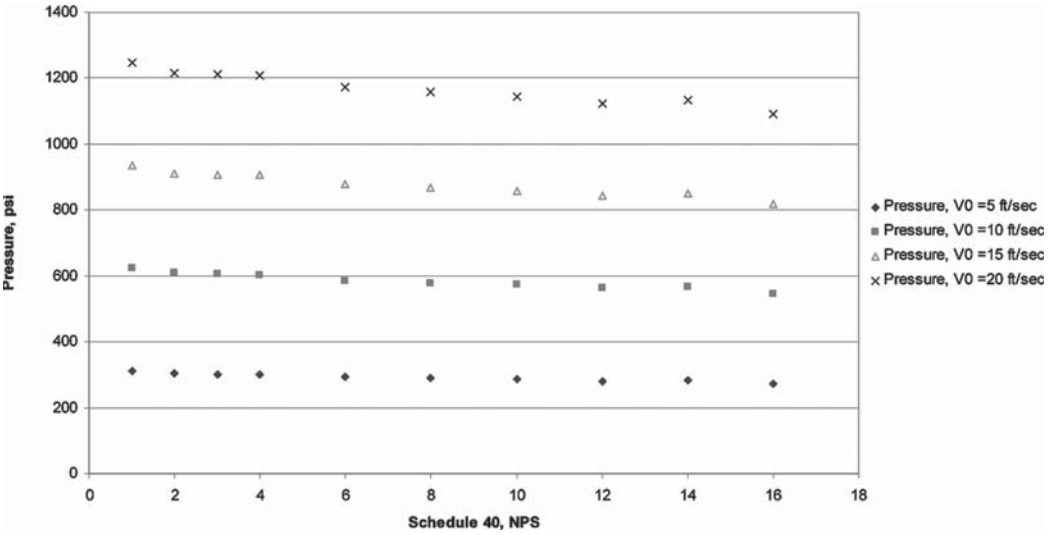


FIG. 8.77 PRESSURES DUE TO A SUDDENLY CLOSED VALVE IN A FIXED-END PIPE

Even so, Fig. 8.78 shows that pipe rupture is not expected for small diameter steel piping designs during valve closure. For example, Grade 60, A106 steel, the hoop stress is always below the bursting strength for sudden valve closures. Even ratcheting cannot cause failure. For another example, brittle A126, 8-in. NPS cast iron pipe may crack when a valve is suddenly closed, and the flow rate equals 10 ft/second. The failure mechanism is assumed to be a crack since the pressure is transient and oscillatory, rather than steady state. However, recognize that these stresses can be doubled near the dead ends of long pipes due to wave reflections.

Also note that the pressures in Fig. 8.77 exceed the maximum design pressures for flanges in many cases. For example, Fig. 3.53 shows that design pressure for class 150 carbon steel flanges is 285 psi. For V_0 equals 5 ft/second, the flange design pressure is exceeded for pipe sizes below Schedule 40, 10-in. NPS. Although Code design requirements may be exceeded, dynamic effects during fluid transients, and conservative design of flanges during hydrostatic tests, imply that flanges will not necessarily leak at these pressures. This observation has merit, since design pressures may be exceeded, even though leaks are not observed during operations. On the other hand, gaskets have failed during water hammer and fatalities have resulted, and dynamic pressure amplification may need to be considered.

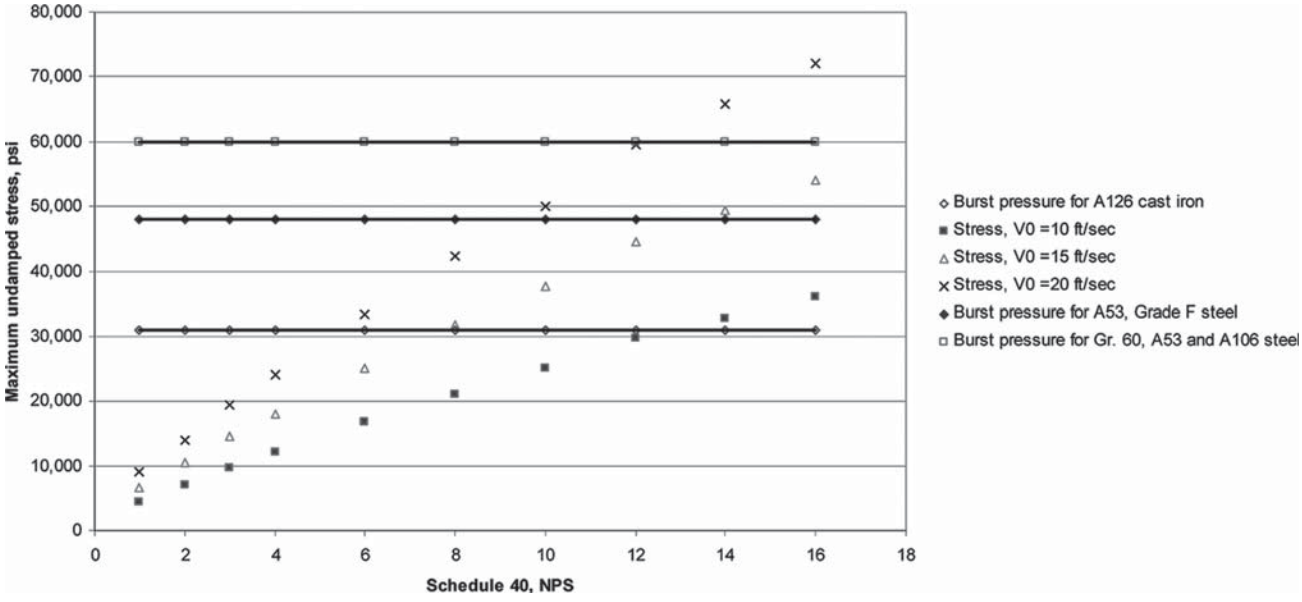


FIG. 8.78 UNDAMPED, ELASTIC, HOOP STRESSES DUE TO A SUDDENLY CLOSED VALVE IN A FIXED-END PIPE

CHAPTER

9

DYNAMIC STRESSES DUE TO BENDING

Dynamic stresses during bending vary due to system geometry. Multiplying the pressure surge magnitude times the pipe cross-sectional area approximates the forces on both elbows and blind flanges. For step pressure surges during water hammer, the DMF < 2 for forces on an elbow in a pipe system. For the step pressure surges on a closed end pipe, an axial force DMF < 4 may exist due to wave reflections at the pipe end, depending on the pipe length and pressure duration. For pipes with U-bends or Z-bends, the forces are also related to the geometry. Although the DMF < 2 at each elbow, the opposing forces may either counter or multiply the DMF, depending on the phase shift in vibrations at opposing elbows. The forces at each elbow act at different times, and accordingly, a phase shift will exist between the opposing forces at the elbows. If the distance between elbows is small, the opposing forces will cancel, and in some cases, the forces will add. In general, few problems can be reasonably approached without the aid of a computer. To provide some insight into dynamic stresses, simple hand calculations are presented here along with an example of a more complicated computer simulation. Also, some graphic techniques to estimate loads due to water hammer are available in ESDU-86015 B [238]. Before examples are presented, equations for frequencies, deflections, and stresses are presented to be used along with single degree of freedom (SDOF) responses.

9.1 DEFORMATIONS, STRESSES, AND FREQUENCIES FOR ELASTIC FRAMES

Several graphs are provided here to approximate stresses for simple elastic frames and simply supported beams. Additional data is available from each of the references as noted with the tables and graphs.

9.1.1 Static Deflections and Reactions for Simply Supported Beams and Elastic Frames

Equations for static reactions and deflections of some structures are presented for simply supported beams in Table 9.1 and elastic frames in Table 9.3. Note that nomenclature used in Tables 9.1 and 9.2 is inconsistent with this text. For elastic frames, U-bends are shown, but data for Z-bends and L-bends was unavailable. Table 9.1 is provided to introduce structural vibrations. To use the formulas in Table 9.2, reactions are calculated, and then the nominal stress is calculated using free body diagrams and the beam formula (Eq. (1.12), $S_b = M \cdot c'/I$).

Also, stresses are noted to vary considerably due to the end constraints. For example, compare a beam with fixed or free ends (Cases 1a and 1b in Table 9.2), where the maximum moments equal $W \cdot L/8$ and $W \cdot L/4$ for fixed and free ends, respectively. This variation between the moments, and therefore stresses, needed to be addressed, since a realistic structural constraint lies between the two conditions of free and fixed ends. For piping design, pipe ends are typically assumed to be fixed, and stress intensification factors are applied to calculate stresses.

9.1.2 Frequencies for Simple Beams

Simply supported beams introduce the more complicated responses of elastic frames by visualizing the response of beam vibrations. Frequencies for a few different beam configurations are listed in Table 9.3 where Den Hartog [209], Pilkey [99], and Young et al [132] provided comprehensive lists of frequencies for springs and beams. For beams, the frequencies may be expressed as

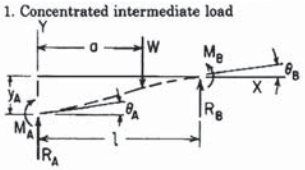
$$\omega_n = \frac{a_n}{(L'')^2} \cdot \sqrt{\frac{E \cdot I \cdot g''}{\left(\frac{W}{L''}\right)}} = \frac{a_n}{(L'')^2} \cdot \sqrt{\frac{E \cdot I \cdot g''}{A \cdot \rho''}} \quad \text{US (9.1)}$$

TABLE 9.1 SHEAR, MOMENT, SLOPE, AND DEFLECTION FORMULAS FOR STRAIGHT ELASTIC BEAMS

(Young et al [132], reprinted by permission of McGraw Hill, Inc.)

NOTATION: W = load (force); w = unit load (force per unit length); M_o = applied couple (force-length); θ_o externally created concentrated angular displacement (radians); Δ_o = externally created concentrated lateral displacement; T_1 and T_2 = temperatures on the top and bottom surfaces, respectively (degrees). R_A and R_B are the vertical end reactions at the left and right, respectively, and are positive upward. M_A and M_B are the reaction end moments at the left and right, respectively. All moments are positive when producing compression on the upper portion of the beam cross section. The transverse shear force V is positive when acting upward on the left end of a portion of the beam. All applied loads, couples, and displacements are positive as shown. All deflections are positive upward, and all slopes are positive when up and to the right. E is the modulus of elasticity of the beam material, and I is the area moment of inertia about the centroidal axis of the beam cross section. γ is the temperature coefficient of expansion (unit strain per degree)

1. Concentrated intermediate load



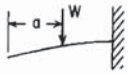
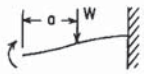
Transverse shear = $V = R_A - W$

Bending moment = $M = M_A + R_A x - W\,\mathrm{H(x\text{-}a)}$

Slope = $\theta = \theta + \dfrac{M_A x}{EI} + \dfrac{R_A x^2}{2EI} - \dfrac{W}{2EI}(\mathrm{H(x\text{-}a)})^2$

Deflection = $y = y_A + \theta_A x + \dfrac{M_A x^2}{2EI} + \dfrac{R_A x^3}{6EI} - \dfrac{W}{6EI}(\mathrm{H(x\text{-}a)})^3$

$\langle x - a \rangle = \mathrm{H(x\text{-}a)}$

End restraints, reference no.	Boundary values	Selected maximum values of moments and deformations
1a. Left end free, right end fixed (cantilever) 	$R_A = 0 \quad M_A = 0 \quad \theta_A = \dfrac{W(l-a)^2}{2EI}$ $y_A = \dfrac{-W}{6EI}(2l^3 - 3l^2 a + a^3)$ $R_B = W \quad M_B = -W(l-a)$ $\theta_B = 0 \quad y_B = 0$	Max $M = M_B$: max possible value $= -Wl$ when $a = 0$ Max $\theta = \theta_A$: max possible value $= \dfrac{Wl^2}{2EI}$ when $a = 0$ Max $y = y_A$: max possible value $= \dfrac{-Wl^3}{3EI}$ when $a = 0$
1b. Left end guided, right end fixed 	$R_A = 0 \quad M_A = \dfrac{W(l-a)^2}{2l} \quad \theta_A = 0$ $y_A = \dfrac{-W}{12EI}(l-a)^2(l+2a)$ $R_B = W \quad M_B = \dfrac{-W(l^2-a^2)}{2l}$ $\theta_B = 0 \quad y_B = 0$	Max $+M = M_A$: max possible value $= \dfrac{Wl}{2}$ when $a = 0$ Max $-M = M_B$: max possible value $= \dfrac{-Wl}{2}$ when $a = 0$ Max $y = y_A$: max possible value $= \dfrac{-Wl^3}{12EI}$ when $a = 0$

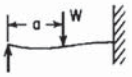
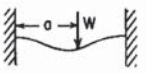
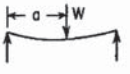
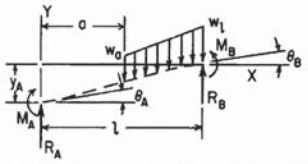
End restraints, reference no.	Boundary values	Selected maximum values of moments and deformations
1c. Left end simply supported right end fixed 	$R_A = \dfrac{W}{2l^3}(l-a)^2(2l+a) \quad M_A = 0$ $\theta_A = \dfrac{-Wa}{4EIl}(l-a)^2 \quad y_A = 0$ $R_B = \dfrac{Wa}{2l^3}(3l^2 - a^2) \quad \theta_B = 0$ $M_B = \dfrac{-Wa}{2l^2}(l^2 - a^2) \quad y_B = 0$	Max $+M = \dfrac{Wa}{2l^3}(l-a)^2(2l+a)$ at $x = a$; max possible value $= 0.174Wl$ when $a = 0.366l$ Max $-M = M_B$: max possible value $= -0.1924Wl$ when $a = 0.5773l$ Max $y = \dfrac{-Wa}{6EI}(l-a)^2\left(\dfrac{a}{2l+a}\right)^{1/2}$ at $x = l\left(\dfrac{a}{2l+a}\right)^{1/2}$ when $a > 0.414l$ Max $y = \dfrac{-Wa(l^2-a^2)^3}{3EI(3l^2-a^2)^2}$ at $x = \dfrac{l(l^2+a^2)}{3l^2-a^2}$ when $a < 0.414l$; max possible $y = -0.0098\dfrac{Wl^3}{EI}$ when $x = a = 0.414l$
1d. Left end fixed, right end fixed 	$R_A = \dfrac{W}{l^3}(l-a)^2(l+2a)$ $M_A = \dfrac{-Wa}{l^2}(l-a)^2$ $\theta_A = 0 \quad y_A = 0$ $R_B = \dfrac{Wa^2}{l^3}(3l-2a)$ $M_B = \dfrac{-Wa^2}{l^2}(l-a)$ $\theta_B = 0 \quad y_B = 0$	Max $+M = \dfrac{2Wa^2}{l^3}(l-a)^2$ at $x = a$; max possible value $= \dfrac{Wl}{8}$ when $a = \dfrac{l}{2}$ Max $-M = M_A$ if $a < \dfrac{l}{2}$: max possible value $= -0.1481Wl$ when $a = \dfrac{l}{3}$ Max $y = \dfrac{-2W(l-a)^2a^3}{3EI(l+2a)^2}$ at $x = \dfrac{2al}{l+2a}$ if $a > \dfrac{l}{2}$: max possible value $= \dfrac{-Wl^3}{192EI}$ when $x = a = \dfrac{l}{2}$
1e. Left end simply supported, right end simply supported 	$R_A = \dfrac{W}{l}(l-a) \quad M_A = 0$ $\theta_A = \dfrac{-Wa}{6EIl}(2l-a)(l-a) \quad y_A = 0$ $R_B = \dfrac{Wa}{l} \quad M_B = 0$ $\theta_B = \dfrac{Wa}{6EIl}(l^2-a^2) \quad y_B = 0$	Max $M = R_A a$ at $x = a$; max possible value $= \dfrac{Wl}{4}$ when $a = \dfrac{l}{2}$ Max $y = \dfrac{-Wa}{3EIl}\left(\dfrac{l^2-a^2}{3}\right)^{3/2}$ at $x = l - \left(\dfrac{l^2-a^2}{3}\right)^{1/2}$ when $a < \dfrac{l}{2}$: max possible value $= \dfrac{-Wl^3}{48EI}$ at $x = \dfrac{l}{2}$ when $a = \dfrac{l}{2}$ Max $\theta = \theta_A$ when $a < \dfrac{l}{2}$: max possible value $= -0.0642\dfrac{Wl^2}{EI}$ when $a = 0.423l$

TABLE 9.1 (CONTINUED)

2. Partial distributed load

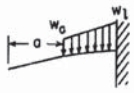
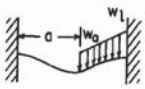
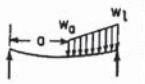


Transverse shear $= V = R_A - w_a\langle x-a\rangle - \frac{w_l - w_a}{2(l-a)}\langle x-a\rangle^2$

Bending moment $= M = M_A + R_A x - \frac{w_a}{2}\langle x-a\rangle^2 - \frac{w_l - w_a}{6(l-a)}\langle x-a\rangle^3$

Slope $= \theta = \theta_A + \frac{M_A x}{EI} + \frac{R_A x^2}{2EI} - \frac{w_a}{6EI}\langle x-a\rangle^3 - \frac{w_l - w_a}{24EI(l-a)}\langle x-a\rangle^4$

Deflection $= y = y_A + \theta_A + \theta_A x + \frac{M_A x^2}{2EI} + \frac{R_A x^3}{6EI} - \frac{w_a}{24EI}\langle x-a\rangle^4 - \frac{(w_l - w_a)}{120EI(l-a)}\langle x-a\rangle^5$

End restraints, reference no.	Boundary values	Selected maximum values of moments and deformations
2a. Left end free, right end fixed (cantilever) 	$R_A = 0 \quad M_A = 0$ $\theta_A = \frac{w_a}{6EI}(l-a)^3 + \frac{w_l - w_a}{24EI}(l-a)^3$ $y_A = \frac{-w_a}{24EI}(l-a)^3(3l+a) - \frac{w_l - w_a}{120EI}(l-a)^3(4l+a)$ $R_B = \frac{w_a + w_l}{2}(l-a)$ $M_B = \frac{-w_a}{2}(l-a)^2 - \frac{w_l - w_a}{6}(l-a)^2$ $\theta_B = 0 \quad y_B = 0$	If $a = 0$ and $w_l = w_a$ (uniform load on entire span), then Max $M = M_B = \frac{-w_a l^2}{2}$ Max $\theta = \theta_A = \frac{w_a l^3}{6EI}$ Max $y = y_A = \frac{-w_a l^4}{8EI}$ If $a = 0$ and $w_a = 0$ (uniformly increasing load), then Max $M = M_B = \frac{-w_l l^2}{6}$ Max $\theta = \theta_A = \frac{w_l l^3}{24EI}$ Max $y = y_A = \frac{-w_l l^4}{30EI}$ If $a = 0$ and $w_l = 0$ (uniformly decreasing load), then Max $M = M_B = \frac{-w_a l^2}{3}$ Max $\theta = \theta_A = \frac{w_a l^3}{8EI}$ Max $y = y_A = \frac{-11 w_a l^4}{120EI}$
2d. Left end fixed, right end fixed 	$R_A = \frac{w_a}{2l^3}(l-a)^3(l+a) + \frac{w_l - w_a}{20l^3}(l-a)^3(3l+2a)$ $M_A = \frac{-w_a}{12l^2}(l-a)^3(l+3a) - \frac{w_l - w_a}{60l^2}(l-a)^3(2l+3a)$ $\theta_A = 0 \quad y_A = 0$ $R_B = \frac{w_a + w_l}{2}(l-a) - R_A$ $M_B = R_A l + M_A - \frac{w_a}{2}(l-a)^2 - \frac{w_l - w_a}{6}(l-a)^2$ $\theta_B = 0 \quad y_B = 0$	If $a = 0$ and $w_l = w_a$ (uniform load on entire span), then Max $-M = M_A = M_B = \frac{-w_a l^2}{12}$ Max $+M = \frac{w_a l^2}{24}$ at $x = \frac{l}{2}$ Max $y = \frac{-w_a l^4}{384EI}$ at $x = \frac{l}{2}$ If $a = 0$ and $w_a = 0$ (uniformly increasing load), then $R_A = \frac{3w_l l}{20}$ $M_A = \frac{-w_l l^2}{30}$ $R_B = \frac{7w_l l}{20}$ Max $-M = M_B = \frac{-w_l l^2}{20}$ Max $+M = 0.0215 w_l l^2$ at $x = 0.548l$ Max $y = -0.001309\frac{w_l l^4}{EI}$ at $x = 0.525l$
2e. Left end simply supported, right end simply supported 	$R_A = \frac{w_a}{2l}(l-a)^2 + \frac{w_l - w_a}{6l}(l-a)^2$ $M_A = 0 \quad y_A = 0$ $\theta_A = \frac{-w_a}{24EIl}(l-a)^2(l^2+2al-a^2) - \frac{w_l - w_a}{360EIl}(l-a)^2(7l^2+6al-3a^2)$ $R_B = \frac{w_a + w_l}{2}(l-a) - R_A$ $\theta_B = \frac{w_a}{24EIl}(l^2-a^2)^2 + \frac{w_l - w_a}{360EIl}(l-a)^2(8l^2+9al+3a^2)$ $M_B = 0 \quad y_B = 0$	If $a = 0$ and $w_l = w_a$ (uniform load on entire span), then $R_A = R_B = \frac{w_a l}{2}$ Max $M = \frac{w_a l^2}{8}$ at $x = \frac{l}{2}$ Max $\theta = \theta_B = \frac{w_a l^3}{24EI}$ Max $y = \frac{-5w_a l^4}{384EI}$ at $x = \frac{l}{2}$ If $a = 0$ and $w_a = 0$ (uniformly increasing load), then $R_A = \frac{w_l l}{6}$ $R_B = \frac{w_l l}{3}$ Max $M = 0.0641 w_l l^2$ at $x = 0.5773l$ $\theta_A = \frac{-7w_l l^3}{360EI}$ $\theta_B = \frac{w_l l^3}{45EI}$ Max $y = -0.00653\frac{w_l l^4}{EI}$ at $x = 0.5195l$

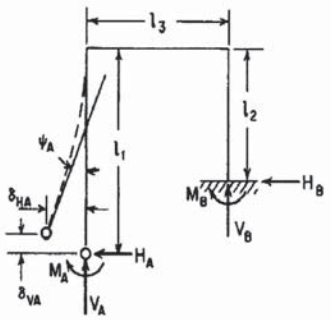
Values for some frequency factors, or beam coefficients, $a_{n,}$ are listed in Table 9.3. Note that for beams, the modal frequencies are not integer multiples, like the longitudinal stresses in a rod with free ends, which was presented in Equation (7.13). Also, note that frequencies are dependent on the end conditions or installation. For example, the beam coefficient varies from 22 to 9.87 for fixed and free-end conditions, respectively, which is a factor of 2.23. In other words, the frequency and maximum stress vary by a factor of 2.23 and ½, respectively, for changes in restraints. Stress intensification factors for piping resolve this discrepancy for stresses, and end correction factors partially address this discrepancy for frequencies.

9.1.3 Frequencies for Elastic Frames

Wachel [223] developed graphs from finite element analysis (FEA) results to determine frame frequencies for

TABLE 9.2 SHEAR, MOMENT, SLOPE, AND DEFLECTION FORMULAS FOR ELASTIC FRAMES (Young et al. [132], reprinted by permission of McGraw Hill, Inc.)

General reaction and deformation expressions for cases 5–12, right end fixed in all eight cases:



Deformation equations:

Horizontal deflection at $A = \delta_{HA} = C_{HH}H_A + C_{HV}V_A + C_{HM}M_A - LF_H$

Vertical deflection at $A = \delta_{VA} = C_{VH}H_A + C_{VV}V_A + C_{VM}M_A - LF_V$

Angular rotation at $A = \psi_A = C_{MH}H_A + C_{MV}V_A + C_{MM}M_A - LF_M$

where $C_{HH} = \frac{l_1^3}{3E_1I_1} + \frac{l_1^3 - (l_1 - l_2)^3}{3E_2I_2} + \frac{l_1^2 l_3}{E_3 I_3}$

$C_{HV} = C_{VH} = \frac{l_2 l_3}{2E_2I_2}(2l_1 - l_2) + \frac{l_1 l_3^2}{2E_3I_3}$

$C_{HM} = C_{MH} = \frac{l_1^2}{2E_1I_1} + \frac{l_2}{2E_2I_2}(2l_1 - l_2) + \frac{l_1 l_3}{E_3 I_3}$

$C_{VV} = \frac{l_2 l_3^2}{E_2I_2} + \frac{l_3^3}{3E_3I_3}$

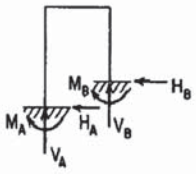
$C_{VM} = C_{MV} = \frac{l_2 l_3}{E_2I_2} + \frac{l_3^2}{2E_3I_3}$

$C_{MM} = \frac{l_1}{E_1I_1} + \frac{l_2}{E_2I_2} + \frac{l_3}{E_3I_3}$

and where LF_H, LF_V, and LF_M are loading terms given below for several types of load

(*Note:* If desired, H_B, V_B, and M_B are to be evaluated from equilibrium equations after calculating H_A, V_A, and M_A)

5. Left end fixed, right end fixed



Since $\delta_{HA} = 0$, $\delta_{VA} = 0$, and $\psi_A = 0$, these three equations are solved simultaneously for H_A, V_A, and M_A:

$$C_{HH}H_A + C_{HV}V_A + C_{HM}M_A = LF_H$$
$$C_{VH}H_A + C_{VV}V_A + C_{VM}M_A = LF_V$$
$$C_{MH}H_A + C_{MV}V_A + C_{MM}M_A = LF_M$$

The loading terms are given below.

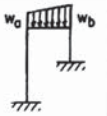
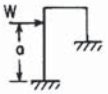
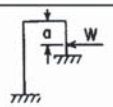
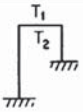
Reference no., loading		Loading terms
5a. Concentrated load on the horizontal		$LF_H = W\left[\frac{l_2}{2E_2I_2}(2l_1 - l_2)(l_3 - a) + \frac{l_1}{2E_3I_3}(l_3 - a)^2\right]$
5b. Distributed load on the horizontal member		$LF_H = w_a\left[\frac{l_2 l_3^2}{4E_2I_2}(2l_1 - l_2) + \frac{l_1 l_3^3}{6E_3I_3}\right] + (w_b - w_a)\left[\frac{l_2 l_3^3}{12E_2I_2}(2l_1 - l_2) + \frac{l_1 l_3^3}{24E_3I_3}\right]$ $LF_V = w_a\left(\frac{l_2 l_3^3}{2E_2I_2} + \frac{l_3^4}{8E_3I_3}\right) + (w_b - w_a)\left(\frac{l_2 l_3^3}{6E_2I_2} + \frac{l_3^4}{30E_3I_3}\right)$ $LF_M = w_a\left(\frac{l_2 l_3^2}{2E_2I_2} + \frac{l_3^3}{6E_3I_3}\right) + (w_b - w_a)\left(\frac{l_2 l_3^2}{6E_2I_2} + \frac{l_3^3}{24E_3I_3}\right)$
5f. Concentrated load on the left vertical member		$LF_H = W\left(C_{HH} - aC_{HM} + \frac{a^3}{6E_1I_1}\right)$ $LF_V = W(C_{VH} - aC_{VM})$ $LF_M = W\left(C_{MH} - aC_{MM} + \frac{a^2}{2E_1I_1}\right)$
5k. Concentrated load on the right vertical member		$LF_H = \frac{W}{6E_2I_2}[3l_1(l_2 - a)^2 - 2l_2^3 - a^3 + 3al_2^2]$ $LF_V = \frac{W}{2E_2I_2}[l_3(l_2 - a)^2]$ $LF_M = \frac{W}{2E_2I_2}(l_2 - a)^2$
5q. Uniform temperature rise: T = uniform temperature T_o = unloaded temperature		$LF_H = (T - T_o)(-\gamma_3 l_3)$ γ = temperature coefficient of expansion (inches/inch/degree) $LF_V = (T - T_o)(\gamma_1 l_1 - \gamma_2 l_2)$ $LF_M = 0$
5r. Uniform temperature differential from outside to inside; average temperature is T_o		$LF_H = (T_1 - T_2)\left[\frac{l_1^2\gamma_1}{2t_1} + \frac{l_2\gamma_2}{2t_2}(2l_1 - l_2) + \frac{l_1 l_3\gamma_3}{t_3}\right]$ $LF_V = (T_1 - T_2)\left(\frac{l_2 l_3\gamma_2}{t_2} + \frac{l_3^2\gamma_3}{2t_3}\right)$ t_1, t_2, and t_3 are beam thicknesses from inside to outside $LF_M = (T_1 - T_2)\left(\frac{l_1\gamma_1}{t_1} + \frac{l_2\gamma_2}{t_2} + \frac{l_3\gamma_3}{t_3}\right)$

TABLE 9.3 VIBRATIONS OF UNIFORM BEAMS WITH LOADS AT THE CENTER OF BEAMS SUPPORTED AT BOTH ENDS OR LOADED AT THE FREE END OF A CANTILEVERED BEAM (Den Hartog [209], reprinted by permission of McGraw Hill, Inc.)

Cantilever or "clamped-free" beam	$a_1 = 3.52$ $a_2 = 22.0$ $a_3 = 61.7$ $a_4 = 121.0$ $a_5 = 200.0$
Simply supported or "hinged-hinged" beam	$a_1 = \pi^2 = 9.87$ $a_2 = 4\pi^2 = 39.5$ $a_3 = 9\pi^2 = 88.9$ $a_4 = 16\pi^2 = 158.$ $a_5 = 25\pi^2 = 247.$
"Free-free" beam	$a_1 = 22.0$ $a_2 = 61.7$ $a_3 = 121.0$ $a_4 = 200.0$ $a_5 = 298.2$
"Clamped-clamped" beam has same frequencies as "free-free"	$a_1 = 22.0$ $a_2 = 61.7$ $a_3 = 121.0$ $a_4 = 200.0$ $a_5 = 298.2$
"Clamped-hinged" beam	$a_1 = 15.4$ $a_2 = 50.0$ $a_3 = 104.$ $a_4 = 178.$ $a_5 = 272.$
"Hinged-free" beam	$a_1 = 0$ $a_2 = 15.4$ $a_3 = 50.0$ $a_4 = 104.$ $a_5 = 178.$

comparison to field measured deflections and vibration velocities. Shell elements were used to describe the pipes, and curved beams were used to describe elbows. Stress predictions and frequencies were both recommended from that work for steel pipe (E = 30,000,000, ρ'' = 0.283), but only frequencies are presented here expressed in terms of Eq. (9.1). Fig. 9.1 to 9.3 provide first-mode frequency factors (a_1), and Table 9.4 provides end correction factors for those frequencies to multiply times Eq. (9.1) to account for frequency changes due to end constraints.

9.2 ELASTIC STRESSES DUE TO BENDING

For pipe installations, the maximum elastic bending stresses due to water hammer can be modeled from step

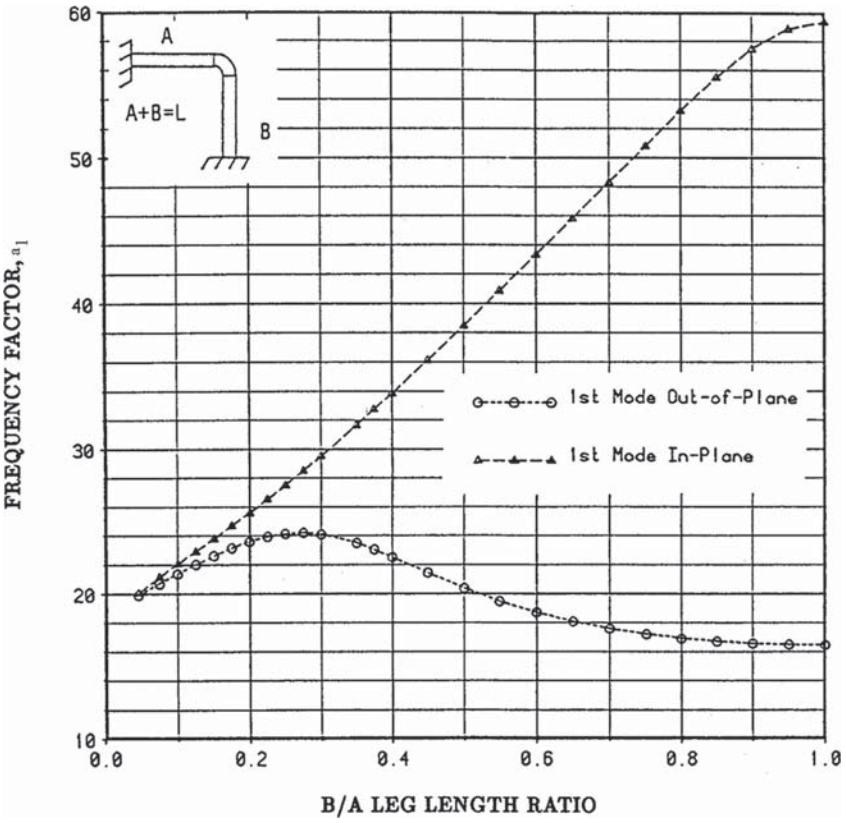


FIG. 9.1 FREQUENCY FACTORS FOR L-BEND PIPING (Wachel et al. [223], reprinted by permission of Engineering Dynamics, Inc.)

responses. The effects of line pack may also be included as an added ramp response, but in general, a step response adequately represents water hammer-induced shock waves for suddenly closed valves. A step response for a pipe with a single elbow is first provided as an example, followed by progressively more complicated examples.

9.2.1 Step Response Calculation for Bending

Example 9.1 Consider a straight pipe with an elbow at the end subjected to water hammer.

This example focuses on a simple theoretical case to demonstrate principles, using Fig. 9.4. This example can only be used to model a pipe attached to a bellows or hose, which has little practical use. A similar example was considered in earlier work by the author, but has been revised to reflect corrections and further developments in theory since that time. When the step pressure shock reaches an elbow ($t = 0$), forces in the x and z directions are instantly applied to impose axial forces and bending moments on the pipe at the fixed end (point A) in addition to hoop stresses traveling around the elbow at the wave front. For this example, a 150-psig pressure surge was assumed, which was much less than the pressure surge expected from closure of a 6-in. nominal pipe size (NPS) valve in the piping. Results are shown in Figs. 8.73 and 8.74, where the only differences between the two figures are the time scales. Calculations are also provided for this example to clarify the use of equations. This example was selected to ensure that stresses remained in the elastic range. In fact, a simple modification to Schedule 40 instead of Schedule 80 pipe for this example changes the maximum stress from 29,399 psi to 46,871 psi, which exceeded yield for many pipe materials.

9.2.1.1 Calculation Assumptions Assume 6-in. Schedule 80 NPS, A106 steel pipe and water at 70°F. Then, $\bar{T} = 0.432$ OD = 6.625 in., ID = 5.761 in., $r_m = 3.53$ in., $E = 29{,}500{,}000$ psi, $\rho_{pipe} = 0.283$ lbm/in.^{3}, $k = 319{,}000$ psi, $I = 40.49$ in.^{4}, metal area, $A = 8.405$ in.^{2}, $S_e = 12{,}500$ psi, and the weight / foot equals 28.57 lbm/ft = 2.38 lbm/in. The pressure across the shock was assumed, such that $P = 150$ psi. Thermodynamic fluid properties were obtained from steam tables from $P_0 = 14.7$ psi to $P = 150$ psig, where $\Delta h = 0.429$ Btu/lbm, $\Delta s = 5.316 \cdot 10^{-5}$ Btu/(lbm·°R). The steps to obtain Figs. 9.5 and 9.6 follow.

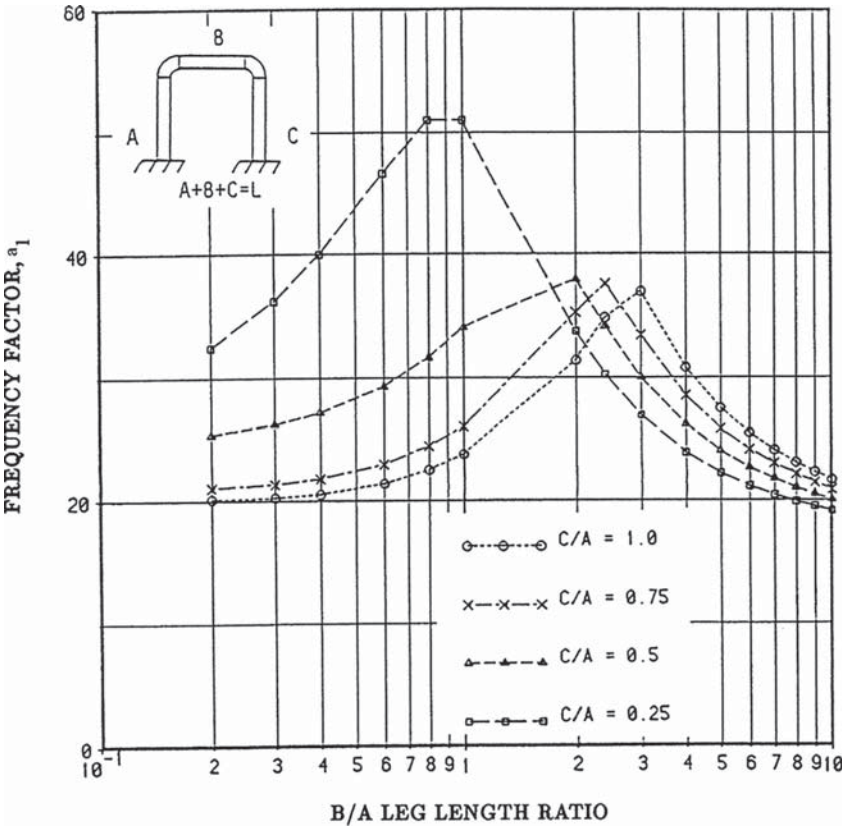


FIG. 9.2 FREQUENCY FACTORS FOR U-BEND PIPING (Wachel et al. [223], reprinted by permission of Engineering Dynamics, Inc.)

9.2.1.2 Axial Stresses Neglecting forces due to V_0, the axial force equals

$$F_z = \frac{P \cdot \pi \cdot \mathrm{ID}^2}{4} = \frac{150 \cdot \pi \cdot 5.761^2}{4} = 3910 \quad \text{US (9.2)}$$

The static axial stress equals

$$\sigma'_z = \frac{F_z}{A} = \frac{3910}{8.405} = 465.2 \text{ psi} \quad \text{US (9.3)}$$

For first-mode frequencies, $F = 1$, and the damping equals

$$\zeta_b = \zeta_z = 0.0053 + 0.0024 \cdot 6 + 0.0166 \cdot R + 0.009 \cdot 1 - 0.0019 \cdot 0 = 0.0287 \quad \text{US (9.4)}$$

The first-mode frequency equals

$$\omega_1 = \frac{n \cdot \pi}{L''} \cdot \sqrt{\frac{A \cdot E \cdot g''}{\left(\frac{W}{L''}\right)}} = \frac{1 \cdot \pi}{48} \cdot \sqrt{\frac{8.405 \cdot 29500000 \cdot 2.68''}{(2.38)}} = 109.37 \quad \text{US (9.5)}$$

Then, the dynamic axial stress shown in Figs. 9.5 and 9.6 equals

$$\sigma_z(t) = \sigma'_z \cdot \left(1 - \frac{e^{-\zeta_z \cdot \omega_z \cdot t}}{\sqrt{1-\zeta_z^2}} \cdot \cos\left(\left(t \cdot \omega_z \cdot \sqrt{1-\zeta_z^2}\right) - a\tan\left(\frac{\zeta_z}{\sqrt{1-\zeta_z^2}}\right)\right)\right)$$

$$= 465.2 \cdot \left(1 - \frac{e^{-0.0287 \cdot 3772.4 \cdot t}}{\sqrt{1-0.0287^2}} \cdot \cos\left(\left(t \cdot 3772.4 \cdot \sqrt{1-0.0287^2}\right) - a\tan\left(\frac{0.0287}{\sqrt{1-0.0287^2}}\right)\right)\right) \quad \text{US (9.6)}$$

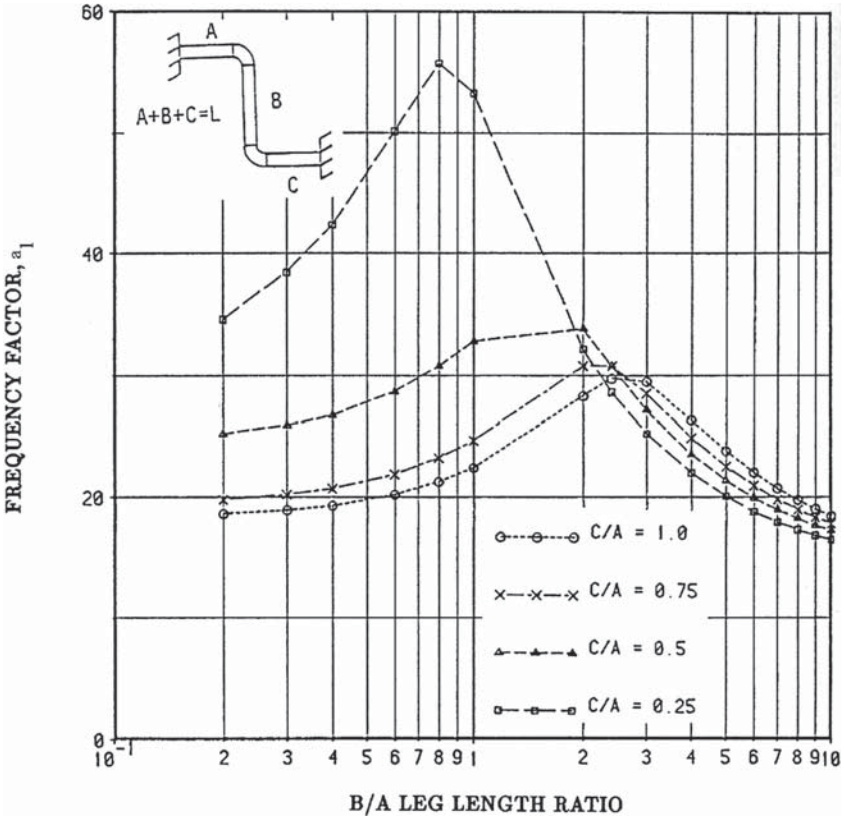


FIG. 9.3 FREQUENCY FACTORS FOR Z-BEND PIPING (Wachel et al. [223], reprinted by permission of Engineering Dynamics, Inc.)

9.2.1.3 Bending Stresses The static bending stress equals

$$\sigma'_b = \frac{M \cdot c'}{I} = \frac{48 \cdot 3910 \cdot (6.625/2)}{40.49} = 15354 \text{ psi} \qquad \text{US (9.7)}$$

The first-mode bending frequency equals

$$\omega_b = \frac{a_n}{(L'')^2} \cdot \sqrt{\frac{E \cdot I \cdot g''}{\left(\frac{W}{L''}\right)}} = \frac{3.52}{(48)^2} \cdot \sqrt{\frac{29500000 \cdot 40.49 \cdot 2.68}{0.0238}}$$

$$= 56.03 rad/\text{second} \qquad \text{US (9.8)}$$

Then, the dynamic bending stress shown in Figs. 9.5 and 9.6 equals

$$\sigma_b(t) = \sigma'_y \, b \cdot \left(1 - \frac{e^{-\zeta_b \cdot \omega_b \cdot t}}{\sqrt{1-\zeta_b{}^2}} \cdot \cos\left(\left(t \cdot \omega_b \cdot \sqrt{1-\zeta_b{}^2}\right) - a\tan\left(\frac{\zeta_b}{\sqrt{1-\zeta_b{}^2}}\right)\right)\right)$$

$$= 15354 \cdot \left(1 - \frac{e^{-0.0287 \cdot 56.03 \cdot t}}{\sqrt{1-0.0287^2}} \cdot \cos\left(\left(t \cdot 56.03 \cdot \sqrt{1-0.0287^2}\right) - a\tan\left(\frac{0.0287}{\sqrt{1-0.0287^2}}\right)\right)\right) \qquad \text{US (9.9)}$$

TABLE 9.4 END CORRECTION FACTORS FOR FREQUENCIES, WELDED END = WELDED INTO A HEADER
(Wachel et al. [223], reprinted by permission of Engineering Dynamics, Inc.)

Piping Configuration	Type of End Conditions	Natural Frequency Calculated on Basis Of Fixed–Ends	End Correction Factor
Straight	Welded–Welded	Fixed–Fixed	0.9 – 1.0
Straight	Welded–Supported	Fixed–Fixed	0.8
Straight	Supported–Supported	Fixed–Fixed	0.7
Straight	Welded–Free	Fixed–Free	0.5 – 1.0
Straight	Supported–Free	Fixed–Free	0.3 – 0.7
Bends	Welded–Welded	Fixed–End	1.0
Bends	Welded–Supported	Fixed–End	0.8
Bends	Supported–Supported	Fixed–End	0.7
Bends	Welded–Change of Plane	Fixed–End	0.8
Bends	Supported–Change of Plane	Fixed–End	0.7
Straight Pipe with Valve		Fixed–Fixed With L = Span Length - Valve Length	1.0

9.2.1.4 Hoop Stresses The static hoop stress equals

$$\sigma'_\theta = \frac{P \cdot r_m}{\bar{T}} = \frac{150 \cdot 3.53}{0.432} = 1225.2 \text{ psi} \quad \text{US (9.10)}$$

The cylindrical frequency for a thin wall tube of average radius r_m equals

$$\omega_\theta = \sqrt{g'' \cdot \frac{\left(\frac{2 \cdot k}{(r_m) \cdot \bar{T}}\right) + \left(\frac{E}{(r_m/2)^2 \cdot (1-\nu^2)}\right)}{\tilde{n}_{pipe} + \frac{(r_m) \cdot \tilde{n}_{water}}{4 \cdot \bar{T}}}}$$

$$= \sqrt{2.68 \cdot \frac{\left(\frac{2 \cdot 315000}{(3.53) \cdot 0.432}\right) + \left(\frac{29500000}{(3.53)^2 \cdot (1-0.29^2)}\right)}{\rho_{pipe} + \frac{(3.53) \cdot 0.035}{4 \cdot 0.432}}}$$

$$= 2989.9 \; rad/\text{second}$$

US (9.11)

Damping for a water-filled tube can be defined by the sum of fluid and structural damping, such that

$$S_r = 2 \cdot \sigma'_\theta = 2 \cdot 1225.17 = 2450.34 \quad \text{US (9.12)}$$

$$D = \left(\frac{S_r}{S_e}\right)^{2.3} + 6 \cdot \left(\frac{S_r}{S_e}\right)^{8} = \left(\frac{2450.34}{12500}\right)^{2.3} + 6 \cdot \left(\frac{2450.34}{12500}\right)^{8} = 0.02$$

US (9.13)

$$\varsigma_s = \frac{D \cdot E}{2 \cdot \pi \cdot S_r^2} = \frac{0.02 \cdot 29500000}{2 \cdot \pi \cdot 2450.34^2} = 0.018 \quad \text{US (9.14)}$$

$$\varepsilon' = \frac{\Delta h - T_0 \cdot \Delta s}{\Delta h} = \frac{0.429 - 529 \cdot 5.316 \cdot 10^{-5}}{0.429} = 0.934$$

US (9.15)

$$\zeta_f = \frac{-\ln(\varepsilon')}{\left(\left(\ln(\varepsilon')^2 + \pi^2\right)^{\frac{1}{2}}\right)} = \frac{-\ln(0.934)}{\left(\left(\ln(0.934)^2 + \pi^2\right)^{\frac{1}{2}}\right)} = 0.012$$

US (9.16)

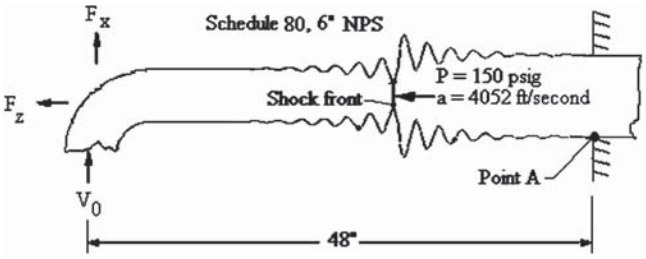


FIG. 9.4 SHOCK IMPINGEMENT ON AN ELBOW

$$\zeta = \frac{-\ln(\varepsilon')}{\left(\left(\ln(\varepsilon')^2 + \pi^2\right)^{\frac{1}{2}}\right)} + \frac{D \cdot E}{2 \cdot \pi \cdot S_r^2} = 0.012 + 0.018 = 0.030$$

US (9.17)

Then, the dynamic bending hoop stress shown in Figs. 9.5 and 9.6 equals

$$\sigma_\theta(t) = \sigma'_\theta \cdot \left(1 - \frac{e^{-0.03 \cdot \omega_\theta \cdot t}}{\sqrt{1-\zeta_\theta{}^2}} \cdot \cos\left(\left(t \cdot \omega_\theta \cdot \sqrt{1-\zeta_\theta{}^2}\right) - a\tan\left(\frac{\zeta\theta}{\sqrt{1-\zeta\theta^2}}\right)\right)\right)$$

$$\left(1 - \frac{e^{-0.03 \cdot 2989.9 \cdot t}}{\sqrt{1-0.03^2}} \cdot \cos\left((t \cdot 2989.9 \cdot \sqrt{1-0.03^2})\right) - a\tan\left(\frac{0.03}{\sqrt{1-0.03^2}}\right)\right)\right) = 1225.2$$

US (9.18)

9.2.1.5 Comparison of Calculated Bending Stress to an FEA Pipe Stress Model Another purpose for this simplified example was to compare theoretical results to commercial software, which in this case was Autopipe®. The calculated bending frequency and maximum undamped bending stress for this example were, in fact, validated and found to be nearly identical to Autopipe® results (Fig. 9.7). To do so, a steep fronted wave traveling at a sonic velocity was modeled. Although hoop and axial stresses could not be validated using Autopipe®, dynamic hoop stresses were validated in paragraph 8.5.4.

9.2.2 Ramp Response for Bending

Rewriting Eq. (7.48), the stresses equal

$$\sigma_\theta(t) = \sigma'_\theta \cdot \left[1 - 3 \cdot e^{\zeta_\theta \cdot \omega_\theta \cdot t} \cdot \frac{\sin(\omega_\theta \cdot t)}{\omega_\theta \cdot t_1} + \frac{\sin(\omega_\theta \cdot (t - t_1))}{\omega_\theta \cdot t_1}\right] \cdot H(t - t_1) + \sigma'_\theta \cdot 3 \cdot e^{\zeta_\theta \cdot \omega_\theta \cdot t} \cdot \left[\frac{t}{t_1} - \frac{\sin(\omega_\theta \cdot (t))}{\omega_\theta \cdot t_1}\right] \cdot H(t_1 - t)$$

US (9.19)

$$\sigma_b(t) = \sigma'_b \cdot \left[1 - e^{\zeta_b \cdot \omega_b \cdot t} \cdot \frac{\sin(\omega_b \cdot t)}{\omega_b \cdot t_1} + \frac{\sin(\omega_b \cdot (t - t_1))}{\omega_b \cdot t_1}\right] \cdot H(t - t_1) + \sigma'_b \cdot e^{\zeta_b \cdot \omega_b \cdot t} \cdot \left[\frac{t}{t_1} - \frac{\sin(\omega_b \cdot (t))}{\omega_b \cdot t_1}\right] \cdot H(t_1 - t)$$

US (9.20)

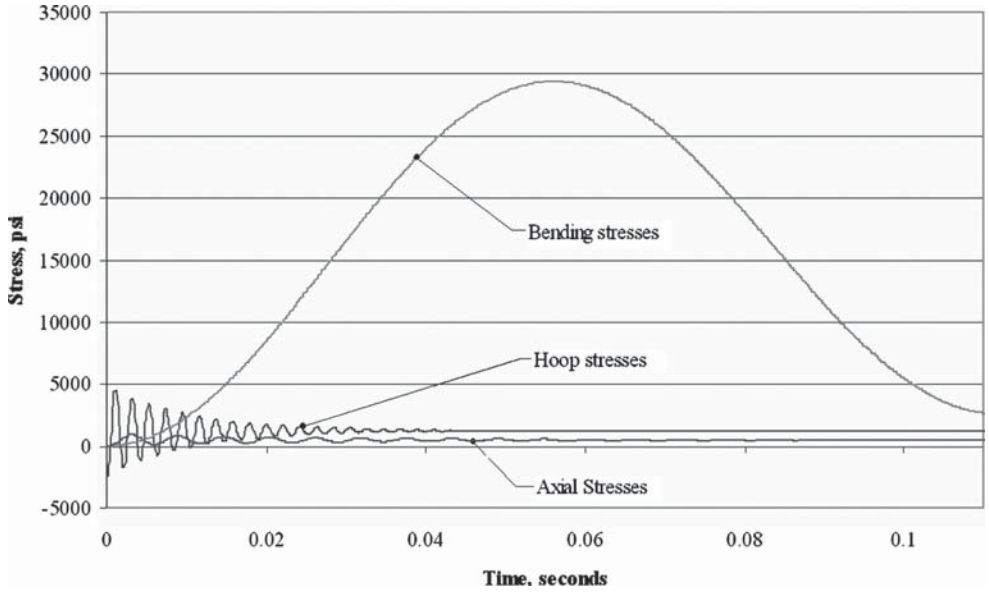


FIG. 9.5 STRESS RESPONSE OF AN ELBOW SUBJECTED TO A STEP PRESSURE SHOCK

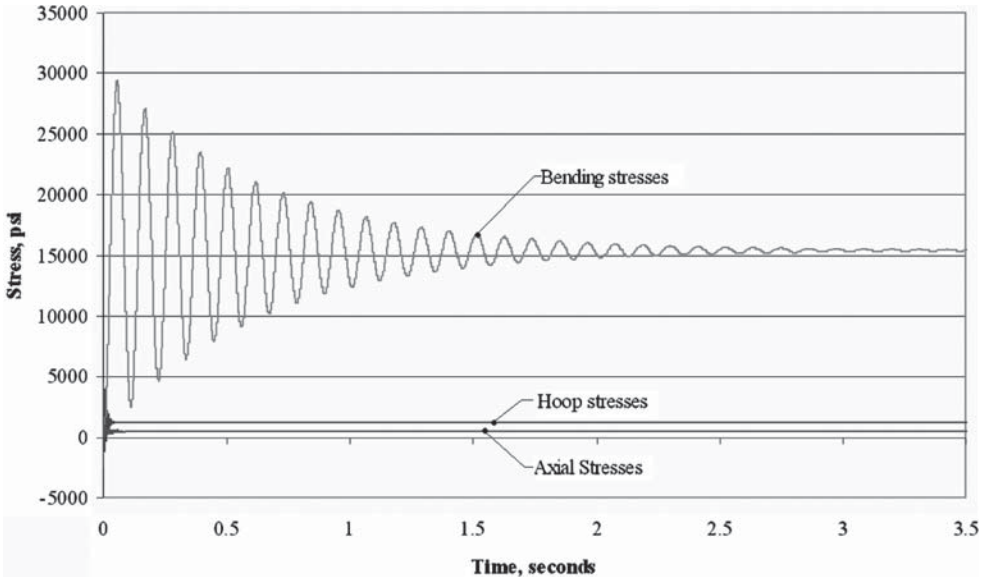


FIG. 9.6 STRESS RESPONSE OF AN ELBOW SUBJECTED TO A STEP PRESSURE SHOCK

$$\sigma_z(t) = \sigma'_z \cdot \left[1 - e^{\zeta_z \cdot \omega_z \cdot t} \cdot \frac{\sin(\omega_z \cdot t)}{\omega_z \cdot t_1} + \frac{\sin(\omega_z \cdot (t - t_1))}{\omega_z \cdot t_1}\right] \cdot H(t - t_1) + \sigma'_z \cdot e^{\zeta_z \cdot \omega_z \cdot t} \cdot \left[\frac{t}{t_1} - \frac{\sin(\omega_z \cdot (t))}{\omega_z \cdot t_1}\right] \cdot H(t_1 - t) \quad \text{US (9.21)}$$

Example 9.2 Determine the effects of a 0.01 second ramp response caused by linear fluid transient pressure changes.

Using the 6-in. NPS, Schedule 80 pipe of Example 9.1, determine the effects of linearly changing fluid transients on dynamic pipe stresses (Fig. 9.8).

Using these three equations, a 0.1-second rise is first considered. Note that the hoop and axial stresses do not overshoot the static stress at all and that the bending stresses are significantly reduced. Since manual valve closure usually takes 0.1 seconds, piping near the valve will see these reductions in stresses. Piping remote from the valve will be affected as a function of the system impedance. As the pipe length increases, the wave front becomes steeper (Fig. 9.9).

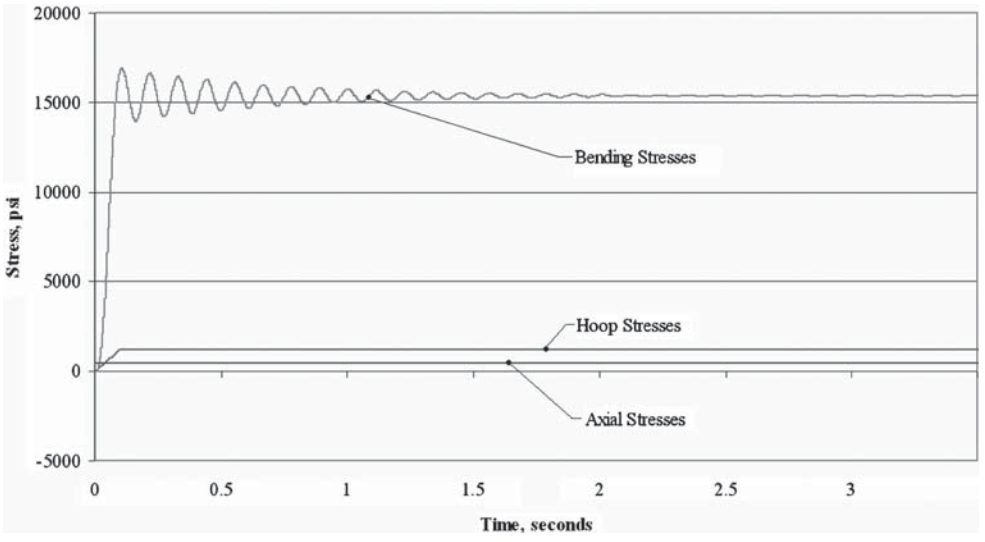


FIG. 9.7 STRESS RESPONSE FOR A 0.1-SECOND RISE TIME

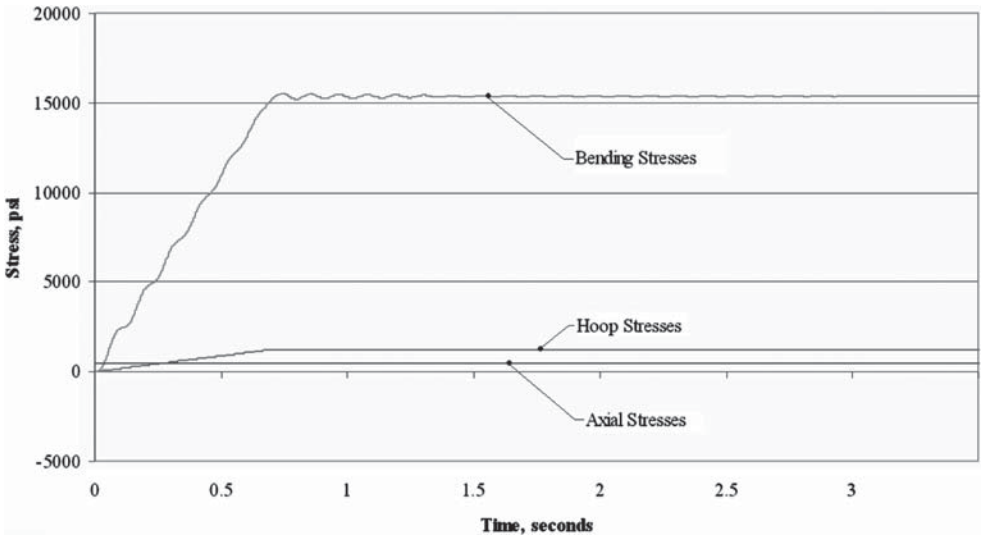


FIG. 9.8 STRESS RESPONSE FOR A 0.7-SECOND RISE TIME

Example 9.3 Determine the effects of a 0.07-second ramp response caused by a linear fluid transient.

A second case, assumes a 0.7-second rise time, again using the 6-in. NPS, Schedule 80 pipe of Example 9.1. Note that the static stress is negligibly overshot when the rise time is less than a second. Also, as rise times increase, the magnitudes of the fluid transients decrease. In other words, a case by case evaluation is required to investigate rise times in terms of valve closure rates and pipe frequency. Even so, this phenomenon provides some explanation of how transient stresses are significantly reduced by seemingly minor system changes.

9.2.3 Impulse Response for Bending

The length of time that a pressure is applied directly influences the pipe stresses, since a pressure impulse is applied to the pipe. Factors such as the length of a pipe, and the distance between elbows, affect the pipe response.

Example 9.4 Consider the effects of pipe length on pipe response.

With respect to pipe length, a shock wave travels the length of the pipe, and either doubles the pressure near the pipe end for a closed pipe or reflects a pressure wave near the vapor pressure of the fluid. In either case, the pipe length is significant. For example, if the pipe is 20 ft long with a dead end, the impulse lasts $2 \cdot L/a$. Consider the same 6-in. pipe of Example 9.1 and that the pipe is still fixed at 48 in. from the elbow, but assume that the length of pipe upstream of the elbow is 20 ft long, and that $V_0 = 10$ ft/second. Assuming that the valve instantly closes, then the change in pressure equals 586.55 psi for fixed-end condi-

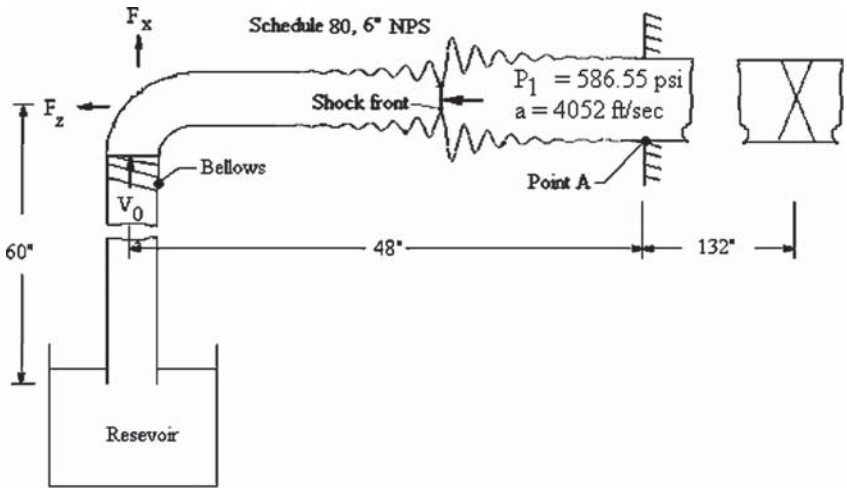


FIG. 9.9 BENDING STRESSES DUE TO REFLECTED PRESSURE WAVES

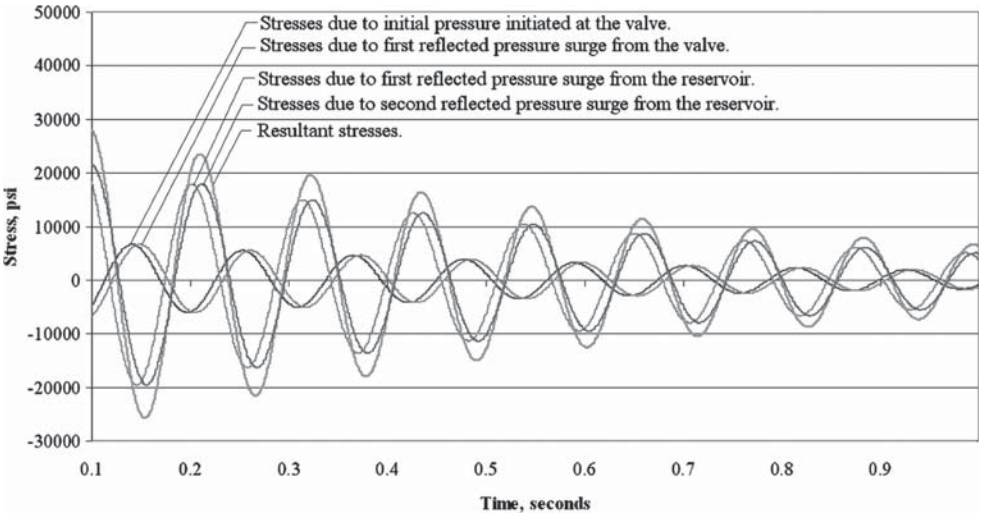


FIG. 9.10 COUPLING OF BENDING STRESSES

tions, and a static bending stress equals 15,291 psi. A six and a half ton force would be expected to damage the pipeline for certain. However, the force on the elbow is related to the impulse time and wave reflections.

Fig. 9.10 provides partial results to explain the stresses due to pressure transients. Neglecting line pack, a shock wave is assumed to be initiated at the valve due to instant closure. Assuming $V_0 = 10$ ft/second, a shock wave traveling at 4052 ft/second away from the closed valve, has a pressure equal to

$$P_1 = \rho \cdot a \cdot V_0 / g = 62.4 \cdot 4052 \cdot 10 / 32.174 = 586.55 \text{ psi} \quad \text{US (9.22)}$$

Using the equations from Example 9.2, the bending stresses can be determined. The elbow is 15 ft from the valve, and the wave travels from the valve to the elbow in 15/a seconds, and the time that the wave strikes the elbow is specified as $t = 0$. The wave passes the elbow, and another wave is reflected from the reservoir. Until the wave returns, the elbow is subjected to $P_1 = 586.55$ psi, and the impulse time $t_1 = 10/a$. At $t = 10/a$, the pressure drops from P_1 to near the vacuum pressure in the pipe, P_{vac}, determined by calculations. For this example, assume that $P_{vac} = -8$ psig. Then, the change in pressure $P_2 = -(586.55 + 8)$ psi. The shock wave returns to the valve and is reflected at a pressure P_1. The process then repeats. Two complete cycles are shown in Fig. 9.10, where the stresses are calculated as follows.

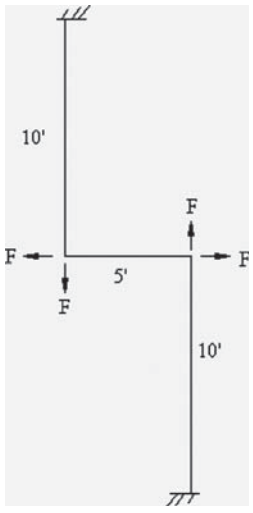


FIG. 9.11 Z-BEND

For each curve, the expression for stresses in a thin wall tube is expressed as

$$\sigma_b(t) = \frac{P \cdot r_m}{\bar{T}} \cdot e^{-\zeta_b \cdot \omega_b \cdot (t - L/a)} \cdot (\cos \omega_b (\omega_b \cdot (t - t_1 - L/a))) -$$
$$\cos(\omega_b \cdot t_1 - L/a) \cdot H(t_1 - t - L/a) +$$
$$\frac{P \cdot r_m}{\bar{T}} \cdot e^{-\zeta_b \cdot \omega_b \cdot (t - L/a)} \cdot (\cos \omega_b (\omega_b \cdot (t - t_1 - L/a)) -$$
$$\cos(\omega_b \cdot t_1 - L/a)) \cdot H(t - t_1 - L/a) \quad \text{US (9.23)}$$

where $t_1 = 10/a$ when $P = P_1$; $t_1 = 30$ for $P = P_2$; $t = L/a = 0$ for the initial pressure from the valve; $t = L/a = 10/4052$ for the first pressure wave reflected from the reservoir; $t = L/a = 40/4052$ for the reflected pressure wave from the valve; and $t = L/a = 50/4052$ for the second reflected pressure wave from the reservoir. Substitution of variables yields Fig. 9.10.

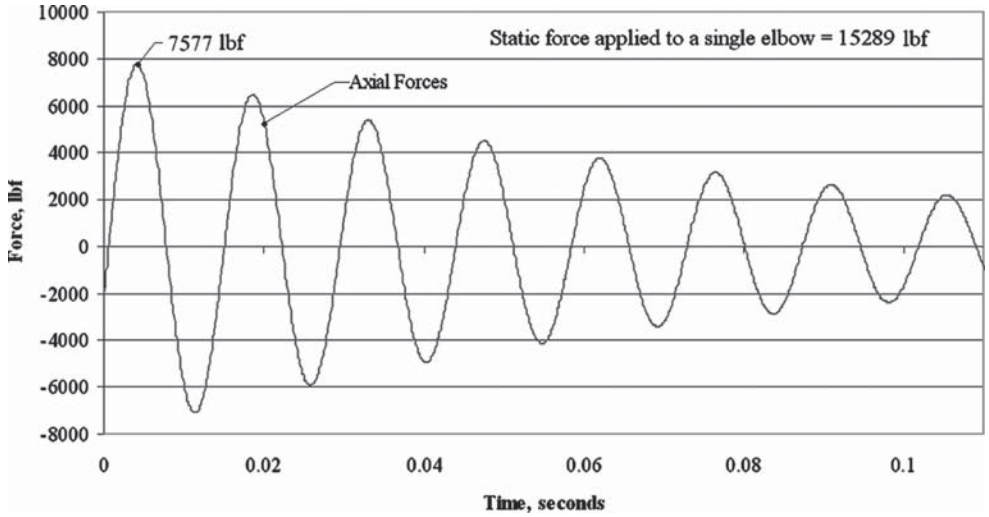


FIG. 9.12 FORCES ON A Z-BEND

9.2.4 Multiple Bend FEA Models

Graphic stress solutions are unavailable for even simple geometry, like Z-bends, but graphic solutions can provide some insight into loads on frames. For example, a Z-bend is considered here.

Example 9.5 Approximate the forces on the Z-bend shown in Fig. 9.11.

The frequency factor, $a_1 = 27.3$ from Fig. 9.3. Then, $\omega_1 = 434.6$ rad/second. A simplification was made by estimating the forces to be equal at the elbows by assuming rigid members. Then, substituting variables from Example 9.1 into Eq. (9.24) yields Fig. 9.12.

$$F(t) = \frac{P \cdot r_m}{\bar{T}} \cdot e^{-\zeta_b \cdot \omega_b \cdot t} \cdot (1 - \cos(\omega_b \cdot t)) - \frac{P \cdot r_m}{\bar{T}} \cdot e^{-\zeta_b \cdot \omega_b \cdot (t - L/a)} \cdot (1 - \cos(\omega_b \cdot t - L/a)) \quad \text{US (9.24)}$$

Equation (9.24) represents the two opposing forces applied to the Z-bend at a time difference equal to $L/a = 5/4052$.

Note that the maximum force is half of the force obtained by applying the static load to a single elbow. Opposing forces at elbows in pipe loops and Z-bends serve to reduce the pipe stresses due to dynamic loads. This

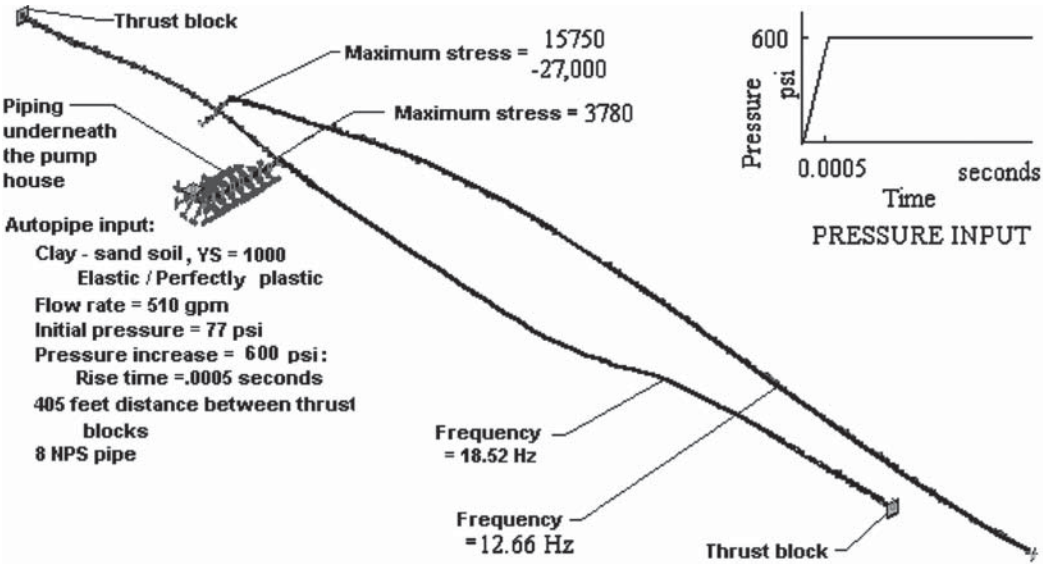


FIG. 9.13 FEA MODEL OF BENDING STRESSES

observation lends a precaution for piping design. An assumption that a pipe end is fixed eliminates the opposing force in a pipe loop and increases the calculated pipe stresses.

9.3 FEA MODEL OF BENDING STRESSES

Example 9.6 Consider an FEA model for bending stresses.

Fig. 9.13 provides the analytical results for bending stresses of an underground ductile iron pipe that failed due to water hammer. The underground pipe was sheared perpendicular to the pipe length. Typical of several failures in 20-ft long, flanged pipes, the failure occurred at the midlength of the pipe span closest to the elbow where the maximum stress occurred. The fatigue strength was exceeded by the bending stresses alone and is considered to be the cause of failure, and the location of the cracks also indicated that a first mode flexural stress may be coupled to the bending stress.

To perform the calculation, a shock wave velocity and maximum pressure was calculated, and input to Autopipe® to obtain the pipe frequency and maximum stresses. This failed pipe was also in the system considered in detail in Examples 5.6, 5.20, 5.22, and 5.27 (paragraphs 5.3.1.4, 5.13, 5.14.4, and 5.17).

9.4 PLASTIC DEFORMATION AND STRESSES DUE TO BENDING

An interesting aspect to water hammer events in steel pipe systems is that ruptures of the pipe are typically not observed. Certainly, there are conditions that can cause rupture due to overload, but pipe systems have been knocked off their supports, piping has been severely bent, and yet, the failures in ductile systems occur at flanges and brittle components attached to the piping. A systematic study of all water hammer damages is outside the scope of this work, but a systematic study has been performed for damages to power plants following earthquakes.

9.4.1 Consideration of Earthquake Damages to Pipe Systems

Adams [239] summarized piping failures in power plants, which were designed to ASME B31.1 and B31.3. Over one million feet of pipe and 10,000 pipe supports were investigated. Using a criterion of any detectable leakage as failure, J. D. Stevenson Associates found that ductile piping did not fail during earthquakes, although pipes may have bent or fallen to the floor from their overhead supports. The only observed failures occurred where brittle components were installed, corrosion damage was evident, or threaded fittings failed. Also, ratcheting was observed in piping, and in one case, a pipe unzipped along a seam weld in a pipe that was not fabricated to code requirements. Adams referenced NUREG/CR0239 [240], EPRI NP-5617, EPRI NP-6593, and EPRI-NP-7000-SL. Even so, recent earthquake damages in Japan may provide additional information on ductile pipe failures during earthquake. Also, further investigation may be required with respect to cracking at reducers in piping during earthquakes.

9.5 SUMMARY OF STRESSES DURING WATER HAMMER

In general, plastic deformation and pipe support damage is a typical result from water hammer in ductile pipe systems, such as steel. Brittle material failure is more common during water hammer events. In all likelihood, many existing piping systems frequently exceed design requirements during operations, since pressure surges are not typically measured. Ratcheting may permit overloads to go unnoticed. If water hammer persists, fatigue failure may occur. Once fatigue commences, many cracks may be present throughout the system, but eliminating the cause of the transient may permit continuous safe operation of a system.

CHAPTER

10

SUMMARY OF WATER HAMMER-INDUCED PIPE FAILURES

Water hammer accidents and damages continue to occur at nuclear and industrial facilities, even at SRS, where I have trained many engineers to identify the causes and effects of water hammer. This text is a start toward a better general education of engineers in this field of study. Another effort to this end, is the writing of an in-process ASME Standard, ASME, B31D - Design Of Piping Systems For Dynamic Loads From Fluid Transients. The Standard is scheduled for completion in 2014, and should be another step toward improved safety and lower operating costs for industrial and municipal facilities.

Water hammer results in fatalities and probably hundreds of millions of dollars in damage during startup, off-normal operations, and long-term operations. Damages occur for different water hammer causes, such as valve and pump operations, keep, and condensate-induced water hammer.

Techniques to assess pressure surges and resulting dynamic pipe stresses are presented in this text. Water hammer induced pressure surges in pipe systems may exceed the design pressure by a factor of six to ten times, or more. Static design bending stresses may be doubled, and hoop stresses may be quadrupled. At the end of a dead end pipe, stresses may again be doubled during water hammer. In short, water hammer may cause pipe stresses to exceed the intended design stresses by more than an order of magnitude. Many pipe cracks in industrial systems are caused by water hammer, and are preceded by valve packing leaks. A common refrain is that pipes fail because they are old. Not so, pipes fail for reasons that can be technically evaluated, and water hammer is a failure mechanism frequently misdiagnosed. Even so, fluid transients occur in all fluid systems, and are not always detrimental to the pipe system.

With respect to valve closure and pump operations in liquid filled systems:

- Water hammer has caused fatigue failures in ductile and brittle components such as concrete or cast iron pipe, cast iron valves, and sight glasses
- Valve closure typically does not cause one-time overload damages in ductile pipes (such as steel), but conditions to cause catastrophic failures may be present during water hammer incidents
- Valve trim, brittle components, and flange gaskets in ductile pipe systems damages have occurred
- Fatigue failures of piping have occurred

Condensate-induced water hammer and slug flow into empty pipes during pump startups tend to produce higher pressures than valve closure. For systems of these types:

- Significant plastic deformations of ductile piping have occurred. In general, overload fracture of a ductile pipe does not occur, but overload fracture of a large-diameter pipe is possible under some conditions, particularly near pipe ends where reflected waves may double the dynamic hoop stresses
- Pipe support damages have occurred
- Flange gaskets, flange bolts, and valves in ductile pipe systems have been damaged, and pipes have been hurled into the air and through building walls
- Catastrophic failures have occurred for brittle components such as cast iron valves and pipe constructed of brittle materials
- Fatalities have occurred during failures of brittle components due to condensate-induced water hammer
- Fatalities have occurred due to flange gasket failures and stripping of flange bolts in ductile steel pipe systems

Following water hammer accidents, obvious piping damages are typically repaired, transients are corrected, and pipe systems are returned to service for most cases, supported by a damage assessment.

Techniques available to perform damage assessments are briefly discussed in this text, supported by more detailed references. For long-term failures in either ductile or brittle materials, cracking due to fatigue may occur after months, or even years, of operation, and the cause of fractures are frequently misdiagnosed. These fatigue failures are often preceded by valve leaks in the system before piping cracks occur. Once a fatigue failure is attributed to water hammer, techniques are available to evaluate continued pipe system use after failure repairs. Specifically, fracture mechanics principles can be applied to assess the system for continued use, provided that the fluid transient loads are adequately reduced. The transient loads on piping are determined by using a dynamic magnification factor. In general, the dynamic magnification factor depends on component type: where DMF < 4 for hoop stresses in a pipe, DMF < 2 for simple bending of a pipe but may be complicated by pipe geometry, and DMF < 2 for valves. To close out this text, a few suggestions on troubleshooting practices and suggested references follow.

10.1 TROUBLESHOOTING A PIPE FAILURE

A principle difficulty in identifying the cause of pipe damage is obtaining a concise operating history of a facility. Water hammer may be the cause of pipe failure, but other factors may contribute to the failure. In fact, one of the primary difficulties in analyzing fatigue failures due to water hammer is the possibility of failure due to other loads or failures due to combined loading. Coupled with the information provided in this text and additional study, a thorough understanding of system operation is paramount. Hopefully, this text provides adequate information for the practicing engineer to better troubleshoot pipe system failures.

A few personal observations to the analyst are in order with respect to the issue of troubleshooting:

- Personally inspect the pipe failure in place, and oversee all subsequent failure analysis
- If available, facility-operating records are the best source of historical information required to understand a failure
- Interviews with operators and technicians provide invaluable insight into a plant's operating history. Frequently, operation records fail to record all observations
- Facility engineers and managers are also a good source of information, but the data they provide is sometimes unintentionally filtered in support of existing explanations and assumptions with respect to pipe failures. Omissions of known facts have often hindered investigations. Scrutinize and record all provided data
- Although schedules may push toward a quickly hazarded guess at the probable cause, do not provide an interpretation of a failure until certain. Credibility decreases rather fast when two or three different guesses are provided before the problem is resolved.
- Although not a technical comment, relationships with the customer are essential. When troubleshooting complex pipe failures, other engineers and managers are frequently responsible for the outcome and liabilities of an investigation. The customer may simply respond, "Not true" after competent results are presented. Teaching the customer or his staff may be required, even if the customer disagrees with reported results. If effective analysis is inhibited by poor communications or poor relationships, significant costs may occur to the analyst, his customer, and affected personnel. An example of this concern was encountered at SRS for the design of a melter system for melting glass for radioactive waste processing. A leak occurred in the melter bus-bar within four minutes of a loud valve-slam due to a shut-down of one of two operating parallel pumps, and X-ray analysis showed that a crack formed internal to the melter at a sharp corner. The melter was redesigned to eliminate this stress raiser. While redesign was in process, the leak increased. Investigation proved that the leak increased when one of two pumps was shut down. Reverse flow occurred through one pump, and fracture growth due to fatigue resulted from water hammer. The engineer in charge did not believe water hammer was the cause, but his management was convinced to change procedures to extend the melter life until the replacement was received. In this case, the failure was corrected by increasing the strength of the part as well as reducing the pressure that caused the failure

10.2 SUGGESTED REFERENCES

Several references provided the education needed to write this book and are frequently referenced to evaluate pipe failures due to fluid transients. In addition to software for fluid transients and pipe design, the following desk top references are suggested.

- *Fluid Transients* [173]
- *Flow of Fluids Through Valves, Fittings, and Pipes* [21]
- *Theory of Vibration With Applications* [212]
- *Roark's Formulas for Stress and Strain* [132]

- *Harris' Shock and Vibration Handbook* [213]
- *Failure of Materials in Mechanical Design* [121]
- *ASME B31.3* [89]
- *Fracture Mechanics* [103]
- *Mark's Standard Handbook for Mechanical Engineers* [33]
- *The Pump Handbook* [53]
- *Gas Dynamics* [14]
- *Instrument Engineers' Handbook* [31]

10.3 RECOMMENDED FUTURE RESEARCH

As noted throughout the text, nearly all topics covered here can be improved with further research. The fundamental water hammer equation has been around for a hundred years, yet computer simulations do not yet adequately describe the fluid mechanics of condensate induced water hammer. The basics of dynamic responses for elastic pipe systems subject to water hammer were presented here, but additional calculations would certainly provide better insight into pipe response and failures. Elastic strains and stresses are reasonably well understood, but the basic mechanisms of plasticity, fatigue, and fracture are not fully understood, and a physical relationship to connect them them has yet to be fully described. Ratcheting and shakedown in piping needs more research before dynamic effects are understood. Additionally, Chapter 8.8.3 discussed the combined effects of fluid transients and trapped flammable gases, where fluid transients are possible causes of explosions in nuclear reactor pipe systems and off-shore oil drilling operations.

When steam systems or pumps are started in nuclear reactors, a sudden pressurization of any accumulated hydrogen in the system can compress the hydrogen and the hydrogen may explode. In some cases, hydrogen may accumulate at high points in the system in reactor cooling systems, and fluid transients may occur during system re-starts or other operations. These two factors may lead to explosions. To describe the mechanics of an explosion in a reactor system, a fluid transient compresses the trapped gas, adiabatic compression causes a temperature increase, and in some cases this temperature increase is sufficient to reach the auto-ignition point of the hydrogen. Similar to a diesel engine the vapor ignites. Depending on the volume of hydrogen, deflagration to detonation transition is possible and an explosion can occur. Essentially, a rapidly moving water column, or slug of fluid, acts as a piston to compress, ignite, and explode a trapped flammable gas. Several unexplained explosions have occurred in Japanese and German nuclear reactor facilities, i.e., Brunsbuettel (2001) and Hamaoka (2001). This theory presents a possible explanation for those explosions (Leishear [237]). This fluid transient/explosion theory may even be related to the Fukushima nuclear reactor disaster (2011), the Three Mile Island nuclear accident (1979), and the Chernobyl nuclear accident (1986). Prior to explosions during these accidents, the accumulation of hydrogen gas was postulated, and conditions to cause water hammer were present according to internet reports by Wikipedia. Therefore, two of the conditions to initiate explosions were probably present in each case.

During off-shore drilling, explosions frequently occur in pipe lines, and this fluid transient/explosion theory is also asserted to contribute to those explosions and resultant fires. To describe the application of the fluid transient/explosion theory, natural gas bubbles of significant size are reported to occasionally fill pipeline sections at the time of explosions. If oil comes up the pipe behind the bubble, the bubble can compress, heat up, ignite, and explode under some conditions. The upper fluid column slows down while the lower water column speeds up to compress the gas between the two moving fluid columns. "Swish, Run, Boom" is the operator response during oil rig explosions and fires, according to internet reports. Swish is the sound that would be heard at the oil rig if there was a gas explosion in the pipe under water as the explosion rushes the oil in the pipeline toward the surface. The operators would have a very short time to run before the exploding gas expands and pushes the oil all the way up to the platform where the operators are stationed, and burning gas and oil reach the piping at the platform. High pressures and forces will be exerted on equipment throughout the pipe system which may damage piping, and explosive shock waves can form if the flaming gas exits the pipe at the platform. This mechanism may have occurred during the Gulf oil spill disaster (2010), and is considered here as a possible cause for repeated pipeline explosions reported at oil rigs across the globe.

The explosion process described here is a possible cause of explosions in several major industrial accidents. All of these accidents potentially share common factors: fluid transients, trapped flammable gases, and explosions with causes that were uncertain or unknown. The explosion cause described here announces a discovery that relates all of these factors. Even so, research is required to experimentally demonstrate and understand this discovery with respect to structural dynamics, explosion mechanics, and specific accidents. The opinion asserted here concludes that there may be serious public risks with respect to pipe system operations, which have not previously been considered. A potential connection between numerous industrial explosions has been presented, which includes accidents at Three Mile Island, Chernobyl, Fukushima, and the Gulf Oil Spill.

APPENDIX

A

NOTATION AND UNITS

A.1 SYSTEMS OF UNITS

Common systems of units are listed in Table A.1 where customary US units are predominantly used throughout this work, and the use of the gravitational constant, g_c, is required for equations. Equations and examples are provided in the text with appropriate conversions to be consistent with customary US units {US: length (in., ft), area (in.^{2}, ft^2), mass (lbm), force (lbf), pressure (psi), flow rate, (gpm), and seconds}. That is, commonly available units are used in examples and equations for this text and are listed in Table A.3 along with abbreviations and symbols. The selection of customary US units may seem somewhat arbitrary, since many units are used in the US. For example, pressure is described by atmospheres, psi, lbf/ft^2, in. of water or mercury. Even so, the more common units encountered in pipe system design were selected for use in this text. Equations are also presented in International System of Units (SI): m, Newton, kg, second} and the English Engineering System {EE: length (in.), area (ft^2), mass (lbm), force (lbf), pressure (lbf/ft^2), flow rate, (ft^3/second), and seconds}. In the text, equations are noted to be US, EE, or SI format, as applicable. In a few cases, viscosities are described in terms of centipoise and centistokes, which are metric quantities related to SI units. Additionally, to adapt the many data formats for units available in the literature, conversions are provided in Table A.2 to convert units. The English Scientific System (ES) of units is also listed in Table A.1, but ES units are not

TABLE A.1 SYSTEMS OF UNITS

Quantity	SI	EE	US	ES
Length, L	m	ft	in.	ft
Area, A	m^2	ft^2	in.^{2}	ft^2
Volume, V'	m^3	ft^3	in.^{3}	ft^3
Time, T	second	second	second	second
Mass, m	kg	lbm	lbm	slug
Force, F	N	lbf	lbf	lbf
Stresses, σ, τ Pressure, P	Pa	lbf/ft^2	psi (lbf/in.^{2})	lbf/ft^2
Weight density, γ	—	lbf/ft^3	lbf/ft^3	lbf/ft^3
Mass density, ρ	kg/m^3	lbm/ft^3	lbm/ft^3	slug/ft^3
Viscosity, μ	Pa second	lbf·second/ft^2	lbf·second/ft^2	lbf·second/ft^2
Viscosity, ν'	m^2/second	ft^2 second	ft^2/second	ft^2/second
Volume, V'	m^3	ft^3	ft^3	ft^3
Velocity, V	m/second	ft/second	ft/second	ft/second
Flow rate, Q	m^3/second	ft^3/second	gpm	ft^3/second
Head, h	M	ft	ft	ft
Power, P'	Watt	ft·lbf/second	hp	ft·lbf/second
Energy, E'	Joule	ft·lbf	ft·lbf	ft·lbf
Elastic modulus, E	kg/m^2	lbf/ft^2	psi	lbf/ft^2

noted in the body of the text. ES units may be substituted in any SI equation since both systems are consistent systems, which do not require the g_c quantity for use.

The text would have certainly been simplified using only the consistent SI system of units, but the fact is that much industry in the US still uses the customary US system of units despite the fact that the SI system is slowly being incorporated into US industry. The EE system would also have been adequate, but customary US units provide a convenient form for equation use. The application of different systems of units was an attempt to broaden the scope of this work, and efforts were made to prevent confusion in the text due to the use of multiple systems of units. Table A.1 shows the relationship between basic quantities used in various systems of units; Table A.2 provides the conversions; and Table A.3 provides the nomenclature and units used in this text.

A.2 CONVERSION FACTORS

Mark's Handbook (Avallone and Baumeister [33] provides a comprehensive list of conversions and constants beyond those used in this text, but common dimensions used in this text are listed along with some of the symbols used here. In short, the following list of conversions provides relationships between the various dimensions required for fluid and solid mechanics as discussed in this text.

TABLE A.2 CONVERSIONS

Acceleration, g		
	g = local gravitational acceleration at sea level, 45 deg latitude. g varies by −0.003 ft/second^2 for each 1000 ft of altitude, and by less than ±0.086 ft for all other latitudes at sea level:	
		US, EE, 32.174 ft/second^2
		SI, 9.80665 m/second^2
	g_c = gravitational constant	
		US, EE, 32.174 (ft·lbm/(second^2·lbf)
		SI, 1.0 (m·kg·second^2)/(N·second^2) Metric, 9.806 (kg_{mass}·m)/(kg_{force}·second^2)
Energy, E		
	1 Btu	778.26 ft·lbf ≈ the energy obtained from burning one wooden match (Lindeburg [57])
	1 Joule	0.7376 ft·lbf
	1 Joule	1 N m
	1 Joule	0.7376 Btu
Enthalpy, h'		
	1 Btu/lbm	2324.4 Joule/kg
Entropy, s'		
	1 Btu/(lbm °R)	4186.8 Joule/(kg °K)
Head, h		
	2.31 ft of water	1 psi = (144 in.^{2}/ft^2)/ρ_w
	13.61 in. of water	1 in., Mercury at 32°F
Head to specific energy, h_v, h_p, h_T, or h_z		
	1 ft	1 (ft·lbf/lbm)/(g/g_c)
	1 m	1 (J/kg)·(1/9.81 m/second^2)
Force, $F = m \cdot a'$		
	1 lbf	4.448 Newton
	1 lbf	1 lbm·(g/g_c)
	1 Newton	1 m·kilogram/second^2
	1 dyne	1 cm·gram/second^2

TABLE A.2 CONVERSIONS (CONTINUED)

Flow rate, Q		
	448.9 gpm	1 ft^3/second
	35.32 ft^3/second	1 m^3/second
Length, L		
	3.281 ft	1 m
Mass, m		
	1 slug (lbf · $second^2$/ft)	g_c·lbm = 32.174 lbm
		2.2046 lbm 1 kg
Mass density, ρ		
	1 g/cm^3	62.42 lbm/ft^3 at 39.2 °F
	1 g/cm^3	1000 kg/m^3
Power, P'		
	1 horsepower	550 ft·lbf/second
	1 horsepower	33,000 ft·lbf/minute
	1 horsepower	0.7062 Btu/second
	1 horsepower	0.7457 kW
	1 watt	1 J/second
	1 watt	1 V·amp
	1 kW	1000 J/second
	1 kW	0.9478 Btu/second
	1 W	1 V amp (1 amp^2·ohm)
Pressure (P), Stress (σ, τ)		
	1 bar	14.504 psi
	1 Pascal	10^{-5} bar
	6.894 Pa	1 psi
	1 atmosphere	14.696 psi at sea level, 59 °F
	1 atmosphere	7.6 m
	1 Pa	1 N/m^2
	29.92 in. mercury	14.696 psia
Volume, V'		
	7.481 gal	1 ft^3 0.02832 m^3
	1 L 10^{-3} m^3	0.264 gal
Velocity, V		
	88 ft/second	60 mi/hour
	60 miles/hour	26.82 m/second
Viscosity (Absolute Dynamic), μ		
	1 centipoise	10^{-3} Pascal second
	47,880 centipoise	1 lbf second/ft^2
	1 centipoise	0.01 Poise
	1 Poise	0.1 N·second/m^2
Viscosity (Kinematic), ν		
	1 ft^2/second	92903.4 centistokes
	1 centistokes	0.01 Stoke
	1 centistoke	10^{-6} m^2/second
	1 Stoke	10^{-4} m^2/second

A.3 NOTATION: VARIABLES, CONSTANTS, AND DIMENSIONS

Some abbreviations and symbols are identical throughout the literature, but prime symbols ("or") are listed in Table A.3 to differentiate similar symbols in this text. For example the letter *a*, is used for the wave speed of a shock wave due to water hammer, and *a*' is used for acceleration, where the letter, *a*, is a common symbol describing each quantity in its respective field. The combination of many different fields of study into a single text requires that this issue be addressed. Separate symbols could be used to describe the two variables, but then, referencing between this text and classic references, or even casual conversations with experts in different fields, becomes confusing. Accordingly, the use of similar symbols is applied to this work for consistency. In a few cases, identical symbols are used when their use is obvious. For instance, the letter, *F*, is used to denote either a force, *F* or degrees Fahrenheit, °F, and stress symbols, σ and τ, are used interchangeably for stresses in either fluids or solids. For text examples, subscripts are used (1, 2, 3, …), and are not all specifically listed in Table A.3.

TABLE A.3 NOTATIONS, ABBREVIATIONS, AND SYMBOLS

a_n, a'	acceleration, ft/second^2
a	crack length, crack depth, in.
a	crack width/2, in.
a	constant
a_n	beam coefficients
a, a_1, a_2, a_3	water hammer shock wave velocity, ft/second
a''	water hammer shock wave velocity, in./second
a_i, a_1-a_7	fracture mechanics constants
A	area, in.^{2}
A_b	total bolting area, in.^{2}
A	elbow sweep radius, in.
A'	arbitrary constant
A''	amplitude
A_0	cross-sectional area, in.^{2}
A_1	upstream pipe area, in.^{2}
A_2	downstream pipe area, in.^{2}
A_0–A_8	constants
ACI	American Concrete Institute
AISC	American Institute of Steel Construction
API	American Petroleum Institute
ASCE	American Society of Civil Engineers
ASHRAE	American Society of Heating, Refrigeration, and Air Conditioning Engineers
ASM	American Society of Metals
ASTM	American Society of Testing and Materials
AWWA	American Water Works Association
B'	constant
b	bending
b	constant
BHP, BHP_1, BHP_2	brake horsepower
Btu	British thermal unit
c	wave velocity, ft/second
c	damping coefficient
c	constant
c	circumference, in.
C	degrees Celsius, Centigrade, °C
C	fracture mechanics constant
c'	maximum distance from the centroid, in.
c''	thread depth correction factor
c_0	velocity (speed) of sound
c_1	constant describing pipe restraint
c_1	dilatational velocity, ft/second
c_2	traction wave velocity, shear wave velocity, ft/second
$c_{critical}$	critical damping coefficient
c_R	surface wave velocity, ft/second
CDVM	classic discrete vapor cavity model
C_H	head correction factor
C_η	efficiency correction factor
cP	centipoise
C_Q	flow rate correction factor
C_p	specific heat, Btu/(lbm·°F)
C_v	flow coefficient for a valve
C_v	specific heat at a constant volume, Btu/(lbm·°F)
C^+	characteristic
C^-	characteristic
$C(t, \omega, \zeta)$	cyclic, harmonic vibration response
d	constant
D	impeller diameter, in.

TABLE A.3 (CONTINUED)

D	bolt circle diameter, in.
D	specific damping energy, in. lbf/(in.^{3}·cycle)
D	inside pipe diameter, in.
D'	derivative control
D_c	distortion coefficient
DMF	dynamic magnification factor
D_{nom}	nominal pipe diameter, in.
D_0	disc diameter, in.
D_1	valve seat opening, in.
D_2	downstream valve opening, in.
e	total strain, in./ft
e	thermal expansion coefficient, in./ft
E	modulus of elasticity, psi
E''	energy, ft·lbf
E'''	quality factor
E_k'	kinetic (specific) energy of a fluid, ft·lbf/lbm
E_k''	kinetic energy, ft·lbf
E_p'	pressure (specific) energy of a fluid, ft·lbf/lbm
E_T'	total (specific) energy, ft·lbf/lbm
E_R	modulus of rigidity, psi
E_T'	total energy, ft·lbf
E_z'	potential (specific) energy of a fluid, ft·lbf/lbm
E_z''	potential energy, ft·lbf
EE	English Engineering System
ES	English Scientific System (English Gravitational System)
f	Darcy friction factor
f	frequency, cycles/second
F	degrees Fahrenheit, °F
F	force, lbf
F_x	spring force, lbf
F_θ	circumferential force, lbf
$F(t)$	forcing function
f''	stress range factor
f_d	damped frequency, cycles/second
f_H	Hazen-Williams friction factor
f'_L	Fanning friction factor for laminar flow
f_m	Manning friction factor for open channels
f_n	Fanning friction factor

TABLE A.3 (CONTINUED)

f_n	natural frequency, cycles/second
f_i	incident wave
f_r	reflected wave
F_r	shear force per unit length, lbf
f_t	transmitted wave
$f(R_K)$	fracture mechanics constant
f_T	Darcy friction factor for turbulent flow
f'_T, f'_{Tr}	Fanning friction factors for turbulent flow
F_x	force in the x direction, lbf
F_y	force in the y direction, lbf
F_z	force in the z direction, axial force, lbf
FEA	finite element analysis
f_1	upstream Darcy friction factor
f_2	downstream Darcy friction factor
F_θ	circumferential force per unit length, lbf
f_1, f_2, f_3...	modal frequencies, cycles/second
G	shear modulus, psi
g	local gravitational acceleration, ft/second^2
g"	local gravitational acceleration, in./second^2
G_1–G_4	fracture mechanics constants
g_c	gravitational constant, ft·lbm/(second^2·lbf)
G_g	mass flux of a gas, lbm/(ft^2·hour)
G_L	mass flux of a liquid, lbm/(ft^2·hour)
gpm	gallon per minute
h	valve stem travel, in.
h	variable head, ft
H	modulus of plasticity, psi
$H(\ldots)$	Heaviside step function
h'	enthalpy, Btu/lbm
h"	film coefficient, Btu/(hour·ft^2·°F)
h_a	head rise, ft
h'_a	head decrease, ft
h_b	barometric head, ft
He	Hedstrom number
h_L	system head loss due to friction, ft
h_{LS}	suction piping head loss, ft
h_{L1}-h_{L5}	head losses due to friction, ft
hp	horsepower

TABLE A.3 (CONTINUED)

h_{pump}	head supplied by a pump, ft
h_s	suction head or suction lift, ft
h_T	total head, ft
$h_{turbine}$	head removed by a turbine, ft
h_v	head loss due to friction of a valve, ft
h_v	head due to vapor pressure
h_w	head when pumping water, ft
Hz	Hertz, cycles per second
h_0	initial head, ft
h_1, h_2	pump head, ft
i	stress intensification factor
I	moment of inertia, in.^{4}
I'	integral control
IBC	International Building Code
i_i	in plane, stress intensification factor
i_o	out of plane, stress intensification factor
in.	inches
I_m	motor moment of inertia, lbf/ft^2
I_p	pump moment of inertia, lbf/ft^2
I_{total}	total mass moment of inertia, lbf/ft^2
$I(t, \omega, \zeta)$	impulse response
ISA	Instrument Society of America
J	Joule
J	polar moment of inertia, in.^{4}
k	bulk modulus of a fluid or solid, psi
k_g	bulk modulus of a gas, psi
k_L	bulk modulus of a fluid, psi
K	degrees Kelvin, °K = °C + 273.15
K	resistance coefficient
k'	spring constant, lbf/ft
k''	spring constant, lbf/in.
k''	thermal conductivity, Btu/(hour·ft^2·°F)
k'''	strength coefficient
K'_d	diameter correction factor
$K_{d,i,j}$	friction losses variables for fittings
K_{eff}	effective fracture toughness, in.$^{1/2}$
kg	kilogram
K'_s	surface finish correction factor
ksi	thousands of pounds force per square in.
K_{thr}	threshold fracture toughness, in.$^{1/2}$
K_I	stress intensity factor, in.$^{1/2}$

TABLE A.3 (CONTINUED)

K_{Ic}, K_{IIc}, K_{IIIc}	fracture toughness, in.$^{1/2}$
$K_{I,res}$	residual fracture toughness, in.$^{1/2}$
K'_L	load correction factor
K_1	upstream resistance coefficient
K_2	downstream resistance coefficient
L	length, ft
L''	length, in.
lbf	pound force
lbm	pound mass
LEFM	linear elastic fracture mechanics
L_s	length between support anchors, ft
L_S	slug length, ft
L_V	void length, ft
m	meter
m	mass
m	fracture mechanics material constant
M	moment, ft·lbf
m'	fluid power law constant, Pascal·second^{n+1}
$\dot{m}$	mass flow rate, lbm/second
max	maximum
M_b	bending moment, ft·lbf
M_i	in plane, moment, ft·lbf
min	minute
min	minimum
M_o	out of plane, moment, ft·lbf
M'_o	plastic hinge, moment, ft·lbf
M_T	torsional moment, ft·lbf
M_z	moment per unit length in the z direction, ft·lbf
MSS	Manufacturer's Standardization Society of Valves and Fittings
Multi-DOF	multiple degree of freedom
M_θ	moment per unit length in the tangential direction, ft·lbf
n	fluid power law constant
n	number of operational cycles
n	rotational speed, rpm
n_R	rated rotational speed, rpm
n	integers, 1,2,3,…
N	Newton
n'	strain hardening exponent
NACE	National Association of Corrosion Engineers

TABLE A.3 (CONTINUED)

NBIC	National Board Inspection Code
N_{design}	predicted number of cycles to failure
NEMA	National Electric Motor Association
NPS	nominal pipe size
NPSHa	net positive suction head required, ft
NPSHr	net positive suction head available, ft
n_S	specific speed
$N, N_1, N_2, \ldots N_j$	number of cycles to failure
OD	outside pipe diameter, in.
psi	lbf per square in.
psia	lbf per square in. absolute
P	pressure, pressure increase across a shock wave, psi
P	pressure gauge symbol
P	pressure cycling regime
P'	proportional control
P'	power, horsepower
Pa	Pascal
P_a	atmospheric pressure, psia
P_{abs}	absolute pressure, psia
PF	power factor
P_g	gauge pressure, psig
P_s	pump suction pressure, psig
P_v	vapor pressure, psia
P_0	initial pressure, psig
P.O.	percent overshoot
P_1, P_2	pressure, psia
P_1, P_2	absolute pressure, psia
q	heat flux, Btu/(hour·ft^2·°F)
Q	fracture mechanics constant
Q_w	volumetric flow rate when pumping water, gpm
Q, Q_1, Q_2	volumetric flow rate, gpm
Q_0	initial volumetric flow rate, gpm
r	radial direction, radial coordinate
r	radius, sweep radius, in.
R	degrees Rankine, °R = °F + 459.67
R'	stress ratio
r_h	hydraulic radius, in.
r_i	inside pipe radius, in.
r_m	average pipe radius, in.
r_o	outside pipe radius, in.
Re	Reynold's number

TABLE A.3 (CONTINUED)

Re_1	upstream Reynold's number
Re_2	downstream Reynold's number
Re_{pl}	Reynold's number for a power law fluid
$R(t, \omega, \zeta)$	ramp response
R1	ratcheting regime
s	installed spring
s	constant
S	stress, allowable stress, psi
s'	entropy, Btu/(lbm °R)
Sa	allowable stress, psi
S'_a	alternating stress, psi
S_b	displacement-controlled bending stress, psi
S_c	pipe stress at ambient conditions, psi
SDOF	single degree of freedom
S_e	fatigue limit, psi
sec	second
SF	service factor
S'_E	calculated stress range, psi
Sh	pipe stress at operating conditions, psi
SI	International System of Units
S_L	longitudinal stress, psi
S_m	mean stress, psi
S_{min}	minimum stress, psi
S_{max}	maximum stress, psi
S_n	fatigue failure stress at $n < N$ cycles, psi
SpG	specific gravity
S_r	range stress, psi
SSU	Sayboldt universal seconds
S_T	pipe stress due to torsion, psi
S_u	ultimate tensile strength, psi
SVZ	single vaporous zone model
S_y	yield strength, psi
$S(t, \omega, \zeta)$	step response
S1	shakedown regime
t	time, seconds
t_o	valve opening time, seconds
T	temperature, °R
T	torque, ft·lbf
T	torsion

TABLE A.3 (CONTINUED)

T	valve closure time, seconds
TFSIM	thermal fluid simulator/MOC program
T_R	rated torque, ft·lbf
$\overline{T}$	pipe wall thickness, in.
$\overline{T}$	film thickness, in.
T_K	temperature, °R or °F
T_L	temperature, °R or °F
$\overline{T}_{min}$	minimum wall thickness, in.
$\overline{T}_{nom}$	nominal wall thickness, in.
$\overline{T}_S$	effective wall thickness, in.
T_0	ambient temperature, °R
t_1	pulse duration, rise time, seconds
u	radial displacement, in.
US	customary U.S. units
V	variable velocity, ft/second
V_{cr}	critical velocity, ft/second
V_f	final velocity, ft/second
V_0	initial velocity, ft/second
V''_0	velocity, in./second
V'	volume, ft^3
V'_g	gas volume, ft^3
V'_L	liquid volume, ft^3
VFD	variable frequency drive
V_r	radial velocity, ft/second
V_S	slug velocity, ft/second
$V''(t)$	vibration response of a structure
V_z	axial velocity, ft/second
V_1	upstream velocity, ft/second
V_2	downstream velocity, ft/second
V_θ	circumferential velocity, feet/second
$V(t, \omega, \zeta)$	vibration response
w	without spring
w	axial displacement, in.
w_a	sum of free and aftershock vibrations, in.
w_p	precursor free vibration, in.
w_{pr}	equals the precursor free vibration, in.
w_1	axial displacement after a shock, in.
w_{1a}	step vibration, in.
w_{2a}	free vibration, in.
w_2	axial displacement before a shock, in.
w_{2p}	equals the precursor free vibration w_2, in.

TABLE A.3 (CONTINUED)

W	weight, lbf ($W = m \cdot g/g_c$, US)
W'	weld strength reduction factor
x	x direction
x	displacement, ft
x''	displacement, in.
x_f	constant, ft
x_h	homogeneous solution for the equation of motion
x_p	particular solution for the equation of motion
XS	extra strong pipe
XXS	extra extra strong pipe
y	y direction
z	axial direction, z coordinate
Z'	elevation, altitude, ft
Z	section modulus, $in.^3$
Z_e	effective section modulus, $in.^3$
Z_{ps}	pressure gauge elevation, ft
Z_1	upstream pipe elevation, ft
Z_2	downstream pipe elevation, ft
α	thermal expansion coefficient
α	angle, radians
α	ratio of operating speed to rated speed
α	flexural resonance constant
β	ratio of upstream to downstream diameters
β	angle, radians
β	ratio of operating torque to rated torque
γ	weight density, lbf/ft^3
γ_g	gas weight density, lbf/ft^3
γ_L	liquid weight density, lbf/ft^3
γ	angle, radians
γ	flexural resonance variable
γ'	wave number, 1/seconds
$\dot{\gamma}'$	shear rate, $second^{-1}$
Δ	total change in length, in.
Δc	change in circumference, in.
Δh	change in head, ft of water
Δh	change in enthalpy, Btu/lbm
Δs	change in entropy, Btu/(lbm·°R)
$\Delta h'$	change in enthalpy, Btu/lbm
ΔK	change in stress intensity factor

TABLE A.3 (CONTINUED)

$\Delta\rho$	change in mass density, lbm/ft^3
ΔP	change in pressure, psi
Δt	change in time, seconds
ΔV	change in velocity, ft/second
ΔT	change in temperature, °F
Δx	displacement, ft
$\Delta x''$	displacement, in.
$\acute{\alpha}$	mass proportional damping coefficient
β	stiffness proportional damping coefficient
δ	deflection, in.
δ	log decrement
ε	surface roughness for pipe, in.
ε	strain, in./in., ft/ft
ε'	thermodynamic efficiency
$\dot{\varepsilon}$	strain rate, in./in./ second
ε_f	equivalent surface roughness for fittings, in.
ε_m	roughness factor for open channels
ε_T	true strain, in./in.
ε_x, ε_y, ε_z	Cartesian orthogonal strains, in./in.
ε_r, ε_θ, ε_z	cylindrical orthogonal strains, in./in.
ε_1, ε_2, ε_3	principal strains, in./in.
ζ	damping coefficient
ζ_s	structural damping coefficient
ζ_f	fluid damping coefficient
ζ_i	modal damping coefficients
ζ_j	orthogonal damping coefficients, x, y, z or r, θ, z
η	pump efficiency
η_φ	motor efficiency
η_w	pump efficiency when pumping water
θ	circumferential (hoop) direction
λ	fluid property parameter
λ	fluid resonance variable
λ	wavelength, ft
λ'	Lame' constant
μ	viscosity or consistency, centipoise
μ	micro
μ_K	viscosity, centipoise
μ_L	viscosity, centipoise
ν	Poisson's ratio

TABLE A.3 (CONTINUED)

ν'	kinematic viscosity, centistokes
ξ	flexural resonance variable
ρ	mass density, lbm/ft^3
ρ''	mass density, lbm/in.^{3}
ρ_w	mass density for water at sea level, 68°F [51] = 62.28 lb mass/ft^3
ρ_g	mass density for a gas, lbm/ft^3
ρ_L	mass density for a liquid, lbm/ft^3
ρ_1	upstream mass density, lbm/ft^3
ρ_2	downstream mass density, lbm/ft^3
σ	stress, psi
σ'	static stress, psi
σ''	surface tension, lbf/ft
$\sigma(t)$	dynamic stress, psi
$\sigma_b(t)$	dynamic bending stress, psi
$\sigma_a(t)$	free vibration stress, psi
σ'_b	static bending stress, psi
σ_e	engineering stress, psi
σ_f	failure stresses, psi
σ_{max}	maximum dynamic stress, psi
σ_{rmax}	maximum dynamic radial stress, psi
$\sigma_P(t)$	precursor free vibration stress, psi
$\sigma_r(t)$	dynamic radial stress, psi
$\sigma_S(t)$	step response stress after a shock, psi
$\sigma_T(t)$	dynamic torsion stress, psi
σ'_T	static torsion stress, psi
σ'_r	static radial stress, psi
σ_t	true stress, psi
$\sigma_z(t)$	dynamic axial stress, psi
σ'_z	static axial stress, psi
σ_{zmax}	maximum dynamic axial stress, psi
σ_x, σ_y, σ_z	orthogonal stresses, psi
$\sigma_{1,}$, σ_2, σ_3	principal stresses, psi
σ_{1m}, σ_{2m}, σ_{3m}	principal mean stresses, psi
σ_{1min}, σ_{2min}, σ_{3min}	minimum principal stresses, psi
σ_{1max}, σ_{2max}, σ_{3max}	maximum principal stresses, psi
$\sigma_\theta(t)$	dynamic hoop stress, membrane stress, psi
σ'_θ	static hoop stress, psi
$\sigma_{\theta max}$	maximum dynamic hoop stress, membrane stress, psi
σ'_1, σ'_2	normal stress on a maximum shear stress plane, psi

TABLE A.3 (CONTINUED)

σ_1, σ_2	successive peak amplitudes, psi
τ	shear stress, psi
τ	ratio of wave speed to critical velocity
τ'	period, seconds
τ'_d	period of damped vibration, seconds
τ'_n	period at the natural frequency, seconds
τ_{max}	maximum shear stress, psi
$\tau_{r\theta}$	hoop shear stress on a radial plane, psi
τ_{rz}	axial shear stress on a radial plane, psi
τ_{zr}	radial shear stress on an axial plane, psi
$\tau_{z\theta}$	hoop shear stress on an axial plane, psi
$\tau_{\theta z}$	axial shear stress on a circumference, psi

TABLE A.3 (CONTINUED)

$\tau_{\theta r}$	radial shear stress on a circumference, psi
τ_{xy}, τ_{yx}, τ_{xz}, τ_{zx}, τ_{yz}, τ_{zy}	orthogonal shear stresses, psi
τ_w	fluid shear stress at the pipe wall, psi
τ_0	fluid shear stress at the pipe centerline, psi
φ	phase angle
ψ	fluid property parameter
ω	radial frequency, radians/second
ω_1, ω_2, ω_3, …	modal frequencies
ω_d	frequency for damped vibration, radians/second
ω_i	modal frequencies
ω_j	orthogonal frequencies, x, y, z or r, θ, z
ω_n	natural radial frequency, radians/second

REFERENCES

References are listed in the order that they are cited, and chapters are also listed where each reference is first cited.

CHAPTER 1

1. Leishear, R. A., 2005, "Dynamic Stresses During Structural Impacts and Water Hammer," PhD Dissertation, University of South Carolina.
2. Leishear, R. A., 2001, "Dynamic Stresses During Water Hammer," Master's Thesis, University of South Carolina.
3. Leishear, R. A., 2007, "Stresses in a Cylinder Subjected to an Internal Shock," vol. 129, ASME Journal of Pressure Vessel Technology, ASME, New York, New York.
4. Leishear, R. A., 2007, "Dynamic Stresses During Water Hammer, A Finite Element Approach," vol. 129, ASME Journal of Pressure Vessel Technology, ASME, New York, New York.
5. Leishear, R. A., 2007, "Derivation of Hoop Stress Equations Resulting from Shock Waves in a Tube," Joint ASME Pressure Vessel and Piping Division Conference, ASME, New York, New York.
6. Leishear, R. A., 2006, "Comparison of Experimental to Theoretical Pipe Strains During Water Hammer," Joint ASME Pressure Vessel and Piping Division/ International Council of Pressure Vessel Technology Conference, ASME, New York, New York.
7. Leishear, R. A., 2006, "Application of a Dynamic Stress Theory to Pipe Leaks," Joint ASME Pressure Vessel and Piping Division/International Council of Pressure Vessel Technology Conference, ASME, New York, New York.
8. Leishear, R. A., 2006, "Experimental Determination of Water Hammer Pressure Transients During Vapor Collapse," Joint ASME Pressure Vessel and Piping Division/International Council of Pressure Vessel Technology, ASME, New York, New York.
9. Leishear, R. A., 2005, "Stresses During Impacts on Horizontal Rods," International Mechanical Engineering Congress and Exposition, ASME, New York, New York.
10. Leishear, R. A., 2005, "Stresses in a Cylinder Subjected to an Internal Shock," Pressure Vessel and Piping Conference, ASME, New York, New York.
11. Leishear, R. A., Morehouse, J., 2004, "Water Hammer Pressure Transients in a Closed Loop System," Joint Heat Transfer and Fluids Engineering Conference, ASME, New York, New York.
12. Leishear, R. A., 2003, "Dynamic Stresses During Structural Impacts," International Mechanical Engineering Congress and Exposition, ASME, New York, New York.
13. Leishear, R. A., Morehouse, J., 2003, "Dynamic Pipe Stresses During Water Hammer, V, Applications," International Mechanical Engineering Congress and Exposition, ASME, New York, New York.
14. Leishear, R. A., Morehouse, J., 2003, "Dynamic Pipe Stresses During Water Hammer, IV, Elastoplasticity in Thick Walled Tubes," ASME/JSME Fluids Conference, ASME, New York, New York.
15. Leishear, R. A., 2002, "Dynamic Pipe Stresses During Water Hammer, III, Complex Stresses," Pressure Vessel and Piping Conference, ASME, New York, New York.
16. Leishear, R. A., 2002, "Dynamic Pipe Stresses During Water Hammer, II, A Vibration Analysis," Pressure Vessel and Piping Conference, ASME, New York, New York.
17. Leishear, R. A., Rhodes, C., Alford, E. A., Young, M., 2002, "Dynamic Pipe Stresses During Water Hammer, I, A Finite Element Analysis," Pressure Vessel and Piping Conference, ASME, New York, New York.
18. Joukowski, N., 1904, "Water Hammer," Proceedings American Water Works Association, vol. 24, Denver, Colorado, pp. 341–424.

CHAPTER 2

19. White, F. M., 1986, "Fluid Mechanics," McGraw Hill, New York, New York.
20. Shames, I. H., 1992, "Mechanics of Fluids," McGraw Hill, New York, New York.

21. Crane, 1988, "Flow of Fluids Through Valves, Fittings, and Pipe, Technical Publication, No. 410," Crane Company, Chicago, Illinois.
22. Slattery, J. C., 1996, "Advanced Transport Phenomena," McGraw Hill, New York, New York.
23. Bird, R. B., Stewart, W. E., Lightfoot, E. N., 2002, "Transport Phenomena," John Wiley and Sons, New York, New York.
24. John, J. E. A., 1984, "Gas Dynamics," Allyn and Bacon, Inc., Newton, Massachusetts.
25. Merzkirch, W., 1974, "Flow Visualization," Academic Press, New York, New York.
26. Nakayama, Y., Boucher, R. F., 1999, "Fluid Mechanics," John Wiley and Sons, New York, New York.
27. Adrian, R. J., 1991, "Particle Imaging Velocimetry for Experimental Fluid Mechanics," Annual Review of Fluid Mechanics, 23, Palo Alto, California.
28. Idelchik, I. E., 1996, "Handbook of Hydraulic Resistance," Begell House, Inc., New York, New York. pp. 556, 557, 565, 568, 569.
29. Tanida, Y., Miyashiro, H., 1992, "Flow Visualization VI," Springer-Verlag, Berlin, Germany.
30. Ahuja, V., Hosangadi, A., Cavallo, P., Shipman, J., "Simulations of Valve Operation in High Pressure Facilities," PVP2007-26629, Pressure Vessel and Piping Conference Proceedings, ASME, New York, New York.
31. Liptak, B. G., Venczel, K., 1982, "Instrument Engineers Handbook," Chilton Book Co., Radnor, Pennsylvania.
32. Harnby, N., Edwards, M. F., Nienow, A. W., 2000, "Mixing in the Process Industries," Reed Publishing, Boston, Massachusetts.
33. Avallone, E. A., Baumeister, T., 1978, 1987, "Marks' Standard Handbook for Mechanical Engineers," McGraw Hill, New York, New York.
34. Govier, G. W., Aziz, K., 1972, "Flow of Complex Mixtures in Pipes," Robert F. Krieger Publishing, Malabar, Florida.
35. Darby, R., 2001, "Chemical Engineering Fluid Mechanics," Marcel Dekker, New York, New York.
36. Leishear, R. A., 2008, "Experimental Bubble Formation in a Large Scale System for Newtonian and Non-Newtonian Fluids," FEDSM2008-55013, ASME Engineering Fluids Conference, New York, New York.
37. Moody, L. F., 1944, "Friction Factors for Pipe Flow," November Transactions of the ASME, vol. 66, New York, New York.
38. B36.10M, 2004, "Welded and Seamless Wrought Steel pipe," American Society of Mechanical Engineers, New York, New York.
39. B36.19M, 2004, "Stainless Steel Pipe," American Society of Mechanical Engineers, New York, New York.
40. ASTM D1785-06, 2006, "Standard Specification for Poly Vinyl Chloride Plastic Pipe, Schedules, 40, 80, and 120," American Society of Testing and Materials, Conshohocken, Pennsylvania.
41. ASTM D2241-05, 2005, "Standard Specification for Poly Vinyl Chloride Pressure Rated Pipe," American Society of Testing and Materials, Conshohocken, Pennsylvania.
42. ASTM B429/B429M-06, 2006, "Standard Specification for Aluminum Alloy Extruded Structural Pipe and Tube," American Society of Testing and Materials, Conshohocken, Pennsylvania.
43. ASTM B88-03, 2003, "Standard Specification for Seamless Copper Water Tube," American Society of Testing and Materials, Conshohocken, Pennsylvania.
44. ASTM B-466, 2007, "Standard Specification for Seamless Copper Nickel Pipe and Tube," American Society of Testing and Materials, Conshohocken, Pennsylvania.
45. ASTM B42-02, 2002, "Standard Specification for Seamless Copper Pipe, Standard Sizes," American Society of Testing and Materials, Conshohocken, Pennsylvania.
46. ANSI/AWWA C115/A21.15-05, 2005, "Flanged Ductile Iron Pipe with Ductile Iron or Gray Iron Threaded Fittings," American Water Works Association, Denver, Colorado.
47. Reid, R. C., Prausnitz, J. M., and Sherwood, T. K., 1977, "Properties of Gases and Liquids," McGraw Hill, New York, New York.
48. Perry, R. H., Green, D. W., Maloney, J. O., 1984, "Perry's Chemical Engineers' Handbook," McGraw Hill, New York, New York.
49. Volk, M. W., 1996, "Pump Characteristics and Applications," Marcel Dekker, New York, New York.
50. "Engineering Data Book," 1990, Hydraulic Institute, Cleveland, Ohio.
51. ASME, 1993, "Steam Tables," ASME Press, New York, New York.
52. Ingersoll Dresser Pumps, 1995, "Cameron, Hydraulic Data," Memphis, Tennessee.
53. Karrasik, I. J., Messina, J. P., Cooper, P., Heald, C. C., 2001, "Pump Handbook," McGraw Hill, New York, New York.
54. Zipparo, V. J., Haen, H., 1993, "Davis' Handbook of Applied Hydraulics," McGraw Hill, New York, New York.

55. Churchill, S. W., Nov. 1977, "Friction Factor Equation Spans All Flow Regimes," Chemical Engineering, McGraw Hill, New York, New York.

56. Miller, D. S., 1978, "Internal Flow Systems," BHRA Fluid Engineering, Bath, England.

57. Lindeburg, M. R., 2006, "Mechanical Engineering Reference Manual," Professional Publications, Belmont, California.

58. ASME B16.9, 2007, "Factory Made Wrought Steel Butt Welding Fittings," American Society of Mechanical Engineers, New York, New York.

59. ASME B16.11, 2008, "Socket Welding and Threaded Forged Steel Fittings," American Society of Mechanical Engineers, New York, New York.

60. ASME B16.5, 2006, "Pipe Flanges and Flange Fittings, NPS ½ - NPS 24," American Society of Mechanical Engineers, New York, New York.

61. ASME B16.42, 1992, "Ductile Iron Pipe Flanges and Flange Fitting Classes 150 and 300," American Society of Mechanical Engineers, New York, New York.

62. Driskell, L., 1983, "Control Valve Selection and Sizing," Instrument Society of America, Research Triangle Park, North Carolina.

63. Varma, V., 1999, "Valve Application, Maintenance, and Repair Guide," TR-105852, EPRI, Palo Alto California.

64. Hutchinson, J. W., 1976, "ISA Handbook of Control Valves," Instrument Society of America, Research Triangle Park, North Carolina.

65. ASME B16-10-2000, "Face to Face and End to End Dimensions of Valves," American Society of Mechanical Engineers, New York, New York.

66. DOE-HDBK-1018/2-93, 1993, "Valve Handbook," Department of Energy, Washington, D. C.

67. Thorley, A. R. D., 1983, "Dynamic Response of Check Valves," 4th International Conference on Pressure Surges, British Hydromechanics Research Association, Bath England.

68. Thorley, A. R. D., 2004, "Fluid Transients in Pipeline Systems," American Society of Mechanical Engineers, New York, New York.

69. ASME, Section I, 2008, "Rules for Construction of Power Boilers," American Society of Mechanical Engineers, New York, New York.

70. ASME, Section IV, 2007, "Rules for Construction of Heating Boilers," American Society of Mechanical Engineers, New York, New York.

71. ASME, Section VIII, 2007, "Boiler and Pressure Vessel Code," American Society of Mechanical Engineers, New York, New York.

72. Crane, 1942, "Flow of Fluids Through Valves, Fittings, and Pipe, Technical Publication, No. 409," Crane Company, Chicago, Illinois.

73. Hooper, W. P., Nov. 1988, "Calculate Head Losses Caused by Change in Pipe Sizes," Chemical Engineering, McGraw Hill, New York, New York.

74. AWWA M11, 2004, "Steel Pipe, A Guide for Design and Installation," American Water Works Association, Denver, Colorado.

75. Abulnaga, B. E., 2002, "Slurry Systems Handbook," McGraw Hill, New York, New York.

76. McKetta, J. J., 1991, "Piping Design Handbook," Marcel Dekker, New York, New York.

77. Crocker, S., King, R. C., 1973, "Piping Handbook," McGraw Hill, New York, New York.

78. Edwards, N. W., Haupt, R. W., Fetzner, D. J., Santana, B. W., 1993, "Evaluation and Acceptance Criteria for ASME Section VIII Vessels and B31.3 Piping Subject to Slug Loading," Journal of Pressure Vessels and Piping, vol. 259, ASME, New York, New York.

79. ANSI/HI, 2002, "Centrifugal Pump Standards," Hydraulic Institute, Parsippany, New Jersey.

80. Blake, J. R., Gibson, D. C., 1987, "Cavitation Bubbles Near Boundaries," Annual Review of Fluid Mechanics, vol. 19, Annual Review of Fluid Mechanics, Palo Alto, California.

81. ANSI/HI, 2002, "Centrifugal/Vertical General Pump Standards," Hydraulic Institute, Parsippany, New Jersey.

82. ASHRAE, 2005, "Fundamentals," American Society of Heating, Refrigeration, and Air Conditioning Engineers, Atlanta, Georgia.

83. Smeaton, R. W., 1997, "Switchgear and Control Handbook," McGraw Hill, New York, New York.

84. Jaeschke, R. L., 1978, "Controlling Power Transmission Systems," Penton/IPC, Cleveland, Ohio.

85. Siskind, C. S., 1963, "Electrical Control Systems in Industry," McGraw Hill, New York, New York.

86. NEMA Standards Publication, 2001, "Application Guide for AC Adjustable Speed Drive Systems," National Electrical Manufacturers Association, Rosslyn, Virginia.

87. Scott, D. S., 1963, "Advances in Chemical Engineering," vol. 4, Academic Press, New York, New York.

88. Hoogendorn, C. J., 1959, "Chemical Engineering Science," vol. 9, Pergammon Press, Oxford, England.

CHAPTER 3

89. "ASME B31.3, Process Piping," 2008, American Society of Mechanical Engineers, New York, New York.

90. "ASME Section VIII, Division 1, "Rules for Construction of Pressure Vessels," American Society of Mechanical Engineers, New York, New York.

91. "2010 ASME Boiler and Pressure Vessel Code, VIII, Rules for Construction of Pressure Vessels, Division 2, Alternative Rules", 2011, American Society of Mechanical Engineers, New York, New York.

92. Becht IV, C. B., 2009, "Process Piping, the Complete Guide to ASME B31.3," American Society of Mechanical Engineers, New York, New York.

93. Antaki, G. A., 2003, "Piping and Pipeline Engineering," Marcel Dekker, New York, New York.

94. Bridgeman, P. W., 1952, "Studies in Large Plastic Flow and Fracture with Special Emphasis on Hydrostatic Pressure," McGraw Hill, New York, New York.

95. Brooks and Choudry, 1993, "Metallurgical Failure Analysis," McGraw Hill Inc., New York, New York.

96. Beaufils, R., Courtin, S., 2011, "Analysis of the Father Experiment with an Engineering Method Devoted to High Cycle Thermal Fatigue," PVP2011-57630, Proceedings of the 2011, Pressure Vessels and Piping Conference, American Society of Mechanical Engineers, New York, New York.

97. Harvey, J. F., 1985, "Theory and Design of Pressure Vessels", Van Nostrand Reinhold, New York, New York.

98. J. F., 1974, "Theory and Design of Pressure Vessels," Van Nostrand Reinhold, New York, New York.

99. Pilkey, W. D., 1994, "Stress, Strain and Structural Matrices," John Wiley and Sons, New York, New York.

100. Marin, J., 1962, "Mechanical Behavior of Materials," Prentice-Hall, Englewood Cliffs, New Jersey.

101. "Metals Handbook," 1987, Ninth Edition, vol. 12, American Society of Testing and Materials, Conshohocken, Pennsylvania.

102. "Metals Handbook," 1974, Eighth Edition, vol. 9, American Society of Testing and Materials, Conshohocken, Pennsylvania.

103. Anderson, T. L., 1995, "Fracture Mechanics: Fundamentals and Applications," CRC Press, Boca Raton, Florida.

104. Henry, G., Hoorstman, D., 1979, "De Ferri Metallographia," V, Fractography and Microfractography, Verlag Stahleisen, Dusseldorf, Germany.

105. Low, J. R., 1949, "Behavior of Metals Under Direct or Nonreversing Loading, Properties of Metals in Engineering," American Society of Testing and Materials, Conshohocken, Pennsylvania.

106. Cooper, W. E., 1957. "The Significance of Tensile Test to Pressure Vessel Design," Welding Journal, American Welding Society, Doral, Florida.

107. ASTM A370, 2012, "Standard Test Methods and Definitions for Mechanical Testing of Steel Products," American Society of Testing and Materials, Conshohocken, Pennsylvania.

108. Boyer, H. E., 1986, "Atlas of Fatigue Curves," American Society for Metals, Metals Park, Ohio.

109. ASME B31T, 2010, Standard Toughness Requirements for Piping, ASME, New York, New York.

110. ASME, Section II, 2011, "Boiler and Pressure Vessel Code," ASME, New York, New York.

111. Flenner, P. D., 2012, "B31 Materials, Fabrication, and Examination, Short Course," ASME, New York, New York.

112. Frey, J., 2012, "Pipe Failure Issues and B31.1 Rules for Operation and Maintenance of Power Piping, Short Course," ASME, New York, New York.

113. Manjoine, M. J., 1944, "Influence of Rate of Strain and Temperature on Yield Stresses of Mild Steel," Journal of Applied Mechanics, ASME, New York, New York.

114. "Metals Handbook," 1990, Tenth Edition, 1, American Society of Testing and Materials, Conshohocken, Pennsylvania.

115. American Society of Metals, 1975, "Metals Handbook," 8th Edition, vol. 10, Metals Park, Ohio.

116. Swanson, S. R., 1974, "Handbook of Fatigue Testing, STP-655," American Society for Testing and Materials, Philadelphia, Pennsylvania.

117. Roth, L. D., 1985, "Ultrasonic Fatigue Testing," Materials Handbook, Ninth Edition, Volume 8, Mechanical Testing, American Society of Testing and Materials, Conshohocken, Pennsylvania.

118. Furuya, Y., Matsuoka, S., Abe, T., Yamaguchi, K., "Gigacycle Fatigue Properties for High-Strength Low-alloy Steel at 100 Hz, 600 Hz, and 20 kHz," Scripta Materilia, Elsevier Science Publishers, Amsterdam, The Netherlands.

119. Grover, H. J., Gordon, S. A., Jackson, L. R., "Fatigue of Metals and Structures," U. S. Government Printing Office, Washington, D. C.

120. Grover, H. J., 1966, "Fatigue of Aircraft Structures," Government Printing Office, Washington, D. C.

121. Collins, J. A., 1993, "Failure of Materials in Mechanical Design," John Wiley and Sons, New York, New York.

122. Leishear, R. A., Stefanko, D. B., Newton, J. D., 2007, "Excitation of Structural Resonance Due to a Bearing Failure," International Mechanical Engineers Conference, American Society of Mechanical Engineers, New York, New York.

123. Section VIII, Division 3, "Alternative Rules for Construction of High Pressure Vessels, Rules for Construction of Pressure Vessels," American Society of Mechanical Engineers, New York, New York.

124. Section III, "Rules for Construction of Nuclear Facility Components," American Society of Mechanical Engineers, New York, New York.

125. Juvinall, R. C., 1967, "Engineering Considerations of Stress, Strain, and Strength," McGraw Hill, New York, New York.

126. Markl, A. R. C., 1952, "Fatigue Tests of Pipe Components," Transactions of the ASME, vol. 74, American Society of Mechanical Engineers, New York, pp. 287–303.

127. Markl, A. R. C., 1947, "Fatigue Tests of Welding Elbows and Comparable Double-mitre Bends," Transactions of the ASME, vol. 69, American Society of Mechanical Engineers, New York.

128. Kapp, J. A., 2009, "Pressure Induced Fatigue, PFP-ASMEEST-07-06-B31 (#3)," American Society of Mechanical Engineers, Standards Technology, New York, New York.

129. BSI, 2011, "PD 5500, Specification for Unfired Fusion Welded Pressure Vessels," British Standards Institution, London, United Kingdom.

130. Kutz, M., 1986, "Mechanical Engineer's Handbook," John Wiley and Sons, New York, New York.

131. Antaki, G. A., 2005, "Fitness-for-Service of Piping, Vessels, and Tanks," McGraw Hill, New York, New York.

132. Young, W. C., Budynas, R. G., 2002, "Roark's Formulas for Stress and Strain," McGraw Hill, New York, New York.

133. M. W. Kellogg Company, 1956, "Design of Piping Systems," John Wiley and Sons, Inc. New York, New York.

134. MSS SP-127, "Bracing for Piping Systems Seismic - Wind - Dynamic Design, Selection, Application," Manufacturers Standardization Society of the Valve and Fitting Industry, Inc., Vienna, Virginia.

135. Peng, L., Peng, T., 2009, "Pipe Stress Engineering," American Society of Mechanical Engineers, Standards Technology, New York, New York.

136. Kannapann, S., 1986, "Introduction to Pipe Stress Analysis," American Society of Heating, Refrigeration, and Air Conditioning Engineers, Atlanta, Georgia.

137. ITT Grinell Corp., 1976, "Piping Design and Engineering," ITT Grinell Corp., Providence, Rhode Island.

138. "ASME B31.1, Power Piping," 2007, American Society of Mechanical Engineers, New York, New York.

139. Antaki, G., 2009, "Alignment of Sustained Load Stress Indices, 17515-R-001," American Society of Mechanical Engineers, Standards Technology, New York, New York.

140. ASCE 7, 2010, "Minimum Design Loads for Buildings and Other Structures," American Society of Civil Engineers, Reston, Virginia.

141. IBC, 2000, "International Building Code," International Codes Council, Falls Church, Virginia.

142. MSS SP-58, 2009, "Pipe Hangers and Supports – Materials, Design, Manufacture, Selection, Application, and Installation," Manufacturers Standardization Society of the Valve and Fitting Industry, Inc., Vienna, Virginia.

143. ACI-318, 2008, "Building Code Requirements for Reinforced Concrete, Appendix D, Anchorage to Concrete," American Concrete Institute, Farmington Hills, Michigan.

144. ACI-349, 2007, "Requirements for Nuclear Related Concrete Structures," American Concrete institute, Farmington Hills, Michigan.

145. AISC, 1989, "Manual of Steel Construction, Allowable Stress Design," American Institute of Steel Construction, Chicago, Illinois.

146. Williams, D. K., Ranson, W. F., 1996, "Pipe Anchor Discontinuity Analysis: Axisymmetric Closed Form Solutions Utilizing Bessel's Functions and Fourier Transforms," PVP-347, Approximate Methods for Design and Analysis of Pressure Vessels and Piping Components, American Society of Mechanical Engineers, New York, New York.

147. Koves, W., 2005, "Design for Leakage in Flange Joints Under External Loads," American Society of Mechanical Engineers, New York, New York.

148. Frikken, D., 2011, "Practical Considerations for Piping Flexibility Analysis in Accordance with ASME B31.3," ASME Short Course, American Society of Mechanical Engineers, New York, New York.

149. Hydraulic Institute, 2000, "Rotary Pump Installation, Operation, and Maintenance," Parsippany, New York.

150. API RP-686, "Recommended Practice for Machinery Installation and Installation Design - Second Edition," American Petroleum Institute, Washington, D. C.

151. "National Board Inspection Code," 2007, National Board, Columbus, Ohio.

152. Nayyar, M., 2012, "Selection and Application of materials for Power piping Systems, Short Course," ASME, New York, New York.

CHAPTER 4

153. Kreyszig, E., 1988, "Advanced Engineering Mathematics," John Wiley and Sons, Inc., New York, New York.

154. Blodgett, O. W., 1966, "Design of Welded Structures," J. F. Lincoln Arc Welding Foundation, Cleveland, Ohio.

155. Merritt, F. S., 1995, "Standard Handbook for Civil Engineers," McGraw Hill, New York, New York.

156. Mendelson, A., 1968, "Plasticity: Theory and Application," Krieger Publishing, Malamar, Florida.

157. Suresh, S., 1998, "Fatigue of Materials," Cambridge University Press, Cambridge, United Kingdom.

158. Landgraf, R. W. 1970, "The Resistance of Metal to Cyclic Deformation," STP-467, American Society for Testing and Materials Philadelphia, Pennsylvania.

159. Bree, J., 1967, "Elastic-Plastic Behavior of Thin Tubes Subjected to Internal Pressure and Intermittent-High Fluxes with Application to Fast Nuclear Reactor Fuel Elements," Journal of Strain Analysis, vol. 2, No. 3. Sage Publishing, Thousand Oaks, Calif.

160. Hodge, P. G., 1959, "Plastic Analysis of Structures," McGraw Hill, New York, New York.

161. Porowski, J. O'Donnell, T., 2008, "Elastic Core Concept in Shakedown Analysis," Pressure Vessels and Piping Conference, PVP2008-61921, American Society of Mechanical Engineers, New York, New York.

162. Bland, D. R., 1956, "Elastoplastic Stresses in Thick-Walled Tubes of Work Hardening Material Subject to Internal and External Pressures and to Temperature Gradients," Journal of the Mechanics and Physics of Materials, vol. 4, ASME, New York, New York.

163. Craig, B. C., Anderson, D. S., 1995, "Handbook of Corrosion Data," ASM International, Materials Park, Ohio.

164. During, E. D. D., 1997, "Corrosion Atlas," Elsevier Science Publishers, Amsterdam, The Netherlands.

165. ASTM E1049-85, "Standard Practices for Cycle Counting in Fatigue Analysis," American Society of Testing and Materials, Conshohocken, Pennsylvania.

166. Barsom, J. M., 1987, "Fracture Mechanics Retrospective, Early Classic Papers," American Society of Testing and Materials, Conshohocken, Pennsylvania.

167. ASME, Section XI, "Rules for Inservice Inspection of Nuclear Power Plant Components," ASME, New York, New York.

168. API 579-1/ASME FFS-1, 2007, "Fitness-For-Service," American Petroleum Institute, Washington, D. C.

169. API 579-2/ASME FFS-2, 2009, "Fitness for Service, Example Problems," American Petroleum Institute, Washington, D. C.

170. "Metals Handbook," 1974, Eighth Edition, vol. 8, American Society of Testing and Materials, Conshohocken, Pennsylvania.

171. McEvily, A. J., 1990, "Atlas of Stress-Corrosion and Corrosion Fatigue Curves," ASM International, Materials Park, Ohio.

CHAPTER 5

172. Parmakian, J., 1963, "Waterhammer Analysis," Dover Publications, New York, New York.

173. Wylie, B. E., Streeter, V. L., 1993, "Fluid Transients in Systems," Prentice Hall, Upper Saddle River, New Jersey.

174. Moody, F. J., 1990, "Introduction to Thermofluid Mechanics," John Wiley and Sons, New York, New York.

175. Chaudry, H., 1987, "Applied Hydraulic Transients," Van Nostrand Reinhold, New York, New York.

176. Larock, B. E., Jeppson, R. W., Watters, G. Z., 2000, "Hydraulics of Pipeline Systems," CRC Press, Boca Raton, Florida.

177. Popescu, M., Arsenie, D., Vlase, P., 2003, "Applied Hydraulic Transients in Hydropower Plants and Pumping Systems," A. A. Balkema Publishers, Lisse, The Netherlands.

178. Ghidaoui, M. S., Zhao, M., McInnis, D. A., Axworthy, D. H., 2005, "A Review of Water Hammer Theory and Practice," vol. 58, Applied Mechanics Reviews, American Society of Mechanical Engineers, New York, New York.

179. Wiggert, D. C., Tijsseling, A. S. 1991, "Fluid transients and Fluid-structure Interaction in Flexible Liquid Filled Piping," Applied Mechanics Review, vol. 54, American Society of Mechanical Engineers, New York, New York.

180. Rollins, J. R., 1986, "Compressed Air and Gas Handbook," Prentice Hall, Englewood Cliffs, New Jersey.

181. Thielsch, H., 1977, "Defects and Failures in Pressure Vessels and Piping," Reinhold Publishing, New York, New York.

182. Arastu, A. H., LaFramboise, W. L., Noble, L. D., Rhoads, J. E., 1999, "Diagnostic Evaluation of a Severe Water Hammer Event in the Fire Protection System," Fluids Conference, American Society of Mechanical Engineers, New York, New York.

183. Suo, L., Wylie, E. B., 1990, "Complex Wavespeed and Hydraulic Transients in Viscoelastic Pipes," vol. 112, Journal of Fluid Engineering, American Society of Mechanical Engineers, New York, New York.

184. Coleman, H. W., Steele, Jr., W. G., 1989, "Experimentation and Uncertainty Analysis for Engineers," John Wiley and Sons, New York, New York.

185. Kobori, T., Yokayama, S., Miyashiro, H., 1955, "Propagation Velocity of Pressure Wave in Pipe Line," Hitachi Hyoron, vol. 37.

186. Contractor, D. N., 1965, "The Reflection of Water Hammer Waves from Minor Losses," Transactions, Series D, vol. 87, American Society of Mechanical Engineers, New York, New York.

187. Holmboe, E. L., 1964, "Viscous Distortion in Wave Propagation as Applied to Waterhammer and Short Pulses," Doctoral Thesis, Carnegie Institute of Technology, Pittsburgh, Pennsylvania.

188. Zielke, W., 1983, "A Short Review of Resistance Laws for Unsteady Flow Through Pipes and Orifices," First Meeting of the IAHR Working Group on the Behavior of Hydraulic Machinery Under Oscillatory Conditions, Milan.

189. Donsky, B., 1961, "Complete Pump Characteristics and the Effects of Specific Speeds on Hydraulic Transients," Journal of Basic Engineering, American Society of Mechanical Engineers, New York, New York.

190. Brown, R. J., Rogers, D. C., 1980, "Development of Pump Characteristics From Field Tests," Journal of Mechanical Design, American Society of Mechanical Engineers, vol. 102, New York, New York.

191. Thorley, A. R. D., Chaudry, A., 1996, "Pump Characteristics for Transient Flow," British Hydrodynamics Research Association, Cranfield, England.

192. Bergant, A., Simpson, A. R., Tijselling, A. S., 2004, "Water Hammer With Column Separation: A Review of Research in the Twentieth Century," CASA-Report 04-34, Department of Mathematics and Computer Science, The University of Eindhoven, The Netherlands.

193. Adamkowski, A., Lewandowski, M., 2009, "A New Method for Numerical Prediction of Liquid Column Separation Accompanying Hydraulic Transients in Pipelines," vol. 131, Journal of Fluids Engineering, American Society of Mechanical Engineers, New York, New York.

194. Lesmez, M. W., Wiggert, D. C., Hatfield, F. J., 1990, "Modal Analysis of Vibrations in Liquid Filled Systems," vol. 112, Journal of Fluid Engineering, American Society of Mechanical Engineers, New York, New York.

CHAPTER 6

195. Brookhaven National Laboratory, 1986, "Report of the Investigation of the Steam Line Accident With Fatal Injuries on October 10, 1986, at Brookhaven National Laboratory Operated by Associated Universities, Inc.," Brookhaven National Laboratory, Upton, New York.

196. Kirsner, W., 1999, "Surviving a Steam Rupture in an Enclosed Space," Heating, Piping and Air Conditioning Engineering Magazine, Cleveland, Ohio.

197. Kirsner, W., 2005, "Condensate Induced Water Hammer in District Steam Systems – Circumstances Resulting in Catastrophic Failures," PVP 2005-71590, American Society of Mechanical Engineers, New York, New York.

198. Green, D. J., 1993, "Technical Evaluation: 300 Area Steam Line Valve Accident, WHC-EP-0667," Westinghouse Hanford Company, Richland, Washington.

199. Merilo, M., 1992, "Water Hammer Prevention, Mitigation, and Accommodation, Volumes 1–6, EPRI NP-6766," Stone and Webster Engineering, Electric Power Research Institute, Palo Alto, California.

200. Van Duyne, D. A., 1996, "Water Hammer Handbook for Nuclear Plant Engineers and Operators," EPRI TR-106438, Electric Power Research Institute, Palo Alto, California.

201. Bjorge, R. W., Griffith, P., 1984, "Initiation of Water Hammer in Horizontal and Nearly Horizontal Pipes Containing Steam and Subcooled Water," Journal of Heat Transfer, vol. 106, American Society of Mechanical Engineers, New York, New York.

202. Spirax Sarco, 1991, "Design of Fluid Systems, Steam Utilization," Allentown, Pennsylvania.

203. Spirax Sarco, 1997, "Design of Fluid Systems, Hook-ups," Allentown, Pennsylvania.

204. Babcock and Wilcox, 1978, "Steam/Its Generation and Use," New York, New York.

CHAPTER 7

205. Leishear, R. A., 2005, "Stresses During Impacts on Horizontal Rods," International Mechanical Engineers Congress and Exposition, American Society of Mechanical Engineers, New York, New York.

206. Graff, K. F., 1991, "Wave Motion in Elastic Solids," Dover Publications, Inc., Mineola, New York.

207. Knopoff, L., 1952, "On Rayleigh Wave Velocities," Bulletin of the Seismological Society of America, vol. 42, El Cerrito, California.

208. Morse, P. M., Ingard, K. U., "Theoretical Acoustics," McGraw Hill, New York, New York.

209. Den Hartog, J. P., 1985, "Mechanical Vibrations," Dover Publications, New York, New York.

210. Kolsky, H., 1963, "Stress Waves in Solids," Dover Publications, New York, New York.

211. Leishear, R. A., 2010, "Higher Mode Frequency Effects on Resonance in Machinery and Structures," PVP2010-25266, Pressure Vessel and Piping Conference, American Society of Mechanical Engineers, New York, New York.

212. Thomson, W. T., 1993, "Theory of Vibrations with Applications," Prentice Hall, Englewood Cliffs, New Jersey.

213. Harris, C. M., Piersol, A. G., 2002, "Harris' Shock and Vibration Handbook," McGraw Hill, New York, New York.

214. Spiegel, M. S., 1967, "Applied Differential Equations," Prentice Hall, Englewood Cliffs, New Jersey.

215. Meirovitch, L. 1997, "Principles and Techniques of Vibrations," Prentice Hall, Upper Saddle River, New Jersey.

216. Lazan, B. J., 1975, "Structural Damping: Energy Dissipation Mechanisms in Structures, with Particular Reference to Material Damping," American Society of Mechanical Engineers, New York.

217. Hadjian, A. T., Tang, H. T., 1986, "Identification of the Significant Parameters Affecting Damping in Piping Systems, in Damping," Hara, F., ed., Pressure Vessels and Piping, vol. 133, American Society of Mechanical Engineers, New York, New York.

218. Thomson, A. G. R., "Acoustic Fatigue Design Data - Part I & Part II," Advisory Group For Aerospace Research And Development, Technical Editing and Reproduction Ltd., 1972.

219. Blevins, R. D., 1990, "Flow Induced Vibrations," Van Nostrand, Reinhold, New York, New York.

220. Wark, K., 1995, "Advanced Thermodynamics for Engineers," McGraw Hill, New York, New York.

CHAPTER 8

221. Dweib, A. H., 2011, "Acoustic Fatigue Assessment of Piping System Components by Finite Element Analysis," PVP-2011-57371, Pressure Vessel Conference, American Society of Mechanical Engineers, New York, New York.

222. Blevins, R. D., 1979, "Formulas for Natural Frequency and Mode Shape," Van Nostrand Rheinhold Co., New York, New York.

223. Wachel, J. C., Szenasi, F. R., Smith, D. R., Tison, J. D., Atkins, K. E., Farnell, W. R., 1993, "Vibrations in Reciprocating Machinery and Piping Systems," Engineering Dynamics Inc., San Antonio, Texas.

224. Leishear, R. A., 2007, "Dynamic Stresses During Water Hammer, A Finite Element Approach," vol. 129, Journal of Pressure Vessel Technology, American Society of Mechanical Engineers, New York, New York.

225. Leishear, R. A., 2007, "Stresses in a Cylinder Subjected to an Internal Shock," vol. 129, Journal of Pressure Vessel Technology, American Society of Mechanical Engineers, New York, New York.

226. Leishear, R. A., 2007, "Derivation for Hoop Stresses Due to Shock Waves in a Tube," PVP2007-26722, Pressure Vessel and Piping Conference, American Society of Mechanical Engineers, New York, New York.

227. Simkins, T. E., 1987, "Resonance of Flexural Waves in Gun Tubes," Technical Report, ARCCB-TR-87008, U. S., Army Armament Research, Development and Engineering Center, Watervliet, New York.

228. Simkins, T. E., 1994, "Amplification of Flexural Waves in Gun Tubes," vol. 172, Journal of Sound and Vibration, Academic Press, Ltd., New York, New York.

229. Beltman, W. M., Burcsu, E. N., Shepherd, J. E., Zuhal, L., 1999, "The Structural Response of Cylindrical Shells to Internal Shock Loading," Journal of Pressure Vessel Technology, vol. 121, American Society of Mechanical Engineers, New York, New York.

230. Herman, G., Mirsky, I., 1956, "Three-Dimensional and Shell Theory Analysis of Axially Symmetric Motions of Cylinders," Journal of Applied Mechanics, American Society of Mechanical Engineers, New York, New York.

231. Timoshenko, S., Woinkowski-Krieger, S., 1959, "Theory of Plates and Shells," McGraw Hill, New York, New York.

232. Barez, F. W., Goldsmith, Sackman, J. L., 1979, (a) "Longitudinal Waves in Liquid Filled Tubes, Theory - I" (b) "Experiments – II," Int. Journal of Mechanical Science, vol. 21, Pergammon Press, Great Britain.

233. Barez, F., 1974, "Longitudinal Waves in Tubes Containing Stationary and Streaming Liquids," PhD Dissertation, University of California, Berkley.

234. Malherbe, M. C., Wing, R. D., Laderman, A. K., Oppenheim, A. K., 1966, "Response of a Cylindrical Shell to Blast Loading," Journal of Mechanical

Engineering Science, vol. 8, Sage Publications, London, Great Britain.

235. Shepherd, J. E., Karnesky, J., Damazo, J., Rusinek, A., 2010, "Plastic Response of Thin-Walled Tubes to Detonation," Pressure Vessel and Piping Conference, PVP2010-25749, American Society of Mechanical Engineers, New York, New York.

236. Naitoh, 2003, "Analysis of Pipe Rupture of Steam Condensing Line at Hamaoka-1," Journal of Nuclear Science and Technology.

237. "Hydrogen Ignition Mechanism for Explosions in Nuclear Facility Pipe Systems," PVP2010-25261, American Society of Mechanical Engineers, New York, New York.

CHAPTER 9

238. ESDU-86015 B, 2011, "Fluid Transients in Pipes. Estimation of Maximum Pressures and Forces in Steam Lines," ESDU – Engineering Sciences Data Unit, London, United Kingdom.

239. Adams, T. M., 2012, "Piping System Earthquake (Seismic) Capacity," ASME B31 Committee Meeting 102 Minutes, J. D. Stevenson and Associates, Inc., Independence, Ohio.

240. NUREG/CR 6358, 2011, "Assessment of United States Industry Structural Codes and Standards for Application to Advanced Nuclear Power Reactors," Nuclear Regulatory Commission, Washington, D. C.

INDEX

Entries are cross referenced using the most common synonymous terms and phrases.

A
ACI-318 [Ref. 143], 179
ACI-349 [Ref. 144], 179
Acoustic velocity, *See* Wave speeds
Affinity laws, 89–90
  Effects from impeller machining, 90, 91
  Flow rate relationships, 89–90
  Head relationships, 89–90
  Horsepower relationships, 89–90
  See also Pump curves
  Speed relationships, 89–90, 91
Air binding of pipes, 113
Air chambers, 255, 278, 279, 280, 285, *See also* Surge tanks
Air entrainment, *See* Centrifugal pumps, *See* Steam jet air entrainment
AISC Manual of Steel Construction [Ref. 145], 179
Allowable stresses, flange bolts, 182, 397
Allowable stresses, flanges, 181–182
Allowable stresses, pipe, 126, 132, 152, 158, 168, 176, 178, 182, 193, 197, 203, 206
  Allowable stresses per B31.3, table, 137–147
  Defined, 3, 161
  Safety factors for allowable stresses in different Codes, 124–125, 136
Aluminum
  See Pipe wall dimensions
  See Tube wall dimensions
Amplitude, *See* Vibration
Anchors, *See* Pipe supports and anchors
Annular mist flow, 110
API 5L, 23, *See also* Pipe wall dimensions
API 579-1/ASME FFS-1 [Ref. 168] and API 579-2 /ASME FFS-2, [Ref. 169], 219, 221–222, 224, 366, 413
  See also Fitness for service
ASCE 7 [Ref. 140], 179
ASME B16.5 [Ref. 60], *See* Fittings, Elbows, tees, crosses, and reducers
ASME B16.9 [Ref. 58], *See* Fittings, Elbows, tees, crosses, and reducers
ASME B16.11, [Ref. 59], *See* Fittings, Elbows, tees, crosses, and reducers
ASME B16.34, *See* Valve Codes
ASME B16.42 [Ref. 61], *See* Fittings, Elbows, tees, crosses, and reducers
ASME B-466 [Ref. 44], *See* Tube wall dimensions
ASME, Boiler and Pressure Vessel Codes
  ASME Section I [Ref. 69], 62, 120
  ASME Section II [Ref. 110], 120, 124, 202
  ASME Section III, 120, 132, 179, 217, 228
  ASME Section IV [Ref. 70], 62, 120
  ASME Section VIII [Ref. 91], 62, 120–121, 180, 209, 217, 326
  ASME Section XI [Ref. 167], 219, 221
  Boiler explosions, 62, 120
  List of Pressure Vessel Codes, 120
ASME, Piping Codes and Standards, 1, 119
  ASME B31.1, Power piping [Refs. 112 and 138], 119, 125, 300, 393
  ASME B31.3, Process piping [Refs. 78, 89, 92, and 148], 119, 120–121, 124, 125, 132, 133–147, 152–159, 161, 163–164, 168–172, 179–182, 185, 201, 206, 214–215, 218, 250, 393, 397
  ASME B31.4, Liquid hydrocarbons and other liquids, 119
  ASME B31.5, Refrigeration piping, 119, 125
  ASME B31.8, Gas transportation and distribution, 119
  ASME B31.9, Building services, 119, 125, 228
  ASME B31.11, Slurry transportation, 119
  ASME B31.12, Hydrogen piping, 119
  ASME B31T, 124, 410, *See also* Toughness requirements
  ASME B36.10M [Ref. 38], 23, *See also* Pipe wall dimensions
  ASME B36.19M [Ref. 39], 23, *See also* Pipe wall dimensions
  List of B31 Piping Codes, 119
  Post construction codes, 119
ASTM B42 [Ref. 45], *See* Pipe wall dimensions
ASTM B88 [Ref. 3], *See* Tube wall dimensions
ASTM D1785 [Ref. 40], *See* Pipe wall dimensions
ASTM D2241 [Ref. 41], *See* Pipe wall dimensions
ASTM B429 [Ref. 42], *See* Pipe wall dimensions and *See* Tube wall dimensions
Atmospheric pressure, values and limits, 98–99
Autofrettage, *See* Plastic deformation
AWWA/ ANSI C115/A21.15 [Ref. 46], *See* Pipe wall dimensions
Axial flow pump, 88, *See also* Centrifugal pumps
Axial stresses, 154, 168
  Dynamic, 325, 326, 337, 338, 340, 385, 389
  Thin wall approximation, due to pressure, 2
  Thick wall approximation, due to pressure, 164
Axial waves, *See* Strain waves

B
B31.1 *See* ASME, Piping Codes and Standards
B31.3 *See* ASME, Piping Codes and Standards
B31.5 *See* ASME, Piping Codes and Standards
B31.9 *See* ASME, Piping Codes and Standards
Ball check valve, *See* Valves
Ball valves, *See* Valves
Basic allowable stress, *See* Allowable stress
Barometric head, defined, 98–99
Bending moment, *See* Moment
Barometric pressure, *See* Atmospheric pressure
Bellows, 167, 168, 171, 291
Bending stresses, 196, 206, 208, 221, 308, 326, 383–384
  B31.3, 161, 163, 170
  Coupling, 391
  Defined, 2
  Dynamic bending stresses, 3, 322, 323, 325, 386, 383–393
  Elastic frames, 381–382, 384–387, 391
  Empty pipes, 178
  Frequencies (beams), 370, 373
  In-plane, 163, 172–173, 175–176
  Limit load, 209
  Maximum DMF for bending stresses, 3, 154
  Out of plane, 163
  See also Plastic deformation
  Static stress equations, 379–381
  See also Stress intensification factors
  Thermal cycling, 203
  Water filled pipes, 177
Bernoulli's equation (extended form also), 5–10, 12, 19, 41, 94, 116, 117, 168, 253, 298
Bingham fluids, 13–15, 34, 38, 74, 253, *See also* Fanning friction factor
Blow down, 233, 297–300
  Flow rate, 297
  Pressure, 298
  Thrust, 300
Brake horsepower, 89, 90, 92, 99, 100, 101, 102, 117
Breathing stresses, defined, 281, 331, *See* Hoop Stresses
Bree diagram, *See* Plastic deformation
British thermal unit, defined, 398
Brittle materials, 121, 124, *See* Tensile testing
Building services, *See* ASME, Piping Codes and Standards
Bulk Modulus
  Defined, 250
  Liquids, 332
    Air entrainment effects, 250–251
    Solids entrainment effects, 250–251
    Table, 32
  Solids, table, 164
  Gases, 250–251, 297
Burst pressure, 201–202, 209, 376, 377
Butterfly valves, *See* Valves

C
Capillarity, 11
Carbon steel, *See* Steel
Cavitation
  Bubbles, 94, 269, 275
  Cavitation erosion, 95–96, 110, 112, 226
  See also Centrifugal pumps
  Defined, 88, 91, 94, 114
  Induced pipe stresses, 94–95
Centrifugal pumps
  Acoustic vibrations, 91
  See also Affinity laws for speed, head, and horsepower relationships
  Air entrainment, 110–112
  See also Brake horsepower
  Cavitation effects on performance, 96–97
  See also Dead head
  See also Efficiency
  Gas entrainment, 110–112
  Heating/overheating during dead-heading, 102
  See Homologous pump curves
  Impeller, 89, 90
  Inertia, 100, 268
  See also Net positive suction head available
  See also Net positive suction head required
  Parallel pumps, 107, 108, 109
  See also Pump curves
  See also Pump nozzles
  Reverse operation, *See* Pump shut-down, *See also* Homologous pump curves
  See also Run out
  Series pumps, 107, 108, 109
  Suction eye, 89, 90
  See Torque
  Vanes, 89, 90
  Vibrations, 323
  See Volumetric flow rate
  Volute, 89, 90
Centroidal axis, defined, 2
Check valves, *See* Valves
Churchill's equation, *See* Darcy friction factors
Close return bends, *See* Resistance coefficients for valves and fittings
Closed loop systems, 86, 106, *See also* System curves
Column separation, 273, 277, 279, 282, *See* Vapor collapse
Compressibility, 6
Concrete pipe, 120, 124, 250
Condensate induced water hammer, 287, 397
  Pipe failures, 287, 288, 290, 291
  Counterflow, 294
  See Fatalities
  See also Fracture mechanics, Failures
  Horizontal pipe, 292–294, 296
  Low pressure discharge, 295, 298
  See also Plastic deformation, Pipe failures
  Preventive actions, 300–301
  Steam pocket collapse, 297
  Steam propelled slug, 295, 298
  See Valve closure
  See also Vapor collapse
  Water cannon, 292
Conservation of mass, 5–6, 245
Consistency of liquids, 13
Contact stresses, 154, 170, 180, 187, 335
Copper nickel tubing, *See* Tube wall dimensions
Copper pipe, *See* Pipe wall dimensions
Copper water tube, *See* Tube wall dimensions
Corrosion
  See Cavitation
  See Fatigue
  See Flow assisted corrosion
  See Stress corrosion cracking
  Types, 228

Corrosion allowance, 155
Counterflow, *See* Condensate induced water hammer
Counterfeit material, 228
Crack propagation, *See* Fracture mechanics
Crane's method, *See* Resistance coefficients for valves and fittings
Creep, 125
Creep, 227, 230
Critical flow, 16, 105, *See also* Turbulence
Critical pressure, 296
Critical temperature, 297
Critical frequency, 345
Critical velocity, 343–347, 349, 351
Crosses, *See* Fittings, Elbows, tees, crosses, and reducers, *See* Resistance coefficients for valves and fittings
Cumulative damage theory, *See* Fatigue
Cup and cone fracture, *See* Tensile testing
Cyclic plasticity, *See* Plastic deformation
Cycloidal response, 314
Cylindrical coordinates, definition, 6, 193, 196, 324, 336

D
Damage mechanisms, defined, 201
Damping
  Damped frequency, 309
  Damping ratio, 309, 310, 311, 312, 313, 316–330, 355
  Fluid damping, 327–330
  Proportional damping, 325–326
  Specific damping energy, 327–329
  Structural damping, 326–329
Darby's method, *See* Resistance coefficients for valves and fittings
Darcy friction factors, 16, 19, 36
  Churchill's equation to describe the Moody diagram, 12, 28, 34, 39, 103
  See also Friction factors
  Moody diagram, 11–12, 16, chart, 17–18, 19, 24, 28, 39, 105
Dead head, definition, 100, 102, 106, 107, 110
Density
  Air, 108
  Bubbles, 94
  Liquid/gas flows, 108
  Liquids, *See* Specific gravity
  Mass density, 2
  Metals, tables, 165–167, 304
  Plastics, table, 167
  Water, 23
  Weight density, 2
Derivative control, *See* PID control
Design flow rates, 1, 88
Diaphragm valve, *See* Valves
Dilatant fluids, 13–15, 34, 253
Differential equations
  Homogeneous solution, 311
  Particular solution, 312
Dispersed bubble flow, 110
Displacement stresses, Displacement controlled stresses, *See* Pipe stresses
Distortion coefficient, *See* Valve actuators
Distortion energy theory, *See* Failure theories
Draw down, 233, 234, 235
Ductile failure, *See* Tensile testing
Ductile iron
  Fittings, *See* Fittings, Elbows, tees, crosses, and reducers
  Pipe, *See* Pipe wall dimensions, *See* Pipe material properties
Ductile materials, 121, 124–125, *See* Tensile testing
Ductile to brittle transition, 124, 127, 128, *See also* Impact tests
Dynamic bending stresses, *See* Bending stresses
Dynamic check valve, *See* Valves
Dynamic amplification factor, *See* Dynamic magnification factors
Dynamic load factor, *See* Dynamic magnification factors
Dynamic magnification factors (DMF), 397
  Damping effects, 329
  Defined, 3–4
  Beams, 323–324, 379
  See Bending stresses
  See also Critical velocity
  Fittings, 369
  Frequency effects, 318–319
  See Hoop stresses
  Load control, 317–318
  Maximum DMF for bending stresses, 3
  Maximum DMF for hoop stresses, 3
  Maximum DMF for Valves, 289
  Percent overshoot relationship, 330
  Pipe
    Long pipe, 331, 336, 337, 340, 349
    Short pipe, 331, 336, 337, 351, 355, 356, 359, 368, 369
  Plastic, 327, 370, 372, 373
  Pressure vessels, 370
  Ramp response, 314
  Relief valve piping, 300
  Rod, 322
  SDOF oscillator, 312
  See also Step response
  Synonyms, 312
  Thermodynamic efficiency relationship, 329
  Valves, 369
Dynamic stresses
  See Axial stresses
  See Bending stresses
  Defined, 2–3
  See also Dynamic stress theory
  See also Dynamic magnification factor
  See Hoop stresses
  See Radial stresses
  See Step response
  See Torsional stress
Dynamic stress theory, 368–369
  Derivation, 351–355
  See Dynamic magnification factors
  See Dynamic stresses
  Experimental results, 356–365
Dynamic viscosity, *See* Viscosity

E
Earthquake loads, 179, 304, 314, 326, 393
Eddy currents, 9, 90
Efficiency
  Pumps, 89, 92, 100–101, 102
  Thermodynamic, 328–330
Elastic core, 204, 205, 207, 208, 210
Elastic follow-up, *See* Plastic deformation
Elastic frames, *See* Bending stresses
Elastic-plastic fracture mechanics, *See* Fracture mechanics
Elastic modulus, *See* Plastic deformation
Elastic water column theory, 242, *See* Water hammer equation

Elbows, *See* Fittings, Elbows, tees, crosses, and reducers, *See* Resistance coefficients for valves and fittings
Elevation head, defined, 7, 117
Elongated bubble flow, 110
Endurance limit, *See* Fatigue
Energy grade line, 11–12, 113, 116
Engineering strain, 121–123, 127, *See also* Tensile testing
Engineering stress, 121–123, 127, *See also* Tensile testing
Enthalpy, 329
Entropy, 329
Equal percentage valves, *See* Valves
Equation of motion, 303, 309, 311, 312, 324, 325, *See also* Vibration
Equivalent pipe length method *See* Resistance coefficients for valves and fittings
Equivalent roughness, 69, *See also* Surface roughness
Erosion, 226, 227
  See also Cavitation
  See also Corrosion
Explosion, 287, 371, 372, 373, 376, 397
External pressure stresses, 202

F
Failure theories, 3
  Bi-axial stress, 196
  Comparison, 193, 198, 199, 200, 201
  See Fatigue
  Maximum Normal stress theory (Rankine), 193, 199, 200
  Octahedral shear stress theory, distortion energy theory (Von Mises), 193, 199, 200, 201
  Maximum shear stress theory (Tresca), 193, 199, 200, 201
  See also Tensile testing
  Tri-axial stress, 196
Fanning friction factors
  Defined, 19
  Fluid flow calculations (Bingham and power law fluids), 34, 38
Fatalities, 235, 287, 288, 397
Fatigue, 193, 197, 199, 201, 204, 209, 220, 225, 226, 227, 235, 313, 325, 327, 331, 334, 355, 365, 367, 372, 374, 393, 397
  Corrosion effects, 153
  Cumulative damage, 214, 215–217
  Curves
    B31.3, 132, 159, 161
    Section VIII, 132, 160–161, 162–163, 218
    Structural stress method, 218–219
  Elastic stress method, 217
  Elastic-plastic stress method, 217–218
  Endurance limit, 3, 121, 128, 129, 130, 131, 132, 133, 148, 151, 152, 153, 197, 199, 211, 215, 216, 217, 218, 222, 327, 365
  Endurance strength, *See* Endurance limit
  Failures, 235–238, 244
  Fatigue limit, *See* Endurance limit
  Frequency effects, 129
  High cycle, 210
  Life, 211–218
  Master curves, 129, 151
  Maximum normal stress theory, 212
  Maximum shear stress theory, 212–213
  Metals, 151, 155
  Octahedral shear stress theory, 213–214
  Pipe data, 155, 156, 157, 158
  Pressure cycling fatigue data, 132, 159
  Pipe failures, 179, 182, 238, 239, 244, 258, 268
  Rain flow counting technique, 214–215
  Size effects, 131–132
  Stress ratio, 129, 150, 164
  Surface effects, 131–132, 152
  Testing techniques, 129, 130, 154, 155
  Thermal fatigue, 148, 210, 211, 227, 229–230
  Uncertainty of data, 150
Fitness for service, 365–367, 397, *See also* API 579-1/ASME FFS-1 and API 579-2, *See also*
Fitting losses, *See* Resistance coefficients for valves and fittings
Fittings, 180, 397
  Elbows, tees, crosses, and reducers, flanged, ASME B16.5, 41, 185, 187
    Class 150 dimensions, table, 50
    Class 300 dimensions, table, 51
  Elbows, tees, crosses, and reducers, ductile iron, ASME B16.42, 41
    Class 150 dimensions, table, 52
    Class 300 dimensions, table, 53
  Elbows, tees, crosses, and reducers, butt welded, table, ASME B16.9, 42–46
  Elbows, tees, crosses, and reducers, socket welded, table, ASME B16.9, 47
  Elbows, tees, and crosses, threaded, table, ASME B16.9, 48
  Street elbows, table, table, ASME B16.11, 49
Flanges, 397
  Allowable stresses, 188
  See also Allowable stresses, flange bolts
  See also Fittings, Elbows, tees, crosses, and reducers, flanged
  See also Moments
  Ratings, forces, moments, and stresses, table, 180–182, 188
  Types, chart, 188
Flexibility analysis, 156, 157, 158, 172–175
Flexibility factor, 171, 180–181
Flexural resonance theory, 367–369
  Derivation 344–345
  Experimental results, 345–348
Float trap, *See* Traps
Flow assisted corrosion, 226, 227, 228
Flow coefficient, 69, 85
Fluid damping, *See* Damping
Flow rate
  See Volumetric flow rate
  See Conservation of mass
  See Design flow rate
Fluid properties
  See Density
  See Specific heats
  See Viscosity
  See also Wave speeds
Fluid transients
  See Blow down
  Computer simulations, *See* Method of characteristics, *See* Mass oscillation technique
  See Condensate induced water hammer
  See Draw down
  See Pump shut-down
  See Pump start-up
  See Resonance
  See Slug flow
  See Valve closure
  See Vapor collapse

Forward travelling wave, 254
Fracture mechanics
  Crack propagation, 221–223, 366
  Elastic-plastic fracture mechanics, 221, 223
  Failures (pipes and valves), 241, 268, 288, 289, 291, 331, 397
  See Fitness for service
  Fracture toughness, 219, 221, 222, 223
  History, 218–219
  Linear elastic fracture mechanics, 219, 221, 223
  Micromechanisms, 223, 224, 225, 288, *See also* Microvoids
  Stress intensity factors, 219, 222, 223
  Stress raisers, 224
  Testing techniques, 222
Fracture toughness, *See* Fracture mechanics
Friction factors for fittings and valves, *See* Resistance coefficients for valves and fittings
Friction factors for pipe
  Defined, 7, 16
  See Darcy friction factors
  See Fanning friction factors
  Non-Newtonian fluids, 36, 38
  Parallel pipes, 40–41
  See also Resistance coefficients for pipes
  Series pipes, 38–40
Friction losses, *See* Resistance coefficients for pipes

G
Gas constant, 297
Gas entrainment, *See* Centrifugal pumps
Gas transportation and distribution, *See* ASME, Piping Codes and Standards
Gasket failures, 288, 397
Gate valves, *See* Valves
Globe valves, *See* Valves
Graphitization, 228
Gravitational constant, defined, 398
Gun tubes, 345–347

H
Hanger loads, *See* pipe supports
Harmonic response
  Defined, 313–318
  PID control, 85
  See Resonance
Head, defined, 1
Head loss, 12, 117
  See also Bernoulli's equation
  Defined, 7
  See also Resistance coefficients for pipes
  See also Resistance coefficients for valves and fittings
Hedstrom number, 38
Henry's Law, 251
High cycle fatigue, *See* Fatigue
Higher mode frequencies, *See* Multi-DOF Systems
Homologous pump curves, 91, 267, 268, 269, 273, 274
Hooke's Law, 121, 197, 324, 341, 352, 353, 356, 365
Hoop stresses
  B31.3, 154–155
  See also Corrosion allowance
  Dynamic hoop stresses, 3, 325, 387–388
  Frequency, 355
  Maximum DMF for hoop stresses, 3, 359
  See also Minimum wall thickness
  Static, thin wall approximation, 2
  Static, thick wall, 156–157
  Step response, 331–340, 351, 352, 353, 354, 384
  Plastic deformation, 208, 370–377
Hooper's method, *See* Resistance coefficients for valves and fittings
Horsepower, *See* Brake horsepower
Hydraulic grade line, 11–12, 113, 270–271, 278
Hydroelectric plants, 235–239, 326, *See also* ASME B31.1
Hydrogen attack, 228
Hydrogen embrittlement, 228
Hydrogen piping, *See* ASME, Piping Codes and Standards
Hydrostatic test, 182, 185, 265, 289, 377
Hyperbolic valves, *See* Valves

I
Impact factor, *See* Dynamic magnification factors
Impact tests, 127, 148–149, *See also* Ductile to brittle transition
Impeller, *See* Centrifugal pumps
Impulse response
  Bending, 390–391
  Derivation, 312–314
  PID control, 85
  Pipe, 338
Induction motors, 99
Inertia, *See* Centrifugal pumps, *See* Moment of inertia, *See* Motors
Inlets, *See* Resistance coefficients for valves and fittings
Integral control, *See* PID control
International Building Code [141]), 179
Inverted bucket trap, *See* Traps

J
Jet pumps, 107, 109
Joukowski's water hammer equation, 1, *See* Water hammer equation

K
Kinematic viscosity, *See* Viscosity
Kinetic energy, defined, 7

L
Lame's constant, 304
Laminar flow, 8–9, 15, 16, 19, 36, 38
Leak before break, 226
Lift check valve, *See* Valves
Limit load analysis
  See also Bending stresses
  See Plastic deformation
Line blockage (plugged piping), 38, 102
Linear elastic fracture mechanics, *See* Fracture mechanics
Linear valves, *See* Valves
Liquid densities, *See* Density
Liquid hydrocarbons and other liquids, *See* ASME, Piping Codes and Standards
Liquid viscosities, *See* Viscosity
Load controlled stress, definition, 154, *See* Pipe stresses, *See* Vibration
Log decrement, *See* Vibration
Longitudinal sustained stresses, *See* Pipe stresses
Loss of ductility, *See* Tensile testing
Low pressure discharge, *See* Condensate induced water hammer

M
Mass density, 397, *See* Density

Mass flow rate, defined, 5
Mass oscillation technique, 253–256
Mass proportional damping, *See* Proportional damping
Master curve, *See* Fatigue
Maxi-max response, *See* Dynamic magnification factors
Maximum Normal stress theory, *See* Failure theories
Maximum shear stress theory, *See* Failure theories
Method of characteristics, 236, 237, 241, 242, 253–258, 261–263, 265, 267, 268, 275, 283
  Alternative methods, 275, 276
Microbiologically induced corrosion (MIC), 228
Microvoids, 125, 221, 224, *See also* Fracture mechanics
Minimum wall thickness, 155, 157
Minor losses, defined, 11, *See* Resistance coefficients for valves and fittings
Mitered pipe bends, 74
Mixed flow pump, 88, *See also* Centrifugal pumps
Modal frequency, *See* Vibration
Modulus of Elasticity, 303, 332, 333, 341
  Definition, 121, 122, 131
  Metals, per B31.3, table, 133–135
  Non-metals, per B31.3, table, 133–135
  Rubber, 228
Moody diagram, *See* Darcy friction factors, *See also* Friction factors
Moment, 2
  Bending, 161, 164, 168, 170, 389–392
  Differential element, 341–342
  Flanges, 180, 182, 191
  In-plane, bending, 163, 170, 173, 175, 176
  Limit load analysis (plastic moment), 207–208
  Out of plane, bending, 163
  Torsional, 161, 164, 168, 170, 171, 174
Moment of inertia, 2, 19, 161, 174
  Polar, 171
Motors
  Current, 99–100
  See Induction motors
  Inertia, 100
  Power factor, 99–100
  Service factor, 99
  Slip, 99
  Speeds, standard, 99
  Starters, 99
Moving bed, *See* Solid/liquid flows
MSS SP-58, *See* Pipe supports and anchors
MSS SP-127, *See* Pipe supports and anchors,
Multi-DOF systems, 319–322

N
Natural frequency, *See* Vibration
Necking, *See* Tensile testing
Needle valves, *See* Valves
Net positive suction head available, 92, 94, 98, 110, 116, 117
Net positive suction head required, 92, 94, 96–98, 110, 116, 117
Newtonian fluids
  Defined, 13
  See also Volumetric flow rate
Nodular iron, *See* Ductile iron
Non-Newtonian fluids
  See Bingham fluids
  See Dilatant fluids
  See also Fanning friction factors
  See Friction factors for pipe
  See Power law fluids
  See Pseudoplastic fluids
  Structural fluids, 13
  See also Volumetric flow rate
Normal stresses, 7, 193–196
Nozzle check valve, *See* Valves

O
Occasional stresses, *See* Pipe stresses
Octahedral shear stress theory, *See* Failure theories
Open channel flow, 113–114
Orifices, *See* Resistance coefficients for valves and fittings
Outlets, *See* Resistance coefficients for valves and fittings
Overload failure, defined, 201

P
Parallel pipes
  See also Centrifugal pumps
  See Fittings, elbows, tees, crosses, and reducers
  See Friction factors for pipe
  See System curves
  See Volumetric flow rate
  See Waves
Participation factor, *See* Vibration
Percent overshoot, 68, 312, 328, 330
Period, *See* Vibration
Phase angle, *See* Vibration
PID control, 84–88
  See also Harmonic response
  See also Impulse response
  See also Proportional control
  See also Ramp response
  See also Step response
  See also Valve actuators
  See also Variable frequency drives
Piezometer tube, 11–12
Pinch valve, *See* Valves
Pipe failures, 397, *See* Failure theories, *See also* Tensile testing, *See* Plastic deformation, *See* Fatigue, *See* Fracture mechanics
Phase angle, *See* vibration
Pipe flow, *See* Bernoulli's equation, *See* Flow rate
Pipe frequency, *See* vibration
Pipe losses
  Diameter effects, 26
  See Resistance coefficients for pipes
  See also Resistance coefficients for valves and fittings
  Steel pipe, aging effects, equation, 26, 28, table, 37
  Temperature effects, 24, 26
  Water flow in steel pipes, table, 37
Pipe resistance, *See* Resistance coefficients for pipes
Pipe stresses
  See Allowable stresses
  See Axial stresses
  See Bending stresses
  Comparison of design stress calculations for different Codes, 176, 178, 179, 182
  Computer programs for calculations, 153
  Defined, 196
  Displacement stresses, Displacement-controlled stresses, defined, 154, 157–158, *See* Bending stresses
  See also Dynamic magnification factors

See Dynamic stresses
See External pressure stresses
See also Flanges, Allowable stresses
See also Flanges, Ratings, forces, moments, and stresses
See Flexibility analysis
See Hoop stresses
See also Moments
Occasional stresses, 157–158
See also Load-controlled stresses
Longitudinal sustained stresses, 157–158
Maximum, 154
Pipe supports and anchors, 397
Design requirements, MSS SP-58, table, 179
Hanger loads, MSS SP-58, table, 185
Failure, 228
Spacing, table, B31.1 and MSS SP-127, 171, 179
Types of supports and anchors, MSS SP-58, 183–184
Pipe, valve, and fitting losses
See Bernoulli's equation
See Fanning friction factors
See Friction factors for pipe
See Equivalent pipe length method for pipe losses
See Resistance coefficients for pipes
See Resistance coefficients for valves and fittings
Pipe wall dimensions
Aluminum pipe, table, ASTM B429, 23
Copper pipe, table, ASTM B42, 27
Ductile iron pipe, table, AWWA/ ANSI C115/A21.15, 28
PVC pipe, table, ASTM D1785, 21
PVC, Pressure rated pipe, table, ASTM D2241, 22
Steel and stainless steel pipe, table, (API 5L, ASME B36.10, ASME B36.19), 20
See also Tube wall dimensions
Piping Codes
API Codes, 67
See also ASME, Piping Codes and Standards
Pitot tube, 11–12
Plastic, 202, 209
Plastic deformation, 303, 308, 365, 393, 397
Autofrettage, 209
Bending stresses, 393
Bree diagram, 205–206, 209–210
See also Burst pressure
Combined stresses, 209
DMF, 379
Elastic core, 204, 205, 207, 208, 210
Elastic follow-up, 203, 228
Failure example, 291
See also Failure theories
See also Hoop stresses
Limit load analysis for bending, 207–208, 209–210, 211
Plastic collapse, plastic flow, 204
Plastic cycling, 203–204, 205
Ratcheting, 204, 205, 206, 207, 209, 370, 377
Shakedown, 203, 205, 206, 207, 208
Spalling, 308
Types, 202, 203
Plastic frequency, 370
Plastic modulus, 203, 371
Plasticity, *See* Plastic deformation
Plates, *See* Vibration
Plug valve, *See* Valves
Pneumatic operators, 77, 84, *See also* Valve actuators
Poisson's ratio, 332, 335, 337, 341, 365, 372
Defined, 121, 136
Metals, table, 164
Polar Moment of inertia, 171
Positive displacement pumps, 88, 110, 303, 276–277
Potential energy, defined, 7
Power, *See* Brake horsepower
Power factor, 92, 100
Power law fluids, 13–15, 36, 38, 74, 253, *See also* Fanning friction factor
Power Piping, *See* ASME, Piping Codes and Standards
Pressure across a shock, 1, *See also* Water hammer equation
Pressure cycling, *See* Fatigue
Pressure drops in piping, *See* Pipe losses
Pressure energy, defined, 7, *See also* Bernoulli's equation
Pressure head, defined, 7, *See also* Bernoulli's equation
Pressure rating, *See* Valves, *See* Flanges, *See also* Hoop stresses
Pressure reducing valves, *See* Pressure regulators
Pressure regulators, 66, 68, 86, 300
Pressure surge due to a suddenly closed valve, *See* Valve closure, *See also* Water hammer equation
Pressure waves, *See* Strain waves
Primary flow, 10
Principal stresses, 193–196, 199, 200, 212, 221
Process Piping, *See* ASME, Piping Codes and Standards
Proportional control *See* PID control
Proportional damping, *See* Damping
Pseudoplastic fluids, 13–14, 34, 253
Pump head, defined, 7, *See also* Bernoulli's equation
Pump curves, 89, 91
See also Centrifugal pumps
See also Net positive suction head available
See also Net positive suction head required
Viscosity effects, 92–94
Pump laws, *See* Affinity laws
Pump nozzles, forces and moments, 182, 191–192, *See also* Moments, *See also* Reactions
Pump shut-down (turbine shut-down)
Corrective actions
See Air chambers
Slow closing valve, 269, 276
VFD control, 279–280, *See also* Variable frequency drives
See Surge tanks
See Water hammer arrestors
Graphic solution, 266, 272
Reverse operation, 89, 235, 240, 266–269, 275, *See also* Homologous pump curves
Pump start-up, 262, 265, 268
PVC Pipe
See Density
See Modulus of elasticity
See Pipe wall dimensions, Pressure rated pipe
See Pipe wall dimensions, PVC pipe
See Thermal expansion coefficients for metals and plastics

Q
Quality factors per B31.3, table, 169

Quick opening valves, *See* Valves

R
Radial flow pump, 88, 89, *See also* Centrifugal pumps
Radial stresses, 195, 196, 326
  Defined, 164
  Dynamic, 335–337, 351
Radial frequency, *See* Vibration
Radial stress, 164, 336, 337
Rain flow counting technique, *See* Fatigue
Ramp response, 85, 313–314, 331, 369, 384, 388–389, 390
Range stress, 129, 327
Rankine theory, *See* Failure theories
Ratcheting, *See* Plastic deformation
Rayleigh proportional damping, *See* Proportional damping
Rayleigh waves, *See* Strain waves
Reactions, 164, 167–168, 179–180, 379
Reducers, *See* Fittings, elbows, tees, crosses, and reducers
Reflected shocks, 389–390
  Fluids, 261, 270
  Solids, 306–308
Refrigeration piping, *See* ASME, Piping Codes and Standards
Relief valves, *See* Valves
Relative roughness, 19, *See also* Surface roughness
Resistance coefficients for pipes, defined, 7, 11–12, *See also* Friction factors for pipe
Resistance coefficients for valves and fittings, 7, 10
  1 K method for valves and fittings (Crane's method), 69, table, 71–75
  2K method for valves and fittings (Hooper's method), 74, table, 71–75
  3K method for valves and fittings (Darby's method), 69, 74, table, 71–75
  Accuracy, 69
  Closing vs. opening of valves, 85
  Colebrook equation, 69
  Equivalent pipe length method, 69, table, 70
  Exits, 40–41, 43, 74
  Flow direction effects, 71–74
  Friction factors for fittings, 75
  Inlets (entrances), 41, 74
  Orifices, 41, 74, 298
  Outlets, 41, 74
  Pipe length effects, 79, 84
  See also Pipe losses
  Throttled valves, 74–83, *See also* Valves
Resonance
  See also Flexural resonance theory
  Fluid resonance, 280, 286
  Solids, 313, 314, 316, 318–321
Reverse travelling wave, 254
Reverse flow, *See* Pump shut-down
Reynold's number, 9, 20, 24, 33, 38, 74, 104, 105
  Defined, 16
  Equation, 19
  See also Viscosity
Reynold's transport theorem, 253
Rigid water column theory, 239, 242, 243, 248
Rods, *See* Vibration
Roughness, *See* Surface roughness
Run out, 105–106, 234–235

S
Safety factors for piping materials, *See* Allowable stresses
Safety valves, *See* Valves
Saltation, *See* Solid/liquid flows
Sayboldt universal second, 14
Seat opening, 75
Secant modulus, 131, *See also* Modulus of elasticity
Secondary flows, 10
Section I, *See* ASME, Boiler and Pressure Vessel Codes
Section II, *See* ASME, Boiler and Pressure Vessel Codes
Section III, *See* ASME, Boiler and Pressure Vessel Codes
Section IV, *See* ASME, Boiler and Pressure Vessel Codes
Section VIII, *See* ASME, Boiler and Pressure Vessel Codes
Section XI, *See* ASME, Boiler and Pressure Vessel Codes
Section modulus, 161, 163
Series pipes
  See also Centrifugal pumps
  See Fittings, elbows, tees, crosses, and reducers
  See Friction factors for pipe
  See System curves
  See Volumetric flow rate
  See Waves
Shakedown, *See* Plastic deformation
Shear modulus, 196, 304
Shear stresses, 171, 180, 333, 193
  Fluids, 7, 13–15, 19, 34, 38
  Solids, 193–194, 196, 198
  Pipe, 171, 180
Shear thickening fluids, *See* Dilatant fluids
Shear thinning fluids, *See* Pseudoplastic fluids
Shock waves
  Elbows, 248
  Parallel pipes, 262, 263, 268–269
  Series pipes, 262, 266–267
  Water, 1
  See also Reflected shocks
  See Shock wave speeds
  See Wave speed equation
Shells, *See* Vibration
Shock wave speeds
  Liquid filled pipes
    Air entrainment effects, chart, 250–251
    Concrete pipe and tunnels, 250
    Equations for wave speeds, 248–250, 331, 339
    Non-metallic pipe, 250
    Steel pipe, chart, 249, 349
    Solid entrainment effects, 250
  Liquids (acoustic velocity), table, 33
  Solids (acoustic velocity), 304
Single degree of freedom systems (oscillators), 308–325, *See* Vibrations
Sinusoidal response, *See* Harmonic response
Siphons, 114–116
Slip, *See* Motor slip
Slow acting valve closure, *See* Valve closure
Slug flow, 110, 114, 233, 234–235, 262, 266, 277, 288, 363–364, 397, *See also* Vapor collapse
Slug formation, *See* Vapor collapse
Slurry transportation, *See* ASME, Piping Codes and Standards

Solid/liquid flows, 114
Spacing of pipe supports, *See* Pipe supports, spacing
Spalling, *See* plastic deformation
Specific damping energy, *See* Damping
Specific energy, defined, 7
Specific gravity
  See also Density
  Liquids, table, 29–30
  Water, chart, 31, table, 32
Specific heats of liquids, 102
Specific speed, 88, 100, 101, 103, 267, 268
Specific volume
  Water, table, 32
Split disc check valve, *See* Valves
Spring constant, 324, *See also* Single Degree of Freedom oscillator, *See also* Vibration
Springs, *See* Vibration
Stainless steel
  See Bulk Modulus
  See Density
  See Pipe wall dimensions
  Stress-strain diagram, 123
Steam hammer, *See* Condensate induced water hammer
Steam jet air entrainment, 289
Steam pocket collapse, *See* Condensate induced water hammer
Steam propelled slug, *See* Condensate induced water hammer
Steam properties, *See* Fluid properties
Steel
  See Bulk Modulus
  See Density
  See Modulus of elasticity
  See Pipe wall dimensions
  Stress-strain diagram, 123
  Types, 126
Stem travel, 75
Step response
  Concrete, 327
  See also Dynamic magnification factor
  See Hoop stress
  PID control, 85–88
  SDOF
    Derivation, 311–312, 324–325
  See also Valve closure
Stiffness proportional damping, *See* Proportional damping
Stoke, 14
Strain, defined, 121, *See* Engineering strain, *See* Tensile testing, *See* True Strain
Strain hardening, and strain hardening exponents, 122, 123, 127, 128
Strain rate effects
  Fluids, 13–15, 34
  Solids, 121, 124, 129, 130, 133, 160, 161, 162, 163
Strain waves
  Distortional waves, 304, 305–308, 336, 337
  Rayleigh waves, 304
  Rods (free and fixed ends), 306–308
  See also Shock waves
  See also Shock wave speeds
  Traction waves, 304, 305
Stratified flow, 110
Street elbows, *See* Fittings
Stress
  See Axial stresses
  See Contact stresses
  See Engineering stress
  See Hoop stresses
  See Normal stresses
  See Pipe stresses
  See Principal stress
  See Radial stresses
  See Shear stresses
  See also Tensile testing
  See True stress
Stress corrosion cracking, 225–226, 227
Stress cube (stresses at a point), 194, 195, 197, 198
Stress intensity factors, *See* Fracture mechanics
Stress intensification factors per B31.3, 163, 170, 171, 176, tables, 180–181
Stress raisers, *See* Fracture mechanics
Stress range factor, 132, 159, 161
Stress ratio, *See* Fatigue
Stress-strain curves, *See* Tensile testing
Stress waves, *See* Strain waves
Structural damping, *See* Damping
Structural fluids, 13, 253
Suction head, defined, 98
Suction eye, *See* Centrifugal pumps
Sudden valve closure, *See* Valve closure, *See also* Water hammer equation
Supports, *See* Pipe supports
Surface roughness, definition and table, 19
Surge tanks, 235, 236, 256, 278–279, 280, 285, *See also* Air chambers
Sustained longitudinal stresses, *See* Pipe stresses
Swing check valve, *See* Valves
System curves, 102–108
  Closed loop systems, 106
  Parallel pipes, 107
  Run out conditions, 106
  Series pipes, 107
  Viscosity effects, 105
Systems of units and conversion factors, 1, 119, 397–399

T
Tees, *See* Fittings, Elbows, tees, crosses, and reducers, *See* Resistance coefficients for valves and fittings
Temperature, personnel safety control, 26
Tensile testing, (tensile stresses), 107, 201, 202, 203, 219, 289, 337
  Brittle fracture, 124, 131, 132, 397
  Cup and cone fracture, 123–124, 125, 126
  Defined, 121–122
  Ductile failure, 126, 397
  See also Engineering strain
  See also Engineering stress
  See also Failure theory
  Loss of ductility, 123, 129
  Necking, 122
  See also Strain rate effects
  Stress-strain curves for metals, 123
Tensile stresses, *See* Tensile testing
Thermal expansion, 138, 142
Thermal expansion coefficients, 136
  Thermal expansion coefficients for metals and plastics per B31.3, table, 168
Thermal fatigue, *See* Fatigue

Thermal stress, 136, 148
Thermodynamic trap, *See* Traps
Thermostatic trap, *See* Traps
Throttled valves, *See* Resistance coefficients for valves and fittings
Tilt check valve, *See* Valves
Torsional stresses, 154, 174, 210, 308, 326
  Defined, 161, 171
  Dynamic, 325
Torque, 99, 100, 101, 102
Toughness requirements
  See also ASME, Piping Codes and Standards, ASME B31T
Transmissibility, *See* Dynamic magnification factors
Trapped air effects, *See* Centrifugal pumps, *See* Air binding, *See* Vapor collapse
Traps, 67
  Float, 64, 67
  Inspection and operation, 301
  Inverted bucket, 65, 67
  Thermodynamic, 66, 68
  Thermostatic, 65, 67–68
Tresca theory, *See* Failure theories
Tri-axial vibrations, *See* vibrations
Troubleshooting practices, 396
True strain, 122, 127, 202
True stress, 122, 127, 202
Tube wall dimensions, *See also* Pipe wall dimensions
  Aluminum tubing, table, ASTM B429, 24
  Copper nickel tubing, table, ASME B-466, 26
  Copper pipe, table, ASTM B42, 27
  Copper water tube, table, ASTM B88, 25
Turbine head, defined, 7, *See also* Bernoulli's equation
Turbulent flow, 8–11, 15, 16, 19, 26, 36, 38, 69, 74, 75, 77, 105, 113

U
Ultimate stress, *See* Ultimate strength
Ultimate strength, 3, 121, 124, 126, 130, 155, 197, 199, 201, 202, 203, 204, 327
  Defined, 122, 124
  Ultimate strengths per B31.3, table, 137–147

V
Valve actuators, 77, 79, 83, 84
  Distortion coefficient, 79, 84
  See also PID control
Valve closure, 397
  See also Rigid water column theory
  Slow acting valve closure, 258, 260, 262, 266, 269, 271
  Sudden valve opening and closure, 1–4, 235, 238, 242–245, 246–248, 258, 259, 261, 270, 374, 377, 397
Valve Codes
  API, 55, 67
  ASME B16.34, 55
Valve stroking, 278, 284
Valves, 397
  Ball valves, 55, 77, 82, 180, 182, 189–190, 262
    Parabolic, 55, 78
    See also Resistance coefficients for valves and fittings
    U-port, 55, 78
    V-port, 55, 78
  Butterfly valves, 56, 77, 80, 81, *See also* Resistance coefficients for valves and fittings
  Check valves
    Ball check, 60
    Dynamic check valve characteristics, 61, 268
    Lift check, 57, 59
    Nozzle check, 60–61
    Piston check, 57, 59
    See also Resistance coefficients for valves and fittings
    Split disc check, 57
    Swing check, 57, 58
    Tilt check, 57, 60
  Diaphragm valves, 56–57
  Dimensions, 43
  Equal percentage valves, 75, 76, 77
  Gate valves, 54–55, 75, 77
    Plate and disc, 79
    Positioned disc, 79
    See also Resistance coefficients for valves and fittings
    Slab type, 79
    V-port, 79
  Globe valves, 54–55, 82, 83
    Angle, 83
    Equal percentage, 80
    Linear, 80
    See also Resistance coefficients for valves and fittings
    Quick opening, 80
    Y-valve, 83
  Hyperbolic valves, 76
  Linear acting valves, 75, 76, 77
  Needle valves, 63, 67
  Pinch valves, 64, 67
  Plug valves, 10–11, 56, 77
    Equal percentage, 78
    Eccentric, 78
    See also Resistance coefficients for valves and fittings
    V-port, 78
  Pressure ratings, 180, 189–190, *See* Valve Codes
  See also Pressure regulators
  Quick opening valves, 76
  Relief valves, 62, 237, 263, 269, 278, 299, 300
  Safety valves, 62, 63
    Safety requirements, ASME Sections I, IV, and VIII, 62
  See also Traps
Vanes, *See* Centrifugal pumps
Vapor collapse, 114, 234, 235, 236–237, 242, 269, 270–271, 273, 275, 276, 278, 279, 287, 297, 357, 363, 365
  Slug formation, 293, 294, 295, 296
  See also Slug flow
  Trapped air effects, 233, 277, 278, 283, *See also* Centrifugal pumps, *See also* Air binding
Variable frequency drives, 91, 99, 100, 234, 275, 278, 365, 366–368
Velocity head, defined, 7, 11, 12, *See also* Bernoulli's equation
Velocity profiles, 8–9
  See also Laminar flow
  See also Turbulent flow
Versed sine response, 314
Vibration
  Aftershock, 350, 355, 356
  Amplitude, 304, 310
  Analyzers, 130–131
  See Bending stresses
  Circular frequency, 305, 307, 309, 321, 323
  Damped frequency, *See* Damping

See Damping
Free vibration, 309, 316
Forced vibration, 311, 315, 316
See also Harmonic response
See also Impulse response
Load control, 314–317, 322–323
Log decrement, 309–310, 355
Modal frequency, 305, 319
See Multi-DOF systems
Natural frequency, 304, 309, 310
Participation factor, 319, 322
Period, 305, 306, 307, 309, 310
Phase angle, 309, 310
Pipe, 332, 333, 334
Plates, 308
Precursor, 350, 353, 355, 356
See also Resonance
Rod, 305–307, 321, 322–323
Shells, 308, 341–343
See also Shock wave speed
See also Single degree of freedom systems
Springs, 319, 321
See also Step response
Tri-axial vibrations, 324
Wave length, 305
Wave number, 305
Vibration response, defined, 3
Vicker's hardness, 210
Viscometers, types, 13–14
Viscosity, 5, 23–24, 26, 88, 108
Dynamic viscosity, defined, 13–15
Equation, 24
Flow rate effects, 102–103, 105
Kinematic viscosity, defined, 13
Liquids, table, 35
Pump performance effects, chart, 92–93
Reynold's number effects, chart, 33
Steam, 34
System curve effects, 105
Units, 13–14
Water, 34
Volumetric flow rate
Defined, 6
Inlet, 41
Newtonian and non-Newtonian fluids, 15–16
Orifice, 41
Outlet, 41
Pumps, 88
Parallel pipes, 40–41
Series pipes, 38–40
Volute, *See* Centrifugal pumps
Von Mises theory, *See* Octahedral shear stress theory
Vortex, 9, 110

W
Water cannon, *See* Condensate induced water hammer
Water hammer arrestors, 280
Water hammer equation
Definition, 1, 234, 235, 272
Derivation, 245–248, 251
Uncertainty, 252
Water horsepower, 92
Water properties
See Density
See Viscosity
Wave flow, 110
Wave length, *See* Vibration
Wave number, *See* Vibration
Wave speed equation, 255, 303, *See also* Shock wave speeds
Wave speeds, *See* Shock wave speeds
Waves, *See* Shock waves
Weight density, 397, *See* Density
Weld joint strength reduction factors per B31.3, table, 170
Wind loads, 179

Y
Yield moment, 207–208
Yield strength, 3, 121, 180, 197, 199, 201, 202, 203, 205, 206, 207, 209, 210, 211, 221, 229, 326, 369, 372, 373, 374
Defined, 122, 123, 124, 126, 130, 132
Dynamic, 370, 371, 375
Yield strengths per B31.3, table, 137–147
Yield stress, liquids, 14, 38, 253
Yield stress, solids, *See* Yield strength
Young's Modulus, *See* Modulus of Elasticity